PROCEEDINGS OF THE 14th INTERNATIONAL CONFERENCE ON ENVIRONMENTAL ENGINEERING, SCIENCE AND MANAGEMENT

MAY 20-21, 2025., BANGSAEN HERITAGE HOTEL, CHON BURI, THAILAND

ISBN : 978-616-94820-0-0

Green Environment & Low Carbon Society Towards Sustainability for Mankind Wellness







EDITORS

Suchat Leungprasert Wanpen Wirojanagud Trakarn Prapaspongsa Pongsak Noophan

Wilasinee Yoochatchaval Kowit Suwannahong Anamai Thetkathuek Pitsanu Pannaracha

PROCEEDING
THE 14th INTERNATIONAL CONFERENCE ON ENVIRONMENTAL ENGINEERING, SCIENCE AND MANAGEMENT

Organized by:

Environmental Engineering Association of Thailand

Faculty of Engineering, Kasetsart University

Faculty of Public Health, Burapha University

Ministry of Higher Education, Science, Research and Innovation

Ministry of Energy

Ministry of Natural Resources and Environment

Pollution Control Department

Department of Local Administration

Department of Climate Change and Environment

Office of Natural Resources and Environmental Policy and Planning

Center for Clean Air Solutions

Thai Health Promotion Foundation

National Research Council of Thailand (NRCT)

Industrial Estate Authority of Thailand

Kasetsart University, Research and Development Institute (KURDI)

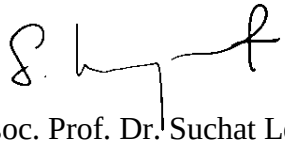
May 20-21, 2025

Message from President of Environmental Engineering Association of Thailand

Environmental Engineering Association of Thailand (EEAT) has continually organized Annual National and International Conferences on Environmental Engineering, Science and Management since 2002 and 2012, respectively. The Conferences will consequently be the knowledge sharing and exchanging platform for academia, researchers, experts and interesting people on the environmental related subjects particularly the evolving subjects on climate change, zero emission, low carbon society, etc. For the year of 2025, it is our great privilege to co-host with the Faculty of Engineering, Kasetsart University, Faculty of Public Health, Burapha University with the generous support of the Ministry of Higher Education, Science, Research and Innovation, Ministry of Energy, Pollution Control Department, Department of Climate Change and Environment, Department of Local Administration, Office of Natural Resources and Environmental Policy and Planning, Center for Clean Air Solutions, Thai Health Promotion Foundation, National Research Council of Thailand (NRCT), Industrial Estate Authority of Thailand, Ministry of Natural Resources and Environment, to organize the 24th National Conference and the 14th International Conference on Environmental Engineering, Science and Management. Knowledgeably, the proceeding is consisted of the qualified abstracts reviewed reviewing by the experts, and full paper had been documented on electronic file, in accordance with the national and international standards. The conference will academically be completed with keynote/guest speakers, oral and poster presentations, as well.

In the meantime, I would like to honestly express my thankfulness to everyone and agencies who collaborate in the presentations of research findings and various supportive private sectors namely, Center for Clean Air Solutions, Thai Health Promotion Foundation, Electricity Generation of Thailand (EGAT), General Environmental Conservation Public Company Limited, Thai Environment Technic Limited : TET, Research Center for Environmental and Hazardous Substance Management (EHSM), Faculty of Engineering, Khon Kaen University, Greenhouse gas Management and Certification Unit, University of Phayao, The Siam Cement Public Company Limited, C.M.P. GROUP, Petro-Instruments Co., Ltd., Therm Engineering Co., Ltd., S.M. Chemical Supplies Co., Ltd., Bara Scientific Co., Ltd., E-Power Service Co., Ltd., Rajamangala University of Technology Thanyaburi, Macro Consultants Co., Ltd., Energy Complex Co., Ltd., United Analyst and Engineering Consultant Co., Ltd., Association of Three Co., Ltd., Bangchak Corporation Public Company Limited, Center of Excellence on Hazardous Substance Management (HSM) of Chulalongkorn University, Siam Wattana Waste Management Co., Ltd., PTT Global Chemical Public Company Limited, Hidaka Yookoo Enterprises Co., Ltd., Modern Dyestuffs & Pigment Co., Ltd., Plus Exploration Company Limited, Hino Motors Manufacturing (Thailand) Ltd., Rajamangala University of Technology Isan, Planet C Co., Ltd., Faculty of Engineering, Kasetsart University, Kasetsart University, Research and Development Institute (KURDI), ENVIR Service Co., Ltd., Innovation Ideas Co., Ltd., UHM Co., Ltd., Calpeda (Thailand) Co. Ltd., Premier Products Public Co., Ltd., Innova Life Co., Ltd., Brara (Thailand) Co., Ltd., Civio Engineering Co., Ltd., Charoen Pokphand Foods Company Limited, NPC Safety and Environmental Service Co., Ltd., Rak Dee Harm Jua Co., Ltd. and Global Environmental Technology Co., Ltd. who provide an exceptional support to make the conference come true.

Finally, I wish both National and International Conferences being achieved with all the ultimate goal.



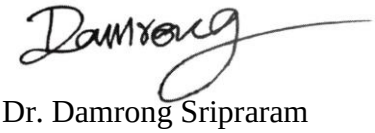
Assoc. Prof. Dr. Suchat Leungprasert
President of Environmental Engineering Association of Thailand

Message from President of Kasetsart University

The National and International Environmental Conferences, organized by the Environmental Engineering Association of Thailand (EEAT), are an important platform for academics and researchers to present their academic work and disseminate environmental knowledge. Such conferences also provide an opportunity for environmental experts and relevant agencies to present their various professional environment issues. In 2025, Kasetsart University, by the Faculty of Engineering, has been honored by EEAT in collaboration with Burapa University by Faculty of Public Health to co-host with the 24th National Environmental Conference, along with the 14th International Environmental Conference on Engineering, Science, and Environmental Management, on 20-21 May 2025 at the Bangsaen Heritage Hotel, Chonburi Province.

Kasetsart University would like to thank EEAT, government agencies and other supporting agencies from the public, educational and private sectors, whose names were mentioned in the message from the president of EEAT for their support in organizing this academic conference, as well as all organizing committees who have handled both the documentation of the academic conference and the preparations for the academic conference, both nationally and internationally, efficiently and effectively.

On behalf of Kasetsart University, I would like to congratulate and thank everyone who participated in presenting research and applied research outcomes, and environmental knowledge. I sincerely hope that this academic conference will be successful in all aspects.



Dr. Damrong Sripraram
President of Kasetsart University

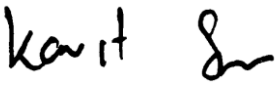
Message from the Dean of Faculty of Public Health, Burapha University

Sustainable development is a vital direction for the national development, that integrates economic growth with environmental conservation and the well-being of communities. Burapha University, by the Faculty of Public Health, has been deeply honored to co-host the 24th National Environmental Conference alongside with the 14th International Conference on Environmental Engineering, Science and Management under the theme "Green Environment and Low-Carbon Society Toward Sustainable Well-being for Humanity held on 20-21 May 2025 at the Bangsaen Heritage Hotel, Chonburi Province.

The National and International Conferences, organized by the Environmental Engineering Association of Thailand (EEAT), is an imperatively academic platform that provides opportunities for academics, researchers, experts, and practitioners from various sectors to exchange knowledge and present academic works, innovations, and experiences related to the environment in economic, social, and community dimensions, especially the concept of "Eco-industry", which is an important mechanism for changing the conventional industrial sector to be environmentally friendly ones; reducing greenhouse gas emissions, promoting the efficient and circular use of resources, in line with the Sustainable Development Goals.

On behalf of Burapha University, we would like to extend our heartfelt gratitude to the EEAT, government agencies, academic institutions, the private sector, and civil society for their invaluable support in organizing this event. We also sincerely thank the organizing committee for their efforts in producing high-quality conference materials and ensuring a professionally prepared and internationally standardized event.

It is with great pleasure that I welcome all participants and contributors who have shared their research, innovations, and practical work in the environmental field. I am confident that this conference will be a driving force for the advancement of environmental knowledge and collaboration, contributing significantly to the nation's sustainable development.



Assoc. Prof. Dr. Kowit Suwannahong
Dean, Faculty of Public Health
Burapha University

ORGANIZING COMMITTEE

CONFERENCE ADVISORS

Assoc. Prof. Dr. Suchat Leungprasert
President, Environmental Engineering Association of Thailand
Assoc. Prof. Dr. Warawut Suadee
Vice President, Environmental Engineering Association of Thailand

CHAIRS

Assoc. Prof. Dr. Wanpen Wirojanagud
Vice President, Environmental Engineering Association of Thailand
Assoc. Prof. Dr. Trakarn Prapaspongsa
Technical Committee Chairman, Environmental Engineering Association of Thailand
Prof. Dr. Wanchai Yodsudjai
Dean, Faculty of Engineering, Kasetsart University
Assoc. Prof. Dr. Watcharin Gasaluck,
President, Burapha University, Thailand
Assoc. Prof. Dr. Kowit Suwannahong,
Dean, Faculty of Public Health, Burapha University

CO-CHAIRS

Prof. Dr. Pongsak Noophan, Kasetsart University
Prof. Dr. Anamai Thetkathuek, Burapha University
Assoc. Prof. Dr. Wilasinee Yoochatchaval, Kasetsart University
Dr. Pissanu Panaracha, Environmental Engineering Association of Thailand

INTERNATIONAL PROGRAM / SCIENTIFIC COMMITTEE

Prof. Kazuei Ishii, Hokkaido University, Japan
Prof. Kang Seoktae, Korean Society of Environmental Engineers, Korea
Prof. Chih-Hsiang Liao, Chia Nan University of Pharmacy and Science, Taiwan
Prof. Chitsan Lin, National Kaohsiung University of Science and Technology, Taiwan
Assoc. Prof. Dr. Tran Duc Huy, Hanoi University of Science and Technology, Vietnam
Ts. Dr. Pramila Tamunaidu, Universiti Teknologi Malaysia, Malaysia
Dr. Bhuvaneswari Kandasamy, SRM University Delhi NCR, India
Dr. Brian James, University of London, UK
Dr. Javier Rioyo, MARE, Ctra. Torres - Reocín, Spain
Dr. Kirandeep Gill, Massachusetts General Hospital and Harvard Medical School, USA
Dr. Kumaresan Lakshmanan, Chennai Institute of Technology, India
Dr. Le Thi Tam, Hanoi University of Science and Technology, Vietnam
Dr. Manimaran Kumar, Saveetha Institute of Medical and Technical Sciences, India
Dr. Nurul Hainiza Binti Abd Razak, Processing and Sustainability Unit,
Engineering & Technology Division, Malaysia
Dr. Phimmavong Kongsy, Souphanouvong University, Lao
Dr. Priyadharsan Arumugam, Institute of Medical Science and Technology Poonamallee campus, India
Dr. Ranjith Rajendran, KSR College of Engineering, India
Dr. Sidxay Makvilay, Ministry of Natural Resources and Environment, Department of Environment, Lao
Mr. Ray Earle, Dublin City University, Ireland
Assoc. Prof. Dr. Wanpen Wirojanagud, Khon Kaen University, Thailand
Assoc. Prof. Dr. Warawut Suadee, Environmental Engineering Association of Thailand, Thailand
Assoc. Prof. Dr. Trakarn Prapaspongsa, Mahidol University, Thailand
Assoc. Prof. Dr. Torpong Kreetachat, University of Phayao, Thailand
Assoc. Prof. Dr. Dondej Tungtakanpoung, Naresuan University, Thailand
Assoc. Prof. Dr. Thammasak Rojviroon, Rajamangala University of Technology Thanyaburi, Thailand
Assoc. Prof. Dr. Kowit Suwannahong, Burapha University, Thailand
Asst. Prof. Dr. Sarun Tejasen, Chulalongkorn University, Thailand
Asst. Prof. Dr. Samonporn Suttibak, Kasetsart University,
Chalermphrakiat Sakon Nakhon Province Campus
Asst. Prof. Dr. Surachai Wongcharee, Faculty of Engineering, Mahasarakham University, Thailand
Dr. Pitsanu Pannaracha, Ramkhamhaeng University, Thailand
Mr. Preeda Vatchratiensakul, Water and Environment Institute for Sustainability,
The Federation of Thai Industries, Thailand

PROCEEDING SUPPORTING STAFFS

Panida Insutha
Suwanna Polyam

Editorial Remark

Environmental Engineering Association of Thailand (EEAT) in collaboration with the Faculty of Engineering, Kasetsart University, Faculty of Public Health, Burapha University as well as Ministry of Higher Education, Science, Research and Innovation, Ministry of Energy, Pollution Control Department, Department of Climate Change and Environment, Department of Local Administration, Office of Natural Resources and Environmental Policy and Planning, Center for Clean Air Solutions, Thai Health Promotion Foundation, National Research Council of Thailand (NRCT), Industrial Estate Authority of Thailand, Ministry of Natural Resources and Environment have very great preference to organize the 24th national conference and the 14th international conference on 20-21 May 2025. The objective of the conference is to be the platform for knowledge management of academia, researchers, experts and interesting people on environmental engineering, science, and management subjects. The academic knowledge derived from the conference would be advantageous to not only the national but also international society for solution of environmental problems encountered since the past up to present.

Regarding the conference document, abstracts and full papers had been considered for presentation and publication through the reviewing process of the experts and editorial team ensuing the national and international standards. The abstracts and full papers were compiled in the proceeding and in the electronic file, respectively. In addition, the conference papers will be selected for publication of the EEAT journal if the papers are knowledgeably appropriate.

On behalf of the editorial team, we would like to express our appreciation to the researchers, academia and experts for preparing abstract, full papers and oral/poster presentation, as well as other interested people for participation to this conference. Moreover, we also would like to specify our acknowledgment to the experts and organizing committee to the productive collaboration for reviewing abstracts/papers, providing considerate comments and recommendations to the authors, and undertaking the completeness of conference document. It is also thankful to the participants, organizing committee who support the conference coming to successfully accomplish our mission.

Editorial Team:
Suchat Leungprasert
Wanpen Wirojanagud
Trakarn Prapaspongsa
Pongsak Noophan
Wilasinee Yoochatchaval
Kowit Suwannahong
Anamai Thetkathuek
Pitsanu Pannaracha

CONTENTS

		Page
20R3-01	Greenhouse Gases Emission Inventory and Investigation of Local Emission Factors: A Case Study of Wastewater Treatment Facility in Thailand Chawakorn Sanusan and Win Trivitayanurak	1
20R3-02	A Study of Characteristics, Origins, and Fates of Ultrafine Particles Over Taichung City, Taiwan Kijpat Thavorn, Win Trivitayanurak and Ta-Chih Hsiao	7
20R3-03	Physical and Chemical Characteristics of Fine and Ultrafine Particulate Matters in Southern Thailand Chanakan Bunyarit, Racha Dejchanchaiwong, Perapong Tekasakul, Nobchonnee Nim, Aree Choodum, Thanita Areerob, Bussakorn Kleangklao, Saysunee Jumrat, Yutthapong Pianroj and Benjalak Boonpeng	13
20R3-04	Examination of Ambient $PM_{2.5}$ Exceedances in Bangkok: Frequency, Duration, and Background Concentration Chaiwat Wilasang, Kasemsan Manomaiphiboon, Jindarat Pariyothon, Natchanok Pala-En and Nishit Aman	19
20R3-05	Evaluating GHG Emissions in 3D Printed House Using a Life Cycle Assessment Hein Htet Zaw and Achariya Suriyawong	26
20R3-06	The Relationship between The PM2.5 Concentrations Correlated with The Meteorological Data Recorded from The Super King Air 350 Aircraft: The Case Study Covers from January 27 to February 7, 2025 Aniruj Akkarapongtrakul, Thanakorn Serisakulthorn, Phayuhaphon Chitcharoen, Warit Planthong, Chanti Detyothin, Marut Ratmanee, Paweena Wessapak, Sirirat Sula, Chaiyaphorn Nilarat, Chadayu Nooddaeng, Anuphong Soksai, Sivarot Putponpai and Thanakrit Wongta	34
20R3-07	Variation of Black Carbon in PM_1 and Its Health Risk Assessment at Low and High-Rise Buildings Nipaporn Auttanate, Nattakit Jintauschariya, Samita kladin, Parkpoom Choomanee, Surat Bualert and Thunyapat Thongyen	43
20R3-08	Chemical Composition of Secondary Organic Aerosol in $PM_{2.5}$ Supannika Salao, Surat Bualert, Parkpoom Choomanee and Thunyapat Thongyen	49
20R3-09	The Impact of Free Public Transit Measures on Urban Traffic and $PM_{2.5}$ Emissions: A Case Study in Thailand Yossakorn Fungkeit, Surat Bualert, Parkpoom Choomanee, Thunyapat Thongyen and Kodchakun Phuangsri	53
20R3-10	Carbon Footprint for Organization: Case Study of Printing and Packaging Factory in Thailand Atchara Pasavanung, Supawadee Polprasert, Withida Patthanaissaranukool and Thanakrit Neamhom	61

20R3-11	Effects of Carbon Capture and Storage (CCS) on Quartz Rock and Groundwater: The case study of Thailand Chanita Sirisaksathaporn, Supreeda Homklin, Sukhuma Chitapornpan, Chatkaew Chailuecha, Pimluck Kijjanapanich, Sulak Sumitsawan, Prattakorn Sittisom, Pharkphum Rakruam, Napat Jakrawatana, Patiroop Pholchan, Sarunnoud Phuphisith, Ekbordin Winijkul and Wanawan Pragot	68
20R3-13	Carbon Footprint for Organization and Reduction of Greenhouse Gas Emission for Faculty of Engineering, Khon Kaen University Krorawan Pankrathoke, Artittayaporn Bunma, Kitirote Wantala and Visanu Tanboonchuy	76
20R3-14	Application of Convective Available Potential Energy (CAPE) for Appropriate Condition on Rain Enhancement in Thailand Ying Li, Parkpoom Choomaneea, Thunyapat Thongyenb and Surat Bualert	80
20R3-15	Carbon Footprint Assessment of Thai Cuisine: Curry and Rice Menus Kanokporn Aree, Santi Phithakkitnukoon, Karn Patanukhom and Sarunnoud Phuphisith	84
20R3-16	Life Cycle Assessment of Drilling Waste Treatment: Comparative Study of Thermal Desorption and Solvent Extraction Bovathanak Leng, Thaksina Poyai, Ratchanan Chamnanmor, Saret Bun and Pisut Painmanakul	89
20R3-18	Rice Waste-based Circular Economy for Green Building Material Products Tanita Cheevaphantusri, Rattanawan Mungkung, Shabbir Gheewala and Napat Jakrawatana	96
20R3-19	Development of Biochar Immobilized Bacteria for Degrading PLA/PBAT/ Starch Bioplastic Luthfia Dwi Rachmani, Christian Adi Pratama and Ekawan Luepromchai	101
20R4-01	Influence of Carbon Nanotube on Physical and Mechanical Properties of Vetiver Root Fiber-Reinforced Bioplastic Composites Pongsathorn Kongkeaw, Peerawit Pasangtiyo, Pichapa Lumpai and Onkanya Panjumlong	108
20R4-03	Investment Analysis of a Circular Economy-based Shopping Mall–Community Food Waste Management Initiative: Financial and Sustainability Perspectives Pawin Sirisinha, Teenan Pisisakulwong, Natthanicha Tayanaraporn, Prasert Akkharaprathomphong and Pisut Painmanakul	116
20R4-05	Life Cycle Assessment of Cellulose Nanofibers Production from Sugarcane Residues Shwe Yie Lin and Trakarn Prapaspongsa	124
20R4-06	Evaluating the Potential of Water Sources in Thailand for Hydrogen Production via Water Electrolysis Sakunthip Hansungnoen, Ekkaphong Chomwong, Ploypailin Romphophak, Prajak Sastaravet, Pattarasiri Fagkaew and Pisut Painmanakul	132
20R4-08	Multi-Factor Analysis of Oil Spill Vulnerability: Integrating Environmental, Socioeconomic, and Policy Perspectives Sataporn Jaisomkom, Saowanee Wijitkosum and Somrudee Meprasert Jitpraphai	139

20R4-09	The variability in soil community and its enzymatic function to plant promotion after biochar addition Mujalin Pholchan, Jearanai Thassana and Khajitmanee Muangprom	148
20R4-10	Promoting Sustainable Waste Management in Coffee Shops: A Case Study of Chiang Mai Phimlapat Jenjai and Sarunnoud Phuphisith	156
20R4-11	Performance of Low-Temperature Thermal Desorption on Drilling Waste Treatment and Recovery Sotheara Huor, Thaksina Poyai, Ratchanan Chamnanmor, Saret Bun and Pisut Painmanakul	162
20R4-12	Study of Food Waste Composition and Generation from Campus Food Vendors: A Case Study of Chiang Mai University Chadaporn Sriwichai, Santi Phithakkitnukoon, Karn Patanukhom and Sarunnoud Phuphisith	170
20R4-13	Dual Effects of Starter Inoculum and Thermal Pretreatment on Oil Palm Mesocarp Fiber for Methane Production in Solid-State Anaerobic Digestion Saengmany Phommakod, Eko Heryadi, Chongkon Poonthawee and Pawinee Chaiprasert	175
20R4-16	The Role of Street Trees in Mitigating Particulate Matter Pollution: A Case Study of PM2.5 and PM10 Concentrations in Urban Street Canyon Pasita Ngowpradit, Wanarat Konisranukul and Yaowatat Boongla	184
20R4-17	Assessment of the Reduction of Greenhouse Gas Emissions from Solid Waste Management for a Large Community Nitaya Kosa, Supatpong Mattaraj, Karnika Ratanapongleka, Wipada Dechapanya, Tiammanee Rattanawerapan Adun Janyalertadun and Sompop Sanongraj	193
20R4-18	People's Perception and Water Consumption Behavior in High Fluoride Risk Area Patcharaporn Somkiattiyot, Aunnop Wongrueng and Sarunnoud Phuphisith	199
20R4-19	Quantifying ESG Impacts on Stock Performance: Evidence from the Thai SET100 Phonthakorn Phreuksa, Warach Saiwilai, Varith Wichienchai, Matnithit Chariyasethapong, Chaidit Sittisunthornwat, Pisut Painmanakul and Vasathon Wongwanich	205
20R5-01	Evaluation of Moving Bed Biofilm Reactor (MBBR) Performance in Treating Weak Domestic Wastewater for Reuse in Agriculture Tongchai Sriwiriyarat and Chanyut Kalakan	213
20R5-02	Application of Corn Straw Biochar for Removal of Heavy Metals from Gold Mining Wastewater Por Yang, Pharkphum Rakruam, Sulak Sumitsawan, Patiroop Pholchan and Pimluck Kijjanapanich	221
20R5-03	Evaluation of Aluminium Fumarate Metal-Organic Framework for Defluoridation of High-Fluoride Contaminated Water Wiratchon Srisom, Sarunnoud Phuphisith, Phacharapol Induvesa, Chalita Ratanatawanate and Aunnop Wongrueng	226

20R5-04	Application of Submerged Nanofiltration Membrane for Treating Natural Organic Matter from Reservoir Water Chamaiporn Nantakham, Takahiro Fujioka, Aunnop Wongrueng and Prattakorn Sittisom	233
20R5-05	Surface Modification of Corn Biochar for Enhancement of Fluoride Adsorption Natthapon Muangmaya, Aunnop Wongrueng and Prattakorn Sittisom	239
20R5-06	Impact of Microplastics on Membrane Fouling for Dissolved Organic Matter Removal from Reservoir Water Thanyapon Kaewjan, Aunnop Wongrueng, Takahiro Fujioka, Prattakorn Sittisom and Pharkphum Rakruam	244
20R5-07	Natural Organic Matter Removal from Ang Kaew Reservoir by using Activated Carbon Natchaya Waisarikam and Pharkphum Rakruam	249
20R5-09	Reduction of Natural Organic Matter and Their Trihalomethane Formation Potential by Alum-coagulation process Suphitcha Tankaew and Pharkphum Rakrum	256
20R5-10	The Removal of Oil Contamination in Water Using Iron Oxide Nanomaterial Artittayaporn Bunma and Visanu Tanboonchuy	261
20R5-11	Decolorization of Dye Wastewater Using Photocatalytic Process Assisted with Titanium-Magnetite Chitosan Beads (TMCB) Nuttaya Pengmuangmool, Soraya Komkiang and Natthapong Proysurin	267
20R5-12	Photocatalytic Degradation of Caffeine in Water using Titanium Dioxide-Coated Materials Warisara Pissadarn, Patiya Kemacheevakul and Surawut Chuangchote	274
20R5-13	Preliminary Study of Benzalkonium Chloride on Growth Rate and Phosphorus Removal Capacity of *Chlorella vulgaris* in Effluent Wastewater Vicheka Chhoeurn and Thunyalux Ratpukdi	280
20R5-14	Treatment of campus wastewater and biomass production using wastewater treatment pond with duckweed Kittin Ruengpattanawiwat, Chart Chiemchaisri, Wilai Chiemchaisri, Tadashi Toyama, Kazuhiro Mori and Masaaki Morikawa	285
20R5-15	Development of Modified Bio-Char From Coconut Husk Base Material Used for Nutrient Removals Shoaib Salman, Nawatch Surinkul, Trakarn Prapaspongsa, Kritsanat Surakit and Sri Shalini Sathyanarayanan	291
20R5-17	Effect of Turbidity on Chlorine Dosage for Algae Removal in Synthetic Raw Water Sokunthea Khim and On-anong Larpparisudthi	300
20R5-18	The Effect of Colloidal Silica Particle on Microfiltration Fouling Gechhor Chea, Chotikoon Bunditboondee and Jenyuk Lohwacharin	305
20R5-19	Enhancing Sustainability in Rice Straw Pulp Production: A Zero Discharge Model Through Biological Treatment and Water Recycling Tiammanee Rattanaweerapan, Supatpong Mattaraj, Wipada Dechapanya, Sompop Sanongraj and Karnika Ratanapongleka	312

20R6-03	Wastewater Treatment Efficiency of Electrocoagulation in the Compressor Industry Ampaporn Jaidee, Chulalak Singharat, Sawarin Suejai, Sakkarin Lajoy and Kowit Suwannahong	318
20R6-04	Composited Mesoporous Biochar Via Slow Pyrolysis Process Prepared from Woods and Plastics Waste as The Raw Precursors Poramed Aungthitipan, Sukanya Hongthong, Pitsanu Pannaracha, Supawan Khantotong and Surachai Wongcharee	326
20R6-05	Application and Characterization of Bone Char Prepared Via Slow Pyrolysis Process and Its Used for Heavy Metal Removal Pornmongkol Tansomros, Janjira Triped, Pitsanu Pannarach, Pathanin Sangaroonand, Chuleeratana Promloa and Surachai Wongcharee	335
20R6-06	Developing Oxygenated Functional Group-Doped Hydrochar from Spent Coffee Grounds via Ultrasonication as a Magnetic Adsorbent for Oily Wastewater Treatment Myint Myat Thuzar, Nattapong Tuntiwiwattanapun and Nurak Grisdanurak	344
20R6-13	Conditional Optimization for Treatment of Wastewater from Ethanal Production Process Using Ozonation Wipada Dechapanya, Nongkran Koonwong, Sompop Sanongraj, Supatpong Mattaraj, Karnika Ratanapongleka and Tiammanee Rattanawerapan	351
20R6-14	Carbon Dioxide Adsorption Efficiency of Pig Bone from Food Waste by the Pyrolysis Process Khemanat Phatrabuddha, Waewprach Tweepharnichkul, Sataporn Kanoksikarin, Montian Songsiam and Kowit Suwannahong	359
21R4-01	Enhancing the Value of Air Filtration Media Fabricated from Natural Waste Materials Jasmin Mayi, Wasna Ngulee, Wikanda Thongnueakhaeng, Peerapol Kaoien, Nantaporn Noosai, Vineeth Vijayan and Supandee Maneelok	364
21R4-02	Long-Term Analysis of PM2.5 Concentrations and Seasonal Variation in Bangkok and Chiang Mai, Thailand: Impacts of COVID-19 Lockdowns and Fire Control Measures Vineeth Vijayan, Supandee Maneelok and Nantaporn Noosai	372
21R4-03	Genotypic and Phenotypic Characterization of ESBL-Producing *E. coli* from Livestock Wastewater and Manure Phub Zam, Thitima Srathongneam, Phongsawat Paisantham, Montakarn Sresung, Supitchaya Theplhar, Nisanart Charoenlap, Paiboon Vattanaviboon, Skorn Mongkolsuk and Kwanrawee Sirikanchana	380
21R4-04	Optimization of batch electrocoagulation process with Al-Fe electrodes in TDS removal using Box-Behnken design for hospital wastewater Suchira Thongson, Raweeporn Pomthong, Suthida Theepharaksapan, Yanika Lerkmahalikit, Khanit Matra and Sirilak Prasertkulsak	386
21R4-05	Analysis of Spatial Distribution Patterns of Non-Communicable Diseases and Risk Factors with GIS in Central Regions of Thailand May Myat Myat Aung, Kritsanat Surakit, Nawatch Surinkul and Romanee Thongdara	394

21R4-06	Assessing Knowledge, Attitudes, and Practices Regarding PM2.5 Among Students at Chulalongkorn University: Implications for Public Health Policy and Education Sophara Chhim, Thammanitchpol Denpetkul and Achariya Suriyawong	402
21R4-07	Treatment of Fishery Wastewater Using a Floating Treatment Wetland Planted with Umbrella Sedge Parichat Supasee, Supreeda Homklin, Satawat Tanarat, Anusorn Boonpoke and Somanat Somprasert	410
21R4-08	Heavy Metals in Fishing Gears and Marine Pollution: A Comprehensive Study on Heavy Metals from Degradation of Fishing Gears, Potential Risks to Marine Environment Khine Yin Nyein, Yotwadee Hawangchu and Dao Janjaroen	416
21R4-09	Upcycling Aluminum Dross into Magnetic Gamma Alumina Adsorbent Thae Su Su Hninn and Vorapot Kannokantapong	424
21R5-01	Plastic Waste Monitoring Via Plastic Product Brand Audit from Marine Debris in Bang Tao Bay, Phuket, Thailand Sineenart Puangmanee and Phaothep Cherdsukjai	432
21R5-02	Effects of Pyrolysis Temperature and Chemical Activation on Characteristics and Yields of Biochar Produced from Coconut Husk Biomass Leangse Meng, Thaksina Poyai, Ratchanan Chamnanmor, Saret Bun and Pisut Painmanakul	438
21R5-03	The Optimal Conditions for Enhancing High Heating Value of Rubberwood Briquettes from Sawdust Residues via Torrefaction Process Sutthipat Khamwichit, Surathai Khamwichit, Weerapol Lapkoed, Nattaya Jaibun, Nattawat Panthong and Wipawee Dechapanya	445
21R5-04	Study of Effecting Factors for Formalin Removal Efficiency in Lab Gross using the Biochar Air Pollution Treatment Unit Surathai Khamwichit, Sutthipat Khamwichit, Arisa Arwaehama, Nareekan Dokket and Wipawee Dechapanya	453
20P-15	Determination of Mechanical, Physical and Microstructural Properties of Hemp Fibers added with Polyacetic Acid Bio Composites Pongsathorn Kongkeaw, Thanin Rudchapo and Apisit Khetcharioen	461
20P-16	Fume Exposure During Arc Welding Practices among Vocational Students: A Case Study Phongsakorn Kumpeera, Pornthip Yenjai and Pongsit Boonruksa	467
20P-18	The Awareness of Residents Regarding Influence on Water Quality in the Local Environment Momone Kanno, Sarunnoud Phuphisith, Yurina Otaki and Masahiro Otaki	473

20R3-01

Greenhouse Gases Emission Inventory and Investigation of Local Emission Factors: A Case Study of Wastewater Treatment Facility in Thailand

Chawakorn Sanusan[1*] and Win Trivitayanurak[1,2]

[1]*Departnment of Environmental and Sustainable Engineering, Faculty of Engineering, Chulalongkorn University, Bangkok 10330, Thailand*
[2]*Professor Aroon Sorathesn, Center of Excellence in Environmental Engineering, Chulalongkorn University, Bangkok 10330, Thailand*
[*]*Phone : (+66)81-069-9009, E-mail : 6572013721@student.chula.ac.th*

ABSTRACT

This study investigates greenhouse gas (GHG) emissions from a wastewater treatment plant (WWTP) in Pattaya, Thailand, with the objective of developing localized emission factors (EFs) for methane (CH_4), nitrous oxide (N_2O), and carbon dioxide (CO_2). Employing both the flux chamber and direct-probe measurement methods, the research quantified emissions across key treatment components and analyzed associated wastewater parameters. Measurements were conducted over two days in September 2024, targeting five points within the activated sludge (AS) system. Results revealed the highest CO_2 emissions from the aeration tank due to aerobic microbial activity, and significant CH_4 and N_2O emissions from the sludge thickening tank linked to anaerobic conditions and nitrification, respectively. The calculated EF of CH_4 was 0.00317 $kgCH_4/kgBOD$ and for N_2O was 0.0035 $gN_2O\text{-}N/kgTKN$—both notably lower than IPCC default values, likely due to efficient treatment and low influent organic and nitrogen content. The study concludes that localized EFs provide more accurate GHG inventories and are essential for Thailand's mitigation strategies under its Nationally Determined Contributions (NDCs) roadmap.

Keywords : greenhouse gas; carbon dioxide (CO_2); methane (CH_4); nitrous oxide (N_2O); emission inventory; emission factor

INTRODUCTION

Greenhouse gases (GHGs) are the contributor of the global boiling crisis. The most significant GHGs are carbon dioxide (CO_2), methane (CH_4), and nitrous oxide (N_2O). CO_2 has been known to play a major part in the global boiling situation for thousands of years and has a very long residence duration in the atmosphere. CH_4 is a short-lived climate pollutant (SLCP) that has had a powerful warming impact approximately 80 times stronger than CO_2 in the 20-year GWP estimate and has a GWP of about 30 over a 100-year peroid. N_2O is a GHG increasingly contributing to global warming. Despite the average N_2O concentration in the atmosphere being around 330 parts per billion (ppb), the IPCC's Sixth Assessment Report (AR6) in 2021 highlighted that N_2O has a significant GWP of 270 for a 100-year time horizon. All these GHGs have been increasing rapidly in the global atmosphere, crucially from the anthropogenic source such as waste and wastewater sector [1].

To address this pressing issue, Thailand has pledged to the Nationally Determined Contributions (NDCs) and published the Thailand's Nationally Determined Contribution Roadmap to Mitigation 2021 – 2030, aimed at reducing 20% (111 $MtCO_2eq$) to 25% of GHG emissions in Thailand. Hence, the Department of Climate Change and Environment (DCCE) of Thailand in cooperation with the Department of Environmental and Sustainable Engineering, Chulalongkorn University aimed to estimate local emission factors (EFs) from wastewater treatment facility to produce a guideline for preparing GHG inventories for community wastewater treatment systems effectively. This study aims to enable organizations to apply these EFs to assess GHG emissions in waste sector. For aerobic wastewater treatment system, various steps may promote anaerobic activity, including primary sedimentation tank and sludge thickening tank. Thousands of journal articles from 1990s – 2020s have reported the concentrations of GHGs especially CH_4 emitted by wastewater treatment plant (WWTP) [2], but not for Thailand yet. Additionally, the study published in 2023 mentioned that CH_4 emissions from the US domestic WWTPs are greater than the current US EPA inventory [3]. Thus there exists a gap in quantifying GHGs from WWTP in Thailand context [4].

For this reason, this research funded under the project of the DCCE titled "Development of greenhouse gas measurement from municipal wastewater treatment system" leads to investigating the GHG emission inventory, calculating the EF, and exploring the GHG mitigation strategy from the activated sludge (AS) wastewater treatment plant using the flux chamber method and the direct-probe measurement method, together with qualitative wastewater data.

METHODOLOGY

Site selection

The chosen study site is the Pattaya WWTP in Chonburi province, Thailand. The plant has a capacity of approx. 65,000 m^3/d. The treatment system is AS with components including an equalization tank, 4 primary sedimentation tanks (approx. 3,700 m^3 per tank), 2 aeration tanks (approx. 4,200 m^3 per tank), 2 final sedimentation tanks (approx. 1,800 m^3 per tank), 2 sludge thickening tanks (approx. 2,820 cm^3 per tank), 4 sludge dewatering machines, and a chlorination pond. The points of measurement are selected as the primary settler, the aeration tank, the final settler, the sludge thickening tank, and the sludge dewatering machine.

Instrumentation

This research utilized a flux chamber, a portable FTIR gas analyzer, a diffusion dryer, a partial difference pressure device, and a flow meter connected via silicone tubing. The flux chamber (Figure 1) is made by polycarbonate (PC) with 40 cm diameter circle area across the flux measurement surface. The employed portable FTIR gas analyzer is the Gasmet GT5000 Terra. Measurements in this study complied with published flux chamber technique and direct-probe measurement technique. The measurement campaign took place on 20 – 21 September 2024, during the mid-day and evening periods.



Figure 1 The flux chamber

The conceptual measurement design on wastewater surface is shown in Figure 2. Moreover, the conceptual measurement design at the sludge thickening tank is represented in Figure 3. For the wastewater grab sampling, the study collected wastewater samples from 4 measurement points including the equalization tank, the center of aeration tank, the chlorination pond, and the sedimentation basin of sludge system. The analyzed wastewater parameters included pH, temperature, BOD_5, COD, TAN, TKN, NO_2^-, NO_3^{2-}, TN, MLSS, MLVSS, and TSS.

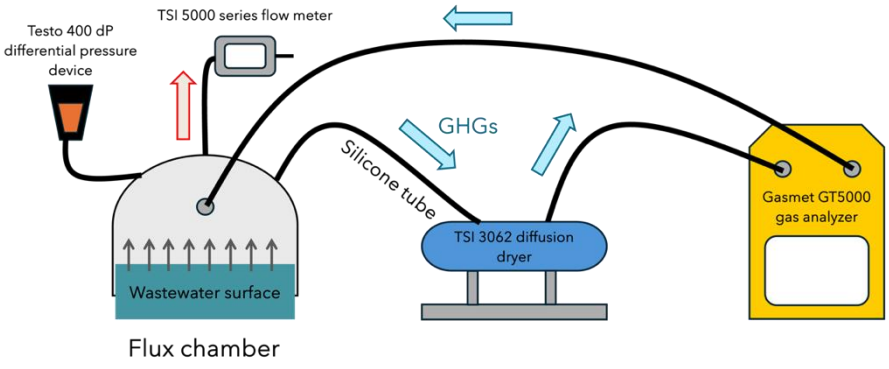


Figure 2 Conceptual design on the wastewater surface

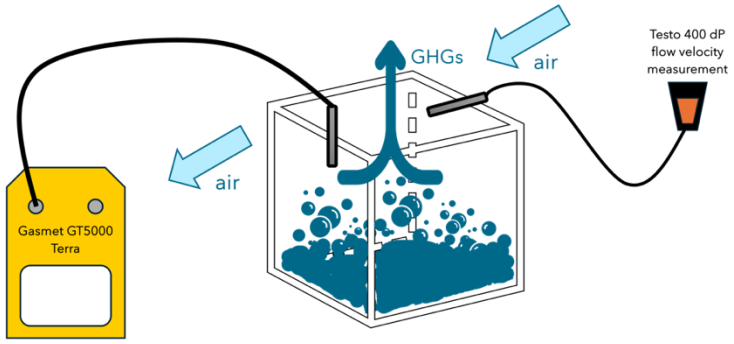


Figure 3 Conceptual design at the sludge thickening tank

Points of measurement

The diagram of the system boundary is represented by Figure 4 that is the quantification points of the GHG emissions from Pattaya wastewater treatment plant and the points of wastewater grab sampling in this study.

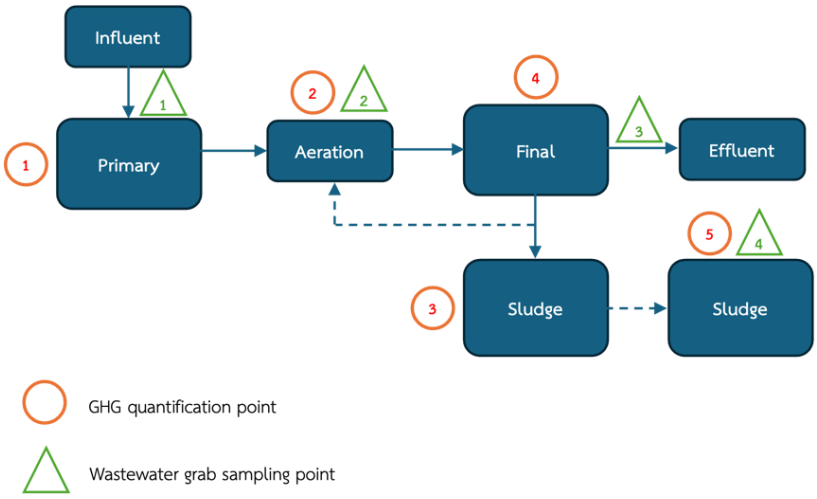


Figure 4 System boundary of GHG emissions from WWTP

Calculation

To calculate GHG emission rate, the GHG data measured as mixing ratios is converted into mass concentration units. Firstly, unit conversion is calculated using the pressure and temperature data under the ideal gas law, as shown in Equation (1).

$$C = \frac{n}{V} = \frac{P \times MW}{R \times T}$$

Where C is GHG concentration in grams per liter (g/L). P is the absolute pressure of a gas in atm, V is the volume it occupies in liter (L), n is the number of atoms and molecules in the gas in mol, and T is its absolute temperature in kelvin (K). Finally, R is the boltzmann constant (universal gas constant) and has the value R equals to 0.082057 L atm K^{-1} mol^{-1}.

After that, the emission flux was calculated following the US EPA method [5], mass concentration would be converted into flux with the known air flow rate and surface area, as shown in Equation (2). Finally, emission rate is the product of the flux and the total emitting area.

$$E = \frac{Q \times C}{A} \quad (2)$$

E is the emission flux of component, in unit of micrograms per square meter-minute (μg/m^2-min). Q is the flow rate of air, in unit of cubic meters per minute (m_3/min). C is the mass concentration of

component, in unit of micrograms per cubic meter ($\mu g/m^3$). Lastly, A is the surface area of flux chamber, in unit of square meters (m^2).

For EF calculations, following the 2019 Intergovernmental Panel on Climate Change (IPCC) Refinement to the 2006 IPCC Guideline for National Greenhouse Gas Inventories using wastewater parameters such as influent rate, BOD, COD, and TKN together with the GHG emission values, focusing on Scope 1 evaluation, in units of $kgCH_4/kgBOD$ of CH_4 and $gN_2O/kgTKN$ of N_2O. The EF of CO_2 was assessed by considering the total annual CO_2 emissions from the treatment system and the influent flow rate. Additionally, the Scope 2 evaluation of GHG emissions from electricity consumption within the WWTP was conducted by multiplying the total electricity usage by the EF of electricity generation in Thailand.

RESULTS AND DISCUSSIONS

From the measurement on 20 – 21 September 2024, during the mid-day and evening periods. Table 1 represents the summary of average GHG concentration analysis from WWTP in miligrams per liter of air (mg/L).

Table 1 The summary of average GHG concentration analysis from WWTP

GHG (mg/L)	Date(*) and period		Primary sed. tank	Aeration tank Near inlet	Aeration tank Midway	Final sed. tank	Sludge thickening tank	Sludge dewatering area
CO_2	1	Mid-day	2.07 ±0.07	22.67 ±4.36	24.62 ±0.69	3.61 ±0.13	1.46 ±0.2	3.44 ±0.002
		Evening	2.91 ±0.19	18.89 ±4.79	13.79 ±2.98	4.63 ±0.22	0.91 ±0.17	0.81 ±0.06
	2	Mid-day	3.94 ±0.16	26.86 ±5.95	25.72 ±0.48	5.59 ±0.52	4.39 ±0.77	0.74 ±0.23
		Evening	2.06 ±0.03	17.64 ±5.12	**	4.69 ±1.64	1.04 ±0.24	**
CH_4	1	Mid-day	0.594 ±0.064	0.086 ±0.084	0.091 ±0.011	0.005 ±0.000	0.080 ±0.012	0.005 ±0.000
		Evening	1.703 ±0.555	0.092 ±0.094	0.089 ±0.033	0.017 ±0.006	0.036 ±0.119	0.002 ±0.000
	2	Mid-day	1.605 ±0.594	0.078 ±0.093	0.101 ±0.003	0.010 ±0.004	0.130 ±0.120	0.002 ±0.058
		Evening	0.383 ±0.032	0.079 ±0.069	**	0.025 ±0.001	0.071 ±0.019	**
N_2O	1	Mid-day	0.00053 ±0.00002	0.00276 ±0.00046	0.00371 ±0.00029	0.00074 ±0.00003	0.00051 ±0.00002	0.00069 ±0.00001
		Evening	0.00060 ±0.00017	0.00340 ±0.00074	0.00180 ±0.00019	0.00082 ±0.00003	0.00036 ±0.00003	0.00040 ±0.00001
	2	Mid-day	0.00066 ±0.00003	0.00389 ±0.00069	0.00355 ±0.00006	0.00068 ±0.00008	0.00033 ±0.00001	0.00028 ±0.00004
		Evening	0.00047 ±0.00003	0.00256 ±0.00078	**	0.00092 ±0.00031	0.00037 ±0.00004	**

* is date of measurement: 1 is 20 September 2024 and 2 is 21 September 2024
** is N/A because of instrument mulfunction and severe whether

The averaged observed concentrations can be highlighted for different emitting points in the WWTP. The highest CO_2 concentration was observed at the aeration tank, reaching 21.51 mg/L near the inlet and 21.38 mg/L midway towards the outlet. This concentration was attributed to the aerobic process carried out by heterotrophic bacteria. Conversely, the sludge thickening tank exhibited a high CH_4 concentration of 0.074 mg/L, while the primary sedimentation tank had a concentration of 1.07 mg/L. These high concentrations were primarily due to the anaerobic process, particularly in the lower regions of the tanks where oxygen and aeration systems are lacking. Furthermore, CH_4 could be released from dissolved CH_4 within wastewater. N_2O concentration was notable at aeration tank (0.0031 mg/L near inlet and 0.0030 mg/L midway toward outlet), the concentration was primarily attributed to nitrification, with a smaller contribution from denitrification that probably was occurred

from sediment at the bottom of tank. The GHG flux measurement results indicated that CO_2, CH_4, and N_2O emission fluxes were highest at the sludge thickening tank, averaging 11,651.27, 441.87, and 2.34 mg/min/m^2, respectively.

Table 2 presents the average GHG emission flux of CO_2, CH_4, and N_2O, with the highest values observed at the sludge thickening tank.

Table 2 The average GHG emission flux on 20 – 21 September 2024

GHGs (mg/min/m^2)	Primary sedimentation tank	Aeration tank	Final sedimentation tank	Sludge thickening tank	Sludge dewatering tank
CO_2	1.31	1.71	1.69	11,700	9.98
CH_4	0.5115	0.0065	0.0073	475.5	0.018
N_2O	0.00027	0.00025	0.00024	2.355	0.00274

From the GHG emission evaluation, the total GHG emission from biochemical processes in wastewater is represented in Table 3. The EF of CH_4 within the AS system from Pattaya WWTP is equal to 0.00317 $kgCH_4$/kgBOD, 4.77 time smaller than the default EF (scope 1) provided by the 2019 IPCC which has value of 0.018 kgCH4/kgBOD due to their low BOD influent and slightly high treatment efficiency that contribute to low CH_4 emissions. While the EF of N_2O is equal to 0.0035 gN_2O-N/kgTKN, extremely smaller than the default 2019 IPCC EF value which was 16 ± 0.012 gN_2O-N/kgTKN. This can be explained by the fact mostly nitrogen and ammonia were oxidized into NO_3^-, and some were collected by bacteria, contributing to small N_2O emissions.

Table 3 Total GHG emission from WWTP on 20 – 21 September 2024

GHGs	Total emission (kg/y)	Total emission ($kgCO_2eq/y$)
CO_2	8,762.25	8,762.25
CH_4	1,087.87	30,460.36
N_2O	1.58	418.7

From these results, it can be concluded that the influent and effluent characteristics (Table 4), particularly those related to GHG emissions especially BOD, significantly influenced the EF of CH_4 which is average BOD (in the influent) was 28.9 mg/L, a low value, and the average BOD removal efficiency is 88.06%, so it results in small amount of CH_4 emissions from the plant. Furthermore, the low average TN of the influent and effluent were 28.6 and 21.4 mg/L, respectively, and high ammonia (in the effluent) and NO_3^- (in the effluent) indicated that mostly ammonia and nitrogen were turned into NO_3^-, rather than N_2O, which consequently impact on the EF of N_2O.

Table 4 Average results of wastewater characteristics from WWTP on 20 – 21 September 2024

Parameter	Influent	Effluent
BOD_5 (mg/L)	28.9	3.45
TAN (mg/L)	15.9	< 0.05
TKN (mg/L)	20.8	2.09
NO_3^{2-} (mg/L)	7.77	19.3
TN (mg/L)	28.6	21.4
Q (m^3/d)	58,923	

However, future study should measure in other AS system plants to obtain more representative data and make it more widely applicable in Thailand. The limitations of this study, including the confined and restricted working area. The points of measurement are not representative of the entire tank, particularly the primary sedimentation tank, final sedimentation tank, and aeration tank. The campaign had a high cost of measurement due to the necessity of renting a portable FITR gas analyzer. The campaign was also conducted during the rainy

season, which could have affected the measured values due to rain and ambient temperature, potentially introducing bias.

CONCLUSION

The primary sources of GHG emissions, including CO_2, CH_4, and N_2O, were primarily emanating from the primary sedimentation tank, aeration tank, and sludge thickening tank. Following this study, the EF of CH_4 and N_2O within the AS WWTP exhibited lower values than the default value prescribed by the IPCC.

This study is the first step in the investigation of GHG inventory for WWTP in Thailand. Further data collection from more WWTPs will contribute to Thailand's local EF (Tier 3), which will ultimately benefit the country's GHG emission mitigation strategy.

ACKNOWLEDGEMENT

This research was supported by the Department of Climate Change and Environment (DCCE). Firstly, I extend my sincere gratitude to my advisor. Dr. Win Trivitayanurak, for their valuable guidance, encouragement, and insightful feedback, which played a crucial role in shaping this work. I would like to express our sincere gratitude to Dr. Orathai Chavalparit and Dr. Jenyuk Lohwacharin for the guidance and support throughout every stage of the project. Additionally, I would like to sincere gratitude to Dr. Chaiyaporn Puprasert for valuable advisement. Additionally, I would also like to thank my partner, brother, family, and friends, whose support and motivation helped me stay focused and committed.

REFERENCE

[1] Intergovernmental Panel on Climate, C. (2023). Climate Change 2021 – The Physical Science Basis: Working Group I Contribution to the Sixth Assessment Report of the Intergovernmental Panel on Climate Change. Cambridge University Press.

[2] Song, C., Zhu, J. J., Willis, J. L., Moore, D. P., Zondlo, M. A., & Ren, Z. J. (2023). Methane Emissions from Municipal Wastewater Collection and Treatment Systems. Environ Sci Technol, 57(6), 2248-2261.

[3] Moore, D. P., Li, N. P., Wendt, L. P., Castaneda, S. R., Falinski, M. M., Zhu, J. J., Song, C., Ren, Z. J., & Zondlo, M. A. (2023). Underestimation of Sector-Wide Methane Emissions from United States Wastewater Treatment. Environ Sci Technol, 57(10), 4082-4090.

[4] Gonzalez, D., Colon, J., Sanchez, A., Gabriel, D. (2022). Multipoint characterization of the emission of odour, volatile organic compounds and greenhouse gases from a full-scale membrane-based municipal WWTP. J Environ Manage, 313, 115002.

[5] USEPA. (1993). Emission Isolation Flux Chamber Sampling.

A Study of Characteristics, Origins, and Fates of Ultrafine Particles Over Taichung City, Taiwan

Kijpat Thavorn[1] Win Trivitayanurak[2] Ta-Chih Hsiao[3]

[1]Graduate Student, Department of Environmental and Sustainable Engineering, Chulalongkorn University, Bangkok 10330, Thailand
[2]Environmental engineering lecturer & Air modeler, Department of Environmental and Sustainable Engineering, Chulalongkorn University
[3]Professor, Graduate Institute of Environmental Engineering, National Taiwan University
Tel : 0982529445, e-mail : kjdome09@gmail.com

ABSTRACT

Ultrafine particles (UFPs), defined as particles smaller than 0.1 μm, pose serious health risks due to their ability to penetrate deep into the respiratory system and bloodstream. However, limited understanding of their emissions, formation, and evolution challenges effective regulation and monitoring. This study investigates the characteristics, origins, and fates of UFPs over Taichung City, Taiwan, using a combination of observational data and regional-scale numerical modeling.

Monitoring data were collected from Tunghai Station in Taichung during April 2021, including particle number size distributions (11–593.5 nm), sulfuric acid concentrations, meteorological parameters, and $PM_{2.5}$ levels. Simulations were conducted using the GEOS-Chem-TOMAS model with GEOS-FP meteorological inputs at 0.25° × 0.3125° resolution. The model includes sectional aerosol microphysics spanning 15 size bins from 2 nm to 2 μm. Four nucleation schemes—binary, ternary, and ion-mediated pathways—were tested to evaluate the sensitivity of new particle formation (NPF) processes.

Spatial analysis revealed elevated UFP concentrations in northeastern Taiwan, influenced by monsoonal winds and inland advection. Time-series comparisons with Scanning Mobility Particle Sizer (SMPS) observations in Taichung showed that the model broadly captured temporal patterns but substantially overestimated UFP magnitudes, with a normalized mean bias exceeding 1000%. The correlation between observed and modeled total particle number concentrations was weak ($R^2 \approx 0.03$), indicating limited skill in reproducing short-term variability. Contour plots from both model and observations showed no distinct NPF events during the study period, possibly due to unfavorable atmospheric conditions or detection limitations.

These findings underscore the importance of refining nucleation schemes and incorporating high-resolution local data to improve model accuracy. This study advances understanding of UFP dynamics in urban environments and highlights key areas for improving air quality modeling and exposure assessments in Taiwan and similar regions.

Keywords : Ultrafine Particles, GEOS-Chem-TOMAS, Nucleation, Air Quality, Taichung, Atmospheric Modeling

INTRODUCTION

Ultrafine particles (UFPs), defined as particulate matter with diameters less than 0.1 μm, are of growing concern due to their adverse health effects. These particles can penetrate deep into the lungs, translocate into the bloodstream, and induce oxidative stress, potentially leading to cardiovascular, respiratory, and neurological diseases [1, 2]. Despite increasing scientific awareness, UFPs remain largely unregulated in most national air quality standards, including those of the U.S. Environmental Protection Agency (EPA) and the European Union (EU). This is primarily due to challenges in measurement, limited long-term data, and an evolving understanding of their health impacts. However, mounting evidence from toxicological and epidemiological studies—supported by organizations such as the World Health Organization (WHO)—suggests that UFPs can trigger systemic inflammation, neurotoxicity, and other adverse outcomes, even at relatively low ambient concentrations.

In contrast to PM2.5 and PM10, which are regulated based on mass concentration, UFPs are more accurately characterized by their number concentration. Conventional air quality monitoring systems largely focus on mass-based metrics such as PM2.5, which fail to capture the high number abundance and dynamic behavior of UFPs. As a result, health risks associated with UFP exposure may be underestimated in current regulatory frameworks. Recent studies have emphasized the importance of particle number concentration (PNC) as a more suitable metric for evaluating UFP exposure and informing public health policy [3].

Advanced chemical transport models such as GEOS-Chem, when coupled with the TwO-Moment Aerosol Sectional (TOMAS) microphysics module, offer a robust framework for simulating aerosol number and mass size distributions [4]. These models are particularly effective in evaluating microphysical processes like nucleation, condensation, and coagulation. Validating model output against high-resolution observational data is essential for enhancing predictive accuracy and improving our understanding of UFP behavior in the atmosphere.

In this study, we investigate the characteristics, sources, and atmospheric evolution of UFPs over Taichung City, Taiwan, by integrating ground-based measurements with GEOS-Chem–TOMAS simulations. Specifically, we aim to identify the key processes driving new particle formation (NPF) events, evaluate the performance of various nucleation schemes, and assess the model's ability to replicate observed UFP dynamics. The findings are expected to enhance UFP representation in regional air quality models and provide insights to support future regulatory and public health strategies.

METHODOLOGY

This study investigates ultrafine particle (UFP) behavior in Taichung, Taiwan, using both observational data and regional-scale modeling for the period April 2021. Particle number size distribution (PNSD) data were acquired from the Tunghai University monitoring site in collaboration with National Taiwan University (NTU), covering a size range of 11–593.5 nm. Sulfuric acid and other meteorological variables, including solar radiation, relative humidity, and PM2.5 concentrations, were monitored to support the analysis of atmospheric conditions influencing UFP formation.

For the modeling component, the GEOS-Chem chemical transport model coupled with the TwO-Moment Aerosol Sectional (TOMAS) microphysics module was employed, following the configurations described by Trivitayanurak et al. (2008) [4] and Bey et al. (2001) [5]. The simulations were conducted using GEOS-FP assimilated meteorological data from NASA's Global Modeling and Assimilation Office, at a nested horizontal resolution of 0.25° × 0.3125°, encompassing the Taiwan region.

The GEOS-Chem-TOMAS framework calculates aerosol number and mass concentrations across 15 discrete size bins ranging from 2 nm to 2 μm. To investigate the sensitivity of UFP formation to different nucleation pathways, four nucleation schemes were evaluated: binary homogeneous nucleation (BHN), ternary homogeneous nucleation (THN), binary ion-mediated nucleation (BIMN), and ternary ion-mediated nucleation (TIMN).

New particle formation (NPF) events were identified based on observed particle growth in the 11–20 nm range, with growth rates determined from changes in geometric mean diameter (Dpg), in line with Dal Maso et al. (2005) [6]. The classification of NPF events was conducted through visual inspection of PNSD surface plots and analysis of nucleation-mode particle evolution, consistent with methodologies outlined by Wang et al. (2023) [7].

Model diagnostics, including nucleation, condensation, and coagulation rates, were used to interpret observed events and assess the capability of each nucleation scheme in reproducing measured UFP trends. These insights are critical for understanding regional-scale UFP dynamics and improving model performance in simulating fine-scale aerosol processes.

RESULTS AND DISCUSSIONS

The GEOS-Chem model simulation for April 2021 illustrates the spatial distribution of total particle number concentrations (PNC) over Taiwan, as shown in Figure 1. The model reveals a pattern of elevated PNC levels in the northeastern regions of Taiwan, consistent with dominant northeasterly winds and the influence of

the northeastern monsoon. Notably, the particle number concentration hotspot appears to shift inland, suggesting the impact of advection on regional aerosol distribution.

To examine temporal variations, we compared model output with ground-based observations from a Scanning Mobility Particle Sizer (SMPS) located in Taichung. Figure 2 displays a time-series contour plot of observed particle number size distributions, highlighting multiple episodes of elevated ultrafine particle (UFP) concentrations below 50 nm. These episodes are attributed to new particle formation (NPF) events likely driven by specific meteorological and precursor gas conditions. Conversely, Figure 3 presents periods of relatively low UFP activity, which may reflect suppressed nucleation due to changes in atmospheric sinks or precursor gas availability.

Figure 4 compares the total particle number concentration (≤ 50 nm) from SMPS measurements (orange line) and GEOS-Chem simulations (blue line). While the model captures some general temporal trends, it significantly overestimates the magnitude of UFP concentrations across nearly all time steps. This discrepancy is quantified by a Normalized Mean Bias (NMB) of +1059.2%, indicating a tenfold average overprediction of observed values. Furthermore, the Root Mean Square Error (RMSE) between model and observations is 27,349,310.67 #/cm³, suggesting large differences in absolute concentrations. The simulation also shows much sharper and more extreme fluctuations than the relatively smoother trends observed in the SMPS data.

A scatter plot in Figure 5 further illustrates the relationship between observed and modeled total UFP concentrations. The correlation is weak, with an R^2 value of 0.0346, indicating that the model explains only 3.46% of the variance in observed UFP data. This extremely limited correlation, combined with the substantial bias and error, strongly suggests that while the model may partially reflect the timing of some UFP events, it fails to capture their actual magnitude and frequency.

To further evaluate particle number dynamics over the month, Figures 6 and 7 present contour plots of particle number size distributions from SMPS observations and GEOS-Chem simulations, respectively. Neither dataset shows prominent new particle formation (NPF) events throughout April 2021, with both exhibiting largely continuous distributions and minimal ultrafine particle growth below 50 nm. This may suggest unfavorable conditions for nucleation during this period or limitations in detection and model sensitivity. However, the simulated distribution still exhibits stronger fluctuations in concentration across sizes and time, reinforcing earlier findings regarding model overestimation and variability.

These discrepancies may arise from multiple sources, including uncertainties in the model's nucleation scheme, simplifications in chemical and physical processes, or inaccuracies in emissions inventories for nucleating precursors. Additionally, the model's resolution and lack of localized meteorological input may limit its ability to resolve small-scale phenomena critical for accurate UFP simulation.

While the World Health Organization (WHO) currently provides air quality guidelines for particulate matter based on mass concentration (e.g., $PM_{2.5}$), there are no established numerical standards for particle number concentrations, especially in the ultrafine range. Nevertheless, exposure to high concentrations of UFPs has been linked to adverse health outcomes due to their ability to penetrate deep into the lungs and enter the bloodstream. The consistent model overestimation underscores the importance of refining model mechanisms to avoid misleading exposure assessments and to support future health risk evaluations.

In future work, efforts will focus on refining nucleation parameterizations, such as by incorporating organic aerosol effects or size-resolved emissions, improving representation of local emissions and meteorology, and incorporating additional observational datasets for model validation and bias correction.

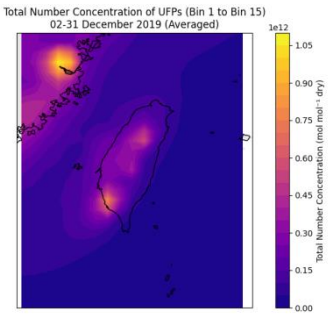


Figure 1 Spatial distribution of total particle number concentration

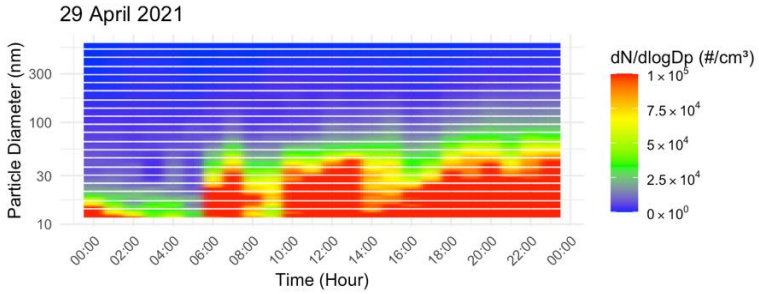


Figure 2 Time-series contour plot of observed particle number size distributions during a high concentration day

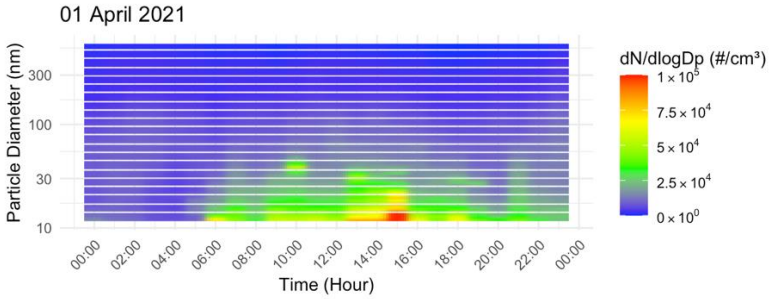


Figure 3 Time-series contour plot of observed particle number size distributions during a low concentration day

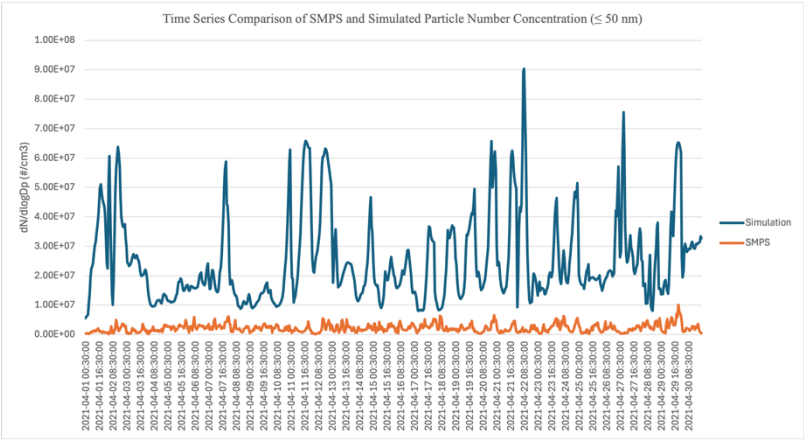


Figure 4 Time Series Comparison of Total Particle Number Concentration (≤ 50 nm)

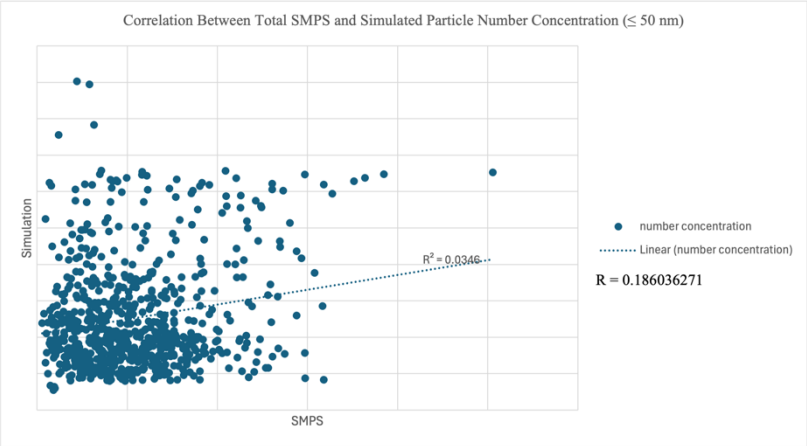


Figure 5 Correlation Between Total SMPS and Simulated Particle Number Concentration (≤ 50 nm)

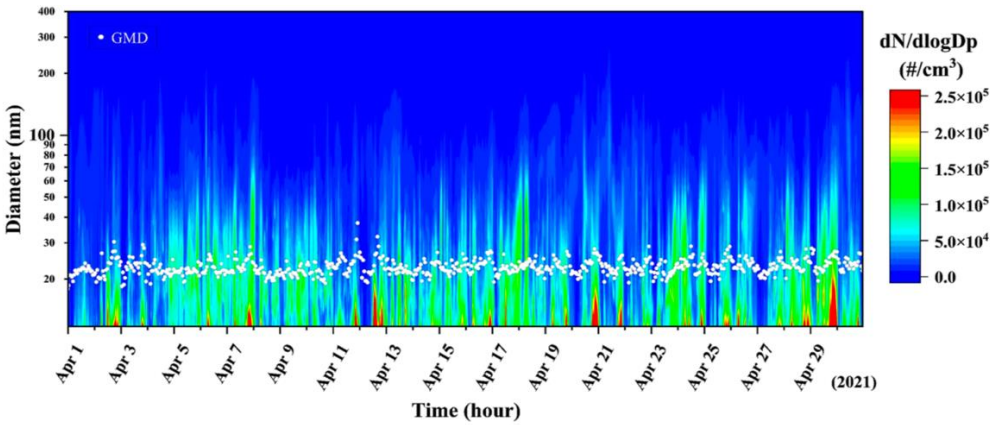


Figure 6. Hourly SMPS contour plot of particle number size distributions observed in Taichung during April 2021. The color scale represents dN/dlogDp (#/cm³).

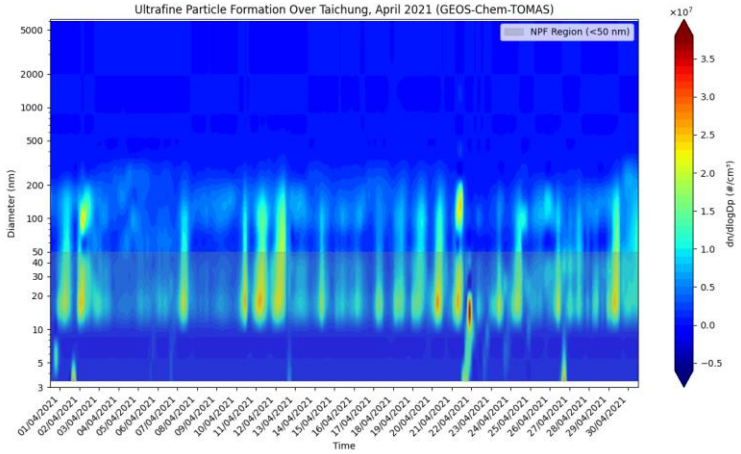


Figure 7. Hourly contour plot of particle number size distributions simulated by the GEOS-Chem-TOMAS model over Taichung during April 2021. The color scale represents dn/dlogDp (#/cm³)

CONCLUSION

This study investigated the spatial and temporal characteristics of ultrafine particle (UFP) number concentrations and size distributions over Taiwan using GEOS-Chem-TOMAS simulations and ground-based SMPS observations from Taichung. The model successfully captured broad spatial patterns of particle number concentration (PNC), including an inland shift of concentration hotspots influenced by the northeastern monsoon and regional advection.

In terms of temporal behavior, the model reproduced some general trends in total UFP number concentration (≤ 50 nm), but substantially overestimated the overall magnitude compared to observations. It also exhibited exaggerated temporal variability, with sharp and frequent fluctuations not reflected in the SMPS data, highlighting challenges in capturing UFP dynamics at local scales.

Correlation analysis further underscored these limitations, with an R^2 of only 0.0346 and a normalized mean bias exceeding 1000%, indicating poor agreement between simulated and observed concentrations. These discrepancies likely stem from uncertainties in nucleation parameterizations, underrepresentation of localized emissions, and limited resolution of meteorological processes.

Contour plots of particle size distributions (Figures 6 and 7) showed no distinct new particle formation (NPF) events in either the simulation or the observations for April 2021. This absence could be attributed to unfavorable atmospheric conditions during the study period or limitations in both model sensitivity and observational resolution.

While the World Health Organization (WHO) provides air quality guidelines for particle mass concentrations (e.g., $PM_{2.5}$), no such standards exist for UFP number concentrations. Given the potential health impacts associated with UFP exposure, model overestimations pose a risk of misinforming exposure assessments and policy decisions.

Overall, these findings highlight the potential of GEOS-Chem-TOMAS for regional air quality analysis but also reveal key areas needing improvement. Future work should prioritize refining nucleation schemes—such as incorporating organic aerosol effects—enhancing the resolution of local emissions and meteorology, and expanding validation datasets, particularly for size-resolved comparisons. Addressing the model's persistent overestimation and weak agreement with observations will be critical to improving its utility for both scientific analysis and public health applications.

ACKNOWLEDGEMENT

The authors would like to thank the Graduate Institute of Environmental Engineering at National Taiwan University for providing access to the GEOS-Chem model output and for their collaborative spirit throughout this research. This work is a result of the collaborative partnership between Chulalongkorn University, Thailand, and National Taiwan University, Taiwan.

REFERENCE

[1] Romieu, I., Castro-Giner, F., Kunzli, N., and Sunyer, J. 2008. Air pollution, oxidative stress and dietary supplementation: a review. *Eur Respir J.* 31(1): 179-197.

[2] Gillespie, P., Tajuba, J., Lippmann, M., Chen, L.-C., and Veronesi, B. 2013. Particulate matter neurotoxicity in culture is size-dependent. *NeuroToxicology.* 36: 112-117.

[3] HEI Panel on Ultrafine Particles. 2013. Understanding the health effects of ambient ultrafine particles. HEI Review Panel on UFPs, Health Effects Institute, Boston, MA.

[4] Trivitayanurak, W., Adams, P.J., Spracklen, D.V., and Carslaw, K.S. 2008. Tropospheric aerosol microphysics simulation with assimilated meteorology: Model description and intermodel comparison. *Atmospheric Chemistry and Physics.* 8: 3149-3168.

[5] Bey, I., Jacob, D.J., Yantosca, R.M., Logan, J.A., Field, B.D., Fiore, A.M., Li, Q., Liu, H.Y., Mickley, L.J., and Schultz, M.G. 2001. Global modeling of tropospheric chemistry with assimilated meteorology: Model description and evaluation. *Journal of Geophysical Research: Atmospheres.* 106(D19): 23073-23095.

[6] Dal Maso, M., Kulmala, M., Riipinen, I., and Wagner, R. 2005. Formation and growth of fresh atmospheric aerosols: Eight years of aerosol size distribution data from SMEAR II, Hyytiälä, Finland. *Boreal Environment Research.* 10: 323-336.

[7] Wang, K., Ma, X., Tian, R., and Yu, F. 2023. Analysis of new particle formation events and comparisons to simulations of particle number concentrations based on GEOS-Chem–advanced particle microphysics in Beijing, China. *Atmos. Chem. Phys.* 23(7): 4091-4104

Physical and Chemical Characteristics of Fine and Ultrafine Particulate Matters in Southern Thailand

Chanakan Bunyarit[1,2], Racha Dejchanchaiwong[1,2]*, Perapong Tekasakul[1,3], Nobchonnee Nim[1], Aree Choodum[4], Thanita Areerob[4], Bussakorn Kleangklao[4], Saysunee Jumrat[5], Yutthapong Pianroj[5], Benjalak Boonpeng[5]

[1]Air Pollution and Health Effect Research Center, Prince of Songkla University, Hat Yai, Songkhla 90112, Thailand

[2]Department of Chemical Engineering, Faculty of Engineering, Prince of Songkla University, Hat Yai, Songkhla 90112, Thailand

[3]Department of Mechanical and Mechatronics Engine

ering, Faculty of Engineering, Prince of Songkla University, Hat Yai, Songkhla 90112, Thailand

[4]Integrated Science and Technology Research Center, Faculty of Technology and Environment, Prince of Songkla University, Phuket Campus, Kathu, Phuket 83120, Thailand

[5]Faculty of Science and Industrial Technology, Prince of Songkla University, Suratthani Campus, Surat Thani 84000, Thailand

**Corresponding author. E-mail address: racha.d@psu.ac.th*

ABSTRACT

The present study aims to study the physical and chemical characteristics of ultrafine ($PM_{0.1}$) and fine ($PM_{2.5}$) during the normal and haze periods in Songkhla, Thailand. Annual $PM_{0.1}$ and $PM_{2.5}$ mass concentrations in Songkhla were 0.9±0.6, and 12.4±6.3 μg/m^3, respectively. PMs concentrations during the haze period in Songkhla were approximately 2 times higher than those during normal period. The levels of particle-PAHs for $PM_{0.1}$ and $PM_{2.5}$ also significantly increased during haze period, about 3 and 4 times higher than those during normal period, respectively. A larger portion of HMW-PAH in both periods indicated the fine particles were the carcinogenic aerosols. The PAH diagnostic ratios for PMs during normal periods indicated a mixed source of vehicle combustion and biomass burning, whereas the major source was biomass burning during the haze periods. Moreover, the result of backward trajectory simulation supported that a major portion of the south and southwest wind during southwest monsoon moved past concentrated hotspots in Sumatra, Indonesia, towards Songkhla. Thus, a regional transboundary haze significant impact on air quality in southern Thailand, as well as many other countries in lower southeast Asia.

Keywords: Fine and ultrafine particles; PAHs; ASEAN Haze

INTRODUCTION

Ultrafine ($PM_{0.1}$) and fine ($PM_{2.5}$) and particles are major air pollution problems that impact human health and the environment. Ebenstein et al. (2017) [1] reported that every 10 μg/m³ increase in $PM_{2.5}$ concentration reduces life expectancy by 0.64 years. Recently, exposure to PM_1 and $PM_{0.1}$ particles have been associated with adverse health effects because they are more harmful to human health than larger particles [2-3]. In lower Southeast Asia (SEA), $PM_{0.1}$ concentration in Indonesia (7-17 μg/m³) was approximately 2-4 times higher than those in Thailand and other countries. PM concentration and other gaseous pollutants in southern Thailand, especially Hat Yai city is not only affected by growing urbanization (traffic, commercial and industrial activities), but also regional transboundary haze, which can be most significant during the southwest monsoon with air masses passing over Sumatra, Indonesia. Chomanee et al. (2020) [1] reported that $PM_{0.1}$ concentration during the 2019 haze period was higher than those during normal period, approximately 2-7 times. Mahasakpan et al. (2023) [5] presented that the main source of $PM_{0.1}$ during the haze period was peat fire burning, accounting for 34%, while during the normal period, it was traffic, accounting for 58%.

Polycyclic aromatic hydrocarbons (PAHs) are significant components of atmospheric pollution, and some PAHs are known to be mutagenic and carcinogenic [6]. United States Environmental Protection

Agency classified 16 PAH compounds as priority pollutants because of their potential toxicity including: 6 low molecular weight PAHs (LMW-PAHs, 2-3 rings) and 10 high molecular weight PAHs (HMW-PAHs, 4-6 rings). Promsiri et al. (2023) [7] reported that $PM_{2.5}$-bounded PAHs concentration of during haze period was about 2-3 times higher than those during normal period. Exposure to PAHs increases the risk of lung cancer and respiratory diseases, which may affect lung function and cause bronchitis [8]. Moreover, diagnostic ratios were used to identify PAH sources [6].

In the present study, the physical and chemical characteristics of ultrafine ($PM_{0.1}$) and fine ($PM_{2.5}$) particles collected during the normal and 2023 haze periods in Songkhla, Thailand were analyzed. Carcinogenic risks from PM-bound PAHs were then evaluated. Diagnostic ratios of PAHs were used to identify the possible sources of PM during the normal and haze periods, supported by tracking backward trajectories (BT) of the air mass transport.

METHODOLOGY

Sampling sites

Sampling site was at Prince of Songkla University (PSU site), (N 7.0068, E 100.4747), located in Hat Yai, Songkhla, Thailand. Hat Yai is an urbanized and industrialized city in southern Thailand. Samples were taken on the top of a sampling station, ~24 m above ground to study atmospheric air quality [9]**.** Air quality in in Hat Yai city are not only affected by the local emission sources including traffic volume, industrial activities, and local agricultural waste burning, but also transboundary haze from neighboring country during southwest monsoon [4]. Location of the sampling site is shown in **Figure 1**.

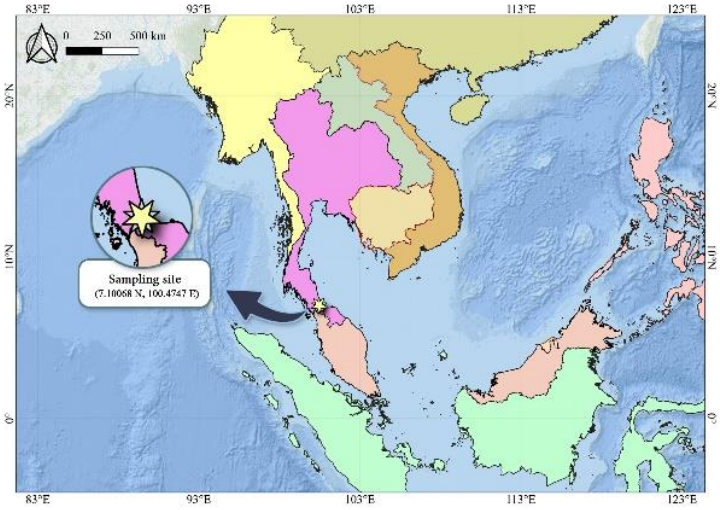


Figure 1 Location of the sampling site.

Physical analysis

PM samples were collected using a nanosampler, operating at a flow rate of 40 L/min for 120 hours during normal period and 72 hours during haze period. Particles were separated into six size ranges from the last stage: <0.1 µm ($PM_{<0.1}$), 0.1-0.5 µm ($PM_{0.1-0.5}$), 0.5-1.0 µm ($PM_{0.5-1}$), 1.0-2.5 µm ($PM_{1-2.5}$), 2.5-10 µm ($PM_{2.5-10}$) and >10 µm ($PM_{>10}$). The particles were collected on a 55-mm quartz fiber filter (2500QAT-UP, Pallfex, USA) in each stage, except the $PM_{0.1-0.5}$ stage, where an inertial filter (IF-stainless-steel filter pack, SUS304, fiber diameter = 9.8 µm) was used.

The QA/QC were controlled for each sampling.

The filters were baked for 1 hr at 350°C to eliminate contaminants. The sample and blank filters before and after sampling were controlled under conditions of RH of 50±5% at a temperature of 25±2°C for 72 hours. The filter was then weighted by a 0.01 mg resolution balance (CP225D, Sartorius, Germany). PM mass concentration (µg/m³) was calculated by the difference of mass of PM collected on the filter (mg) divided by the total air volume of sampling (m³).

Chemical characteristic analysis

PAHs analysis

PAHs were extracted using an ultrasonic extraction technique. The extracted solutions were filtered through a PTFE syringe filter (0.45 μm), then added 50 μL of dimethyl sulfoxide and used a rotary evaporator to evaporate it until it nearly dried about (~50 μL). The residue was redissolved in 450 μL acetonitrile and then filtered again through a PTFE syringe filter. 16-PAHs were determined using high performance liquid chromatograph (HPLC, Agilent-1100, USA) with coupled diode array and fluorescence detectors (HLPC-DAD/FLD). A linear correlation between the 16-PAHs-mix standard solution concentrations (Supelco, Catalog number 4-8743, Germany) and peak areas was found with R^2 values higher than 0.999 for all PAH compounds. 16 PAH compounds are shown in **Table 1**.

Table 1 16 PAH compounds.

Group	PAH compounds	Symbols
LMW	Naphthalene	Nap
	Acenaphthylene	Act
	Acenaphthene	Ace
	Fluorene	Fle
	Phenanthrene	Phe
	Anthracene	Ant
HMW	Fluoranthene	Flu
	Pyrene	Pyr
	Benzo[a]anthracene	BaA
	Chrysene	Chr
	Benzo[b] Fluoranthene	BbF
	Benzo[k] Fluoranthene	BkF
	Benzo[a]Pyrene	BaP
	Dibenzo[a,h]anthracene	DBA
	Benzo[g,h,i]peryrene	BghiPe
	Indeno[1,2,3-cd}pyrene	IDP

PAHS diagnostic ratios

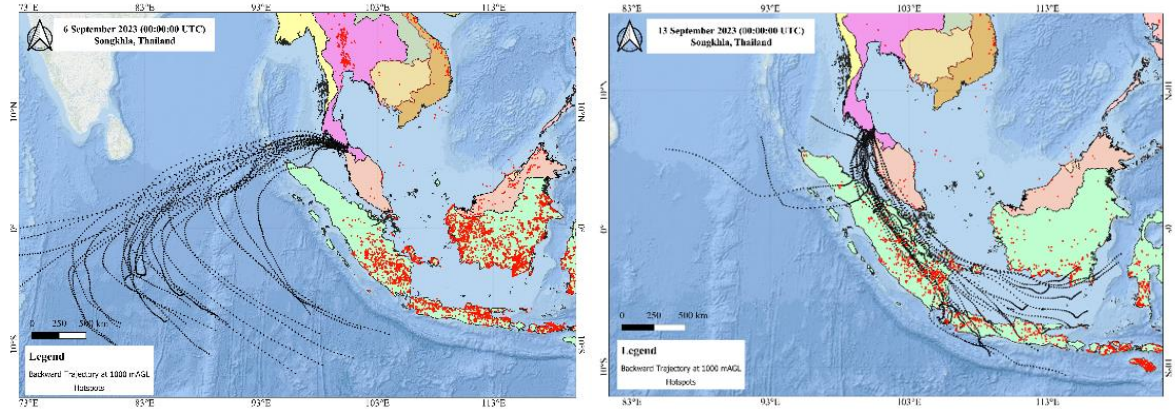
Diagnostic ratios of (Flu/(Flu+Pyr) and BaA/(BaA +Chr) were used to identify the potential PAH sources of fine ($PM_{2.5}$) and ultrafine ($PM_{0.1}$) particles during normal and haze periods. Here, the PAH ratios of BaA/(BaA+Chr) > 0.35 and Flu/(Flu + Pyr) > 0.5 indicated strong biomass burning, whereas the ratios of BaA/(BaA+Chr) < 0.35 and Flu/(Flu + Pyr) ratio < 0.5 indicated strong combustion fuel as a source [10][11].

RESULTS AND DISCUSSIONS

Backward trajectory simulation

Air mass transport from sources to receptors was simulated to observe 120-hours backward trajectories (BT) of air at 1000m above ground level (AGL) using the Hybrid Single-Particle Langrangian Integrated Trajectory Model version 4 (HYSPLIT4) [12]. Hotspot from open biomass burning were obtained from Earthdata (2025) [13].

BT simulation results over Hat Yai, southern Thailand during normal and haze periods were presented in **Figure 2.** The BT during normal periods showed that the east and northeast wind carried clean air, from the Gulf of Thailand to southern Thailand (**Figure 2a**). The BT simulations during haze periods showed the southwest-bound air mass movement, passing through some hotspots in northern Sumatra to Hat Yai (**Figure 2b**). This agrees with previous studies showing significant enhancements in $PM_{2.5}$ concentrations over lower SEA during the southwest monsoon [4-7].

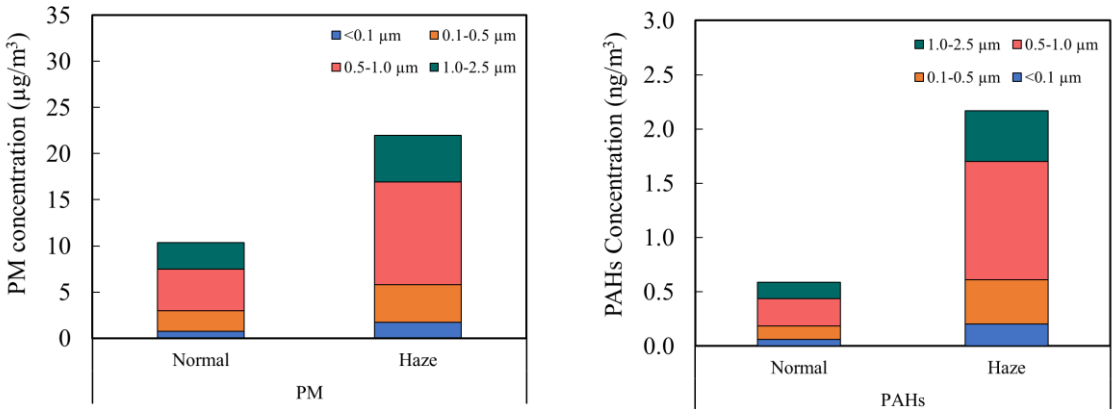


(a) (b)

Figure 2 The backward trajectories during (a) normal and (b) haze periods.

Size-segregated PM concentrations

Size-segregated PM concentrations during the normal and haze periods in Hat Yai Songkhla, Thailand are shown **in Figure 3(a)**. Annual $PM_{0.1}$ and $PM_{2.5}$ mass concentrations were 0.9±0.6 and 12.4±6.3 μg/m^3, respectively. $PM_{0.1}$ and $PM_{2.5}$ concentration during haze period were approximately 2 times higher than those during normal period. The $PM_{2.5}$ level did not exceed Thailand's standard (37.5 μg/m^3). The abundant of PM concentrations during the normal and haze period were found in particle size range 0.5-1 μm, accounting into 44% and 50%, respectively.



(a) PM mass concentrations (b) PAH mass concentrations

Figure 3 Size-segregated PM and PAH mass concentrations during normal and haze periods.

PM-bound PAH characteristics

The average PAH concentrations in $PM_{0.1}$ and $PM_{2.5}$ during the haze period were approximately 3 and 4 times higher than those during the normal period, respectively, as shown in **Figure 3(b)**. The PAH concentrations in the particle size range of 0.5-1 μm in normal and periods occupied up to 49% and 51% of PAH concentrations in $PM_{2.5}$, respectively. This was consistent with Mahasakpan et al. (2023) [5] and Dejchanchaiwong et al. (2020) [6] who reported that the highest average PAH concentrations in southern Thailand during 2019 haze period were found in the $PM_{0.5–1.0}$ size range. The findings indicated that PAHs were dominated by particles in the size range of <1 μm.

The individual PAH profiles in $PM_{0.1}$ and $PM_{2.5}$ during the haze period is shown in **Figure 4**. HMW-PAHs (4-6 rings) in $PM_{0.1}$ and $PM_{2.5}$ contributed 76.7 and 78.4% for normal period and 77.8% and 82.2% for haze period and respectively. HMW-PAHs concentrations in $PM_{0.1}$ during haze periods slightly increased as compared to normal period.The predominant of LMW-PAHs (2-3 ring) during normal and haze periods was Nap. BbF, DBA, BghiPe and IDP were the most abundant for HMW-PAHs (4-6 ring) during normal period, BbF and BghiPe were also dominated in the HMW-PAHs during haze period.

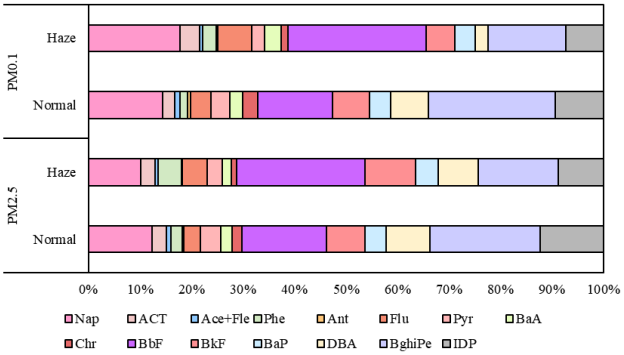


Figure 4. Individual PAH profiles in $PM_{0.1}$ and $PM_{2.5}$ during the normal and haze period.

Source identification

The PAHs diagnostic ratios are commonly used as chemical trackers to identify sources of PAHs. In the present study, Diagnostic ratios of BaA/(BaA +Chr) and Flu/(Flu + Pyr) were used to identify the potential PAH sources of $PM_{0.1}$ and $PM_{2.5}$ during the normal and haze periods. The emission sources of $PM_{0.1}$ and $PM_{2.5}$ during normal and haze periods are showed in **Figure 5**. The results showed that the main sources of $PM_{0.1}$ and $PM_{2.5}$ during normal period were a mixed source of vehicle combustion and biomass burning. This agrees with a previous study of Dejchanchaiwong et al. (2020) [6], who reported the sources of $PM_{0.1}$ are a mix of vehicle combustion and biomass burning even when biomass burning dominates. The values during haze period (red triangles) for both PM were in upper right quadrant. This ratio indicated that the major source of $PM_{0.1}$ and $PM_{2.5}$ during haze periods was biomass burning. This is similar trend to previous studies [4-7].

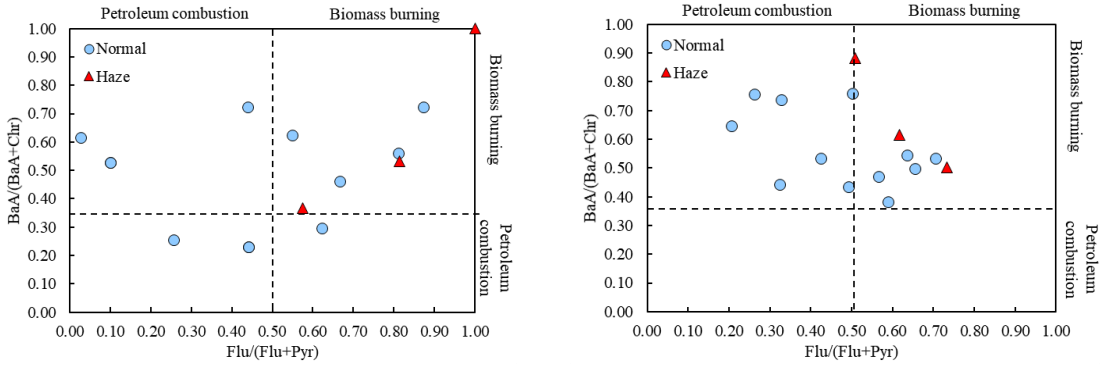


Figure 4 PAHs diagnostic ratios during normal and haze periods for (a) $PM_{0.1}$ and (b) $PM_{2.5}$

CONCLUSION

Physical and chemical characteristics of fine and ultrafine particles in Songkhla, southern Thailand during 2023 normal and haze periods were investigated. We conclude:

- $PM_{0.1}$ and $PM_{2.5}$ concentrations during haze period were approximately 2 times higher than those during normal period.
- Average PAH concentrations in $PM_{0.1}$ and $PM_{2.5}$ during haze period were approximately 3 and 4 times higher than those during normal period, respectively.
- HMW-PAHs (4-6 rings) are mainly associated with $PM_{0.1}$ and $PM_{2.5}$, accounting for 56.1-88.3% and 59.7-88.2%, respectively.
- The PAH diagnostic ratios for $PM_{0.1}$ and $PM_{2.5}$ during normal period indicated a mixed source of petroleum combustion and biomass burning, whereas the major sources were biomass burning during haze period.

Thus, a regional transboundary haze significant impact on air quality in southern Thailand, as well as many other countries in lower southeast Asia.

ACKNOWLEDGEMENT

This research has received funding support from the NSRF via the Program Management Unit for Human Resources & Institutional Development, Research and Innovation [grant number B42G670042].

REFERENCE

[1] Ebenstein, A., et al. 2017. New evidence on the impact of sustained exposure to air pollution on life expectancy from China's Huai River Policy. Proceedings of the National Academy of Sciences. 114 (39): 10384–10389.

[2] Díaz-Robles, L. A., et al. 2014. Health risks caused by short term exposure to ultrafine particles generated by residential wood combustion: A case study of Temuco, Chile. Journal of Environment International. 66: 174–181.

[3] Potter, N. A., et al. 2021. Particulate Matter and Associated Metals: A Link with Neurotoxicity and Mental Health. Journal of Atmosphere. 12 (4): 425.

[4] Chomanee, J., et al. 2020. Physicochemical and toxicological characteristics of nanoparticles in aerosols in southern Thailand during recent haze episodes in lower southeast Asia. Journal of Environmental Sciences. 94: 72–80.

[5] Mahasakpan, N., et al. 2022. Fine and ultrafine particle- and gas-polycyclic aromatic hydrocarbons affecting southern Thailand air quality during transboundary haze and potential health effects. Journal of Environmental Sciences. 124: 253–267.

[6] Dejchanchaiwong, R., et al. 2020. Impact of transport of fine and ultrafine particles from open biomass burning on air quality during 2019 Bangkok haze episode. Journal of Environmental Sciences. 97: 149–161.

[7] Promsiri, P., et al. 2022. Transboundary haze from peatland fires and local source-derived PM2.5 in Southern Thailand. Atmospheric Environment. 294: 119512.

[8] Ho, A. F. W., et al. 2019. Time-Stratified case crossover study of the association of outdoor ambient air pollution with the risk of acute myocardial infarction In the context of seasonal exposure to the Southeast Asian Haze problem. Journal of the American Heart Association. 8 (6).

[9] U.S.EPA, 2011. Exposure Factors Handbook Report No. EPA/600/R-09/052F. prepared by U.S. Environmental Protection Agency, Research Triangle Park, NC

[10] Yunker, M. B., et al. 2002. PAHs in the Fraser River basin: a critical appraisal of PAH ratios as indicators of PAH source and composition. Journal of Organic Geochemistry. 33 (4): 489–515.

[11] Yang, Y., et al. 2010. Seasonal variation, sources, and gas/particle partitioning of polycyclic aromatic hydrocarbons in Guangzhou, China. Journal of The Science of the Total Environment. 408 (12): 2492–2500.

[12] Air Resources Laboratory. 2024. HYSPLIT model. https://ready.arl.noaa.gov

[13] Earthdata. 2025. NRT VIIRS 375 m Active Fire product. https://earthdata.nasa.gov/firms.

20R3-04

Examination of Ambient $PM_{2.5}$ Exceedances in Bangkok: Frequency, Duration, and Background Concentration

Chaiwat Wilasang[1,2], Kasemsan Manomaiphiboon[1,2*], Jindarat Pariyothon[3], Natchanok Pala-En[4], Nishit Aman[5]
[1]*The Joint Graduate School of Energy and Environment, King Mongkut's University of Technology Thonburi, Thailand*
[2]*Center for Energy Technology and Environment, Ministry of Higher Education, Science, Research and Innovation, Thailand*
[3]*Department of Social and Applied Science, King Mongkut's University of Technology North Bangkok, Thailand*
[4]*Ministry of Natural Resources and Environment, Thailand*
[5]*Department of Environmental and Sustainable Engineering, Chulalongkorn University, Thailand*
[*]*E-mail: kasemsan.man@kmutt.ac.th*

ABSTRACT

Thailand recently revised the ambient air standards of $PM_{2.5}$ from 50 μg m^{-3} to 37.5 μg m^{-3} for daily (24-h) concentration and from 25 μg m^{-3} to 15 μg m^{-3} for annual concentration. This study examined the frequency and duration of $PM_{2.5}$ exceedance events based on the previous and current daily standards and also investigated background $PM_{2.5}$ level ($BPM_{2.5}$) that reflects the influences of natural processes and pollutant transport, as opposed to local anthropogenic sources. Hourly $PM_{2.5}$ observations in recent years at two monitoring stations (P52 and P59) in Bangkok were obtained from the Pollution Control Department and used in the analysis. They were quality-checked and then converted to a daily scale. Here, the run theory was applied to identifying $PM_{2.5}$ events, and a Hidden Markov Model was used to estimate BPM_2 (only in the dry season). It was found that most exceedances occur in the dry season, with a decreasing trend under each of the previous and current standards. The current (i.e., stricter) standard naturally detects more events and exceedances, with longer durations and shorter clean-day gaps. Dry-season $BPM_{2.5}$ has a declining trend at both stations. For dry-season $\Delta PM_{2.5}$ (defined as average $PM_{2.5}$ - average $BPM_{2.5}$), each station has a decreasing trend, suggesting the positive outcome of local emission controls over the recent years in Bangkok. It should be noted that this study presented here is part of ongoing research, and the results are still considered preliminary.

Keywords : $PM_{2.5}$; air quality standard; exceedances; frequency; duration; background $PM_{2.5}$ concentration

INTRODUCTION

Bangkok often experiences air pollution whose extent exceeds national ambient standards. It is driven by various emissions, urbanization, and certain weather conditions favorable for the intensification of air pollution. $PM_{2.5}$ is an important regulated air pollutant in Thailand and globally, which poses health risks, contributes to reduced atmospheric visibility, and influences weather and climate through both direct and indirect effects. In Thailand, the daily (24-h) and annual average standards of $PM_{2.5}$ have recently been lowered to be stricter, from 50 μg m^{-3} to 37.5 μg m^{-3} and from 25 μg m^{-3} to 15 μg m^{-3} [1], respectively. The current standards correspond to those recommended by the World Health Organization (WHO)'s Interim Target 3 [2]. Here, the frequency and duration of a $PM_{2.5}$ event (defined as a consecutive period with daily exceedances) in Bangkok due to the previous (PRV) and current (CUR) daily standards were examined. The background concentration of $PM_{2.5}$ (shortly, $BPM_{2.5}$) is of further interest, which is a pollutant level in an area not induced by local anthropogenic sources within but influenced mainly by local natural processes and/or pollutants transported from elsewhere [3, 4]. These $PM_{2.5}$ characteristics are relevant information for air quality management.

DATA AND METHODS

Hourly $PM_{2.5}$ data at two air quality monitoring stations (P52 and P59) in Bangkok, operated by the Pollution Control Department (PCD) (Figure 1), were obtained. Their surrounding backgrounds are roadside and general area, respectively. The data periods cover eight seasonal years (2016-2023) for P52 and nine (2015-2023) seasonal years for P59. A seasonal year starts in the dry season and ends in the wet season. For example, for the seasonal year 2000, the dry season includes November 2019 to April 2020, while the wet season includes

May 2020 to October 2020. The probable measurement range of $PM_{2.5}$ is from 0.1 μg m^{-3} to 1,000 μg m^{-3} [5], used for data screening. Any missing hourly values at one station were gap-filled using a generalized additive mixed model (GAMM) and the corresponding non-missing values (when available) from the other station. At least 90% of the data are required for computing statistics; otherwise, the results are assigned as missing. The run theory [6] was applied to identifying $PM_{2.5}$ events. A $PM_{2.5}$ event is defined as the period of consecutive days with daily $PM_{2.5}$ exceedance. For each event, start/end days, duration (number of days), $PM_{2.5}$ intensity (as mean), frequency, and clean-day gap (the number of days between the event and its previous or next event). Here, they were computed using the PRV and CUR individually. To estimate $BPM_{2.5}$, the Hidden Markov Model (HMM) clustering was utilized to analyze the temporal pattern of a daily $PM_{2.5}$ time series and then identify distinct pollution states [4, 7]. The time series was first detrended on a daily scale and then de-seasonalized. The latter step involves subtraction with mean $PM_{2.5}$ values by day-of-week for each month of the year, resulting in daily $PM_{2.5}$ anomalies used as the input to HMM. The model parameters were estimated using maximum likelihood estimation (MLE) via the expectation-maximization (EM) algorithm. The EM algorithm iteratively alternates between estimating the expected log-likelihood (E-step) and maximizing it (M-step). This process continues iteratively until reaching a maximum number of iterations (NIT) or minimizing the difference (ε) between successive log-likelihood estimates. Following Martín et al. (2020) and Rizos et al. (2022), NIT = 2,000 and $\varepsilon = 10^{-8}$ [4, 7]. HMM also requires the optimal number of clusters (here, called pollution states) based on the given data, which was selected based on the Bayesian Information Criterion (BIC). HMM was here carried out using the "hmmlearn" package in Python.

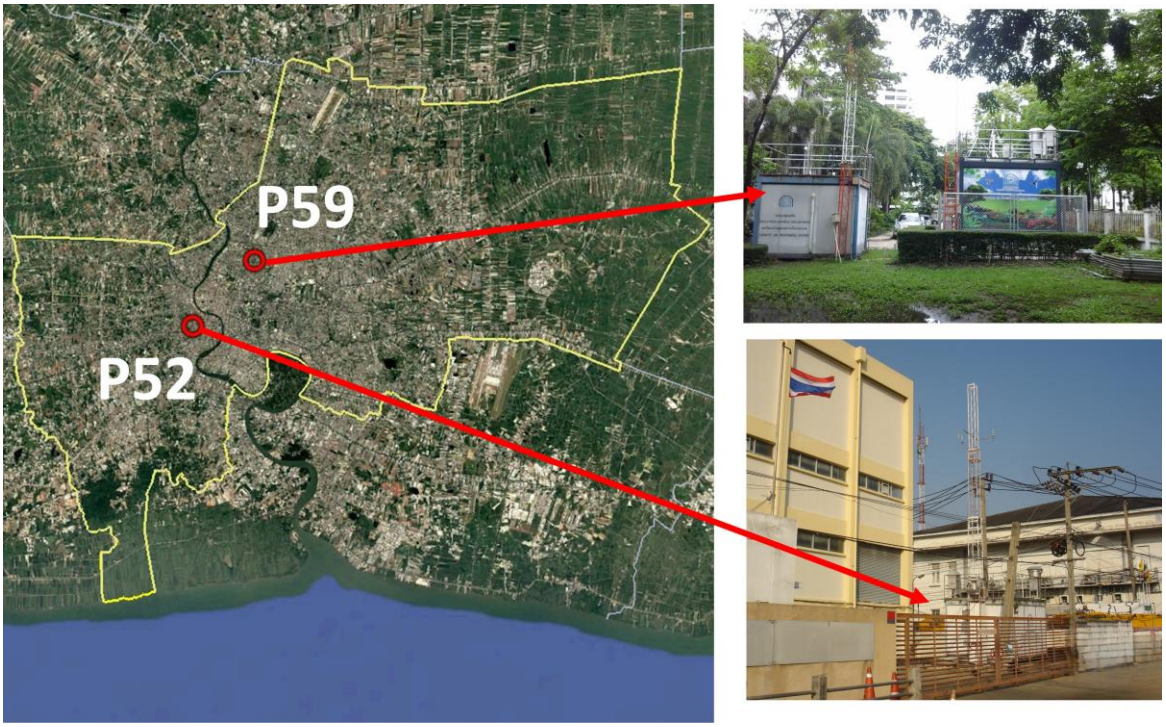


Figure 1 PCD stations considered in the study.

RESULTS AND DISCUSSION

$PM_{2.5}$ events and exceedances occur mostly in the dry season (Figure 2), during which the weather often becomes stagnant with relatively low planetary boundary layer height or mixing height. Its dry-season trends due to PRV and CUR are shown to be significantly (at a 0.05 level) negative or decreasing at both stations. Stricter CUR yields more $PM_{2.5}$ events. The duration of $PM_{2.5}$ event and the clean-day gap between two events are summarized in Figures 3 and 4. Under CUR, it is seen from both stations that event duration is longer while the clean-day gap becomes shorter, while clean-day gap tends to be shorter. As for dry-season $BPM_{2.5}$, a total of five temporal states or clusters were found and chosen as optimal for the daily $PM_{2.5}$ time series at each station

(Figure 5). They are labeled as States 1-5, corresponding to low to high $PM_{2.5}$ levels. The five original states were here simplified by being grouped into three pollution levels (Figure 6): States 1 and 2 combined as Level 1 (low or background), Level 2 (moderate) as States 3 and 4 combined, and Level 3 (high) as State 5. At P59, Level 1 shares the largest occurrence (48% of total days), while P52 has Level 2 occurring the most (53%). Given P52 being the roadside station, it is expected to be more exposed to local traffic sources. Dry-season $BPM_{2.5}$ shows a decreasing trend at both stations (Figure 7a). Annual dry-season $BPM_{2.5}$ at P59 is consistently lower than at P52, possibly due to P59 being in a well-urbanized and commercial area (as part of the city center) and that $PM_{2.5}$ is expected to be more locally constrained and responsive. As for $BPM_{2.5}$ days, the number of days registered as Level 1 (background), it has a declining trend at P52 but approximately no trend at P59 (Figure 7b). The latter reasonably suggests persistent influence on $PM_{2.5}$ from local sources. In view of $\Delta PM_{2.5}$, computed as average $PM_{2.5}$ minus average $BPM_{2.5}$, it shows a decreasing trend at each station (Figure 8), potentially suggesting the positive outcome of local emission controls over the recent years in Bangkok.

CONCLUSIONS

This study attempts to examine how the previous and current daily $PM_{2.5}$ standards impact the frequency and duration of $PM_{2.5}$ events and to statistically determine the background $PM_{2.5}$ condition in order to better understand the effectiveness of local emissions in Bangkok at two different sites. The applied methods are shown to be useful to support the objectives and can be improved or enhanced in the future. It is noted that this study is part of ongoing research, and the results presented here are still considered preliminary.

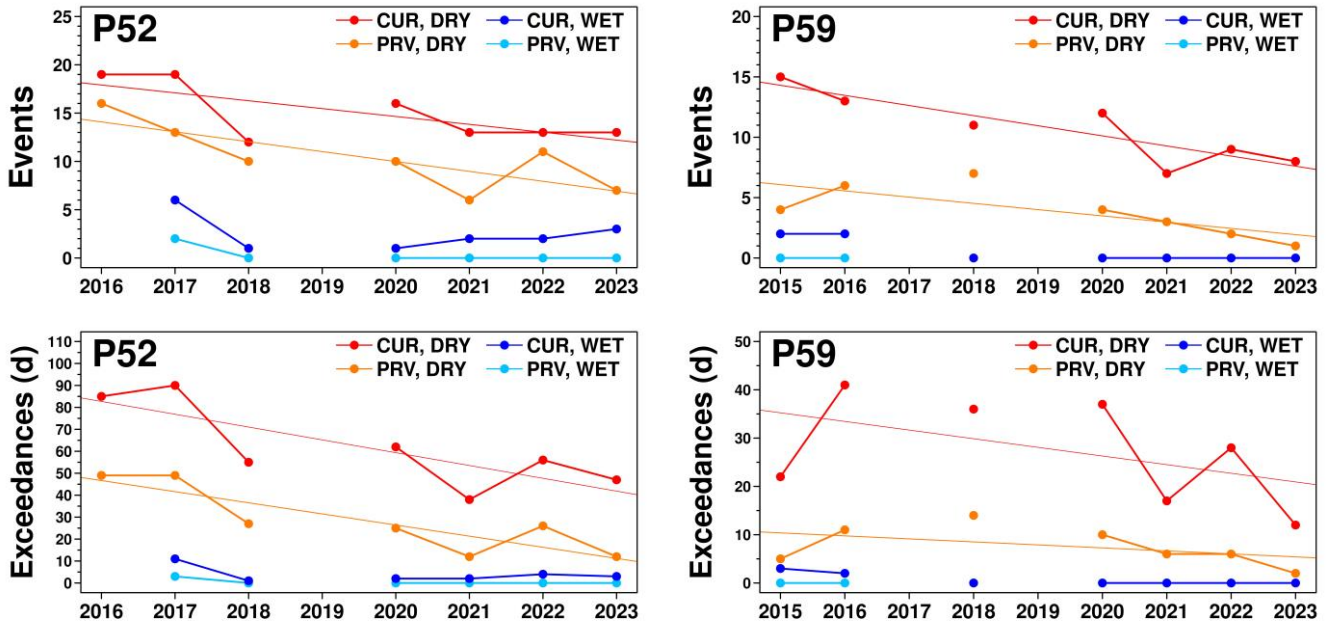


Figure 2 Trends in dry-season events and daily exceedances.

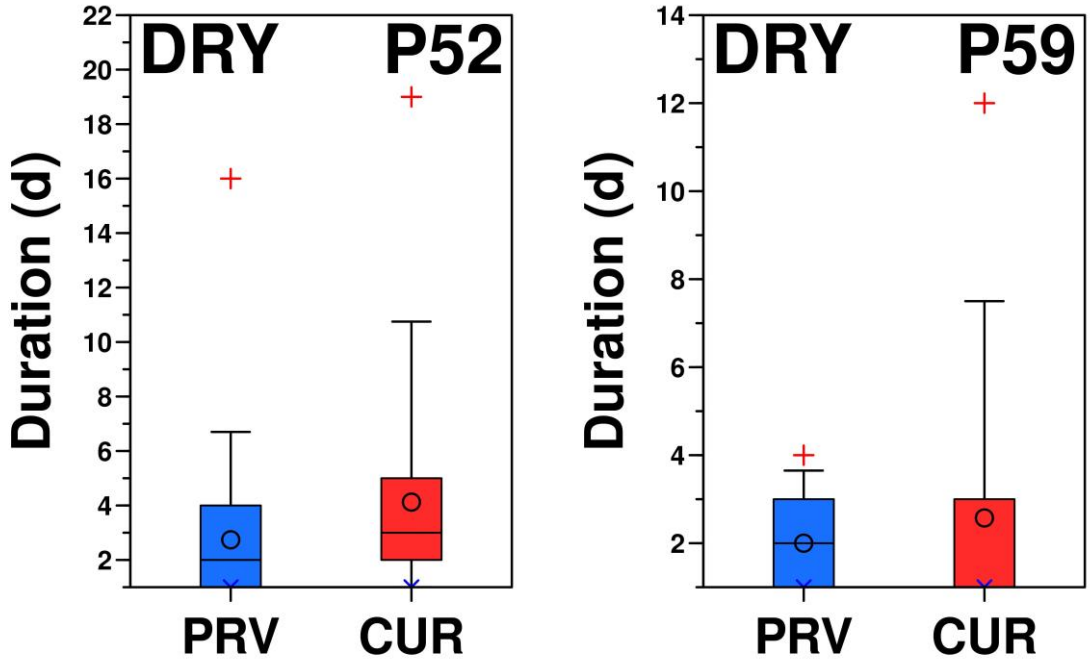


Figure 3 Duration of dry-season $PM_{2.5}$ event at each station by standard. For each box, the top, middle, and bottom lines mark the 75th, 50th (median), and 25th percentiles, respectively, and the circle is the mean. The red and blue symbols are the maximum and minimum, respectively.

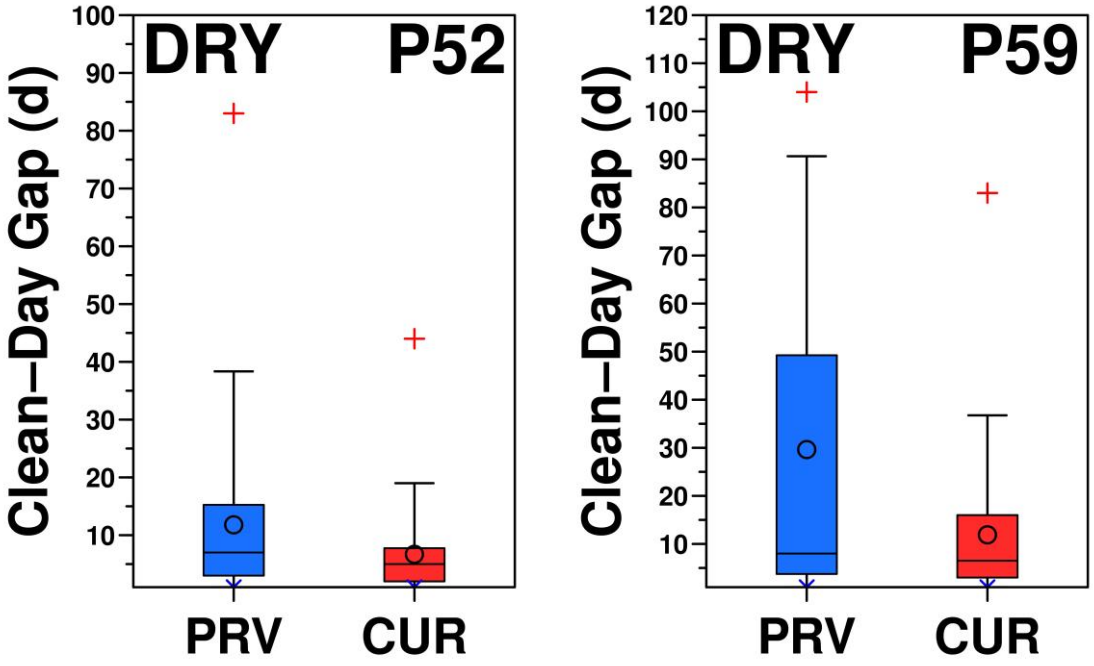
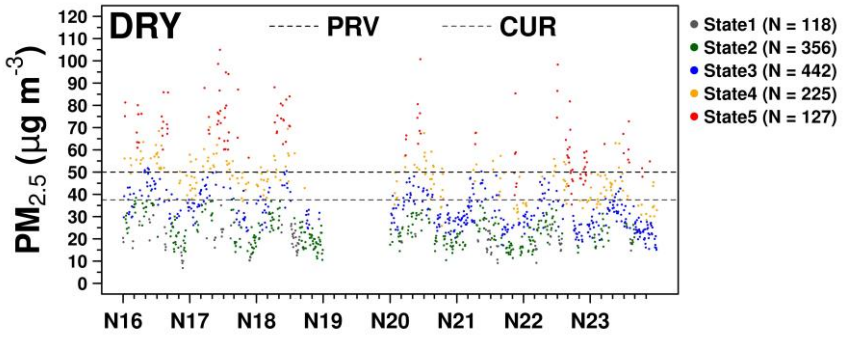


Figure 4 Dry-season clean-day gap at each station by standard.

a) P52



b) P59

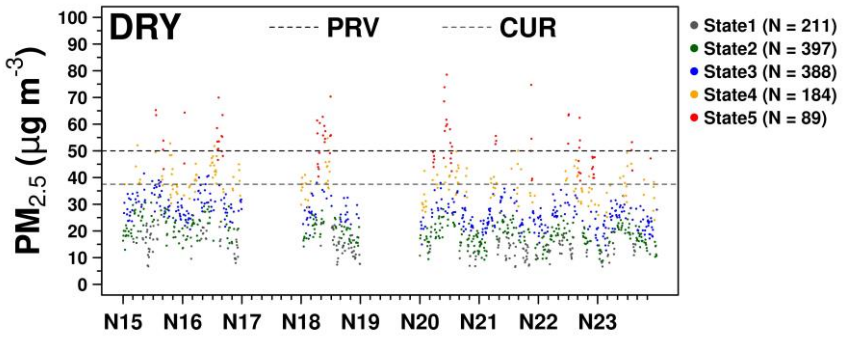
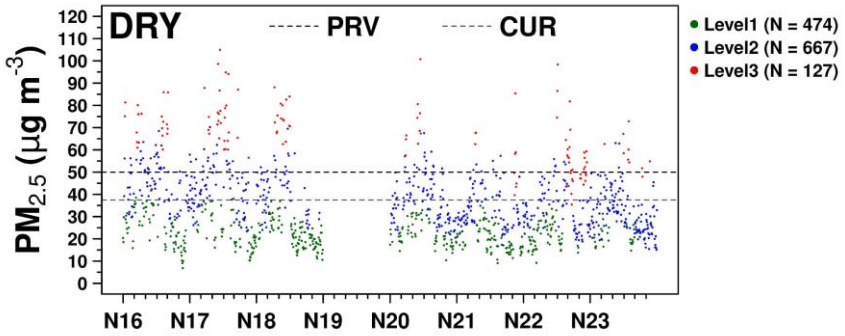


Figure 5 Daily $PM_{2.5}$ time series in dry season by five states

a) P52



b) P59

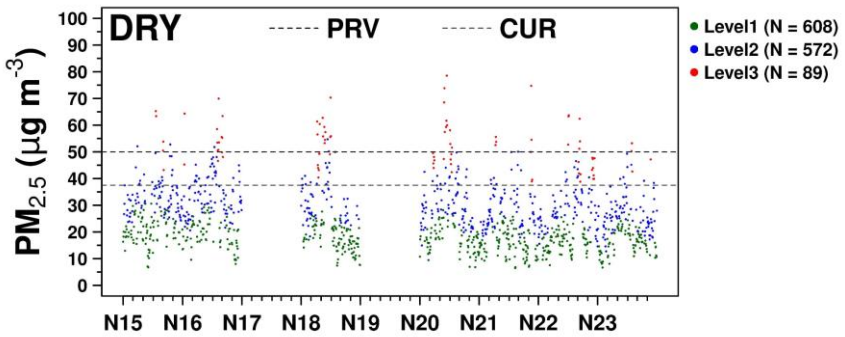


Figure 6 Daily $PM_{2.5}$ time series in dry season by pollution level at each station.

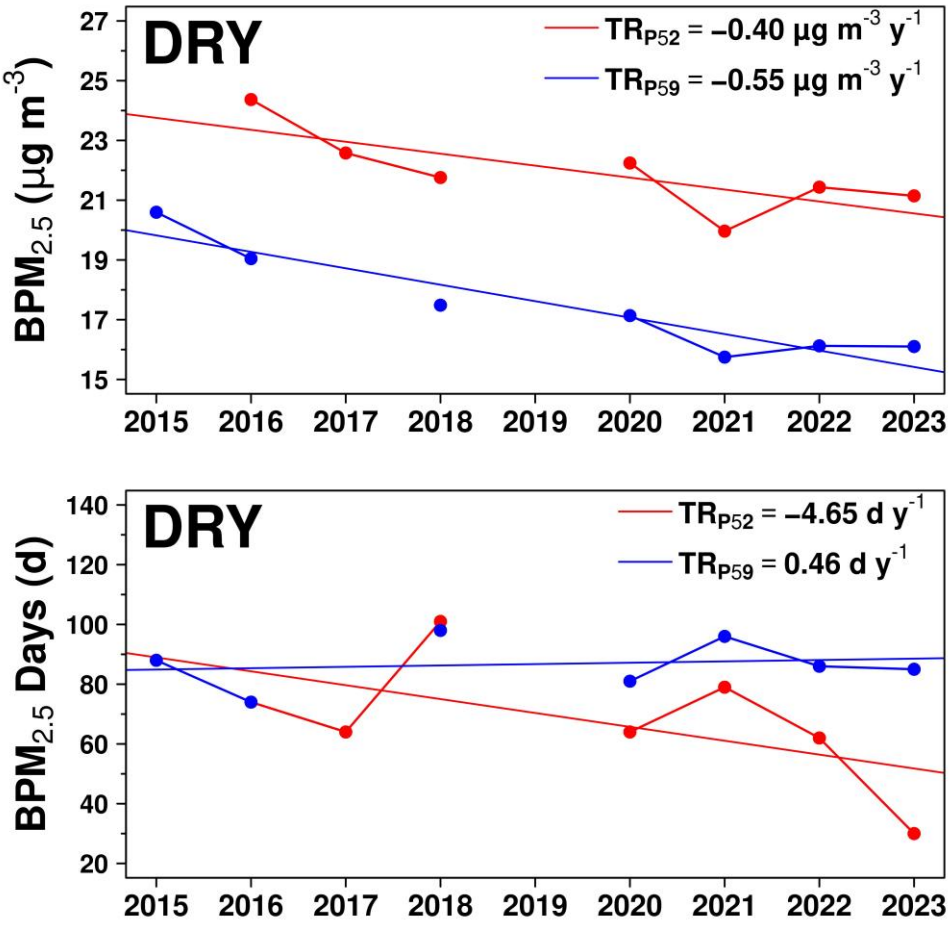


Figure 7 Trends in dry-season $BPM_{2.5}$ (top) and $BPM_{2.5}$ days (bottom) at each station.

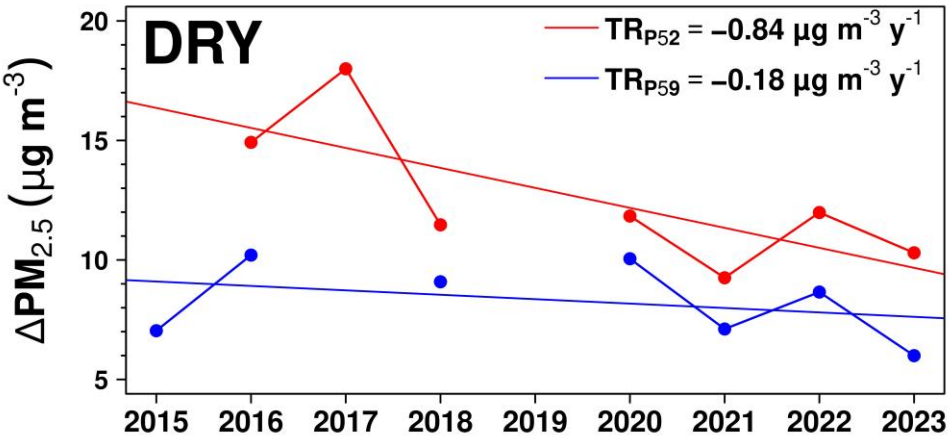


Figure 8 Trends in dry-season $\Delta PM_{2.5}$ (average $PM_{2.5}$ - average $BPM_{2.5}$) at each station.

ACKNOWLEDGEMENTS

The authors thank the Pollution Control Department for the provided air quality data. This study is part of ongoing research supported by the Joint Graduate School of Energy and Environment. The first author has received a postdoctoral fellowship from King Mongkut's University of Technology Thonburi.

REFERENCES

[1] NEB. 2022. Designation of Ambient $PM_{2.5}$ Standards. National Environmental Board (in Thai).
[2] WHO. 2021. WHO Global Air Quality Guidelines. World Health Organization.
[3] WHO. 1980. Glossary on Air Pollution. World Health Organization.
[4] Martín-Cruz, Y., Vera-Castellano, A., G´omez-Losada, A. 2020. Characterization of background particulate matter concentrations using the combination of two clustering techniques in zones with heterogeneous emission sources. Atmospheric Environment, 243; 117832.
[5] Aman, N., Manomaiphiboon, K., Pala-En, N., Devkota, B., Inerb, M., Kokkaew, E. 2023. A study of urban haze and its association with cold surge and sea breeze for Greater Bangkok. International Journal of Environmental Research and Public Health. 20; 3482.
[6] Yevjevich, V.M. 1967. An objective approach to definitions and investigations of continental hydrologic droughts. Hydrology Paper No. 23, Colorado State University, US.
[7] Rizos, K., Meleti, C., Kouvarakis, G., Mihalopoulos, N., Melas, D. 2022. Determination of the background pollution in the Eastern Mediterranean applying a statistical clustering technique. Atmospheric Environment. 276; 119067.

20R3-05

Evaluating GHG Emissions in 3D Printed House Using a Life Cycle Assessment

Hein Htet Zaw[1*], and Achariya Suriyawong[2]

[1*]*Master student, Department of Environmental and Sustainable Engineering, Faculty of Engineering, Chulalongkorn University, Bangkok 10330, Thailand.*
E-mail: heinhtetzaw31101997@gmail.com
[2]*Asst. Professor, Department of Environmental and Sustainable Engineering, Faculty of Engineering, Chulalongkorn University, Bangkok 10330, Thailand.*
E-mail: Achariys.S@Chula.ac.th

ABSTRACT

This research examines CO_2 emissions linked to the use of 3D printing in constructing a single building, with a focus on carbon dioxide (CO_2) emissions. The purpose is to evaluate the environmental impact of 3D printed buildings using a Life Cycle Assessment approach that spans from material sourcing to onsite assembly. Emissions from raw material production, energy consumption during construction, and transportation activities were quantified. The results reveal that raw material production, particularly the use of cement-based materials, contributes the most to GHG emissions, followed by energy consumption and transportation. The results emphasize the need for selecting eco-friendly materials and adopting energy-conscious construction techniques. This study provides valuable insights into the environmental implications of 3D printing in construction and serves as a foundation for future research on optimizing sustainability in this emerging field.

Keywords: 3D printing, greenhouse gas emissions, carbon footprint, life cycle assessment (LCA), sustainable construction, environmental impact

1. INTRODUCTION

Globally, the construction industry is responsible for approximately 40% of energy use and 30% of greenhouse gas emissions, highlighting its critical role in sustainability [1]. As the demand for sustainable development increases, new technologies such as 3D printing have emerged as potential solutions to reduce the environmental impact of the construction sector. 3D printing, also known as additive manufacturing, constructs structures by layering materials based on digital designs, allowing for customized and precise architecture, and compared to conventional construction, 3D printing can significantly cut down on material use, reduce build time, and accommodate intricate architectural features [2]. 3D printing technology holds the potential to address the growing need for more sustainable and efficient construction practices by optimizing material usage and reducing energy consumption during the construction phase [3].

Despite these potential benefits, the environmental implications of 3D printing in construction are not fully understood, particularly regarding its contribution to CO_2 emissions. While some studies have explored the potential energy savings and waste reduction associated with 3D printed buildings, there remains a significant gap in research when it comes to a holistic life cycle assessment (LCA) of technology's environmental impact. Most prior research centers on material innovations and the technical development of 3D printing applications in the construction sector [4], but comprehensive studies analyzing GHG emissions, including embodied carbon, during the entire life cycle of a 3D printed building are limited [5]. Due to limited data, it remains challenging to quantify the potential of 3D printing in lowering carbon emissions in the construction sector, particularly in large-scale projects such as multi-story buildings.

This research aims to fill this gap by evaluating the GHG emissions associated with the construction of a single building using 3D printing technology. The study applies a cradle-to-onsite construction life cycle assessment (LCA) framework to quantify CO_2 emissions arising from three major phases of the construction process: raw material production, energy consumption during construction, and transportation activities. This approach will provide a comprehensive understanding of the carbon footprint of 3D printed buildings and identify areas for improvement in reducing emissions.

The findings contribute to the growing discourse on low-carbon construction technologies and offer valuable insights for stakeholders seeking to implement environmentally responsible building practices. By

focusing exclusively on 3D printed structures, this research highlights the unique challenges and potentials of this emerging construction method within the broader context of sustainable development goals.

2. LITERATURE REVIEW

The use of 3D printing in construction has evolved significantly over the past decade, transforming from a conceptual technology into a viable method for building structures. This technique involves building components layer-by-layer from digital models, a hallmark of additive manufacturing in the construction industry, which in the context of construction, includes houses and buildings [6]. In construction, 3D printing supports faster build cycles, reduced resource waste, and the creation of complex, bespoke forms with greater resource efficiency [7].

However, despite these benefits, 3D printing in construction also presents various challenges, particularly concerning its environmental impact. One of the main concerns is the energy consumption associated with the printing process. The curing and setting stages of cement-based 3D printing require considerable energy, contributing to high overall energy use [8]. This energy use can lead to high CO_2 emissions if powered by non-renewable energy sources. The materials commonly used in 3D printing, such as concrete and polymers, often have high embodied carbon content, which may negate the environmental benefits gained from reduced material waste [9]. Thus, while 3D printing offers the potential for reducing material waste, its overall environmental benefit must be assessed more thoroughly to understand its full impact on greenhouse gas emissions.

This study aims to quantify CO_2 emissions generated during the construction of a 3D printed residential structure by applying a Life Cycle Assessment (LCA) methodology, following a cradle-to-onsite construction framework, focusing on key stages such as raw material production, energy use, transportation, and waste generation. Emission factors from the IPCC will be used for accuracy, and transportation emissions will be estimated based on material quantities, distance, and transport modes. Results will be compared with conventional construction data to assess the carbon footprint of 3D printed buildings and identify opportunities for environmental improvement.

2.1. Life Cycle Assessment (LCA) in Construction

Life Cycle Assessment (LCA) is a widely used methodology to assess the environmental impacts of a product or process from its inception to its end-of-life (ISO 14040, 2006). In the construction industry, LCA has been applied to evaluate the environmental impacts of buildings, focusing on key factors such as energy use, material sourcing, waste generation, and emissions [10]. The use of LCA in construction has enabled researchers to identify the most impactful stages of a building's life cycle, highlighting areas where interventions can reduce carbon footprints [11].

In the realm of 3D printing, Life Cycle Assessment (LCA) serves as a valuable framework for evaluating environmental impacts across various stages of construction. Multiple studies have applied LCA methodologies to 3D printed buildings, aiming to quantify CO_2 emissions related to raw material extraction, energy use during production, and waste generation. These findings highlight the importance of adopting a cradle-to-site approach to comprehensively assess the environmental implications of 3D printed structures, as illustrated in the following figure [12].



Figure 1 LCA Perspective in 3D Printed Building Construction

3. METHODOLOGY

This study employs a cradle-to-onsite construction Life Cycle Assessment (LCA) approach, which evaluates the environmental impact of a building from the extraction of raw materials through to the construction phase. The cradle-to-onsite method is particularly suitable for this research as it focuses on the carbon emissions associated with the production, transportation, and use of materials in the construction of a 3D printed house, while excluding the operational phase (post-construction). This framework allows for a detailed analysis of emissions during critical construction stages, ensuring a comprehensive understanding of the carbon footprint of 3D printed buildings (ISO 14040, 2006). To provide a comprehensive understanding of the environmental impact, a comparative analysis is included, contrasting the emissions of 3D-printed houses with previous studies of conventional construction. Additionally, limitations of the study include potential deviations in real-world construction practices, variations in material properties based on supplier specifications, and the exclusion of indirect emissions from equipment manufacturing or workforce transportation. The scope of the research is as follows:

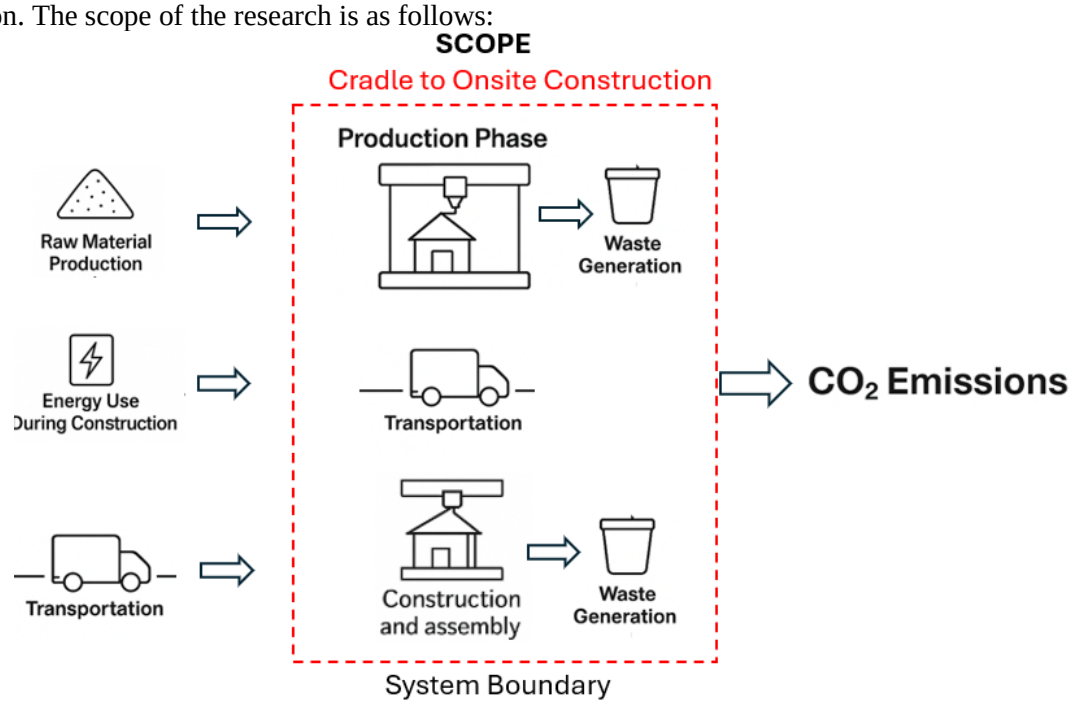


Figure 2 Scope of the Study

3.1. Data Collection

Data for this study was gathered from a variety of sources to quantify the emissions at each stage of the construction process. Key data points include:

- **Material Quantities**: The quantities of raw materials used in the construction, such as concrete, metals, and polymers, were based on the building design and industry-standard material specifications.
- **Energy Consumption**: The energy required during the construction process, including the operation of 3D printing equipment, was estimated using the power consumption data of typical 3D printing systems.
- **Transportation**: Emission factors for transportation were calculated based on the quantity of materials, the distance between production sites and the construction site, and the mode of transport.
- **Waste Generation**: Data on material waste generated during the printing process was collected from manufacturers and industry reports on 3D printing in construction.

3.3. Functional Unit

The functional unit of this study is defined as the construction of a single 3D printed residential building. Carbon dioxide (CO_2) emissions are quantified in kilograms per square meter of building area (kg CO_2/m^2) to ensure consistency and comparability. This unit of measurement allows for the normalization of emissions across various phases of construction and building configurations, providing a standardized basis for evaluating the environmental impact of 3D printed construction.

3.4. Emission Factors

To calculate the CO_2 emissions for each category (material production, energy consumption, and transportation), standard emission factors are applied. These emission factors are derived from industry database IPCC guidelines [13, 14] and relevant literature on CO_2 emissions from construction activities :

Table 1 Emission Factors for Construction Activities and Waste Generation

Category	Emission Factor	Unit	Source
Material Production	Cement Production: 0.9 kg CO_2/kg cement produced	kg CO_2/kg	IPCC 2006 Guidelines, Volume 2, Chapter 2
	Steel Production: 1.8 kg CO_2/kg steel produced	kg CO_2/kg	IPCC 2006 Guidelines, Volume 3, Chapter 2
Energy Consumption	Electricity (average): 0.233 kg CO_2/kWh	kg CO_2/kWh	IPCC 2006 Guidelines, Volume 2, Chapter 2
	Diesel Fuel Combustion: 2.68 kg CO_2/liter	kg CO_2/liter	IPCC 2006 Guidelines, Volume 2, Chapter 2
Transportation	Heavy-Duty Truck (diesel): 0.15 kg CO_2/ton-km	kg CO_2/ton-km	IPCC 2006 Emission Factor Database
	Light-Duty Truck (diesel): 0.12 kg CO_2/ton-km	kg CO_2/ton-km	IPCC 2006 Emission Factor Database 2006
Waste Generation	Landfill Disposal (general): 0.25 kg CO_2/kg waste	kg CO_2/kg	IPCC 2006 Guidelines, Volume 5
	Recycling (general): -0.15 kg CO_2/kg waste	kg CO_2/kg	IPCC 2006 Guidelines, Volume 5
3D Printing Waste [15]	Material Waste during Printing: 0.05 kg CO_2/kg print material	kg CO_2/kg	Ferro et al., 2021
	Recycling 3D Printed Material: -0.10 kg CO_2/kg material	kg CO_2/kg	Ferro et al., 2021

3.5. Calculation for Carbon Footprint

To calculate the CO_2 emissions for each category (material production, energy consumption, and transportation), standard emission factors were applied. These calculation formulas and emission factors were derived from industry database IPCC guidelines and relevant literature on CO_2 emissions from construction activities.

3.5.1. Material Production Emissions

For 3D printed construction method, the CO_2 emissions from material production were calculated using the following formula [13]:

$$EC = \sum (Q_i \times EF_i) \quad (1)$$

Where:

- EC: Embodied Carbon (kg CO_2)
- Q_i: Quantity of material i (kg)
- EF_i: Emission factor for material i (kg CO_2/kg)

Emission Factors [14, 15]:

- Cement: 0.87 kg CO_2 per kg
- Steel: 1.77 kg CO_2 per kg
- Aggregates: 0.048 kg CO_2 per kg
- Timber: 0.25 kg CO_2 per kg

The emissions for each material are calculated by multiplying the quantity used in the construction by the corresponding emission factor.

3.5.2. Energy Consumption Emissions

Energy consumption during construction operations, including concrete mixing, material handling, and machinery operations, was calculated as follows [13]:

$$EE = V \times ECu \times EFe \quad (2)$$

Where:

- EE: Energy Emissions (kg CO_2)
- V: Concrete volume (m^3)
- ECu: Energy consumption per unit volume (kWh/m^3) = 80 kWh/m^3 [16]
- EFe: Emission factor of electricity (kg CO_2/kWh)

3.5.3. Transportation Emissions

Transportation emissions were calculated using the formula [17]:

$$TE = M \times D \times EFt \quad (3)$$

Where:

- TE: Transportation Emissions (kg CO_2)
- M: Mass of material transported (tons)
- D: Distance (km) = 100 km
- EFt: Emission factor (kg CO_2/ton-km)

Emission Factors:

- Heavy-duty truck (diesel): 0.15 kg CO_2/ton-km [18]
- Light-duty truck (diesel): 0.12 kg CO_2/ton-km [19]

3.5.4. Total Emissions

The total CO_2 emissions for the construction process are derived by summing the emissions from material production, energy consumption, and transportation.

$$TE_{total} = EC + EE + TE \quad (4)$$

Where:

- TE_{total}: Total Emissions (kg CO_2)
- EC: Emissions from material production
- EE: Emissions from energy consumption
- TE: Emissions from transportation

For the 3D printed building method, the total emissions calculation will include the sum of emissions from materials, energy consumption, and transportation, based on the specific quantities and construction processes involved in 3D printing. Emission factors will be applied to each category such as material production, energy use during construction, and transportation which use data specific to the 3D printing method, ensuring a comprehensive assessment of the environmental impact.

4. RESULTS AND DISCUSSIONS

The study quantifies the CO_2 emissions associated with the construction of a single 3D printed building. The emissions were assessed across four key categories: Construction, Raw Materials, Transportation, and Energy Consumption. The results are summarized in the table below:

Table 1 Results of Embodied Carbon

Type	Construction (kg of CO_2)	Product			Waste Generation (kg of CO_2)	Total Carbon Emission (kg of CO_2)
		Raw Materials (kg of CO_2)	Transportation (kg of CO_2)	Energy Consumption (kg of CO_2)		
3D Printed (Single)	11,200.83	37,274.43	2,763.83	8,428.50	233.05	59,900.64

The total carbon emissions from the construction of a single 3D printed building amounted to 59,900.64 kg of CO_2, comprising emissions from onsite construction activities, raw material production, energy consumption, transportation, and waste generation. Onsite construction contributed 11,200.83 kg CO_2, a relatively low figure due to the efficiency of 3D printing, which reduces labor requirements and minimizes material waste through precise deposition. In contrast, emissions from raw materials were significantly higher, totaling 37,274.43 kg CO_2, largely due to the intensive use of cement is a major contributor to carbon emissions despite the material efficiency of the printing process. Transportation-related emissions were moderate at 2,763.83 kg CO_2, reflecting the reduced need for material movement compared to traditional methods, although the transportation of heavy equipment and essential construction inputs remained necessary. Energy consumption during construction generated 8,428.50 kg CO_2, primarily from the operation of printing machinery and support equipment. While more efficient than conventional construction, the energy demand of 3D printing still presents an area for improvement. Overall, despite its advantages in material efficiency and waste reduction, the 3D printing process is still heavily impacted by emissions from cement-based raw materials, underscoring the need for sustainable alternatives in future applications. The comparison table is presented as follows:

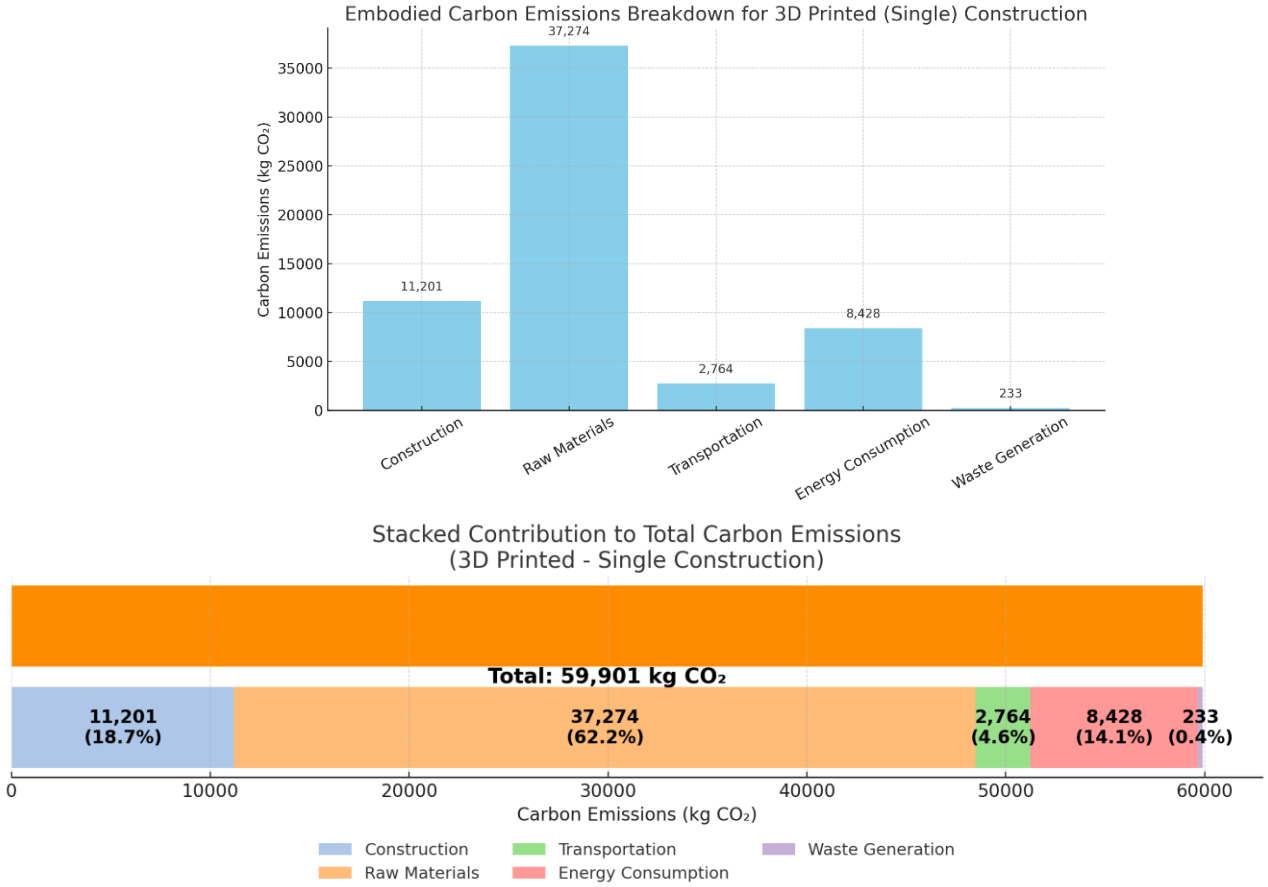


Figure 3 Comparison of Various Parameters in 3D Printed Construction (kg CO_2)

4.6. Comparison with Conventional Methods

In comparison, conventional concrete and steel construction emits 100,000–150,000 kg CO_2, with 60–70% attributed to cement and steel production by Tongwane (2015) and Drewniok (2023) [20, 21]. While 3D printing reduces emissions through efficient material use and on-site fabrication, its high cement content remains a major carbon source by Han (2021) [5].

Energy emissions from 3D printing (8,428.50 kg CO_2) are lower than those in conventional construction, which involves energy-intensive processes like batching, mixing, and steel fabrication. Cement alone contributes about 8% of global CO_2 emissions (IPCC, 2006) [13]. Nonetheless, large-scale 3D printers still require significant energy input.

Transportation emissions (2,763.83 kg CO_2) are minimized with 3D printing due to on-site production, whereas conventional methods can attribute 10–20% of lifecycle emissions to transportation by Sandanayake (2017) [22].

Waste emissions from 3D printing are also lower (233.05 kg CO_2), thanks to precise deposition, compared to conventional practices that waste up to 20% of materials by Ferro (2022) [15].

Both methods are challenged by cement's carbon footprint, but ongoing research into low-carbon binders and recycled materials offers promising pathways for emissions reduction by Machado (2025) [23].

CONCLUSION

This study presents a comprehensive Life Cycle Assessment (LCA) of CO_2 emissions associated with the construction of a single 3D-printed building. The results show that the raw materials phase is the largest contributor to CO_2 emissions, followed by energy consumption and transportation, with total emissions amounting to 59,900.64 kg. These findings highlight the importance of developing strategies to reduce the environmental impact of 3D-printed buildings, particularly by addressing emissions from material sourcing, energy use, and transportation. While 3D printing demonstrates advantages in efficiency and waste reduction, its sustainability potential hinges on further advancements in material selection, the use of renewable energy, and transportation logistics. Compared to conventional construction methods, 3D printing can significantly reduce CO_2 emissions due to reduced formwork, lower labor requirements, and decreased transportation needs. The insights from this study contribute to the growing body of research on the sustainability of 3D-printed buildings and offer guidance for future efforts to reduce the carbon footprint of construction, supporting the transition to more eco-friendly and energy-efficient building practices.

ACKNOWLEDGEMENT

I would like to express my sincere gratitude to all those who contributed to this study. A special acknowledgment goes to EEAT for their invaluable support in organizing the conference, providing a platform to share and discuss these findings. Finally, I am grateful for the resources and tools that made this study possible.

REFERENCE

[1] R. T. Masyhur, A. H. Alias, N. A. Haron, and Z. Zulkafli, "A systematic review on green practices in the Malaysian construction industry: Status, challenges, key motivations, rating systems and technology evolution," *Energy and Buildings,* p. 114550, 2024.

[2] M. Khan and C. McNally, "Recent developments on low carbon 3D printing concrete: Revolutionizing construction through innovative technology," *Cleaner Materials,* p. 100251, 2024.

[3] M. Sovetova and J. K. Calautit, "Thermal and energy efficiency in 3D-printed Buildings: Review of geometric Design, materials and printing processes," *Energy and buildings,* p. 114731, 2024.

[4] A. Hassan, T. Alomayri, M. F. Noaman, and C. Zhang, "3D Printed Concrete for Sustainable Construction: A Review of Mechanical Properties and Environmental Impact," *Archives of Computational Methods in Engineering,* pp. 1-31, 2025.

[5] Y. Han, Z. Yang, T. Ding, and J. Xiao, "Environmental and economic assessment on 3D printed buildings with recycled concrete," *Journal of Cleaner Production,* vol. 278, p. 123884, 2021.

[6] I. Akhrif, F. Z. Oulkhir, M. El Jai, N. Rihani, N. C. Igwe, and S. E. Baalal, "Earth-based materials 3D printing, extrudability and buildability numerical investigations," *Progress in Additive Manufacturing,* pp. 1-33, 2025.

[7] D. Dey, B. Panda, Y. Shukla, and R. Rawal, "A comprehensive assessment of thermal performance of 3D printed concrete lattice walls," *Progress in Additive Manufacturing,* pp. 1-18, 2025.

[8] T. Zat, S. L. Schuster, E. S. Duarte, N. D. F. Daudt, R. C. D. Cruz, and E. D. Rodríguez, "Rheological properties of high-performance concrete reinforced with microfibers and their effects on 3D printing process," *Journal of Building Engineering,* p. 112406, 2025.

[9] J. A. Martínez-Sánchez, F. Comino, P. E. Romero, and M. R. de Adana, "Design, development and performance evaluation of a 3D-printed desiccant wheel using poly-lactic acid and wood filaments for sustainable HVAC systems," *Building and Environment,* p. 112889, 2025.

[10] L. J. Hurst and T. S. O'Donovan, "Embodied impacts of key materials for UK decarbonised domestic retrofit: Differences between sources of embodied carbon and embodied energy data," *Energy and Buildings,* vol. 319, p. 114515, 2024.
[11] H. Xu, J. I. Kim, and J. Chen, "Improved framework for estimating carbon emissions from prefabricated buildings during the construction stage: life cycle assessment and case study," *Building and Environment,* p. 112599, 2025.
[12] H. Hosamo, G. B. Coelho, E. Buvik, S. Drissi, and D. Kraniotis, "Building sustainability through a novel exploration of dynamic LCA uncertainty: Overview and state of the art," *Building and Environment,* p. 111922, 2024.
[13] H. Eggleston, L. Buendia, K. Miwa, T. Ngara, and K. Tanabe, "2006 IPCC guidelines for national greenhouse gas inventories," 2006.
[14] I. Change, "2006 IPCC guidelines for national greenhouse gas inventories," *Institute for global environmental strategies, Hayama, Kanagawa, Japan,* 2006.
[15] D. Falliano, L. Restuccia, and G. A. Ferro, "Biochar addition for 3DCP: a preliminary study," *Procedia Structural Integrity,* vol. 41, pp. 699-703, 2022.
[16] C. Orozco, S. Tangtermsirikul, T. Sugiyama, and S. Babel, "Examining the endpoint impacts, challenges, and opportunities of fly ash utilization for sustainable concrete construction," *Scientific reports,* vol. 13, no. 1, p. 18254, 2023.
[17] I. Ipcc, "Guidelines for national greenhouse gas inventories," *Prepared by the National Greenhouse Gas Inventories Programme. Eggleston HS, Buendia L, Miwa K, Ngara T, Tanabe K, editors. Published: IGES, Japan,* 2006.
[18] X. Song *et al.*, "Carbon emissions in China's steel industry from a life cycle perspective: Carbon footprint insights," *Journal of Environmental Sciences,* vol. 148, pp. 650-664, 2025.
[19] F. Tornese, A. L. Carrano, B. K. Thorn, J. A. Pazour, and D. Roy, "Carbon footprint analysis of pallet remanufacturing," *Journal of Cleaner Production,* vol. 126, pp. 630-642, 2016.
[20] M. Tongwane, S. Piketh, L. Stevens, and T. Ramotubei, "Greenhouse gas emissions from road transport in South Africa and Lesotho between 2000 and 2009," *Transportation Research Part D: Transport and Environment,* vol. 37, pp. 1-13, 2015.
[21] M. P. Drewniok *et al.*, "Mapping material use and embodied carbon in UK construction," *Resources, Conservation and Recycling,* vol. 197, p. 107056, 2023.
[22] M. Sandanayake, G. Zhang, S. Setunge, W. Luo, and C.-Q. Li, "Estimation and comparison of environmental emissions and impacts at foundation and structure construction stages of a building–A case study," *Journal of cleaner production,* vol. 151, pp. 319-329, 2017.
[23] N. B. Machado, J. D. Silvestre, and R. A. Bohne, "Embodied GHG emissions of reinforced concrete and timber structures: Relevance, driving factors and target values," *Building and Environment,* vol. 275, p. 112753, 2025.

20R3-06

The Relationship between The $PM_{2.5}$ Concentrations Correlated with The Meteorological Data Recorded from The Super King Air 350 Aircraft: The Case Study Covers from January 27 to February 7, 2025

Aniruj Akkarapongtrakul[1*] Thanakorn Serisakulthorn[1] Phayuhaphon Chitcharoen[2] Warit Planthong[2] Chanti Detyothin[3] Marut Ratmanee[4] Paweena Wessapak[1] Sirirat Sula[1] Chaiyaphorn Nilarat[1] Chadayu Nooddaeng[5] Anuphong Soksai[5] Sivarot Putponpai[5] and Thanakrit Wongta[5]

[1]Scientist, Department of Royal Rainmaking and Agricultural Aviation, Bangkok 10900, Thailand*
[1]Scientist, Department of Royal Rainmaking and Agricultural Aviation, Bangkok 10900, Thailand
[2]Rain making pilot, Department of Royal Rainmaking and Agricultural Aviation, Bangkok 10900, Thailand
[3]Expert on applied atmospheric science Research and Development, Department of Royal Rainmaking and Agricultural Aviation, Bangkok 10900, Thailand
[4]Director of Information Technology Center, Department of Royal Rainmaking and Agricultural Aviation, Bangkok 10900, Thailand
[5]Electrician, Department of Royal Rainmaking and Agricultural Aviation, Bangkok 10900, Thailand
[*]Phone : 089 436 1516, E-mail : akkarapongtrakul.a@gmail.com

ABSTRACT

This research focused on the concentration of fine particulate matter with a diameter less than 2.5 micrometers ($PM_{2.5}$) in the vicinity of Don Mueang Airport, Bangkok, at altitudes up to 3000 meters (approximately 10000 feet). The study connected the amounts of $PM_{2.5}$ to weather factors such as air pressure, temperature, wind speed, and wind direction, using a Super King Air 350 aircraft. The data was collected during an elevation rate of 5 meters per second from January 29 to February 7, 2025 (0400 UTC), and on February 1-2, 2025, at 1700 UTC. The results indicated that the average $PM_{2.5}$ level at the ground reached 68.2 µg/m³ on January 31, 2025, while the concentration measured from the SKA aircraft was 5615 #/cm³. The pattern of fluctuations in $PM_{2.5}$ particulate matter on the surface is evident. The readings obtained from ground stations and research aircraft are congruent. Furthermore, during the night, $PM_{2.5}$ particulate matter concentrations are 18–34 percent lower than those observed during the day. Dust concentration often diminishes with increasing altitude. Furthermore, atmospheric dust in the Bangkok region is prevalent below 1500 meters, with temperature inversions rising by 1 °C to 4 °C with height, while elevated air pressure tends to augment surface dust concentration. The wind predominantly blows from the southeast during the day and from the northeast at night. The wind speed during the day mostly ranges from 4 to 8 m/s, accounting for 52 %, while at night, it is lighter, ranging from 2 to 4 m/s, accounting for 48 % of the surface-level wind measurements at 3000 meters. Moreover, wind velocity influences the fluctuations in dust levels. The research shows that the amount of $PM_{2.5}$ particles measured from January 29 to February 7, 2025, matches the levels found by the research aircraft and the weather conditions.

Keywords : Department of Royal Rainmaking and Agricultural Aviation, $PM_{2.5}$, Passive Cavity Aerosol Spectrometer Probe, Super King Air 235 Aircraft, Meteorology

INTRODUCTION

Due to its small size and ability to get into the respiratory system, $PM_{2.5}$, or fine particulate matter with an aerodynamic diameter of 2.5 micrometers, is a major air quality issue. $PM_{2.5}$ is emitted by both natural and anthropogenic sources, including fossil fuel combustion and biomass burning. [1-4]

Meteorological factors heavily influence variations in air quality. Many places only have air quality issues during certain seasons or days. Recently, the impact of $PM_{2.5}$ dust during the northeast monsoon, which brings cold and dry air from China during early November to mid-November, has been characterized by elevated air pressure and reduced temperature. Furthermore, high pressure impedes the buoyancy of air masses, resulting in dust particles that do not disperse freely from their origin. Furthermore, as high air pressure diminishes, the reduced wind velocity results in the dust particles' travel being slower than usual. This has led to severe smog in Bangkok and its surrounding areas. This smog is caused by fine particulate matter pollution, biomass burning, and particulate matter pollution from other human activities [5-7], as well as extensive burning in neighboring countries during winter. Even when the emissions of air pollutants don't fluctuate greatly, the smog persists. Residents of the Bangkok Metropolitan Region, Thailand, have long

encountered issues related to particulate matter. Researchers have identified it as a pivotal region for $PM_{2.5}$-related concerns within the Bangkok Metropolitan Region [8]. Numerous research studies examine the $PM_{2.5}$ particulate matter concentrations in Bangkok and surrounding areas. Most studies examine the quantity of dust particles, their concentrations, and the chemical compounds that contribute to fine particulate matter, which impacts the health of many Bangkok residents. However, there is currently no research conducted in Thailand that assesses the distribution of dust and quantifies its concentration at varying altitudes.

Measurements of aerosol concentration and size distribution must be precise to investigate how atmospheric aerosols affect the climate and human health. Through light scattering, the Passive Cavity Aerosol Spectrometer (PCASP) is a very sensitive tool for finding out the concentration and size of aerosols [8].

The Department of Royal Rainmaking and Agricultural Aviation has additional missions. The department not only conducts royal rainmaking operations but also gathers swift and precise data on the impact of small dust particles ($PM_{2.5}$) on public health in Thailand. The department achieves such goals through research and study. It has examined meteorological data at 0400 UTC daily from January 27 to February 7, 2025, and at 1700 UTC on February 1 and 2, 2025, at Don Mueang international airport, as well as instruments for measuring $PM_{2.5}$ particles. The team operates an SKA aircraft equipped with a PCASP probe to monitor particulate matter less than 2.5 micrometers in diameter for targeted research purposes. This research seeks out how many and what sizes of particles between 0.1 and 2.5 micrometers are present in Bangkok and nearby areas up to 10000 feet (about 3000 meters) high so we can compare these amounts with readings from ground stations and look at weather data to see if there are any connections during air quality measurements taken from January 29 to February 7, 2025.

METHODOLOGY

This research looked at weather data to see how it relates to the increase of $PM_{2.5}$ particles in Bangkok and nearby areas from January 29 to February 7, 2025, using Super King Air 350 aircraft No. 2012. The aircraft departed from Hua Hin Airport in Prachuap Khiri Khan Province at 0300 UTC to assess the dimensions of particulate matter smaller than 2.5 micrometers, executing a touch-and-go navigation at Don Mueang airport at 0400 UTC. Subsequently, it took off from U-Tapao Airport for another touch-and-go at 1700 UTC, ascending at a rate of 1000 feet per minute (5 m/s) while crossing the regions of Bangkok, Nonthaburi, Nakhon Pathom, Samut Sakhon, and Samut Songkhram, operating at altitudes exceeding 10000 feet to investigate the concentration and vertical distribution of dust particles. The PCASP sensor checks how many $PM_{2.5}$ dust particles are in the air and on the ground, finding particles that are between 0.1 and 3 micrometers. It also gathers important weather information from the AIMMS sensor, like air pressure, humidity, temperature, wind speed, and wind direction. Select particles smaller than 2.5 micrometers to match with the weather data collected, and then compare the measurements from the day (0400 UTC) and night (1700 UTC). Select particles smaller than 2.5 micrometers to ensure alignment with the recorded meteorological data, then compare measurements taken throughout the day (0400 UTC) and night (1700 UTC).

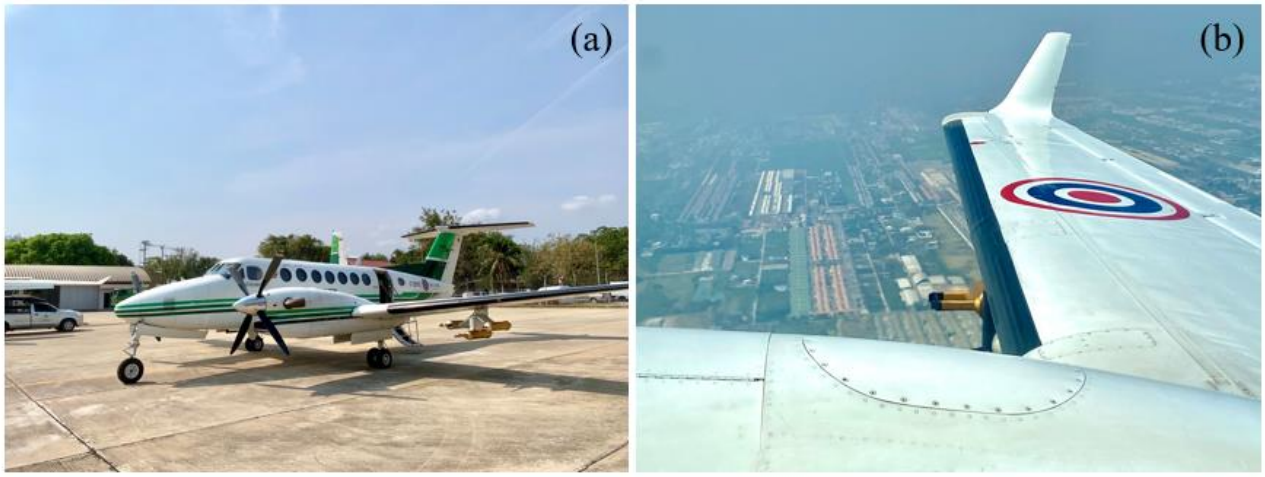


Figure 1. (a) The Super King Air 350 aircraft before the particle assessment operation and meteorological data, Hua Hin District, Prachuap Khiri Khan Province. (b) The PCASP sensor measures parameters at an altitude of 2000 feet above Bangkok and its surroundings

RESULTS AND DISCUSSIONS

The information gathered from the Super King Air 350 aircraft in Bangkok, which looked at the levels of small particles ($PM_{2.5}$) and weather data, matched the $PM_{2.5}$ dust readings from 7 stations close to Don Mueang Airport. The distribution of dust captured within the passenger compartment of the research aircraft are observable both during the daytime (Figure 2(a)) and at night (Figure 2(b)).



Figure 2 shows the distribution of particulate matter in the atmosphere over Bangkok and in the air on February 1, 2025. (a) daytime (0400 UTC), altitude 4000 feet, and (b) nighttime (1700 UTC), at 3000 feet.

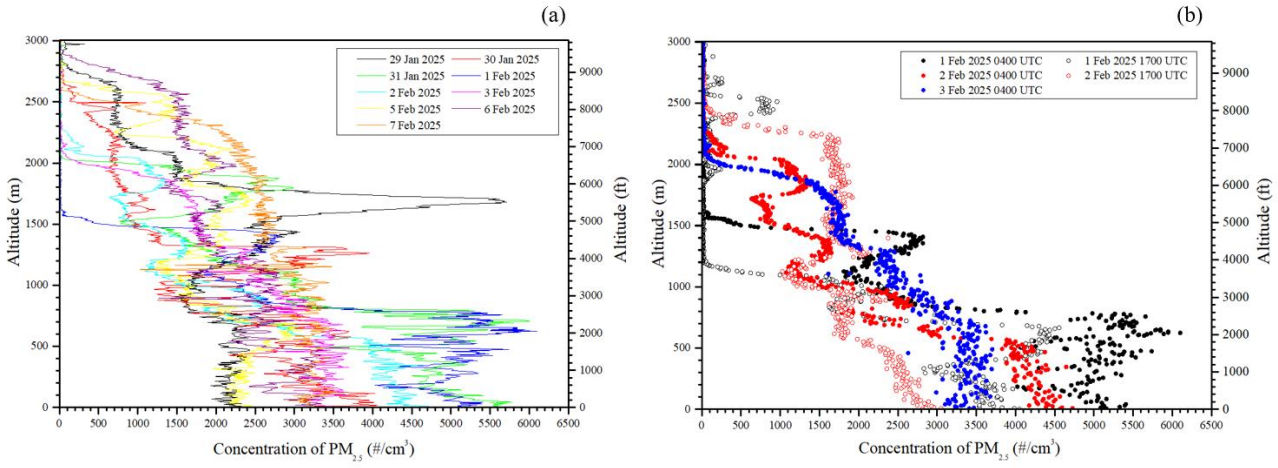


Figure 3 displays the levels of tiny particles in the air at 10000 feet. (a) $PM_{2.5}$ levels recorded from January 29 to February 7, 2025, before noon (local time), and (b) $PM_{2.5}$ levels from February 1 to 3, 2025, comparing the morning (0400 UTC) and evening (1700 UTC) measurements

Figures 3(a) and 3(b) illustrate the distribution of $PM_{2.5}$ particulate matter at several altitudes surrounding Don Mueang international airport, Bangkok. The dispersion of tiny dust particles diminishes with elevation. Throughout both day and night, dust concentration levels approach zero at an altitude of around 3000 meters (around 10000 ft). According to Figure 3(a), the $PM_{2.5}$ dust concentration at 0400 UTC on January 29, 2025, is 2212 #/cm³, which is projected to rise on January 30-31, 2025, reaching surface concentration values of 3961 #/cm³ and 5615 #/cm³, respectively. Subsequently, the $PM_{2.5}$ particulate matter recorded by the SKA aircraft exhibits a consistent decline from 0400 UTC on February 1-7, 2025, with the lowest concentration occurring on February 5, 2025, at 2280 #/cm³. Refer to the specifics in Table 1. The $PM_{2.5}$ particulate matter in the atmosphere surrounding Don Mueang Airport has a high concentration. The deposition of dust near the surface may result from incomplete combustion of engines, building activities, or other causes [2, 5-9].

When comparing the $PM_{2.5}$ dust levels at Don Mueang airport during the measurement period by the SKA aircraft, it was found that the $PM_{2.5}$ levels at night, recorded at 1700 UTC, were lower than those during the day at 0400 UTC, as shown in Figure 3(b). On February 1, 2025, the daytime $PM_{2.5}$ dust levels were between 5100 and 5400 #/cm^3 (solid black dots), which were higher than the nighttime levels of 3000 to 4000 #/cm^3 (transparent black dots). On February 1, 2025, the daytime $PM_{2.5}$ dust concentration values ranged from 5100 to 5400 #/cm^3 (solid black dots), surpassing the nighttime values of 3000 to 4000 #/cm^3 (transparent black dots). Similarly, on February 2, 2025, the daytime values ranged from 4200 to 4700 #/cm³ (solid red dots), exceeding the nighttime values of 2700 to 3100 #/cm³ (transparent red dots). The $PM_{2.5}$ dust concentration data from the SKA research aircraft matches the average concentration values collected from the surface station at Don Mueang airport, Bangkok, as shown in Figure 4.

Figure 4 shows the average levels of $PM_{2.5}$ particles at 7 stations near Don Mueang airport from January 29 to February 7, 2025, during the times when SKA aircraft were operating at Don Mueang international airport, Bangkok, between 0400 UTC (daytime) and 1700 UTC (nighttime). The average $PM_{2.5}$ particulate matter concentration near Don Mueang Airport from January 29 to 31, 2025, exhibited an upward trend, with values of 30.7 µg/m³ on January 29, 48.6 µg/m³ on January 30, and 68.2 µg/m³ on January 31. Subsequently, the mean concentration value on the surface of Don Mueang Airport A decline occurred from February 1 to February 7, 2025, with the minimum average concentration recorded on February 5, 2025, at 32.4 µg/m³, as seen in Table 1. When comparing the $PM_{2.5}$ levels from February 1 to February 3, 2025 (marked in red box), it was found that the average concentration at night (1700 UTC) was lower than during the day, with readings of 54.4 µg/m³ on February 1 at 0400 UTC and 42.0 µg/m³ on February 2 at 0400 UTC. The nighttime values were lower than the daytime concentrations by 18 and 34 percent, respectively, for February 1 and 2, 2025.

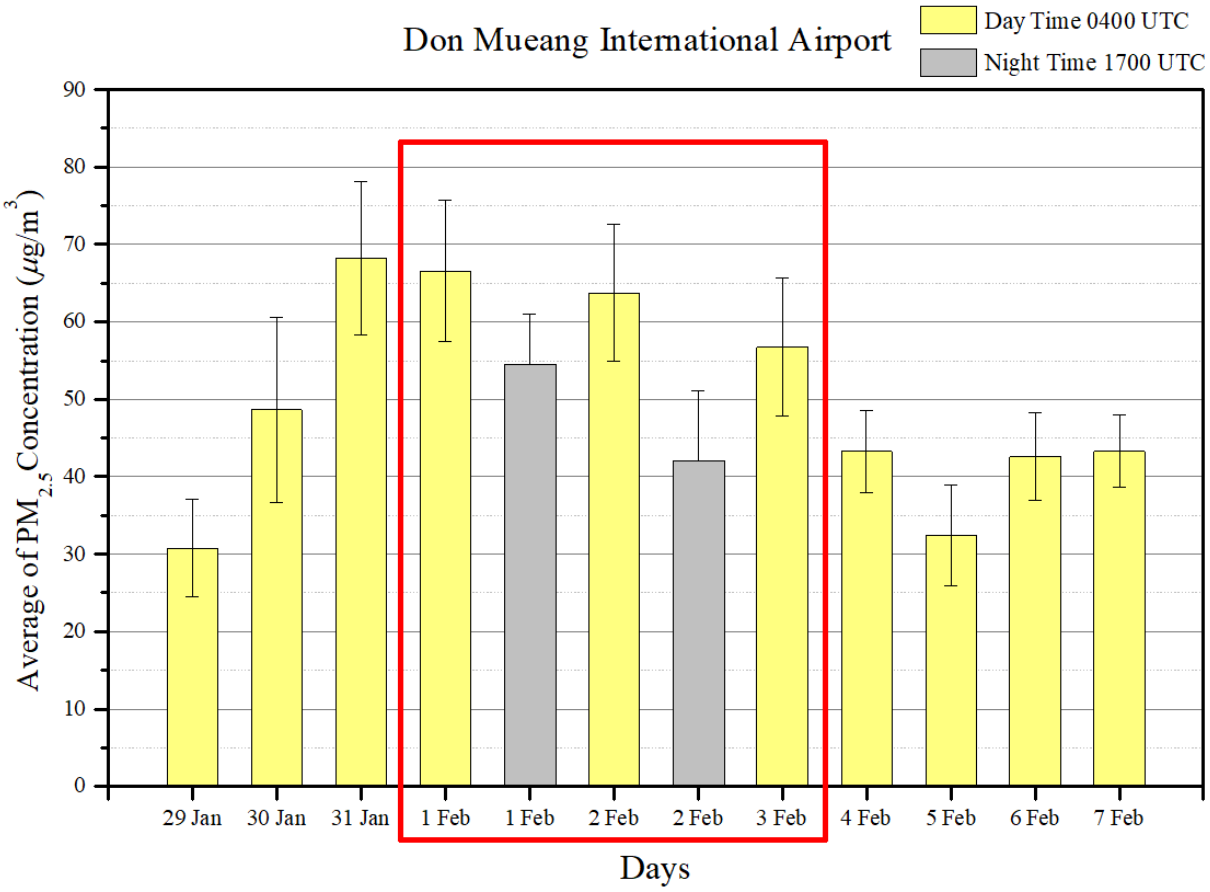


Figure 4 illustrates the average concentration of $PM_{2.5}$ particulate matter at 7 stations close to Don Mueang airport, Bangkok (22t, bkp120t, bkp74t, bkp97t, bkp98t, bkp130t, and bkp75t stations).

Table 1: Average of concentration measured from air pollution station and SKA probe at surface-50 meters values 29 January–7 February 2025

Day (Time)	Concentration by measured SKA probe at surface – 50 meters	Concentration from measured by air pollution Station
	#/cm^3	μg/m^3
29 Jan 2025 (1700 UTC)	2212	30.7
30 Jan 2025 (1700 UTC)	3961	48.6
31 Jan 2025 (1700 UTC)	5615	68.2
1 Feb 2025 (1700 UTC)	5246	66.6
1 Feb 2025 (0400 UTC)	3618	54.4
2 Feb 2025 (1700 UTC)	4481	63.8
2 Feb 2025 (0400 UTC)	2842	42.0
3 Feb 2025 (1700 UTC)	3316	56.7
4 Feb 2025 (1700 UTC)	No measurements were taken today.	43.2
5 Feb 2025 (1700 UTC)	2280	32.4
6 Feb 2025 (1700 UTC)	3218	42.6
7 Feb 2025 (1700 UTC)	3244	43.3

Figure 5 shows tiny particles smaller than 2.5 micrometers are spread out, based on temperature values taken by the SKA research aircraft at heights of up to 3000 meters. The buoyancy of $PM_{2.5}$ dust, as measured by the SKA research aircraft, diminished in the region where the dew point temperature and ambient temperature increased between 700 and 800 meters (2400-2600 feet). In a different region, at an elevation of 1650-1750 meters (5700-5850 feet), the dust, which had been progressively accumulating, diminished markedly. In the final region, at an elevation of 2600-2800 meters (8800-9200 feet), the dust exhibited a low density with a concentration of roughly 700 #/cm³ as the ambient temperature rose. Conversely, the dew point temperature fell markedly. The dust diminished abruptly. The number rapidly approaches zero; in other words, ambient temperature and dew point temperature influence the retention of $PM_{2.5}$ particulate matter, supported by research, including studies on temperature inversion [2, 5, 10-15].

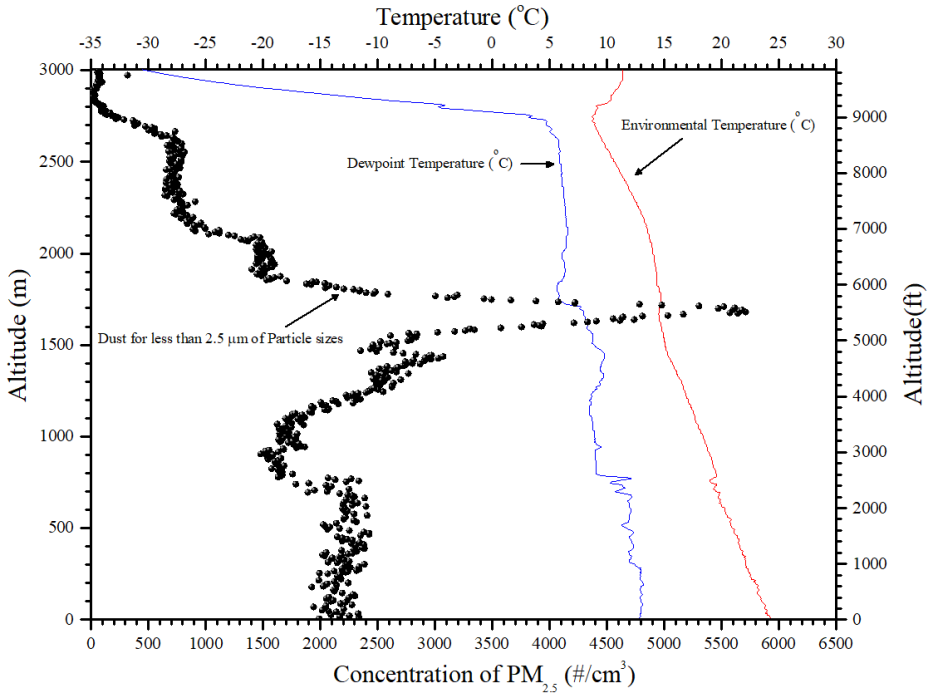


Figure 5 shows concentrations of particulate matter less than 2.5 micrometers, dew point temperature, and ambient temperature at ground surface altitudes of 10000 feet (3000 meters), January 29, 2025.

Figures 6(a) and 6(b) illustrate the ambient temperature values at surface altitudes up to 3000 meters in height. The ambient temperature generally decreases with elevation daily. Upon examining the surface temperature at Don Mueang airport during daytime, as illustrated in Figure 6(a), it was observed that on January 29, 2025, the surface temperature registered at 24.2 °C. Subsequently, from January 30 to February 3, 2025, the temperatures rose to 26.0 °C, 28.1 °C, 29.2 °C, 29.8 °C, and 30.9 °C, respectively. The ambient temperature at the surface of Don Mueang airport then increased. A declining trend is observed on February 3, 2025, with a surface temperature of 27.3 °C, and from February 5 to 7, 2025, with surface temperatures of 27.3 °C, 28.1 °C, and 29.0 °C, respectively. Upon examining Figure 6(b), it is observed that the nocturnal surface temperature values (represented by the black and red dotted lines) on February 1 and 2, 2025, are lower than the diurnal temperatures, which are both recorded at 27.0 °C on those days.

The temperature decline patterns between day and night (Figure 6(a) and Figure 6(b)) exhibit distinct variations. Upon examining the temperature graph throughout the day, as seen in Figure 6(a), it was observed that the ambient temperature line exhibits an undulating pattern at altitudes below 1300 meters. Temperature remains stable (change less than 1 °C) until a considerable rise occurs (change of 1-4 °C) at altitudes over 1500 meters. We observed a lesser rise in ambient temperature during the night than during the day. A temperature variation of 1-4 °C occurred at altitudes of 100-500 meters, and a similar rise of 1-4 °C was seen at altitudes of 2500-2800 meters, attributed to the heat emitted from the Earth's surface. At elevated altitudes, thermal buoyancy resulting from the Earth's heat transmission renders the heat layer above the surface discernible.

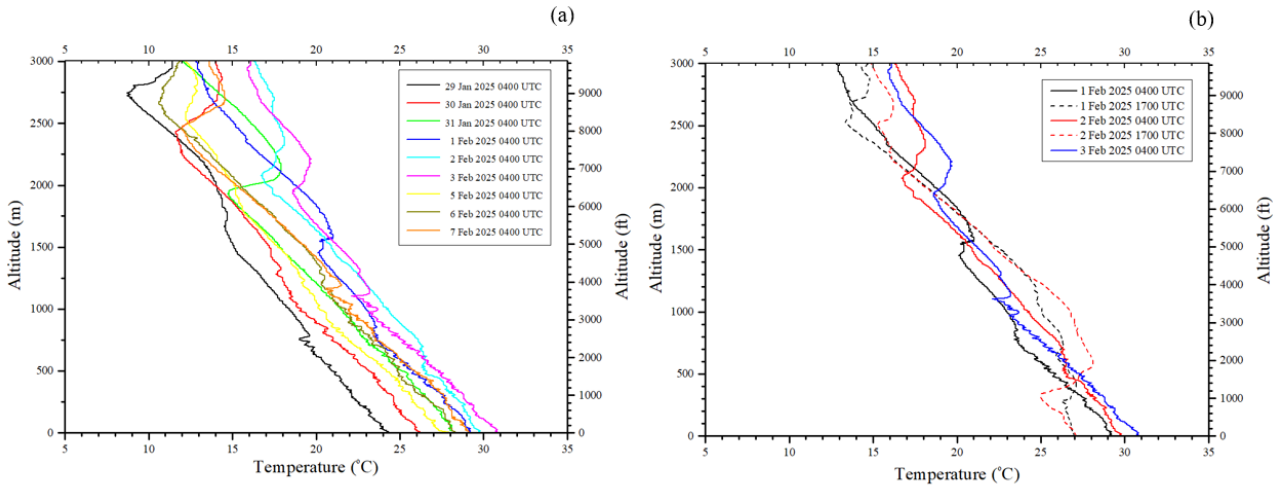


Figure 6 presents the temperature recorded by the SKA aircraft at ground level-3,000 m at Don Mueang Airport. (a) temperature measurements from 29 January to 7 February 2025 (daytime 0400 UTC) and (b) temperature measurements from 1 to 3 February 2025 throughout daytime (0400 UTC) and nighttime (1700 UTC)

Figure 7 indicates the air pressure documented by the Super King Air 350 aircraft at Don Mueang airport, extending to an altitude of 350 meters (approximately 1000 feet), in relation to the height of the tallest structure in the Bangkok region, the Magnolia Waterfront Residences at Icon Siam Condominium, which stands at 317.95 meters, during the period from 29 January to 7 February 2025. The pressure at the airport surface was observed to range from 1009 to 1017 hPa, as seen in Figure 7(a). Throughout the daytime (0400 UTC), atmospheric pressure generally diminishes with increasing altitude. At the surface level, the pressure measurements were recorded as follows: 1017 hPa (29 January 2025), 1013.8 hPa (30 January 2025), 1011.7 hPa (31 January 2025), 1010.4 hPa (1-2 February 2025), 1008.9 hPa (3 February 2025), 1010.2 hPa (5 February 2025), 1011.1 hPa (6 February 2025), and 1011.8 hPa (7 February 2025). Furthermore, it was observed that the pressure at 1700 UTC during the night on 1 and 2 February 2025 was lower than that of the daytime. Previous studies indicate that air pressure plays a crucial role in exacerbating atmospheric pollution. Air pressure alone does not influence the retention of $PM_{2.5}$ dust. Additional parameters include dust amount and source, temperature, wind speed, air flow coefficient, air lift, precipitation, and air instability index [3, 5, 15].

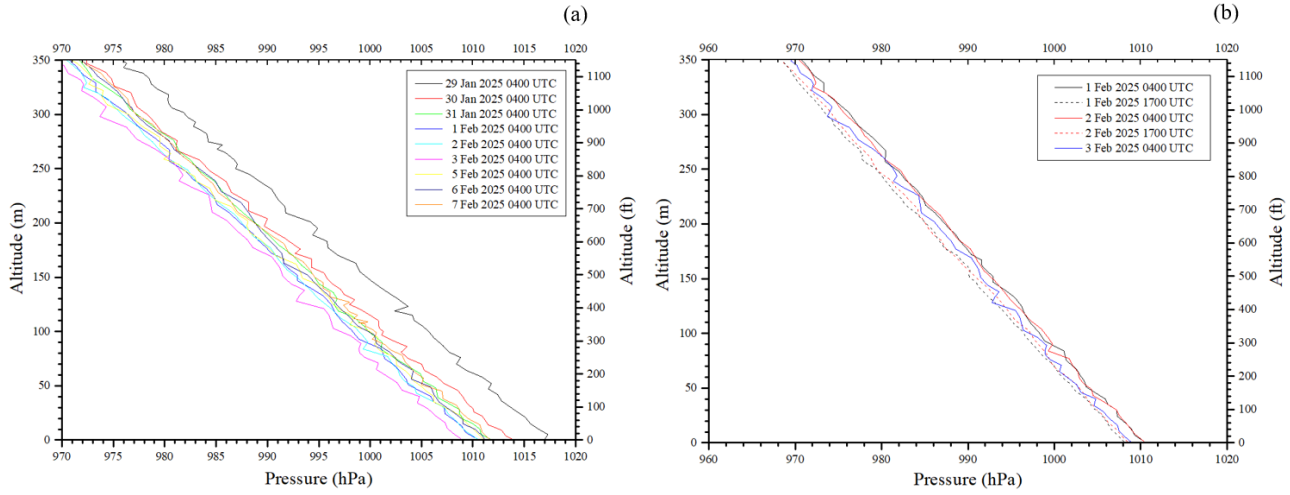


Figure 7 depict air pressure recorded by SKA aircraft at ground level-350 meters at Don Mueang Airport. (a) air pressure measured from 29 January to 7 February 2025 (daytime 0400 UTC) and (b) air pressure measured from 1 to 3 February 2025 during the day (0400 UTC) and at night (1700 UTC)

The wind speed and wind direction measured by the SKA aircraft at Don Mueang Airport at ground level to 3000 meters altitude during the day are depicted in Figure 8(a) (0400 UTC) and at night in Figure 8(b) (1700 UTC). The wind direction was predominantly southeasterly during the day from January 29 to February 7, 2025. The wind speed at an altitude of 0-3000 meters was primarily in the 4-8 m/s (yellow and orange) range during the day, which accounted for 52% of the measured speed. In the meantime, the wind was primarily northeasterly during the nights of February 1–2 at 1700 UTC (Figure 8(b)), with a predominant speed of 2–4 m/s (green), which accounted for 48 percent of the wind speed measurements. The second wind, which was 4 to 8 m/s, accounted for 28 percent of the wind speed measurements.

The vertical distribution and concentration of $PM_{2.5}$ dust were compared to the vertical wind speed on February 1, 2025, at night (1700 UTC), as demonstrated in Figure 8(a). The ground-level $PM_{2.5}$ dust had a concentration of approximately 3600 #/cm³ (solid red line) and a wind speed of approximately 3.5 m/s (gray area). It is evident that the particulate value decreased as the wind speed at different levels increased. Conversely, the particulate concentration increased at higher altitudes as the speed decreased. At an altitude of approximately 1200 meters, the particulate concentration decreased to nil during the night. On February 2, 2025, at 0400 UTC, the wind speed at the ground level was substantially lower during the day than at night (Figure 9(b)). The wind speed was 1 m/s, and the dust concentration was higher during the night. The concentration value is 5100 #/cm³, and the distribution of $PM_{2.5}$ dust indicated that the value decreased within the 700-1400 meters height range. Subsequently, the concentration value decreased until it reached zero at elevations of 1500 meters or higher. It is evident that the $PM_{2.5}$ dust held at Don Mueang Airport was at an altitude of less than 1500 meters during both day and night. The dust ascended to a height of approximately 400 meters during the day, which was marginally higher than at night. The wind speed significantly influenced the concentration of $PM_{2.5}$ particulate at various measured heights. [9, 16-17]

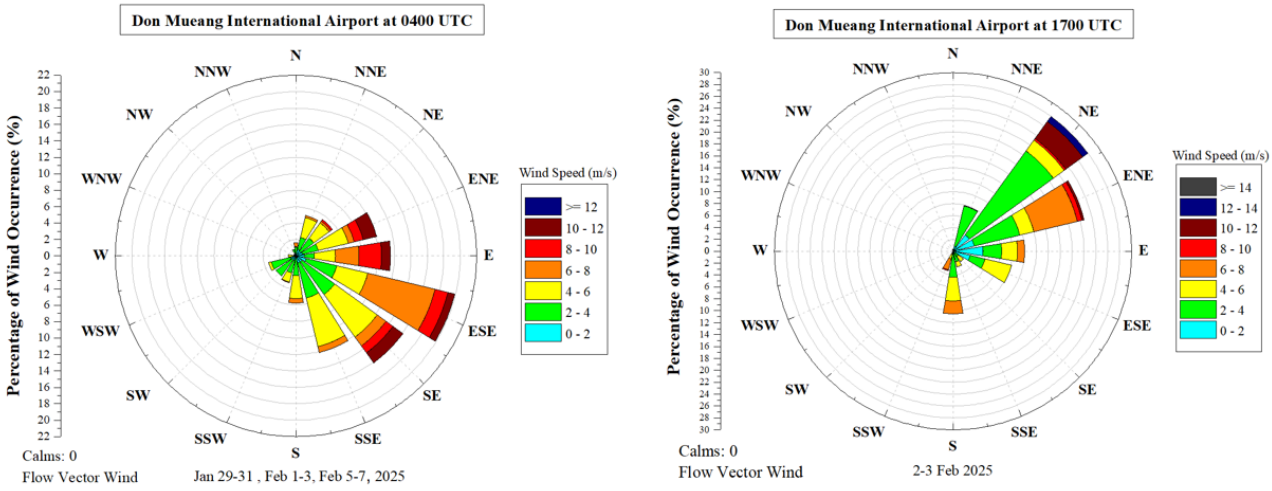


Figure 8. Wind speed and wind direction measured by SKA aircraft at ground level–3000 m at Don Mueang Airport (a) 29 January–7 February 2025 (daytime 0400 UTC) and (b) 1–2 February 2025 (nighttime 1700 UTC)

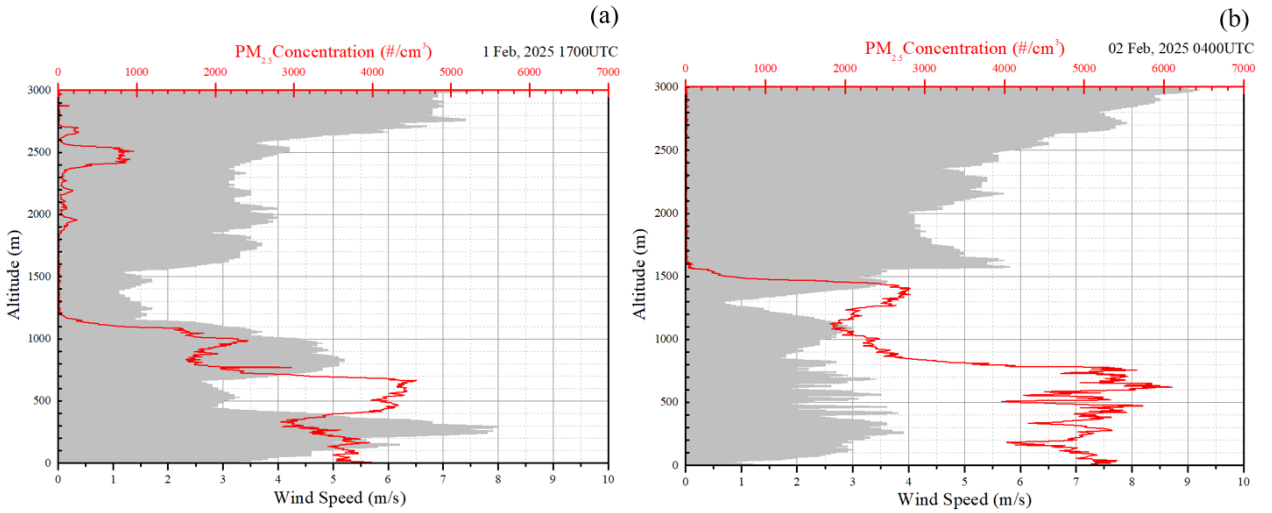


Figure 9 demonstrates the correlation between wind speed and wind direction recorded by SKA aircraft at an altitude of 3000 meters above ground level at Don Mueang airport: (a) nighttime (1700 UTC), 1 February 2025, and (b) nighttime (0400 UTC), 2 February 2025.

CONCLUSION

The results drawn from the flights for measuring air quality and the assessment of $PM_{2.5}$ particulate dispersion in the Bangkok region, completed during both the day and night, are as follows:

1. The daily pattern of $PM_{2.5}$ particles showed that the dust was found below 2800 meters during the day and 2700 meters at night, and the amount of $PM_{2.5}$ matched what was measured at the surface station at Don Mueang Airport.

2. Temperature inversion affects dust retention at different altitudes. On the other hand, air pressure influences the concentration of dust at the surface. The concentration of $PM_{2.5}$ tends to rise with increased pressure.

3. The wind predominantly originates from the southeast during the day (0400 UTC) and from the northeast at night (1700 UTC). Furthermore, wind speed influences the fluctuations in $PM_{2.5}$ particulate matter by dispersing dust within the atmosphere. At low wind speeds, dust concentrations are elevated, whereas strong winds result in decreased concentrations.

ACKNOWLEDGEMENT

I express my gratitude to the Department of Royal Rainmaking and Agricultural Aviation for the upper air quality data from the Omkoi rainmaking station in Chiang Mai province and to the Pollution Control Department for the daily and monthly $PM_{2.5}$ data. I extend my gratitude to the Director-General of the Department of Royal Rainmaking and Agricultural Aviation, as well as the applied atmospheric science specialists, for their assistance with the $PM_{2.5}$ identified by the Super King Air 350 probe for investigation. I am truly thankful to the head of the Rainmaking Weather Monitoring and Development Division for granting access to the radar station and the data for the study, as well as to all executives for their support and assistance throughout the research process. I extend my gratitude to the scientists at the Southern Rainmaking Operation Center for their assistance with this project.

REFERENCE

[1] Belis, C.A., Karagulian, F. and Larsen, B.R. 2013. Critical review and meta-analysis of ambient particulate matter source apportionment using receptor models in Europe. Atmospheric Environment. 69: 94-108.

[2] Seinfeld, J.H. and Pandis, S.N. 2016. Atmospheric Chemistry and Physics: From Air Pollution to Climate Change. John Wiley & Sons. New York.

[3] Ali, M.U., Liu, G. and Yousaf, B. 2019. A systematic review on global pollution status of particulate matter-associated potential toxic elements and health perspectives in urban environment. Environmental Geochemistry and Health. 41: 1131-1162.

[4] Yue, H., He, C. and Huang, Q. 2020. Stronger policy required to substantially reduce deaths from $PM_{2.5}$ pollution in China. Nature Communications. 11: 1462.

[5] Narita, D., Oanh, N.T.K., Sato, K., Huo, M., Permadi, D.A., Chi, N.N.H., Ratanajaratroj, T. and Pawarmart, I. 2019. Pollution characteristics and policy actions on fine particulate matter in a growing Asian economy: The case of Bangkok Metropolitan Region. Atmosphere. 10: 227.

[6] McMurry, P.H. 2000. A review of atmospheric aerosol measurements. Atmospheric Environment. 34(12-14): 1959-1999.

[7] Bahareh, K., Mohammad, R. and Mansouri, D. 2020. Comprehensive temporal analysis of temperature inversions across urban atmospheric boundary layer of Tehran within 2014-2018. Modeling Earth Systems and Environment. 967-982.

[8] Li, D., Liao W., Rigden A.J., Liu, X., Wang, D., Malyshev, S. and Shevliakova, E. 2019. Urban heat island: Aerodynamics or imperviousness ?. Science Advances., 5(4).

[9] Li, Y., and Chao, J. 2018. Theoretical urban heat island circulation in the temperature inversion profile. Atmosphere 9: 98.

[10] Thi, T.T., Thi, T.T. and Thi T.L., Duc H. N. and Binh M.Tu. 2019. Temperature inversion and air pollution relationship, and its effects on human health in Hanoi City, Vietnam. Environmental Geochemistry and Health, 41: 929-937.

[11] Iacobellis, S.F., Norris, J.R., Kanamitsu, M. and Tyree, A.M. 2009. Climate variability and California low-level temperature inversions. In California Climate Change Center. Scripps Institution of Oceanography. 1-48.

[12] Ji, D.S., Wang, Y.S., Wang, L.L., Chen, L.F., Hu, B. and Tang, G.Q. 2012. Analysis of heavy pollution episodes in selected cities of northern China. Atmospheric Environment, 50: 338-348.

[13] Boming, L., Xin, M.,Yingying M., Hui, L., Shikuan, J., Ruonan, F. and Wei, G. 2022. The relationship between atmospheric boundary layer and temperature inversion layer and their aerosol capture. Atmospheric Research 271: 106121.

[14] Wang, W., He, J., Miao, Z. and Du, L. 2021. Space-Time Linear Mixed-Effects (STLME) model for mapping hourly fine particulate loadings in the Beijing-Tianjin-Hebei region, China. The Journal of Cleaner Production. 292: 125993.

[15] Yin, P., Guo, J., Wang, L., Fan, W., Lu, F., Guo, M. And Dong, Z., 2020. Higher risk of cardiovascular disease associated with smaller size-fractioned particulate matter. Environmental Science & Technology Letters. 7 (2): 95-101.

[16] Subrata, K.D., Tanaya, T., K.N. Um., Murali, K., Sanjoy K.S. 2021. Characteristics of temperature inversion from radiosonde measurements in the Western Ghats region. Atmospheric Research. 250: 105391.

[17] Zhu, Y., Ma, Y., Liu, B., Xu, X., Jin, S.and Gong, W., 2021. Retrieving the vertical distribution of $PM_{2.5}$ mass concentration from lidar via a random forest model. In: IEEE Transactions on Geoscience and Remote Sensing. 60.

20R3-07

Variation of Black Carbon in PM_1 and Its Health Risk Assessment at Low and High-Rise Buildings

Nipaporn Auttanate[1], Nattakit Jintauschariya[1], Samita kladin[1], Parkpoom Choomanee[1*], Surat Bualert[1], Thunyapat Thongyen[2]

[1]*Department of Environmental Science, Faculty of Environment, Kasetsart University, Bangkok, Thailand*

[2]*Department of Technology and Management, Faculty of Environment, Kasetsart University, Bangkok, Thailand*

[*]*Phone :* +86-277-7689, *E-mail :* parkpoom.choom@ku.th

ABSTRACT

This study conducted a comprehensive analysis of the distribution and health implications of particulate matter (PM), with a specific focus on PM_1, in the urban atmosphere of Bangkok. Particulate matter samples were collected at three distinct heights (30 and 110 meters) at the Microclimate and Air Pollution Monitoring Station, Faculty of Environment, Kasetsart University. The study evaluated the health impacts associated with PM_1 inhalation. Results revealed significant vertical variations in PM_1 concentrations, with mean levels of 57.70 ± 2.67 μg/m³ at 30 meters and 51.14 ± 1.30 μg/m³ at 110 meters. The maximum PM_1 concentration was recorded at 148.38 μg/m³ at the 30-meter elevation. Ambient air temperature ranged from 20.50°C to 32.25°C, while relative humidity (RH) varied between 35.86% and 79.36%. Wind speed demonstrated a positive correlation with altitude, whereas PM_1 concentrations exhibited an inverse relationship, consistent with atmospheric dispersion dynamics. Black carbon (BC) constituted approximately 12% of the total PM_1 concentration. The health impact assessment indicated no non-carcinogenic risks from black carbon exposure (HQ<1). Cancer risk levels were low across all age groups, with the highest risk observed in older adults aged 65–95 years. During heavy haze periods, mean PM_1 concentrations exceeded Thailand's $PM_{2.5}$ standard (37.5 μg/m³) by approximately twofold. Despite limited research on PM_1 exposure risks in Thailand, this study provides novel insights into vertical particulate dispersion patterns and their implications for urban health management. These findings underscore the need for evidence-based strategies to mitigate adverse health outcomes, particularly in densely populated metropolitan areas and high-rise residential environments where atmospheric stagnation exacerbates pollution accumulation.

Keywords : black carbon; PM_1; risk assessment; low and high-rise buildings

INTRODUCTION

Air pollution is a major global contributor to health complications and mortality, particularly due to fine particulate matter. Rapid urbanization and industrial expansion have intensified infrastructure development, including transportation networks, commercial buildings, and high-rise residential complexes. These activities generate significant fine particulate emissions, while urban spatial configurations impede air mass circulation and wind patterns, reducing ventilation efficiency. Consequently, this leads to the accumulation of airborne pollutants and particulate matter in urban environments. Particulate matter with a diameter not exceeding 1 micrometer (PM_1) constitutes a distinct category within the particulate classification system, which includes $PM_{2.5}$ (particles smaller than 2.5 micrometers) and PM_{10} (particles smaller than 10 micrometers). PM_1 accounts for 70–90% of $PM_{2.5}$ by mass, highlighting its significance as a primary contributor to fine particulate air pollution [1]. The dispersion of fine particulate matter is associated with spatial variability, particularly in contemporary urban settings. The growth of urban societies and the increasing popularity of apartment-style housing, driven by urban expansion and a rising population residing in multi-story buildings, enhance the vertical distribution of particulate matter. This, in turn, affects the exposure of urban populations to air pollution in metropolitan areas [2,3]. The configuration of urban buildings, such as structures flanking roads, can create wind circulation patterns that trap particulates and hinder their vertical dispersion. Additionally, roadside obstacles like trees and constructions act as barriers, preventing particles from mixing with air at higher altitudes [4]. Other factors, including urban planning layouts, topography, wind direction, temperature, and spatial distribution patterns of buildings, influence changes in particulate concentration with increasing height. Furthermore, the dispersion and concentration of PM_1 are affected by meteorological conditions, pollution sources, and seasonal variations.The chemical composition of particulate matter can vary significantly due to the influence of emission sources, weather conditions, and particulate dispersion. The carbonaceous components of particulate matter consist of elemental carbon (EC), also

known as black carbon, and organic carbon (OC), which account for approximately 10% and 45% of the mass of $PM_{2.5}$ and PM_{10}, respectively. Notably, in urban fine particulate matter, particularly PM_1, black carbon is the second most abundant component, comprising about 21% of the mass, following organic aerosol (OA), which constitutes approximately 49% of the mass [5].

Bangkok's rapid vertical urbanization, characterized by clustered high-rise developments and intensified land use, has created spatially heterogeneous microenvironments with distinct air pollution profiles. Black carbon (BC) particles, ranging in size from approximately 10 nanometers to 1 millimeter, contain elemental carbon (EC) at less than 60% of their total particulate mass. Polycyclic aromatic hydrocarbons (PAHs) serve as the primary carcinogenic components in these particles, which originate from vehicle exhaust emissions produced by the combustion of diesel, gasoline, and other petroleum-derived fuels [6]. Especially concerning are ultrafine particles ($PM_{0.1}$), as these particles can infiltrate the bronchioles and alveoli in the lungs, posing significant health risks. Key health issues associated with black carbon include cancer, which arises from the formation of DNA-damaging substances, leading to mutations in genes. Respiratory toxicity results from abnormal immune responses involving eosinophils and mast cells, causing airway inflammation. Cardiovascular toxicity includes conditions such as coronary artery disease. Furthermore, black carbon particles cause damage to various organs through mechanisms that remain poorly understood [7]. While ground-level PM_1 pollution in Bangkok is well-documented, limited research exists on vertical BC variability across elevated urban structures or its health implications for high-rise population, a critical gap given that 63% of Bangkok's residential units now occupy buildings above 15 floors (45 meters). Bangkok's northern districts (e.g., Chatuchak, Phaya Thai) prioritize high-rise residential complexes, whereas southern zones (e.g., Din Daeng, Pathum Wan) exhibit mixed-use congestion with dense commercial hubs and transportation networks. This dichotomy creates divergent BC exposure pathways: northern areas face infiltration from adjacent expressways (e.g., Vibhavadi Rangsit Road), while southern sectors endure direct emissions from idling traffic in superblock-design thoroughfares. Compounding this, biomass burning from informal settlements and construction activities notably diesel-powered machine. Recent $PM_{2.5}$ peaks (119 μg/m³ in January 2025) [7] correlate with a 22% rise in cardiovascular mortality among outdoor workers, while indoor BC concentrations in high-rises (1,572 ng/m³) remain underestimated due to inadequate ventilation standards [9]. Vulnerable populations, including low-income groups displaced to traffic-corridor suburbs, face dual exposure risks, ground-level commuting, and residual UFP infiltration in aging residential towers [10] .

This study addresses significant knowledge gaps by investigating the spatiotemporal variability of black carbon across Bangkok's vertical urban landscape and quantifying the resultant health disparities. The findings will inform the development of targeted air quality policies, including emission controls and ventilation guidelines for high-rise dwellers, thereby contributing to improved environmental health outcomes.

METHODOLOGY

Study location and sample collection

For the monitoring of PM_1 and meteorological data, measurements were conducted and collected at two distinct elevations: 30 meters and 110 meters above ground level at the Microclimate and Air Pollution Monitoring Station (KU Tower), as well as a spatial survey within a 5-kilometer radius surrounding the KU Tower. (Figure 1.)

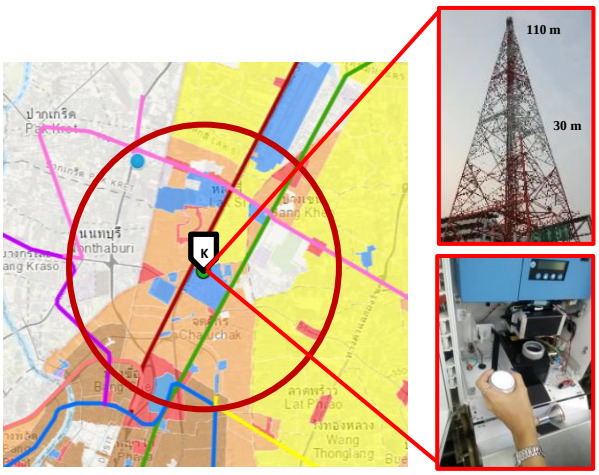


Figure. 1 KU Tower Sampling site (5 km radius) and Bangkok city plan (Latitude:13.854529 N, Longitude: 100.570012 E)

PM_1 samples were collected between January to February 2025 (heavy haze period). The sampling was conducted using a Thermo Fisher Scientific ADR-1500 Area Dust Monitor, which employs a light-scattering technique to measure particulate concentrations. PM_1 particles were captured on 37 mm quartz microfiber filters. Following collection, the filters were stored in a refrigerated environment at approximately 4°C to preserve sample integrity before subsequent analysis. After that, the Quartz Fiber filter sample was analyzed using SootScan™ Model-OT21 to analyze the amount of black carbon in PM_1. An optical transmissometer technique to determine the amount of black carbon uses wavelengths of light 880 nm for BC quantification [11], equation (1) expresses the Beer-Lambert law as shown below, and equation (2) expresses b_{att} in units of inverse megameters (Mm^{-1}) (2).

$$I = I_0 e^{-(b_{att} \times L)} \tag{1}$$

$$b_{att} = \frac{\text{Area (m}^2\text{)}}{\text{Volume (m}^3\text{)}} \times \ln\left(\frac{I}{I_0}\right) \times 10^6 \tag{2}$$

equation (3) expresses the BC concentration (μg/m^3) is calculated using b_{att} at 880 nm and $\sigma_{att}[\lambda]$ (m^2/g)

$$\text{BC concentration } (\mu g/m^3) = \frac{b_{att}\ (Mm^{-1})}{\sigma_{att}(\lambda)(m^2 g^{-1})} \tag{3}$$

Health Risk Assessment

Black carbon from diesel combustion emissions from automobile exhaust is classified as carcinogenic to humans (Group 1) by the International Agency for Research on Cancer (IARC), which is associated with an increased risk of developing lung cancer. Consequently, this study aims to conduct a comprehensive health risk assessment of black carbon in PM_1, focusing on inhalation exposure risk evaluation. This assessment encompasses the calculation of Chronic Daily Intake (CDI) (4), Hazard Quotient (HQ) for non-carcinogenic risks (5), and Carcinogenic Risk (CR) (6) for five distinct population groups. The evaluation of these metrics will provide insights into the potential health impacts of black carbon exposure on different demographics.

Table 1 Body weight (BW) and inhalation rate (IR) [12]

Group	Age (year)	Males		Females	
		BW	IR	BW	IR
Children	11 to <23	58.6	17.23	50.0	13.28
Youth	23 to <30	70.9	17.48	59.2	13.67
Young adult	30 to <40	71.5	16.88	58.7	13.68
Adult	40 to <65	71.1	16.24	58.8	12.31
Older adult	65 to <96	68.9	12.96	57.2	9.80

Chronic Daily Intake (CDI) is a metric for estimating long-term exposure to toxic substances. The CDI calculation involves key factors: concentration of black carbon (C) (mg/m^3), inhalation rate (IR) (m^3/day), exposure frequency (EF) (days/year), exposure duration (ED) (year), body weight (BW) (kg), and averaging time (AT) (days).

$$CDI = (C \times IR \times EF \times ED) / (BW \times AT) \tag{4}$$

The Hazard Quotient (HQ) is a risk assessment metric used to evaluate the potential for non-cancer health hazards from exposure to contaminants. It is calculated as the ratio of potential exposure to a substance and the reference concentration (RfC) at which no adverse effects are expected. For black carbon (BC), the RfC is defined as 5×10^{-3} mg/m³ by the USEPA. An HQ value less than 1 indicates no non-carcinogenic risk, while a value greater than 1 suggests potential non-carcinogenic health risks

$$HQ = CDI / RFC \tag{5}$$

The carcinogenic risk (CR) associated with black carbon (BC) in PM_1 is calculated using the Cancer Slope Factor (CSF), which quantifies the inhalation toxicity of BC or soot. The CSF value for BC is typically set at $1.1\ (mg/kg/day)^{-1}$ [13]. As Thailand has yet to establish specific guidelines for hazardous exposure levels of

black carbon, the health impact assessment in this study was conducted using the criteria set forth by the New York State Department of Health as a reference framework.

$$CR = CDI \times CSF \quad (6)$$

According to the criteria established by the New York State Department of Health, cancer risk is categorized into five levels: $CR \geq 10^{-1}$ (very high); (2) $10^{-3} \leq CR < 10^{-1}$ (high); (3) $10^{-4} < CR \leq 10^{-3}$ (moderate); (4) $10^{-6} < CR \leq 10^{-4}$ (low); and (5) $CR \leq 10^{-6}$ [14].

RESULTS AND DISCUSSIONS

PM_1 and Black Carbon Concentration

The sampling area (KU Tower) covers Lak Si, Bang Khen and Chatuchak districts, consisting of yellow zone (low-density residential zone), orange zone (medium density residential zone) and red areas (commercial zone), respectively. (Land use zoning plan of Bangkok). From the Digital Elevation Model (DEM), it is shown that within a 5-kilometer radius, the area has an elevation exceeding 30 meters above the average ground level, approximately 42.50 meters. This categorizes the structures in the area as High-Rise Buildings under the Building Control Act B.E. 2522 (1979) of Thailand.

The mean mass concentration of PM_1 from January to February 2025 (heavy haze period). The average concentrations at 30 m., and 110 m. were 57.70±2.67 μg/m^3 (11.91-148.38 μg/m^3), and 51.14±1.30 μg/m^3 (11.10-121.14 μg/m^3), respectively. The study findings indicate that the vertical distribution of PM_1 concentrations decreases with increasing altitude. This contrasts with the research conducted by Roostae et al. (2024), which examined the vertical distribution of particulate matter in Tehran, Islamic Republic of Iran, and found that particulate matter concentrations increased with altitude [15]. Urban areas with dense traffic, industrial activities, and faulty vehicle emissions (e.g., diesel engines) contribute significantly to PM_1 levels [16].

Table 2. Vertical variation of PM_1 in Bangkok

Level	PM_1 (μg/m^3)	BC(μg/m^3)	PM_1/BC
30 m.	57.70±2.67	6.54±1.43	12.19
110 m.	51.14±1.30	5.61±0.47	12.12

The proportion of black carbon within PM_1 was approximately 12% of the total PM_1 concentration, suggesting that the particulate matter in the area is predominantly derived from combustion-related activities. These sources likely include emissions from diesel vehicles, the utilization of fossil fuels, biomass burning, and industrial combustion processes, which are known to contribute significantly to black carbon emissions.

Meteorological data

Meteorological data are presented in Table 3. The average temperature across two altitude levels during the heavy haze period ranged between 26–27°C, with the lowest recorded temperature of 20.50°C at an altitude of 110 meters. The maximum average relative humidity at the 110-meter altitude was 53.54%, while the average wind speed increased with altitude, which corresponded to the average concentration of particulate matter.

Table 3. Meteorological data during the heavy haze period at 30 m. and 110 m. levels

Meteorological parameter	30 m.		110 m.	
	Mean±S.D	Min-Max	Mean±S.D	Min-Max
Wind speed (m/s)	1.95±0.49	0.86-4.83	2.78±0.17	1.30-6.00
Temperature (°C)	27.31±2.54	20.88-32.25	26.83±2.19	20.50-31.57
RH (%)	52.97±9.94	35.86-77.09	53.54±8.39	37.14-79.36
Wind direction (Deg.)	159.55±10.86	67.25-322.25	155.63±20.44	35.33-233.00

Health risk assessment

The health impact assessment of exposure to black carbon from PM_1, as presented in Table 4., revealed no non-carcinogenic risks (HQ<1). The cancer risk level (CR) across all age groups, as well as among males and females, was categorized as low. However, the study indicated that females exhibited higher risks of exposure

compared to males across two altitude levels. Among females residing or exposed to black carbon at altitudes above 30 meters (high-rise buildings), the highest cancer risk was observed in the older adult group aged 65–96 years.

Table 4. Predicted non-cancer risk (HQ) and carcinogenic risk (CR) levels of black carbon.

Height (m)	Group	Males			Females		
		CDI	HQ	CR	CDI	HQ	CR
< 30 m.	Children	7.90E-04	1.58E-01	7.18E-04	7.14E-04	1.43E-01	6.49E-04
	Youth	6.63E-04	1.33E-01	6.02E-04	6.21E-04	1.24E-01	5.64E-04
	Young adult	6.35E-04	1.27E-01	5.77E-04	6.26E-04	1.25E-01	5.69E-04
	Adult	6.14E-04	1.23E-01	5.58E-04	5.63E-04	1.13E-01	5.12E-04
	Older adult	5.06E-04	1.01E-01	4.60E-04	4.60E-04	9.21E-02	4.19E-04
> 30 m.	Children	6.78E-04	1.36E-01	6.16E-04	6.12E-04	1.22E-01	5.57E-04
	Youth	5.68E-04	1.14E-01	5.17E-04	5.32E-04	1.06E-01	4.84E-04
	Young adult	5.44E-04	1.09E-01	4.95E-04	5.37E-04	1.07E-01	4.88E-04
	Adult	5.27E-04	1.05E-01	4.79E-04	4.83E-04	9.65E-02	4.39E-04
	Older adult	4.34E-04	8.67E-02	3.94E-04	3.95E-04	7.90E-02	3.59E-04

Most studies conducted in Thailand focus on assessing the health impacts of $PM_{2.5}$ exposure. Findings from studies during 2020–2029 indicate that the hazard quotient (HQ>1) was particularly significant among infants, who exhibited acute and higher risks compared to other groups. These elevated risks are primarily attributed to behavioral patterns, environmental conditions, and physiological factors [17]. Although the study also reported low HQ values (HQ<1), the pathophysiological mechanisms of black carbon exposure from fine particulate matter remain critical issues that warrant further investigation, control measures, and ongoing monitoring of environmental and public health impacts.

CONCLUSION

The findings of this study highlight the critical need for targeted urban health management policies that account for the vertical distribution of fine particulate matter (PM_1) in densely populated environments such as Bangkok. The significant variation in PM_1 concentrations at different heights, coupled with elevated levels during haze events, indicates the potential for disproportionate exposure risks among residents of high-rise buildings. Although current health risk assessments suggest limited carcinogenic and non-carcinogenic threats from black carbon, the sustained exposure to elevated PM_1 concentrations remains a pressing concern, particularly for vulnerable populations such as the elderly. Future urban health policies should incorporate vertical air quality monitoring into routine surveillance systems and prioritize the development of adaptive mitigation strategies, such as enhancing natural ventilation in high-rise structures, regulating emission sources near residential zones, and promoting green infrastructure to improve atmospheric dispersion. These evidence-based interventions will be essential to mitigate health risks and support sustainable urban living in the face of escalating air pollution challenges.

ACKNOWLEDGEMENT

This study was funded by the “Atmospheric Science Research Group (ASRG)” and the Faculty of Environment, Kasetsart University, Bangkok, Thailand.

. ……

REFERENCE

[1] Chen G, Li S, Zhang Y, Zhang W, Li D, Wei X, et al. Effects of ambient PM_1 air pollution on daily emergency hospital visits in China: an epidemiological study. The Lancet Planetary Health. 2017;1(6):221-9.

[2] Han S, Zhang Y, Wu J, Zhang X, Tian Y, Wang Y, et al. Evaluation of regional background particulate matter concentration based on vertical distribution characteristics. Atmospheric Chemistry and Physics Discussions. 2015;15:14889-921.

[3] Zheng T, Li B, Li X-B, Wang Z, Li S-Y, Peng Z-R. Vertical and horizontal distributions of traffic-related pollutants beside an urban arterial road based on unmanned aerial vehicle observations, Building and Environment. Building and Environment. 2021;187.

[4] Liu X, Shi X-Q, He H-D, Li X-B, Peng Z-R. Vertical distribution characteristics of particulate matter beside an elevated expressway by unmanned aerial vehicle measurements. Building and Environment. 2021:108330.

[5] Werden BS, Giordano MR, Mahata K, Islam MR, Goetz JD, Puppala SP, et al. Submicron Aerosol Composition and Source Contribution across the Kathmandu Valley, Nepal, in Winter. ACS Earth Space Chem. 2023;7:49-68.

[6] Boffetta P, Jourenkova N, Gustavsson P. Cancer risk from occupational and environmental exposure to polycyclic aromatic hydrocarbons. Cancer Causes Control. 1997;8(3):444-72.

[7] Niranjan R, Thakur AK. The Toxicological Mechanisms of Environmental Soot (Black Carbon) and Carbon Black: Focus on Oxidative Stress and Inflammatory Pathways. Front Immunol. 2017;8:763.

[8] Inthorn, D., Sidtitoon, N., Silapanuntakul, S. and Incharoensakdi, A. 2002. Sorption of mercury, cadmium and lead in aqueous solution by the use of microalgae. Science Asia. 28(3): 253-261.

[9] Inthorn, D., Singhakarn, C. and Khan, E. Decolorization of reactive dyes by pre-treated Flute reed (phargmites karka (Retz). At 34th Mid-Atlantic Industrial & Hazardous Conference, Annual Mid Atlantic Industrial and Hazardous Waste Conference at Rugers University, New Jersey, USA on September 20-21, 2002.

[10] Polprasert, C. 1996. Organic Waste Recycles. John Wiley & Sons Inc., New York.

[11] Inthorn, D. Heavy metal removal. In: Kojima, H. and Lee, Y.K. Photosynthetic Microorganisms in Environmental Biotechnology, Springer-Verlag, 2001; 111-135.

[12] Agency USEP. Exposure Factors Handbook: 2011 Edition (Final Report). 2011 ed2011.

[13] Lin W, Dai J, Liu R, Zhai Y, Yue D, Hu Q. Integrated assessment of health risk and climate effects of black carbon in the Pearl River Delta region, China. Environ Res. 2019;176:108522.

[14] D. O. H. DOH Procedure for Evaluating Potential Health Risks for Contaminants of Concern. In: Health consultation: hopewell precision area groundwater contamination site town of east Fishkill DC, New York, in: Appendix C., editor.: New York State Department of Health; 2012.

[15] Roostaei V, Abbasi A, Gharibzadeh F, Faridi S, Naddafi K, Yunesian M, et al. Vertical Distribution of Air Particulate Matter (PM_1, $PM_{2.5}$, and PM_{10}) in Different Regions of Tehran. Aerosol and Air Quality Research. 2024;24(10):240036.

[16] Majewski G, Rogula-Kozłowska W, Rozbicka K, Rogula-Kopiec P, Mathews B, Brandyk A. Concentration, Chemical Composition and Origin of PM_1: Results from the First Long-term Measurement Campaign in Warsaw (Poland). Aerosol and Air Quality Research. 2018;18.

[17] Amnuaylojaroen T, Parasin N. Future Health Risk Assessment of Exposure to $PM_{2.5}$ in Different Age Groups of Children in Northern Thailand. Toxics [Internet]. 2023; 11(3).

20R3-08

Chemical Composition of Secondary Organic Aerosol in $PM_{2.5}$

Supannika Salao[1], Surat Bualert[1*], Parkpoom Choomanee[1] and Thunyapat Thongyen[2]

[1]*Department of Environmental Science, Faculty of Environment, Kasetsart University, Bangkok, Thailand*
[2]*Department of Technology and Management, Faculty of Environment, Kasetsart University, Bangkok, Thailand*

**Phone : +81-803-9899, E-mail : surat.b@ku.ac.th*

ABSTRACT

This study investigates the chemical composition of secondary organic aerosols (SOA) in $PM_{2.5}$ samples collected from roadside area at Ngam Wong Wan gate 3, Kasetsart University, Bangkok, Thailand. The $PM_{2.5}$ samples were collected for 24-hour from 18-24 december 2024. The results showed that $PM_{2.5}$ concentrations ranging from 26.922 to 59.649 $\mu g.m^{-3}$. The diurnal patterns characterized by peak concentrations during early morning (04:00-08:00) and night hours (22:00-24:00), indicating significant influence from urban traffic. Chemical analysis using methanol/dichloromethane (9:1) extraction revealed predominance of succinic acid and phthalic acid. Phthalic acid, typically the second most abundant diacid in urban roadside $PM_{2.5}$, originates from both direct combustion emissions and atmospheric degradation of aromatic hydrocarbons such as naphthalene. Additional organic acids identified included various benzenedicarboxylic acids, pentanetetracarboxylic acid, butenoic acid derivatives, furandicarboxylic acid, and other complex organic compounds. This study provides valuable insights into the composition of SOA in urban $PM_{2.5}$, contributing to better understanding of air pollution sources and formation mechanisms in heavily trafficked urban environments.

Keywords: $PM_{2.5}$, secondary organic aerosol, dicarboxylic acids, urban air pollution, traffic emissions.

INTRODUCTION

Air pollution from fine particulate matter is still an important problem that needs to be managed and solved, in urban areas with dense population and heavy traffic. Bangkok is currently still experiencing continuous air pollution problems every year from fine aerosols, especially secondary organic aerosols (SOA), which are found to be a component of fine dust particles smaller than 2.5 microns ($PM_{2.5}$) [1] and are an important component that affects air quality, reduces visibility, blocks out solar radiation, and causes cloud condensation nuclei (CCN) [2]. SOA does not come from direct sources, but it is caused by the chemical reaction of volatile organic compounds (VOCs) in the atmosphere with other gases in the atmosphere [3]. VOCs come from human activities, such as vehicle exhaust emissions or from industrial sector. However, traffic sources are considered the main source of VOCs in urban areas such as Bangkok and other pollutants in the city lead to the formation of SOA [4]. There are many factors that affect the concentration of SOA, such as the source, the reaction mechanism of the precursor pollutants in the atmosphere, meteorological condition, which affect the accumulation, distribution in the atmosphere and changes in the characteristics and severity of air pollution problems, such as the situation in Bangkok, it was found that during February - March of each year, the $PM_{2.5}$ in the atmosphere exceeds the ambient air quality standard of Thailand. In urban areas, traffic is the main source of VOCs and other pollutants that lead to the formation of SOA. However, identifying the source of SOA remains a major challenge, as SOA has a complex composition and continuously changing in atmosphere. The organic fraction of $PM_{2.5}$ has been extensively investigated in recently, mainly finding molecular marker to finding information on the origin

sources. Fraction of dicarboxylic acids has been widely used as tracer for identification of primary and secondary sources of precursors. In addition, the lack of effective methods to separate complex sources with diverse pollution sources also requires the development of methods that can separate traffic SOA from other sources in urban areas.

METHODOLOGY

$PM_{2.5}$ sample were collected near roadside area Ngam Wong Wan gate 3 of Kasetsart University, Bangkok, Thailand (Figure 1). The sampling site located in urban area surrounded by heavy traffic roads (Ngam Wong Wan road). $PM_{2.5}$ samples were colleted from 18 - 25 November 2024. The sampling was done for 24 h from 9:00 a.m. to 9:00 a.m. of the next day. Each sample collected on quartz fiber filters (Whatman, USA) with flow rate 1.52 $L.min^{-1}$. Before the sampling quartz fiber filters was prebaked in oven at 350 ◦C for 1 h to eliminate organic contaminants. After the sampling quartz fiber filters were kept at -20 ◦C before the chemical analysis.

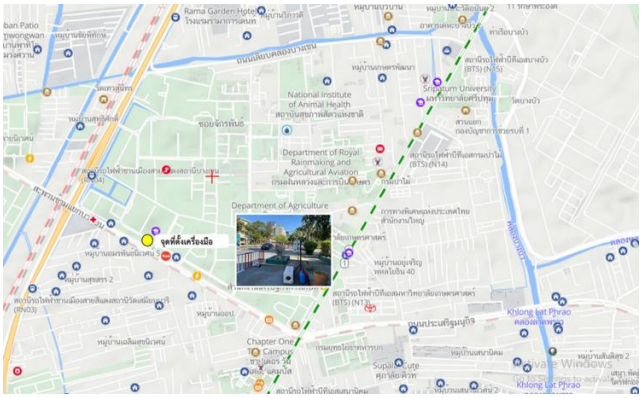


Figure 1. particulate matter ($PM_{2.5}$) sampling area near Ngam Wong Wan gate 3, Kasetsart University

The chemical analysis of dicarboxylic acids in $PM_{2.5}$ has been described in previous studies [5] [6] [7]. Briefly, the filter was extracted with a mixture of dichloromethane/methanol (1: 9, v/ v, 10 mL) under ultrasonication 60 min. The filtered extract was concentrated with pure nitrogen gas. After the dried extracts silylated with 40 µL of N,O-bis-(trimethylsilyl) trifluoroacetamide (BSTFA) containing 1% trimethylsilyl chloride and pyridine 10 µL for 1.5 h at 70°C. The result derivative was diluted with 100 µL of isooctane containing the recovery standard (hexadecane). The GC/MS was performed using an Agilent Technologies Network GC/MS system (7890 GC with 5973 mass selective detector). The column used was a ZB-5MSplus column (L= 30 m, I.D. = 0.25 mm, df = 0.25 µm film thickness (USA). High purity helium was the carrier gas with a velocity of 1.0 $mLmin^{-1}$.

RESULTS AND DISCUSSIONS

The average 24 h concentration of $PM_{2.5}$ near roadside show in table 1, the concentration of $PM_{2.5}$ range between 26.922-59.649 µ $g.m^{-3}$. Figure 2 reveals distinct diurnal patterns in $PM_{2.5}$ concentrations, characterized by an early morning peak (04:00-08:00) when concentrations reach their highest levels, followed by decrease during midday hours (10:00-14:00), and then increase during evening hours (16:00-24:00) with a secondary peak occurring around 22:00-24:00. This distribution suggests that $PM_{2.5}$ levels are heavily influenced by daily human activities, particularly morning and evening traffic patterns. The result of dicarboxylic acids and related SOA have been investigated in the urban atmosphere, the study found that when using a solvent mixture of methanol/dichloromethane (9:1) at a volume of 10 ml for extraction, the $PM_{2.5}$ chemical analysis of organic acids in $PM_{2.5}$ shown that predominance succinic acid and phthalic acid, phthalic acid is often the second most abundant diacid in urban roadside $PM_{2.5}$ sample. This aromatic acid is

direct emitted from combustion sources and has been considered to generate in atmosphere by atmospheric degradation of aromatic hydrocarbon such as naphthalene [5]. Additionally, other types of acids were found, including dicarboxylic acids; 1,2-benzenedicarboxylic acid, butyl 2-methylpropyl ester, 1,3-benzenedicarboxylic acid (isophthalic acid), propanedioic acid, monocyclohexyl-, 2,5-furandicarboxylic acid and benzenebutanoic acid, 2-carboxy-tricarboxylic acid; 1,2,4,5-benzenetetracarboxylic acid and 1,3,3,5-pentanetetracarboxylic acid ketocarboxylic acids; butanoic acid, 3-methyl-2-oxo-, bis(trimethylsilyl), propanoic acid, 2-oxo-3-(trimethylsilyloxy)-, butanoic acid, 3-oxo-, 2,2,2-trifluoroethyl and cyclooctaneacetic acid, 2-oxo-.

Table 1. Concentration of $PM_{2.5}$ roadside area Ngam Wong Wan gate 3 of Kasetsart University.

Date	**$PM_{2.5}$ ($\mu g.m^{-3}$)**
18 December 2024	26.922
19 December 2024	39.518
20 December 2024	52.152
21 December 2024	34.397
22 December 2024	38.916
23 December 2024	59.649
24 December 2024	44.548

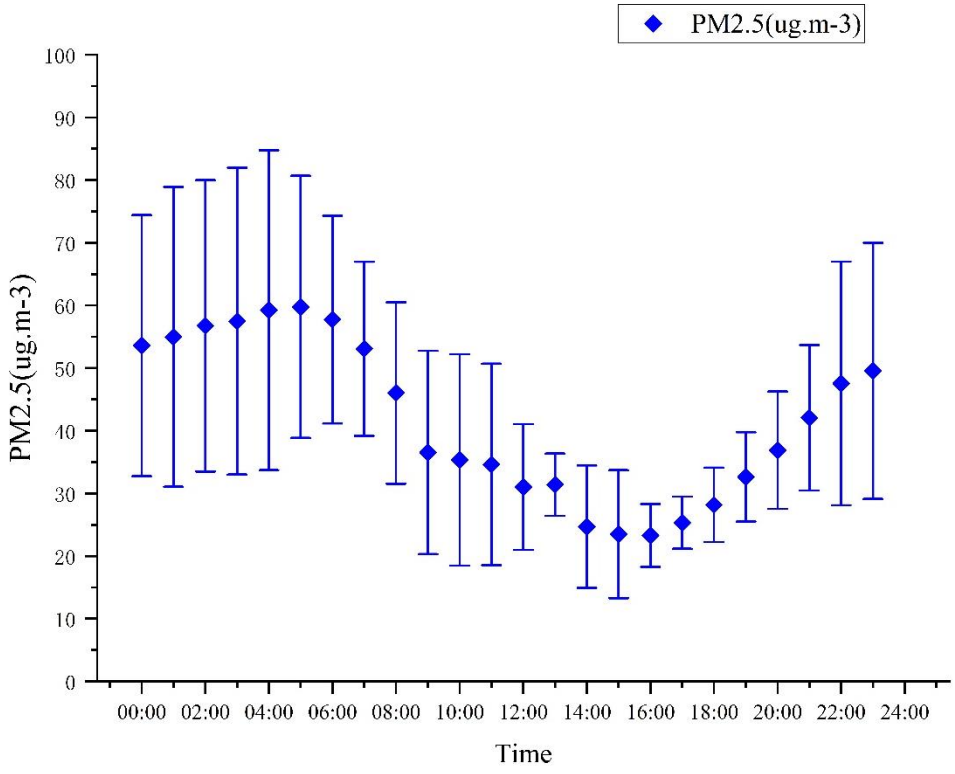


Figure 2. diurnal patterns in $PM_{2.5}$ concentrations

CONCLUSION

This study investigated the concentration patterns and chemical composition of $PM_{2.5}$ in a roadside environment at Kasetsart University, Bangkok. The findings reveal distinctive diurnal variations in $PM_{2.5}$ concentrations, with pronounced peaks during early morning hours (04:00-08:00) and evening to night hours (16:00-24:00), with a secondary peak around 22:00-24:00. These patterns strongly correlate with urban traffic flow, particularly during morning and evening rush hours, demonstrating the significant impact of vehicular emissions on urban air quality. The chemical analysis of $PM_{2.5}$ samples using methanol/dichloromethane (9:1) extraction identified succinic acid and phthalic acid as the predominant organic compounds. Phthalic acid, typically the second most abundant diacid in urban roadside samples, originates from both direct combustion emissions and atmospheric degradation of aromatic hydrocarbons. The presence of these compounds, along with various other identified organic acids, confirms the significant contribution of traffic-related secondary organic aerosol formation in the urban atmosphere. These results enhance our understanding of $PM_{2.5}$ composition in urban environments and highlight the importance of traffic emission control in air quality management strategies. The identified chemical markers can serve as tracers for source apportionment studies and aid in developing more effective pollution mitigation measures for urban areas with heavy traffic density like Bangkok.

ACKNOWLEDGEMENT

This research was funded by Kasetsart University through the Graduate School Fellowship Program; the Atmospheric Science Research Group (ASRG); and the Faculty of Environment, Kasetsart University, Bangkok, Thailand.

REFERENCE

[1] Vodicka P, Kawamura K, Deshmukh DK, Pokorna P, Schwarz J, Zdimal V. Anthropogenic and biogenic tracers in fine aerosol based on seasonal distributions of dicarboxylic acids, sugars and related compounds at a rural background site in Central Europe. Atmospheric Environment. 2023;299:119619.

[2] Wiedensohler, A., Cheng, Y., Nowak, A., Wehner, B., & Achtert, P. (2008). Rapid aerosol particle growth and increase of cloud condensation nucleus activity by secondary aerosol formation and condensation: a case study for regional air pollution in northeastern China. *J. Geophys. Res.*, 114, 1-13.

[3] Wang, S., Wu, D., Wang, X., Fung, J. C. H., & Yu, J. Z. (2013). Relative contributions of secondary organic aerosol formation from toluene, xylenes, isoprene, and monoterpenes in Hong Kong and Guangzhou in the Pearl River Delta, China: an emission-based box modeling study. *Journal of Geophysical Research: Atmospheres*, 118, 507 - 519.

[4] Lui, K. H., Lau, Y.-S., Poon, H. Y., Organ, B., Chan, M.-N., Guo, H., . . . Ho, K. F. (2023). Characterization of chemical components of fresh and aged aerosol from vehicle exhaust emissions in Hong Kong. *Chemosphere*, 333, 138940.

[5] Kawamura K. Identification of C2-C10 .omega.-oxocarboxylic acids, pyruvic acid, and C2-C3 .alpha.-dicarbonyls in wet precipitation and aerosol samples by capillary GC and GC/MS. Analytical Chemistry. 1993;65(23):3505-11.

[6] Pietrogrande MC, Bacco D. GC–MS analysis of water-soluble organics in atmospheric aerosol: Response surface methodology for optimizing silyl-derivatization for simultaneous analysis of carboxylic acids and sugars. Analytica Chimica Acta. 2011;689(2):257-64.

[7] Pietrogrande MC, Bacco D, Chiereghin S. GC/MS analysis of water-soluble organics in atmospheric aerosol: optimization of a solvent extraction procedure for simultaneous analysis of carboxylic acids and sugars. Analytical and Bioanalytical Chemistry. 2013;405:1095-104.

[8[Kawamura K, Bikkina S. A review of dicarboxylic acids and related compounds in atmospheric aerosols: Molecular distributions, sources and transformation. Atmospheric Research. 2016;170:140-60.

[9] Kawamura K, Yasui O. Diurnal changes in the distribution of dicarboxylic acids, ketocarboxylic acids and dicarbonyls in the urban Tokyo atmosphere. Atmospheric Environment. 2005;39(10):1945-60.

[10] Tkacik DS, Lambe AT, Jathar S, Li X, Presto AA, Zhao Y, et al. Secondary organic aerosol formation from in-use motor vehicle emissions using a potential aerosol mass reactor. Environ Sci Technol. 2014;48(19):11235-42.

20R3-09

The Impact of Free Public Transit Measures on Urban Traffic and $PM_{2.5}$ Emissions: A Case Study in Thailand

Yossakorn Fungkeit[1] Surat Bualert[2*] Parkpoom Choomanee[3] Thunyapat Thongyen[4] and Kodchakun Phuangsri[5]

[1]Graduate student; Department of Environmental Science, Faculty of Environment, Kasetsart University, Bangkok, Thailand; [2]Associate Professor, Department of Environmental Science, Faculty of Environment, Kasetsart University, Bangkok, Thailand; [3]Assitant Professor, Department of Environmental Science, Faculty of Environment, Kasetsart University, Bangkok, Thailand; [4]Assitant Professor, Department of Technology and Management, Faculty of Environment, Kasetsart University, Bangkok, Thailand; [5]Department of Geology, Chulalongkorn University*

**Corresponding author: Tel : 0818039899 , E-mail : surat.b@ku.th*

ABSTRACT

Transportation is a major contributor to fine particulate ($PM_{2.5}$) emissions in Thailand, particularly in congested urban areas. These emissions not only degrade air quality but also have broader economic impacts by limiting individuals' ability to participate in daily activities. This study aims to investigate atmospheric $PM_{2.5}$ emissions through short-term observations conducted along the inbound section of the Sirat Expressway a key urban tollway leading to central Bangkok during the morning rush hour (06:00–09:00). The study compares traffic conditions and $PM_{2.5}$ emissions before and during the implementation of free public transit measures $PM_{2.5}$ emissions were estimated using the U.S. EPA's Motor Vehicle Emission Simulator (MOVES), a widely recognized tool for modeling mobile source emissions. The monitoring period included both regular working days and days when the free public transportation policy was active. Results indicate that $PM_{2.5}$ concentrations peaked consistently at 07:00-08:00 across all study days. During regular working days, traffic volume was significantly higher and average speeds were lower, resulting in greater $PM_{2.5}$ mass emissions. In contrast, the introduction of free public transit reduced traffic congestion, improved speed distribution, and led to a decrease in $PM_{2.5}$ emissions. Findings suggest that the free public transport policy contributed to emission reductions by alleviating peak-hour traffic bottlenecks. Additionally, other concurrent policies such as work-from-home (WFH) measures likely played a supportive role in lowering traffic volume and associated emissions. This study highlights the potential effectiveness of short-term public transit incentives in improving urban air quality and supports the consideration of long-term sustainable transportation strategies in $PM_{2.5}$ management.

Keywords : $PM_{2.5}$; Free Public Transport Measures ; Air Quality ; Urban Expressway Traffic ; MOVES

INTRODUCTION

Air quality in Thailand has continued to deteriorate for several days due to high levels of fine particulate matter ($PM_{2.5}$) from agricultural waste burning and transport emissions. This problem is particularly severe in densely populated urban areas with heavy traffic [1]. In addition, meteorological factors between November and February disrupt the distribution of air masses, leading to what is known as the "Haze season" typically occurring during winter in Thailand with extremely high $PM_{2.5}$ levels in January and February. (Thai Meteorological Department, 2022) [2]. The air pollution usually occurs during winter in Thailand, with extremely high levels in January and February. In urban areas, primary air pollutants (i.e., PM, SOx, NOx, NH_4^+) are directly emitted from anthropogenic sources such as motor vehicle exhaust, agricultural waste burning, and industrial processes, combined with unfavorable meteorological conditions that limit atmospheric dispersion [3].

Fine particulate matter is a major health problem in the modern world, with serious negative impacts on human health, ecosystems, and the economy. Different sources of PM result in variations in its chemical and physical composition, leading to differing levels of toxicity that have a direct impact on many health issues [4]. In addition, environmental impacts of pollution are becoming more serious every day. These factors affect the economy, notably through the loss of opportunities for individuals to participate in their regular daily lives [5].

Transportation is a major source of fine particle emissions, particularly in congested urban areas. To address this issue, the Prime Minister of Thailand has introduced an urgent measure to mitigate $PM_{2.5}$ pollution by offering free public transportation, including electric trains and buses operated by the Bangkok Mass Transit Authority (BMTA). The primary objective of this initiative is to reduce the use of private vehicles, which are a major source of air pollution. Free public transport measures can help reduce the number of cars on the road and increase travel speeds, both of which are directly linked to $PM_{2.5}$ emissions from vehicles. [6]

The US-EPA's Motor Vehicle Emission Simulator (MOVES) is a modeling tool developed by the U.S. Environmental Protection Agency to estimate air pollutant emissions from mobile sources. Originally designed to predict vehicle emission outcomes under various traffic behaviors and vehicle conditions across different study scenarios, MOVES is now also applied to assess the effectiveness of greenhouse gas mitigation measures in the transportation sector. By focusing on air quality improvement, the effect of transport policies such as driving restrictions [7], road pricing schemes [8], and gasoline regulations [9] have been widely discussed. Likewise, the effect of new public transportation infrastructure supply on air quality has been extensively investigated. This is the case for new urban public transportation openings and expansions, as well as improvements in service, speed, and routing. However, little is known about the effects of low-cost or free-of-charge public transportation financing schemes on air quality [10][11].

Therefore, this study aims to investigate atmospheric fine particle emissions through short-term observations at an urban center expressway with heavy traffic, both before and during the implementation of free public transit measures. Additionally, it aims to demonstrate the potential of these measures in controlling $PM_{2.5}$ emissions based on MOVES, which is a state-of-the-science emission modeling system that estimates emissions for mobile sources at the national, county, and project level for criteria air pollutants, greenhouse gases, and air toxics. Changes in human traffic activities due to the free public transit measures allowed for objective testing and evaluation of variations in urban $PM_{2.5}$ emissions. To assess $PM_{2.5}$ levels, measurements taken before and during the implementation of the measures were compared, with a focus on the haze season. Finally, we report the efficiency of free public transit measures in reducing $PM_{2.5}$ levels in Thailand.

METHODOLOGY

Site Description, Timeline and Meteorology

This study focuses on the inbound section of the Sirat Expressway (tollway) leading to central Bangkok, covering a distance of 0.384 kilometers with three lanes and a shoulder (latitude: 13.819624N; longitude: 100.549576E), as shown in Figure 1. Two study periods were selected: regular working days (January 20–22, 2025) and working days with the free public transport measure (January 27–29, 2025). Both periods were observed during Thailand's morning rush hour (approximately 06:30–09:30), which is typically very busy on working days. The measured meteorological temperature and relative humidity (RH) (DMA875, LSI Lastem Milano, Italy) data were obtained from the Air Pollutants Monitoring Tower at

Kasetsart University (KU Tower) at a height of 30 meters above ground level (latitude: 13.854529N; longitude: 100.570012E) [12].



Figure 1. the Sirat Expressway (tollway) leading to central Bangkok, covering a distance of 0.384 kilometers (yellow line).

Speed and traffic volume

This study investigates traffic speed based on the speed limits applied to elevated expressways in Thailand. For four-wheeled vehicles, including passenger cars and pickup trucks, the speed limit is 100 km/h. For trucks with a gross weight over 2,200 kilograms and buses with more than 15 seats, the speed limit is 80 km/h. School buses or student transport vehicles are limited to a maximum speed of 65 km/h. Vehicles with an 80 km/h speed limit include vans, buses, and trucks, while trailers are subject to a 60 km/h speed limit. Traffic was observed using CCTV footage provided by Bangkok Expressway and Metro (BEM), analyzed through photo review and manual traffic counting conducted at continuous 30-minute intervals. Vehicle types were categorized for input into the MOVES model as follows: Motorcycle, Passenger Car, Passenger Truck, Light Commercial Truck, Other Buses, Transit Bus, and Single Unit Short-haul Truck. Both study periods were observed during the morning rush hour from 06:00 to 09:00. However, according to Thai regulations, trucks are prohibited from using expressways between 05:00 and 09:00. As a result, these vehicle types were absent during the observation period, as shown in Figure 2 and 3.

$PM_{2.5}$ in Ambient Air collection

This study also monitored actual PM2.5 concentrations, as measured based on light scattering using the Tapered Element Oscillating Microbalance (TEOM) 1405 DF (Thermo Fisher Scientific Inc., Waltham, MA, USA). The instrument was installed on the rooftop of the Faculty of Environment building at a height of 30 meters above ground level, which helps to minimize direct interference from traffic emission sources [13].

Traffic-Based $PM_{2.5}$ Emission Estimation with MOVES

For the MOVES model input, the fuel formulation is based on the default dataset corresponding to the Euro-5 standard. Vehicle age distribution and fuel consumption data for each vehicle type are referenced from the Department of Land Transport's annual report for the fiscal year 2024. The vehicle age distribution is as follows: less than 1 year (4.07%), 1 year (6.02%), 2 years (5.94%), 3 years (5.27%), 4 years (4.84%), 5 years (5.54%), 6 years (5.42%), 7 years (4.97%), 8 years (4.34%), 9 years (4.11%), 10 years (4.25%), 11 years (4.99%), 12 years (5.15%), 13 years (4.36%), 14 years (3.06%), 15 years (2.82%), 16 years (2.45%), 17 years (2.74%), 18 years (2.66%), 19 years (2.26%), 20 years (1.99%), 21 years (2.49%), 22 years (2.28%), 23 years (1.92%), 24 years (1.58%), 25 years (1.43%), and more than 25 years (3.04%).

The distribution of vehicle fuel types is as follows: Gasoline (67.54%), Diesel (28.47%), Liquefied Petroleum Gas – LPG (1.19%), Compressed Natural Gas – CNG (0.55%), Electricity (1.05%), and Hybrid and other fuel types (1.19%). [14].

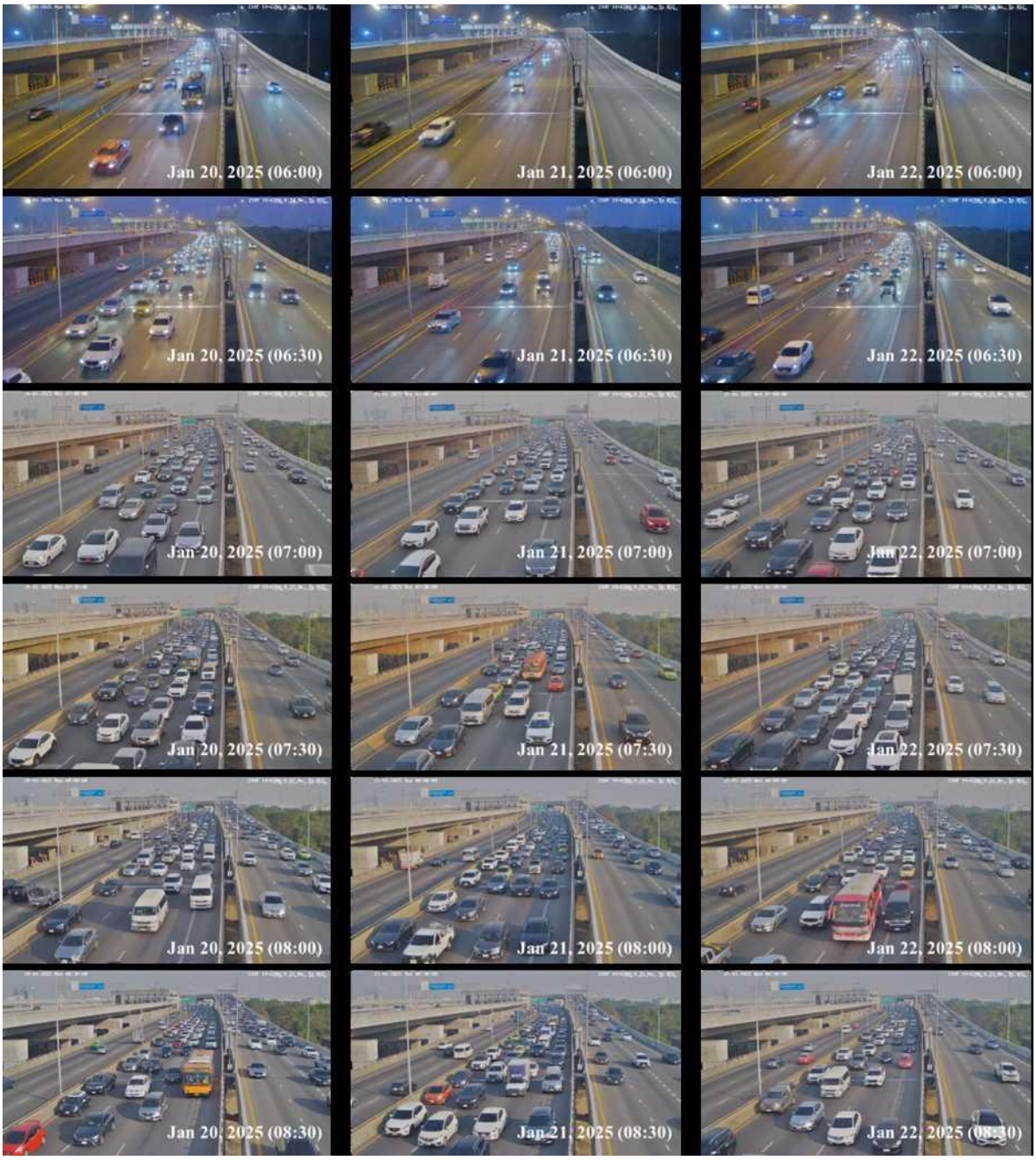


Figure 2. Hourly traffic monitoring on the Sirat Expressway (06:00–09:00) during regular working days (Jan 20–22, 2025).



Figure 3. Hourly traffic monitoring on the Sirat Expressway (06:00–09:00) during free public transport days (Jan 27–29, 2025).

Table 1. Important MOVES model inputs that influence the emission rates output [15][16].

Input	**Data preparation**	**Emission rate sensitivity**
Meteorology	Temperature and RH from local weather station	Peak sensitivity
Vehicle Kilometers Traveled	From travel demand models or real time traffic data	Very high sensitivity
Driving cycles	Driving patterns from local vehicle activity data	High sensitivity
Vehicle age maintenance data	From regional environmental agencies regulations	Medium sensitivity
Fuel formulation and supply	From regional environmental agencies regulations	Medium sensitivity

Average Speed Distribution	From travel demand models or real-time traffic data	Medium sensitivity
Vehicle fuel consumption	From department of motor vehicle registration	Low sensitivity
Activity fractional distribution	From travel demand models or real-time traffic data	Very low sensitivity

RESULTS AND DISCUSSIONS

$PM_{2.5}$ concentration trend

$PM_{2.5}$ concentrations under the free public transport measure were analyzed for diurnal variation, as shown in Table 2. The observed concentrations reflected typical peak traffic patterns during morning rush hours (06:30 to 09:30), with notable changes observed after the implementation of the free public transport measure. Across all study days, the highest $PM_{2.5}$ concentrations consistently occurred at 08:00. During the regular working days, the highest concentration was approximately 86.49 µg/m³ on Wednesday at 08:00, while the lowest was 65.56 µg/m³ on Wednesday at 06:00. Following the introduction of the free public transport measure, a reduction in mean $PM_{2.5}$ concentration at 08:00 was observed: a decrease of 32.95 µg/m³ on Monday, 53.89 µg/m³ on Tuesday, and 60.32 µg/m³ on Wednesday, compared to the corresponding days during the regular working period. The lowest concentrations under the free public transportation measure were recorded at 08:00 on Monday, with a value of 12.35 µg/m³, consistent with improved traffic flow conditions and enhanced atmospheric dispersion typically occurring in the early morning.

Table 2. $PM_{2.5}$ concentration during regular working days and free public transport days

Date & Time	Regular working days			Free public transport days		
	$PM_{2.5}$ (µg/m³)	**Temp. (°C)**	**RH (%)**	**$PM_{2.5}$ (µg/m³)**	**Temp. (°C)**	**RH (%)**
Mon. 06:00	48.60	22.8	59	16.63	22.4	59
Mon. 07:00	49.10	22.2	61	16.08	21.6	58
Mon. 08:00	45.30	21.7	62	12.35	21.4	57
Tue. 06:00	76.48	22.4	62	28.84	21.4	59
Tue. 07:00	80.55	21.9	64	26.34	21.3	58
Tue. 08:00	81.26	22.1	62	27.37	21.3	57
Wed. 06:00	65.56	22.1	67	31.36	20.9	59
Wed. 07:00	77.63	21.6	70	25.97	20.7	60
Wed. 08:00	86.49	22.7	62	26.17	21.1	59

Impact of free transit on drive cycles

The study of traffic volume and speed on the selected route revealed that, during regular working days, expressway traffic exhibited higher volumes and lower average speeds compared to the period with the free public transportation measures. In both periods, passenger cars accounted for the largest proportion of vehicles, comprising 93% of the total traffic volume. The most congested period was between 07:00 and 08:00 AM, during which the lowest average speed was observed on regular working days at 7.24 km/h. In contrast, during the same hour under the free public transport measures, the average speed increased to 7.77 km/h, with a reduction of 448 vehicles, as shown in Figure 4.

When analyzing the overall traffic during the observation period under the free public transportation scheme, the average speed increased significantly to 40.91 km/h, while the total traffic volume dropped to 34,370 vehicles. This contrasts with the regular working days, where the average speed was 24.09 km/h and the traffic volume reached 65,416 vehicles. Based on these traffic outcomes, the MOVES-based $PM_{2.5}$ emission forecasts indicate a corresponding reduction in emissions, reflecting the positive impact of the free public transportation measures.

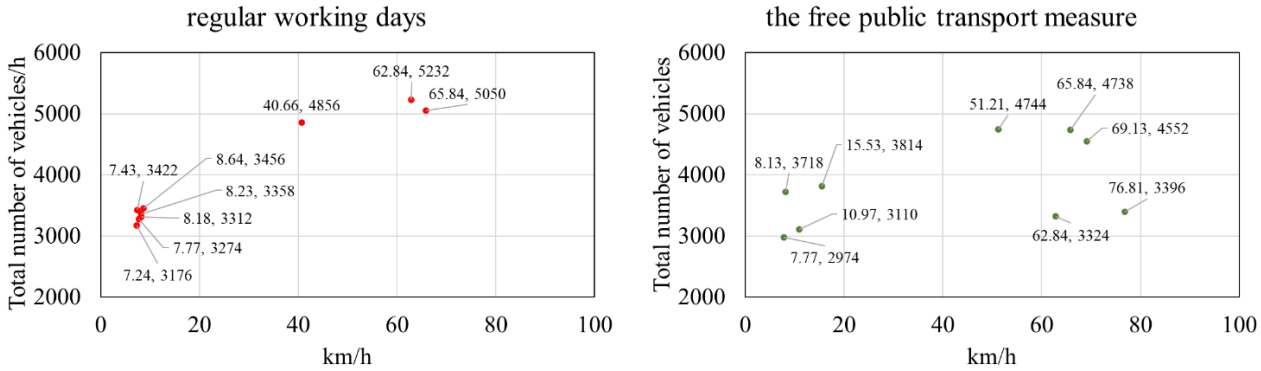


Figure 4. Relationship between traffic volume and speed during regular working days and free public transport measures

Comparison of $PM_{2.5}$ emission for the free public transport measure

The $PM_{2.5}$ mass emissions throughout the study period, as shown in Table 3, demonstrate a clear relationship between traffic speed, volume, and emission levels. During the morning rush hours of the regular working days, the average $PM_{2.5}$ emission was 7.88 grams. In contrast, under the free public transport days, the average emission decreased to 5.65 grams. When analyzed by time period, $PM_{2.5}$ emissions during 07:00–08:00 and 08:00–09:00 on regular working days were higher than those during 06:00–07:00. This can be attributed to increased traffic volume and lower average speeds during peak hours. On the other hand, during the free public transport days, the highest $PM_{2.5}$ emissions were observed between 07:00 and 08:00. This reflects the reduction in overall traffic volume and a more evenly distributed traffic flow, avoiding excessive congestion during a single peak hour. Since this study was conducted during the period when Thailand was under $PM_{2.5}$ pollution control, it is possible that additional air pollution reduction measures, such as the Work from Home (WFH) policy enforced by various organizations, also contributed to the decrease in traffic volume.

Table 3. $PM_{2.5}$ mass emission during regular working days and free public transport days

Date & Time	$PM_{2.5}$ Mass Emission (grams)	
	Regular working days	Free public transport days
Mon. 06:00	4.73	4.38
Mon. 07:00	9.85	8.73
Mon. 08:00	9.70	7.12
Tue. 06:00	4.16	3.59
Tue. 07:00	9.12	7.57
Tue. 08:00	9.51	2.51
Wed. 06:00	3.98	3.80
Wed. 07:00	9.46	10.45
Wed. 08:00	10.37	2.70

CONCLUSION

Free public transport measures help reduce traffic volume on expressways during rush hours. When traffic volume decreases during these hours, total daily, monthly, and annual traffic volume also decreases, leading to a reduction in greenhouse gas emissions and an increase in traffic speed. As traffic speed increases, $PM_{2.5}$ emissions from combustion decrease. To maximize $PM_{2.5}$ reduction during this period, it is recommended to promote work-from-home measures to further reduce traffic volume for those who still need to work in person. In addition, an economic feasibility study of implementing free public transportation measures could support long-term policy decisions by evaluating the cost-effectiveness of the program (health cost saving, transport operating costs, etc.) in relation to the reduction of urban air pollution.

ACKNOWLEDGEMENT

This study was supported by the Bangkok Expressway and Metro (BEM) for CCTV traffic data, and funded by the Atmospheric Science Research Group and the Faculty of Environment, Kasetsart University, Bangkok, Thailand.

REFERENCE

[1] Carlisle,A.,&Sharp, N. (2001).Exercise and outdoor ambient air pollution. British Journal of Sports Medicine ,35(4),214 222.

[2] Thai Meteorological Department. 2025. Seasonal in Thailand. URL https://www.tmd.go.th (accessed 14 March 2025).

[3] Rattanapotanan, T., Thongyen, T., Bualert, S., Choomanee, P., Suwattiga, P., Rungrattanaubon, T., Utavong, T., Phupijit, J., & Changplaiy, N. (2023). Secondary sources of $PM_{2.5}$ based on the vertical distribution of organic carbon, elemental carbon, and water-soluble ions in Bangkok. *Environmental Advances*, *11*, 100337. https://doi.org/10.1016/j.envadv.2022.100337

[4] WHO, 2019. Ambient (Outdoor) Air Pollution. World Health Organization, Retrieved 1 February 2025 from https://www.who.int/news-room/fact-sheets/detail/ambient- (outdoor)-air-quality-and-health.

[5] EEA, 2021. Air Quality Standards. European Environment Agency, Retrieved 1 February 2025 from https://www.eea.europa.eu/themes/air/air-quality-concentrations/airquality-standards

[6] Gu, Y., & Yung, R. (2023). *Free rides to cleaner air? Examining the impact of massive public transport fare discounts on air quality.* Transportation Research Part D: Transport and Environment, 118, 103938.

[7] Davis, L.W., 2021. Estimating the price elasticity of demand for subways: Evidencefrom Mexico. Reg. Sci. Urban Econ. 87, 103651.

[8] Percoco, M., 2013. Is road pricing effective in abating pollution? Evidence from milan.Transp. Res. D 25, 112–118.

[9] Auffhammer, M., Kellogg, R., 2011. Clearing the air? The effects of gasoline contentregulation on air quality. Amer. Econ. Rev. 101 (6), 2687–2722.

[10] Lu, H., Zhu, Y., Qi, Y., Yu, J., 2018. Do urban subway openings reduce PM2.5concentrations? Evidence from China. Sustainability 10 (11), 4147.

[11] Li, S., Liu, Y., Purevjav, A.-O., Yang, L., 2019. Does subway expansion improve airquality? J. Environ. Econom. Manage. 96, 213–235.

[12] Choi,D.,Beardsley, M.,Brzezinski, D., Koupal, J.,Warila,J.,2010. MOVES sensitivity analysis: the impacts of temperature and humidity on emissions. In:Presentedat the 19th Annual International Emission Inventory Conference, Ann Arbor, MI.

[13] Saiohai, J., Bualert, S., Thongyen, T., Duangmal, K., Choomanee, P., & Szymanski, W. W. (2023). Statistical PM2.5 prediction in an urban area using vertical meteorological factors. *Atmosphere*, *14*(3), 589. https://doi.org/10.3390/atmos14030589

[14] USEPA, 2017. Dynamometer Drive Schedules [WWW Document]. US EPA. Retrieved 1 February 2025. https://www.epa.gov/vehicle-and-fuel-emissions-testing/dynamometer-driveschedules

[15] US EPA (2021). *MOVES3 Technical Guidance: Using MOVES to Prepare Emission Inventories for State Implementation Plans and Transportation Conformity.* U.S. Environmental Protection Agency, Office of Transportation and Air Quality. https://www.epa.gov/moves

[16] Liu,H.,Chen, X.,Wang, Y.,Han, S.,2013.Vehicle emission and near-road air quality modeling for Shanghai, China :based on global positioning system data from taxis and revised MOVES emission inventory. Transp. Res. Rec. 1, 38–48. http://dx.doi.org/10.3141/2340-05.

20R3-10

Carbon Footprint for Organization: Case Study of Printing and Packaging Factory in Thailand

Atchara Pasavanung[1,2] ,Withida Patthanaissaranukool[1,2], Thanakrit Neamhom[1,2], Supawadee Polprasert[1,2*]

[1] *Department of Environmental Health Sciences, Faculty of Public Health, Mahidol University, Bangkok, 10400, Thailand*
[2] *Center of Excellence on Environmental Health and Toxicology (EHT), OPS, MHESI, Bangkok 10400, Thailand*
***** *Corresponding author: Supawadee Polprasert, Phone 0845272277, Fax 023548525, E-mail address: supawadee.pol@mahidol.ac.th*

ABSTRACT

The purpose of this study is to identify the carbon footprint associated with all activities in a printing and packaging production facility. Additionally, it aims to provide guidelines for organizations in this industry to reduce their carbon emissions. Researching carbon emissions from printing and packaging factories offers a valuable opportunity for Thailand to progress toward carbon neutrality and achieve its sustainable development goals. By examining the high energy consumption and the raw materials used in these processes, more effective strategies for reducing emissions can be developed. The activity data on all production and office operations are collected over the course of one year, from January to December 2024. This data will encompass both direct and indirect sources of GHG emissions, in accordance with the TGO guidelines. The results indicate that in 2023, the carbon footprint of the printing and packaging production factory is expected to reach 4,105.79 tons of CO_2e per year. The main source of carbon emissions in our operations comes from purchased electricity (Scope 2), which amounts to 2,256.55 tons of CO_2e per year. Following this, indirect emissions categorized under Scope 3 total 1,094.54 tons of CO_2e per year. Scope 3 emissions include those from purchased goods and services, fuel and energy-related activities, waste generated, as well as downstream transportation and distribution. Direct carbon emissions (Scope 1) are the least significant, contributing approximately 754.70 tons of CO_2e per year, primarily because most machines in the factory operate using electricity. Incorporating solar energy, utilizing high-efficiency appliances like air conditioning and lighting, and adopting energy-saving initiatives are crucial for reducing overall power consumption. Since implementing solar energy, there has been a significant reduction in electricity usage compared to 2022, with a decrease of approximately 502.4 tons of CO_2e per year.

Keywords : carbon footprint for organization; printing and packaging; global warming; greenhouse gas emission; carbon emission

INTRODUCTION

Global warming is a critical worldwide issue that must be urgently addressed. This problem is caused by the rise in temperature resulting from various human activities that disrupt the balance of greenhouse gas (GHG) emissions. An increase in temperature is the most instant effect of global warming, which in turn leads to climate change [1]. This significant problem has become a global challenge, leading to a consensus to reduce greenhouse gases [2]. Thailand is a member country actively participating in efforts to reduce greenhouse gas emissions and address climate change in collaboration with the international community through its National Determined Contributions (NDCs) [3]. The issue is especially important in today's rapidly changing consumer landscape. Many consumers are increasingly looking for products and safe for their health and the environment. This growing demand for eco-friendly packaging, particularly biodegradable options such as paper-based, pouches and cartons, has resulted in a significant increase in the adoption of sustainable packaging solutions. The packaging industry is essential for the production processes in the food, beverage, tourism, and export sectors. The packaging industry is expected to keep growing due to several

factors, such as rising demand for flexible packaging, expansion in the food sector, and a shift towards sustainable products. In Thailand, both the packaging and printing industries are on the rise, with packaging accounting for 60% and printing for 40% of the market. Researching carbon emissions from printing and packaging factories offers Thailand a valuable opportunity to move toward carbon neutrality and achieve its sustainable development goals. By examining the high energy consumption and raw materials used in these processes, this study aims to identify the carbon footprint associated with all activities within a printing and packaging production facility. Additionally, it also aims to provide guidelines for organizations in this industry to sustainably reduce their carbon emissions.

METHODOLOGY

The printing and packaging production factory employs 400 workers, divided into two shifts: the morning shift runs from 8:00 a.m. to 5:30 p.m., while the night shift operates from 8:00 p.m. to 5:00 a.m. Additionally, the office department consists of 148 employees and operates from 8:30 a.m. to 5:30 p.m. The summary of operational boundaries is illustrated in Figure 1. The activity data on all production and office operations are collected over the course of one year, from January to December 2024. This data includes both direct and indirect sources of greenhouse gas (GHG) emissions, in accordance with the guidelines set by the Thailand Greenhouse Gas Management Organization (TGO). The GHG emissions of an organization are categorized into three scopes:

Scope 1: Direct GHG emissions from stationary, mobile combustion equipment, and fugitive emissions.

Scope 2: Indirect GHG emissions from purchased electricity

Scope 3: Other indirect GHG emissions include four categories:

- Category 3.1 - Purchased Goods and Services,
- Category 3.3 - Fuel and Energy-Related Activities,
- Category 3.5 - Waste Generated in Operations, and
- Category 3.9 - Downstream Transportation and Distribution.

The amount of GHG emissions is calculated based on CO_2 equivalent using Equation 1.

$$\text{GHG emission} = \text{Activity Data} \times \text{Emission Factor} \quad (1)$$

Where,

GHG Emission	is the amount of greenhouse gas emissions (tons CO_2e per year)
Activity Data	is the activities that cause greenhouse gas emissions.
Emission Factor	is a constant value used to convert activity data into the amount of greenhouse gas emissions

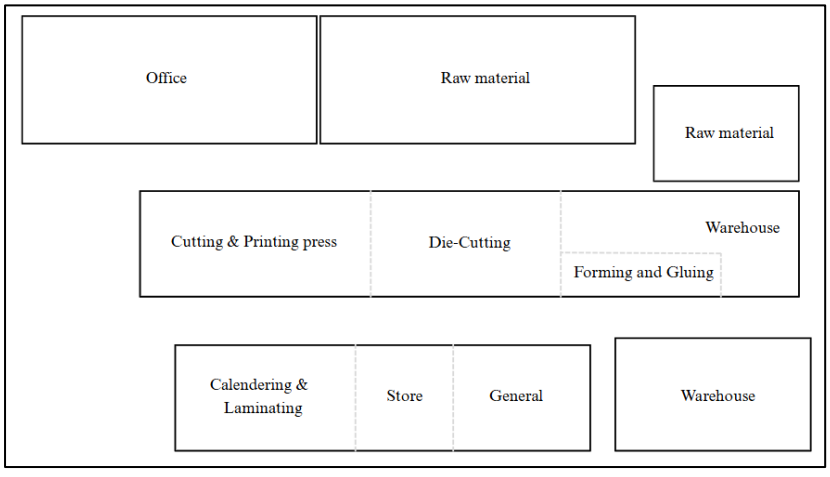


Figure 1 The system boundary of the printing and packaging factory

In the printing industry, the production process is typically divided into two main stages: Label Production and Packaging Production, both of which primarily utilize paper as the main raw material. The key shared steps in both processes are as follows: 1.Cutting Paper is cut to the required dimensions based on product specifications. 2. Printing Press or content are printed onto the paper surface. Upon completion of these steps, the production process may proceed with additional operations depending on the specific product type and customer requirements. These subsequent processes may include:

1. Calendering – The printed paper is passed through rollers to smooth the surface and enhance print quality.

2. Die-Cutting – The material is cut into specific shapes using a custom-made die designed for that particular product. This ensures high precision and product-specific consistency.

3. Slicing – In certain cases, printed materials can be directly sent to the slicing process without undergoing further finishing steps. This is typically applicable to products such as instant noodle cup lids and beverage labels.

4. UV Coating – This is a critical surface finishing technique enhances both appearance and durability, and can produce either a high-gloss or matte finish.

5. Corrugated Laminating – This process involves adhering a printed top sheet onto a corrugated board, combining visual appeal with structural strength. It is commonly used for packaging boxes of products such as cameras or automotive parts.

6. Folding and Gluing – As the final stage in the post-press process, this step uses automated machines to fold and apply adhesive, securing the structure. It is essential for high-speed production, such as toothpaste packaging.

7. Hot Stamping – A relief printing technique that uses heat and pressure to transfer foil onto the paper surface for decorative or branding purposes.

8. Stripping – The process of removing excess paper from a die-cut workpiece using a stripping unit, which cleanly ejects waste material. The packaging and printing production process is shown in Figure 2.

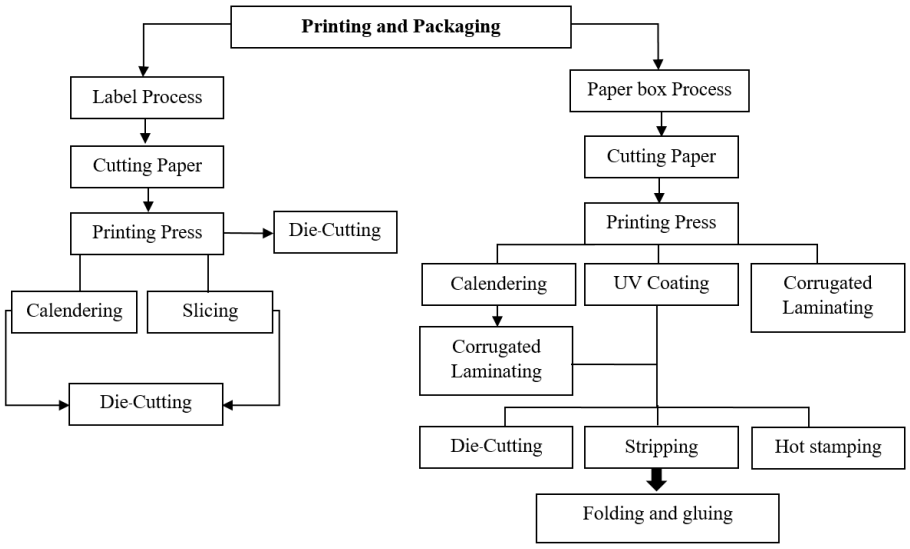


Figure 2 The packaging and printing production processes

RESULTS AND DISCUSSIONS

In 2023, the carbon footprint of the printing and packaging production factory is estimated to be 4,105.79 tons of CO_2eq per year. The results for three scopes are displayed in Table 1 and **Figure 3**.

Table 1 The amount of carbon emissions

Activity	Amount	Unit	Emission Factor	Source	Carbon Emission (ton CO_2eq/year)
Scope 1 Direct carbon emission					
Stationary combustion					
Diesel for fire pump	195	L	2.7078	[4]	0.53
Lawn mower Gasohol 91	10	L	2.1894	[4]	0.02
Mobile combustion					
Business travel E-85	1,655	L	2.2394	[4]	3.71
Gasohol 95	20,322	L	2.2394	[4]	45.51
Benzene 95	120	L	2.2394	[4]	0.27
Benzene 91	49	L	2.2394	[4]	0.11
Diesel	4134	L	2.7406	[4]	11.32
Lawn mower Gasohol 91	25	L	2.2719	[4]	0.06
Forklift –LPG	7,920	kg	3.1134	[4]	24.66
Septic tank system	1,775.19	kgCH_4	28	[4]	49.71
Fugitive Emissions					
R22	313.26	kg	1760	[4]	551.34
R32	42	kg	677	[4]	28.43
R407C	22	kg	1774	[4]	39.03
Fertilizer	3	kg	1.0335	[4]	0.003
Scope 2 Indirect GHG emissions					
Purchased electricity	4,514,000	kWh	0.4999	[4]	2256.55
Scope 3 Other indirect GHG emissions.					
Category 3.1 Purchased Goods and Services					
Toluene	1,907.4	kg	0.9551	[4]	1.82
A4	763.90	kg	2.1020	[4]	1.61
Water supply	21,756	m^3	0.7948	[4]	17.29
Toilet paper	763.9	kg	2.1020	[5]	1.61
Isopropyl alcohol	22,941	kg	2.4	[6]	55.06
Category 3.3 Fuel – and energy related activities					
Fuel – and energy-related	4,514,000	kWh	0.0987	[4]	445.53
Category 3.5 Waste generated in operations					
Solid Waste	146,000	kg	0.7933	[4]	115.82
Category 3.9 Downstream Transportation and Distribution					
Product distribution-diesel	166,313.5	L	2.7406	[4]	455.80

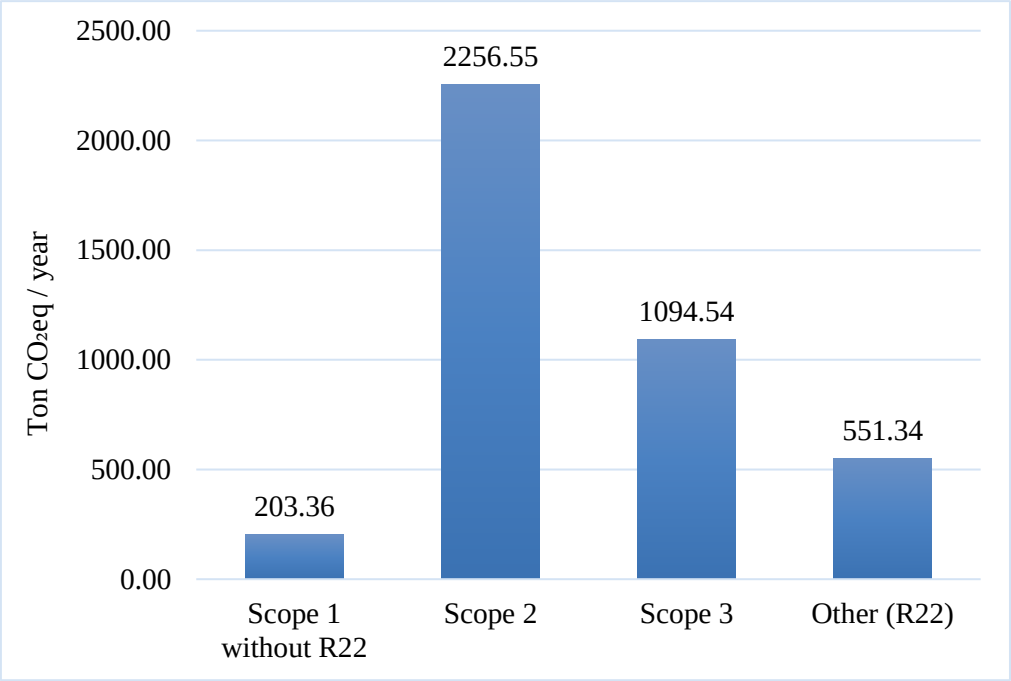


Figure 3 Amount of Carbon emission in the printing and packaging industry

The direct carbon emissions from Scope 1 amount to approximately 754.70 tons CO_2e, with R22, used as a refrigerant, being the largest contributor in this scope. Notably, the biggest portion of carbon emissions comes from Scope 2, which totals 2,256.55 tons CO_2e annually, primarily due to the electricity consumption of printing and packaging machines, air conditioning, and other electricity appliances, etc. There has been a significant reduction in electricity consumption compared to 2022, decreasing by approximately 411.9 tons CO_2e per year as a result of adopting solar energy. For Scope 1, the primary fuel used is gasohol 95, totaling 20,322 liters, followed by diesel at 4,134 liters. The company operates 24 vehicles, consisting of 23 gasoline-powered vehicles and one diesel-powered vehicle. Among these, three vehicles are designated for general use, while 21 vehicles are used for business contacts with customers on a shared basis. Therefore, it is important to reduce fuel consumption during business commuting by prioritizing online communication instead of in-person travel. The website and product catalog require comprehensive renovation to ensure easy access for ordering products and to reduce unnecessary sales travel. Moreover, refrigerant (R22) should be replaced with an alternative that has low global warming potential and is not harmful to the ozone layer. The company has a total of 101 air conditioners. This includes 81 units that use R22 refrigerant, 17 units that use R32 refrigerant, and 3 units that use a different refrigerant. In addition, the company operates 102 machines, which consist of 11 calendering machines, 10 industrial printing machines, 10 paper-cutting machines, 26 die-cutting machines, 8 forming and gluing machines, 9 air compressors, 8 film machines, and 20 other machines. Moreover, there are 2,302 light bulbs currently in use. These include 2,065 T8 36-watt bulbs, 204 T5 28-watt bulbs, 22 units of 150-watt light fixtures, and 11 units of 200-watt light fixtures, all of which consume a significant amount of electricity. It is important to incorporate solar energy, implement high-efficiency appliances such as air conditioning and lighting, and adopt energy-saving initiatives to reduce overall power consumption. The largest source of indirect carbon emissions in Scope 3 comes from downstream transportation and distribution, which amounts to 455.80 tons of CO_2e. To mitigate these emissions, it is crucial to optimize the logistics system for distributing products downstream. This can be accomplished by ensuring that goods and services

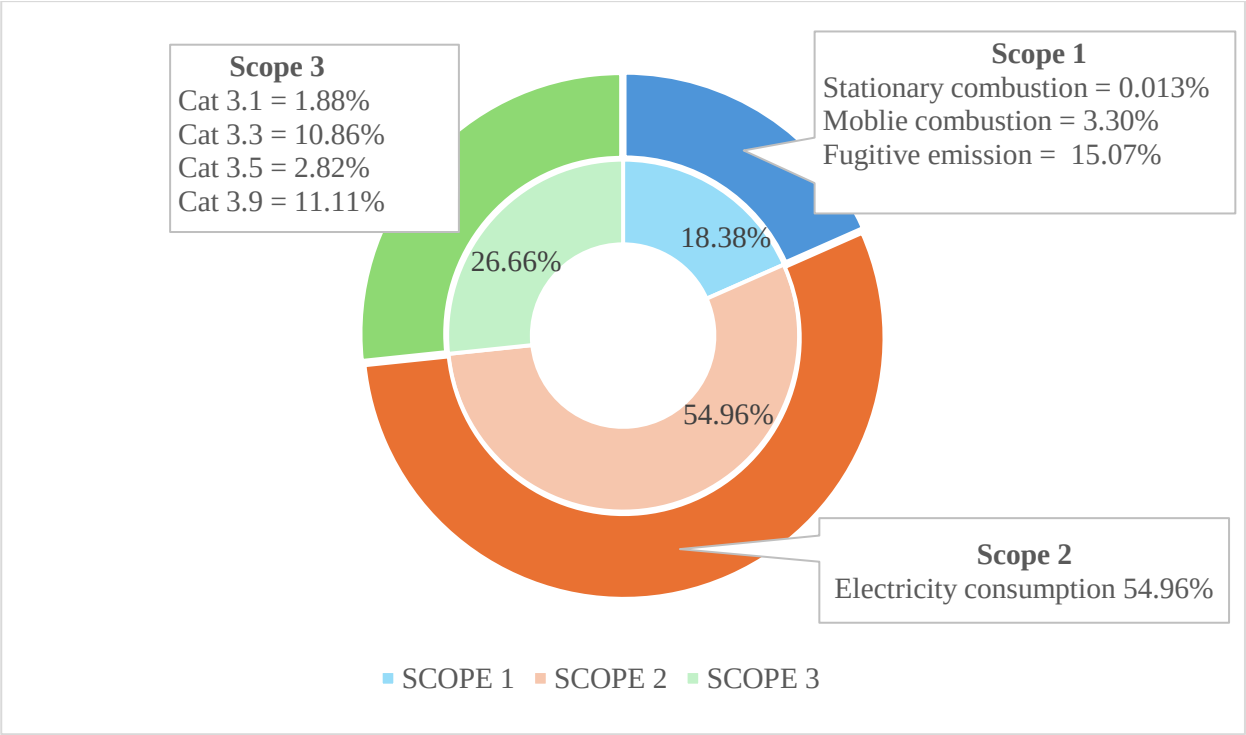


Figure 4 The contribution of carbon emissions from each scope in the Printing and Packaging Factory

In contrast, the research on carbon emissions in China's steel industry reported that in 2019, China's steel industry emitted approximately 2,326.16 million tons of CO_2. Fossil fuel combustion during the steel production process was identified as the primary source of these emissions, accounting for 71.15% under Scope 1. Additionally, emissions from purchased electricity contributed to 17.77%. These findings indicate that the main activity in this industry involves fuel combustion for power generation used in steel production, while electricity is primarily used for minor activities, such as office routines. To reduce carbon emissions in the steel industry, it is essential to optimize the energy structure by increasing the share of non-fossil energy sources in power generation. This approach aligns with global decarbonization strategies and supports the industry's commitment to achieving net-zero emissions targets [8]. A study on the carbon footprint of a news broadcasting organization conducted in the Netherlands revealed that travel and transport in scope 3 are the largest contributors to CO_2 emissions, accounting for 71.7% of the total emissions, which amounts to 166.26 tons of CO_2eq per year. This category includes air travel, domestic travel, outsourced travel, and commuter travel. To reduce greenhouse gas emissions, the study recommends encouraging employees to work from home when possible and promoting the use of electric vehicles, as these measures could significantly lower CO_2 emissions [9]. The amount of carbon emissions is directly linked to the primary activities of the organization. It is essential to declare all activities for thorough self-evaluation and to identify effective strategies for reducing carbon emissions.

CONCLUSION

The Printing and Packaging Factory contributes to carbon emissions through both direct and indirect greenhouse gas outputs from its operations. Addressing these emissions is essential to promote a more sustainable and responsible manufacturing process, particularly in Scope 1 and Scope 2. It is important to effectively manage fuel and electricity consumption by reducing usage and exploring alternatives. Vehicles should transition to electric options. Additionally, online communication needs improvement to enhance interactions with customers. The website and product catalog require comprehensive renovation to ensure

easy access for ordering products and to reduce unnecessary sales travel. Besides, refrigerant (R22) should be replaced with an alternative that has low global warming potential and is not harmful to the ozone layer. Considering an expansion of solar energy to meet almost all factory electricity needs is essential. Moreover, it is essential to employ highly efficient electrical machines and equipment to enhance performance and reduce energy consumption. By implementing clean technology principles, organizations can significantly minimize the use of raw materials. This approach not only conserves resources but also effectively decreases the amount of waste generated, contributing to a more sustainable and environmentally friendly operation.

ACKNOWLEDGEMENT

This research was partially supported by a grant from the Center of Excellence on Environmental Health and Toxicology (EHT), OPS, Ministry of Higher Education, Science, Research and Innovation. The authors would like to express their sincere gratitude to the Executive Director of the printing and packaging factory for providing all necessary data for the carbon emission calculations. The authors declare no conflicts of interest or personal relationships that could have influenced the findings reported in this paper.

REFERENCE

[1] Nidhiben P, Maksims F, Francesco R. Carbon footprint evaluation tool for packaging marketplace. Environ Clim Technol. 2023;27:368-78.

[2] Sakcharoen T,Niyommaneerat W, Silalertruksa T. Towards low-carbon travel trips through carbon footprint: A case study of marine tourism in Sichang Island, Thailand. Cleaner Eng Technol. 2024;23:100840.

[3] United Nations Development Programme (UNDP). Climate finance handbook to the Thai Parliament [Internet]. 2024 Aug [cited 20 Jan 2025Availablefrom:https://www.undp.org/sites/g/files/zskgke326/files202408/UNDP_Thailand_%28ENG%29%20Climate%20Finance%20Handbook%20to%20the%20Thai%20Parliament.pdf

[4] Emission Factor for CFO and CFP [Internet]. [cited 1 Feb 2025]. Available from: http://thaicarbonlabel.tgo.or.th

[5] Gemechu ED, Butnar I, Gomà-Camps J, Pons A. A comparison of the GHG emissions caused by manufacturing tissue paper from virgin pulp or recycled waste paper. Int J Life Cycle Assess [Internet]. 2013 Sep;18(8):1618–28. Available from: https://www.researchgate.net/publication/257680097_A_comparison_of_the_GHG_emissions_caused_by_manufacturing_tissue_paper_from_virgin_pulp_or_recycled_waste_paper

[6] Raymond MJ, Slater CS, Savelski MJ. LCA approach to the analysis of solvent waste issues in the pharmaceutical industry. Green Chem. 2010;12(10):1826–34. doi:10.1039/c003666h.

[7] Thailand Greenhouse Gas Management Organization. Carbon footprint for organization [Internet]. Bangkok: TGO; 2018 [cited 1 Feb 2025]. Available from: http://www.tgo.or.th/

[8] Song X, Du S, Deng C, Shen P, Xie M, Zhao C, Chen C, Liu X. Carbon emissions in China's steel industry from a life cycle perspective: Carbon footprint insights. *J Environ Sci (China)*. 2023;128:72–85. doi:10.1016/j.jes.2023.04.027.

[9] Fouladvand J, Oudendijk R, Hooimeijer M, Derks R, Berndsen S. Carbon footprint of a news broadcasting organisation. *Sustain Prod Consum*. 2023;39:257-68. doi: 10.1016/j.spc.2023.05.004.

20R3-11

Effects of Carbon Capture and Storage (CCS) on Quartz Rock and Groundwater: The case study of Thailand

Chanita Sirisaksathaporn[1], Supreeda Homklin[2], Sukhuma Chitapornpan[2], Chatkaew Chailuecha[2], Pimluck Kijjanapanich[3], Sulak Sumitsawan[3], Prattakorn Sittisom[3], Pharkphum Rakruam[3], Napat Jakrawatana[3], Patiroop Pholchan[3], Sarunnoud Phuphisith[3], Ekbordin Winijkul[4], and Wanawan Pragot[2*]

[1]Master student, School of Energy and Environment, University of Phayao, 19 Moo 2 Maeka, Muang, Phayao, 56000, Thailand

[2]Lecturer, School of Energy and Environment, University of Phayao, 19 Moo 2 Maeka, Muang, Phayao, 56000, Thailand

[3] Lecturer, Department of Environmental Engineering, Faculty of Engineering, Chiang Mai University 239, Huay Kaew Road, Muang District, Chiang Mai 50200, Thailand

[4] Lecturer, Environmental Engineering and Management, Asian Institute of Technology, 58 Phahonyothin Rd., Khlong Luang, Pathum Thani 12120, Thailand

[*] Corresponding author Phone : +66855979855, E-mail : wanawan.pr@up.ac.th

ABSTRACT

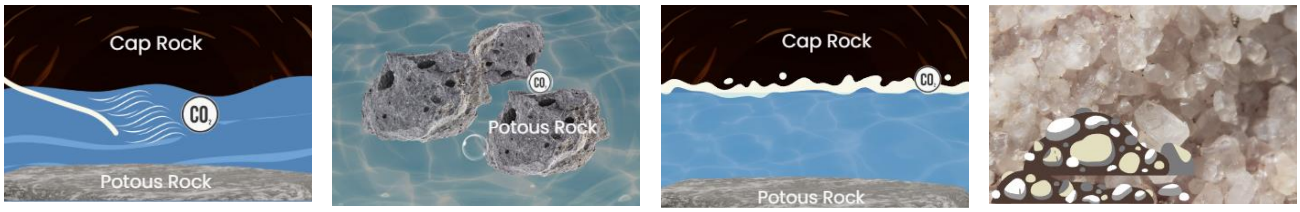
Carbon Capture and Storage (CCS) is a process focused on reducing greenhouse gas emissions by capturing carbon dioxide from its sources and storing it deep underground in rock formations for long-term storage. This paper focus on the effect of carbon capture and storage on quartz rock and groundwater in Thailand. The rocks from this resource could be suitable for CO_2 storage as its porous physical structure, mineral composition, strength and erosion resistance. The quartz rocks were sampling from the Korat basin, Thailand. Synthesis groundwater water was prepared using the references data of the groundwater sampling from the same point of this quartz rocks. The synthetic groundwater with saturated CO_2 gas dissolution was prepared by bubbling the CO_2 gas until it saturated (pH~5). After that, quartz rock was soaked in this water over a period of 28 days under atmospheric condition. The study demonstrated significant changes in both pore fluid and solid phases over a study period. The effect on pore fluid phase showed the rapid increase in pH, total dissolved solid (TDS), and conductivity at the beginning and relatively stable with a bit upward trend revealing the dissolution trapping and mineral trapping process. Meanwhile, increases in alkalinity, hardness, and heavy metals (Fe, Mn, Cu, Zn, Pb, As) were observed due to the acidic properties of CO_2 dissolved in water that leached of minerals and heavy metals from the quartz rock samples. Solid phase results confirmed the mineral trapping process occurring in experimental system. The dry mass of rocks increased by 0.18% within the calcite crystal morphology showed enhancement and the suspended solid (SS) increased from 0.5 to 6 mg/L. Although the study is based on a short-term experiment, it highlights the importance of understanding and preparing for potential impacts from the carbon capture and storage process.

Keywords : Carbon Capture and Storage (CCS), Quartz rock, Groundwater contamination, Mineral trapping

INTRODUCTION

Technological innovations nowadays have made life more convenient in many areas, such as agriculture, transportation, and industry. his has led to increased CO_2 emissions, resulting in global warming and environmental issues such as climate change, rising temperatures, and more severe natural disasters. To address these problems, many countries, including Thailand, recognize the importance of reducing greenhouse gas (GHG) emissions. One of the widely accepted technologies is Carbon Capture and Storage (CCS), a process that captures CO_2 from emission sources and stores it in underground rock formations or other suitable sites to reduce the amount of CO_2 in the atmosphere [1].

Carbon Capture and Storage (CCS) is a technology to reduce CO_2 emissions and mitigate the impacts of global warming. However, there are concerns about the risk of CO_2 leakage from underground storage sites, which could occur due to cracks in the rock formations or degradation of underground water sources that may become contaminated by CO_2. Therefore, careful monitoring and research are necessary to ensure that this technology can be safely and sustainably used in the long term [2].



a. Structural and stratigraphic trapping | b. Residual trapping | c. Dissolution trapping | d. Mineral trapping

Figure 1 Carbon dioxide capture processes of carbonation interactions

The CO_2 injection during CCS process affects the change in gas phase, pore fluid and solid phase. These changes continuously create the surrounding impact of CO_2 on water and rock in the long-term carbonation interactions [3]. The interaction type includes 1) structural and stratigraphic trapping, 2) residual trapping, 3) dissolution trapping, and 4) mineral trapping.

Structural and stratigraphic trapping (Figure 1a) is the primary mechanism for inhibiting the migration of CO_2 from the injection point to other subsurface sites. which is undesirable for storage. CO_2 displaces water in the pores and is trapped in areas with restricted movement, with natural seals ensuring the gas doesn't escape.

Residual trapping (Figure 1b) occurred capillary forces trap CO_2 when injected into water-saturated rock layers. CO_2 displaces water in the pores and is trapped in areas with restricted movement, with natural seals ensuring the gas doesn't escape.

Dissolution trapping (Figure 1c) when CO_2 dissolves into the water within the geological formation. The dissolved CO_2 forms carbonic acid (H_2CO_3), which then dissociates into bicarbonate (HCO^{3-}) and carbonate (CO_3^{2-}) ions. his increases the density of CO_2, making it more effectively trapped. The process works best in environments with high salinity and low temperatures, which help CO_2 dissolve more and be trapped in the water, reducing the chances of it escaping from the rock formation.

Mineral trapping (Figure 1d) is a process that involves injecting CO_2 into rocks containing minerals that can react with CO_2 such as calcium (Ca^{2+}) and magnesium (Mg^{2+}) [4]. Mineral trapping is one of the most permanent methods of CO_2 sequestration, offering a sustainable and effective way to mitigate CO_2 emissions by locking the gas into long-lasting mineral deposits.

As quartz has a porous physical structure along with its mineral composition, it plays a significant role in enhancing carbon dioxide (CO_2) storage capabilities. Quartz, primarily composed of silicon dioxide, often coexists with minerals like feldspar that contain calcium (Ca) and magnesium (Mg). These elements are crucial for chemical reactions that facilitate CO_2 mineralization, a process that ensures long-term CO_2 storage [3]. The examples of the conversion of CO_2 into stable carbonate minerals are calcite ($CaCO_3$) and magnesium carbonate ($MgCO_3$), which ensures long-term CO_2 storage [5]. This process occurs when CO_2, in the form of carbonic acid (H_2CO_3), reacts with minerals containing calcium or magnesium, forming new, dissolution-resistant minerals. The ability of quartz-rich formations to support the process of CO_2 storage in

the form of mineral trapping is crucial for the effectiveness of geological CO_2 sequestration, playing an important role in mitigating climate change [6]. Research has shown that the geochemical interactions in these formations can lead to the formation of stable carbonates, further strengthening their role in CO_2 storage [7]. The challenges remain in studying the long-term stability of these geological formations, as well as the potential for CO_2 leakage from the storage site. Therefore, ongoing research and monitoring are essential to ensure the safety and long-term effectiveness of CO_2 storage, ensuring its sustainability in the long run.

Experiments have shown that the initial mineral composition and water chemistry have significantly affected the reaction [8,9]. Calcite and dolomite primarily characterize the initial phase. Dissolved CO_2 in water reduces the pH of groundwater, and the chemistry of the water affects the stability and transformation of minerals after CO_2 injection [10], The process enhancing rock dissolution and leaching of ions such as Ca^{2+}, Mg^{2+}, Pb^{2+}, As^{2+}, and Zn^{2+}[11]. This contamination impacts groundwater quality, affecting its taste, smell, and color, and leads to a decline in water quality [12]. Furthermore, the process increases levels of Total Dissolved Solids (TDS), bicarbonate (HCO^{3-}), and sulfite (SO_3^{2-}), while Oxidation Reduction Potential (ORP) remains stable[13] . These impacts underscore the need for careful monitoring and management of CCS processes to protect groundwater resources and maintain water quality in affected areas. This paper focus on the effect of carbon capture and storage on quartz rock and groundwater in Thailand.

METHODOLOGY

Synthesis groundwater

Synthesis water was prepared using the references data of the groundwater sampling from the well number of 5705D015 in Korat basin, Mueang Nakhon Ratchasima, Nakhon Ratchasima, Thailand that contained 19 mg/L of magnesium ion (Mg^{2+}) and 39 mg/L of calcium ion (Ca^{2+}) [14]**.** The synthesis water groundwater used for the experiment was prepared using deionized water (DI), which is water that has undergone a process to remove impurities. The pH of the water samplings was then adjusted to 5 by bubbling the CO_2 gas until saturated. After that, quartz rock samples were soaked in synthetic groundwater with saturated carbon dioxide gas dissolution. The experiments were done under atmospheric conditions and accurately observe the changes in the quartz over time of 28 days.

The chemical and physical composition of the synthetic groundwater was analyzed both before and after the 28 days rock immersion experiment. Temperature, total dissolved solid (TDS), pH, and conductivity were measured daily using the Multi-parameter PCS Tester 35#ECPCSTEST35. The filtrated sample with a GF/C glass microfiber filter were then measured suspended solid (SS), alkalinity (Alk), hardness, total organic compounds (TOC), and heavy metals were analyzed monthly.

Quartz rock

In Thailand, quartz is mainly found in the northern and northeastern areas, especially in the Korat Plateau and some areas in the east, where it is often found with feldspar. The quartz rocks were sampling from the Korat basin, Mueang Nakhon Ratchasima, Nakhon Ratchasima, Thailand**.** A quartz sample was chosen and cut into rough cubic pieces at the size of 30 x 33 x 48 cm. to observe the changes during the experiment.

The chemical and physical composition of the quartz rock was analyzed both before and after the 28-day soaking experiment. Two parameters were measured: 1) the total mass of the rock and 2) the mineral composition using X-ray diffraction (XRD). This experiment was designed to provide insights into the progressive changes that occur in quartz rocks when exposed to CO_2 saturated synthetic groundwater. By varying the exposure duration, we aim to understand how the interaction with CO_2 evolves over time and its effects on rock weathering and mineral formation.

RESULTS AND DISCUSSIONS

The results of the effect of carbon capture and storage (CCS) on quartz rock and groundwater in this study can be categorized into the effect to 1) pore fluid phase occurring in the synthetic groundwater with saturated CO_2 dissolution and 2) solid phase occurring in quartz rock. Testing parameters, methods and the results for liquid phase and solid phase were present in Table 3.

Table 3 Result of testing parameters and methods for synthetic groundwater with saturated CO_2 dissolution and quartz rock

Testing	Day 0	Day 28	Test method
Pore fluid phase			
pH	5.25	8.49	Multi-parameter PCS Tester 35#ECPCSTEST35
Conductivity (µS/cm)	90.5	176.7	
TDS (mg/L)	64.1	125.0	
Alk (mg/L)	6.60	28.00	Titration method
Hardness (mg/L)	66.80	80.00	
TOC	-1.543	-13.080	Combustion catalytic oxidation method
Fe (mg/L)	nd	<0.05	Atomic Absorption Spectrometry
Mn (mg/L)	nd	<0.04	
Cu (mg/L)	nd	<0.03	
Zn (mg/L)	<0.04	0.10	
Pb (mg/L)	nd	<0.05	
Cr (mg/L)	nd	nd	
As (mg/L)	<0.002	<0.002	
Solid phase			
SS (mg/L)	0.5	6.0	Gravimetric method
Mass (g)	70.6854	70.8098	Gravimetric method
Quartz (%)	98.2	97.3	XRD, BrukerD8 Advance diffractometer, ICDD method
Calcite (%)	1.8	2.7	

Pore fluid phase

After 28 days of soaking quartz rock samples in synthetic groundwater saturated with dissolved carbon dioxide gas, the distinguish changes in liquid were observed. Figure 3 showed the changes in water physical and chemical properties in the liquid phase during the samplings period. The temperature throughout the experiment were at 26.7ºC with only minor fluctuations of ±0.61°C.

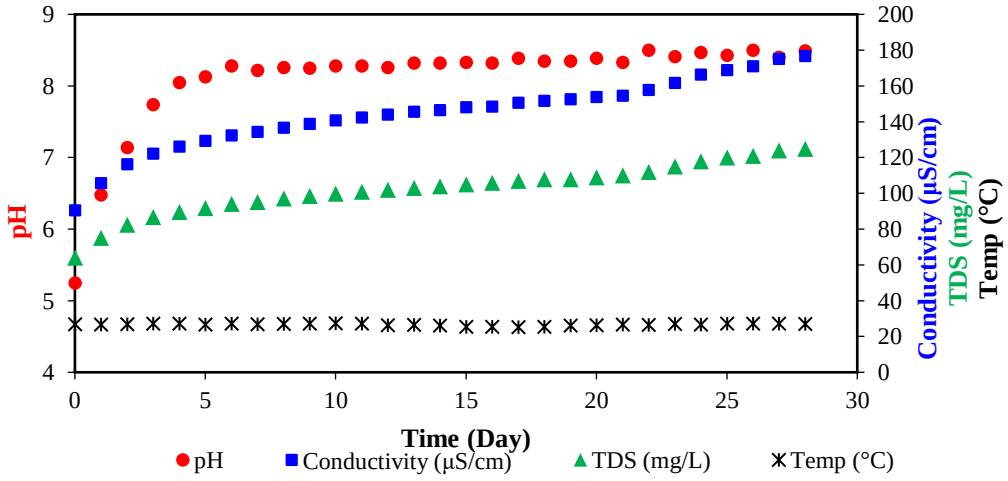


Figure 3 Temperature**,** pH, TDS, and conductivity of water sample over 28 days period

At the beginning after injecting CO_2 gas into the synthetic groundwater, CO_2 was transferred in the water and formed the liquid form dissolved CO_2. This hydrolysis process of CO_2 formed carbonic acid (H_2CO_3) which caused the pH drop to about 5, as shown in the following equations:

$$CO_2(g) \leftrightharpoons CO_2\,(aq) \qquad \textbf{Equation 1}$$

$$CO_2\,(aq) + H_2O(l) \leftrightharpoons H_2CO_3^-(aq) \qquad \textbf{Equation 2}$$

The dissolution of CO_2 led to an increase in the concentration of various ions, such as Ca^{2+}, Mg^{2+} and bicarbonate (HCO_3^-) in the water. Then, there was a rapid increase in the pH, conductivity, and TDS in the first five days due to the reaction between the carbonate and hardness (Ca^{2+} and Mg^{2+}) and of the synthetic groundwater. This process caused mineral trapping that the dissolution was transformed into other minerals by chemical precipitation process, as represented by the following equations:

$$Ca^{2+,}\,Mg^{2+} + CO_3^{2-}\,(aq) \rightarrow CaCO_3\,(s), MgCO_3\,(s) \qquad \textbf{Equation 3}$$

After that the pH was relatively stable after day at around 8-8.5 for the rest of the period, indicating a buffering reaction or the dissolution of alkaline minerals. Meanwhile, increases in conductivity, TDS, SS, alkalinity, hardness, and heavy metals (Fe, Mn, Cu, Zn, Pb, As) were observed due to the acidic properties of CO_2 dissolved in water. This led to the leaching of minerals and heavy metals from the quartz rock samples. The values of TDS and conductivity after approximately 20 days of experimentation showed a continuous upward trend that suggested that reactions between the minerals in the rock and synthetic groundwater were continuously undergoing. The reactions mentioned above are expressed as follows.

$$H^+ + \text{Quartz rock} \rightarrow Ca^{2+}, Mg^{2+} + \text{heavy metal} \qquad \textbf{Equation 4}$$

The results showed slight changes and continued upward trends due to the experiment duration of 28 days is too short for the stabilization phase of the reaction between quartz rock and CO_2 dissolution. To observe clearer and stable results, a testing period of 2-10 years is required to allow the reactions occurring in the CO_2 dissolution process and mineral precipitation to fully take place, enabling effective carbon sequestration through mineral trapping [15].

Solid phase

Three significant physical changes were observed after 28 days of soaking quartz rock samples in synthetic groundwater saturated with dissolved carbon dioxide gas. The dry mass increased by 0.18%, and the calcite structure within crystal morphology showed enhancement in the XRD. Figure 4 revealed the calcite content increased by 0.9%, from 1.8% on day 0 to 2.7% on day 28. This change indicated physical alterations resulting from the reaction between the rock and the water, leading to the formation and mineral precipitation of calcite. These changes suggested that CO_2 injection influenced both the pore fluid and the solid phase of the rock. The interaction between elements in the rock and carbonate ions in CO_2 saturated synthetic groundwater led to compositional changes due to the mineralization process. During mineralization, divalent metal ions (M^{2+}) bond with carbonate ions, resulting in precipitation and the formation of stable carbonate minerals [16]. In this case, calcite ($CaCO_3$) is the primary mineral formed inside quartz rock structure.

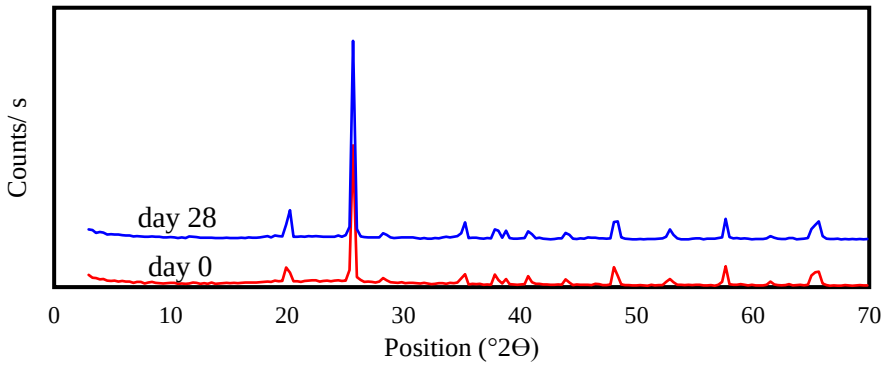


Figure 4 X-ray diffraction (XRD) of quartz rock before and after experiment

Moreover, Figure 5 represented the occurrent of the small white precipitate in the sediments and beneath or around the edges of the rock and the increase of SS from 0.5 mg/l to 6 mg/l confirmed the mineral trapping process of divalent metal ions (M^{2+}) bond with carbonate ions as presented in Equation 3. The minerals in quartz rock are abundant, and when a reaction occurs, it leads to the leaching of these minerals. This process results in the formation of heavy metals in a dissolved form in the water, which then precipitate and form solid compounds [15].

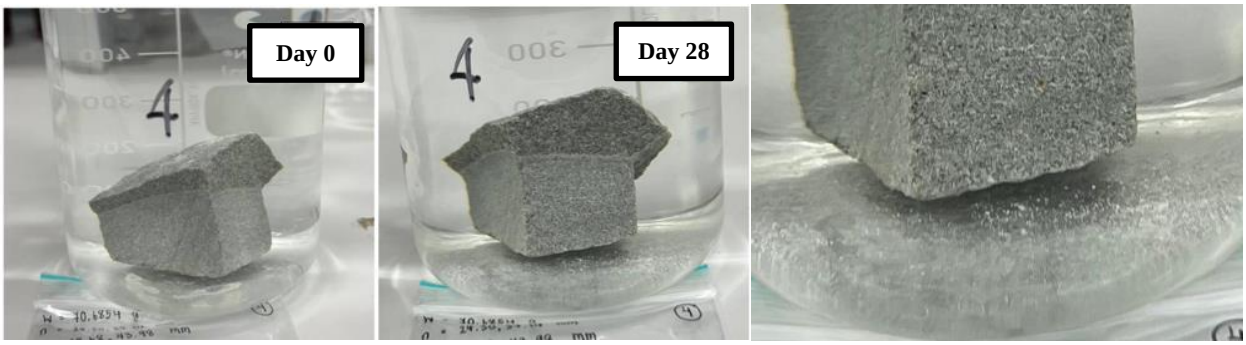


Figure 5 An experiment of soaking quartz rock in synthetic groundwater for a period of day 0 and day 28.

In CO_2 storage through mineral trapping, CO_2 gas is converted into solid carbonate minerals, such as magnesite or calcite. When CO_2 reacts with synthetic groundwater, carbonic acid (H_2CO_3) is formed, increasing the acidity of the water. Carbonic acid is a weak acid that dissociates immediately, as shown in the equation for the acidification of synthetic groundwater [15]. The process of carbon mineralization of quartz consists of the following steps:

1. Gaseous CO_2 dissolved in water to form bicarbonate and carbonate ions. The dissociation of CO_2 in the groundwater maked the solution corrosive to materials in contact with it due to the formation of carbonic acid (pH decreases to approximately 3-5) [17,18].
2. Cations such as Ca^{2+}, Mg^{2+}, and Heavy metal were released into the solution due to mineral dissolution.
3. Stable carbonates are formed through ionic reactions at higher pH. The pH increases back due to the dilution of CO_3^{2-}(aq) in the groundwater. Subsequently, carbonate ions and divalent cations combined to form carbonate minerals (precipitation). The synthetic groundwater continued to react with various minerals, such as Ca and Mg, in the rock to normalize the pH. This led to reactions with carbonate minerals, resulting in the formation of $CaCO_3$, along with the production of bicarbonate, which occured in pore fluid of underground reservoirs.

CONCLUSION

The study on the effect of carbon capture and storage (CCS) on quartz rock and groundwater from the Korat basin in Thailand demonstrated significant changes in both pore fluid and solid phases over a 28-day experiment.

In the pore fluid phase, after initial CO_2 dissolution lowered the pH to around 5, there was a rapid increase in pH, conductivity, and TDS during the first five days due to reactions between carbonate and hardness elements in the synthetic groundwater. The pH eventually stabilized around 8-8.5, indicating buffering reactions or dissolution of alkaline minerals. The continuous upward trend in TDS and conductivity even after 20 days suggests ongoing reactions between rock minerals and groundwater. Moreover, the study shows that CO_2 injection causes the leaching of heavy metals such as iron (Fe), manganese (Mn), copper (Cu), and zinc (Zn) from quartz rocks into the groundwater. This could pose environmental and health risks if not carefully monitored, especially if the contaminated water is used for drinking or agricultural purposes.

In the solid phase, three significant physical changes were observed to confirm mineral trapping processes. Firstly, a 0.18% increase in dry mass. Secondly, enhanced calcite structure from 1.8% to 2.7% as confirmed by XRD analysis in the crystal morphology. Finally, the formation of white precipitates and increase in suspended solids from 0.5 mg/L to 6 mg/L.

The findings demonstrate that CO_2 injection influences both the pore fluid and solid phases through mineralization processes, where divalent metal ions bond with carbonate ions to form stable carbonate minerals, primarily calcite ($CaCO_3$). However, the 28-day experimental period is considered too short for the complete stabilization of reactions between quartz rock and CO_2 dissolution. A longer testing period of 2-10 years would be necessary to fully observe the carbon sequestration through mineral trapping processes.

The study provides important insights into the carbon mineralization process in quartz rock, including CO_2 dissolution, mineral dissolution releasing cations, and the formation of stable carbonates through ionic reactions at higher pH levels.

ACKNOWLEDGEMENT

This work has partially received funding support from the National Scientific Research Fund via the Program Management Unit for Human Resources & Institutional Development, Research and Innovation (grant no. B40G660032), Chiang Mai University.

REFERENCE

[1] Burnside NM, Naylor M. Review and implications of relative permeability of CO_2/brine systems and residual trapping of CO_2. International Journal of Greenhouse Gas Control 2014;23:1–11. https://doi.org/10.1016/j.ijggc.2014.01.013.

[2] Gholami R, Raza A, Iglauer S. Leakage risk assessment of a CO_2 storage site: A review. Earth Sci Rev 2021;223:103849. https://doi.org/https://doi.org/10.1016/j.earscirev.2021.103849.

[3] Zhao X, Liao X, Wang W, Chen C, Rui Z, Wang H. The CO_2 storage capacity evaluation: Methodology and determination of key factors. Journal of the Energy Institute 2014;87:297–305. https://doi.org/https://doi.org/10.1016/j.joei.2014.03.032.

[4] Kim K, Kim D, Na Y, Song Y, Wang J. A review of carbon mineralization mechanism during geological CO2 storage. Heliyon 2023;9. https://doi.org/10.1016/j.heliyon.2023.e23135.

[5] Li Z, Lv Y, Liu B, Fu X. Reactive Transport Modeling of CO_2-Brine–Rock Interaction on Long-Term CO_2 Sequestration in Shihezi Formation. Energies (Basel) 2023;16. https://doi.org/10.3390/en16020670.

[6] Fentaw JW, Emadi H, Hussain A, Fernandez DM, Thiyagarajan SR. Geochemistry in Geological CO_2 Sequestration: A Comprehensive Review. Energies (Basel) 2024;17. https://doi.org/10.3390/en17195000.

[7] Jedli H, Hedfi H, Jbara A, Bouzgarrou S, Slimi K. Mineralogical and Geochemical Characteristics of Caprock Formations Used for Storage and Sequestration of Carbon Dioxide. Journal of Minerals and Materials Characterization and Engineering 2015;03:409–19. https://doi.org/10.4236/jmmce.2015.35043.

[8] Zhao Y, Wu S, Chen Y, Yu C, Yu Z, Hua G, et al. CO_2-Water-Rock Interaction and Pore Structure Evolution of the Tight Sandstones of the Quantou Formation, Songliao Basin. Energies (Basel) 2022;15. https://doi.org/10.3390/en15249268.

[9] Ahmat K, Cheng J, Yu Y, Zhao R, Li J. CO_2-Water-Rock Interactions in Carbonate Formations at the Tazhong Uplift, Tarim Basin, China. Minerals 2022;12. https://doi.org/10.3390/min12050635.

[10] Chang R, Kim S, Lee S, Choi S, Kim M, Park Y. Calcium carbonate precipitation for CO_2 storage and utilization: A review of the carbonate crystallization and polymorphism. Front Energy Res 2017;5. https://doi.org/10.3389/fenrg.2017.00017.

[11] Zhao X, Deng H, Wang W, Han F, Li C, Zhang H, et al. Impact of naturally leaking carbon dioxide on soil properties and ecosystems in the Qinghai-Tibet plateau. Sci Rep 2017;7. https://doi.org/10.1038/s41598-017-02500-x.

[12] Wei Y, Maroto-Valer M, Steven MD. Environmental consequences of potential leaks of CO2 in soil. Energy Procedia, vol. 4, Elsevier Ltd; 2011, p. 3224–30. https://doi.org/10.1016/j.egypro.2011.02.239.

[13] Fagorite V, Chijioke F, Opara A, Onyekuru S, Oguzie E. Environmental and safety issues associated with geological carbon storage: a review. EuroMediterr J Environ Integr 2022;7. https://doi.org/10.1007/s41207-022-00328-0.

[14] Arif M, Zhang Y, Iglauer S. Shale wettability: Data sets, challenges, and outlook. Energy and Fuels 2021;35. https://doi.org/10.1021/acs.energyfuels.0c04120.

[15] Fentaw JW, Emadi H, Hussain A, Fernandez DM, Thiyagarajan SR. Geochemistry in Geological CO2 Sequestration: A Comprehensive Review. Energies (Basel) 2024;17. https://doi.org/10.3390/en17195000.

[16] Ma J, Zhu X, Liu D, Wang S, Xue L, Li Q, et al. Effects of simulation leakage of CCS on physical-chemical properties of soil. Energy Procedia, vol. 63, Elsevier Ltd; 2014, p. 3215–9. https://doi.org/10.1016/j.egypro.2014.11.347.

[17] Li W, Nan Y, You Q, Jin Z. CO2 solubility in brine in silica nanopores in relation to geological CO2 sequestration in tight formations: Effect of salinity and pH. Chemical Engineering Journal 2021;411:127626. https://doi.org/https://doi.org/10.1016/j.cej.2020.127626.

[18] Bashir A, Ali M, Patil S, Aljawad MS, Mahmoud M, Al-Shehri D, et al. Comprehensive review of CO2 geological storage: Exploring principles, mechanisms, and prospects. Earth Sci Rev 2024;249. https://doi.org/10.1016/j.earscirev.2023.104672.

20R3-13

Carbon Footprint for Organizati on and Reduction of Greenhouse Gas Emission for Faculty of Engineering, Khon Kaen University

Krorawan Pankrathoke[1], Artittayaporn Bunma[1], Kitirote Wantala[2,3], and Visanu Tanboonchuy[1,3*]

[1]Department of Environmental Engineering, Faculty of Engineering, Khon Kaen University, Khon Kaen, Thailand

[2]Department of Chemical Engineering, Faculty of Engineering, Khon Kaen University, Khon Kaen, Thailand [3]Research Center for Environmental and Hazardous Substance Management (EHSM), Khon Kaen University, Thailand

[*]Phone : 043-009700 E-mail : visanu@kku.ac.th

ABSTRACT

This research evaluates the greenhouse gas (GHG) emissions at the Faculty of Engineering, Khon Kaen University (KKU), for the year 2024, totaling 2,611.99 tons of CO_2-equivalent emissions. The emissions are categorized into Scope 1 (695.65 tCO_2eq), Scope 2 (1,031.20 tCO_2eq), and Scope 3 (886.14 tCO_2eq). Scope 1 emissions are relatively low, primarily due to the implementation of the Activated Sludge (AS) method in wastewater treatment, which effectively mitigates methane emissions. Scope 2 emissions are largely driven by electricity consumption, while Scope 3 emissions are influenced by construction activities and staff commuting, with factors such as the large workforce and distance of staff residences contributing to higher emissions. The findings suggest key strategies for emission reduction, including enhancing energy efficiency, transitioning to renewable energy sources, and promoting sustainable commuting practices. The study underscores the importance of comprehensive strategies to reduce the carbon footprint and contribute to sustainability goals.

Keywords : greenhouse gases; climate change; carbon footprint; Khon Kaen Universiy; sustainability

INTRODUCTION

The greenhouse gas (GHG) emissions have become a global concern as nations, industries and institutions work to combat climate change and advance the cause of environmental sustainability, the GHG emissions have emerged as a global issue. According to the United Nations Environment Programme (UNEP), GHG emissions must be halved by 2030 to limit global warming to 1.5°C [1]. To meet this challenge, institutions, organizations, and individuals alike are being called upon to take responsibility for their carbon footprints and contribute to mitigation efforts.

Universities play a unique role in this global effort. Beyond their educational and research missions, they function as large-scale organizations with substantial energy use, transportation demands, and waste generation. As centers of innovation and leadership, universities are well-positioned to demonstrate environmental responsibility and inspire systemic change. In recent years, higher education institutions around the world have initiated sustainability programs and conducted assessments of their environmental impacts, including carbon footprint evaluations [2,4].

Khon Kaen University (KKU), one of Thailand's leading academic institutions, has committed to becoming a "Green University" by combining sustainability into its operations. Various strategies have been applied, including energy efficiency measures, renewable energy adoption, and environmental awareness programs [3]. Within KKU, the Faculty of Engineering stands out as a major contributor to the university's resource consumption and carbon emissions. This is attributed to its extensive facilities, high energy demands in laboratories and classrooms, and ongoing construction activities to support academic growth.

Recognizing the importance of informed and strategic action, this study aims to assess the carbon footprint of the Faculty of Engineering using the official guidelines provided by the Thailand Greenhouse Gas Management Organization (TGO) [6]. The assessment categorizes emissions into Scope 1 (from direct sources such as fuel and waste), Scope 2 (electricity consumption), and Scope 3 (indirect sources including commuting, waste disposal, and procurement) [7]. By quantifying emissions across these scopes, the research identifies key contributors and proposes a roadmap for reducing the environmental impact. The results are intended to serve as both a baseline and a catalyst for institutional action toward achieving long-term carbon neutrality.

METHODOLOGY

This study follows the TGO Carbon Footprint for Organization Calculation Guidelines (2020), aligned with the Greenhouse Gas Protocol and IPCC 2006 Guidelines [6,7].
Emissions are categorized into:

- Scope 1: Direct emissions from on-site fuel combustion, university vehicles, and wastewater treatment
- Scope 2: Indirect emissions from purchased electricity.
- Scope 3: Other indirect emissions from waste, commuting, and construction.

3.1 Data Collection

Data was gathered from facility records, electricity bills, transportation logs, construction reports, and staff surveys. The following equation was used:

$$\text{Emissions} = \text{Amount of Activity} \times \text{Emission Factor (EF)} \quad (1)$$

where "Amount of Activity" represents the quantity of energy used or fuel consumed, and "EF" converts activity data into emissions (kg CO_2eq) [5].

3.2 Boundary and Assumptions

The boundary includes all buildings and infrastructure managed by the Faculty of Engineering. Emissions from shared utilities were prorated based on area and usage intensity.

RESULTS AND DISCUSSION

Table 1 GHG Emissions by Scope (2024)

Scope	Emission Source	tCO_2eq	% of Total
Scope 1	Stationary combustion	0.05	0.00
	Vehicles	11.80	0.70
	Septic tank	607.80	1.30
	Wastewater	0.00	0.00
	Refrigerators	75.97	4.53
	Total Scope 1	**695.65**	**26.63**
Scope 2	Electricity	1030.20	61.50
	Total Scope 2	**1030.20**	**61.50**
Scope 3	Office materials	15.83	0.95
	Tap water	43.14	2.57
	Related activities from Scope 1 and 2	63.35	3.78
	Commuting	352.88	13.67
	Construction	257.32	15.36
	Waste management	5.84	0.35
	Business travel by car	30.49	1.17
	Business travel by air	117.30	6.54
	Total Scope 3	**886.14**	**33.93**
	Total Scope 1, 2 and 3	**2,611.99**	**100.00**

Scope 1 Direct emissions were mainly from septic tanks and backup generators. The use of Activated Sludge (AS) systems reduced methane emissions compared to traditional treatment methods.

Scope 2 Electricity accounted for 1030.20 tCO_2eq. Laboratories and office buildings were the largest consumers. Although KKU has installed solar panels on some rooftops, renewable energy still covers less than 5% of total demand [3].

Scope 3 The highest emissions were from commuting (staff and students using private vehicles) and the construction of a new food center. These findings are consistent with global trends in higher education institutions [4,5].

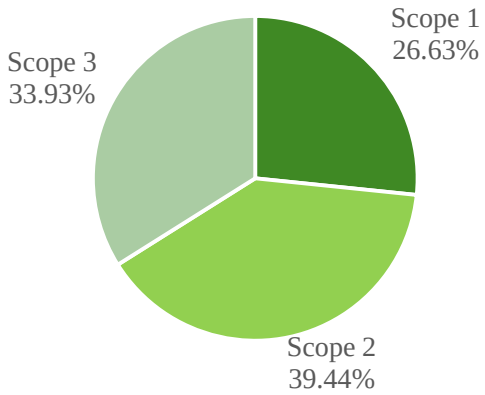


Figure 1 Emission Breakdown by Scope

Mitigation Strategies

1 Transportation

To promote sustainable mobility, Khon Kaen University has already implemented a fully electric shuttle bus system within the campus, significantly reducing greenhouse gas emissions from internal transportation. Further enhancements include establishing a campus-wide bicycle-sharing program to reduce reliance on personal vehicles. A dedicated carpooling application for staff and students can also help lower carbon emissions by encouraging shared travel. Moreover, enhancing public transportation linkages to the campus will increase accessibility and reduce the number of private vehicles commuting to the university.

2 Energy Efficiency

Improving energy efficiency across campus is crucial. This includes replacing fluorescent lighting with energy-efficient LED alternatives, upgrading existing HVAC systems, and installing smart sensors to optimize energy use. Additionally, expanding on-site renewable energy sources, such as rooftop solar panels, can significantly reduce the university's dependency on fossil fuels.

3 Sustainable Construction

Future construction projects should prioritize sustainability by using low-carbon materials such as fly ash concrete. Incorporating building energy simulations during the design phase can help minimize energy consumption throughout a building's lifecycle, ensuring that new developments align with environmental goals.

4 Policy Recommendations

Institutional policies play a key role in driving change. It is recommended to integrate carbon footprint reduction strategies into the faculty's strategic plans to ensure long-term commitment. Furthermore, providing incentives for individuals and departments that make low-carbon choices will encourage widespread participation in sustainability efforts.

Table 2 Comparison of GHG Emissions: Faculty of Engineering, Khon Kaen University; KKU (2024) and Faculty of Engineering, Kasetsart University; KU (2010-2011) [8]

Scope	KKU (2024) %	KU (2010-2011) %
Scope 1	26.63	4.42
Scope 2	39.44	62.35
Scope 3	33.93	33.23

Compare greenhouse gas emissions between the Faculty of Engineering at Khon Kaen University (KKU) and Kasetsart University (KU), notable differences in the distribution of emissions emerge. At KU, electricity consumption (Scope 2) accounts for the largest share—over 62% of total emissions—likely reflecting the university's larger scale in terms of students, staff, and equipment. Meanwhile, Scope 1 emissions at KU are relatively low at only 4.42%, suggesting fewer direct emission sources such as on-site fuel use or wastewater treatment.

While, KKU shows a more evenly spread emission. While electricity use (Scope 2) still contributes the highest portion at 39.44%, direct emissions (Scope 1) are more significant, making up 26.63% of the total. This may be due to the presence of systems like anaerobic wastewater treatment and vehicle usage within the faculty.

Interestingly, both institutions report similar proportions of Scope 3 emissions—approximately 33%—which include commuting, office materials, and waste management. This shared pattern highlights a mutual opportunity to reduce emissions through behavioral changes and more sustainable practices in daily operations.

These differences emphasize that each institution has its own unique challenges and strengths in tackling emissions. Adapted strategies, especially in energy use and commuting, will be essential to make meaningful progress toward lower carbon footprints.

CONCLUSION

This study concludes that the total greenhouse gas (GHG) emissions from the Faculty of Engineering at Khon Kaen University (KKU) in 2024 amounted to 2,611.99 tCO_2eq. Among the various emission sources, Scope 2 emissions, primarily from electricity consumption, were the largest contributor (1,030.20 tCO_2eq). Scope 1 emissions (695.65 tCO_2eq) were relatively low, primarily due to the implementation of the Activated Sludge system in wastewater treatment, which effectively reduces methane release. In contrast, Scope 3 emissions were significant, mainly driven by construction activities and the commuting patterns of university personnel.

ACKNOWLEDGEMENT

I would like to express my sincere gratitude to the Faculty of Engineering, Khon Kaen University, for providing the essential resources and support required to conduct this study. My heartfelt appreciation also extends to the staff of the Faculty of Engineering, KKU, for their valuable assistance in data collection and their continuous support throughout the research process.

REFERENCE

[1] IPCC. 2022. Sixth Assessment Report. Intergovernmental Panel on Climate Change. Available at: https://www.ipcc.ch. Accessed on April 5, 2025.
[2] Fraser, M. and Hite, R. 2014. Sustainability in Universities. Journal of Environmental Education, 45(2): 105-117.
[3] Khon Kaen University. 2022. Sustainability Report. Available at: https://www.kku.ac.th. Accessed on April 5, 2025.
[4] MIT Office of Sustainability. 2021. Campus Carbon Assessment. Massachusetts Institute of Technology.
[5] University of Cambridge. 2020. Environmental Sustainability Report. University of Cambridge
[6] Thailand Greenhouse Gas Management Organization (TGO). 2020. Carbon Footprint for Organization Calculation Guidelines. Available at: https://www.tgo.or.th. Accessed on April 5, 2025.
[7] IPCC. 2006. 2006 IPCC Guidelines for National Greenhouse Gas Inventories. Available at: https://www.ipcc.ch. Accessed on April 5, 2025.
[8] Chutima Sukanan. 2012. Carbon Footprint for Organization and Reduction of Greenhouse Gas Emissions for Faculty of Engineering, Kasetsart University. Kasetsart University.

20R3-14

Application of Convective Available Potential Energy (CAPE) for Appropriate Condition on Rain Enhancement in Thailand

Ying Li[1], Parkpoom Choomaneea[2], Thunyapat Thongyenb[3] and Surat Bualert [4*]

[1]*Graduate student, Department of Environmental Science, Faculty of Environment, Kasetsart University, Bangkok, Thailand*
[2]*Assitant Professor, Department of Environmental Science, Faculty of Environment, Kasetsart University, Bangkok, Thailand*
[3] *Assitant Professor, Department of Technology and Management, Faculty of Environment, Kasetsart University, Bangkok, Thailand*
[4*]*Associate Professor, Department of Environmental Science, Faculty of Environment, Kasetsart University, Bangkok, Thailand*
[*]*Corresponding author: Tel : 0818039899, e-mail : Surat.b@ku.ac.th*

ABSTRACT

This study investigates the application of Convective Available Potential Energy (CAPE) to identify optimal atmospheric conditions for rain enhancement in Chiang Mai, Thailand. Using five years of upper-air sounding data (2018–2024, excluding 2022 due to no data recrod) from the Chiang Mai station, through Universal RAwinsonde Observation Program (RAOB) to derive Convective Available Potential Energy (CAPE) and Convective Inhibition (CIN) from Skew-T diagrams. Results revealed that the highest CAPE values (~1000 J/kg) occurred during June–September, indicating strong atmospheric instability conducive to convection, while the lowest values (~100 J/kg) in January and December reflected stable conditions. CIN exhibited an inverse relationship with CAPE, with minimal inhibition during high-CAPE months. These findings suggest that the monsoon season (June–September) may be less suitable for rain enhancement due to naturally high convective activity. Further study in other stations in Thailand will be conducted in order to learn the behavior of CAPE deeply and apply for appropriate condition on rain enhancement.

Keywords : Climate Change, CAPE, CIN, Atmospheric energy, Rain enhancement

INTRODUCTION

The water cycle on Earth is a natural phenomenon primarily driven by processes such as evaporation, condensation, and precipitation. However, Climate change, land use changes, and urbanization have been significantly influenced this cycle worldwide, resulting in extreme weather events, including floods and droughts [1-3]. Rising temperature disrupts the water cycle processes and contributes for more evaporation, which cause in either floods or droughts [4]. Human activities, rapid and unplanned land-use, also contribute to the vulnerability to flood and drought risks [5].

Given the challenges posed by climate change and urbanization, to address the growing water resource shortages and precipitation enhancement, many countries conducted the cloud seeding and rain enhancement technologies as potential solutions [6-8]. In Thailand, early studies on warm-rain enhancement demonstrated that seeding warm convective clouds with calcium chloride particles could significantly increase rainfall [9]. More recently, low-frequency acoustic waves have emerged as a promising tool for rain enhancement, particularly in China, where they have been successfully applied for fog dispersal and other weather modification purposes due to their cost-effectiveness and environmental sustainability [10]. Research in the United States (US) showed that Cloud seeding efficiency is significantly influenced by the microphysical properties of clouds, particularly the concentration and size distribution of ice nuclei, which determine the effectiveness of precipitation enhancement techniques [11].

Weather modification research has been ongoing since the 1950s, with traditional methods primarily focusing on cloud seeding to induce precipitation. This process involves dispersing substances such as silver iodide, potassium iodide, dry ice, and hygroscopic materials like salt into the atmosphere to promote cloud condensation [12]. Successful implementation of rain enhancement requires a comprehensive analysis of cloud characters and hygroscopic particles [13].

In addition, atmospheric energy dynamics play a crucial role in shaping weather patterns and climate systems. The energy transformations occurring during cloud formation have risen the significant attention, particularly convective available potential energy (CAPE) and convective inhibition (CIN). CAPE has been widely used to quantify the atmospheric capacity to support the upward movement of air parcels, leading to cloud formation and severe thunderstorms [14, 15]. While CIN represents the energy needed to lift a parcel to above the level of free convection. It provides a measure of the stability in the lower troposphere that often prevents deep moist convection from happening [16].

CAPE has been extensively studied worldwide to understand its influence on precipitation patterns and its relationship with thunderstorm development. Malik analyzed CAPE alongside the spatial distribution of precipitation and temperature across 45 stations in Pakistan from 1987 to 2016, revealing that regions with higher CAPE values also experienced elevated temperatures and increased rainfall [17]. Similarly, Sahu has explored the climatological variations of CAPE and Convective Inhibition (CIN) in India by using ERA-5 data from 1987 to 2016, providing valuable insights for forecasters to better understand convective activity [18].

Despite significant global advancements in the study of Convective Available Potential Energy (CAPE), its application in Thailand, particularly within the context of rain enhancement operations, remains underexplored. This study seeks to bridge this critical gap by conducting a comprehensive analysis of the climatological environment and seasonal variations of CAPE dynamics in Chiang Mai Province, a region characterized by its unique topographical and meteorological conditions. By examining the relationship between CAPE, local precipitation patterns, and temperature fluctuations, this research aims to understand the atmospheric energy mechanisms that influence convective activity and cloud formation. The findings of this study are expected to provide a foundational reference for future CAPE-related research in Thailand, offering valuable insights into the atmospheric conditions that are most conducive to effective rain enhancement.

.

METHODOLOGY

Upper air sounding data spanning five years (2018-2024, except year 2022) from the Chiangmai station were obtained from the University of Wyoming's website (http://weather.uwyo.edu/upperair/sounding). Additionally, 29 years of climatological data (1992–2021) were collected from the Thailand Meteorological Department (TMD). Using the 29-year dataset, average monthly rainfall, evaporation, and temperature were calculated to identify the wet, dry, and transition periods. Furthermore, average monthly humidity and temperature were analyzed and compared. The upper air sounding data were processed using the Universal RAwinsonde Observation Program (RAOB) to derive Convective Available Potential Energy (CAPE) and Convective Inhibition (CIN) from Skew-T diagrams. RAOB is the world's most innovative sounding software. Automatically decodes data from over 100 different formats and plots data on 12 interactive displays including skew-Ts. Produces displays of over 200 atmospheric parameters including CAPE and CIN.

RESULTS AND DISCUSSIONS

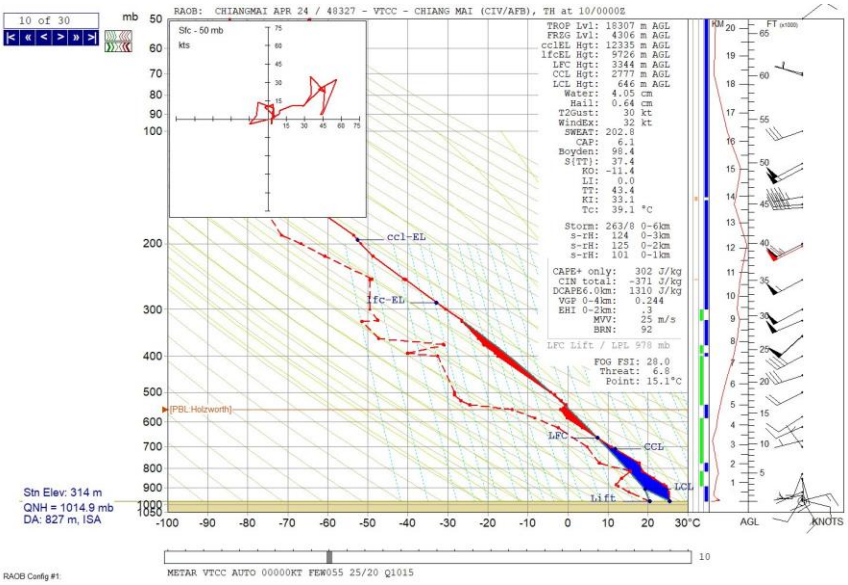


Figure 1. Sounding Graph in Chingmai in 24 April, 2024

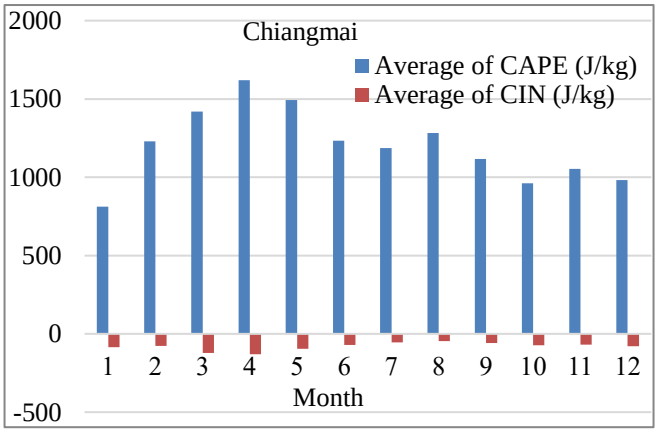


Figure 2. Average CAPE and CIN in Chiangmai (2018-2024)

The sounding data were ploted in RAOB program and the Skew-T was showed in Figure 1.

Figure 2 shows that the average values of CAPE and CIN over a period of 12 months in Chiangmai from 2018 to 2024 excpet year 2022 due to no data record, which measures the amount of energy available for convection, indicates a significant variation through the period. The highest average CAPE values were observed during June, July, August and September, reaching around 1000 J/kg, probably implying a period of strong atmospheric instability. In contrast, the lowest CAPE values were happened in January and December, with values dropping to 100 J/kg, which indicating a more stable atmosphere with less potential for convection. It might not a proper condition for rain enhancement operation.

CIN, which represents the energy required to overcome the inhibition of convection, exhibits an inverse relationship with CAPE. The lowest CIN values are observed in during the months (June, July, August and September) with the highest CAPE, indicating a higher likelihood of convective events. However, the highest CIN values occurred in March, followed by April and February, showing the chance of less convective activity.

CONCLUSION

In conclusion, the analysis of CAPE values over a 12-month period in Chiang Mai showed that the highest average CAPE values were observed during June, July, August and September, reaching around 1000 J/kg, reveals that it is not a proper time for rain enhancement activity. These founding are valuable for weather forecasting and risk assessment, particularly in regions prone to convective storms. It also could be a meteological reference for the rain enhancement operation. Further research could explore the impact of long-term climate trends on these convective parameters to better understand potential conditions for rain enhancement . However, the data of year 2022 was absent due to no available data record for upper air sounding in Thailand for Chiangmai station. The study will continue to collect and analyze the CAPE and CIN in the nine stations in Thailand for further study. The variations on CAPE and CIN during the rain enhancement process will be observed and studied as well.

ACKNOWLEDGEMENT

This research was funded by Kasetsart University through the Graduate School Fellowship Program; the Atmospheric Science Research Group (ASRG); and the Faculty of Environment, Kasetsart University, Bangkok, Thailand.

REFERENCE

1. Beshir, A.A. and J. Song, *Urbanization and its impact on flood hazard: the case of Addis Ababa, Ethiopia.* Natural Hazards, 2021. **109**(1): p. 1167-1190.
2. Gu, Z., et al., *Relationship Between Urbanization–Induced Land Use Changes and Flood Risk: Case Study in Chiang Mai, Thailand.* Water, 2025. **17**(3): p. 327.
3. van der Wiel, K. and R. Bintanja, *Contribution of climatic changes in mean and variability to monthly temperature and precipitation extremes.* Communications Earth & Environment, 2021. **2**(1): p. 1.
4. Lee, H., et al., *Climate change 2023: synthesis report. Contribution of working groups I, II and III to the sixth assessment report of the intergovernmental panel on climate change*. 2023: The Australian National University.
5. Huang, S., et al., *Urbanization amplified asymmetrical changes of rainfall and exacerbated drought: Analysis over five urban agglomerations in the Yangtze River Basin, China.* Earth's Future, 2023. **11**(2): p. e2022EF003117.
6. French, J.R., et al., *Precipitation formation from orographic cloud seeding.* Proceedings of the National Academy of Sciences, 2018. **115**(6): p. 1168-1173.
7. Kim, C., et al., *An Overview of Cloud Seeding Experiments for Precipitation Enhancement over the Northern Part of the Korean Peninsula and Their Future Prospects.* Russian Meteorology and Hydrology, 2023. **48**(8): p. 704-712.
8. Wehbe, Y., et al., *Rethinking water security in a warming climate: rainfall enhancement as an innovative augmentation technique.* npj Climate and Atmospheric Science, 2023. **6**(1): p. 171.
9. Silverman, B.A. and W. Sukarnjanaset, *Results of the Thailand Warm-Cloud Hygroscopic Particle Seeding Experiment.* Journal of Applied Meteorology, 2000. **39**(7): p. 1160-1175.
10. Wang, M., et al., *Evaluation the Effect of Acoustic Wave on Rainfall Enhancement in Low-frequency Acoustic Field*, in *AGU Fall Meeting Abstracts*. 2021: New Orleans, LA. p. H25ZA-03.
11. Al Homoud, M., et al., *Assessment of the Cloud Seeding Efficiency over Tom Green County Texas, USA.* Atmosphere, 2024. **15**(12): p. 1506.
12. Langmuir, I., *THE PRODUCTION OF RAIN BY A CHAIN REACTION IN CUMULUS CLOUDS AT TEMPERATURES ABOVE FREEZING.* Journal of Atmospheric Sciences, 1948. **5**(5): p. 175-192.
13. Cotton, W.R., *Aerosol-Induced Invigoration of Cumulus Clouds—A Review.* Atmosphere, 2024. **15**(8): p. 924.
14. Allen, J.T., D.J. Karoly, and K.J. Walsh, *Future Australian Severe Thunderstorm Environments. Part II: The Influence of a Strongly Warming Climate on Convective Environments.* Journal of Climate, 2014. **27**(10): p. 3848-3868.
15. Brooks, H.E., *Severe thunderstorms and climate change.* Atmospheric Research, 2013. **123**: p. 129-138.
16. Chen, J., et al., *Changes in Convective Available Potential Energy and Convective Inhibition under Global Warming.* Journal of Climate, 2020. **33**(6): p. 2025-2050.
17. Malik, S., et al., *Convective available potential energy (CAPE) in Pakistan and its association with precipitation and temperature.* Theoretical and Applied Climatology, 2021. **146**(1): p. 191-212.
18. Sahu, R., et al., *Pre-monsoon Thunderstorm Season Climatology of Convective Available Potential Energy (CAPE) and Convective Inhibition (CIN) over Eastern India.* MAUSAM, 2022. **73**(3): p. 565-586.

20R3-15

Carbon Footprint Assessment of Thai Cuisine: Curry and Rice Menus

Kanokporn Aree[1], Santi Phithakkitnukoon[2], Karn Patanukhom[3], and Sarunnoud Phuphisith[4*]

[1] Master's Student, Department of Environmental Engineering; [2] Associate Professor, Department of Computer Engineering; [3] Assistant Professor, Department of Computer Engineering; [4] Assistant Professor, Department of Environmental Engineering, Faculty of Engineering, Chiang Mai University, Chiang Mai 50200, Thailand.*
[*]Phone : +66(0)53944192, E-mail: sarunnoud.p@cmu.ac.th

ABSTRACT

The demand for food production is expected to increase significantly as the global population continues to grow, placing pressure on the food system and the environment. The current food system is a major contributor to global warming and requires a transition towards more sustainable food production and consumption. This study assessed the carbon footprint of menu consumption, covering the emissions from ingredient acquisition to the cooking process. A total of 82 Thai curry and rice menus were analyzed and categorized by meat type, e.g., pork, poultry, fish, and cooking methods, e.g., frying, boiling, and steaming. The average CF was found to be highest in poultry-based dishes (3.34 ± 1.18 gCO_2e/g), followed by pork (3.21 ± 1.45 gCO_2e/g), and lowest in fish-based (1.47 ± 0.78 gCO_2e/g). In contrast, the average CF of non-meat dishes was 2.67 ± 1.97 gCO_2e/g. Key CF contributors varied by dish type, with meat and eggs being the most carbon-intensive ingredients. LPG consumption, which varied across different cooking methods, also influenced the CF emission. Modifying menu composition and being aware of LPG consumption in the cooking process could lessen the CF of the menu. The results reinforce the need for an integrated approach in the food industry that considers ingredients and cooking methods, aiming to develop sustainable food systems that align with global climate goals and enhance public health.

Keywords : Life Cycle Assessment; Carbon Footprint; Food production; Thai Cuisine; Sustainability

INTRODUCTION

Modern food systems encompass multiple stages, including production, transportation, processing, packaging, storage, retail, consumption, food loss, and waste management [1]. This system plays a critical factor for human health, and ensuring sufficient food supply is the foundation of well-being [2]. The United Nations projected that the global population would reach 9.7 billion by 2050, necessitating a 70% increase in food production to meet rising demand [3]. However, food production and consumption processes significantly contribute to environmental issues [4]. Current dietary should be improved to enhance sustainability and reduce environmental impacts. This includes minimizing food waste, which accounts for one-third of global food production. Ensuring food security while maintaining sustainability presents a significant challenge [5]. The Sustainable Development Goals, the second goal is advocating food security and the promotion of sustainable food production. [6]. Different dietary patterns have varying environmental impacts, emphasizing the need to shift consumption habits to mitigate these effects. Adopting more sustainable dietary choices can help reduce the environmental footprint of food production and contribute to long-term global sustainability [7].

The agricultural sector covers approximately 37% of the earth's land surface and is a major source of methane and nitrous oxide emissions, accounting for 52% and 84% of global anthropogenic emissions, respectively [8]. These are greenhouse gases (GHG) and lead to global warming crisis. Significant emissions for ruminants are explained mainly by methane emissions from enteric fermentation which makes animal-based food products significantly more impactful than plant-based alternatives in terms of their environmental footprint [9].

Given that the current food system is a major contributor to global warming, it is imperative to transition towards more sustainable food production methods and encourage environmentally responsible consumption behaviors. This study aims to evaluate the carbon footprint (CF) of meal consumption. The CF information can reveal opportunities for reducing the average carbon footprint of food products. Providing consumers with CF information on menus helps to encourage consumer decision-making in food selection to make climate-friendly food choice.

METHODOLOGY

This study was scoped into curry and rice menus. The menus were surveyed from food vendors at Chiang Mai University during August – September 2024. Then, the recipes and cooking time were extracted from an online cooking recipe-sharing platform called "Wongnai." All menus were categorized based on ingredients (e.g., with meat and without meat) and cooking methods (e.g., stirred-fried, boiled, etc.). The CF of menus was calculated covering the emissions from ingredient acquisition to cooking process (cradle to gate), using eq. 1. The calculation excluded the transport emissions of ingredients to kitchens.

$$CF = \frac{\sum_{i=1}^{n}(X_i \times EF_i) + Y_L \times EF_L}{X_T} \quad \text{—eq 1}$$

Here, CF is the amount of carbon footprint of the menu (gCO_2e/g)., X_i is the weight of ingredient i used in the menu (g)., EFi is the emission factor of the ingredient i (gCO_2e/g)., Y_L is the weight of LPG used in the menu (g), EF_L is the emission factor of LPG including the emissions from acquisition and combustion in cooking process (gCO_2e/g). The weight of LPG used is calculated by multiplying the total cooking time in minutes by the LPG consumption rate. All cooking methods were assumed to have the same rate of 1.67 grams per minute, which was determined from the experiments conducted in this study. X_T is the total weight of ingredients (g). All emission factors were from the Thai National LCI Database, TIIS-MTEC-NSTDA and the TGO certified carbon footprint products. If the emission factors were unavailable in the national database, the study first considered whether the weight of the ingredient was less than 5% of the total weight. If so, the ingredient was excluded from the calculation. If the weight of the ingredient accounted for more than 5% of the total weight, a similar ingredient's emission factor was used instead. All calculations were done using Microsoft Excel version 2501 Build 16.0.18429.20132.

RESULTS AND DISCUSSIONS

1. Menu categories

A total of 82 menus were observed and categorized into meat-based and non-meat-based menus. The meat-based included 29 pork dishes, 21 poultry dishes and six fish dishes. The remaining 26 menus were non-meat based. Based on cooking method, the menus were classified into seven categories: 45 stir-fried dishes, 22 boiled dishes, nine fried dishes, two steamed dishes, two grilled dishes, one simmered dish and one baked dish.

2. CF of curry and rice menus

Regardless of the cooking method, poultry dishes exhibited the highest average CF (3.34 ± 1.18 gCO_2e/g), followed by pork (3.21 ± 1.45 gCO_2e/g), non-meat dishes (2.67 ± 1.97 gCO_2e/g), and fish (1.47 ± 0.78 gCO2e/g), as shown in Figure 1. The primary contribution to CF varies by meat-type. Chicken meat was the highest contribution in almost all poultry dishes (20 out of 21 dishes or 95%). Pork ranked the highest contribution, at 72% of the total pork-based dishes. For the fish-based dishes, LPG was the dominant contributor for 50% of fish dishes; the other 33% had their largest contribution from fish and 17% had from eggs. As for non-meat based, eggs showed the most significant emissions in 58% of the total non-meat-based dishes, instant noodles and glass noodles (15%), LPG (15%), and green vegetables (12%).

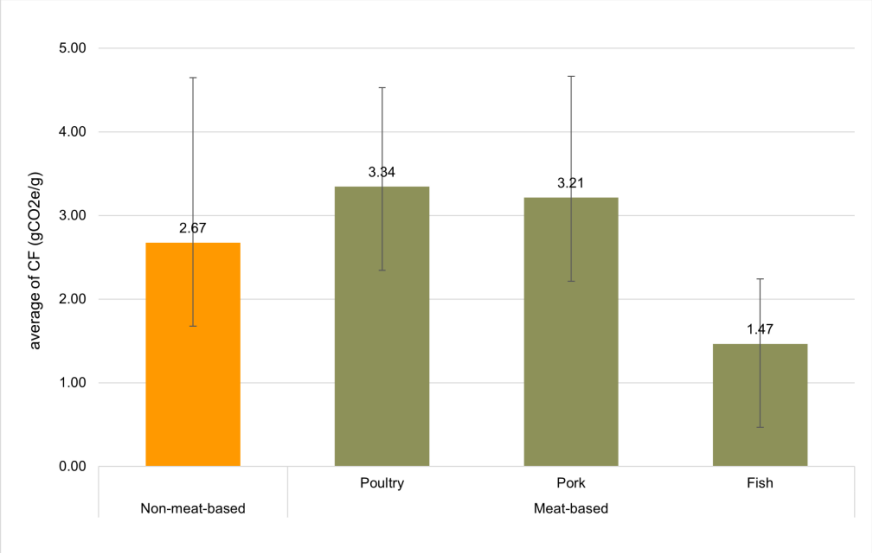


Figure 1 CF of meat-based and non-meat dishes

In meat-based dishes, the highest CF was found on the menu stewed pork and egg in brown sauce (6.49 gCO_2e/g), followed by and clear soup with egg and minced pork menu (6.09 gCO_2e/g). In contrast, Choo Chee curry with fish was the lowest CF menu (0.80 gCO_2e/g). The dishes with high CF typically contain pork and eggs, as shown in **Figure 2,** both are ingredients associated with high GHG. For non-meat based, the highest CF dish was sweet and sour fried boiled eggs (7.78 gCO_2e/g), while the lowest CF menu was stir-fried vegetables (0.49 gCO_2e/g). This indicates that eggs are a key contributor to GHG among non-meat dishes. Opting for a diet that choosing fish or vegetables as an alternative could contribute to lowering emissions.

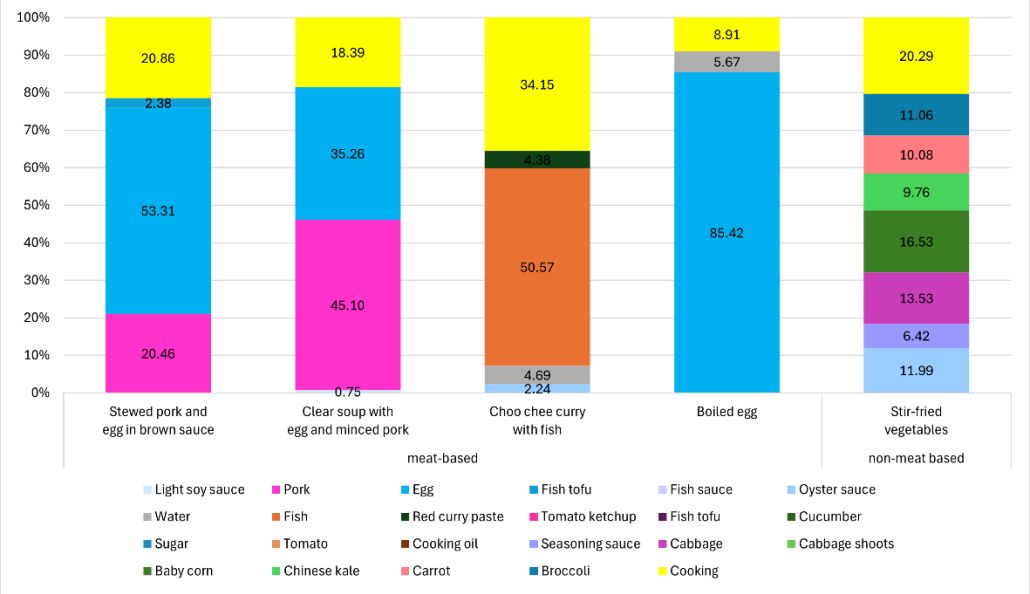


Figure 2 GHG contributing composition in some selected menus

Our findings are consistent with the previous studies. The study by Leuenberger et al. [10] reported that meat-based dishes generated higher GHG emissions, on average 3 $kgCO_2e$/serving, and poultry or pork ranged from 1.5 to 2 $kgCO_2e$/serving. While the vegetarian dishes had 0.9 $kgCO_2e$/serving. Another study by Volanti et al. [11] showed that the meat, fish and dairy dishes had high CF, ranging from 3 to 24 gCO_2e/g, with the highest value at beef. Fruit and vegetables had a smaller CF than 2 gCO_2e/g.

Considering the cooking methods, that consumed LPG varied, **Figure 3** presents that fried dishes had the highest CF (4.83 ± 1.83 gCO_2e/g), followed by steamed (4.28 ± 0.54 gCO_2e/g), grilled (3.66 ± 2.93 gCO_2e/g), stir-fried (2.52 ± 1.31 gCO_2e/g), boiled (2.92 ± 1.54 gCO_2e/g), simmered (2.22 gCO_2e/g), and baked (2.06 gCO_2e/g). Carefully considering the footprint contribution of LPG usage, it showed that grilled dishes had the highest contribution from LPG usage (55%), followed by baking (32%), boiled (24%), steamed (24%), stir-fried (20%), fried (17%), and stewed (10%). This result should be cautious, as there were few menus cooked steamed, grilled, simmered, and baked in our study, as described above.

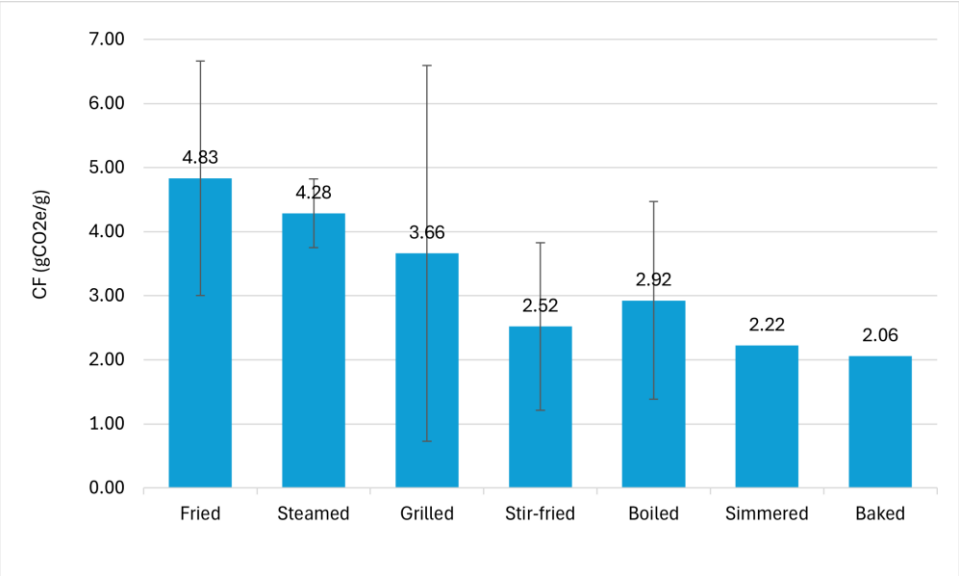


Figure 3 CF of menus by cooking methods

Our results show that meat-based dishes, particularly poultry and pork, had higher CF than fish and vegetarian options. This is consistent with global trends highlighting the environmental impact of meat production. By shifting towards plant-based diets, individuals can substantially reduce their carbon emissions. Introducing CF information on menus can influence consumer choices, encouraging shifts towards more sustainable options. Such transparency in menu labeling can drive significant behavioral changes, supporting broader climate change mitigation efforts. Additionally, our findings reveal that the LPG could be a significant CF contributor, such as fish dishes, where LPG accounts 50% of the total CF portion. The estimation assumed that all cooking methods use the same rate of LPG consumption, differing only in the cooking time.

CONCLUSION

The present study evaluated the GHG associated with different curry and rice menus. The emissions covered from raw material acquisition to cooking process. The findings indicated that meat-based dishes had higher CF. Shifting dietary behaviors can contribute to reducing greenhouse gas emissions. The outcome of the present study could raise consumers awareness of the need to encourage environmentally friendly menu choices, promoting sustainable food consumption.

The limitations of this study primarily stem from its restricted data collection scope and the inherent variability in recipes. Furthermore, the carbon footprint calculations did not encompass emissions associated with the transportation of ingredients to the kitchen, and food waste generation, e.g., from cooking and after consumption. Incorporating transportation and food-related emissions into the carbon footprint analysis would offer a more holistic view of the total environmental impact, guiding more targeted strategies for reducing GHG in the food sector. In addition, future investigations could expand the scope of data collection to include a broader array of recipes and culinary practices, enhancing the generalizability of the findings.

ACKNOWLEDGEMENT

This project is funded by National Research Council of Thailand (NRCT).

REFERENCE

[1] World Bank. (2019). Agriculture, forestry, and fishing, value added (% of GDP). World Bank national accounts data, and OECD National Accounts data files. World Bank Group. Retrieved from https://www.ipcc.ch/srccl/chapter/chapter-5/

[2] Kanauchi, M., & Kanauchi, K. (2018). The World Health Organization's Healthy Diet Indicator and its associated factors: A cross-sectional study in central Kinki, Japan. *Preventive Medicine Reports*, 12, 198–202. https://doi.org/10.1016/j.pmedr.2018.09.011

[3] Food and Agriculture Organization (FAO). (2009). *Global agriculture towards 2050*: The challenge. Food and Agriculture Organization of the United Nations Forum.

[4] Notarnicola, B., Tassielli, G., Renzulli, P. A., Castellani, V., & Sala, S. (2017). Environmental impacts of food consumption in Europe. *Journal of Cleaner Production*, 140, 753–765. https://doi.org/10.1016/j.jclepro.2016.06.080

[5] Nikkhah, A., Firouzi, S., Dadaei, K., & Van Haute, S. (2021). Measuring circularity in food supply chain using life cycle assessment; refining oil from Olive Kernel. Foods, 10(590). https://doi.org/10.3390/foods10030590

[6] United Nations. (n.d.). Sustainable Development Goal 2. Retrieved April 4, 2025, from https://sdgs.un.org/goals/goal2

[7] Swain, M., Blomqvist, L., McNamara, J., & Rivers, N. (2018). Reducing the environmental impact of global diets. Science of The Total Environment, 610–611, 1207–1209. https://doi.org/10.1016/j.scitotenv.2017.08.125

[8] Smith, P., Martino, D., Cai, Z., Gwary, D., Janzen, H., Kumar, P., McCarl, B., Ogle, S., O'Mara, F., Rice, C., Scholes, B., Sirotenko, O., Howden, M., McAllister, T., Pan, G., Romanenkov, V., & Smith, J. (2007). Greenhouse gas mitigation in agriculture. Philosophical Transactions of the Royal Society B: Biological Sciences, 363(1492), 789–813. https://doi.org/10.1098/rstb.2007.2184

[9] Carlsson-Kanyama, A., & González, A. D. (2009). Potential contributions of food consumption patterns to climate change. American Journal of Clinical Nutrition, 89(5), 1704S–1709S. https://doi.org/10.3945/ajcn.2009.26736AA

[10] Leuenberger, M., Jungbluth, N., & Büsser, S. (n.d.). *Environmental impact of canteen meals: Comparison of vegetarian and meat-based recipes*. ESU-services Ltd. Retrieved from https://esu-services.ch/fileadmin/download/leuenberger-2010-meals-LCAfood.pdf

[11] Volanti, M., Arfelli, F., Neri, E., Saliani, A., Passarini, F., Vassura, I., & Cristallo, G. (2021). Environmental impact of meals: How big is the carbon footprint in the school canteens? *Foods* **2022**, *11*(2), 193; https://doi.org/10.3390/foods11020193

20R3-16

Life Cycle Assessment of Drilling Waste Treatment: Comparative Study of Thermal Desorption and Solvent Extraction

Bovathanak Leng[1], Thaksina Poyai[2], Ratchanan Chamnanmor[3], Saret Bun[4] and Pisut Painmanakul[5,6,7*]

[1]Master student; [3]Doctoral student; [5]Professor, Department of Environmental and Sustainable Engineering, Faculty of Engineering, Chulalongkorn University, Bangkok 10330, Thailand

[2]Lecturer, Department of Environmental Engineering, Faculty of Engineering, Kasetsart University, Bangkok 10900, Thailand

[4]Professor, Water and Environmental Engineering, Faculty of Hydrology and Water Resources Engineering, Institute of Technology of Cambodia, Phnom Penh, Cambodia

[6]Director, Carbon Institute for Sustainability, Chulalongkorn University, Bangkok 10330, Thailand

[7]Head, Center of Excellence in Treatment Technology and Management of Petroleum Contaminants and Environmental Pollution, Chulalongkorn University, Bangkok 10330, Thailand

[*]Phone : 089 413 1392, E-mail : bvathanak.leng@gmail.com

ABSTRACT

The oil and gas industry generates a large volume of drilling waste which poses serious environmental and economic challenges. Traditional disposal methods such as landfilling and ocean dumping have been banned in many regions due to their associated environmental concerns. Therefore, this study investigated the environmental performance of two alternative treatment methods for managing drilling waste: (1) thermal desorption and (2) solvent extraction using ethyl lactate (EL). A comprehensive Life Cycle Assessment (LCA) was conducted to quantify the environmental impacts of each scenario, employing the ReCiPe 2016 methodology within the SimaPro software. The assessment covered 18 midpoint impact categories and 3 endpoint damage indicators. The findings showed that Scenario 1 (thermal desorption) consistently produced the lowest environmental impacts across all 18 midpoint categories and all three endpoint indicators. In contrast, Scenario 2 (solvent extraction using EL) demonstrated the highest impacts of the total environmental burden in both midpoint and endpoint categories due to the high volumes uses of chemical solvent required while in Scenario 1, the treatment by thermal desorption used only the electricity, minimizing low impacts to the environment. These findings indicate that thermal desorption is an environmentally sustainable method for treating drilling waste, compared to solvent washing.

Keywords: Drilling waste treatment, Solvent extraction, Thermal desorption, Life cycle assessment

INTRODUCTION

The oil and gas industry generates a large volume of drilling waste which poses serious environmental and economic challenges. Drilling waste consists of two main types: drilling fluids and drill cuttings. Drilling fluids are the liquid that is used to lubricate and cool the drilling bit, stabilize the well bore, and control sub-surface pressure. Its important role is to pump down the hole and transport the drill cuttings that produce from the drilling of boreholes while extracting up to the surface [1]. Drill cuttings are a mixture of rock fragments and drilling fluids which are considered to be the byproducts, generated during the process of drilling the oil [2]. These kinds of wastes contain many toxic components, including hydrocarbons, heavy metals, and other hazardous substances, which require effective and safe management. The traditional disposal methods of drilling waste such as ocean dumping and landfilling, have been banned due to several environmental concerns such as soil contamination, water pollution, and adverse effects on marine ecosystem [3, 4]. To respond with these problems, the treatment of drilling waste has emerged as one of the most effective approaches for managing this type of waste. Various treatment methods have been investigated including cuttings re-injection, stabilization/solidification, bioremediation, thermal treatments and solvent extraction. Thermal desorption is a process of using heat to evaporate organic contaminants from the media, and reduce the waste volume especially use to treat hydrocarbon content in drilling waste management [1]. This technology has become greatly popular for treating oil-based drill cuttings (OBDCs) because of the high removal efficiency, short treatment time, less secondary pollution, and reusable of processed products [5-7]. After thermal treatment, the total petroleum hydrocarbon (TPH) contents in dried solids can be reduced to <1% (mass percent) within the temperature ranges from 250 to 350 °C [1, 8].

Another treatment method which is the solvent extraction/washing, is a separation technique that uses liquid solvent to selectively remove contaminants from a solid material [9]. The solvent washing can be considered to be another appealing option by using the solvent to wash or clean the contaminated drilling waste due to its lower energy requirement, rapid treatment, and ease of operation [10]. The study from Poyai (2020), investigated that the use of organic solvents such as ethyl lactate (EL), ethyl acetate (EA) and ethylene glycol (EG) to treat the contaminated drill cuttings and the result showed using EL can remove 87 % of total petroleum hydrocarbons (TPHs) [10]. That is why thermal desorption and solvent extraction has shown to be the most promising paths that could be applied in managing these wastes. Moreover, the environmental performance of drilling waste management needs to be considered.

Life Cycle Assessment (LCA) is a tool used for evaluating the environmental impacts of the whole process of a product's life cycle [11]. LCA can be used to determine how a product has the impacts to the environment, starting from the first stage of raw materials, through production and use, all the way to its disposal stage. A study from Hu (2021), showed that the investigation of using LCA on drilling waste treatment by thermal desorption, starting from extraction until treatment, contributed different impacts to the environment and the study as well provided insights for selecting treatment methods that had low-impact to the environment [12]. Therefore, by using the LCA in managing the drilling waste, the study could provide insights into sustainable waste management strategies, and support the adoption of environmental solutions for oil and gas industries. The objective of the study was to conduct the LCA to quantify the environmental impacts of two drilling waste management scenarios: (1) the treatment of drilling waste via thermal desorption and (2) the treatment of drilling waste by solvent extraction.

METHODOLOGY

A systematic research framework was developed to evaluate the environmental impacts of the two treatment processes. The study conducted the LCA following the ISO 14040 and 14044 standards, which involved four stages: goal and scope definition, life cycle inventory, life cycle impact assessment, and result interpretation as seen in Figure 1 [13, 14].

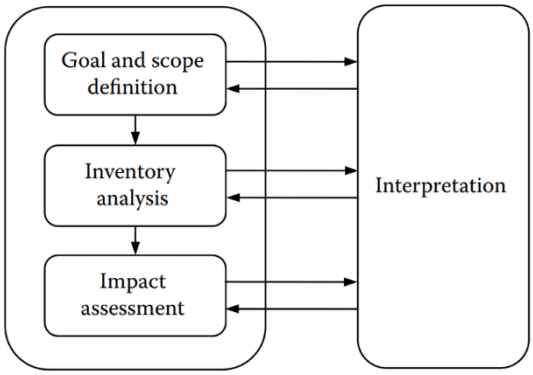


Figure 1 The four iterative phases of life cycle assessment

Goal and scope definition

- **Scenario 1**

The goal was to assess the environmental performance of the treatment of drilling waste by using thermal desorption process. The scope included the transportation of drilling waste from extraction source, and the thermal treatment stage. It covered a gate-to-gate system. On-site drilling activities, wastewater treatment plant, and the disposal of the drilling waste were excluded from the study. The functional unit of the first scenario was 1,000 tons of drilling waste. The system boundary of Scenario 1 was shown in Figure 2.

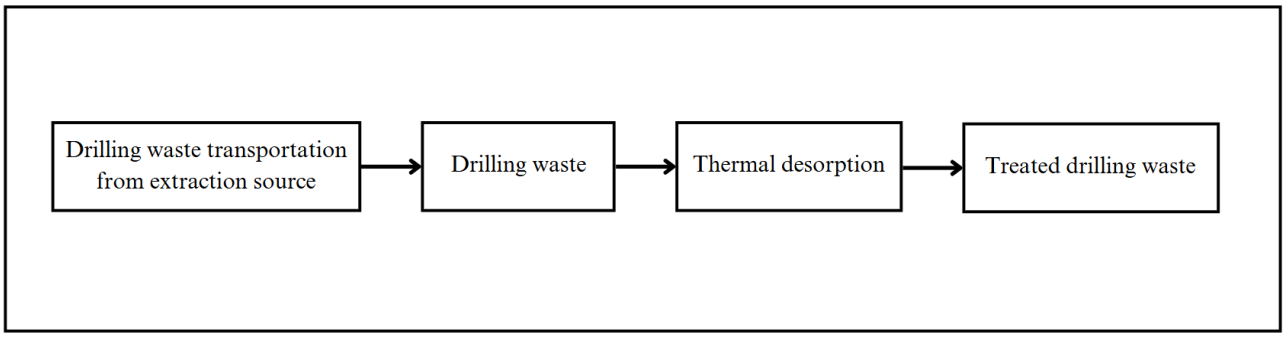


Figure 2 The system boundary of Scenario 1: drilling waste treated by thermal desorption

- **Scenario 2**

This scenario aimed to evaluate the environmental impacts of drilling waste treatment by using a solvent extraction method. According to the study from Poyai (2020) which investigated the effectiveness of three solvents: ethyl lactate (EL), ethyl acetate (EA), and ethylene glycol (EG), in extracting total petroleum hydrocarbons (TPHs) from drill cuttings [10]. Among them, ethyl lactate achieved the highest TPH removal efficiency at 87%, outperforming the other two solvents. Therefore, in this scenario, the use of EL-based washing to treat drilling waste was studied. However, due to the lack and unavailability data of ethyl lactate (EL), the data ethyl acetate (EA) was selected as a substitute for the data of EL in the LCA modeling instead. This substitution is justified based on the chemical and functional similarities between EL and EA. Both solvents are short-chain esters with comparable molecular structures and solvent properties [15, 16]. Ethyl acetate is also recognized as a low-toxicity, biodegradable solvent and is widely used in industrial applications, its production data more readily available, transparent, and consistent for use in LCA modeling [17]. The scope in this scenario consisted of the transportation of drilling waste from extraction source, and the solvent extraction stage with the use of ethyl acetate-based washing. It covered a gate-to-gate approach. On-site drilling activities, wastewater treatment plant, and the disposal of the treated drilling waste were excluded from the study. The functional unit of Scenario 2 was 1,000 tons of drilling waste. The system boundary of Scenario 2 was shown in Figure 3.

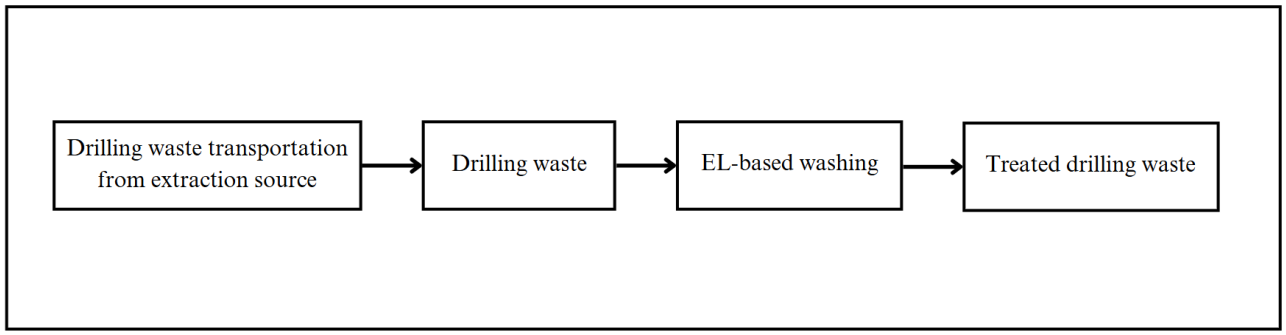


Figure 3 The system boundary of Scenario 2: drilling waste treated by solvent extraction

Life cycle inventory

The required inventory data consisted of the associated inputs (raw materials, resources, energy consumption) and outputs (products, emissions, waste). The quantities of raw materials, energy usage, and waste generation were gathered as primary data. Emissions from the thermal treatment process were sourced from secondary data, found in existing literature and scientific studies. For the first scenario, energy input data for thermal desorption were calculated based on pilot-scale operations, while gaseous emissions were derived from previous studies [12, 18]. In the second scenario, both input and output data were calculated through pilot-scale experiments. The Ecoinvent database v3.10 was used and chosen based on its relevance to Thailand's location, and for data unavailable for Thailand, the Rest of the World (RoW) dataset was used to minimize uncertainty in the assessment results. The life cycle inventory data of both scenarios were listed in Table 1.

Table 1 Life cycle inventory for treatment of drilling waste in 1000 tons.

Scenario	Items	Process/activity Equipment/material	Energy/material/distance	Unit	Reference
Both	Transportation	Lorry 16-32 metric ton	370	km	Calculated
1	Inputs	**Thermal desorption**			
		Turbine motor	37×10^4	kWh	Calculated
		Vacuum pump	37×10^4	kWh	Calculated
		Coolant pump	23×10^4	kWh	Calculated
		Thermal glass reactor	12×10^4	kWh	Calculated
	Outputs	**Gaseous emissions**			
		Particulates	107.8	kg	Previous studies [10, 13]
		CO_2	23.2	kg	
		CO	7.3	kg	
		CH_4	2.8	kg	
		NO_x	68.4	kg	
		SO_2	14.6	kg	
2	Inputs	**Solvent extraction**			
		Stirrer/mixer	192×10^3	kWh	Calculated
		Ethyl lactate	412×10^4	kg	Calculated
		Water	10^7	kg	Calculated
	Outputs	**Separated water**			
		Wastewater	10^7	kg	Calculated
		Spent solvent			
		TPH-contaminated solvent	412×10^4	kg	Calculated

Life cycle impact assessment

In this study, SimaPro™ 9.6.0.1 software was employed as a tool for evaluating the impacts of products, and processes throughout the entire life cycle with the use of The ReCiPe 2016 (H) v1.1 assessment method. The hierarchist perspective was used in ReCiPe method for defining the problem-oriented midpoints and the damage-oriented endpoint assessments. Both scenarios assessed 18 midpoint impacts including global warming (kg CO_2-eq), stratospheric ozone depletion (kg CFC-11-eq), ionizing formation (kBq Co-60-eq), ozone formation human health/terrestrial ecosystem (kg NO_x-eq), fine particulate matter formation (kg $PM_{2.5}$-eq), terrestrial acidification (kg SO_2-eq), freshwater eutrophication (kg P-eq), marine eutrophication (kg N-eq), terrestrial ecotoxicity (kg 1,4-DCB), freshwater ecotoxicity (kg 1,4-DCB), marine ecotoxicity (kg 1,4-DCB), human carcinogenic toxicity (kg 1,4-DCB), human non-carcinogenic toxicity (kg 1,4-DCB), land use ($m^2 \times$ yr annual cropland-eq), mineral resource scarcity (kg Cu-eq), fossil resource scarcity (kg oil-eq), and water consumption (m^3 water-eq consumed). 3 endpoint impacts consisted of human health (disability-adjusted life year, DALY), ecosystem (biodiversity in terms of disappeared fraction of species on an area during a year, species/yr), and resource scarcity (USD 2013).

Result interpretation

This stage of the LCA involved analyzing and interpreting the results obtained from the life cycle inventory and impact assessment to evaluate the environmental impacts of both scenarios. The interpretation phase of the LCA provided conclusions as it identified which treatment processes or scenarios that had the greatest environmental impact by assessing both midpoint and endpoint indicators. Additionally, this stage also compared the current study with previous LCA studies involving different treatment technologies to evaluate overall environmental performances.

RESULTS AND DISCUSSIONS

Impacts of midpoint characterization

The 18 midpoints impact categories were assessed using ReCiPe 2016 Midpoint (H) v1.09 method. As illustrated in Figure 4, the use of two treatment methods in treating drilling waste associated with different environmental impacts. In Scenario 1, thermal desorption exhibited the lowest impacts in all 18 categories, with all values remained below approximately 10%. In contrast, the use of EL in solvent extraction in Scenario 2, demonstrates the highest environmental impacts across all categories, with values consistently at 100%. This indicated that the solvent extraction method resulted in the most significant environmental burden. The high environmental impacts observed in Scenario 2 (EL-based washing) were primarily due to the large quantities of solvents required to extract or wash the petroleum hydrocarbon contaminants from the drilling waste. Ethyl lactate was considered as non-environmentally friendly chemicals. Their production, use, and disposal were associated with significant environmental burdens, contributing heavily to categories such as global warming potential, toxicity, and resource depletion. In contrast, Scenario 1 (Thermal desorption) relied on the use of electricity to heat the contaminated drilling waste. This approach minimized the introduction of harmful substances into the life cycle and significantly reduced environmental impacts in all categories evaluated. As a result, thermal desorption represented the most sustainable option among the three techniques.

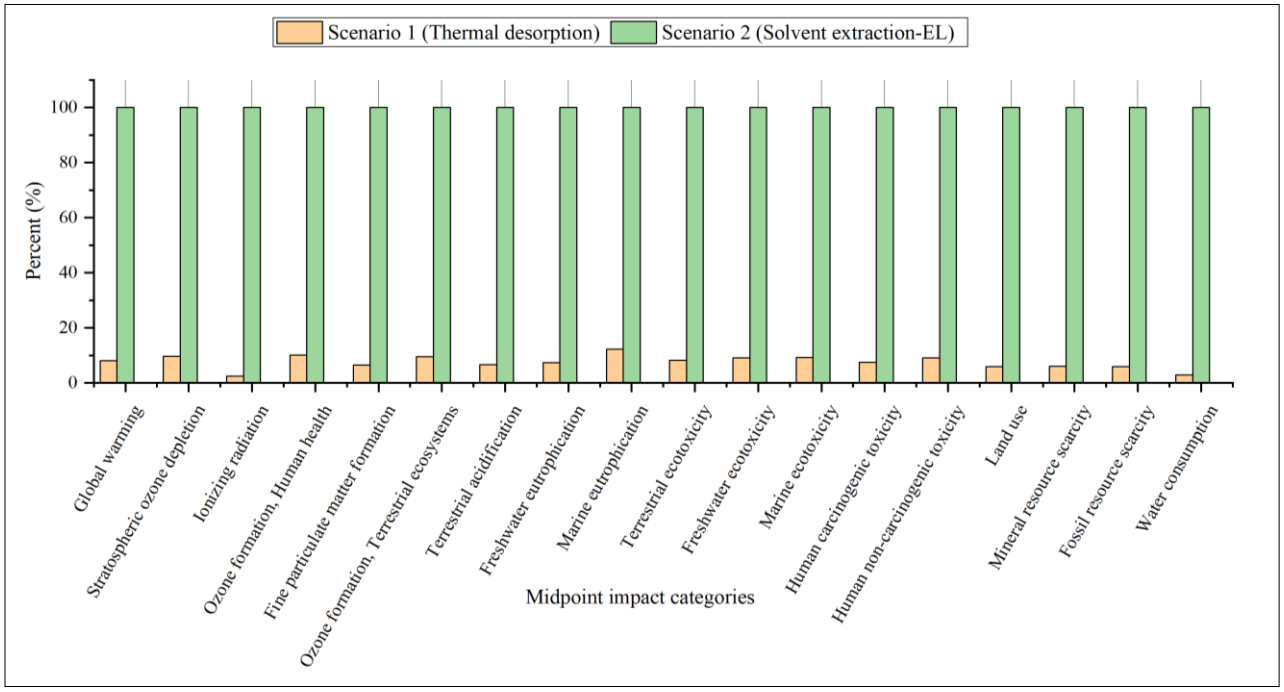


Figure 4 Midpoint impacts for the treatment of drilling waste in both scenarios

Impacts of endpoint damage assessment

The life cycle impacts of endpoint damage assessments of using thermal desorption and solvent extraction were shown in Figure 5. The results were expressed as relative percentage contributions across three endpoint categories of human health, ecosystems, and resources. Scenario 1 resulted the lowest impacts across all three damage categories, while Scenario 2 showed the highest impacts with the use of EL-based washing solvent. Treating 1,000 tons of drilling waste using the EL-based in solvent extraction method led to damages of 0.05 DALY to human health, 9.14×10^5 species/year to ecosystem biodiversity, and 2610 USD2013 in resource depletion as shown in Table 2. A total of 0.05 DALY indicated that the treatment process caused a health burden equivalent to losing 18.25 days of healthy life across the affected population. A value of 9.14e-05 species·year meant that the process contributed to a 0.0000914 annual loss of species, while numerically small, reflected cumulative ecological degradation that could become significant at large scales. A value of 2610 USD2013 reflected the estimated future economic burden caused by extracting non-renewable resources for this treatment process. In comparison, the damages associated with thermal desorption was approximately 7% of those caused by EL-based method.

Table 2 The endpoint impact scores of both scenarios

Damage category	Unit	Impact scores of Scenario 1	Impact scores of Scenario 2
Human health	DALY	0.033	0.05
Ecosystems	species.yr	5.61×10^5	9.14×10^5
Resources	USD2013	1827.95	2610.81

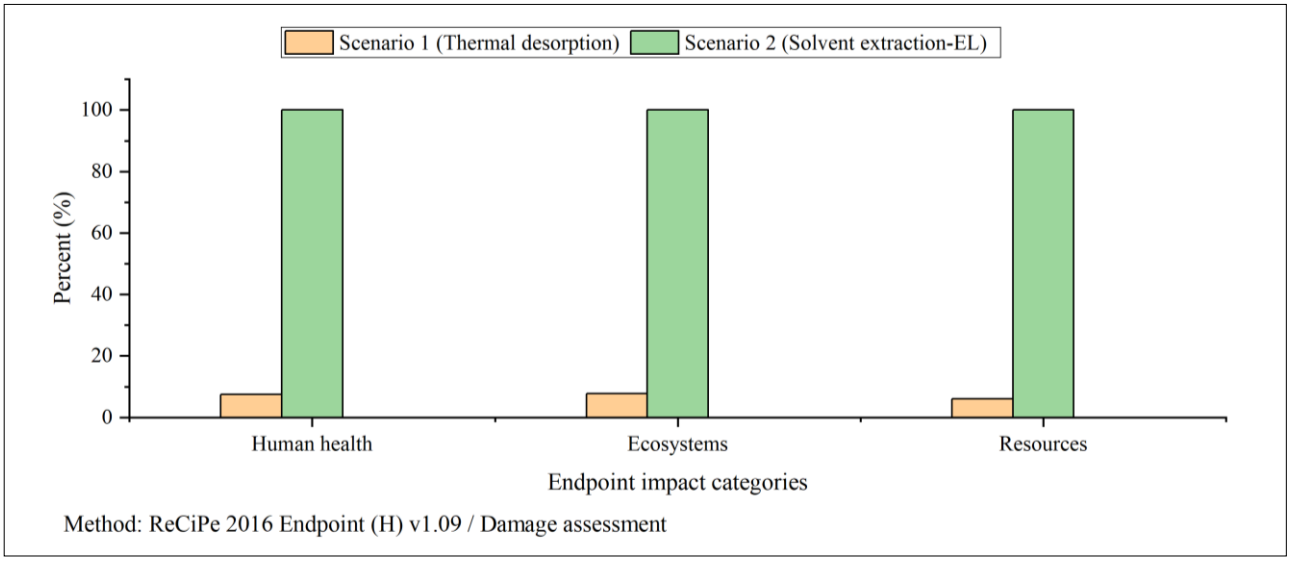


Figure 5 Endpoint impacts of the two scenarios for drilling waste treatment

Comparison study

Given the substantial environmental impacts associated with the use of ethyl lactate (EL) solvent, this section focused only in comparing the thermal desorption method with the findings from previous studies. As global warming potential (GWP) is considered the most critical impact category, the discussion here were limited to this indicator. In our study, the use of thermal desorption to treat one ton of drilling waste generated 84.5 kg CO_2-eq GHG emission. According to the study from Hu (2021), it reported that treatment of one ton of dill cuttings using three low-temperature thermal desorption (LTTD), including thermomechanical cuttings cleaner (TCC), screw-type dryer (STD), and rotary drum dryer (RDD), produced 177.2 kg, 294.4 kg, and 255.3 kg CO_2-eq GHG emission, respectively [12]. The lower CO_2 emissions observed in our study were primarily attributed to the use of electricity as the energy source. Specifically, the assessment was conducted based on Thailand's electricity grid, which relied on natural gas as the main source of electricity generation. In contrast, the study of using three LTTD to treat drill cuttings, utilized diesel-based electricity generation, resulting in significantly higher CO_2 emissions from their processes. Another study from Lemming et al. (2016) also assessed the GHG emission of trichloroethene contaminated-soil, treated by thermal desorption which released 180 kg CO_2-eq emission [19]. Compared to our study, the higher CO_2 emissions reported in this paper could be attributed to its location in Denmark, where a significant portion of the electricity was generated from coal, leading to greater carbon emissions than in our study.

CONCLUSION

The study conducted a comprehensive life cycle assessment (LCA) to evaluate the environmental impacts of two drilling waste treatment methods, which were thermal desorption and solvent extraction using ethyl lactate. The findings clearly demonstrated that thermal desorption of Scenario 1 offered the lowest environmental impacts across all 18 midpoint categories and 3 endpoints damage indicators, making it the most sustainable treatment option. On the other side of using EL in solvent extraction, the result showed significantly higher environmental burdens due to the large volumes of chemical solvents required.

Therefore, thermal desorption is the most environmentally sustainable and low-impact technology for managing petroleum-contaminated drilling waste.

ACKNOWLEDGEMENT

The author would like to thank Prof. Pisut, Dr. Thaksina, Ms. Ratchanan, and Prof. Saret for their continuous guidance, insightful advice, and unwavering support throughout the research journey.

REFERENCE

[1] Ball, A.S., R.J. Stewart, and K. Schliephake, A review of the current options for the treatment and safe disposal of drill cuttings. Waste Management & Research, 2012. 30(5): p. 457-473.
[2] de Almeida, P.C., O.d.Q.F. Araújo, and J.L. de Medeiros, Managing offshore drill cuttings waste for improved sustainability. Journal of cleaner production, 2017. 165: p. 143-156.
[3] Magalhães, M.O.L., et al., The effects of oil well drill cuttings on soil and rice plant development (Oryza sativa) under two redox conditions. Bulletin of environmental contamination and toxicology, 2014. 92: p. 311-316.
[4] Puiseux, A., A. Guillou, and T. Merzi. Overview of drill cuttings management options through modeling, monitoring and life cycle assessment. in SPE International Conference and Exhibition on Health, Safety, Environment, and Sustainability? 2020. SPE.
[5] Jones, T., M. Sanders, and B. Chambers. Improvements in the analysis of thermally recovered drilling fluid base oils from drilled cuttings. in SPE International Conference and Exhibition on Health, Safety, Environment, and Sustainability? 2002. SPE.
[6] Stephenson, R., et al., Thermal Desorption of Oil from Oil-Based Drilling Fluids Cuttings: Processes and Technologies. SPE Asia Pacific Oil and Gas Conference and Exhibition. 2004.
[7] Zhang, X. and A. Yao, Pilot experiment of oily cuttings thermal desorption and heating characteristics study. Journal of Petroleum Exploration and Production Technology, 2019. 9: p. 1263-1270.
[8] Murray, A.J., et al. Friction-based thermal desorption technology: Kashagan development project meets environmental compliance in drill-cuttings treatment and disposal. in SPE Annual Technical Conference and Exhibition? 2008. SPE.
[9] Hall, D.W., J.A. Sandrin, and R.E. McBride, An overview of solvent extraction treatment technologies. Environmental Progress, 1990. 9(2): p. 98-105.
10. Poyai, T., et al., Solvent-based washing as a treatment alternative for onshore petroleum drill cuttings in Thailand. Science of the Total Environment, 2020. 718: p. 137384.
[11] Shaked, S., et al., Environmental life cycle assessment. 2015: CRC Press.
[12] Hu, G., et al., Life cycle assessment of low-temperature thermal desorption-based technologies for drill cuttings treatment. Journal of Hazardous Materials, 2021. 401: p. 123865.
[13] ISO, Environmental management-Life cycle assessment-Requirements and guidelines. Vol. 14044. 2006a: ISO.
[14] ISO, Environmental management-life cycle assessment-principles and framework. 2006b: International Organization for Standardization.
[15] Erişir, E. and E. Gümüşkaya, An Environmentally Friendly Solvent for Cellulose Acetate Production: Ethyl Lactate. Bartın Orman Fakültesi Dergisi. 26(3): p. 271-283.
[16] Bermejo, D.V., et al., Effect of cosolvents (ethyl lactate, ethyl acetate and ethanol) on the supercritical CO2 extraction of caffeine from green tea. The Journal of Supercritical Fluids, 2016. 107: p. 507-512.
[17] Bories, C., et al., LCA case study: comparison between independent and coproduction pathways for the production of ethyl and n-butyl acetates. The International Journal of Life Cycle Assessment, 2018. 23: p. 251-266.
[18] Ogbuagu, D.H., A.C. Esinulo, and S.E. Job, Evaluation of treatment efficiency of drilling waste with thermal desorption technique. International Journal in IT & Engineering, 2016. 4(4): p. 39-45.
[19] Lemming, G., et al., Environmental impacts of remediation of a trichloroethene-contaminated site: life cycle assessment of remediation alternatives. Environmental science & technology, 2010. 44(23): p. 9163-9169.

20R3-18

Sustainability Assessment of Circular Economy Products from Rice Wastes

Tanita Cheevaphantusri[1*] , Rattanawan Mungkung[2] , Shabbir Gheewala[3], and Napat Jakrawatana[4]

[1] Sustainable Energy and Resources Engineering (TAIST program), Kasetsart University, Bangkok 10900, Thailand; [2]Associate Professor, Department of Environmental Technology and Management, Faculty of Environment, Kasetsart University, Bangkok, Thailand; [3]Professor, The Joint Graduate School of Energy and Environment, King Mongkut's University of Technology Thonburi, Bangkok, Thailand; [4]Associate Professor, Department of Environmental Engineering, Faculty of Engineering, Chiang Mai University, Chiang Mai, Thailand*

[*]Phone :0869792585, E-mail : tanita.ch@ku.th

ABSTRACT

The bio-circular-green (BCG) economy model has been introduced by the Thai government to promote a circular economy and encourage the development of value-added products through resource use efficiency. Thailand produces approximately 21 million tons of milled rice annually, generating a significant amount of rice wastes that has not been effectively utilized. The study conducted a comprehensive sustainability assessment of two rice wastes products— rice husk ash (RHA) blended concrete block and rice straw (RS) brick using life cycle assessment (LCA), eco-efficiency, material circularity indicator (MCI), and cost benefit analysis (CBA) tools. The LCA results identified that raw material acquisition was the major hotspot for all impact categories for RHA-blended concrete block while the production phase was the primary hotspot in all impact categories for RS bricks except photochemical oxidation. The eco-efficiency results based on GWP were 0.17 USD/kgCO_2e for RHA-blended concrete blocks and 2.7 USD/kgCO_2e for RS brick. The MCI results for RHA-blended concrete block was 0.4, higher than the MCI for conventional concrete blocks, while RS bricks achieve an MCI of 0.5, indicating a higher degree of circularity. The cost benefit analysis (CBA) revealed that RHA-blended concrete block achieved a CBA of 2.2, indicating a profit gained whereas RS brick only receives a CBA of 0.9, indicating a loss. The results show that improved environmental performance could increase eco-efficiency, increase circularity, and strengthen economic feasibility, which in turn supports income generation for local communities, as reflected in the CBA. However, balancing these factors could be a challenge, and recommendations are provided to improve the overall sustainability performance of the products and promote more sustainable circular products.

Keywords : Life cycle assessment; Eco-efficiency; Material circularity indicator; Cost-benefit analysis, BCG model; Rice waste

INTRODUCTION

The Thai government has recently introduced the BCG Model Strategic Plan (2021-2026) to promote sustainable use of biological resources, strengthen local economies, enhance the competitiveness of Thai industries, and build resilience to global change. The BCG economy encourages industries to leverage technology and innovation to improve efficiency, reduce waste, and develop high-value products and services that enable circularity and sustainability. Since the agriculture industry employs over 12 million people or around 50% of the entire country's workforce, Thailand has put emphasis on the transformation of low commodities to high-value products [1]. Thus, leading to more research focusing on the effective utilization of agricultural waste.

Another major industry, the building industry consumes over 30% of natural resources and generates around 25% of solid waste at the global scale. In Thailand, it accounts for approximately 36% of the overall resource consumption. The production of building materials like cement is highly energy-intensive, consumes significant natural resources, and emits large amounts of greenhouse gases (GHGs), contributing to environmental degradation and pollution-related issues [2]. The construction industry represents a fundamental sector within the circular economy, with ongoing research dedicated to identifying and developing potential circular materials. Among these, rice waste has emerged as a promising substitute for cement and bricks due to its pozzolanic properties, helping reduce reliance on virgin raw materials and contributing to greenhouse gas (GHG) emission reduction while also adding values. This study aimed to assess the technical and financial feasibility of using rice waste in building materials in particular for local communities. It was the first attempt to integrate various life cycle-based sustainability tools - Life Cycle

Assessment (LCA), Eco-efficiency, Material Circularity Indicator (MCI), and Cost-Benefit Analysis (CBA) to comprehensively evaluate the circularity and sustainability performances of rice waste-based building materials in Thailand. The information in this research could be useful for supporting decision makers in promoting sustainable development and improving resource use efficiency of circular economy products in line with Thailand's BCG economy model.

METHODOLOGY

Studied products:

Rice husk ash (RHA)-blended concrete blocks and rice straw (RS) bricks were selected to assess their feasibility for community-level manufacturing to respond to the BCG economy model for local communities.

Scope of study:

The system boundary is from cradle to gate.

Sustainability assessment tools:

LCA study: The LCA was conducted according to the ISO 14040 and 14044 standards. The functional unit was set as 1 m^3 of RHA-blended concrete blocks and RS bricks. Five impact categories were considered, which were climate change (GWP), acidification (AP), eutrophication (EP), depletion of abiotic resources (ADP), and photochemical oxidation (PCOP). The life cycle impact assessment method was based on CML 2001[3].

Eco-efficiency Assessment: The eco-efficiency assessment was conducted according to the ISO 14045:2012 as the ratio of product value based on the selling price of products to the life cycle environmental impacts obtained from the LCA study.

Material Circularity Indicator: The MCI assessment method was based on the Ellen MacArthur Foundation guideline [2]. It is a tool to calculate the degree of circularity of a product; MCI ranges between 0-1; 0 representing a fully linear product and 1, a fully circular product.

Cost Benefit Analysis: CBA is a decision-making tool used to evaluate the overall economic viability of investment by comparing its total expected costs with its total expected benefits. It is expressed as a ratio of the net present value (NPV) of benefit and cost. A discounting rate of 2%—reflecting the Thai government bond interest rate in 2025—is applied to account for the time value of money. The CBA is performed over a period of 5 years.

RESULTS AND DISCUSSIONS

The LCA results identified raw material acquisition as the major hotspot for all impact categories in the RHA-blended concrete block, with the highest impact in GWP of 280 $kgCO_2e$ (90%) and ADP of 1,339 MJ (72%) (Figure 1). These impacts are primarily due to the calcination process in cement production. The clinkerization stage is particularly energy-intensive, requiring the burning of clinker at extremely high temperatures [4]. In addition, the consumption of coal and natural gas during this process is a major source of emissions, while the release of SO_2 and NO_x significantly contributes to AP and PCOP [5][6]. By replacing primary cement with hydraulic cement (i.e., a type of cement that has lower clinker content due to substitution of supplementary cementitious materials like limestone, fly ash, and slag by 10%), the overall GWP and ADP of the RHA-blended concrete block could be decreased by 38% and 28%, respectively (Figure 2).

For RS bricks, the production phase was the primary hotspot across all impact categories except PCOP, mainly due to the high electricity consumption of machinery in small-scale operations. GWP contributes as the highest environmental impact of 557 $kgCO_2e$ (63%) and 6,766 MJ (55%) (Figure 3). Assuming the production can be upscaled and more advanced technology can be adopted, the electricity consumption could potentially be reduced by 10% and lowering the overall GWP and ADP by 7% and 5%, respectively. A 30% reduction in electricity consumption could further decrease GWP by 21% and ADP by 16% (Figure 3).

The eco-efficiency of the products was calculated using their selling prices: \$45/m^3 for RHA-blended concrete blocks (\$0.20 per block) and \$1,399/m^3 for RS bricks (\$0.47 per brick). The eco-efficiency based on global warming potential (GWP) was 0.16 USD/$kgCO_2e$ for RHA-blended concrete blocks, which is lower than the non-hollow concrete blocks produced by a local manufacturer (0.22 USD/$kgCO_2e$) (Table 1). However, the eco-efficiency value can be enhanced to 0.26 USD/$kgCO_2e$ by substituting primary cement with hydraulic cement. The RS brick exhibited a substantially higher eco-efficiency value of 1.8 USD/$kgCO_2e$, surpassing comparable industry products such as medium-density fiberboard (MDF) with urea-formaldehyde (UF)-E0 and UF-Carb 1,

despite its comparatively higher GWP (Table 1). Reducing energy consumption by 30% could possibly lower its GWP to 620 $kgCO_2e$, and increasing its eco-efficiency value to 2.3 USD/$kgCO_2e$.

The RHA-blended concrete block had an MCI value of 0.4, higher than conventional market products. The RS bricks achieved an MCI of 0.5, indicating greater material circularity (Table 2).

The capital cost for producing RHA-blended concrete blocks primarily involves the installation of a mixer and pressing machine ($4,687). Other operation costs include the raw material production and transportation costs, and the labor cost ($14,551). With this setup, the maximum production capacity can reach 144,000 blocks per year. The product's low price of 0.24 USD per block led to a CBA ratio of 2.2, suggesting that the investment is financially feasible for community-led project.

For the RS brick, the capital costs included expenses for equipment such as aluminum plates, small steel rods, crushing, mixing, pressing, and trimming machines ($11,140). This provides a maximum production capacity of 36,864 bricks per year. The overall operating costs is $17,613, with isocyanate accounting for nearly half of the investment costs ($6,994). This resulted in a CBA ratio of 0.9, indicating a loss. Since chemical adhesives are essential for binding the particleboards, they significantly contributed to the high production cost. Although much research has been done on the utilization of natural binder, there are still constraints in terms of product's quality, costs, and availability. Due to high production cost, the community could further explore producing another product such as furniture using the same material. This could potentially target a niche market that values environmentally friendly products at a higher price point.

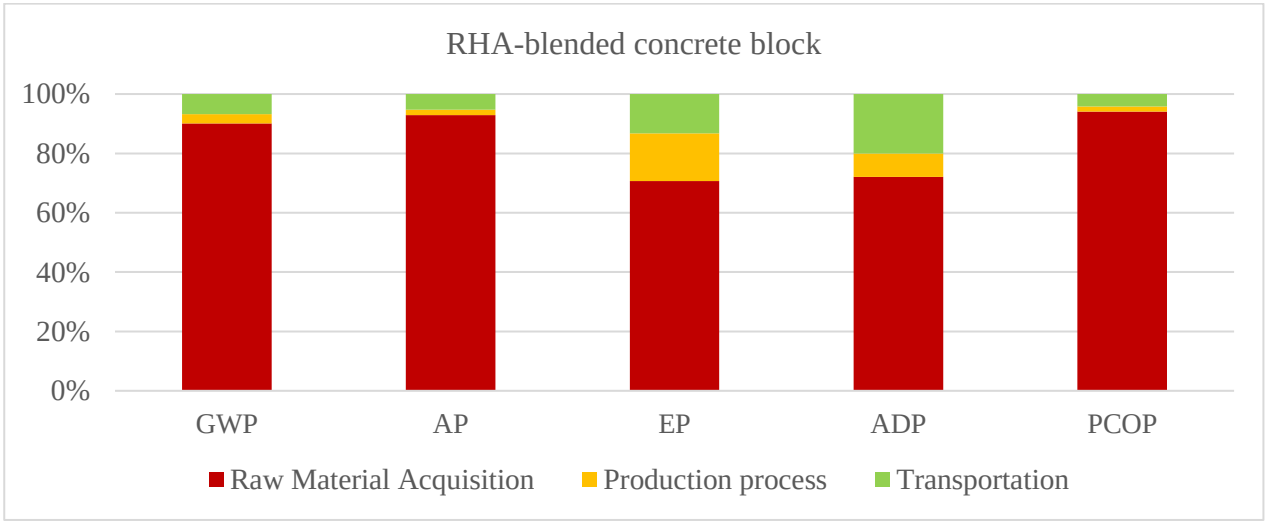


Figure 1. Contribution analysis of environmental impacts across life cycle stages of RHA-blended concrete block

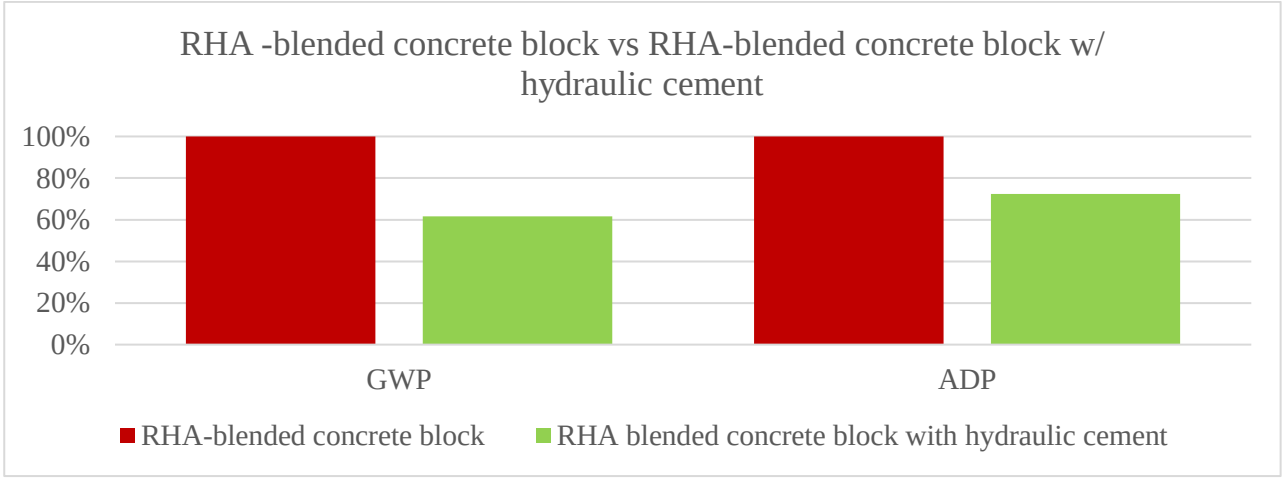


Figure 2. Environmental impacts of RHA-blended concrete block vs RHA-blended concrete block with hydraulic cement

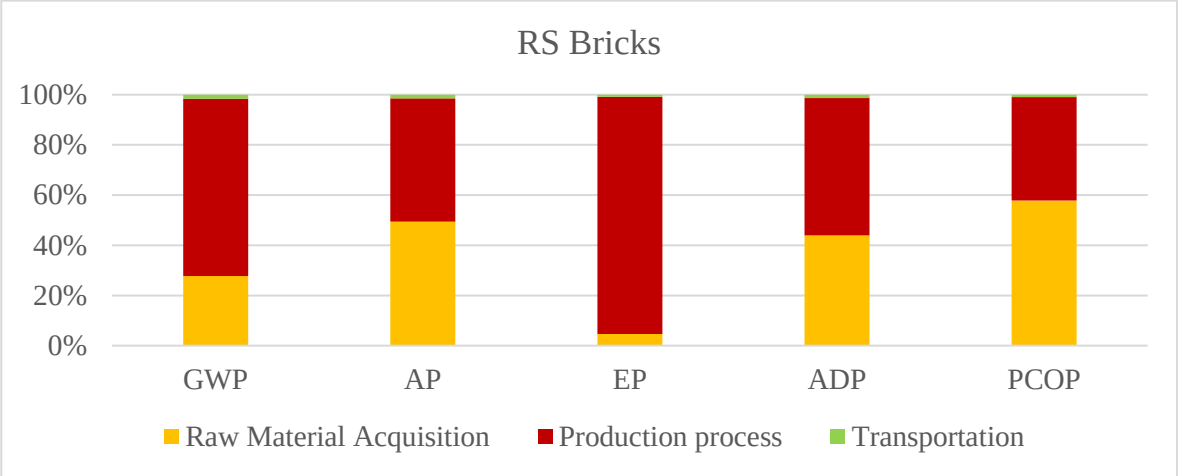


Figure 3. Contribution analysis of environmental impacts across life cycle stages of RS bricks

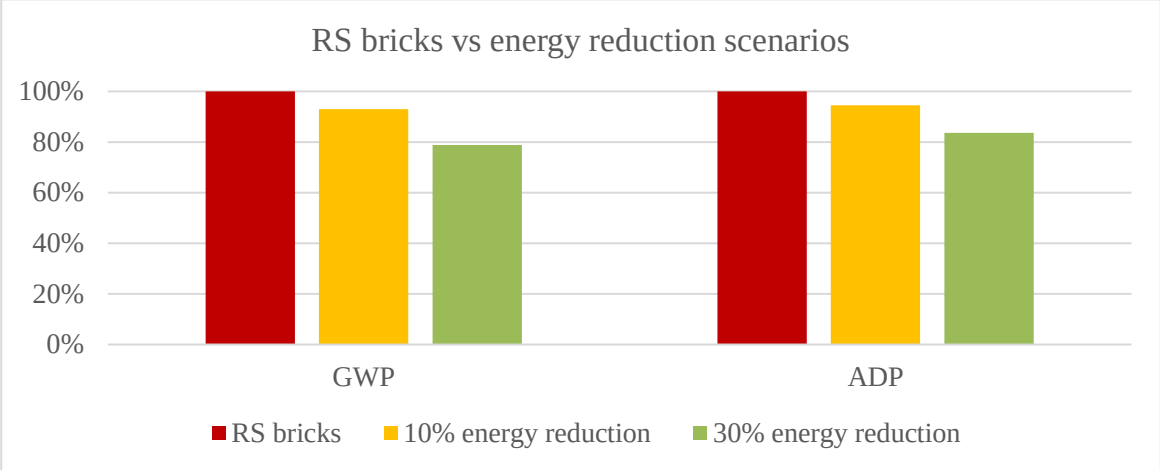


Figure 4. Environmental impacts of RS bricks vs energy reduction scenarios

Table 1. Eco-efficiency values of circular products

Product	**Price (USD)**	**GW ($kgCO_2e$)**	**Eco-eff. (USD/$kgCO_2e$)**
RS brick comparison			
RS brick with 30% energy reduction	1,399	620	2.26
*RS brick	1,399	773	1.78
[1]MDF UF-E0	235	746	0.32
[1]MDF UF-Carb 1	235	668	0.35
RHA-blended concrete block comparison			
*RHA-blended concrete block	45	280	0.16
Non-hollow concrete block	35	157	0.22
RHA-blended concrete block w/ hydraulic cement	45	172	0.26

*This study

[1]Data obtained from Thailand Greenhouse Gas Organization (TGO). The CFP of all products were verified in 2019. E0: Formaldehyde (F) <0.07ppm, E1: F<0.10ppm, Carb 1: F<0.18ppm

GW: Global warming

Table 2 MCI results

Parameter	Conventional NH concrete block	RHA-blended concrete block	RS bricks
V	618,333	344,406	1,382
M	1,097,705	1,097,705	13,824
$W=W_0$	1,097,705	1,097,705	13,824
Fs	-	0.5	0.90
Fr	0.44	0.2	-
Cr	-	-	-
X	1.0	1.0	1.0
F(X)	0.9	0.9	0.9
LFI	0.78	0.66	0.55
MCI	**0.30**	**0.41**	**0.51**

CONCLUSION

The utilization of rice waste in building materials not only reduces the environmental impacts but also improves the eco-efficiency values. However, more sustainable products may not always be economically feasible for community-level projects due to high initial investment costs. Addressing these challenges requires stronger collaboration between communities, private entities, and the public sector to support the development and adoption of circular building material products from rice wastes. Among different products studied, RHA-blended concrete blocks showed a strong potential for community-led project due to their higher eco-efficiency compared to similar products, with a payback period within the first year. However, the initial investment of approximately 20,500 USD in the first year poses a financial challenge for small local communities. Therefore, securing external funding from the government or private organizations is recommended to support community-led production.

ACKNOWLEDGEMENT

Financial support was provided by National Research Council of Thailand under the Thailand Advanced Institute of Science and Technology and Tokyo Institute of Technology (TAIST-Tokyo Tech) Program.

REFERENCES

[1] "Bcg Model: Fostering Sustainable Development in Thai Economy." National Science and Technology Development Agency (NSTDA), accessed June 5, 2024, https://www.nstda.or.th/en/images/pdf/BCG_Booklet1.pdf.

[2] Ellen Macarthur Foundation. (2019). Methodology: An approach to measuring circularity. Ellen Macarthur Foundation. https://emf.thirdlight.com/link/3jtevhlkbukz-9of4s4/@/preview/1?o

[3] Di Giuseppe, Elisa, Marco D'Orazio, Guangli Du, Claudio Favi, Sébastien Lasvaux, Gianluca Maracchini, and Pierryves Padey. "A Stochastic Approach to Lca of Internal Insulation Solutions for Historic Buildings." Sustainability 12, no. 4 (2020). https://doi.org/10.3390/su12041535.

[4] Dahanni, H., A. Ventura, L. Le Guen, M. Dauvergne, A. Orcesi, and C. Cremona. "Life Cycle Assessment of Cement: Are Existing Data and Models Relevant to Assess the Cement Industry's Climate Change Mitigation Strategies? A Literature Review." Construction and Building Materials 411 (2024). https://doi.org/10.1016/j.conbuildmat.2023.134415.

[5] Li, Chen, Suping Cui, Zuoren Nie, Xianzheng Gong, Zhihong Wang, and Norihiro Itsubo. "The Lca of Portland Cement Production in China." The International Journal of Life Cycle Assessment 20, no. 1 (2014): 117-27. https://doi.org/10.1007/s11367-014-0804-4.

[6] Noviani, Lilis, Eko Haryono, and Wahyu Supartono. "Environmental Impact Analysis of Pcc Cement Products (Portland Composite Cement) Using Lca (Life Cycle Assessment)." IOP Publishing (2023). https://doi.org/doi:10.1088/1755-1315/1190/1/012003.

20R3-19

Development of Biochar Immobilized Bacteria for Degrading PLA/PBAT/Starch Bioplastic

Luthfia Dwi Rachmani[1], Christian Adi Pratama[2] and Ekawan Luepromchai[3]

[1*] *Graduate student, Department of Microbiology, Faculty of Science, Chulalongkorn University, Bangkok 10330, Thailand.*

[2] *Graduate student, International Program in Hazardous Substance and Environmental Management (IP-HSM), Graduate School, Chulalongkorn University, Bangkok 10330, Thailand.*

[3]*Associate Professor, Center of Excellence in Microbial Technology for Marine Pollution Treatment (MiTMaPT), Chulalongkorn University, Bangkok 10330, Thailand*

[*]*Phone : 065-613-4330, E-mail : ekawan.l@chula.ac.th*

ABSTRACT

Efforts to reduce conventional plastic use focus on replacing them with bioplastics. PLA/PBAT/starch, a common bioplastic blend exhibits excellent physical properties while remaining compostable. However, it still takes a long time to degrade. A bacterial consortium, EAc, consisting of *Nocardiodes zeae* EA12, *Stenotrophomonas pavanii* EA33, *Gordonia desulfuricans* EA63, and *Chitinophaga jiangningensis* EA02, has been shown to degrade high molecular weight PLA. However, to improve bacterial stability during biodegradation, immobilization is needed to protect them. Biochar, a natural material, has shown potential as a carrier for bacterial immobilization. In the present study, the immobilization process was performed on three types of biochar: bamboo, eucalyptus, and cassava, which were selected based on differences in their physicochemical properties. Eucalyptus biochar showed the highest bacterial absorption (77.59 ± 0.78%) with 7.90 ± 0.31 Log CFU/g of total viable bacteria. However, the bamboo biochar exhibited the highest esterase and protease activities. This was probably due to the high silica concentration in bamboo biochar, which can interact with the ionic groups of extracellular enzymes and maintain their activities. The immobilized bacteria were then applied to bioplastic biodegradation for 30 days in an aqueous medium. Bamboo biochar yielded the best PLA/PBAT/starch biodegradation results with 9.5 ± 0.67% weight loss. The result corresponded with the highest biofilm formation (9.76 ± 0.077 Log CFU/cm³), esterase activity (0.0458 ± 0.003 U/mL), and protease activity (0.52 ± 0.059 U/mL) in the present of immobilized bamboo biochar. In contrast, the abiotic control group showed minimal degradation with a weight loss of 0.187 ± 0.0002%. These results suggest that bamboo biochar is a promising carrier for immobilizing EAc consortium, which can be effectively employed in the biodegradation of PLA/PBAT/starch bioplastics. Future study will focus on the bacterial stability and resilience to environmental stress during bioplastic biodegradation process in composting systems.

Keywords : Biodegradation; Immobilization; Biochar; Bioplastic; Bacterial consortium

INTRODUCTION

Plastic is a major environmental pollutant, primarily due to its slow degradation process, which can take decades or even centuries [1]. Despite ongoing efforts to mitigate plastic pollution, one promising solution is the substitution of conventional plastics with bioplastics. Bioplastics possess natural biodegradable properties, which can contribute significantly to reducing environmental pollution [2]. The primary components of bioplastics are typically a blend of polylactic acid (PLA) and polybutylene adipate terephthalate (PBAT), as this combination enhances its mechanical strength, resistance, and hydrophilicity [3, 4]. This blend can be strengthened by adding starch as a reinforcing agent, which improves the material's biodegradability and processing properties. Because they resemble traditional plastics, PLA/PBAT/starch-based bioplastics have become a major player in the biodegradable plastic market [3].

To address the issue of bioplastic waste accumulation, a biodegradation process utilizing microorganisms can be employed to mitigate its environmental impact through a more sustainable approach. The effectiveness of bioplastic degradation can be enhanced by introducing specific bioplastic degrading bacteria. A recent study by Mistry et al. [5] isolated *Chitinophaga jiangningensis* EA02, *Nocardioides zeae* EA12, *Stenotrophomonas pavanii* EA33, and *Gordonia desulfuricans* EA63, which were later combined into a consortium called EAc and demonstrated their ability to degrade high molecular weight PLA plastic in

compost. These bacteria adhere to the surface of the bioplastic and possess the ability to secrete extracellular enzymes including protease, lipase, and esterase to aid in the hydrolysis process. The resulting breakdown products are subsequently assimilated by the bacteria as a carbon source, with carbon dioxide and water produced as byproducts [5, 6].

However, the introduction of free-cell bacteria into the degradation system can lead to several challenges, including competition with indigenous microorganisms and rapid environmental changes that may result in a reduction in microbial cell populations and a decline in biodegradation efficiency. One potential solution to address these issues is the immobilization of bacteria. Bacterial immobilization is a method for capturing bacterial cells in a matrix and protecting them from direct contact with the environment [7]. Various types of matrixes can be used to immobilize bacteria. One matrix that can be used is biochar. Biochar is carbonaceous materials produced from carbon rich substances by pyrolysis method or thermal incineration (≤700°C) in an oxygen-limited atmosphere. In addition, biochar has advantages over other microbial carriers such as being carbon-rich and highly stable [8, 9]. However, biochar has various different properties such as total porous, zeta potential, functional group, and specific surface, and there has no report using biochar as bacterial carrier in bioplastic composting process. The use of biochar as a bacterial immobilization carrier for bioplastic-degrading bacteria was therefore expected to increase survival rates and maintain bacterial performance in degrading bioplastics in the long-term degradation process. In addition, the biochar can improve soil quality when applied to the environment because biochar itself can increase crop yield and soil fertility [10, 11].

Thus, this study evaluated the process of immobilizing bacterial consortium EAc on different types of biochar and determined the biodegradation of PLA/PBAT/Starch bioplastic using the immobilized bacteria in liquid medium. The efficiency of immobilized bacteria was determined from bioplastic weight reduction, biofilm formation on the bioplastic surface, esterase, and protease activity after 30 days of incubation.

METHODOLOGY

1. Biochar preparation

Three types of biochar, namely bamboo, eucalyptus, and cassava rhizomes were obtained from Thai Carbon Company Limited with the pyrolysis temperature ±680°C for 3h. Each biochar differs in its biomass constituent properties such as cassava is rich in hemicellulose, eucalyptus is rich in cellulose, while bamboo was chosen because of its high silica content in the biomass [12-14], which may affect bacterial immobilization. Biochar was ground and sieved to obtain a particle size of 0.3–2 mm, and then washed with deionized water to remove small particles. The sample was dried at 60°C before undergoing double sterilization to ensure that no viable bacteria remained inside.



a) b) c)

Fig. 1 Biochar sample a) bamboo, b) eucalyptus, and c) cassava

2. Bacterial consortia immobilization

Briefly, 5% (w/v) biochar was added to 50 mL of degradation basal media (DBM) which consists of KH_2PO_4 0.7 g/L, K_2HPO_4 1.4 g/L, $NaNO_3$ 8.0 g/L, NH_4NO_3 3.0 g/L, NaCl 0.01 g/L, $MgSO_4 \cdot 7H_2O$ 0.7 g/L, $CaCl_2 \cdot 2H_2O$ 0.01 g/L, $FeSO_4 \cdot 7H_2O$ 0.005 g/L, MnSO4.H2O 0.005 g/L, yeast extract 0.005 g/L, and 0.05

mL/L of trace elements consisting of CuSO4.H2O 0.5 g/L, MoNa2O4·2H2O 0.06 g/L, and ZnSO4·7H2O 0.5 g/L, and gelatin 3 g/L. The DBM also contained a mixture of *Chitinophaga jiangningensis* EA02, *Nocardia zeae* EA12, *Stenotrophomonas pavanii* EA33, and *Gordonia desulfuricans* EA63, with a concentration of 10^7 CFU/mL and a ratio of 1:1:1:1 (v/v/v/v) (initial OD600 1.0). The immobilization was carried out for 24 h on a shaker at 150 rpm. The immobilized biochar was separated using centrifuge at 8000 x g for 10 min, washed with sterile saline water to remove unattached bacteria, and dried in laminar airflow to fix the bacteria onto the biochar. Then, the samples were analyzed for percent bacterial absorption, total attached bacteria and enzyme analysis (i.e. esterase and protease).

3. Biodegradation of bioplastic using immobilized bacteria consortia

The biodegradation assay was conducted using 50 mL of DBM supplemented with 3 g/L gelatin and 3 pieces (3x3x0.0037 cm^3) of surface sterilized PLA/PBAT/Starch bioplastic manufactured by Thai Wah Public Company. 5 g of immobilized cells were added to the system and incubated for 30 d at room temperature, 150 rpm. Free cells with bioplastic were also used in order to compare the results with immobilized EAc on biochar. Abiotic control (media with bioplastic and biochar only) and biotic control (free cells without bioplastic) were included in the experiment. Analysis of biodegradation assay included weight loss of bioplastics, biofilm formation, and enzyme analysis as described below.

After 30 days, the bioplastic was separated from the medium. The bioplastic was analyzed for biofilm formation and weight loss, while the medium was analyzed for enzyme activity. To measure the weight loss, the attached biofilm on the plastic surface was removed by immersing the sample in 2% (w/v) SDS for 1 hour, followed by 95% ethanol for 30 minutes, and then dried overnight in a dehydrator. The sample was later weighed to determine the weight loss.

For the esterase activity assay, 30 µL of p-nitrophenyl solution was added to a 96-well plate, followed by 200 µL of pH 7 phosphate buffer and 20 µL of the cell-free supernatant. The mixture was incubated at 30°C for 30 minutes, and the OD405 was measured. Esterase activity was defined as the rate at which p-nitrophenol was enzymatically released from the substrate at a rate of 1 mole per mL per minute. The standard curve for this measurement was constructed using p-nitrophenol at varying concentrations.

Protease activity was assessed using the Sigma Aldrich protocol. In summary, 90 µL of 0.65% casein substrate and 20 µL of cell-free supernatant were incubated for 10 minutes, followed by the addition of 90 µL trichloroacetic acid and further incubation at 30°C for 30 minutes. After centrifugation, 40 µL of the supernatant was transferred to a new plate, and 90 µL of sodium carbonate and 20 µL of Folin-Ciocalteu's reagent were added. The mixture was incubated for 30 minutes, and the OD660 was measured. Protease activity was represented by the production of 1 µmole of tyrosine per mL per minute. A standard curve was prepared using L-tyrosine. All experiments were conducted in triplicate.

RESULTS AND DISCUSSIONS

1. Effect of biochar on immobilization

Each type of biochar possessed unique physicochemical properties that influenced its interaction with microorganisms. For example, cassava-derived biochar was notably rich in hemicellulose, eucalyptus biochar was abundant in lignocellulose, and bamboo biochar was characterized by a high silica content [13, 14]. These inherent differences in the biochemical composition of biochar significantly impacted its ability to serve as a substrate for microbial colonization and immobilization. In addition to the organic composition, the surface characteristics of biochar, such as its total surface area and porosity, played crucial roles in the immobilization process. The larger the surface area and the more porous the biochar, the greater its capacity for bacterial attachment and subsequent biofilm formation, which were essential for effective immobilization. In the present study, it was observed that eucalyptus biochar exhibited the highest levels of total absorption and bacterial attachment (Table 1). This was attributed to the superior porosity and surface area of eucalyptus biochar compared to the other biochar types. Previous research supported these findings, reporting that eucalyptus biochar demonstrated the highest total porosity and surface area when compared to cassava, bamboo, and other types of biochar [15–17]. However, the bamboo biochar exhibited the highest esterase and protease activities compared to the other biochars. This was probably due to the high silica concentration in bamboo biochar, which can interact with the ionic groups of extracellular enzymes and maintain their activities [13].

Total porosity and surface area affected the process of bacterial immobilization by providing more space for bacterial attachment. The process of immobilizing bacteria on biochar began with bacteria filling the biochar pores, and adhesion occurred through physical adsorption driven by Van der Waals forces, which caused an attraction between the hydrogen bonds of the microorganisms and the biochar [18]. The immobilization process continued with the formation of a biofilm by the microorganisms, which allowed the bacteria to adhere to the inner surface and the pores of the biochar [19, 20].

Table 1 Bacterial consortia immobilization on biochar for 24 h

Biochar	Absorbed bacteria (%)	Bacterial attachment (Log CFU/g)	Esterase activity (U/mL)	Protease activity (U/mL)
Bamboo	76.57±3.99	6.79±0.44	0.0724±0.009	0.749±0.175
Eucalyptus	77.59±0.78	7.90±0.31	0.046±0.012	0.509±0.103
Cassava	76.93±0.99	7.73±0.57	0.0401±0.006	0.498±0.054

2. Bioplastic degradation by immobilized bacteria

The form of the bioplastic after 30 days of incubation changed, with the free-cell condition producing the smallest fragments compared to the other samples (Fig. 1d). However, under the immobilized biochar treatment, bamboo exhibited the most significant change, producing smaller plastic fragments than the other immobilized biochar treatments (Fig. 1a–c). The decreased fragment size correlated with a higher percentage of weight loss (Fig. 2a). The free-cell EAc consortium showed the highest bioplastic biodegradation efficiency with an 11.6% weight loss, which was likely due to the high level of contact between the cells and the plastic surface. This degradation efficiency was comparable to that observed with the immobilized consortia on bamboo biochar. Among the immobilized systems, bamboo biochar exhibited the highest weight loss ($9.5 \pm 0.67\%$), followed by eucalyptus biochar ($2.5 \pm 0.56\%$) and cassava biochar ($1.9 \pm 0.60\%$). In contrast, the abiotic control group showed minimal bioplastic degradation with a weight loss of $0.187 \pm 0.0002\%$.

A similar trend was observed for biofilm formation, as depicted in Fig. 2b. However, the sample using eucalyptus biochar showed a decrease in the number of bacteria in the biofilm, as indicated by the total absorption and total attached bacteria results (Table 1). This may have occurred because, in the case of bamboo biochar, both bacteria and enzymes were immobilized, allowing the bioplastic to undergo hydrolysis first, which made it more accessible for the bacteria to utilize as a carbon source, thereby increasing the bacterial number. Higher biofilm formation indicated a greater capacity of bacteria to colonize and adhere to the surface of bioplastics, facilitating their use of bioplastics as a carbon source [21].

The biodegradation process began when bacteria first attached to the surface of the plastic and formed a biofilm to facilitate adhesion. After forming the biofilm, the bacteria could then secrete their extracellular enzymes to help break down the long polymer chains into smaller molecules (e.g., oligomers, dimers, and monomers). These small molecules could be depolymerized and used for microbial uptake and growth, allowing them to pass through semipermeable membranes and eventually undergo mineralization in the cells. The monomers in the cells were then either mineralized into CO_2 and H_2O [22, 23].

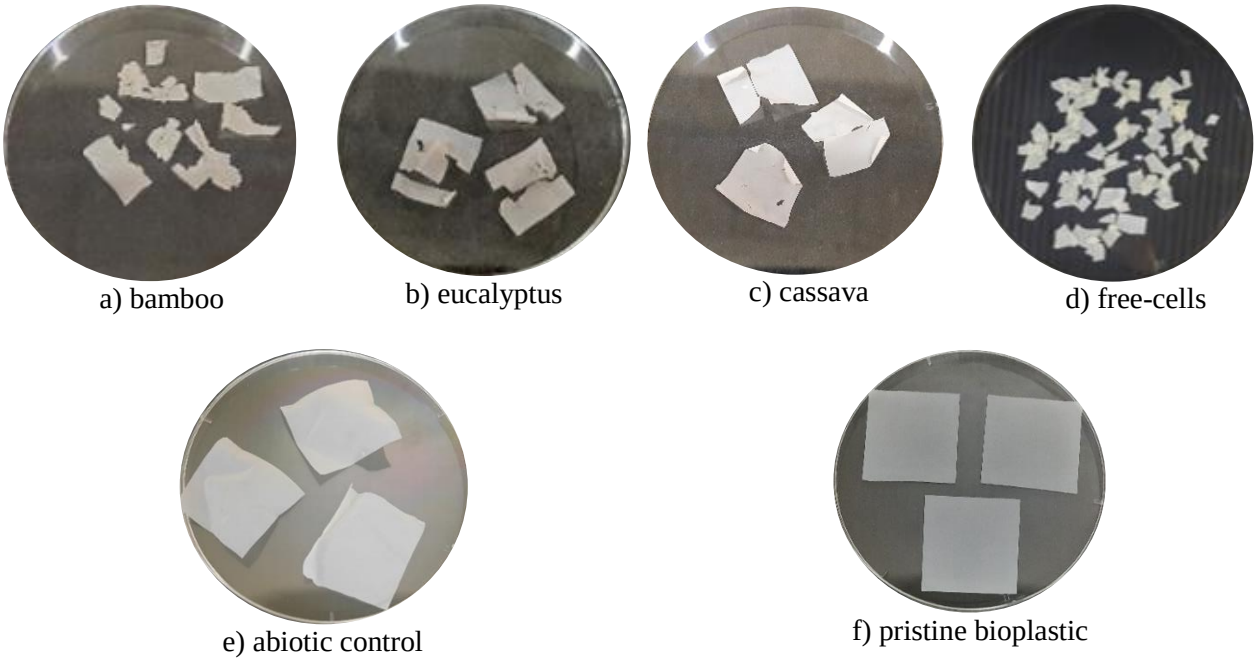
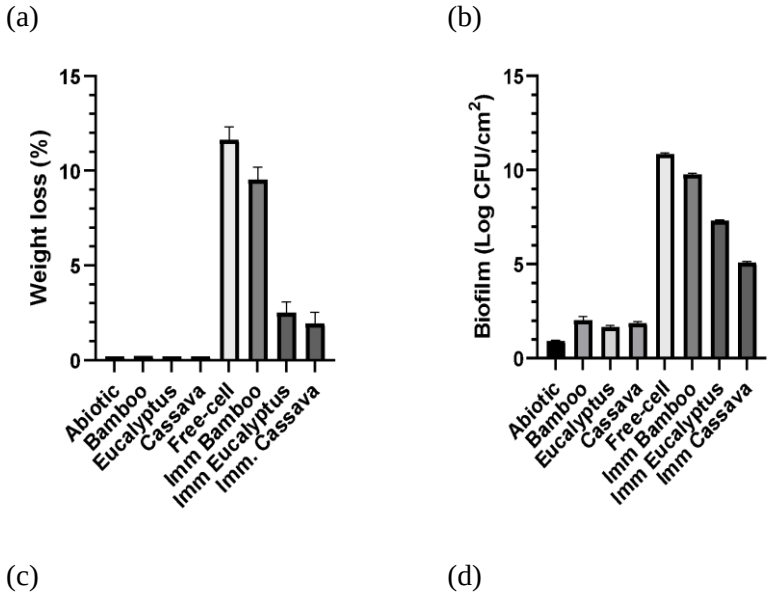


Fig. 1 Biodegradation of bioplastic after 30 days using EAc consortium immobilized in a) bamboo, b) eucalyptus, and c) cassava biochars, comparing to d) free-cells, e) abiotic control, and f) pristine bioplastic.

Among the immobilized cells, bamboo biochar had the highest enzyme activities (Fig. 2c and d). This result suggested that bamboo biochar was capable of immobilizing both of the bacterial cells and extracellular enzymes. The immobilization of these enzymes maintained their activities and enhanced the biodegradation process by facilitating the depolymerization of long polymer chains in bioplastics, making them more accessible for bacterial assimilation [24].



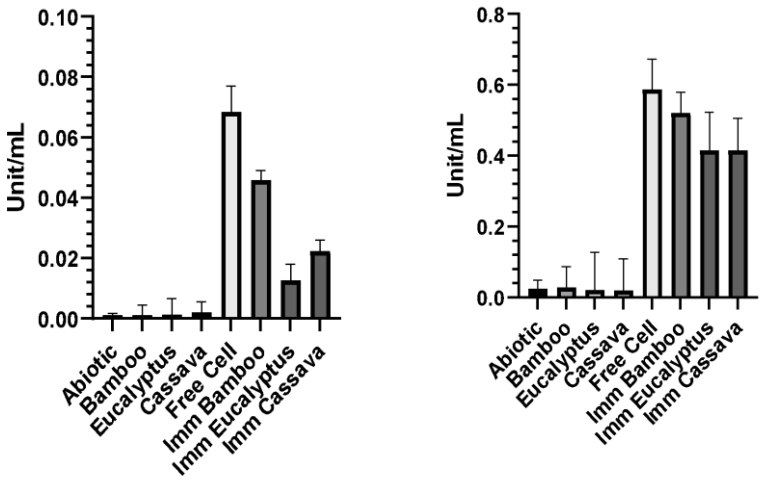


Fig. 2 Activities of immobilized cells, free cells, and biochar after 30 days: bioplastic weight loss (a), biofilm (b), esterase activity (c), and protease activity (d).

In the biodegradation process, esterase was one of the hydrolytic enzymes that could cut the ester bond and create a cleavage in the chain to mediate the degradation process [25, 26]. Meanwhile, protease was one of the enzymes that catalyzed the degradation of both PLA and PBAT, leading to the formation of lactic acid and small molecules [27, 28].

CONCLUSION

Biochar immobilization of bacterial consortium EAc was effectively conducted, with bamboo biochar showing the most promising bioplastic degradation results. The results were corresponded with the highest biofilm formation, esterase activity, and protease activity in the present of immobilized bamboo biochar. Although, the immobilized bamboo biochar had lower activities than the free-cells in an aqueous medium. The immobilized EAc on bamboo biochar was intended for use in composting systems, where it was expected to enhance bacterial stability and resilience to environmental stress. The future work will focus on the efficiency of immobilized biochar during the bioplastic biodegradation process in composting systems.

ACKNOWLEDGEMENTS

The authors would like to acknowledge the Office of the Permanent Secretary for Higher Education, Science, Research and Innovation for financial support and the Department of Microbiology, Faculty of Science, Chulalongkorn University for facilities and equipment. Luthfia Dwi Rachmani also thanks Chulalongkorn University for providing the scholarship for ASEAN and Non-ASEAN country.

REFERENCE

1. Nayanathara Thathsarani Pilapitiya, P.G.C. and A.S. Ratnayake, *The world of plastic waste: A review.* Cleaner Materials, 2024. **11**: p.100220.
2. Carvalheira, M., B.C. Marreiros, and M.A.M. Reis, *Acids (VFAs) and bioplastic (PHA) recovery*, in *Clean Energy and Resource Recovery*. 2022. p. 245-254.
3. Caputo, P., et al., *Reinforcement of Polylactic Acid / Poly Butylene Adipate-co-Terephthalate blends by starch addition: A coupled computational and experimental study.* Colloids and Surfaces A: Physicochemical and Engineering Aspects, 2024. **685**: p. 133159.
4. Park, D.I., et al., *Rheological Characteristics of Starch-Based Biodegradable Blends.* Polymers (Basel), 2023. **15**(8): p. 1953
5. Mistry, A.N., et al., *Bioaugmentation with a defined bacterial consortium: A key to degrade high molecular weight polylactic acid during traditional composting.* Bioresour Technol, 2023. **367**: p. 128237.
6. Amobonye, A., P. Bhagwat, S. Singh, and S. Pillai, *Plastic biodegradation: Frontline microbes and their enzymes.* Sci Total Environ, 2021. **759**: p. 143536.

7. Zhang, W., et al., *Efficient nitrate removal by Pseudomonas mendocina GL6 immobilized on biochar.* Bioresour Technol, 2021. **320**(Pt A): p. 124324.
8. Bhattacharya, T., et al., *Advances and prospects for biochar utilization in food processing and packaging applications.* Sustainable Materials and Technologies, 2024. **39**: p. 100831
9. Schommer, V.A., et al., *Techniques and mechanisms of bacteria immobilization on biochar for further environmental and agricultural applications.* Microbiol Res, 2024. **278**: p. 127534.
10. Singh Yadav, S.P., et al., *Biochar application: A sustainable approach to improve soil health.* Journal of Agriculture and Food Research, 2023. **11**: p. 100498
11. Jiang, Y., et al., *A global assessment of the long-term effects of biochar application on crop yield.* Current Research in Environmental Sustainability, 2024. **7**: p. 100247
12. Chen, X., et al., *Total utilization of lignin and carbohydrates in Eucalyptus grandis: an integrated biorefinery strategy towards phenolics, levulinic acid, and furfural.* Biotechnology for Biofuels, 2020. **13**(1): p. 1-10
13. Chaturvedi, K., et al., *Bamboo for producing charcoal and biochar for versatile applications.* Biomass Convers Biorefin, 2023: p. 1-27.
14. Minister Obonukut, S.A.a.A.J., *Biochar from Cassava Waste: A Paradigm Shift from Waste to Wealth*, in *Biochar- Productive Technologies, Properties and Applications*, M. Bartoli, Editor. 2023. p. 1-28.
15. Masís-Meléndez, F., et al., *Variability of Physical and Chemical Properties of TLUD Stove Derived Biochars.* Applied Sciences, 2020. **10**(2): p. 507.
16. Singh, R., et al., *High surface area Eucalyptus wood biochar for the removal of phenol from petroleum refinery wastewater.* Environmental Challenges, 2021. **5**: p. 100353.
17. Kamolklang, L., P. Seekhumlek, A. Kaeokan, and A. Watcharenwong, *Synthesis of Cassava Rhizome Biochar for Methomyl Adsorption.* Thai Environmental Engineering Journal, 2024. **38**(3): p. 11-28.
18. Dong, X., et al., *Mechanisms of adsorption and functionalization of biochar for pesticides: A review.* Ecotoxicol Environ Saf, 2024. **272**: p. 116019.
19. Zhou, Y., et al., *Production and beneficial impact of biochar for environmental application: A comprehensive review.* Bioresour Technol, 2021. **337**: p. 125451.
20. Sun, T., et al., *Bacterial compatibility and immobilization with biochar improved tebuconazole degradation, soil microbiome composition and functioning.* J Hazard Mater, 2020. **398**: p. 122941.
21. Howard, S.A. and R.R. McCarthy, *Modulating biofilm can potentiate activity of novel plastic-degrading enzymes.* NPJ Biofilms Microbiomes, 2023. **9**(1): p. 72.
22. Luo, Y., Z. Lin, and G. Guo, *Biodegradation Assessment of Poly (Lactic Acid) Filled with Functionalized Titania Nanoparticles (PLA/TiO(2)) under Compost Conditions.* Nanoscale Res Lett, 2019. **14**(1): p. 56.
23. Cai, Z., et al., *Biological Degradation of Plastics and Microplastics: A Recent Perspective on Associated Mechanisms and Influencing Factors.* Microorganisms, 2023. **11**(7): p. 1661
24. Mohanan, N., Z. Montazer, P.K. Sharma, and D.B. Levin, *Microbial and Enzymatic Degradation of Synthetic Plastics.* Front Microbiol, 2020. **11**: p. 580709.
25. Noor, H., et al., *Insight on esterase from Pseudomonas aeruginosa strain S3 that depolymerize poly(lactic acid) (PLA) at ambient temperature.* Polymer Degradation and Stability, 2020. **174**: p. 109096
26. Kim, S.H., et al., *Application of liquid-based colorimetric method for high throughput screening of bioplastic-degrading strains using esterase assay.* Anal Biochem, 2024. **685**: p. 115390.
27. Qiu, Y., et al., *Enhancing biodegradation efficiency of PLA/PBAT-ST20 bioplastic using thermophilic bacteria co-culture system: New insight from structural characterization, enzyme activity, and metabolic pathways.* J Hazard Mater, 2024. **477**: p. 135426.
28. Janczak, K., et al., *Comparative studies on the effectiveness of proteases and enzymes from dietary supplements in the degradation of polylactide (PLA).* International Biodeterioration & Biodegradation, 2025. **196**: p. 105950

20R4-01

Influence of Carbon Nanotube on Physical and Mechanical Properties of Vetiver Root Fiber-Reinforced Bioplastic Composites

Pongsathorn Kongkeaw[1*], Peerawit Pasangtiyo [2], Pichapa Lumpai[2] and Onkanya Panjumlong [2]

[1] Program of Physics, Faculty of Science and Technology , Rajabhat Maha Sarakham University, Maha Sarakham 44000, Thailand.
[2] Program of Science, Faculty of Education , Rajabhat Maha Sarakham University, Maha Sarakham 44000, Thailand.
[*]E-mail : pongsathorn.ko@rmu.ac.th

ABSTRACT

This research investigates the influence of carbon nanotubes (CNTs) on the physical and mechanical properties of vetiver root fiber-reinforced polylactic acid (PLA) bio composites. A composite formulation with a 90:10 ratio of PLA to vetiver root fibers was prepared with varying concentrations of CNTs (2, 4, 6, 8, and 10% by weight). Control samples of pure PLA, PLA with vetiver fibers only, and PLA with CNTs only were also fabricated for comparative analysis. The samples were characterized by tensile strength, flexural strength, density, water absorption, thickness swelling, and thermal stability. Results revealed that pure PLA exhibited the highest tensile strength (10.37±0.88 MPa), which decreased with increasing CNT content, reaching a minimum at 6% CNTs before slightly recovering at higher concentrations. This behavior was attributed to CNT agglomeration and interfacial incompatibility between hydrophobic CNTs and hydrophilic natural fibers. Similarly, flexural properties followed comparable trends, with lowest values at 6% CNTs. Physical properties showed that density increased with CNT content, while water absorption and thickness swelling peaked at 6% CNTs before decreasing at higher concentrations. Thermogravimetric analysis demonstrated enhanced thermal stability at higher CNT loadings due to the barrier effect and improved heat distribution. This research demonstrates the potential of CNT-reinforced vetiver root fiber bio composites as environmentally friendly materials with tailorable properties for various applications.

Keywords: Composites, Carbon Nanotubes, Vetiver Root Fibers, Mechanical Properties, Thermal Stability

INTRODUCTION

His Majesty King Bhumibol Adulyadej the Great (Rama IX) initiated and promoted the Vetiver Development and Campaign Project for soil and water conservation since 1991, recognizing the special properties of vetiver grass in preventing soil erosion [1]. Vetiver grass has a deep, strong root system that grows vertically and branches into a dense network, effectively anchoring soil, preventing erosion, and maintaining soil moisture [2, 3]. Studies on the mechanical properties of vetiver roots have shown they are strong, resistant to tensile forces and bending, highly flexible, and can withstand curvature stress well [4, 5]. These properties give vetiver roots high potential for use as reinforcement material in various composite materials, especially in the development of bio-hybrid composites that focus on integrating natural materials with biopolymers to enhance performance.

Polylactic Acid (PLA) is a widely popular biopolymer used in bioplastic production, as it is made from renewable resources such as plant starch or sugar from corn, cassava, or sugarcane [6, 7]. PLA has good mechanical properties, such as high stiffness and tensile strength [8, 9]. However, PLA has significant limitations, including high brittleness, low impact resistance, and insufficient moisture resistance for use in harsh environments [10]. Reinforcement with natural fibers combined with nano-particle additives is therefore an effective approach to improve these deficient properties.

Carbon Nanotubes (CNTs) are nanomaterials with outstanding mechanical and electrical properties, extremely high strength, excellent flexibility, light weight, and good thermal and electrical conductivity [11]. Adding even a small amount of CNTs (0.1-5% by weight) to polymer composite systems can significantly improve the mechanical properties of materials [12]. CNTs function as a network for distributing forces within composite materials, reducing crack formation and propagation, and increasing the ability to withstand various forces such as tensile, compressive, and bending forces [13, 14].

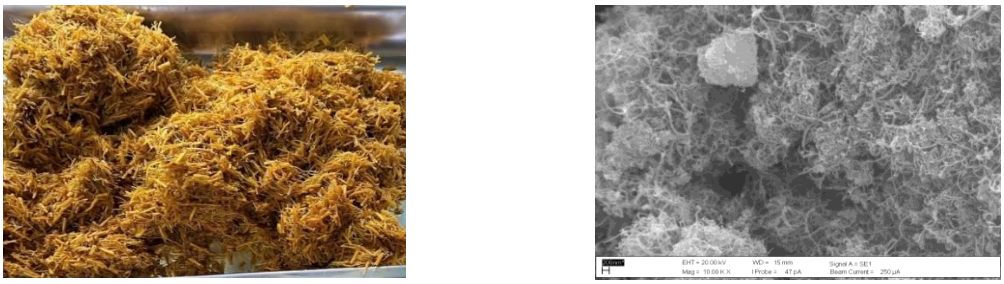
The combination of natural fibers from vetiver roots with CNTs in a PLA matrix represents an innovative approach to developing eco-friendly high-performance bio composites. Literature reviews have shown that reinforcement with appropriate amounts of CNTs can increase tensile strength by up to 30-45% and elastic modulus by 15-60% compared to neat polymers [13, 15], while natural fibers help increase toughness and impact resistance of the materials [16].

The research on "Influence of Carbon Nanotube on Physical and Mechanical Properties of Vetiver Root Fiber-Reinforced Bioplastic Composites" not only aims to study the improvement of mechanical properties of materials but also promotes the utilization of local resources that are not main economic crops to create economic value addition. This aligns with the Bio-Circular-Green Economy (BCG Model) concept that the Thai government is promoting for sustainable development [17]. Using vetiver grass in the bioplastic industry not only helps reduce production costs due to being an inexpensive and locally available raw material but also promotes environmental conservation according to the royal initiative.

Additionally, the developed bio composites have potential applications in several industries, such as the automotive industry for interior decorative parts requiring strength and light weight, the packaging industry for packaging requiring high mechanical properties and biodegradability, and the eco-friendly construction materials industry. This research is therefore significant in terms of materials science and technology, community economic development, and sustainable environmental conservation.

METHODOLOGY

The raw materials prepared for this research included upland vetiver grass (*Vetiveria Nemoralis A. Camus*), Roi-Et variety, collected from Ban Pla Bu village, Nong Saeng sub-district, Wapi Pathum district, Maha Sarakham province, Thailand. The root section of the vetiver grass was used in this study as shown in Figure 1**(**a). The first step involved preparing and separating the vetiver root fibers by washing them with plain water and then sun-drying. Subsequently, the dried roots were cut using a simple cutting machine to obtain fibers with diameters ranging between 200-300 µm, widths of approximately 1-2 mm, and lengths of about 20-40 mm. In the next step, the fiber surface was modified by soaking in 0.5% by volume concentration of sodium hydroxide solution for 2 h at room temperature. The fibers were then washed with distilled water, and the water condition was verified to have a neutral pH using a pH meter. Afterward, the fibers were dried in a hot air oven at 60°C for 24 h to achieve an average moisture content of 4-13%. Meanwhile, the matrix was prepared from Polylactic Acid (PLA) supplied by GLOBAL BIOPOLYMERS, Bangkok, Thailand. The multi-walled carbon nanotubes (MWCNTs) utilized in this experimental study were of high purity (>95 wt%) with inner diameters ranging from 3-5 nm and outer diameters of 8-15 nm as shown in Figure 1**(**b). These nanotubes were synthesized using the Chemical Vapor Deposition (CVD) method, which is recognized for producing high-quality carbon nanostructures with controlled dimensions and properties. The MWCNTs were commercially procured from AliExpress, China, and were selected based on their dimensional experimental outcomes.consistency and high purity to ensure reliable experimental outcomes.



(a) (b)

Figure 1 Raw materials (a)vetiver root fibers (b) SEM micrograph of CNTs

Preparation of Bioplastic Composite Materials

For this research, a base formulation with a ratio of 90:10 %wt between PLA and vetiver root fibers was established. Carbon nanotubes (CNTs) were subsequently incorporated into this base mixture at varying concentrations of 2, 4, 6, 8, and 10 %wt according to the experimental conditions. Additionally, control samples were prepared for comparative analysis, consisting of pure PLA (100 %wt), PLA reinforced only with vetiver root fibers, and PLA reinforced only with CNTs, to serve as standards for comparing various properties of the composite materials. The composite materials were processed using a closed-system mixer at a temperature of 200°C for 6 min. These temperature and time parameters were optimized to ensure uniform distribution of the constituent materials, particularly the dispersion of carbon nanotubes within the polymer matrix. The selected temperature was appropriate for the melting of PLA while preventing thermal degradation of the natural fibers and carbon nanotubes. Following the mixing process, all samples were finely ground using a material grinder to produce uniform, small plastic granules suitable for subsequent injection molding.

Specimen Fabrication and Testing

The finely ground composite granules were then injection molded using an injection molding machine at 180°C to produce test specimens according to ASTM standard dimensions. The injection molding temperature was optimized to ensure proper melting and flow of the composite material without causing degradation of the components. The fabricated specimens were subjected to mechanical property testing, including tensile strength tests according to ASTM D638 standard and flexural strength tests according to ASTM D790 standard, using a universal testing machine. For physical property testing, specimens were prepared according to Thai Industrial Standard (TIS 876-2547) to evaluate density, thickness swelling, and water absorption, which are key parameters indicating dimensional stability and moisture resistance of the composite materials. To ensure statistical reliability, five replicate specimens were tested for each experimental condition in all mechanical and physical property tests. Thermal property testing to determine the decomposition temperature of the composite materials was conducted using Thermogravimetric Analysis (TGA), with testing temperatures ranging from 30 to 850°C to encompass the thermal decomposition range of all components in the composite materials.

Statistical Analysis

The microstructural study of the composite materials was performed using Scanning Electron Microscopy (SEM) to analyze the adhesion characteristics between the polymer matrix and reinforcing materials, the distribution of vetiver root fibers, and the quality of carbon nanotube dispersion within the composite structure. This morphological analysis provided important information regarding the relationship between microstructural features and the observed mechanical and physical properties. All test data were presented as mean values with standard deviations and analyzed for statistical differences using one-way Analysis of Variance (ANOVA) at a 95 percent confidence level (α =0.05) to assess the statistical significance of differences observed between experimental groups. The significance criterion was established at $P < 0.05$, which enables accurate and reliable interpretation of the influence of carbon nanotube concentration on various properties of the vetiver root fiber-reinforced bioplastic composites.

RESULTS AND DISCUSSIONS

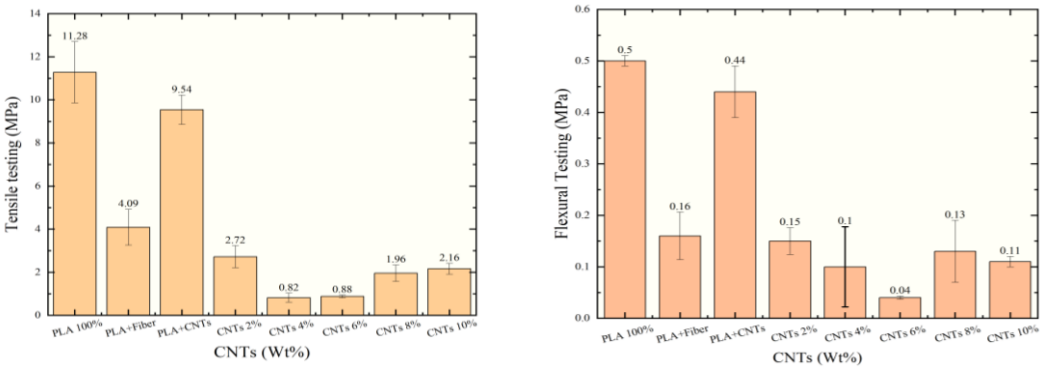
Table 1. Physical and mechanical average values of tests performed.

Sample	Density (g/cm^3)	Water absorption (%)	Thickness Swilling (%)	Tensile strength (MPa)	Tensile modulus (MPa)	Flexural strength (MPa)	Flexural modulus (MPa)
PLA 100%	0.435±0.03	4.31±0.99	4.13±0.91	10.37±0.88	208.33±8.96	0.50±0.010	5.33±0.76
PLA+ Fiber	0.543±0.05	2.06±0.09	5.18±1.05	4.55±0.73	195.50±5.63	0.16±0.046	5.00±1.32
PLA+ CNTs	0.560±0.06	5.92±1.20	7.55±1.35	9.93±0.57	202.50±6.5	0.44±0.04	5.67±0.29
CNTs 2% wt	0.424±0.07	5.00±1.07	3.23±0.63	2.27±0.51	192.83±3.51	0.15±0.02	5.17±0.58
CNTs 4% wt	0.400±0.03	4.32±1.37	5.25±0.37	1.03±0.21	196.00±8.79	0.10±0.07	3.17±1.26
CNTs 6% wt	0.691±0.11	7.3±1.05	6.34±1.69	0.88±0.06	142.50±11.5	0.04±0.00	1.83±0.76
CNTs 8% wt	0.623±0.07	3.43±0.91	3.64±0.75	2.00±0.21	151.83±16.6	0.13±0.06	5.00±0.50
CNTs 10% wt	0.740±0.18	3.74±0.45	3.11±1.28	2.21±0.18	198.33±5.03	0.11±0.01	4.50±0.87
p-value	0.002*	0.000*	0.001*	0.000*	0.000*	0.000*	0.001*

where *is significantly difference at $p<0.05$

Statistical analysis of the data in Table 1 reveals p-values less than 0.05 ($p<0.05$) for all experimental conditions, indicating statistically significant differences between group means at a 95% confidence level. The analysis confirms that pure PLA has the highest tensile strength (10.37±0.88 MPa), significantly different from all composite types. The addition of vetiver root fibers alone significantly reduced tensile strength (4.55±0.73 MPa). Furthermore, matrix is more uniform. However, as CNT content increases, agglomeration occurs, incorporating CNTs into the PLA/vetiver root fiber system resulted in

significantly lower tensile strength compared to pure PLA, though slight increases were observed at 8% and 10% CNTs concentrations**.**



(a) (b)

Figure 2 Mechanical Properties (a) Tensile strength (b) Flexural strength

1.Mechanical properties

The tensile strength Figure 2(a) illustrates the relationship between CNT content and tensile strength, showing a significant decreasing trend as carbon nanotube concentration increases in the composite material. Pure PLA (100%) exhibited the highest tensile strength at 11.28 MPa, followed by PLA+CNTs at 9.54 MPa. The vetiver root fiber and carbon nanotube composite (PLA+Fiber+CNTs) demonstrated a continuous decline in tensile strength with increasing carbon nanotube content, reaching its lowest value of 0.58 MPa at 6% wt CNTs. Subsequently, the tensile strength slightly increased to 1.96 MPa and 2.16 MPa at CNT concentrations of 8% wt and 10% wt, respectively. This phenomenon can be explained by the theory of carbon nanotube dispersion in polymer matrices. As described by [18], at lower CNT concentrations, nanotube dispersion in the creating defect sites within the composite structure that serve as failure initiation points when subjected to tensile forces [19]. Additionally, the reduction in tensile strength may result from the incompatibility between hydrophobic carbon nanotubes and hydrophilic vetiver root fibers, leading to interfacial voids and reduced load transfer efficiency between the matrix and reinforcing materials [20]. Nevertheless, the slight increase in tensile strength at 8% and 10% CNT content may be attributed to the formation of an interconnected network at higher concentrations, enhancing load-bearing capacity, which aligns with findings by [21] that high-concentration CNTs can form continuous networks and increase strength.

The Flexural strength Figure 2(b) illustrates the relationship between CNTs content and flexural strength, demonstrating a declining trend as CNTs concentration increases in the composite material. Pure PLA (100%) exhibited the highest flexural strength at 0.50 MPa, followed by PLA+CNTs at 0.44 MPa, while the composite material containing only vetiver root fibers (PLA+Fiber) showed a significantly reduced flexural strength of 0.16 MPa compared to pure PLA. When examining composite materials with various CNTs concentrations, the flexural strength showed a continuous decrease from 0.15 MPa at 2% wt CNTs to 0.10 MPa at 4% wt CNTs, reaching its lowest value of 0.04 MPa at 6% wt CNTs. Subsequently, the flexural strength slightly increased to 0.13 MPa and 0.11 MPa at CNTs concentrations of 8% wt and 10% wt, respectively. This phenomenon can be explained by theories of dispersion and interaction between component materials in composites. As [22] described, the reinforcement efficiency of carbon nanotubes depends on their dispersion and adhesion to the polymer matrix. When CNTs content increases, the likelihood of agglomeration also increases, creating stress concentration points and reducing load transfer efficiency [23].

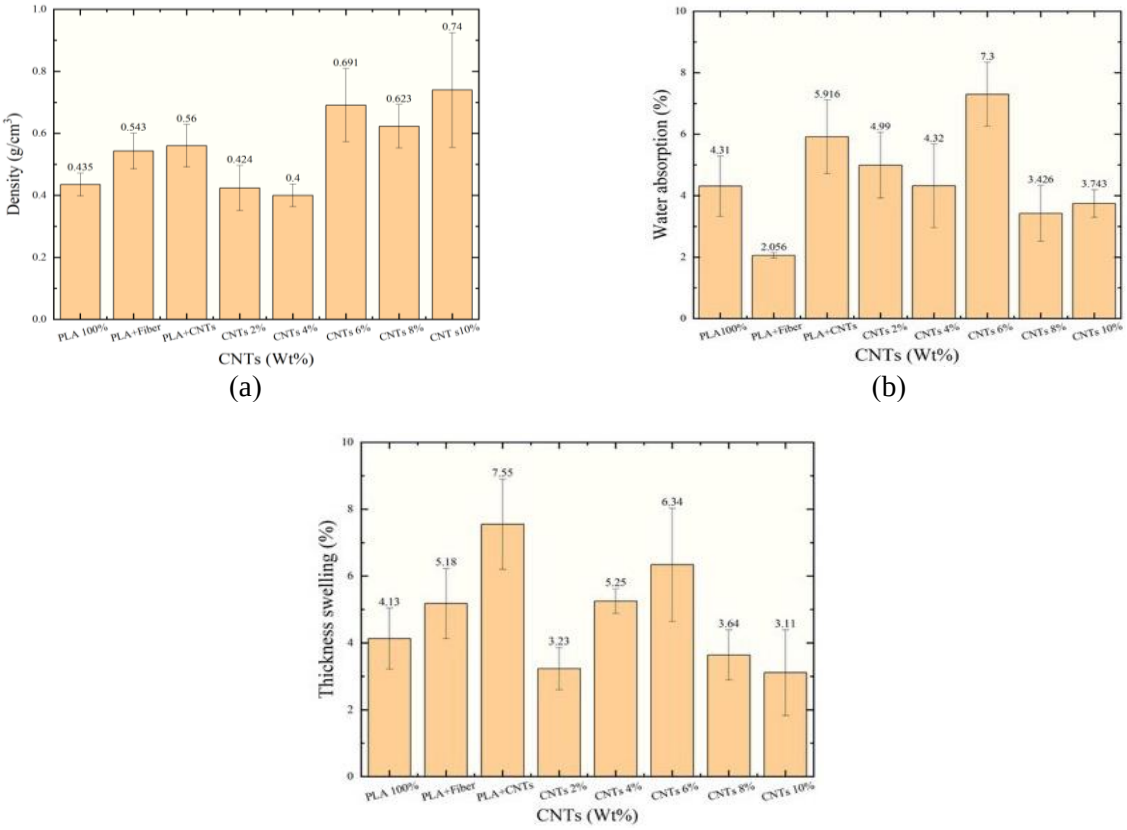


Figure 3 . Physical properties of Bioplastic composites (a) Density (b) Water absorption and (c) Thickness swelling

2.Physical properties test

Analysis of the relationship between carbon nanotube content and physical properties of the composite materials revealed several significant trends. Figure 3(a) shows that density values tend to increase with increasing CNTs content, rising from 0.435 g/cm³ in pure PLA to 0.740 g/cm³ at 10% CNTs. This increase is attributed to the higher density of CNTs compared to the polymer matrix, which aligns with research by Karthik Babu Nilagiri Balasubramanian et al. [24] who found that nano-fillers enhance the density of composites. Figure 3(b) demonstrates that water absorption varies with CNTs concentration, reaching its maximum at 6% wt CNTs (7.3%) and decreasing at 8-10% wt CNTs (3.43-3.26%). This phenomenon can be explained by the dispersion theory and network formation of CNTs. Bharti et al. [25] explained that at low to moderate concentrations, CNTs create voids that serve as water pathways, while at higher concentrations, a continuous network reduces water penetration. Figure 3(c) shows that thickness swelling correlates closely with water absorption, with maximum values occurring in CNTs+PLA (7.55%) and 6% wt CNTs (6.34%), followed by a decrease at 8-10% wt CNTs (3.64-3.11%). Statistical analysis in Table 1 indicates p-values less than 0.05 for all parameters, confirming statistically significant differences between experimental groups. A positive correlation was observed between water absorption and thickness swelling, consistent with findings by Ashori et al. [26] who reported that water absorption leads to composite material swelling due to water molecule infiltration into the polymer structure.

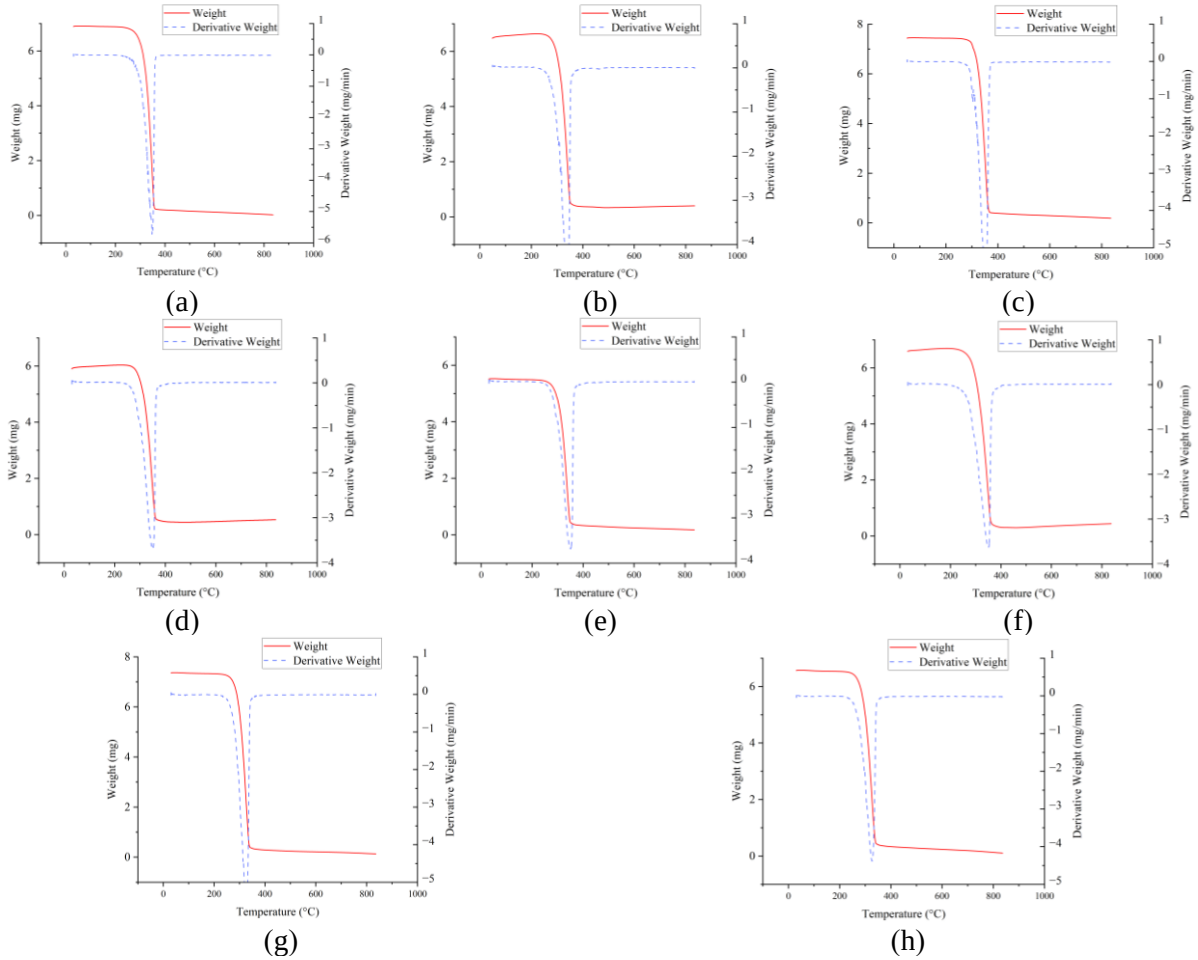


Figure 4. Decomposition temperature of Bioplastic composites (a) PLA100%wt (b) PLA+Fiber (c)PLA+CNT (d)CNT 2%wt (e) CNT4% wt (f) CNT6% wt (g) CNT8% wt (h) CNT10% wt

3.Thermal properties test

Figure 4 presents the thermal decomposition profiles of various bioplastic composites analyzed using Thermogravimetric Analysis (TGA). All samples exhibit similar decomposition patterns, with the primary weight loss occurring in the temperature range of approximately 300-400°C, corresponding to the degradation of the PLA matrix as evidenced by the sharp drops in the weight curves and corresponding peaks in the derivative weight curves. Pure PLA (Figure 4a) shows a single-step decomposition with maximum degradation at approximately 350°C, consistent with the thermal breakdown of PLA. The PLA+Fiber composite (Figure 4b) demonstrates a slightly more complex degradation pattern, with the fiber component likely contributing to a minor secondary decomposition process. The addition of CNTs to PLA (Figure 4c) appears to maintain a thermal profile similar to pure PLA, indicating minimal interference with the polymer's thermal degradation mechanisms. When examining various CNT concentrations (Figures 4d-h), a trend emerges where higher CNT content (particularly at 8 %wt and 10 %wt, Figures 4g-h) results in slightly enhanced thermal stability, as indicated by the shifted decomposition temperatures. This improvement can be attributed to the barrier effect of well-dispersed CNTs, which impede the release of volatile degradation products and retard mass loss during heating [27]. Additionally, the high thermal conductivity of CNTs facilitates more efficient heat distribution throughout the composite, potentially delaying localized thermal degradation [28]. These results demonstrate that carbon nanotube materials can enhance the thermal stability of polymer composites.

CONCLUSION

This study demonstrates that carbon nanotube content significantly influences the physical and mechanical properties of vetiver root fiber-reinforced PLA bio composites. The incorporation of CNTs exhibited a non-linear effect on composite performance, with 6% CNT concentration representing a critical threshold where mechanical properties reached their minimum values before improving at higher concentrations. This behavior can be attributed to competing mechanisms of CNT agglomeration,

interfacial interactions, and network formation within the polymer matrix. While tensile and flexural strengths decreased compared to pure PLA, the density and thermal stability improved with increasing CNT content. The thermal analysis revealed that higher CNT loadings (8-10%) enhanced the composite's thermal resistance through barrier effects and improved heat distribution. Water absorption and thickness swelling showed a correlation with CNT content, peaking at 6% before decreasing at higher concentrations due to the formation of a continuous CNT network that reduced water penetration. These findings contribute to understanding the complex interactions between natural fibers, biopolymers, and nanomaterials, offering insights for developing sustainable bio composites with tailored properties for applications in packaging, automotive components, and eco-friendly construction materials, aligning with the Bio-Circular-Green Economy model for sustainable development.

ACKNOWLEDGEMENT

The authors would like to acknowledge the financial support provided by the Science, Research and Innovation Fund, Fundamental Fund (FF.) for the fiscal year 2025.

REFERENCE

[1] Adulyadej, B., & Board, O. o. t. R. D. P. 1996. 50 Years of Development Work According to the Initiatives of His Majesty King Bhumibol Adulyadej of Thailand. Office of the Royal Development Projects Board.

[2] Gnansounou, E., & Raman, J. K. 2018. A review on bioremediation potential of vetiver grass. In E. Gnansounou (Ed.), Springer Singapore (pp. 127-140).

[3] Mohiuddin, A. 2022. Effectiveness of vetiver for landslide prevention in hilly areas of Chattogram metropolitan. .

[4] Jandyal, T., & Shah, M. Y. 2024. An experimental investigation on the effect of vetiver grass root system on the engineering properties of soil. Life Cycle Reliability and Safety Engineering, 13(3), 335-350.

[5] Pattnaik, S. S., Behera, D., Nanda, D., Das, N., & Behera, A. K. (2025). Green chemistry approaches in materials science: physico-mechanical properties and sustainable applications of grass fiber- reinforced composites. Green Chemistry, 27(10), 2629-2660.

[6] Kumari, S. V. G., Pakshirajan, K., & Pugazhenthi, G. 2022. Recent advances and future prospects of cellulose, starch, chitosan, polylactic acid and polyhydroxyalkanoates for sustainable food packaging applications. International Journal of Biological Macromolecules, 221, 163-182.

[7] Taib, N.-A. A. B., et al. 2023. A review on poly lactic acid (PLA) as a biodegradable polymer. Polymer Bulletin, 80(2), 1179-1213.

[8] Bledzki, A. K., Jaszkiewicz, A., & Scherzer, D. 2009. Mechanical properties of PLA composites with man-made cellulose and abaca fibres. Composites Part A: Applied Science and Manufacturing, 40(4), 404-412.

[9] Graupner, N., Herrmann, A. S., & Müssig, J. 2009. Natural and man-made cellulose fibre-reinforced poly (lactic acid) (PLA) composites: An overview about mechanical characteristics and application areas. Composites Part A: Applied Science and Manufacturing, 40(6-7), 810-821.

[10] Zhao, X., Liu, J., Li, J., Liang, X., Zhou, W., & Peng, S. 2022. Strategies and techniques for improving heat resistance and mechanical performances of poly (lactic acid) (PLA) biodegradable materials. International Journal of Biological Macromolecules, 218, 115-134.

[11] Syduzzaman, M., Islam Saad, M. S., Piam, M. F., Talukdar, T. A., Shobdo, T. T., & Pritha, N. M. 2025. Carbon nanotubes: Structure, properties and applications in the aerospace industry. *Results in Materials*, *25*, 100654.

[12] Al-Maharma, A. Y., Sendur, P., & Al-Huniti, N. 2018. Critical review of the dominating the fracture toughness of CNT reinforced polymer composites. *Materials Research Express*, *6*(1), 012003.

[13] Ali, A., Koloor, S. S. R., Alshehri, A. H., & Arockiarajan, A. (2023). Carbon nanotube characteristics and enhancement effects on the mechanical features of polymer-based materials and structures–A review. Journal of Materials Research and Technology, 24, 6495-6521.

[14] Mendoza Reales, O. A., & Dias Toledo Filho, R. 2017. A review on the chemical, mechanical and microstructural characterization of carbon nanotubes-cement based composites. Construction and Building Materials, 154, 697-710.

[15] Shan, L., et al. 2023. The effects of nano-additives on the mechanical, impact, vibration, and buckling/post-buckling properties of composites: A review. Journal of Materials Research and Technology, 24, 7570-7598.

[16] Al-Maharma, A. Y., & Sendur, P. 2018. Review of the main factors controlling the fracture toughness and impact strength properties of natural composites. *Materials Research Express*, *6*(2), 022001.

[17] T. National Science and Technology Development Agency. "Bio-Circular-Green Economy to be declared a national agenda." https://www.nstda.or.th/thaibioeconomy/1 38-bio-circular-green-economy-to-be-declared-a-national-agenda.html.[Accessed 31 March 2025].

[18] Ma, P.-C., Siddiqui, N. A., Marom, G., & Kim, J.-K. 2010. Dispersion and functionalization of carbon nanotubes for polymer-based nanocomposites: A review. Composites Part A: Applied Science and Manufacturing, 41(10), 1345-1367.

[19] Spitalsky, Z., Tasis, D., Papagelis, K., & Galiotis, C. 2010. Carbon nanotube–polymer composites: Chemistry, processing, mechanical and electrical properties. Progress in Polymer Science, 35(3), 357-401.

[20] Nurazzi, N. M., Asyraf, M. R. M., Fatimah Athiyah, S., Shazleen, S. S., Rafiqah, S. A., Harussani, M. M., Kamarudin, S. H., Razman, M. R., Rahmah, M., Zainudin, E. S., Ilyas, R. A., Aisyah, H. A., Norrrahim, M. N. F., Abdullah, N., Sapuan, S. M., & Khalina, A. 2021. A Review on Mechanical Performance of Hybrid Natural Fiber Polymer Composites for Structural Applications. *Polymers*, *13*(13), 2170

[21] Papageorgiou, D. G., Li, Z., Liu, M., Kinloch, I. A., & Young, R. J. 2020. Mechanisms of mechanical reinforcement by graphene and carbon nanotubes in polymer nanocomposites. Nanoscale, 12(4), 2228-2267.

[22] Fu, S.-Y., Feng, X.-Q., Lauke, B., & Mai, Y.-W. 2008. Effects of particle size, particle/matrix interface adhesion and particle loading on mechanical properties of particulate–polymer composites. Composites Part B: Engineering, 39(6), 933-961.

[23] Thostenson, E., Li, C., & Chou, T. 2005. Nanocomposites in context. Composites Science and Technology, 65(3-4), 491-516.

[24] Nilagiri Balasubramanian, K. B., & Ramesh, T. 2018. Role, effect, and influences of micro and nano-fillers on various properties of polymer matrix composites for microelectronics: A review. Polymers for Advanced Technologies, 29(6), 1568-1585.

[25] Arora, B., & Attri, P. 2020. Carbon Nanotubes (CNTs): A Potential Nanomaterial for Water Purification. *Journal of Composites Science*, *4*(3), 135.

[26] Ashori, A., Sheshmani, S., & Farhani, F. 2013. Preparation and characterization of bagasse/HDPE composites using multi-walled carbon nanotubes. Carbohydrate Polymers, 92(1), 865-871.

[27] Su, S. P., Xu, Y. H., China, P. R., & Wilkie, C. A. 2011. Thermal degradation of polymer–carbon nanotube composites. In *Polymer–Carbon Nanotube Composites* (pp. 482–510).

[28] Mohd Nurazzi, N., Asyraf, M. R. M., Khalina, A., Abdullah, N., Sabaruddin, F. A., Kamarudin, S. H., Ahmad, S., Mahat, A. M., Lee, C. L., Aisyah, H. A., Norrrahim, M. N. F., Ilyas, R. A., Harussani, M. M., Ishak, M. R., & Sapuan, S. M. (2021). Fabrication, Functionalization, and Application of Carbon Nanotube-Reinforced Polymer Composite: An Overview. *Polymers*, *13*(7), 1047.

20R4-03

Investment Analysis of a Circular Economy-based Shopping Mall–Community Food Waste Management Initiative: Financial and Sustainability Perspectives

Pawin Sirisinha[1*], Teenan Pisisakulwong[1], Natthanicha Tayanaraporn[1], Prasert Akkharaprathomphong[2] and Pisut Painmanakul[3]

[1]Undergraduate Student; [2]Assistant Professor, Department of Industrial Engineering, Faculty of Engineering, Chulalongkorn University, Bangkok 10330, Thailand
[3]Professor, Department of Environmental and Sustainable Engineering, Faculty of Engineering, Chulalongkorn University, Bangkok 10330, Thailand
[*]Phone : 093-137-2742, E-mail : pawin.sir@gmail.com

ABSTRACT

Thailand is facing a growing food waste management issue, with per capita food waste rising from 79 kg in 2021 to 86 kg in 2024, exceeding the global average by 9%. Despite this, inefficient disposal practices persist, with 57% of food waste being sent to landfills, the least desirable option according to the FAO. This study explores a sustainable food waste management model through a co-investment partnership between a shopping mall and the National Housing Authority (NHA), assessed from both financial and sustainability perspectives. In this model, the shopping mall invests $10,200 in a food waste dehydrator to process on-site waste, which is then transported to the community. The NHA funds a $4,500 anaerobic digester and a $12,123 black soldier fly larvae farming facility to convert the waste into biogas, animal feed, and other value-added products. Over a three-year period, financial analysis shows a positive Net Present Value (NPV) of $9,157 and an Internal Rate of Return (IRR) of 22% for the shopping mall, while the NHA incurs a financial loss with an NPV of –$77,901, due to lower revenue from carbon credit. The NHA's participation remains justified given its status as a state-owned enterprise focused on delivering public value rather than financial gain. Despite the financial imbalance, the project yields significant sustainability value. The Social Return on Investment (SROI) analysis shows strong results, with returns of 11.11 and 6.81 times the initial investment for the shopping mall and NHA, respectively. Therefore, this project remains overall feasible, combining financial and sustainability benefits that support its long-term impact.

Keywords: SROI; circular economy; food waste management; investment analysis

INTRODUCTION

Food waste has become a critical global issue, contributing significantly to environmental, social, and economic challenges. Each year, global consumption generates over 1.1 billion tons of food waste, producing approximately 4.4 $GtCO_2e$ emissions, which account for 8% of total anthropogenic emissions [1]. Thailand faces significant challenges in food waste management, mirroring global trends. According to the United Nations Environment Programme (UNEP), the country's per capita food waste has increased notably from 79 kg in 2021 to 86 kg in 2024, surpassing the global average by 9%. Moreover, food waste management in Thailand remains inefficient, with approximately 57% of food waste being disposed of through landfilling — a method classified by the FAO as the least desirable [2]. A major drawback of landfill disposal is the emission of methane (CH_4), a greenhouse gas with a Global Warming Potential 27 times higher than that of carbon dioxide (CO_2) [3]. Additionally, this method can cause unpleasant odors and foster the spread of pathogens, further exacerbating environmental and public health concerns.

To address these challenges, the National Housing Authority (NHA) has initiated "the food waste management for a circular economy in communities and shopping centers project". This initiative promotes a circular economy approach by integrating food waste management between housing communities and shopping centers. The model involves transporting dehydrated food waste from shopping centers to local communities, where it is processed alongside household waste through two primary methods: anaerobic digestion and black soldier fly (BSF) larvae farming. Anaerobic digestion converts household food waste into

biogas and organic soil amendments, while BSF larvae farming transforms blended food waste into high-protein animal feed. The project is currently in its pilot phase at the shopping district in Pathumwan, Bangkok, and the Klong Chan National Housing Community [4].

Anaerobic digestion and BSF larvae farming represent sustainable food waste management methods integrated into the project model. Anaerobic digestion involves microorganisms decomposing food waste in oxygen-free conditions, producing biogas—comprising 60%-70% methane and 30%-40% carbon dioxide—alongside nutrient-rich digestate usable as soil amendment [5]. Despite its proven success in countries like the UK, where over 94 facilities generate approximately 220 MW of energy from food waste digestion, Thailand still faces challenges scaling up this technology, with most projects remaining in pilot stages. For example, a facility in Nakhon Ratchasima produces only 0.8 MW from 88 tons of food waste per day [6]. In parallel, BSF larvae farming offers an efficient method to convert organic waste into high-protein animal feed. BSF larvae decomposes organic material, thriving in warm and humid environments (24-30°C) [7]. These complementary approaches not only mitigate environmental impacts but also create economic opportunities through renewable energy generation and sustainable animal feed.

Since the primary goal of this project is to generate long-term social and environmental benefits rather than financial profit, it is essential to assess its overall value beyond traditional financial metrics. Social Return on Investment (SROI) is a comprehensive framework designed to measure the social, economic, and environmental impact of an investment. Developed by the Roberts Enterprise Development Fund, SROI builds on the principles of cost-benefit analysis by integrating social impact assessment as a fundamental component [8]. This framework has been extensively used in waste management initiatives. For example, a waste management and composting project by PT Badak NGL in India achieved an SROI of 1.59, considering factors like increased environmental awareness, reduced landfill waste, and decreased reliance on chemical fertilizers [9]. Similarly, Thailand's Send Plastic Home project, which promotes plastic waste separation and recycling, reported an SROI of 8.45, highlighting its significant impact on waste reduction and behavioral change [10]. The Learning Center and Waste Bank project in Saraburi, Thailand, reported an SROI of 2.65, highlighting the multifaceted benefits of structured waste management. These included strengthened community relations through active involvement, economic growth driven by job creation and increased income, reduced landfill transportation costs, and improved environmental outcomes through decreased household waste and overall waste disposal [11].

This study aims to assess project feasibility based on financial return and environmental, social, and economic return by using Net Present Value (NPV), Payback Period (PP), Internal Rate of Return (IRR) and Social Return on Investment (SROI) analysis.

METHODOLOGY

Stakeholder Analysis

To assess the feasibility of the project, a comprehensive project analysis was conducted. This process began with reviewing the project details from internal reports and engaging in discussions with the project leader, Professor Dr. Pisut Painmanakul, who is overseeing the food waste management initiative linking community areas and shopping centers. Subsequently, field visits were carried out to observe the existing challenges, environmental conditions, and the expectations of various stakeholders. The purpose of this phase was to identify key stakeholders, analyzing their interests, roles, influence, and relationships within the context of food waste management for a circular economy in communities and shopping centers project.

Financial Analysis

This phase focuses on assessing the feasibility of the investment from a business and profitability perspective. The financial returns were categorized into two types: increased revenue and cost reduction. In this project, the analysis only considered direct costs, for example capital expenditure and operational costs, while indirect or opportunity costs were excluded. After determining all costs and returns, the next step was to assess cost-effectiveness through the following methods:

1. Net Present Value (NPV) is the difference between the present value of returns expected annually throughout the project and the present value of costs. The project is considered viable for investment if NPV > 0, meaning that the benefits should outweigh the costs.

2. Payback Period (PP) indicates the time needed to recoup the initial investment. A shorter payback period is preferred, though this can vary depending on the project type.

3. Internal Rate of Return (IRR) determines the interest rate or discount rate that makes the NPV of the project equal to zero. The investment is deemed acceptable if the calculated IRR exceeds the discount rate.

SROI Analysis

Social Return on Investment (SROI) analysis was used to assess the project's impact from a sustainability perspective based on one year of project outcomes. Unlike the financial analysis, which focuses solely on economic returns, SROI incorporates both social and environmental benefits. The analysis methodology followed the SROI Network framework as shown in Figure 1 [12].

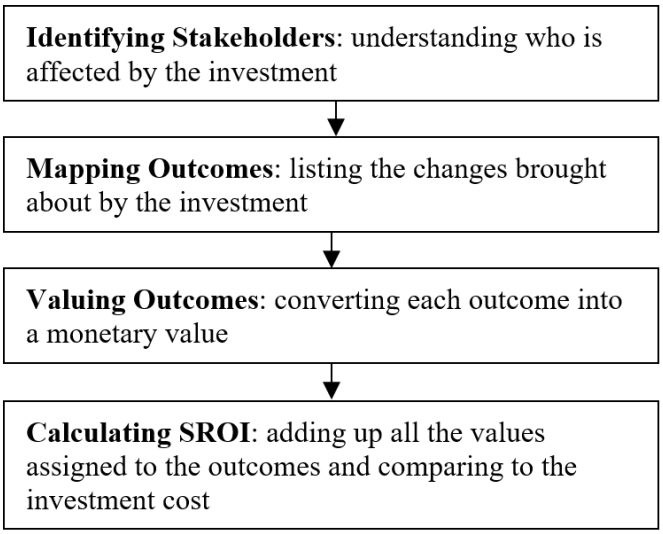


Figure 1 The procedures of the SROI analysis

To assess the project's impact, key stakeholders and their roles were first identified. The outcomes for each stakeholder were then evaluated holistically, considering economic, environmental, and social aspects.

Non-financial outcomes were monetized using financial proxies, allowing for a comprehensive valuation. To ensure the analysis did not overstate the project's returns, four key parameters were applied:

- Deadweight: The extent to which outcomes would have occurred without the project.
- Attribution: The portion of outcomes attributable to external factors.
- Displacement: Any negative effects resulting from the project's positive impacts elsewhere.
- Drop-off: The reduction in benefits over time.

Finally, the SROI for each investor was calculated using Equation (1), where the financial value of outcomes includes adjustments reflecting those four parameters.

$$SROI = \frac{Financial\ value\ of\ outcomes}{Investment\ cost} \quad (1)$$

RESULT AND DISCUSSIONS

Stakeholder Analysis

Table 1 outlines the stakeholders involved in the project, detailing their roles and whether they should be included in the Social Return on Investment (SROI) analysis based on the direct benefits they receive. Out of seven stakeholders, only three are identified as key stakeholders due to their significant contributions to the project.

Table 1 Stakeholder Involvement and Consideration in SROI Analysis

Stakeholder	Involvement	Should be Considered in SROI
Shopping mall	- Collect food waste - Dehydrate food waste	**Included,** it directly benefits from reduced food waste management costs and a lower organizational carbon footprint.
Food Waste Transport Service Provider	- Transport dried food waste from the shopping mall to the community	Excluded, the provider can offer services to any customer and is not uniquely impacted by this project.
Community	- Collect food waste - Processes food waste into value-added products (community enterprise)	**Included,** the community directly benefits from increased income and reduced living expenses by using the value-added products created.
NHA	- Lead the project implementation	**Included**, it directly benefits from carbon credit and improved performance of the communities under its care.
Bangkok Metropolitan Administration (BMA) / Municipality	- Previously managed the shopping mall's food waste	Excluded, public organizations do not have profit-seeking objectives and are not directly financially impacted.
BMA / Municipality Employees	- Previously handled food waste transport from the shopping mall	Excluded, employees continue to receive the same contractual wages regardless of the reduction in food waste from the mall.
Food Waste Collectors for Animal Feed	- Independent individuals who collect food waste to sell for animal feed, especially for pigs	Excluded, in an urban shopping mall context, food waste is typically sent directly for disposal rather than being distributed to individual collectors.

Table 2 Investment Responsibilities and Expected Benefits for Key Stakeholders

Stakeholder	Costs/Investments	Expected Benefits
Shopping mall	- Food waste dehydrator ($10,200)	- Reduced waste management costs - Improved environmental performance
Community (Community Enterprise)	- Cost of transporting food waste from shopping centers - Cost of adding value to food waste	- Improved quality of life and economic status from increased income and reduced expenses
NHA	- Anaerobic digestor ($4,500) - Black soldier fly farming facility ($12,123)	- Improved environmental performance - Carbon credit from community waste management as an alternative to landfilling

The project follows a co-investment model designed to create a win-win situation, where both investment burdens and benefits are shared among stakeholders, as illustrated in Table 2. Firstly, the National Housing Authority (NHA) serves as the project leader, receiving direct benefits from carbon credits and improvements in the performance of the communities under its care. The shopping mall plays an active role in collecting and dehydrating food waste. Since the community enterprise hires a service provider to transport dehydrated food waste, the shopping mall directly benefits from reduced waste management costs and a lower organizational carbon footprint.

Finally, the community is involved in collecting food waste and, through community enterprises, add value by processing it. Dehydrated waste from the mall, mixed with a small amount of hydrated waste from the community, is used for black soldier fly larvae farming. The remaining community waste is fermented in an anaerobic digestor to produce biogas and soil amendments.

Financial Analysis

The financial analysis of the National Housing Authority (NHA) and the shopping mall is presented in Figures 2 and 3, respectively. The analysis, conducted over a three-year project period using a 3% discount rate based on government bond yields, shows a Net Present Value (NPV) of $9,157 for the shopping mall and a negative NPV of –$77,901 for the NHA. The shopping mall achieves an Internal Rate of Return (IRR) of 22%, with payback occurring by the second year. This financial feasibility of the shopping mall is crucial to inviting it as a partner and implementing the project. In contrast, the NHA incurs a financial loss due to its larger share of investment and lower revenue from carbon credits. Despite this, the NHA's participation is justified, as its role is focused on delivering public value rather than financial returns.

	Year 0	Year 1	Year 2	Year 3
Average carbon credit price from management projects (USD/tCO2e)	0.00	3.00	3.00	3.00
Amount of carbon credits (tCO2e)	0.00	15.61	15.61	15.61
Revenue (USD)	0.00	46.84	46.84	46.84
Labor costs (USD/year)	0.00	9,000.00	9,000.00	9,000.00
Electricity costs (USD/year)	0.00	18.21	18.21	18.21
Variable raw material costs for food waste fermentation (USD/year)	0.00	11,636.14	11,636.14	11,636.14
Maintenance cost for anaerobic digester (10% of initial cost) (USD/year)	0.00	450.00	450.00	450.00
Maintenance cost for farming facility (5% of initial cost) (USD/year)	0.00	606.15	606.15	606.15
Operational Expenditure (USD)	0.00	21,710.51	21,710.51	21,710.51
Cost of anaerobic digester (USD)	4,500.00	0.00	0.00	0.00
Cost of farming facility with breeding stock (USD)	12,123.00	0.00	0.00	0.00
Capital Expenditure (USD)	16,623.00	0.00	0.00	0.00
Profit(Loss)	-16,623.00	-21,663.66	-21,663.66	-21,663.66

Figure 2 Financial analysis of NHA

	Year 0	Year 1	Year 2	Year 3
Waste management cost (USD/kg)	0.00	0.24	0.24	0.24
Amount of food waste (kg)		43,324.11	43,324.11	43,324.11
Cost Saving (USD)	0.00	10,397.79	10,397.79	10,397.79
Electricity costs (USD/kg waste)	0.0000	0.0585	0.0585	0.0585
Electricity costs (USD)	0.00	2,534.27	2,534.27	2,534.27
Maintenance cost for dehydrator (10% of initial cost) (USD/year)	0.00	1,020.00	1,020.00	1,020.00
Operational Expenditure (USD)	0.00	3,554.32	3,554.32	3,554.32
Cost of dehydrator (USD)	10,200.00	0.00	0.00	0.00
Capital Expenditure (USD)	10,200.00	0.00	0.00	0.00
Profit(Loss)	-10,200.00	6,843.46	6,843.46	6,843.46

Figure 3 Financial analysis of the shopping mall

SROI Analysis

Table 3 illustrates outcomes, indicators, and financial proxies for each stakeholder. The shopping mall experienced two primary benefits. First, there was an improvement in its environmental performance. This was quantified based on the reduction in carbon footprint of the organization and monetized based on an average carbon credit price. Second, the mall achieved cost savings in waste management by reducing expenses related to landfill disposal. These savings were calculated by comparing the cost of dehydrated food waste against the traditional cost of transporting and landfilling.

The community benefited both economically and socially. By participating in value-added processes, such as composting and black soldier fly larvae farming, the community generated additional income from selling these products. Furthermore, households in the community reduced energy expenses by using methane produced from anaerobic digestion as an alternative to LPG. The financial proxy for this saving was determined by equating methane energy output to the LPG equivalent and applying market prices, minus operating costs.

The NHA, as the project initiator, realized significant environmental outcomes. By facilitating the diversion of food waste from landfills, the NHA reduced greenhouse gas emissions in managed communities. These reductions, certified as carbon credits, provided a direct financial benefit when valued at the average carbon credit price from waste management projects.

Table 3 Outcome, indicator, and financial proxy for each stakeholder

Stakeholders	Outcome	Indicator	Financial Proxy
Shopping mall	Improved environmental performance	Reduction in the organization's carbon footprint	Greenhouse gas emissions avoided from landfilling food waste (tCO2e) × Carbon Pricing (Baht/tCO2e)
	Reduced waste management costs	Decrease in food waste management expenses	Total food waste (kg) × [Cost of conventional disposal (Baht/kg) – Cost of food waste dehydrating (Baht/kg)]
Community	Improved livelihood and economic status	Income from selling value-added products	[(Volume of liquid fertilizer (liters) × Market price (Baht/liter)) + (Amount of compost (kg) × Market price (Baht/kg)) + (Weight of larvae (kg) × Market price (Baht/kg))] – Transportation costs – Farming operating costs
	Reduced expenses by using biogas instead of LPG	Decrease in LPG usage costs	[Volume of methane produced (kg) × Equivalent LPG energy conversion × LPG market price (Baht/kg)] – Anaerobic digestor operation costs
NHA	Improved environmental performance of managed communities	Reduction in greenhouse gas emissions	[GHG reduction from anaerobic digestion (tCO2e) + GHG reduction from farming (tCO2e)] × Average carbon credit price from waste management projects (Baht/tCO2e)

Considering the benefits from 3 years of project life, the monetized values of the outcomes are shown in Table 4. The biggest benefit proportion is by far attributed to the community, accounting for 78.93% of the total benefits. This is primarily driven by the improved livelihood and economic status from the initiative, which is valued at $73,286. The shopping mall follows with a 20.94% benefit proportion, largely due to reduced waste management costs of $23,591. The NHA represents a smaller share of the total benefits at 0.12%, mainly from improved environmental performance in the communities it manages, valued at $140.

Table 4 Estimation of financial value generated from the project

Stakeholders	Outcome (3 years)	Monetized Value	Benefit proportion (%)
Shopping mall	Improved environmental performance	$133	20.94%
	Reduced waste management costs	$23,591	
Community	Improved livelihood and economic status	$73,286	78.93%
	Reduced expenses by using biogas instead of LPG	$16,123	
NHA	Improved environmental performance of managed communities	$140	0.12%

In the Social Return on Investment (SROI) analysis, four key factors—deadweight, attribution, displacement, and drop-off—were assessed to ensure the accuracy of impact valuation. For this project, all four factors were determined to be zero based on the following considerations:

Deadweight: The project outcomes, particularly the diversion of food waste from landfills and the generation of value-added products, would not have occurred without this initiative. Prior to the project, food waste was sent directly to landfills, confirming that all observed benefits are fully attributable to the project's implementation.

Attribution: The positive outcomes achieved—such as reduced carbon emissions, improved waste management, and community economic benefits—are fully credited to the project. No other external initiatives or interventions contributed to these specific impacts during the project timeline.

Displacement: The project did not cause any negative shifts or replace benefits elsewhere. For example, the use of food waste for black soldier fly larvae farming did not reduce the availability of resources for other existing uses, nor did the biogas production impact other energy sources negatively.

Drop-off: Given the nature of the project's ongoing operations and the continuous generation of value-added products (e.g., compost, biogas, larvae), the benefits are expected to remain consistent throughout the three-year project life. No decline in impact is anticipated over time, provided that operations are maintained.

However, if this project is scaled up into rural areas, displacement may become a factor. In rural settings, individuals who currently collect food waste from shopping malls and markets to feed livestock, particularly pigs, may lose access to this valuable resource, potentially increasing their cost of living. This potential negative impact should be carefully considered when evaluating the feasibility of future expansions. Table 5 presents the SROI values for the base case and scenarios where 25%, 50%, and 75% of the food waste from shopping malls or markets were collected by these individuals. These scenarios provide insight into the potential social and economic implications of scaling the project in rural areas.

Table 5 Displacement value and SROI of each scenario

Scenario	Displacement Value*	SROI		
		Overall	Shopping mall	NHA
Base case	$0	4.22	11.11	6.81
25%	$25,994	3.25	8.56	5.25
50%	$51,989	2.28	6.01	3.69
75%	$77,983	1.32	3.46	2.12

* Food waste can be used as 1:1 substitute for pig feed, priced at 0.8 USD/kg.

CONCLUSION

This study evaluated the investment potential of a circular economy-based food waste management initiative. The financial analysis confirmed the project's profitability for the shopping mall. Using a 3% discount rate over a three-year project period, the shopping mall achieved a Net Present Value (NPV) of $9,158 and an Internal Rate of Return (IRR) of 22%, with payback occurring by the second year. In contrast, the National Housing Authority (NHA) recorded a negative NPV of –$77,901, primarily due to its larger investment share and lower revenue from carbon credits. Despite this, the NHA's participation remains justified given its role as a state-owned enterprise focused on delivering public value rather than financial profit. The Social Return on Investment (SROI) analysis revealed substantial social and environmental impacts. Over a three-year period, the shopping mall realized returns of 11.11 times its initial investment, while NHA achieved a return of 6.81 times its investment. These strong results reflect the project's effectiveness in generating meaningful economic, social, and environmental benefits for stakeholders and communities. For scaling up in rural areas, potential displacement effects on local food waste collectors should be carefully considered, as their access to waste for animal feed may be disrupted.

REFERENCE

[1] H. Forbes, E. Peacock, N. Abbot, and M. Jones. 2024. Food Waste Index Report 2024. United Nations Environment Programme, Nairobi.

[2] D. Nikomborirak, T. Srisuwannaket, and C. Liumpetch. 2019. A Study on the Management of Surplus Food in order to Reduce Food Waste for Thailand. Thailand Development Research Institute, Bangkok.

[3] IPCC. IPCC Global Warming Potential Values. [Online]. Available: https://ghgprotocol.org/sites/default/files/2024-08/Global-Warming-Potential-Values%20%28August%202024%29.pdf.

[4] P. Painmanakul. 2023. Food waste management guideline for circular economy in community and shopping mall. Program Management Unit for Competitiveness, Bangkok.

[5] F. Xu, Y. Li, X. Ge, L. Yang, and Y. Li. 2018. Anaerobic digestion of food waste–Challenges and opportunities. Bioresource technology. 247: 1047-1058.

[6] C. Banks, S. Heaven, Y. Zhang, and U. Baier. 2018. Food waste digestion: anaerobic digestion of food waste for a circular economy. International Energy Agency, Paris.

[7] S. Photharin. 2020. Manual for Promoting and Developing Farmers' Potential with Innovation for Environmental Management. Kasetsart University, Sakon Nakhon.

[8] M. Maldonado and M. Corbey. 2016. Social Return on Investment (SROI): a review of the technique. Maandblad Voor Accountancy en Bedrijfseconomie. 90(3): 79-86.

[9] Y. Gunawan, B. Eko, R. Yudistyana, and D. T. Putri. 2021. Organic Waste Management Program Evaluation: A SROI and Action Research. Economics Development Analysis Journal. 10(3): 243-254.

[10] T. Poyai, P. Pongpunpurt, U. Leknoi, P. Painmanakul, and N. Chawaloesphonsiya. 2024. Plastic waste management in urban areas: Key takeaways from the “Send Plastic Home” project in Bangkok, Thailand. Process Safety and Environmental Protection. 190: 1222-1232.

[11] P. Sridan, P. Surapolchai, T. Plainlaor, A. Tanyaim, N. Hounnaklang, O. Zongram, and Y. Hawangchu. 2024. Social Return on Investment (SROI) from the Community Waste Bank Implementation under the Learning Center of Systematic Waste Management Innovation According to the Circular Economy Concept. Applied Environmental Research. 46(1).

[12] J. Nicholls, E. Lawlor, E. Neitzert, and T. Goodspeed. 2012. A guide to social return on investment. The SROI Network, Liverpool.

20R4-05

Life Cycle Assessment of Cellulose Nanofibers Production from Sugarcane Residues

Shwe Yie Lin[1], and Trakarn Prapaspongsa[1,*]

[1]*Master Student;* [1,*]*Associate Professor,* [1]*Department of Civil and Environmental Engineering, Faculty of Engineering, Mahidol University, Salaya, Nakhon Pathom 73170, Thailand.*
**Corresponding author, Phone: (+66) 2 889 2138, E-mail: trakarn.pra@mahidol.ac.th*

ABSTRACT

Sugarcane residues, a major agricultural residue burned in Thailand, has high cellulose content. Converting sugarcane residues into cellulose nanofibers offers an eco-friendly pathway to valorize agricultural waste, ultimately promoting Thai sugarcane and sugar industry as key players in advancing the Bio-Circular-Green economy. However, the assessment of the environmental sustainability of converting biomass into bioproducts is essential. This study used a life cycle perspective to compare the environmental impacts of eighteen production methods for cellulose nanofibers from sugarcane residues, evaluating climate change impact at the mid-point level, damage to three Areas of Protection: human health, ecosystem quality and resource scarcity and total damage cost on three Areas of Protection. The system boundary was from the cradle-to-gate. The functional unit, "one kilogram of cellulose nanofibers," was used. High-pressure homogenization and microfluidization resulted in the lower environmental impacts because of their lower overall energy consumption. The etherification and sonification method was the worst production method, showing significantly higher environmental impacts and damage cost compared to the mechanical, low-energy method, which was the best-performing. The environmental impacts varied dramatically between production methods, with climate change impact ranging from 1.6 to 1,000 kg CO_2-eq/kg of cellulose nanofibers, human health from 2.5×10^{-6} to 1.5×10^{-3} DALYs/kg of cellulose nanofibers, ecosystem quality from 7×10^{-9} to 4×10^{-6} species·year/kg of cellulose nanofibers, and resource scarcity from 0.1 to 90 USD/kg of cellulose nanofibers. The total damage costs also showed huge variation, ranging from around 8 to 5,160 Thai Baht/kg of cellulose nanofibers. Methods with enzymatic and mechanical processes showed the lowest impact across all categories. Methods involving 2,2,6,6-Tetramethylpiperidinyloxy oxidation, etherification, and sonification showed the highest impacts due to their reliance on chemicals and energy-intensive steps. Within homogenization methods, low-energy processes (e.g., low-energy homogenization) were environmentally sustainable compared to high-energy ones. Sonification-based methods were the least sustainable, with the highest impacts in all categories. The assessment left out the economic and social aspects. These show significant opportunities to carry out a more comprehensive evaluation of CNF production systems to strengthen their relevance to sustainable real-world adoption.

Keywords: life cycle assessment; sugarcane residue; cellulose nanofibers; biomaterial

INTRODUCTION

Nanocellulose from renewable sources like wood pulp and agricultural waste offers an eco-friendly, low-carbon alternative to petroleum-based counterparts [1]. Sugarcane trash has a high cellulose content (34-48%) [2], making it a valuable resource for producing cellulose nanofibers. As sugarcane crop residue accounted for more than 10% of over 8 million tonnes of agricultural residue burned in Thailand [3], producing cellulose nanofibers from sugarcane trash could serve as an environmentally sustainable pathway for valorizing biomass waste in the sugarcane industry, ultimately promoting Thai sugarcane and sugar industry as key players in advancing the Bio-Circular-Green economy (BCG). Sugarcane biorefineries facilitate the co-production of valuable products from sugarcane waste [4]. Consequently, sugarcane biorefineries adhere to the principles of a circular bioeconomy [5] by minimizing waste generation, enhancing resource efficiency, and fostering sustainable value chains within the sugarcane sector [6], making them crucial for advancing the concept of a BCG. However, the assessment of the environmental sustainability of converting biomass into bioproducts is essential. Life cycle assessment has been used to

assess the environmental impact of processes, sequences, or treatment technologies used to extract biomaterial from agricultural waste [7]. This study aims to assess and compare the life cycle environmental impacts of different production routes for cellulose nanofibers from sugarcane trash. The functional unit, "one kilogram of cellulose nanofibers," was chosen to facilitate comparisons between production methods.

METHODOLOGY

Life cycle Assessment

This study used a life cycle perspective to compare the environmental impacts of various production methods for CNF from sugarcane trash, evaluating climate change impact at the mid-point level and all three damage categories (human health damage, ecosystem damage, and resource scarcity damage) at the end-point level. The environmental impact assessment was from a cradle-to-gate perspective. The system boundary included the cultivation and harvesting of sugarcane using the green cane harvesting technique, which avoids preharvest cane burning and producing CNF from sugarcane trash from green cane harvesting. The assessment also considered the environmental impact of producing chemicals and fuels necessary for agricultural (sugarcane plantation) and subsequent industrial stages (cellulose nanofiber production). The functional unit, "one kilogram of cellulose nanofibers," was chosen to facilitate comparisons between production methods. Figure 1 shows the system boundary of the study. The ReCiPe 206 method was used because it quantifies both midpoint impacts and damage to three Areas of Protection: human health, ecosystem quality and resource scarcity. Calculations were carried out on SimaPro Software version 9.5.01 (PRé Consultants bv, Amersfoort, The Netherlands).

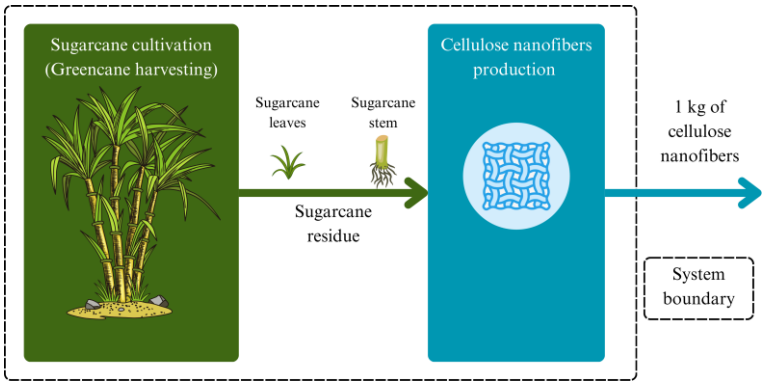


Figure 1 System boundary.

Numerous studies have outlined various mechanical methods for producing CNF from biomass, including high-pressure homogenization, microfluidization, ball milling, steam explosion, ultrasonication, and high-speed blending [7]. These approaches have shown consistent performance in processing [7]. This study considered 18 methods for producing CNF. Each method incorporates different pretreatments and mechanical processes. This study includes a wide range of processing approaches, from homogenization and mechanical methods to advanced techniques such as microfluidization and sonication.

These methods are S1: Enzymatic treatments and homogenization [8], S2: Alkaline pretreatment, 2,2,6,6-Tetramethylpiperidinyloxy (TEMPO) oxidation, and high-pressure homogenization [7], S3: Alkaline pretreatment, lime juice hydrolysis, and high-pressure homogenization [7], S4: Etherification and homogenization [9], S5: Homogenization, high energy [10], S6: Homogenization, low energy [10], S7: Homogenization, medium energy [10], S8: Organosolv pretreatment, lime juice hydrolysis, and high-pressure homogenization [7], S9: Organosolv pretreatment, TEMPO oxidation, and high-pressure homogenization [7], S10: TEMPO oxidation and homogenization I [11], S11: TEMPO oxidation and homogenization II [9], S12: Mechanical, high energy [12], S13: Mechanical, low energy [12], S14: Carboxymethylation pretreatments and microfluidization [10], S15: Enzymatic pretreatments and microfluidization [10], S16: Etherification and sonification [9], S17: TEMPO oxidation and sonication [9], and S18: TEMPO oxidation and ultrasonication [11].

Damage cost assessment

Environmental impact valuation scheme used by Kaenchan and Gheewala [13] was used, i.e., Equation (1) and (3) to evaluate the damage cost on the human health and ecosystems. Equation (2) and (4) were used to calculate damage cost on human health and ecosystems in the year of interest, y.

$$\text{Damage cost on human health}_{2011} = \text{Damage cost factor}_{\text{Human health, 2011}} \times \text{Human health damage} \quad (1)$$

$$\text{Damage cost on human health}_{y} = \text{Damage cost on human health}_{2011} \times (1+r)^{(y-2011)} \quad (2)$$

$$\text{Damage cost on ecosystems}_{2011} = \text{Damage cost factor}_{\text{Ecosystems damage, 2011}} \times \text{Ecosystems damage} \quad (3)$$

$$\text{Damage cost on ecosystems}_{y} = \text{Damage cost on ecosystems}_{2011} \times (1+r)^{(y-2011)} \quad (4)$$

Where, $\text{Damage cost factor}_{\text{Human health, 2011}}$ = 512,000 Thai Baht (THB)/DALY

$\text{Damage cost factor}_{\text{Ecosystems damage, 2011}} = 2.137\times10^{8}$ THB/species.year

r = the average inflation rate of Thailand between 2011 and y, based on the inflation rate from The World Bank.

For the damage cost on the resource scarcity, Equation (5) and (6) were used.

$$\text{Damage cost on resource scarcity}_{2013} = \text{Exchange rate}_{2013} \times \text{Resource scarcity damage} \quad (5)$$

$$\text{Damage cost on resource scarcity}_{y} = \text{Damage cost on resource scarcity}_{2013} \times (1+r)^{(y-2013)} \quad (6)$$

Where, r = the average inflation rate of Thailand between 2013 and y based on the inflation rate from The World Bank.

Finally, the total damage cost in y was calculated by

$$\text{Total damage cost}_{y} = \text{Damage cost on human health}_{y} + \text{Damage cost on ecosystems}_{y} + \text{Damage cost on resource scarcity}_{y} \quad (7)$$

RESULTS AND DISCUSSION

Environmental performance comparison of various cellulose nanofibers production methods

Methods with enzymatic and mechanical processes showed the lowest impact across all categories. Methods involving TEMPO oxidation, etherification, and sonification showed the highest impacts due to their reliance on chemicals and energy-intensive steps. Within homogenization methods, low-energy processes (e.g., low-energy homogenization) were environmentally sustainable compared to high-energy ones. Sonification-based methods were the least sustainable, with the highest impacts in all categories.

Numerous studies have outlined various mechanical methods for producing CNF from biomass, including high-pressure homogenization, microfluidization, ball milling, steam explosion, ultrasonication, and high-speed blending [7]. These approaches have shown consistent performance in processing [7]. However, they are typically associated with high energy demands, posing significant challenges for large-scale CNF production [7]. Notably, high-pressure homogenizers and microfluidizers have been found to considerably lower the overall energy requirements in the CNF manufacturing process [14]. Recent studies

have explored nanocellulose production, showing that combining mechanical and chemical methods lowers energy use [14].

The worst and best methods for CNF production from sugarcane residue for each impact can be found in **Table 1**.

Table 1 Worst and best methods for cellulose nanofibers (CNF) production from sugarcane residue.

Impact	Worst/Best method	Impact value	Unit
Climate change	**S16:** Etherification and sonification	1,000	kilogram carbon dioxide equivalent (kg CO_2-eq)/kg of CNF
	S13: Mechanical, low energy	1.6	kg CO_2-eq/kg of CNF
Human health	**S16:** Etherification and sonification	1.5×10^{-3}	Disability adjusted life years/kg of CNF
	S13: Mechanical, low energy	2.5×10^{-6}	Disability adjusted life years/kg of CNF
Ecosystem quality	**S16:** Etherification and sonification	4×10^{-6}	species.year/kg of CNF
	S13: Mechanical, low energy	7×10^{-9}	species.year/kg of CNF
Resource scarcity	**S16:** Etherification and sonification	90	United States dollar 2013/kg of CNF
	S13: Mechanical, low energy	0.1	United States dollar 2013/kg of CNF
Total damage cost	**S16:** Etherification and sonification	5160	Thai Baht/ kg of CNF
	S13: Mechanical, low energy	7.5	Thai Baht/ kg of CNF

The worst production method.
The best production method.

Climate change

There were high variations in the climate change impact across various production methods, primarily resulting from differences in energy consumption and chemical use. **Figure 2** shows the climate change impact across the various production methods.

S16: Etherification and sonification showed the highest impact, followed by S17: TEMPO oxidation and sonication. In these methods, energy consumption accounted for the largest share of emissions, contributing over 800 kg CO_2-eq/kg of CNF. Besides, chemical use further increased the impact. These findings showed that sonification-based methods had high greenhouse gas emissions due to their high energy demands. S13: Mechanical, low-energy treatment showed the lowest impact, at 1.6 kg CO_2-eq/ kg of CNF, with energy consumption accounting for most of the impact. S15: Enzymatic pretreatments and microfluidization resulted in a GWP of 3.20 kg CO_2-eq/kg of CNF, primarily driven by energy use. These results suggest that enzymatic and low-energy mechanical treatments are the most favorable options for climate change impact. Several scenarios showed high contributions from chemical use, highlighting the substantial environmental burden associated with chemical-intensive processes, necessitating strategies for reducing or substituting high-emission reagents.

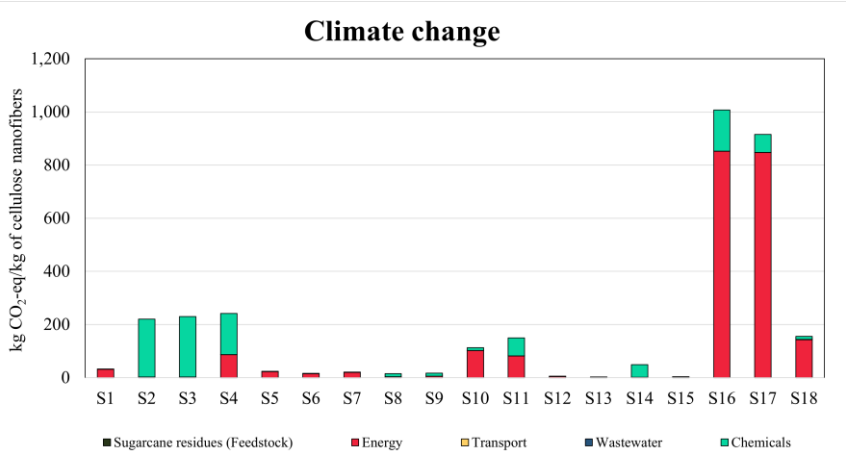


Figure 2 Climate change impact, measured in kilogram carbon dioxide equivalent (kg CO_2-eq)/kilogram of cellulose nanofibers across the various production methods.

Human health

The primary contributors to human health damage were energy consumption and chemical usage, with some methods having substantially higher impacts due to their intensive energy consumption and chemical use. **Figure 3 (a)** shows the human health damage across the various production methods.

Methods with extremely high human health damage were S16: Etherification and sonification, and S17: TEMPO oxidation and sonication, at over 1×10^{-3} DALY/kg of CNF. In both methods, energy consumption was the dominant contributor, showing sonification-based methods had a substantial human health damage due to their intensive energy requirements. S13: Mechanical, low-energy treatment had the lowest human health damage, followed by S15: Enzymatic pretreatments and microfluidization. In both methods, energy use was the primary factor. Several methods showed notable human health damage from high chemical usage.

Ecosystem quality

Across various methods, there were high variations in ecosystem damage depending on energy consumption, chemical usage, and feedstock use. The most critical contributors to ecosystem damage were energy use and chemical usage, with some methods showing disproportionately high impacts due to their intensive resource demands. **Figure 3 (b)** shows the ecosystem damage across the various production methods.

Methods with the highest ecosystem damage were S16: Etherification and sonification, and S17: TEMPO oxidation and sonication, at around 4×10^{-6} species.year/ kg of CNF, with energy consumption being the dominant contributor. These results highlight that sonification-based treatments showed high ecosystem damage due to their high energy demands. S13: Mechanical, low-energy had the lowest ecosystem damage at 7×10^{-9} species.year/ kg of CNF, followed by S15: Enzymatic pretreatments and microfluidization. In these cases, energy use was also the primary contributor. These findings suggest that low-energy mechanical and enzymatic treatments were the most favorable for ecosystem damage. Several methods also showed relatively high ecosystem damage due to high chemical usage. These results show that high ecosystem damage is also associated with chemical-intensive use.

Resource scarcity

Across various methods, there were high variations in resource scarcity damage depending on energy consumption, and chemical usage. The most critical contributors to resource scarcity damage were energy

use and chemical usage, with certain methods showing disproportionately high impact due to their intensive resource demands. **Figure 3 (c)** shows the resource scarcity damage across the various production methods.

Methods with the highest resource scarcity damage were S16: Etherification and sonification, and S17: TEMPO oxidation and sonication, at 92 USD2013/kg of CNF, and 70 USD2013/kg of CNF, respectively, with energy consumption being the dominant contributor. These results highlight that sonification-based treatments showed high resource scarcity damage due to their high energy demands. S13: Mechanical, low energy had the lowest impact at 0.12 USD2013/kg of CNF, followed by S15: Enzymatic pretreatments and microfluidization at 0.26 USD2013/kg of CNF. In these cases, energy use was also the primary contributor. These findings suggest that low-energy mechanical and enzymatic treatments were the most favorable for resource scarcity damage. Several methods also showed relatively high resource scarcity damage due to high chemical usage. These results show that high ecosystem damage is also associated with chemical-intensive use.

Total damage cost

The comparative assessment of damage costs associated with various production methods showed that methods involving high-energy consumption and chemical usage tend to have significantly higher damage costs. Methods involving sonification, particularly S16: Etherification and sonification, and S17: TEMPO oxidation and sonication, had the highest total damage costs. Methods such as S13: Mechanical, low energy, and S12: Mechanical, high energy showed the lowest damage costs. **Figure 3 (d)** shows the total damage cost across the various production methods.

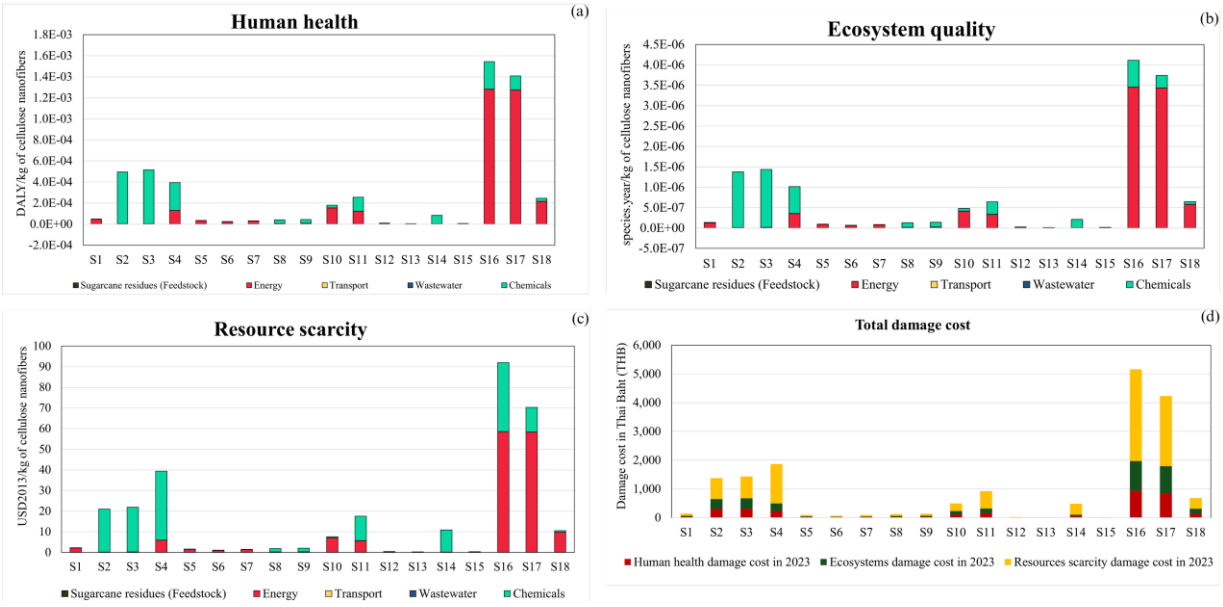


Figure 3 Impact on (a) human health, measured in disability adjusted life years (DALY)/kilogram of cellulose nanofibers, (b) ecosystem, measured in species.year/kilogram of cellulose nanofibers, (c) resource scarcity, measured in United States dollar 2013 (USD2013)/kilogram of cellulose nanofibers, and (d) total damage cost, measured in Thai Baht (THB)/kilogram of cellulose nanofibers across the various production methods.

CONCLUSONS

This study compared the life cycle environmental impact of various CNF production methods from sugarcane trash, evaluating climate change impact at the mid-point level and all three damage categories (human health damage, ecosystem damage, and resource scarcity damage) at the end-point level. Moreover, the total damage cost on the human health, ecosystem quality and resource scarcity were also evaluated. The environmental impacts varied dramatically between production methods, with climate change impact ranging

from 1.6 to 1,000 kg CO_2-eq/kg of cellulose nanofibers, human health from 2.5×10^{-6} to 1.5×10^{-3} DALYs/kg of cellulose nanofibers, ecosystem quality from 7×10^{-9} to 4×10^{-6} species·year/kg of cellulose nanofibers, and resource scarcity from 0.1 to 90 USD/kg of cellulose nanofibers. The total damage costs also showed large variation, ranging from around 8 to 5,160 Thai Baht/kg of cellulose nanofibers. Mechanical and enzymatic methods consistently showed lower impacts across all categories, including climate change, human health, ecosystem quality, and resource scarcity. Chemical-intensive processes such as TEMPO oxidation and etherification, particularly when combined with energy-intensive techniques like sonification, had significantly higher impacts. These findings highlight the importance of prioritizing mechanical and enzymatic methods for environmentally sustainable cellulose nanofiber production.

This study solely focused on the environmental impact comparison of CNF production methods from sugarcane residues. There are several limitations that show important research opportunities. The assessment was restricted to the environmental dimension, leaving economic and social aspects such as cost-benefit ratios or techno-economic feasibility; the assessment of the socio-economic implications for sugarcane and CNF industries—including shifts in agricultural and production practices, labor dynamics, and local development; industrial-scale viability—including scalability challenges, cost-effectiveness, and environmental profiles in commercial settings, to strengthen their relevance to sustainable real-world adoption. These gaps present significant opportunities to build upon this work and develop a more comprehensive evaluation of CNF production systems.

ACKNOWLEDGEMENTS

The authors gratefully acknowledge the financial support provided by the Faculty of Graduate Studies, Mahidol University under the Grant to Support Graduate Students in Academic Presentations in Thailand (Fiscal Year 2025). The research is also supported by the National Research Council of Thailand (NRCT) under the Research Team Promotion Grant project entitled "Moving towards carbon neutrality and sustainability of food, feed, fuel through BCG using life cycle thinking" (Grant No. N42A650550) as well as partially supported by the Faculty of Graduate Studies and Graduate Studies of Mahidol University Alumni Association. It was also supported by Worldwide University Network (WUN) (Research Development Fund – 2022) under the project entitled “Towards Net Zero and Sustainable Cities with Resource Optimization, Circular Economy and Research Network (NZS CITIES)”.

References

1. Ansari, M.M., et al., *Nanocellulose derived from agricultural biowaste by-products– Sustainable synthesis, biocompatibility, biomedical applications, and future perspectives: A review.* Carbohydrate Polymer Technologies and Applications, 2024. **8**: p. 100529.
2. Powar, R.V., et al., *End-Use Applications of Sugarcane Trash: A Comprehensive Review.* Sugar Tech, 2022. **24**(3): p. 699-714.
3. FAO, *Emissions from Crops*. 2021.
4. Singh, S.P., et al., *Sugarcane wastes into commercial products: Processing methods, production optimization and challenges.* Journal of Cleaner Production, 2021. **328**: p. 129453.
5. Mandegari, M.A., S. Farzad, and J.F. Görgens, *Recent trends on techno-economic assessment (TEA) of sugarcane biorefineries.* Biofuel Research Journal, 2017. **4**(3): p. 704-712.
6. Wagh, M.S., et al., *Valorisation of agro-industrial wastes: Circular bioeconomy and biorefinery process – A sustainable symphony.* Process Safety and Environmental Protection, 2024. **183**: p. 708-725.
7. Haroni, S., et al., *Sustainable production of cellulose nanofiber from sugarcane trash: A quality and life cycle assessment.* Industrial Crops and Products, 2021. **173**: p. 114084.
8. *Lactic acid, its salts and esters exports by country* 2021.

9. Li, Q., et al., *Nanocellulose Life Cycle Assessment.* ACS Sustainable Chemistry & Engineering, 2013. **1**(8): p. 919-928.
10. Arvidsson, R., D. Nguyen, and M. Svanström, *Life Cycle Assessment of Cellulose Nanofibrils Production by Mechanical Treatment and Two Different Pretreatment Processes.* Environmental Science & Technology, 2015. **49**(11): p. 6881-6890.
11. Gallo Stampino, P., et al. *Comparative Life Cycle Assessment of Cellulose Nanofibres Production Routes from Virgin and Recycled Raw Materials*. Molecules, 2021. **26**, DOI: 10.3390/molecules26092558.
12. Moon, D., et al., *Evaluation of Energy Consumption and Greenhouse Gas Emissions in Preparation of Cellulose Nanofibers from Woody Biomass.* Transactions of the ASABE, 2013. **56**(3): p. 1061-1067.
13. Kaenchan, P. and S. Gheewala, *Budget constraint and the valuation of environmental impacts in Thailand.* The International Journal of Life Cycle Assessment, 2017. **22**.
14. Klemm, D., et al., *Nanocellulose as a natural source for groundbreaking applications in materials science: Today's state.* Materials Today, 2018. **21**(7): p. 720-748.

20R4-06

Evaluating the Potential of Water Sources in Thailand for Hydrogen Production via Water Electrolysis

Sakunthip Hansungnoen[1], Ekkaphong Chomwong[1], Ploypailin Romphophak[2*], Prajak Sastaravet[3]
Pattarasiri Fagkaew[4] and Pisut Painmanakul[5]

[1]ndergraduate Student, Department of Environmental Engineering, Faculty of Engineering, Chulalongkorn University, Bangkok 10330, Thailand; [2]Researcher, Department of Environmental Engineering, Faculty of Engineering, Chulalongkorn University, Bangkok 10330, Thailand; [3]Lecturer, Faculty of Environmental Science, Ramkhamhaeng University, Bangkok 10240, Thailand;*
[4]Lecturer, Department of Sanitary Engineering, Faculty of Public Health, Mahidol University, Bangkok 10400, Thailand; [5]Professor, Department of Environmental Engineering, Faculty of Engineering, Chulalongkorn University, Bangkok 10330, Thailand
[*]Phone: 086-3234765, Fax: +6622187903, E-Mail: r.ploypailin@gmail.com

ABSTRACT

This study evaluates the potential of water sources in Thailand for hydrogen production via water electrolysis. The objective is to identify suitable regions for hydrogen production by assessing factors such as freshwater availability, renewable energy potential, water quality, seawater quality, port size, and industrial estate distribution. These factors are crucial for selecting areas for Proton Exchange Membrane (PEM) electrolysis, which requires stable water resources and renewable energy. Data were collected from government agencies, including Royal Irrigation Department of the Ministry of Agriculture and Cooperatives, Ministry of Energy, and Pollution Control Department of Ministry of Natural Resources and Environment. The study identified nine provinces with favorable conditions for establishing hydrogen production facilities, supported by water treatment systems for electrolysis. The findings highlight Thailand's potential to develop a sustainable green hydrogen industry, contributing to the nation's goal of carbon neutrality by 2050. The study emphasizes the importance of improving water management and expanding renewable energy infrastructure to support the clean energy transition.

Keywords: green hydrogen; hydrogen production; water source; electrolysis; renewable energy

INTRODUCTION

Energy and environmental changes are global issues, leading to a wide range of natural disasters, such as floods, landslides, and droughts, that are consistent with global climate change. An analysis by NASA of global surface temperature changes generally matches independent analyses by the National Oceanic and Atmospheric Administration (NOAA) and other research groups. The results show that the world is 1.47 degrees Celsius warmer than the long-term average between 1951 and 1980 [1]. The warmest year on record is expected to be 2024, largely due to the burning and use of fossil fuels, particularly oil and petroleum. In 2024, global fossil fuel use released 37.4 billion tons of carbon dioxide (CO_2), an increase of 0.8% from the previous year [2]. Reducing greenhouse gas emissions is therefore an important task, particularly in reducing the use of fossil fuels.

Currently, renewable energy is being developed to replace fossil fuels, such as hydropower, wind power, solar power, and biogas. However, they are not flexible enough for production. Therefore, finding technologies to reduce these shortcomings is important today. Green hydrogen is something obtained from the process of separating water with electricity from renewable energy. It can meet the flexibility of current renewable energy because hydrogen provides high energy when burned, can be stored for a long time, comparable to fossil fuels, and has convenient and flexible transportation.

The use of hydrogen energy has been developed in many countries, especially in Europe. The European Union (EU) sees that hydrogen will become a very important energy source in the future because it is clean energy and can be extracted from water, which can be recycled. The (EU) estimates that by 2030, hydrogen will be used to generate energy in the EU up to 665 TWh, or 6 percent of the total energy in the European Union, and by 2050, hydrogen will be used to generate energy up to 2,250 TWh, or 24 percent of the energy needed in the EU [3].

Thailand has a goal to be carbon neutral in 2050. The use of green hydrogen energy in the electricity generation sector at a proportion of 10%-75% by 2050 will be beneficial to achieving the goal of carbon neutrality in 2050 by reducing carbon emissions from electricity generation by more than 42% from the present [4].

Thailand has high potential for hydrogen production due to its abundant water sources, both freshwater and seawater, as water is a key element for hydrogen production. However, hydrogen production does not solely depend on water; it also relies on other factors. Therefore, this study focuses on identifying suitable areas in Thailand or areas with potential for establishing hydrogen production plants. This assessment will serve as a preliminary evaluation to identify areas with potential in various aspects, using multiple criteria for decision-making, such as water quantity and quality, transportation, industrial estates, and renewable energy in the area. Therefore, the assessment of the potential for establishing a hydrogen industry is crucial for developing the clean energy industry, reducing dependence on foreign energy, and aligning with the national energy policy.

METHODOLOGY

Study of provinces in Thailand that have coastal areas and large freshwater sources, with the main provinces being in the East, West and South, which are adjacent to the Gulf of Thailand and Andaman coasts. The area has a total size of 82,626.3 km^2, covering 15 provinces: Trat, Chanthaburi, Rayong, Chonburi, Chachoengsao, Phetchaburi, Prachuap Khiri Khan, Surat Thani, Nakhon Si Thammarat, Songkhla, Narathiwat, Ranong, Phuket, Krabi, and Trang, as shown in Figure 1.

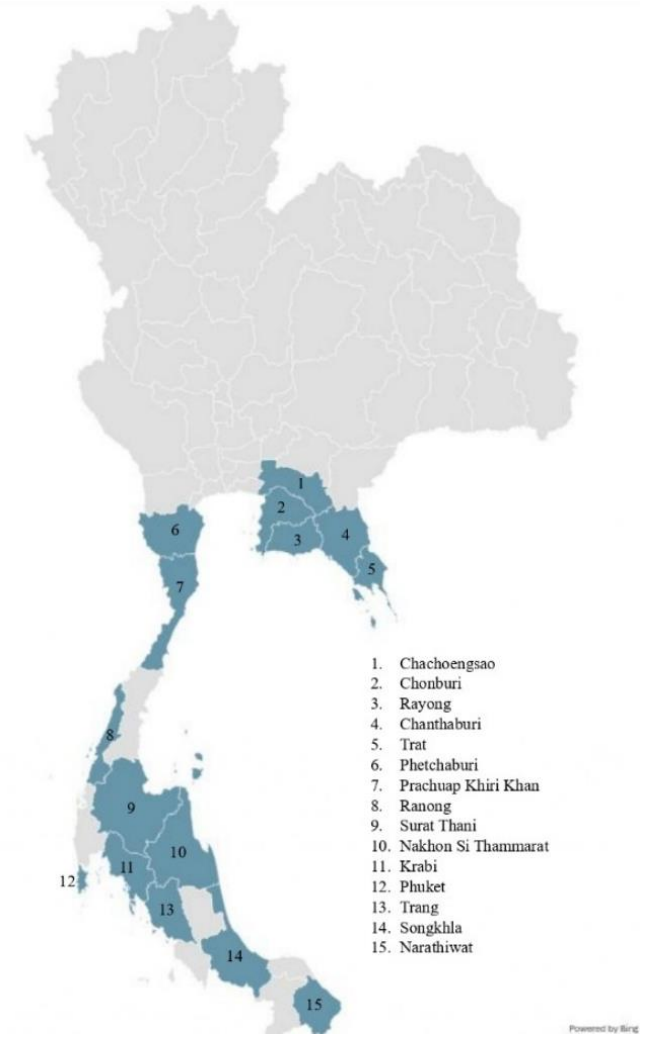


Figure 1 15 Selected Provinces for Hydrogen Production Study in Thailand

The region is typically characterized by tropical rainforests with an average temperature of around 30 °C. The dry season is from December to May, with little or no rainfall, followed by the rainy season from April to November, with rainfall ranging from 1200 - 4500 mm. In addition, the region also has high potential for solar power generation, with most areas having ground radiation of about 5 kW/m^2, which can be used to produce green hydrogen.

This study considered the principles for selecting green hydrogen production sites as shown in Table 1. Six main criteria were considered: freshwater availability, renewable energy potential, freshwater quality, seawater quality, port size, and industrial estate distribution. The focus is on the quantity of available freshwater and renewable energy.

Table 1 Criteria for Evaluating the Potential of Provinces for Hydrogen Production

Criteria	Weight	Performance level		
		1	2	3
Freshwater Availability	3	Usable water volume < 14 million m³	Usable water volume between 14 – 41 million m³	Usable water volume > 41 million m³
Renewable Energy Potential	3	Electricity generation capacity < 30 MW	Electricity generation capacity between 30 – 100 MW	Electricity generation capacity > 100 MW
Freshwater Quality	2	Poor (meets <50% of the standard)	Fair (meets 50% - 80% of the standard)	Good (meets >80% of the standard)
Seawater Quality	2	Poor (meets <50% of the standard)	Fair (meets 50% - 80% of the standard)	Good (meets >80% of the standard)
Port Size	1	Small port (capacity < 20 Gross Tons)	Medium port (capacity between 20 - 500 Gross Tons)	Large port (capacity > 500 Gross Tons)
Industrial Estate Distribution	1	1 industrial estate	2 - 9 industrial estates	More than 13 industrial estates

Notes

- Usable Water Volume refers to the remaining water volume after deducting the amount used for various activities, such as agriculture.
- Potential Levels are divided into three levels, with a higher level indicating better potential.
- Weight represents the importance of each criterion in the evaluation.

The rationale for Weight Assignment

This project prioritizes freshwater availability and renewable energy potential the most, as it focuses on Green Hydrogen production, which relies on electrolysis. This process requires a large volume of water and energy from renewable sources.

Explanation of Criteria

The criteria for evaluating the suitability of a location for green hydrogen production are based on specific parameters, as outlined below:

Freshwater Availability and Renewable Energy Potential

The criteria for usable water volume and power generation capacity are derived from the data distribution of 15 provinces, with usable water volumes ranging from 2.5 to 57.0 million m^3 and power generation capacities ranging from less than 30 MW to more than 100 MW. These ranges reflect the data distribution in the context of available resources and energy production.

Freshwater Quality and Seawater Quality

Water quality is assessed based on the percentage of parameters that meet the standards. For freshwater, there are 12 parameters evaluated, and for seawater, 19 parameters. These include factors

like DO, EC, turbidity, total solids, and various contaminants. The quality is classified as poor, fair, or good, depending on how many of the parameters meet the standards.

Quality Classification of Freshwater Quality:

- Good: > 80% pass → 10 - 12 parameters meet the standard
- Fair: 50% - 80% pass → 7 - 9 parameters meet the standard
- Poor: < 50% pass → 1 - 6 parameters meet the standard

Quality Classification of Seawater Quality:

- Good: > 80% pass → 15 - 19 parameters meet the standard
- Fair: 50% - 80% pass → 7 - 14 parameters meet the standard
- Poor: < 50% pass → 1 - 6 parameters meet the standard

Port Size

Ports in Thailand used for gas transport typically have a capacity of around 500 Gross Tons. Therefore, ports larger than this capacity are categorized as Performance Level 3.

Industrial Estate Distribution

The distribution of industrial estates in the 15 studied provinces forms the basis for this criterion. Songkhla has 1 industrial estate, while Rayong and Chonburi have more than 13. This is reflected in the performance levels to indicate the readiness of each region for industrial development.

Sources of Data

The necessary data were obtained from relevant government agencies, official websites, and other sources as summarized in Table 2. The data have been adapted for use in this study.

Table 2 Data Sources for Evaluating the Potential of Provinces for Hydrogen Production

Data Type	Source	Description / Notes
Freshwater Availability	Royal Irrigation Department	Data on usable water volume in different regions [5]
Renewable Energy Potential	Ministry of Energy	Data on power plants and their electricity generation capacity [6]
Freshwater Quality	Water Database System, Pollution Control Department	Data on freshwater quality parameters [7]
Seawater Quality	Pollution Control Department	Data on seawater quality parameters [8]
Port Size	Marine Department	Data on port sizes and cargo handling capacity [9]
Industrial Estate Distribution	Thai Franchise Center	Data on the number and distribution of industrial estates [10]

To assess the suitability of the 15 selected provinces for hydrogen production, a comprehensive evaluation was conducted based on multiple key factors. Freshwater availability from both reservoirs and surface water sources was analyzed, as it is essential for electrolysis in hydrogen production. Additionally, the potential for renewable energy was assessed to evaluate the capacity of renewable energy sources, which are crucial for sustainable hydrogen production. Furthermore, the quality of both freshwater and seawater was examined using various environmental parameters to determine their suitability for industrial applications. Port size and industrial estate distribution were also considered to assess the logistical infrastructure and level of industrial development in each province. All the data will be stored in Table 3.

Table 3 Assessment of Water Resources and Infrastructure for Hydrogen Production in Thailand

No.	Province	Reservoir/Dam	Capacity (Million m^3)	Usable Water Volume (Million m^3)	Renewable Power (MW)	Freshwater Quality Compliance (parameter)	Seawater Quality Compliance (parameter)	Ports with Size 500 Gross Tons (Number)	Ind. Estates (Number)
1	Trat	Khlong Sano	65	15-26 (Avg: 20.50)	5.00	5	16	-	-
2	Chanthaburi	Khlong Thung Phle	80	35-45 (Avg: 40.00)	34.65	8	17	-	-
3	Rayong	Prasae	295	41-67 (Avg: 57.00)	30.50	5	12	5	13
4	Chonburi	Bang Phra	117	4-7 (Avg: 5.50)	69.45	7	13	74	13
5	Chachoengsao	Khlong Si Yat	295	16-23 (Avg: 19.50)	68.34	5	15	16	-
6	Phetchaburi	Kaeng Krachan	710	5-13 (Avg: 9.00)	225.18	11	12	2	-
7	Prachuap Khiri Khan	Pranburi	391	31-40 (Avg: 35.50)	110.89	9	13	2	-
8	Surat Thani	Ratchaprapa	5638	1000-2260 (Avg: 1630.00)	343.59	8	13	25	-
9	Nakhon Si Thammarat	Huai Nam Sai	80	15-38 (Avg: 26.50)	202.41	8	13	5	-
10	Songkhla	Khlong Sadao	56.74	23-34 (Avg: 28.50)	75.48	8	15	19	1
11	Narathiwat	Near Ban	3	2-3 (Avg: 2.50)	15.50	8	15	1	-
12	Ranong	Hat Som Paen	10	2-4 (Avg: 3.00)	1.50	5	14	1	-
13	Phuket	Bang Wad	10.2	3-6 (Avg: 4.50)	13.00	8	13	3	-
14	Krabi	Bang Kam Plad	16	3-6 (Avg: 4.50)	66.71	9	14	5	-
15	Trang	Tha Ngiew	18	3-5 (Avg: 4.00)	21.18	7	14	6	

RESULTS AND DISCUSSIONS

Based on the assessment of the potential of the hydrogen production area, the analysis was carried out in five areas: Freshwater availability, Freshwater Quality, Freshwater Quality, Renewable energy capacity, Port capacity and Industrial Estate, with the weighting of each criterion to correspond to the requirements of the green hydrogen production.

Table 4 Potential Assessment Score Table for Six Aspects

No.	Province	Criteria						
		Freshwater availability	Freshwater Quality	Seawater Quality	Renewable energy capacity	Port capacity	Industrial Estate	Total
1	Trat	2	1	3	2	2	0	10
2	Chanthaburi	2	2	3	2	2	0	11
3	Rayong	3	1	2	2	3	3	14
4	Chonburi	2	2	2	4	3	3	16*
5	Chachoengsao	2	1	3	4	3	0	13
6	Phetchaburi	1	3	2	6	3	0	15
7	Prachuap Khiri Khan	2	2	2	4	3	0	13
8	Surat Thani	3	2	2	6	3	0	16*
9	Nakhon Si Thammarat	2	2	2	6	3	0	15
10	Songkhla	2	2	2	4	3	1	14
11	Narathiwat	1	1	3	2	3	0	10
12	Ranong	1	2	3	2	3	0	11
13	Phuket	1	2	2	2	3	0	10
14	Krabi	1	2	2	4	3	0	12
15	Trang	1	2	2	2	3	0	10

* Provinces with the highest disregard scores

From Table 4, it shows the evaluation scores of the hydrogen production potential of provinces in Thailand using multiple-choice criteria. It was found that the provinces with the highest scores were Chonburi and Surat Thani, both with scores of 16 points. When considering each component, Chonburi stands out more in terms of industrial estates, which will affect the convenience of use. On the other hand, Surat Thani does not have industrial estates, making Chonburi more potential than Surat Thani, despite having the same score. The next provinces with high potential are Phetchaburi and Nakhon Si Thammarat, both scoring 15 points. Phetchaburi is prominent in renewable energy, which allows us to produce green hydrogen, but it has a small amount of water and may require additional water from other sources. Nakhon Si Thammarat excels in all aspects similarly to Phetchaburi, but when compared to freshwater quality, Nakhon Si Thammarat has worse water quality than Phetchaburi, which may result in higher water treatment costs. The provinces with the least potential are Trat, Narathiwat, Phuket, and Trang, all scoring only 10 points. The weakness of these four provinces is renewable energy. If we want to produce green hydrogen, more renewable energy may need to be added. The specific weakness of Narathiwat, Phuket, and Trang is the small amount of water, which may not be sufficient for hydrogen production throughout the year. Additional water may need to be sourced from other places, such as seawater or other reservoirs within the province, which will increase costs. The specific weakness of Trat province is water quality, as it has the worst water quality, which directly affects the water treatment system before production, making the cost of improving water quality higher than other areas.

However, the study of these 6 components is only a preliminary assessment. In the next phase, there may be a need to evaluate the costs associated with hydrogen production, such as the water quality improvement systems for freshwater sources, which are a key factor for production. The hydrogen production system uses PEM, which requires high-quality water, significantly affecting the production cost. The required water quality is deionized (DI) water [11], which in the water treatment system, must use reverse osmosis (RO) and electrodeionization (EDI) systems to make the water quality equal to DI water [12].

CONCLUSION

The assessment of hydrogen production potential by electrolysis in Thailand is an assessment of several important factors for the green hydrogen production process, especially the amount of water and renewable energy power plants. It was found that Chonburi Province, which has the highest potential, has complete factors in terms of production and utilization, and is the best strategic location for hydrogen production. The provinces with the lowest potential are Trat, Narathiwat, Phuket, and Trang. In addition, all areas must improve water quality to obtain water quality that can produce hydrogen. The results of this study serve as a guideline for policymakers and investors to develop Thailand's hydrogen economy in line with the national energy plan and the goal of net-zero greenhouse gas emissions by 2025.

ACKNOWLEDGEMENT

This work was supported by a project grant from the Faculty of Environmental Engineering and Sustainability, Chulalongkorn University. We would like to thank lecturers from Chulalongkorn University, Mahidol University, and Ramkhamhaeng University

REFERENCE

[1] NASA. Vital Signs of the Planet: Global Temperature. Available at: https://climate.nasa.gov/vital-signs/global-temperature/?intent=111 (Accessed: 04/03/2025).

[2] Kasikorn Research Center. CO2 Emissions and Their Impact. Available at: https://www.kasikornresearch.com/th/analysis/k-social-media/Pages/CO2-CIS3567-FB-2025-03-06.aspx (Accessed: 04/03/2025).

[3] Thai Industrial Standards Institute (TISI). Hydrogen Energy Regulations. Available at: https://appdb.tisi.go.th/tis_devs/regulate/eu/pdf/Hydrogen_Energy_070964.pdf (Accessed: 04/03/2025).

[4] SCB Economic Intelligence Center. In Focus: Hydrogen in the PDP 2024. Available at: https://www.scbeic.com/th/detail/file/product/9514/gxj1pwggl2/In-focus-Hydrogen-in-the-PDP-2024-20240628.pdf (Accessed: 04/03/2025).

[5] Royal Irrigation Department (RID), Thailand. 2024. Reservoir and Water Resource Data. Available at: https://app.rid.go.th/reservoir/

[6] Department of Alternative Energy Development and Efficiency (DEDE), Thailand. 2024. Renewable Energy Potential GIS Data. Available at: https://gis.dede.go.th/gallery-map-list.aspx

[7] Department of Water Resources (DWR), Thailand. 2024. National Water Resource Management System. Available at: https://rwater.mnre.go.th/front/main/Home

[8] Pollution Control Department (PCD), Thailand. 2024. Marine Water Quality Data. Available at: https://pcd.gdcatalog.go.th/es/dataset/_11_05_marinequality/resource/56278561-21d9-4d66-b7d0-9bf685a13fc2

[9] Marine Department (MD), Thailand. 2024. Maritime Transport and Port Information. Available at: https://md.go.th

[10] Industrial Estate Authority of Thailand (IEAT). 2022. List of Industrial Estates in Thailand. Available at: https://www.ieat.go.th/web-upload/

[11] Becker, H., Murawski, J., Shinde, D. V., Stephens, I. E. L., Hinds, G., & Smith, G. (2023). Impact of impurities on water electrolysis: a review. *Sustainable Energy & Fuels*, 7, 1565. Available at: https://pubs.rsc.org/en/content/articlepdf/2023/se/d2se01517j (Accessed: 04/03/2025).

[12] Lekhajaroenkul, T., Supapa, S., & Yanpirat, P. (Year). Technical and economic feasibility analysis on the installation of purified water system by electrical ion discharger instead of ion resin exchanger: A case study of purified water plant generation system for pharmaceutical processing. *Korean Journal of Business Economics (KBEJ)*. Available at:https://ph01.tci-thaijo.org/index.php/kbej/article(Accessed: 04/03/2025).

20R4-08

Multi-Factor Analysis of Oil Spill Vulnerability: Integrating Environmental, Socioeconomic, and Policy Perspectives

Sataporn Jaisomkom[1], Saowanee Wijitkosum[2], and Somrudee Meprasert Jitpraphai[3,4*]

[1] *Maritime Administration, Gruduate School, Chulalongkorn University, Bangkok 10330, Thailand*
[2] *Sustainable Evironment Research Institute, Chulalongkorn University, Bangkok 10330, Thailand*
[3] *Department of Marine Science, Faculty of Science, Chulalongkorn University, Thailand*
[4] *Center of Excellence in Microbial Technology for Marine Pollution Treatment (MiTMaPT), Faculty of Science, Chulalongkorn University, Bangkok 10330, Thailand*
[*] *Phone : +66 (0) 2 2185394-5, Fax : +66 (0) 2 2550780, E-mail: somrudee.j@chula.ac.th*

ABSTRACT

Oil spills impact marine ecosystems, public health, and economic activities. Chonburi Province, located in Thailand's Eastern Economic Corridor (EEC), is crucial to the nation's economy and aims for sustainable growth. Oil spill vulnerability assessment is essential for guiding preparedness, resource allocation, and mitigation strategies to enhance coastal resilience. This study examines the interactions among critical oil spill influencing factors and vulnerability in Chonburi Province using the Analytical Hierarchy Process (AHP). A panel of 13 experts—including government officials, oil industry professionals, and academics—conducted pairwise comparisons. Fifteen key factors were considered: spill frequency, recurrence in the same area, oil properties, spill volume, incident scene and timing, sea surface currents and wind, tide, human coastal activities, coastline type, marine fauna mobility, coastal ecosystem resilience, availability of oil removal equipment, operator expertise, and response plans. The results show that the mitigation factor is the most important for oil spill vulnerability. The three highest-weighted factors—Plans for Responding and Dealing with Situations (M3), Knowledge, Skills, and Abilities of Operators (M2), and Equipment and Tools for Removing Oil (M1)—highlight the key elements of an effective spill response. These findings confirm that emergency response planning, trained operators, and proper oil removal equipment are essential for reducing oil spill risks and ensuring quick and efficient cleanup. These findings emphasize the importance of proactive planning, preparedness, and policy development to minimize oil spill impacts and strengthen coastal resilience.

Keywords: Oil spill vulnerability; Analytical Hierarchy Process (AHP); Anthropogenic risk factors; Gulf of Thailand; Marine pollution

INTRODUCTION

Oil spills pose significant risks to marine ecosystems, public health, and economic activities [1]. The leading causes of oil spills at sea include operations within the oil and petroleum industries, ship collisions, illegal oil dumping, untreated waste disposal, and transportation activities. While the target of SDG 14—'Reduce Marine Pollution and Protect and Restore Ecosystems' [2] aims to address such challenges, the question remains: how can marine pollution, like oil spills in Chonburi, be effectively resolved? Chonburi Province, situated within Thailand's Eastern Economic Corridor (EEC), is a region highly vulnerable to the environmental risks posed by intensive marine activities.

Moreover, Chonburi has been classified as a high-risk area by the Pollution Control Department [3]. Between 1997 and 2023, 57 oil spills were recorded [4]. The most frequent spill locations were ports, coastal areas (Figure 1), and regions with heavy maritime traffic (Figure 2). The majority of spills involved fuel oil used in ships (diesel and gasoline), accounting for 23 incidents or 40.35% of the total. The next most common cause was oil spills (light oil and heavy oil) that washed ashore, comprising 21.05% of the total.

Additionally, many oil spills have unknown sources and quantities, making them difficult to manage. Large oil spills (over 1,000 tons) are often caused by ship collisions or ship strikes near Shark Rock. These incidents are comparatively easier to manage because the polluters are identifiable.

Vulnerability assessments are critical steps in preparing to mitigate the negative impacts of disasters and reducing associated risks [5]. These assessments serve as a foundation for allocating management resources across preparedness, response, recovery [6], and disaster minimization efforts. Identifying factors that influence vulnerability is essential for effective risk management.

Various tools exist for identifying and analyzing these factors, with the Analytical Hierarchy Process (AHP) being one of the most reliable and effective decision-making methods. AHP has been widely applied to environmental risk analysis, including flood risk in the Upper Tigris Basin [7], drought risk in the Lam Ta Kong Watershed [8], and landslide susceptibility in Ethiopia's highlands [9]. Similarly, research on oil spill vulnerability has utilized various tools (e.g., SAR images, ESI, AIS, GIS, XGBoost, Random Forest, SES, EWM, AHP) depending on the characteristics of each area (Table 1). While some studies use more complex mathematical models, these can pose limitations in certain areas [12, 15]. However, tools vary in complexity, offering both simple and advanced options.

Table 1 Relavent research using factor analysis.

Study Area	Tools	Factors				
		Incident information	Vessels and Ports information	Area information	Dynamic information	Adaptation/ Mitigation
Bohai Gulf, China [10] (damage assessment)	SAR Image	✓		✓	✓	
Coastal of Japan [11]	Likelihood Analysis	✓	✓	✓	✓	
Arctic marine areas [12]	Bayesian networks	✓		✓	✓	
South Sumatera, Indonesia [13]	ESI			✓		
Coastal of China [14]	AIS and GIS	✓	✓	✓		
Coastal of England [15]	XGBoost and Random Forest	✓	✓	✓		
Coastal of Peru [16]	SES		✓	✓	✓	
Bohai Gulf, China [17] (risk assessment)	GIS and EWM	✓	✓	✓		
North of the Shandong Peninsula, China [18]	AHP and GIS		✓	✓	✓	✓

Several methods for vulnerability assessment, such as AHP, are both straightforward and effective. However, no studies have specifically analyzed oil spill vulnerability factors using AHP in the Gulf of Thailand, particularly in the Chonburi area. This research employs AHP to identify key vulnerability factors associated with oil spills in Chonburi. Due to its strategic importance and the environmental risks it faces, Chonburi represents an ideal case study for assessing oil spill vulnerability. The study synthesizes and evaluates these factors to establish guidelines and preventive measures for planning, preparedness, problem-solving, impact reduction, damage mitigation, and policy development.

METHODOLOGY

1. Study Area. Chonburi Province covers approximately 5,069 km² (Figure 1) and serves as a major economic and industrial hub with heavily congested vessel routes. Figure 2 illustrates the density of water traffic in the study area, showing that during December to March, the eastern Gulf of Thailand experiences calm waves, making it ideal for sea transport and travel. This period results in increased maritime traffic in Chonburi Province [19].

The province hosts key ports, refineries, and petrochemical industries, along with a 160 km coastline containing ecologically sensitive areas such as coral reefs, mangroves, and fisheries, all of which are highly vulnerable to oil spill contamination. Additionally, Chonburi features diverse coastline types [20] and is home to popular tourism destinations, including Pattaya.

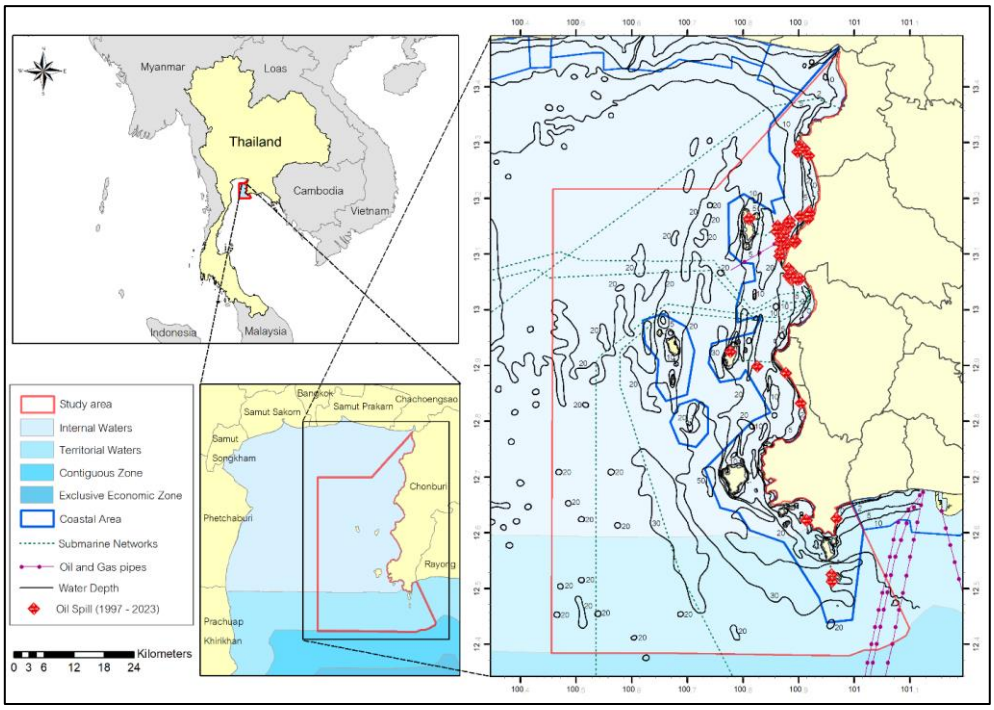


Figure 1 The study area.

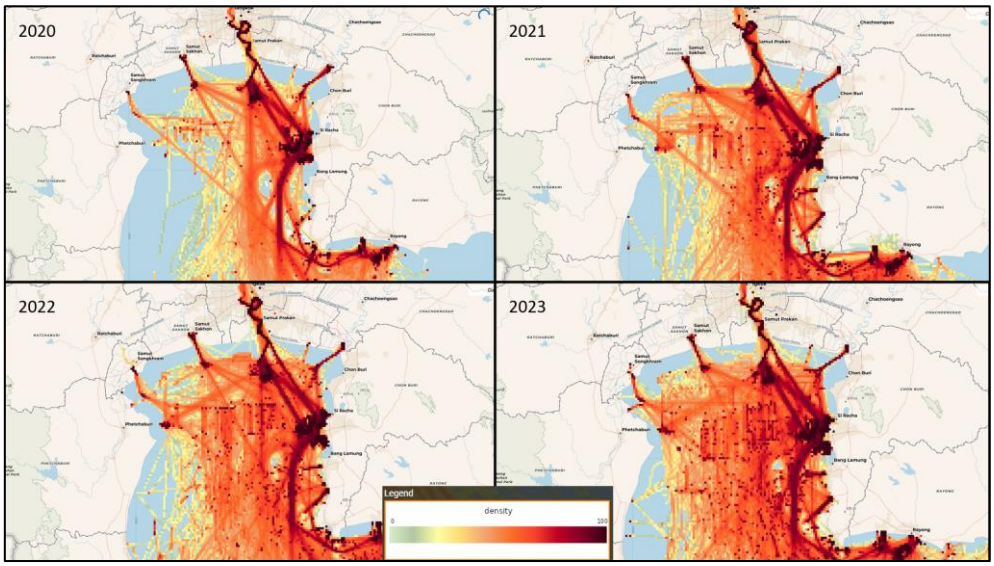


Figure 2 Vessel routes during December of 2020 - 2023 [19].

2. Identifying Vulnerability Factors. Vulnerability factors were identified through content analysis, synthesis based on the definition of vulnerability [21], relevant research presented in Table 1, field observations, and interviews with local officers. These five methods were grouped into three main factors and further divided into fifteen sub-factors.

1) Exposure Factors (E) refer to any factors that lead to the impact of oil spills on the population or marine and coastal resources within the study area. There are nine factors:

1.1) Frequency of oil spills (E1) refers to the recurrence of oil spill incidents within a defined time period.

1.2) Incidence of recurrence in the same area (E2) refers to the repeated occurrence of oil spills in the same location within a period when the situation remains unresolved or uncontrolled, and the spills are caused by different polluters.

1.3) Type and properties of spilled oil (E3) refer to the classification and characteristics of oil resulting from petroleum production.

1.4) Spill volume (E4) refers to the total quantity of oil released during a spill incident.

1.5) Scene of the incident (E5) refers to the specific location where the oil spill occurred.

1.6) Time of the incident (E6) refers to the specific timing when the oil spill occurred.

1.7) Sea surface currents and wind (E7) refer to the movement of water masses and atmospheric winds over the sea, including the effects of local winds and monsoons.

1.8) Tide (E8) refers to the cyclical rise and fall of sea levels caused by gravitational forces exerted by the moon and the sun.

1.9) Human coastal activities (E9) refer to the impact of oil spills on marine and coastal activities, with varying degrees of severity depending on the situation.

2) Sensitivity Factors (S) refer to any factors that make the marine ecosystem in the area susceptible to impacts from oil spills. There are three factors:

2.1) Types of coastline (S1) refer to the various characteristics of coastlines, including rocky shores, sandy beaches, and mangroves.

2.2) The locomotion ability of marine fauna (S2) refers to the mobility and movement capacity of marine organisms.

2.3) Resilience of coastal ecosystems (S3) refers to the varying levels of sensitivity exhibited by different types of coastal ecosystems, such as seagrass beds, coral reefs, and mangroves, in response to the impacts of oil spills.

3) Mitigation Factors (M) refer to any factors that influence the ability to respond effectively to oil spills. There are three factors:

3.1) Equipment and tools for removing oil (M1) refer to the availability and preparedness of resources, including booms, oil dispersants, vessels, and aircraft, used for oil spill cleanup.

3.2) Knowledge, skills, and abilities of operators (M2) refer to the expertise and competency of personnel, as well as the number of individuals, involved in oil spill response operations.

3.3) Plans for responding and dealing with situations (M3) refer to practical and applicable response plans that are established to address oil spill incidents.

Once the factors relevant to the study were identified, they were analyzed and prioritized using the AHP process.

3. Analytical Hierarchy Process (AHP).

AHP was used to rank vulnerability factors systematically. By breaking the problem into a hierarchy reflecting vulnerability characteristics, each factor was thoroughly assessed. Analyzing and prioritizing these factors involved four key steps:

3.1 Structuring the decision problem into a hierarchical model. The decision problem is structured as a hierarchical model, breaking it down into its vulnerability characteristics. This model includes three levels: the goal, criteria, and alternatives (Figure 3).

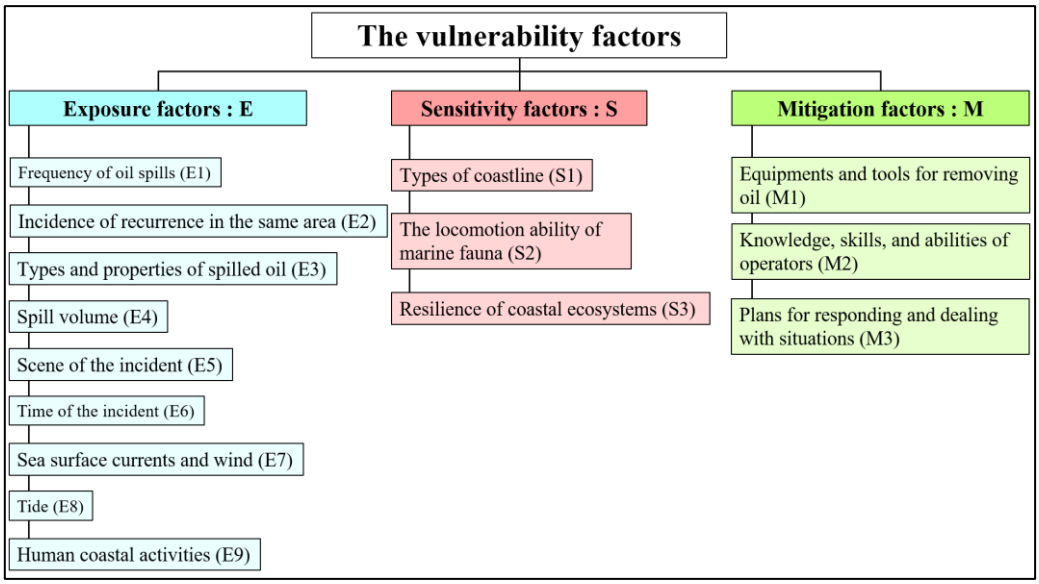


Figure 3 The vulnerability factors.

3.2 Making pairwise comparisons and obtaining the judgment matrix. A group of 13 experts compared the factors in this study. These experts included local government practitioners and policymakers, representatives from the oil industry, and academics. They came from organizations such as Marine Office 6 (Chonburi), Environment and Pollution Control Office 13 (Chonburi), Marine and Coastal Resources Office 2 (Chonburi), and the Chonburi Provincial Maritime Enforcement Office. Other participants included the Chonburi Port Security Control Center, Thai Maritime Enforcement Command Center (Thai-MECC Region 1), First Naval Area Command (NAC 1), and Chonburi Fisheries Provincial Office. Industry representatives were from Thai Oil Public Company Limited and PTT Oil and Retail Business Public Company Limited. The academics specialized in areas like Chemical Oceanography, Physical Oceanography, and Marine Technology.

Experts compare and rate each factor using a rating scale [22]. A factor with a higher rating is considered more significant than one with a lower rating. These ratings are used to create a judgment matrix, where each entry (a_{ij}) follows three rules: $a_{ij} > 0$; $a_{ij} = 1/a_{ji}$; and $a_{ii} = 1$ for all i. If the matrix satisfies the condition $a_{ij} = a_{ik} * a_{kj}$ for all entries, it is considered consistent. If not, the inconsistency level is measured using the consistency ratio (CR) [22].

3.3 Verifying factor weights and consistency of comparisons. Factor weights of the elements are calculated from the judgment matrices using the eigenvector method (EVM). When EVM is applied, the consistency ratio (CR) can be computed. A CR value below 0.1 is considered acceptable. If the CR for a matrix exceeds 0.1, judgments should be reassessed, with RI set to 1.59 for a 15-factor matrix, following the formula [22].

$$CR = CI/RI \quad (1)$$

Where the consistency index (CI) is measured through the following formula [22]

$$CI = \frac{\lambda_{max} - n}{n-1} \quad (2)$$

3.4 Aggregating weights across various levels. The overall vulnerability weights were determined by combining the factor weights across various hierarchical levels.

RESULTS AND DISCUSSIONS

Weights were determined through AHP analysis based on 105 pairwise comparisons. All comparison matrices had consistency ratios below 0.1, ensuring reliable judgments. **Plans for Responding and Dealing with Situations (M3)** was identified as the highest priority (weight = 0.191), as it ensures effective coordination, quick resource deployment, and spill containment. **Knowledge, Skills, and Abilities of Operators (M2)** ranked second (weight = 0.175), highlighting the need for trained personnel to handle

equipment and execute cleanup operations efficiently. Regular training helps operators adapt to unpredictable spill conditions. **Equipment and Tools for Removing Oil (M1)** was the third priority (weight = 0.145), covering essential resources like containment booms, skimmers, and dispersants for rapid response. Proper maintenance and strategic positioning of these tools further enhance spill mitigation. Other factors were prioritized accordingly, as shown in Figure 3.

The primary vulnerability factor identified is mitigation, which directly affects oil spill response effectiveness. Research findings from all expert groups were settled in agreement. This study highlights three critical elements for effective oil spill management: response plans (M3), operators' knowledge, skills, and abilities (M2), and equipment and tools for oil removal (M1). These findings align with numerous studies that underscore the importance of robust response plans to ensure an organized and precise reaction to oil spills. Well-coordinated plans minimize redundancy, accelerate response times, and enable complete spill removal before significant damage occurs to marine and coastal resources. However, a response plan alone is insufficient. The expertise of operators and the availability of appropriate equipment and tools are essential, as oil spill situations demand specialized intervention. These factors are pivotal in reducing errors and improving the success rate of spill management.

While spill volume (E4) and coastline type (S1) play a significant role in shaping response strategies, these factors mainly help operators allocate resources effectively for each situation and are considered of lesser importance. Environmental factors, such as sea surface currents and winds (E7), tidal currents (E8), and the location of the incident (E5), add challenges by influencing oil distribution and complicating cleanup efforts. Since these factors are uncontrollable and often change during an incident, they are given lower priority in vulnerability assessments. Instead, operators must remain adaptable and continuously monitor the situation. Thus, the findings underscore the importance of flexible and adaptive response strategies.

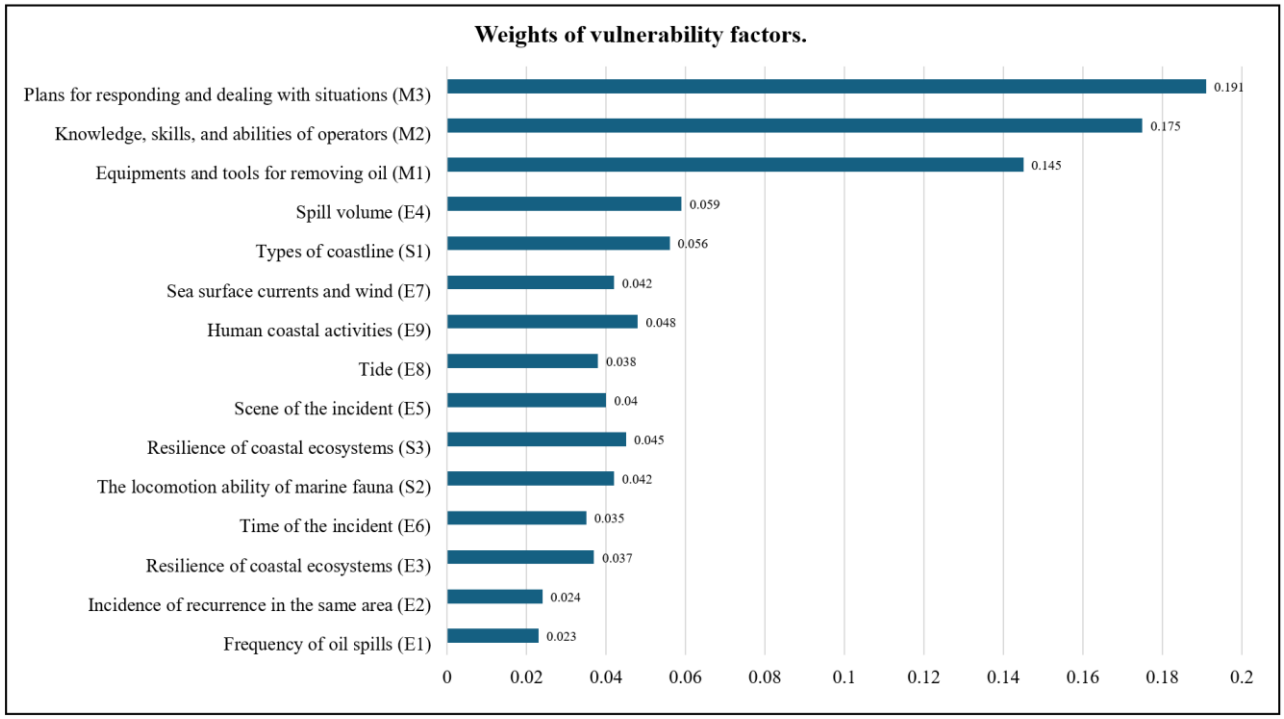


Figure 3 Weights of vulnerability factors.

Analysis results from each expert group revealed that all groups ranked mitigation factors as the highest priority. However, the subsequent rankings varied. Experts from government agencies prioritized the exposure factor, Spill Volume (E4). For sensitivity factors, they placed greater importance on Types of Coastline (S1) over other sensitivity factors, as oil volume and coastal characteristics influence preparedness for response and cleanup efforts when oil slicks approach the coastline. The oil industry prioritized the exposure factors Human Coastal Activities (E9) and Scene of the Incident (E5), as these directly impact the

industry's oil transportation routes. Academics focused more on sensitivity factors, ranking Resilience of Coastal Ecosystems (S3) and Types of Coastline (S1) higher than exposure factors, emphasizing their influence on the recovery of marine and coastal ecosystems.

These findings are consistent with previous research on vulnerability assessments, such as the Drought Vulnerability study focusing on the Lam Ta Kong Watershed, which defined factors based on spatial context and locality. Vulnerability is characterized by three main components: exposure, sensitivity, and adaptive capacity. In the drought vulnerability assessment, ten factors were grouped into four categories: geographical, natural, climatic, and anthropogenic—representing the core elements of vulnerability. The study identified precipitation, the number of precipitation days, and land use as critical factors influencing drought. Among these, land use had a particularly significant impact on watershed drought, emphasizing the importance of land use management as a strategy to mitigate the effects of drought [9].

Similarly, in assessing oil spill vulnerability, three key components—exposure, sensitivity, and adaptability—were used to define influencing factors. A total of 23 oil spill-related factors were categorized into these three groups. **Exposure indicators** included potential oil spill risk sources that could affect mariculture areas. **Sensitivity indicators** represented the inherent characteristics of mariculture areas and factors impacting the environment's self-purification capacity. **Adaptability indicators** focused on oil spill response capacity, such as the availability of response equipment. Vulnerability was analyzed across sub-zones of mariculture areas by examining exposure, sensitivity, adaptability, and overall vulnerability to oil spills. These factors were spatially assessed and classified into five levels: extremely low, relatively low, medium, relatively high, and extremely high. The findings identified four distinct mariculture zones. Zone 3, located in the Miaodao Archipelago, demonstrated higher exposure, sensitivity, and adaptability compared to other zones. This was due to the presence of numerous oil wells and channels, the effects of ocean current velocity and wave height, and the proximity of emergency equipment. As a result, Zone 3 showed the lowest overall vulnerability to oil spill stress [18].

Chonburi Province is a key contributor to Thailand's economic development and a vital part of the Eastern Economic Corridor. Situated along the Gulf of Thailand—a semi-enclosed sea—the province faces environmental challenges, including oil spills, which worsen existing marine issues such as water pollution from microplastics, heavy metals, and plankton blooms. Recent oil spills have compounded marine pollution, adversely affecting marine transportation, coastal activities, recreation, and the aquaculture industry. Vulnerability assessments are essential for developing effective guidelines and preventive measures to address oil spills. These assessments are shaped by regional physical characteristics, biological conditions, human activities, and policy frameworks. A comprehensive oil spill vulnerability assessment, which considers environmental, human, and response-related factors, is critical for improving preparedness, resource allocation, and mitigation strategies. Ultimately, such assessments will strengthen coastal resilience and enhance the effectiveness of response efforts.

CONCLUSION

This study highlights the importance of mitigation factors—such as response plans, operator skills, and oil removal equipment—in reducing oil spill vulnerability in Chonburi province. Exposure and sensitivity factors also affect how oil spills impact the environment and economy. Since Chonburi is a high-risk, economically important area, strong preparedness, trained personnel, and effective response strategies are essential. These findings align with Sustainable Development Goal 14 (SDG 14: Life Below Water), which focuses on protecting marine ecosystems. Good oil spill management helps achieve SDG 14.1, which aims to reduce marine pollution. Improving coastal resilience also supports global sustainability efforts by protecting biodiversity and supporting economic stability. By strengthening response plans, training operators, and using resources efficiently, we can reduce environmental damage and support long-term sustainability. As Chonburi continues to grow, prioritizing sustainable oil spill prevention will help preserve marine ecosystems and protect coastal communities for the future.

ACKNOWLEDGEMENT

This research is supported by Thai Maritime Enforcement Command Center (Thai-MECC) scholarship and the Center of Excellence in Microbial Technology for Marine Pollution Treatment (MiTMaPT).

REFERENCE

[1] International Maritime Organization (IMO). 2019. Participant's Manual IMO Model Course on Oil Pollution, Preparedness, Response and Cooperation, 3rd Edition: IMO.

[2] United Nations. 2023. Sustainable Development Goals. https://sdgs.un.org/goals [22 March 2025]

[3] Pollution Control Department. 2010. Predicting the movement of oil spills in the sea, impacts on natural resources and solutions. Kotchakorn Publishing Limited Partnership., Bangkok.

[4] Marine Department. 2023. Data and Statistics. https://md.go.th/category/data-andstatistics/page/34/?95 [15 May 2024]

[5] Fuchs, S., Birkmann, J., and Glade, T. 2012. Vulnerability assessment in natural hazard and risk analysis: current approaches and future challenges. Nat Hazards. 64(3): 1969–1975.

[6] Orru, K., Hansson, S., Gabel, F., Tammpuu, P., Krüger, M., Savadori, L., and Rhinard, M. 2022. Approaches to 'vulnerability' in eight European disaster management systems. Disasters. 46(3): 742–767.

[7] Kaya, B. 2025. Dynamic and Scalable Flood Risk Assessment Using GIS, AHP, and Novel Fuzzy AHP: A Case Study of the Upper Tigris Basin. Research Square. (2025): 1-16.

[8] Kukuntod, N., and Wijitkosum, S. 2024. Interaction of drought-influencing factors for drought mitigation strategies in Lam Ta Kong Watershed, Khorat Plateau. Heliyon. 10(2024): 1-15.

[9] Sisay, T., Tesfaye, G., Jothimani, M., Reda, T. M., and Tadese, A. 2024. Landslide susceptibility mapping using combined geospatial, FR and AHP models: a case study from Ethiopia's highlands. Discover Sustainability. 5(1): 1-25.

[10] Wei, L., Hu, Z., Dong, L., and Zhao, W. 2015. A damage assessment model of oil spill accident combining historical data and satellite remote sensing information: A case study in Penglai 19-3 oil spill accident of China. Beijing, China. Marine Pollution Bulletin. 91(2015): 258-271.

[11] United Nations Environment Programme (UNEP). 2017. Risk Assessment of Oil Spill Incident: Focusing on Likelihood Analysis in the NOWPAP Region - MERRAC Technical Report No. 36.

[12] Nevalainen, M., Helle, I., and Vanhatalo, J. 2017. Preparing for the unprecedented – Towards quantitative oil risk assessment in the Arctic marine areas. Marine Pollution Bulletin. 114(2017): 90-101.

[13] Rustandi, Y.; Damar, A.; Rakasiwi, G.; Afandy, A.; Hamdani, A.; Mulyana, D. Environmental sensitivity index mapping as aprevention strategy against oil spill pollution: A case study on the coastal area of South Sumatera Province in Indonesia. At IOP Conference Series: Earth and Environmental Science at Penang, Malaysia on January 10, 2020.

[14] Zhu, G., Xie, Z., Xu, H., Wang, N., Zhang, L., Mao, N., and Cheng, J. 2022. Oil spill Environmental Risk Assessment and Mapping in Coastal China Using Automatic Identification System (AIS) Data. Sustainability. 14(2022): 1-16.

[15] Rawson, A., Brito, M., and Sabeur, Z., 2021. Spatial Modeling of Maritime Risk Using Machine Learning. Risk Analysis. 42(10): 2291-2311.

[16] Flores-Medina, P., Sepp-Neves, A., Coppini, G., and Morales-Caselles, C. 2022. Strategic environmental sensitivity mapping for oil spill contingency planning in the Peruvian marine-coastal zone. Science of the Total Environment. 852(2022): 1-11.

[17] Wang, Y., Du, P., Liu, B., and Wu, X. 2023. Geographic information system-based comprehensive oil spill risk assessment in China's Bohai Sea. Frontiers in Marine Science. 10(2023): 1-11.

[18] Wang, Y., Du, P., Liu, B., and Wu, X. 2023. Vulnerability of mariculture areas to oil-spill stress in waters north of the Shandong Peninsula, China. Ecological Indicators. 148(2023): 1-12.

[19] Thai Maritime Enforcement Command Center. 2025. Heatmap. https://seavision.volpe.dot.gov/ [5 January 2025]

[20] PEMSEA. 2013. Environmental Sensitivity Index (ESI) Atlas of the Gulf of Thailand. PEMSEA Resource Facility, Philippines.

[21] Intergovernmental Panel on Climate Change (IPCC). 2001. Climate Change 2001: Impacts, Adaptation, and Vulnerability: Contribution of Working Group II to the Third Assessment Report of the Intergovernmental Panel on Climate Change. Cambridge University Press, Cambridge.

[22] Saaty, T. L. 1980. The Analytic Hierarchy Process: Planning, Priority Setting, Resources Allocation. McGraw-Hill, London.

20R4-09

The Variability in Soil Community and Its Enzymatic Function to Plant Promotion after Biochar Addition

Mujalin Pholchan[1*], Jearanai Thassana[1], and Khajitmanee Muangprom[1]

[1]*Researcher, Environmental Technology, Maejo University, Chiangmai 50290, Thailand.*
[*]*Phone : 0 5387 3870, Fax : 0 5387 3827, E-mail : mujalin@mju.ac.th*

ABSTRACT

The widespread use of chemical inputs in contemporary agriculture has raised concerns regarding long-term soil health and sustainability. Biochar (BC), a carbon-rich byproduct of biomass pyrolysis, presents a viable alternative, offering improvements in soil structure, nutrient retention, and microbial activity. This study investigates the effects of modified biochar on soil microbial diversity and associated metabolic pathways that contribute to soil fertility and plant productivity. Five soil samples (D1–D5) were collected from agricultural sites for microbial community profiling. Metagenomic DNA was extracted and analyzed using QIIME2. A total of 371 microbial species were identified across samples. D1 exhibited dominance of Proteobacteria, Acidobacteriota, and Halobacterota. In contrast, D2–D5 showed increased abundance of Firmicutes and Actinobacteriota, with the emergence of phyla such as WPS-2 and the enrichment of functional genera including the ammonia-oxidizing bacterium MND1. Bacilli were detected in all samples, with the highest relative abundance observed in D5 (8.34%). Notably, Bacillus sp.—a component of the applied BC—was more abundant in D4 (0.12%) and D5 (0.58%) than in D1 (0.02%), indicating BC's potential to retain and promote beneficial microbial taxa. Microbial richness was highest in D2 (4887 OTUs), exceeding that of the control (D1, 4517 OTUs), confirming the diversity-enhancing effect of BC. D4 exhibited the most distinct microbial community (3403 OTUs). Functional annotation revealed increased abundance of proteins such as COG1595 and key enzymes including EC:2.7.7.7 and EC:1.6.5.3, which are associated with nucleotide synthesis and redox metabolism. The metabolic pathway PWY-3781 was most prominent post-BC application, with pathways PWY-7111, PWY-6277, and PWY-6122 also enriched in D3 compared to D1.These findings demonstrate that biochar promotes microbial diversity, enhances beneficial microbial populations, and activates key metabolic pathways, thereby contributing to improved soil quality and supporting sustainable agricultural practices.

Keywords : biochar, microbial diversity, metabolic pathways, plant growth, soil fertility

INTRODUCTION

Contemporary agriculture relies on chemicals to achieve high-quality yields. However, the long-term and repeated use of chemicals in the same area not only decreases soil quality but also disrupts and damages the soil microbial system. Therefore, the shift towards using biological materials instead of chemicals is an alternative that should be given attention.

Biochar is an agricultural waste from the pyrolysis process. It is an environmentally friendly biological material at a low cost that has been widely applied in environmental studies due to its various properties e.g. high carbon content, large surface area, high cation exchange capacity, and stable structure [1]. Due to its adsorption capacity, biochar is an effective biological material for eliminating contaminants [2], including heavy metal pollutants [3] and organic contaminants such as dyes [4]. Moreover, biochar is also used to improve soil quality and promote plant growth. Biochar has been used to examine soil properties and the growth of plants. It helps increase the pH of the soil and promotes higher final biomass, root biomass, plant height, and number of leaves [5].

In addition, biochar also affects the microbiome within the soil. It contributes to increasing the diversity of the soil microbiome [6] e.g. the increase in Bacillus and Pseudomonas by up to 100% [7] that plays a role in promoting plant growth and nutrient cycling. Some studies have also shown that biochar can increase soil enzyme activity, such as urease activity by 23.1%, alkaline phosphatase activity by 25.4%, and dehydrogenase activity by 19.8% [8].

However, most studies focus on short-term impacts, while long-term changes in microbial diversity, abundance, and functions remain unclear. While biochar can enhance microbial activity, its effects on specific microbial metabolic pathways, such as carbon and nitrogen cycling, need more investigation.

This study focuses on the effects of modified biochar (BC) addition changes on soil microbial diversity and investigates metabolic pathways that promote plant growth and soil quality.

METHODOLOGY

Soil samples (D1 control without BC, D2 paddy field 1, D3 paddy field 2, D4 eggplant field, and D5 long yard bean field) from agricultural areas after plantation were collected for microbial diversity analysis. They were preserved in the 50 mL centrifuge tube with absolute ethanol at the ratio of 1:1 (by volume) and stored at − 20 ◦C prior to DNA extraction. Total DNA was extracted from the soil sample using the nucleospin® soil (Bio-rad laboratories, USA) following the manufacturer's instructions. The DNA samples were then sent for metagenomic sequencing analysis which was performed on Illumina HiSeq platform by Novogene Biological Information Technology (Tianjin, China). 16 S rRNA genes of distinct 16SV3–V4 regions were amplified used specific primers with the barcode. All PCR reactions were carried out with Phusion® High-Fidelity PCR Master Mix (New England Biolabs) and sequencing libraries were generated using NEBNext Ultra DNA Library Pre ® Kit for Illumina. The library quality was assessed on the Qubit@ 2.0 Fluorometer (Thermo Scientific) and Agilent Bioanalyzer 2100 system. Sequences analysis were performed by Uparse software (Uparse v7.0.1001) (Edgar, 2013). Sequences with ≥97% similarity were assigned to the same OTUs. Representative sequence for each OTU was screened for further annotation. Alpha and Beta diversity analysis were calculated with QIIME2. and displayed with R software (Version 2.15.3). Venn and Flower diagram, Ternary plot as well as were relative abundances also generated [9].

RESULTS AND DISCUSSIONS

The microbial diversity analysis using the Metagenomic method in all soil samples revealed the presence of both Bacteria and Archaea. From Figure 1, which indicates the evolutionary relationships of microorganisms in each phylum and the abundance of microbial groups in the soil samples (D1 – D5) through a phylogenetic tree, various dominant microbial communities were identified (65 phyla, 154 classes, 331 orders, 434 families, 732 genera, and 371 species) such as *Bacillus* and *Alicyclobacillus* (Phylum Firmicutes), *Sphingomonas* (Phylum Proteobacteria), and *Nitrospira* (Phylum Nitrospirota).

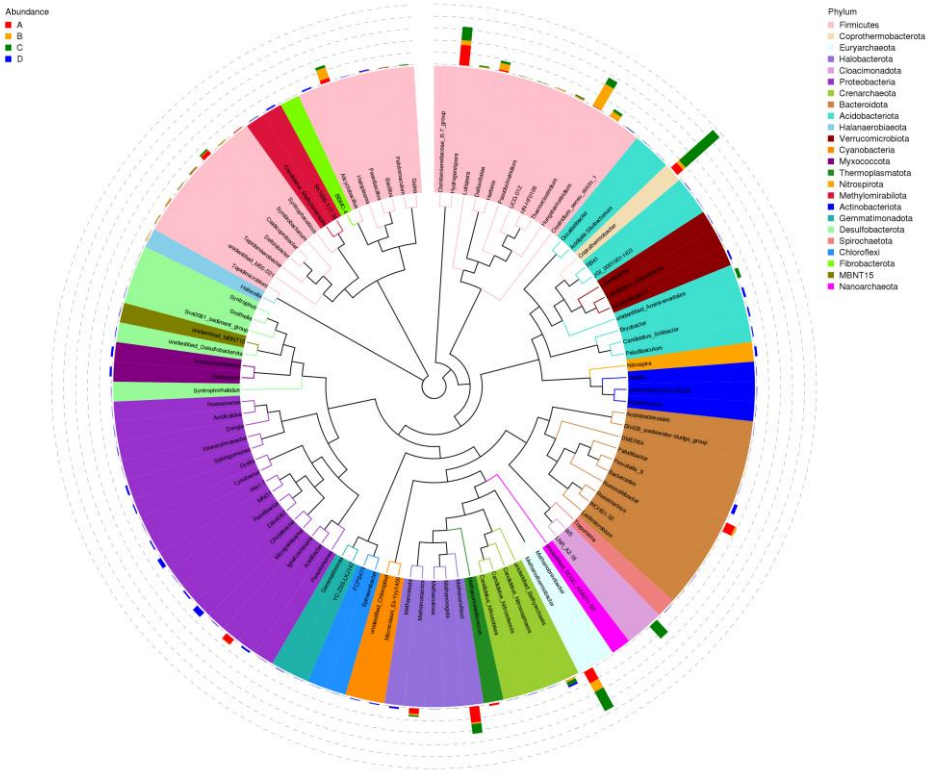


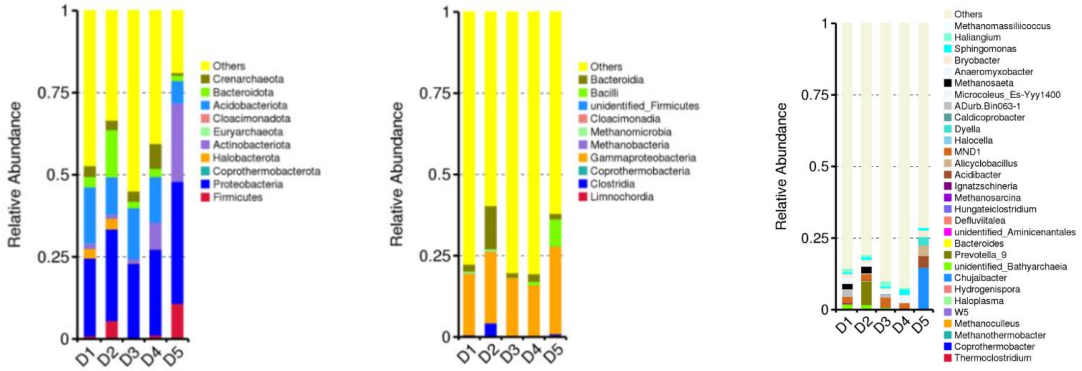
Figure 1 Phylogenetic tree and the abundance of the soil samples (D1 – D5)

The relative abundance of soil samples in Figure 2 have 10 dominant microbial phyla. In control (D1) before BC were applied, Proteobacteria, Acidobacteriota, and Halobacterota were the most abundant microbial phyla. Proteobacteria are functions related to carbon, nitrogen, and sulfur cycling. Acidobacteriota survive in acidic environments and influencing nitrogen, phosphorus, and plant growth dynamics [10]. And Halobacterota,

which is Archaea that survive in high-salinity environments and can promote plant growth [11]. According to the results, the soil from D1 is in extreme condition, which should improve for better microbial growth.

The dominant genus after BC addition (D3) is Ammonia-oxidizing bacterium (MND1) (3.29%). Ammonia-oxidizing bacteria (AOB) plays a role in promoting root cytokinin synthesis that contributes to enhancing plant growth. Additionally, AOB is the primary bacteria in soil nitrification, leading to an increase of release nitrate (NO_3^-) in the soil [12]. The increased abundance of MND1 after BC addition indicates that biochar helps to enhance the population of beneficial soil microorganisms. This coincides with the extended and well-developed root systems observed in the samples where biochar was applied, indicating improved agricultural performance (data not shown).

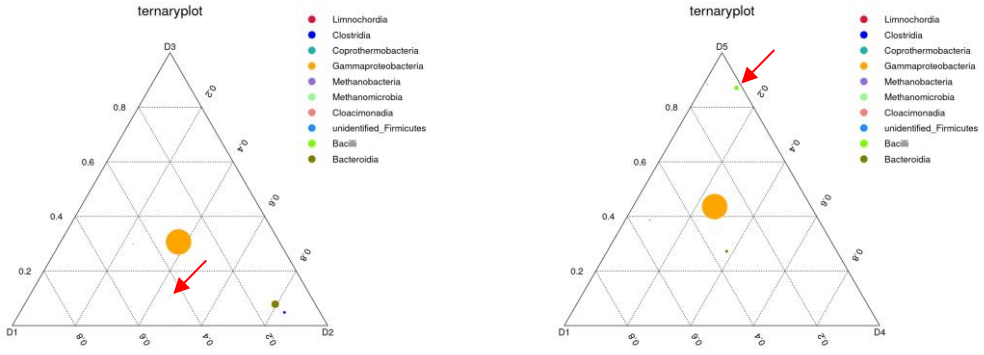
In the areas where modified biochar (BC) were applied (D2-D5), relative abundance results showed an increase in microbial populations, along with new microbial phyla. For instance, *Candidatus* phylum Eremiobacterota (WPS-2), which is commonly found in bare soil environments [13], was detected after the addition of BC. It was found that the Firmicutes population increased in D2, D4 and D5, representing the phylum of BC-associated microorganisms in this study. Actinobacteriota populations significantly increased in D3 and D4. Similarly, a study on clay soil reported an increase in Actinobacteriota after applying biochar at 20 t/m³ [14].



(a) (b) (c)

Figure 2 Relative abundances of major taxonomic groups from soil samples
(a) phylum level (b) class level (c) genus level

In Figure 3 shown that Bacilli (Phylum Firmicutes) is mostly found in D5 (8.34%), D4 (1.06%), D2 (0.18%), D1 (0.18%), and D3 (0.04%) respectively. This can improve the soil microenvironment by modulating the microbial community and soil quality through water and nutrient retention within the soil, as well as reducing soil salinity. Resulting in the enhancement of plant growth and an increase in yield [15]. According to the results, BC used in this study are a mixed culture (*Bacillus* sp.) that found in mostly test areas, it can imply that biochar can retain and maintain the soil-improving microorganisms in varying environmental conditions. Meanwhile, the microbial populations of D3 is decrease due to unsuitable soil conditions for microbial growth.



(a) (b)

Figure 3 Ternary plot of soil samples
(a) D1, D2, D3 (b) D1, D4, D5

These results align with research on biochar and bioorganic fertilizer (BOF) containing *Bacillus* sp., which similarly enhanced microbial diversity in saline-alkaline soil, comparable to the BC used in this study. The study found Actinobacteriota present in soils both with and without biochar and BOF. Moreover, Firmicutes population also increased after biochar or BOF application [16], consistent with the above experimental results.

The research demonstrated that biochar and BOF alter microbial diversity and community structure, with the application of both biochar with BOF resulting in more effective improvements than either biochar or BOF alone [16]. Indicating that the BC addition in this study supports the efficient application of biochar.

The highest microbial diversity is D2 (n=4887), whereas the lowest is D5 (n=1436). In comparison, D2 has higher microbial diversity than D1 (n=4517), shown in Figure 4. Regarding, the above research indicates that biochar significantly enhances soil microbial diversity [6]. Therefore, it can be concluded that biochar has a contribution to increasing microbial diversity. Although this study was a one-time application of biochar and its short-term effects may not have a significant impact on soil bacterial communities, it did enhance certain soil conditions. These improvements included an increase in soil pH, enhanced soil moisture retention, higher concentrations of potassium and phosphorus, and an increase in cation exchange capacity (CEC). However, in terms of the long-term effects of biochar application, Zhang et al. (2022) found that biochar significantly improved soil fertility and increased the relative abundance of Proteobacteria, while the abundance of Acidobacteria decreased.

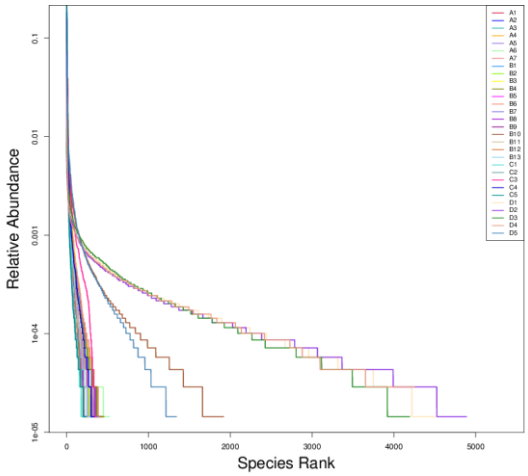


Figure 4 Species Rank showing Relative abundance of soil samples (D1 – D5)

However, there is specificity of microorganisms that depends on the environmental conditions. According to the quantity of microorganisms, as shown in Figure 5, the highest and lowest specifics and differences of microorganisms are D4 (3403 OTUs) and D5 (1280 OTUs) respectively. According to the experimental results, 3 microbial species were found in all soil samples: *Bacillus* sp., *Clostridium* sp. (*Clostridium sensu stricto 1*), and *Arenimonas* sp. In addition, unidentified_Chloroplast was also found in all soil samples, which due to residual genetic material from Cyanobacteriia.

Upon the addition of BC, a significant increase in *Bacillus* sp. was observed in D4 (0.0012054) and D5 (0.0057687) compared to D1 (0.0001722). As D1, D2, and D3 samples are collected from paddy fields, there is a higher correlation in soil microbiomes than D4 and D5 as shown in Figure 5. Conversely, following the addition of BC, changes in microbial diversity were observed, there is no presence identical microorganisms in D2–D3–D4–D5 (0), despite these soil samples are of the same type but cultivated with different plants. This clearly indicates that BC addition contributes to enhancing microbial diversity.

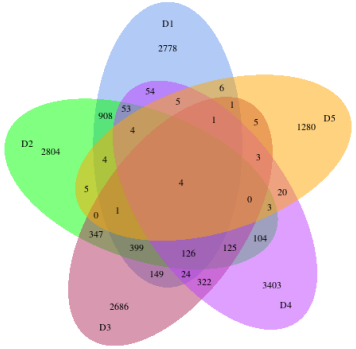


Figure 5 Venn diagram of soil samples

The analysis of enzymes or metabolic pathways can predict soil health and fertility. The functions of various enzymes can refer to a significant role in energy transfer, organic matter breakdown, and nutrient cycling from soil microorganisms. The enhancement of enzyme activity would affect the metabolic pathways of bacteria, leading to several reaction end-products based on their different functional contributions. The results of enzyme analysis from 5 soil samples revealed that D1 contained 10 distinct enzymes and Clusters of Orthologous Groups (COGs). The most abundant enzyme and COG found in D1 were EC:1.6.5.3 and COG0438, respectively. As shown in Table 1, the enzymes that increased after BC addition were EC:2.7.7.7, EC:3.6.4.12, EC:1.6.5.3, EC:2.1.1.72, and EC:1.2.7.11.

EC:2.7.7.7 is directly responsible for DNA synthesis and involved in transferring phosphorus-containing groups, specifically nucleotidyl transferases. EC:3.6.4.12 are also called molecular motors. This enzyme involved in unwinding DNA during DNA replication, DNA repair and recombination, chromosome segregation, and transcription initiation. Recently discovered that DNA helicases may involve in plant DNA recombination, as their abundance becomes prominent during the meiotic prophase of plants [17]. Additionally, DNA helicases is associated with the hydrolysis of phosphoric ester bonds in polynucleotides. EC:1.6.5.3 is an energy-conserving enzyme complex (Complexes I, 1, 2, 3), which is the first phosphorylation site of mitochondria and the respiratory complexes. This enzyme belongs to the hydrolase and amidase groups that are responsible for catalyzing the hydrolysis of the amide bond between the carbonyl group and the nitrogen atom. EC:1.6.5.3 was the most abundant enzyme in samples D1–D4, except for D5. EC:2.1.1.72 is responsible for producing a species-characteristic methylation pattern on adenine residues in a specific short base sequence in the host cell DNA, and is associated with S-adenosylmethionine–protein-arginine N-methyltransferases. And EC:1.2.7.11 is an essential enzyme in microbial one-carbon metabolism, belonging to the 2-oxoacid oxidoreductase group. This enzyme oxidatively decarboxylates different 2-oxoacids to form their CoA derivatives.

The results indicate that the increase in EC:2.7.7.7 reflects an enhancement in DNA synthesis, suggesting that BC contributes to the growth of microbial populations in the soil. Additionally, the higher levels of EC:1.6.5.3 compared to other enzymes demonstrate that the main activity in all soil samples is electron exchange that occurs in the electron transport chain of oxidative phosphorylation.

Table 1 Comparison of prominent enzymes from soil samples

Enzyme Commission (EC) number	Accepted Name	Soil samples				
		D1	D2	D3	D4	D5
EC:2.7.7.7*	DNA-directed DNA polymerase	0.013315	0.013435	0.013768	0.012851	0.012729
EC:3.6.4.12*	DNA helicase	0.011838	0.012217	0.012156	0.011122	0.011131
EC:1.6.5.3*	NADH:ubiquinone reductase	0.014261	0.013716	0.014998	0.014136	0.012556
EC:1.2.7.3	2-oxoglutarate synthase	0.003573	0.003992	0.003460	0.002429	0.001763
EC:2.7.13.3	histidine kinase	0.009984	0.009620	0.010220	0.009129	0.010377
EC:2.7.7.6	DNA-directed RNA polymerase	0.005981	0.005886	0.005858	0.006145	0.005445
EC:3.5.1.28	N-acetylmuramoyl-L-alanine amidase	0.001646	0.001979	0.001638	0.001739	0.002381
EC:5.2.1.8	peptidylprolyl isomerase	0.008104	0.008900	0.007880	0.007046	0.006900
EC:2.1.1.72*	site-specific DNA-methyltransferase (adenine-specific)	0.003819	0.003882	0.004042	0.003782	0.002511
EC:1.2.7.11*	2-oxoacid oxidoreductase (ferredoxin, OFOR)	0.002606	0.002802	0.002557	0.001996	0.001566

Note: (*) The increased enzyme after BC addition.

Interestingly, the analysis of COGs (Table 2) shown that COGs highly increased after BC addition were COG0745, COG1595, and COG1132. COG0745 belongs to the OmpR family and is involved in transcription as a DNA-binding response regulator with REC and winged-helix (wHTH) domains. The abundance of COG0745 increased Obviously in D3 – D5. COG1595 belongs to the sigma24 family and is involved in transcription as a DNA-directed RNA polymerase specialized sigma subunit. The abundance of COG1595 increased in all soil samples after the addition of BC. And COG1132 is a transport protein associated with the ABC-type multidrug and LPS transport system, specifically the ATPase and permease component MsbA. Its abundance increased Obviously in D3 – D5. From the experimental results, the analysis of COGs revealed the metabolic activity and corresponding essential proteins of the bacterial community, with COG1595 identified as a key protein in the soil with BC addition.

Table 2 Comparison of prominent COGs from soil samples

COGs number	Classification	Accepted Name	Soil samples				
			D1	D2	D3	D4	D5
COG0438*	TRANSFERASE	Lipopolysaccharide 1,6-galactosyltransferase	0.006011	0.005790	0.006285	0.005686	0.005220
COG1131	TRANSPORT PROTEIN	Ribosome-associated ATPase	0.003302	0.003157	0.003546	0.003429	0.003814
COG0745	TRANSCRIPTION	DNA-binding response regulator	0.003535	0.003512	0.003603	0.003609	0.004415
COG0642	TRANSFERASE	Signal transduction histidine kinase	0.005481	0.005205	0.005756	0.005157	0.004529
COG1595*	TRANSCRIPTION	DNA-directed RNA polymerase specialized sigma subunit	0.003755	0.003787	0.004022	0.003930	0.004142
COG1132*	TRANSPORT PROTEIN	-	0.002134	0.002103	0.002310	0.002238	0.002301
COG1028	OXIDOREDUCTASE	NAD(P)-dependent dehydrogenase	0.004781	0.004389	0.005080	0.005100	0.005066
COG0451	ISOMERASE	Nucleoside-diphosphate-sugar epimerase	0.004911	0.004375	0.005100	0.004508	0.003938
COG0840	SIGNALING PROTEIN	Methyl-accepting chemotaxis protein (MCP)	0.001795	0.002027	0.001589	0.001252	0.001522
COG1136	MEMBRANE PROTEIN	-	0.002867	0.002682	0.002856	0.002441	0.002435

Note: (*) The increased COGs after BC addition.

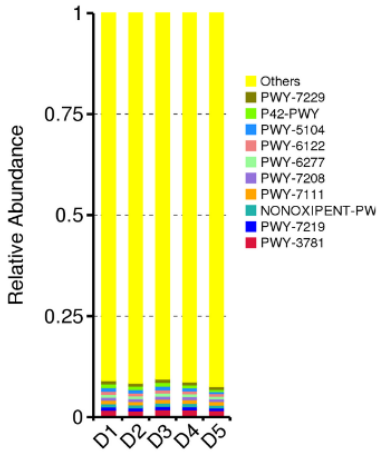


Figure 6 Prediction analysis of metabolic pathways in soil samples

The prediction analysis of metabolic pathways is the analysis within soil samples using PICRUSt2. The most 10 abundant metabolic pathways are shown in Figure 6. According to the metabolic pathway analysis of the samples after BC addition (D3), there was a noticeable increase in the proportion of metabolic pathways compared to the control without BC (D1). The most abundant metabolic pathway found in all samples was PWY-3781, or Aerobic Respiration I (cytochrome c). PWY-3781 is an aerobic respiration pathway that parallels the transport of electrons from the oxidation of NADH, leading to ATP synthesis. This metabolic pathway is performed in plants, animals, and some bacteria via complexes I-IV. Complex I accepts NADH, while complex II accepts the TCA cycle intermediate succinate. The flow of electrons causes protons to be pumped from the matrix side to the intermembrane space, creating a proton gradient. These protons then flow back through the ATP-synthesizing complex in the mitochondrial or bacterial inner membrane, resulting in ATP synthesis. In microorganisms, NADH:ubiquinone oxidoreductases can also catalyze the reoxidation of cytosolic NADH to regenerate NAD^+ such as *Saccharomyces cerevisiae* [1 8 -2 1]. This is consistent with the above experimental results that showed the presence of EC:1.6.5.3 (Table 1).

Moreover, the metabolic pathways that increased after BC addition were PWY-7111, PWY-6277, and PWY-6122. PWY-7111 is the Pyruvate Fermentation to Isobutanol (engineered) pathway, where isobutanol is a higher alcohol and a by-product of yeast fermentation. This metabolic pathway is commonly engineered in microbial hosts such as *Saccharomyces cerevisiae*, *Escherichia coli*, and *Bacillus subtilis*. In this pathway, the last two reactions of the Ehrlich pathway are combined with the pathway for valine biosynthesis from pyruvate through the mutual intermediate 3-methyl-2-oxobutanoate to produce isobutanol [2 2 , 2 3]. PWY-6277 is the superpathway of 5-aminoimidazole ribonucleotide (AIR) biosynthesis. This metabolic pathway's end product is

5-amino-1-(5-phospho-β-D-ribosyl)imidazole (AIR), which is a key intermediate in the biosynthesis of purine nucleotides and thiamine. AIR is synthesized from 5-phospho-α-D-ribose 1-diphosphate (PRPP) through 5 steps. PWY-6122 is the 5-aminoimidazole ribonucleotide biosynthesis II pathway, which parallels the PWY-6277 as it also produces AIR as the end product. However, this metabolic pathway is found in *E. coli*, as the third step is catalyzed by a different enzyme compared to PWY-6277. The metabolic pathways that increased after BC addition are associated with the production of various compounds, such as isobutanol and AIR.

According to the results, both the abundance of soil microbiome and microbial diversity were observed, along with the effectiveness of BC on soil microorganisms. Additionally, enzymes and metabolic pathways were observed as well. By examining the changes in metabolic pathways, several observations can be used for further research, such as soil quality, microbial activity and diversity, as well as soil enzyme activity. The results indicate that BC contributed to increasing microbial diversity and populations in soil, leading to enhanced microbial activity and an increase in enzyme quantities, which are linked to important metabolic pathways that promote plant growth and soil quality. However, the scope of the research is limited in terms of the range of biochar addition and the investigation of long-term effects and beneficial microorganisms, so further studies are required within this context.

CONCLUSION

The microbial diversity analysis results of soil samples (D1-D5) revealed 65 phyla, 154 classes, 331 orders, 434 families, 732 genera, and 371 species. Before the addition of BC (D1), Proteobacteria, Acidobacteriota, and Halobacterota were the most abundant microbial phyla, indicating that the soil was in an extreme condition. Regarding the soil after the addition of BC (D2-D5), there was an increase in the populations of Firmicutes and Actinobacteriota, along with new microbial phyla, such as WPS-2, and dominant genera, such as ammonia-oxidizing bacterium (MND1) (3.29%), which is a primary bacterium in soil nitrification.

Additionally, Bacilli have been found as well (D5 (8.34%), D4 (1.06%), D2 (0.18%), D1 (0.18%), and D3 (0.04%)), which are microorganisms that can improve the soil microenvironment. *Bacillus* sp. was observed in D4 (0.12%) and D5 (0.58%) compared to D1 (0.02%). Since BC used in this study is a mixed culture of *Bacillus* sp., it can be implied that biochar can retain and maintain soil-improving microorganisms under varying environmental conditions and also indicates that biochar helps to enhance the population of beneficial soil microorganisms. The results showed that the highest microbial diversity is in D2 (n=4887), which is higher than in D1 (n=4517). Therefore, it can be concluded that BC contributes to increasing microbial diversity. And also found that D4 (3403 OTUs) has the highest specifics and differences in microbiome.

Moreover, COG1595 is a key protein in the soil after BC addition, and it was also found that enzymes, including EC:2.7.7.7 and EC:1.6.5.3, increased after BC addition. This increase suggests that BC contributes to the enhancement of DNA synthesis, leading to an increase in microbial populations in the soil. Furthermore, the main activity of the soil microbiome involves electron exchange, which occurs in the electron transport chain of oxidative phosphorylation.

The most prominent metabolic pathway is PWY-3781 (Aerobic Respiration I (cytochrome c)), which aligns with the presence of EC:1.6.5.3. After the addition of BC (D3), several metabolic pathways increased compared to the control without BC (D1). The metabolic pathways that increased include PWY-7111, PWY-6277, and PWY-6122. In conclusion, biochar can support soil-improving microorganisms and increase microbial populations that enhance microbial activity, resulting in greater microbial diversity and improved soil fertility, which in turn supports better plant health and growth.

ACKNOWLEDGEMENT

This research was financially supported by the Fundamental Fund in the year 2024 no. MJU 1-67-08-002.

REFERENCE

[1] Rizwan, M., et al., *Mechanisms of biochar-mediated alleviation of toxicity of trace elements in plants: a critical review.* Environ Sci Pollut Res Int, 2016. **23**(3): p. 2230-48.

[2] Kaetzl, K., et al., *Slow sand filtration of raw wastewater using biochar as an alternative filtration media.* Scientific Reports, 2020. **10**: p. 1229.

[3] Yang, W., et al., *Adsorption of copper(II) and lead(II) from seawater using hydrothermal biochar derived from Enteromorpha.* Mar Pollut Bull, 2019. **149**: p. 110586.

[4] Park, J.-H., et al., *Adsorption/desorption behavior of cationic and anionic dyes by biochars prepared at normal and high pyrolysis temperatures.* Colloids and Surfaces A: Physicochemical and Engineering Aspects, 2019. **572**.

[5] Carter, S., et al., *The Impact of Biochar Application on Soil Properties and Plant Growth of Pot Grown Lettuce (Lactuca sativa) and Cabbage (Brassica chinensis).* Agronomy, 2013. **3**: p. 404-418.

[6] Xu, W., et al., *Global meta-analysis reveals positive effects of biochar on soil microbial diversity.* Geoderma, 2023. **436**: p. 116528.

[7] Gebisa, L., *Effects of Biochar Application on Beneficial Soil Organism Review*. 2018.

[8] Pokharel, P., Z. Ma, and S. Chang, *Biochar increases soil microbial biomass with changes in extra- and intracellular enzyme activities: a global meta-analysis.* Biochar, 2020. **2**.

[9] Edgar, R.C., *UPARSE: highly accurate OTU sequences from microbial amplicon reads.* Nature Methods, 2013. **10**(10): p. 996-998.

[10] Gonçalves, O.S., et al., *Insights into plant interactions and the biogeochemical role of the globally widespread Acidobacteriota phylum.* Soil Biology and Biochemistry, 2024. **192**: p. 109369.

[11] Hernández-Canseco, J., et al., *Plant Growth-Promoting Halobacteria and Their Ability to Protect Crops from Abiotic Stress: An Eco-Friendly Alternative for Saline Soils.* Agronomy, 2022. **12**(4): p. 804.

[12] Wang, X.-L., et al., *Unveiling the dual role of heterotrophic ammonia-oxidizing bacteria: enhancing plant regrowth through modulating cytokinin delivery.* Frontiers in Microbiology, 2023. **14**.

[13] Sheremet, A., et al., *Ecological and genomic analyses of candidate phylum WPS-2 bacteria in an unvegetated soil.* Environ Microbiol, 2020. **22**(8): p. 3143-3157.

[14] Zhang, J. and J.-L. Shen, *Effects of biochar on soil microbial diversity and community structure in clay soil.* Annals of Microbiology, 2022. **72**(1): p. 35.

[15] Xia, H., et al., *Study of the mechanism by which Bacillus subtilis improves the soil bacterial community environment in severely saline-alkali cotton fields.* Science of The Total Environment, 2025. **958**: p. 178000.

[16] Gu, Y.-y., et al., *Effect of biochar and bioorganic fertilizer on the microbial diversity in the rhizosphere soil of Sesbania cannabina in saline-alkaline soil.* Frontiers in Microbiology, 2023. **14**.

[17] Sarwat, M. and N. Tuteja, *Chapter 7 - DNA Helicase-Mediated Abiotic Stress Tolerance in Plants*, in *Biochemical, Physiological and Molecular Avenues for Combating Abiotic Stress Tolerance in Plants*, S.H. Wani, Editor. 2018, Academic Press. p. 103-115.

[18] Feng, Y., et al., *Structural insight into the type-II mitochondrial NADH dehydrogenases.* Nature, 2012. **491**(7424): p. 478-82.

[19] Marres, C.A., S. de Vries, and L.A. Grivell, *Isolation and inactivation of the nuclear gene encoding the rotenone-insensitive internal NADH: ubiquinone oxidoreductase of mitochondria from Saccharomyces cerevisiae.* Eur J Biochem, 1991. **195**(3): p. 857-62.

[20] Luttik, M.A., et al., *The Saccharomyces cerevisiae NDE1 and NDE2 genes encode separate mitochondrial NADH dehydrogenases catalyzing the oxidation of cytosolic NADH.* J Biol Chem, 1998. **273**(38): p. 24529-34.

[21] Small, W.C. and L. McAlister-Henn, *Identification of a cytosolically directed NADH dehydrogenase in mitochondria of Saccharomyces cerevisiae.* J Bacteriol, 1998. **180**(16): p. 4051-5.

[22] Savrasova, E.A., et al., *Use of the valine biosynthetic pathway to convert glucose into isobutanol.* J Ind Microbiol Biotechnol, 2011. **38**(9): p. 1287-94.

[23] Blombach, B. and B.J. Eikmanns, *Current knowledge on isobutanol production with Escherichia coli, Bacillus subtilis and Corynebacterium glutamicum.* Bioeng Bugs, 2011. **2**(6): p. 346-50.

20R4-10

Promoting Sustainable Waste Management in Coffee Shops: A Case Study of Chiang Mai

Phimlapat Jenjai[1] and Sarunnoud Phuphisith[2*]

[1] Graduate student, Gruduate School, Chiang Mai University; [2] Assistant Professor, Department of Environmental Engineering, Faculty of Engineering, Chiang Mai University, Chiang Mai 50200, Thailand.
[*]Phone :+66 53 94 4192, E-mail : sarunnoud.p@cmu.ac.th

ABSTRACT

This study explored waste generation and its management practices in coffee shops, focusing on spent coffee grounds (SCG) and single-use packaging. Fifty coffee shops in Mueang District, Chiang Mai Province, Thailand, were interviewed using a semi-structured questionnaire for SCG disposal methods, packaging usage, and environmental strategies. Of the fifty shops interviewed, 66% fell into the micro-enterprise category, while the remaining 34% were small enterprises. The results showed that the daily average SCG generation was 3.57 ± 2.05 kg per shop. Most shops separated SCG from general waste, of which 28% discarded them to landfills. PET and paper cups were commonly used. PET cups were mostly found with a printed screen design. Shop size and service strategies also affected waste generation. The findings underline the opportunities to encourage the repurposing of SCG in the city, foster sustainable packaging, and raise environmental awareness. Future policies should incorporate behavioral segmentation and provide stronger support for sustainable production and consumption.

Keywords: coffee shop, spent coffee grounds, waste management, GHG emissions, sustainable packaging

INTRODUCTION

Coffee is one of the most popular beverages worldwide, leading to a global issue related to food waste generation [1]. Coffee shop sustainability depends on various factors, including waste management practices and entrepreneurs' perspectives on reducing environmental impact [2]. Spent coffee grounds (SCG) is one crucial waste generated as the most common biomass waste [1]. Common management methods of SCG include incineration and sanitary landfilling, but these methods result in resource loss and environmental pollution [3]. SCG is a nutrient-rich resource that can be repurposed and other value-added applications, including composting, raw materials for bioplastics, and biorefinery [4]. Recent studies highlight the potential of SCG in contributing to circular bioeconomy strategies by converting organic waste into high-value products through biorefinery technologies [5]. However, the practical implementation of such sustainable approaches at the local level particularly among small-scale coffee businesses remains limited [4]. Factors such as lack of infrastructure, logistical constraints, and insufficient awareness among shop owners hinder the reuse of SCG [3]. Although the reuse of SCG in small-scale operations is still emerging, academic studies have demonstrated that SCG possess versatile properties such as richness in polysaccharides, proteins, phenolics, and lipids which make them suitable for low-cost valorization pathways including composting, bioadsorbents, and incorporation into biocomposite materials [4], [5]. These approaches align with circular economy principles and offer promising routes for sustainable waste management even at the community level. Promoting small-scale SCG valorization, especially in coffee shops, can therefore offer an environmentally responsible waste management alternative while supporting broader sustainability goals. In this context, exploring the current SCG disposal practices of local coffee shops can provide insights into their awareness and readiness for adopting more circular and sustainable waste management models.

Single-use packaging is another important waste generated from coffee shops. In 2023, Thailand generated approximately 3.03 million tons of single-use plastic waste per year, accounting for 11.25% of municipal solid waste. About 25% of plastic waste was recycled or repurposed, while 72% was disposed of through landfill along with other municipal waste. Additionally, 3% of the plastic waste remained unmanaged and accumulated in the environment [6]. Improper disposal or negligence in managing plastic waste contributes to environmental pollution and greenhouse gas emissions, further exacerbating the global climate crisis. Plastic cups, which are widely used in takeaway beverage services, constitute a significant portion of single-use plastic waste. Despite being technically recyclable, plastic cups are rarely collected and recycled in practice. This is largely due to contamination from leftover beverages, the lightweight and bulky

nature of the cups, and their low resale value factors that make collection and processing economically unviable for most recycling businesses. Additionally, plastic cups are often made from various plastic types. When mixed in unsorted waste streams, they require costly separation processes. The lack of source separated waste in communities further reduces the recyclability of these materials [7]. As a result, plastic cups are typically disposed of through landfilling or informal dumping, contributing to long-term environmental degradation and resource inefficiency.

Coffee is a major economic crop in Chiang Mai, benefiting from its favorable climate. As a result, the province has been designated as a target area under the Bio-Circular-Green model to enhance coffee production efficiency, increase its value, and promote sustainability in an environmentally friendly manner [8]. Additionally, the government has introduced policies to establish Chiang Mai as a "City of Coffee", recognizing its rapid growth and the widespread presence of coffee shops offering diverse service models [9]. This study aimed to explore the sustainability of waste management in coffee shops in Mueang District, Chiang Mai, focusing on SCG and single-use packaging waste. The objectives included assessing the current disposal practices, comparing waste generation by enterprise size, and estimating a city-wide environmental impact in terms of greenhouse gas emissions from the current disposal practices. The findings of the present study could support ways towards a more sustainable and circular waste management practices within the local coffee sector.

METHODOLOGY

2.1 Data Collection

Face-to-face interviews were conducted with 50 coffee shops in Mueang District, Chiang Mai Province, as illustrated in **Figure 1,** from December 2024 to January 2025. The interviews were structured using a questionnaire consisting of four sections: 1) general shop information 2) SCG generation and its waste management 3) types of packaging use and their waste management 4) promotion and service strategies that related to waste reduction initiatives. The strategies included (a) a promotion or discount for bringing own reusable cups, (b) offering plastic bags for orders, (c) offering paper bags for orders, (d) providing waste separation bins in the service areas.

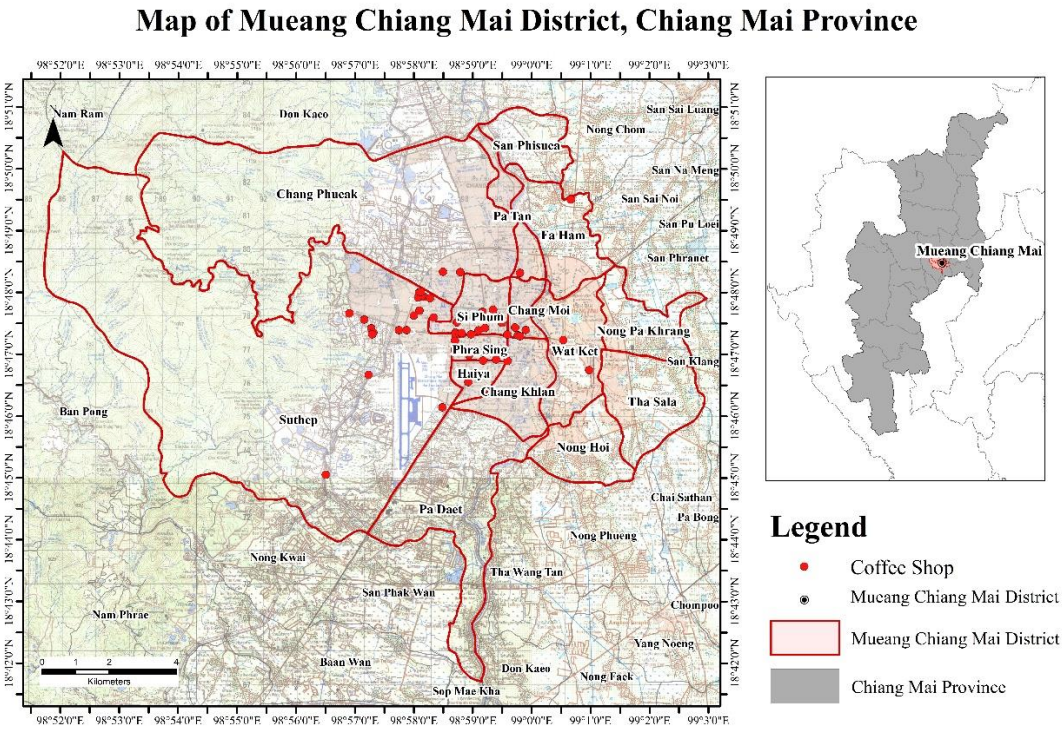


Figure 1 Locations of the interviewed coffee shops in Mueang Chiang Mai District, Chiang Mai Province (created by ArcMap version 10.7.1)

2.2 Data Analysis

All data analyses were conducted using Microsoft Excel version 2501. Descriptive analysis was conducted to explore observable trends and patterns in waste generation and sustainability practices. A comparison was made among the interviewed shops. The study categorized coffee shops into two enterprise sizes based on the number of employees classification: micro enterprises and small enterprises. A micro enterprise is defined as a business with no more than five employees, and a small enterprise employs no more than 30 individuals [10].

Furthermore, the emission of greenhouse gas (GHG) was estimated for the current waste management and anticipated for Chiang Mai province, using Equation (1).

$$GHG\ emission = W \times EF \quad (1)$$

Where, GHG emission is the emission from landfilling ($kgCO_2e$/day), W is a total weight of waste generated per day (kg/day), and EF is the emission factor of landfilling adapted from TGO, 2022 [11]. EF = 2.53 tCO_2e/t for SCG and EF = 2.93 tCO_2e/t for paper cup. The average values of waste generated from the surveyed shops were used to estimate total daily waste generation and GHG emissions for Chiang Mai Province. The total number of registered coffee shops in Chiang Mai province was extracted from OpenStreetMap. As of 25 January, there were 719 shops.

RESULTS AND DISCUSSIONS

1. Daily SCG generation and waste management

About 56% of the interviewees were males, had an average age of 35.1 ± 7.3 years old, 80% held a bachelor's degree, and 70% of the interviewees were business owners. About 66% of the interviewed shops were classified as size micro-enterprises.

The daily average SCG generation was 3.57 ± 2.05 kg per shop, or 0.04 ± 0.01 kg per cup sold. The small enterprises produced a larger average of 4.32 ± 2.00 kg per shop than the micro enterprises, generated an average of 3.18 ± 1.99 kg per shop. However, the difference was not significant (t-test = 1.918, n_1 = 33, n_2 =17, $p > 0.05$).

The study by Filimonau et al. (2019) reported that larger-scale coffee shops tend to generate more food waste due to broader menus and higher service intensity [12]. Furthermore, the environmental behavior of coffee shop operators, including their awareness and engagement with waste issues, plays a critical role in determining waste management practices [2]. These insights suggest that beyond enterprise size, behavioral and managerial factors are essential to shaping sustainability outcomes in the coffee sector.

Regarding SCG management, most shops (84%) separated SCG from general waste. Of this number, about 28% was solely disposed of for municipal solid waste collection, another 28% was given away for free to others, another 28% was utilized, and 16% was sold to others, as shown in **Figure 2**. The interviews showed that coffee shop owners and operators were aware of the value of SCG, which can be utilized in various applications. The common answers included using SCG as a soil conditioning, an ingredient of soap or exfoliating scrubs, and a deodorizer. Despite a considerable amount of SCG being generated daily, 28% of the shops disposed of it to landfills affecting GHG emission contribution.

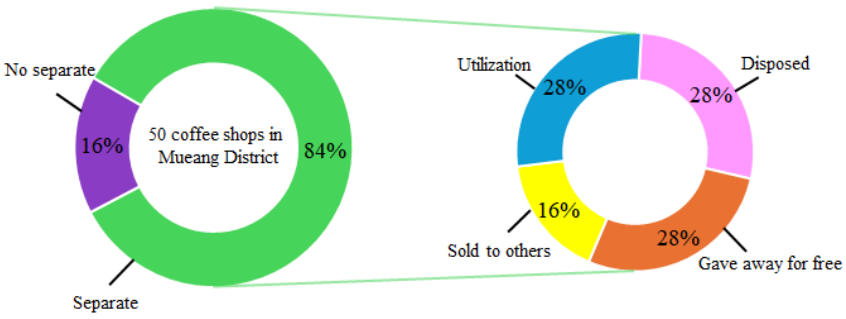


Figure 2 Disposal and utilization of SCG

2. Packaging use and waste management practices

The study categorized packaging use based on service types. For the eat-in service, the ceramic cup was the most used (90%) among the interviewed shops, followed by glass (60%), and Polyethylene Terephthalate (PET) plastic cups (40%), as shown in **Figure 3**. For takeaway orders, 94% of the shops offered PET plastic cups, 86% double-wall paper cups, and 4% corrugated paper cups. The result indicates that while ceramic and glass cups were commonly available for dine-in customers, PET plastic cups remain the dominant choice for takeaway, highlighting the reliance on single-use packaging in coffee shops.

All interviewed shops offered straws, of which 90% offered conventional plastic straws, and 10% provided biodegradable alternatives. The study categorized lid use based on menu types. All lids used for iced coffee were made from 100% PET plastic. Lids used for hot coffee included 46% Polystyrene (PS), 32% Polypropylene (PP), and 16% Polylactide (PLA), providing biodegradable alternatives.

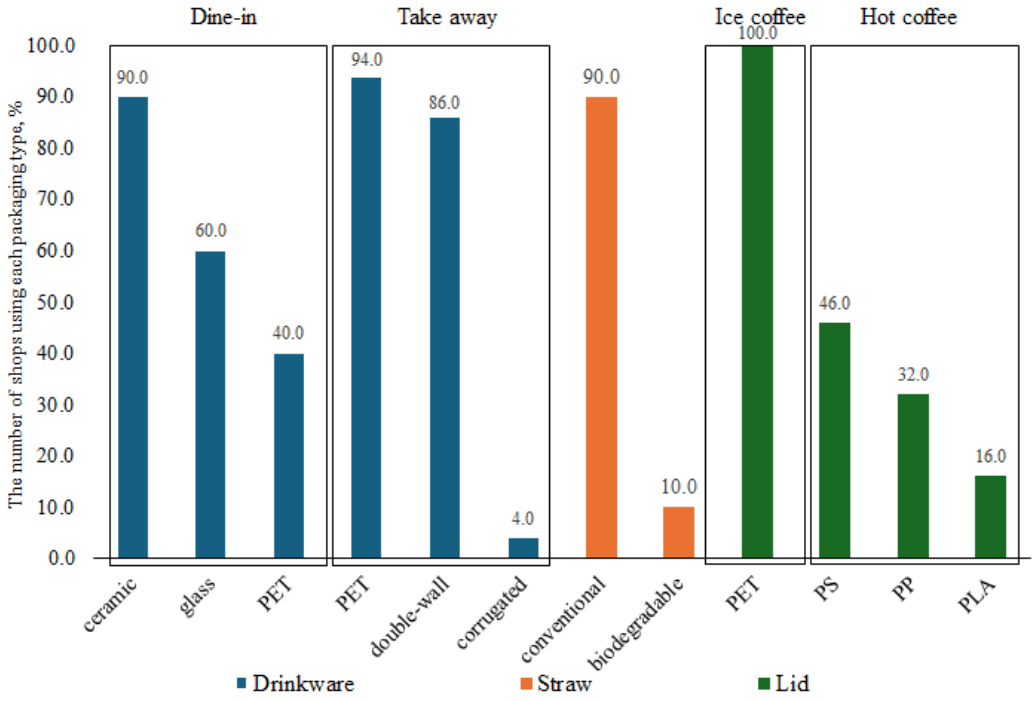


Figure 3 Types of packaging used in the interviewed coffee shops

The interview showed that 54% of the shops did not separate waste before disposal and disposed of it to a municipal waste management service. The remaining 46% implemented waste separation: 32% disposed of the separated waste to the municipal waste management service, and 14% sold the recyclables to waste buyers.

Although PET plastic cups are recyclable, the survey found that PET cups were often neglected by the waste buyers due to food contamination and printed screens on the plastic cups. About 82% of the interviewed shops served their drinks in printed screen cups. The printed screens reduce PET recycling value. To enhance recyclability, eliminating printed designs on PET cups should be promoted and environmental-friendly design and consumer awareness should be called for when choosing environmentally-friendly products.

Considering the single-use packaging consumption, micro enterprises used an average of 48.55 ± 37.96 PET cups per day and 10.94 ± 17.88 paper cups per day, while small enterprises used 47.65 ± 40.28 PET cups per day and 6.41 ± 7.62 paper cups per day.

3. Promotion and service strategies

About 30% of the interviewed shops offered discounts to customers who bring their reusable cups. The limited adoption reasons included the shops already setting low prices and hygienic concerns.

Most of the shops (86%) provided plastic bags for takeaway orders, and 28% offered paper bags as an alternative. The widespread use of single-use bags contributes to unnecessary waste, often driven by customer demand. This presents an opportunity to emphasize the need to reduce reliance on single-use

packaging. Encouraging both consumers and coffee shop operators to be more aware of sustainable consumption could mitigate unnecessary waste generation.

Regarding the provision of waste bins, 66% of the interviewed shops had no waste bin in their service areas, while 32% provided a mixed-waste type bin, and only 2% offered various bins for waste segregation. The survey suggests that most coffee shops lack effective waste management practices for packaging disposal. Government agencies must play a more active and structured role in plastic waste management. This includes establishing clear regulations that mandate waste segregation at source, providing financial or tax incentives for businesses adopting sustainable packaging, enforcing producer responsibility schemes, and investing in public recycling infrastructure. The absence of legally binding requirements for plastic waste separation and recycling in Thailand has hindered long-term progress. Therefore, comprehensive policy frameworks and effective enforcement mechanisms are essential to support sustainable practices and reduce environmental impacts.

4. GHG emissions from SCG and packaging management

Based on the average SCG generated from the interviewed coffee shops in the present study, the total amount of SCG generated is estimated at 2,5667 kg per day. If all SCG were to be disposed of through landfilling, the resulting GHG emissions from SCG daily greenhouse gas emissions were calculated as approximately 6,494 kg CO_2e per day. However, according to the current SCG management practices identified in the survey, 28% of SCG was landfilled, leading to a daily emission of 1,818 kg CO_2e. It is important to note that the total number of coffee shops considered in the estimation is limited to those registered as coffee shops, not including restaurants that may offer coffee.

In addition to organic waste, packaging waste from single-use cups was also assessed. On average, each coffee shop generated approximately 0.72 kg of PET cups and 0.11 kg of paper cups per day. When extrapolated to the provincial level, this corresponds to an estimated total of 520 kg of PET cups and 81 kg of paper cups per day. As a result of the interview, PET and paper cups were currently disposed of through municipal landfill systems. Considering the GHG emission due to paper cup decomposition in landfill, an estimated GHG emission was about 238 kg CO_2e per day.

Although PET cups resist to biodegradation limiting the GHG effect, they present substantial and long-lasting environmental challenges. PET is a highly durable material, capable of persisting in terrestrial and marine environments for several centuries, with estimates ranging up to 450–500 years before complete degradation [13]. PET is technically recyclable, its environmental benefits have been significantly constrained by low collection rates, contamination issues, and the lack of effective recycling infrastructure in many regions. In most cases, PET packaging including disposable cups is designed for short-lived applications and discarded within a year of production. Despite its recyclability, practical limitations such as inadequate sorting technologies, insufficient source separation, lack of public awareness, and logistical inefficiencies have hindered the successful diversion of PET waste from landfills [14]. These systemic barriers not only undermine the effectiveness of current recycling efforts but also reflect the broader unsustainability of prevailing plastic use patterns particularly in regions where circular economy policies are still in their infancy. These factors highlight the need for more effective upstream strategies including plastic reduction, reuse systems, and improvements in circular economy infrastructure to mitigate the long-term ecological impacts of PET plastic cups.

The findings from this study reveal critical insights into the relationship between enterprise characteristics and waste generation patterns in Chiang Mai's coffee sector. While small enterprises produced more SCG on average, micro enterprises tended to use more single-use plastic and paper cups. This contrast may stem from differences in operational models, customer service styles, or consumption habits. Moreover, extrapolating the results to a city-wide scale emphasizes the significance of even small daily emissions: about 2.5 metric tons of CO_2e per day, primarily from SCG, could be reduced through valorization strategies such as composting or biochar production.

Further support the conclusion that entrepreneurs' awareness and environmental values significantly affect waste management outcomes. These insights indicate that policy interventions should target not only physical infrastructure but also mindset and behavior through education and incentives. [2]

CONCLUSION

This study examined waste management in coffee shops in Mueang District, Chiang Mai, focusing on spent coffee grounds and single-use packaging. While most shops separated SCG from general waste, only a portion was effectively reused. PET and paper cups were widely used among micro and small enterprises. As crucial waste generated from coffee shops, SCG showed a significant source of GHG emissions by landfilling managed and the persistence of PET cups in the environment raises long-term concerns. Extrapolating these findings to the city-wide level reveals that Chiang Mai's coffee sector may contribute approximately 2,056 kg CO_2e per day and 3,168 kg of total waste daily, highlighting the cumulative environmental burden. Adopting the repurposing strategies can significantly reduce waste and GHG emissions from landfills, contributing to environmental sustainability. Importantly, behavioral differences such as reuse awareness and service models appeared to shape waste generation patterns more strongly than enterprise size alone. To address this, both shop-level and policy-level strategies are needed, including support for composting, reusable packaging, waste separation, and sustainable design. Strengthening regulatory enforcement, incentivizing waste reduction strategies, and investing in recycling infrastructure are crucial steps toward achieving sustainable urban waste management.

ACKNOWLEDGEMENT

The author is profoundly grateful for the support from the Graduate School, Chiang Mai University. The author also wishes to acknowledge the Faculty of Engineering and the Department of Environmental Engineering, Chiang Mai University, for their academic guidance and continued support throughout this study. Appreciation is further extended to the coffee shop owners in Mueang District, Chiang Mai, for their cooperation and for providing the data used in this research.

REFERENCE

[1] Garcia, C.V. and Kim, Y.-T. 2021. Spent Coffee Grounds and Coffee Silverskin as Potential Materials for Packaging: A Review. Journal of Polymers and the Environment. 29(6): 2372–2384.

[2] Alfarizi, M., Samputra, P.L. and Arista, N.I.D. 2023. Role of entrepreneur's perspective of waste management for coffee shop sustainability. Problems and Perspectives in Management. 21(4): 502–515.

[3] Zhao, S., Wang, T., Zhu, L., Xu, P., Wang, X., Gao, L. and Li, D. 2019. Analysis of suspended microplastics in the Changjiang Estuary: Implications for riverine plastic load to the ocean. Water Research. 161: 560–569.

[4] Franca, A.S. and Oliveira, L.S. 2022. Potential Uses of Spent Coffee Grounds in the Food Industry. Foods. 11(14): 2064.

[5] Banu, J.R., Kavitha, S., Kanna, R.Y., Kumar, M.D., Preethi, A., Atabani, A.E. and Kumar, G. 2020. Biorefinery of spent coffee grounds waste: Viable pathway towards circular bioeconomy. Bioresource Technology. 302: 122821.

[6] Pollution Control Department, Ministry of Natural Resources and Environment. 2024. Thailand State of Pollution Report 2023. Available at: https://www.pcd.go.th/publication (Accessed: 15 February 2025).

[7] Pollution Control Department, Ministry of Natural Resources and Environment. 2018. Thailand's Roadmap on Plastic Waste Management 2018–2030. Available at: https://www.pcd.go.th/garbage/ (Accessed: 2 April 2025).

[8] Chiang Mai Provincial Agriculture and Cooperatives Office, Office of the Permanent Secretary for Ministry of Agriculture and Cooperatives. 2024. Chiang Mai Provincial Development Plan (2023-2027). Available at: https://www.opsmoac.go.th/chiangmai (Accessed: 15 February 2025).

[9] Siri, R. 2022. International tourist perception on coffee shop in Chiang Mai, Thailand. MFU Connexion. 6(2): 232-262.

[10] Office of Small and Medium Enterprises Promotion (OSMEP). 2019. Ministerial Regulation on the Definition of Micro, Small and Medium Enterprises B.E. 2019. Available at: https://www.sme.go.th/uploads/file/download-20201118145003.pdf (Accessed: 2 April 2025).

[11] Thailand Greenhouse Gas Management Organization (Public Organization). 2022. Guidelines for Carbon Footprint Calculation and Reporting for Organizations (8th edition, 6th revision). Available at: https://www.tgo.or.th (Accessed: 6 April 2025).

[12] Filimonau, V., Krivcova, M. and Pettit, F. 2019. An exploratory study of managerial approaches to food waste mitigation in coffee shops. International Journal of Hospitality Management. 76: 48–57.

[13] Andrady, A.L. 2011. Microplastics in the marine environment. Marine Pollution Bulletin. 62(8): 1596–1605.

[14] Hopewell, J., Dvorak, R. and Kosior, E. 2009. Plastics recycling: challenges and opportunities. Philosophical Transactions of the Royal Society B: Biological Sciences. 364(1526): 2115–2126.

20R4-11

Performance of Low-Temperature Thermal Desorption on Drilling Waste Treatment and Recovery

Sotheara Huor[1], Thaksina Poyai[2], Ratchanan Chamnanmor[3], Saret Bun[4] and Pisut Painmanakul[5,6,7*]

[1]Master student ,[3]Doctoral student; [5]Professor, Department of Environmental and Sustainable Engineering, Faculty of Engineering, Chulalongkorn University, Bangkok 10330, Thailand

[2]Lecturer, Department of Environmental Engineering, Faculty of Engineering, Kasetsart University, Bangkok 10900, Thailand

[4]Professor, Water and Environmental Engineering, Faculty of Hydrology and Water Resources Engineering, Institute of Technology of Cambodia, Phnom Penh, Cambodia

[6]Director, Carbon Institute for Sustainability, Chulalongkorn University, Bangkok 10330, Thailand

[7]Professor, Center of Excellence in Treatment Technology and Management of Petroleum Contaminants and Environmental Pollution, Chulalongkorn University, Bangkok 10330, Thailand

[*]Phone: (66) 08 9413 1392, E-mail: sothearahuor56@gmail.com

ABSTRACT

The oil and gas industry plays a vital role in global energy supply, with drilling operations generating significant waste, particularly contaminated drilling mud. Improper disposal of this waste poses serious environmental and health risks due to hazardous components like hydrocarbons and chemical additives. To address the issue, this study aims to evaluate the effectiveness of low-temperature thermal desorption (LTTD) in drilling mud treatment and recovery, enhancing contaminant reduction and material recovery. A 2-liter single-layer glass reactor was used to treat authentic drilling mud at different temperatures. In the thermal desorption process, 600 milliliters of well-mixed drilling mud were gradually heated from room temperature up to 300°C in incremental steps (150°C, 200°C, 250°C, and 300°C). Oil recovery was monitored at each stage, with heating continued until no further increase in recovered oil volume was observed, ensuring maximum extraction efficiency. Proximate and ultimate analyses were conducted to determine the composition and energy content of the drilling mud, while gas chromatography-mass spectrometry (GC-MS) was used to evaluate hydrocarbon recovery. Thermogravimetric analysis (TGA) monitored thermal stability and decomposition behavior, providing comprehensive insights into the effectiveness of the thermal desorption process. The results demonstrated high volatile content and substantial heating value of the drilling mud sample, with GC-MS and TGA confirming effective hydrocarbon release below 300°C. Oil recovered at 100–150°C consisted of light hydrocarbons and alcohols, indicating early volatile removal. At 200–250°C, mid-weight hydrocarbons like C14–C19 became dominant, showing improved recovery. The heaviest fractions and highest alkane content were extracted at 250–300°C, confirming it as optimal for desorption. Furthermore, X-ray diffraction (XRD) analysis indicated that key minerals of drilling mud fine particles remained structurally stable after treatment. These findings suggest the practicality of LTTD in drilling waste treatment and hydrocarbon recovery, preventing environmental damage and aligning with the circular economy.

Keywords: Drilling waste, Thermal treatment, Petroleum hydrocarbons, Resource recovery

INTRODUCTION

The oil and gas industry plays a vital role in the global economy by supplying essential energy sources such as gasoline, diesel, and jet fuel, which support transportation, heating, and electricity generation. In addition to its energy contributions, the industry significantly influences economic development and infrastructure growth. Onshore drilling operations begin with site preparation, including geological surveys and permitting, followed by the construction of a drilling rig to establish the wellbore. Throughout the drilling process, drilling fluids are circulated to cool the drill bit, transport cuttings, and maintain borehole stability [1]. Drilling fluids are typically categorized into three types based on their continuous phase: water-based drilling fluids (WBDFs), oil-based drilling fluids (OBDFs), and synthetic-based drilling fluids (SBDFs) [2]. While WBDFs and OBDFs use water and oil as their base, respectively, SBDFs are composed of synthetic compounds such as esters, olefins, and paraffins. These synthetic fluids are increasingly adopted in challenging and high-pressure drilling environments due to their superior

lubrication properties [3]. As drilling progresses, drilling mud becomes contaminated with drill cuttings and chemical additives, resulting in a complex waste stream that requires appropriate management [1]. Improper disposal of this waste poses serious environmental and health risks. Contaminants such as hydrocarbons, particularly polycyclic aromatic hydrocarbons (PAHs), can persist in the environment, degrade soil and water quality, and pose carcinogenic and toxic threats to human health [4, 5]. Therefore, effective treatment of drilling waste is necessary to minimize its environmental impact and enable the recovery of valuable resources.

Several technologies have been developed for drilling waste management, including re-injection, stabilization/solidification, bioremediation, and thermal treatments [2]. Among these, thermal desorption has emerged as a promising method due to its rapid processing time, high oil recovery efficiency, and ability to reduce hazardous waste volume. In comparison, stabilization/solidification methods produce materials suitable for disposal but lack resource recovery potential. Bioremediation, while environmentally friendly, tends to be slower and less effective for hydrocarbon-rich waste [6-8]. Incineration and pyrolysis are effective but require higher energy input and may generate harmful emissions [3, 9]. Thermal desorption, particularly low-temperature thermal desorption (LTTD), offers an optimal balance between treatment efficiency and environmental performance. Operating typically between 200°C and 350°C, LTTD volatilizes moisture and hydrocarbons, allowing for the recovery of valuable components such as diesel and short-chain oils used in drilling fluids [10-13]. Due to its lower energy requirements and ability to retain valuable materials, LTTD is considered a favorable option for drilling waste treatment. However, most previous research has relied on synthetic waste samples, limiting practical applicability. This study, therefore, addresses this gap by evaluating the effectiveness of LTTD technology in the treatment and recovery of authentic drilling mud. The findings aim to improve the efficiency of the thermal desorption process in reducing petroleum-based contaminants and recovering valuable materials from the waste stream.

METHODOLOGY

Experimental set-up

In this study, a 2-liter single-layer glass reactor is utilized as a thermal desorption unit for treating various types of drilling waste. The reactor features several key components that contribute to the efficiency of the process. A stirring motor ensures uniform mixing and heating of the waste, crucial for consistent desorption. An electric heating jacket provides the necessary heat, regulated by a controller that adjusts temperature and stirring parameters. As contaminants are vaporized, a condenser cools the vapors back into a liquid, which is then collected in a 1L collection bottle. Temperature is continuously monitored by a thermometer sleeve to maintain desired operating conditions. Additionally, a vacuum pump significantly enhances the process by decreasing the reactor's internal pressure, which assists in moving the vapor to the condenser. This setup successfully removes volatile contaminants from drilling waste under controlled conditions.



Figure 1. A 2-liter single-layer glass reactor

Experimental procedure

In the thermal desorption process, the drilling mud sample was thoroughly mixed to ensure homogeneity across the sample. Subsequently, 1 liter of this well-mixed drilling mud was processed in a thermal reactor that had been prepared in advance. The experiment commenced by gradually heating the

drilling mud starting from room temperature, initially to 100°C. This was followed by incremental increases in temperature, moving to 150°C, then to 200°C, subsequently to 250°C, and finally reaching 300°C. At each of these temperature points, the process was closely monitored to observe the accumulation of oil in the collection vessel. Monitoring continued at each stage until there was no further increase in oil volume, indicating that the extraction of oil at each respective temperature had maximized, thus ensuring optimal recovery of oil from the drilling mud at various thermal levels.

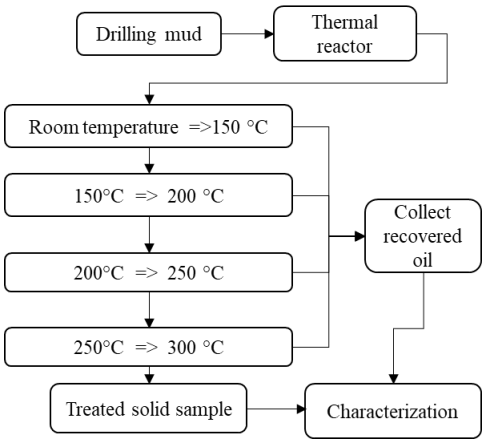


Figure 2. Operational conditions for the LTTD process

Analytical parameters

In this study, several analytical methods are employed. Proximate analysis is utilized to measure moisture content, volatile matter, fixed carbon, and ash content. Ultimate analysis assesses the elemental composition of the waste, which includes carbon, hydrogen, nitrogen, sulfur, and oxygen. The heating value is determined to ascertain the energy content of the waste. Chemical profiles of recovered are analyze by gas chromatography equipped with a mass spectroscopy detector (GC-MS) to observe the concentration of hydrocarbons before and after treatment. Additionally, thermogravimetric analysis (TGA) is applied to monitor the thermal stability and decomposition of waste. These methods collectively provide a comprehensive evaluation of the desorption process's effectiveness.

RESULTS AND DISCUSSION

Drilling mud characteristics

In this study, authentic drilling mud collected from the fluid return flow during drilling at an onshore operation in Phitsanulok Province, Thailand is being used. These drilling mud samples consist of a mixture of liquid and solid phases and exhibit a brown color. The appearance of these drilling mud samples is illustrated in Fig.3.



Figure 3. Physical appearance of drilling mud waste

Table 1 outlines the proximate and elemental analyses, along with the heating value of the drilling mud. The proximate analysis reveals a moisture content of 7.96%, a volatile matter content of 68.95%, fixed carbon at 0.56%, and ash at 22.53%. In terms of elemental compositions, the drilling mud contains 49.90% carbon, 9.47% hydrogen, 0.12% nitrogen, 1.30% sulfur, and oxygen by difference at 39.21%. The higher

heating value (HHV) of the mud is recorded at 27.02 MJ/kg, indicating its potential energy content which is critical for applications involving energy recovery. In the study by Duan et al., 2024, drilling mud features a significantly lower moisture content at 7.96% compared to 12.73% and a higher volatile matter at 68.95% compared to 48.6%. These characteristics suggest that drilling mud could allow for more efficient energy recovery by reducing the need to evaporate moisture and by providing more volatiles for combustion. Moreover, Drilling mud's carbon content is considerably higher at 49.90% compared to 27.7%, indicating a richer hydrocarbon base, which aligns with its higher heating value of 27.02 MJ/kg versus 11.6 MJ/kg. Additionally, the ash content in drilling mud is lower at 22.53% compared to 34.31%, which could lead to fewer disposal issues and reduced inorganic residue after.

Table 1. Proximate analysis, elemental analysis, and heating value of drilling muds.

Properties of the drilling mud	**Measured value**
Proximate analysis (wt%)	
moisture	7.96
volatile	68.95
fixed C	0.56
ash	22.53
Elemental analysis (%)	
C	49.90
H	9.47
N	0.12
S	1.30
O*	39.21
HHV (MJ/kg)	27.02

O by difference*

The thermal behavior of the raw drilling mud was examined using thermogravimetric analysis (TGA) and derivative thermogravimetry (DTG), as shown in Figure 4. A notable weight loss occurred between 100°C and 250°C, indicating the release of moisture and volatile organic compounds in the raw sample. This corresponds with a sharp DTG peak, reflecting the maximum rate of thermal decomposition within this range. Beyond 250°C, the TGA curve shows gradual stabilization, and the DTG signal flattens, suggesting that most volatile components had decomposed, and only thermally stable residues remained. These results confirm that significant thermal degradation of drilling mud primarily occurs below 300°C, supporting the relevance of this range for efficient low-temperature thermal desorption.

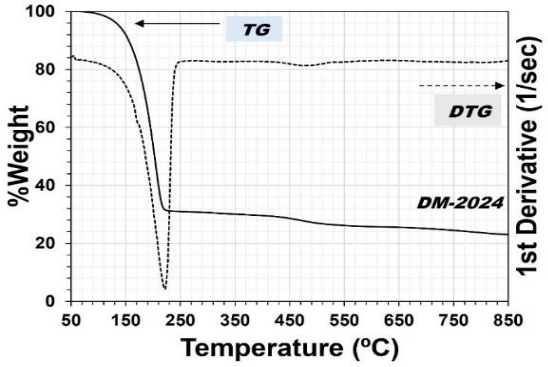


Figure 4. Thermal degradation of drilling mud samples analyzed by TGA

Compositions of the treated drilling mud

The XRD pattern of the solid residue obtained from drilling mud treated at 300°C, shown in Figure 5, offers insights into the mineralogical stability of key components after thermal desorption. The presence of sharp diffraction peaks indicates that the crystalline structure of major minerals remains intact at this temperature. Barite ($BaSO_4$), a common weighting agent in drilling fluids, is clearly identified, confirming its high thermal stability below 500°C [14]. Quartz (SiO_2), commonly found in drill cuttings, is also present and known for its chemical resilience [15]. Calcite ($CaCO_3$), often used as a bridging or pH-modifying agent, is likewise detected, consistent with its decomposition starting above 600°C [16]. These results suggest that thermal treatment at 300°C does not significantly alter the structure of these minerals, supporting their stability under LTTD conditions and indicating the potential for safe handling or reuse of the residue.

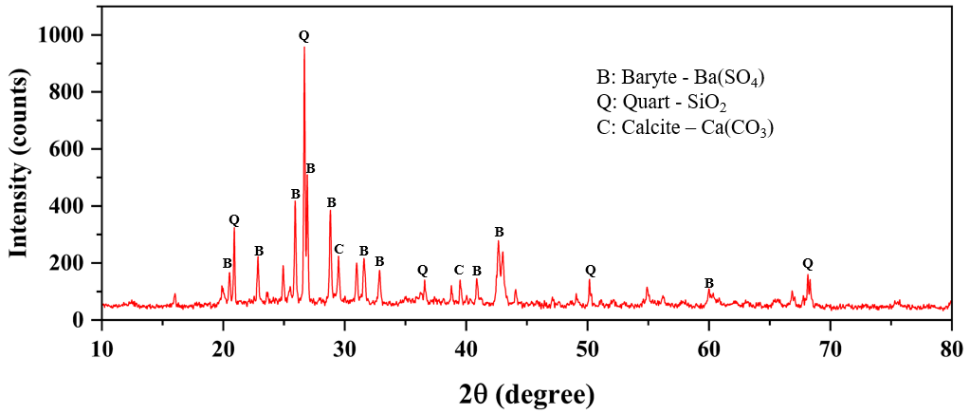


Figure 5. XRD of treated drilling mud at 300°C

The thermal degradation behavior of drilling cuttings pre-treated at various temperature intervals—100–150°C, 150–200°C, 200–250°C, and 250–300°C—was analyzed using TGA and DTG. As shown in Figure 6, the sample treated at 100–150°C exhibited the highest weight loss and most prominent DTG peak, indicating that a large portion of volatiles, particularly hydrocarbons and moisture, remained due to insufficient pre-treatment. The 150–200°C sample showed slightly reduced weight loss and DTG intensity, suggesting partial removal of lighter hydrocarbons, but significant volatile content still remained [17]. In contrast, samples treated at 200–250°C and 250–300°C demonstrated a substantial decrease in both weight loss and DTG peak intensity, reflecting effective desorption of volatile materials during thermal treatment. The 250–300°C sample showed the least thermal degradation, confirming that most labile compounds had been removed, with only thermally stable residues remaining. These findings indicate that volatile removal efficiency increases with temperature, and up to 300°C is effective for eliminating the majority of hydrocarbons. The diminishing DTG response also shows that further heating beyond 300°C contributes minimally to mass loss, aligning with energy optimization goals. Compared to the raw sample, which showed greater weight loss and a strong DTG peak between 100°C and 250°C, the treated samples demonstrate the efficiency of staged low-temperature desorption. While the untreated mud retained more volatiles, the 250–300°C sample exhibited higher thermal stability and minimal remaining volatiles, confirming that most decomposable compounds were removed. This supports 300°C as an optimal upper limit for balancing effective oil removal with energy efficiency, consistent with previous findings [11, 18].

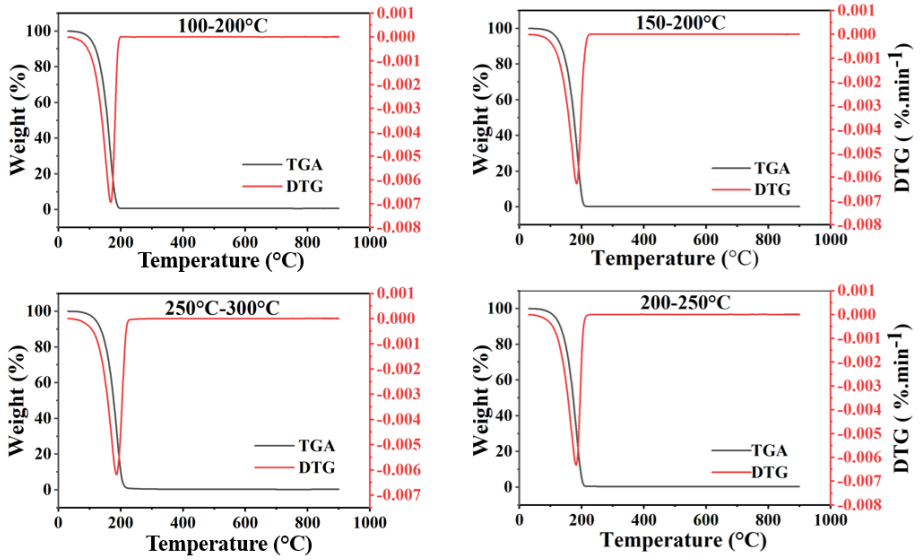


Figure 6. The TGA and DTG curves

Figure 7 shows the volume of liquids extracted from drilling mud at different temperature intervals, highlighting the effectiveness of the thermal desorption process. Initially, from room temperature to 150°C, the process predominantly extracts water, totaling 40 ml, alongside 20 ml of lighter oils. This early stage effectively removes moisture and the most volatile oil fractions, suggesting that lower temperatures are mainly beneficial for evaporating water and light hydrocarbons.

As the temperature increases to 150–200°C, oil recovery shifts toward heavier fractions, with 56 ml of oil extracted and no water present, indicating that mid-range temperatures are more effective at volatilizing hydrocarbons that are less volatile at lower temperatures. This trend continues at higher intervals, with 175 ml recovered between 200–250°C and peaking at 200 ml between 250–300°C. These findings highlight that the 200–300°C range is critical for efficiently mobilizing and extracting denser and more complex hydrocarbon compounds. Careful temperature control during thermal desorption is therefore essential to maximize oil recovery while minimizing residual waste and environmental impact.

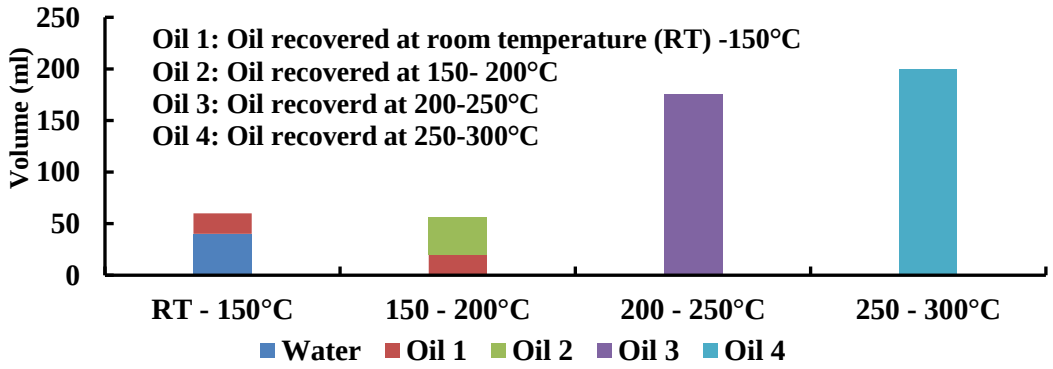


Figure 7. Volume of recovered oil at each temperature

The GC-MS analysis highlights key trends for optimizing thermal desorption of drilling mud. Data from Tables 2 and 3 reveal that specific temperature ranges significantly influence oil recovery efficiency and the extent of residual oil contamination. The findings show that alkanes, which form a significant component of the oil content, increase with temperature, achieving maximum volatilization at 250-300°C. This suggests that higher temperatures are necessary for recovering heavier alkanes but could be less energy-efficient and potentially degrade sensitive compounds. Notably, lighter compounds such as alcohols and alicyclic hydrocarbons demonstrate optimal recovery at lower temperatures, specifically between 150-200°C

[19], suggesting that these settings are sufficient for their effective extraction and can help minimize energy use.

In terms of oil recovery, the carbon number distribution shows that mid-range hydrocarbons (C10–C14) dominate across all temperature ranges, with a notable increase in heavier fractions (C20–C28) at the highest temperatures. This suggests that while most oil components can be effectively recovered below 250°C, higher temperatures are necessary for the volatilization of heavier compounds. [20, 21]. However, at the highest temperature range (250-300°C), while achieving the highest alkane content (79.10%), the emergence of small amounts of nitrogenous compounds indicates the onset of thermal cracking, suggesting a focused recovery of heavy hydrocarbon fractions.

The temperature range of 150–200°C allows for efficient recovery of lighter and mid-range hydrocarbons with lower energy input. However, the 250–300°C range shows greater potential for more complete desorption, particularly of heavier fractions, and may be favorable in applications where thorough oil removal is prioritized over energy efficiency.

Table 2. GC-MS compound class distributes across temperature ranges

Categories	*RT-150°C	150-200°C	200-250°C	250-300°C
Alcohol	9.32%	9.85%	3.02%	1.28%
Alicyclic Hydrocarbon	24.13%	16.50%	16.11%	13.79%
Alkane	59.02%	69.51%	66.70%	79.10%
Alkene	5.35%	2.00%	8.22%	2.96%
Carboxylic acid	1.63%	0.78%	1.40%	2.04%
Ketone	0.55%	0.00%	0.07%	0.27%
Ether	0.00%	1.35%	4.43%	0.01%
Nitrogenous compound	0.00%	0.00%	0.06%	0.57%

**RT: Room temperature*

Table 3. Carbon Number Distribution Across Temperature Ranges

Carbon number	*Rm-150°C	150-200°C	200-250°C	250-300°C
C_3-C_{10}	4.92%	8.65%	4.98%	7.10%
C_{11}-C_{13}	72.33%	71.84%	64.59%	50.55%
C_{14}-C_{19}	21.12%	15.07%	24.06%	39.74%
C_{20}-C_{28}	1.59%	4.36%	1.98%	2.37%

**RT: Room temperature*

CONCLUSION

This study demonstrated the effectiveness of low-temperature thermal desorption (LTTD) for treating drilling mud, highlighting its potential for environmental remediation and resource recovery. The results showed that oil and moisture removal occur below 300°C, with the most significant weight loss and hydrocarbon volatilization detected between 150°C and 300°C. Proximate and ultimate analyses confirmed the high energy content and volatile matter of the drilling mud, supporting its suitability for thermal treatment. TGA and DTG analyses validated that temperatures beyond 300°C offer minimal benefit, indicating that this threshold is sufficient for efficient desorption. GC-MS results revealed that lighter hydrocarbons are recovered at lower temperatures, while heavier alkanes peak between 250–300°C. XRD patterns showed that mineral structures remained stable post-treatment, suggesting the residue's potential for safe reuse. Overall, this study supports LTTD as an energy-efficient method for treating drilling waste, with 300°C identified as an optimal upper limit for balancing recovery and energy use.

ACKNOWLEDGEMENT

This study was supported by the scholarship program for ASEAN or Non-ASEAN Country supported by Chulalongkorn University.

REFERENCE

[1] O. J. Ochulor, O. O. Sofoluwe, A. Ukato, and D. D. Jambol, "Technological advancements in drilling: A comparative analysis of onshore and offshore applications," *World Journal of Advanced Research and Reviews,* vol. 22, no. 2, pp. 602-611, 2024.

[2] G. Hu, H. Liu, A. Rana, J. Li, S. Bikass, K. Hewage, and R. Sadiq, "Life cycle assessment of low-temperature thermal desorption-based technologies for drill cuttings treatment," *Journal of Hazardous Materials,* vol. 401, p. 123865, 2021, doi: 10.1016/j.jhazmat.2020.123865.

[3] A. S. Ball, R. J. Stewart, and K. Schliephake, "A review of the current options for the treatment and safe disposal of drill cuttings," *Waste Management & Research,* vol. 30, no. 5, pp. 457-473, 2012, doi: 10.1177/0734242X11419892.

[4] D. Jagwani, A. Kulkarni, P. Shukla, D. S. Ramteke, and H. D. Juneja, "PAH composition of Water Based Drilling Mud and drill cuttings in the offshore region, east coast of India," *Bulletin of environmental contamination and toxicology,* vol. 87, pp. 550-555, 2011, doi: 10.1007/s00128-011-0340-x.

[5] T. G. Ambaye, A. Chebbi, F. Formicola, S. Prasad, F. H. Gomez, A. Franzetti, and M. Vaccari, "Remediation of soil polluted with petroleum hydrocarbons and its reuse for agriculture: Recent progress, challenges, and perspectives," *Chemosphere,* vol. 293, p. 133572, 2022, doi: 10.1016/j.chemosphere.2022.133572

[6] A. Wojtanowicz, "Oilfield waste disposal control," *Environmental Technology in the Oil Industry,* pp. 167-198, 2016.

[7] E. Diplock, D. Mardlin, K. Killham, and G. Paton, "Predicting bioremediation of hydrocarbons: laboratory to field scale," *Environmental Pollution,* vol. 157, no. 6, pp. 1831-1840, 2009.

[8] A. B. Guerra *et al.*, "Metagenome enrichment approach used for selection of oil-degrading bacteria consortia for drill cutting residue bioremediation," *Environmental Pollution,* vol. 235, pp. 869-880, 2018, doi: 10.1016/j.envpol.2018.01.014.

[9] J. V. Milato, R. J. França, and M. R. M. Calderari, "Co-pyrolysis of oil sludge with polyolefins: Evaluation of different Y zeolites to obtain paraffinic products," *Journal of Environmental Chemical Engineering,* vol. 8, no. 3, p. 103805, 2020.

[10] J. E. Vidonish, P. J. Alvarez, and K. Zygourakis, "Pyrolytic remediation of oil-contaminated soils: reaction mechanisms, soil changes, and implications for treated soil fertility," *Industrial & Engineering Chemistry Research,* vol. 57, no. 10, pp. 3489-3500, 2018.

[11] P. Falciglia, M. Giustra, and F. Vagliasindi, "Low-temperature thermal desorption of diesel polluted soil: influence of temperature and soil texture on contaminant removal kinetics," *Journal of hazardous materials,* vol. 185, no. 1, pp. 392-400, 2011, doi: 10.1016/j.jhazmat.2010.09.046.

[12] D. N. Richardson, "Review of variables that influence measured concrete compressive strength," *Journal of materials in civil engineering,* vol. 3, no. 2, pp. 95-112, 1991.

[13] R. L. Stephenson, S. Seaton, R. McCharen, E. Hernandez, and R. B. Pair, "Thermal desorption of oil from oil-based drilling fluids cuttings: processes and technologies," in *SPE Asia Pacific Oil and Gas Conference and Exhibition*, 2004: SPE, pp. SPE-88486-MS, doi: 10.2118/88486-MS.

[14] O. Á. Omoniyi and S. Mubarak, "Potential usage of local weighting materials in drilling fluid a substitute to barite," *Int J Innov Res,* vol. 3, no. 13, p. 493, 2014.

[15] E. I. Kovaleva, M. Guchok, V. Terekhova, V. Demin, and S. Y. Trofimov, "Drill cuttings in the environment: possible ways to improve their properties," *Journal of Soils and Sediments,* vol. 21, pp. 1974-1988, 2021.

[16] K. S. Karunadasa, C. Manoratne, H. Pitawala, and R. Rajapakse, "Thermal decomposition of calcium carbonate (calcite polymorph) as examined by in-situ high-temperature X-ray powder diffraction," *Journal of Physics and Chemistry of solids,* vol. 134, pp. 21-28, 2019.

[17] X. Duan *et al.*, "A TGA-FTIR study on the pyrolysis of oil-based drilling cuttings and the influence of its solids on pyrolysis characteristics," *Journal of Environmental Chemical Engineering,* vol. 12, no. 3, p. 112846, 2024.

[18] H. Liu, J. Li, M. Zhao, Y. Li, and Y. Chen, "Remediation of oil-based drill cuttings using low-temperature thermal desorption: Performance and kinetics modeling," *Chemosphere,* vol. 235, pp. 1081-1088, 2019, doi: 10.1016/j.chemosphere.2019.07.047.

[19] G. A. Olah and Á. Molnár, *Hydrocarbon chemistry*. John Wiley & Sons, 2003.

[20] Y. Sun, J. Cao, M. Wang, Z. Yang, H. Wu, J. Shang, and J. Ma, "Chemical composition of headspace vapor from volatilization of ten petroleum samples," *Fuel,* vol. 396, p. 135299, 2025.

[21] J. G. Speight, "Chapter 3—Hydrocarbons from crude oil," *Handbook of industrial hydrocarbon processes,* pp. 95-142, 2020.

20R4-12

Study of Food Waste Composition and Generation from Campus Food Vendors: A Case Study of Chiang Mai University

Chadaporn Sriwichai[1], Santi Phithakkitnukoon[2], Karn Patanukhom[3] and Sarunnoud Phuphisith[4*]
[1]Graduate student, Department of Environmental Engineering, Faculty of Engineering, Chiang Mai University, Chiang Mai 50200, Thailand; [2]Associate Professor, Department of Computer Engineering, Faculty of Engineering, Chiang Mai University, Chiang Mai 50200, Thailand; [3]Assistant Professor, Department of Computer Engineering Faculty of Engineering, Chiang Mai University, Chiang Mai 50200, Thailand; [4]Assistant Professor, Department of Environmental Engineering, Faculty of Engineering, Chiang Mai University, Chiang Mai 50200, Thailand
[*]Phone : 053 944 192 , E-mail : sarunnoud.p@cmu.ac.th

ABSTRACT

This study aims to evaluate food waste generation and its composition from the cooking process of curry and rice menus to promote sustainable production and consumption. Data were collected from ten food vendors located at cafeterias in Chiang Mai University for two working day weeks each, using the direct weighing method. The results showed that food waste was generated the most during the preparation stage. Daily food waste generation ranged from 0.53 – 5.17 kg and 0.002-0.029 kg/plate sold. Avoidable and unavoidable ratios differed by shop. Components of food waste varied depending on the menu and the practices of each vendor. None of the surveyed shops separated food waste, making it difficult to use to its maximum benefit.

Keywords : Food Waste; Avoidable; Unavoidable; Waste management; Thai Cuisine

INTRODUCTION

Food is one of the most essential factors for human consumption to sustain life. When food is produced, it often generates food waste; More than one third of food produced is waste [1], affecting food scarcity and environmental issues. Food waste may be occurred from leftover food or food scraps that occur in various steps, from harvesting to cooking. All food waste has an impact on the economy and the environment, including hunger, food shortages, resource waste and greenhouse gas emissions from food waste management. Therefore, studying ways to reduce and prevent food waste is an important issue in promoting sustainable consumption, which will be beneficial in reducing production costs, reducing negative environmental impacts and reducing unnecessary resource waste.

Food waste can be generated from many sources, such as households, wholesale and retail stores, hotels, restaurants, and others. Each source may have different amounts and components of food waste [2] which are affected by the size, the type of cooking, the efficiency of stock management and kitchen plan, and the behavior of operators. Food waste can be divided into avoidable and unavoidable. Avoidable refers to food waste that is still edible, which may be leftovers, discarded, or unused. It may come from trimming during the preparation of ingredients before cooking or during the cooking process, such as carrot scraps that are trimmed to be used as a garnish on a dish, or meat scraps, etc. [3]. Unavoidable refers to food-related components that are not intended for human consumption. Examples of inedible parts include bones, shells, and seeds. Unavoidable parts do not include packaging [4].

The food service sector is one of the major sources of food waste, with many factors contributing to food waste generation. The study by Filimonau et al. (2023) [5] reported that the size and type of restaurant affect the amount of food waste generated, and the composition of food waste generated varies from type to type. The efficiency of restaurant management, kitchen management plans, and the behavior of restaurant operators, such as planning for ingredient preparation, checking product labels before purchasing to avoid expiration before use and having to discard, purchasing ingredients in excess, etc.

The present study focused on the generation of in-kitchen waste in Thai cuisine. We investigated the amount and composition of food waste generated from the cooking process, covering stocking ingredients, preparing, cooking and ready to serve. We also surveyed the current food waste management practices to promote food waste reduction and preventive measures.

METHODOLOGY

This study targeted curry and rice food vendors as this type of food category uses various ingredients and processes. Food waste generation and composition data were collected from ten food vendors located at cafeterias in Chiang Mai University for two working day weeks each, beginning on October 4, 2024, and ending on January 31, 2025. The direct weighing method was employed and food waste was classified into avoidable and unavoidable categories. Food waste was also accessed by ingredient types, i.e., vegetable scraps, meat, starch, and eggshells. In addition, the operators were asked about their cooking experiences, steps in producing food waste and how it was managed. All data was analyzed using Microsoft Excel version 2019.

RESULTS AND DISCUSSIONS

1. Food waste composition and generation rate

General data of the food vendors surveyed are shown in Table 1. About 75% of the food vendors had more than 10 years of cooking experience. Most of them prepared and cooked all meals in the cafeteria kitchen

Table 1 General data of the surveyed food vendors

ID	Cooking Experience (years)	Plate sold (per/day)	Cooking at cafeteria kitchen* (%)
CR1	20	300	100
CR2	20	300	100
CR3	20	150	20
CR4	10	100	50
CR5	2	100	100
CR6	20	300	100
CR7	13	100	20
CR8	15	150	50
CR9	20	200	20
CR10	30	200	20

*Some food vendors prepared and cooked at cafeteria only, some food vendors partly prepared and cooked at their houses.

The average amount of daily food waste generation ranged from 0.53 – 5.17 kg, as shown in **Figure 1**. Considering the amount of plate sold daily, the food waste generation varied from 0.002-0.029 kg/day/plate sold, as shown in **Figure 2,** It is noticeable that sales volume does not affect the amount of food waste generated per day by curry and rice food vendors. The shops CR1, CR2, and CR6 had the same amount of daily plate sold, but the amount of daily food waste generated was different. The shop CR1 had less food waste generation because the food vendors used their trimmed vegetable scraps to cook other menus instead of throwing them away. The CR2 was a popular shop for selling boxed lunches, resulting in a higher amount of food waste generated per day than both shops. Shops CR3 and CR8 had the same plate sold, but CR8 had higher amount of food waste generation because all cooking processes were done at the university cafeteria kitchen. The shop CR3, on the other hand partly prepared and cooked from outside. Shops CR4, CR5, and CR7 had the same plate sold, but the amount of food waste was different. CR5 has the least amount of food waste because the food vendors buy and sell trimmed ingredients, so the amount of food waste is less than the other two food vendors.

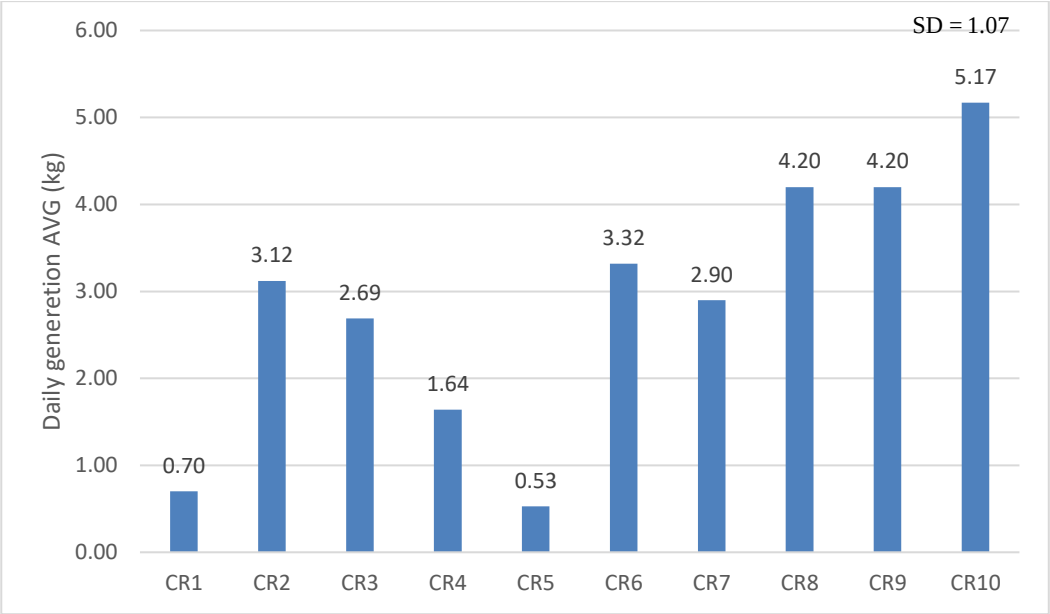


Figure 1 The daily average amount of food waste generation

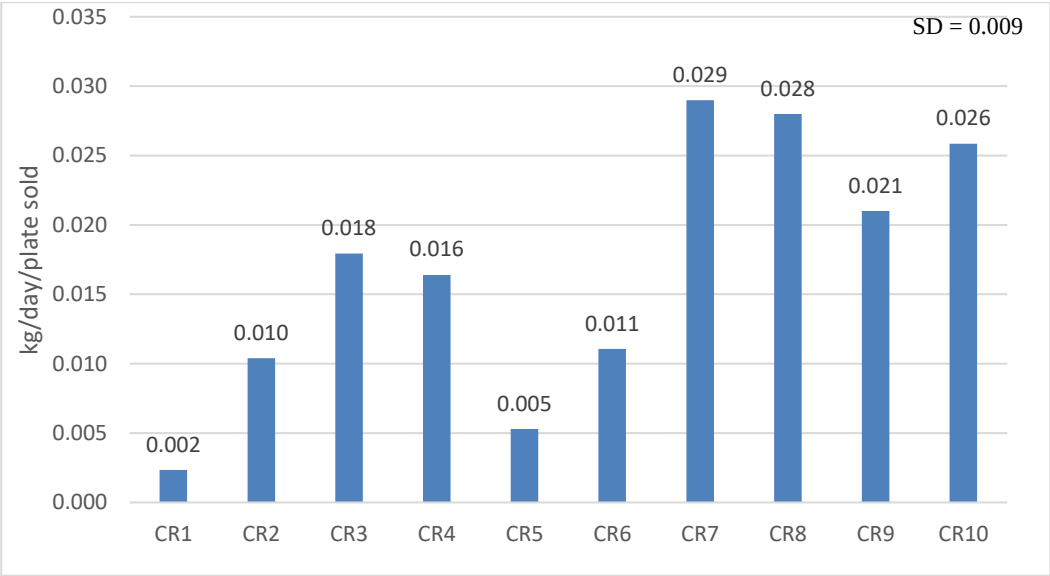


Figure 2 The daily average amount of food waste generation per plate sold

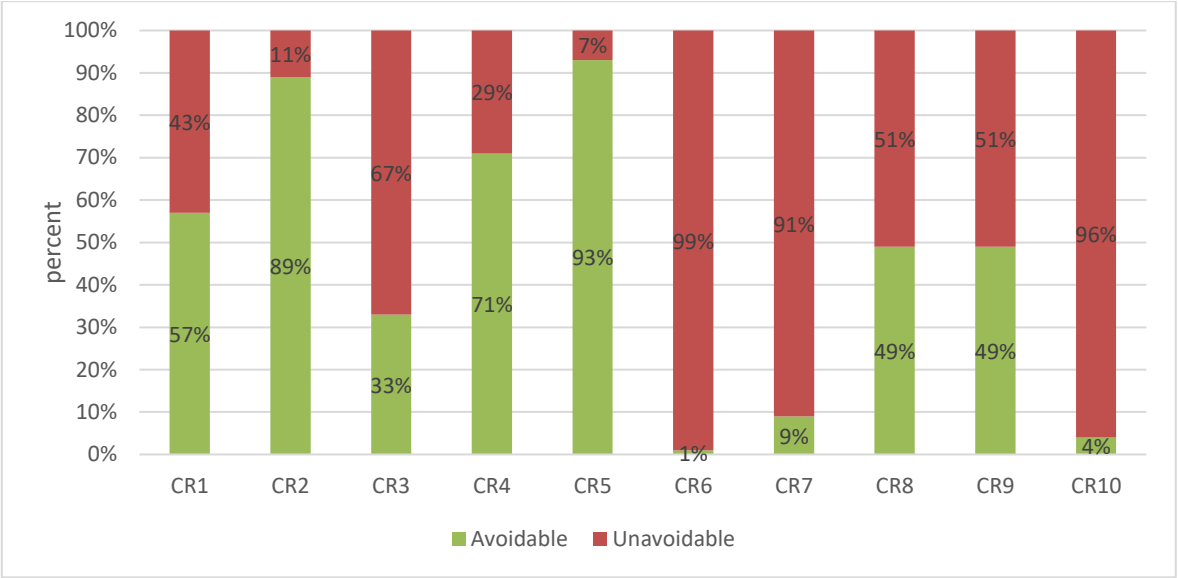


Figure 3 Avoidable and unavoidable compositions in food waste

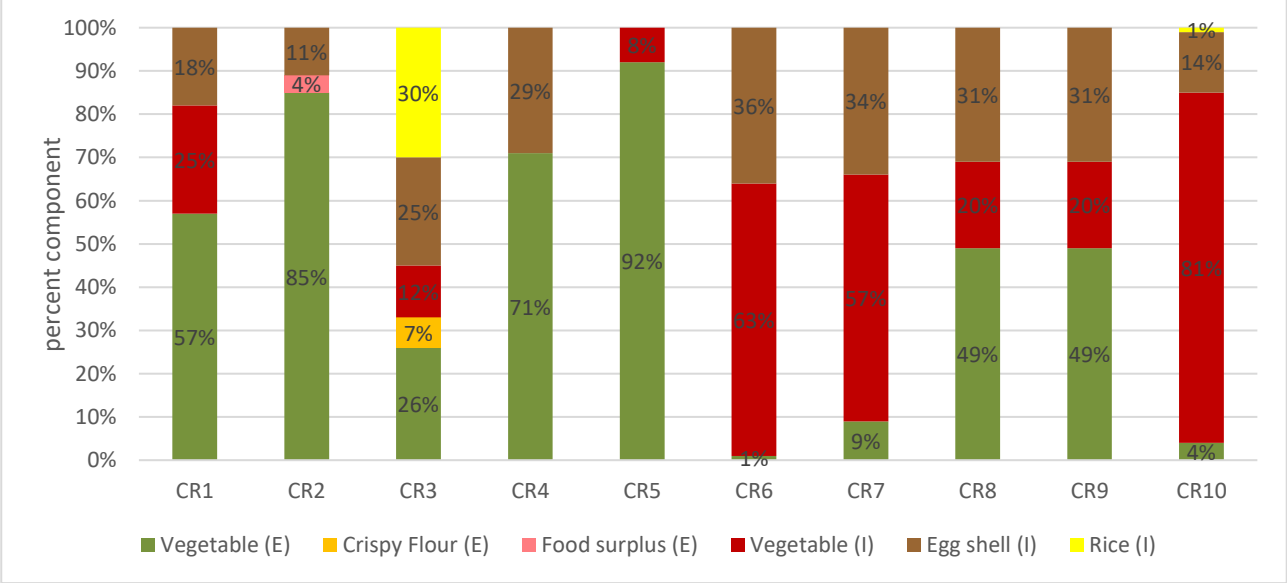


Figure 4 Component details in food waste

In average, the preparation of ingredients was the highest source of food waste generation, accounting for 95% of the total waste generated. The second source of food waste occurred in cooking process (4%), and ready-to-serve (1%). This is consistent with previous research [5]. The composition between avoidable and unavoidable parts varied, as shown in **Figure 3.** About half of the surveyed shops generated unavoidable parts over avoidable parts. The dominant was vegetable scraps, which could be avoided, at 44% on average, unavoidable vegetable scraps, at 36%, eggshells, at 25%, burnt rice scraps, at 16 %, crispy dough scraps at 8%, and ready-to-serve food, at 4%, as shown in **Figure 4**.

2. Food waste management methods

All the surveyed shops did not separate food waste and disposed of it mixed with general waste. The shops mentioned about the limited kitchen space; placing several bins for separation was impossible and separating waste takes time. Most vendors (93%) threw away all the generated food waste at the university bins while only 7% separated their food waste for composting.

CONCLUSION

The present study assessed food waste generation from curry and rice cooking. The preparation stage was the key source of food waste generation. Food vendors generated unavoidable more than avoidable parts, with vegetables being the most commonly found component. Components of food waste varied depending on the menu and the practices of each vendor. None of the surveyed shops separated food waste, resulting in food waste mixed with general waste, making it difficult to use to its maximum benefit.

ACKNOWLEDGEMENT

This project is funded by National Research Council of Thailand (NRCT). The authors would like to sincerely thank the Department of Environmental Engineering, Faculty of Engineering, Chiang Mai University for their kind cooperation in providing facilities.

REFERENCE

[1] FAO, 2013.Food wastage footprint Impacts on natural resources.

[2] รัตนาวรรณ มั่งคั่ง, 2023. ขยะอาหาร วิธีการประเมินปริมาณขยะอาหาร ดัชนีขยะอาหาร และเส้นฐานขยะอาหารระดับชาติ – กรุงเทพฯ

[3] WRAP, 2023, Household Food And Drink Waste In The United Kingdom 2021/22

[4] United Nations Environment Programme, 2021. Food Waste Index Report 2021. Nairobi.

[5] Filimonau, V., Algboory, H., Mohammed, N. K., Kadum, H., Qasem, J. M., & Muhialdin, B. J. (2023). Food waste and its management in the foodservice sector of a developing economy: An exploratory and preliminary study of a sample of restaurants in Iraq. *Tourism Management Perspectives*, *45*, 101048. https://doi.org/https://doi.org/10.1016/j.tmp.2022.101048

[6] Jayasekara, A. P, et al., 2024. Mapping pre-consumer food waste in quick service restaurants on a university campus: Two Australian case studies. *Journal of Cleaner Production*, *434*, 139978

Dual Effects of Starter Inoculum and Thermal Pretreatment on Oil Palm Mesocarp Fiber for Methane Production in Solid-State Anaerobic Digestion

Saengmany Phommakod[1], Eko Heryadi[1,2], Chongkon Poonthawee[3] and Pawinee Chaiprasert[1*]

[1]*Biotechnology Program, School of Bioresources and Technology, King Mongkut's University of Technology Thonburi, Tha Kham, Bangkhunthian, Bangkok, 10150, Thailand*

[2]*Department of Chemical Engineering, Faculty of Engineering, Mulawarman University, Samarinda 75123, Indonesia*

[3]*Excellent Center of Waste Utilization and Management, Pilot Plant Development and Training Institute, King Mongkut's University of Technology Thonburi, Tha Kham, Bangkhunthian, Bangkok, 10150, Thailand*

[*]*Corresponding author: Tel : (66)2-470-7525, Fax : (66)2-452-3455, e-mail : pawinee.cha@kmutt.ac.th*

ABSTRACT

Palm oil is the world's largest used in vegetable oil. During the processes of crude oil production, oil palm mesocarp fiber (OPMF) is one of the significant solid waste generations. OPMF is the lignocellulosic solid residue from processes of palm fruit cooking and pressing during extraction of crude palm oil. Although OPMF contains high amounts of cellulose (33%), hemicellulose (22%), and lignin (21%), its utilization as feedstock for biomethane production is hampered by its recalcitrant to degrade this complex structure. This study evaluated dual effects on how active various sources of seed inoculums from anaerobic treatment of palm oil mill effluent (POME), cow manure (CM), and swine manure (SM) as well as OPMF hydro-pretreatment using heat or thermal energy as from crude palm oil industry. The thermal pretreatment of OPMF with sterilized hot water (SHW) and boiling hot water (BHW) were conducted to examine the enhancement of methane production and compared to non-pretreatment. A biochemical methane potential (BMP) assay was performed in both effects using OPMF as the feedstock. Within 30 d of incubation, the potential methane yield produced at 355, 168, and 162 mL/gVS using CM, POME, and SM inoculum, respectively. BMP of CM showed 2 times higher potential than POME and SM. The methane production rate for CM, POME, and SM was 18.8; 6.8, 5.8 mL/d, respectively. Whereas the SHW and BHW pretreatment of OPMF showed slight effect on methane production. Furthermore, CM inoculum was used in modified solid inclined (MSI) reactor for anaerobic digestion fed with raw OPMF (62% TS). The methane production rate and yields from OPMF were 9.2 L/d and 266 L/KgVS, respectively, within 30 days digestion period. This high solid-state MSI reactor shows the high capability to degrade the solid waste of OPMF for methane production.

Keywords: biochemical methane potential; hydro-heat pretreatment; inoculum seed; oil palm mesocarp fiber; solid-state anaerobic digestion

INTRODUCTION

Palm oil mills are the largest industrial sectors in various food products, such as cooking oil, margarine, shortenings in baking, and confectionery fats including oleochemicals and biodiesel industries. The global production of crude palm oil (CPO) reached 73 million tons in 2022. The ASEAN region is the major palm oil producing area and the most important exporters to global markets. Recently, Thailand holds the third place of world CPO producers (4.6%) below Indonesia (57.6%) and Malaysia (24.9%) [1]. During the processes of CPO production, palm oil industries generate a large number of wastewaters as palm oil mill effluent and solid wastes. Various forms of solid wastes generated from palm oil mill industry, for example oil palm empty fruit bunch (23.5%), oil palm mesocarp fiber (13.5%), oil palm shell (5.0%), oil palm decanter cake (3.5%), and others (14.5%) [2]. These massive by-products of waste in the form of liquid and solid fractions are turning out to be the main source of pollution and high environmental impact for the sustainability of the palm oil industry. Normally, palm oil mill effluent was treated by anaerobic digestion (AD) for biomethane production. Where solid wastes, the residual lignocellulosic biomasses are recalcitrant to natural degradation and unusable in the plantation sector. Lignocellulosic material represents a plentiful organic resource which will be a high potential feedstock for production of renewable biogas energy through AD [3].

Oil palm mesocarp fiber (OPMF) is one of solid wastes requiring more study to treat and utilize for valuable products. OPMF is generated from cooking and pressing process of the palm fruits after the extraction of palm oil. The fiber characteristics in terms of cellulose, hemicellulose, and lignin content are 21.41, 21.77, and 30.33%, respectively with 62.29% total solids, 8.63% ashes, and 9.99% extractives. Fibrous materials of OPMF containing high lignocellulosic materials will decrease the hydrolysis step in the AD process due to the physical barrier provided by lignin, hemicellulose, and crystalline of cellulose [4].

The biodegradability of lignocellulosic OPMF in AD is influenced by various factors, such as efficacy hydrolytic microorganisms as inoculum seed, cellulose crystallinity, accessible surface area, degree of cellulose polymerization, and the presence of lignin [5]. To overcome these pain points, suitable inoculum sources with effective microbial consortium and pretreatment methods are commonly applied to enhance the hydrolysis rate of lignocellulose before through acidogenesis, acetogenesis, and methanogenesis for methane production. Several pretreatment methods such as steam explosion, biological pretreatment, and diluted acid pretreatment have been proposed and used to improve the biodegradability for enhancing methane production [5]. The destruction of lignocellulosic structure occurred by pretreatment, which normally applied before hydrolysis step. Pretreatment increased surface area, removed lignin and disrupted cellulose structure which could enhance the efficiency in hydrolysis step. There were several methods of lignocellulosic pretreatment but only a few methods had potential as cost effective and able to apply in industries. It is not only cost effectiveness and applicable methods were concerned but lignocellulosic properties after pretreatment are also considered. However, hydrothermal pretreatment has gained attention due to its chemical-free, minimal equipment erosion, short reaction time, and low generation of inhibitors that may affect microbial activity [6]. The moist heat temperature might affect to breakdown lignocellulosic structure. In addition, hydro-heat pretreatment of OPMF was chosen to apply in this study due to its applicable steam (100-121°C) in palm oil mill. This method can use the existing steam in the factory. No extra energy cost be paid by this application. Moreover, an efficacy anaerobic microbial consortium plays a vital role in the AD system, efficiency of methane production relies on the compatibility and potential interaction between microorganisms and the available substrates.

Out of all bioconversion technologies for biofuel and bioenergy production, AD is a cost-effective technology that has been implemented worldwide for commercial production of electricity, heat, and compressed natural gas from organic materials [7]. Based on total solid (TS) content in AD system, the common types of reactors can be classified into wet ($\leq$10%TS), semi-dry (10-20%TS) and dry or solid-state ($\geq$20%TS) AD systems. These technologies have been intensively studied for biogas production from lignocellulosic biomasses. The development of solid-state AD was aimed to reduce water consumption, increase organic loading, small reactor volumes, less mixing requirement, and lower cost of energy [8, 9]. The methane yields of perennial crop and agricultural residues were higher than those derived from yard wastes and woody biomass. No significant difference between methane yields between liquid AD and solid-state AD except for paper were found. However, low methane production might be affected from the high content and complex structure of fibrous material that extends the achievable microbial degradation of cellulose and hemicellulose reflecting in negatively related to methane yields [10].

This research is aimed to explore the methane production potential from OPMF using a various anaerobic microbial seed through biochemical methane potential (BMP) assay. Thermal pretreatment was implemented on the OPMF under water to enhance its degradability. Two different thermal pretreatments were performed, namely boiling hot water (BHW) and sterilized hot water (SHW). Furthermore, a solid-state AD of OPMF was conducted using the best conditions of microbial seed and thermal pretreatment, aiming at examining the effectiveness of solid-state AD from OPMF for methane production with proposed modified solid inclined (MSI) reactor. The process performance and stability of the MSI reactor were studied. This technology of solid-state AD for palm oil solid wastes could be promising to commercial use in the palm oil industry sectors.

METHODOLOGY

Oil Palm Mesocarp Fiber

The raw OPMF was used as feedstock which obtained from the palm oil mill factory located at Eastern part of Thailand. After collecting, OPMF was put in the plastic bag and stored at 4°C before further study. The OPMF sample was milled in a knife mill and sieved to a size of 1-2 mm prior use. The characteristics of OPMF were 62% of total solid (TS), 95% of volatile solid (VS), 5% of ash, 14% of oil, 33% of cellulose, 22% of hemicellulose and 21% of lignin.

Inoculum Sources

Three inoculums were used as follows i) microbial sludge of anaerobic continuous stirred tank reactor treating palm oil mill effluent (POME) collected from Eastern part of Thailand, ii) cow manure (CM), and iii) swine manure (SM) which both manures collected from Bangkok, Thailand. Microbial inoculums from animal manure were prepared by suspension in water at ratio 1:1 by weight, then the suspended microorganisms in liquid fraction were collected to use as inoculums. The characteristics of POME, CM, and SM were contained 31.04, 74.10, and 39.75 g/L of suspended solid (SS), 22.24, 51.85, and 26.65 g/L of volatile suspended solid (VSS), and 0.72, 0.70, and 0.67 ratio of VSS/SS, respectively. Three inoculums were assayed for BMP of OPMF.

Pretreatment Methods

Boiling hot water (100°C, 14.7 psi) and sterilized hot water (121°C, 15 psi) were applied to pretreat OPMF with adding distilled water at ratio 1:1 by weight for 10 min. The using of this temperature range was simulated by using excess steam heat from palm oil processing for pretreatment, offering cost savings by eliminating the need for extra heat sources and payments. The pretreated OPMF was characterized. The pretreated samples (OPMF-BHW and OPMF-SHW) and the non-pretreated sample (OPMF-NP) with the selected inoculum were further used for BMP assay.

Biochemical Methane Potential Assay

The assay of BMP was conducted in triplicate using a 100 mL serum bottle with the inoculum to substrate ratio (ISR) of 2 based on the weight of VS [11]. Concentration of OPMF sample was 0.6% VS. The liquid volume was adjusted using basal medium at pH 7.0 with final working volume at 80 mL. The anaerobic condition was set and incubated at 37°C. The biogas production and composition were determined. A modified Gompertz equation was fitted to the CH_4 cumulative data [12]. By using the equation model, the production potential, maximum production rate and the lag phase of the reaction were determined.

AD of Solid-State Content of OPMF in the Modified Solid Inclined (MSI) Reactor

The suitable inoculum and pretreatment method of OPMF from above study was applied in MSI reactor. The 23.5 L lab-scale MSI reactor was constructed of two compartments of upper (15.3 L) and bottom (8.1 L) separating by inclined base stainless steel (30° slope) with 4.0 mm pores distributing throughout the plate as shown in **Figure 1**. The upper part with 9 L working volume hold 3 kg of OPMF, 3 kg of inoculum, and the space for spraying of liquid leachate. The bottom part was for 3 L of leachate. The ISR was 1:1 by weight. This system was operated at an ambient temperature (30-33°C) in batch mode with liquid leachate recirculation once a day. The selected OPMF and inoculum was conducted and investigated the MSI reactor performance and stability during AD.

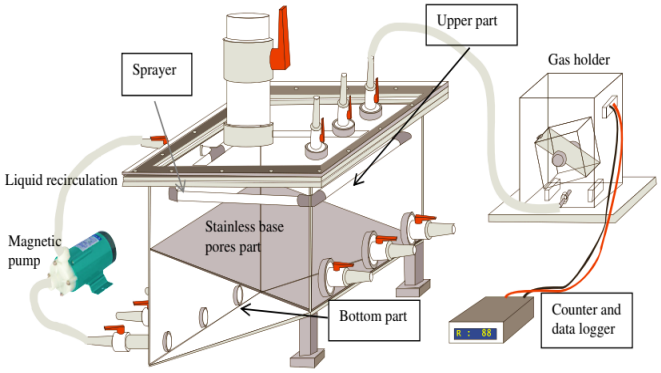


Figure 1 Lab-scale modified solid inclined reactor [13]

Analytical Methods

pH, TS, VS, oil and grease, chemical oxygen demand (COD), total volatile fatty acids (TVA), and alkalinity were analyzed according to the procedures by the American Public Health Association (APHA) standard methods [14]. The cellulose, hemicellulose, and lignin contents were analyzed using a Fibretherm® (Gerhardt GmbH Co Ltd). The daily biogas volume was measured using water replacement method. The content of methane and carbon dioxide in the biogas was analyzed by gas chromatography (Shimadzu, Class-GC 14B, Japan) with a Porapak-N column equipped with a thermal conductivity detector [15].

Statistical Analysis

Data from the effect of inoculum and pretreatment on AD of OPMF (TS, VS and COD), solid residues (oil, cellulose, hemicellulose, and lignin) and kinetic data in the BMP assay and MSI reactor during incubation were statistically analyzed using analysis of variance (ANOVA) followed by Tukey's LSD (least significant difference). The means and standard deviation were presented, and the significant differences were set at $P < 0.05$.

RESULTS AND DISCUSSIONS

BMP of OPMF using Various Inoculums

During the first 15 days of incubation, the cumulative methane production from CM was higher than POME, and SM in 2 and 10 times, respectively (**Figure 2**). According to kinetic data (**Table 1**), maximum methane production of CM, POME and SM was 356, 168, and 162 mL/gVS within 30, 40, and 50 days, respectively. CM produced higher methane production rates (18.8 mL/d) than POME (6.8 mL/d) and SM (5.8 mL/d). In addition, CM had shorter lag time (0.24 d) than POME (0.36 d) and SM (10.51 d). These results indicate that CM is the suitable inoculum for methane production from high lignocellulosic material of OPMF. Gu et al [16] and Dhamodharan et al [17] were also reported that microbial inoculum from CM has the highest ability to degrade rice straw and food waste for methane production among other livestock manure and anaerobic microbial sludge, respectively.

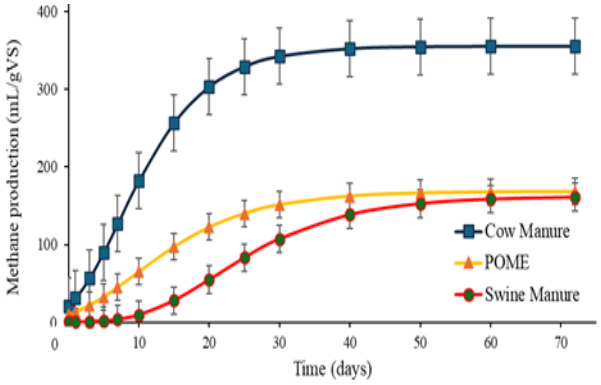


Figure 2 Cumulative methane production from various inoculums

Table 1 Kinetic data of BMP assay with various inoculums

Parameters	POME		
	POME	CM	SM
Lag time (d)	0.36±0.02[a]	0.24±0.01[b]	10.51±0.65[c]
Max methane production date (d)	40[a]	30[b]	50[c]
Methane production rate (mL/d)	6.76±0.06[a]	18.83±1.00[b]	5.77±0.33[c]
Methane yield (mL/gVS)	168.43±1.19[a]	355.83±0.61[b]	162.18±0.28[c]
r^2	0.970±0.00	0.997±0.00	0.980±0.00

Means with different letters are significantly different (Tukey's LSD, $P < 0.05$)

Effect of Pretreatment on Methane Production from OPMF

Characteristics of OPMF Samples

OPMF has a high bulky characteristic with high fiber contents. Lignocellulose content will depend on the types of lignocellulosic biomass. Rice straw, corn stover, and wheat straw had higher content of cellulose and hemicellulose but similar lignin content comparing to OPMF [6]. Pretreatments of BHW and SHW slightly effect on the partial solubilization of lignocelluloses in OPMF compared to OPMF-NP. The remaining contents of cellulose, hemicellulose, and lignin including oil in OPMF-SHW were lower than OPMF-BHW and OPMF-NP as shown in **Table 2**. OPMF-SHW can solubilize lignocelluloses and oil better than lower ones (OPMF-BHW and OPMF-NP). The thermal solubilization of biomass occurs in water and affects the physicochemical properties of water. Organic materials are insoluble in water under ambient conditions, water can be a good solvent for non-polar organic materials under supercritical conditions. An increase in the ionic character of water (hydronium and hydroxide ions) can facilitate acid–base-catalyzed reactions [18].

Table 2 Composition of non-pretreated and pretreated OPMF

	Composition ((g/kg*)					
Substrate	TS	VS	Cellulose	Hemicellulose	Lignin	Oil
OPMF-NP	622.90±5.8	588.83±2.1	206.99±5.3	138.53±0.5	130.19±1.0	27.97±0.2
OPMF-BHW	597.65±1.9	553.88±3.7	196.75±6.8	128.43±6.7	123.95±8.2	25.03±0.1
OPMF-SHW	559.36±2.5	518.08±1.0	154.96±6.0	111.85±4.8	113.28±1.4	22.23±0.1

*per kg wet basis of OPMF sample

BMP Assays of OPMF Samples

For determination of methane potential of OPMF-NP, OPMF-BHW, and OPMF-SHW, CM was selected for inoculum in this experiment. **Figure 3** shows that methane production from the pretreated OPMF-BHW (366 mL/gVS), OPMF-SHW (369 mL/gVS), and non- pretreated OPMF-NP (340 mL/gVS) were not much different.

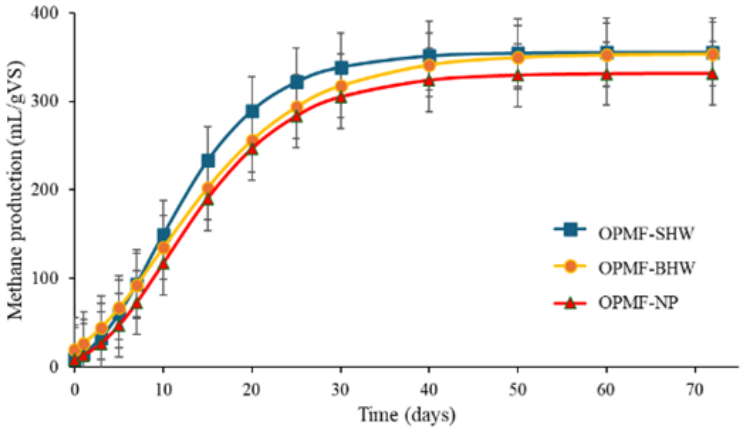


Figure 3 BMP assay for non-pretreated and pretreated OPMF sample

Hemicellulose, the branched and amorphous polysaccharide with the heteropolymer structures in lignocellulose, has been almost completely degraded in all OPMF samples (**Figure 4**). Similar result was found in lignin removal. Cellulose and oil were partially removed 70-85% and 60-75%, respectively. The removal of organic matters in OPMF-BHW, OPMF-SHW, and OPMF-NP were not significantly different among them. These results are reflected in BMP assays.

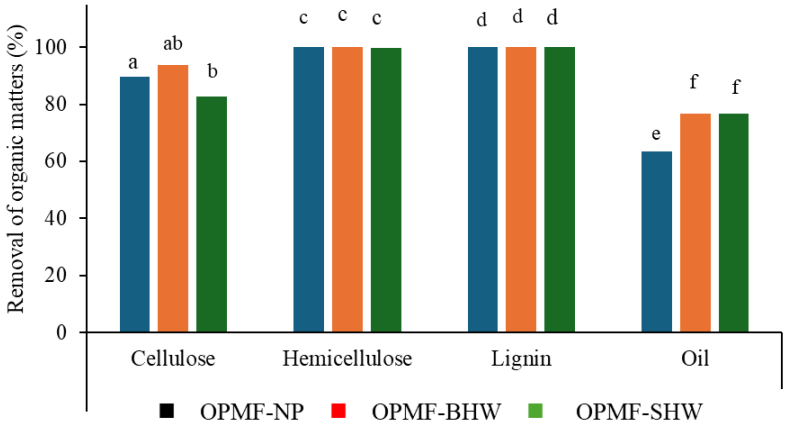


Figure 4 Removal of organic matters from BMP assay of OPMF using CM, inoculum. This graph represents the repeated measures ANOVA ($P < 0.05$) comparing the mean values, columns labelled with different letters are significantly different (Tukey's LSD, $P < 0.05$).

The OPMF sample has a high crystallinity index at 67.2%. In this form of cellulose structure is recalcitrant for biodegradation. Therefore, OPMF having a rigid fiber structure containing high cellulose content and oil, the biodegradation of lignocellulose by anaerobic microorganisms was quite difficult when using relatively low temperature pretreatment at 100-121°C. Whereas the thermal pretreatment of oil palm

decanter cake (OPDC) with BHW shows the positive effect for enhancing the methane production from the study of Eko and Chaiprasert [13]. It was noticed that the structure and content of cellulose in lignocellulosic biomass including oil should be the factors effect on pretreatment method to breakdown of these compounds.

Performance and Stability of Solid-State MSI reactor in Methane Production from OPMF

According to the experiment, MSI reactor was fed with raw OPMF (62% TS, 95% VS, and 1.18% TKN) and CM inoculum in a batch system. High composition of organic content with 95% VS containing 101.2 g/L of total COD (CODt).

Process Stability

The parameters of pH, TVA, and alkalinity were monitored during the incubation time. The MSI reactor was incubated for 60 days of digestion period. The initial pH was recorded at 7.08 with 1,200 mg/L of TVA, and 5,350 mg/L of alkalinity. Values of pH, TVA, alkalinity, and ratio of TVA/alkalinity during 30 and 60 days of MSI operation were 7.6 and 7.5, 600 and 200 mg/L, 4,300 and 4,000 mg/L, and 0.14 and 0.05, respectively (**Table 3**). pH was quite stable in neutral range. Ratio of TVA/alkalinity was lower than 0.4 with high buffer capacity (high alkalinity) and lower TVA. These results reflected that MSI reactor was quite stable during AD of OPMF. This range of pH (7.00±0.5) and TVA/alkalinity ratio (below than 0.4) are suitable for AD microorganisms and minimizes the inhibition of the AD process, reflecting the process stability [19].

Table 3 Stability of MSI reactor

Parameters	**Period of AD**	
	30 d	**60 d**
pH	7.6±0.2	7.5±0.1
TVA (mg/L)	600±100	200±30
Alkalinity (mg/L)	4,300±20	4,000±10
TVA/ Alkalinity	0.14±0.01	0.05±0.01

Process Performance

The effectiveness of MSI reactor for treating the solid-state OPMF was monitored between 30 and 60 days of incubation. Organic matters were slowly degraded. Removal of TS, VS, and CODt during 30 and 60 days were 7 and 10%, 36 and 39%, and 20 and 35%, respectively (**Figure 5a**). While removal of cellulose, hemicellulose, lignin, and oil were not significantly different between 30 and 60 d with 38, 42, 1-5, and 85%, respectively (**Figure 5b**). The removal of organic matters occurred during 30 d and no further degradation due to recalcitrant structure of lignocellulosic OPMF making it hardly to degrade.

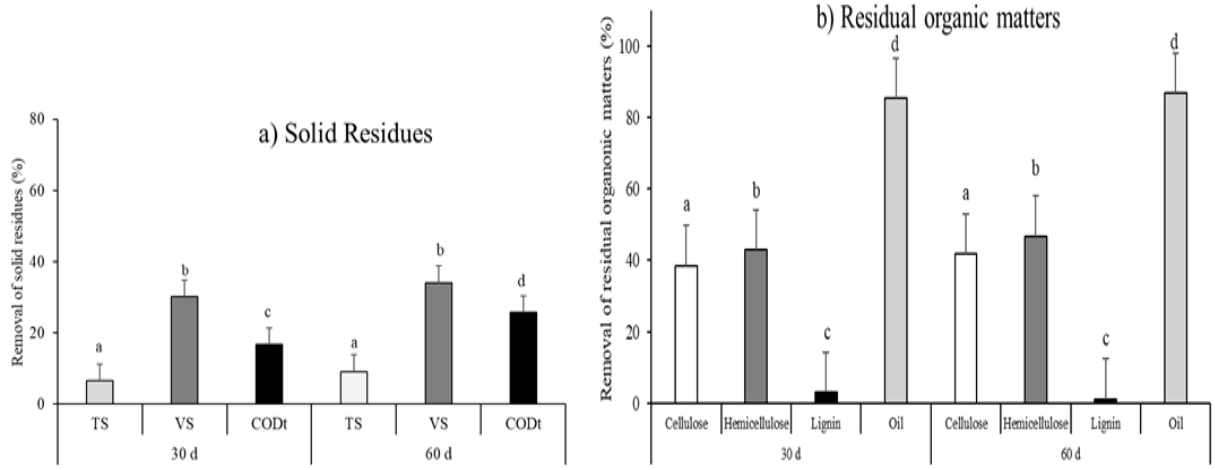


Figure 5 Removal of solid residues (a) and organic matters (b) in OPMF. This graph represents the repeated measures ANOVA ($P < 0.05$) comparing the mean values, columns labelled with different letters are significantly different (Tukey's LSD, $P < 0.05$).

Low biodegradation of OPMF resulted in low biogas production from high solid content in MSI reactor with ISR of 1:1. The biogas and methane production were stable within 30 days (**Figure 6**). Methane production rate, methane production potential, and methane yield for OPMF were 9.2 L/d, 160 L, and 266 L/KgVS, respectively (**Table 4**). In addition, Chaikitkaew et al [20] reported the methane yield and organic matter removal of high solid-AD of OPMF with 25% TS content at different ISR ratio of 1:2 and 1:6 were 140 and 112 L/kgVS and 80 and 42% in 45 d of incubation time, respectively. The ISR ratio had an effect on methane reduction. Thus, to enhance methane production in MSI reactor for the future study, ISR ratio in high solid content reactor should firstly be optimized. In addition, switching from a batch to a fed-batch feeding mode in an MSI reactor, if feasible, can lead to a higher feedstock loading rate and a more efficient semi-continuous operation by allowing controlled nutrient addition and product removal.

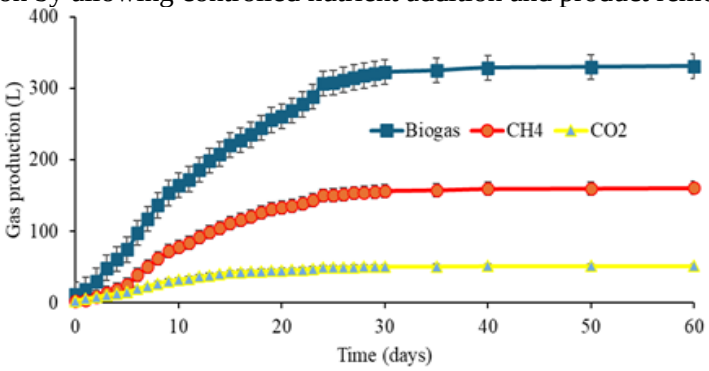


Figure 6 Production of gas during AD of OPMF

Table 4 Kinetic data of OPMF on MSI reactor

Kinetic parameters	unit	Period of AD	
		30 d	60 d
Lag time	d	1.89	1.88
Maximum methane production rate	L/d	9.21	9.18
Methane production potential	L	159.89	160.19
Methane yield	L/KgVS	266.01	241.43
r^2		0.997	0.997

The methane yield determined by a BMP assay is indeed a widely used and reliable indicator of a feedstock's potential for methane production through AD. Normally, BMP test using feedstock or substrate at 0.5-1.0% VS (low solid content) for determination of methane production. It measures the maximum volume of methane gas that can be produced from a substrate, typically expressed as volume of methane per weight of VS. BMP value is affected by a number of factors such as type and composition of substrate, substrate concentration, ISR, temperature, and mixing. Some methane yield values from BMP test reported from the literature searches are shown in **Table 5**. Methane yields from various organic substrates vary significantly depending on their composition and biodegradability. Lignin-rich organic waste produced a much lowest yield of 200 L/kg VS, likely due to its recalcitrant structure. In an MSI reactor with a high solid content (62% TS with 95% VS), methane production was observed to be slightly lower.

Table 5 Comparison of methane yield from OPMF and another lignocellulosic biomass by BMP assay

Substrates	Methane yield (L/kg VS)	References
Rice straw	350	[21]
Maize silage and straw	312	
Lignin-rich organic waste	200	
Food waste	396	
Oil palm mesocarp fiber (OPMF)	355-365	This study
Oil palm mesocarp fiber (OPMF)*	266 (high solid content, MSI reactor)	

* Not determined by BMP assay but monitored from reactor

CONCLUSION

Source of microbial inoculum was an important factor to accelerate AD of OPMF. CM inoculum shows the best performance in AD compared to POME and SM. BHW and SHW pretreatment at low temperature (100-121 °C) and pressure (14.7-15.0 psi) show less effect on OPMF pretreatment. High solid content MSI reactor for methane production from OPMF can be enhanced and applied in the future if the optimized ISR and fed batch feeding mode will be applied and conducted. Using a MSI reactor for high-solid AD of OPMF offers a promising pathway to high methane yield, enabling the palm oil industry to achieve economic sustainability and environmental responsibility through a circular economy approach.

ACKNOWLEDGEMENT

The authors gratefully acknowledge the financial support by King Mongkut's University of Technology Thonburi (KMUTT), Thailand Science Research and Innovation (TSRI), and National Science, Research and Innovation Fund (NSRF) Fiscal year 2567 Grant number FRB670016/0164.

REFERENCES

[1] Sowcharoensuk, C. 2023. Thailand Industry Outlook 2024-26: Palm Oil Industry. Krungsri Research. 1-77.

[2] Ng, F., Yew, F., Basiron, Y. and Sundram, K. 2012. A renewable future driven with Malaysia palm oil-based green technology. Journal of Oil Palm & The Environment. 2: 1-7.

[3] Patinvoh, R.J., Osadolor, O.A., Chandolias, K., Sarvari Horvath, I. and Taherzadeh, M.J. 2017. Innovative pretreatment strategies for biogas production. Bioresource Technology. 224: 13-24.

[4] Costa, A.G., Pinheiro, G.C., Pinheiro, F.G.C., Dos Santos, A.B., Santaella, S.T. and Leitão, R.C. 2013. Pretreatment strategies to improve anaerobic biodegradability and methane production potential of the palm oil mesocarp fibre. Chemical Engineering Journal. 230: 158-165.

[5] Peral, C. 2016. Biomass Pretreatment Strategies (Technologies, Environmental Performance, Economic Considerations, Industrial Implementation). in: Biotransformation of Agricultural Waste and By-Products. 125-160.

[6] Ahmad, F., Silva, E.L. and Varesche, M.B.A. 2018. Hydrothermal processing of biomass for anaerobic digestion – A review. Renewable and Sustainable Energy Reviews. 98: 108-124.

[7] Zheng, Y., Zhao, J., Xu, F. and Li, Y. 2014. Pretreatment of lignocellulosic biomass for enhanced biogas production. Progress in Energy and Combustion Science. 42: 35-53.

[8] Yang, L., Xu, F., Ge, X. and Li, Y. 2015. Challenges and strategies for solid-state anaerobic digestion of lignocellulosic biomass. Renewable and Sustainable Energy Reviews. 44: 824-834.

[9] Ge, X., Xu, F. and Li, Y. 2016. Solid-state anaerobic digestion of lignocellulosic biomass: Recent progress and perspectives. Bioresource Technology. 205: 239-49.

[10] Brown, D., Shi, J. and Li, Y. 2012. Comparison of solid-state to liquid anaerobic digestion of lignocellulosic feedstocks for biogas production. Bioresource Technology. 124: 379-86.

[11] Hansen, T.L., Schmidt, J.E., Angelidaki, I., Marca, E., Jansen, J., Mosbaek, H. and Christensen, T.H. 2004. Method for determination of methane potentials of solid organic waste. Waste Management. 24(4), 393-400.

[12] Lo, H.M., Kurniawan, T.A., Sillanpaa, M.E., Pai, T.Y., Chiang, C.F., Chao, K.P., Liu, M.H., Chuang, S.H., Banks, C.J., Wang, S.C., Lin, K.C., Lin, C.Y., Liu, W.F., Cheng, P.H., Chen, C.K., Chiu, H.Y. and Wu, H.Y. 2010. Modeling biogas production from organic fraction of MSW co-digested with MSWI ashes in anaerobic bioreactors. Bioresource Technology. 101(16): 6329-35.

[13] Eko, H. and Chaiprasert, P. 2020. Enhancement of methane production from high solid anaerobic digestion of pretreated palm oil decanter cake using a modified solid inclined reactor. Journal of Chemical Technology & Biotechnology. 95(3): 781-790.

[14] APHA/AWWA/WEF. 2017. Standard Methods for the Examination of Water and Wastewater, American Public Health Association. Washington, DC, USA.

[15] Panichnumsin, P., Nopharatana, A., Ahring, B.K. and Chaiprasert, P. 2012. Enhanced Biomethanation in Co-Digestion of Cassava Pulp and pig manure using a two-phase anaerobic system. Journal of Sustainable Energy & Environment. 3: 73-79.

[16] Gu, Y., Chen, X., Liu, Z., Zhou, X. and Zhang, Y. 2014. Effect of inoculum sources on the anaerobic digestion of rice straw. Bioresource Technology. 158: 149-55.

[17] Dhamodharan, K., Kumar, V. and Kalamdhad, A.S. 2015. Effect of different livestock dungs as inoculum on food waste anaerobic digestion and its kinetics. Bioresource Technology. 180: 237-41.
[18] Elliott DC. 2011. Hydrothermal Processing, Thermochemical Processing of Biomass: Conversion into Fuels. In: Brown RC, editor. Chemicals and Power. Chichester, UK: John Wiley & Sons, Ltd. 200–231
[19] Jabeen, M., Zeshan, Yousaf, S, Haider, M.R. and Malik, R.N. 2015. High-solids anaerobic co-digestion of food waste and rice husk at different organic loading rates. International Biodeterioration and Biodegradation. 102: 149–153.
[20] Chaikitkaew, S., Kongjan, P., O-Thong, S. 2015. Biogas production from biomass residues of palm oil mill by solid state anaerobic digestion. Energy Procedia. 79: 838-844.
[21] Khalid, A., Arshad, M., Anjum, M., Mahmood, T. and Dawson, L. 2011. The anaerobic digestion of solid organic waste. Waste Management. 31(8): 1737–1744.

The Role of Street Trees in Mitigating Particulate Matter Pollution: A Case Study of $PM_{2.5}$ and PM_{10} Concentrations in Urban Street Canyon

Pasita Ngowpradit[1*], Wanarat Konisranukul[2] and Yaowatat Boongla[2]

[1]Graduate student ; [2]Assist. Prof., Faculty of Science and Technology, Thammasat University.*
Phone: 02-564-4482, E-mail : kwanarat@gmail.com

ABSTRACT

This study evaluates the effectiveness of street trees in reducing particulate matter ($PM_{2.5}$ and PM_{10}) concentrations in an urban street canyon along Sukhumvit Road, Samut Prakan Municipality, Thailand. Field measurements were conducted at pedestrian level (1.5 m height) across three sidewalk microenvironments: beneath tree canopies, between trees, and in open, non-vegetated areas. Real-time particle counters monitored PM levels, temperature, humidity, and wind speed over a two-week period. Results demonstrated consistently lower PM concentrations on sidewalk with street trees. Relative Difference in Concentration (RDC) analysis revealed negative values for 70.8% of $PM_{2.5}$ (17/24) and 75.0% of PM_{10} (18/24) measurements, with average reductions of 3.74% and 4.11%, respectively, beneath tree canopies. Statistical analysis (ANOVA) confirmed significant PM_{10} reduction ($p = 0.030$), while $PM_{2.5}$ differences were marginally non-significant ($p = 0.058$). Tree canopies also moderated microclimate conditions, lowering ambient temperature by 0.33°C and wind speed by 0.83 m/s compared to non-vegetated areas. These findings highlight street trees as effective, sustainable interventions for urban air quality improvement, particularly for coarse particle (PM_{10}) mitigation. The study provides actionable insights for urban planners and policymakers advocating nature-based solutions in high-density built environments.

Keywords : street trees; PM2.5; PM10; urban; street canyon

INTRODUCTION

The use of green infrastructure to mitigate particulate pollution and enhance environmental quality in urban areas has gained significant recognition. Empirical studies have established a significant correlation between urban green space coverage and reduced ambient particulate matter (PM) concentrations [1–4]. In recent years, the role of street trees in reducing the adverse effects of particulate matter (PM) in urban areas has been increasingly recognized, particularly among researchers focused on improving air quality in the built environment. However, the impact of street trees on particle concentrations in built-up street canyons is complex [5]. Their effectiveness in capturing particulate matter and influencing local airflow, which may either enhance or inhibit pollutant dispersion depends on various factors [6-7].

Numerous field studies support the premise that increased vegetation coverage generally correlates with lower particulate pollution levels in urban settings [2][4][8]. Trees function as natural filters, intercepting airborne particles and absorbing gaseous pollutants, while specific spatial arrangements can alter wind patterns or create localized microclimates that facilitate pollutant removal [9]. Nevertheless, contradictory findings indicate that vegetation, including urban tree canopies, may exhibit limited PM reduction efficacy under certain conditions [10-11]. For example, Gromke et al. [12] reported that larger tree crowns and reduced spacing between street trees can elevate PM concentrations along canyon walls due to restricted airflow. Similarly, dense foliage has been shown to reduce wind speeds, inadvertently promoting PM accumulation in some scenarios [13]. These conflicting findings highlight the dual role of street trees. While trees can act as protective barriers against traffic emissions at the pedestrian level, their planting designs critically influence wind dynamics and pollutant dispersion [14]. Consequently, optimizing green infrastructure requires careful consideration of these trade-offs to maximize air quality benefits.

Meteorological conditions further complicate this relationship. Parameters such as humidity, temperature, precipitation, wind speed, and direction differentially affect PM concentrations across particle size fractions [15,16]. As Yanling et al [17] demonstrated, these variables drive spatio-temporal PM variability by influencing pollutant accumulation and dispersion processes. Additionally, large-scale weather patterns and various meteorological factors interact with local meteorological conditions to shape $PM_{2.5}$ and PM_{10} pollution patterns [18–20], adding another layer of complexity to urban air quality dynamics.

In this context, this study investigates the impact of street trees on PM concentrations through direct measurements of $PM_{2.5}$ and PM_{10} levels in street canyons with and without tree cover in Samut Prakan Municipality, a high-density urban area experiencing worsening particulate pollution. The main objective is to assess how the presence or absence of street trees in the urban environment affects air quality, particularly $PM_{2.5}$ and PM_{10} at the pedestrian level. Concurrent measurements of wind velocity, temperature, and humidity were conducted to identify key influencing factors and support the interpretation of pollution patterns. Over the past 2–3 years, Samut Prakan has recorded an average of 30 annual exceedances of the $PM_{2.5}$ standard [21], highlighting the urgency of evidence-based solutions. The findings aim to provide urban planners and designers with actionable insights for deploying street trees as sustainable PM mitigation tools.

METHODOLOGY

Study area

This study examines the impact of street trees on $PM_{2.5}$ and PM_{10} levels along Sukhumvit Road, a major traffic corridor in Samut Prakan Municipality. Meteorological data from the urban district of Samut Prakan recorded a mean air temperature of 28.4°C, relative humidity of 74%, and a mean wind speed of 3.89 m/s. In 2022, the highest 24-hour average $PM_{2.5}$ concentration reached 108 µg/m³—nearly triple Thailand's 24-hour standard (37.5 µg/m³)—while the annual mean likewise exceeded the national limit (15 µg/m³). These violations correlate with the area's characteristics, including its high building density, diverse land-use activities, and consistently heavy traffic volume throughout the day. Structurally, Sukhumvit Road is a six-lane, concrete-paved road with opposing traffic lanes. The roadside is primarily lined with commercial buildings, government offices, and residential areas and an aspect ratio of approximately 0.5. Vegetation coverage varies, with some sections densely treed while others lack greenery entirely, as shown in Figure 1. This variation provides a framework for assessing the influence of tree cover on air quality in both vegetated and non-vegetated sections.

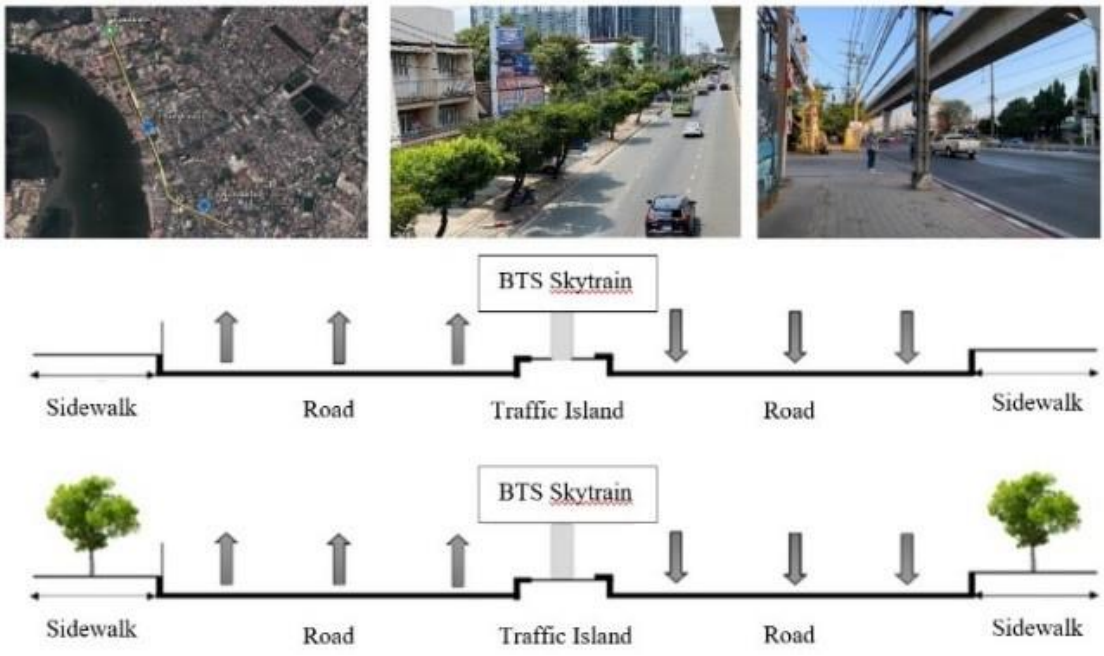


Figure 1 Characteristics of Sukhumvit Road

Methods

To investigate the effect of street trees, sampling sites with similar background concentrations were selected along Sukhumvit Road. Field measurements were carried out on the sidewalks of three segments of Sukhumvit Road in Samut Prakan Municipality, as shown in Figure 2. Since the road runs north to south, each sampling point was placed on the sidewalk within the street canyon on the leeward side of the prevailing wind direction to minimize the direct influence of roadside trees on pollutant concentrations [22].

Measurements were taken at a height of 1.5 meters above ground level, with three sampling points per road segment: (1) beneath tree canopy, (2) between two trees, and (3) in open areas without tree. Each segment was at least 100 meters long and included three sampling points located on the same side of the road. The sampling points without trees were positioned at least 25 meters away from any trees

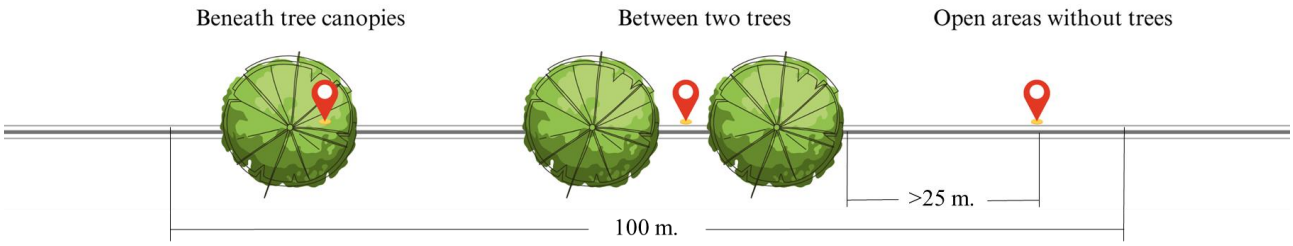


Figure 2 Field measurements were carried out on the three segments of sidewalks with three sampling points per road segment: (1) beneath tree canopy, (2) between two trees, and (3) in open areas without trees.

Data Collection and Analysis

To achieve the research objectives, this study investigates the influence of street trees on particulate matter (PM) concentrations by measuring $PM_{2.5}$ and PM_{10} levels using real-time particle counters (CEM DT-9880, ±5% accuracy) along Sukhumvit Road. In each segment, $PM_{2.5}$, PM_{10}, and microclimatic factors, including relative humidity, temperature, and wind speed, were simultaneously recorded at three sidewalk sampling points: beneath tree canopies, between two trees, and in open areas without trees. Both PM and microclimate data were logged every five minutes. Data collection was conducted between January 20, 2022, and February 7, 2022, from 07:00 am. to 6:00 pm. on both weekdays and weekends, with five sampling days per segment over a two-week period covering all three segments.

The relative difference in concentration (RDC) was used to quantify the influence of street trees on particle concentrations ($PM_{2.5}$ and PM_{10}) at pedestrian level [20]. RDC was calculated as the difference in particle concentrations between tree-covered and open areas, as shown in Equation (1). Statistical analysis was performed using one-way ANOVA and the least significant difference (LSD) test to evaluate the effects of street trees on PM concentrations and microclimatic variables, using SPSS software.

$$RDC = \frac{C_{tree} - C_{ref}}{C_{ref}} \times 100 \qquad \text{Equation (1)}$$

where C_{tree} is the particle concentration at area with tree ($\mu g/m^3$)
C_{ref} is the particle concentration at area without tree/between tree ($\mu g/m^3$)

RESULTS AND DISCUSSIONS

PM Concentration and PM2.5/PM10 Ratio

$PM_{2.5}$ and PM_{10} concentrations along Sukhumvit Road were analyzed using hourly field data collected between 7:00 AM and 6:00 PM over a two-week period. The spatiotemporal variability of the $PM_{2.5}/PM_{10}$ ratio was examined based on these hourly measurements to better understand the dynamics of particulate matter distribution throughout the day. The results revealed that peak particulate concentrations occurred during morning rush hours (7:00–9:00 AM) across all sampling points. Beneath tree canopies, $PM_{2.5}$ and PM_{10} peaked at 45.70 $\mu g/m^3$ and 73.47 $\mu g/m^3$, respectively, at 7:00 AM, before gradually declining to their lowest levels at noon (35.24 $\mu g/m^3$ for $PM_{2.5}$ and 56.00 $\mu g/m^3$ for PM_{10} at 12:00 PM). Open areas without tree cover exhibited similar diurnal trends but with slightly higher concentrations, reaching maxima of 47.05 $\mu g/m^3$ ($PM_{2.5}$) and 74.96 $\mu g/m^3$ (PM_{10}) at 7:00 AM and minima of 34.80 $\mu g/m^3$ ($PM_{2.5}$) and 55.82 $\mu g/m^3$ (PM_{10}) at 2:00 PM. The most pronounced variability was observed between trees, where peak concentrations were highest (48.91 $\mu g/m^3$ $PM_{2.5}$ and 77.48 $\mu g/m^3$ PM_{10} at 8:00 AM). Across all sites, particulate matter concentrations were consistently lowest during early afternoon hours (12:00–2:00 PM), as illustrated in Figure 2.

$PM_{2.5}/PM_{10}$ ratios were subsequently calculated (Figure 2). The results indicate that the ratios across the three sites—beneath tree canopies, between two trees, and in open areas without trees—ranged from 0.620 to 0.657, 0.623 to 0.636, and 0.574 to 0.640, respectively. The highest ratio (0.657) was observed beneath tree canopies, suggesting that street trees may selectively reduce PM_{10} through leaf deposition, thereby increasing the relative proportion of $PM_{2.5}$ [23-24]. In contrast, open areas without trees exhibited a

narrower ratio range (0.623–0.636), indicating greater stability, likely due to the absence of vegetation-driven particle filtration [25]. The most variable ratios (0.574–0.640) were recorded between trees, where the lowest value (0.574) suggests intermittent PM_{10} dominance. This variability may result from airflow disturbances in tree gaps, which could promote coarse particle resuspension or uneven pollutant dispersion [26].

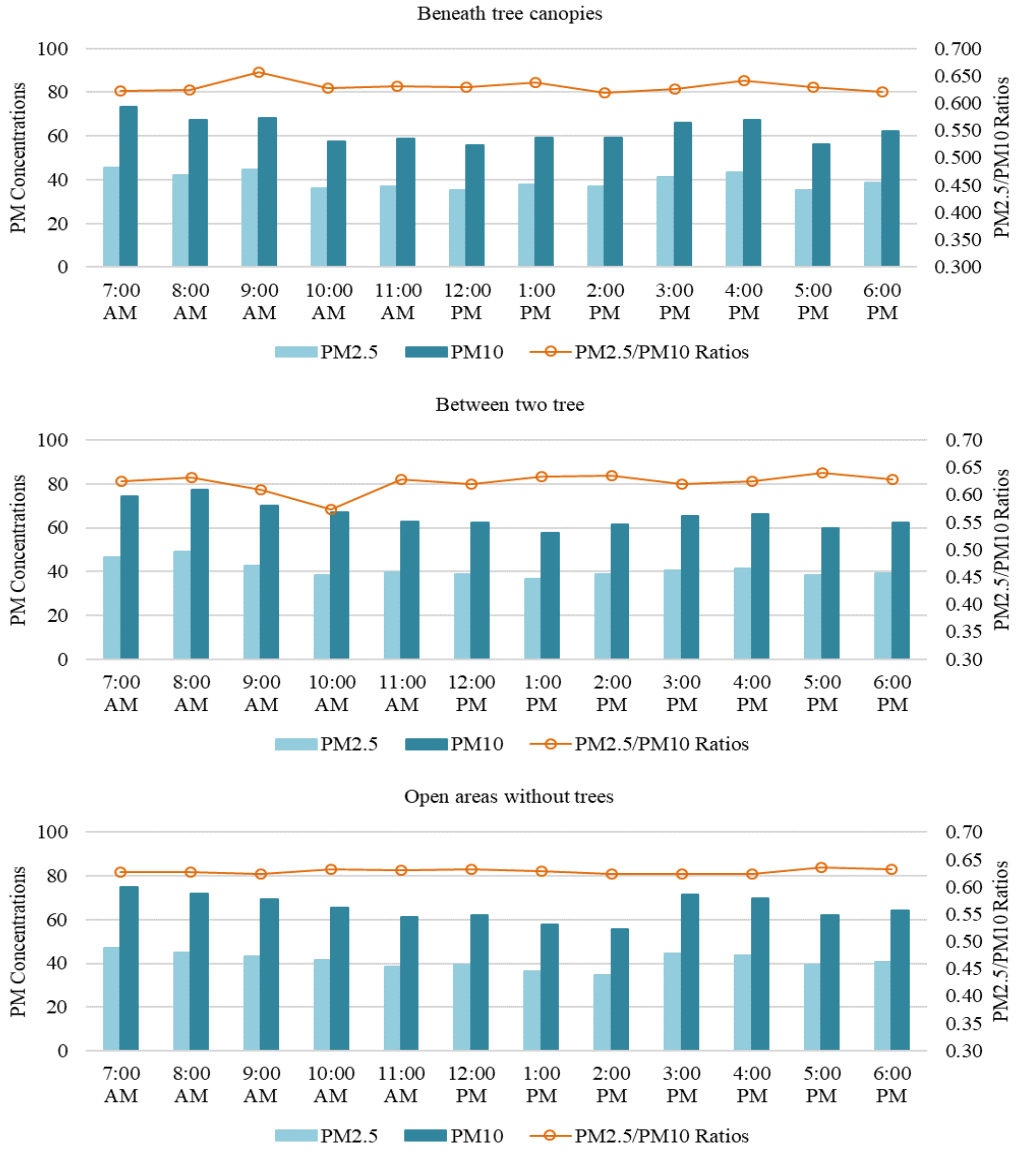


Figure 3 PM Concentrations and ratios of the PM2.5/PM10 on Sukhumvit Road

PM Concentration and RDC

Figure 4 presents the hourly $PM_{2.5}$ and PM_{10} concentrations along Sukhumvit Road, accompanied by their corresponding RDC values. The results demonstrate that street trees significantly influence particulate matter levels. The highest reduction of $PM_{2.5}$ beneath trees was found at 10:00 AM (RDC_BTC = -12.49%), and at 8:00 AM for between two trees (RDC_BWT = -13.99%). These times correspond with relatively lower $PM_{2.5}$ concentrations at vegetated sites compared to tree-free areas. A similar trend is evident for PM_{10} concentrations, where the most pronounced reductions occurred at 10:00 AM as well, with beneath tree canopies reaching -11.87% and between two trees as low as -14.16%. These values are slightly more substantial than those observed for $PM_{2.5}$ at the same time, suggesting that tree canopies and vegetated areas are particularly effective at capturing larger particulate matter. In addition, as shows in figure 4, during the early morning hours (7:00–9:00 AM), $PM_{2.5}$ concentrations beneath trees were occasionally comparable to or

slightly higher than those in treeless area (WT), particularly at 9:00 AM. This may be due to limited airflow under the canopy, which can temporarily trap pollutants. This pattern reversed after 9:00 AM, when PM concentrations at non-vegetated sites exceeded those at vegetated locations. The temporal variations in RDC values reflect dynamic interactions between traffic emissions, wind patterns, and vegetation structure.

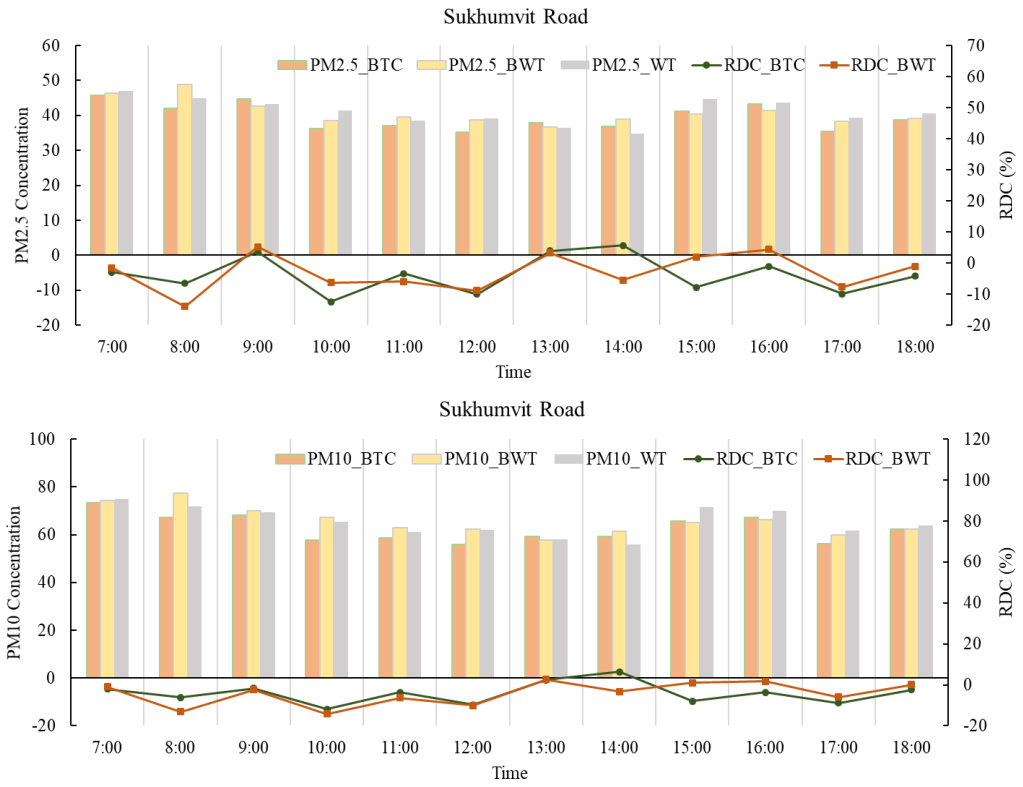


Figure 4 illustrates the PM2.5 and PM10 concentration from 7:00 a.m. to 6:00 p.m. on Sukhumvit Road. BTC, BTT and WT represent Beneath Tree Canopy, Between Two Trees, and Without Tree.

As illustrated in Figure 5, the RDC values for $PM_{2.5}$ and PM_{10} along Sukhumvit Road were predominantly negative, demonstrating consistently lower particulate matter concentrations at vegetated locations compared to non-vegetated areas. Specifically, 17 of 24 RDC values for $PM_{2.5}$ (9 beneath tree canopies [BTC] and 8 between trees [BWT]) were negative, while 18 of 24 values for PM_{10} showed the same trend. On average, $PM_{2.5}$ concentrations were reduced by approximately 3.74% beneath tree canopies (BTC) and 2.99% between trees (BWT), while PM_{10} concentrations were reduced by about 4.11% beneath tree canopies and 4.27% between trees. These findings clearly indicate that both fully and partially vegetated areas significantly reduce PM levels relative to tree-free zones, with PM_{10} showing the most pronounced reduction. The results underscore the efficacy of urban vegetation, particularly tree canopies, in mitigating particulate pollution—an effect that is more substantial for coarse particles (PM_{10}) than fine particles ($PM_{2.5}$).

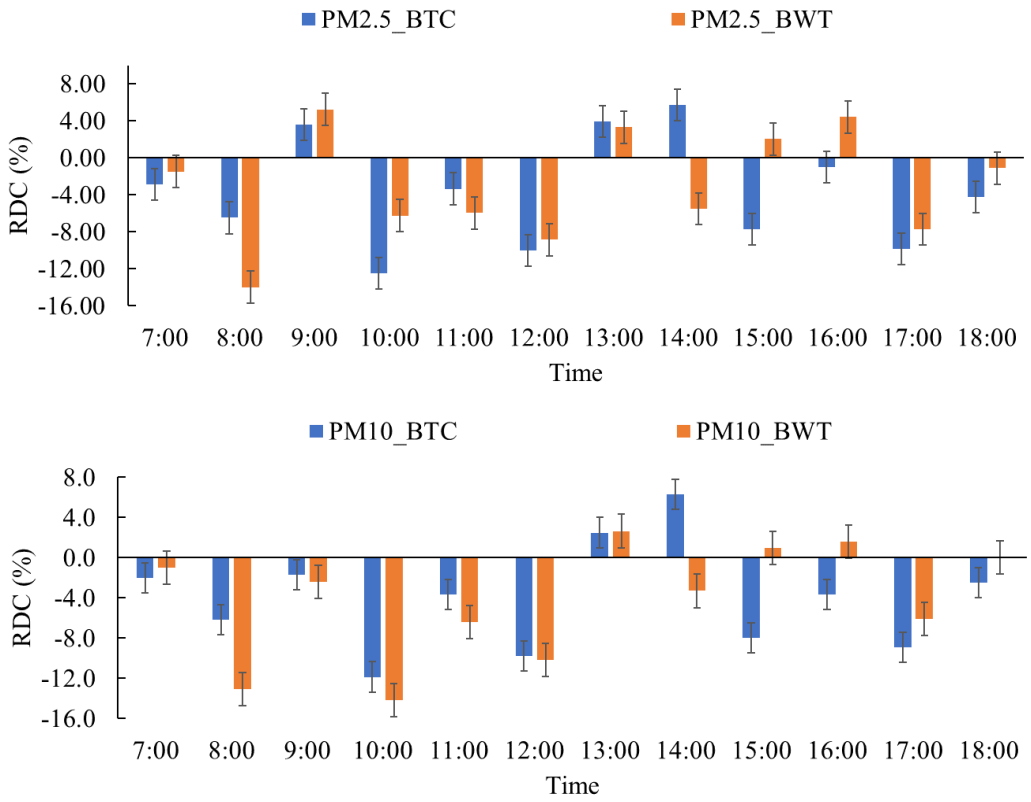


Figure 5 RDC values for PM $_{2.5}$ and PM $_{10}$ at different times on Sukhumvit Road. Where BTC, BTT and WT represent Beneath Tree Canopy, Between Two Trees, and Without Tree, respectively.

The effect of Tree on PM and Microclimate

ANOVA was conducted to determine whether there were variations in PM concentrations and microclimate among the sampling points (beneath tree canopy, between two trees, and open areas without trees). The results revealed differences in particulate matter concentrations ($PM_{2.5}$ and PM_{10}) across the three sampling points. For $PM_{2.5}$, the mean concentration was lowest under tree canopies (39.45 µg/m³), slightly higher in open areas (41.00 µg/m³), and comparable between trees (40.71 µg/m³). The one-way ANOVA shows that these differences were not statistically significant at the 0.05 level ($p = 0.058$), indicating that while trees may slightly reduce $PM_{2.5}$ levels, the effect was not strong enough to be conclusive. In contrast, PM_{10} concentrations showed clearer variation across sites. The lowest mean was observed under tree canopies (62.51 µg/m³), followed by the between trees (64.84 µg/m³), and highest in open areas (65.18 µg/m³). The ANOVA test for PM_{10} yielded a statistically significant result ($p = 0.030$), suggesting that tree canopies significantly reduce PM_{10} levels compared to open areas. These findings indicate that street trees are more effective at mitigating larger particles (PM_{10}), possibly due to their capacity to intercept coarse dust particles, while the effect on finer particles like $PM_{2.5}$ may be influenced by additional factors such as wind flow and atmospheric dispersion.

The results revealed significant effects of tree canopies on the urban microclimate. Trees significantly reduced air temperature ($F = 13.168$, $p < 0.001$), with the lowest mean temperature observed under tree canopies (31.07°C), compared to areas without trees (31.40°C, $p < 0.001$). Wind speed was also significantly lower beneath tree canopies (1.54 m/s) than in areas without trees (2.37 m/s, $p < 0.001$) and between trees (2.08 m/s, $p < 0.001$). However, no significant difference was found in relative humidity across the three sampling conditions ($F = 1.873$, $p = 0.154$). Mean differences in microclimatic variables (temperature, humidity, and wind speed) were further examined using LSD post hoc multiple comparisons (see Table 1).

Table 1 LSD multiple comparison tests for determining the effect of trees on the concentration of PM and Microclimate

Comparison (I - J)	Dependent variables									
Sampling Points	$PM_{2.5}$		PM_{10}		Temperature		Humidity		Wind speed	
	M-diff (I-J)	Sig	M-diff (I-J)	Sig	M-diff (I-J)	Sig	M-diff (I-J)	Sig	M-diff (I-J)	Sig
BTC-BTT	-1.25703	0.070	-2.33636	0.016*	-0.33151	0.000*	0.64693	0.106	-0.25846	0.000*
BTC- WT	-1.55095	0.027*	-2.67384	0.008*	-0.39319	0.000*	0.69348	0.083	-0.54061	0.000*
BTT-WT	0.29396	.676	0.33747	0.934	-06168	0.088	-0.04655	0.907	0.28214	0.000*

BTC, BTT and WT represents Beneath Tree Canopy, Between Two Trees, and Without Tree, respectively. M−Diff represents the mean difference *The Mean difference is significant at the 0.05 level (P value= 0.05)

The findings confirm that tree canopies significantly reduce both $PM_{2.5}$ and PM_{10} concentrations while also lowering temperatures and wind speeds, underscoring their role in urban microclimate regulation. These results align with previous studies showing that trees significantly influence local thermal conditions, particularly by providing shade and reducing surface and air temperatures at the pedestrian level [27]. Additionally, the observed reduction in wind speed is consistent with existing literature describing how trees act as windbreaks, decreasing wind flow and turbulence in street canyons [28]. In contrast, the lack of significant variation in humidity may be attributed to the already high baseline humidity commonly found in tropical cities, where atmospheric moisture is near saturation, limiting further influence from vegetation [29]. It is also possible that the scale or density of tree cover in the study area was insufficient to generate measurable changes in ambient humidity.

Conclusion

This study examined the impact of street trees on PM2.5 and PM10 concentrations within a high-density street canyon in Samut Prakan. Results indicate that tree-covered locations effectively mitigate PM pollution at the pedestrian level (1.5 m), with the lowest concentrations observed under tree canopies, followed by areas between trees, and areas without trees. The findings also suggest that street trees can play a meaningful role in improving urban air quality by reducing particulate matter concentrations, particularly PM_{10}. Given the significant reduction of PM_{10} and the observed trends in $PM_{2.5}$ under tree canopies, urban policymakers should consider integrating tree planting into air quality management strategies, especially along high-traffic roads. Promoting the use of dense, broad-leaved species with effective canopy coverage could enhance the interception of airborne particles and improve thermal comfort for pedestrians. However, as this study was conducted on a specific stretch of Sukhumvit Road in Samut Prakan Municipality, its generalizability may be limited. To strengthen policy development, future research should expand the geographic scope by including multiple urban districts with varying built environments, traffic patterns, and vegetation types.

REFERENCE

[1] Thapsaeng, N, Konisranukul, W. and Jirakhajornkul, S. 2018. The Influence of Urban Green Spaces on Airborne Particulate Matter Pollution. In Proceedings of Research Articles. The 6th National and International Academic Conference on Educational Innovation for Sustainable Social Development, Northeasthern University (NEUNIC).

[2] Yli-Pelkonen et al. 2017. Urban forests near roads do not reduce gaseous air pollutant concentrations but have an impact on particles levels, Landsc. Urban Plann, 158; 39–47.

[3] Chen et al. 2019. Effects of neighborhood green space on PM2.5 mitigation: Evidence from five megacities in China, Build. Environ, 156; 33–45.

[4] Irga, P.J., Burchett, M.D. and Torpy, F.R. 2015. Does urban forestry have a quantitative effect on ambient air quality in an urban environment? Atmos Environ, 12(15); 173–181.

[5] Miao, Y., Zhou, W., Qiu, L., and Liu, H. 2020. How the morphology of urban street canyons affects suspended particulate matter concentration at the pedestrian level: An in-situ investigation. Sustainable Cities and Society, 55; 102042.

[6] Buccolieri et al., 2018. Review on urban tree modelling in CFD simulations: Aerodynamic, deposition and thermal effects. Urban Forestry & Urban Greening, 31; 212–220.

[7] Chen, X., Pei, T., Zhou, Z., Teng, M., He, L., Luo, M., and Liu, X. 2015. Efficiency differences of roadside greenbelts with three configurations in removing coarse particles (PM_{10}): A street scale investigation in Wuhan, China. Urban Forestry & Urban Greening, 14(2); 354–360.

[8] Buccolieri, R., Gromke, C., Di Sabatino, S., and Ruck, B. (2009). Aerodynamic effects of trees on pollutant concentration in street canyons. Science of the Total Environment, 407(17); 5247–5256.

[9] Diener, A. and Mudu. 2021. How can vegetation protect us from air pollution? A critical review on green spaces' mitigation abilities for air-borne particles from a public health perspective - with implications for urban planning Science of The Total Environment, 796; 148605.

[10] Setälä, H., Viippola, V., Rantalainen, A., Pennanen, A., and Yli-Pelkonen, V. 2013. Does urban vegetation mitigate air pollution in northern conditions? Environmental Pollution, 183; 104–112.

[11] Brantley, H. L., Hagler, G. S., Deshmukh, P. J., and Baldauf, R. W. 2014. Field assessment of the effects of roadside vegetation on near-road black carbon and particulate matter. Science of the Total Environment, 468–469; 120–129.

[12] Gromke, C., and Ruck, B. 2012. Pollutant concentrations in street canyons of different aspect ratio with avenues of trees for various wind directions. Boundary-Layer Meteorology, 144(1); 41–64.

[13] Wania, A., Bruse, M., Blond, N., and Weber, C. 2012. Analysing the influence of different street vegetation on traffic-induced particle dispersion using microscale simulations. Journal of Environmental Management, 94(1); 91–101.

[14] Zhu, C., and Zeng, Y. 2018. Effects of urban lake wetlands on the spatial and temporal distribution of air PM_{10} and $PM_{2.5}$ in the spring in Wuhan. Urban Forestry & Urban Greening, 31; 142–156.

[15] Li, X., Ma, Y., Wang, Y., Liu, N., and Hong, Y. 2017. Temporal and spatial analyses of particulate matter (PM_{10} and $PM_{2.5}$) and its relationship with meteorological parameters over an urban city in northeast China. Atmospheric Research, 198; 185–193.

[16] Wang, J. et al. 2023. Impact analysis of meteorological variables on PM2.5 pollution in the most polluted cities in China. Heliyon, 9(7).

[17] Xu, Y., Xue, W., Lei, Y., Huang, Q., Zhao, Y., Cheng, S., Ren, Z., and Wang, J. 2020. Spatiotemporal variation in the impact of meteorological conditions on $PM_{2.5}$ pollution in China from 2000 to 2017. Atmospheric Environment, 224; 117215.

[18] Chen, L., Liu, C., Zhang, L., Zou, R., and Zhang, Z. 2018. Variation in tree species ability to capture and retain airborne fine particulate matter (PM2.5). Scientific Reports, 7; 3206.

[19] Miao, Y., Li, Y., & Zhang, Y. (2017). The impact of urban green spaces on particulate matter pollution in metropolitan areas. Environmental Pollution, 229, 186–194.

[20] Miao, C. et al. 2021. Seasonal effects of street trees on particulate matter concentration in an urban street canyon. Sustain. Cities Soc, 73.

[21] Air and Noise Quality Management Division. 2022. Report on the status and management of air and noise pollution in Thailand for the year 2022. Bangkok.

[22] N. Zhan, G. Lyu, X. Li, S. Zhang. 2020 Study on air pollutants distribution in street canyons affected by interaction of hedgerows and trees. Environ. Sci. Technol., 43 (6); 101-107.

[23] Nowak, D. J., et al. 2013. Modeled PM2.5 removal by trees in ten U.S. cities and associated health effects. Environmental Pollution, 178; 395-402.

[24] Jeanjean, A. P. R., et al. 2017. Air quality affected by trees in real street canyons: The case of Marylebone neighbourhood in central London. Urban Forestry & Urban Greening, 22; 41-53.

[25] Zhang, K., Batterman, S., and Dion, F. 2011. Vehicle emissions in congestion: Comparison of work zone, rush hour and free-flow conditions. Atmospheric Environment, 45(11); 1929–1939.

[26] Morakinyo, T. E., and Lam, Y. F. 2016. Simulation study of dispersion and removal of particulate matter from traffic by urban trees. Atmospheric Environment, 132; 120-128.

[27] Rahman, M. A., Stratopoulos, L. M. F., Moser-Reischl, A., Zölch, T., Häberle, K.-H., Rötzer, T., Pretzsch, H., and Pauleit, S. 2020. Traits of trees for cooling urban heat islands: A meta-analysis. Building and Environment, 170; 106606.

[28] Abhijith, K. V., Kumar, P., Gallagher, J., McNabola, A., Baldauf, R., Pilla, F.and Pulvirenti, B. 2017. Air pollution abatement performances of green infrastructure in open road and built-up street canyon environments. A review. Atmospheric Environment, 162**;** 71–86.

[29] Liu, J., Zheng, B., Xiang, Y., & Fan, J. 2022. The Impact of Street Tree Height on PM2.5 Concentration in Street Canyons: A Simulation Study. Sustainability, 14(19); 12378.

20R4-17

Assessment of the Reduction of Greenhouse Gas Emissions from Solid Waste Management for a Large Community

Nitaya Kosa[1], Supatpong Mattaraj[2], Karnika Ratanapongleka[2], Wipada Dechapanya[2], Tiammanee Rattanawerapan[2], Adun Janyalertadun[2] and Sompop Sanongraj[2,*]

[1]*Graduate student, Environmental Engineering Program, Department of Chemical Engineering, Faculty of Engineering, Ubon Ratchathani University, Ubonratchathani 34190, Thailand;*

[2*]*Lecturer, Faculty of Engineering, Ubon Ratchathani University, Ubonratchathani 34190, Thailand.*

[*]*Phone : 0918271088, Fax : 045 353333., E-mail : sompop.s@ubu.ac.th*

ABSTRACT

Greenhouse gas (GHG) emissions from municipal solid waste (MSW) significantly contribute to climate change, particularly through methane (CH_4) and carbon dioxide (CO_2) emissions from landfills. This study evaluates the potential for GHG emissions reduction through improved solid waste management practices in Ban Non Sung, Khun Han district, Sisaket province, Thailand. Data were collected from October 2019 to September 2020, covering 1,586 residents across 340 households. Waste segregation at source included composting, bio-fermentation, animal feed conversion, and recycling. GHG emissions reductions were calculated based on national methodologies. Results showed that 69.27% of sorted waste was organic, with per capita sorted waste generation of 0.07 kg/day. The total estimated GHG emissions reduction was 41,111.78 kg CO_2eq/year (0.96 kg CO_2eq per kg sorted waste). Animal feed conversion was the most effective method, accounting for 40.89% of total reduction, followed by composting (18.81%) and bio-fermentation (18.04%). Additionally, national data from 2020–2023 indicated a steady increase in source-sorted waste and corresponding GHG reductions, emphasizing the role of community-based waste initiatives in meeting national climate goals. The findings support the integration of sustainable waste practices to significantly mitigate GHG emissions in large communities.

Keywords : Greenhouse gas (GHG) emissions; solid waste management; waste segregation at source; GHG reductions; community-based waste initiatives

INTRODUCTION

Greenhouse gas (GHG) emissions have become one of the most pressing global environmental issues due to their significant contribution to climate change and global warming. The Intergovernmental Panel on Climate Change (IPCC) reports that human activities, particularly in the energy, agriculture, and waste sectors, are the primary sources of GHG emissions worldwide. Methane (CH_4), carbon dioxide (CO_2), and nitrous oxide (N_2O) are the main greenhouse gases emitted into the atmosphere, with CH_4 having a global warming potential approximately 25 times higher than CO_2 over a 100-year period [1]. Among these sources, solid waste management (SWM) has received increasing attention, especially in developing countries where rapid urbanization and population growth have intensified waste generation and its environmental impacts.

In Thailand, municipal solid waste (MSW) generation continues to rise annually, driven by increased economic activity, changing consumption patterns, and lack of effective waste segregation at the source. There are many open-dump landfill sites which still wait for the proper management [2]. According to the Pollution Control Department (PCD), Thailand generated approximately 25.37 million tons of MSW in 2020, of which only a fraction was properly segregated and treated [3]. A significant portion of this waste, especially organic matter, ends up in landfills, where anaerobic decomposition results in the release of CH_4. Therefore, improving waste management practices, particularly at the community level, presents a practical and impactful opportunity for GHG emissions reduction.

Modern approaches to sustainable solid waste management focus on waste minimization, source segregation, recycling, composting, and energy recovery. These strategies not only extend the lifespan of landfills but also contribute to climate change mitigation through the reduction of GHG emissions. In particular, the diversion of organic waste from landfills to processes such as composting, bio-fermentation, and animal feed conversion has been proven to substantially reduce CH_4 emissions [4]. Furthermore, community-based initiatives that promote awareness, participation, and behavioral change among residents have shown promising results in enhancing the efficiency of waste management systems.

The Ministry of Natural Resources and Environment (MNRE) of Thailand has acknowledged the critical role of SWM in achieving the targets set in the Thailand National Greenhouse Gas Reduction Plan (2021–2030), which aligns with the country's commitment under the Paris Agreement [5]. As part of this strategy, increasing the rate of waste segregation at source and promoting organic waste treatment technologies are key priorities. The Thailand Greenhouse Gas Management Organization (TGO) has also developed specific methodologies for calculating GHG reductions from waste management activities, providing a standardized framework for monitoring and evaluation [6].

This study focuses on assessing the potential for GHG emissions reduction through community-driven solid waste management in Ban Non Sung, Khun Han district, Sisaket province, Thailand. The selected community represents a typical semi-urban area where household-level waste practices can have a measurable environmental impact. By examining the composition of solid waste, identifying the proportion of recyclable and organic fractions, and calculating the GHG emissions reduction based on actual management practices, this research aims to provide data-driven insights for scaling similar initiatives across other communities in Thailand.

The results from this study are expected to contribute to the growing body of knowledge on sustainable waste practices in the context of climate change mitigation. Furthermore, they can support policymakers and local governments in designing evidence-based programs that promote environmentally responsible behavior and community engagement in line with national and global sustainability goals.

METHODOLOGY

This study assesses waste composition and calculates the GHG emissions reduction achieved through different waste management practices. Data collection was conducted from October 2019 to September 2020, covering a population of 1,586 residents across 340 households. Waste segregation methods were analyzed, including organic waste processing through composting, bio-fermentation, and animal feed conversion, along with recycling efforts for glass, plastic, paper, and metals. GHG emissions reductions were calculated based on the methodologies provided by the Ministry of Natural Resources and Environment of Thailand [7]. The reduction in greenhouse gas (GHG) emissions resulting from the implementation of organic waste management activities can be calculated using Equation 1:

$$\text{GHG Emission Reduction } (kgCO_2eq) = (\text{Activity Data}_{before} \times \text{Emission Factor}_{before}) - (\text{Activity Data}_{after} \times \text{Emission Factor}_{after}) \quad \text{Eq. 1}$$

Where:

- Activity Data (kg) refers to the amount of organic waste managed, based on data from Ban Non Sung village, moo 1, Non Sung subdistrict, Khun Han district, Sisaket province.
- Emission Factor ($kgCO_2eq/kg$) refers to the greenhouse gas emission factor [6]

In addiiton, the potential GHG emissions reduction from municipal waste management was analized**.** This analysis was conducted at the national level, using the results from this study on source-based waste management practices with active community participation as a representative model. The aim was to estimate the broader potential impact of scaling up similar community-based initiatives across the country, thereby assessing their contribution to national GHG mitigation targets.

RESULTS AND DISCUSSIONS

Overaal, Ban Non Sung village, moo 1, Non Sung subdistrict, Khun Han district, Sisaket province, serves as a national model for community-based solid waste management and operates an exemplary waste-recycling bank system. The village waste management diagram is summarized as shown in Figure 1. The community separates waste at the source into four categories: organic, recyclable, general, and hazardous waste. A key strength of the village lies in its decentralized organic waste management: each household is encouraged to handle their organic waste on-site through composting, bio-fermentation, or by using it as animal feed. These practices help reduce the volume of waste needing external collection while promoting local food production, such as homegrown vegetables using composted fertilizer as shown in Figure 2. Recyclables are deposited monthly at the community waste-recycling bank as shown in Figure 3, with proceeds contributing to a welfare fund. General waste is creatively made community products (as shown in Figure 4) or reused when possible or collected for disposal at an RDF facility. Hazardous waste is separated and managed responsibly. To improve waste logistics, the village has established 19 designated community drop-off points (as shown in Figure 5) where residents are

encouraged to bring general and hazardous waste in sealed plastic bags at scheduled times. These points have replaced the previous door-to-door collection system, fostering better waste segregation, community participation, and resource recovery. The village promotes strong waste discipline through regular community meetings, public announcements, local regulations, and incentive-based participation. This integrated system not only reduces environmental impact but also strengthens community engagement and social welfare through structured cooperation and shared responsibility.

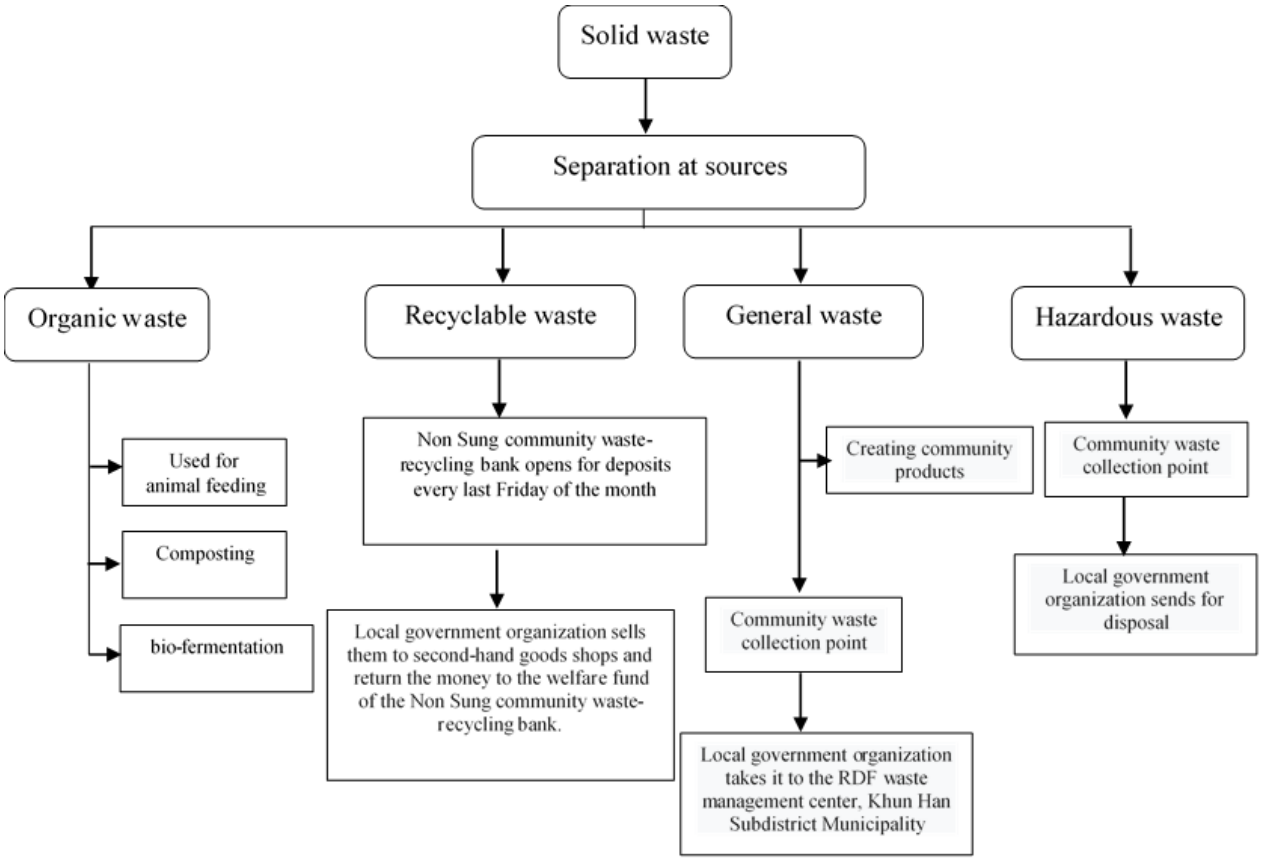


Figure 1 Waste management diagram of Ban Non Sung community, village No. 1, Non Sung subdistrict, Khun Han district, Sisaket province



Figure 2 Homegrown vegetables



Figure 3 Community waste-recycling bank



Figure 4 Community products from waste



Figure 5 Community drop-off point for general and hazardous waste

The study found that the composition of solid waste that has been sorted out at the source for a large community with a population of 1,586 people for the fiscal year 2020 had 42,715.65 kg including organic and food waste, representing 69.27 %, followed by recycable waste accounting for 30.73 % (as shown in Figure 6). Figure 6 presents the composition of sorted waste in the studied community. Organic waste accounts for the highest proportion, followed by glass and plastic. The daily per capita sorted waste generation was 0.07 kg (~0.34

kg/household), and total GHG emissions reduction from waste management activities was estimated at 41,111.78 kg CO_2eq per year (0.96 kg CO_2eq per kg sorted solid waste).

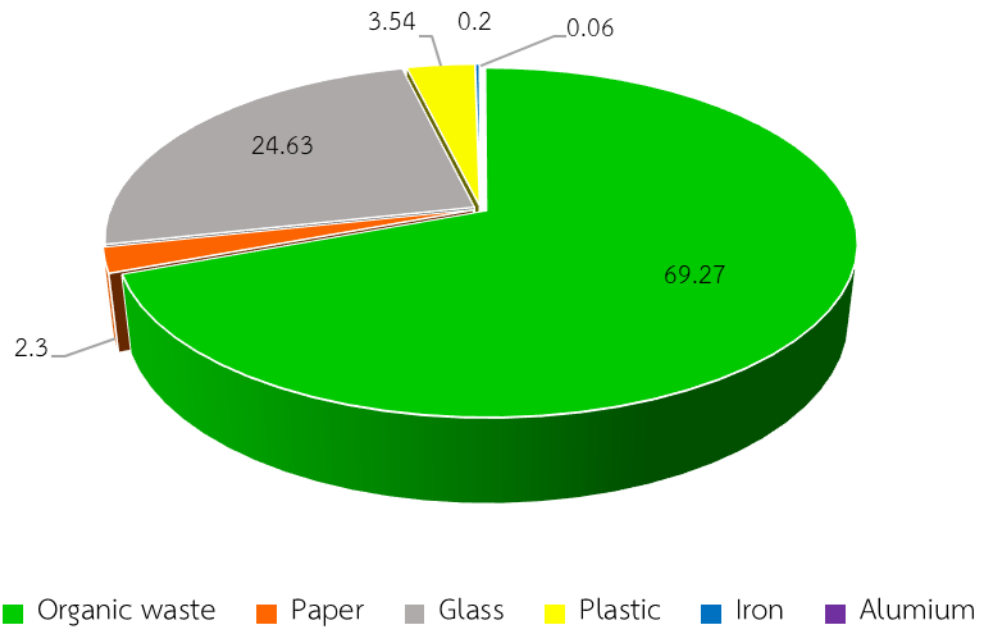


Figure 6 % Sorted Waste Composition in the Studied Community

The most effective method for reducing GHG emissions was utilizing food and vegetable scraps for animal feed, contributing to a reduction of 16,812.09 kg CO2eq (40.89%). Composting and bio-fermentation contributed to reductions of 7,733.82 kg CO2eq (18.81%) and 7,414.60 kg CO2eq (18.04%), respectively. Table 1 summarizes the reductions in GHG emissions achieved through different waste management methods.

Table 1 Anual GHG Emissions Reduction from Waste Management Methods

Waste Management Method	GHG Reduction (kg CO_2eq)	Percentage Reduction (%)
Animal Feed Conversion	16,812.09	40.89
Composting	7,733.82	18.81
Bio-Fermentation	7,414.60	18.04

To provide an updated assessment in Thailand, secondary data from 2020-2023 was analyzed as shown in Table 2 revealing trends in sorted solid waste (at source) and its corresponding impact on GHG reduction. In Table 2, the results indicate a gradual increase in waste generation, with a corresponding rise in GHG emissions reduction due to improved waste management strategies. This highlights the importance of continued community-driven waste initiatives in achieving sustainability goals according to Thailand's National Greenhouse Gas Reduction Plan (2021-2030) [8].

Table 2 Generated and sorted solid waste during year 2020-2023 in Thailand

Year	Solid Waste Generated (million-ton, Mt)	Sorted Solid Waste at Source (million-ton, Mt)	Anual GHG Emissions Reduction* (Mt CO_2eq)
2020	25.37	8.36	8.02
2021	24.98	7.89	7.57
2022	25.70	8.80	8.45
2023	26.95	9.31	8.94

*Calculated based on this study

CONCLUSION

Effective sorted solid waste management plays a crucial role in mitigating GHG emissions in large communities. The adoption of strategies such as organic waste processing for animal feed, composting, and bio-fermentation has significantly contributed to emission reductions. Additionally, the analysis of organic waste trends from 2020-2023 emphasizes the necessity of sustained efforts in community-driven waste initiatives to further reduce environmental impact.

ACKNOWLEDGEMENT

We would like to thank the Khun Han subdistrict municipality office, and the Non Sung Community, village No. 1, Khun Han district, Sisaket province, for their kindness in providing information on waste management operations, as well as Ubon Ratchathani University for their support in implementing the project.

REFERENCE

[1] IPCC, 2021. Climate Change 2021: The Physical Science Basis. Contribution of Working Group I to the Sixth Assessment Report of the Intergovernmental Panel on Climate Change. https://www.ipcc.ch/report/ar6/wg1/

[2] Sanongraj S, Rattanaweerapan T, Dechapanya W., 2023. Production and characteristics of refuse derived fuel from open-dump solid waste. Bioresource Technology Reports; 22:1-6.

[3] Pollution Control Department, Thailand, 2019. National Solid Waste Report. https://www.pcd.go.th

[4] United Nations Environment Programme (UNEP), 2016. Global Waste Management Outlook. https://www.unep.org/resources/report/global-waste-management-outlook

[5] Ministry of Natural Resources and Environment, Thailand, 2021. Thailand National Greenhouse Gas Reduction Plan (2021–2030). https://www.boi.go.th/upload/content/National%20Solid%20Waste%20Management%20Plan-Thailand.pdf

[6] Thailand Greenhouse Gas Management Organization (TGO), 2021. Greenhouse Gas Calculation Methodologies. https://tver.tgo.or.th/database/public/methodologies/

[7] Ministry of Natural Resources and Environment, Thailand, 2020. Waste Management and GHG Mitigation Strategies; https://www.boi.go.th/upload/content/National%20Solid%20Waste%20Management%20Plan-Thailand.pdf?utm_source=chatgpt.com

[8] Ministry of Natural Resources and Environment, 2021. Thailand National Greenhouse Gas Reduction Plan, 2021-2030; https://www.boi.go.th/upload/content/National%20Solid%20Waste%20Management%20Plan-Thailand.pdf?utm_source=chatgpt.com

20R4-18

People's Perception and Water Consumption Behavior in High Fluoride Risk Area

Patcharaporn Somkiattiyot[1], Aunnop Wongrueng[2] and Sarunnoud Phuphisith[3*]
[1]*Graduate student, Department of Environmental Engineering, Faculty of Engineering, Chiang Mai University, Chiang Mai 50200, Thailand*
[2]*Associate Professor, Department of Environmental Engineering, Faculty of Engineering, Chiang Mai University, Chiang Mai, Thailand 50200*
Phone: 094-4299656, E-mail: aunnop@eng.cmu.ac.th
[3*]*Assistant Professor, Department of Environmental Engineering, Faculty of Engineering, Chiang Mai University, Chiang Mai, Thailand 50200*
[*]*Phone :+66 53 94 4192, E-mail : sarunnoud.p@cmu.ac.th*

ABSTRACT

People living in many rural areas of Thailand experience high fluoride concentrations in groundwater. Defluoridation technologies are needed to reduce the chance of being affected by fluorosis-related illnesses, such as dental and skeletal fluorosis. Demand is particularly significant in areas where groundwater is the primary or sole drinking water source. In addition to the availability of technologies, people's awareness of fluoride risk and acceptance of the defluoridation system are also essential to their daily water consumption. The present study examined people's awareness of fluoride effects and their water consumption behaviors in high fluoride-risk areas in San Kamphaeng District, Chiang Mai, Thailand. The interview results from 205 respondents showed that despite most respondents' desire for a defluoridation system for their daily water consumption, they had a low understanding and awareness of the fluoride risk and its contamination in their groundwater resources. Education and awareness about the threats of fluoride contamination in water must be promoted to fill the gap between people's understanding of fluoride risk and contamination and their choices for everyday water use.

Keywords: People perception, Water consumption behavior, Fluoride contamination, Groundwater and Tap water

INTRODUCTION

In many areas in the world, groundwater is used to produce drinking water because it is of better quality and less microbial contamination than surface water. Additionally, some regions have few sources of surface water or contaminated surface water. Therefore, groundwater is a better source of raw water for drinking water. However, due to geochemical properties, ground water can occasionally become naturally contaminated. The two main examples of naturally occurring contaminants in groundwater are fluoride and arsenic. The presence of fluoride in drinking water can reduce the incidence of dental caries when its concentration lies in the optimal range of 0.5-0.7 mg/L [1]. However, excessive fluoride consumption causes dental and skeletal fluorosis. In several areas of Thailand, including rural communities of Chiang Mai, groundwater is dramatically contaminated by fluoride; its concentration is often above the maximum threshold of 1.5 mg/L recommended by the World Health Organization [2], causing dental and skeletal fluorosis in communities.

Fluoride removal from water can be achieved through coagulation, ion exchange, reverse osmosis, and adsorption. However, the adoption of these techniques remains low. Behavioral factors influencing people's safer water consumption in fluoride-contaminated areas are crucial determinants.

The objective of this study examined people's awareness of fluoride-free water and their water consumption behaviors in high fluoride-risk areas to foster public health impacts and the importance of choosing safe water for daily use. The methods described below can help communities of the Buak Khang to switch towards the consumption of fluoride-safe water and people's awareness of high fluoride risk in groundwater.

METHODOLOGY

The study area was Buak Khang Municipality, San Kamphaeng District, Chiang Mai, Thailand. (**Figure 1**) The area experienced a high fluoride risk with fluoride contamination in groundwater ranging from 0.7 to 10 mg/L [3]. Data was collected from 15 May 2024 to 31 December 2024 by contacting

community leaders to invite residents to participate in the survey and face-to-face interviews voluntarily. The questionnaire was reviewed and approved by the Chiang Mai University Research Ethics Committee (CMUREC No. 67/172). The selection criteria for participants include being Thai, at least 20 years old, residing in high fluoride-risk areas for at least 3 months, and willing to participate in the survey.

The questionnaire included four parts: Part 1 was about personal information. Part 2 was asked about understanding fluoride risk and its effects on water contamination. Part 3 was about water consumption behavior and water sources for drinking and cooking. This part also included the expenses for water use. Lastly, part 4 was about the questions on technology acceptability; this referred to the defluoridation system to treat water before consumption. Such technology acceptability is very important, especially in areas with excessively high fluoride levels in water. The community's acceptance and adoption of these technologies directly impact public health and the long-term sustainability of fluoride-safe water management. All data was analyzed using Microsoft Excel (version 2404 Build 16.0.17531.20120).

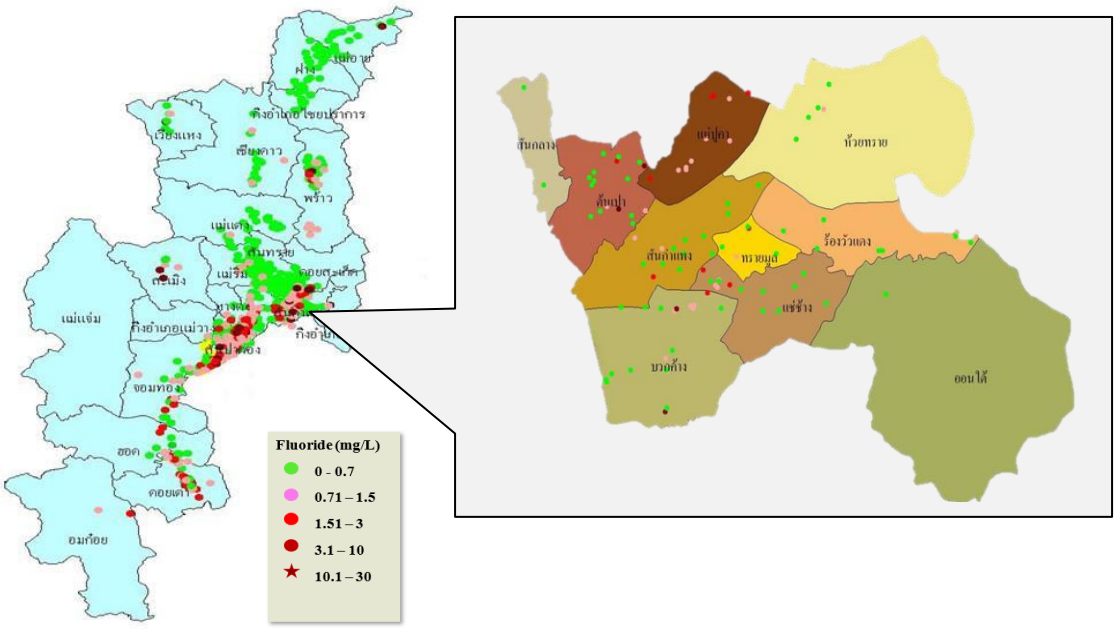


Figure 1 Fluoride contamination in groundwater in San Kamphaeng District.

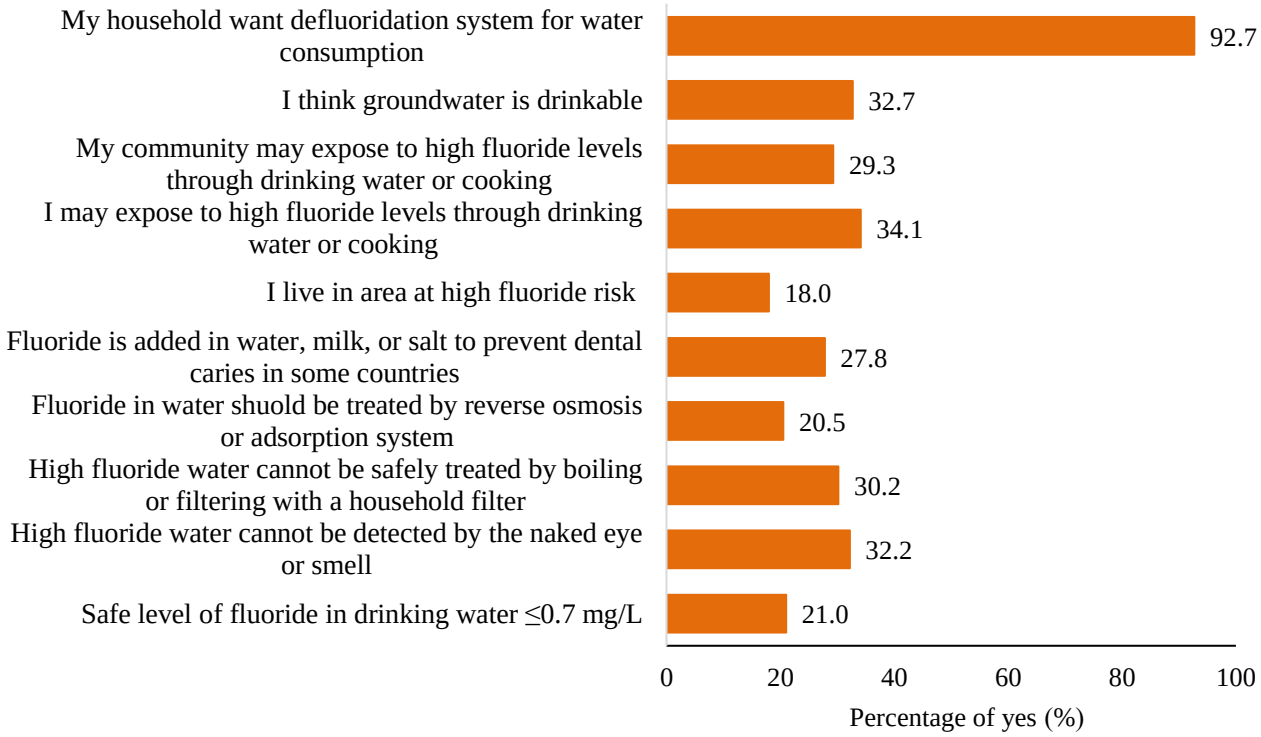
RESULTS AND DISCUSSIONS

A total of 205 residents participated in the survey, and their socio-demographic characteristics are presented in **Table 1.** Most of the participants were female (60.5%), the average age of participants was 56 years, and they had been living in fluoride-risk areas for 46 years on average. Most of them have careers as employees (56.1%), personal business (20.0%), farmer (13.2%), housekeeper (3.4%) and elderly people (1.0%) respectively.

Table 1 Participants' characteristics.

Socio-demographic characteristics		**Value**
Total respondents (N)		205
Gender (%)	Male	38.0
	Female	60.5
	Unspecified	1.5
Age (year)	Mean±S.D.	56.7±11.7
Living period (year)	Mean±S.D.	46.9±18.5
Career (%)	Personal Business	20.0
	Employee	56.1
	Housekeeper	3.4
	Farmer	13.2
	Elderly people	1.0
	Unspecified	6.3

Figure 2 shows the respondents' understanding of fluoride contamination in water and their perceived risk of high fluoride contamination. It was found that (21.0%) knew that the safe level of fluoride in drinking water is ≤0.7 mg/L, (32.2%) knew that water with high fluoride cannot be detected by the naked eye or smell and (30.2%) knew that water with high fluoride cannot be removed by boiling or filtering with a household filter. Also found that, only 20.5% knew that a reverse osmosis or adsorption system should be used to remove fluoride, (27.8%) knew that in some countries, fluoride is added to water, milk, or salt to prevent tooth decay, (18.0%) knew that they lived in a high-fluoride risk area, (34.1%) believed that they might be exposed to high levels of fluoride from drinking water or cooking water, (29.3%) believed that their community might be exposed to high levels of fluoride from drinking water or cooking water and (32.7%) thought that groundwater was drinkable. From the study results, it can be concluded that most respondents had low levels of understanding and awareness of the risks of fluoride contamination in water. Most respondents (92.7%) desired a defluoridation system to remove fluoride from their consumption. This implies a gap between



people's understanding of fluoride risk and water quality in the area.

Figure 2 Understating of fluoride contamination in water and risk (N=205).

Figure 3 shows the levels of fluoride contamination in the groundwater of the study area and the respondents' drinking water sources. Most respondents bought water for daily drinking: bottled water (67.7 %), and vending machines (13.7%). Small respondents (2.3%) drank water from filtered systems. Some respondents used groundwater, especially in the villages with high fluoride levels (0.71-10 mg/L), Buak Khang Moo 1, Roi Phrom, Rong Kong Khoa, Buak Khang Moo 2, Ban Du, and Ko Sa Laemg. Demonstrating that the respondents in the villages with high fluoride levels are under distressful fluorosis health problems. The health impacts of fluoride are not acute but chronic, which means that prolonged exposure to high fluoride doses is required to adversely affect human beings. The occurrence of dental fluorosis is directly dependent on the groundwater fluoride content as well as with the dietary intake of fluoride containing water for drinking purposes [4]. Recent studies reported high levels of fluoride intake would cause detrimental health effects such as dental fluorosis, skeletal fluorosis, and hypertension [5]. However, the severity of the fluoride toxicity may vary depending on its concentration in groundwater, ingestion rate, the longevity of fluoride exposure as well as local climate (air temperature: a key driver of daily water intake). For instance, exposure to groundwater fluoride levels above the safe limit led to the

development of dental fluorosis (1.5-3 mg/L), skeletal fluorosis (3-6 mg/L), and bone crippling (>6 mg/L) in human individuals [6].

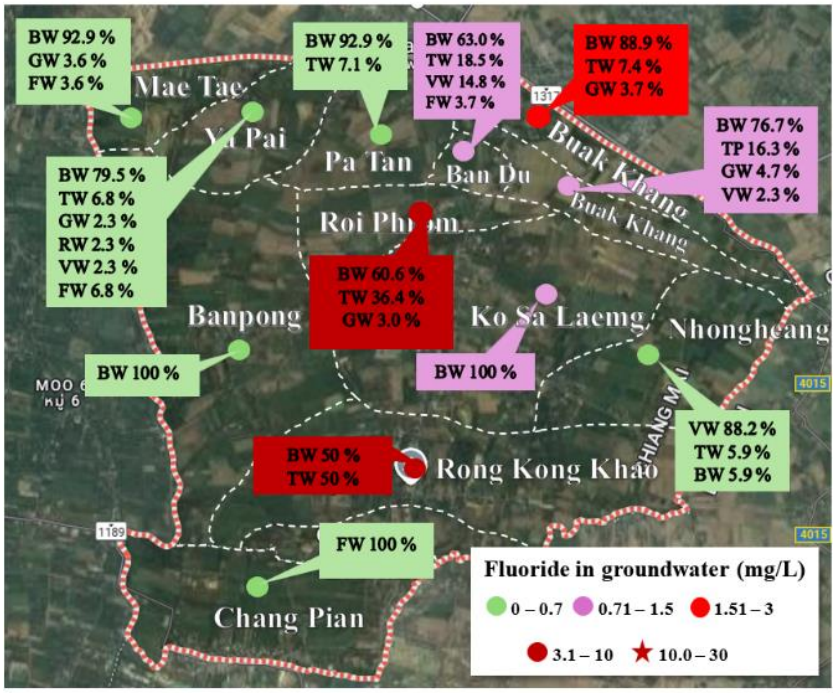


Figure 3 Source of drinking water consumption in study area.
Description: RW=Rainwater, GW=Ground water, TW=Tap water, BW=Bottled water, VW=Vending machine water, FW=Filtered water home use

Most respondents used bottled water (42.3%) and tap water (37.5%) for cooking. Groundwater used for cooking (4.4%) had a higher percentage than for drinking. In Roi Phrom village, where high fluoride content in groundwater, 14.3% of the respondents used groundwater for their cooking (**Figure 4**). Using groundwater or tap water contaminated with fluoride as high as 10 mg/L can be harmful to health in the long term. When fluoride-containing water is used to soak rice or boil vegetables, fluoride accumulates in the rice or vegetables, causing indirect fluoride intake from food and could be a significant source of daily fluoride intake. Thus, the fluoride intake from food cooked in boiling water is comparable to or greater than intake from drinking water. [7].

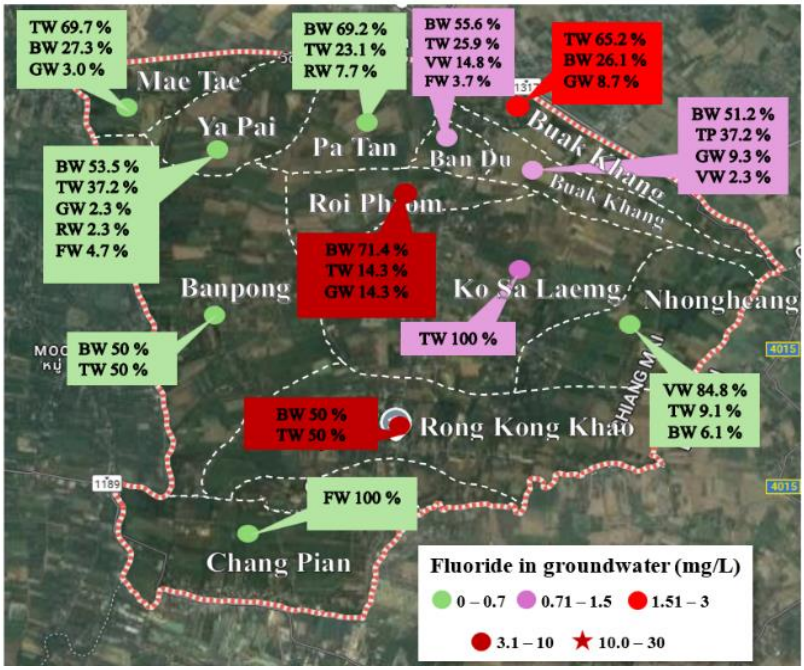


Figure 4 Source of cooking water consumption in study area.
Description: RW=Rainwater, GW=Ground water, TW=Tap water, BW=Bottled water, VW=Vending machine water, FW=Filtered water home use

Table 2 shows the expenses on drinking water consumption reported in this study was 174.4±241.9 Bath per month and the mean expense for cooking water consumption was 182.0±286.1 Bath per month. The mean total expense on drinking water consumption and cooking water consumption of participants was 356.4±398.9 Bath per month.

Table 2 Expense for water use.

Item	Unit	Mean±S.D.
For drinking water	Bath/month	174.4±241.9
For cooking water	Bath/month	182±286.1
Total expense	Bath/month	356.4±398.9
Expected monthly expense for water use	Bath/person/month	162.4±510.2

The respondents' satisfaction with the color, odor, and taste of the current water used is shown in **Table 3**. Median scores satisfied were at the level of 5 (out of 6) for all parameters. The independent t-test analysis shows that the satisfaction with the color, odor and taste of drinking water were indifferent between males and females (p>0.05). For cooking water use, there is a significant difference in taste between males and females (t= -1.981, df=200, p=0.049), females showed a lower score than males. But there were no differences in color and odor satisfactions.

Table 3 Perception on water consumption (N=205).

Drinking water	Mean±S.D.	Median
Color	4.6±1.5	5
Odor	4.4±1.7	5
Taste	4.7±1.3	5
Cooking water		
Color	4.1±2.0	5
Odor	3.8±2.1	5
Taste	4.1±1.9	5

Response level provide: 6 = strongly satisfied to 1 = strongly dissatisfied.

CONCLUSION

The research findings indicate that most participants in high fluoride risk areas had quite a low understanding of fluoride in water and were less aware of the vulnerability and severity of fluoride contamination. Most used bottled water for daily consumption. Still, groundwater and tap water were used in some areas with high fluoride contamination, implying a high chance of exposure to high fluoride intake from their daily water. Access to fluoride-safe water is a basic human necessity and a fundamental human right. Education and awareness about the dangers of fluoride contamination in water must be promoted.

ACKNOWLEDGEMENT

The authors would like to thank both two Mr. Suchart Tapun in Banbuakkhang school and community leader in Buakkhang municipality for help and convenience and all interview participants for their precious comments. This research was supported Teaching Assistant and Research Assistant Scholarships support from Chiang Mai University. We would like to express our sincere thanks to Department of Environmental Engineering, Faculty of Engineering, Chiang Mai University for invaluable supports in terms of facilities and scientific equipment.

REFERENCE

[1] World Health Organization. “Guidelines for drinking – Water quality: Chemical fact sheet”. 2004 Geneva. Switzerland.

[2] Surveillance information system. “Fluoride content in drinking water”. 2025. Intercountry Centre for Oral Health. Thailand.

[3] Chamnanprai S., R., et al. 2020. Surveillance of fluoride content in drinking water in the northern part of Thailand. Intercountry Centre for Oral Health.

[4] Das K., Puppala H., et al. 2025. Community level vulnerability of groundwater fluoride contamination and exposure by the application of multi-criteria model. Journal of Hazardous Materials Advances. doi.org/10.1016/j.hazadv.2024.100555.

[5] Yousefi et al, 2018b. Health risk assessment to fluoride in drinking water of rural residents living in the Poldasht city, Northwest of Iran. Ecotoxicol. Environ. 148, pp. 426-43, doi.10.1016/j.ecoenv.2017.10.057.

[6] World Health Organization. “Fluoride and Oral Health: Report on Oral Health Status and Fluoride Use”. 1994 Geneva. Switzerland.

[7] Sawangjang B., Takizawa S., et al. 2023. Re-evaluating fluoride intake from food and drinking water: Effect of boiling and fluoride adsorption on food. Journal of Hazardous Materials.doi.org/10.1016/j.jhazmat.2022.130162.

20R4-19

Quantifying ESG Impacts on Stock Performance: Evidence from the Thai SET100

Phonthakorn Phreuksa[1*] Warach Saiwilai[1] Varith Wichienchai[1] and Matnithit Chariyasethapong[1]

Chaidit Sittisunthornwat[2] Pisut Painmanakul[3] and Vasathon Wongwanich[4]

[1]Undergraduate Student, Department of Environmental Engineering, Faculty of Engineering, Chulalongkorn University, Bangkok 10330, Thailand;

[2]Graduate Student, Innovative Engineering for Sustainability Program, Faculty of Engineering, Chulalongkorn University, Bangkok 10330, Thailand
[3]Professor, Department of Environmental Engineering, Faculty of Engineering, Chulalongkorn University, Bangkok 10330, Thailand
[4]11th Grade Student KIS International School
*Phone: 080-1546956, E-Mail: pphonthakorn.work@gmail.com

ABSTRACT

Environmental, Social, and Governance (ESG) factors are increasingly believed to influence corporate financial performance. This paper investigates how ESG scores relate to stock returns in Thailand's SET100 index from 2021 to 2023. We employ a Fama–French three-factor model as a baseline and then augment it with Bloomberg's ESG scores (range 0–10) for each stock as an additional explanatory variable. The regression results identify which stocks have statistically significant ESG coefficients, interpreted as "return-based ESG scores." We then construct portfolios sorted by these ESG coefficients – including portfolios using all stocks and using only stocks with significant ESG loadings ($p < 0.10$) to compare performance. Portfolio performance metrics (mean return, volatility, Sharpe ratio) are analyzed to evaluate whether ESG-based screening yields superior risk-adjusted returns. The findings indicate that incorporating ESG factors provides incremental insight into stock performance: a number of SET100 stocks show significant positive ESG coefficients, and portfolios tilted toward high return-based ESG scores exhibit slightly higher risk-adjusted returns than their low-ESG counterparts. These results suggest that, in this sample, investors could have achieved marginally better Sharpe ratios by favoring companies with strong ESG characteristics. The study contributes quantitative evidence that ESG factors can be integrated into investment analysis in emerging markets, helping businesses and investors balance sustainability considerations against financial costs.

INTRODUCTION

In recent years, ESG investing has moved into the mainstream as stakeholders debate whether sustainable business practices improve or hinder financial performance. A large-scale meta-analysis of over 2000 studies found that the majority (around 58%) reported a positive relationship between ESG criteria and corporate financial performance, with only a small minority (~8%) finding a negative relationship [1]. This aligns with stakeholder theory, which argues that responsible practices can enhance firm value by reducing risks and building trust. On the other hand, a traditional view posits a potential trade-off: resources spent on ESG might detract from profits, implying lower returns (the "costly sustainability" hypothesis). The net impact of ESG on investor returns thus remains an empirical question, especially in emerging markets where evidence is still limited.

Thailand provides a useful testing ground for this issue. The Stock Exchange of Thailand (SET) has actively promoted sustainability, for example by introducing the Thailand Sustainability Investment (THSI) list and the SET ESG Index of high-ESG firms [8]. Many Thai companies now report ESG metrics, and international

rating agencies (like Bloomberg and MSCI) assign ESG scores to Thai firms. However, local investors and corporate managers may still question whether higher ESG performance translates into tangible financial benefits such as stock outperformance or lower risk. Prior studies on the Thai market have started to explore this. For instance, Prinyapon et al. (2022) grouped Thai stocks into ESG and non-ESG portfolios and found that the ESG portfolio earned a significantly positive Jensen's alpha (abnormal return) while the non-ESG portfolio did not, indicating better performance for ESG stocks [2]. This suggests that, at least historically, Thai companies with strong sustainability profiles tended to outperform their peers on a risk-adjusted basis. Nonetheless, such analyses often treat ESG as a binary inclusion factor. There is a need for more granular, quantitative insight into how much ESG characteristics contribute to returns and whether this can be captured in an investment strategy.

This paper aims to extend the understanding of ESG impacts on stock performance through a financial lens, focusing on the SET100 index constituents. We specifically ask: Do stocks with higher ESG ratings earn superior risk-adjusted returns, and can an ESG factor improve traditional asset pricing models? We answer this by employing the Fama–French three-factor model (which accounts for market, size, and value effects) as a baseline for expected returns [7], and then examining whether adding an ESG score factor significantly explains any remaining variation in returns. By quantifying the ESG effect as a regression coefficient for each stock, we obtain a "return-based ESG score," analogous to the approach of Jin (2020) who used fund alphas from factor regressions as ESG performance measures [3]. We then sort stocks by these return-based ESG scores to form portfolios and test if high-ESG-score portfolios outperform low-score portfolios on a risk-adjusted basis.

The contributions of this study are threefold. First, it provides empirical evidence from an emerging market on integrating ESG metrics into asset pricing models, complementing recent efforts to construct ESG factors for Thailand [4]. Second, it demonstrates a methodology to investors for extracting quantitative "ESG alpha" signals from standard ESG ratings, potentially guiding portfolio selection in a more nuanced way than a simple ESG/non-ESG split. Third, it offers business stakeholders insight into whether capital markets in Thailand are rewarding ESG efforts with better stock performance. By clearly quantifying the ESG-return relationship, the results can help corporate decision-makers weigh the costs of ESG initiatives against the potential benefit of a lower cost of capital or higher investor demand. The rest of the paper is organized as follows: Methodology describes the data, models, and portfolio construction. Results and Discussion presents the regression findings and portfolio performance, interpreting the economic significance and addressing potential concerns. Conclusion summarizes the implications for investors and firms, and suggests areas for further research.

METHODOLOGY

Data Sources: Our sample covers the 100 companies comprising the SET100 index (a broad index of large-cap Thai stocks) during the period January 2021 to December 2023. We obtained monthly stock price data for these firms and calculated monthly total returns. Price data were adjusted for corporate actions such as dividends or splits where applicable, to ensure returns reflect total shareholder return. We also obtained ESG scores for each company from Bloomberg. Bloomberg's ESG score is an overall measure (on a 0 to 10 scale) of how well a firm manages material ESG issues, with higher scores indicating better ESG performance [6]. These scores are updated annually; in our dataset we have an ESG score for each company for 2021, 2022, and 2023. We matched the scores to monthly returns by assigning each firm's score for a given calendar year to all months of that year. For example, a stock with ESG score 4.5 in 2021 and 5.0 in 2022 would have 4.5 as its ESG variable for January–December 2021 returns and 5.0 for January–December 2022 returns, and so on.

Before analysis, we performed basic data cleaning. If a stock was not listed for the entire period (e.g. newly added to SET100 in mid-2021 or delisted early), we included it only for the months it was actively trading and required a minimum of 12 months of data for reliable regression. Monthly returns were expressed in percentage terms. We also obtained or constructed the Fama–French three factors for the Thai market. Specifically, we required: (1) the market excess return (market index return minus risk-free rate), (2) the SMB (Small-minus-Big) size factor, and (3) the HML (High-minus-Low book-to-market) value factor [7]. In absence of an official Fama–French dataset for Thailand, we approximated these factors using available data: the market factor was proxied by the SET100 index return minus the 1-month Thai government bond yield (as risk-free rate), the SMB factor was constructed from the return differential between an index of small-cap stocks (e.g. sSET index) and large-cap stocks (SET50 index), and HML was proxied by the return differential between a portfolio of high book-to-price stocks and low book-to-price stocks within the SET100 (using published financial ratios to sort stocks). While these proxy constructions have limitations, they capture the broad size and value effects in the Thai market. All returns and factor values are in local currency (Thai Baht) terms.

Regression Models: For each stock *i* in the SET100, we first estimate a baseline time-series regression using the Fama–French three-factor model:

$$R_{i,t} - R_{f,t} = \alpha_i + \beta_{M,i}(R_{M,t} - R_{f,t}) + \beta_{S,i}SMB_t + \beta_{V,i}HML_t + \epsilon_{i,t}$$

where $R_{i,t}$ is the stock's monthly return in month *t*, $R_{f,t}$ is the risk-free rate (proxied by the 1-month bond yield) in month *t*, $R_{M,t}$ is the return of the market index (SET100) in month *t*, and SMB and HML are the size and value factors for month *t*. The coefficients $\beta_{M,i}$, $\beta_{S,i}$, $\beta_{V,i}$ capture the stock's exposure to market, size, and value factors respectively, and α_i is the intercept (Jensen's alpha) for stock *i*. We estimated this model by ordinary least squares (OLS) using the 36 monthly observations from 2021–2023 for each stock.

Next, we estimated an extended model that includes the ESG score as an additional factor:

$$R_{i,t} - R_{f,t} = \alpha'_i + \beta'_{M,i}(R_{M,t} - R_{f,t}) + \beta'_{S,i}SMB_t + \beta'_{V,i}HML_t + \gamma_i\, ESG_{i,t} + \epsilon'_{i,t}$$

Here $ESG_{i,t}$ is the ESG score for stock *i* in month *t* (which, as noted, is a piecewise constant value that can change at the start of each year). The new coefficient γ_i is of primary interest – it measures the sensitivity of stock *i*'s return to its ESG score, controlling for the usual risk factors. Intuitively, if γ_i is positive and significant, it suggests that stock *i*'s high ESG rating contributes to higher excess returns, beyond what traditional factors would predict. A negative γ_i would imply the opposite – a high ESG score is associated with lower returns, after accounting for risk factors. It is worth noting that since ESG scores do not vary monthly, there is a risk of multicollinearity between $ESG_{i,t}$ and the intercept term. In effect, $\gamma_i \times ESG_{i,t}$ for a given stock is like an additional constant (or a step function changing annually). To mitigate instability, we centered the ESG variable by subtracting the cross-sectional mean ESG score each year. This way, γ_i captures the return impact of having an ESG score above or below the yearly average.

We interpret the estimated γ_i as a return-based ESG score for the stock. This concept mirrors that of returns-based style analysis, where factor loadings can indicate implicit characteristics. In the ESG context, prior research has termed similar regression-derived measures as returns-based ESG scores [3]. A positive γ_i can be seen as an "ESG alpha" – the stock's return is higher with a higher ESG rating, implying the company's sustainability profile is being rewarded by investors. Conversely, a negative γ_i would mean the stock's returns tend to be lower when ESG is higher, perhaps indicating an ESG-related cost or investor avoidance of that stock despite its ESG strength (which could occur if, for example, high ESG stocks are overvalued and subsequently underperform). A value of $\gamma_i = 0$ means the stock's performance is neutral to ESG – its returns are fully explained by conventional factors alone. In the language of Jin (2020), a zero returns-based

ESG score indicates neutrality to systematic ESG risk, a positive score indicates hedging or lower exposure to ESG risks, and a negative score implies higher exposure to ESG risk [3].

After estimating the extended model, we recorded each stock's ESG coefficient γ_i and its t-statistic and p-value. We identified which stocks had statistically significant ESG coefficients at the 10% level ($p < 0.10$), noting the sign and magnitude. We also compared the adjusted R-squared of the extended model to the baseline model for each stock to see if adding ESG improved the explanatory power. On average, there was a small uptick in R^2 when including ESG, suggesting a modest increase in explained variance by incorporating the ESG factor.

Portfolio Construction: To evaluate whether ESG screening based on our regression results can enhance portfolio performance, we constructed several test portfolios of the SET100 stocks. All portfolios were formed at the end of the sample period (December 2023) using the full-sample regression estimates (thus effectively an in-sample analysis). While an out-of-sample test would be ideal to confirm predictability, our aim here is to see how a portfolio tilted towards certain ESG characteristics would have performed during 2021–2023. Note that while the SET100 index comprises 100 stocks, two companies were excluded from our analysis due to missing data, so all performance statistics refer to a final sample of 98 stocks. The portfolios and their formation criteria are as follows:

1. High vs Low ESG-Coefficient Portfolios (All Stocks): We ranked all 98 stocks by their estimated ESG coefficient γ_i. The High-ESG-Coefficient portfolio consists of the 20 stocks with the highest γ_i values (i.e. those most positively sensitive to ESG score), equally weighted. The Low-ESG-Coefficient portfolio consists of the 20 stocks with the most negative (or lowest) γ_i values, equally weighted. These represent extreme quintiles. We also formed a Middle portfolio of the remaining 58 stocks for reference. We then calculated the monthly returns of these portfolios over the 2021–2023 period by averaging the constituent stocks' monthly returns (rebalancing monthly to equal weights). This yields a time series of portfolio returns, from which we compute performance metrics. This approach tests whether, in retrospect, the stocks that had strong positive ESG effects (high γ_i) delivered better performance than those with strong negative ESG effects.
2. Significant-ESG Stocks Portfolio: We created a portfolio comprising only the stocks that had an ESG coefficient significant at the 10% level or better ($p < 0.10$) in the extended regression. This Significant-ESG portfolio is equally weighted among those significant names (there were 20 such stocks out of 100, as discussed later). For comparison, we also look at the complement: a portfolio of stocks with non-significant ESG coefficients (the other 78 stocks). This analysis checks whether focusing on stocks where ESG impact is more statistically robust yields different performance. Essentially, if our regression successfully identified a subset of stocks where ESG truly adds alpha, then the significant-ESG portfolio might outperform the rest.

Performance Evaluation: For each portfolio, we calculated the mean return, volatility, and Sharpe ratio over the 2021–2023 period. The mean return is annualized (geometric average of monthly returns multiplied by 12), the volatility is the annualized standard deviation of monthly returns (multiplying the monthly std. dev by $\sqrt{12}$), and the Sharpe ratio is computed as (mean return−Rf)/volatility, where R_f is the average risk-free rate over the period. For simplicity, we used the average Thai 1-month yield (approximately 0.3% per annum in 2021 rising to ~1% in 2023, averaging ~0.6% over the period) as R_f. We also examined the return distributions (skewness, drawdowns) for any major differences in downside risk between portfolios.

Throughout the analysis, we are mindful of statistical limitations. With only 36 monthly observations, the power to detect significance is limited, and some results could be sample-specific. We include ESG at a 10% significance threshold to be slightly more inclusive given the low power (a conventional 5% threshold might miss potentially interesting moderate signals). We also performed basic regression diagnostics: checking residual plots for non-random patterns, and ensuring no single month (such as the COVID-19 rebound in

early 2021 or the volatile market in 2022) unduly influenced results. No severe violations were found, though we caution that the time span includes unusual market conditions (pandemic recovery and inflationary pressures) that might not generalize.

RESULTS AND DISCUSSIONS

ESG Regression Coefficients: After running the extended Fama–French + ESG regressions for all SET100 stocks, we found that the ESG coefficient γ_i estimates ranged from about -1.33 to +0.48. A positive value means the stock's excess return tends to be higher when its ESG score is higher (relative to peers), and negative means the stock did worse with a higher ESG score. Out of 100 stocks, 20 stocks had γ_i coefficients that were statistically significant at the 10% level or better (approximately 13 at 5% level). Notably, 14 of these significant coefficients were positive, and only 6 were negative. This indicates that for a subset of companies, there is evidence that better ESG ratings contributed to higher returns, even after controlling for market, size, and value factors. The positive significant γ_i were typically in the range of +0.01 to +0.29. For example, a large Thai bank in our sample had $\gamma_i \approx +0.05$ ($p < 0.01$), suggesting that for each one-point increase in its ESG score, the bank's excess monthly return was about 0.05% higher. Over a year, if its ESG score were, say, 2 points above average, this would correspond to roughly $0.05\% \times 12 \times 2 \approx 1.20\%$ higher annual excess return attributed to ESG – a material but not overwhelming contribution.

For the majority of stocks (78 out of 98) γ_i was not statistically different from zero. This does not necessarily mean ESG has no effect for those stocks; it might be that any ESG impact is too small to detect or the score didn't vary enough. It's also plausible that for many companies, ESG performance was largely in line with peers (i.e., not a differentiator in returns). Our findings here resonate with those of Marupanthorn et al. (2024), who found that introducing an ESG "Best-minus-Worst" factor improved the model fit for Thai stock returns [4]. In our case, instead of a constructed factor, we directly used firm-level scores, but the outcome is similar: ESG considerations have a detectable, if small, impact on returns.

Interpreting the economic meaning: these γ_i coefficients can be viewed as each stock's *ESG premium or discount*. A stock with a high positive γ_i effectively enjoyed a premium for good ESG – its returns were higher than expected given its risk exposures, aligning with the idea that investors reward sustainability (or that the company's ESG practices led to superior performance). A high negative γ_i would imply an ESG-related discount or cost – perhaps investors weren't willing to pay as much for its ESG profile, or the firm's ESG initiatives hurt short-term profits. However, we caution that correlation is not causation; a positive ESG coefficient doesn't prove that ESG initiatives caused higher returns – it could be that a well-run company excels both financially and in ESG (an omitted variable like management quality could drive both). Yet, the fact that we controlled for major risk factors and still see ESG making a difference is suggestive that ESG could be an independent source of return variation. This return-based measure essentially treats ESG as another risk factor – akin to how "quality" or "momentum" factors are treated in factor investing. In fact, some researchers argue ESG overlaps with quality factors (high ESG companies often have better governance, prudent management, etc.).

To address a likely question from reviewers: How are Bloomberg's ESG scores used in this analysis, and do they add quantitative investment insight? We explicitly used Bloomberg's scores as numerical inputs in our regression model as described. Bloomberg's ESG score, being based on disclosed data and measured on a consistent 0–10 scale, allowed us to compare ESG intensity across companies [6]. By including it in a regression, we translated these scores into "ESG betas" or return contributions, which is a novel quantitative insight beyond just saying "ESG firms did well." It identifies *which* firms' high ESG performance aligned with higher returns. This method moves beyond correlation by controlling for other factors, thereby providing investors a clearer signal: for example, if two stocks both had 20% returns, but one had a significant positive ESG coefficient, it implies part of its return is associated with ESG—which might persist

if ESG continues to be rewarded. This is valuable for an investor constructing an ESG-tilted portfolio or a fund manager justifying ESG integration by showing a linkage to performance. It essentially quantifies the abstract concept of "ESG impact" in units of return. Such quantitative insights complement traditional ESG analysis and respond to calls for integrating ESG into factor models [4].

Portfolio Performance: Table 1 summarizes the performance of the various portfolios we constructed. Below we discuss the key comparisons (all returns are annualized for ease of interpretation):

Table 1. Portfolio Performance of ESG-Screened Groups (Top 20, Middle, and Bottom 20 Stocks)

Portfolio	Annualized Return	Annualized Volatility	Share Ratio
Top 20	0.1472	0.1629	0.8669
Middle	0.0390	0.1225	0.2690
Bottom 20	0.0796	0.1514	0.4864

High vs Low ESG-Coefficient Portfolios: The High-ESG portfolio (top 20 stocks by γ_i) achieved an average return of 14.72% per year with annualized volatility of 16.29%, yielding a Sharpe ratio of 0.87 (using 0.6% risk-free). In contrast, the Low-ESG portfolio (bottom 20 stocks) returned 7.96% per year with volatility 15.14%, for a Sharpe ratio of 0.49. The High-ESG group not only earned a higher average return, but interestingly had volatility roughly on par with (slightly higher than) the Low-ESG group. The result was a noticeably better risk-adjusted return. To gauge significance, we looked at the difference in monthly returns: the High-ESG minus Low-ESG portfolio had an average excess return of about 0.56% per month. While this result is not statistically significant at conventional levels (e.g. $p < 0.05$), the economic difference—roughly a 6.76% annual incremental excess return—could be meaningful for investors. These results tentatively support the view that screening for stocks with strong return-based ESG scores could improve portfolio outcomes. It aligns with prior findings that ESG-screened portfolios can match or beat the market on a risk-adjusted basis [2]. The top group clearly demonstrates superior risk-adjusted performance relative to both the middle and bottom groups, even though the middle group's performance is particularly poor. This pattern underscores that the greatest differentiation in performance—and the strongest signal for an "ESG premium"—appears at the extremes of the ESG score distribution.

Table 2. Portfolio Performance of ESG-Significant Groups (Significant and Non-Significant)

Portfolio	Annualized Return	Annualized Volatility	Share Ratio
Significant ESG	0.0580	0.1168	0.4451
Non-Significant ESG	0.0713	0.1347	0.4844

Significant-ESG vs Non-Significant ESG: When we split the SET100 stocks according to the statistical significance of the regression-derived ESG coefficient (using a threshold of $p < 0.10$), the performance numbers reveal an interesting nuance. The portfolio composed of stocks with significant ESG coefficients—representing 18 stocks—delivered an annualized return of 5.80%, with an annualized volatility of 11.68%, and a resulting Sharpe ratio of 0.4451. By contrast, the portfolio consisting of the remaining 82 stocks, for which the ESG coefficient was not statistically significant, achieved a higher annualized return of 7.13% with 13.47% annual volatility, yielding a Sharpe ratio of approximately 0.4844. These results indicate that, on average, the non-significant group exhibited slightly better performance in both absolute and risk-adjusted terms than the significant ESG portfolio. Although one might expect that stocks showing a statistically robust ESG effect would perform better, the observed differences suggest that—at least in this sample—the broader universe (which naturally benefits from diversification) may compensate for the absence of a clearly detectable ESG premium at the individual level. In other words, while a focus on statistically significant ESG coefficients provides a purer signal regarding the ESG-return relationship, it may also result in a more concentrated portfolio that suffers from higher idiosyncratic risk. Therefore, even though the significant group shows a measurable ESG effect, its modest economic edge (or even slight

underperformance on a risk-adjusted basis) indicates that, in practice, investors might achieve a more balanced outcome by either combining both groups or by adopting a more continuous screening approach.

In summary, across these portfolio tests, ESG-based screening did not hurt performance and in fact showed a slight improvement in risk-adjusted returns. The high-ESG portfolios yielded Sharpe ratios about 0.1 to 0.2 points higher than the low-ESG counterparts over this period. While the differences are not statistically extreme, there is no evidence of an ESG performance penalty; if anything, the bias was towards a benefit. This aligns with the consensus from global research that incorporating ESG does not sacrifice returns, and can even enhance them in certain contexts [1]. Our results specifically provide a quantitative investment insight: by using the regression-derived ESG coefficient, one can create a more nuanced ESG portfolio that potentially captures alpha from ESG, rather than simply excluding low-rated companies arbitrarily. For example, instead of excluding all companies below an ESG score threshold (which might drop many firms without considering their return profile), an investor could target those companies where ESG seems to drive returns (high γ_i). This approach balances both financial performance and sustainability – a key point for practitioners.

Robustness and Limitations: We acknowledge several limitations in our analysis. The sample period of three years is short; the results could be sensitive to specific market cycles (for example, the post-COVID recovery favored certain sectors). ESG scores themselves did not vary much year-to-year for many firms, limiting the statistical power in time-series regressions. A longer sample, as data become available, would help solidify the conclusions. We also treated the ESG score as an additive linear factor; it's possible the relationship is non-linear or interacts with other factors (maybe ESG matters only in certain industries or during downturns). We did a brief check by interacting ESG with the market factor in regressions (to see if high ESG stocks have different beta in downturns) and found no strong pattern, but this could be explored more. Another point is that our portfolio tests were in-sample — an investor in 2021 would not have known the 2021–2023 γ values. A more realistic approach would be to use 2021–2022 data to predict 2023 performance, etc.

Lastly, transaction costs and real-world constraints (e.g., some large investors can't deviate too much from the index) could erode the excess returns from ESG screening. In our hypothetical portfolios, we assumed monthly rebalancing and equal weights, which in practice would incur costs. However, since ESG scores change only annually, an ESG-tilted strategy wouldn't need high turnover beyond maybe annual reshuffling, which is manageable. Concentration is another consideration: the more one narrows down to "ESG winners," the more one might sacrifice diversification [3]. Our significant-ESG portfolio had only 20 stocks; a real fund might not want such a concentrated bet. There is a balance to strike between the level of ESG screening and portfolio diversification, as Jin (2020) emphasizes [3].

CONCLUSION

This study examined the impact of ESG factors on stock performance for Thai SET100 firms through a quantitative lens. By incorporating Bloomberg's ESG scores into a Fama–French factor regression for each stock, we derived return-based ESG coefficients that measure how much a company's ESG performance contributes to its stock returns. We found that a subset of companies had significantly positive ESG coefficients, indicating that their sustainability practices aligned with higher returns beyond traditional risk premia. Conversely, only a few showed negative impacts. Using these coefficients for portfolio construction, we observed that portfolios favoring stocks with strong ESG return profiles achieved slightly higher average returns and Sharpe ratios than those skewed toward low-ESG-profile stocks over the 2021–2023 period. Although the outperformance was not extreme, it suggests an ESG-focused strategy did not harm returns and may have provided a modest benefit, including potential downside risk reduction during market stress.

For investors, these findings demonstrate a practical way to integrate ESG considerations: by treating ESG as an additional factor in investment analysis, one can identify which stocks might yield an "ESG alpha." Rather than relying on exclusion lists or broad ESG indices, investors can use regression-based insights to fine-tune their portfolios. The evidence from Thailand's market contributes to the global conversation that ESG integration can be compatible with fiduciary duty and return objectives [1].

For businesses and policymakers, the results carry an encouraging message: good ESG performance is associated with favorable financial outcomes, at least to a mild extent, in the eyes of the market. This means investments in sustainability might pay off not just in societal terms but also via investor recognition and possibly a lower cost of capital. However, the nuanced outcome – with many firms showing no clear ESG effect – also implies that simply having a high ESG score is not a guarantee of stock market rewards. Quality of implementation, industry context, and maintaining competitiveness remain key. Companies should pursue ESG initiatives that also strengthen their core business, thereby aligning ethical and financial imperatives.

In conclusion, the evidence from the Thai SET100 suggests that ESG factors do have a quantifiable impact on stock performance, and that impact can be harnessed in investment strategies for improved risk-adjusted returns. This bridges a gap by providing local-market empirical support to the notion that "sustainable investing" and "profitable investing" need not be at odds. Future research could extend this work by examining longer time horizons, exploring individual E, S, and G pillar scores for differential effects, and testing the approach in other emerging markets. As data quality improves and more firms embrace ESG reporting, the ability to pinpoint how sustainability translates to financial performance will only grow, enabling both investors and companies to make more informed decisions in pursuit of sustainable growth.

ACKNOWLEDGEMENT

The authors thank the organizers and reviewers of the EEAT Conference for their valuable feedback, which helped improve the clarity and rigor of this paper. We also acknowledge Bloomberg L.P. for providing ESG rating data via the Bloomberg Terminal, and the Stock Exchange of Thailand for access to historical stock price and financial data. Their support was instrumental in conducting this research. Any errors or omissions are our own.

REFERENCE

[1] Friede, G., Busch, T., & Bassen, A. (2015). ESG and Financial Performance: Aggregated Evidence from More Than 2000 Empirical Studies. Journal of Sustainable Finance & Investment, 5(4), 210–233. DOI:10.1080/20430795.2015.1118917

[2] Prinyapon, Y., Nittayagasetwat, A., & Nittayagasetwat, W. (2022). Performance of ESG Stocks: Case of Stock Exchange of Thailand. NIDA Business Journal, 31(June–Nov), 55–72.

[3] Jin, I. (2020). ESG-Screening and Factor-Risk-Adjusted Performance: The Concentration Level of Screening Does Matter. Journal of Sustainable Finance & Investment, 11(4), 303–324 (published 2021).

[4] Marupanthorn, P., Termsaithong, T., Wangpratham, N., Koryanyong, J., Chanpiwat, C., & Pathomsathit, C. (2024). Development of ESG Factors for Enhancing Factor Model in the Thai Stock Market. SSRN Working Paper, Feb 2024.

[5] Fama, E. F., & French, K. R. (1993). Common Risk Factors in the Returns on Stocks and Bonds. Journal of Financial Economics, 33(1), 3–56.

[6] Bloomberg L.P. (2020). Bloomberg ESG Scores – Methodology Overview. [Online]. Bloomberg Professional Insights.

[7] Investopedia (2023). Fama and French Three-Factor Model. Investopedia.com (accessed 2025).

[8] Stock Exchange of Thailand (2015). Thailand Sustainability Investment (THSI) Initiative – SET News Release.

20R5-01

Evaluation of Moving Bed Biofilm Reactor (MBBR) Performance in Treating Weak Domestic Wastewater for Reuse in Agriculture

Tongchai Sriwiriyarat[1*] and Chanyut Kalakan[2]

[1]Associate Professor, Department of Chemical Engineering, Faculty of Engineering, Burapha University, Chonburi 20131, Thailand*
[2]Assistant Professor, Department of Civil Engineering, Faculty of Engineering, Burapha University, Chonburi, 20131, Thailand
[*]Phone: 038-10-2222 ext. 3404, E-mail: sriwiri@buu.ac.th

ABSTRACT

Wastewater reuse presents a viable solution for water conservation and nutrient recycling in agriculture to resolve the rising water demand in Thailand's Eastern Economic Corridor (EEC). This study evaluated a full-scale Moving Bed Biofilm Reactor (MBBR) system for treating domestic wastewater and developed a compact, cost-effective, small-scale MBBR system for septic tank effluent treatment. Both systems consisted of two MBBR reactors followed by a clarifier, filtration, and disinfection. The full-scale system achieved high nitrification efficiency (97.2±4.4%) with minimal nitrite accumulation and effluent nitrate concentrations of 20.5±6.9 mg N/L. Most ammonium nitrogen was nitrified in the first MBBR reactor, with nitrification rates of 0.36 g N/m²/day in MBBR #1 and 0.02 g N/m²/day in MBBR #2, indicating low nitrogen loading. The small-scale system removed 56.4±12.3% of ammonium, but nitrite accumulated (9.4±10.6 mg N/L), likely due to oxygen limitations. Higher nitrification rates (0.68 and 0.50 g N/m²/day) reflected its higher nitrogen load. Phosphate removal was minimal in both systems. Effluent total suspended solids (TSS) were 11.8±9.6 mg/L (full-scale) and 22±11.2 mg/L (small-scale), meeting secondary treatment standards. The full-scale system used UV disinfection, while chlorination trials in the small-scale system eliminated coliforms with a chlorine dosage of 12 mg/L. Both full-scale and small-scale systems produced effluent suitable for agricultural reuse, supporting water conservation and nutrient recycling. Further aeration and phosphorus removal optimization could enhance treatment efficiency and agricultural benefits.

Keywords : SDG6; Water shortage; Moving Bed Biofilm Reactor; Agriculture reuse; Septic tank

INTRODUCTION

Global water demand is projected to increase by 20% to 30% by 2050 (5,500-6,000 km^3/year), with about 70% attributed to agriculture. Agricultural water requirements are expected to increase by 60% by 2025 [1]. In 2015, the United Nations (UN) established 17 Sustainable Development Goals (SDGs), including SDG6 (Clean Water and Sanitation), which emphasizes safe wastewater treatment and reuse [2]. Thailand has committed to achieving these SDGs by 2030 [3]. However, water shortages in Thailand's Eastern Economic Corridor (EEC), including Chachoengsao, Chonburi, and Rayong provinces, are expected due to industrial expansion, population growth, tourism, and agriculture. By 2036, water demand in the EEC region is forecasted to reach 8.0×10^8 m^3/year by 2027 and 1.0×10^9 m^3/year. This study proposes wastewater recycling to increase domestic water availability and to reduce dependence on freshwater sources [4]. Currently, wastewater engineering has increasingly adopted the concept of reusing wastewater in various activities or recycling pollutants within wastewater as valuable resources [5]. Consequently, recovering and reusing nutrients from wastewater has become a topic of great interest for a nutrient circular economy framework [6]. Treated effluent can be reclaimed for agricultural irrigation, alleviating agricultural water demand, maximizing resource recovery, minimizing environmental impact, and aligning with SDG6 targets.

Among several wastewater treatment systems, the Moving Bed Biofilm Reactor (MBBR) system is a promising technology for reliably treating wastewater so that effluent can meet effluent quality standards under various conditions. It uses biofilm-supporting media to immobilize bacteria, forming layers that enhance microbial activity. The MBBR system offers a compact design, small footprint, and high specific surface area, so it makes particularly advantageous; therefore, the MBBR system can support elevated organic loading rates (OLRs) while maintaining a short hydraulic retention time (HRT) [7].

This study evaluated a full-scale MBBR system for treating domestic wastewater for agricultural reuse and developed a compact, cost-effective, small-scale MBBR for septic tank effluent. Both systems aim to offer sustainable solutions for centralized and decentralized wastewater treatment while ensuring compliance with agricultural water quality standards.

METHODOLOGY

Full-scale MBBR System Configuration and System Operation

A full-scale two-stage MBBR system was constructed at the Northern Saensuk wastewater treatment plant consisting of two MBBR reactors (MBBR #1 and #2), a coagulation-flocculation unit, a lamella clarifier, a sand filter, and a UV disinfection unit as illustrated by Figure 1. After the domestic wastewater passed the bar screen, the wastewater was pumped at 50 m^3/day into the first MBBR reactor (a total volume of 20 m^3 and an effective volume of 14.14 m^3). Then, it flowed to the second MBBR reactor (14.14 m^3), resulting in a hydraulic retention time (HRT) of 13.6 hours. Each MBBR reactor contained 30% (v/v) plastic media (4.24 m^3), as illustrated by Figure 2(a), with a diameter of 2.5 mm, a thickness of 10 mm, and a bulk specific surface area of 500 m^2/m^3. The surface area loading rate (SALR) of 4 g BOD_5/m^2/day was used to determine the media amount in the MBBR #1 to achieve BOD removal efficiency of greater than 90% [11]. Firstly, the nitrification rate of 1 g N/m^2/day was used to determine the media volume (3 m^3) in the second MBBR reactor. However, the same media volume (4.24 m^3) of the first MBBR tank was chosen for use in the second MBBR reactor; therefore, the design nitrification rate was 0.71 g N/m^2/day. The pH and DO meters were installed in the first MBBR #1 to measure real-time pH and DO. The aeration was supplied with fine bubble diffusers at a specific energy consumption of 0.17-0.25 kWh/m^3 to provide the air to maintain the DO concentrations of about 3.0-4.0 mg/L and suspend the reactor's media.

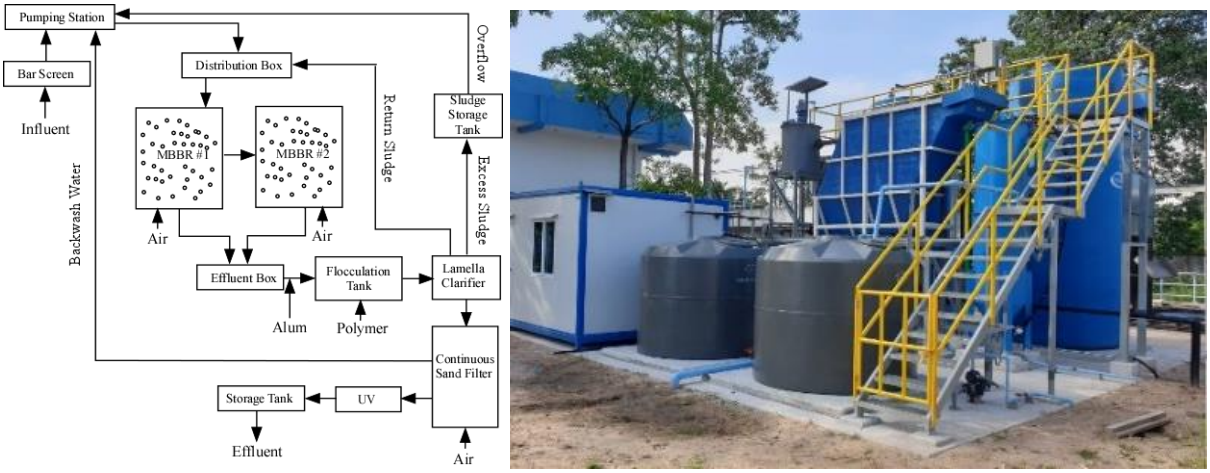


Figure 1 A full-scale MBBR wastewater treatment system located at the Northern Saensuk wastewater treatment plant

A static mixer and a flocculation tank were installed between the second MBBR and clarifier to increase the floc sizes with alum and polymer. However, the coagulation/flocculation unit was disabled in this study to save energy and chemicals due to much less suspended solids observed in both MBBR reactors. Therefore, the solids in the effluent from the second MBBR reactor were directly settled in the lamella settler with a 120 m^3/day capacity to achieve an 80% solids removal efficiency. An air diaphragm pump with a capacity of 15 L/min was used to pump the sludge to the sludge storage tank. The remaining suspended solids were filtered in the continuous sand filter with a filtration rate of 5.0 m^3/m^2/hr. The continuous sand filter was operated to filter the effluent continuously and backwash simultaneously. The backwash water was sent back to the pumping station. The clear effluent was disinfected by a UV sterilizer unit with a capacity of 2.7 m^3/hr.

Small-scale MBBR System Configuration and System Operation

Figure 3(a) presents a diagram of a compact, two-stage, small-scale MBBR system constructed from four 200-L tanks consisting of a storage tank, two MBBR reactors, and a clarifier, as shown in Figure 3(b). All materials were purchased locally and inexpensively to build the system locally and economically. The

wastewater storage tank was used as the equalization tank for wastewater collected from the second chamber of the septic tank system located at the back of a building at Piboonbumpen Demonstration School, Burapha University. A small pump is installed inside the tank to continuously stir and prevent the suspended solids from settling. Wastewater from the storage tank was pumped at 1200 L/day into the first 200-L MBBR reactor with an effective volume of 190 L, as illustrated by Figure 3(c), and then flowed to the second 200-L MBBR reactor (190 L), providing a nominal HRT of 7.6-hour. The design SALR of each MBBR reactor was 4 g BOD_5/m^2/day. Each reactor contains 40% (v/v) of the same plastic media, a higher volume than the full-scale system, to address high nitrogen concentrations in the influent. An air pump with an airflow rate of 100 L/min and air pressure of 0.04 MPa was used to connect three circular diffusers with a 13-cm diameter to supply DO and suspend the media in each reactor. The wastewater flowed from MBBR #2 to the 6-inch-diameter polyvinyl chloride (PVC) tube installed in the center of the clarifier. The tube was filled with a filter brush (14 cm in diameter and 60 cm in length) to filter large particulates. The suspended solids accumulated in the bottom zone and were periodically drained out. The remaining suspended solids were filtered again with the plastic media floating at the top of the tank, as shown in Figure 3(d). Effluent (Figure 3(e)) from the clarifier was stored in the tank for chlorination. In Thailand, the locally produced laundry bleach brand "Haiter" containing 6% (w/w) sodium hypochlorite, was employed as a disinfectant in this study because users can purchase it from local stores. The bleach was injected into a 6-inch tube installed at the center of the effluent tank. The bleach was mixed with effluent by air bubbles supplied by the air pump and kept inside the tank for additional contact time before flowing out from the effluent tank.



(a) (b)

Figure 2 Biofilm formation on the media in the MBBR systems

Measurement and Analyses

After both systems were successfully constructed and fed with seeding sludge from the local nearby activated sludge wastewater treatment system, the samples were collected from both systems for parameter analyses including Total chemical oxygen demand (TCOD), soluble chemical oxygen demand (SCOD), total suspended solids (TSS), ammonium (NH_4^+), nitrite (NO_2^-), nitrate (NO_3^-), and phosphate (PO_4^{3-}) according to the Standard Methods for Water and Wastewater Examinations [10]. TCOD and SCOD were measured with the closed reflux with titration method; the NH_4^+, NO_2^-, NO_3^-, and PO_4^{3-} were analyzed with phenate, colorimetric method, and brucine colorimetric method with UV-spectrophotometer, respectively. All data in this study were presented as mean ± standard deviation (SD).

RESULTS AND DISCUSSIONS

Influent Wastewater Characteristics

Table 1 shows the influent wastewater characteristics of domestic wastewater from Saensuk municipality and the septic tank of a school building. The domestic wastewater was found to have lower ammonium and phosphate concentrations than septic tank effluent due to combined sewers and dilution [8]. This suggests that septic tank effluent may be a more valuable local agricultural nutrient source. As indicated by the SD values in Table 1, nutrient (nitrogen and phosphorus) and COD levels in the influent feeding to the small MBBR system also fluctuated during summer because the building was unoccupied by students, reducing wastewater volume and altering the wastewater composition.

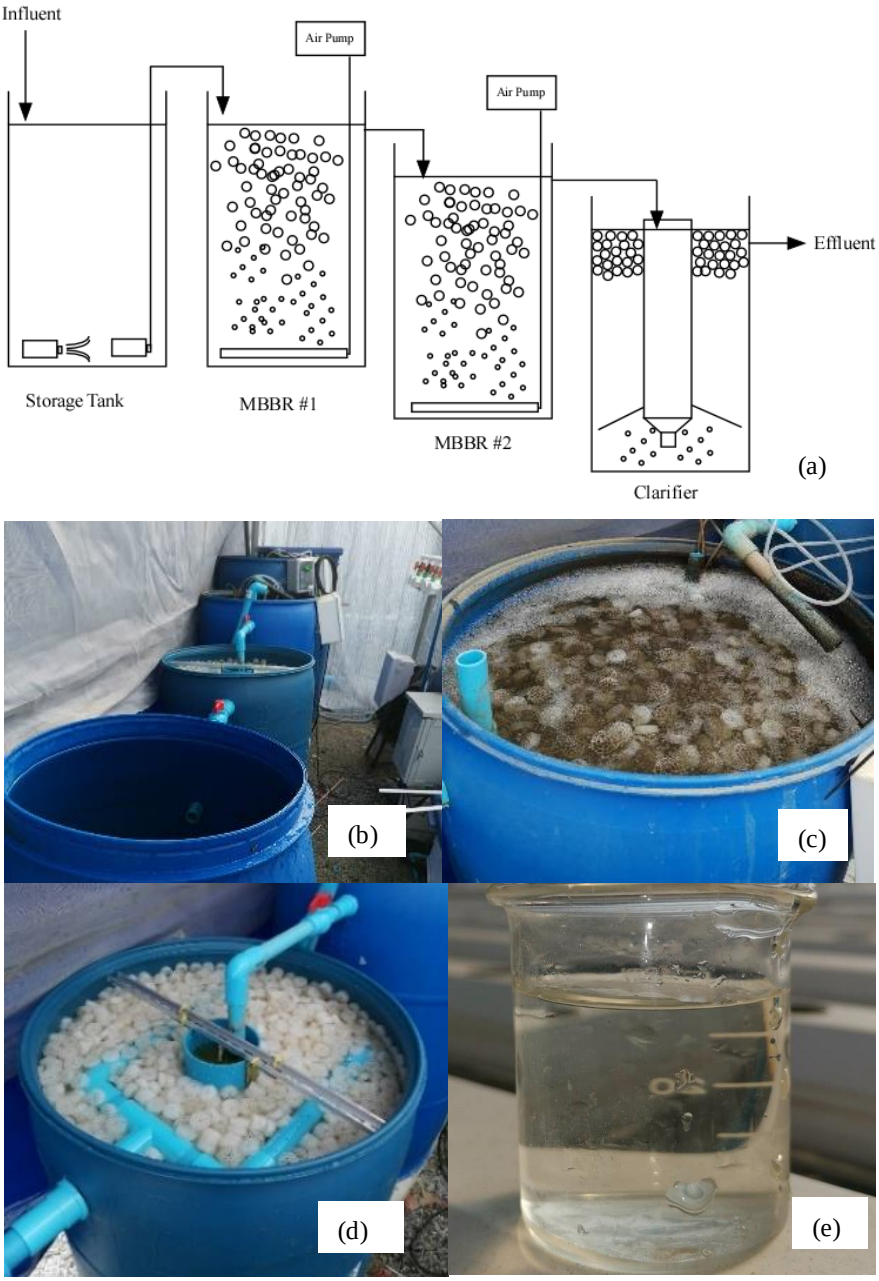


Figure 3 A small MBBR wastewater treatment system at Piboonbumpen Demonstration School, Burapha University

Table 1 Influent wastewater characteristics from the full-scale and compact MBBR wastewater treatment systems

Parameters	Full-scale MBBR		Small-scale MBBR	
	Avg.	S.D.	Avg.	S.D.
TCOD (mg COD/L)	80.0	0.0	64.6	20.3
NH_4^+-N (mg N/L)	21.4	1.5	76.7	24.4
NO_2^--N (mg N/L)	0.0	0.0	1.0	1.1
NO_3^--N (mg N/L)	0.1	0.3	1.1	1.7
TSS	35.6	41.9	61.7	37.1
PO_4^{3-}-P (mg P/L)	4.1	1.9	23.1	7.0
pH	7.2	0.1	7.6	0.2

MBBR System Performances for COD Removal and Nitrification

For over 3-4 months of operation, the full-scale and small-scale MBBR systems eliminated all COD (100% removal efficiencies) in the wastewater due to the low influent COD concentration. The COD mass balances around each reactor of the full-scale MBBR system, as shown in Figure 4, indicate that most organic matters of about 4.2±0.6 kg COD/day were removed in the first MBBR reactor of the full-scale MBBR system. The actual SALR of 1.19 g BOD_5/m^2/day was achieved in the first MBBR, assuming a BOD_5/COD ratio of 0.6 [8]. Also, it was found that the COD was completely removed in the first MBBR reactor of the small-scale MBBR system with 81.6±23.2 g COD/day and the SALR of 1.28 g BOD_5/m^2/day. The SALR rate of the full-scale system was approximately the same as the small-scale MBBR system. No COD was found in the second stage of both MBBR systems, as shown in Figure 4. According to WEF [11], both systems were classified as low-rate MBBR, and a BOD removal efficiency of greater than 90% was expected. The low-rate MBBR is typically used to remove organic matter prior to the nitrification in the second stage of the two-stage MBBR system [11].

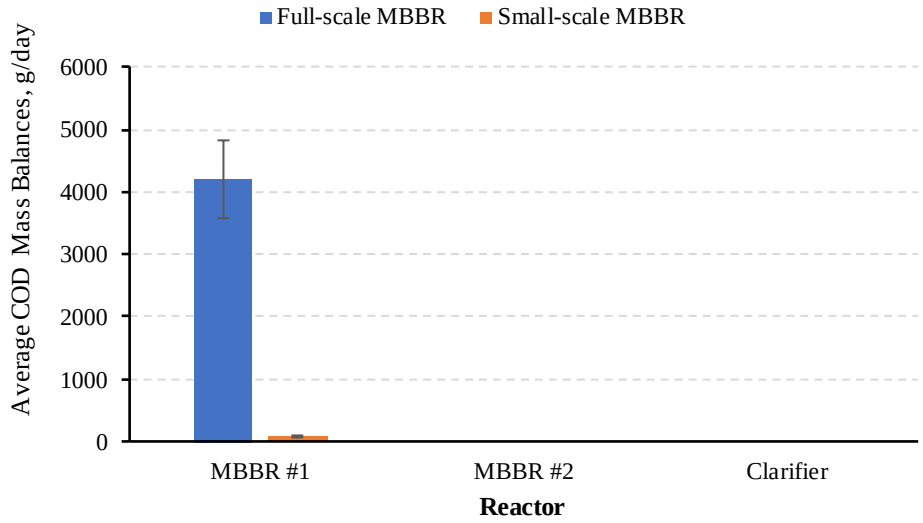


Figure 4 COD mass balances in (a) the full-scale MBBR system and (b) the small MBBR system

In the full-scale MBBR system, according to Figure 5(a), nitrification achieved the removal efficiencies of 97.2±4.4%, producing nitrate concentrations of 20.5±6.9 mg N/L without nitrite accumulation. It was found that most ammonium nitrogen was nitrified in the first MBBR reactor (0.77±0.31 kg N/day) to nitrite (0.10±0.09 kg N/day) and then to nitrate nitrogen (0.64±0.19 kg N/day), respectively, due to low ammonium nitrogen in the domestic wastewater. The nitrification rate in the MBBR #1 and MBBR #2 reactors were 0.36 and 0.02 g N/m^2/day, respectively. It is evident that most ammonium removal occurred in MBBR #1, which aligns with the higher nitrification rate (0.36 g N/m^2/day) compared to MBBR #2. The lower activity in MBBR #2 suggests that ammonium was nearly depleted after MBBR #1, reducing substrate availability for nitrifiers in the second stage. Additionally, the low nitrogen loading in the system indicates that the biofilm carriers were not fully utilized, which may explain the lower nitrification rate in the second MBBR. Minimal nitrite was accumulated in this reactor, but it was later completely nitrified to nitrate in the second MBBR reactor. It appears that the MBBR system was underloaded concerning the nitrogen loading. The high nitrification efficiency in the full-scale MBBR system suggests that the reactors operated under favorable conditions for ammonium oxidation and subsequent nitrite oxidation. The observed low nitrite accumulation confirms that complete nitrification was achieved, likely due to sufficient oxygen availability and a well-established nitrifying biofilm.

In contrast, the small-scale MBBR system exhibited lower nitrification performances as indicated by lower ammonium removal efficiency of 56.4±12.3%. Substantial residual ammonium in the effluent at the concentrations were 35.3±18.8 mg N/L. Both MBBR #1 and MBBR #2, as illustrated by Figure 5(b), contributed to nitrification with nitrification rates of 0.68 and 0.50 g N/m^2/day, respectively. These rates were significantly higher than those in the full-scale system, likely due to the higher nitrogen loading. The accumulation of nitrite (9.4±10.6 mg N/L) in the small-scale system suggests an imbalance between ammonium oxidation and nitrite oxidation. Figure 6 reveals the variations in ammonium, nitrite, and nitrate concentrations found in effluents according to the variations of ammonium nitrogen in the influent. This

phenomenon is commonly associated with oxygen limitation, as ammonia-oxidizing bacteria (AOB) outcompete nitrite-oxidizing bacteria (NOB) under low dissolved oxygen (DO) conditions. Higher ammonium concentrations further support this hypothesis, as ammonium oxidation is an oxygen-intensive process. The variation in nitrite levels indicates that nitrification efficiency may be unstable under fluctuating operating conditions. Furthermore, the elevated nitrate concentrations (22.2±11.2 mg N/L) in the small-scale system indicate that nitrification was still occurring but was not as complete as in the full-scale system. The presence of residual ammonium and nitrite in the effluent suggests that optimizing aeration and hydraulic retention time (HRT) could improve the performance of the small-scale reactor.

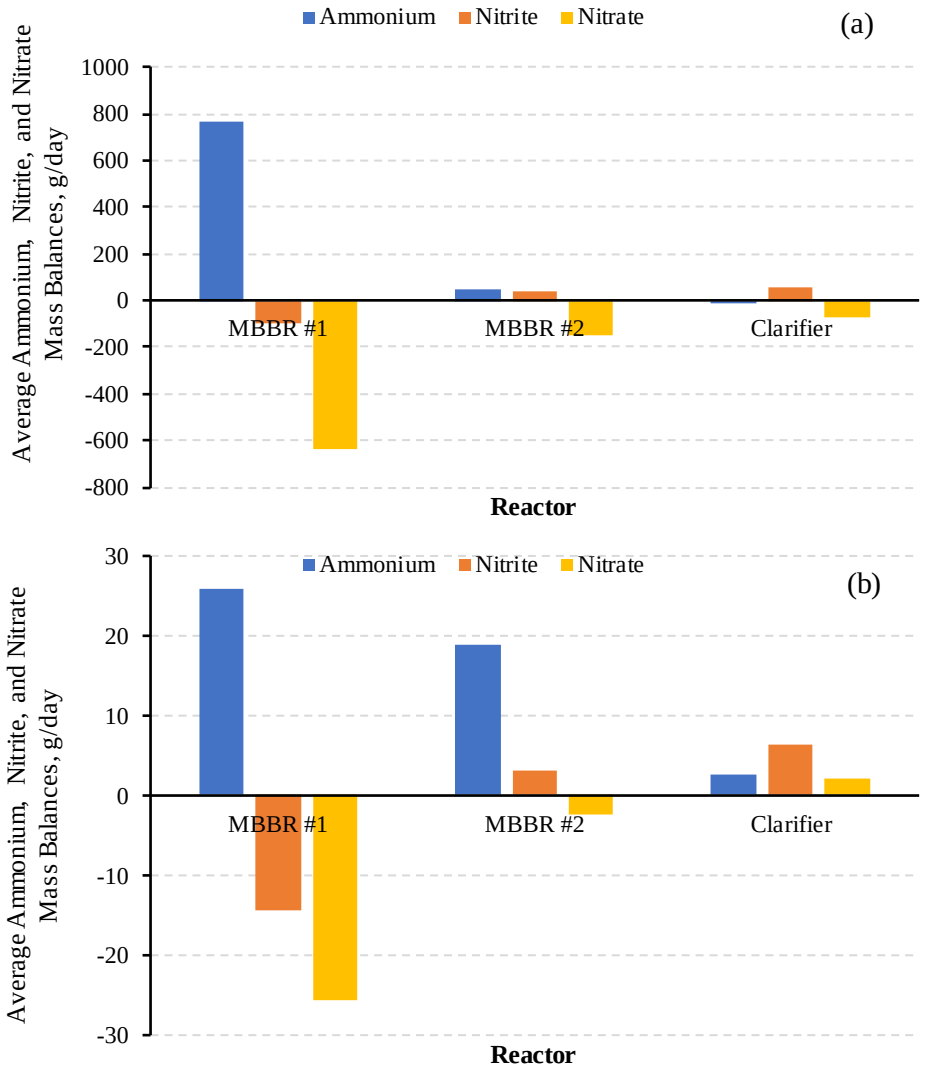


Figure 5 Ammonium, nitrite, and nitrate nitrogen mass balances in (a) the full-scale MBBR system and (b) the small MBBR system

In addition, both systems demonstrated minimal phosphorus removal, likely due to the absence of specific phosphorus removal mechanisms such as enhanced biological phosphorus removal (EBPR) or chemical precipitation. Supplementary treatment, such as chemical dosing with ferric chloride or alum, could be considered if phosphorus reduction is a concern. The total suspended solids (TSS) concentrations in the full-scale and small-scale systems effluents were 11.8±9.6 mg SS/L and 22±11.2 mg SS/L, respectively. The lower TSS in the full-scale system suggests better solids separation, potentially due to the sand filtration. The TSS levels in both systems meet typical effluent standards for secondary treatment. Effluent disinfection was performed using UV in the full-scale system; however, bacterial examination was not conducted, leaving the effectiveness of pathogen removal unknown. Future monitoring of microbial indicators such as total coliforms (TCB) and fecal coliforms (FCB) is recommended to validate UV disinfection performance. In the small-scale system, chlorination trials indicated complete disinfection, with no detectable TCB, FCB, or

residual chlorine after 60 minutes of contact with a 12 mg/L chlorine dosage. While effective, this dosage is relatively high, probably due to the reactions with other compounds in the effluents. Optimization of chlorine application could be explored to minimize chemical use while maintaining disinfection efficacy. According to U.S. EPA guidelines, secondary-treated and disinfected wastewater must meet the following criteria for reuse in non-food crop irrigation: ≤ 30 mg/L BOD, ≤ 30 mg/L TSS, ≤ 200 fecal coliforms/100 mL, and ≥ 1 mg/L residual chlorine. Since both MBBR systems met these standards, they present feasible options for agricultural water and fertilizer reuse. However, additional filtration or advanced disinfection methods may be necessary for applications requiring stricter pathogen control.

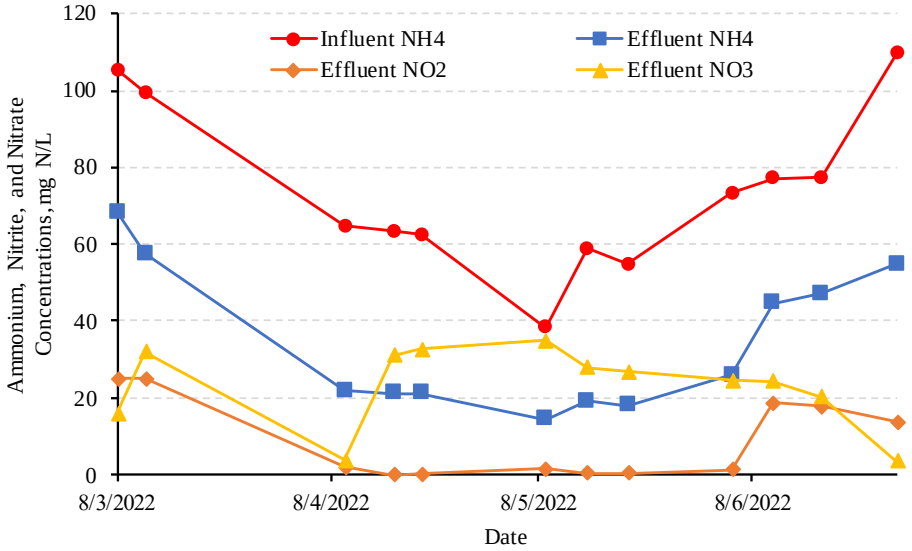


Figure 6 Variation in ammonium, nitrite, and nitrate nitrogen concentrations in a small MBBR system

Cost-Effective Analysis of MBBR Systems for Agricultural Reuse

Using locally available and cost-effective materials, a small-scale wastewater treatment system was constructed and installed at Piboonbumpen Demonstration School, Burapha University. The total construction cost, excluding labor, was approximately 20,000 THB, with capital expenses mainly from the plastic media costs and operational expenses primarily from electricity usage of two small water pumps (23W each, operating 24 hours/day, 1.10 kWh/day), a DC pump for wastewater intake (300W, operating 1 hour/day, 0.44 kWh/day) and two small aeration pumps (120W each, operating 24 hours/day, 5.76 kWh/day). The total electricity consumption was 7.30 kWh/day (~220 kWh/month). Using the Provincial Electricity Authority's calculation tool, the estimated electricity cost is 883.50 THB/month or 29.45 THB/day. The treatment cost per cubic meter of wastewater is 24.5 THB/m^3. For comparison, if a farmer uses tap water for agricultural purposes at 1.2 m^3/day (36 m^3/month), the estimated water bill is 673.24 THB/month (22.44 THB/day or 18.7 THB/m^3) based on Chonburi's water tariffs. Tap water is 2.06 THB/day, cheaper than treated wastewater. However, considering the nitrogen and phosphorus content in the treated effluent, which reduces fertilizer needs, the net treatment cost can be lower. For instance, with an effluent flow rate of 1,200 L/day, nitrogen content is 63.7 g/day, and phosphorus is 28.8 g/day. If the flow rate increases to 1,500 L/day, the treatment cost drops to 19.6 THB/m^3, with a hydraulic retention time of 6.1 hours, maintaining similar treatment efficiency. At this flow rate, tap water costs 19.5 THB/m^3, making 1,500 L/day the cost-effective threshold for operation. Reducing flow rates is not recommended as it increases the per-unit treatment cost and may affect system performance. Expanding the system's capacity or increasing media content beyond 40% could possibly improve efficiency.

For the full-scale MBBR system at Saensuk (North) wastewater treatment facility, electricity consumption is 80 kWh/day (~2,400 kWh/month), costing 9,730.65 THB/month. With a current flow rate of 50 m^3/day, the electricity cost per cubic meter is 6.5 THB/m^3. Comparing this to tap water costs for 1,500 m^3/month (~43,470 THB/month), reclaimed water could reduce expenses by 4.5 times. Furthermore, the treated effluent contains 1,100 g/day of nitrogen and 150 g/day of phosphorus, essential nutrients for agriculture. In addition, enhancing the MBBR system to treat more wastewater would reduce treatment costs and environmental pollution. Upgrading the system to produce water of near-potable quality could allow its

reuse for various community activities, saving four times the water costs and alleviating water shortages in the Eastern Economic Corridor (EEC).

CONCLUSIONS

This study confirms the feasibility of using a full-scale and a small-scale MBBR system for treating wastewater for agricultural reuse. The full-scale system demonstrated high nitrification efficiency (97.2±4.4%), effectively converting ammonium to nitrate with minimal nitrite accumulation. In contrast, the small-scale system exhibited partial nitrification with some nitrite accumulation, likely due to oxygen limitations. However, both systems achieved complete organic removal and met effluent quality standards for non-food crop irrigation. While phosphorus removal was minimal, the treated effluent contained nitrogen and phosphorus nutrients that could reduce the need for synthetic fertilizers, enhancing the cost-effectiveness of wastewater reuse. Energy consumption analysis revealed that increasing the influent flow rate could further optimize operating costs, lowering the cost per cubic meter of treated water. Additionally, comparisons with tap water costs showed that wastewater reuse could be a financially competitive alternative, particularly when considering the added benefit of nutrient recycling. The study highlights MBBR technology as a sustainable and cost-effective wastewater treatment option, particularly for decentralized applications in agriculture. Expanding wastewater reuse applications beyond irrigation could further enhance sustainability, aligning with global water conservation goals and supporting SDG 6 in reducing water shortage.

ACKNOWLEDGMENT

This work is financially supported by the National Research Council of Thailand (Grant No. KM 47/2564 and Project No. 464042-ODU08).

REFERENCES

[1] Boretti, A. and Rosa, L. 2019. Reassessing the projections of the world water development report. npj Clean Water. 2:15.

[2] United Nations. The sustainable development goals (SDGs). United Nations. Retrieved February 5, 2025, from https://sdgs.un.org/goals.

[3] United Nations Thailand. Sustainable development goals in Thailand. United Nations Thailand. Retrieved February 5, 2025, from https://thailand.un.org/en/sdgs.

[4] Suksaroj, T.T., Jha, N.K., Chuanpongpanich, S., Siriraksophon, W., Kwanyuen, B. and Suksaroj, C. 2024. Strategy development for domestic water use reduction in special economic zone of Thailand through water user perception and factor analysis. Environmental and Sustainability Indicator. 21: 100344.

[5] Fernandes, E. and Marques, R.C. 2023. Review of water reuse from a circular economy perspective. Water. 15(5): 848.

[6] Soo, A. and Shon, H.K. 2024. A nutrient circular economy framework for wastewater treatment plants. Desalination. 592:118090.

[7] Leyva-Díaz, J.C., Martín-Pascual, J., Muñío, M.M., González-López, J., Hontoria, E. and Poyatos, J.M. 2014. Comparative kinetics of hybrid and pure moving bed reactor membrane bioreactors. Ecological Engineering. 70(7): 227-234.

[8] Phanwilai, S., Noophan, P., Li, C.W. and Choo, K.H. 2022. Efficacies of nitrogen removal and comparisons of microbial communities in full-scale (pre-anoxic systems) municipal water resource recovery facilities at low and high COD:TN ratios. Water. 14(5): 720.

[9] U.S. Environmental Protection Agency. 2012. Guidelines for Water Reuse (EPA/600/R-12/618). U.S. Environmental Protection Agency, Washington, D.C.

[10] American Public Health Association (APHA), American Water Works Association (AWWA), & Water Environment Federation (WEF). 2012. Standard Methods for the Examination of Water and Wastewater (22nd ed.). American Public Health Association, Washington D.C.

[11] Water Environment Federation (WEF). 2010. Biofilm Reactors: WEF Manual of Practice No. 35. McGraw Hill, New York.

20R5-02

Application of Corn Straw Biochar for Removal of Heavy Metals from Gold Mining Wastewater

Por Yang[1, 2*], Pharkphum Rakruam[3], Sulak Sumitsawan[3], Patiroop Pholchan[3] and Pimluck Kijjanapanich[3]

[1*] Lecturer, Department of Civil engineering, Faculty of engineering, Souphanouvong University, Luang Prabang 0600, Laos.
[2] Graduate student, Department of Environmental Engineering, Faculty of Engineering, Chiang Mai University, Chiang Mai 50200, Thailand;
[3] Assistant Professor, Department of Environmental Engineering, Faculty of Engineering, Chiang Mai University, Chiang Mai 50200, Thailand.
[*]Corresponding author: Tel : 0825645135, Fax : 053 210328, E-mail: yangporching06@yahoo.com

ABSTRACT

This study aims to solve the environmental issue of contamination of heavy metals from mining wastewater by using biochar as an absorbent. Biochar was pyrolyzed from rice straw at 700°C for 2 h using a tube-type electrical furnace under 150 mL/min of N_2 gas and a heating rate of 20 °C/min. This experiment investigated the removal of Cu, Ni, and Zn from the synthetic wastewater using biochar from corn straw to remove the heavy metals from mining wastewater. The result indicates that the removal efficiency of Cu is the highest at 93.98%, and the adsorption capacity of Cu, Ni, and Zn is 4.19, 2.30, and 5.97 mg/g for corn straw biochar. The competitive adsorption of heavy metals was observed during this experiment, such as Zn > Cu > Ni. The adsorption kinetics of Cu, Ni, and Zn on corn straw biochar is fitted to the pseudo-second-order kinetic model.

Keywords: Agriculture waste; Biochar; Corn straw; Heavy metal; Mining wastewater;

INTRODUCTION

Recently, the mining industry of Laos is expected to play a crucial role in the increase of the national revenue, economic growth, and driving forces for the local community development [1]. The gold mining activity has an impact on the environment in the form of land degradation, deforestation, soil erosion, acid drainage, water pollution, air pollution, and heavy metals. The main pollution from the gold mining project is the acid mine drainage, which contains heavy metals from the tailing pond. Wastewater from the gold mining tailing contains high concentrations of the heavy metals and cyanide. The discharge of toxic elements from the tailings and other mine waste is core environmental contamination from gold mines. The infiltration of water through sulfide-containing tailings piles and ponds, surface and underground workings, waste, and development rock leads to the discharge of large volumes of metals like Zn, Cu, Pb, As, Ni, and sulphate ions into stream and river ecosystems [2,3]. This results in acid mine drainage (AMD) being created with severe harmful effects on the receiving water bodies. Heavy metal contamination and acid mine drainage are the most significant environmental concerns where waste materials containing metal-rich sulfides from mining activity have been kept or discarded [4]. The water pollution from the gold mining tailings pond was a solution that has a high heavy metal ion, and there are various technologies for treatment. The methods for remediating heavy metals from water include physicochemical methods, chemical precipitation, coagulation and flocculation, electrochemical treatments, ion exchange, membrane filtration, electrodialysis, and adsorption. However, these technologies suffer from a range of disadvantages, stretching from inefficiency in removing pollutants at low concentrations and completely converting pollutants into biodegradable or less toxic byproducts; not being suitable for all heavy metal removal; sludge generation; formation of metal hydroxide; high energy and chemical consumption; process complexity; and high maintenance and operation expenses. [5,6].

Adsorption is one of the frequently used techniques for heavy metal removal due to its simple operation, wider range of adsorbent availability, high accessibility, and easy design by selecting appropriate adsorbents based on adsorption capacity, efficiency, availability, and cost of adsorbent materials. Adsorption is a suitable technology for small communities or can be applied on a large scale in permeable reactive barriers (PRB). Biochar, which has excellent adsorption ability and economic and environmental benefits[7] , can be used for heavy metals removal from mining wastewater. An efficient and viable treatment process

should meet both economic and environmental requirements to be marketed and applied in large scale. The incorporation of low-cost and available materials in different treatment process could decrease the global treatment cost and increase the process efficiency [6]. This study chose corn straw as agricultural waste for the biochar production because this material is available and prevalent, especially in Southeast Asia. While this material can cause greenhouse gas emissions if it is burned in the open field.

The point of this experiment was to find out how well biochar can remove heavy metals like Cu, Ni, and Zn from gold mining wastewater and how well it can absorb these metals. This study used corn straw biochar, pyrolyzed at 700°C, as the adsorbent.

METHODOLOGY

1. Biochar production

The corn straw was collected from the local farm in Mae Faek, San Sai District, Chiang Mai Province, Thailand. Firstly, the rice straw was air- dried and cut to size <2 cm. Then, it was washed by demineralized water and dried in the oven at 60°C. The dried sample was pyrolyzed at 700°C for 2 h using a tube-type electrical furnace under 150 mL/min of N_2 gas and a heating rate of 20 °C/min.

2. Chemical

A mixed stock solution of Cu, Ni, and Zn was prepared by dissolving their respective salts copper sulfate ($CuSO_4 \cdot 5H_2O$), nickel sulfate ($NiSO_4 \cdot 6H_2O$), and zinc sulfate ($ZnSO_4 \cdot 7H_2O$) in deionized water at a concentration of 100 mg/L and dilution concentration of each element as needed for the experiment.

3. Experiment

Batch adsorption experiments were carried out at room temperature in 250 mL Erlenmeyer flasks. The samples were agitated at 200 rpm on an orbital shaker in order to enhance the contact between the adsorbent and the adsorbate. Batch heavy metals adsorption experiments were carried out using 150 mL of the synthetic mining wastewater with concentrations of Cu, Ni, and Zn at 5, 14, and 21 mg/L, respectively [8]. The initial pH of the synthetic mining wastewater was maintained at pH= 5 using sodium hydroxide or sulfuric acid solution. The adsorbent dosage of 1 g/L was used in this experiment. The samples were collected in 60 mL and filtered at the contact times of 5, 10, 15, 30, 60, 120, 240, 480, 720, and 1440 min. Heavy metal was determined by Flame Adsorption Atomic Spectroscopy.

4. Calculations of adsorption

The heavy metal uptake per gram of sorbent and the percentage removal were calculated according to the following equations (1) [9]:

$$q_t = \frac{(C_0 - C_t)V}{m} \quad (1)$$

The metal removal efficiency of the treatment system at any time during operation was calculated based on the inlet and the outlet effluent concentrations as follows:

$$\% \text{ Removal} = \frac{(C_0 - C_t) * 100}{C_0} \quad (2)$$

Where the q_t is the amount (mg/g) of heavy metals adsorbed, C_0 and C_t are the initial and time concentrations of heavy metals (mg/L), respectively, V is the volume of solution (mL), and m is the weight of the biochar (g) used for the experiment.

5. Sorption kinetics

5.1 Pseudo-first-order kinetic model

The linearized form of the pseudo-first-order kinetic model was applied to the experimental data to describe the kinetics of heavy metals sorption [10]. This equation is given below:

$$\log(q_e - q_t) = \log q_e - \left(\frac{k_1}{2.303}\right) t \quad (3)$$

Where q_t and q_e are the amount of solute adsorbed per mass of sorbent (mg/g) at any time and equilibrium, respectively, and k_1 is the rate constant of first-order sorption (1/min). The straight-line plot of $\log(q_e-q_t)$ against t gives $\log(q_e)$ as slope and intercept equal to $k_1/2.303$. Hence the amount of solute sorbed per gram of sorbent at equilibrium (q_e) and the first-order sorption rate constant (k_1) can be evaluated from the slope and the intercept.

5.2 Pseudo-second-order kinetic model

The Lagergren pseudo-second-order kinetic model was applied to the experimental data to describe the kinetics of heavy metals sorption. The model is represented by [11]:

$$\frac{t}{q_t} = \frac{1}{k_2 q_e^2} + \left(\frac{1}{q_e}\right) t \quad (4)$$

The initial sorption rate is defined by the following equation 5

$$h = k_2 q_e^{\ 2} \quad (5)$$

Where k_2 is the rate constant, q_t is the metal uptake capacity at any time t

RESULTS AND DISCUSSIONS

This study showed the removal of heavy metals from corn straw biochar adsorption. The removal efficiency of Cu, Ni, and Zn at contact time 12 h was 93.98, 16.52, and 34.45%, respectively, as shown in Figure 1. The study achieved the adsorption capacity of Cu, Ni, and Zn, which were 4.19, 2.30, and 5.97 mg/g, respectively, as illustrated in Figure 2. Meanwhile, this study was shown the competitive adsorption of heavy metals in wastewater like Zn > Cu > Ni for corn straw biochar. The competitive adsorption of Cu > Ni was similar to the reported use of date seed biochar [12] and Waste WS (Juglans regia L.) biochar [13].

The parameters for the adsorption kinetics of corn straw biochar were calculated, as displayed in Table 1. The higher values of correlation coefficients are 1.000, 0.979, and 0.989 for the pseudo-second-order model, and 0.981, 0.425, and 0.857 for the pseudo-first-order model for Cu, Ni, and Zn, respectively.

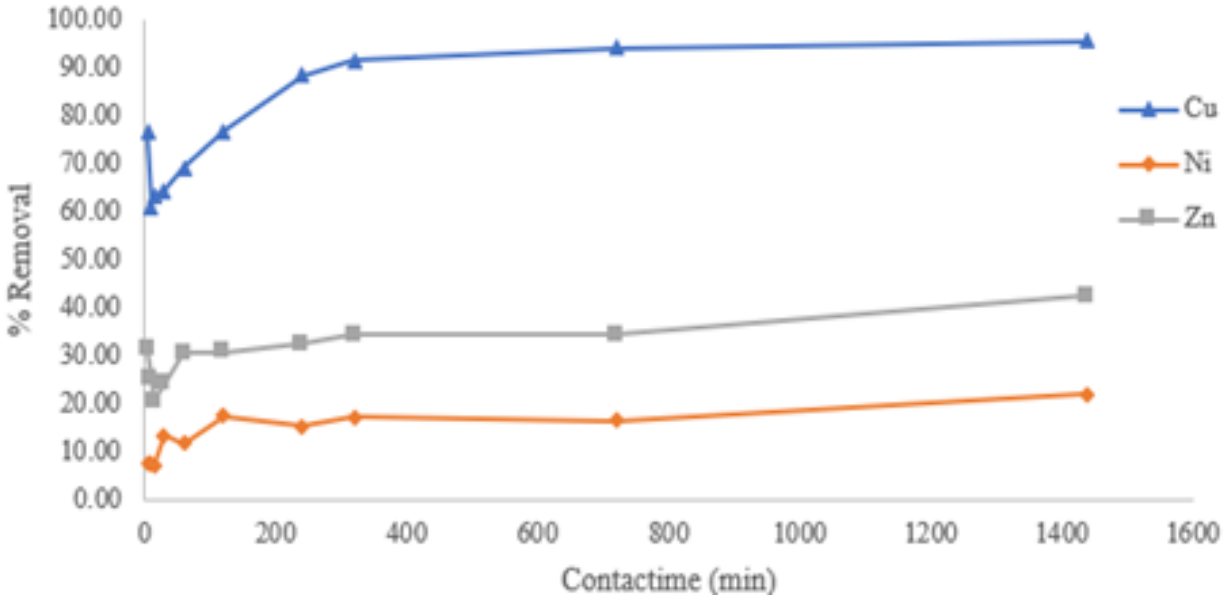


Figure 1. Heavy metals removal efficiency by corn straw biochar adsorption.

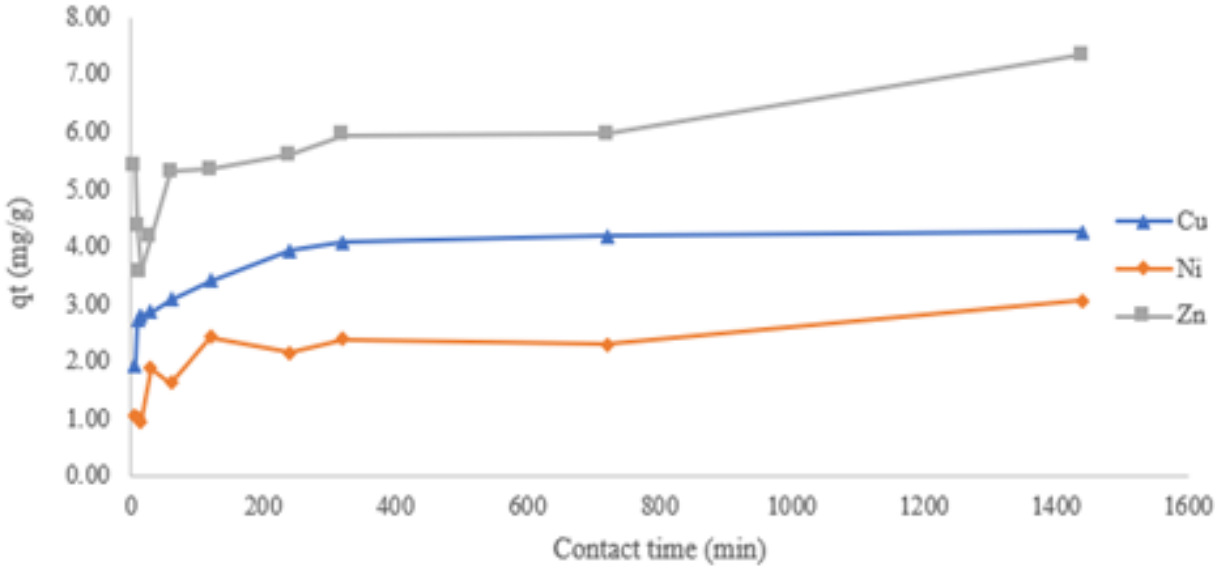


Figure 2. Heavy metals capacity adsorption by corn straw biochar adsorption**.**

Table 1. The adsorption kinetics of corn straw biochar on heavy metals adsorption for the pseudo-first-order model and the pseudo-second-order model.

Heavy metal	Pseudo-first -order model			Pseudo-Second -order model		
	q_e (mg/g)	k_1 (g/mg/min)	R^2	q_e (mg/g)	k_2 (g/mg/min)	R^2
Cu	1.828	0.008	0.981	4. 297	0.015	1.000
Ni	1.288	0.015	0.425	2.976	0.007	0.979
Zn	2.337	0.012	0.857	7.189	0.004	0.989

CONCLUSION

This study shows the removal efficiency and adsorption capacity of corn straw biochar. The maximum removal efficiency of Cu was 95.54%. The adsorption kinetics of corn straw biochar on heavy metal adsorption was fitted with the pseudo-second-order model.

ACKNOWLEDGEMENT

The study was financially supported by the Ministry of Education and Sport, Lao PDR especially the SSHEP Project under Asian Development Bank and Department of Environmental Engineering, Chiangmai University. The author gratefully to all staff in Department of Environmental Engineering for helping for be the successful of this research.

REFERENCE

[1] Chansavath BOPHA and Kongkham CHANTHAVICHITH, Mineral resources in Lao PDR. Proceeding of the international conference on Geology of Thailand: Tawards Sustainable Development and Sufficience Economic, 2007, P 194-198.

[2] Durkin, T.V.; Herrmann, J.G. Focusing on the Problem of Mining Wastes: An Intro- duction to Acid Mine Drainage, EPA Seminar Publication No. EPA/625/R-95/007. Available online: http://technology.infomine. com/enviromine/publicat/amdintro.html (accessed on 11 Jua 2016).

[3] Edwards, K.J.; Bond, P.L.; Gihring, T.M.; Banfield, J.F(2000). An archaeal iron-oxidizing extreme acidophile important in acid mine drainage. Science, volume 287, pp:1796–1799.

[4] Concas, A.; Ardau, C.; Cristini, A.; Zuddas, P.; Cao, G. (2006). Mobility of heavy metals from tailings to stream waters in a mining activity contaminated site. Chemosphere, volume 63, pp: 244-253.

[5] Acheampong.A.M, Meulepasa.W.J.R and Lensa.L.N.P (2009). Removal of heavy metals and cyanide from gold mine wastewater. *J Chem Technol Biotechnol* 2010; volume 85: pages 590–613. (www.interscience.wiley.com) DOI 10.1002/jctb.2358

[6] Enaime.G , Baçaoui.A, Yaacoubi.A and Lübken.M, 2020. Review Biochar for Wastewater Treatment-Conversion Technologies and Applications. Appl. Sci. 10, 3492; doi:10.3390/app10103492. www.mdpi.com/journal/applsci

[7] Patra.M. J, Panda.S.S and Dhal.K.N, 2017. Biochar as a low-cost adsorbent for heavy metal removal: a review. International Journal of Research in Biosciences. Volume 6. Issue 1, pp:1-7.

[8] Fernández-González.R, Martín-Lara.M.A, Iáñez Rodríguez. I, Calero.M (2018). Removal of heavy metals from acid mining effluents by hydrolyzed olive cake. Bioresource Technology 268, page169–175.

[9] Acheampong, M. A., J. P. C. Pereira, R. J. W. Meulepas & P. N. L. Lens, 2011. Biosorption of Cu(II) onto agricultural materials from tropical regions. *Journal of Chemical Technology & Biotechnology,* 86, 1184-1194.

[10] Abdelwahab O, 2007. Kinetics and isotherm studies of copper II removal from wastewater using various adsorbents. *Egypt J Aquatic Res* **33**:125–143.

[11] Ho YS and McKay G,1999. Pseudo-second-order model for sorption processes. *Process Biochem* 34 :451-465.

[12] Mahdi, Z., Q. J. Yu & A. El Hanandeh (2018) Competitive adsorption of heavy metal ions (Pb^{2+}, Cu^{2+}, and Ni^{2+}) onto date seed biochar: batch and fixed bed experiments. Separation Science and Technology, 54, 888-901.

[13] Ivanchenko, A., O. Soroka, D. Yelatontsev & V. Panasenko (2025) Heavy metal ions removal from an aqueous solution using an adsorbent derived from walnut shell: Equilibrium, kinetic and thermodynamic studies. Desalination and Water Treatment, 321.

20R5-03

Evaluation of Aluminium Fumarate Metal-Organic Framework for Defluoridation of High-Fluoride Contaminated Water

Wiratchon Srisom[1], Sarunnoud Phuphisith[2] , Phacharapol Induvesa[3] , Chalita Ratanatawanate[4] and Aunnop Wongrueng[5*]

[1]Graduate student, Department of Environmental Engineering, Faculty of Engineering, Chiang Mai University, Thailand ; [2] Assistant Professor, Department of Environmental Engineering, Faculty of Engineering, Chiang Mai University, Chiang Mai 50200, Thailand; [3]Lecturer, Department of Environmental Science, Faculty of Science, Silpakorn University, Nakhon Pathom 73000, Thailand; [4]National Nanotechnology Center (NANOTEC), National Science and Technology Development Agency (NSTDA), Thailand; [5] Associate Professor, Department of Environmental Engineering, Faculty of Engineering, Chiang Mai University, Chiang Mai 50200, Thailand*

[*]Phone : : (+66)53-944192, E-mail : aunnop@eng.cmu.ac.th

ABSTRACT

Removal of fluoride from water in areas with high fluoride problems has become a major problem as high levels of fluoride exposure cause bone and tooth problems. Nowadays, the adsorption method as one of the most effective methods of removing pollutants has attracted increasing attention among chemists and environmental researchers. However, one challenge is the design and development of more efficient adsorbents and their practical application in problem areas. The adsorption performance of Aluminum Fumarate (AlFu) for removal of fluoride was studied and the influence of some experimental factors, such as effects of pH, adsorbent dose as well as adsorption capacity, adsorption kinetics, adsorption isotherm and study the effective removal of fluoride ions from actual contaminated water (Groundwater runs). The theoretical maximum adsorption capacities based on the Freundlich isotherm were found to be 0.52 mg/g under constant conditions. The fluoride removal of AlFu MOF adsorbent in actual contaminated water (Groundwater runs) from sampling location 1 and sampling location 2 was up to 84 and 86%, respectively.

Keywords: adsorbent; aluminum Fumarate; metal-organic frameworks; fluoride; fluorosis

INTRODUCTION

Groundwater has fluoride from either human or natural sources [1]. Because groundwater flows through a range of geological formations over its complicated flow history, water can become contaminated. One of the main causes of endemic fluorosis is hydrogeochemical processes. High fluoride concentrations in groundwater have been reported to be supported by low calcium and high bicarbonate alkalinity [2, 3]. Even though the human body needs it in trace quantities, if it reaches the maximum permissible limit of 1.5 mg/L, it can be extremely dangerous [4, 5]. In Thailand, fluoride levels are dangerous if they exceed the maximum permissible value of 0.7 mg/L. High fluoride causes major bone problems and fluorosis [1, 6]. Therefore, reducing fluoride from groundwater has long been a research issue.

Metal-organic frameworks (MOFs) have increased appeal in the present-day academic research. The strength of combining organic and inorganic chemistry is shown by MOFs, which represent the summit of chemical structural perfection. They stand out from other traditional techniques in the field of study by their exceptional surface area, incredibly high adsorption capacity, and variable characteristics. In addition to having an abundance of reactive sites, they are frequently recycled and reversed. In relation to fluoride stability in solution, reversibility, and adsorption kinetics, MOFs perform better than normal adsorbents [7]. The factors that affect its effectiveness and optimal conditions are key to its standing as one of the most desired defluoridation adsorbents.

This study aims to use Aluminum Fumarate (AlFu) MOF adsorbent to remove fluoride from drinking water. The effects of pH, adsorbent dose as well as adsorption capacity, adsorption kinetics, adsorption isotherm and study the effective removal of fluoride ions from actual contaminated water (Groundwater runs) are also thoroughly examined.

METHODOLOGY

1. Water collecting

Groundwater containing high fluoride concentration in Chiang Mai Province was collected and shown in Figure 1. Fluoride concentration was analyzed by fluoride ion selective electrode. Other parameters i.e., pH, EC, and TDS were measured by using portable meters.

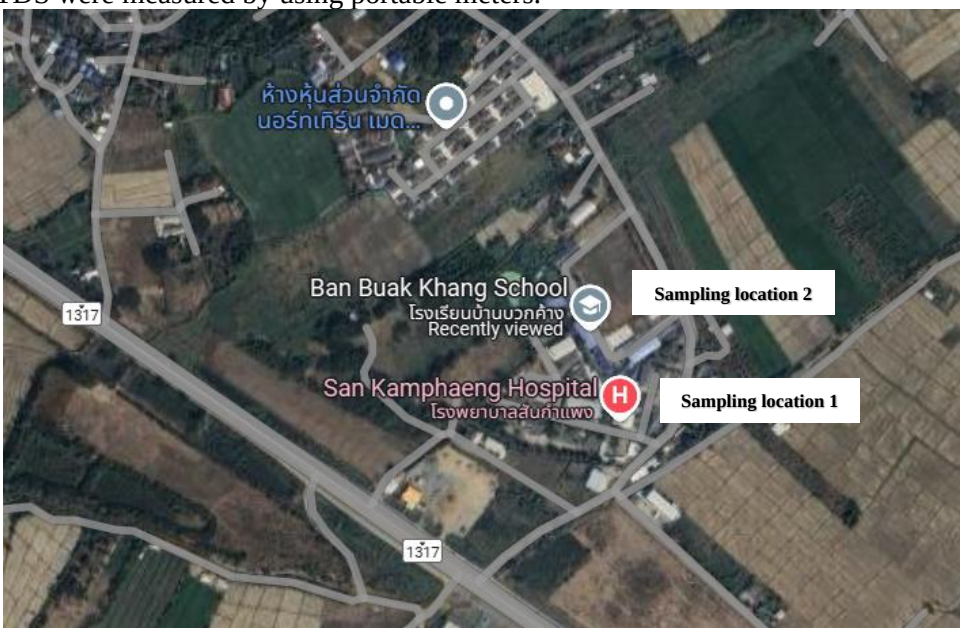


Figure 1 Sampling location

2. Synthesis of water

Synthetic water used prepared from Sodium Fluoride (NaF). Dissolved in DI water makes to a fluoride concentration of 5.0 mg/L. Which is close to the fluoride concentration found in natural groundwater.

3. Synthesis of adsorbent

Aluminum Fumarate (AlFu) MOF adsorbent was synthesized in the laboratory from National Nanotechnology Center, Thailand (NANOTEC).

4. Adsorption study

4.1 Point of zero chart (PZC)

A batch equilibrium method was applied for determining the PZC of absorbent. The absorbent of 5 g/L was shaken with 50 mL of deionized water at 250 rpm for 24 hours and the pH was varied from 3.0 to 12.0 using 0.1 N of hydrochloric acid or 0.1 N of sodium hydroxide. After that the initial pH was measured. After 24 hours, the final pH was measured. Then, a relationship between the initial pH and the final pH will be plotted. Finally, the PZC of AlFu MOF will be obtained from the common plateau of the plot.

4.2 The equilibrium of MOFs dose

The equilibrium of AlFu MOF dose was studied in a batch condition. It was conducted by varying the AlFu MOF dose from 1 to 20 g/L and they mixed synthetic fluoride water concentration 5 mg/L in 50 mL of flasks with AlFu MOF dose 1, 5, 10, 15 and 20 g/L at pH 7.5. After then, sample mixture will be shaken at 250 rpm, 24 hours at room temperature. After the equilibrium time, the samples were filtered through a nylon syringe filter with a pore size of 0.22 µm to separate the water solution and the AlFu MOF. The solution was analyzed for their remaining fluoride concentration by Ion specific electrode.

4.3 Adsorption isotherm

The adsorption isotherm was studied by varying the initial concentration of fluoride from 1 to 100 ppm by synthetic fluoride water at pH 7.5. Then, sample mixture will be shaken at 250 rpm, 24 hours at room temperature. After the equilibrium time, the samples were filtered through a nylon syringe filter with a pore size of 0.22 µm to separate the water solution and the AlFu MOF. The solution was analyzed for their remaining fluoride concentration by Ion specific electrode.

4.4 Adsorption kinetic

The adsorption kinetics of fluoride was studied in a batch condition. It was conducted by varying the adsorption time from 0 to 48 hours. In addition, the equilibrium fluoride concentration was based by on the isotherm study result with the equilibrium AlFu MOF dose at pH 7.5. Then, the samples mixed with AlFu

MOF shaken at 250 rpm at room temperature. After the set time, they were filtered through a nylon syringe filter with a pore size of 0.22 µm to separate the water solution and the MOFs. The solution was analyzed for their remaining fluoride concentration by Ion specific electrode.

4.5 Study the effective removal of fluoride ions from actual contaminated water (Groundwater runs)

The effective removal of fluoride ions from actual contaminated water was based by on the isotherm study result with the equilibrium AlFu MOFs dose and kinetic study result with fluoride concentration of 5 mg/L, After the set time, they were filtered through a nylon syringe filter with a pore size of 0.22 µm to separate the water solution and the MOFs. The solution was analyzed for their remaining fluoride concentration by Ion specific electrode.

RESULTS AND DISCUSSIONS

Experimental results of water sample characteristics are presented in Table 1. The fluoride concentration in groundwater at sampling location 1 and 2 was 4.25±0.07 mg/L and 9.45±0.18 mg/L, respectively. It was found that the concentration of fluoride was very high exceeding the quality standard for groundwater used for consumption, with no more than 0.7 milligrams of fluoride per liter. This groundwater cannot be directly used for drinking and for cooking.

Table 1 Water samples characteristics

Sampling location	Parameter			
	pH	EC (µs/cm)	TDS (mg/L)	F (mg/L)
1	8.01	644	322	4.25±0.07
2	8.14	610	305	9.45±0.18

The point of zero charges (PZC) of AlFu MOF adsorbent was investigated by considering the common plateau of the plot of the relationship between the initial pH solution and final pH solution after 24 h in Figure 2. The point of 0 charge (pH_{pzc}) of AlFu MOF adsorbent was approximately 7.0. This is explained by the fact that the material becomes neutrally charged at pH 7.0 and that the AlFu MOF becomes negatively charged at higher pH values. The AlFu MOF's positive charge at a lower pH promotes fluoride adsorption easier [8]. Additionally, it is possible to exchange OH^- by F^- nucleophilically at low pH values.

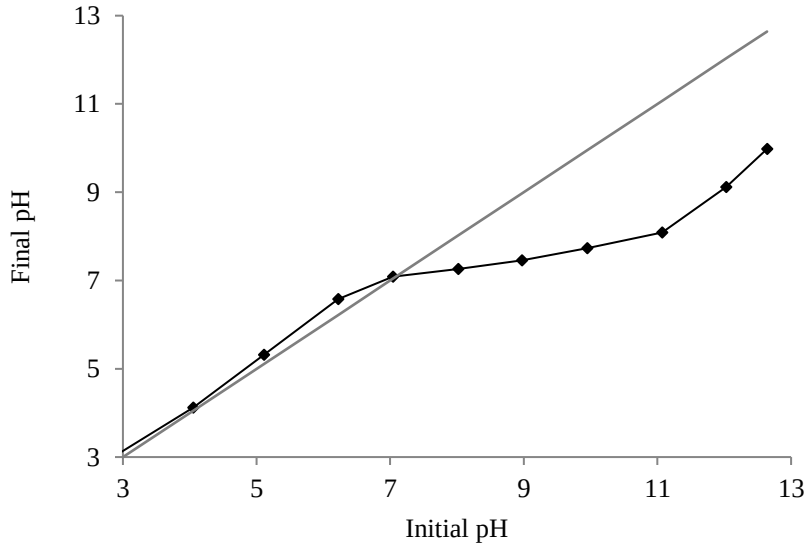


Figure 2 pH_{pzc} result of AlFu MOF adsorbent

The results of optimum adsorbent dose are shown in Figure 3, which is at the condition of 5 g/L at room temperature for 24 hours with shaking at 250 rpm. In addition, when the adsorbent dosage was increased, the adsorption results were stable.

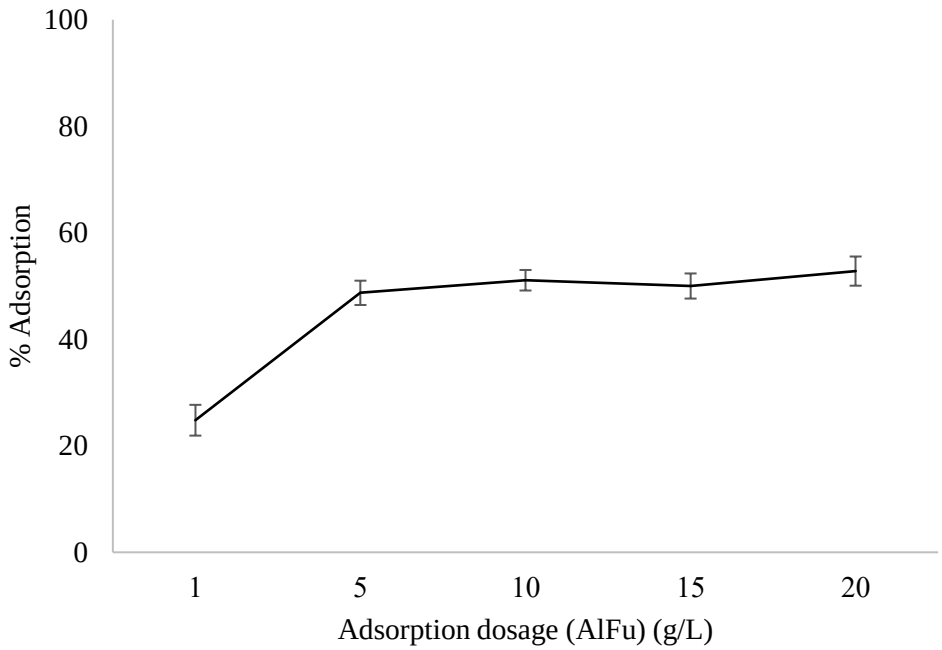


Figure 3 Effect of adsorbent dose on adsorption

Table 2 shows that the Freundlich isotherm provides a better fit than the Langmuir isotherm at room temperature (298 K) for fluoride concentrations from 1 to 100 mg/L. This table shows that the main adsorption mechanism is heterogeneous adsorption, as the Freundlich isotherm provides a better fit.

Table 2 Adsorption Isotherm of AlFu MOF

Material	Linear isotherm		
AlFu	K_p (L/g)	R^2	
	0.0746	0.9752	
	Langmiur isotherm		
	q_m (mg/g)	K_L (L/mg)	R^2
	1.9790	2.4425	0.9918
	Freundlich isotherm		
	K_F (mg/g)	1/n	R^2
	5.6964	0.9158	0.9979

The kinetic studies in this research indicate that the adsorption process is highly fast, with adsorption beginning quickly in the initial stage and widespread intra-particle diffusion occurring at the beginning of the adsorption step. Because the particles are microporous, the first phase of adsorption is the most efficient. After 30 minutes, surface adsorption begins slowly and reaches equilibrium after 48 hours of operation as shown in Figure 4. The kinetic parameters are shown in Table 3, and it can be seen that the adsorption follows pseudo second order kinetics, since the regression coefficient (R^2) in this instance was 0.9983, whereas in first order, it is only 0.8904. As a result, the adsorption process can be described as second order kinetics, indicating that the rate-limiting step is chemisorption involving valency forces via electron sharing or exchange with the adsorption [9]. The value of Q_m at fluoride concentrations of 5.0 mg/L was 0.52 mg/g. The rate constants for pseudo first and second order kinetics are k_1 = 0.1746 min^{-1} and k_2 = 0.0783 g/mg, respectively

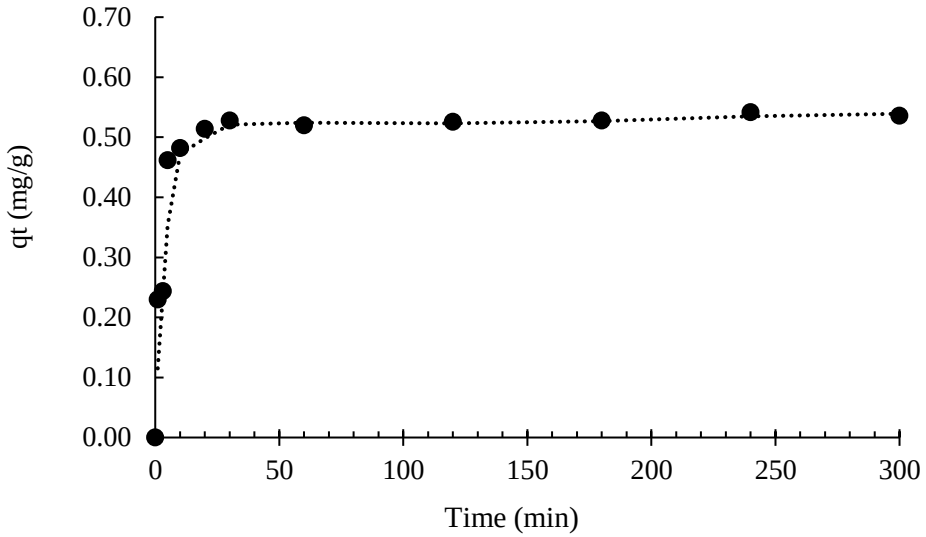


Figure 4 Adsorption kinetic of AlFu MOF

Table 3 Adsorption kinetic of AlFu MOF

Material	Pseudo-first-order			
	Q_m (mg/g)	k_1 (min^{-1})	q_{1cal} (mg/g)	R_1^2
	0.5200	0.1746	0.3459	0.8904
	Pseudo-second-order			
AlFu	k_2 (g/mg/min^{-1})	q_{2cal} (mg/g)	h (mg/g/min)	$t_{1/2}$ (min)	R_2^2
	0.0783	0.6111	0.0292	20.9074	0.9983

The initial concentrations of fluoride in groundwater were 4.25 mg/L and 9.45 mg/L, respectively. The fluoride concentration was determined to be extremely high, above Thailand's quality limit of no more than 0.7 mg of fluoride per liter. The fluoride removal of AlFu MOF adsorbent in actual contaminated water (Groundwater runs) from sampling location 1 and sampling location 2 in Figure 5 were up to 84 and 86%, respectively. The sampling location 1 was able to reduce the fluoride contamination in the water to below the drinking water standard in Thailand, but the sampling location 2 still exceeded the level at 0.7 mg/L.

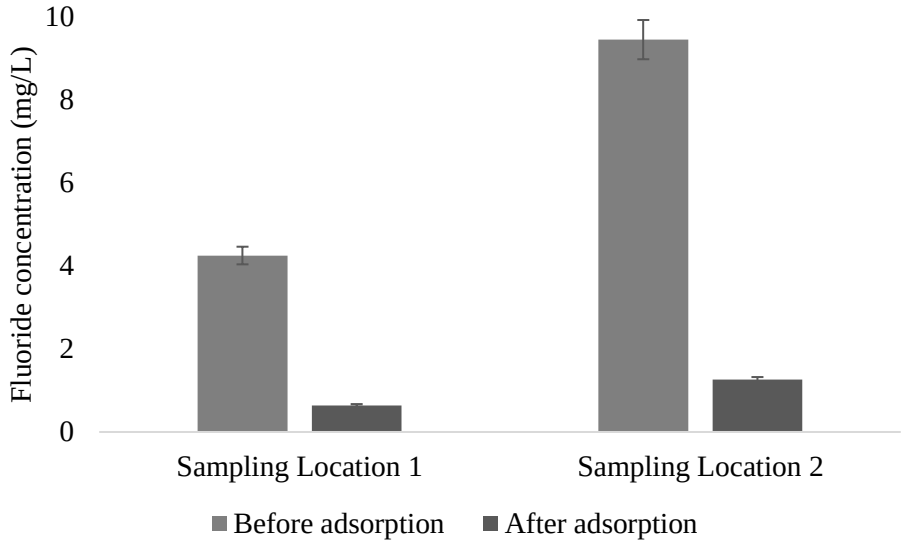


Figure 5 Removal of fluoride ions from actual contaminated water (Groundwater runs)

A study of comparability was carried out to determine the performance of the AlFu MOF over other conventional adsorbents for fluoride removal. Table 6 shows that the AlFu MOF has a significantly higher adsorption capacity than others such as CNP_0.2NaOH_600 [10] and Pyrolusite (PA-1) [11]. Therefore, a little amount of AlFu MOF can drastically reduce fluoride levels in drinking water.

Table 4 Comparing of AlFu MOF with other reported materials for fluoride removal.

Adsorbent	Adsorption condition			Qm (mg/g)	Ref.
	pH	Dosage (g/L)	Equilibrium time (min)		
CNP_0.2NaOH_600	8.0	5	120	0.20	[10]
Pyrolusite (PA-1)	7.0	15	60	0.11	[11]
Acid-Pyrolusite (PA-2)	7.0	15	60	0.58	[11]
ZIF-7	-	-	-	0.90	[12]
Zr-MOF-801	2-10	-	30-150	19.42	[13]
AlFu	8.0	5	30	0.52	This study

CONCLUSION

Aluminium fumarate (AlFu MOF) has been found to be a good adsorbent for fluoride in groundwater in risk areas. The adsorption capacity was found to be 0.52 mg/g at 298 K. Adsorption studies confirmed the Freundlich isotherm model and a Pseudo-second-order reaction supported by Kinetic studies. The fluoride removal of AlFu MOF adsorbent in actual contaminated water (Groundwater runs) from sampling location 1 and sampling location 2 was up to 84 and 86%, respectively.

ACKNOWLEDGEMENT

This research work was partially supported by Chiang Mai University and the Graduate School of Chiang Mai University and received Teaching Assistant and Research Assistant Scholarships support from Chiang Mai University. We would like to express our sincere thanks to the Department of Environmental Engineering, Faculty of Engineering, Chiang Mai University for invaluable support in terms of facilities and scientific equipment.

REFERENCE

[1] Meenakshi and R.C. Maheshwari, Fluoride in drinking water and its removal. Journal of Hazardous Materials, 2006. 137(1): p. 456-463.

[2] Bulusu, K.R. and B.N. Pathak, Discussion on water defluoridation with activated alumina. Environ. Eng. Div, 1980. 106 (2): p. 466–469.

[3] Hem, J.O., Study and Interpretation of the Chemical Characteristics of Natural Water. U.G. Geological Survey Water Supply Paper, 1959: p. 1473.

[4] Pontie, M., et al., Fluorine and the environment, in: Alain Tressaud (Ed.). Advances in Fluorine Science, 2006. Vol. 2.

[5] WHO, Chemical fact sheets: fluoride guidelines for drinking water quality Incorporation First Addendum, Recommendations. Geneva, 2006. Vol. 1: p. 375–377.

[6] Chatterjee, S. and S. De, Adsorptive removal of fluoride by activated alumina doped cellulose acetate phthalate (CAP) mixed matrix membrane. Separation and Purification Technology, 2014. 125: p. 223-238.

[7] Kadhom, M. and B. Deng, Metal-organic frameworks (MOFs) in water filtration membranes for desalination and other applications. Applied Materials Today, 2018. 11: p. 219-230.

[8] Karmakar, S., et al., Aluminium fumarate metal-organic framework: A super adsorbent for fluoride from water. Journal of Hazardous Materials, 2016. Vol. 303: p. 10-20.

[9] Aly, Z., Graulet, A., Scales, N., & Hanley, T. Removal of aluminium from aqueous solutions using PAN-based adsorbents: characterisation, kinetics, equilibrium and thermodynamic studies. Environmental science and pollution research international, 2014. 21(5), 3972–3986. https://doi.org/10.1007/s11356-013-2305-6.

[10] Somkiattiyot, P., et al., Enhanced Fluoride Removal from Groundwater Using Napier Grass-Derived Adsorbent: Experimental and DFT Study. TRENDS IN SCIENCES, 2025. 22(3): 9217

[11] Induvesa, P., et al., A. Adsorption of Fluoride onto Acid-Modified Low-Cost Pyrolusite Ore: Adsorption Characteristics and Efficiencies. Int. J. Environ. Res. Public Health, 2022. 19, 17103. https://doi.org/10.3390/ijerph192417103

[12] Tan, T.L., et al., Adsorptive, kinetics and regeneration studies of fluoride removal from water using zirconium-based metal organic frameworks. RSC Adv, 2020. 10 (32), 18740–18752.

[13] Zhao, X., et al., The stability and defluoridation performance of MOFs in fluoride solutions. Microporous Mesoporous Mater, 2014. 185, 72–78.

20R5-04

Application of Submerged Nanofiltration Membrane for Treating Natural Organic Matter from Reservoir Water

Chamaiporn Nantakham[1, 2] Takahiro Fujioka[3] Aunnop Wongrueng[4] and Prattakorn Sittisom[5*]

[1]Master student, Department of Environmental Engineering, Faculty of Engineering, Chiang Mai University, Chiang Mai 50200, Thailand; [2]Multidisciplinary and Interdisciplinary School, Chiang Mai University, Chiang Mai 50200, Thailand; [3]Graduate School of Engineering, Nagasaki University, 1-14 Bunkyo-machi, Nagasaki, 852-8521, Japan; [4]Ph.D., Associate Professor, Department of Environmental Engineering , Faculty of Engineering, Chiang Mai University, Chiang Mai 50200, Thailand; [5]Ph.D., Assistant Professor, Department of Environmental Engineering , Faculty of Engineering, Chiang Mai University, Chiang Mai 50200, Thailand

[*]Phone : 053-944-192, E-mail : prattakorn.s@cmu.ac.th

ABSTRACT

Water contamination issues affect the quality of water supplies and are primarily caused by the ongoing expansion and development of residential areas and industries. Chlorine is a commonly used chemical in conventional treatment systems for disinfection due to its affordability and widespread availability. However, disinfection by-products, which are formed from the reaction between organic substances in water sources and disinfectants, can negatively impact human health. One such DBP is trihalomethane, which is classified as a human carcinogen. This study evaluates the effectiveness of submerged nanofiltration membranes compared to conventional treatment systems in removing natural organic matter. Water samples were collected every three days from Angkaew Reservoir using the grab sampling method. The membrane system was operated with a peristaltic pump at a constant permeate flux of 11 $L/m^2 \cdot h$. All samples were analyzed for physical and chemical characteristics at the Environmental Engineering Laboratory, Chiang Mai University. The findings indicate that the NF270 membrane successfully reduced turbidity, electrical conductivity, total dissolved solids, UV absorbance at 254 nm, dissolved organic carbon, and trihalomethane formation potential by 93–98%, 36–65%, 36–65%, 74–89%, 68–80%, and 66.54%, respectively. The conventional treatment system, in contrast, not only failed to effectively remove ions but also increased their concentrations in the water. The NF270 membrane demonstrated superior ion removal capabilities compared to the conventional system. Consequently, under stable operating conditions, this study demonstrates that surface water can be effectively treated using nanofiltration membranes to produce high-quality water.

Keywords: disinfection by-products; nanofiltration; natural organic matter; submerged membrane; trihalomethanes

INTRODUCTION

The demand for tap water is continuously increasing. Additionally, water contamination problem are exacerbated by the ongoing expansion and development of urban housing, industrial activities, and surface runoff. Therefore, effective water management is essential maintaining water quality. In conventional treatment system, chlorine is commonly used as a disinfectant. However, disinfection by-products (DBPs) are formed when chlorine reacts with natural organic matter (NOM) present in the water. These DBPs are considered carcinogenic and may pose significant risks to human health. Among the most concerning DBPs are trihalomethanes (THMs) [1]. Potential health risks associated with DBPs include congenital abnormalities, early pregnancy loss, and an increased incidence of bladder cancer. DBPs have been identified in association with the use of the four primary disinfectants—chlorine, chloramines, ozone, and chlorine dioxide—as well as with newer disinfection technologies such as ultraviolet (UV) treatment followed by post-chlorination [2, 3].

Nanofiltration (NF) membranes have a wide range of applications, with wastewater treatment and drinking water production being among their primary uses. NF membranes are versatile and can be employed to treat various water sources, including groundwater, surface water, and wastewater. Additionally, they are often utilized as a pre-treatment step in seawater desalination processes, enhancing overall system efficiency and membrane lifespan [4]. The widespread application of membrane technologies has contributed significantly to the reduction of particulate matter and NOM concentrations in drinking

water. The effectiveness of these membrane-based treatments depends on several factors, including membrane type, physicochemical properties, module configuration, operating conditions, and overall system efficiency [5]. Particulate and dissolved pollutants, such as synthetic organics, salts, hardness, pathogenic bacteria, and DBP precursors are effectively eliminated by NF membranes. Additionally, in terms of regulating dissolved organic matter (DOM) , membrane separation competes with other cutting-edge treatments like granular activated carbon (GAC) when used in conjunction with the current water treatments. Additionally, membrane separation is competitive in the economy of the future because of the ensuing technological advancements [6]. Sentana *et al*. [7] reported that the amounts of DBPs in natural waters decreased when nanofiltration membranes were used. Three commercial NF membranes—models NF270, NF90 (Dow Chemical Inc.), and Desal-HL-51 (GE Water)—have been used to investigate the manufacturing potential of trihalomethane and haloacetic acid (THMFP and HAAFP). The NF90 membrane reduced more than 90% of the possibility of generating dibromochloromethane and bromodichloromethane. The NF270 and Desal-HL-51 membranes decreased less THMFP. A submerged membrane system is used to separate suspended particles, microbes, and other contaminants. The operation of a submerged membrane system involves submerging the membrane module directly into water. The submerged membrane technology takes far less space than the conventional treatment system. Additionally, this system has outstanding fouling resistance [8]. This study compared the effectiveness of submerged NF membrane to minimize disinfection by-product precursors with the conventional treatment system. This study was conducted at Angkaew reservoir in Chiang Mai University, Thailand in 2024.

METHODOLOGY

Experimental protocols

Water samples were collected from Angkaew Reservoir every three days over a two-week experiment period. The samples were subsequently analyzed for physical and chemical characteristics at the Department of Environmental Engineering, Chiang Mai University. The laboratory-scale was operated at a constant permeate flux of approximately 11 L/m^2.h and maintained at a feed temperature of 20 °C. Daily, 200 mL of permeate was collected and immediately analyzed for water quality parameters. Dissolved organic carbon (DOC) analysis was performed on a weekly basis, with samples stored under refrigeration until analysis. The trihalomethane formation potential (THMFP) was analyzed once during the experiment. Membrane cleaning was carried out every six days by gently scrubbing the membrane surface with a sponge prior to initiating a new experimental cycle.

Analysis

The electrical conductivity and total dissolved solids were measured using a portable conductivity analyzer (Starter 300C, OHAUS Corporation, USA). Every sample underwent turbidity analysis (Merck, Turbiquant 1100 IR, Sigma-Aldrich Canada Co., or Millipore (Canada) Ltd., Canada). A 0.45-micron nylon membrane filter was used to pre-filter each sample. A TOC analyzer was used to measure the DOC (Multi N/C 3100, Analytikjena, Germany, Standard Method 5310). A UV/VIS spectrophotometer (Lambda365, Perkin Elmer, Perkin Elmer Inc., Boston, MA, USA, Standard Method 5910B) was also used to measure the sample's ultraviolet absorbance at 254 nm (UV254). In a tea-colored bottle with sample water, add a 10% chlorine solution, and then leave it in the dark for a whole day. A gas chromatograph (GC) with an electron capture detector (GC-ECD) system (Agilent 4890D (EPA 551.1)) was utilized to analyze the concentration of the top layer of Methyl Tertiary Butyl Ether (MTBE).

Nanofiltration membrane and module

This study employed the NF270 nanofiltration membrane (DuPont/FilmTec, Midland, MI, USA), with a total effective filtration area of 56 cm^2. The membrane was operated in a submerged configuration using an outside-in filtration mode. Initially, the pure water flux was determined by filtering deionized water through the submerged NF270 membrane. Subsequently, the collected water samples were analyzed and subjected to the filtration process.

RESULTS AND DISCUSSIONS

Quality of water in reservoir

The pH values of the water samples fell within the neutral range, between 7.5 and 8.5. The raw water quality parameters are summarized in **Table 1**. While the electrical conductivity (EC) and total dissolved solids (TDS) of the raw water were within acceptable limits, its turbidity exceeded the standard threshold. The concentration of DOC was measured at 3.55 mg/L, and the UV254 was 0.0947 cm^{-1}. The specific ultraviolet absorption (SUVA) index was calculated by dividing the UV254 absorbance value by the DOC

concentration and multiplying the result by 100 [9]. The SUVA value below 2 L/(mg·m) typically indicated that the organic matter is predominantly composed of aliphatic hydrocarbons or non-humic substances with low hydrophobicity. In contrast, a SUVA value above 2 L/(mg·m) suggests the presence of hydrophobic and hydrophilic NOM, aromatic hydrocarbons, or aquatic humic substances [10]. The calculated SUVA value for this water source was 2.66 L/(mg·m), indicating that the organic matter present was primarily humic in nature, with a significant proportion of aromatic hydrocarbon structures.

Table 1 Characteristics of a water source.

Parameters	Unit	Value	Standard*
pH	s.u.	8.48 ± 0.48	6.5-8.5
EC	µS/cm	141.0 ± 5.30	<500**
TDS	mg/L	70.3 ± 2.54	<600
Turbidity	NTU	11.36 ± 1.62	<4
UV254	cm^{-1}	0.0947 ± 0.01	-
DOC	mg/L	3.55 ± 0.22	-

*Water supply quality standard in Thailand

**Guidelines of Drinking Water Quality, 4th ed.; World Health Organization (WHO)

Operational stability

Minimal fouling occurred during the experiment when surface water was directly treated using NF at a low permeate flux, resulting in a slight increase in transmembrane pressure (TMP) from 90 to 92 kPa **(Figure 1)**. Following membrane cleaning, the TMP exhibited a modest decrease, indicating that the system operated in a relatively stable manner throughout the experiment. In the previous study, Fujioka *et al*. [8] indicated that the TMP increased from 35 to 37 kPa. Given that many of Thailand's water sources are characterized by high concentrations of organic matter and turbidity, the relatively high TMP observed in this study is not unexpected. Nonetheless, the TMP increase of approximately 2 kPa observed in both studies suggests that the low and stable permeate flux operation was a key factor contributing to this moderate fouling. Despite variations in the quality of the water sources, the system demonstrated consistent performance throughout the experiment.

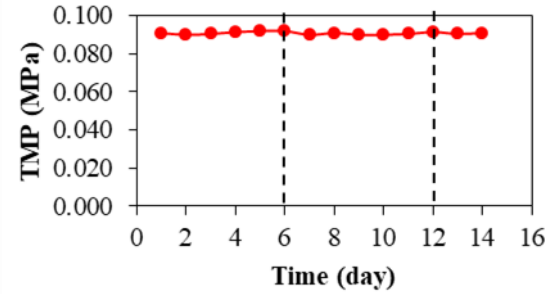


Figure 1 Transmembrane pressure (TMP) changes that occur when the reservoir is treated with NF at low permeate flux.

Membrane efficiency

The EC and TDS values of the pre-entry water range from 134.0 to 148.1 µS/cm and 66.7 to 73.5 mg/L, respectively. For the water treated by the NF270 membrane, EC and TDS values ranged from 49.2 to 88.2 µS/cm and 25.0 to 44.2 mg/L, respectively. The removal efficiencies for EC and TDS were observed to be between 36–65% **(Figure 2a)**. These findings indicate that, although the NF270 membrane effectively reduces EC and TDS, the permeate conductivity remains relatively high. This suggests that the NF membrane is more efficient in rejecting divalent ions than monovalent ions [8] [11]. Nevertheless, the treated water's electrical conductivity value was below the WHO maximum (500 µS/cm), which is the limit for electrical conductivity in drinking water.

The UV254 and DOC results are presented in **Figure 2b**. The submerged NF membrane system demonstrated a high efficacy in rejecting organic compounds, with removal efficiencies ranging from 74% to 89%. This rejection corresponded to organic molecules, such as aromatic hydrocarbons and compounds containing double bonds, as inferred from the characteristics of the raw water. Throughout the operation, the NF membrane was effective in rejecting organic materials with a molecular weight cut-off (MWCO) between 200 and 1000 Da [12]. Consequently, the accumulation of organic matter in the feed tank increased

over time. Furthermore, the permeate quality remained highly consistent, exhibiting a very low UV254 value. This suggests that the NF270 membrane is effective in rejecting small particles, particularly aromatic and double-bonded molecules. The NF270 membrane demonstrated a substantial DOC removal efficiency ranging from 68% to 80%, indicating its ability to reject certain organic matter dissolved in the water. The DOC value of the resulting permeate was significantly lower, further supporting the conclusion that dissolved organic materials are effectively rejected by the NF270 membrane. Additionally, the specific ultraviolet absorbance (SUVA) index decreased from 2.66 to 1.87 L/(mg·m), reflecting a reduction in the concentration of humic substances. Given that humic compounds share characteristics with polyaromatic hydrocarbons in aqueous environments, these results suggest that the NF270 membrane can effectively reject such compounds as well.

The turbidity of the feed water ranged from 9.17 to 13.54 NTU. Throughout the duration of the experiment, the turbidity of the permeate remained consistently low, ranging from 0.20 to 0.76 NTU. The results indicated that the NF270 membrane was highly effective in removing turbidity from surface water, achieving removal efficiencies between 93% and 98% when employed directly, without any pre-treatment **(Figure 2c)**. These findings demonstrate that the NF270 membrane is particularly efficient in removing larger particles responsible for turbidity in water sources.

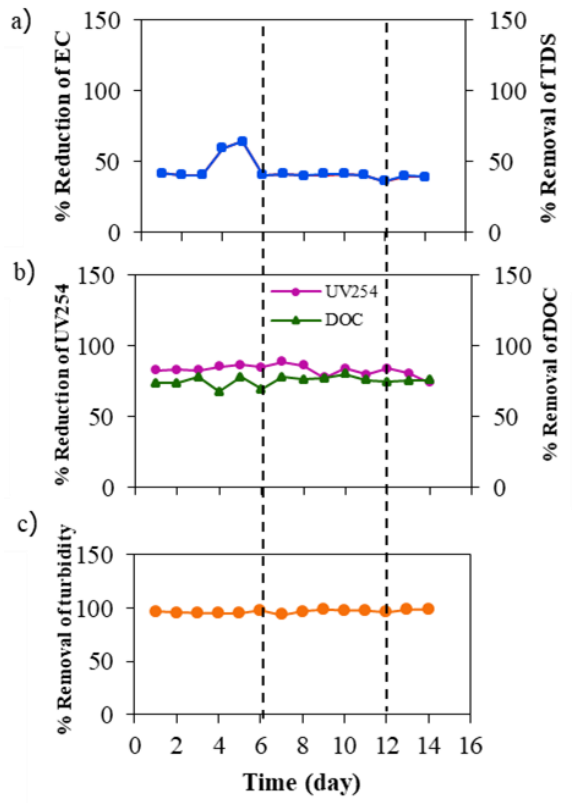


Figure 2 Membrane efficiency in removing (a) EC and TDS, (b) UV254 and DOC, and (c) turbidity over a period of 14 days.

Trihalomethane Formation Potential (THMFP)

THMs comprise four principal compounds: chloroform (CF), bromodichloromethane (BDCM), dibromochloromethane (DBCM), and bromoform (BF). The concentrations of total trihalomethanes (TTHMs) detected in this water source are summarized in **Table 2**. Among the DBPs identified, only two THM species—BDCM and CF—were present. The presence of bromide, a key precursor for brominated THMs, is most plausibly attributed to naturally occurring bromine in groundwater. This bromide can migrate upward and mix with surface water, particularly in regions characterized by bromide-rich geological formations or soil strata. [13]. With respect to THMFP, the presence of natural organic matter in water sources plays a critical role in the formation of THMs, as these compounds are produced when organic constituents react with chlorine during the disinfection process. Evaluating THMFP also provides insights into the characteristics of DOM present in the water. Analytical results revealed a TTHMs concentration of 789.73 ppb in the untreated water source. Following treatment with a submerged NF270 membrane, TTHM levels were reduced by 66.54%. Specifically, the concentrations of CF and BDCM decreased by 51.66% and

84.4%, respectively. Notably, the molecular weight cut-off (MWCO) of the NF270 membrane exceeds the molecular weights of common THM species (CF = 119.4 g/mol, BDCM = 163.8 g/mol, DBCM = 208.3 g/mol, and BF = 252.7 g/mol), indicating that mechanisms other than size exclusion—such as adsorption or diffusion—may contribute to the observed reductions [14]. Consequently, NF270 removes THMs through the mechanisms of surface adsorption, initial membrane fouling, and gaps between polymer chains [15]. The overall THM ratio for this water source was calculated to be 7.5, exceeding recommended safety thresholds. This finding underscores the necessity of removing NOM from the source water prior to chlorination to minimize the formation of THMs during disinfection. Treatment using the NF270 membrane resulted in a permeate with a guideline value (GV) of 1.7. Although the NF270 membrane demonstrated a substantial reduction in TTHM concentrations, the GV of the treated water remained above the acceptable limit of 1.0, indicating that the permeate may still be unsuitable for direct human consumption without further treatment or post-processing.

Table 2 THMFP in raw water and permeate water.

Samples	Species of THMs (ppb)				TTHMs (ppb)
	CF	BDCM	DBCM	BF	
Raw	430.71	359.02	ND [b]	ND [b]	789.73
Permeate	208.19	56.02	ND [b]	ND [b]	264.21
Guideline [a]	300	60	100	100	

[a] Guidelines for Drinking Water Quality, 4th ed.; World Health Organization (WHO)

[b] ND = Not detected, if the concentration was lower than 10 ppb (< 10 µg/L)

Comparison between the conventional treatment system and submerged NF system

Sriboonnak *et al*. [16] pointed out that the conventional water treatment systems had an efficiency of removing UV254 and DOC at 74.63% and 58.02%, respectively. The result shows that the efficiency of previous studies is in the same range of removal efficiency as NF, which indicated that NF had higher removal efficiency depending on the water quality. Moreover, Sriboonnak's study showed that the electrical conductivity in water after conventional treatment increased from 172.4 to 196.3 µS/cm. The result indicated that the ions in water cannot be eliminated by the conventional treatment system as shown in **Table 3**. In contrast, the NF system can reject only a small number of ions in the water, even though permeate has a relatively high electrical conductivity (< 88.2 µS/cm). Furthermore, Sriboonnak's research revealed that the disinfection procedure in conventional system considerably raised the amount of THMs in the water. NOM and THMFP of water treatment processes were studied by Wong *et al*. (2007) [17]. The results indicated that after water treatment, the MSR plant had a removal efficiency of 44%. On the other hand, the NF system had a better efficiency and was successful in lowering THMs by 66.54%. Overall, the findings show that NF is a more successful method than the conventional treatment for removing dissolved organic and ions.

Table 3 Analysis of the differences between conventional treatment systems and the submerged membrane technology.

Parameters	Unit	NF270 membrane	Conventional treatment system	Standard*
EC	µS/cm	74.1	196.3	<500**
TDS	mg/L	37.9	-	<600
Turbidity	NTU	0.32	-	<4
UV254	cm^{-1}	0.0153	0.0300	-
DOC	mg/L	0.79	2.30	-

*Water supply quality standard in Thailand

**Guidelines of Drinking Water Quality, 4th ed.; World Health Organization (WHO)

CONCLUSION

This membrane system had very high turbidity removal efficiency (> 93%). Even though NF270 membranes also had low efficiency in monovalent ion rejection, causing EC and TDS values to remain high (36-65%). The NF270 membrane is effective in eliminating DOC by 68-80% and can also reduce THMFP by up to 68.48%. In addition, the removal of principal water quality indicators (e.g., UV254) by the NF270 membrane was 74-89%, depending on the water source's quality, which indicates the concentration of humic acid, which has a structure of aromatic rings. When evaluating how well the NF270 membrane system performs in comparison to the conventional treatment system, it was found that conventional treatment

methods raise the concentration of certain ions in the water. Consequently, this study demonstrates that, in terms of system performance, when operating steadily, direct surface water treatment using an NF membrane can provide superior water quality. This improvement in water quality not only enhances the safety for consumption but also minimizes the need for additional chemical treatments often required in conventional systems. Therefore, adopting NF membrane technology could significantly benefit communities relying on surface water sources for their drinking water supply. Future studies may conduct further comparative economic studies to determine the cost-effectiveness of using this system to replace the conventional system.

ACKNOWLEDGEMENT

This research work was partially supported by the Faculty of Engineering, Chiang Mai University. The authors also thank the received Teaching Assistant and Research Assistant Scholarships support from Chiang Mai University. We would like to sincerely thank Chiang Mai University's Faculty of Engineering, Department of Environmental Engineering, for their significant cooperation in providing facilities and scientific equipment.

REFERENCE

[1] WHO. 2011. Guidelines for drinking-water quality. Published 4 ed. 38: 104-8.
[2] Richardson, SD., Plewa, MJ., Wagner, ED., Schoeny, R. and DeMarini, DM. 2007. Occurrence, genotoxicity, and carcinogenicity of regulated and emerging disinfection by-products in drinking water: a review and roadmap for research. Mutation Research/Reviews in Mutation Research. 636(1-3): 178-242.
[3] Hua, G. and Reckhow, David A. 2007. Characterization of disinfection byproduct precursors based on hydrophobicity and molecular size. Environmental science & technology. 41(9): 3309-3315.
[4] Hilal, N., Al-Zoubi, H., Darwish, N.A., Mohamma, A.W. and Arabi, AM. 2004. A comprehensive review of nanofiltration membranes: Treatment, pretreatment, modelling, and atomic force microscopy. Desalination. 170(3): 281-308.
[5] Howe, KJ., Marwah, A., Chiu, K-P. and Adham, SS. 2006. Effect of coagulation on the size of MF and UF membrane foulants. Environmental Science & Technology. 40(24): 7908-7913.
[6] Eriksson, P., Kyburz, M. and Pergande, W. 2005. NF membrane characteristics and evaluation for sea water processing applications. Desalination. 184(1-3): 281-294.
[7] Sentana, I., Rodríguez, M., Sentana, E., M'Birek, C. and Prats, D. 2010. Reduction of disinfection by-products in natural waters using nanofiltration membranes. Desalination. 250(2): 702-706.
[8] Fujioka, T., Ngo, M.T.T., Makabe, R., Ueyama, T., Takeuchi, H., Nga, T.T.V. et al. 2021. Submerged nanofiltration without pre-treatment for direct advanced drinking water treatment. Chemosphere. 265: 129056.
[9] Krasner, S.W., Westerhoff, P., Chen, B., Rittmann, B.E., Nam, S.-N. and Amy, G. 2009. Impact of wastewater treatment processes on organic carbon, organic nitrogen, and DBP precursors in effluent organic matter. Environmental science & technology. 43(8): 2911-2918.
[10] Edzwald, J.K. and Tobiason, J.E. 1999. Enhanced coagulation: US requirements and a broader view. Water Science and technology. 40(9): 63-70.
[11] Maroufi, N. and Hajilary, N. 2023. Nanofiltration membranes types and application in water treatment: a review.Sustainable Water Resources Management. 9(5): 142.
[12] Baker, R.W. 2023. Membrane technology and applications.Published: John Wiley & Sons.
[13] Davis, S.N., Fabryka-Martin, J.T. and Wolfsberg, L.E. 2004. Variations of bromide in potable ground water in the United States. Ground Water. 42(6): 902-909.
[14] Gang, D., Clevenger, T.E. and Banerji, S.K. 2003. Relationship of chlorine decay and THMs formation to NOM size. Journal of hazardous materials. 96(1): 1-12.
[15] Albatrni, H., Qiblawey, H. and El-Naas, M.H. 2021. Comparative study between adsorption and membrane technologies for the removal of mercury. Separation and purification technology. 257: 117833.
[16] Sriboonnak, S., Induvesa, P., Wattanachira, S., Rakruam, P., Siyasukh, A., Pumas, C. et al. 2021. Trihalomethanes in water supply system and water distribution networks. International Journal of Environmental Research and Public Health. 18(17): 9066.
[17] Wong, H., Mok, K.M. and Fan, X.J. 2007. Natural organic matter and formation of trihalomethanes in two water treatment processes. Desalination. 210(1-3): 44-51.

20R5-05

Surface Modification of Corn Biochar for Enhancement of Fluoride Adsorption

Natthapon Muangmaya[1], Aunnop Wongrueng[2], Prattakorn Sittisom[3*]

[1]Master student, Department of Environmental Engineering, Faculty of Engineering, Chiang Mai University, Chiang Mai 50200, Thailand. [2]Ph.D., Associate Professor, Department of Environmental Engineering, Faculty of Engineering, Chiang Mai University, Chiang Mai 50200, Thailand. [3]Ph.D., Assistant Professor, Department of Environmental Engineering, Faculty of Engineering, Chiang Mai University, Chiang Mai 50200, Thailand.*
[*]Phone : 053944131, E-mail : prattakorn.s@cmu.ac.th

ABSTRACT

Fluoride contamination in drinking water remains a significant environmental and public health challenge. This study investigates the synthesis of biochar from agricultural corn waste and its application for fluoride removal. Three biochar variants were synthesized: unmodified, $CaCl_2$-modified, and $MgCl_2$-modified, with modification concentrations of 0.5, 0.75, and 1.0 M. Batch adsorption experiments indicated that $CaCl_2$-modified biochar exhibited the highest fluoride removal efficiency, ranging from 60 to 65%, significantly outperforming $MgCl_2$-modified biochar (19 to 27%) and unmodified biochar (1.8%). The superior performance of the $CaCl_2$-modified biochar can be attributed to enhanced electrostatic interactions between the positively charged surface sites and fluoride ions, facilitated by the larger atomic radius of calcium. Fixed-bed column studies, conducted under the optimal batch conditions, revealed a breakthrough point at 24 hours. The Carbon Usage Rate (CUR) was determined to be 0.69 g/L, indicating that 0.69 grams of biochar are required to produce 1 liter of clean water. These findings underscore the potential of modified corn waste biochar as a sustainable, low-cost adsorbent for fluoride removal in water treatment systems.

Keywords : Fluoride; Modified Biochar; Adsorption

INTRODUCTION

Fluoride is a naturally occurring element that is ubiquitously distributed in the environment and can enter water sources through the leaching of fluoride-bearing minerals. Common minerals contributing to fluoride dissolution in water include biotite, topaz, granite, basalt, syenite, and shale [1]. The presence of fluoride in drinking water has both beneficial and adverse health effects, contingent on its concentration. Human exposure to fluoride primarily occurs via the consumption of drinking water [2]. The World Health Organization (WHO) specifies that the permissible fluoride concentration in drinking water should range between 0.5 and 1.5 mg/L [3]. At low concentrations (0.4–1.0 mg/L), fluoride is essential for promoting bone mineralization and enhancing dental enamel strength [4]. However, excessive fluoride intake can lead to fluorosis and disrupt calcium and phosphorus metabolism in the human body [2].

A variety of technologies have been developed for the removal of fluoride from contaminated water, including adsorption, ion exchange, chemical precipitation, electrolysis, dialysis, and electrodialysis [2]. Among these, adsorption is widely regarded as one of the most efficient and cost-effective methods [2]. The effectiveness of the adsorption process is predominantly influenced by the type of adsorbent material utilized. In recent years, there has been growing interest in the use of environmentally friendly and sustainable adsorbents derived from agricultural waste materials.

Corn cultivation is prevalent in northern Thailand, generating a substantial quantity of agricultural residues post-harvest. Farmers commonly dispose of these residues by open burning due to its convenience and rapidity. However, this practice contributes significantly to air pollution and environmental degradation. To address these issues, this study aims to convert corn waste into biochar via pyrolysis, a thermochemical process that not only mitigates air pollution but also enhances the value of agricultural waste.

The objective of this research is to synthesize biochar from corn residues and assess its potential for fluoride adsorption from contaminated water.

METHODOLOGY

Preparation of adsorbent

Biochar adsorbents were synthesized from agricultural waste materials, specifically corn stalks, leaves, and cobs, following three distinct modification protocols: (i) unmodified biochar, (ii) $CaCl_2$-modified biochar at concentrations of 0.5 M, 0.75 M, and 1.0 M, and (iii) $MgCl_2$-modified biochar at concentrations of 0.5 M, 0.75 M, and 1.0 M. The materials were subjected to pyrolysis at 600°C for 1 hour. After pyrolysis, the resulting biochar was ground using a mortar and pestle to achieve a particle size ranging from 40 to 100 mesh. The biochar was then sequentially washed with deionized water until a neutral pH equilibrium was reached.

Preparation of synthetic fluoride solution

Analytical grade sodium fluoride (NaF) was used to prepare a 5 mg/L fluoride stock solution, with deionized water serving as the solvent.

Batch study

Batch adsorption experiments were carried out in 250 mL Erlenmeyer flasks, each containing 100 mL of the prepared fluoride solution. The adsorbent dosage was maintained at 0.50 g per flask. The suspensions were agitated using a shaker (GFL3170, Gesellschaft für Labortechnik mbH, Germany) at 200 rpm for 24 hours at ambient temperature, with the pH maintained between 7 and 8. Post-adsorption fluoride concentrations were measured using fluoride ion-selective electrodes (4-Star Benchtop, Orion, USA). All experiments were performed in triplicate to ensure statistical reliability.

Column Adsorption study

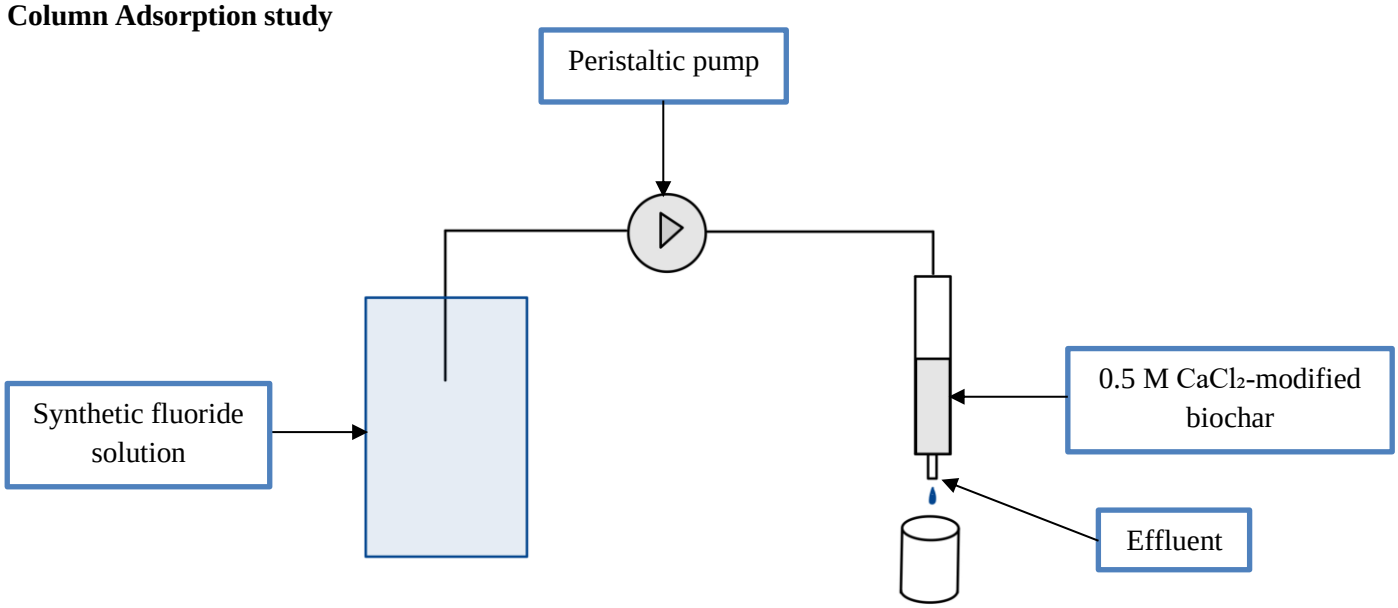


Figure 1 Experimental setup

Fixed-bed column studies were conducted under the optimal conditions determined from batch experiments. The adsorbent was systematically packed into a glass column and operated at ambient temperature. The influent fluoride solution was introduced at the column inlet using a calibrated peristaltic pump (Masterflex L/S, USA) at a flow rate of 10 mL/min. Effluent samples were collected at predetermined intervals and analyzed for fluoride concentration using ion-selective electrodes (4-Star Benchtop, Orion, USA). The breakthrough experiments were carried out until the effluent concentration approached that of the influent, indicating near-saturation of the adsorbent bed.

RESULTS AND DISCUSSIONS

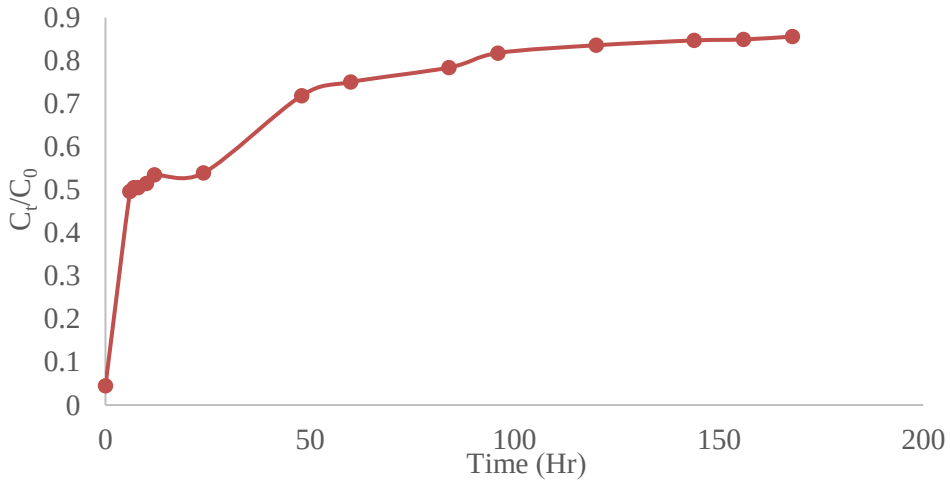
Batch Adsorption Studies

Table 1 Adsorption Efficiency of the Adsorbent.

Sample	C_t/C_0	Removal%
Unmodified	0.98	1.80
$CaCl_2$ 0.5 M	0.38	61.81
$CaCl_2$ 0.75 M	0.39	60.99
$CaCl_2$ 1 M	0.34	65.91
$MgCl_2$ 0.5 M	0.80	19.71
$MgCl_2$ 0.75 M	0.76	24.02
$MgCl_2$ 1 M	0.74	26.28

The comparative analysis of fluoride removal efficiencies across the three biochar variants revealed significant disparities in their adsorption capabilities (Table 1). The modified biochars demonstrated markedly superior performance relative to the unmodified biochar. Specifically, biochars modified with $CaCl_2$ and $MgCl_2$ exhibited enhanced fluoride removal efficiencies, achieving removal rates of 60–65% and 19–27%, respectively. In contrast, the unmodified biochar exhibited a significantly lower fluoride adsorption capacity, with an efficiency of only 1.8%. The enhanced fluoride removal efficiency observed in the $CaCl_2$- and $MgCl_2$-modified biochars can be attributed to the introduction of additional positive surface charges, which facilitate electrostatic interactions with the negatively charged fluoride ions. Further comparative evaluation of the modified biochars revealed that the $CaCl_2$-modified biochar outperformed the $MgCl_2$-modified biochar in fluoride removal, achieving efficiencies in the range of 60–65%, compared to 19–27% for the latter. The superior performance of the $CaCl_2$-modified biochar may be attributed to the larger atomic radius of calcium relative to magnesium. The increased atomic size of calcium results in reduced nuclear attraction, which enhances its ability to release electrons and interact more effectively with fluoride ions compared to magnesium [5]. Consequently, $CaCl_2$-modified biochar exhibited a significantly higher fluoride adsorption capacity than the $MgCl_2$-modified biochar. When compared to other established fluoride removal technologies, such as ion exchange with manganese carbonate (which achieves removal efficiencies of over 90%) [6], nanofiltration (up to 95% removal), and reverse osmosis (up to 99% removal) [7], the fluoride removal performance of the synthesized biochar is comparatively lower. However, these conventional methods are associated with substantially higher production and maintenance costs, as well as more complex operational and maintenance requirements, when compared to the relatively simple, cost-effective adsorption process employed in this study.

Column Adsorption study



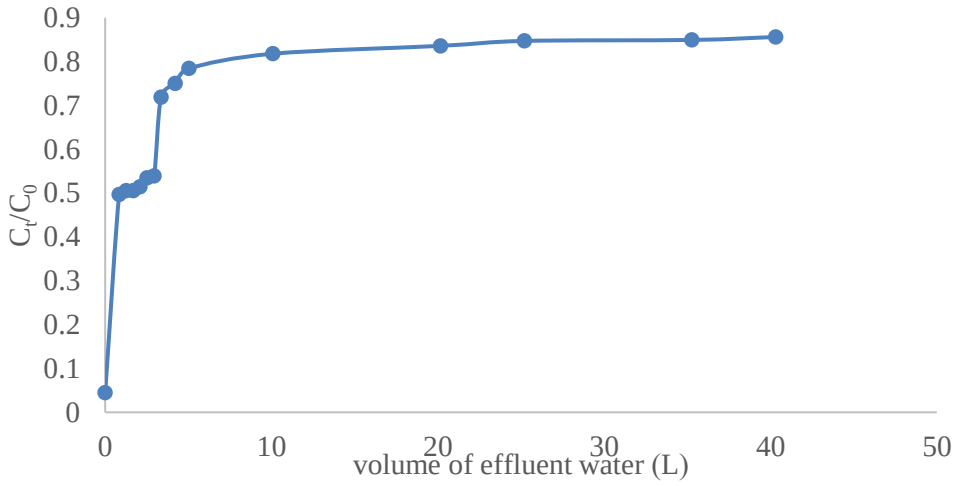


Figure 1 (A)Breakthrough curve at a final fluoride concentration with time. (B) Breakthrough curve at a final fluoride concentration with volume of effluent water.

The breakthrough curve analysis (Figure 1) revealed distinct phases in the adsorption process for the 0.5 M $CaCl_2$-modified biochar. During the initial phase (0-10 hours), the column exhibited optimal performance, characterized by negligible fluoride breakthrough, indicating efficient mass transfer and abundant active adsorption sites. Between 10 and 50 hours, a progressive increase in effluent fluoride concentration was observed, signaling the onset of bed saturation. This behavior aligns with the classical breakthrough pattern observed in fixed-bed adsorption systems, where the gradual depletion of available binding sites results in reduced removal efficiency. The breakthrough profile suggests that the mass transfer zone progresses through the column over time, eventually leading to the full saturation of the adsorbent bed. From the analysis shown in Figure 1, the breakthrough point was identified at 24 hours. This value was subsequently used to calculate the Carbon Usage Rate (CUR), which quantifies the required amount of adsorbent to produce a specified volume of clean water. The calculated CUR was determined to be 0.69 grams per liter (g/L), indicating that 0.69 grams of biochar is required to produce 1 liter of clean water [8].

CONCLUSION

This study demonstrates a significant enhancement in fluoride removal efficiency through the physicochemical modification of corn-derived biochar. The calcium chloride modification protocol, in particular, proved highly effective, resulting in a substantial increase in fluoride adsorption capacity, with removal efficiencies reaching 65.91% at a 1 M $CaCl_2$ concentration. This represents a marked improvement over the unmodified biochar, which exhibited minimal adsorption capabilities. The efficacy of the calcium-modified biochar was validated through extensive batch studies, while continuous flow column experiments revealed a characteristic breakthrough curve occurring between 10 and 50 hours of operation for the 0.5 M $CaCl_2$-modified biochar. These findings not only highlight the potential of modified corn biochar as an effective fluoride adsorbent but also emphasize the critical role of surface modification in enhancing adsorption performance. This research contributes to the development of sustainable, agriculture-based adsorbents for fluoride removal and lays the groundwork for future optimization studies in water treatment technologies.

ACKNOWLEDGEMENT

This research was kindly supported by the Department of Environmental Engineering, Chiang Mai University, which provided essential research facilities, laboratory space, and the necessary equipment and instruments required for the experimental work.

REFERENCE (Please see format of the reference in the Manuscript Format and Style)

[1] Bhatnagar, A., Kumar, E. and Sillanpää, M. 2011. Fluoride removal from water by adsorption—a review. Chemical Engineering Journal. 171(3): 811-840.

[2] Roy, S., Ghosh, P., Mondal, N.K., Mukherjee, S. and Datta, J.K. 2017. Calcium impregnated activated charcoal: Optimization and efficiency for the treatment of fluoride containing solution in batch and fixed bed reactor. Process Safety and Environmental Protection. 109: 18-29.

[3] World Health Organization. 2022. Guidelines for drinking-water quality: incorporating the first and second addenda. World Health Organization.
[4] Loganathan, P., Vigneswaran, S., Arulrajah, A., Kandasamy, J. and Bolan, N.S. 2013. Defluoridation of drinking water using adsorption processes. Journal of Hazardous Materials. 248: 1-19.
[5] Zumdahl, S.S., Zumdahl, S.A. and DeCoste, D.J. 2020. Chemistry: An atoms first approach. Cengage Learning.
[6] Zhao, Y., Yu, Y., Fu, F., Ma, J. and Liu, C. 2022. Self-assembled embedding of ion exchange materials into nanofiber-based hydrogel framework for fluoride capture. Chemical Engineering Journal. 431: 134201.
[7] Tahaikt, M., El Haddi, A., Kherbeche, A., Taky, M., El Rhilassi, A., Barka, N., Cuerda-Correa, E.M. and Alaoui, A. 2021. Technical-economic comparison of nanofiltration and reverse osmosis in the reduction of fluoride ions from groundwater: Experimental, modeling, and cost estimate. Desalination and Water Treatment. 216: 83-95.
[8] De Luca, P., Carbone, G., Rizzo, L., Ragusa, A., and Sorrentino, A. 2021. Semi-continuous adsorption processes with multi-walled carbon nanotubes for the treatment of water contaminated by an organic textile dye. Applied Sciences. 11(4): 1687

20R5-06

Impact of Microplastics on Membrane Fouling for Dissolved Organic Matter Removal from Reservoir Water

Thanyapon Kaewjan[1,2], Aunnop Wongrueng[3*], Takahiro Fujioka[4], Prattakorn Sittisom[5] and Pharkphum Rakruam[5]

[1]*Master student, Department of Environmental Engineering, Faculty of Engineering, Chiang Mai University, Chiang Mai 50200, Thailand*

[2] *Multidisciplinary and Interdisciplinary School Chiang Mai University, Chiang Mai Thailand, 50200, Thailand*

[3*] *Ph.D., Associate Professor, Department of Environmental Engineering , Faculty of Engineering, Chiang Mai University, Chiang Mai 50200, Thailand*

[4]*Graduate School of Engineering, Nagasaki University, 1-14 Bunkyo-machi, Nagasaki, 852-8521, Japan*

[5]*Ph.D., Assistant Professor, Department of Environmental Engineering , Faculty of Engineering, Chiang Mai University, Chiang Mai 50200, Thailand*

[*]*Phone : 053-944192, E-mail : aunnop@eng.cmu.ac.th*

ABSTRACT

One of the most significant environmental challenges is plastic waste, particularly microplastics, which contaminate freshwater sources used for human consumption. These microplastics may impact both human health and ecosystems. This study employs submerged nanofiltration membrane technology to investigate how microplastics influence the removal of dissolved organic matter from reservoir water. The experimental setup was designed to simulate a real-world scenario in which untreated surface water, potentially contaminated with microplastics, is filtered to remove dissolved organic matter. The NF270 membrane was tested under low-pressure conditions in this research. According to the results, the system required only physical cleaning to operate continuously throughout the experiment. There was no discernible difference in membrane flux between the first and final cycles of system operation. Despite the presence of microplastics, the submerged nanofiltration membrane system remained effective in removing dissolved organic matter from untreated surface water. This study demonstrates the potential of submerged nanofiltration membrane technology to address the challenges posed by freshwater contamination from microplastics. Furthermore, it suggests that nanofiltration membranes could be a valuable technique for improving water quality and protecting both the environment and public health from the harmful effects of microplastics.

Keywords : nanofiltration; submerged membrane; dissolved organic matter; microplastic; fouling

INTRODUCTION

One of the major environmental issues requiring immediate international response is plastic pollution. Plastic waste undergoes both biotic (microbe-assisted biodegradation) and abiotic (UV-induced photodegradation or weathering degradation caused by wind and waves) processes in the environment [1]. These activities result in the creation of smaller plastic pieces known as microplastics.

Microplastics (MPs) are small plastic particles measuring less than 5 mm in size. They can be composed of various polymers and exhibit different morphologies, including spheroid, fragment, and fiber forms. Primary microplastics are intentionally manufactured and incorporated into products to enhance specific qualities (e.g., microbeads are added to household and personal care products for their abrasive effect). In contrast, secondary microplastics are generated when larger plastic objects weather and degrade, often due to improper disposal or mishandling of waste [2].

Microplastics in drinking water can pose several hazards, and there are three types that are of particular concern: physical particles; chemicals, including monomers, additives, and sorbed substances; and biofilms. The effects of chemicals can vary depending on the dosage and the method of exposure (e.g., ingestion, inhalation, or injection) [3].

When microplastics are present in water, they can impact human health through consumption. Therefore, the removal of microplastics before consumption is essential. Advanced water treatment technologies, such as membrane filtration processes, have gained widespread acceptance and are now globally established. Membrane filtration can effectively reduce the concentration of microplastics in water

[4]. These systems can remove organic matter dissolved in water as well as microplastics that contaminate the water [5]. However, the effects of microplastics on membrane filtration are not yet fully understood.

This study investigates the impact of microplastics on membrane fouling during the removal of dissolved organic matter in reservoir water using submerged nanofiltration membranes.

METHODOLOGY

The NF270 membrane (DuPont/Filmtec, Midland, MI, USA) was used in this study. The flow direction was designed to be outside-in, and the membrane was applied in submerged membrane filtration. Water samples were measured for pH using the pH210K, Laqua 200 series (Horiba, Japan). Additionally, a sensor probe (Starter 300C, Conductivity Portable, OHAUS Corporation, USA) was used to measure electrical conductivity (EC) and total dissolved solids (TDS). To quantify turbidity, a turbidity meter (Merck, Turbiquant 1100 IR, Sigma-Aldrich Canada Co., or Millipore (Canada) Ltd., Canada) was used. Following the standard procedure 5310 for dissolved organic carbon (DOC) measurement [6], the DOC of water samples was determined using a total organic carbon analyzer (Multi N/C 3100, Analytikjena, Germany). A UV-Vis spectrophotometer (Lambda 365, PerkinElmer, Korea) was also used to evaluate the sample's ultraviolet absorbance at 254 nm (UV254) using standard Method 5910B [6], the ultraviolet absorption method.

A batch system was employed to operate the submerged nanofiltration membrane. The experiment was conducted in four cycles, with two batches per cycle, using feed waters with microplastic concentrations of 0, 10, 100, and 1000 ppm, respectively. Physical cleaning was performed on the NF membranes every two batches. In this experiment, a scrub sponge was used to clean the membrane.

RESULTS AND DISCUSSIONS

1. Quality of raw water

Table 1 displays the raw water quality characteristics of Ang Kaew Reservoir. Ang Kaew Reservoir is the primary water source for Chiang Mai University's water supply. The pH values of the raw water samples ranged from 7.5 to 8.5, which is within the neutral pH range. When compared to the water supply quality standards, the EC, TDS, and turbidity values were found to be within the acceptable range. Samples with SUVA values ranging from 2 to 4 L/mg·m exhibited a medium UV–254 concentration of both aquatic humic and non-humic substances [7]. This suggests that the organic matter in the raw water analyzed in this study consisted of a mixture of aquatic humic and non-humic components.

Table 1 Quality of raw water

Parameter	Unit	Value	Standard*
pH	s.u.	8.18 ± 0.48	6.5-8.5
EC	μS/cm	247.3 ± 25.76	< 500**
TDS	mg/L	123.0 ± 12.67	< 600
Turbidity	NTU	12.02 ± 1.68	< 4
UV–254	1/cm	0.1192 ± 0.01	-
DOC	mg/L	4.84 ± 0.47	-
SUVA	L/mg·m	2.48 ± 0.19	-

* Standard inferred to Water supply quality standards in Thailand

** Guidelines for Drinking-Water Quality, 4th ed.; World Health Organization (WHO)

2. Quality of permeate water

2.1 Effect of MPs on membrane fouling

The membrane flux in the submerged nanofiltration membrane system is shown in Figure 1. The membrane flux value was relatively stable throughout the trial period; stable flux values were in the range of 0.31 $m^3/m^2 \cdot d$ to 0.35 $m^3/m^2 \cdot d$. Since this change in membrane flux was not significant, the system could be operated continuously in each batch before physical cleaning. Therefore, it was assumed that the stability of the flux was probably related to the irregular structure in the cake layer, which was accompanied by the biofilm formation due to biological processes in the layer [8].

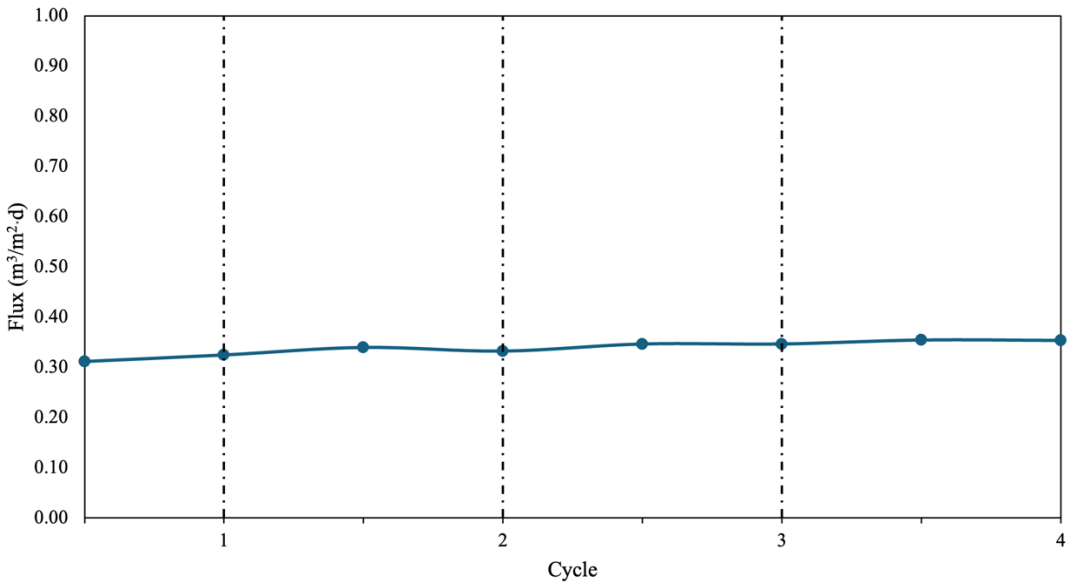


Figure 1 The membrane flux of the system in the presence of microplastics.

2.2 Effect of membrane fouling on dissolved organic matters removal

The percentage of UV–254 and DOC removal by the submerged nanofiltration membrane system is shown in Figure 2. Although the previous membrane flux values did not directly indicate membrane fouling, the effect of organic matter in the raw water was analyzed. The UV–254 parameter is a qualitative water test standard that can be used to quickly estimate the amount of organic matter in water. Another such parameter is DOC, which represents the total amount of organic carbon in a water sample that has been filtered through a 0.45 μm filter.

The results showed that the concentration of organic materials in the submerged nanofiltration membrane system with added microplastics was slightly higher, even after physical cleaning [9]. In this experiment, the percentage of UV–254 removal in the first batch was 98.57%, which decreased to 90.26% in the last batch. Similarly, the DOC removal in the first batch was 91.15%, but in the last batch, this decreased to 88.37%. These results suggest that the membrane system became clogged when contaminated with higher concentrations of microplastics. Nevertheless, as demonstrated by the UV–254 and DOC removal percentages, the membrane was still able to efficiently remove organic matter, even when fouled.

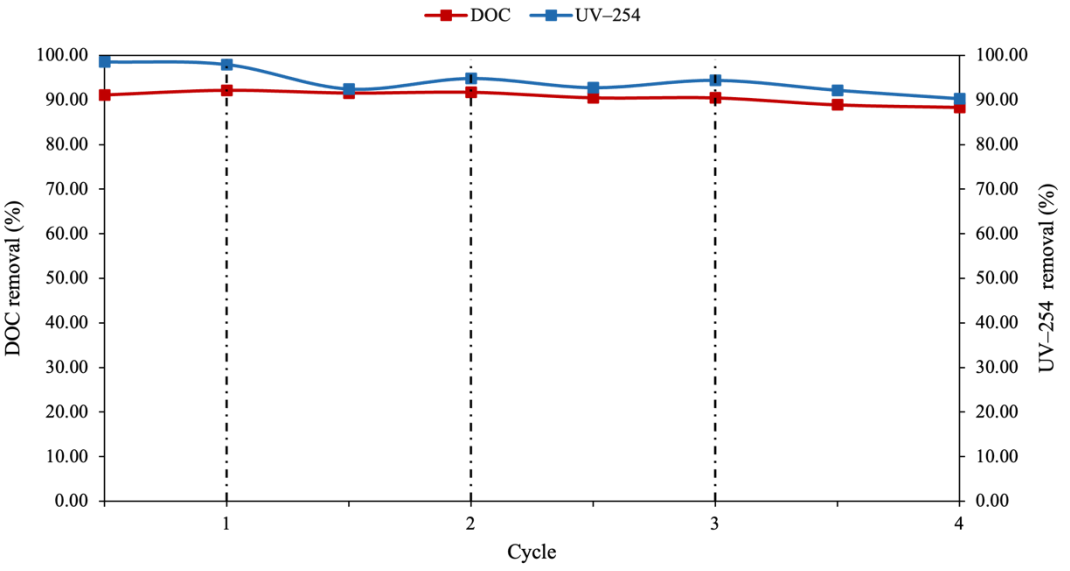


Figure 2 The percentage of UV–254 and DOC removal in the submerged nanofiltration membrane system.

The efficiency of the membrane in removing physical contaminants is shown in Figure 3. The submerged nanofiltration membrane system demonstrated an EC removal efficiency ranging from 49.15% to 60.56%, and a TDS removal efficiency ranging from 48.71% to 59.80%. In contrast, the turbidity removal efficiency was much higher, ranging from 97.76% to 99.28%. Although EC and TDS were not removed to extremely high levels, the quality of these feed water parameters remained within the standard range, as shown in Table 1.

The turbidity of the permeate water remained stable, with values ranging from 0.18 to 0.35 NTU. According to the results of the experiment, the submerged nanofiltration membrane system demonstrated a high percentage of turbidity removal efficiency, ranging from 97.76% to 99.28%, when applied to surface water treatment. The experiment confirmed that this approach was effective in eliminating turbidity without any pretreatment, even when carried out during the rainy season. Furthermore, the system efficiently removed microplastic particles contaminating the feedwater. This study demonstrated that nanofiltration membranes can effectively treat surface water and remove microplastics [5]. The pH value of the permeate water remained within the neutral range of 7.5 to 8.5, in accordance with water supply quality standards in Thailand (Section: Quality of Raw Water in Table 1).

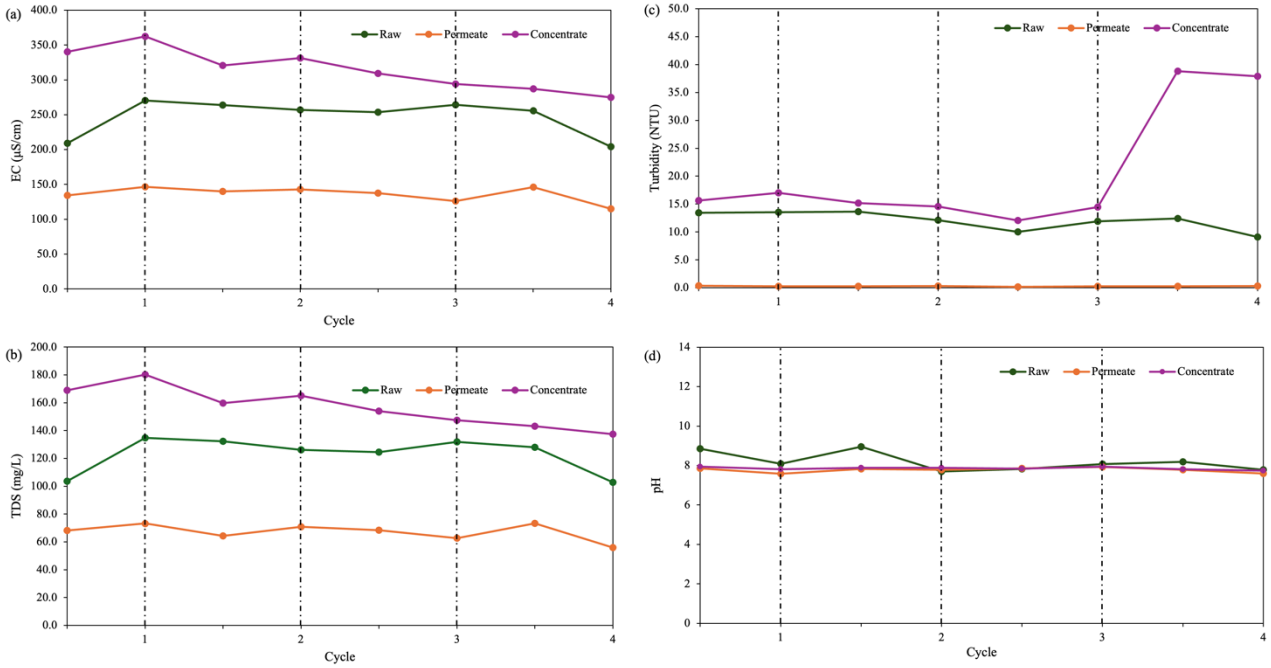


Figure 3 Quality of submerged nanofiltration membrane: (a) EC, (b) TDS, (c) turbidity, and (d) pH during the direct NF treatment of the reservoir water with a submerged nanofiltration membrane system.

CONCLUSION

The submerged flat sheet nanofiltration membrane system in this study operated under low-pressure conditions and did not require pre-treatment. The study found that, despite increased microplastic contamination, the change in flux was minimal compared to the initial flux. The increased concentration of microplastics had a significant effect on membrane fouling, which in turn affected the removal of dissolved organic matter from reservoir water. However, the NF270 membrane remained effective in removing dissolved organic matter, including DOC, UV–254, EC, and TDS, from raw water. Therefore, this research confirms that microplastics do impact the membrane system's ability to remove dissolved organic matter from reservoir water, even without the need for pre-treatment.

ACKNOWLEDGEMENT

This work was supported by Teaching Assistant and Research Assistant Scholarships from Chiang Mai University. The valuable discussions with Assoc. Prof. Dr. Aunnop Wongrueng, Department of Environmental Engineering, Faculty of Engineering, Chiang Mai University, are gratefully acknowledged.

REFERENCE

[1] Isabella Gambino, F. B., Tiziana Grassi, Alessandra Panicoand Antonella De Donno. 2022. Occurrence of Microplastics in Tap and Bottled Water: Current Knowledge. Int J Environ Res Public Health. 19(9): 5283-5298.

[2] Microplastics. 29 February 2024]; Available from:https://plasticseurope.org/sustainability/plastics-health/microplastics/.

[3] Microplastics in drinking-water. Geneva: World Health Organization; 2019. Licence: CC BY-NC-SA 3.0 IGO.

[4] Pivokonsky, M., Cermakova, L., Novotna, K., Peer, P., Cajthaml, T., & Janda, V. 2018. Occurrence of microplastics in raw and treated drinking water. Sci Total Environ. 643: 1644-1651.

[5] Severino, A., Russo, B., Lavorato, C., Argurio, P., Figoli, A., Molinari, R., & Poerio, T. 2025. Integrated nanofiltration and photocatalytic processes for the removal of polystyrene nanoplastics waste in water. Separation and Purification Technology, 360, 131232.

[6] Billy B. Potter, J. C. W. (2012). USEPA method 415.3: Quantifying TOC, DOC, and SUVA. AWWA Water Sci, 104(6).

[7] Edzwald, J.K. and J.E. Tobiason. 1999. Enhanced coagulation: US requirements and a broader view. Water Sci Technol. 40(9): 63-70.

[8] Peter-Varbanets, M., Hammes, F., Vital, M., Pronk, W., 2010. Stabilization of flux during dead-end ultra-low pressure ultrafiltration. Water Res. 44 (12), 3607–3616.

[9] Li, L., Liu, D., Song, K., & Zhou, Y. 2020. Performance evaluation of MBR in treating microplastics polyvinylchloride contaminated polluted surface water. Mar Pollut Bull, 150, 110724.

20R5-07

Natural Organic Matter Removal from Ang Kaew Reservoir by using Activated Carbon

Natchaya Waisarikam [1,2] and Pharkphum Rakruam[3*]

*[1]Graduate School, Chiang Mai University, Chiang Mai 50200, Thailand, Thailand; [2]Graduate student, Department of Environmental Engineering, Faculty of Engineering, Chiang Mai University, Chiang Mai 50200; [3]Assistant Professor, Department of Environmental Engineering, Faculty of Engineering, Chiang Mai University, Chiang Mai 50200; Corresponding author: *Phone: 053 – 944 192, E-mail: pharkphum@eng.cmu.ac.th*

ABSTRACT

Natural organic matter (NOM) is a heterogeneous mixture of organic compounds found in aquatic environments, originating from decomposing plant and animal materials. Its presence in water sources poses significant challenges to water treatment processes, as it can react with disinfectants to form harmful disinfection by-products (DBPs), such as trihalomethanes (THMs) and halo acetic acids (HAAs), which are linked to adverse health effects. Among the various NOM removal techniques, adsorption using activated carbon is widely recognized for its high efficiency and minimal secondary pollution. This study evaluates the adsorption efficiency and kinetic behavior of NOM removal using commercial activated carbon. Surface water from Ang Kaew reservoir was used as raw water. Adsorption experiments were conducted at varying adsorbent dosages (0.0125–0.150 g), and NOM concentrations were measured using NOM surrogate parameters including dissolved organic carbon (DOC) and ultraviolet absorbance at 254 nm (UV-254). The results showed that increasing the adsorbent dose improved NOM removal efficiency, with the highest DOC removal of 60% achieved at an optimal dosage of 0.75 g/L. The adsorption kinetics were analyzed using pseudo-first order and pseudo-second order models. The experimental data best fitted the pseudo-second-order model ($R^2 = 0.9989$), indicating that the adsorption process is governed by chemisorption involving electron exchange mechanisms. These findings highlight the potential of commercial activated carbon for effective NOM removal, contributing to improved water treatment practices. Further research on adsorption mechanisms and long-term performance evaluation is recommended to optimize its application in large-scale water treatment systems.

Keywords: natural organic matter; total organic carbon; adsorption; commercial activated carbon

INTRODUCTION

Natural organic matter (NOM) containing all the organic materials that come from withering plants, animals and their degradation products, is prevalently existing in aquatic, terrestrial and marine environments [1]. Natural organic matter (NOM) is a complex matrix of heterogeneous organic material present in all natural waters. It is derived from decaying terrestrial plants and as a byproduct of bacteria, algae, and aquatic plants. It can be classified as either particulate organic matter, retained by a 0.45 μm filter, or dissolved organic matter which is NOM passing through a 0.45 μm filter. NOM is introduced in water sources through interactions between the hydrologic cycle, biosphere and geosphere. The amount and characteristics of NOM vary with source, level of degradation, season, climate and geology. To better understand the role of NOM in water treatment, characterization of NOM in the raw water is necessary. Simple techniques such as color, total organic carbon (TOC), dissolved organic carbon (DOC), chemical oxygen demand (COD), pH, turbidity, and ultraviolet absorbance at 254 nm (UV-254) are commonly employed by water treatment facilities in their quality control. UV-254 is an important parameter for measurement throughout the drinking water treatment process. UV-254 provides an indication of the concentration of organic matter, specifically those that contain aromatic rings or unsaturated bonds (double and triple) in their molecular structures. Many organic compounds occurring naturally in the environment, such as humic substances, are aromatic and exist in high concentrations in surface water. These compounds are known to be a major precursor of DBP formation. Therefore, UV-254 provides one of the best indications of water's potential to form DBPs upon chlorine addition and should be monitored throughout the treatment process to ensure organics are removed [2].

Due to the complexity of origin, the composition and concentration of NOM in the environments are varied according to the different backgrounds, locations and other factors such as climate and human activities. Generally, NOM is a complex heterogeneous mixture of organic substances with different molecule sizes, physical and chemical properties, and various functional groups, including aromatic,

aliphatic, phenolic and quinone structures. The presence of NOM causes numerous problems in water treatment and distribution systems. NOM interacts with disinfectants forming harmful disinfection by-products (DBPs), reduces water quality by causing unpleasant odors, tastes and color in raw drinking water, promotes bacterial reproduction and biofilm formation within drinking water distribution systems and increases coagulant and disinfectant doses, which consequently increases sludge volumes and production of DBPs. The latter poses numerous public health concerns to water utilities, since their consumption in drinking water is linked to the development of various cancers and a variety of adverse reproductive outcomes. It has been reported that an increasing amount of NOM pollution has been found in the past several decades in raw water supplies, which has caused various problems with water quality in different aspects such as reacting with the disinfectants and producing undesired Disinfection by-products (DBPs) such as trihalomethanes (THMs) and halo acetic acids (HAAs). The World Health Organization (WHO) set the guideline value for DBPs in drinking water not to exceed 100 $\mu g L^{-1}$.

Many strategies have been developed to remove NOM, including coagulation, membrane separation, biosorption, etc. [3]. Among the various techniques available, adsorption method is deserving as promising techniques to remove NOM from water due to its low consumption of energy, simple operation, high efficiency, low cost and less likely to cause secondary pollution as well as the wide suitability for purified water [4]. Activated carbon is a well-known and efficient adsorbent that is commonly used in the environmental aspects that can remove organic carbon from drinking water. This research aims to investigate the efficiency and kinetic models on NOM removal by using activated carbon.

METHODOLOGY

Characterization of commercial activated carbon

The commercial activated carbon from DC Fine chemicals were used as adsorbents. The particle size of commercial activated carbon is in the range of 100-250 μm. The characteristics of the adsorbent, including specific surface area (BET surface area) and pore diameter, were analyzed. Brunauer–Emmett–Teller (BET) method is based on the adsorption and desorption principle developed by Stephen Brunauer, Paul Emmett, and Edward Teller, and it is considered one of the best methods for the analysis of surface area [5].

NOM removal experiment

Surface water from Ang Kaew Reservoir, Chiang Mai, Thailand was collected in January 2025 and used as water sample. About 200 mL of water samples were added to the volumetric flask containing commercial activated carbon in the range of 0.0125 to 0.150 g. Next, it was shaken at 200 rpm under room temperature for 1 hr. After that, the samples were filtered by 0.45 μm nylon syringe filter. NOM concentration in water samples were measured by using NOM surrogate parameters including dissolved organic carbon (DOC) concentrations and ultraviolet absorbance at 254 nm (UV-254). DOC concentrations were analyzed by TOC analyzer and UV-254 was analyzed by UV-VIS Spectrophotometer. After that, Specific ultraviolet absorbance (SUVA) was calculated. SUVA is the absorbance of ultraviolet light in a water sample at a specified wavelength that is normalized for dissolved organic carbon (DOC) concentration that is used to measure the aromatic character of dissolved organic matter by detecting density of electron conjugation which is associated with aromatic bonds [6]. SUVA was investigated by calculating following equation 1.

$$\text{SUVA } (L \bullet m^{-1} \bullet mg^{-1}) = 100 \times \left[\frac{UV254}{DOC}\right] \quad (1)$$

Adsorption kinetic experiment

The adsorption kinetics experiment was investigated by using 0.0250 g of commercial activated carbon in 200 mL of water sample. The adsorption kinetic was conducted by shaking at 200 rpm under room temperature for 1 hour. The water samples were collected at various times including 0.5, 1, 3, 5, 10, 20, 30, 40, 50, and 60 mins. The collected water samples were filtered through a 0.45 μm nylon syringe filter and analyzed for NOM concentration by Total Organic Carbon (TOC) analyzer. The kinetics model was investigated by plotting graphs of linear equations of pseudo-first order and pseudo-second order in Equation (2) and Equation (3), respectively.

$$\log (Q_e - Q_t) = \log Q_e - \left(\frac{k_1}{2.303}\right)t \quad (2)$$

where:

q_t = Adsorbed amount at time t(mg/g)
q_e = Adsorbed amount at equilibrium (mg/g)
k_1 = Pseudo-first order rate constant (min^{-1})
t = Time (min)

$$\frac{t}{Q_t} = \frac{1}{k_2 Q_e^2} + \frac{t}{Q_e} \quad (3)$$

where:

k_2 = Pseudo-second order rate constant (g/mg·min)

RESULTS AND DISCUSSIONS

Characterization of commercial activated carbon

BET surface area and average pore diameters of commercial activated carbon were 740.47 m^2/g and 3.442 nm, respectively.

Table 1 The result of BET surface area and average pore diameter of commercial activated carbon from DC Fine chemicals

Materials	**S_{BET} (m^2/g)**	**pore diameter (nm)**
Commercial activated carbon	740.47	3.442

From table 1, it was found that BET surface area and pore diameter of commercial activated carbon are high. In general, high S_{BET} and abundant porous structures could provide higher surface area and more active sites, which enhance adsorption capacity [7].

NOM removal experiment

The removal efficiency of DOC concentration and UV-254 are shown in Figure 1, 2 and 3, respectively. From Figure 1, it illustrates the effect of varying carbon dosage on DOC concentration in raw water. Initially, with no carbon treatment (0 g/L), the DOC level is highest at 3.41 mg/L. A significant reduction is observed even at a low carbon dosage of 0.0129 g/L, bringing the DOC down to 2.16 mg/L, indicating high removal efficiency at the early stage of carbon addition. As the dosage increases, the DOC continues to decrease but at a slower rate, reaching 1.74 mg/L at 0.0249 g/L and gradually dropping to 1.42 mg/L at the highest dosage of 0.1498 g/L.

From these results, it was found that increasing dose of carbon could lead to more effective treatment. The removal efficiency of DOC concentration from Ang Kaew Reservoir was increased with increasing dose of absorbent. The highest DOC removal was 60% under the maximum dose of adsorbent at 0.75 g/L. Moreover, the results of UV-254 showed that the absorbance of UV-254 decreased with increasing activated carbon. When considering the results in Figures 1, 2, and 3, it was found that carbon dosage at 0.1245 g/L had the highest removal percentage of DOC and provided the most cost-effective balance between removal efficiency and resource usage.

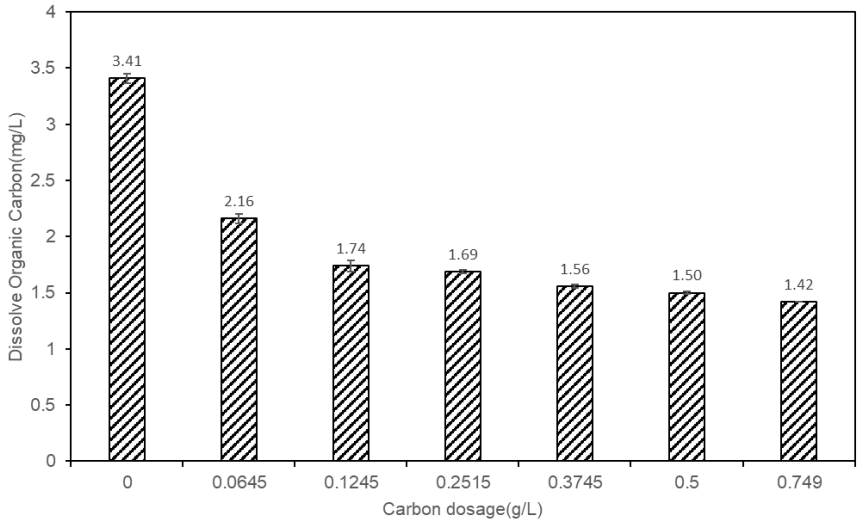


Figure 1 The effect of various carbon dosages on DOC concentration in raw water

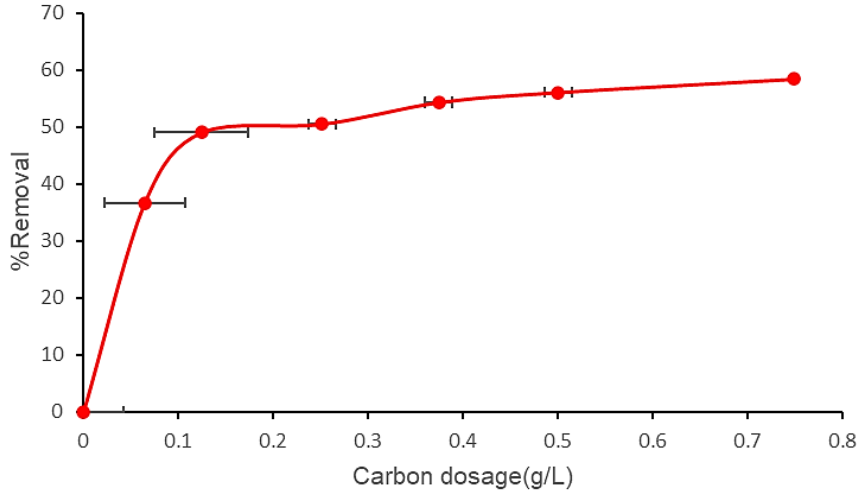


Figure 2 Percent DOC removal efficiency at various carbon dosage

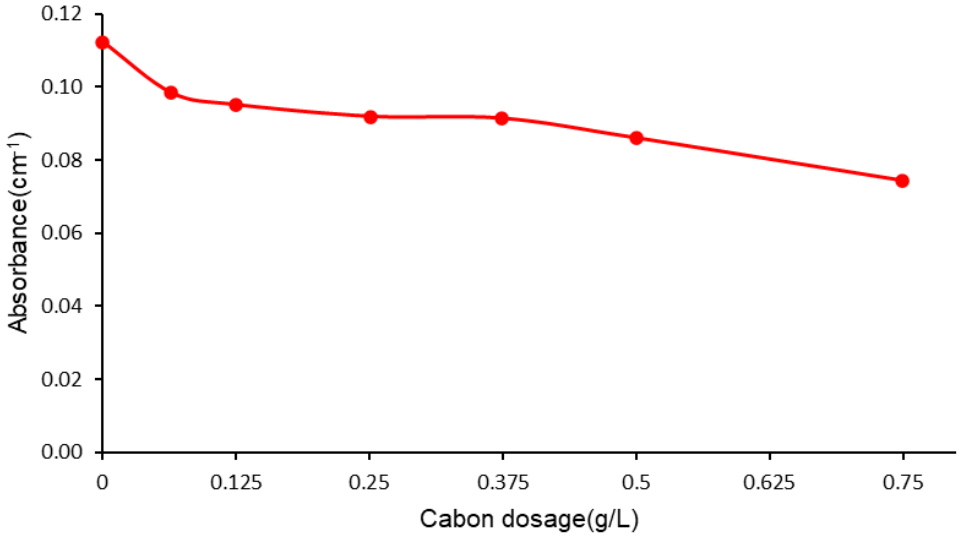


Figure 3 The absorbance changed of carbon dosages after absorbed NOM from Ang Kaew Reservoir by UV-254

The specific ultraviolet absorbance (SUVA) was calculated which is an indicator of the aromaticity and character of organic compounds in raw water. The results of SUVA are shown in Figure 4. The SUVA value in raw water was 3.294 which indicated that organic matter in raw water was contianed aliphatic and aromatic as humic substances. When raw water was adsorbed by actvated carbon, the SUVA was increasing to 4.554-5.859 at different carbon dosage. The SUVA higher than 4 indicated that the organic matter was contained mostly aromatic as humic substances. Thus, it can be concluded that the adsorption with activated carbon preferentially removes organic matter in term of aliphatic.

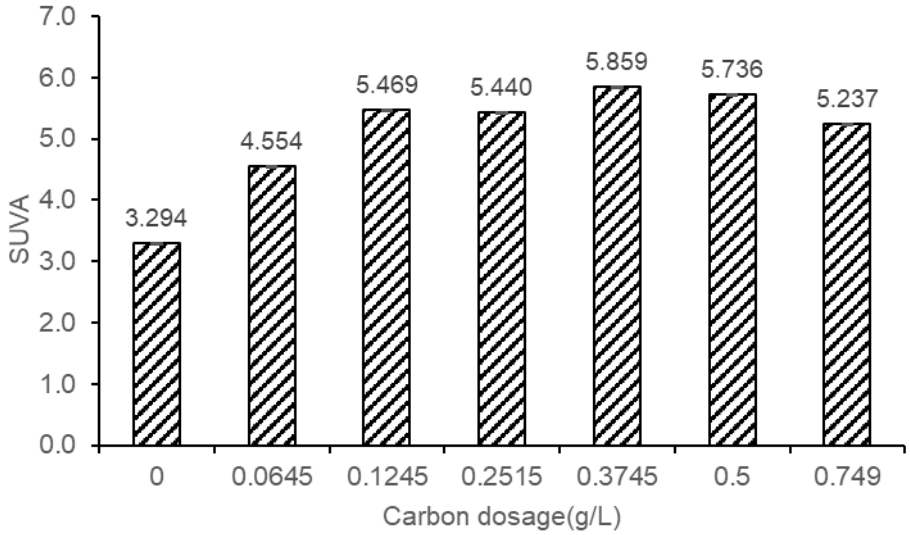


Figure 4 The SUVA changed of carbon dosages after absorbed NOM from Ang Kaew Reservoir

The comparison of removal efficiency of organic matter in this research and other related research was concluded in Table 2. This research was using absorption method for Ang Kaew Reservoir water with initial DOC level at 3.41 mg/L and achieved a removal efficiency of 60%. This result was consistency with the other research that using adsorption method for Ping River water, Chiang Mai, Thailand and groundwater near landfill site, Chiang Mai, Thailand which achieved almost 60% of DOC removal. Furthermore, this result was compared to other removal methods as in-line coagulation followed by ceramic membrane filtration of Ping River. It was found that using in-line coagulation followed by ceramic membrane filtration yielded a higher removal efficiency of 68.5% which demonstrated the highest efficiency in removing DOC concentration from raw water.

Table 2 The comparison of removal efficiency of dissolved organic carbon in raw water

Source	**Method**	**DOC in raw water (mg/L)**	**Removal Efficiency (%)**	**UV-254 absorbance after treatment (cm^{-1})**
Ang Kaew Reservoir	Absorption (This research)	3.41	60	0.0744
Ping River	In-line Coagulation + Ceramic Membrane [8]	2.30	68.5	0.0220
Ping River	Absorption [9]	1.93	60	0.0614
Landfill Site	Absorption [10]	3.37	58	0.0614

Adsorption kinetic experiment

The plotting of pseudo-first order and pseudo-second order of commercial activated carbon are shown in Figure 5 and Figure 6, respectively.

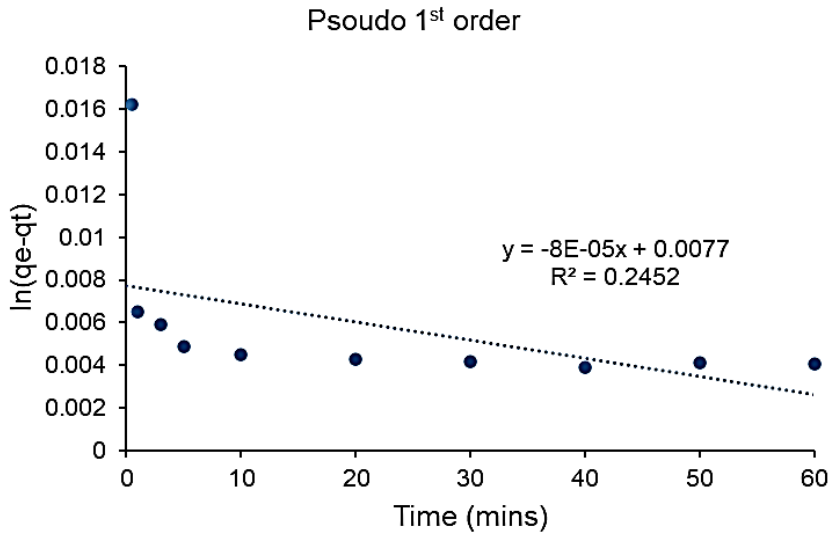


Figure 5 Linear equations of pseudo-first order of commercial activated carbon on DOC removal

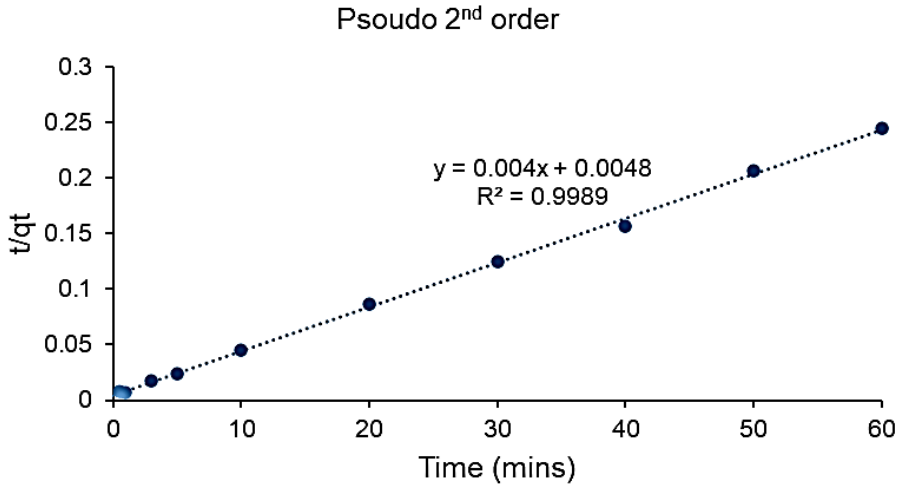


Figure 6 Linear equations of pseudo-second order of commercial activated carbon on DOC removal

From the linear plot, it was found that the obtained correlation coefficient (R^2) was 0.2452 and 0.9989, respectively. Therefore, it can conclude that the adsorption of DOC by using commercial activated carbon was fitted with pseudo-second order. It can be described that the adsorption mechanism on commercial activated carbon is caused by chemical forces (Chemisorption) and depends on the number of available adsorption sites and involves stronger interactions, such as covalent or ionic bonding, rather than just physical attraction [11].

CONCLUSION

BET surface area of commercial activated carbon was 740.47 m^2/g and average pore diameter was 3.442 nm. Commercial activated carbon at optimal dosage (0.1245 g/L) had a high removal efficiency of DOC concentration at 48.97%. The organic matter in term of aliphatic was mostly removed by adsorption with activated carbon. In terms of kinetic models, it fits with pseudo-second order. Thus, the adsorption mechanism of this absorbent was chemisorption.

ACKNOWLEDGEMENT

This research was partially funded by the Graduate School of Chiang Mai University and received Teaching Assistant and Research Assistant Scholarships support from Chiang Mai University.

REFERENCE

[1] Chen, J., Gu, B., LeBoeuf, E. J., Pan, H. and Dai, S. 2002. Spectroscopic characterization of the structural and functional properties of natural organic matter fractions. Chemosphere 48: 59-68.

[2] inc., R. t., 2025. UV254. Retrieved April 8, 2025, from https://realtechwater.com/parameters/uv254/.

[3] Feng, H., Liang, Y. N. And Hu, X. 2022. Natural organic matter (NOM), an underexplored resource for environmental conservation and remediation. Materials Today Sustainability 19: 100159.

[4] Elsharkawy, K., Radwan, M. and El-Aswar, E. I. 2025. Unveiling the role of rubber seals in the generation of decentralized disinfection by-products in chlorinated water distribution systems. Chemosphere 372: 144094.

[5] Khan, I., Saeed, K. And Khan, I. 2019. Nanoparticles: properties, applications and toxicities. Arabian Journal of Chemistry.12(7):908–31.

[6] Bourbonniere, R. A. 2009. Review of Water Chemistry Research in Natural and Disturbed Peatlands. Canadian Water Resources Journal. 34 (4): 393–414.

[7] Rakruam, P. and Wattanachira, S. 2014. Reduction of DOM fractions and their trihalomethane formation potential in surface river water by in-line coagulation with ceramic membrane filtration. Journal of Environmental Sciences 26: 529-536.

[8] Wudthigarn, C., Wongrueng, A., Rakruam, P. And Wattanachira, S. 2015. Removal of Dissolve Organic Matter by Activated Carbon Adsorption. Proceeding of International Conference on Environmental Engineering, Science and Management. May 27-29. Chiang Mai, Thailand.

[9] Yimyam, K et al.2015. Reduction of Disinfection by-Products (DBPs) Precursors by Activated Carbon Adsorption. Proceeding of International Conference on Environmental Engineering, Science and Management. May 27-29. Chiang Mai, Thailand.

[10] Rouquerol, F., Avnir, D., Fairbridge, C. W., Everett, D. H., Haynes, J. M., Pernicone, N., Ramsay, J. D., Sing, K. S. W. and Unger, K. K. 1999. Recommendations for the characterization of porous solids. Pure and Applied Chemistry, 71(8), 1591-1625.

[11] Ahmad, A. A., Hameed, B.H. and Aziz, N. 2007. Adsorption of direct dye on palm ash: kinetic and equilibrium modeling. Journal of Hazardous Materials. 141, 70-76.

20R5-09

Reduction of Natural Organic Matter and Their Trihalomethane Formation Potential by Alum-coagulation Process

Suphitcha Tankaew[1], Pharkphum Rakruam[2]

[1] Master student, Department of Environmental Engineering, Faculty of Engineering, Chiang Mai University, Chiang Mai 50200, Thailand; [2] Ph.D., Assistant Professor, Department of Environmental Engineering, Faculty of Engineering, Chiang Mai University, Chiang Mai 50200, Thailand
[*]Phone: 053 – 944 192, E-mail: pharkphum@eng.cmu.ac.th

ABSTRACT

This study evaluated the effectiveness of the coagulation process in reducing turbidity, organic matter, and trihalomethane formation potential (THMFP) in raw water using potassium alum as a coagulant at concentrations of 20, 30, 40, 50, and 60 mg/L. The results showed that the raw water had a turbidity of 2.71 NTU, a total organic carbon (TOC) concentration of 2.91 mg/L, and a UV254 absorbance of 0.0812 cm^{-1}. After coagulation, the maximum reduction in turbidity was 84.8% at a coagulant concentration of 40 mg/L, the maximum reduction in TOC was 59.1% at 50 mg/L, and the maximum reduction in UV254 absorbance was 81.2% at 60 mg/L. Additionally, after the coagulation process and chlorination for 24 hours, the THMFP values were decreased from 663.83 µg/L in raw water to 145.46, 192.36, 198.93, 206.79, and 188.51 µg/L at coagulant concentrations of 20, 30, 40, 50, and 60 mg/L, respectively. The study concluded that the coagulation process with potassium alum effectively improves water quality by significantly reducing turbidity, organic matter, and THMFP formation potential.

Keywords: Coagulation; Natural organic matter; Trihalomethanes Formation Potential

INTRODUCTION

Water is an essential resource for sustaining life in natural ecosystems. It's utilized in daily activities for both domestic use and consumption reflecting its fundamental importance. Beyond fulfilling basic needs, water also plays a vital role in maintaining ecological balance, supporting nutrient cycling, and regulating the Earth's climate system [1]. Nevertheless, despite its critical significance, many natural water sources today are increasingly affected by pollution and contamination caused by human activities. These include industrial discharges, agricultural runoff, and urban development, all of which contribute directly to the deterioration of water quality. One of the most significant factors impacting water quality is Natural Organic Matter (NOM), a complex mixture of organic compounds that originates from natural sources.

Natural organic matter in water originates from natural sources and anthropogenic activities, including plant decomposition, animal remains, microbial activity, and wastewater from industrial and domestic sources [2]. The presence of natural organic matter contributes to undesirable color, odor, and taste, leading to water pollution and necessitating treatment to meet potable water standards. Various methods are employed for natural organic matter removal including coagulation-flocculation, filtration, oxidation, adsorption, and biological treatment. This study focuses on the coagulation process which is a widely adopted water treatment process in Thailand due to its cost-effectiveness, operational simplicity, and efficiency in treating large water volumes. Coagulation effectively reduces total organic carbon (TOC) and UV-254 [3, 4], which serve as indicators of natural organic matter and precursors to disinfection by-products (DBPs), particularly trihalomethanes (THMs), carcinogenic compounds formed through chlorine interactions [5].

This research aims to mitigate natural organic matter in surface water and minimize DBP formation by employing alum as a coagulant in the coagulation process.

METHODOLOGY

Raw water characteristics

Raw water samples were collected from Angkaew Reservoir, Chiang Mai, Thailand in January 2025. Then, it was analyzed for natural organic matter concentration by determining the total organic carbon (TOC) concentration, ultraviolet absorbance of the samples at 254 nm (UV-254), and trihalomethane formation potential (THMFP).

Coagulation experiment

The coagulation experiment was conducted by using the Jar test (Phipps & Bird 7790-950, Phipps & Bird lnc., USA). The water sample was added to a 1000 ml beaker. Then, the potassium alum which was used as a coagulant was added to the beaker at various concentrations at 0, 20, 30, 40, 50, and 60 mg/L, respectively. After that, the rapid mixing was conducted at 150 rpm for 1 minute followed by slow mixing at 50 rpm for 20 minutes, and allowed to settle for 30 minutes. The water samples were collected and analyzed for natural organic matter concentration and their trihalomethane formation potential. A TOC analyzer (Multi N/C 3100, Analytikjena, Germany, Standard Method 5310) was used to measure TOC in water samples. A UV/VIS spectrophotometer (Lambda365, Perkin Elmer, Perkin Elmer Inc., Boston, MA, USA, Standard Method 5910B) was used to measure the ultraviolet absorbance of the samples at 254 nm(UV254). Trihalomethane formation potential was analyzed according to the EPA 551.1 method. A 10% concentrated chlorine solution was added to the amber bottle and incubated in the dark for 24 hours. Then, a gas chromatography (GC) system with electron capture detection (GC-ECD) (Agilent 4890D) was used to analyze the top-layer concentration of MTBE.

RESULTS AND DISCUSSIONS

Characteristics of raw water

The raw water characteristics from Ang Kaew Reservoir are shown in **Table 1**. The turbidity of the raw water was 2.70 NTU, with a pH of 7.4. The concentration of total organic carbon (TOC) was 2.91 mg/L, and the ultraviolet absorbance at a wavelength of 254 nanometers (UV254) was 0.0812 cm^{-1}. This indicates the presence of organic matter in the water, which increases the potential for the formation of Trihalomethanes (THMs).

Table 1 Characteristics of raw water

Parameter	unit	value
Turbidity	NTU	2.70
pH	-	7.4
TOC	mg/L	2.91
UV-254	cm^{-1}	0.0812

The trihalomethane formation potential (THMFP) of raw water was 663.83 µg/L, which consisted of two compounds including Chloroform (CF) at 609.25 µg/L and Bromodichloromethane (BDCM) at 54.58 µg/L, respectively. These values exceed the World Health Organization (WHO) standards for THMs, which set the total THMs limit at 300 µg/L, with specific limits for chloroform at 300 µg/L and bromodichloromethane at 60 µg/L.

Reduction of organic matter

The results of the coagulation process showed that the turbidity decreased from 2.71 NTU in raw water to 0.85, 0.66, 0.41, 0.58, and 0.75 NTU at coagulant doses at 20, 30, 40, 50, and 60 mg/L, respectively. The results indicate that turbidity was reduced by a maximum of 84.8% at a concentration of 40 mg/L.

For the reduction of organic matter, the TOC concentration was decreased from 2.91 mg/L in raw water to 1.63, 1.39, 1.27, 1.19, and 1.20 mg/L at coagulant dosages 20, 30, 40, 50, and 60 mg/L, respectively as shown in **Figure 1**(a). From the obtained results, it was found that the highest TOC reduction was 59.1% when 50 mg/L of coagulants was applied. The absorbance at a wavelength of 254 nanometers (UV-254) was reduced from 0.0812 to 0.0247, 0.0156, 0.0199, 0.0175, and 0.0153 cm^{-1} at coagulant dosages 20, 30, 40, 50, and 60 mg/L, respectively as shown in **Figure 1**(b).

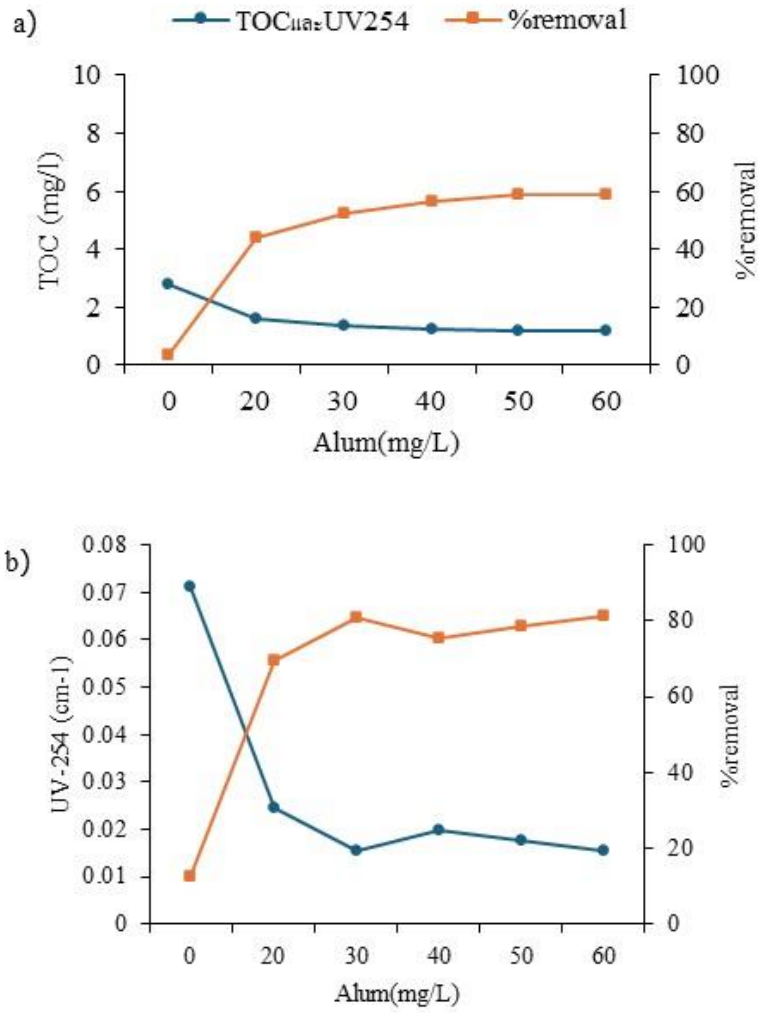


Figure 1. Removing efficiency of (a) TOC and (b) UV-254 by alum coagulation

The obtained results were consistent with the results of [6], which concluded that the increase of alum resulted in the increase of reduction efficiency for turbidity, total organic carbon (TOC), and absorbance at a wavelength of 254 nanometers (UV254) in water.

Compared to previous studies [7] using poly aluminum chloride (PAC) combined with ozonation before precipitation, which achieved TOC reductions of 28–38% and UV absorption values of 48–73%, this study using alum alone achieved TOC reductions of up to 59.1% and UV reductions of up to 81.2%, indicating similar or even better performance than more sophisticated processes. Although ozone slightly increased the efficiency (4–10% for TOC), it required higher infrastructure and operating costs. This study therefore demonstrates that alum remains an effective and cost-effective alternative for surface water treatment, especially in resource-constrained areas.

Reduction of THMFP

Raw water and coagulated water were subjected to chlorination for 24 hours. The potential for trihalomethane formation (THMFP) of raw water was 663.83 ug/L and reduced to 145.46, 192.36, 198.93, 206.79, and 188.51 µg/L at coagulant dosages of 20, 30, 40, 50, and 60 mg/L, respectively. Additionally, there are two types of THMs were detected, including chloroform and bromodichloromethane, as shown in Figure 2. The results indicate that coagulation with alum effectively reduces the potential for trihalomethane formation (THMFP) in raw water, consistent with [8]. The reduction in dissolved organic carbon (TOC) and absorbance at a wavelength of 254 nanometers (UV254) further supports this finding [9]. However, when the coagulant dosage increases beyond a certain level, the removal efficiency tends to stabilize or increase only slightly.

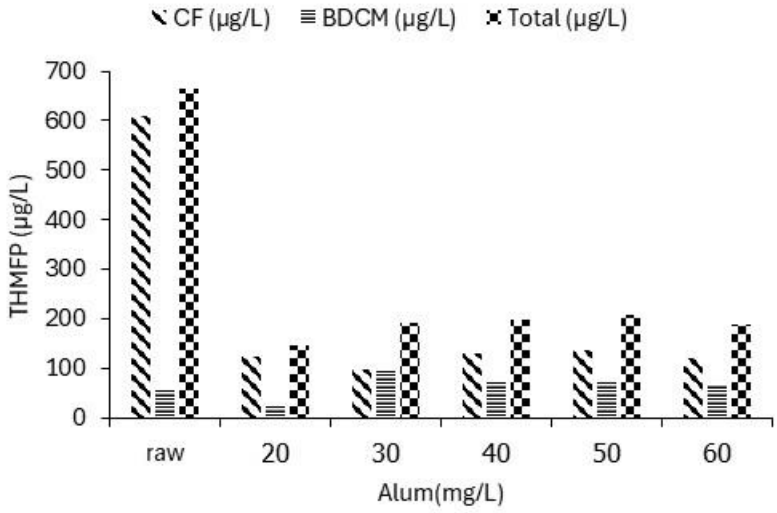


Figure 2. THMFP after coagulation at various dosages

The specific THMFP in raw water and coagulated water at various doses were calculated based on the THMFP and TOC concentration. It is a measure of how much Trihalomethane (THM) can be formed per unit of organic matter. The results of specific THMFP are shown in Figure 3. From the results, it was found that the specific THMFP in raw water was highest. This indicated that the organic matter in raw water was highly reactivity to form THMs. Whereas the specific THMFP in coagulated water was lower than those in raw water in all alum dosage. It can be indicated that the remaining organic matter after coagulated was lower reactivity to form THMs. The organic matter that was removed by coagulation process was highly active species.

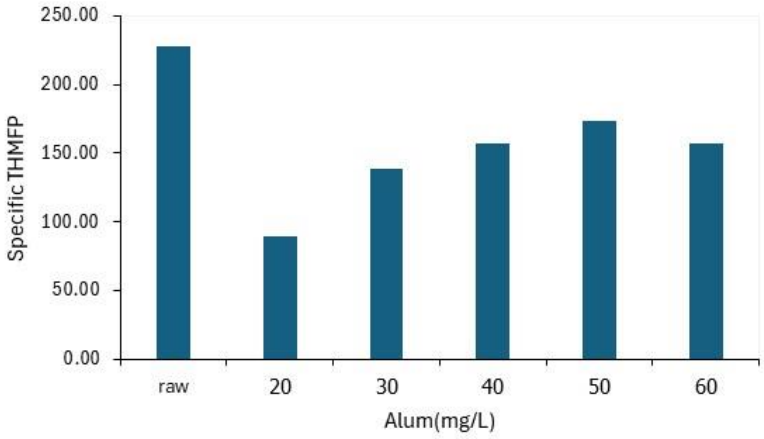


Figure 3. Specific THMFP

CONCLUSION

The concentration of total organic carbon (TOC) was reduced by 59.1% at a coagulant dosage of 50 mg/L, while the absorbance at a wavelength of 254 nanometers (UV254) decreased by 81.2% at 60 mg/L. Although the 50 mg/L dosage removes TOC slightly better, the 60 mg/L dosage achieves a similar TOC reduction while significantly improving the removal of UV254. Thus, the optimal dose for TOC and UV254 reduction was 60 mg/L. Regarding the potential for trihalomethane formation (THMFP), using alum at a concentration of 20 mg/L significantly reduced THMFP from 663.83 µg/L to 145.46 µg/L. This result demonstrates that the use of coagulants effectively reduces the amount of organic matter that reacts with chlorine, which serves as a precursor to the formation of trihalomethanes (THMs). The specific THMFP indicated that coagulation process with alum can removed organic matter that high reactivity to form THMs.

ACKNOWLEDGEMENT

This research was supported by the Department of Environmental Engineering, Chiang Mai University, in terms of providing facilities, laboratory space, as well as necessary equipment and experimental tools essential for conducting the research.

REFERENCE

[1] Acreman, M. 1999. Water and ecology: Linking the earth's ecosystems to its hydrological cycle. Revista CIDOB d'Afers Internacionals. Núm.: 45–46, Agua y desarrollo.

[2] Ibrahim, N. and Aziz, H. 2014. Trends on natural organic matter in drinking water sources and its treatment. International Journal of Scientific Research in Environmental Sciences. 2: 94–106.

[3] Knap-Bałdyga, A. and Żubrowska-Sudoł, M. 2023. Natural organic matter removal in surface water treatment via coagulation—Current issues, potential solutions, and new findings. Sustainability. 15. DOI: 10.3390/su151813853.

[4] Matilainen, A., Gjessing, E.T., Lahtinen, T., Hed, L., Bhatnagar, A. and Sillanpää, M. 2002. Removal of NOM in the different stages of the water treatment process. Environment International. 28(6): 457–465.

[5] Richardson, S.D., Plewa, M.J., Wagner, E.D., Schoeny, R. and DeMarini, D.M. 2007. Occurrence, genotoxicity, and carcinogenicity of regulated and emerging disinfection by-products in drinking water: A review and roadmap for research. Mutation Research/Reviews in Mutation Research. 636(1): 178–242.

[6] Qin, J.-J., Oo, M.H., Lee, H. and Choong, S.Y. 2006. Impact of coagulation pH on enhanced removal of natural organic matter in treatment of reservoir water. Separation and Purification Technology. 49(3): 295–298.

[7] Dąbrowska, L. 2020. Removal of trihalomethane (THM) precursors from water during coagulation enhanced by ozonation. Desalination and Water Treatment. 199: 198–204.

[8] Selcuk, H., Yildiz, I. and Yildiz, M. 2007. DBPs formation and toxicity monitoring in different origin water treated by ozone and alum/PAC coagulation. Desalination. 210(1): 31–43.

[9] An, Y., Yu, G., Ma, F. and Wang, Y. 2017. Simultaneous removal of phosphorus and dissolved organic matter from a sludge in situ reduction process effluent by coagulants. RSC Advances. 7(67): 42305–42311.

20R5-10

The Removal of Oil Contamination in Water Using Iron Oxide Nanomaterial

Artittayaporn Bunma[1] and Visanu Tanboonchuy[1,2*]

[1]*Department of Environmental Engineering, Faculty of Engineering, Khon Kaen University, Khon Kaen, Thailand*
[2]*Research Center for Environmental and Hazardous Substance Management (EHSM), Khon Kaen University, Khon Kaen, Thailand*
[*]*Corresponding author: Tel : 043 009 700 e-mail : visanu@kku.ac.th*

ABSTRACT

Contamination of water sources by petroleum hydrocarbons and volatile organic compounds (VOCs), particularly the BTEX group (benzene, toluene, ethylbenzene, and xylene), represents a critical environmental concern due to their toxicity, persistence, and potential health risks. This study explores the synthesis and application of iron oxide (Fe_3O_4) nanoparticles for the removal of petroleum based contaminants, with Gasoline 91 selected as the model compound. Characterization of the material revealed a high specific surface area of 206.85 m^2/g as determined by the Brunauer Emmett Teller (BET) method. The nitrogen adsorption desorption isotherm exhibited a clear hysteresis loop, indicative of a mesoporous to macroporous structure with interconnected pore networks. The average pore diameter was approximately 4.24 nm, with dominant pores ranging from 1.9 to 2.16 nm, highlighting the material's capability to adsorb small molecular compounds. These structural characteristics suggest that the material is well suited for adsorption and catalytic applications. Magnetic characterization using a VersaLab magnetometer showed that the highest magnetization (36.53 emu/g) was achieved under optimal synthesis conditions (pH 10, Stirring rate 650 rpm, Tempureture 55°C), demonstrating sufficient magnetic responsiveness for external field manipulation. UV-Vis spectrophotometric analysis at 290 nm confirmed significant oil removal efficiency, with Gasoline 91 concentration decreasing from 100 mg/L to 41.86 mg/L within 30 minutes.

Keywords : Iron Oxide Nanomaterial, Oil Removal, BTEX, Nano adsorbent

INTRODUCTION

The contamination of oil and volatile organic compounds (VOCs), particularly from benzene, toluene, ethylbenzene, and xylene (BTEX), represents a critical environmental concern due to their detrimental effects on aquatic ecosystems and public health. BTEX compounds are commonly found in wastewater generated by the oil and gas industries, particularly from crude oil refining and petrochemical production, especially near oil refineries, chemical plants, and fuel stations [1]. The storage of fuel in underground tanks at service stations, designed to save space and reduce fire hazards, necessitates stringent safety measures to prevent leakage, which may pose risks to groundwater and surrounding ecosystems [2].

BTEX leakage from underground storage systems can occur due to material degradation over time, corrosion from chemical reactions or environmental conditions such as temperature and humidity, or mechanical damage resulting from vehicular impacts or natural disasters like earthquakes. Such structural failures may cause BTEX compounds to rapidly migrate into soil and groundwater. Due to their high volatility and moderate water solubility, BTEX compounds can easily spread through soil, surface water, and groundwater systems. Their presence in these environments poses serious health risks, including mucous membrane irritation, respiratory issues, and neurological disorders. Notably, benzene is a well-established carcinogen linked to leukemia [2]. The toxicity and partial solubility of BTEX in water underscore their environmental threat [3].

Managing and remediating oil spills is a complex and challenging process, as oil can readily spread in water and adhere to various surfaces [4]. Conventional oil spill cleanup methods often involve the use of chemical dispersants to reduce oil water interfacial tension, enhancing dispersion in water [5]. However, the use of such chemicals may lead to secondary pollution of soil and water. Additionally, oil sorbents made

from synthetic or natural fibers may generate difficult to manage solid waste, creating long term disposal challenges. To mitigate oil contamination, recent research has focused on developing efficient and environmentally friendly technologies and materials. One promising approach is the use of nanomaterials, particularly iron oxide nanoparticles, which can effectively adsorb and remove BTEX compounds, thereby reducing their spread to uncontaminated areas [6].

This study aims to address groundwater contamination using gasoline as a representative pollutant. The remediation strategy involves the use of a composite of iron oxide nanoparticles as the adsorbent. Iron oxide nanoparticles are known for their high oil adsorption capacity, making them an efficient and sustainable solution for oil adsorption. This approach helps reduce the volume of disposable sorbent waste. The research supports the development of sustainable technologies for managing petroleum contamination and contributes to long term environmental remediation strategies. Therefore, the synthesis of iron oxide nanoparticles represents a promising approach for effectively treating water contaminated with Gasoline 91. This not only helps mitigate water pollution but also supports the development of sustainable environmental management technologies for the future.

METHODOLOGY

This study involves the synthesis of iron oxide nanoparticles using chemical reagents, including ferric chloride ($FeCl_3 \cdot 6H_2O$), ferrous chloride ($FeCl_2 \cdot 4H_2O$), sodium hydroxide (NaOH), and hydrochloric acid (HCl). The synthesized nanoparticles are characterized using a VersaLab magnetometer to measure magnetic properties, Brunauer Emmett Teller (BET) method and a UV-Vis spectrophotometer for absorption analysis.

The synthesis process follows the co-precipitation method as described by Rajput et al. (2015). In this procedure, $FeCl_3$ and $FeCl_2$ are dissolved in a 2:1 molar ratio in hydrochloric acid (HCl) and degassed distilled water. Sodium hydroxide (NaOH) is gradually added until the pH reaches 8.0 shown in Figure 1, resulting in the formation of black magnetic nanoparticles. These nanoparticles are separated using a magnetic field, washed with deionized water, and dried at 50°C.

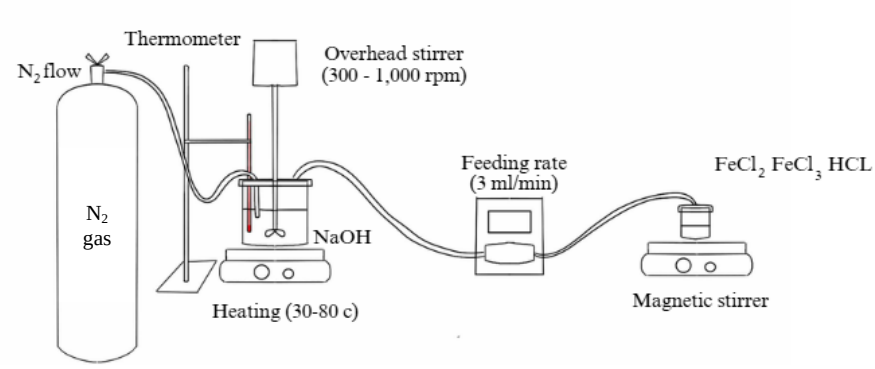


Figure 1 experiment laboratory scale setup

To optimize synthesis conditions, the Box-Behnken Design (BBD) is employed, using three independent variables: X_1 (pH range 7–13), X_2 (stirring rate 300–1000 rpm), and X_3 (temperature 30–80°C) shown in Table 1. A total of 15 experiments are conducted, and the magnetic properties (Y, emu/g) are compared to determine the optimal conditions. The synthesized nanoparticles are then tested for oil adsorption efficiency, with performance evaluation conducted using UV-Vis spectrophotometry at 290 nm.

Table 1 Consideration of appropriateness in the Box-Behnken Design synthesis.

Variable	Low (-)	High (+)
X_1: pH	7	13
X_2: Stirring rate (rpm)	300	1000
X_3: Temperature (°C)	30	80

The adsorption kinetic experiments were systematically performed to evaluate the efficiency of Fe_3O_4 nanoparticles in the removal of Gasoline 91 from aqueous media. The initial concentration of Gasoline 91 was established at 100 mg/L, and its residual concentration was quantitatively monitored at predetermined time intervals over a 30 min experimental period. The linear equation is expressed as follows equations (1) and (2). The experimental kinetic data were analyzed using both the pseudo-first order and pseudo-second order kinetic models. were applied to illustrate the reaction rate of adsorption process

Pseudo-first order model:

$$\ln(q_e - q_t) = \ln q_e - k_1 t \quad (1)$$

Pseudo-second order model:

$$\frac{t}{q_t} = \frac{1}{k_2 q_e^2} + \frac{1}{q_e} t \quad (2)$$

Where q_e represents the adsorption capacity of the adsorbent at equilibrium ($mg \cdot g^{-1}$), q_t is amount of adsorbate absorbed on the adsorbent surface at the time ($mg \cdot g^{-1}$), K_1 and K_2 are the rate constants for the pseudo-first order and pseudo-second order models, respectively.

RESULTS AND DISCUSSION

Contamination by petroleum-based pollutants and volatile organic compounds (VOCs), such as benzene, toluene, ethylbenzene, and xylene (BTEX), represents a significant environmental issue, threatening both aquatic ecosystems and human health. Therefore, the development of effective and sustainable technologies for oil removal from water sources has become increasingly important. Among emerging solutions, the use of magnetic nanomaterials, particularly iron oxide nanoparticles (Fe_3O_4), has gained considerable attention due to their excellent adsorption capabilities and magnetic properties, which allow for efficient separation and recovery without generating secondary waste.

In this study, Fe_3O_4 nanoparticles were synthesized and characterized to investigate their potential for oil removal from water. The results revealed that the magnetic properties of the nanoparticles were highly dependent on synthesis conditions, including pH, reaction temperature, and stirring speed. Magnetization values ranged from 15.18 to 36.53 emu/g, with the highest magnetization achieved at pH 10, 55°C, and 650 rpm. In contrast, lower temperature (30°C) and slower agitation (300 rpm) under the same pH condition resulted in significantly reduced magnetization (15.18 emu/g) as shown in Table 2. These findings highlight the crucial role of both thermal and kinetic energy in influencing nanoparticle formation. Furthermore, the synthesized Fe_3O_4 nanoparticles exhibited superparamagnetic behavior, enabling rapid and precise external manipulation using magnetic fields. This property greatly enhances their practicality in environmental applications, especially in the targeted adsorption and removal of oil pollutants from water, providing a cleaner alternative to conventional treatment methods.

Characterization using the Brunauer Emmett Teller (BET) method revealed that the material had a high specific surface area of 206.85 m^2/g. The nitrogen adsorption–desorption isotherm showed a distinct hysteresis loop, indicating a mesoporous to macroporous structure with interconnected pore networks. These structural features contribute to enhanced adsorption performance, as they facilitate the diffusion and

retention of pollutant molecules within the pore system. The BET C constant was also notably high (82.585), suggesting strong interactions between nitrogen and the surface of the material, and confirming the presence of high-energy adsorption sites. Analysis of the pore size distribution further indicated that the material predominantly exhibited mesoporous characteristics with some microporous features, having an average pore diameter of 4.24 nm and dominant pore sizes in the range of 1.9 to 2.16 nm. These properties make the nanoparticles especially effective for adsorbing small molecules, such as those found in gasoline and VOCs, thereby underscoring their suitability for use in environmental remediation and catalytic applications.

Table 2 Experimental design matrix and magnetization of iron oxide nanoparticles

Run Order	X_1: pH	X_2: Stirring rate (rpm)	X_3: Temperature (°C)	Magnetization(emu/g)
1	7	300	55	31.41
2	10	300	80	30.32
3	10	1000	30	22.01
4	10	650	55	36.53
5	13	650	30	26.84
6	13	300	55	28.21
7	10	650	55	36.5
8	7	1000	55	34.64
9	13	650	80	18.77
10	7	650	30	30.97
11	10	650	55	34.65
12	7	650	80	31.0
13	10	300	30	15.18
14	10	1000	80	30.6
15	13	1000	55	30.14

The concentration of Gasoline 91 present in the aqueous solution was quantitatively analyzed by monitoring its absorbance at specific time intervals. This methodological approach enabled accurate determination of the temporal changes in pollutant concentration throughout the course of the study.

The experimental findings revealed a consistent and gradual decline in the concentration of Gasoline 91 as the reaction time progressed. Initially, at time zero (0 min), the concentration was recorded at 100 mg/L, which served as the baseline for comparison. Over the subsequent 30 min period, a significant reduction in concentration was observed, culminating in a final value of 41.86 mg/L. This steady decrease in concentration over time clearly indicates the progressive removal or degradation of Gasoline 91 from the solution, which can be attributed to the effectiveness of the adsorption or treatment process employed in the study.

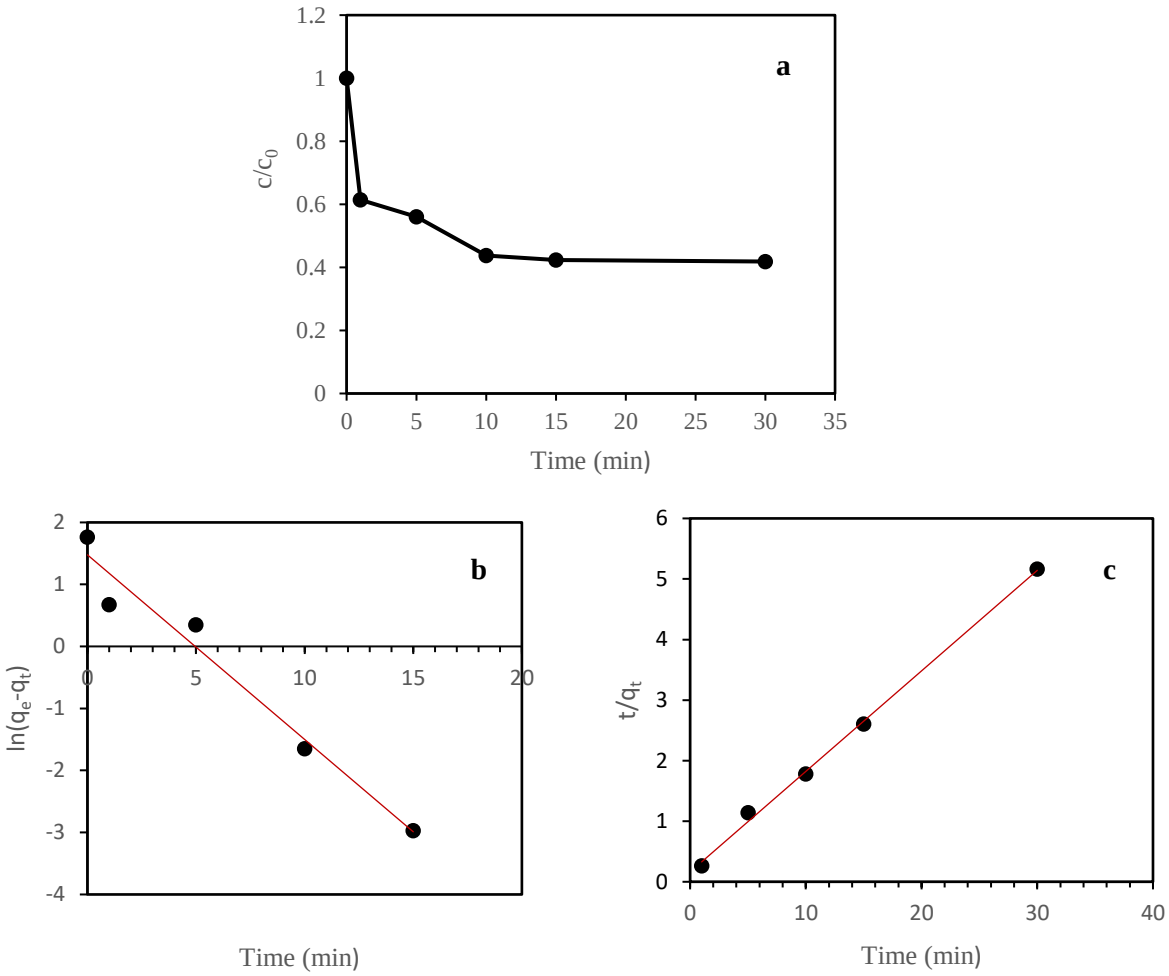


Figure 2 Adsorption kinetic of Gasoline 91 removal by iron oxide nanoparticles (a) Adsorption kinetic, (b) Pseudo-first order model, and (c) Pseudo-second order model

This indicates that Gasoline 91 transformation over time. The plot of concentration versus time exhibited a decreasing curve, reflecting a rapid decline in concentration during the initial period, followed by a gradual stabilization as time progressed. The removal of gasoline using iron oxide nanoparticles is adsorption capacity increased rapidly, likely due to the abundance of available active porous on the iron oxide nanoparticles surface. As the active sites became saturated, the adsorption rate gradually decreased, approaching equilibrium around 30 min.

The adsorption mechanism and rate-limiting steps, two kinetic models were applied: pseudo-first order and pseudo second order. The kinetic plots and parameters are shown in Figure 2 and Table 3

Table 3 Kinetic Parameters for Gasoline 91 removal by iron oxide nanoparticles

Kinetics model	Parameter	Iron oxide nanoparticles
Pseudo-first order	q_e ($mg \cdot g^{-1}$)	4.3802
	K_1 (min^{-1})	0.2978
	R^2	0.9664
Pseudo-second order	q_e ($mg \cdot g^{-1}$)	6.0240
	K_2 ($g/mg \cdot min^{-1}$)	0.1697
	R^2	0.9978

The adsorption kinetics of Gasoline 91 onto iron oxide nanoparticles were best fitted by the pseudo-second-order model, which exhibited strong agreement with experimental data throughout the adsorption process especially during the initial rapid uptake (0–15 min) and equilibrium phases (30 min). In contrast, the pseudo-first-order model systematically underestimated adsorption capacities, demonstrating its inadequacy for this system. The robustness of the pseudo-second order model was further validated by its high correlation coefficient ($R^2 = 0.9978$), as detailed in Table 3.

CONCLUSION

This study successfully synthesized iron oxide nanoparticles under optimized conditions, resulting in a high level of efficiency in removing Gasoline 91 contamination from water. Additionally, these nanoparticles can be easily separated from the water using an external magnetic field, providing a simple and efficient method for recovery. The kinetic adsorption was explained by the pseudo second order model, with a correlation coefficient (R^2) of 0.9978, which suggests that the adsorption step is a rate limiting step in the adsorption process.

ACKNOWLEDGEMENT

The author would like to express gratitude to Department of Environmental Engineering Faculty of engineering, Khon Kean University and Research Instrument Center Khon Kaen University for supporting the laboratory and equipment used in this research.

REFERENCES

[1] Aghdam, E.M., Hassani, A.H., and Khosravi, M. 2015. Environmental impact of BTEX compounds in groundwater contamination: A review. *Environmental Science and Pollution Research*, 22(9): 7094–7112.

[2] Nourmoradi, H., Foroghi, M., and Farhadkhani, M. 2012. Health effects of benzene exposure: A systematic review. *Environmental Health Perspectives*, 120(3): 370–378.

[3] Mohammadi, M., Nasseri, S., and Nabizadeh, R. 2020. Removal of BTEX from aqueous solutions using innovative adsorption techniques. *Journal of Environmental Management*, 256: 109–118.

[4] Ogbezode, O., Wang, Y., and Chen, X. 2023. Application of iron oxide nanoparticles in environmental remediation and biomedical fields. *Nanomaterials*, 13(1): 100–120.

[5] Srinewat, S., et al. 2022. Magnetic properties of iron oxide nanoparticles and their application in wastewater treatment. *Journal of Science and Technology*, 30(4): 405–420.

[6] Wongsaprom, K. 2013. Iron oxide nanoparticles and their role in contaminant removal from water. *Journal of Environmental Science Research*, 22(2): 115–130.

20R5-11

Decolorization of Dye Wastewater Using Photocatalytic Process Assisted with Titanium-Magnetite Chitosan Beads (TMCB)

Nuttaya Pengmuangmool[1], Soraya Komkiang[1], and Natthapong Proysurin[1*]

[1]Environmental Health Program, Faculty of Public Health, Naresuan University, Phitsanulok,65000, Thailand
**Phone : (66) 847553713 , E-mail : natthapongp@nu.ac.th*

ABSTRACT

The textile industry is a large-scale industry where dyeing is a crucial process. The dyeing process uses huge amounts of water, resulting in wastewater containing dye components that must be treated before being released into the environment. This research focuses on the treatment of dye wastewater using a photocatalytic process with Titanium Dioxide containing Magnetite and Chitosan in the form of beads (TMCB). The experiments were conducted on synthetic dye wastewater containing Reactive Blue-19 dye and ran continuously for 180 minutes. The results showed a maximum efficiency of 55% in synthetic dye wastewater at a concentration of 40 mg/L and pH 11. The study of reusability showed that the titanium dioxide-magnetite-chitosan beads could be reused for 4 cycles. The kinetics of the photocatalytic process followed a first-order reaction with a photocatalytic reaction rate constant (k) of 0.0032 $min^{-1.}$

Keywords: Decolorization; Reactive dye; Photocatalytic degradation; Titanium-Magnetite Chitosan Beads; Titanium dioxide; Dye-containing wastewater

INTRODUCTION

The fast fasion industry globally produces 10% of carbon dioxide emissions [1]. Moreover, textile industry in fast fasion trends generates huge amount of dye wastewater and toxic chemicals especially dyeing and printing processes. that can affect environmental issues and human health risks such as skin irritation, cancer, and reproductive [2]. Therefore, wastewater from textile industry is concerned to be treated before discharging into water bodies.

There are several removal methods such as physical, biological, chemical treatment methods. Each technique has its own advantage and disadvantage. However, chemical treatment method especially advance oxidation processes (AOPs) posses the efffective method such as the photocatalytic process was widely applied for diverse organic pollutants and has been applied for dye removing in wastewater [3]. Normally, titanium dioxide was employed in this process as a catalyst for producing hydroxyl radical as oxidizing agent. However, titanium dioxide was applied in suspended form which has limitation of collection after treatment.

Therefore, this research aimed to investigate the removal of dye wastewater using a photocatalytic process employing composite materials of titanium dioxide and magnetite particle in form of chitosan beads to facilitate collection, and reusability. The study investigates optimum conditions of photocatalytic process and evaluates the reusability of the treated beads in dye removal and the kinetics of the photocatalytic process were examined.

METHODOLOGY

Experimental set up

The photocatalytic experiment was conducted in laboratory scale. Photocatalytic reactor were set up in dark chamber to prevent light penetration and 16 Watt UV- C lamp was applied as energy source. Oxygen was aerated in each beaker of 50 mL of synthetic dye solution. Synthetic dye wastewater containing Reactive Blue-19 was applied throughout experiment as shown in Figure 1.

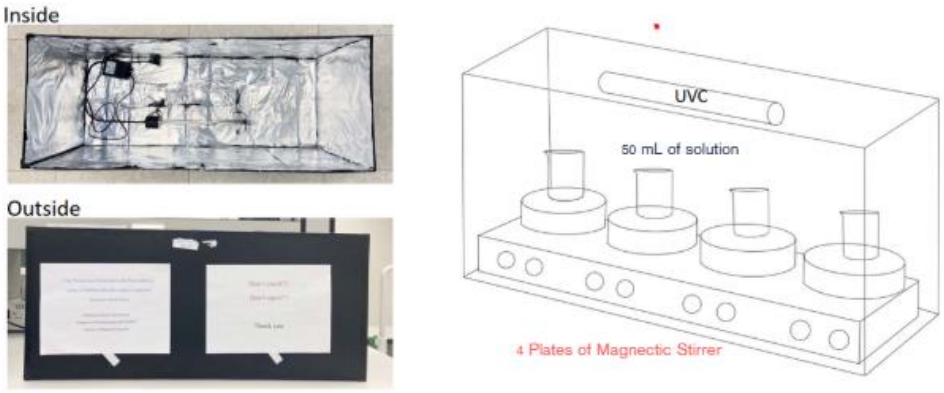


Figure 1 Schematic Diagram of Photocatalytic Process

Preparation of Titanium-magnetite chitosan beads (TMCBs)

Magnetite particles were prepared from mixture solution of Ferric Choride ($FeCl_3$) and Ferrous Sulfate ($FeSO_4$) in molar ratio of 1:1 and dropped into 2 M NaOH until pH 11 to form fine magnetite particles (Fe_3O_4) and then particles were washed with DI water and dried in oven at 105 ºC for 4 hours [4]. Mixture of titanium dioxide and chitosan was prepared by dissolving 4 g of chitosan powder in 4% of 50 mL of acetic acid and then stirred it for 2 hours and 1 g of titanium dioxide was mixed into chitosan solution and the mixture was degassed in ultrasonic bath for 20 minutes. Titanium-magnetite chitosan beads (TMCBs) were formed by adding 3 g. of magnetite particles in titanium dioxide and chitosan slurry and dropped in 0.5 M NaOH using syringe dropping. TMCBs were cleaned with DI water and chilled in refrigerator at 5 ºC for 24 hours to form the beads before using them in the experiment [5].

Investigation of optimum conditions

Optimum conditions that affect removal efficiency using photocatalytic process assisted with TMCBs such as pH, initial dye concentration, TMCB dose and contact time were carried out as shown in Table 1. Reusability of TMCBs was also tested in this experiment.

Table 1 Variation of optimum conditions

Conditions	Unit	Variation
pH	-	5,7,9 and 11
Initial dye concentration	mg/L	5, 10, 15 and 20
TMCB dose	g	2, 3 and 4
Contact time	min.	15, 30, 45, 60, 90, 120, 150 and 180

Samples of synthetic wastewater were filtered using membrane filter 0.45 µm and analyzed the absorbance using UV-Vis spectrophotometer at maximum wavelength of 595 nm. and compared with standard curve to convert to dye concentration. The removal efficiency (% Removal) of each condition was calculated as shown in equation 1.

$$\% \textbf{ Removal} = \frac{C_0 - C_t}{C_0} \times 100 \quad (1)$$

where % Removal is removal efficiency (%)

C_0 is initial dye concentration (mg/L)

C_t is remaining dye concentration (mg/L)

Kinetics

Kinetics of photocatalytic reaction using TMCBs were explained employing psuedo-first order and psuedo-second order as shown in equation 2 and equation 3, respectively.

$$\ln \frac{C_t}{C_0} = k_1 t \quad (2)$$

$$\frac{1}{C_0} = k_2 t + \frac{1}{C_t} \quad (3)$$

where k_1 is kinetic rate constant of psuedo-first order reaction (min^{-1})

k_2 is kinetic rate constant of psuedo-first order reaction (mg/L/min)

t is time (minute)

RESULTS AND DISCUSSIONS

Effect of contact time

The photocatalytic process performance was investigated for contact time from 15 to 180 minutes. Figure 2 indicates that increasing contact time affects removal efficiency of photocatalytic processes because longer contact time allows expansion of reaction between dye molecules and reactive species. From Figure 2, it can be seen that the removal efficiency of dye can be reached to 55% at contact time of 180 minutes.

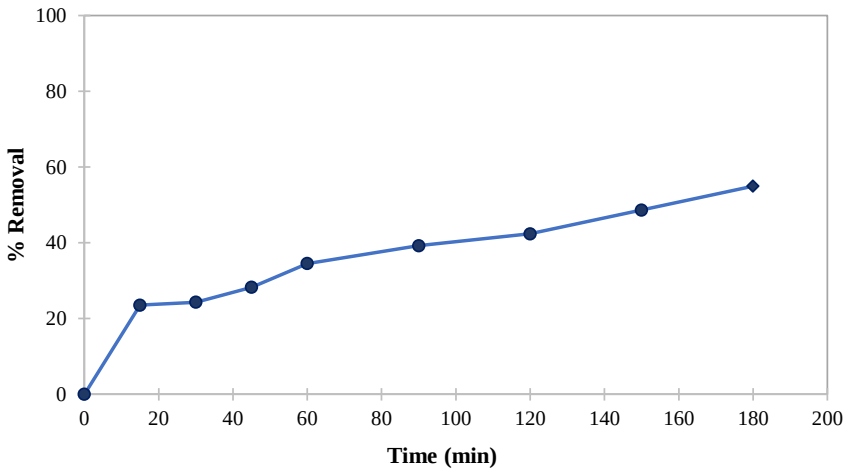


Figure 2 Effect of Contact Time on Dye Removal Efficiency
(C_0 = 10 mg/L, pH 7, TMCB 4 g)

Effect of solution pH

The solution pH affects dye degradation in terms of degradation mechanism. The effect of the solution pH on the rate of photocatalytic process was investigated within the range of 5-11. As Figure 3, increment of pH solution led to removal efficiency. Dye removal efficiency showed good performance at the alkaline condition, and it was highest at 66% at pH 11. This is attributed to increased highly reactive species especially hydroxyl radical (˙OH) by the titanium dioxide catalyst in basic condition and it enhances dye degradation. This result is in accordance with previous work, which reported maximum dye removal efficiency of 80% at pH 11 [6].

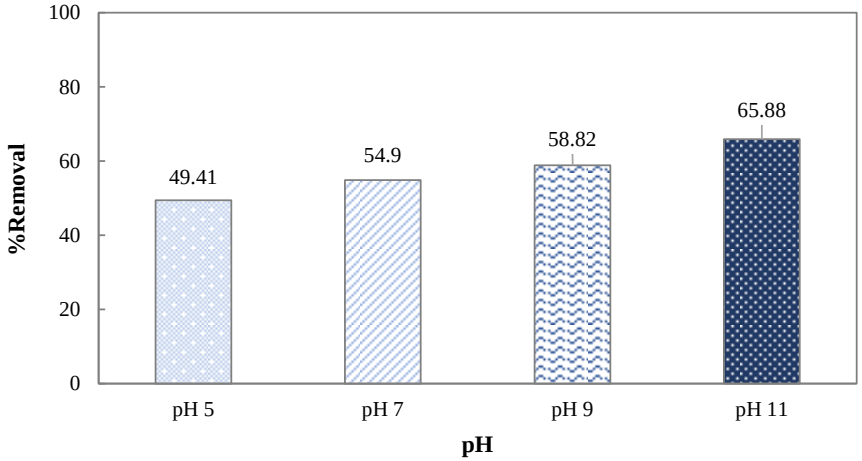


Figure 3 Effect of pH Solution on Dye Removal Efficiency
(C_0 = 10 mg/L, TMCB 4 g, Contact time 180 min.)

Effect of initial dye concentration

Initial dye wastewater concentration of 40 mg/L gave the highest removal efficiency of 55 % as shown in Figure 4. This is attributed to altered dye adsorption behavior at high concentrations and sufficient UV-C light penetration of the catalyst surface during photocatalysis. This result correlated with previous study, which found increased removal percentages at initial dye concentrations of 180-240 mg/L compared to 100 mg/L [7]

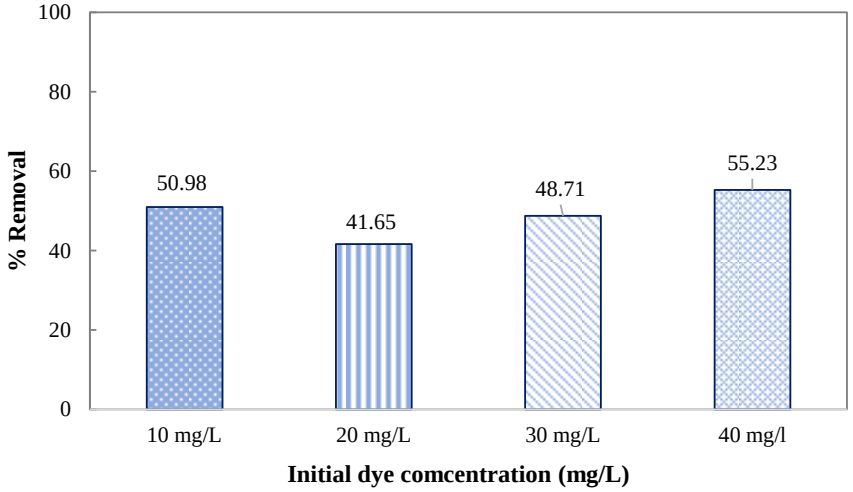


Figure 4 Effect of Initial Dye Concentration on Dye Removal Efficiency
(Contact time 180 min., TMCB 4 g, pH 11)

Effect of TMCB dose

According to Figure 5, increment of catalyst dosage affects dye degradation. The amount of 4 g of TMCB gave the highest dye removal efficiency at 46% compared to 2 g which showed removal percentage of 26%. This is because the increased amount of photocatalyst results in high active sites and the specific surface area and led to resulting in degradation rate due to increased hydroxyl radical.

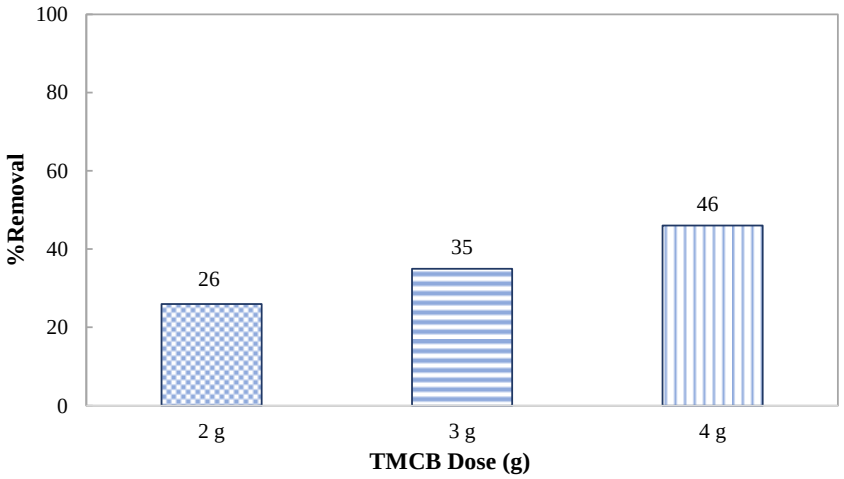


Figure 5 Effect of Initial Dye Concentration on Dye Removal Efficiency
(Contact time 180 min., pH 11, C_0 =40)

Reusability

The cyclic experiment was carried out to investigate the reusability of the TMCB. It can be reused for 4 cycles and give similar removal efficiency of 46%, 52%, 46%, and 51% at cycle 1-4, respectively as shown in Figure 6. The slight fluctuations in removal percentages between cycles are attributed to magnetite powder in the beads being washed out due to oxidation and irradiation on the catalyst.

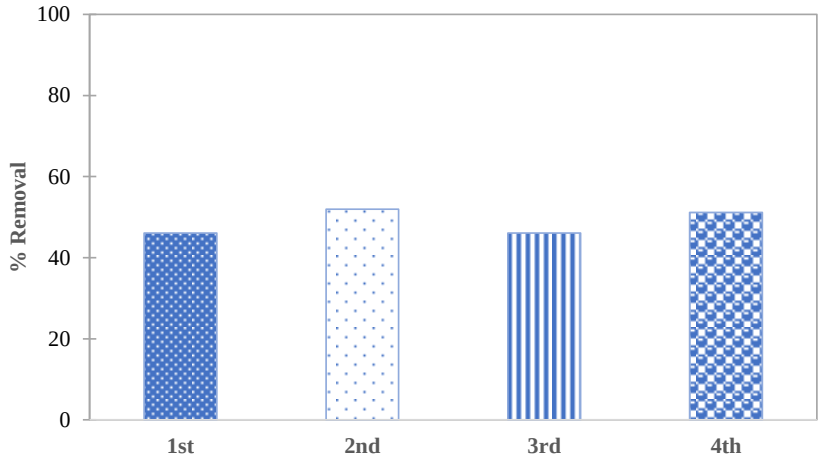


Figure 6 Reusability of TMCB in Different Cycle on Dye Removal Efficiency

Photocatalytic degradation kinetics

The kinetic study of the degradation reactions was investigated quantitatively using the pseudo-first-order and pseudo-second-order kinetics. Kinetics of the photocatalytic process using TMCBs were examined using contact time and dye concentration as illustrated in Figure 7. The kinetics of the photocatalytic process followed the first-order reaction equation according to previous research [8] with reaction constant (k) of 0.0032 min^{-1}.

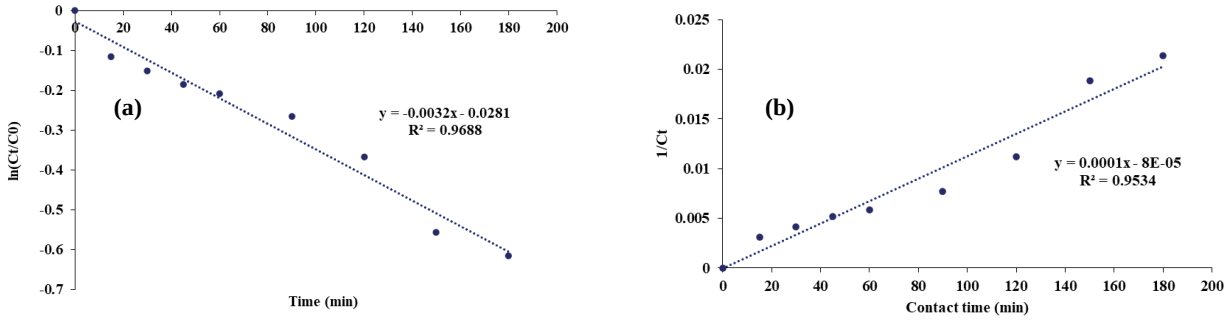


Figure 7 Kinetics of the Photocatalytic Process Using TMCBs
(a) pseudo-first-order (b) pseudo-second-order reactions

CONCLUSION

TMCBs were used as a catalyst for assisting the photocatalytic process of dye wastewater. Optimum conditions of the experiment found that the highest efficiency was 55% in synthetic dye wastewater at a concentration of 40 mg/L and pH 11 with contact of 180 min. The reuse of titanium dioxide mixed with magnetite and chitosan beads could be reached by 4 cycles. The photocatalytic process fitted with pseudo-first order reaction. Overall, TMCBs is a promising catalyst for photocatalytic degradation of dye from wastewater.

ACKNOWLEDGEMENT

The research was partially funded by the Environmental Health Division, Faculty of Public Health, Naresuan University.

REFERENCE

[1] Li, Z., Zhou, Y., Zhao, M., Guan, D., & Yang, Z. (2024). The carbon footprint of fast fashion consumption and mitigation strategies-a case study of jeans. Science of The Total Environment, 924, 171508.

[2] Al-Tohamy, R., Ali, S. S., Li, F., Okasha, K. M., Mahmoud, Y. A. G., Elsamahy, T., ... & Sun, J. (2022). A critical review on the treatment of dye-containing wastewater: Ecotoxicological and health concerns of textile dyes and possible remediation approaches for environmental safety. Ecotoxicology and environmental safety, 231, 113160.

[3] Samsami, S., Mohamadizaniani, M., Sarrafzadeh, M. H., Rene, E. R., & Firoozbahr, M. (2020). Recent advances in the treatment of dye-containing wastewater from textile industries: Overview and perspectives. Process safety and environmental protection, 143, 138-163.

[4] Milidrag, G. P., Nikić, J., Gvoić, V., Mandić, A. K., Agbaba, J., Bečelić-Tomin, M., & Kerkez, D. (2022). Photocatalytic degradation of magenta effluent using magnetite doped TiO_2 in solar parabolic trough concentrator. Catalysts, 12(9), 986.

[5] Rosdiana, E. A., Prasetya, N. B. A., & Gunawan, G. (2023). Synthesis and characterization of TiO_2-chitosan beads and its application as a degradation agent of methylene blue. Trends in Sciences, 20(9), 6670-6670.

[6] Sirirerkratana, K., Kemacheevakul, P., & Chuangchote, S. (2019). Color removal from wastewater by photocatalytic process using titanium dioxide-coated glass, ceramic tile, and stainless steel sheets. Journal of Cleaner Production, 215, 123-130.

[7] Chairungsri, W., Pholchan, P., Sumitsawan, S., Chimupala, Y., & Kijjanapanich, P. (2023). Photocatalytic degradation of textile dyeing wastewater using titanium dioxide on a fixed substrate: Optimization of process parameters and continuous reactor tests. Sustainability, 15(16), 12418.

[8] Siddique, M., Khan, R., Khan, A. F., & Farooq, R. (2014). Improved Photocatalytic Activity of TiO_2 Coupling Ultrasound for Reactive Blue 19 Degradation. Journal of the chemical society of Pakistan, 36(1).

20R5-12

Photocatalytic Degradation of Caffeine in Water using Titanium Dioxide-Coated Materials

Warisara Pissadarn[1], Patiya Kemacheevakul[1,2*], Surawut Chuangchote [2,3]

[1] Department of Environmental Engineering, Faculty of Engineering, King Mongkut's University of Technology Thonburi, 126 Prachauthit Rd., Bangmod, Thungkru, Bangkok 10140, Thailand [2]Research Center of Advanced Materials for Energy and Environmental Technology (MEET), King Mongkut's University of Technology Thonburi, 126 Prachauthit Rd., Bangmod, Thungkru, Bangkok 10140, Thailand [3]Department of Tool and Materials Engineering, Faculty of Engineering, King Mongkut's University of Technology Thonburi, 126 Prachauthit Rd., Bangmod, Thungkru, Bangkok 10140, Thailand
[*]Corresponding author: Tel: 024709360, e-mail: patiya.kem@kmutt.ac.th

ABSTRACT

Caffeine is a widely consumed stimulant that is increasingly detected in aquatic environments due to its persistence and the inefficiency of conventional wastewater treatment processes in removing it completely. Its presence in water bodies poses ecological risks, including adverse effects on aquatic organisms at concentrations as low as 0.91 mg/L. This study explores the photocatalytic degradation of caffeine using titanium dioxide (TiO_2)-coated substrates, specifically glass beads, alumina balls, and ceramic balls, synthesized via the sol-gel method. The prepared materials were characterized using scanning electron microscopy (SEM) and energy-dispersive X-ray spectroscopy (EDS) to assess surface morphology and the distribution of TiO_2. Photocatalytic experiments were conducted using synthetic wastewater containing 3.6 mg/L of caffeine under three experimental conditions: (i) in the dark (adsorption), (ii) under UV-C irradiation without a catalyst (photolysis), and (iii) under UV-C irradiation with TiO_2-coated materials (photocatalysis). Caffeine degradation was monitored using high-performance liquid chromatography (HPLC). Results indicated that ceramic balls exhibited the highest TiO_2 adherence due to their rougher surface texture and achieved a degradation efficiency of 99.47% after 360 min of UV-C exposure. In comparison, glass beads and alumina balls achieved degradation efficiencies of 90.19% and 67.37%, respectively. The enhanced performance of the ceramic balls is attributed to their greater surface area, which facilitates stronger TiO_2 binding and provides more active sites for photocatalytic reactions. These findings demonstrate the potential of TiO_2-coated ceramic balls as an effective and economical approach for the removal of caffeine from wastewater. This study contributes to the development of advanced treatment technologies and suggests a promising pathway for integrating photocatalytic materials into large-scale wastewater treatment systems. Further research is warranted to evaluate the scalability and long-term performance of this method under real-world industrial conditions.

Keywords : caffeine degradation; titanium dioxide; photocatalysis; wastewater treatment; ceramic ball

INTRODUCTION

Caffeine ($C_8H_{10}N_4O_2$) is a natural stimulant found in coffee, tea, soft drinks, and medications [1-2]. Due to its high production volume and extensive use, it leads to significant environmental contamination. The average daily global caffeine consumption is approximately 70 mg per person, and it is frequently detected in surface water, groundwater, and wastewater from treatment plants [3-4]. Major sources of environmental caffeine include human excretion, coffee processing wastewater, and industrial waste. In the human body, caffeine is mostly metabolized in the liver, with the remainder excreted in urine, contributing to wastewater contamination [1, 5]. Additionally, coffee processing releases caffeine into the environment through residues and wastewater, with concentrations ranging from 0.022 to 3.594 mg/L [6].

The increasing presence of caffeine in environmental matrices such as water highlights the widespread reach of its contamination. This widespread occurrence is concerning as caffeine is not only a pollutant but also a substance that can affect the health of aquatic ecosystems. It has been recognized that contaminants like caffeine, when present in high enough concentrations, can interfere with the natural processes of aquatic organisms. These disturbances can affect reproduction, growth, and behavior, further exacerbating the ecological imbalance. Moreover, since caffeine does not readily degrade in the environment, it remains in water systems for extended periods, making it a persistent contaminant. The accumulation of caffeine in water bodies could potentially impact water quality and pose risks to human and animal health through bioaccumulation.

Caffeine residues in water often exceed the capacity of wastewater treatment processes to degrade them, which results in bioaccumulation in aquatic organisms. This accumulation can lead to ecological risks such as impaired regenerative capacity and increased mortality in aquatic species. Long-term exposure to trace levels of caffeine has been associated with oxidative stress, cellular damage, and adverse impacts on the health and viability of aquatic species. Caffeine is stable in water, with a reported half-life of 100 to 240 days, which prolongs its presence in aquatic systems. As a result, effective monitoring and mitigation strategies are necessary to address its environmental impact [7].

Caffeine's environmental impact has been widely studied, leading to the development of methods to completely remove or reduce its concentration. Traditional technologies have limitations, but advanced oxidation processes (AOPs) are considered highly effective. AOPs utilize reactive oxygen species, such as hydroxyl (OH•) radicals, to degrade contaminants like caffeine into non-toxic substances [8]. One notable AOP method is heterogeneous photocatalytic degradation, which uses titanium dioxide (TiO_2) as a photocatalyst. TiO_2 is favored for its stability, non-toxicity, corrosion resistance, and affordability. In this method, TiO_2 absorbs UV light to generate hydroxyl radicals that oxidize pollutants [4, 9-10]. The efficiency of TiO_2/UV degradation is influenced by factors including organic load, catalyst amount, reactor design, temperature, pH, UV exposure time, light intensity, and ionic species [10]. TiO_2 exists in three forms: anatase, rutile, and brookite, with anatase being the preferred form due to its stability and ease of synthesis [11-12]. The sol-gel technique is commonly used to synthesize TiO_2 nanoparticles, enhancing their crystallinity and surface area [13].

This research investigated the factors affecting the effectiveness of caffeine degradation through photocatalytic processes using titanium dioxide-coated materials. The materials used are glass beads, alumina balls, and ceramic balls, which are prepared via the sol-gel method. Titanium dioxide was coated onto these prepared materials, and the effectiveness of caffeine degradation was tested under various conditions, including the absence of light, light without a photocatalyst, and light with a photocatalyst. The performance of caffeine removal was compared to determine the optimal conditions. Moreover, this approach could eliminate the extra costs associated with the removal process.

METHODOLOGY

This study investigated the photocatalytic degradation of caffeine in aqueous solutions using titanium dioxide (TiO_2)-coated materials, specifically glass beads, alumina balls, and ceramic balls. The process began with the synthesis of a TiO_2 sol using the sol-gel method. Polyvinylpyrrolidone (PVP) was dissolved in methanol and stirred for 30 min. Titanium (IV) n-butoxide and ACA were then added to the mixture under continuous stirring. The solution was then stirred further, resulting in a cloudy yellow homogeneous mixture, indicating successful sol formation. This sol was used to coat the support materials via the dip-coating technique. Each material was immersed in the TiO_2 solution to ensure uniform coating and then dried to remove residual solvents. Subsequently, the coated materials were calcined at 500°C for 2 h to enhance crystallinity, adhesion, and photocatalytic properties.

The coated materials were characterized using scanning electron microscopy (SEM) to analyze surface morphology and coating distribution, and energy-dispersive X-ray spectroscopy (EDS) to confirm elemental composition, particularly the presence of titanium and oxygen. These characterization techniques verified the successful deposition of TiO_2 on the surface of the materials.

A synthetic caffeine solution with a concentration of 3.6 mg/L was prepared to simulate wastewater contamination. The photocatalytic activity was assessed under three experimental conditions: in the absence of light (dark conditions), under UV-C light without any catalyst (photolysis), and under UV-C light in the presence of TiO_2-coated materials (photocatalysis). In all experimental setups, the reactions were conducted

in petri dishes, with each dish containing 10 mL of the caffeine solution. In the dark condition, the catalyst was added to the caffeine solution and kept in darkness to evaluate adsorption; samples were collected every 60 min for 120 min. In the photolysis experiment, only UV-C light was used without any catalyst, and samples were taken every 60 min over 360 min. In the photocatalysis experiment, the TiO_2-coated materials were first mixed with the caffeine solution in the dark until adsorption equilibrium was reached. Then, UV-C lamps were switched on, and samples were collected at 60-minute intervals for a total of 360 min.

Caffeine concentrations in all samples were determined using high-performance liquid chromatography (HPLC), with a limit of detection (LOD) of 0.005 mg/L, ensuring precise and accurate analysis. The experiments were carried out in a custom-made photocatalytic reactor chamber with dimensions of 30 cm × 60 cm × 40 cm (width × length × height). Two UV-C lamps (18 W each, Philips) were positioned 15 cm above the reaction zone, and mounted on the ceiling of the chamber. A shaker was placed at the bottom to maintain solution homogeneity during irradiation, and a ventilation fan was installed on the chamber's side to regulate the temperature by dissipating heat generated by the UV lamps.

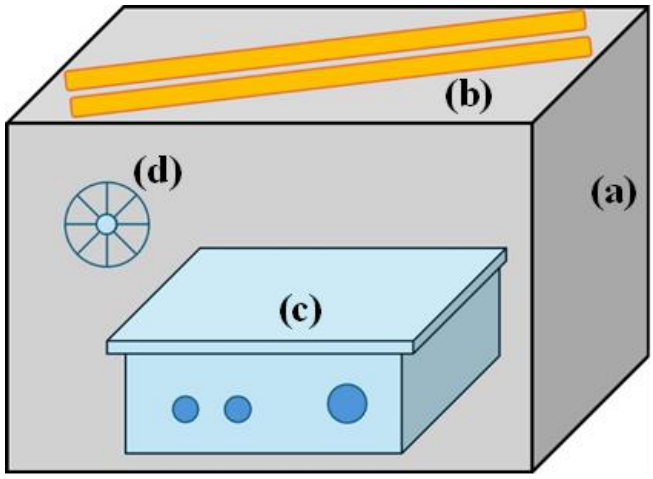


Figure 1 Photocatalytic Reactor: (a) plastic box, (b) UV-C lamp, (c) orbital shaker, and (d) ventilation fan.

RESULTS AND DISCUSSIONS

The surface morphologies of three distinct materials, namely glass beads, ceramic balls, and alumina balls, were extensively analyzed using scanning electron microscopy (SEM), and the results are illustrated in Figure 2. The SEM images clearly indicated a noticeable difference in the surface characteristics of the three materials. Specifically, the surface of the glass bead appeared relatively smooth, exhibiting a uniform texture with minimal irregularities. In contrast, the ceramic ball displayed a surface with much more pronounced roughness, with visible grooves and protrusions that significantly differentiated it from the glass bead. The alumina balls, while also displaying some rough texture, exhibited a surface that was rougher than the glass beads but somewhat smoother compared to the ceramic balls. These distinct surface textures provided the basis for further analysis of the adhesion of TiO_2 coatings on these materials.

Upon coating with titanium dioxide (TiO_2), all three materials demonstrated a thin film layer of TiO_2 adhering to their surfaces. However, the extent of TiO_2 attachment varied significantly among the tested materials. Notably, the ceramic balls demonstrated the strongest adhesion, with SEM images revealing a more uniform and robust TiO_2 coating compared to the glass beads and alumina balls. The adhesion behavior of TiO_2 on the support materials was further corroborated by energy-dispersive X-ray spectroscopy (EDS) analysis, which revealed higher titanium (Ti) content on the surface of the ceramic balls compared to the other substrates. This observation was particularly interesting, as it suggested that the surface properties of the materials played an important role in the adhesion process. Rough surfaces possess various grooves, irregularities, and microscopic features that increase the total surface area available for TiO_2 particles to attach. These surface features offer more space for the TiO_2 particles to secure themselves firmly.

Additionally, these grooves and irregularities can enhance the mechanical locking of the particles into place, making it much more difficult for the TiO_2 coating to detach over time. In cases where chemical bonding occurs, such as in the sol-gel coating techniques commonly used for TiO_2 deposition, rough surfaces offer more sites for the formation of chemical bonds between the TiO_2 and the material surface. This provides additional stability and ensures better long-term adhesion [14-15].

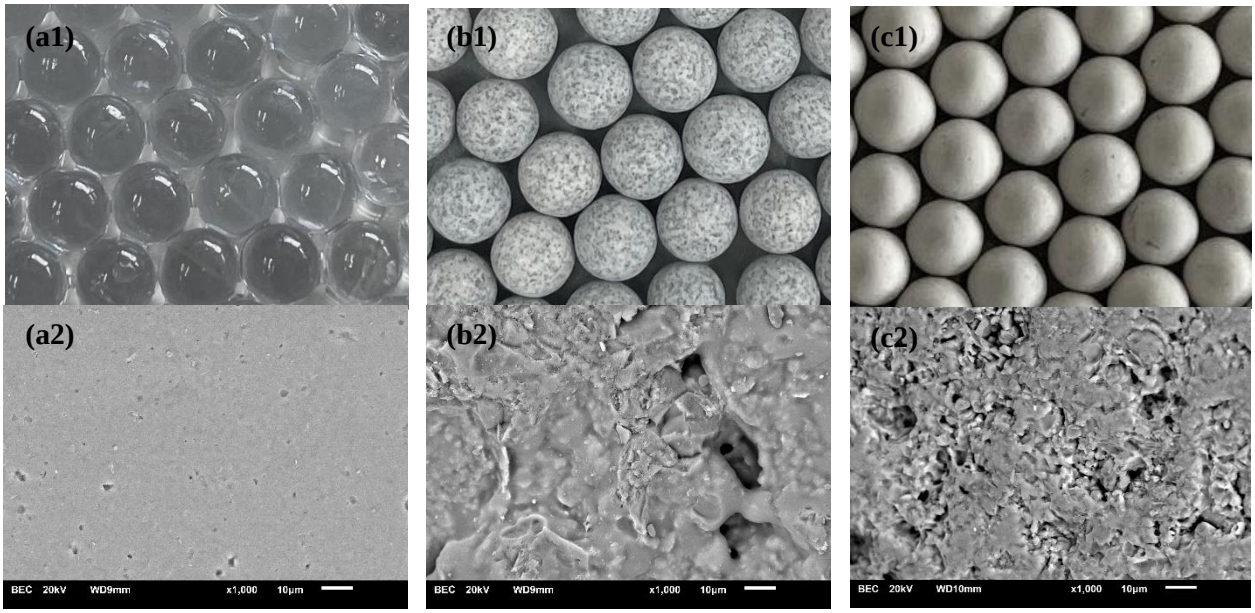


Figure 2 SEM images of bare materials and TiO_2-coated materials: (a1) glass beads, (a2) surface of a glass bead, (b1) ceramic balls, (b2) surface of a ceramic ball, (c1) alumina balls, (c2) surface of an alumina ball.

Following the TiO_2 coating, the photocatalytic degradation of caffeine using these materials was studied under UV-C irradiation, with an initial caffeine concentration of 3.6 mg/L. For the dark condition for 120 min to test caffeine adsorption, it was found that all three materials did not adsorb caffeine. As for the photolysis experiment, where UV-C light was irradiated for 6 h, no caffeine degradation was observed either, as shown in Figure 3. For the photocatalytic experiments, the samples were exposed to UV-C irradiation for 360 min in the presence of TiO_2-coated materials. The degradation of caffeine was measured and analyzed using high-performance liquid chromatography (HPLC). The results indicated that the TiO_2-coated ceramic balls achieved the highest degradation efficiency at 99.47%, followed by the TiO_2-coated glass beads at 90.19%. In contrast, the TiO_2-coated alumina balls exhibited a significantly lower degradation efficiency of 67.37%. These findings, illustrated in Figure 4, clearly demonstrate that the ceramic balls exhibited the highest photocatalytic degradation efficiency, which can be attributed to their rougher surface texture. The increased surface roughness likely provided a greater number of active sites for TiO_2 attachment, thereby enhancing the overall photocatalytic performance of the material.

The significantly higher degradation efficiency observed for the ceramic balls is attributed to their rough surface texture and material composition, which facilitated stronger TiO_2 attachment compared to the other substrates. The results confirm that surface morphology and material composition play a critical role in determining not only the adhesion of TiO_2 coatings but also the overall photocatalytic performance. This insight has important implications for the design and implementation of photocatalysts in both environmental and industrial wastewater treatment applications.

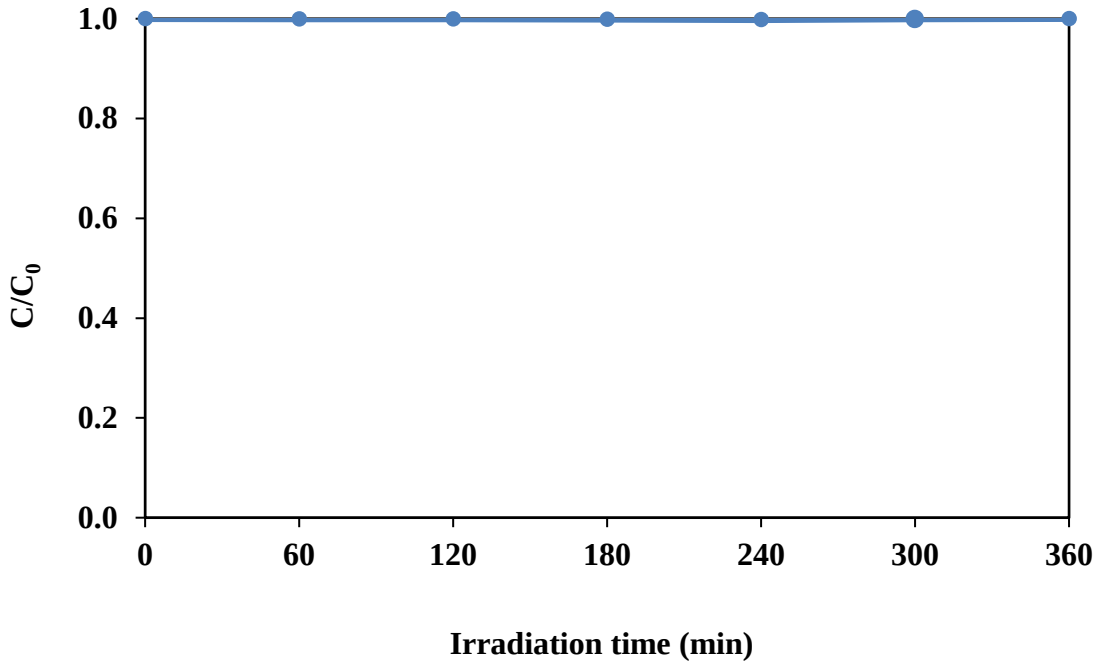


Figure 3 Photolysis degradation of 3.6 mg/L caffeine under UV-C irradiation

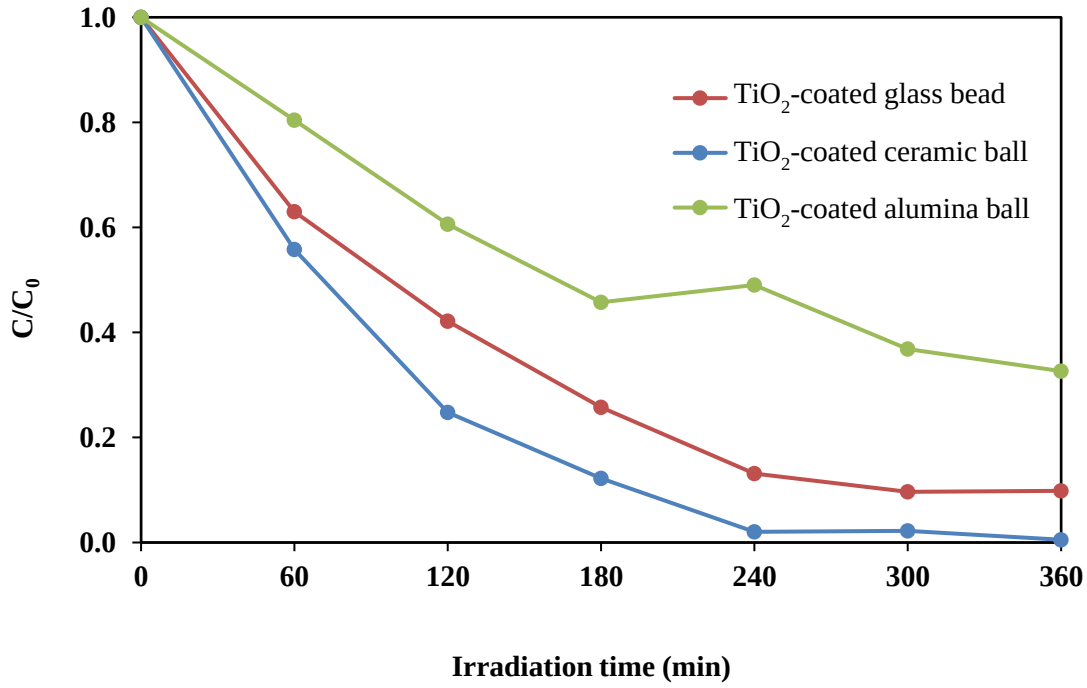


Figure 4 Photocatalytic degradation of 3.6 mg/L caffeine under UV-C irradiation.

CONCLUSION

The results showed that TiO_2-coated ceramic balls exhibited the highest caffeine degradation efficiency among the tested materials. This superior performance is attributed to the rough surface of the ceramic balls, which provides a greater surface area and more active sites for TiO_2 adhesion, resulting in better photocatalyst dispersion and stronger binding. These structural advantages facilitated more efficient photocatalytic activity under UV-C irradiation, enabling the reduction of caffeine concentration in synthetic

wastewater from an initial level of 3.6 mg/L to below 0.91 mg/L. This final concentration falls within environmentally safe limits and is considered non-toxic to aquatic organisms, particularly fish, as it does not interfere with their foraging behavior or reproductive cycles. As a result, TiO_2-coated ceramic balls are a promising material for integration into wastewater treatment systems aimed at removing pharmaceutical contaminants such as caffeine. Their high photocatalytic efficiency, combined with the material's durability and relatively low cost, also presents a potential for cost-effective and sustainable treatment solutions. In addition, the use of ceramic balls minimizes catalyst loss and simplifies recovery, offering practical advantages for long-term operations. Future research should focus on optimizing the coating process, assessing catalyst reuse potential, and investigating the performance of these materials in actual industrial wastewater. Evaluating scalability, reactor design, and long-term environmental impact will be critical to advancing the practical application of TiO_2-coated ceramic balls in full-scale wastewater treatment plants.

ACKNOWLEDGEMENT

This work was partly supported by King Mongkut's University of Technology Thonburi (KMUTT), Thailand Science Research and Innovation (TSRI), and National Science, Research and Innovation Fund (NSRF) Fiscal year 2025 Grant number FRB680074/0164.

REFERENCE

[1] Raj R., et al. (2021) Removal of caffeine from wastewater using electrochemical advanced oxidation process: A mini review. *Case Studies in Chemical and Environmental Engineering*, 4, 100129.

[2] Korekar G., et al. (2019) Occurrence, fate, persistence, and remediation of caffeine: A review. *Environmental Science and Pollution Research*, 27(28), 34715–34733.

[3] Buerge I. J., et al. (2003) Caffeine, an anthropogenic marker for wastewater contamination of surface waters. *Environmental Science & Technology*, 37(4), 691–700.

[4] Ghosh M., et al. (2019) Solar photocatalytic degradation of caffeine with titanium dioxide and zinc oxide nanoparticles. *Journal of Photochemistry and Photobiology A: Chemistry*, 377, 1–7.

[5] Castillo M., et al. (2021) Occurrence and risk of caffeine in aquatic environments: A review. *Environmental Advances*, 5, 100103.

[6] Muangmora R., et al. (2023) Photocatalytic degradation of pharmaceuticals from water using nitrogen-doped titanium dioxide coated on fiberglass cloth. *Journal of Cleaner Production*, 397, 136487.

[7] Li S., et al. (2020) Risks of caffeine residues in the environment: Necessity for a targeted ecopharmacovigilance program. *Chemosphere*, 243, 125343.

[8] Kanakaraju D., et al. (2018) Advanced oxidation process-mediated removal of pharmaceuticals from water: A review. *Journal of Environmental Management*, 219, 189–207.

[9] Akpan U., & Hameed B. (2009) Parameters affecting the photocatalytic degradation of dyes using TiO_2-based photocatalysts: A review. *Journal of Hazardous Materials*, 170(2–3), 520–529.

[10] Sujatha G., et al. (2020) UV Light-Irradiated photocatalytic degradation of coffee processing wastewater using TiO_2 as a catalyst. *Environments*, 7(6), 47.

[11] Pelaez M., et al. (2012) A review on the visible light active titanium dioxide photocatalysts for environmental applications. *Applied Catalysis B: Environmental*, 125, 331–349.

[12] Scarpelli D., et al. (2018) Anatase to rutile phase transition in TiO_2 nanocrystals: Effects on the photocatalytic and antibacterial activities. *Journal of Materials Science*, 53(17), 12720–12730.

[13] Singh J., & Mehata M. S. (2019) Recent progress in sol–gel synthesis and applications of TiO_2: A review. *Journal of Sol-Gel Science and Technology*, 92(1), 84–104.

[14] Hosseini, Z.S., Haghparast, F., Masoudi, A.A., and Mortezaali, A. 2021. Enhanced visible photocatalytic performance of un-doped TiO2 nanoparticles thin films through modifying the substrate surface roughness. *Materials Chemistry and Physics* 279: 125530.

[15] Kumar, A., Saxena, V.K., Thangavel, R., and Nandi, B.K. 2022. A dual effect of surface roughness and photocatalysis of crystalline TiO2-thin film for self-cleaning application on a photovoltaic covering glass. *Materials Chemistry and Physics* 289: 126427.

20R5-13

Preliminary Study of Benzalkonium Chloride on Growth Rate and Phosphorus Removal Capacity of *Chlorella vulgaris* in Effluent Wastewater

Vicheka Chhoeurn[1*], Thunyalux Ratpukdi[2]

[1*]Graduate student; [2] Associate Professor, Department of Environmental Engineering, Faculty of Engineering, Khon Kaen University, Khon Kaen 40002, Thailand
[*]*Phone : 0970057869, E-mail : vicheka.c@kkumail.com*

ABSTRACT

Effluent wastewater is a major environmental concern due to its high nutrient content, particularly phosphorus, which can promote algal blooms and lead to eutrophication. To mitigate this issue, phosphorus—one of the key nutrients responsible for eutrophication—must be effectively controlled. In recent years, especially during the COVID-19 pandemic, the use of antimicrobial agents such as benzalkonium chloride (BKC) has increased significantly. These compounds may impact biological processes in wastewater treatment, including nutrient removal by microalgae. The objective of this study is to investigate the ability of *Chlorella vulgaris* to remove phosphorus in the presence of BKC. In this study, *C. vulgaris* was cultured under different BKC concentrations. Preliminary tests showed that cell viability was negatively affected at BKC concentrations ranging from 1 to 3 mg/L, whereas a low concentration (0.05 mg/L) slightly promoted algal growth. In a 12-day experiment, phosphorus removal efficiency was compared between two conditions: 3 mg-P/L with 0.1 mg-BKC/L and 3 mg-P/L without BKC. The results showed that *C. vulgaris* removed 19.28% of phosphorus without BKC and 15.46% with BKC. These findings indicate that even in the presence of low concentrations of BKC, *C. vulgaris* retains the ability to remove phosphorus, with no significant difference observed between the two conditions. This study suggests that microalgae-based treatment systems may remain effective for phosphorus removal despite the presence of antimicrobial agents like BKC in wastewater.

Keywords: BKC, Effluent Wastewater, *Chlorella vulgaris*

INTRODUCTION

The treated effluent domestic wastewater one of the major concerns in aquatic environmental due to the nutrients in discharge water. The concentration on nitrogen (N) and phosphorus (P) for the treated effluent were (6.6 to 11.46) mg/L and (0.62 to 1.62) mg/L, respectively [1]. Excessive amount of N and P in the water ecosystem could promotes eutrophication also known as algae-bloom. Between these two nutrients, phosphorus is a main limiting nutrient for mitigating eutrophication [2]. Concentrations of phosphorus higher than 0.1 mg P/L are sufficient to cause eutrophication [3].

Many studies demonstrate that the use of microalgae for the removal of nitrogen and phosphorus is a great potential due to the ability of microalgae that can uptake nitrogen and phosphorus to produce biomass [4].

Recently, the use of antimicrobial agents has increased particularly, during and after the COVID-19 pandemic. Benzalkonium chlorides (BKC) is one the antimicrobials that have been used as disinfectants against viruses, bacteria, algae, and fungi due to their long half-life. The antibacterial mechanism of BKC is generally believed to involve by their distinct hydrophobic and hydrophilic properties, which interact with the negatively charged cell membranes, leading to cell disruption and inhibition of cell division [5].

BKC as disinfectants have been detected in various sources, including municipal wastewater, surface water, groundwater, reclaimed water, sludge, sediment, roof runoff, and dust collected from residential homes in 13 counties. Concentrations reached a maximum of 30 mg/L in roof runoff water samples and 421 µg/g in indoor dust soil samples [5]. The presence of BKC residue in wastewater has an impact on algae. [6] found that 3-48 mg/L of dodecyl dimethyl benzyl ammonium chloride (one of BKC) significantly inhibited the photosynthesis of *Chlorella sp.* However, the effect of BKC on nutrient uptake, particularly P, has not been investigated.

Therefore, this study aims to determine the inhibitory effect of BKC on the growth of *Chlorella vulgaris* and evaluate the effects of BKC on the phosphorus removal potential of *Chlorella vulgaris*. *Chlorella sp.* was chosen as it is well-known green microalgae that has been reported to uptake phosphorus in the natural environment and wastewater effectively. Moreover, *Chlorella vulgaris* is a common species of green algae with a small cell of globular structure that is highly adaptable to various environmental conditions and produces high biomass [7].

METHODOLOGY

The standard Blue-Green 11 Medium (BG 11) was used as the medium for microalgae growth and synthesis wastewater while N and P were adjusted to obtain the concentration needed for experiments. BKC (8% w/v) was obtained from K.C. Chemitech Co., Ltd., Thailand.

Chlorella vulgaris TISTR8580 was purchased from Thailand Institute of Scientific and Technological Research, Thailand. *Chlorella vulgaris* was cultivated at room temperature in an incubator under 12h light on and 12h off condition. *C. vulgaris* was grown in 300 mL of sterile BG 11 medium using a 500-mL Erlenmeyer flask. Microalgae cells used in the experiments were collected at the exponential growth period. The microalgae cells were centrifuged 5000 rpm for 5 min and supernatant was discarded. Then, the microalgae cells were resuspended in deionized water, followed by centrifuging. This rinsing step was repeated 3 times.

The experiment in this study was divided into three main parts. The first part aimed to investigate the effect of BKC on the viability of *C. vulgaris* under a nutrient-free condition (only deionized water). The second part preliminary investigated P removal efficiency with and without BKC. BG11 medium was used as synthetic wastewater, with N adjusted to 10 mg/L and P concentration of 3.0 mg/L. The BKC concentration of 0.1 mg/L was used.

Algae cell number was counted using hemocytometer. To analyze P, the Stannous chloride method combined with persulfate digestion (4500-P), Standard Methods for the Examination of Water and Wastewater, is used. Moreover, the optical density at 680 nm was used to establish a relationship with the microalgae cell number.

RESULTS AND DISCUSSIONS

Figure 1 illustrates microalgae *C. vulgaris* growth under BKC exposure. The control and 0.05 mg/L BKC conditions showed a similar pattern with a slight decrease in cell number, while 0.1 mg/L of BKC resulted in a more negative decrease in cell compared to control. At higher concentrations of 1 mg/L and 3 mg/L, a significant reduction of cells was observed. These results indicate that high BKC concentrations lead to pronounce declining in cell numbers.

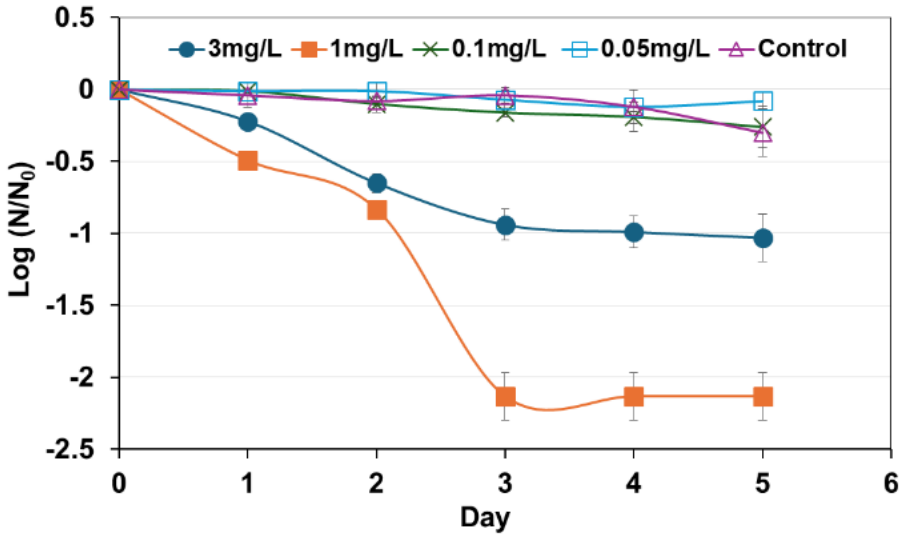


Figure 1 Effect of BKC on *C. vulgaris* cell number in deionized water**.**

Figure 2 shows the viability of *C. vulgaris* in response to BKC. A BKC concentration of 0.05 mg/L had no negative effect on cell viability (82.48%) and even appeared to promote cell growth. In contrast, 0.1 mg/L reduced viability to 50%, which was similar to the control (no BKC). At higher concentrations of 1 mg/L and 3 mg/L, cell viability decreased sharply to 0.59% and 9.42%, respectively. Since BKC at 0.1 mg/L did not significantly affect cell viability, this concentration was selected for the subsequent experiment on phosphorus removal.

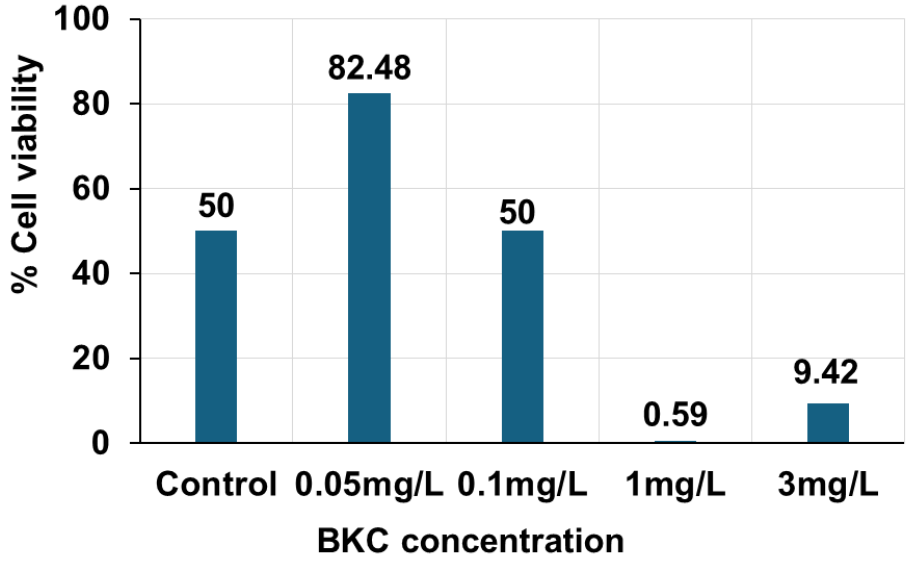


Figure 2 Microalgae cell viability at day 5.

For cell numbers in BG11 medium with and without BKC (P = 3.0 mg-P/L), it was found that BKC (0.1 mg/L) did not affect the cell number compared to the BG11 medium without BKC (Figure 3). The results in Table 1 showed the phosphorus removal by *C. vulgaris* in BG11 media with and without BKC (0.1 mg/L). Over 12 days, phosphorus removal efficiency reached 19.28% without BKC and 15.46% with BKC, suggesting a slight inhibitory effect of BKC on phosphorus uptake. However, based on a paired t-test, the difference in phosphorus removal was not statistically significant (p = 0.48). Despite this minor difference, *C. vulgaris* demonstrates resilience in phosphorus removal even in the presence of low BKC concentrations.

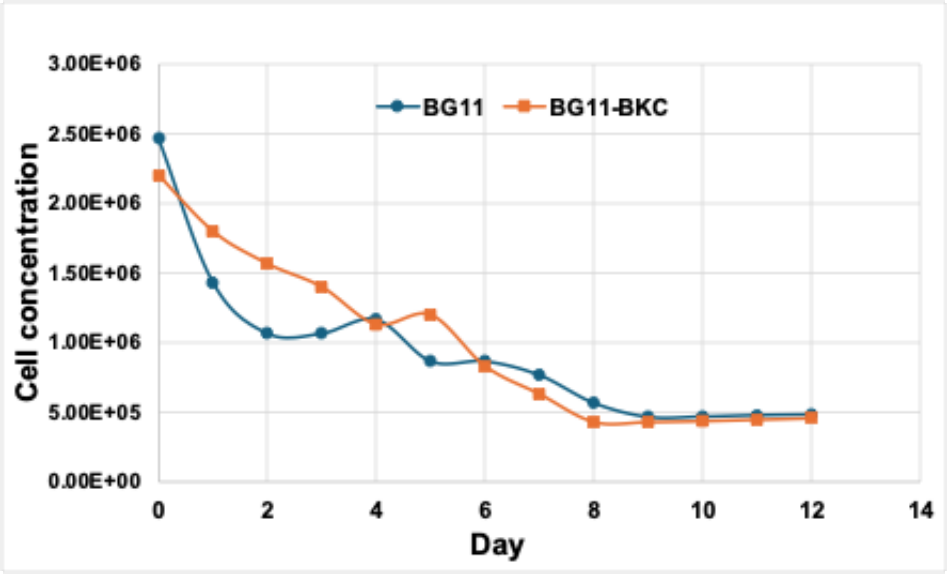


Figure 3 Comparison of *C. vulgaris* cell number in BG11 Medium with and without BKC (P = 3.0 mg-P/L, BKC = 0.1 mg/L).

Table 1 Phosphorus removal by *C. vulgaris* with the presence of BKC

Day	No BCK		BKC 0.1 mg/L	
	P conc. (mg/L)	% Removal	P conc. (mg/L)	% Removal
0	2.80 ± 0.15	-	2.91±0.11	-
3	2.71 ± 0.06	3.21	2.90±0.15	0.34
6	2.74 ± 0.12	2.14	2.60±0.20	10.65
9	2.50 ± 0.18	10.71	2.56±0.20	12.02
12	2.26 ± 0.17	19.28	2.46±0.07	15.46

(BG11 Medium, P = 3.0 mg-P/L, ± is standard deviation)

To further quickly observe the cell numbers in our experiment we developed the relationship between cell numbers of *C. vulgaris* and optical density at wavelengths 680 nm (OD680). It was found that *C. vulgaris* cell number has a good correlation with the OD680 with R^2 of 0.897 (Figure 4).

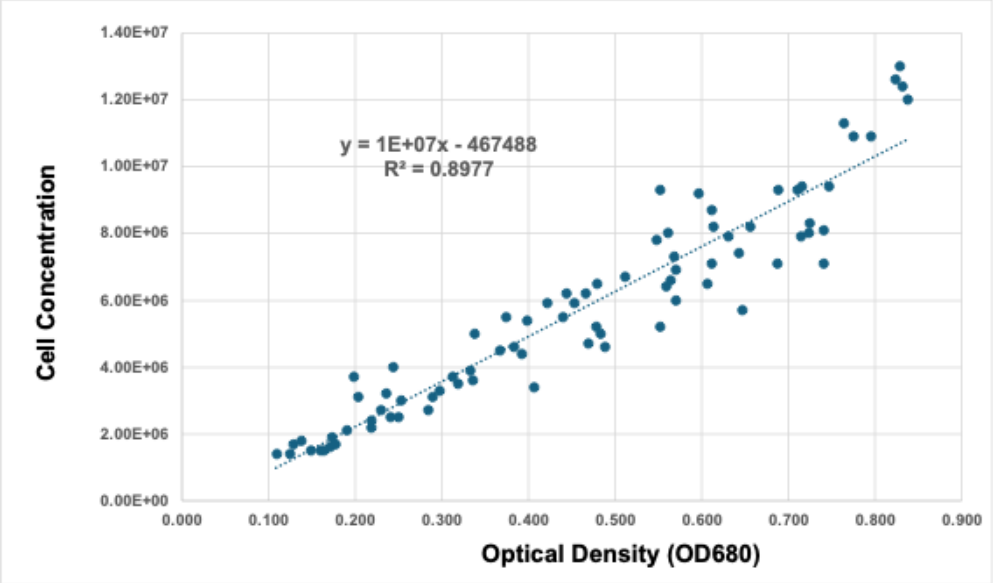


Figure 4 The correlation between cell concentration and optical density measured at 680 nm.

CONCLUSION

Benzalkonium chloride (BKC) significantly impacts *Chlorella vulgaris* at concentrations above 0.1 mg/L, severely reduced cell viability. While low BKC concentrations (0.1 mg/L) only slightly inhibited phosphorus removal efficiency, the microalgae demonstrated resilience in nutrient uptake capabilities. These findings suggest *C. vulgaris* can potentially be utilized in wastewater treatment systems with low BKC concentrations. As mentioned earlier, this is preliminary study. To obtain the more comprehensive effect of BKC, higher BKC concentrations with different P concentrations should be investigated.

ACKNOWLEDGEMENT

I gratefully acknowledge the Faculty of Engineering, Khon Kaen University, for providing access to laboratory facilities and technical support. Special thanks are extended to Assoc. Prof. Dr. Thunyalux Ratpukdi for his invaluable guidance and encouragement throughout this study. This research was fully supported by the KKU Scholarship for ASEAN and GMS Countries Personnel.

REFERENCE

[1] Noophan, P., Paopuree, P., Kanlayaras, K., Sirivithayapakorn, S., & Techkarnjanaruk, S. 2009. Nitrogen Removal Efficiency at Centralized Domestic Wastewater Treatment Plants in Bangkok, Thailand. Environment Asia. 2(2):30-35.

[2] Schindler, D. W.; Carpenter, S. R.; Chapra, S. C.; Hecky, R. E.; Orihel, D. M. Reducing Phosphorus to Curb Lake Eutrophication is a Success. *Environ. Sci. Technol.* **2016**, *50* (17), 8923–8929. https://doi.org/10.1021/acs.est.6b02204.

[3] Lavrinovičs, A., Mežule, L., & Juhna, T. 2020. Microalgae starvation for enhanced phosphorus uptake from municipal wastewater. Algal Research, 52: 102090.

[4] Li, G., Bai, X., Li, H., Lu, Z., Zhou, Y., Wang, Y., Cao, J., & Huang, Z. (2019). Nutrients removal and biomass production from anaerobic digested effluent by microalgae: A review. In *International Journal of Agricultural and Biological Engineering* (Vol.12, Issue 5, pp. 8–13). Chinese Society of Agricultural Engineering. https://doi.org/10.25165/j.ijabe.20191205.3630

[5] Liao, M., Wei, S., Zhao, J., Wang, J., & Fan, G. 2023. Risks of benzalkonium chlorides as emerging contaminants in the environment and possible control strategies from the perspective of ecopharmacovigilance. Ecotoxicology and Environmental Safety. 266: 115613.

[6] Ge, Y., Chen, J., Xue, Y., Xing, W., Zhang, L., Lu, X., Liu, J., Li, F., & Yang, Q. 2024. Elimination of inhibitory effects of dodecyl dimethyl benzyl ammonium chloride on microalgae in wastewater by cocultivation with a newly screened microbial consortium. Science of the Total Environment, 919: 170676.

[7] Magee, E., Zhou, W., Yang, H., & Zhang, D. 2013. The effect of biochar application in microalgal culture on the biomass yield and cellular lipids of chlorella vulgaris. In Chemeca 2013: Challenging Tomorrow. Engineers Australia. https://search.informit.org/doi/10.3316/informit.882702302963923.

20R5-14

Treatment of campus wastewater and biomass production using wastewater treatment pond with duckweed

K. Ruengpattanawiwat[1*], C. Chiemchaisri[2], W. Chiemchaisri[2], T. Toyama[3], K. Mori[3], M. Morikawa[4]

[1]Graduate student, Department of Environmental Engineering, Faculty of Engineering, Kasetsart University, Bangkok, Thailand; [2]Professor, Department of Environmental Engineering, Faculty of Engineering, Kasetsart University, Bangkok, Thailand, [3]Professor, Graduate Faculty of Interdisciplinary Research, University of Yamanashi, Kofu, Japan, [4]Professor, Graduate School of Environmental Science, Hokkaido University, Sapporo, Japan*
[*]Phone: 0957195816, E-mail: kittin.ru@ku.th

ABSTRACT

This study investigates the use of duckweed (*Spirodela polyrhiza)* for campus wastewater treatment at the central wastewater treatment system of Kasetsart University. The research focuses on duckweed biomass production and organic and nutrient removals from wastewater. The experiment was carried out in bench-scale units operated in parallel comparing the treatment unit without and with duckweed. In both units, hydraulic retention time (HRT) was controlled at 4 days. The experiment unit with duckweed was operated with 100% duckweed coverage and duckweed biomass was harvested twice a week. The experimental results revealed improved organic carbon and nutrient removals in the duckweed unit. In terms of biomass production, the average biomass production rate was 6.5 g-dry weight/m^2/day during which average chemical oxygen demand (COD), total Kjeldahl nitrogen (TKN), and phosphate (PO_4^{3-}) removal efficiencies were 55%, 30%, and 25%, respectively. These findings indicate that duckweed can enhance the performance of wastewater treatment while offering the additional benefit of generating biomass for further utilization.

Keywords: duckweed; *Spirodela polyrhiza*; campus wastewater; wastewater treatment; biomass production

INTRODUCTION

Duckweed, a rapidly growing aquatic plant, is an eco-friendly solution for wastewater treatment and biomass production due to its high nutrient uptake efficiency. It effectively removes key nutrients such as nitrogen and phosphorus which helps prevent environmental issues such as eutrophication caused by excess nutrients in water. In wastewater treatment ponds, suspended solids (SS) are removed through sedimentation whereas biodegradation of organic substances takes place in bulk water. Duckweed coverage at the pond surface may limit oxygen diffusion, but its roots promote oxygen transfer and support the biodegradation of organic matter at the rhizosphere. Meanwhile, nitrogen removal occurs through duckweed uptake, ammonia volatilization, and nitrification-denitrification reaction at the duckweed root zone. Previous studies have shown that duckweed, such as *Lemna sp.* and *Spirodela* sp. reduce organic substances in terms of biochemical oxygen demand (BOD), chemical oxygen demand (COD), solid particles in terms of turbidity, and total suspended solids as well as nutrients such as nitrate and phosphate [1-3]. The growth rate of duckweed, wastewater concentration, and climate conditions significantly affected nutrient removal efficiencies. The pilot-scale research with *Lemna* sp. also highlighted that biofilm in the system enhanced nitrogen removal by supporting nitrifying and denitrifying bacteria [4]. Despite its known benefits in wastewater treatment, the performance of duckweed-based wastewater treatment can vary depending on its operating and environmental conditions, e.g. operation mode, duckweed species, influent characteristics, temperature, etc. [4,5]. To realize actual performance on pollutant removals and biomass production under local operating conditions in Thailand, this study was performed using *Spirodela polyrhiza* applied to the treatment of real wastewater of Kasetsart University, Bangkhen campus. The study focused on examining the role of duckweed in enhancing organic and nutrient removals as well as its growth and biomass production during its application in wastewater treatment.

METHODOLOGY

Experimental system

Two plug-flow type wastewater pond units (1.38 m length, 0.83 m width, 0.20 m water depth) having a working volume of 200 l each with their schematic shown in Figure 1 are installed. The first unit (R1) is the control experiment operating without duckweed and the second unit (R2) with duckweed provided over its entire water surface (Figure 2). The experimental units were fed continuously with campus wastewater at a 50 l/d flow rate to maintain a hydraulic retention time (HRT) of 4 days in the system. The chemical characteristics of campus wastewater are as follows, pH of 7.5 - 7.9, COD of 90 – 150 mg/l, SS of 30 – 60 mg/l, TKN of 30 - 60 mg/l, PO_4^{3-} of 0.5 - 4 mg/l. During the operation period of 3 months, light intensity supplied to the units was determined as 8000 – 20000 lux whereas dissolved oxygen (DO) in the bulk water varied between 0.5-2 mg/l.

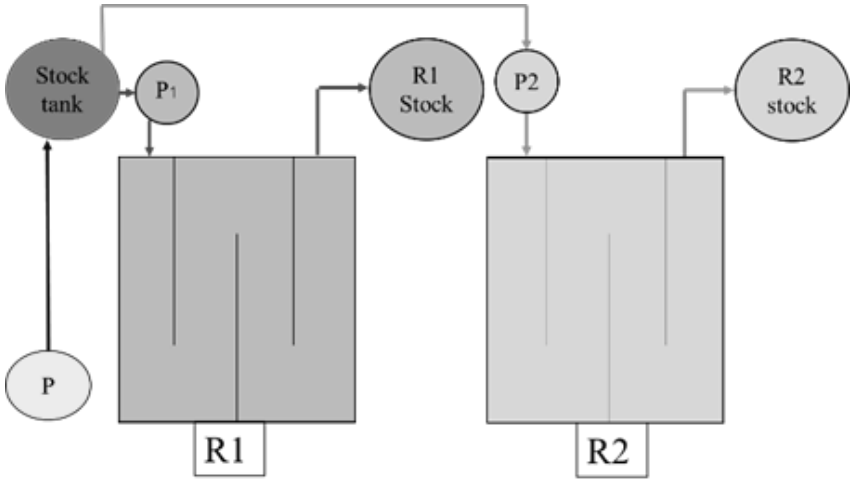


Figure 1 Schematic of Reactor 1 (R1) and Reactor 2 (R2)

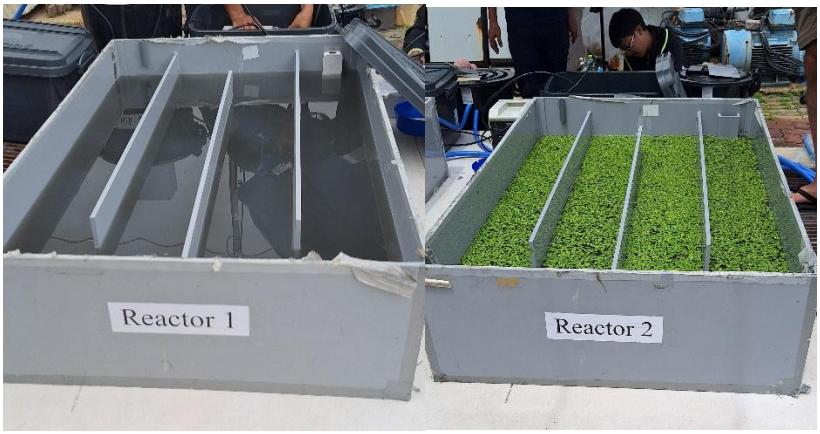


Figure 2 Photographs of R1 and R2

Duckweed biomass production

Indigenous duckweed (*Spirodela polyrhiza*) obtained from the effluent pond of a food processing factory in Thailand (Figure 3) was acclimatized to the campus wastewater for about 2 months before using in the experiment unit. At the beginning of the experiment, the duckweed was provided covering 100% of the water surface in R2, and its biomass was allowed to increase naturally during the experiment. To determine and maintain the growth of duckweed, duckweed biomass was measured twice a week during which regular harvesting was performed to maintain the biomass at 100% of water surface coverage. The harvested duckweed was measured for its wet and dry (at 65^{o}C overnight) weight and biomass production rate was determined in g dry weight/m^2 of reactor surface area/day unit.



Figure 3 *Spirodela polyrhiza* duckweed used in this study

Water quality analysis

Influent and effluent water qualities were analyzed twice a week to determine chemical oxygen demand (COD), total Kjeldahl nitrogen (TKN), and phosphate (PO_4^{3-}) concentrations to evaluate their removal efficiencies. Moreover, pH, DO, electrical conductivity (EC), and total dissolved solids (TDS) were also regularly monitored. The analyses were performed following the Standard Method for the Examination of Water and Wastewater [6].

RESULTS AND DISCUSSIONS

Duckweed biomass production in campus wastewater

The growth of *Spirodela polyrhiza* duckweed was found to increase during the initial period and became relatively stable after 9 days of operation. Its biomass production rate had an average value of 6.5 g-dry weight/m^2/day, which is equivalent to 23.7 ton-dry weight/ha/year) over the whole experimental period whereas the highest biomass production of 9 g-dry weight/m^2/day was observed at 37 days (Figure 4). At this growth rate, the doubling time of duckweed biomass was determined as 3.4 days. Compared to previous studies, this growth rate and doubling time fall within the normal range in wastewater [7], similar to that reported for diluted sewage [8].

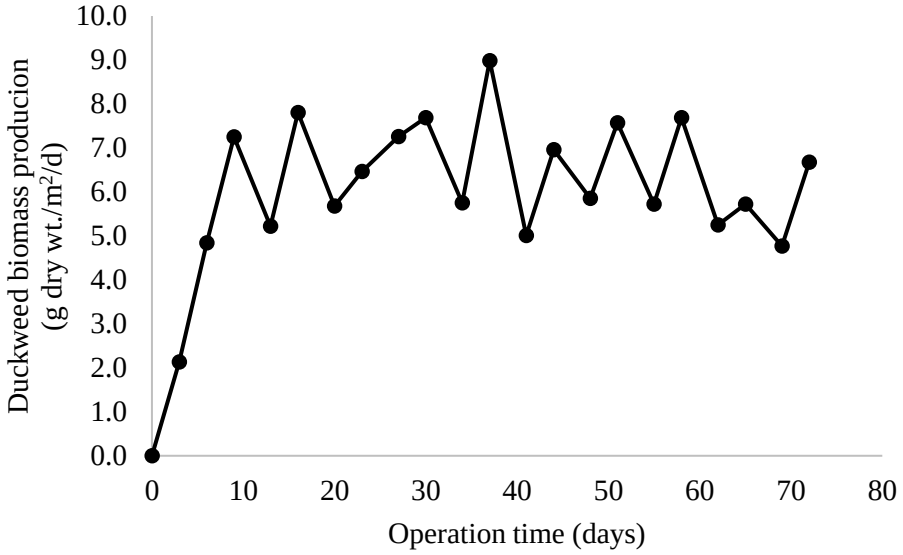


Figure 4 Duckweed biomass production

Treatment performance in duckweed pond

Figure 5 shows the variations of COD concentrations in the influent and effluent of R1 and R2 during the experimental period. Even though the influent was found to highly fluctuated, especially at the beginning of the experiment, the effluent concentrations were relatively stable especially in R2 with the presence of duckweed. A stable operation could be achieved after about 2 weeks of operation during which organic removals in terms of COD in duckweed pond (R2) were reached at 50–65% level, significantly higher than those in the control system (R1) which were kept at about 30-40%. These results suggest that the presence of duckweed helps improve organic removals during its treatment, possibly through enhanced aerobic biodegradation of organic substances by the associated microorganisms to duckweed roots. Li et al [9] revealed that the presence of *Spirodela* sp. duckweed led to improved organic removal and the degree of its humification during wastewater treatment. Ozengin and Elmaci [10] also observed a gradual improvement of organic (COD) removal by duckweed (*Lemna minor* L.) treating municipal wastewater for 20 days during which microorganisms were gradually adapting to wastewater.

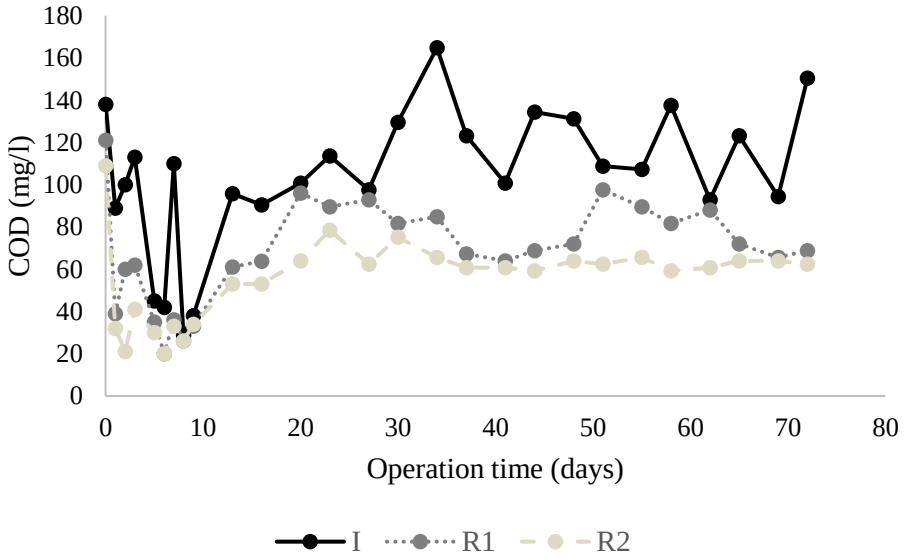


Figure 5 Variations of COD concentrations in the influent (I) and effluent from the experimental units without (R1) and with duckweed (R2)

Nutrient removal efficiencies of the duckweed pond in terms of TKN and PO_4^{3-} were evaluated and compared with the control system. Figures 6 and 7 present the variations in TKN and PO_4^{3-} in the influent and effluent of R1 and R2 over the operation period, respectively. While the influent TKN fluctuated significantly in a range of 27-59 mg/l, the effluent concentrations from both reactors varied correspondingly. During the experimental period, stable TKN removals were achieved at 25-35% in R2, better than those of 20-30% achieved in R1. Enhancement of N removal could be attributed to its uptake for duckweed biomass production. For PO_4^{3-}, its influent concentrations tend to decrease over time from 4 to 1 mg/l during which the duckweed pond removed about 15-20% whereas they were 5-10% in the pond without duckweed. Relatively low concentrations and removal percentages of PO_4^{3-} coincident with stable duckweed biomass production observed after 20 days of the experiment (Figure 4) suggest that phosphorus could be the limiting factor of duckweed growth in this study.

Table 1 summarizes the treatment performance in terms of COD, TKN, and PO_4^{3-} in R1 and R2 during its stable operation. It can be clearly seen that R2 exhibited superior performance in pollutant removals across all three parameters. Therefore, the study reveals the beneficial effect of duckweed in the treatment of campus wastewater whereas duckweed biomass can also be achieved as its by-product.

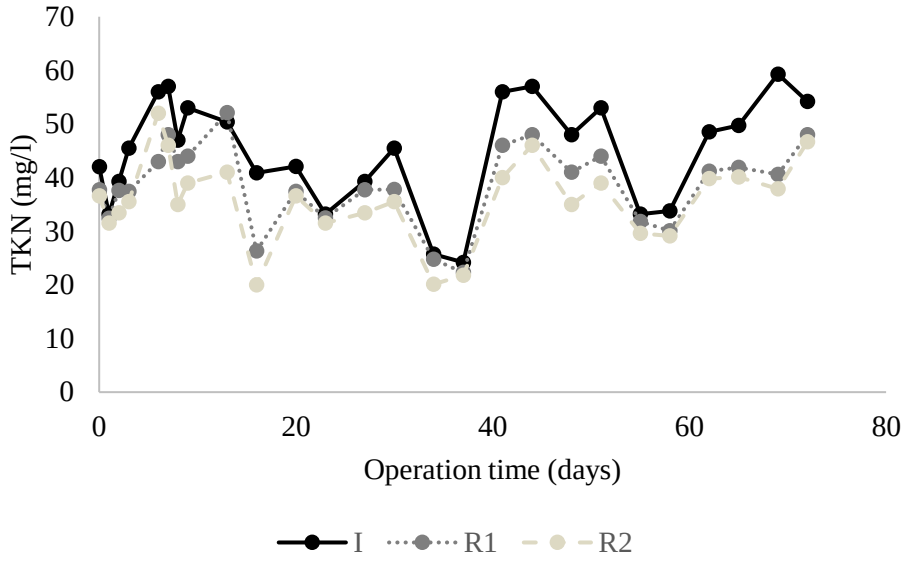


Figure 6 Variations of TKN concentrations in the influent (I) and effluent from the experimental units without (R1) and with duckweed (R2)

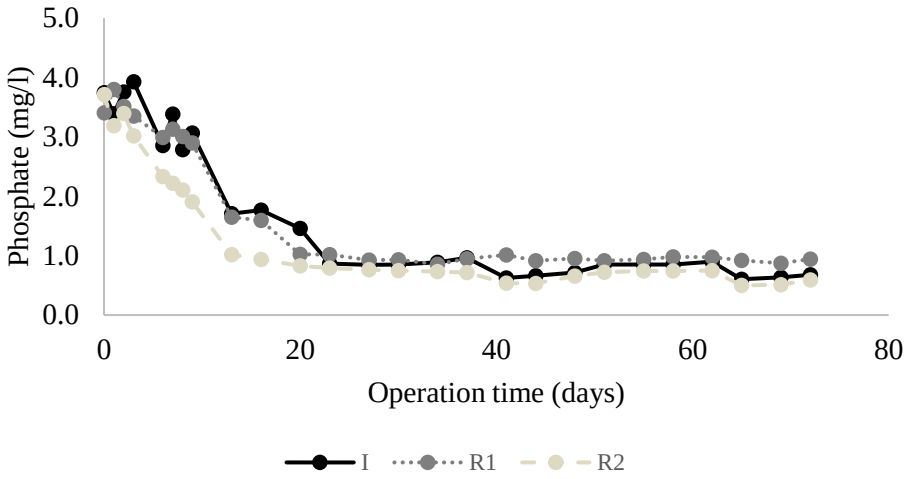


Figure 7 Variations of PO_4^{3-} concentrations in the influent (I) and effluent from the experimental units without (R1) and with duckweed (R2)

Table 1 Average COD, TKN, and PO_4^{3-} concentrations and their removals (%R) in the experimental units without (R1) and with duckweed (R2) during steady operation

	COD (mg/l)	%R	TKN (mg/l)	%R	PO_4^{3-} (mg/l)	%R
Influent	103.7±33.7		45.3±10.4		1.7±1.2	
Effluent R1	78.0±12.3	33.0±16.1	39.0±8.3	13.0±9.1	1.6±0.9	6.8±4.2
Effluent R2	63.1±6.2	45.9±9.0	35.4±7.8	21.0±10.0	1.1±0.7	21.3±11.5

CONCLUSION

Spirodela polyrhiza duckweed was found successfully applied to purify the campus wastewater of Kasetsart University. A maximum biomass production rate of 9 g-dry weight/m^2/day was achieved at day 37 of operation whereas it was averaged at 6.5 g-dry weight/m^2/day over the entire experimental period. This biomass production was possibly limited by the availability of PO_4^{3-} in the influent.

In terms of treatment efficiency, the treatment pond with duckweed achieved COD removal of up to 65%, along with TKN and PO_4^{3-} removal of 35% and 30%, respectively. They are considerably better than those in the pond without duckweed. These findings indicate that duckweed can contribute effectively to the reduction of pollutants in wastewater, highlighting its potential for environmental applications. This study implies that *Spirodela* sp. can be considered a sustainable and environmentally friendly option for wastewater remediation. Thus, duckweed-based wastewater treatment systems not only improve water quality performance but also contribute to resource recovery in terms of biomass production.

ACKNOWLEDGEMENT

This work was carried out as an activity under a research project entitled Development of the Duckweed Holobiont Resource Values towards BCG Economy supported by the Japan International Cooperation Agency (JICA) and Japan Science and Technology Agency (JST). The authors would like to thank the central wastewater treatment system of Kasetsart University for providing campus wastewater in this study.

REFERENCE

[1] Dalu, J.M. and Ndamba, J. (2003). Duckweed based wastewater stabilization ponds for wastewater treatment (a low cost technology for small urban areas in Zimbabwe). Physics and Chemistry of the Earth, 28, 1147–1160.

[2] Al-Hashimi, M.A. and Joda, R.A. (2010). Treatment of domestic wastewater using duckweed plant. Journal of King Saud University- Engineering Sciences, 22(1), 11-18.

[3] Xu, J. and Shen, G. (2011). Growing duckweed in swine wastewater for nutrient recovery and biomass production. Bioresource Technology, 102, 848–853.

[4] Dinh, T.T.U., Soda, S., Nguyen, T.A.H., Nakajima, J. and Cao, T.H. (2020). Nutrient removal by duckweed from anaerobically treated swine wastewater in lab-scale stabilization ponds in Vietnam. Science of the Total Environment, 722, 137854.

[5] Zhao, Y., Fang, Y., Jin, Y., Huang, J., Ma, X., He, K., He, Z., Wang, F. and Zhao, H. (2015). Microbial community and removal of nitrogen via the addition of a carrier in a pilot-scale duckweed-based wastewater treatment system. Bioresource Technology, 179, 549–558.

[6] APHA, AWWA, WEF (2005). Standard Methods for the Examination of Water and Wastewater. 21th Edition. New York.

[7] Mohedano, R.A., Costa R.H.R., Taraves, F.A. and Belli Filho, P. (2012). High nutrient removal rate from swine wastes and protein biomass production by full-scale duckweed ponds. Bioresource Technology, 112, 98-104.

[8] Iwano, H., Hatohara, S., Tagawa, T., Tamaki, H., Li, Y. and Kubota, K. (2020). Effect of treated sewage characteristics on duckweed biomass production and microbial communities. Water Science and Technology, 82(2), 292-302.

[9] Li, L., Liu, M., Wu, M., Jiang, C., Chen, X., Ma, X., Liu, J., Li, W., Tang, X. and Li, Z. (2017). Effects of duckweed (*Spirodela polyrhiza*) remediation on the composition of dissolved organic matter in effluent of scale pig farms. Journal of Environmental Sciences, 55, 247-256.

[10] Ozengin N. and Elmaci A. (2007). Performance of duckweed (*Lemna minor* L.) on different types of wastewater treatment. Journal of Environmental Biology, 28(2), 307-314.

20R5-15

Development of Modified Bio-Char from Coconut Husk Base Material Used for Nutrient Removals

Shoaib Salman[1*], Nawatch Surinkul[2], Trakarn Prapaspongsa[3], Kritsanat Surakit[4], and Sri Shalini Sathyanarayanan[5]

[1]Master Student; [2]Assistant Professor, [3]Associate Professor, [4] Lecturer, [5]Foriegn Expert*
Department of Civil and Environmental Engineering, Faculty of Engineering, Mahidol University, Salaya, Nakhon Pathom, Thailand.
[*]Phone: +66 627197003, E-mail: shoaib.sal@student.mahidol.edu

ABSTRACT

Nutrient contamination, specifically the excess concentrations of ammonia and phosphorus in water bodies, has increased the demand for sustainable water treatment solutions. This research investigates the development of modified Biochar derived from coconut husks for adsorbent, a sustainable, low-cost, and widely available biomass. Various techniques, including Fourier-transform infrared spectroscopy (FTIR), Brunauer-Emmett-Teller (BET) surface area analysis, and scanning electron microscopy (SEM), were employed to determine the chemical and structural properties of the Biochar. Raman spectroscopy was employed to assess the surface area and degree of graphitization. Furthermore, adsorption capacity investigates the characteristics of the Biochar adsorbent. A self-sustained carbonization combustion method was used in a reactor made of heat-resistant bricks to convert coconut husk into Biochar. Further modification was performed using zeolite and lime, which enhanced the Biochar's ability to adsorb nutrients such as ammonia and phosphorus. Biochar has shown the ability to remove approximately 50% of ammonia and phosphorus from solutions with concentrations of 15 mg/L and 10 mg/L, respectively. After modifying the Biochar, the removal efficiency was significantly enhanced, reaching between 70% and 90%. Raman spectroscopy analysis of the Biochar revealed a G-band to D-band ratio of approximately 0.75 to 0.80, indicating a moderate absorbance level. This suggests that the modification enhanced the Biochar's ability to adsorb these contaminants effectively. This could apply to high-nutrient wastewater. Adsorption tests were performed under varying conditions, including retention time and nutrient concentrations. The effluent of the wastewater treatment was used as the influent of this study. It revealed that the removal efficiency of 70–90% of nutrients from agricultural wastewater effluents meets wastewater standards. This research contributes to effective nutrient removal by providing a cost-effective, sustainable, and eco-friendly solution based on modified coconut-based biomass, transforming waste into resources, and advancing wastewater treatment technology.

Keywords: modified Biochar, nutrient removal, agricultural wastewater, and coconut-based biomass.

INTRODUCTION

Water pollution resulted from the rapid development of industry and community without proper management. Consequently, water availability and quality have become one of the significant environmental challenges of the 21st century due to a rapid increase in population, industrialization, agricultural development, and urbanization. The high-nutrient wastewater when discharged without treatment in the water bodies the water bodies got contaminated. . It was observed that the parameters of water samples that were collected from the pig farm were majorly affected by chemical oxygen demand (COD) concentration, pH, Temperature, dissolved oxygen (DO), electrical conductivity (EC), and total dissolved solids (TDS), total Kjeldahl nitrogen (TKN), ammonia nitrogen (NH_3–N), and Phosphate phosphorous (PO_4^{-3}-P) [1]. High levels of nutrients such as ammonia nitrogen (NH_3–N) and Phosphate phosphorus (PO_4^{-3}-P) can lead to several environmental and public health issues. Some of them are described: Eutrophication involves excessive growth of algae and plants because of the nutrients. When these aquatic plants die and decompose, they deplete water quality and create a dead zone [2]. Algal Blooms grow due to high nutrient levels and harmful algae such as cyanobacteria. This can contaminate drinking water supplies and recreational areas [3]. Various options have been available for wastewater treatment, one is material adsorption.

The green coconut husk is abundant in Thailand and available free of charge as compared to other coconut biomasses, as it is considered waste generated from various sectors. Biochar from green coconut husk can be a cost-effective solution for the treatment of agricultural wastewater, and the adsorption process helps

remove contaminants from agricultural wastewater [4]. Biochar is one of the most suitable materials as it is carbon-rich, especially when derived from agricultural wastes. Biochar is used for the treatment and has a high capability towards adsorption of contaminants [5] [6]. Coconut Biochar's distinguishing properties include high porosity, carbon-rich, high aromatization degree, and strong anti-decomposition [7] [8]. The Biochar produced from combustion has an adsorption capacity ranging from 0.15 to 5.09 mg·N/g for ammonia adsorption [9]. Phosphate adsorption ranges from 1.37 to 193 mg P/g, with an average value of 28.90 mg P/g [10]. However, this research focused on the development of Biochar from green coconut husk and modification with zeolite and lime for adsorbent. This research presents a comparative analysis of the adsorption capacities of Biochar and Modified Biochar.

METHODOLOGY

This research focused on developing a low-cost, efficient adsorbent for treating high-nutrient wastewater using low-cost materials, such as coconut husk modified with zeolite and lime. Coconut biomass was obtained from the surrounding area of Nakhon Pathom province, Thailand. The coconut biomass samples were dried under the sun for about 1 week. Low-cost materials such as Zeolite and lime are also obtained from local shops. Then, coconut biomass samples underwent combustion at 300 °C – 500 °C to convert them into Biochar, and low-cost materials (zeolite and lime) were mixed with the Biochar to modify and enhance its adsorption capacity. The research was divided into three phases.

Phase I: Development of Biochar:

In the preliminary phase of the research, Biochar was prepared from green coconut husk using a self-sustained carbonization method in a pilot-scale brick reactor. Initially, approximately 10 green coconuts, with a total weight of 4130 grams, were placed under the sun for one week to allow moisture content to evaporate, leaving the husk dry and suitable for combustion. After drying, the husk's weight was reduced to 1,590 grams. The combustion process involved a mixture of pine leaves, dry grass, sawdust, straw, and husk, which were utilized to fuel the combustion of the green coconut husk at temperatures ranging from 300°C to 500°C over one day. This process yielded approximately 154 grams of Biochar. Additionally, Brunauer-Emmett-Teller (BET) analysis was performed to determine the particle size, pore volume, and surface area of the produced Biochar.

Phase II: Preparation and Characterization of Biochar

In this phase, Biochar was modified using zeolite and lime in varying ratios of (Biochar: Zeolite: Lime) 1:1:1, 1:2:1, 1:1:2, 1:2:2, 2:1:1, and 1:0:0 using a weight of 1 gram per 100 ml of sample. Adsorption experiments were conducted to identify the optimal conditions, focusing on variables such as the initial concentration of the adsorbate and the retention time, which ranged from 0 to 120 minutes, with 5-minute intervals. The adsorption experiments were conducted using a synthetic solution containing ammonia nitrogen (NH_3-N) and Phosphate phosphorus (PO_4^{-3}-P), with concentrations of 15 mg/L and 10 mg/L, respectively, which are representative of agricultural wastewater. Characterization of the Biochar and modified Biochar was carried out using Raman spectroscopy, scanning electron microscopy (SEM), Fourier-transform infrared (FTIR) spectroscopy, and Brunauer-Emmett-Teller (BET) analysis. These tests were conducted to evaluate key properties such as surface area, particle size, pore volume, and adsorption capacity of the Biochar materials.

Phase III: Application to Agriculture Wastewater

The low-cost modified Biochar was produced on a lab scale, with a focus on optimizing the hydraulic retention time (HRT) of 2 hours and a (Biochar: Zeolite: Lime) ratio of 2:1:1 using a weight of 1 gram per 100 ml of sample, as determined in Phase II. This phase mainly targeted the removal efficiency of ammonia and phosphorus from pig farm wastewater effluent.

RESULTS AND DISCUSSIONS

1. Physical structure and characteristics of Biochar and Modified Biochar

1.1 Raman spectroscopy

Figure 1. a represents Raman spectroscopy analysis of Biochar gives a G/D band intensity ratio of approximately 75-80%, indicating a moderate value of the graphitic structure, which suggests its potential effectiveness for adsorption applications. The existence of graphitic and disordered structures represents

adsorbents' ability to adsorb a range of organic and inorganic contaminants, offering potential for wastewater treatment. This makes Biochar a promising material for various environmental and industrial applications.

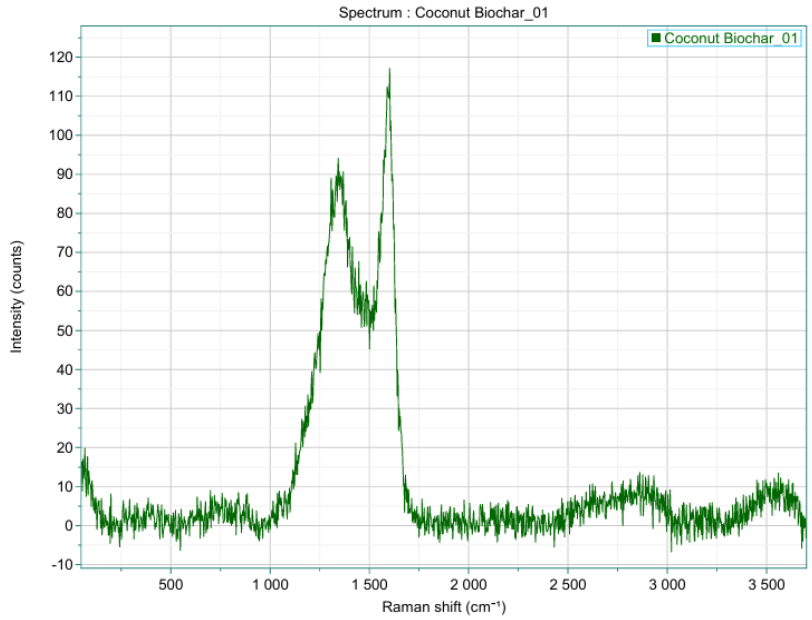


Figure 1.1.a. Raman Spectroscopy of Biochar

Figure 1.b represents Raman spectroscopy analysis of Modified Biochar of ratio 2:1:1 (Biochar: zeolite: lime), demonstrating an increased adsorption effectiveness following modification. We can observe that modification has increased the O-H stretching vibration, indicating hydroxyl group presence which forms hydrogen bonds that help to enhance the hydrophilic nature, surface area, reactivity, and surface interactions. These interact with adsorbate and enhance adsorption capacity.

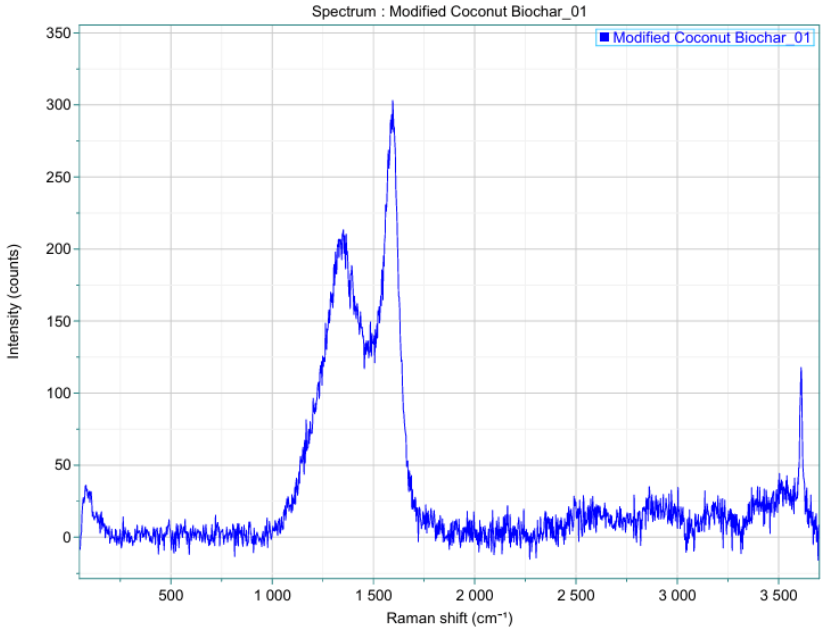


Figure 1.1.b. Raman Spectroscopy of Modified Biochar

1.2 Scanning Electron Microscope (SEM)

Figure 1.2.a illustrates the microstructure of Biochar at 200X magnification and a scale bar of 100 µm, obtained using scanning electron microscopy (SEM). The surface of the Biochar appears rough, with the

presence of small pores, indicating a porous nature. Following modification with zeolite and lime at a ratio (Biochar: Zeolite: Lime) 2:1:1, increases additional micro-pores, further improving the material's overall surface texture. **Figure 1.2.b** demonstrates a significant increase in surface area, which enhances its adsorption capacity and enables greater interaction between the Biochar and contaminants. This modification effectively increases the porosity and surface characteristics, making the Biochar more suitable for various adsorption applications.

A B

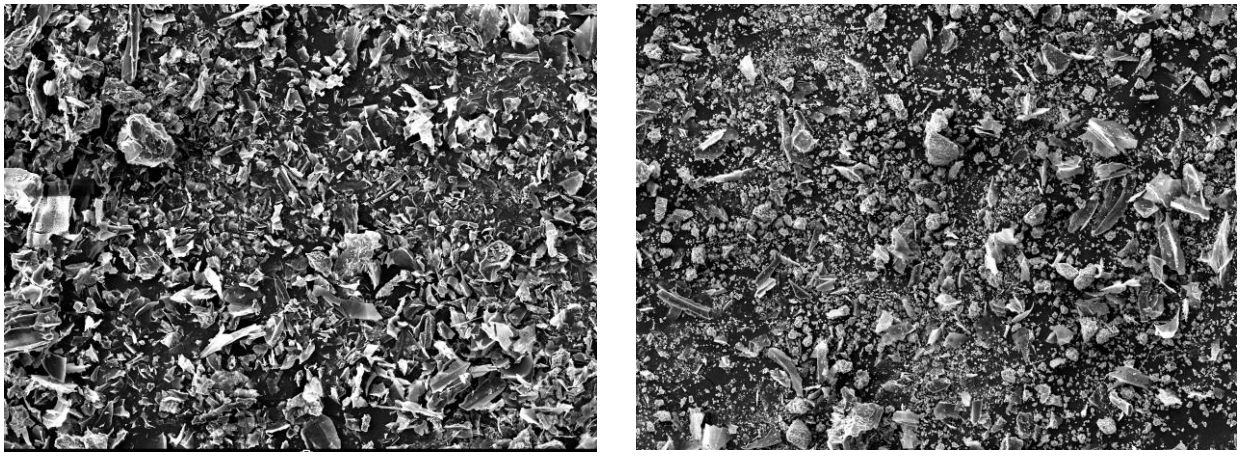


Figure 1.2. Scanning electron microscope (SEM) view under 200X magnification and a scale bar of 100 µm. Of Biochar (A) and Modified Biochar (B)

1.3 Fourier Transform Infrared Spectroscopy (FTIR)

FTIR analysis indicates the chemical composition, functional groups, and structural features presence of hydroxyl (–OH) groups, and O-H stretching vibration. In **Figure 1.3.a,** the broad peak at 3350.26 cm^{-1} represents the O-H stretching vibration of hydroxyl groups (–OH) in Biochar. We can predict the weak and less ordered hydrogen bonding due to the broadness of the peak. In a modified Biochar of ratio (Biochar: Zeolite: Lime) 2:1:1, the sharp peak at 3639.81 cm^{-1} represents hydroxyl (–OH) stretching in hydrogen-bonded and this sharp peak represents stronger hydroxyl groups. The zeolite and Lime result in sharp peaks. The variations suggest that the modification has increased the surface chemistry of the Biochar, due to the presence of more reactive surface groups, which is illustrated in **Figure 1.3.b.**

A **B**

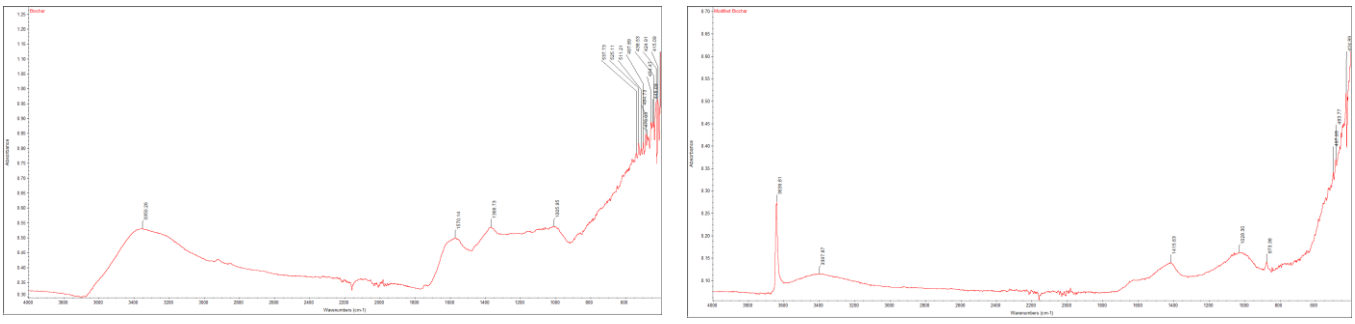


Figure 1.3.a. Fourier Transform Infrared Spectroscopy (FTIR) of Biochar (A) and Modified Biochar (B)

1.4 Brunauer-Emmett-Teller (BET)

The Brunauer-Emmett-Teller (BET) analysis of low-cost adsorbents, Biochar, and Modified Biochar (with a mixing ratio of Biochar: Zeolite: Lime at 2:1:1), was conducted to investigate their surface properties. The surface area of Biochar was found to be **0.5948 m^2/g**, while the surface area of Modified Biochar increased to **4.2379 m^2/g**, indicating a significant enhancement in surface area due to the modification by zeolite and lime as they filled the pores and increased surface area. The pore volume of Biochar was measured at **0.007374 cm^3/g**, compared to **0.034183 cm^3/g** for the modified sample, demonstrating a significant increase in pore volume. The enhanced pore volume contributed to the improvement of the efficiency of nutrient adsorption.

Furthermore, the pore size of Biochar was **49.2144 nm**. In contrast, the modified sample exhibited a reduced pore size of **30.3851 nm**, suggesting a more refined and potentially more effective porous structure in the modified Biochar. This can enhance the Biochar's adsorption capacity, especially for smaller molecules. These findings highlight the structural modifications effected by the zeolite and lime, which could enhance the material's suitability for adsorption applications.

Physical Properties	Biochar	Modified Biochar
Surface Area	0.5948 m^2/g	4.2379 m^2/g
Pore Volume	0.007374 cm^3/g	0.034183 cm^3/g
Pore size	49.2144 nm	30.3851 nm

2. Nutrient Removal by Biochar and Modified Biochar

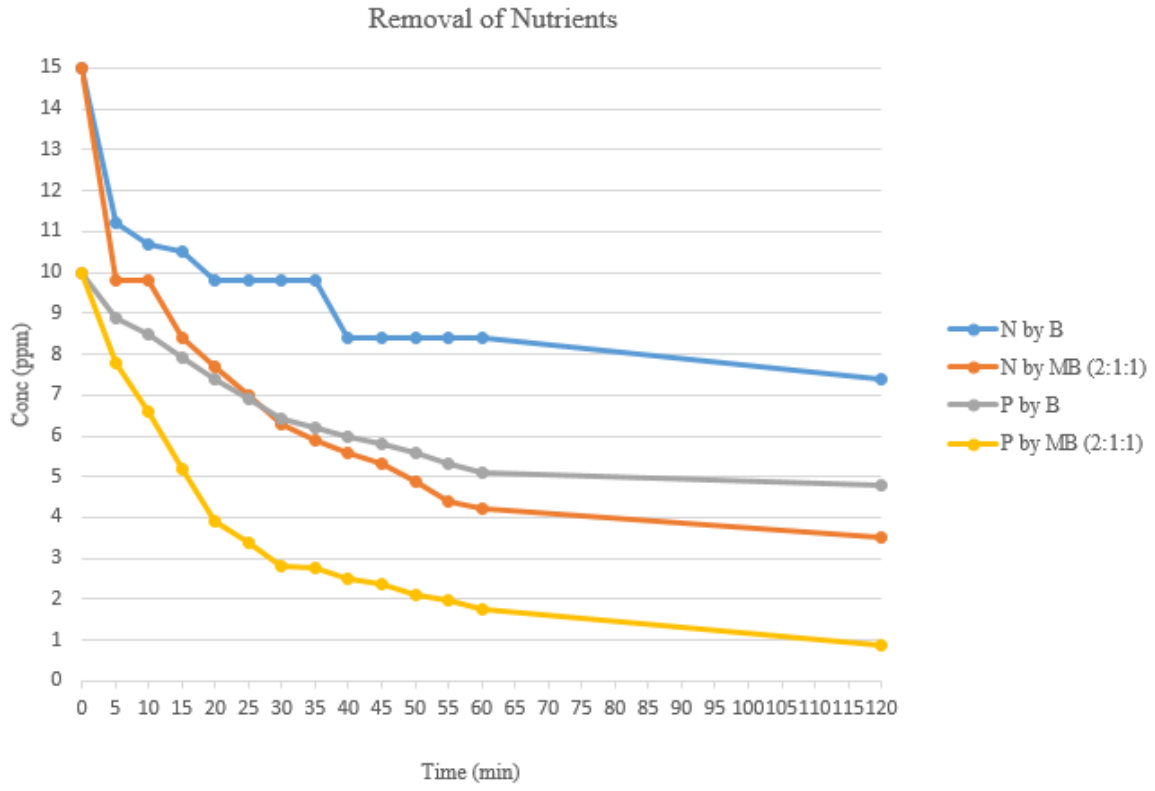


Figure 2 Results of NH_3- N and PO_4^{-3}- P Removal

Figure 2 illustrates the variation in nutrient removal at different time intervals, with an initial NH_3-N concentration of 15 mg/L and a PO_4^{-3}- P concentration of 10 mg/L. Comparing the performance of both Biochar and Modified Biochar with a 2:1:1 ratio (Biochar: Zeolite: Lime) using a weight of 1 gram per 100 ml of sample. These results were observed over 120 minutes.

At time 0, NH_3-N was 15 mg/L and a PO_4^{-3}- P was 10 mg/L. After 5 minutes of time interval, modified Biochar reduced the NH_3-N concentration to 9.8 mg/L and the PO_4^{3-}-P concentration to 7.8 mg/L; on the other hand, Biochar, which had reduced the concentration to 11.2 mg/L for NH_3-N and 8.9 mg/L for PO_4^{3-}-P. Biochar and modified Biochar both continue to reduce concentration, after 60 minutes NH_3 -N concentration with Biochar reaches 8.4 mg/L, while Modified Biochar reduces it further to 4.2 mg/L. Similarly, the PO_4^{3-}-P concentration is lowered by Modified Biochar, with a concentration of 1.75 mg/L at 60 minutes compared to 5.1 mg/L for Biochar.

At 120 minutes, the NH_3-N concentration using Biochar is reduced to 7.4 mg/L, while Modified Biochar achieves a significantly lower value of 3.5 mg/L. For phosphorus removal, Biochar reaches 4.8 mg/L, whereas Modified Biochar reduces the concentration effectively to 0.89 mg/L. These results depict the adsorption capacity and efficiency of Modified Biochar in removing both ammonia and phosphorus.

B denotes Biochar, MB denotes Modified Biochar, N denotes NH_3-N, and P denotes PO_4^{-3}-P in **Figure 2.**

Table 1: Removal Efficiency of Biochar and Modified Biochar in Synthetic Solution

Type of Nutrient	Modified Biochar (Biochar:Zeolite:Lime)	Influent Concentration (mg/L)	Effluent Concentration (mg/L)	Removal %	Adsorption Capacity (mg/g)
NH_3- N	1:0:0	15	7.4	50.66	0.76
NH_3- N	2:1:1	15	3.5	76.65	1.15
PO_4^{-3}- P	1:0:0	10	4.8	52.0	0.52
PO_4^{-3}- P	2:1:1	10	0.89	91.1	0.911

Table 1 presents the removal efficiency of Biochar and Modified Biochar, along with a comparison of their respective nutrient removal percentages. When Biochar is used in a 1:0:0 ratio (Biochar: Zeolite: Lime), it achieves an ammonia removal efficiency of 50.66%. However, the modification of Biochar of ratio 2:1:1 (Biochar: Zeolite: Lime) using a weight of 1 gram per 100 ml of sample, enhances its removal efficiency, increasing it to 76.65%. Regarding phosphorus removal, Biochar achieves a removal rate of 52%, while Modified Biochar shows a significantly higher removal efficiency, reaching approximately 91.1% at 2 hours. By using the adsorption capacity equation, we can calculate the adsorption capacity of nutrients.

Table 2: Removal Efficiency of Biochar and Modified Biochar in Agriculture Wastewater.

Type of Nutrient	Modified Biochar (Biochar:Zeolite:Lime)	Influent Concentration (mg/L)	Effluent Concentration (mg/L)	Removal %	Adsorption Capacity (mg/g)
NH_3- N	1:0:0	5.98	3.04	49.0	0.29
NH_3- N	2:1:1	5.98	1.167	80.4	0.48
PO_4^{-3}- P	1:0:0	0.963	0.438	54.5	0.52
PO_4^{-3}- P	2:1:1	0.963	0.1098	88.59	0.085

Table 2 represents the removal efficiency of NH_3-N and PO_4^{-3}-P in agricultural wastewater by using Biochar and Modified Biochar. When Biochar is used in a 1:0:0 ratio (Biochar: Zeolite: Lime), it achieves an ammonia removal efficiency of 49.0%. However, the modification of Biochar of ratio 2:1:1 (Biochar: Zeolite: Lime) using a weight of 1 gram per 100 ml of sample enhances its removal efficiency, increasing it to 80.4%. Regarding phosphorus removal, Biochar achieves a removal rate of 54.5%, while Modified Biochar shows a significantly higher removal efficiency, reaching approximately 88.59% at 2 hours.

3. Adsorption Isotherm

The relationship between the initial concentrations of ammonia nitrogen (NH_3-N) and phosphate phosphorus (PO_4^{-3}–P) and their respective concentrations over time was observed using adsorption isotherms. These isotherms describe the equilibrium relationship between the amount of adsorbate adsorbed per unit mass of adsorbent (q_e) and the equilibrium concentration of the adsorbate in solution (C_e). The equilibrium data for the adsorption of ammonia nitrogen and phosphate phosphorus onto Biochar and Modified Biochar were analyzed using the Langmuir and the Freundlich isotherm models. The Freundlich isotherm plots exhibited strong linear correlations, as indicated by high R^2 values, and provided a better fit than the Langmuir model. However, both isotherm models demonstrated a good fit to the experimental data, suggesting they are suitable for describing the adsorption behavior in this study.

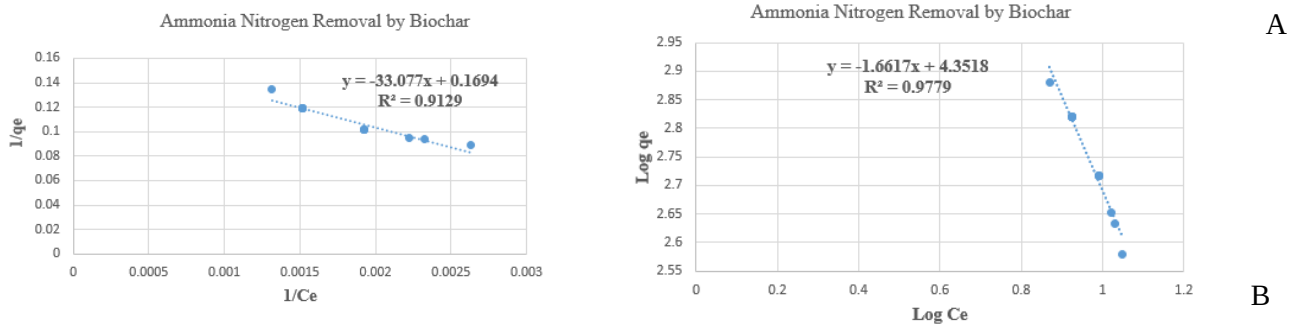
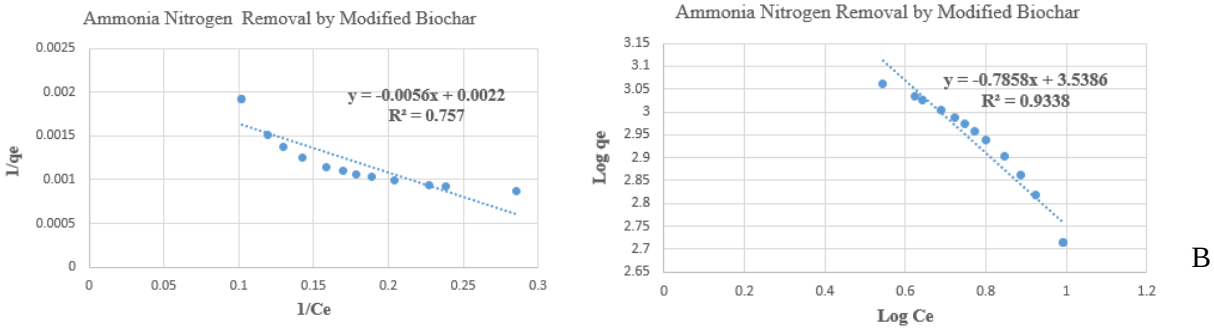


Figure 3. Langmuir (A) and Freundlich (B) Adsorption Isotherms for Ammonia Nitrogen Removal by Biochar

A



B

Figure 4. Langmuir (A) and Freundlich (B) Adsorption Isotherms for Ammonia Nitrogen Removal by Modified Biochar A B

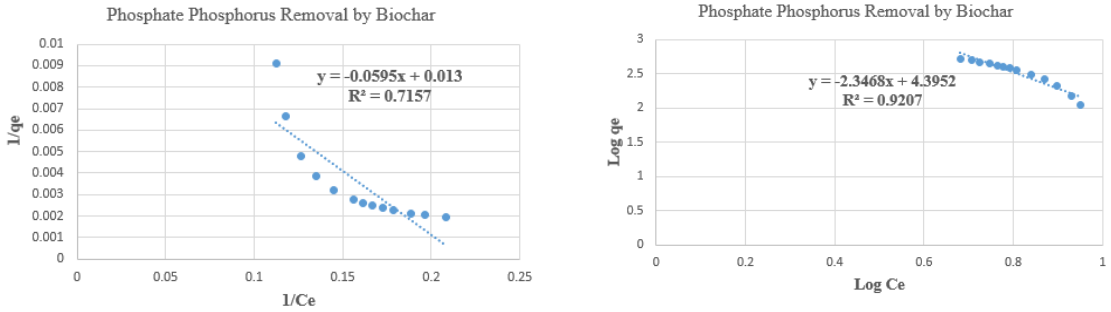
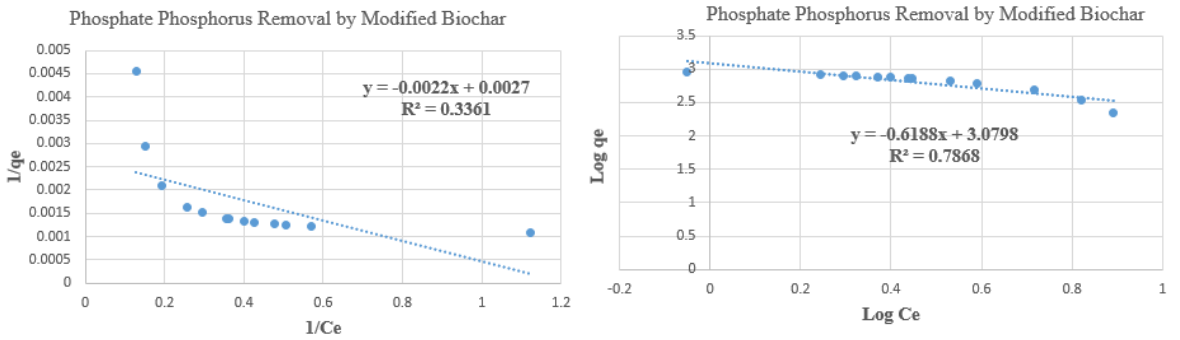


Figure 5. Langmuir (A) and Freundlich (B) Adsorption Isotherms for Phosphate Phosphorus Removal by Biochar



A

B

Figure 6. Langmuir (A) and Freundlich (B) Adsorption Isotherms for Phosphate Phosphorus Removal by Modified Biochar.

CONCLUSION

In conclusion, this research provided a comparative analysis of the adsorption capacities of Biochar and Modified Biochar for nutrient removal, such as NH_3-N and PO_4^{-3}-P, from agricultural wastewater. The results demonstrate a significant increase in the removal % of Biochar after modification from zeolite and Lime at a ratio of 2:1:1 (Biochar: Zeolite: Lime) using a weight of 1 gram per 100 ml of sample. After a contact time of 2 hours for NH_3-N, it increased from 49.0% to 80.4%, and for PO_4^{-3}-P, it increased from 54.5% to 88.59%. These findings highlight the importance of Biochar from green coconut husk for nutrient removal and its modification. Furthermore, the nutrient-enriched Biochar can be repurposed as a promising fertilizer for agricultural fields.

ACKNOWLEDGEMENT

This study was conducted as part of thesis research and was financially supported by the Environmental and Water Resources Engineering Program at the Department of Civil and Environmental Engineering, Faculty of Engineering, and the Faculty of Graduate Studies, Mahidol University.

REFERENCE

[1] Celia De La Mora-Orozco, I. J.-A.-T.-L.-A.-R. (2018). Removing Organic Matter and Nutrients from Pig Farm Wastewater with a Constructed Wetland System. International Journal of Environmental Research and Public Health.

[2] JoAnn M. Burkholder, D. A. (2007). Seagrasses and eutrophication. Journal of Experimental Marine Biology and Ecology, 46-72.

[3] Kevin G. Sellner, G. J. (2003). Harmful algal blooms: causes, impacts, and detection. Journal of Industrial Microbiology and Biotechnology, 383–406.

[4] S. Mandal, A. K. (2016). Application of Biochar Produced From Biowaste Materials for Environmental Protection and Sustainable Agriculture Production. Environmental Materials and Waste.

[5] Vo Cong Minh, N. T. (2023). Production of Biochar from Coconut Husks for Adsorption of Heavy Metals in Water. Philippine Journal of Science.

[6] Samyuktha S. Kolluru, S. A. (2021). Heavy metal removal from wastewater using nanomaterials-process and engineering aspects. Process Safety and Environmental Protection, 323-355.

[7] James E. Amonette, S. J. (2009). Biochar for Environment Management. Routledge.

[8] Spokas, K. (2013). Biochar: The science behind the hype. United States, Minnesota: Department of Agriculture.

[9] Kyoung S. Ro, I. M. (2015). Removing Gaseous NH3 Using Biochar as an Adsorbent. Agriculture, 991-1002.

[10] Ming Zhang, G. S. (2020). Evaluating biochar and its modifications for the removal of ammonium, nitrate, and phosphate in water. Water Research.

20R5-17

Effect of Turbidity on Chlorine Dosage for Algae Removal in Synthetic Raw Water

Sokunthea Khim[1,2], On-anong Larpparisudthi[3*]

[1]Master student, Department of Environmental and Sustainable Engineering, Faculty of Engineering, Chulalongkorn University, Bangkok 10330, Thailand
[2]Faculty of Hydrology and Water Resources Engineering, Institute of Technology of Cambodia, Russian Federation Blvd., P.O. Box 86, Phnom Penh, Cambodia
[3]Assistant Professor, Department of Environmental and Sustainable Engineering, Faculty of Engineering, Chulalongkorn University, Bangkok 10330, Thailand*
[*]Corresponding author: Tel : 081 641 0060, E-mail : onanong.l@chula.ac.th

ABSTRACT

The overgrowth of algae in freshwater has become a challenge and concern for the treatment facilities, which can lead to reduce the water quality and water scarcity. There are many algae species, among those *Scenedesmus* is one of the commonly found green microalgae that belong to the Chlorophyceae class, which is under the phylum of Chlorophyta. Chlorine is widely used as a disinfectant to kill germs or pathogens in the water by damaging the cell membrane and cell organs. High turbidity might drop the effectiveness of the water treatment process. In this study, the varied dosage of chlorine was used to find the effective concentration for inactivation *Scenedesmus sp.* in the water. From the results, 10 mg/L of chlorine reduces the Chlorophyll-a in water sample from 56.72 μg/L to 37.53 μg/L in 30 min, but when there was more turbidity, the removal efficiency slightly decreased. Therefore, this study proves that turbidity can decrease the inactivation of algae cells and increase the amount of chlorine demand, which can lead to the increase of disinfection byproducts.

Keywords : algae; turbidity; chlorine; *Scenedesmus sp*; chlorophyll-a

INTRODUCTION

Water is essential for human well-being, but it is also considered as an important factor for supporting aquatic life in the ecosystem as well [1]. The growth of the population is leading to an increase in freshwater consumption, while only around 0.3% of the world's water resources are accessed [2]. In the last few decades, water pollution has become an issue regarding water quality, causing problems by reducing the supply of water for consumption, sanitation, and drinking. This affects human health, all living organisms, and the aquatic ecosystem in the water body.

In recent years, surface water pollution has become a significant issue, with algae blooms being a primary concern. Algae blooms in the water sources are a natural phenomenon generated by the overgrowth of the phytoplankton population in water bodies, also known as eutrophication [3]. During the early 1990s, a survey of lakes all over the world discovered that 28% of lakes in Africa, 48% of lakes in North America, 41% of water bodies in South America, 54% of Asian lakes, and 53% of European lakes were eutrophic [4]. The algae blooms in water sources are caused by natural sources and untreated wastewater discharge from industry, households, and agriculture, which results in excessive nitrogen and phosphorus levels in seas, rivers, lakes, and reservoirs, leading to eutrophication [5]. Those nutrients flow into the watershed due to the discharge of wastewater from domestic or untreated water from industrial areas, animal livestock, and fertilizer usage in agriculture [6]. Temperature increases also play an important role by providing better conditions for algae growth and releasing nutrients from sediment more easily than usual. In general, a high amount of algae was found in the dry season rather than the rainy season due to the shallow depth of water [7]. The high concentration of phytoplankton and particulate matter in algae blooms can block the light penetration in the water column, which decreases the light availability [8]. Algae growth can harm the growth and development of aquatic plants, although those aquatic plants were not destroyed, while the change in biodiversity can cause global warming, which supports the overgrowth of phytoplankton [9]. The safety of drinking water will be threatened by algae blooms in water sources. The challenges and cost of treating algae-contaminated water by using conventional drinking water techniques require more consideration, and the safety of water quality cannot be guaranteed [10].

Chlorine is one of the potential oxidizing agents that could inactivate bacterial and other microorganisms in the water. In general, disinfectants such as chlorine have been used at high concentrations to achieve a quick rate of death. Chlorine enters cells when it is mostly present as hypochlorous acid, inactivating them by damage to the cell wall and membrane [11]. During eutrophication, algae in the water can cause high turbidity that leads to a decrease in the removal efficiency of the water treatment process, which threatens water quality [12]. However, the high turbidity in water can reduce the inactivation performance of chlorine because the particles can absorb it and reduce the concentration of chlorine in the treatment process. The main purpose of this study is to focus on removing algae species when the water has high turbidity and limit the dose of chlorine used as pre-treatment.

METHODOLOGY

Algae cultivation

The algae species used as a representative in this study are *Scenedesmus sp.*, which were obtained from the Department of Marine Science, Faculty of Science, Chulalongkorn University. *Scenedesmus sp* were cultured by using the BG-11 medium, then grown at room temperature conditions and air supply by utilizing the air pump to provide carbon dioxide (CO_2) for algae to do photosynthesis. The algae species were incubated under 14:10 hours per day as light and dark cycle of artificial light from fluorescent lamps in the range 5000 lux, which is a suitable light condition for algae growth. To synthesize the water sample, bentonite was used to increase the amount of turbidity in the water by adding it until the turbidity reached 50 NTU. Then, algae species were added to the water and diluted to a cell density of about 1.0 ($\pm$0.5) x 10^6 cells/ml.

Jar test experiment

The jar test was used to determine the effective amount of chlorine that could inactivate the algae cells. The different amounts of chlorine were varied, such as 0.2, 0.5, 1, 2, 5, and 10 mg/L, to find the optimal dosage by using 500 ml of water sample poured into a beaker and stirring at 100 rpm. The chlorine stock solution was prepared by NaClO, and the water samples of each concentration were sampled at 30 min, 1 hour, and 2 hours.

Analytical methods

Chlorophyll-a (Chl-a) and optical density (OD_{680}) is analyzed by an ultraviolet-visible (UV-vis) spectrophotometer. To know the biomass of algae in the water, Chl-a was measured since it is an indicator that shows the green pigment in plants. The water samples were filtered using a cellulose acetate filter membrane and then extracted with a 90% acetone solution. After that, the absorbance measurement was taken at 630, 647, 664, and 750 nm, the results of each wavelength were calculated by Equation 1.

$$\text{Chl-a } (\mu g/L) = \frac{[11.85*(E_{664}-E_{750})-1.54*(E_{647}-E_{750})-0.08*(E_{630}-E_{750})]*S}{L*V} \quad \text{(Equation 1)}$$

Where
S: volume of acetone used for the extraction (ml)
V: is the volume of water filtered (L)
L: is the path length of cuvette (cm)

RESULTS AND DISCUSSIONS

Effect of Duration

When varying concentrations of chlorine added to the water, the dosage of chlorine has an effect on the OD_{680} of algae over the exposure time as shown in Fig. 1. The value of OD_{680} absorbance decreased with the exposure time as more reaction time and more reactive oxidation species were produced that generate the oxidation performance [13]. From Fig.1, when adding chlorine dosages of 5 mg/L and 10 mg/L, the algae inactivation was 15.30% and 20.40%, respectively, after 30 minutes of chlorination. After 1 hour and 2 hours, the OD_{680} of algae at 5 mg/L and 10 mg/L chlorine dosage decreases from 16.32% to 23.46% and 18.36% to 24.48%. When chlorine added into the water for a long period, the prolonged contact time between chlorine and algal cells can lead to strong damage on the cell nucleic acids inside the cell membrane. With the chlorine dose of 10 mg/L, the OD_{680} of algae was decreased from 0.098 to 0.078 after 2 hours of a retention time. The chlorine damaged the membrane of algae cells when increase both the chlorine

dose and oxidation time. The performance of the chlorine dosage can lead to stress on the algae and break the cell structure [14].

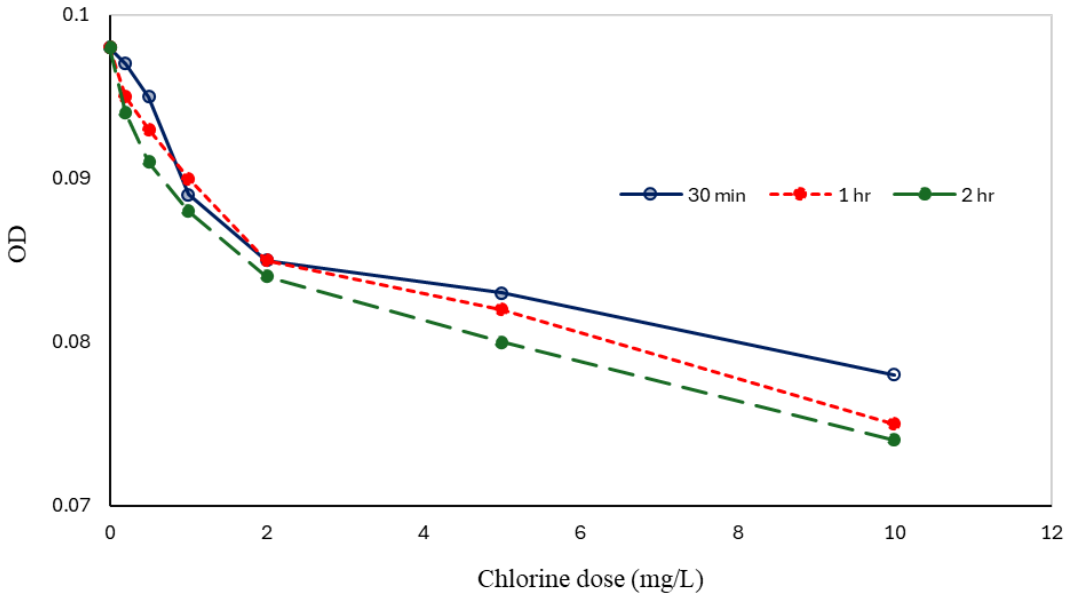


Fig. 1: The optical density at the varied times (30 min, 1 hr, and 2 hr)

Effect of Chlorine Dose on the Inactivation of *Scenedesmus sp.*

Adding chlorine to the water as a disinfectant would inactivate the algae species in the water. Chlorine is widely regarded as a nonselective oxidant that interacts with a wide range of biological components and influences metabolic processes.

Figure 2 shows the results between Chl-A and the chlorine dosage at different of sampling times. The results show that the increase of chlorine dosage results in the decrease of Chl-A as well as the increase of exposure time. However, at lower chlorine dose such as 0.2 and 0.5 mg/L, the results show slightly reduced compared to those of higher dose. At 0.2 mg/L of chlorine dosage, the Chl-A was slightly declined from 56.73 µg/L to 54.94, 51.91, and 50.24 µg/L after 30 min, 1 hr, and 2 hrs, respectively. While the removal efficiency increased from 16.69% to 44.11% after chlorination for 2 hours, with a chlorine concentration of 10 mg/L. These are caused by chlorine alters the cell membrane, causing proteins and RNA to escape from the cell and damaging the outer membrane [15]. At the higher dosage of chlorine, it leads to the production of more hydrochloric and hypochlorous acids that disrupt the structure of proteins in the cell, allowing it to repair itself back to normal, as amino acids and RNA are redistributed within the cell. According to [16], chlorine is able to damage the algae cell membrane through the oxidative process that breaks the nucleic acids, proteins, amino acids, cell walls, and other lipids, resulting in a loss of viability for the microorganism. Thus, this can indicate that the higher concentration of chlorine is able to inactivate algae cells more effectively than the lower dose during the chlorination process for water treatment, because chlorine is one of the most effective disinfectants for damaging the enzymes inside the cytoplasm [13]. Based on the experiment, the dosage of chlorine can lead to a huge difference in the removal of the algae species in the water treatment when the concentration of chlorine increases.

Effect of turbidity on chlorine dose

Turbidity is a measurement of particles in water, including silt, clay, algae, bacteria, and other microorganisms. Figure 3 shows the results of Chl-A at different of sampling time of 5 mg/L and 10 mg/L of chlorine dosage. When compared the results in Figure 2 with those of Figure 3 at the same chlorine concentration and duration, it is shown that the inactivation of *Scenedesmus sp.* decreased when there was turbidity in water. At 10 mg/L of chlorine dosage, the Chl-A in the water sample with 50 NTU turbidity decreased from 59.69 to 42.504 µg/L at 2 hr, while the water sample without turbidity decreased from 56.73 to 31.706 µg/L, respectively. From figure 3, at a duration of 30 min and 5mg/L of chlorine dosage, the amount of Chl-A showed a small reduction in

inactivation of algae species because the cell was slowly damaged when the turbidity in the water was high, which required a higher dose of chlorine to be added. Turbidity can affect the chlorine performance when the particle concentration is high, as it might be able to absorb or react with chlorine.

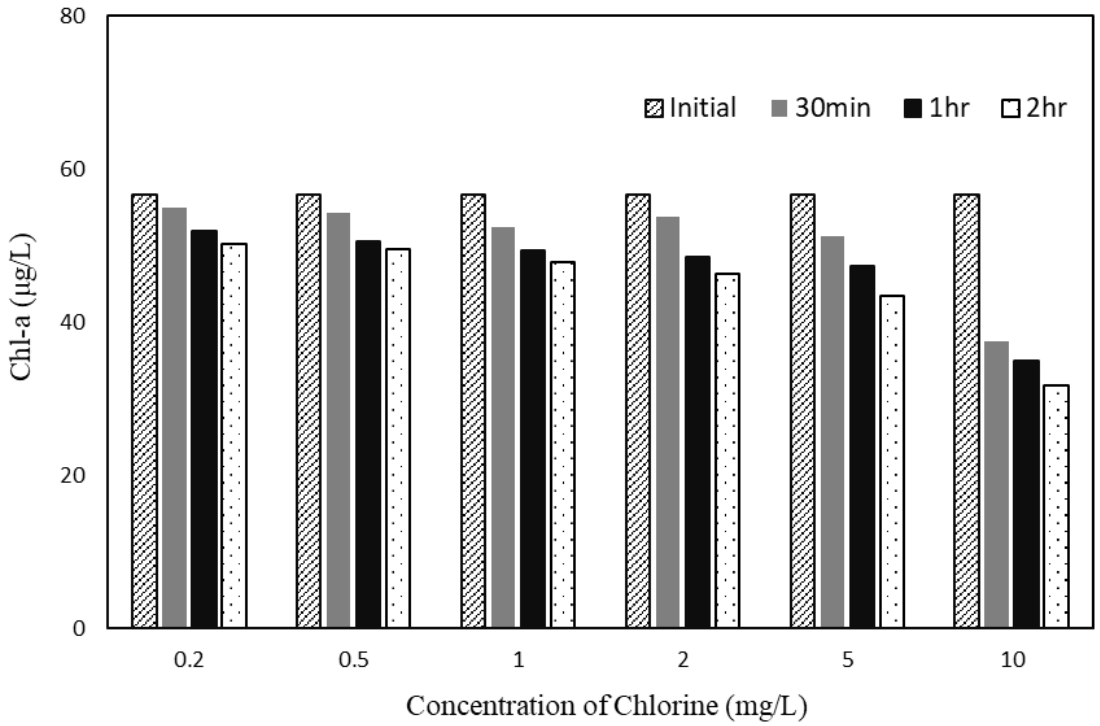


Fig. 2: The amount of Chl-a at varied doses of Cl_2

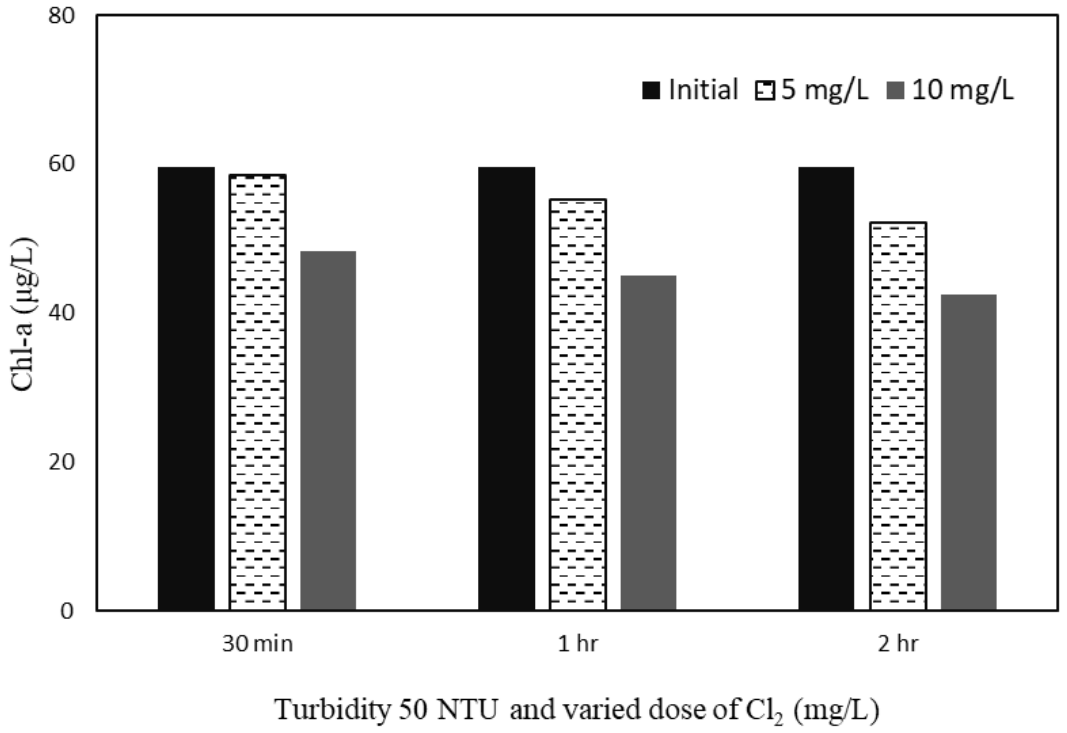


Fig. 3: The amount of Chl-a treated with turbidity

CONCLUSION

In conclusion, this study has shown that using chlorine as the pre-treatment in the water treatment process is effective in inactivating the *Scenedesmus sp*. The inactivation of algae cells shows good performance when the dose of chlorine is 10 mg/L, which can remove species up to 44.11% in 2 hr. On the other hand, the removal effectiveness can be impacted by the high turbid water, which reduces the removal effectiveness, and requires a higher dose of chlorine. The huge concentration of chlorine may result in good removal of the phytoplankton, but using too much chlorine can lead to disinfection byproducts. Thus, to address the challenge of eutrophication in the water, when it has high particles, it is necessary to study more due to the turbidity, which can reduce the removal efficiency by decreasing the water quality after treatment.

ACKNOWLEDGEMENT

The authors thankfully the Department of Environmental and Sustainable Engineering, Faculty of Engineering, Chulalongkorn University, for this research and the program for ASEAN or Non-ASEAN countries provided by Chulalongkorn University for scholarship funding.

REFERENCE

[1] L. Anatolia S.M. Exposto, M. Nahak Lino, J. A.C. Quim, M. Juvi Goncalves, and H. Pereira Vicente, "Efforts To Improve Clean Water Quality To Support Community Health," KESANS : International Journal of Health and Science, vol. 1, no. 3, pp. 236-251, 2021.

[2] Z. Kılıç, "The importance of water and conscious use of water," International Journal of Hydrology, vol. 4, no. 5, pp. 239-241, 2020.

[3] S. Merel, D. Walker, R. Chicana, S. Snyder, E. Baurès, and O. Thomas, "State of knowledge and concerns on cyanobacterial blooms and cyanotoxins," Environment International, vol. 59, pp. 303-327, 2013/09/01/ 2013.

[4] J. J. Beaulieu, T. DelSontro, and J. A. Downing, "Eutrophication will increase methane emissions from lakes and impoundments during the 21st century," Nat Commun, vol. 10, no. 1, p. 1375, Mar 26 2019.

[5] J. Zhang, W. Ni, Y. Luo, R. Jan Stevenson, and J. Qi, "Response of freshwater algae to water quality in Qinshan Lake within Taihu Watershed, China," Physics and Chemistry of the Earth, Parts A/B/C, vol. 36, no. 9, pp. 360-365, 2011/01/01/ 2011.

[6] X. Yang, X. Wei, X. Xu, Y. Zhang, J. Li, and J. Wan, "Characteristics of Dissolved Organic Nitrogen in the Sediments of Six Water Sources in Taihu Lake, China," Int J Environ Res Public Health, vol. 16, no. 6, Mar 14 2019.

[7] M. D. Giripunje, A. B. Fulke, K. Khairnar, P. U. Meshram, and W. N. Paunikar, "Review of Phytoplankton Ecology in Freshwater Lakes of India.," Lakes, Reservoirs and Ponds, vol. 7(2), pp. 127–141, 2013.

[8] J. Lan, P. Liu, X. Hu, and S. Zhu, "Harmful Algal Blooms in Eutrophic Marine Environments: Causes, Monitoring, and Treatment," Water, vol. 16, no. 17, 2024.

[9] A. K. Tiwari and D. B. Pal, "Chapter 11 - Nutrients contamination and eutrophication in the river ecosystem," in Ecological Significance of River Ecosystems, S. Madhav, S. Kanhaiya, A. Srivastav, V. Singh, and P. Singh Eds.: Elsevier, 2022, pp. 203-216.

[10] Y. Peng et al., "Algae removal characteristics of the ultrasonic radiation enhanced drinking water treatment process," Journal of Water Process Engineering, vol. 55, p. 104154, 2023/10/01/ 2023.

[11] P. J. García–Nieto, E. García–Gonzalo, J. R. Alonso Fernández, and C. Díaz Muñiz, "Forecast of chlorophyll-a concentration as an indicator of phytoplankton biomass in El Val reservoir by utilizing various machine learning techniques: A case study in Ebro river basin, Spain," Journal of Hydrology, vol. 639, p. 131639, 2024/08/01/ 2024.

[12] J. Jin, W. Xia, P. Hu, and H. Yang, "Efficient removal of algae and turbidity from water by a composite coagulant composed of a cationic starch and attapulgite," Science China Technological Sciences, vol. 65, no. 12, pp. 2979-2989, 2022, doi: 10.1007/s11431-022-2123-3.

[13] Y. Chen et al., "UV-assisted chlorination of algae-laden water: Cell lysis and disinfection byproducts formation," Chemical Engineering Journal, vol. 383, p. 123165, 2020/03/01/ 2020,

[14] J. Sun, L. Bu, L. Deng, Z. Shi, and S. Zhou, "Removal of Microcystis aeruginosa by UV/chlorine process: Inactivation mechanism and microcystins degradation," Chemical Engineering Journal, vol. 349, pp. 408-415, 2018,

[15] M. Mizozoe, M. Otaki, and K. Aikawa, "The Mechanism of Chlorine Damage Using Enhanced Green Fluorescent Protein-Expressing Escherichia coli," Water, vol. 11, no. 10, 2019,

[16] R. Cheswick, G. Moore, A. Nocker, F. Hassard, B. Jefferson, and P. Jarvis, "Chlorine disinfection of drinking water assessed by flow cytometry: New insights," Environmental Technology & Innovation, vol. 19, 2020.

The Effect of Colloidal Silica Particle on Microfiltration Fouling

Gechhor Chea[1,2] Chotikoon Bunditboondee[3] and Jenyuk Lohwacharin[4*]

[1]Master student, Department of Environmental and Sustainable Engineering, Faculty of Engineering, Chulalongkorn University, Bangkok 10330, Thailand
[2]Faculty of Hydrology and Water Resource Engineering, Institute of Technology of Cambodia, Phnom Penh, Cambodia
[3]Postdoctoral researcher, Department of Environmental and Sustainable Engineering, Faculty of Engineering, Chulalongkorn University, Bangkok 10330, Thailand
[4]Associate Professor, Department of Environmental and Sustainable Engineering, Faculty of Engineering, Chulalongkorn University, Bangkok 10330, Thailand*
[*]Phone : (66) 98-2-218-6671, Fax : (66) 2-218-6666 E-mail : jenyuk.l@chula.ac.th

ABSTRACT

Microfiltration membranes are widely utilized in water and wastewater treatment due to their effectiveness in removing micrometer-sized particles, including suspended solids and large bacteria. Understanding particle behaviors is critical in evaluating membrane fouling mechanisms in microfiltration systems. This study investigates the effect of silica with varying manganese concentrations on particle aggregation and size distribution over time, with the aim of identifying conditions that promote the smallest particle size with significant aggregation, representing a worst-cast fouling scenario. Jar test experiment is conducted by measuring the pH of tap water, particle size and standard deviation were analyzed at 1, 10, 30, and 60 minutes. The concentration of 0.2 mg/L of Mn^{2+} with 100 mg/L of silica in 30 minutes of reaction time, indicating dense and compact floc formation. Although the sorting quality at 30 minutes was moderately varied, it remained acceptable for evaluating aggregation performance during active phase. Selecting the 30 minutes condition with the smallest D_{50} simulates the most challenging scenario for MF membrane. The worst-case condition provides valuable insight for future studies on membrane system.

Keywords : silica; manganese; particle size; aggregation; dispersion; membrane filtration

INTRODUCTION

Microfiltration membrane has been a popular technology in water and wastewater treatment, which can remove the micrometer sized matters, suspended particles, large bacteria with their pore size ranging from 0.1 to 1 μm [1]. Moreover, MF has known to use in variety applications such as food and beverage industry, ultrapure water, plasmapheresis, water treatment and wastewater treatment [2]. Microfiltration membrane presents the operational challenge such as membrane fouling, causing by particulate and colloidal fouling, organic or inorganic fouling on the surface or inside pore size of membrane. The organic and inorganic species in the feed water tend to deposit and clog on the surface membrane, leading to lower the quality and quantity of the permeate flux, efficiency of the membrane operation [3], reduce the lifespan of the membrane, increase the energy consumption, and maintenance cost. Silica and manganese are commonly found in natural water [4]. Colloids silica and manganese colloidal is considered one of the most complex fouling in terms of their particle size [3, 5]. Silica generally exists in water in three different forms such as colloidal, particulate, and dissolved silica [6], and colloidal silica has been reported to cause the severe fouling [7]. In addition, manganese colloidal are commonly found on membrane as foulants and incomplete of manganese particles in the pretreatment steps may cause severe fouling problems [4]. MF encountered the fouling, resulting in flux decline when the particles is being deposit inside the pore of the membrane or at the membrane surface [2], which is a operational challenge. One of the most severe problems for the membrane performance is a membrane fouling, which caused to reduce the water flux and increase the operational cost [8]. Moreover, fouled MF happen when the accumulate of the colloidal particles presented on the surface or within pore membrane [9-11], which impacted from the feed water characteristics, solution chemistry, membrane properties, and operational conditions [12]. Previous studies on the individual behaviors of silica and manganese particles on microfiltration technologies are documented. However, there is a limited understanding of how manganese ions influence the floc formation of colloidal silica under varying environmental conditions, including changes in contaminant concentrations. By addressing the gap, this research aims to determine the floc size of colloidal silica particles formed from the interaction of silicate anions with manganese ions, which is beneficial for an understanding the optimal floc size that guide the

design and operation of microfiltration to balance filtration efficiency and fouling. In addition, it is established the worst-case scenario condition for the further research for the investigation of membrane fouling, enhancing the understanding of how extreme situations affect filtration system performance.

METHODOLOGY

Materials

Silicon dioxide (CAS: 14808-60-7) and Manganese II sulfate 1-hydrate $MnSO_4$. H_2O (CAS: 10034-96-5) are used as the fouling agent in the experiment. The concentration of the SiO_2 and Manganese stock solution was adjusted to 500 mg/L and 2 mg/L, respectively. Ultrapure water (Milli-Q) was used to prepare all stock solution. Sodium hydroxide and Hydrochloric acid were used for pH adjustment. Ultrafiltration membrane was used for pre-filtered tap water.

Synthetic Water Preparation

Tap water were prepared by using ultrafiltration membrane to remove the contaminants (pH=8.7). All test s were conducted at room temperature. In all experiments, 1M of NaOH and HCL were used for pH adjustment for stock solutions.

Stock solutions containing 500 mg/L of SiO_2 were prepared by using Silicon dioxide (CAS: 14808-60-7). To simulate the stock solution to the originally pH of tap water, 20 millimoles of NaOH was added into solution for mixing in 24 hours to completely dissolved the silica. Stock solution containing 2 mg/L of Mn^{2+} was prepared by using sulfate monohydrate ($MnSO_4.H_2O$), stock solution was prepared by dissolution of $MnSO_4.H_2O$ in water.

Experimental Procedure

Jar Test in **Figure 1** is carried out as a batch test, accommodating a series of six beakers together with six spindle steel paddles. 500 mL of tap water were filled into 6 beakers by measuring pH of tap water. Tap water was prepared by using UF membrane filtration to avoid the contaminants, preventing the effect of experiment.100 mg/L of stock solution, which is completely dissolved were added into each beaker, there were a different final pH in each vessel. Add the pH adjusting reagent into tap water in the reaction vessels to reach the original tap water's pH and stir the solution. The same amount of SiO_2 concentration is added with varying concentration of manganese set at 0.002 mg/L, 0.01 mg/L, 0.02 mg/L, 0.07 mg/L, 0.2 mg/L, 0.4 mg/L. Start homogenisation mixing 100 rpm immediately after added the concentration of manganese in 1 minutes. After the mixing time has elapsed, take small sample from each beaker to measure the size distribution for the rapid mixing. The slow mixing is conducted at 40 rpm for 10, 30, and 60 minutes at room temperature. It is advantageous to take small amount of sample from each beaker to immediately measure the size distribution. The pH was measure immediately after the time is elapsed. Record all input and measured parameters in data sheet. Particle size distribution were analyzed using Dynamic Scattering (DLS).

Among various methods of measuring particle size, Dynamic Light Scattering (DLS) has gained popularity due to its ability to quickly assess the complete particle size distribution [4]. All samples were analyzed within 3 minutes of sample collection to reduce the possibility of further particle aggregation.

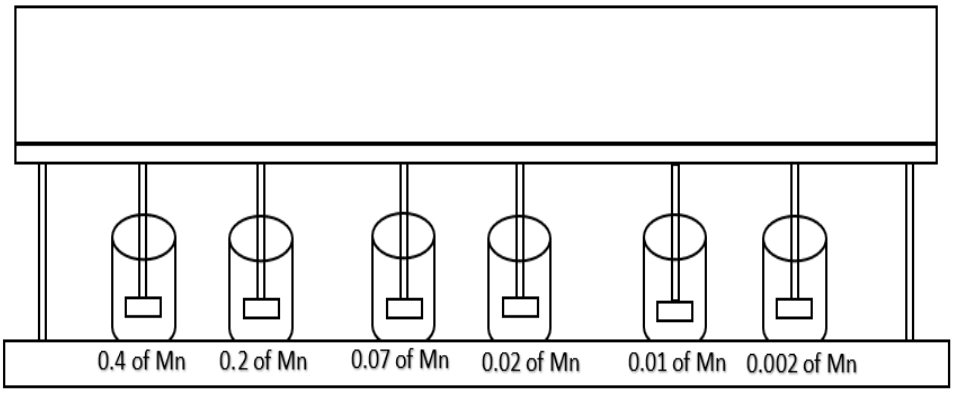


Figure 1 Jar Test Apparatus

Filtration resistance and cake formation calculation

In membrane filtration, the accumulation of silica particles on the membrane surface leads to the formation of a cake layer [3], which is significantly contributes to hydraulic resistance. This resistance directly impacts the filtration efficiency by reducing permeate flux and increase the required operating pressure. The following equation is used to calculate the cake resistance (R_c):

$$R_c = \frac{\alpha \,.\, C \,.\, V}{A} \quad \text{(Eq. 1)}$$

where R_c : cake resistance (m^{-1}); α: specific cake resistance (m/kg); C: concentration of particles in feed (kg/m^3); V: filtrate volume (m^3); A: Filtration area (m^2)
The specific cake resistance "α" can be calculation by:

$$\alpha = 180 \frac{(1-\epsilon)}{\epsilon^3} \frac{1}{\varphi_v{}^2 d_p{}^2 \rho_s} \quad \text{(Eq. 2)}$$

where ϵ: porosity of the cake; φ_v : volume shape factor; d_p: particle diameter (representing the average particle size of the particle forming the cake); ρ_s: solid density of the particle (kg/m^3). The **Table 1** exhibits few theoretical values of volume shape factor for known shape.

Table 1 Theoretical values of volume shape factors for known shape [13]

Shape	Volume shape factor
Spherical	1
Cubic	0.81
Plate like	0.51
Needle	0.29 to 0.2

RESULTS AND DISCUSSIONS

Analytical Parameter

The initial pH of tap water which is prepared by UF membrane was approximately 8.5 to 8.7 before Jar test experiment. **Table 2** show the pH value after Jar test, all samples were measured at various times intervals (1, 10, 30, and 60 minutes). Most samples showed a gradual decline in pH over time, especially within 30 minutes due to the chemical reaction occurring which reducing the pH. After 30 minutes, pH values in most samples stabilized and remained closed to 8.2 to 8.25 range, indicate the system reach equilibrium in 60 minutes. pH is a critical parameter in water treatment process, as it influences the size distribution and stability of particle in suspension. In this study, the addition of silica and manganese during experiment, slightly changes in pH were observed. However, this variation remained within the acceptable range of tap water as recommended by the World Health Organization.

Table 2 pH value of tap water after Jar test experiment

Time (min)	pH					
	B1	**B2**	**B3**	**B4**	**B5**	**B6**
1	8.12	8.38	8.3	8.62	8.57	8.58
10	8.1	8.25	8.23	8.29	8.3	8.35
30	8.05	8.1	8.21	8.19	8.2	8.11
60	8.05	8.2	8.25	8.22	8.23	8.23

Note: B1 = Sample was prepared with 100 mg/L of SiO_2 and 0.002 mg/L of Mn^{2+}
B2 = Sample was prepared with 100 mg/L of SiO_2 and 0.01 mg/L of Mn^{2+}
B3 = Sample was prepared with 100 mg/L of SiO_2 and 0.02 mg/L of Mn^{2+}
B4 = Sample was prepared with 100 mg/L of SiO_2 and 0.07 mg/L of Mn^{2+}
B5 = Sample was prepared with 100 mg/L of SiO_2 and 0.2 mg/L of Mn^{2+}
B6 = Sample was prepared with 100 mg/L of SiO_2 and 0.4 mg/L of Mn^{2+}

Particle Size Analysis

Figure 2 shows the particle-size distribution during Jar test experiments for 60 minutes. Low Mn^{2+} concentrations 0.002 mg/L shows minimal change in D_{50} over time, indicating insufficient ionic strength to promote significant particle bringing or neutralization. Moderate Mn^{2+} concentration (0.01 to 0.07 mg/L), exhibit a significant increase in D_{50}, peaking around 20 to 30 minutes, then sharply decrease. Therefore, the particle-size distribution depends on the detection of particles [14], a noticeable in particle size was observed to be decreased due too the aggregation and subsequent sedimentation of larger floc. During the measurement time, flocs grow in size and density, which tend to settle down and making them undetectable during particle size analysis, resulting in a lower measured D_{50}. In addition, high manganese concentrations (0.2 and 0.4 mg/l), show relatively low and stable D_{50} value throughout the experiment, indicating ineffective floc formation. The graph in **Figure 2** illustrates the noticeable change of particle size after 30 minutes, repeated experiment of 100 mg/L of silica with 0.02 mg/L and 0.2 mg/L of Mn^{2+} were conducted.

Figure 3 (a) illustrate the changes in median particle size (D_{50}) over time for both the original and duplicate experiments. Both trails show a peak in D_{50} at 30 minutes and return close to zero again in both trails due to the particle settling or disaggregation during measurement time. Moreover, good agreement in both experiment supports the repeatability and reliability of the measurement. **Figure 3 (b)** presents the change in median particle size over time for two trails. At the initial time of 1 minute, trail 2 shows a higher D_{50}, while trail 1 begins with a much lower D_{50}, which is the different in initial particle presence between two trails due to the different sampling point. The trail 2 was sampling at the bottom of the baker, while trail 1 was in the middle before measure the particle size. At 60 minutes, both line show very low D_{50} value implied that either particles remained dispersed or larger particles settled out and were not detected in suspension. The slight increase in trail 1 at 30 minutes due to the aggregation, but the absence of this behavior in trail 2 is not consistently reproducible. These concentration of manganese with silica is not significantly promote particle growth, particles formed tend to disperse or settle quickly.

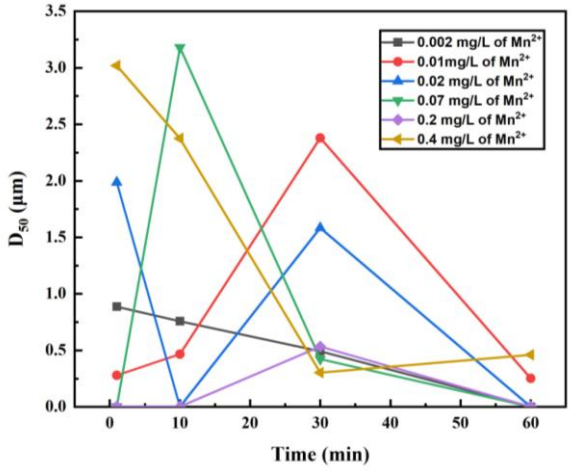


Figure 2 Particle Size Distribution

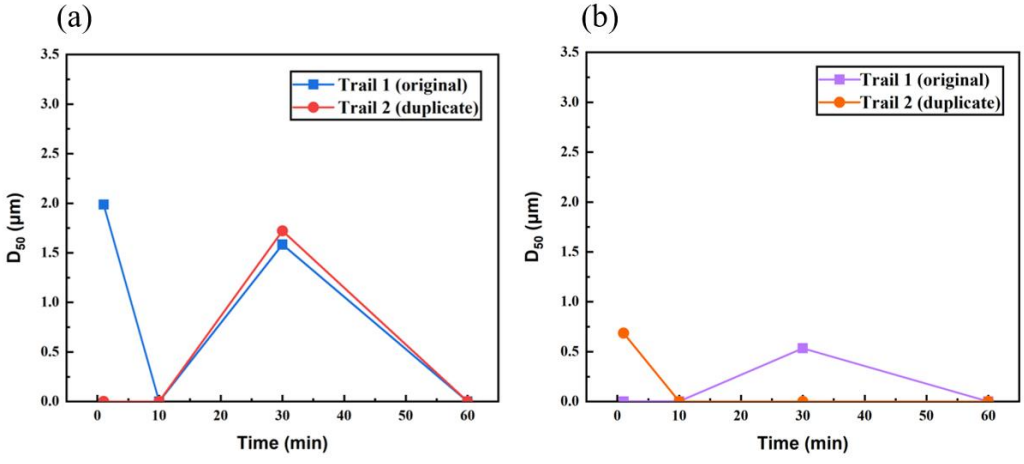


Figure 3 Particle Size Distribution: (a) Particle size distribution of 100 mg/L of SiO_2 with 0.002 mg/L of Mn^{2+}; (b) Particle size distribution of 100 mg/L of SiO_2 with 0.2 mg/L of Mn^{2+}

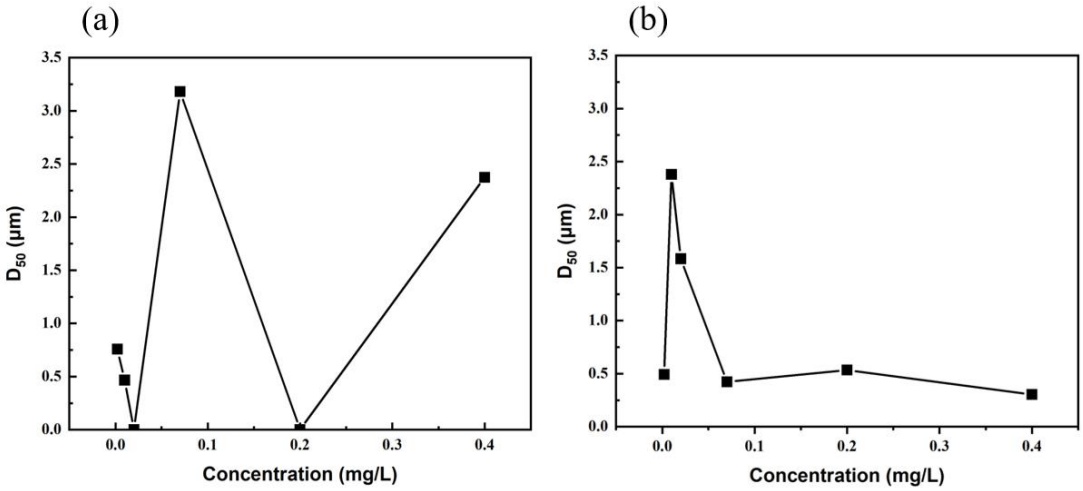


Figure 4 Particles Size Distribution: (a) Particles size distribution of 100 mg/L of SiO_2 with varying Mn^{2+} concentration in 30 minutes; (b) Particles size distribution of 100 mg/L of SiO_2 with varying Mn^{2+} concentration in 60 minutes

Table 3 Standard deviation value of particle size

Time (min)	Std. Dev.					
	B1	**B2**	**B3**	**B4**	**B5**	**B6**
1	2.327	0.1097	0.634	0.679	0.608	2.089
10	0.2239	2.173	1.040	1.611	1.251	1.161
30	0.745	2.874	2.102	0.2486	0.726	0.946
60	0.00009	0.2630	0.00009	0.00009	0.00009	0.373

Figure 4 (a) illustrates the particles size (D_{50}) of silica with varying Mn^{2+} concentrations in 30 minutes. D_{50} sharply increase at 0.7 mg/L of Mn^{2+} with 100 mg/L of SiO_2 concentration, indicate the strong particle aggregation at this concentration. This is likely the optimum point for aggregation, where manganese ions effectively promote flocculation or bridging between particles. At 0.2 mg/L, particles size drops to near zero, indicate a collapse of aggregation behavior, while the particles reaggregation occur at 0.4 mg/L of Mn^{2+}, potentially due to excess irons facilitating bridging once again.

Figure 4 (b) indicate significant particles formation at very low concentration of Mn^{2+} at 0.002 mg/L with SiO_2 concentration. Initial low level of Mn^{2+} in 60 minutes may enhance aggregation, while further addition of Mn^{2+} could lead to destabilization which is decrease particle size. At higher concentrations, the manganese may oversaturate particle surface, preventing further bridging and leading to smaller, more disperse particles. The concentration and time that best for the smallest particles with significant aggregation is 0.2 mg/L at 30 minutes, a sharp drop in particle size after reaching at peak 0.07 mg/L was shown that the aggregation has occurred, and particle may have flocculated into large clusters that settle out or are no longer detected in the suspended phase. In 60 minutes, although a similar trend is seen, some re-dispersion of aggregation might have occurred, indicate less stable or less compact aggregation over time. The value of standard deviation is shown in **Table 3**. Based on the SD value, sorting improves over time by 60 minutes which is indicating stabilization of particle size distribution [15]**.** By 60 minutes, nearly all samples are well sorted, evidential that the particle in 60 minutes is not well aggregated. Although all samples were well sorted in 60 minutes, but 30 minutes is acceptable and meaningful as the time point for significant aggregation, even if sorting is not yet fully stabilized. The level of sorting in 30 minutes is acceptable for analyzing aggregation efficiency, although the SD values at 30 minutes are not all “very well sorted”, most samples fall within “moderately” to “moderately well sorted” ranges.

Hydraulic Resistance and cake resistance measurement

Based on previous studies, the porosity of cake formed by silica particles flocculated with metal ions such as Mn^{2+} typically ranges between 0.55 and 0.70, depending on floc structure, concentration, and aggregation time [16]. In this study, a cake porosity value of 0.6 was assumed based on typical ranges reported for flocculated silica-manganese particle. The silica is in crystalline form, commonly crystalline structure includes cubic, hexagonal, and tetragonal. The cubic has been selected in this calculation. The specific cake resistance values indicate a moderately resistant cake structure, which is consistent with partially compressible flocs formed by the aggregation of silica in the presence of low concentrations of Mn^{2+}. The hydraulic resistance value remained below 10^{13} m^{-1}, indicating that cake formation was present but not serve. Hydraulic resistance is calculated in **Table 4.**

Table 4 Volume shape factor and PSD measurements of the particle

N.o	Shape	Volume shape factor	Particle size distribution		Specific cake resistance (m/kg)	Hydraulic resistance (m^{-1})
			D_{50} (µm)	Std. Dev.		
B1	Cubic	0.81	0.492	0.745	8.07×10^{11}	3.74×10^{10}
B2			2.380	2.874	0.345×10^{11}	0.16×10^{10}
B3			1.584	2.102	0.779×10^{11}	0.361×10^{10}
B4			0.423	0.2486	10.92×10^{11}	5.06×10^{10}
B5			0.534	0.726	6.85×10^{11}	3.18×10^{10}
B6			0.303	0.946	21.28×10^{11}	9.89×10^{10}

CONCLUSION

An understanding of particle size behavior in water is crucial in membrane filtration because it is directly influencing the fouling potential, which affects the efficiency, lifespan, and operating cost of the filtration system. This study has progressed the understanding of the mixing SiO_2 with varying Mn^{2+} concentration. It has also highlighted the behavior of particle size has formed in different time and concentration to see the smallest particle size with significant particle aggregation, intentionally create a challenge scenario for the filtration system, beneficial for further studies to evaluate the membrane's behavior under extreme fouling condition, develop more effective cleaning protocol, evaluate different membrane materials or pore size for resistance severe fouling. Additional further work may include the investigation of the membrane fouling in terms of particle size.

ACKNOWLEDGEMENT

The author thanks to ASEAN and non-ASEAN scholarship program. This research was partially funded by the Kurita Asia Research Grant 2023, 23Pth009, provided by Kurita Water and Environment Foundation.

REFERENCE

[1] S. F. Anis, R. Hashaikeh, and N. Hilal, "Microfiltration membrane processes: A review of research trends over the past decade," *Journal of Water Process Engineering*, vol. 32, 2019.

[2] M. Mulder, *Basic principles of membrane technology*. Springer science & business media, 2012.

[3] Y. Jang *et al.*, "Colloidal silica fouling mechanism in direct-contact membrane distillation," *Desalination*, vol. 527, 2022.

[4] S. L. D. Kenari, "Size and Zeta Potential of Oxidized Iron and Manganese in Water Treatment: Influence of pH, Ionic Strength, and Hardness," 2016.

[5] A. R. P. Pizzichetti, C. Pablos, C. Álvarez-Fernández, K. Reynolds, S. Stanley, and J. Marugán, "Evaluation of membranes performance for microplastic removal in a simple and low-cost filtration system," *Case Studies in Chemical and Environmental Engineering*, vol. 3, 2021, doi: 10.1016/j.cscee.2020.100075.

[6] A. Antony, J. H. Low, S. Gray, A. E. Childress, P. Le-Clech, and G. Leslie, "Scale formation and control in high pressure membrane water treatment systems: A review," *Journal of membrane science*, vol. 383, no. 1-2, pp. 1-16, 2011.

[7] W. Arras, N. Ghaffour, and A. Hamou, "Performance evaluation of BWRO desalination plant—a case study," *Desalination*, vol. 235, no. 1-3, pp. 170-178, 2009.

[8] N. Porcelli and S. Judd, "Chemical cleaning of potable water membranes: A review," *Separation and purification technology*, vol. 71, no. 2, pp. 137-143, 2010.

[9] E. M. Vrijenhoek, S. Hong, and M. Elimelech, "Influence of membrane surface properties on initial rate of colloidal fouling of reverse osmosis and nanofiltration membranes," *Journal of membrane science*, vol. 188, no. 1, pp. 115-128, 2001.

[10] C. Visvanathan, "Studies on colloidal membrane fouling mechanisms in crossflow microfiltration," *Journal of membrane science*, vol. 45, no. 1-2, pp. 3-15, 1989.

[11] G. Belfort, R. H. Davis, and A. L. Zydney, "The behavior of suspensions and macromolecular solutions in crossflow microfiltration," *Journal of membrane science*, vol. 96, no. 1-2, pp. 1-58, 1994.

[12] C. Y. Tang, T. Chong, and A. G. Fane, "Colloidal interactions and fouling of NF and RO membranes: a review," *Advances in colloid and interface science*, vol. 164, no. 1-2, pp. 126-143, 2011.

[13] D. Bourcier *et al.*, "Influence of particle size and shape properties on cake resistance and compressibility during pressure filtration," *Chemical Engineering Science*, vol. 144, pp. 176-187, 2016.

[14] C. Zhang, J. Lohwacharin, and S. Takizawa, "Properties of residual titanium dioxide nanoparticles after extended periods of mixing and settling in synthetic and natural waters," *Sci Rep*, vol. 7, no. 1, p. 9943, Aug 30 2017, doi: 10.1038/s41598-017-09699-9.

[15] P. Philip E. Plantz, "Explanation of Data Reported by Microtrac Instruments ".

[16] K. J. Howe and M. M. Clark, *Coagulation pretreatment for membrane filtration*. American Water Works Association, 2002.

20R5-19

Enhancing Sustainability in Rice Straw Pulp Production: A Zero Discharge Model Through Biological Treatment and Water Recycling

Tiammanee Rattanaweerapan[1*], Supatpong Mattaraj[1], Wipada Dechapanya[1], Sompop Sanongraj[1], and Karnika Ratanapongleka [1]

[*1]Department of Chemical Engineering, Faculty of Engineering, Ubon Ratchathani University, Ubonratchathani, Thailand.
[*]*Phone : 0873779599, E-mail : Tiammanee.r@ubu.ac.th*

ABSTRACT

The utilization of rice straw, an agricultural byproduct, in pulp production provides an environmentally sustainable alternative to wood-based materials. However, the pulping process generates wastewater with high concentrations of organic pollutants, such as BOD, COD, and lignin, which exceed regulatory discharge limits. This study demonstrated the potential of biological treatment using *Bacillus subtilis* for reducing organic pollutants in rice straw pulping wastewater. Optimal treatment was achieved with 15% dilution of wastewater where the concentration of BOD and COD were 510, 670 mg/L, respectively, and a microbial concentration of 30% (m/v). The BOD and COD removal efficiencies were 83.53% and 66.75%, respectively. Additionally, the water recycling experiment revealed that up to 50% of treated water could be reused in the pulping process without a significant impact on water quality. The findings support the development of a zero-discharge model that promotes environmental sustainability and resource conservation in agro-industrial applications.

Keywords : rice straw pulping; biological wastewater treatment; *Bacillus subtilis*; zero discharge; water recycling

INTRODUCTION

The escalating depletion of wood resources and intensifying environmental concerns have prompted a surge in the exploration of alternative, non-wood pulp sources. Among these, rice straw, an abundant agricultural byproduct, has garnered considerable attention as a promising feedstock for pulp production [1]. Often regarded as an agricultural waste, rice straw is typically underutilized or subjected to open burning, a practice that contributes significantly to air pollution and the emission of greenhouse gases. By harnessing rice straw for pulp manufacturing, the paper industry can address two pressing challenges: mitigating environmental degradation and ensuring the availability of a sustainable raw material. However, the pulping of rice straw generates wastewater laden with organic pollutants, including lignin, phenolic compounds, and suspended solids. These pollutants frequently exceed regulatory discharge limits, posing substantial risks to aquatic ecosystems and public health if not treated adequately. Conventional treatment methods, whether chemical or physical, are often cost-prohibitive, energy-intensive, and lead to the generation of toxic sludge or secondary pollutants [2]. In contrast, biological treatment utilizing *Bacillus subtilis* offers a promising, cost-effective, and environmentally sound alternative. This bacterium is renowned for its potent enzymatic activity, which facilitates the degradation of various organic pollutants, including lignin and cellulose derivatives [3]. Furthermore, *Bacillus subtilis* is non-pathogenic, exhibits resilience under varying environmental conditions, and produces minimal secondary waste [4].

This study investigates the efficacy of *Bacillus subtilis* in treating wastewater generated from rice straw pulping, while integrating a recycling system to achieve a zero-discharge model. This approach not only minimizes waste generation but also conserves water resources, thereby contributing to the broader objectives of circular economy practices within agro-industrial sectors. The research aims to establish a scalable and sustainable wastewater management model for pulp production, ensuring compliance with environmental regulations and fostering long-term industrial sustainability.

METHODOLOGY

Wastewater Sample Preparation : The wastewater generated in the production of the pulp comes from two stages: hot-chemical pulping and washing processes. For the wastewater treatment experiment with *Bacillus subtilis*, wastewater from the hot-chemical pulping process is used, while wastewater recycling is used from the pulp washing process.. Preliminary analysis focused on BOD, COD, and pH.

Microbial Preparation : *Bacillus subtilis*, obtained in powdered form from a local chemical supplier, was used for the treatment experiments.

Wastewater Treatment Experiments : The wastewater, initially exhibiting a high pH, was adjusted to a range of 6–9 before further treatment. The study comprised two phases; wastewater was diluted to 15%, 25%, and 40% (v/v) and treated in 30-liter plastic tanks. Samples were collected on days 0, 5, 10, and 20 to analyze BOD, COD, and pH. The dilution level with the highest removal efficiency was selected for further microbial proportion analysis. The second phase was the optimization of microbial proportion: two microbial concentrations, 10% and 30% (m/v), were tested and compared with the control (0%*Bacillus subtilis*). Treatment was performed in 30-liter tanks, with samples collected on days 0, 5, 10, and 20 to assess BOD and COD removal efficiency.

Water-Recycle Experiment: For water recycling, wastewater from the washing process was mixed with tap water at 20%, 30%, and 50% ratios before reuse in the pulping process. Key parameters were analyzed before and after treatment, including pH, COD, and lignin content.

RESULTS AND DISCUSSIONS

According to the study, the raw wastewater exhibited excessive contaminant levels, necessitating dilution before biological treatment (Table 1). The high pH (12.62), BOD (2,922 mg/L), and COD (20,466 mg/L) of the undiluted wastewater rendered it unsuitable for direct microbial degradation. Dilution of wastewater at concentrations of 15, 25, and 40% reduced BOD and COD values as shown in Table 1, and to be suitable for the growth of *Bacillus subtilis*, the pH values were adjusted to be as similar and neutral as possible.

Table 1. Characteristics of the raw and diluted wastewater samples before treatment

Parameters	Raw wastewater	Proportion of wastewater		
	100%	**15%**	**25%**	**40%**
BOD (mg/L)	2,922	510	600	840
COD (mg/L)	20,466	670	1,341	2,170
pH	12.62	7.10	7.00	7.10

Wastewater Dilution Optimization : Figure 1 shows that dilution significantly reduced pollutant concentrations to within treatable ranges for *Bacillus subtilis*. Among the three tested dilution levels,15%, 25%, and 40%, the 15% dilution exhibited the highest removal efficiency for both BOD and COD. BOD removal performed well during the first 5 days of the experiment (Figure 1(a)). COD was well achieved during the 10 days of the experiment (Figure 1 (b)), while the pH value tended to increase from about 7 to about 8.5 (Figure 1 (c)). This may be due to the products from organic degradation by *Bacillus subtilis* contain substances that have basic properties [5]. With the initial concentration of 510 and 670 for BOD and COD, respectively, BOD was reduced by 83.53%, while COD removal reached 66.75%, indicating efficient microbial activity at lower initial pollutant concentrations. This result confirms that excessive organic loading can inhibit microbial processes, a finding consistent with previous work by Worku et al. (2023) [1]. They emphasized the importance of maintaining moderate BOD levels for optimal biodegradation. Similarly, Kumar et al. (2022) [2] demonstrated that a BOD range of 500–600 mg/L offers ideal conditions for

effective biological treatment using Bacillus cereus. In our study, Bacillus subtilis showed comparable performance, with added benefits of broader tolerance and safer handling.

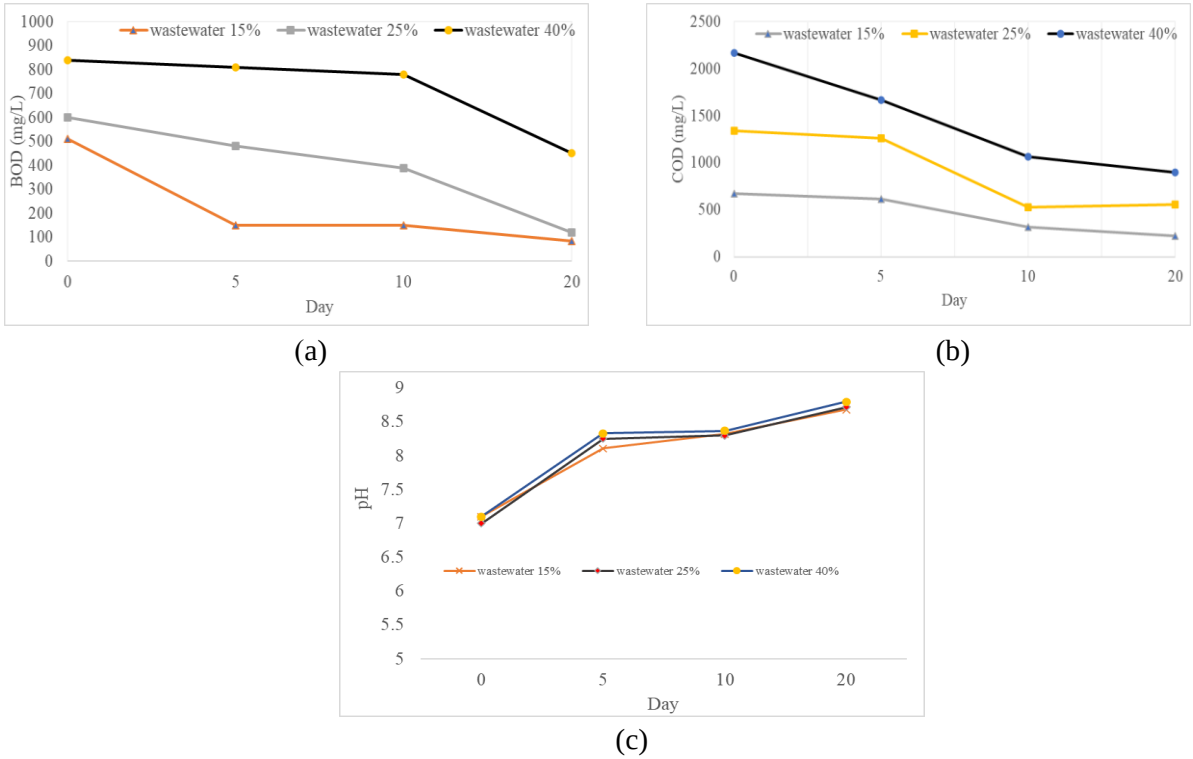


Figure 1 Changes in BOD (a), COD (b), and pH (c) of treatment wastewater experiment by using various dilutions (15%, 25%, and 40%)

Microbial Proportion Optimization: In the second phase, optimizing the microbial concentration (10% vs 30% m/v) further improved degradation rates. Figure 2 (a) and (b) show the decrease of BOD and COD concentration from the initial to the final experiments. The microbial concentration of 10%, 30%, and 0% has COD values starting at 790, 840, and 870 after 20 days. COD values decreased to 39, 54, and 132, respectively. BOD Starting at 413, 471, and 407, after 20 days, BOD values decreased to 97, 103, and 263, respectively. The pH value increases from day 0 to day 5 and then starts to equilibrium condition. The BOD treatment efficiency of 10%, 30%, and 0% microbial filling rates was 76.38%, 77.96%, and 35.38%, respectively. Though both concentrations effectively reduced pollutants, a 30% concentration yielded slightly better results in the early stages, suggesting faster microbial acclimatization and substrate consumption. However, the long-term performance differences were marginal, indicating that a lower microbial dosage might be more cost-effective for industrial-scale operations without compromising treatment efficiency. therefore, it can be said that 10% of microbial concentration is enough for this wastewater treatment.

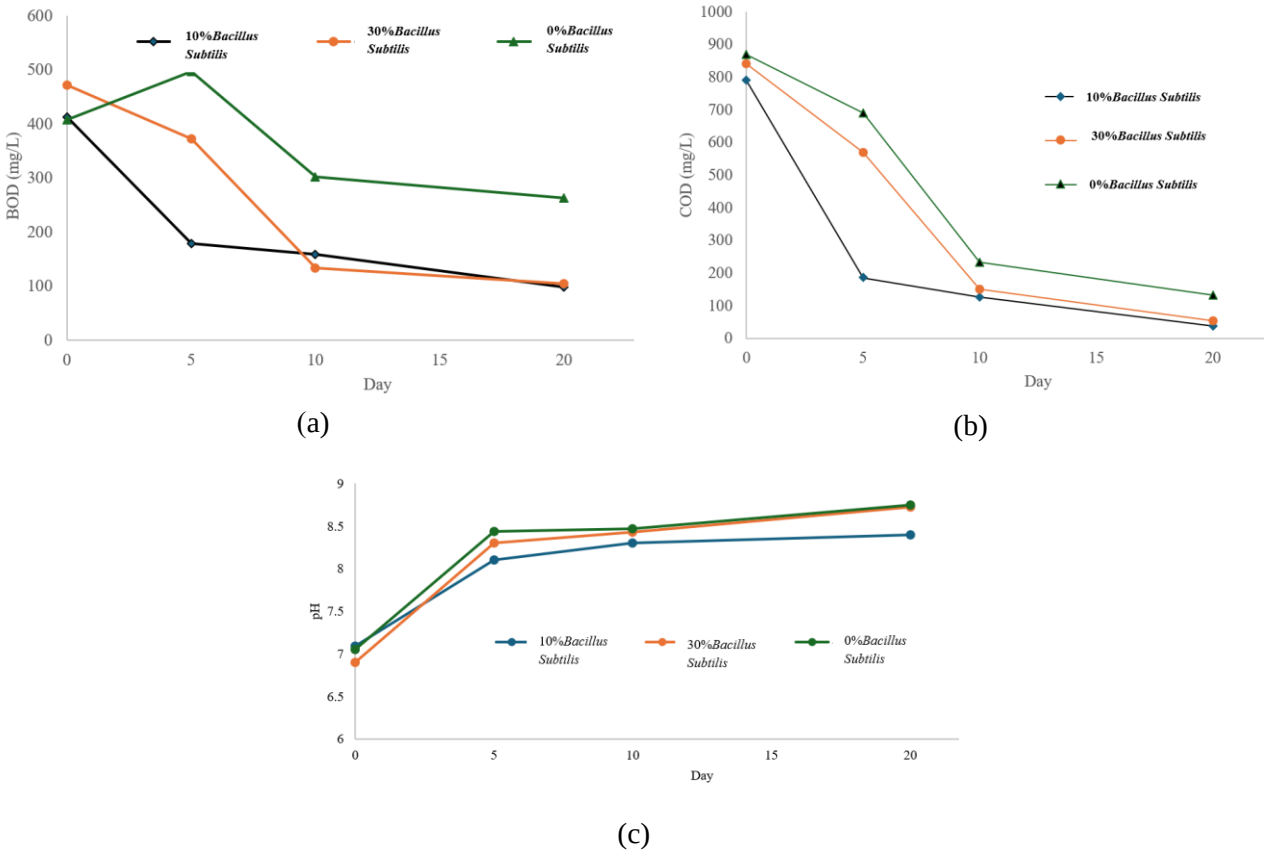


Figure 2 Changes in BOD (a), COD (b), and pH (c) of wastewater treatment experiments by using various microbial concentrations (10%, 30%, and 0%)

Water Recycling Potential

The water recycling experiments explored the reuse potential of treated wastewater in the pulping process. When mixed with fresh tap water in ratios of 20%, 30%, and 50%, the effluents exhibited varying pH, COD, and lignin contents (Table 2). The COD value is directly proportional to the percentage of recycling. This is due to the composition of the substances present in the washing water used. The addition of more recycled water results in an increase in the pH value of wastewater from the hot-chemical process and may affect the removal of lignin, causing lignin to be removed from the rice stubble pulp and dissolved in the wastewater. The lignin content is higher when recycled water is used in a higher proportion, as can be seen that 50% lignin can be dissolved almost as high as using a new solution (0% recycling), as shown in Figure 3. Despite effective BOD and COD removal, lignin remained a persistent challenge. Its resistance to microbial degradation and tendency to accumulate over multiple cycles could impact product quality and system stability. Future enhancements may include integrating advanced oxidation or membrane filtration to address residual lignin and non-biodegradable substances in long-term recycling setups.

Table 2. Key parameters of wastewater from the recycling experiments.

Samples	pH	COD (mg/L)	Lignin (%w/v)
Effluent from the washing process	11.78	1,576	0.20
Effluent from the hot-chemical pulping by water recycling			
0%	12.93	22,883	5.22
20%	12.27	14,550	3.53
30%	12.31	16,350	3.85
50%	12.33	17,883	3.94

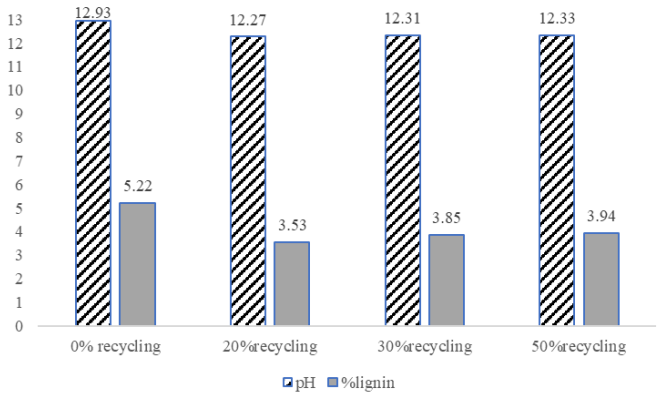


Figure 3 The soluble lignin and pH relationship in recycling wastewater

The zero-discharge diagram of rice straw pulp production : From this study, the zero-discharge model of rice straw pulp production can be written as a diagram as follows (Figure 4). The diagram illustrates a zero-waste discharge system in paper production from rice stubble, emphasizing efficient wastewater management and recycling. The process begins with hot-chemical pulping of rice stubble, which generates wastewater. This wastewater is treated biologically using *Bacillus subtilis*, a bacterium that helps degrade organic pollutants. The treated water is then recycled back into the system, supplying the hot-chemical pulping, washing, and possibly the paper production stages. This closed-loop water system ensures that no wastewater is discharged into the environment. By integrating biological treatment and water reuse, the process not only minimizes environmental impact but also promotes sustainability and resource efficiency.

CONCLUSION

This study demonstrated the potential of biological treatment using *Bacillus subtilis* for reducing organic pollutants in rice straw pulping wastewater. Optimal treatment was achieved with 15% dilution of wastewater where the concentration of BOD and COD were 510, 670 mg/L, respectively, and a microbial concentration of 30% (m/v). The BOD and COD removal efficiencies were 83.53% and 66.75%, respectively. Water recycling experiment, revealing that up to 50% of treated water could be reused in the pulping process without a significant impact on water quality. The findings support the development of a zero-discharge model that promotes environmental sustainability and resource conservation in agro-industrial applications.

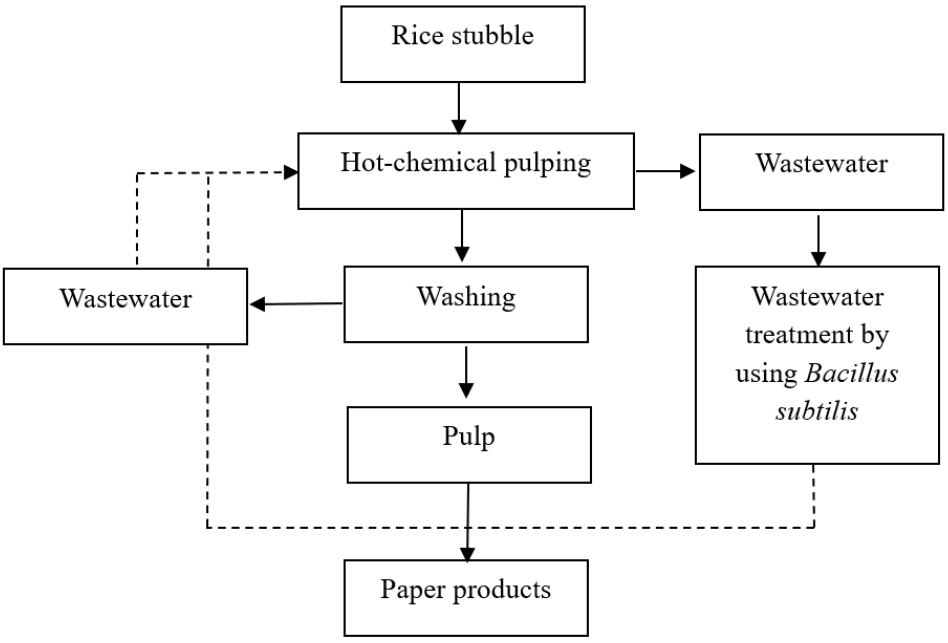


Figure 4 The zero discharge diagram of rice straw pulp production

ACKNOWLEDGEMENT

The authors would like to thank our colleagues at the Department of Environmental Engineering for their valuable insights and support throughout the study. Special thanks to the funding and technical support teams who contributed to the wastewater treatment and water recycling experiments. This work would not have been possible without the collaboration and encouragement of all involved.

REFERENCE

[1] Limenew Abate Worku, Archana Bachheti, Rakesh Kumar Bachheti , Cristiano E. Rodrigues Reis, and Anuj Kumar Chandel. 2023. Agricultural Residues as Raw Materials for Pulp and Paper Production: Overview and Applications on Membrane Fabrication. Membranes.13.228.

[2] Rajesh Kumar, Anjali Singh, Annapurna Maurya, Pooja Yadav, Ashutosh Yadav, Pankaj Chowdhary, Abhay Raj. 2022. Effective bioremediation of pulp and paper mill wastewater using *Bacillus cereus* as a possible kraft lignin-degrading bacterium. Bioresources Technology. 352.127076.

[3] Rafiu Olasunkanmi Yusuf, Zainura Zainon Noor, Mohd Ariffin Abu Hassan, Samuel Enahoro Agarry, Bamidele Ogbe Solomon. 2012. A comparison of the efficacy of two strains of Bacillus subtilis and Pseudomonas fragii in the treatment of tannery wastewater. Desalination and Water Treatment.51.3189–3195.

[4] T. Siddharth, P. Sridhar, V. Vinila, R.D. Tyagi. 2021. Environmental applications of microbial extracellular polymeric substance (EPS): A review. Journal of Environmental Management 287. 11228.

[5] Amira Hassan Al-Abdalall and Eida Marshid Al-Khaldi. 2016. Production of alkaline proteases by alkalophilic Bacillus subtilis during recycling animal and plant wastes. African Journal of Biotechnology. 15(47). 2698-2702.

20R6-03

Wastewater Treatment Efficiency of Electrocoagulation in the Compressor Industry

Ampaporn Jaidee[1]Chulalak Singharat[2] Sawarin Suejai[2] Sakkarin Lajoy[3] and Kowit Suwannahong[4*]

[1] Environment Officer Siam Compressor Industry Co., Ltd,[2] Undergraduate student (B.Sc. in Environmental Health) Public Health, Burapha University, [3]Manager- Sustainability Development Department, Siam Compressor Industry Co., Ltd, [4] Associate Professor, Dean of the Faculty of Public Health, Burapha University
[*]Phone : [1]0840081459,[4]0619516639, E-mail :[1]ampapornj@siamcompressor.com, [4*]kowit.su@go.buu.ac.th.*

ABSTRACT

Water is an essential resource for industrial processes. The innovation approach for reclaimed water is a choice for sustainable wastewater management. This research aims to identify a sustainable and cost-efficient solution for wastewater treatment by comparing coagulation-flocculation and electrocoagulation methods in the compressor production industry. In particular, the wastewater comes from different sources such as part washing, dipping, deionized water systems, cooling towers, and cleaning. The study compares the efficiency of coagulation-flocculation and electrocoagulation wastewater treatment methods and assesses both systems' carbon footprint using experimental studies. The study found that coagulation-flocculation is more effective in reducing turbidity than Electrocoagulation, with reductions of 96.43% and 81.88%, respectively. However, Electrocoagulation is more effective in reducing total dissolved solids (TDS), achieving a 5.80% reduction. The coagulation-flocculation results in a substantially higher increase in conductivity than Electrocoagulation. Specifically, coagulation-flocculation leads to a 43% increase in conductivity after 120 minutes. In addition, wastewater treatment using coagulation-flocculation produces 72% more sludge than Electrocoagulation during the same sedimentation period of 120 minutes. Regarding treatment costs, which include electricity usage, sludge treatment, and chemical expenses, the electrocoagulation method is associated with a lower overall cost, amounting to 36.94 baht per cubic meter. In contrast, the coagulation-flocculation method has a total cost of 95.78 baht per cubic meter. A limitation of Electrocoagulation is that the pH of water must be maintained within the range of 6-8 to ensure good water quality after treatment. Regarding treatment costs, which include electricity usage, sludge treatment, and chemical expenses, the electrocoagulation method is associated with a lower overall cost, amounting to 36.94 baht per cubic meter. In contrast, the coagulation-flocculation method has a total cost of 95.78 baht per cubic meter. A limitation of Electrocoagulation is that the pH of water must be maintained within the range of 6-8 to ensure good water quality after treatment. The research outcome is beneficial for developing environmentally friendly wastewater treatment approaches, reducing chemical usage, and minimizing greenhouse gas emission impacts. The limitation of pH levels may make electrocoagulation systems unsuitable for wastewater sources with fluctuating pH values. However, if this parameter can be controlled, it will help reduce environmental impacts and lower wastewater treatment costs.

Keywords: Wastewater Treatment, Coagulation-flocculation, Electrocoagulation, Carbon Footprint

INTRODUCTION

In the compressor production process, wastewater is generated from parts washing systems, Dipping, Deionized water systems, cooling towers, and cleaning. The effluents from these sources primarily contain chemicals, heavy metals, oils, and surfactants. Acidic and alkaline substances originating from chemicals used in the regeneration of the water treatment system are also present. Therefore, it essential for the company to implement a wastewater treatment system to regulate and manage the effluents generated from its production processes, ensuring that the quality of the treated water complies with established standards before discharge into external water sources. Currently, the company uses a coagulation-flocculation treatment system, with main chemicals including $FeCl_3$, $Ca(OH)_2$, and Polymer, [2] [3] generating large amounts of sludge and high chemical consumption, subsequently leading to increased operational costs. To address this issue, the study aims to compare the efficiency of coagulation-flocculation and electrocoagulation wastewater treatment methods and evaluate the carbon footprint associated with each system through experimental studies.

METHODOLOGY

This comparative experiment of the efficiency between coagulation-flocculation and electrocoagulation wastewater treatment establishes the following performance indicators: (1) treatment cost per cubic meter of water, (2) volume of sludge generated, and (3) treatment duration. The parameters measured include pH, total dissolved solids (TDS), turbidity, and electrical conductivity as shown in Figure 1 and 2. In addition, operational data are collected to assess the carbon footprint per cubic meter of wastewater treated following the guidelines of the Carbon Footprint Products issued by the Thailand Greenhouse Gas Management Organization (Public Organization), or TGO .

Coagulation-flocculation Concept

The principle of coagulation-flocculation involves the formation and aggregation of precipitates. The chemicals used are referred to as coagulants, typically divided into two main categories. The first includes inorganic metal salts, such as aluminium sulfate (alum), ferrous sulfate, and ferric chloride. The second category comprises pre-polymerized coagulants, including poly aluminium chloride (PAC), poly aluminium sulfate (PAS), and polyaluminium chlorosulfate (PACS) [3]

In this study, ferric chloride ($FeCl_3$) and calcium hydroxide ($Ca(OH)_2$) were used as chemical coagulants, while an anionic polymer was applied during the flocculation process[2] as shown in Figure 1.

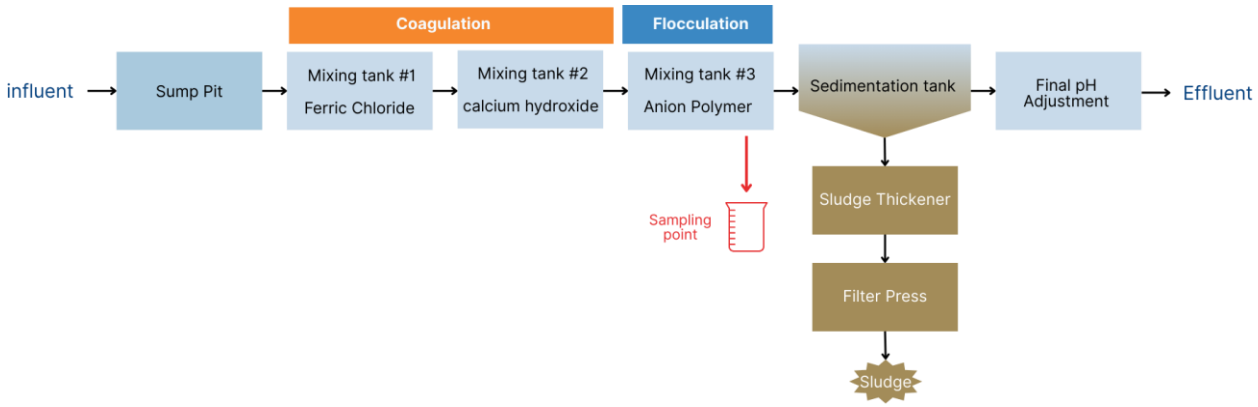


Figure 1 Coagulation-flocculation ($FeCl_3$, $Ca(OH)_2$, and Polymer) Diagram

Electrocoagulation Concept

The electrocoagulation system comprises an electrolytic cell containing an anode and a cathode, which are externally connected to a direct current power source and submerged in an electrolyte solution. [6] The fundamental principles of the electrocoagulation are as follows: [4]

1) A redox reaction occurs: oxidation at the anode, causing metal ions to be released, while reduction occurs at the cathode, producing hydrogen gas.
2) Destabilization of dissolved particles or substances in water happens through the neutralization of charges—contaminants with opposite charges are attracted to the metal ions from the anode, leading to neutral particles that more easily aggregate into flocs.
3) These larger flocs are removed either by sedimentation or flotation. Hydrogen gas generated at the cathode helps lift the flocs to the water surface, making them easier to separate.

In this study, the electrocoagulation unit was integrated with the existing coagulation–flocculation treatment system. The reactor receives influent water from the sump pit and, after treatment, transfers the effluent to the sedimentation tank. The aluminum metal was used as the electrode, and the oxidation-reduction reactions involved are defined as follows: [6]

Anode Reaction……....$Al \rightarrow Al^{3+} + 3e^-$

Cathode Reaction…….$2H_2O + 2e^- \rightarrow H_2(g) + 2OH^-$

Overall Reaction……...$Al^{3+} + 3H_2O \rightarrow Al(OH)_3 + 3H^+$



Figure 2 Electrocoagulation Reactor

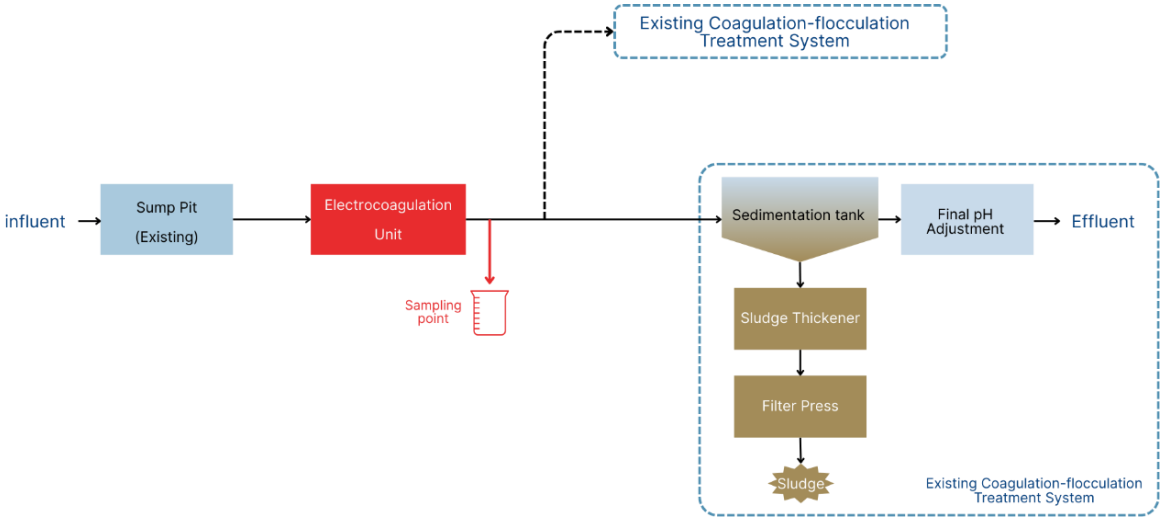


Figure 3 Electrocoagulation integrated installed with Coagulation-flocculation Diagram

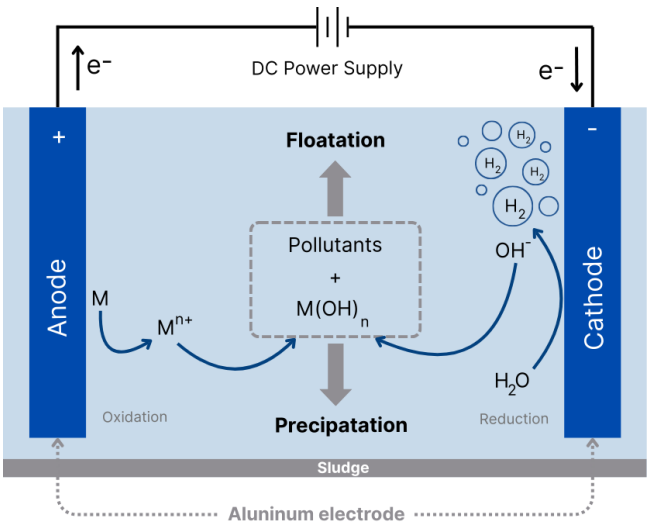


Figure 4 Schematic of Electrocoagulation Concept [1][4][5]

RESULTS AND DISCUSSIONS

Wastewater Treatment Efficiency

The study found that coagulation-flocculation is more effective in reducing turbidity than Electrocoagulation, with reductions of 96.43% and 81.88%, as shown in figure 5. Also, the coagulation-flocculation can settle and achieve a removal efficiency of 93.19% after 20 minutes of mixing, indicating a faster settling rate than Electrocoagulation.

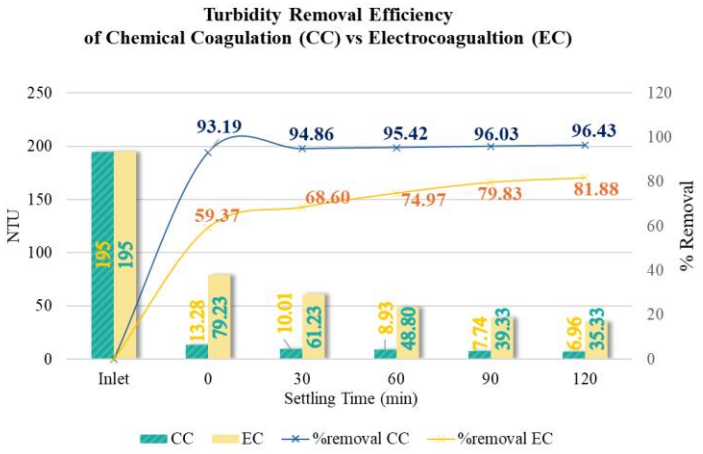


Figure 5 Comparison results of Turbidity Removal Efficiency of Coagulation-flocculation and Electrocoagulation

However, Electrocoagulation is more effective in reducing total dissolved solids (TDS), achieving a 5.80% reduction, as shown in figure 6—coagulation-flocculation results in a substantially higher increase in conductivity than Electrocoagulation. Specifically, coagulation-flocculation leads to a 43% increase in conductivity after 120 minutes, as shown in Figure 7.

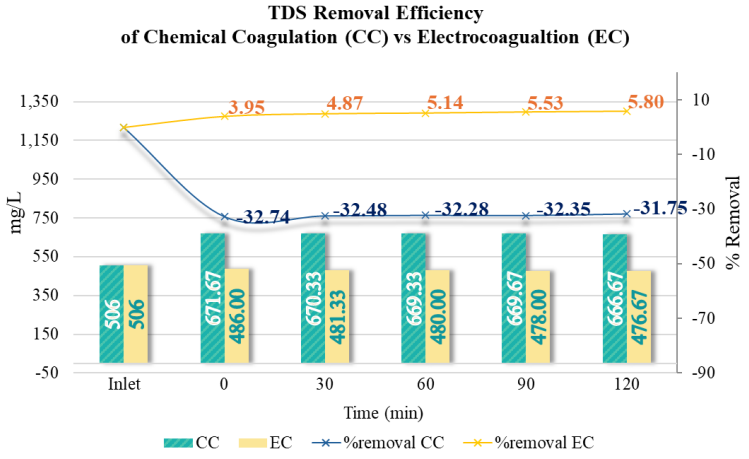


Figure 6 Comparison results of Total Dissolved Solid Removal Efficiency of Coagulation-flocculation and Electrocoagulation

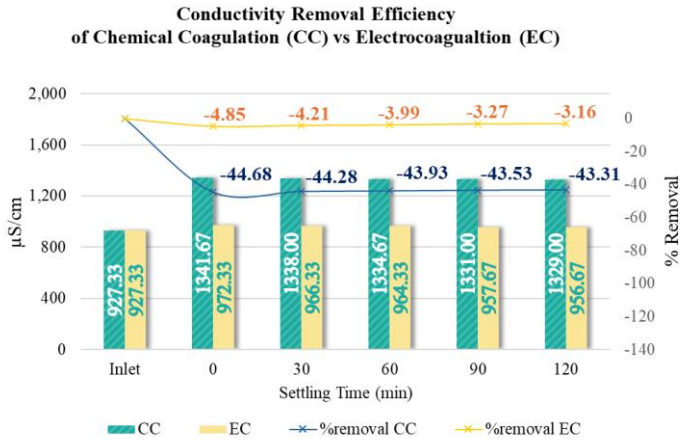


Figure 7 Comparison results of Conductivity Removal Efficiency of Coagulation-flocculation and Electrocoagulation

Both treatment methods showed relative stability for the pH values, with no noticeable change compared to the influent water, as shown in Figure 8.

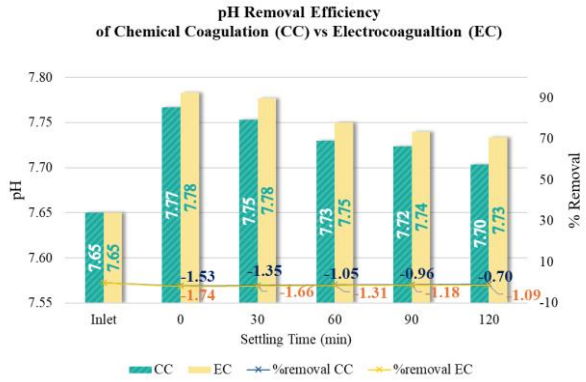


Figure 8 Comparison results of pH Removal Efficiency of Coagulation-flocculation and Electrocoagulation

In addition, wastewater treatment using coagulation-flocculation produces 72% more sludge than Electrocoagulation during the same sedimentation period of 120 minutes, as shown in figure 9 and figure 10.

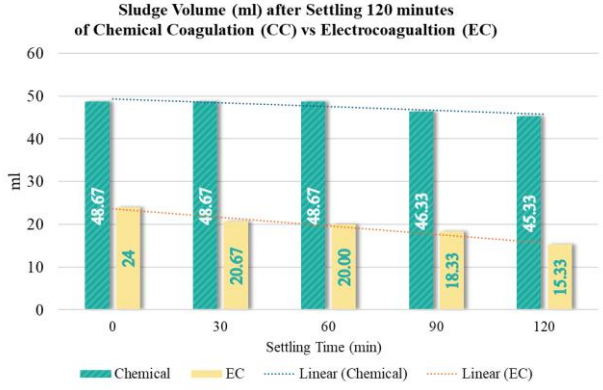


Figure 9 Comparison results of Sludge Volume after Settling of Coagulation-flocculation and Electrocoagulation

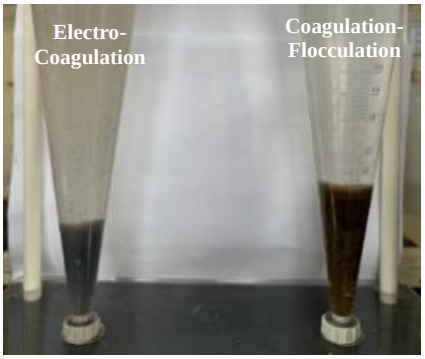


Figure 10 Sludge Volume of Coagulation-flocculation and Electrocoagulation

Wastewater Treatment Cost

Regarding treatment costs, which include electricity usage, sludge treatment, and chemical expenses, the electrocoagulation method is associated with a lower overall cost, amounting to 36.94 baht per cubic meter. In contrast, the coagulation-flocculation method costs 95.78 baht per cubic meter, as shown in Table 1.

Table 1 Comparison Operation Cost per cubic meter (THB) of Coagulation-flocculation and Electrocoagulation

Operation Cost (THB/m^3)	Treatment Method	
	Coagulation-flocculation	**Electrocoagulation**
Electricity Cost	0.11	4.11
Sludge Treatment Cost*	91.93	32.83
Chemical Cost	3.74	-
Total Operation Cost	95.78	36.94

* Calculate the wet weight of sludge after settling 120 min

Regarding preventive maintenance, the sludge filter press used in the coagulation-flocculation method requires filter cloth replacement once a year, costing approximately 31,298 THB annually. In the electrocoagulation method, oxidation-reduction reactions occur on the metal electrodes, which must be replaced at least every two months to maintain adequate performance, resulting in an annual cost of approximately 409,620 THB. However, if the electrocoagulation system is optimized in capacity, flow rate, electric current/voltage [5], and the electrical polarity direction switching, the electrode replacement frequency could be reduced.

Carbon Footprint of Coagulation-flocculation and Electrocoagulation Treatment Method

The system boundary is defined as Cradle-to-Gate for the carbon footprint assessment of the Coagulation-flocculation and Electrocoagulation treatment method. The functional unit is one cubic meter of wastewater treated by each method. The life cycle inventory includes data from a 10-day sampling experiment on operational inputs and outputs, such as electricity and chemical consumption, sludge generation, and greenhouse gas (GHG) emissions from the treatment systems.

The results of the assessment as shown in Figure 11; the carbon footprint of electrocoagulation method is 0.89 $kgCO_2e/m^3$and Coagulation-flocculation method is 1.35 $kgCO_2e/m^3$

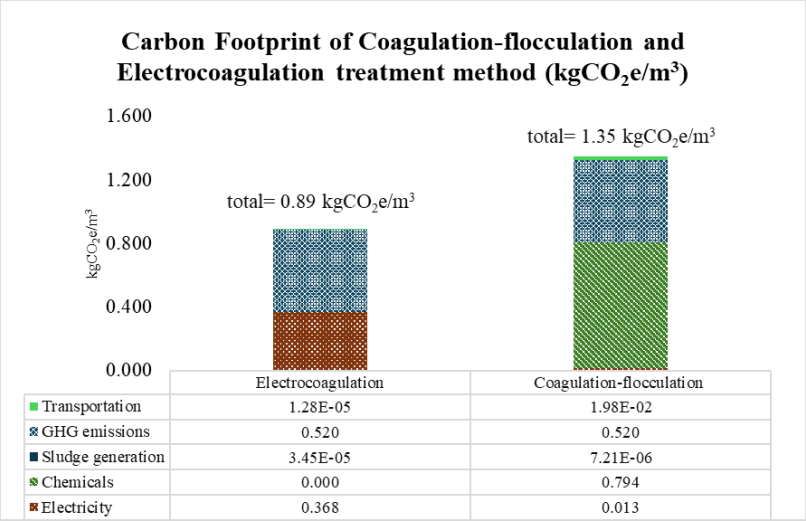


Figure 11 Carbon Footprint of Coagulation-flocculation and Electrocoagulation Treatment Method

Limitation & Recommendation

The coagulation-flocculation method can operate over a wide range of influent pH values. However, when the pH is too low or too high, it can lead to excessive chemical consumption and increased sludge generation. The influent pH must be in the neutral range for Electrocoagulation to ensure suitable conditions for the electrochemical reactions and coagulation process. Therefore, a limitation of Electrocoagulation is that the water's pH must be maintained within the range of 6-8 to ensure good water quality after treatment. Within this pH range and this experiment, optimal treatment efficiency requires a voltage of 50V, an electric current of 18-50A, and a flow rate of 3 m^3/hr. However, the operation factors depend on the condition of the Influent, such as turbidity, electrical conductivity, and suspended solids. Moreover, there are operational system factors, including the type of power source, reaction time, electrode spacing, and current density. [5]

The Electrocoagulation is suitable for treating effluent with a pH within the neutral range and under stable conditions with consistent wastewater quality parameters. This allows for the optimization of operational factors for the electrocoagulation method, such as electric current and voltage or water flow rate, making the treatment process easier to manage. Therefore, implementing an electrocoagulation system is one of the potential post-treatment solutions for treating wastewater that has already undergone primary treatment, as shown in Table 2.

Concerning occupational health and safety, it is essential to implement preventive measures to reduce the risk of chemical exposure in the station, especially during the manual addition of chemicals into the storage tank. The electrocoagulation system requires metal electrode replacement to maintain the treatment efficiency. The lifting equipment, such as hoists, should be installed at the workstation to facilitate operation and reduce ergonomic risk exposure for operators. Also, preventive maintenance might expose the risk of electrical shock if there are no appropriate safety measures and training.

Table 2 Comparison Advantage and Limitation of Coagulation-flocculation and Electrocoagulation Operation from experiment study

Category	Treatment Method	
	Coagulation-flocculation	**Electrocoagulation**
Treatment Efficiency	High efficiency in removing turbidity with a higher settling rate	Removing turbidity with a slower settling rate
Suitable pH range of Influent	Wide range pH (approx.4-12)	Neutral Range (6-8)
Preventive Maintenance	Annually Filter Cloths Replacement	Metal Electrode Replacement at least every 2 months*
Occupational Health and Safety	Chemical Risk Exposure, especially during the manual addition of chemical	Ergonomic Risk Exposure when replacing metal electrode frequently

* Depends on optimized operation factors such as capacity, flow rate, electric current/voltage, and the electrical polarity switching

CONCLUSION

This study is beneficial for developing environmentally friendly wastewater treatment approaches, reducing chemical usage, sludge generation, and minimizing greenhouse gas emission impacts, as evidenced by the lower carbon footprint assessment result. The limitation of pH levels may make electrocoagulation systems unsuitable for wastewater sources with fluctuating pH values. The workplace must evaluate and ensure that the influent water quality is in the neutral range and should be under stable conditions to facilitate the optimized operation for the operator. Also, safety risks and preventive measures, such as lifting equipment, the number of related operators, and safety and operation training, must be considered. However, if this parameter can be controlled, it will help reduce environmental impacts and lower wastewater treatment costs.

ACKNOWLEDGEMENT

The authors acknowledge with appreciation of the providing the workplace, necessary facilities, and staff for the experiment study by Siam Compressor Industry Co., Ltd., Chonburi 20230, and the guidance, laboratory instrument, and academic support granted by the Faculty of Public Health, Burapha University, Chonburi 20131, Thailand.

REFERENCE

[1] Gholami, M., Tyagi, R., Vanrolleghem, P. and Drogui, P. 2022. A comparison of artificial intelligence models for predicting phosphate removal efficiency from wastewater using the electrocoagulation process. Digital Chemical Engineering. 4: 100043. 10.1016/j.dche.2022.100043.

[2] Omnya, A., El-Battrawry, Mervat, A., El-Sonbati**,** Ebtesam M., El-Awadly & Talaat A. (2020). Study on Ferric Chloride Coagulation Process and Fenton's Reaction for Pretreatment of Dairy Wastewater. Current Science International. 9(1): 87-96.

[3] Sunbundit, A., Changchai, N. (2018). The paint factory's wastewater: COD removal by chemical precipitation method. RMUTSB Academic Journal. 6(2): 171-181.

[4] Sintusopa, N. (2020). Treatment of melanoidin in wastewater by using Electrocoagulation. Available from http://sutir.sut.ac.th:8080/jspui/bitstream/123456789/9198/2/Fulltext.pdf (cited March 18, 2025).

[5] Boinpally, S., Kolla, A., Kainthola, J., Kodali, R. and Vemuri, J. 2023. A state-of-the-art review of the electrocoagulation technology for wastewater treatment. Water Cycle. 4: 26–36.

[6] Garomsa, F.S., Berhanu, Y.M., Desta, W.M. and Bidira, F. 2024. Indigenous bio-coagulant assisted electrocoagulation process for the removal of contaminants from brewery wastewater: Performance evaluation and response surface methodology optimization. Heliyon. 10(22): e40394.

Composited Mesoporous Biochar Via Slow Pyrolysis Process Prepared from Woods and Plastics Waste as The Raw Precursors

Poramed Aungthitipan[1], Sukanya Hongthong[2], Pitsanu Pannarach[3], Supawan Khantotong[3] and Surachai Wongcharee[4]*

[1]Mater candidate; field of Civil Engineering, Faculty of Engineering, Mahasarakham University, Khamriang, Kantarawichai, Mahasarakham 44150, Thailand.
[2]Lecturer; Department of Mechanical Engineering, Faculty of Arts and Science, Chaiyaphum Rajabhat University, Chaiyaphum 36000, Thailand
[3]Lecturer; Faculty of Engineering, Ramkhamhaeng University, Bangkok 10240, Thailand
[4]Assistant Professor; Field of Environmental Engineering, Faculty of Engineering, Mahasarakham University, Khamriang, Kantarawichai, Mahasarakham 44150, Thailand
[*]Phone : 0886620962, E-mail : Surachai.w@msu.ac.th

ABSTRACT

A composite material is created by combining two or more distinct materials to produce a new material with improved properties. In this study, wood and polypropylene (PP) plastic were utilized to form a composite biochar. In this composite, wood particles serve as the reinforcing phase, while the plastic functions as the matrix, contributing structural integrity. This alternative composite biochar was produced by co-pyrolyzing wood and PP plastic. The results revealed that the physical and chemical characteristics of the resulting WP biochar were significantly enhanced, with a specific surface area reaching approximately 42.46 m²/g. Elemental analysis identified carbon (C) and oxygen (O) as the primary constituents. Isotherm analysis showed a Type III isotherm pattern, indicating the presence of mesoporous and macroporous structures. FTIR analysis confirmed the presence of key functional groups such as hydroxyl (-OH), carboxyl (-COOH), carbonyl (C=O), aliphatic C–H, and aromatic C=C bonds characteristic features of carbon-rich materials. These findings suggest that WP biochar has strong potential for water and wastewater treatment applications due to its high porosity and reactive surface chemistry. In essence, WP biochar produced through biomass carbonization exhibits high carbon content and a porous architecture. When incorporated into composites, it can enhance material performance, including improved mechanical strength, greater thermal stability, and enhanced adsorption capabilities. However, challenges such as the cost and availability of biomass feedstocks, the scalability of production processes, and the need for further research and pilot projects have contributed to the slow adoption of this technology. Nonetheless, utilizing wood and plastic waste as raw materials for biochar production through a modified anaerobic furnace with a slow pyrolysis process offers a promising and sustainable approach.

Keywords: biochar; plastic waste; wood; slow pyrolysis

INTRODUCTION

Biochar is a type of charcoal that is produced from organic biomass, such as agricultural waste, wood chips, or other plant materials [1-3]. It is created through a process called pyrolysis, which involves heating the biomass in the absence of oxygen [4, 5].This prevents the biomass from fully combusting and instead converts it into a stable form of carbon. The production of biochar has been practiced for centuries, primarily for agricultural purposes. It is often used as a soil amendment to improve soil fertility and enhance plant growth [6].Biochar has a highly porous structure, which allows it to retain water and nutrients in the soil, making them more available to plants. It also provides a habitat for beneficial microorganisms and can improve soil structure over time[7]. In addition to its agricultural benefits, biochar is also considered a carbon-negative material. When biomass is converted into biochar, the carbon that would have been released into the atmosphere as carbon dioxide is effectively sequestered in the biochar[8]. This makes biochar a potential tool for carbon dioxide removal and climate change mitigation. Biochar can be used in various applications beyond agriculture. It has been explored as a filtration medium for water and air purification, as a component in animal feed to improve digestion and reduce emissions, and as a material for construction and energy production[9].Thailand, like many other countries, faces significant challenges related to plastic

waste. The country has been grappling with a high rate of plastic consumption and inadequate waste management systems, leading to environmental pollution and negative impacts on public health [10]. Thailand has a robust plastic manufacturing industry, and plastic consumption is widespread across various sectors, including packaging, agriculture, and tourism. Unfortunately, a substantial portion of the plastic waste generated in the country ends up in landfills, water bodies, and natural environments. Several factors contribute to the plastic waste problem in Thailand [11]. 1. Single-use plastic consumption: The use of single-use plastics, such as plastic bags, straws, and food containers, is prevalent in Thailand. These items are often used for short periods and then discarded, leading to a significant volume of plastic waste. 2.Inadequate waste management infrastructure: Thailand faces challenges in waste collection, sorting, and recycling. Some areas lack proper waste management infrastructure, which results in plastic waste being disposed of improperly or ending up in waterways. 3.Plastic leakage from informal recycling sectors: Thailand has a significant informal recycling sector, where waste pickers collect and sort recyclable materials, including plastics. However, due to limited resources and infrastructure, some of these operations may contribute to plastic leakage and improper disposal practices.



Figure 1 Plastic waste from the production of recycled plastic pellets factory.

Wood is a natural, renewable resource that comes from trees. It is a versatile material with a wide range of applications and has been used by humans for various purposes for thousands of years. Wood is a natural, fibrous material derived from the stems, branches, and roots of trees. It is composed primarily of cellulose, hemicellulose, and lignin, which provide its structural properties. Wood has been used by humans for various purposes for centuries and continues to be an important resource today[12]. Types of Wood: Wood can be classified into two main categories: hardwood and softwood. Hardwood comes from deciduous trees (e.g., oak, maple, mahogany) and is generally denser, more durable, and used for furniture, flooring, and high-quality woodworking. Softwood comes from coniferous trees (e.g., pine, spruce, cedar) and is lighter, less dense, and commonly used for construction, framing, and paper production[13]. Structure and Properties: Wood has a complex cellular structure that contributes to its unique properties. It consists of long, fibrous cells arranged in growth rings. The structure provides strength, flexibility, and the ability to absorb and release moisture. Wood exhibits characteristics such as hardness, grain pattern, color, and dimensional stability, which can vary depending on the species[14, 15]. Wood is versatile material with a wide range of applications. It is commonly used in construction for structural elements, such as beams, posts, and trusses. Wood is also used for furniture, cabinetry, flooring, doors, windows, and decorative items. Additionally, it serves as a renewable energy source in the form of firewood and biomass for heating and power generation[16]. Wood is a renewable resource when harvested responsibly. Sustainable forestry practices, including reforestation and selective logging, ensure the long-term availability of wood while maintaining forest ecosystems. Certification systems, such as the Forest Stewardship Council (FSC), help promote sustainable wood sourcing and responsible forestry practices. It's important to balance the use of wood with sustainable practices to protect forests, maintain biodiversity, and ensure the long-term availability of this valuable resource. Responsible sourcing, proper waste management, and recycling or repurposing wood products also contribute to minimizing the environmental impact of wood use.

Therefore, this research aimed to study the combination of wood and plastic waste to produce biochar in order to deal with water contamination. The chemical and physical structures of composite biochar prepared from waste and plastic waste from the production of recycled plastic pellets were explored for the use and application for water, wastewater and/or air pollutant treatment. The characterization was analyzed via SEM-EDX, BET, and FTIR.

METHODOLOGY

Composite biochar preparation

Wood precursors (Fig. 2) were sourced from construction and demolition activities, including scrap lumber from construction sites and packaging materials from demolished structures. Recycling and repurposing this wood waste as feedstock for biochar production helps reduce overall waste, minimizes environmental impact, and supports the creation of value-added products. The plastic waste (polypropylene, PP) used in the study was obtained from a recycled plastic pellet production facility located in Chaiyaphum Province, Thailand. The raw materials were processed to specific sizes: plastic PP was cut to approximately 0.5–2.0 cm, while wood pieces measured around 10–15 cm in length. Both materials were dried at 105 °C for 24 hours to remove moisture. A mixture ratio of 4 parts wood to 1 part plastic waste by weight (approximately 1 kg in total) was loaded into a modified pyrolysis reactor (outer diameter: 0.6 m, height: 2.5 m) operating under oxygen-limited conditions. The pyrolysis was conducted using LPG as fuel, with the temperature ramped at a rate of 10 °C per minute and held at target temperatures of 300 °C, 400 °C, and 500 °C for one hour each. After the pyrolysis process, the reactor was allowed to cool naturally to room temperature. The resulting mixed biochar (Fig. 1) was then ground using a marble mortar to obtain a fine powder, which was stored for subsequent analyses including SEM-EDX, BET surface area measurements, and FTIR spectroscopy.



Figure 2 Images: a) Polypropylene (PP), b)Woods, c) WP based biochar after pyrolysis and d) WP based-biochar after milling

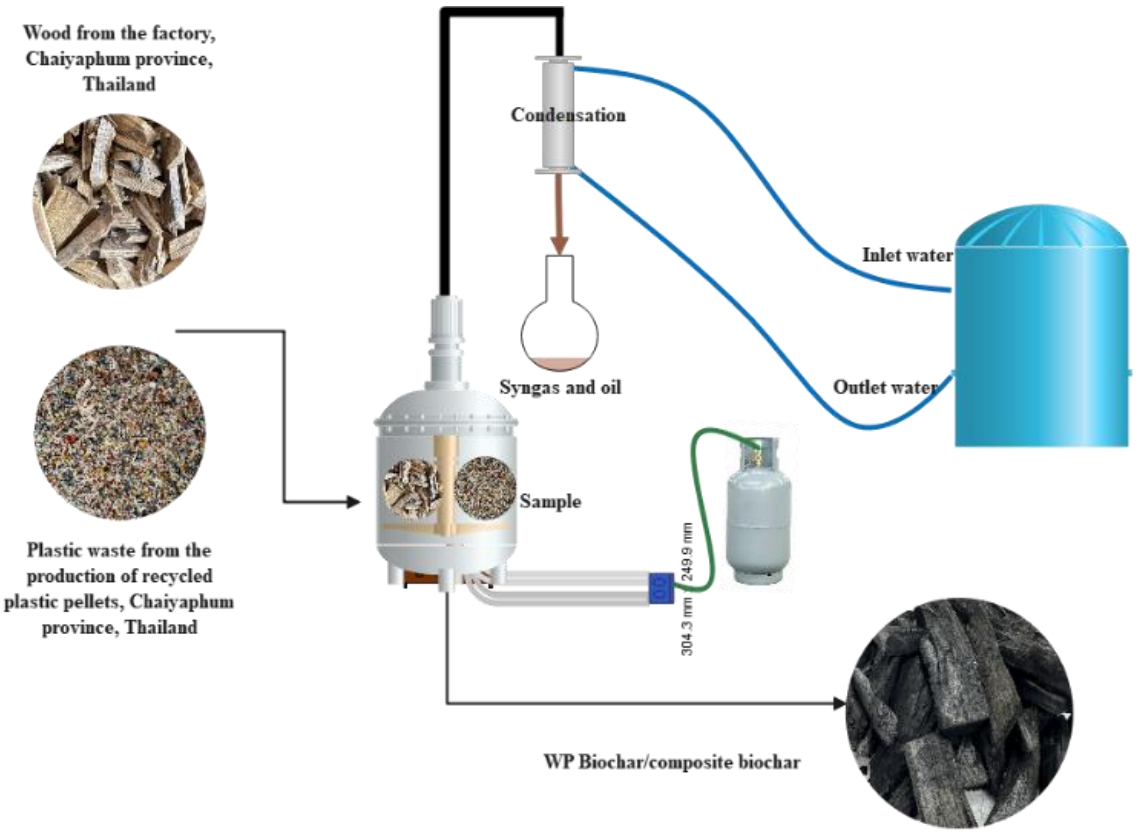


Figure 3 Schematic of the production of composite wood and plastics waste

Characterization of composite biochar/WP biochar

SEM-EDX stands for Scanning Electron Microscopy with Energy Dispersive X-ray Spectroscopy was used to provide detailed information about the topography, morphology, and composition of the material being analyzed. EDX corresponds to specific elements present in the sample, and their energy was used to identify and quantify the elemental composition of the material obtained. BET stands for Brunauer-Emmett-Teller and was applied to measure the specific surface area, pore size distribution, pore volume and adsorption isotherm of porous materials. Fourier Transform Infrared Spectroscopy (FTIR) is a technique used to analyze the chemical composition and molecular structure of a sample obtained by measuring its interaction with infrared light of mid-infrared region (2.5 to 25 micrometers or 4000 to 400 cm^{-1} By comparing the spectrum of the composite biochar with reference spectra or spectral databases that can identify functional groups, determine the presence of specific chemical bonds, and analyze the chemical composition of the composite biochar.

RESULTS AND DISCUSSIONS

SEM-EDX

The elemental analysis of WP (wood-plastic composite) biochar, as presented in Table 1, highlights the significant influence of pyrolysis temperature on the chemical composition of the biochar. Notably, the carbon content increases steadily with rising temperatures—starting from 72.48% at 300 °C, to 84.98% at 400 °C, and reaching a peak of 92.03% at 500 °C. This trend reflects the progressive carbonization of the feedstock, whereby increasing temperatures drive off more volatile matter, resulting in a biochar with a higher fixed carbon content and improved stability. Concurrently, the oxygen content decreases from 19.51% at 300 °C to 3.32% at 500 °C, indicating greater devolatilization and deoxygenation at higher pyrolysis temperatures. This reduction in oxygen is typical of biochar undergoing enhanced aromatization and condensation of carbon structures, leading to a more graphitic and thermally stable material. In terms of minor elements, aluminum (Al) and calcium (Ca) show irregular trends. Aluminum is notably present at 300 °C (5.31%) and reappears at 500 °C (3.43%), but is absent at 400 °C, suggesting possible interactions or transformations at that intermediate temperature. Conversely, calcium is highest at 300 °C (2.70%) and decreases with temperature, becoming undetectable at 500 °C. This could imply volatilization or conversion to non-detectable forms. Chlorine (Cl), undetected at 300 °C, appears at 400 °C (1.14%) and slightly increases at 500 °C (1.22%), possibly due to the thermal decomposition of plastic components, which often release chlorine-containing compounds at higher temperatures. Overall, the biochar produced from wood-plastic composites displays increasingly carbon-rich characteristics as pyrolysis temperature rises, supporting its suitability for applications requiring high fixed-carbon content, such as adsorbents or soil amendments. The presence of inorganic elements, particularly at lower temperatures, may also influence its behavior in environmental or catalytic uses.

Table 1 Element analysis for WP biochar

Temp.	Element				
	C (%)	**O** (%)	**Al** (%)	**Ca** (%)	**Cl** (%)
300 °C	72.48	19.51	5.31	2.70	-
400 °C	84.98	10.42	-	2.14	1.14
500 °C	92.03	3.32	3.43	-	1.22

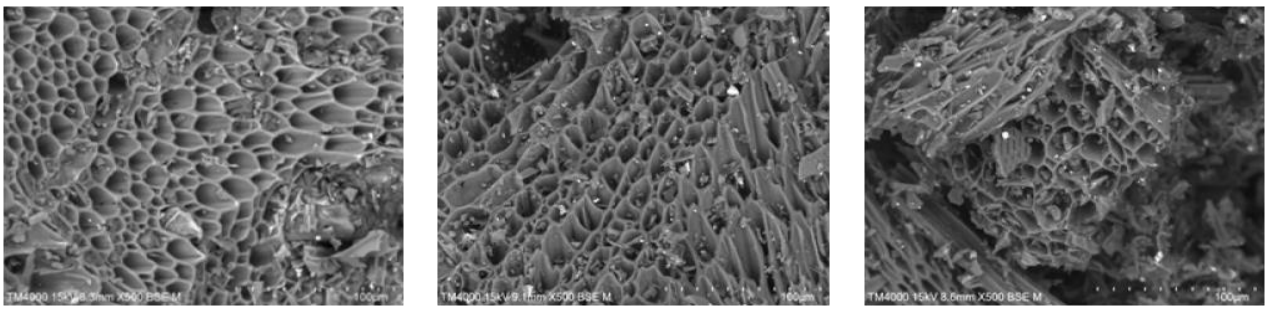
The surface morphology of WP biochar varies significantly with pyrolysis temperature, as shown in Fig. 4. At 300 °C (Fig. 4a), the SEM image reveals a well-developed porous structure following 1 hour of pyrolysis, indicating effective pore formation at this moderate temperature. Such porosity is crucial for applications requiring high surface area, such as adsorption and catalysis. However, as the pyrolysis temperature increases to 400 °C and 500 °C (Fig. 4b and 4c), the biochar structure becomes denser and less porous. This decline in porosity is likely due to the thermal degradation and collapse of pore walls or fusion of structural elements, which can block or shrink existing pores. These morphological changes emphasize the critical role of activation parameters particularly temperature, time, and method in shaping the physical characteristics of biochar. The choice of raw material also influences these outcomes, as it determines how the material responds to heat and structural breakdown. By carefully controlling these factors, it is possible to tailor the pore size distribution and specific

surface area of the biochar to suit specific functional applications, including environmental remediation, catalytic support, and energy storage.

In contrast, the sample treated at 400°C (middle image) shows a noticeably rougher and more irregular structure. The pores appear collapsed or partially deformed, and the cell walls exhibit a more granular texture. These features indicate the onset of substantial hemicellulose degradation and partial delignification, leading to increased porosity and surface exposure. The disruption of the matrix at this stage enhances accessibility to cellulose fibers, which is beneficial for downstream biochemical processes such as enzymatic hydrolysis.

By 500°C (right image), the biomass structure is significantly compromised. The micrograph reveals a dense, fractured, and disordered arrangement of collapsed and broken cell walls. The porous framework seen at lower temperatures has nearly disappeared, replaced by aggregated fibrous debris and fused fragments. This level of degradation points to extensive breakdown of hemicellulose, softening and migration of lignin, and potential disruption of cellulose crystallinity. While this degree of treatment maximizes the exposure of cellulose for biochemical applications, it also results in substantial loss of structural integrity.

Overall, the figure effectively demonstrates how thermal treatment at increasing temperatures leads to progressive breakdown of the lignocellulosic matrix. Lower temperatures (300°C) preserve the natural structure, while higher temperatures (300–500°C) promote porosity and reactivity at the cost of mechanical stability. The choice of treatment conditions should thus be tailored to the intended application whether preserving fiber strength for composites or enhancing digestibility for biofuel production.

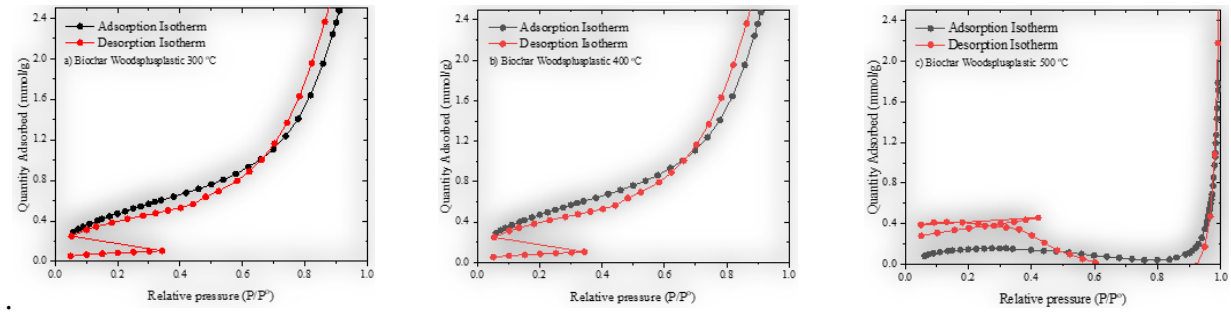


a) b) c)

Figure 4 SEM-EDX images: a) 300 ^{O}C b) 400 ^{O}C, and c) 500 ^{O}C

WP biochar isotherm analysis

The adsorption isotherms and model fits presented in the figure illustrate the enhanced adsorption performance of modified WP biochar compared to its raw form. The experimental isotherm (left plot) shows a markedly higher adsorption capacity for the modified biochar, particularly at increased equilibrium concentrations (Ce), indicating its improved affinity toward the adsorbate. The Langmuir model (middle plot), which assumes monolayer adsorption on a homogeneous surface, fits the data well especially for the modified biochar suggesting that surface modification has increased the number of active sites or enhanced their uniformity. In contrast, the Freundlich model (right plot), which accounts for heterogeneous surface energies and multilayer adsorption, also demonstrates a reasonable fit, particularly for the raw biochar, indicating a variety of adsorption sites with differing affinities. The improved performance of the modified biochar can be attributed to changes such as increased surface area, enhanced porosity, or the introduction of functional groups that provide additional binding sites. Overall, the results confirm that surface modification significantly enhances the adsorption capability of WP biochar, making it more effective for potential applications in pollutant removal from aqueous environments.



a) b) c)

Figure 5 Isotherm of WP biochar: a) 300 ^{O}C b) 400 ^{O}C, and c) 500 ^{O}C

Specific surface area, pore size and total pore volume of biochar

Table 2 presents the specific surface area, total pore volume, and average pore diameter of WP biochar produced at different pyrolysis temperatures. The data indicate that pyrolysis temperature has a significant influence on the textural properties of the biochar. At 400 °C, the WP biochar exhibited the highest surface area (42.4650 m^2/g) and total pore volume (0.112128 cm^3/g), suggesting that this temperature is optimal for developing porous structures with accessible surface sites. This enhanced porosity is likely due to the effective volatilization of organic components and partial decomposition of plastic and wood fractions at this intermediate temperature, leading to the formation of micro- and mesopores. In contrast, the surface area and pore volume decreased markedly at 500 °C, indicating possible pore collapse or structural shrinkage due to more intense thermal degradation and carbonization. Meanwhile, the average pore diameter increased at 500 °C (24.64 nm), implying a shift toward fewer but larger pores, which might not be as effective for adsorbing smaller molecules. At 300 °C, both surface area (16.6242 m^2/g) and pore volume (0.045739 cm^3/g) were relatively low, suggesting incomplete devolatilization and limited pore development. Overall, the results suggest that pyrolyzing WP biochar at 400 °C yields the most favorable structural characteristics for adsorption applications, balancing surface area and pore structure.

Table 2 Specific surface area, pore size and total pore volume of WP biochar obtained

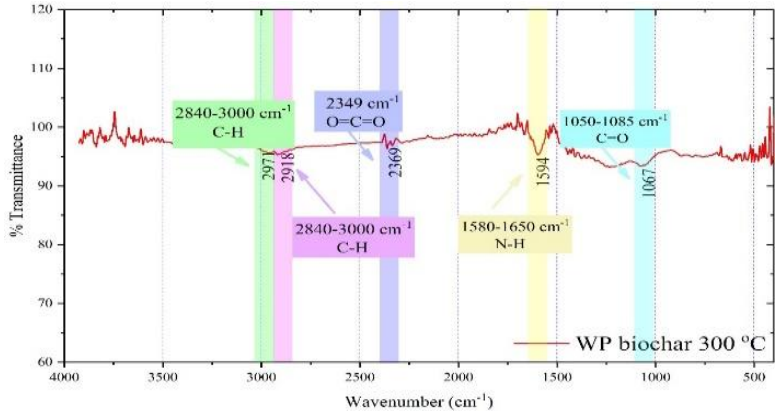
Temperature	300 °C	400 °C	500 °C
Surface Area (m^2/g)	16.6242	42.4650	11.9697
Total pore volume (cm^3/g)	0.045739	0.112128	0.013309
Average pore diameter (nm)	21.53	11.53	24.64

FTIR analysis-Functional groups study of the produced materials

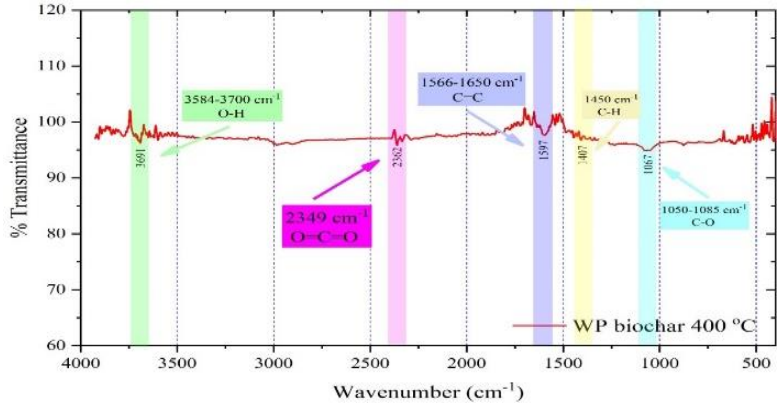
The FTIR spectra of WP biochar produced at different pyrolysis temperatures (300 °C, 400 °C, and 500 °C) reveal significant changes in functional groups as the temperature increases. At 300 °C, the biochar shows strong absorption bands corresponding to aliphatic C–H stretching (2840–3000 cm^{-1}), carbon dioxide-related O=C=O stretching (2349 cm^{-1}), N–H bending (1580–1650 cm^{-1}), and C–O stretching (1050–1085 cm^{-1}), indicating the presence of various oxygenated and nitrogen-containing functional groups. This suggests a relatively low degree of carbonization and a high presence of volatile compounds. As the pyrolysis temperature increases to 400 °C, a notable O–H stretching band (3584–3700 cm^{-1}) appears, along with continued presence of O=C=O, but the emergence of a strong C=C stretching band (1566–1650 cm^{-1}) indicates the beginning of aromatic ring formation. This transition marks the partial decomposition of less stable groups and the start of structural reorganization. At 500 °C, the spectrum further evolves with diminished aliphatic and oxygenated groups and a more pronounced C=C aromatic band, signifying enhanced aromaticity and carbonization. The reduced intensity of O=C=O and C–O bands confirm the loss of volatile, oxygen-rich functionalities, reflecting the formation of a more thermally stable and carbon-rich material. Overall, the FTIR analysis illustrates the progressive transformation of biomass into a more graphitic structure with increasing pyrolysis temperature.

Table 3 Comparative table summarizing the key functional group changes in WP biochar across the three pyrolysis temperatures (300 °C, 400 °C, and 500 °C)

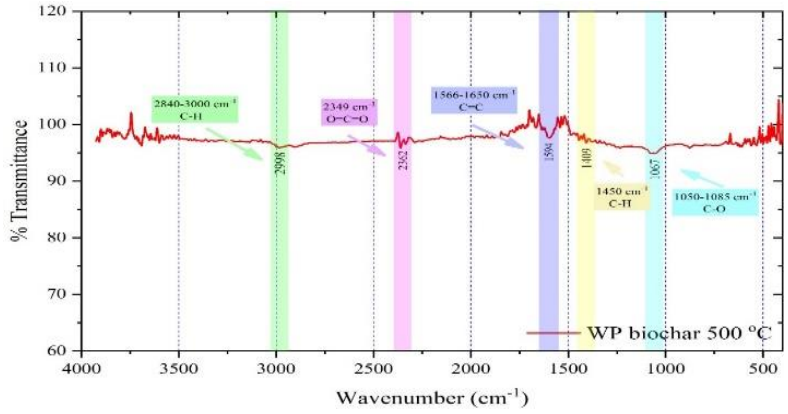
Wavenumber (cm^{-1})	Functional Group	Assignment	300 °C	400 °C	500 °C
2840–3000	C–H stretching	Aliphatic hydrocarbons	Present (strong)	Present	Present (weaker)
3584–3700	O–H stretching	Hydroxyl groups	Absent	Present (strong)	Absent
2349	O=C=O stretching	CO_2 / carbonates	Present	Present	Weaker
1580–1650 / 1566–1650	N–H bending / C=C stretching	Amines / Aromatic rings	Present (N–H)	Present (C=C)	Present (stronger)
1450	C–H bending	Alkyl group deformation	Absent	Present	Present
1050–1085	C–O stretching	Alcohols, ethers, esters	Present (strong)	Present	Present (weaker)



a)



b)



c)

Figure 6 FTIR images of WP biochar: a) 300 ^{O}C b) 400 ^{O}C, and c) 500 ^{O}C

CONCLUSION

The WP biochar was produced through slow pyrolysis of a composite of wood and plastic waste at temperatures of 300 °C, 400 °C, and 500 °C. The resulting biochar were found to be carbon-rich, with carbon contents of 72.48%, 84.98%, and 92.03%, respectively, highlighting an increasing trend with higher pyrolysis temperatures. Elemental analysis revealed that the main constituents in the biochar included carbon (C), oxygen (O), aluminum (Al), calcium (Ca), and chlorine (Cl), though the presence of some elements varied depending on temperature. Nitrogen adsorption–desorption isotherms for WP biochar indicated a Type III isotherm, which is intermediate between Type I and Type II. This type of isotherm is characteristic of mesoporous materials with moderate surface areas and pore volumes, where adsorption increases gradually and eventually levels off. BET surface area analysis showed that the WP biochar produced at 400 °C exhibited the highest specific surface area of 42.4650 m²/g, suggesting that this temperature is optimal for pore development. The average pore diameter of WP biochar ranged from approximately 11 to 25 nm, confirming their mesoporous nature. In terms of surface chemistry, FTIR analysis identified common functional groups such as hydroxyl (–OH), carboxyl (–COOH), carbonyl (C=O), aliphatic C–H bonds, and aromatic C=C bonds. These functional groups contribute to the biochar's reactivity and adsorption potential. Overall, WP biochar demonstrates favorable physical and chemical characteristics, especially at 400 °C that make it suitable for applications such as pollutant adsorption.

ACKNOWLEDGEMENT

The authors would like to thank, acknowledge and express gratitude that this research was financially supported by the Faculty of Engineering, Mahasarakham University in providing an opportunity to pursue this research work. The authors also thank the Department of Environmental Engineering and Research Centers for their laboratory support.

REFERENCE

[1] [Huang, W.-H., D.-J. Lee, and C. Huang, *Modification on biochars for applications: A research update.* Bioresource technology, 2021. **319**: p. 124100.

[2] Li, H., et al., *Mechanisms of metal sorption by biochars: Biochar characteristics and modifications.* Chemosphere, 2017. **178**: p. 466-478.

[3] Yargicoglu, E.N., et al., *Physical and chemical characterization of waste wood derived biochars.* Waste management, 2015. **36**: p. 256-268.

[4] Ronsse, F., et al., *Production and characterization of slow pyrolysis biochar: influence of feedstock type and pyrolysis conditions.* Gcb Bioenergy, 2013. **5**(2): p. 104-115.

[5] Apaydin-Varol, E., E. Pütün, and A.E. Pütün, *Slow pyrolysis of pistachio shell.* Fuel, 2007. **86**(12-13): p. 1892-1899.

[6] Sohi, S.P., et al., *A review of biochar and its use and function in soil.* Advances in agronomy, 2010. **105**: p. 47-82.

[7] Amonette, J.E. and S. Joseph, *Characteristics of biochar: microchemical properties.* Biochar for environmental management: Science and technology, 2009. **33**.

[8] Woolf, D., et al., *Sustainable biochar to mitigate global climate change.* Nature communications, 2010. **1**(1): p. 56.

[9] Cha, J.S., et al., *Production and utilization of biochar: A review.* Journal of Industrial and Engineering Chemistry, 2016. **40**: p. 1-15.
[10] Bureecam, C., T. Chaisomphob, and P.-Y. Sungsomboon, *Material flows analysis of plastic in Thailand.* Thermal Science, 2018. **22**(6 Part A): p. 2379-2388.
[11] Kofoworola, O.F. and S.H. Gheewala, *Estimation of construction waste generation and management in Thailand.* Waste management, 2009. **29**(2): p. 731-738.
[12] Jane, F.W., *The structure of wood.* The structure of wood., 1970(2nd ed.(rev.)).
[13] Ruffinatto, F., A. Crivellaro, and A.C. Wiedenhoeft, *Review of macroscopic features for hardwood and softwood identification and a proposal for a new character list.* IAWA journal, 2015. **36**(2): p. 208-241.
[14] Nilsson, T. and R. Rowell, *Historical wood–structure and properties.* Journal of Cultural Heritage, 2012. **13**(3): p. S5-S9.
[15] Migneault, S., et al., *Effects of processing method and fiber size on the structure and properties of wood–plastic composites.* Composites Part A: Applied Science and Manufacturing, 2009. **40**(1): p. 80-85.
[16] Timilsina, N., et al., *Tree biomass, wood waste yield, and carbon storage changes in an urban forest.* Landscape and Urban Planning, 2014. **127**: p. 18-27.

20R6-05

Application and characterization of bone char prepared via slow pyrolysis process and its used for heavy metal removal

Pornmongkol Tansomros[1], Janjira Triped[2], Pitsanu Pannarach[3], Pathanin Sangaroonand[4], Chuleeratana Promloa[5] and Surachai Wongcharee[6]*

[1]Mater candidate; field of Civil Engineering, Faculty of Engineering, Mahasarakham University, Khamriang, Kantarawichai, Mahasarakham 44150, Thailand.
[2]Lecturer; Department of Science, Faculty of Arts and Science, Chaiyaphum Rajabhat University, Chaiyaphum 36000, Thailand
[3]Faculty of Engineering, Ramkhamhaeng University, Bangkok 10240, Thailand
[4]Sukhothai Thammathirat Open University (STOU), Nonthaburi 11120, Thailand
[5]Sustainable Infrastructure Research and Development Center (SIRDC), Department of Civil Engineering, Faculty of Engineering, Khon Kaen University (KKU), Khon Kaen 40002, Thailand
[6]Assistant Professor; Field of Environmental Engineering, Faculty of Engineering, Mahasarakham University, Khamriang, Kantarawichai, Mahasarakham 44150, Thailand
[*]Phone : 0886620962, E-mail : Surachai.w@msu.ac.th

ABSTRACT

This study explores the production and characterization of cow bone char via slow pyrolysis at temperatures of 300°C, 400°C, and 500°C, with a focus on its potential for heavy metal adsorption, specifically copper (Cu II) ions. The bone char was analyzed for its physical and chemical properties, including surface area, porosity, and functional groups, using techniques such as SEM-EDX, FTIR, and BET. The adsorption efficiency of the biochar was evaluated across a copper concentration range of 0-250 mg L^{-1}. Results revealed that the adsorption capacity increased steadily with higher pyrolysis temperatures, reaching a maximum of 63 mg g^{-1} for biochar prepared at 500°C. SEM images and BET analysis indicated that higher temperatures resulted in an increase in surface area and porosity, while FTIR analysis demonstrated the transformation of organic and inorganic components during pyrolysis. The study concluded that the biochar prepared at 500°C exhibited the highest adsorption capacity and superior performance in removing Cu(II) ions, emphasizing the critical role of pyrolysis temperature in enhancing the material's suitability for environmental remediation. These findings offer important insights for optimizing biochar preparation conditions for heavy metal removal and water purification applications.

Keywords: Cow; Bone, Biochar, Slow pyrolysis, Adsorption

INTRODUCTION

The amount of bone waste is steadily increasing, and with the rising global meat production, particularly in certain countries, it is expected that by 2026, bone waste will continue to grow. This increase in meat production is directly linked to the higher availability of discarded bones [1]. The amount of bone waste generated depends on several factors, including local slaughtering and processing methods, the demand for bone-derived products, and the waste management systems in place in different regions. Discarded cow bone, much like those from oxen, can be repurposed for various uses across different industries, depending on regional practices and cultural preferences. Bone char, a material primarily composed of calcium phosphate, is created by heating bones at high temperatures in the absence of oxygen (a process known as charring). This process transforms the bones into a porous, carbon-rich material that has a wide range of applications. Bone char are commonly used in purification processes, such as water filtration, due to its ability to remove impurities, including heavy metals and toxins [2]. It is also used in soil improvement to enhance soil fertility by adding calcium and phosphorus, two essential nutrients for plant growth. Additionally, bone char is utilized in decolorization processes, particularly in the sugar industry, to remove colorants from raw sugar during its refining process.

In a similar fashion, biochar is a carbon-rich material produced by the pyrolysis (heating in the absence of oxygen) of various organic feedstocks, including agricultural waste, wood chips, and animal bones. Biochar offers numerous environmental and agricultural benefits [3]. It is used as a soil amendment to

improve soil structure, increase water retention, and promote microbial activity, leading to improved plant health and increased crop yields [4]. Biochar is also known for its ability to sequester carbon, making it an effective tool in mitigating climate change by capturing and storing atmospheric carbon for long periods [5]. Bone char and biochar share the benefit of being sustainable materials that can be produced from waste products, turning organic materials that might otherwise be discarded into valuable resources for agriculture, environmental conservation, and industrial processes [6]. While bone char is more specialized for uses related to calcium and phosphorus enrichment, biochar is widely praised for its role in enhancing soil health and its potential in climate change mitigation through carbon sequestration [7].

Biochar is a type of charcoal produced from biomass materials through a process called pyrolysis [11]. It is a carbon-rich solid material that is created by heating biomass in the absence of oxygen [12]. The resulting biochar can be used for various purposes and has gained attention for its potential environmental and agricultural benefits [13]. Biochar can be made from a variety of biomass feedstocks, including agricultural waste, wood chips, forestry residues, and even animal manure [13]. Different types of biomass can yield biochar with varying properties, which may influence its suitability for specific soil types and agricultural practices [14].

Slow pyrolysis is a process of thermal decomposition of organic materials, such as biomass or waste, in the absence of oxygen at relatively low temperatures[15]. It is a form of pyrolysis that occurs at a slower rate compared to other pyrolysis methods. In slow pyrolysis, the biomass or organic material is heated to temperatures typically ranging from 350 to 700 degrees Celsius [16] (662 to 1292 degrees Fahrenheit) [16]. The absence of oxygen prevents complete combustion and allows for the production of biochar, volatile gases, and bio-oil or pyrolysis oil [17]. Slow pyrolysis has certain advantages over other pyrolysis methods [18]. It allows for a more controlled decomposition process, resulting in higher-quality biochar with greater stability and enhanced carbon sequestration potential [19]. Additionally, slow pyrolysis can produce a higher yield of biochar compared to faster pyrolysis methods [20].

Therefore, this research aimed to produce the biochar from cow bone obtained from abattoirs using a modified anaerobic furnace. Physical and chemical properties were also studied via SEM-EDX, FITR and BET (porosity and surface area) and adsorption capacity was also explored.

METHODOLOGY

Bone char preparation

Waste bones were sourced from an abattoir in Mahasarakham province, Thailand, for the preparation of pyrolysis and biochar from both cow bones. The selected feedstock was first cleaned using tap water and then boiled to ensure that no residue remained inside or on the bones. After boiling, the bones were allowed to dry at room temperature, as shown in Figure 1. Once dried, the bones were transferred to a reactor (diameter: 60 cm, height: 2.5 m) for slow pyrolysis. Prior to pyrolysis, the bones were weighed to 1 kg per cycle. Pyrolysis was carried out at temperatures of 300°C, 400°C, and 500°C for one hour per cycle. After each pyrolysis cycle, the bones were allowed to cool down to room temperature, as illustrated in Figure 2. The resulting bone char was then crushed or milled into a fine powder and stored in a desiccator for further physical and chemical characterization.

Study the chemical and physical structure

The physical and chemical structure of the samples was analyzed using Fourier Transform Infrared Spectroscopy (FTIR), a technique that identifies the chemical composition of materials based on their interaction with infrared light [21]. Infrared light, which has longer wavelengths than visible light, is absorbed by the molecules in a sample, causing them to vibrate [22]. FTIR (model: Bruker INVENIO Platinum ATR) works by measuring the absorption of infrared light at various wavelengths. The sample is exposed to infrared light, and the light that passes through is detected and analyzed. The resulting spectrum provides valuable information about the molecular bonds present in the sample [23] [24]. Scanning Electron Microscopy (SEM) was employed to examine the morphology and composition of the materials at both micro- and nanoscale levels [25]. In combination with Energy Dispersive X-ray Spectroscopy (SEM-EDX, model: Tabletop Microscopes TM4000II / TM4000Plus II), this technique is used to determine the elemental composition of the sample [26]. SEM-EDX provides both qualitative and quantitative information about the elements present in a sample and their relative abundances [27]. Additionally, the surface area, isotherm, and porosity of the samples were analyzed using Brunauer-Emmett-Teller (BET) analysis (model: Micromeritics TriStar II Plus), which is a tool used for determining these physical properties.

Adsorption capacity

This study investigates the adsorption characteristics of synthetic copper solution using variables such as time, pH, cow bone char quantity, and copper concentration. A stock solution of copper citrate (2000 mg L-1) was prepared, with a consistent concentration of 100 mg L^{-1} used for all trials. In the time-dependent experiments, 1 g of cow bone char was added to 10 Erlenmeyer flasks containing 100 mg L^{-1} copper citrate. The flasks were shaken and left for varying durations (0-180 min). After filtering the solutions through a 0.45 GF/C filter, the Cu (II) concentration was measured using an ICP-OES (Optima 8000, Perkin Elmer). The amount of Cu (II) adsorbed at equilibrium (q_e, mg g^{-1}) was calculated the adsorption capacity For the adsorption isotherm study, copper citrate solutions were prepared with initial concentrations of 100 mg L^{-1}, which were then adjusted to 0-250 mg L^{-1}. One gram of cow bone char was added to each flask, and the mixtures were allowed to react for 24 h. After filtering, the Cu (II) concentration in the filtrates was measured as described earlier. The solutions were stored at temperatures below 4°C for further analysis.



Figure 1 Photographic images of raw material; Cow bone

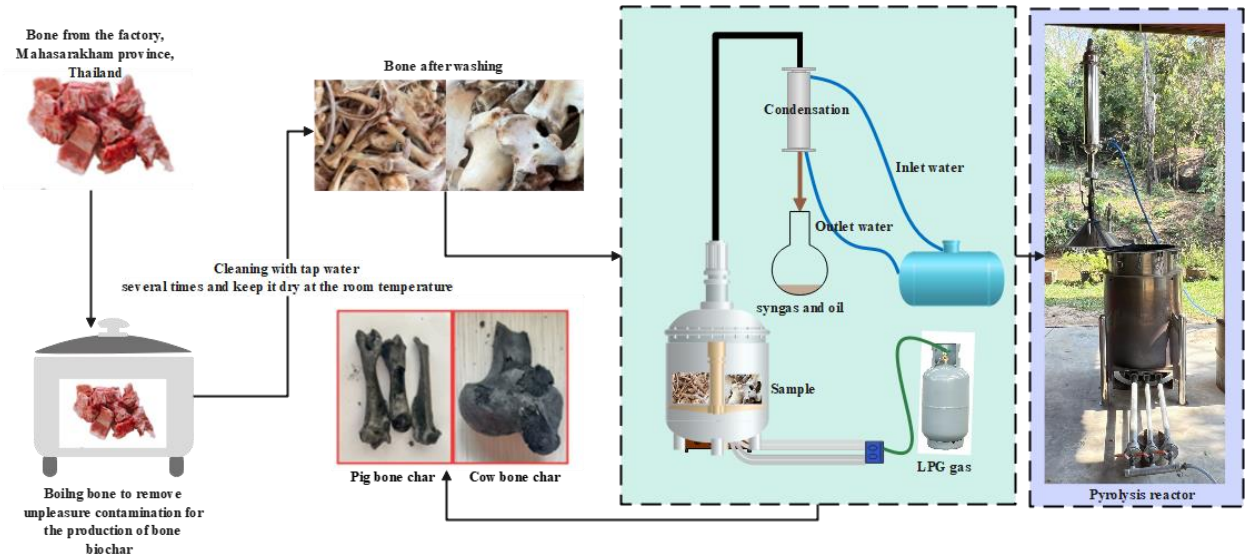


Figure 2 Preparation of bone char

RESULTS AND DISCUSSIONS

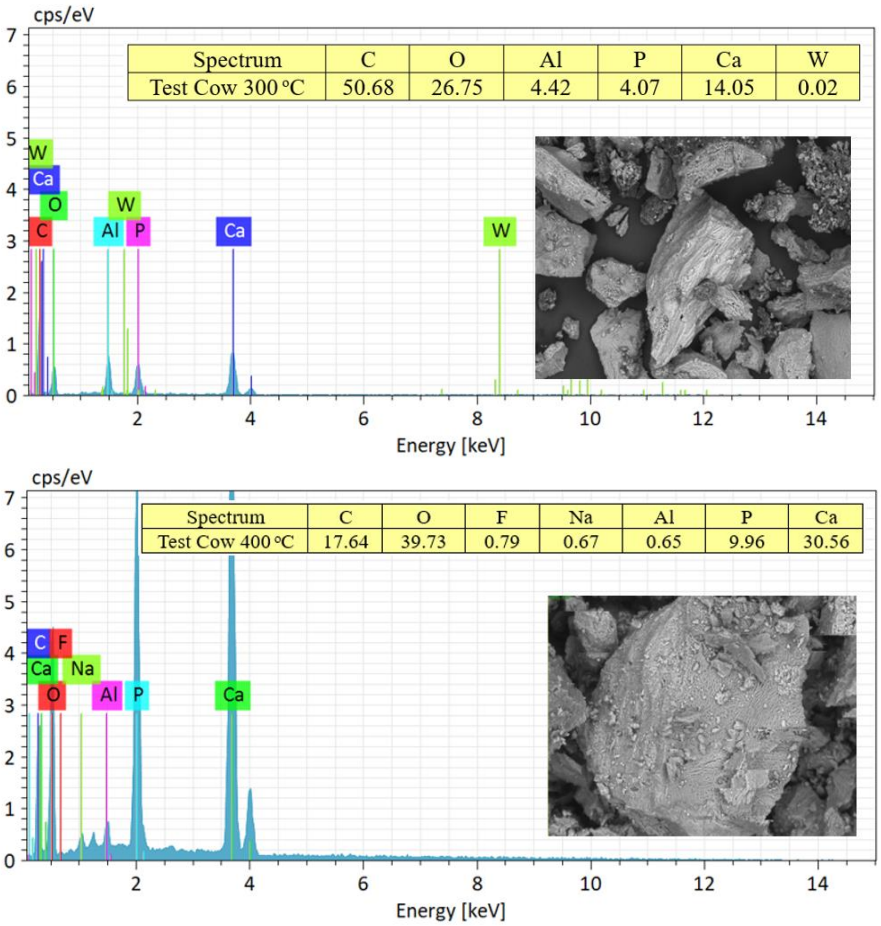
SEM-EDX

The Energy Dispersive X-ray Spectroscopy (EDX) analysis (Figure 3) of cow bone char at different pyrolysis temperatures (300°C, 400°C, and 500°C) reveals significant changes in the elemental composition, which impact its suitability for various applications. At 300°C, the spectra show high concentrations of carbon (C) (~40%), oxygen (O) (~25%), and calcium (Ca) (~30%), indicating the retention of substantial organic material, including proteins and collagen, in the char. The prominent peaks for phosphorus (P) (~3%) and aluminum (Al) (~2%) reflect the presence of mineral components characteristic of bone, with calcium phosphate being the dominant mineral. The relatively high oxygen content suggests incomplete pyrolysis and residual moisture in the char.

As the pyrolysis temperature increases to 400°C, the carbon (~30%) and oxygen (~15%) peaks decrease, signaling the breakdown of organic matter. The emergence of fluorine (F) (~1%) and sodium (Na) (~1%) suggests that pyrolysis conditions facilitate the release of mineral salts and other inorganic compounds. While calcium (~40%) and phosphorus (~2%) remain relatively stable, the phosphorus content slightly decreases due to the breakdown of phosphate groups. The increase in mineral elements, such as calcium, indicates that a more stable, mineral-rich structure is forming as organic materials continue to decompose.

At 500°C, the carbon (~15%) and oxygen (~5%) content further decreases, and the char becomes predominantly mineral-based, with calcium (Ca) (~50%) and phosphorus (P) (~4%) as the major components. The appearance of new elements like magnesium (Mg) (~2%) and chlorine (Cl) (~1%) indicates further mineral transformation or incorporation of additional elements during pyrolysis. The reduction of organic content and the increase in mineral concentration at higher temperatures enhance the char's stability and make it more suitable for applications that require a high mineral content, such as adsorption of contaminants and soil enhancement.

This trend underscores the influence of pyrolysis temperature on the elemental composition of bone char, highlighting how higher temperatures lead to a more mineral-rich material, which is beneficial for environmental and agricultural applications, while lower temperatures result in a carbon-rich char suitable for different uses. The results demonstrate that by adjusting pyrolysis conditions, bone char can be tailored for specific applications that leverage its organic or mineral content.



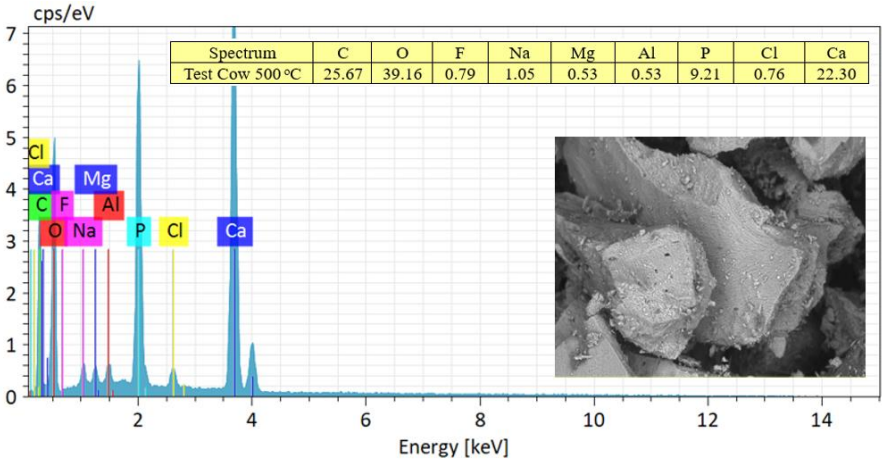
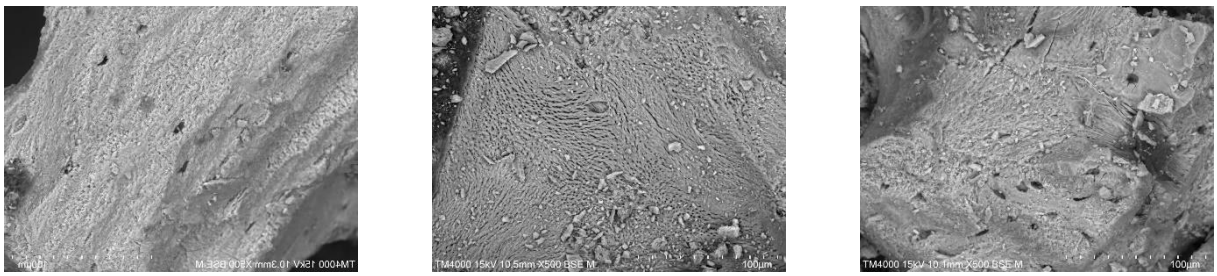


Figure 3 Depicted SEM-EDX image of Cow biochar

The provided Scanning Electron Microscopy (SEM) images (Figure 4) of cow bone char at different pyrolysis temperatures (300°C, 400°C, and 500°C) reveal the significant morphological and structural changes that occur with increasing temperature. At 300°C, the bone char retains much of its original organic structure, appearing relatively smooth and compact. This suggests that the pyrolysis process at this temperature has not yet fully decomposed the organic components, and the surface remains less porous with minimal changes to the bone's mineral structure. As the temperature increases to 400°C, the surface becomes rougher and more irregular, indicating that organic material, such as collagen and proteins, has begun to break down, exposing more of the inorganic mineral components. This rough texture and the increased surface area are important for enhancing the material's ability to adsorb contaminants in applications like water treatment or soil amendment. By 500°C, the bone char undergoes a more complete decomposition of organic material, resulting in a highly porous structure with significant cracks and surface irregularities. The increased porosity and roughness at this temperature suggest a higher degree of mineral crystallization, particularly in calcium phosphate structures, which improves the material's ability to interact with adsorbates. These morphological changes indicate that as the pyrolysis temperature increases, the bone char becomes more effective for applications that require higher surface area and enhanced adsorptive capacity, such as environmental remediation or soil enhancement. The SEM images highlight the critical role of pyrolysis temperature in transforming the bone char's physical and chemical properties, making it more suitable for industrial and environmental uses as the temperature increases.



a) b) c)

Figure 4 SEM-EDX for Cow bone char; a) 300 °C, b) 400 °C and c) 500 °C

Cow bone char N_2 adsorbed isotherm analysis

Figure 5 provided displays adsorption isotherms for cow bone char samples processed at three different pyrolysis temperatures: 300°C, 400°C, and 500°C. These curves illustrate the relationship between the amount of copper ions adsorbed onto the cow bone char and the equilibrium concentration of copper in the solution, providing insights into the adsorption capacity of the material at varying temperatures. At each temperature, the isotherms show a typical Langmuir-type adsorption behavior, where the adsorption increases with the copper concentration in solution, eventually plateauing as the surface sites of the bone char become saturated. The shape of the isotherms suggests that adsorption occurs on a homogeneously distributed surface and that the number of available active sites decreases as the char becomes more saturated with copper ions. Notably, the isotherms at

higher pyrolysis temperatures (400°C and 500°C) exhibit a higher adsorption capacity compared to the 300°C sample. This suggests that increased pyrolysis temperature enhances the adsorptive properties of cow bone char by increasing its surface area and porosity, as seen in the earlier SEM analysis. The higher temperatures are likely to promote the formation of more mineral-rich sites, such as calcium phosphate, which are more effective in binding heavy metals like copper. The 500°C sample appears to have the highest adsorption capacity, reflecting the char's increased mineral content and more developed surface texture, which facilitates better interaction with the copper ions. These adsorption trends emphasize the critical role of pyrolysis temperature in altering the structural and chemical properties of bone char, particularly its adsorption efficiency. The results suggest that higher pyrolysis temperatures result in bone char with enhanced adsorptive characteristics, which could make it a more effective material for environmental applications, particularly in removing heavy metals from contaminated water or soil. This trend also underscores the importance of optimizing pyrolysis conditions to achieve the desired properties for specific industrial and environmental applications.

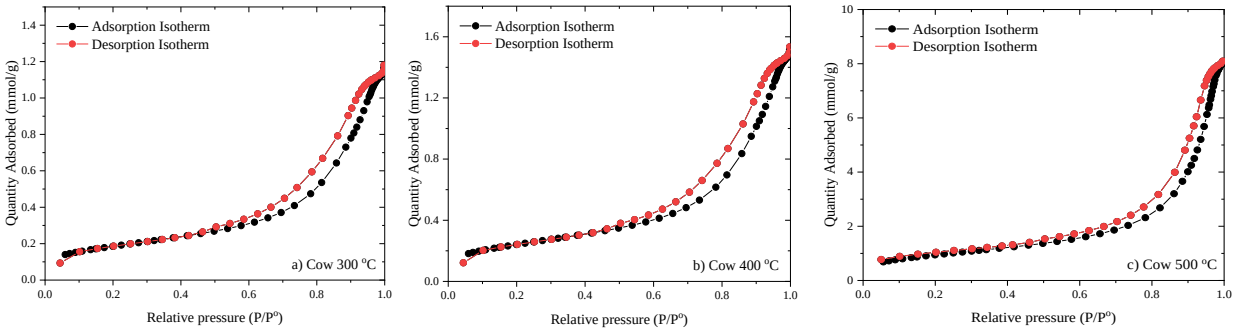


Figure 5 N_2 adsorbed isotherm analysis of cow bone char

Specific surface area, pore size and total pore volume of biochar

Table 2 illustrates the impact of pyrolysis temperature on the surface area, total pore volume, and average pore diameter of cow bone char. At 300°C, the char has a relatively low surface area (14.98 m^2/g), moderate total pore volume (0.0396 cm^3/g), and an average pore diameter of 10.57 nm, indicating limited porosity and organic material retention. At 400°C, the surface area increases to 21.99 m^2/g, with a higher pore volume (0.0518 cm^3/g), though the pore diameter decreases to 9.42 nm, suggesting the formation of smaller pores. At 500°C, the surface area reaches 77.31 m^2/g, the pore volume decreases to 0.0247 cm^3/g, and the average pore diameter increases to 13.51 nm, indicating the development of larger pores and a mineral-enriched structure. Overall, increasing pyrolysis temperature enhances surface area and porosity, with the 500°C char showing the most significant improvements, making it ideal for applications requiring high surface area and adsorption capacity.

Table 2 Specific surface area, pore size and total pore volume of cow bone char

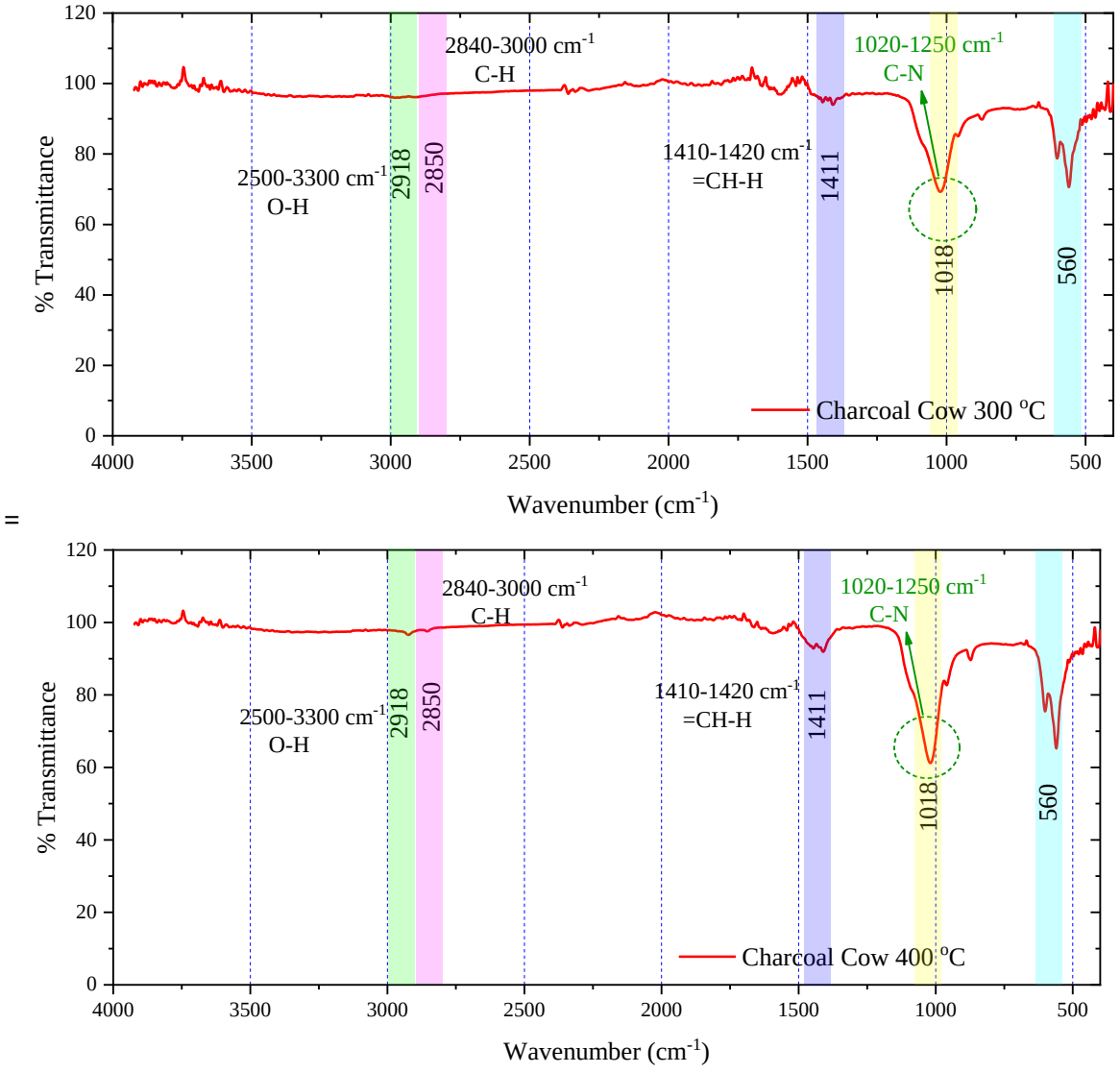
Temperature	**Cow bone char**		
	300 °C	**400 °C**	**500 °C**
Surface Area (m^2/g)	14.9827	21.9863	77.3060
Total pore volume (cm^3/g)	0.039574	0.051779	0.024676
Average pore diameter (nm)	10.5653	9.4202	13.5099

FTIR analysis-Functional groups study of the produced materials

The FTIR spectra (Figure 6) of cow bone char processed at 300°C, 400°C, and 500°C reveals the transformation of organic and inorganic components with increasing pyrolysis temperature. At 300°C, the spectra show prominent C-H and C-N stretching bands (around 2918 cm^{-1} and 2850 cm^{-1}) indicating the retention of organic material. The C-N stretching band at 1020-1250 cm^{-1} suggests nitrogen-containing compounds, while the 560 cm^{-1} peak reflects mineral components. At 400°C, there is a reduction in organic peaks, and the mineral peaks become more prominent, indicating increased mineralization. By 500°C, the organic functional groups are nearly decomposed, and the spectrum is dominated by mineral-related peaks, particularly calcium phosphate. This transformation demonstrates that higher pyrolysis temperatures enhance the mineral content of bone char, making it more suitable for applications requiring stability and adsorption capacity.

Adsorption studies

The adsorption capacity of cow bone char for copper removal was evaluated at pyrolysis temperatures of 300°C, 400°C, and 500°C, across a copper concentration range of 0-200 mg L^{-1}, as shown in Figure 8c. The results revealed a steady increase in adsorption capacity from 7 mg g^{-1} to 62 mg g^{-1} within this concentration range. Beyond this, adsorption capacity plateaued, particularly between 200-250 mg L^{-1}, indicating the approach of equilibrium. Notably, the biochar produced at 500°C exhibited the highest adsorption capacity, reaching 63 mg g^{-1}, outperforming the char prepared at lower temperatures. While biochar at 300°C and 400°C also demonstrated effective adsorption, the 500°C biochar consistently exhibited superior performance, emphasizing the critical role of pyrolysis temperature in enhancing the material's ability to remove Cu(II) ions. This study confirms that higher pyrolysis temperatures significantly improve the adsorption capacity of bone char, making it a promising candidate for heavy metal removal in environmental remediation. The findings contribute valuable insights for optimizing biochar preparation conditions, enhancing its efficacy in water purification and heavy metal adsorption applications.



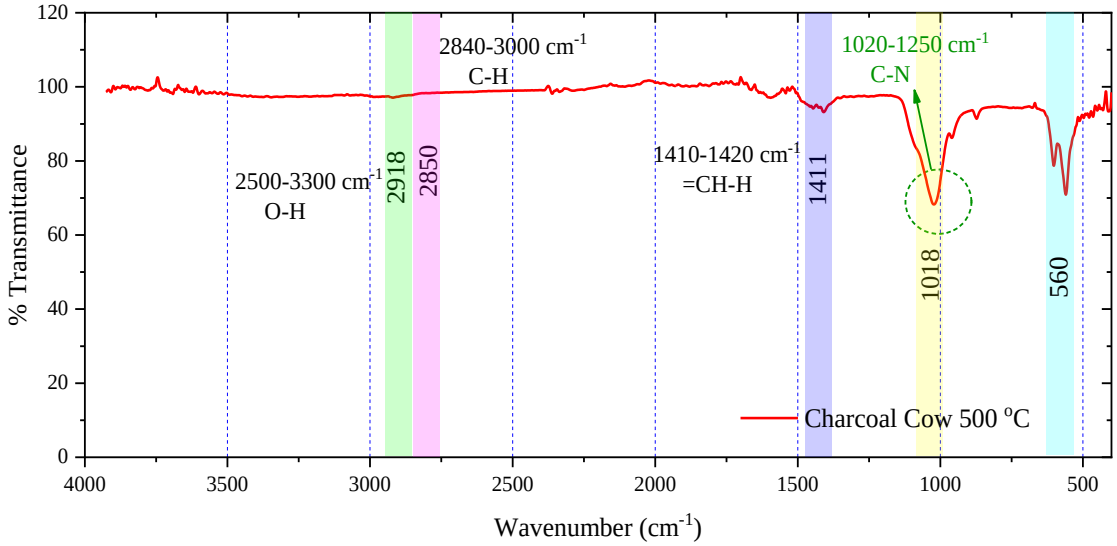


Figure 6 FTIR of Cow bochar via slow pyrolysis process

CONCLUSION

This study investigated the production and characterization of cow bone char derived through slow pyrolysis at temperatures of 300°C, 400°C, and 500°C, and its potential application for heavy metal adsorption, specifically for the removal of Cu (II) ions. The results demonstrated that increasing pyrolysis temperature significantly enhanced the surface area, porosity, and mineral content of the bone char, with the 500°C sample exhibiting the highest adsorption capacity. The biochar prepared at 500°C showed superior performance in copper removal, reaching an adsorption capacity of 63 mg g^{-1}, outpacing the char produced at lower temperatures. This study highlights the critical role of pyrolysis conditions in optimizing the physical and chemical properties of biochar, particularly for environmental remediation. The findings underscore the effectiveness of cow bone char as an adsorbent material, especially when processed at higher temperatures, and provide important insights for future research and practical applications in water purification and the removal of heavy metals from contaminated environments.

ACKNOWLEDGEMENT

The authors would like to thank, acknowledge and express gratitude that this research was financially supported by the Faculty of Engineering, Mahasarakham University in providing an opportunity to pursue this research work.

REFERENCE

[1] Alkurdi, S.S., et al., Bone char as a green sorbent for removing health threatening fluoride from drinking water. Environment international, 2019. **127**: p. 704-719.

[2] Jayathilakan, K., et al., *Utilization of byproducts and waste materials from meat, poultry and fish processing industries: a review.* Journal of food science and technology, 2012. **49**: p. 278-293.

[3] Zimmer, D., et al., *Bone char vs. S-enriched bone char: Multi-method characterization of bone chars and their transformation in soil.* Science of the Total Environment, 2018. **643**: p. 145-156.

[4] Alipal, J., et al., *A review of gelatin: Properties, sources, process, applications, and commercialisation.* Materials Today: Proceedings, 2021. **42**: p. 240-250.

[5] Karim, A.A. and R. Bhat, *Gelatin alternatives for the food industry: recent developments, challenges and prospects.* Trends in food science & technology, 2008. **19**(12): p. 644-656.

[6] Hsu, D.-j., et al., *Essential and toxic metals in animal bone broths.* Food & nutrition research, 2017. **61**(1): p. 1347478.

[7] Wusan, D., *Ancient Chinese Thought of Character Formation Modern Logo Design.* Leonardo, 2014. **47**(2): p. 183-185.

[8] Wasswa, J., J. Tang, and X. Gu, *Utilization of fish processing by-products in the gelatin industry.* Food Reviews International, 2007. **23**(2): p. 159-174.

[9] Sohi, S.P., et al., *A review of biochar and its use and function in soil.* Advances in agronomy, 2010. **105**: p. 47-82.

[10] SUKUMARAN, A., *ADSORPTION OF AMMONIUM PURPURATE USING COCUNUT SHELLCHARCOL AS BIOCHAR.* 2021.
[11] Tripathi, M., J.N. Sahu, and P. Ganesan, *Effect of process parameters on production of biochar from biomass waste through pyrolysis: A review.* Renewable and sustainable energy reviews, 2016. **55**: p. 467-481.
[12] Kambo, H.S. and A. Dutta, *A comparative review of biochar and hydrochar in terms of production, physico-chemical properties and applications.* Renewable and Sustainable Energy Reviews, 2015. **45**: p. 359-378.
[13] Sparrevik, M., et al., *Environmental and socioeconomic impacts of utilizing waste for biochar in rural areas in Indonesia–a systems perspective.* Environmental science & technology, 2014. **48**(9): p. 4664-4671.
[14] Siedt, M., et al., *Comparing straw, compost, and biochar regarding their suitability as agricultural soil amendments to affect soil structure, nutrient leaching, microbial communities, and the fate of pesticides.* Science of the Total Environment, 2021. **751**: p. 141607.
[15] Goyal, H., D. Seal, and R. Saxena, *Bio-fuels from thermochemical conversion of renewable resources: a review.* Renewable and sustainable energy reviews, 2008. **12**(2): p. 504-517.
[16] Garcia-Perez, M. and J. Metcalf, *The formation of polyaromatic hydrocarbons and dioxins during pyrolysis: A review of the literature with descriptions of biomass composition, fast pyrolysis technologies and thermochemical reactions.* 2008.
[17] Miranda, N.T., et al., *Sugarcane bagasse pyrolysis: A review of operating conditions and products properties.* Renewable and Sustainable Energy Reviews, 2021. **149**: p. 111394.
[18] Chen, D., J. Zhou, and Q. Zhang, *Effects of heating rate on slow pyrolysis behavior, kinetic parameters and products properties of moso bamboo.* Bioresource Technology, 2014. **169**: p. 313-319.
[19] Xiao, R., et al., *Recent developments in biochar utilization as an additive in organic solid waste composting: A review.* Bioresource Technology, 2017. **246**: p. 203-213.
[20] Zhang, Z.X., J. Wu, and W.F. Chen, *Review on prepation and application of biochar.* Advanced Materials Research, 2014. **898**: p. 456-460.
[21] Theophanides, T., *Introduction to infrared spectroscopy.* Infrared Spectroscopy-Materials Science, Engineering and Technology, 2012: p. 1-10.
[22] Hsu, C.-P.S., *Infrared spectroscopy.* Handbook of instrumental techniques for analytical chemistry, 1997. **249**.
[23] Dutta, A., *Fourier transform infrared spectroscopy.* Spectroscopic methods for nanomaterials characterization, 2017: p. 73-93.
[24] Bialkowski, S.E., *Photothermal spectroscopy methods for chemical analysis*. Vol. 177. 1996: John Wiley & Sons.
[25] Bettinger, C.J., R. Langer, and J.T. Borenstein, *Engineering substrate topography at the micro-and nanoscale to control cell function.* Angewandte Chemie International Edition, 2009. **48**(30): p. 5406-5415.
[26] Utsunomiya, S. and R.C. Ewing, *Application of high-angle annular dark field scanning transmission electron microscopy, scanning transmission electron microscopy-energy dispersive X-ray spectrometry, and energy-filtered transmission electron microscopy to the characterization of nanoparticles in the environment.* Environmental science & technology, 2003. **37**(4): p. 786-791.
[27] Bayuseno, A. and W.W. Schmahl, *Understanding the chemical and mineralogical properties of the inorganic portion of MSWI bottom ash.* Waste Management, 2010. **30**(8-9): p. 1509-1520.

20R6-06

Developing Oxygenated Functional Group-Doped Hydrochar from Spent Coffee Grounds via Ultrasonication as a Magnetic Adsorbent for Oily Wastewater Treatment

Myint Myat Thuzar[1], Nattapong Tuntiwiwattanapun[2], Nurak Grisdanurak[3]

[1]*Graduate School, International Program in Hazardous Substance and Environmental Management, Chulalongkorn University, Bangkok 10330, Thailand.*
[2]*Researcher, Sustainable Environmental Research Institute, Chulalongkorn University, Bangkok 10330, Thailand.*
[3]*Co-author, Center of Excellence in Environmental Catalysis and Adsorption, Faculty of Engineering, Thammasat University, Pathum Thani 12121, Thailand*
[*]*Phone : +66-2-218-8137, Fax : ……., E-mail :* Nattapong.t@chula.ac.th

ABSTRACT

Oil spills pose significant environmental challenges, affecting aquatic ecosystems, human health, and water resources. Among treatment methods, adsorption has gained considerable attention due to its efficiency in removing oil contaminants from water. While numerous adsorbents derived from agricultural, food, and industrial waste have been explored, their application in open water is often limited by difficulties in spent adsorbent recovery. In this study, Spent Coffee Grounds (SCGs) were utilized to produce a magnetic adsorbent with high oil adsorption capacity and easy recovery. The SCGs underwent hydrothermal carbonization (HTC) at 220°C for 120 minutes, followed by ultrasonication-assisted activation to enhance surface morphology. The activated hydrochar was then magnetized using a cold precipitation technique, and its diesel removal efficiency was evaluated in artificial seawater. Characterization results showed that the magnetic hydrochar exhibited a surface area of 2.25 m^2/g and a pore volume of 0.011 cm^3/g, significantly higher than raw hydrochar (0.5189 m^2/g) and activated hydrochar (2.2582 m^2/g). FTIR analysis confirmed the activation of oxygenated functional groups via HTC and ultrasonication. Iron (Fe) was incorporated into the hydrochar using $FeCl_3 \cdot 6H_2O$ and $FeSO_4 \cdot 7H_2O$ at a 2:1 molar ratio, with Fe concentrations of 0.2 M, 0.25 M, and 0.3 M. While Fe loading improved magnetization, excessive Fe content increased surface hydrophilicity, leading to reduced oil adsorption, as evidenced by contact angle measurements. The optimal Fe concentration (0.2 M) resulted in a maximum diesel removal efficiency of 98.99%. These findings demonstrate that Fe-modified SCG-based hydrochar is an effective, sustainable, and easily recoverable adsorbent for oil spill remediation.

Keywords: Spent Coffee Grounds (SCGs), O-Doping, Magnetic Hydrochar, Oil Spill, Adsorption.

1. INTRODUCTION

Oily waste pollution is one of the most serious environmental concerns today. That can be caused not only by human errors but also by pipeline failures, oil transfers between vessels, etc., This incident generates numerous environmental and ecological impacts[1]. As well as oily wastewater is produced by various industries, including metal processing industries, edible oil refineries, petrochemical industries, and domestic wastewater, etc., which can affect the environment, human health, and contaminate drinking water and groundwater resources. Toxic compounds, such as phenols, petroleum hydrocarbons, and polycyclic aromatic hydrocarbons, can be found in oily wastewater, which inhibits both plant and animal development and increases the chemical and biological oxygen demand in water bodies[2]. As the industrial economy continues to expand, wastewater treatment remains a necessary challenge. Nowadays, numerous techniques are employed to remove oily wastewater from various sources including physical, chemical, electro/photo-catalysis, adsorption, and advanced oxidation processes (AOPs). The adsorption process has gained attention as a more suitable method widely applied in various wastewater treatment due to its cost-effectiveness and environmentally friendly[3]. Recent studies have highlighted the advantages of using natural and synthetic sorbents, polyurethane, polypropylene, and modified activated carbons, which possess high adsorption capacities and minimize secondary pollution. Among the various feedstocks, Spent coffee grounds (SCGs)

are the residual wastes generated after brewing the coffee which has steadily increased because it is one of the most traded commodities with over 9.2 million tons produced globally[4]. Spent Coffee Grounds (SCGs) are composed of 8.6-13.3% cellulose, 30-40% hemicellulose, 25-35% lignin, 10-20% fats, 6.7-13.6% proteins and 2.5% polyphenols. As a result of containing a variety of organic compounds, SCGs can be transformed into value-added products to remove the various contaminants. Delil, A.D.(2019) reported that SCGs under ultrasonication activation for 24 hr without chemical activation could be able to remove Cd(II) in 96%[5]. Edathil, A.A., et al. (2018) reported that magnetic coffee waste by dispersing Fe_3O_4 nanoparticles could remove 99.56% and 99.3% of Pb(II) upon Fe loading in varying concentrations [6]. Hussain et al. (2020) demonstrated the magnetic biochar from spent coffee grounds achieved a high Cadmium (II) removal efficiency of 96%, with the maximum adsorption capacity 10.42 mg/g. This efficiency is attributed to various functional groups, including oxygen Fe-O functional groups, making it a viable, low-cost adsorbent for wastewater treatment [7].

Hydrothermal carbonization has attracted significant attention because the process requires less energy, minimizes the environmental impact, and enhances the carbon content of the produced hydrochar. Hydrochar is the carbon-rich material derived from hydrothermal carbonization of bio-feedstocks such as agricultural wastes, food wastes, and industrial residuals[8]. However, the surface area of the hydrochar has low surface area and porosity which limit in adsorption performance. Therefore, it is required to activate or modify of the surface area in hydrochar to enhance the adsorption efficiency. By integrating magnetic materials through activated hydrochar, magnetic hydrochar has gained attention that significantly enhances the high efficiency in the removal of contaminants in wastewater treatment. Recent studies have investigated the modification of adsorbents to enhance their removal efficiency and magnetic adsorbents which mostly highlight their adsorption capacity and ease of separation through surface modification using an external magnetic field[9]. Several methods have been used to synthesize magnetic hydrochar, including co-precipitation, thermal decomposition, microemulsion, and hydrothermal synthesis. Compared to other methods, co-precipitation is a simple and cost-effective method for producing magnetic hydrochar embedded with Fe_3O_4 nanoparticles which has been widely applied in the removal of the contaminants from the wastewater. Magnetization via co-precipitation process has been showed that increase the specific surface area and porosity of the hydrochar[10].

The abundance of the oxygenated functional groups of hydrochar made it suitable to adsorb the iron oxide precursors, resulting in strong magnetic power properties. To further improve the iron oxide precursors of hydrochar, expanding the surface area while maintain the abundance of oxygenated functional groups will be more interesting. Therefore, applying ultrasonication to activate the hydrochar before magnetization could enhance the exposure of functional groups on the surface of the carbon materials. Ultrasound treatment can effectively create materials with a multistage pore structure and an adjustable micropore-to-mesopore ratio. The activated hydrochar produced through ultrasonication exhibits enhanced characteristics that increase surface area and functional groups, and improve its performance as an adsorbent for contaminants, making it effective in water treatment processes[11]. In this study, ultrasonication combined with iron integration on hydrochar will be employed to modify surface functional groups, enhancing the adsorption capacity of iron precursors to produce strong and porous magnetic hydrochar suitable for oily wastewater treatment. Rana N. Malhas (2023) studied that the maximum oil removal efficiency upon increasing the carbon avocado peel adsorbent dose (1.5 g – 7 g) and the adsorption capacity was 66-90% for Crude oil, 45-68% for Diesel, 35-56% for Kerosene, and 19-45% for Gas oil respectively[12].

In this context, ultrasonication combined with iron integration on hydrochar will be employed to modify surface functional groups, enhancing the adsorption capacity for iron precursors, and producing strong and porous magnetic hydrochar suitable for oily wastewater treatment.

The objectives of this study are to investigate the effects of hydrothermal temperature and ultrasonication activation on the surface properties of the hydrochar adsorbent. Then, the selected activated hydrochar was magnetized and evaluated the diesel removal from oily wastewater.

2. MATERIALS and METHODOLOGY

2.1 Preparation of Hydrochar and Activation

Five grams of SCGs and DI water in liquid to solid (L/S) ratio of 10:1 (mL/g) was mixed in the stainless-steel autoclave reactor which was heated at 220˚C for 120 mins at a heating rate of 5˚C/min. Once the reaction was completed, the obtained hydrochar (HC-220) was washed several times with DI water and dried at 105˚C. Further activation was conducted via ultrasonication treatment in an ultrasonication bath (Elma, Trassonic T 700/H) for 120 mins, named HC_US 120 and the sample was rinsed with DI water several times and dried at 105˚C to produce magnetic hydrochar. The hydrochar yield was calculated using eq (1).

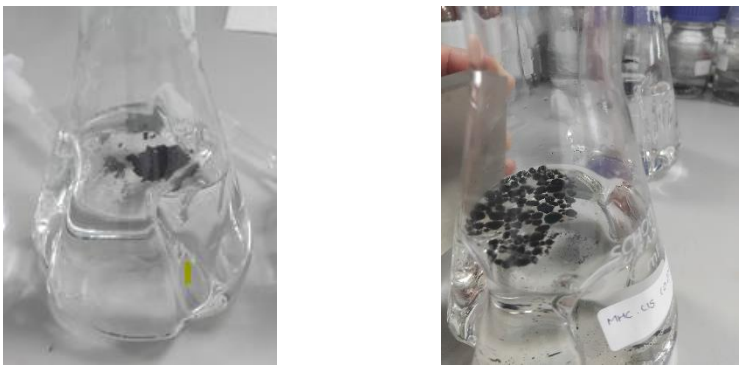
$$\text{Hydrochar Yield (\%)} = \frac{\text{Weight of hydrochar}}{\text{Weight of biomass}} \times 100 \quad (1)$$

2.2 Preparation of Magnetic Hydrochar

Three grams of selected activated hydrochar will be added to the iron solution in the mixture of $FeCl_3.6H_2O$ and $FeSO_4.7H_2O$ at 2:1 molar ratio with varying concentrations in 0.2M, 0.25M, and 0.3M by co-precipitation process. Then, 0.1M of NaOH solution was added until the pH dropped to pH 10. The magnetic hydrochar (MHC) was washed with DI water until pH reached pH 7 and dried overnight at 80˚C for further application.

2.3 Residual Diesel Oil in Artificial Seawater

The optimal amount of selected magnetic hydrochar was applied to diesel oil adsorption in artificial seawater, which had a mixture of NaCl, $MgSO_4$, $MgCl_2$, $CaCl_2$, and KCl in a certain ratio. The experiment was conducted using 200 mL of artificial seawater and 2 g of diesel oil. After adding 0.1 g of adsorbent, the mixture was shaken at 150 rpm for 30 minutes, as shown in Fig. 1. Then, the solid-liquid fraction was separated, and the liquid sample was extracted with hexane in a 1:1 ratio, filtered through 0.45μm syringe filters to remove any particulate matter, and quantified the residual oil concentration using gas chromatography with flame ionization detection (GC-FID).



(a) (b)

Figure 1: Removal of Diesel Oil Using Magnetic Hydrochar (a) Before Adsorption (b) After Adsorption

The adsorption capacity, Q_e (mg g-1) and adsorption efficiency E (%) was estimated by Eq (2), (3).

$$Q_e = \frac{(C_0 - C_e)V}{m} \quad (2)$$

$$E = \frac{C_0 - C_e}{C_0} \times 100 \quad (3)$$

Where C_0 and C_e (mg/L) is the initial and equilibrium concentration of the petroleum oil, respectively; m is the mass (g) of dry adsorbent used in experiments; V is the volume (L) of the solution.

2.3 Characterization of Adsorbents

The specific surface area and porosity of HC, HC_US, and MHC were analyzed by the Brunauer-Emmett-Teller (BET) method. The surface functional groups of hydrochar and magnetic hydrochar will be analyzed using Fourier Transform Infrared (FT-IR) Spectroscopy within the spectral range of 4000–400 cm^{-1}. The magnetic properties of the magnetic adsorbent will be evaluated by inhouse method using the magnetic bar (magnetic holding of 8 kg). The wettability of Magnetic hydrochar was analyzed using the water contact angle (WCA).

3. RESULTS AND DISCUSSIONS

3.1 Physio-Chemical Characterization of adsorbents

The Brunauer-Emmett-Teller (BET) can analyze the specific surface area of the adsorbents. The results indicated that hydrothermal treatment and ultrasonication activation enhanced the surface area and pore volume of SCGs as shown in Table 1. The hydrothermal carbonization enhanced the surface area and pore volume by hydrolysis, dehydration, decarboxylation, aromatization, and polymerization. Applying an ultrasonication on the hydrochar (HC) can increase both surface area and pore volume due to pore cleaning and the values are quite decrease comparing with the other adsorbents upon the different temperature [13]. In addition, magnetic hydrochar with higher Fe concentration under sonication treatment exhibits the highest surface area, reaching to 2.2582 m^2/g which indicates that iron interaction improves the surface's porosity and enhances high removal efficiency. This might be due to the alkaline conditions of the co-precipitation process, which could extract lignin from Hydrochar.

Table 1 BET surface area, pore volume and water contact angle of hydrochar and magnetic hydrochar

Sample	Surface Area (m2/g)	Pore Volume (cm3/g)	Water Contact Angle
SCG	0.2249	0.00004	-
HC-220	0.5189	0.004826	-
HC_US - 120	0.6732	0.004439	-
MHC_US -0.2	0.7042	0.005475	97.6˚
MHC_US -0.25	1.8094	0.010732	108˚
MHC_US -0.3	2.2582	0.01105	74.6˚

The physical characteristics of adsorbents, particularly the pH, play a critical role in the adsorption process. Hydrochar exhibited a lower pH range of 3.5-4 compared to the SCG which had a range of pH 4-5, and this decrease is likely due to the decomposition of cellulose, hemicellulose and lignin into organic acids under elevated temperature. In contrast, the synthesis of magnetic hydrochar involved the addition of alkali solution, which increased the pH range to 9-13 which is the formation of pure magnetite (Fe_3O_4). The Fe_3O_4 nanoparticles formed through co-precipitation of Fe^{2+} and Fe^{3+} ions interact with oxygen-containing functional groups, which can modify the surface properties of the adsorbents. The magnetic precursor used in chemical co-precipitation is a combination of Fe2+ and Fe3+, with the preparation reaction proceeding as follows:

$$Fe^{2+} + 2Fe^{3+} + 8OH^- \longrightarrow Fe_3O_4 + 4H_2O \quad (1)$$

FTIR was analyzed to identify the functional groups in hydrochar, activated hydrochar, and magnetic hydrochar within the spectra 4000 – 400 cm^{-1} and the result is shown in Fig: 2. The O-H stretching was found in peaks between 3300 cm^{-1} and 3500 cm^{-1} for all materials which indicates the presence of hydroxyl functional groups[14]. The O-H stretching band around 3400 cm-1 was prominent in SCGs and remained moderately found in HC and HC_US, reflecting partial retention of surface hydroxyl groups after hydrothermal and ultrasonic treatment. However, MHC_US (0.3M) exhibited significantly higher O-H

intensity, which correlates with its observed higher water solubility and hydrophilicity compared to lower Fe concentrations in MHC_US (0.2M and 0.25M). In addition, the peak at 2850 cm^{-1} - 2920 cm^{-1} corresponds to C-H stretching, indicating the presence of aliphatic hydrocarbon with medium stretching intensity in all samples but slightly decrease due to the decomposition of aliphatic components. Additionally, the C=O stretching band (1700 cm^{-1}) and C=C stretching band (1600 cm^{-1}) were slightly increased in MHC_US samples as Fe concentration compared to HC and HC_US due to magnetization can enhance carbonyl interactions and affect surface oxidation. The C-O stretch groups were observed at 1050-1250 cm^{-1} and became more pronounced with increasing Fe concentration, which indicated the coordination between Fe and oxygen-containing groups. After magnetization, Fe-O stretching was detected at 500 cm^{-1} - 600 cm^{-1} in MHC samples, which verified the presence of iron oxide in MHC_US[15]. The increasing intensity of this peak with higher Fe concentrations supports the successful magnetization process. These spectral changes, including the reduction in O–H, C=O, and C–O band intensities alongside the appearance of Fe–O stretching, suggest significant surface chemical modifications that enhance the oxygenated functional groups.

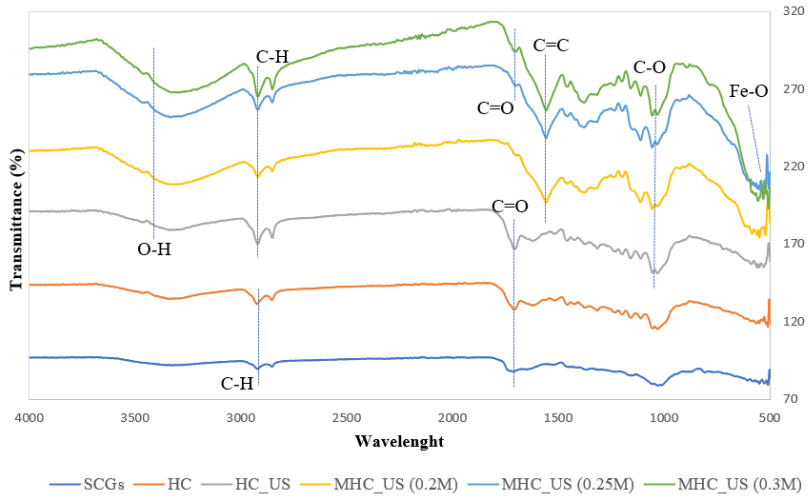
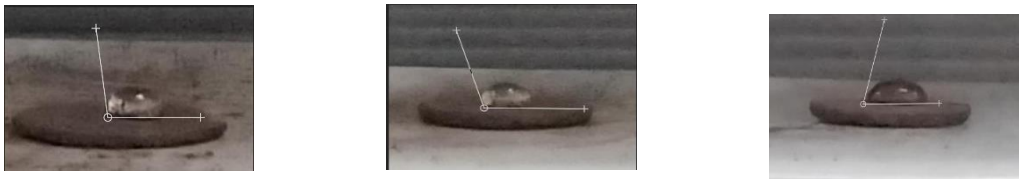


Figure 2 FTIR Spectra of SCGs, HC. HC_US, MHC_US

The wettability of the Magnetic hydrochar was analyzed using the water contact angle (WCA). WCA greater than 90˚ indicates hydrophobicity, while WCA below 90˚ signifies hydrophilicity. The adsorbent was placed, and a droplet of water was slowly dropped using a pipette. The contact angle values for MHC_US (0.2) and MHC_US (0.25) were recorded at 97.6˚ and 108˚, respectively in Table 1 and confirmed their hydrophobic nature. In contrast, MCH_US (0.3) exhibited a lower WCA of 74.6˚, indicating a transition toward hydrophilicity in Fig: 3. This reduction in WCA might be the activation process that facilitated surface oxidation due to the breakdown of C-H and C-C bonds, leading to an increase in oxygen-containing functional groups, which can enhance the surface polarity and water affinity. Additionally, the presence of Fe-OH species in magnetic hydrochar may have contributed to a further reduction in hydrophobicity.



(a) MHC_US (0.2M) (b) MHC_US (0.25M) (c) MHC_US (0.3M)

Figure 3: Water Contact Angle of Magnetic Hydrochar

The magnetic properties in magnetic hydrochar are characterized by using the reference magnetic bar (magnetic holding of 8 kg), which will be used to hold 1 g of the magnetic adsorbent. The weight of the non-magnetic part of the magnetic adsorbent will be recorded. Then, the distance between the reference magnetic bar and the magnetic adsorbent was extended using the additional paper. The thickness of the paper and the weight of the non-magnetic part of the magnetic adsorbent will be recorded until the weight of the non-magnetic part exceeds 50%. The relationship between the thickness of the paper and the weight of the non-magnetic part will be used to calculate the thickness of paper that provides 50% of the weight of the non-magnetic part. Such distance will be used to report the magnetic power of magnetic adsorbents. As a result, the magnetic hydrochar with low Fe loading exhibited a significant increase in the thickness of the paper, 11.61 cm, which suggests stronger magnetic attraction compared to other samples at 5.19 cm and 1.88 cm, respectively. Therefore, this analysis can predict the magnetic strength of an adsorbent on the thickness of the paper with a higher thickness value, which can indicate strong magnetization.

3.2 Removal of Diesel Oil from Artificial Seawater

The diesel oil removal efficiency of different magnetic hydrochar varied significantly with Fe concentration. MHC_US-0.2 and MHC_US-0.25 exhibited the removal efficiency in 98.99% and 56.45% respectively, as shown in Table 2. In contrast, MHC_US-0.3 showed a sharp decline to 28.25%. Additionally, MHC_US-0.2 remained floating on the water surface due to its hydrophobicity. In contrast, the increased Fe concentration in MHC_US-0.3 likely contributed to its reduced oil adsorption performance, which may have increased hydrophilicity and reduced oil affinity. This trend was further supported by residual oil analysis by GC-FID after extracting with hexane in the adsorbent, where MHC_US-0.2 retained 1.980 g of oil, indicating efficient adsorption capacity. On the other hand, MHC-US-0.3 had retained 0.567 g, suggesting a lower uptake of oil and influence of hydrophilic surface characteristics.

Table 2 Diesel-oil removal efficiency using 0.1 g of magnetic hydrochars

Sample	Initial Oil (g)	Residual Oil (g)	Removal %
MHC_US-0.2	2.00	1.98	98.99
MHC_US-0.25	2.00	1.129	56.45
MHC_US-0.3	2.00	0.567	28.25

4. CONCLUSION

This study successfully developed magnetic SCG hydrochar as an effective oil adsorbent for open-water applications. HTC and ultrasonication enhanced the surface area, pore volume, and oxygenated functional groups, facilitating Fe precursor adsorption and resulting in strong magnetic properties. Among the tested materials, MHC_US-0.2 exhibited the highest adsorption capacity (1.98 g/g) and removal efficiency (98.99%), while MHC_US-0.3 showed significantly lower adsorption (0.567 g/g) due to increased Fe concentration and hydrophilic surface characteristics. Although Fe incorporation improves magnetization, excessive Fe loading can induce surface oxidation and hydrophilicity, thereby reducing oil removal efficiency. Future research should focus on optimizing Fe deposition and surface functionalization to enhance hydrophobicity and adsorption performance for more efficient oil spill remediation. Additionally, the environmental sustainability of magnetic adsorbents at commercial scale necessitates consideration of their end-of-life management. While incineration and landfilling are common disposal methods, their long-terms safety implications are still under evaluation and require further investigation.

ACKNOWLEDGEMENT

The work was financially supported by the International Postgraduate Program in Hazardous Substance and Environmental Management, Graduate School, Chulalongkorn University.

REFERENCES

1. Malhas, R., et al., *Application of magnetic separation for oil spill remediation and recovery in Kuwait sea water.* Desalination and Water Treatment, 2021. **209**: p. 114-120.
2. Medeiros, A.D.L.M.d., et al., *Oily Wastewater Treatment: Methods, Challenges, and Trends.* Processes, 2022. **10**(4): p. 743.
3. Wang, Z., et al., *Biomass-Derived Porous Carbonaceous Aerogel as Sorbent for Oil-Spill Remediation.* ACS Applied Materials & Interfaces, 2016. **8**(48): p. 32862-32868.
4. Yousuf M. Al-Awadhi, S.P., *Coffee Waste Biochar: A Widely Available and Low-cost Biomass for Producing Carbonaceous Water Treatment Adsorbents.* Chemical Engineering Transactions, 2022. **92**.
5. Delil, A.D., *Optimization of Adsorption for the Removal of Cadmium from Aqueous Solution Using Turkish Coffee Grounds.* International Journal of Environmental Research, 2019. **13**: p. 861-878.
6. Edathil, A.A., et al., *Novel magnetic coffee waste nanocomposite as effective bioadsorbent for Pb(II) removal from aqueous solutions.* Journal of Environmental Chemical Engineering, 2018. **6**(2): p. 2390-2400.
7. Hussain, N., et al., *Cadmium (II) removal from aqueous solution using magnetic spent coffee ground biochar: Kinetics, isotherm and thermodynamic adsorption.* Materials Research Express, 2020. **7**(8): p. 085503.
8. Huishan Meng, Z.C., *Magnetic hydrochar for sustainable wastewater management.* npj Material Sustainability, 2025.
9. Sayğılı, G.A. and H. Sayğılı, *Fabrication of a magnetic hydrochar composite via an in situ one-pot hydrocarbonization strategy for efficient herbicide removal.* Diamond and Related Materials, 2022. **128**: p. 109302.
10. Hung-Suck Park, G.S., *Adsorption Characteristics of Modified Magnetic Coffee Waste for Removal of Tetracycline from Water.* 2020.
11. Madusari, S., *Hybrid Hydrothermal Carbonization and Ultrasound Technology in Oil Palm Biomass for Hydrochar Production.* ChemBioEng, 2022. **10**.
12. Rana N. Malhas, K.W.A., *Oil Removal from Polluted Seawater using Carbon Avocado Peel as Bio-Absorbent.* European Journal of Enginnering and Technology Research, 2023. **8**.
13. Venkatesan, S., et al., *Evaluation of the production of hydrochar from spent coffee grounds under different operating conditions.* Journal of Water Process Engineering, 2022. **49**: p. 103037.
14. Patiño, A.A.B., V.L. Lassalle, and M.F. Horst, *Magnetic hydrochar nanocomposite obtained from sunflower husk: A potential material for environmental remediation.* Journal of Molecular Structure, 2021. **1239**: p. 130509.
15. Yi, Y., et al., *Magnetic biochar for environmental remediation: A review.* Bioresource Technology, 2020. **298**: p. 122468.

20R6-13

Conditional Optimization for Treatment of Wastewater from Ethanol Production Process Using Ozonation

Wipada Dechapanya[1,*], Nongkran Koonwong[2], Sompop Sanongraj[1], Supatpong Mattaraj[1], Karnika Ratanapongleka[1], and Tiammanee Rattanawerapan[1]

[1*]*Lecturer, Faculty of Engineering, Ubon Ratchathani University, Ubonratchathani 34190, Thailand.*

[2]*Undergraduate student, Environmental Engineering Program, Department of Chemical Engineering, Faculty of Engineering, Ubon Ratchathani University, Ubonratchathani 34190, Thailand;*

[*]*Phone : 0885944017, Fax : 045 353333., E-mail : wipada.d@ubu.ac.th*

ABSTRACT

This study aimed to determine the optimal conditions for removing COD and color from ethanol production effluent using the ozonation process. The investigation employed Response Surface Methodology (RSM) with a Central Composite Design (CCD) model, focusing on two key variables: ozone dosage rate (900, 1,200, and 1,500 mg/hr) and contact time (60, 90, and 120 minutes). The results showed that the highest COD and color removal efficiencies—62.93% and 75.92%, respectively—were achieved at an ozone dosage of 1,500 mg/hr and a contact time of 120 minutes. Based on the ANOVA statistical analysis of the treatment results, the Quadratic Model and the Linear Model were found to be suitable for describing the relationship between the variables (ozone dosage rate and contact time) and the COD and color removal efficiencies of effluent from a UASB tank using the ozonation process. According to the model, the optimal conditions for maximum treatment efficiency were an ozone dosage rate of 1,500 mg/hr and a contact time of 116.881 minutes, which predicted COD and color removal efficiencies of 63.99% and 75.79%, respectively. To validate these findings, a series of experiments were conducted under the recommended optimal conditions. The average COD removal efficiency observed was 62.99±0.68%, which closely aligns with the model prediction, with a deviation of only 1.602%. Similarly, the average color removal efficiency was 73.22±0.62%, showing a minor deviation of 3.514% from the predicted value. These results confirm the reliability and suitability of the CCD model in optimizing the ozonation process for treating effluent from ethanol production.

Keywords : ozonation process; ethanol production wastewater; Response Surface Methodology; Central Composite Design;

INTRODUCTION

The ethanol industry is a sector that requires a large amount of water in its production process, starting from the preparation of raw materials, which involves washing and cleaning before being processed into a starch solution. The process then moves on to boiling, fermentation, and distillation, respectively. The wastewater generated from production contains high levels of COD, BOD, and color, while having a low pH (high acidity), making it difficult to treat [1]. This leads to negative impacts on surrounding communities, such as the discharge of wastewater into rivers or ethanol wastewater overflowing into residential areas. The overflowing wastewater is characterized by a brown color, an unpleasant odor, and chemical contamination. These issues not only affect local communities but also pose significant environmental concerns [2].

Currently, the ethanol industry often adopts anaerobic wastewater treatment systems. These systems help reduce costs by eliminating the need for aeration and generating less sludge, thereby lowering sludge disposal expenses. Additionally, anaerobic treatment can produce biogas, mainly composed of methane gas, which can be used as fuel or an alternative energy source within the factory, leading to further energy cost savings [3]. Nevertheless, although anaerobic systems are widely utilized in ethanol wastewater treatment, the treated water often has a brown color and high COD levels that do not meet discharge standards. There are also issues related to unpleasant odors. To address these problems, various treatment methods have been explored, including membrane filtration, activated carbon adsorption, ozonation, and the Fenton process. Each method has its limitations depending on the treatment process. Previous studies have shown that ozonation is effective in removing color and organic substances from ethanol production wastewater [4]. Therefore, this research was conducted to study the optimal conditions for treating wastewater from the

ethanol production process using the ozonation method, by comparing the water quality before and after treatment.

Ozonation is currently used in wastewater treatment, as it does not produce toxic byproducts in the treated water. This process involves removing pollutants in the form of biologically non-degradable organic compounds through a chemical reaction using ozone. Ozone is a powerful oxidizing agent capable of breaking down complex organic molecules. Additionally, ozone is an unstable gas that can decompose into oxygen, releasing various radicals such as hydroxyl radicals (OH•) and superoxide anion (O_2^-). These radicals are highly reactive and act as strong oxidizing agents, readily reacting with various substances. The use of ozone in degrading organic matter in water reduces the toxicity of these compounds and enhances their biodegradability [5, 6]. Furthermore, COD and many colored and complex organics are broken into smaller, less colored or colorless compounds. Ozone is also a powerful disinfectant, making it highly effective in eliminating pathogens [7]. The key reactions in the ozonation process for wastewater treatment occur through both direct and indirect oxidation mechanisms. In direct oxidation, ozone reacts directly with certain organic and inorganic compounds via electrophilic attack, particularly targeting functional groups such as double bonds, activated aromatic rings, or amines, as illustrated in Equation 1. In indirect oxidation, ozone decomposes in water, especially under alkaline conditions, to generate hydroxyl radicals (OH•), which are highly reactive and non-selective oxidants (Equations 2–6). Once formed, these hydroxyl radicals can rapidly oxidize a wide range of organic pollutants, often more efficiently than ozone itself, as shown in Equation 7 [8].

$$O_3 + \text{pollutant} \rightarrow \text{oxidized products} + \text{byproducts} \quad (1)$$

$$O_3 + OH^- \rightarrow HO_2^- + O_2 \quad (2)$$

$$HO_2^- \leftrightarrow O_2^- + H^+ \quad (3)$$

$$O_3 + O_2^- \rightarrow O_3^- + O_2 \quad (4)$$

$$O_3^- + H^+ \leftrightarrow HO_3 \quad (5)$$

$$HO_3 \rightarrow OH\bullet + O_2 \quad (6)$$

$$OH\bullet + \text{pollutant} \rightarrow \text{oxidized products} + H_2O \quad (7)$$

This study focused on two primary variables influencing pollutant removal efficiency: ozone dosage rate and contact time. To evaluate their effects and interactions, the Central Composite Design (CCD) approach was utilized through the Design Expert software. This statistical method enabled a structured assessment of how these factors impact treatment performance. Moreover, the integration of advanced analytical tools and computational techniques has significantly improved the ability to determine the most effective treatment parameters. Design Expert's Response Optimizer feature further aids in forecasting and confirming the optimal conditions for achieving maximum removal efficiency.

METHODOLOGY

This research emphasizes determining the optimal conditions for treating wastewater from the ethanol production process using the ozonation method. The study commenced with the collection of wastewater samples to analyze their characteristics (color, pH, and COD). An experimental design was then developed based on the principles of RSM. Treated water samples were analyzed to evaluate treatment efficiency and validate the accuracy of the mathematical model generated by the software. The characteristics of the wastewater sample were analyzed according to standard methods, as displayed in Table 1 [9]. Based on primary research, two key process variables, ozone dosage rate and contact time, were

adjusted to values of 900, 1,200, and 1,500 mg/hr, and 60, 90, and 120 minutes, respectively [4, 10]. The ozone dosage rate generated by the ozone generator was analyzed following the standard method [9].

Table 1. Parameters and methods for analyzing characteristics of wastewater from ethanol production

Parameter	Analysis method
pH	pH Meter
COD (mg/L)	Closed Reflux Colorimetric Method
Color	ADMI Method

The optimization process using RSM involves designing a structured set of experiments where key variables are systematically adjusted. The experimental data are then used to develop a mathematical model that illustrates the relationship between the independent variables (factors) and the dependent variable (response). This model enables the prediction of the response outcome based on different combinations of factor levels. Additionally, it plays a crucial role in determining the optimal conditions for enhancing contaminant removal, reducing chemical oxygen demand (COD), and improving the color and odor quality of the treated wastewater [11–13]. The RSM model is typically represented by the following equation [14].

$$y = \beta_0 + \sum_{i=1}^{k} \beta_i x_i + \sum_{i=1}^{k} \beta_{ii} x_i^2 + \sum \sum_{i<j} \beta_{ij} x_i x_j + \varepsilon \quad (8)$$

Where y is the model response, β_0 is the intercept, β_i are the linear coefficients for each independent variable, β_{ii} are the quadratic coefficients for the squared terms of each independent variable, β_{ij} are the interaction coefficients between the variables X_i and X_j, X_i and X_j are the independent variables, k is the number of independent variables, and ε is the error term. This equation is essential for understanding the impact of changes in process variables on the response and plays a crucial role in process optimization.

RESULTS AND DISCUSSIONS

The preliminary analysis of the wastewater samples revealed that the effluent from the ethanol production process contains relatively high levels of pollution, particularly in terms of COD and color, as shown in Table 2. This indicates a significant load of organic and inorganic substances in the wastewater [10]. The effluent appears as dark brown water with black sludge, as illustrated in Figure 1.

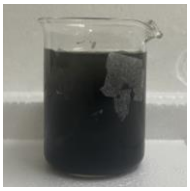


Figure 1 Wastewater sample from ethanol production

Treatment of wastewater sample from ethanol production using ozonation

The study on the efficiency of COD and color removal from ethanol production wastewater using the ozonation process showed that color could be reduced to 154 ADMI, and COD to 1,740.01 mg/L. The resulting color value meets the industrial effluent standards set by the Ministry of Industry, while the COD value exceeds the permissible limit. Additionally, experimental results revealed an increase in the pH of the treated water, as shown in Table 3. The rise in pH is attributed to the formation of hydroxide ions (OH^-) during the reaction, leading to a condition where the concentration of hydroxide ions [OH^-] is greater than that of hydronium ion [H_3O^+] resulting in a more basic solution and, consequently, a higher pH after treatment [15]. Figure 2 illustrates the physical characteristics of the wastewater sample and treated water. As seen from the figure, the color of the water sample changed from dark brown to lightly cloudy white.

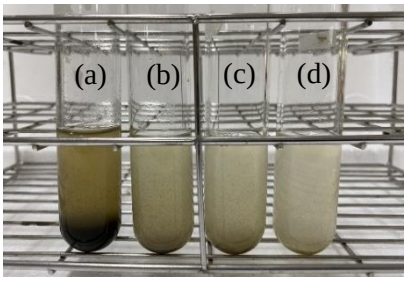


Figure 2 Physical characteristics of the wastewater sample and treated water at different contact times (a) 0 min, (b) 60 min (c) 90 min (d) 120 min

Table 2 Wastewater characteristics from ethanol production

Parameters	Average value before treatment	Average value after treatment	Standard values of effluent discharge [16]
pH	7.59	8.68	5.5 – 9.0
COD	4,830 mg/L	1,740.01 mg/L	≤ 120 mg/L
Color	573 ADMI	154 ADMI	≤ 300 ADMI

A comparison between the experimental results and the predicted values for COD and color removal efficiencies obtained from the Design-Expert software is demonstrated in Table 3. The results indicate that the predicted values closely match the experimental data. Similarly, the color removal efficiencies obtained from both the experimental results and the Design-Expert predictions are also comparable, as shown in Table 3, further confirming the model's accuracy. The highest COD and color removal efficiencies were observed at an ozone dosage rate of 1,500 mg/hr and a contact time of 120 minutes, achieving 62.93% and 75.92% removal efficiencies, respectively. In contrast, the lowest removal efficiencies were found at an ozone dosage rate of 900 mg/hr and a contact time of 60 minutes, with COD and color removal rates of 11.86% and 62.54%, respectively.

Table 3 Comparison between experimental and predicted values of removal efficiency

No.	Ozone dosage rate (mg/hr)	Contact time (min)	Removal efficiency (%)			
			COD		Color	
			Experiment	Prediction	Experiment	Prediction
1	900	60	14.14±3.07	11.86	62.37±1.90	62.54
2	900	90	40.63±4.29	42.21	70.52±0.14	70.20
3	900	120	51.59±1.26	53.10	72.96±1.41	73.11
4	1200	60	22.74±1.78	29.19	63.74±0.22	63.29
5	1200	90	56.52±0.73	53.34	72.96±0.69	73.11
6	1200	90	54.39±5.32	53.34	72.91±3.44	71.17
7	1200	90	55.06±6.89	53.34	71.15±3.59	71.17
8	1200	90	55.48±2.07	53.34	69.75±0.17	71.17
9	1200	90	52.20±6.73	53.34	68.22±1.99	71.17
10	1200	120	59.14±3.31	58.02	74.73±0.19	74.31
11	1500	60	50.70±5.02	46.53	64.18±4.39	64.46
12	1500	90	59.09±1.01	64.46	73.12±1.88	72.57
13	1500	120	63.32±1.28	62.93	75.65±1.42	75.92

Statistical analysis

Based on the experimental results using the RSM, the data from Table 3 were used to identify the most appropriate mathematical model for predicting COD and color removal efficiencies in ethanol production wastewater treated by the ozonation process. The model summary statistics indicated that the quadratic model, with an adjusted R^2 value of 0.9209, was selected to describe the relationship between the process variables (ozone dosage rate and contact time) and COD removal efficiency. The linear model was suggested for the prediction of color removal efficiency. Statistical analysis revealed that the equation for the percentage of COD removal had an F-value of 41.02 and a P-value of < 0.0001. Since the P-value is less than 0.05, this indicates that the model is statistically significant and suitable for explaining the relationship between COD removal efficiency and the studied variables in the ozonation process. Furthermore, the coefficient of determination (R^2) was found to be 0.9535, as presented in Table 4, indicating that 95.35% of the experimental data can be explained by the predicted values from the mathematical model [17]. A high R^2 value signifies high accuracy in the model's predictive capability. Similarly, the adjusted R^2 (Adj R^2) was 0.9303, which is higher than the minimum acceptable value of 0.64, suggesting that the model is well-suited for predicting COD removal. The predicted R^2 (Pred R^2) was 0.7701, with a difference of only 0.1602 from the Adj R^2. Since this difference is less than 0.2, it implies that the model has no significant problems regarding prediction adequacy [18, 19]. Furthermore, the coefficient of variation (C.V.) was 8.40%, which is below the 10% threshold, indicating that the predictive model has good repeatability and precision. Additionally, the adequacy precision was 21.9545, as shown in Table 4. Since this value is greater than 4, it demonstrates that the model is reliable [9].

For color treatment, the statistical analysis revealed that the equation for the percentage of color removal had an F-value of 41.56 and a P-value of < 0.0001, which is less than 0.05. This indicates that the model is statistically significant and suitable for explaining the relationship between the color removal efficiency and the investigated factors in the ozonation process. When examining the coefficient of determination (R^2), a value of 0.9205 was obtained, as shown in Table 5, indicating that 92.05% of the experimental data can be explained by the mathematical model's predictions [17]. A high R^2 value suggests high accuracy in the model's ability to predict outcomes, which is essential in mathematical modeling for experimental design. In general, R^2 values range from 0 to 1, and a good model should have an R^2 value close to 1. Likewise, the adjusted R^2 (Adj R^2) was found to be 0.8637, which exceeds the minimum acceptable value of 0.64, confirming the model's suitability. The predicted R^2 (Pred. R^2) was 0.8560, differing from the Adj R^2 by only 0.0077. Typically, this difference should not exceed 0.2, indicating that the model has no significant issues regarding prediction reliability [18, 19]. Moreover, the coefficient of variation (C.V.) was only 2.28%, which is well below the 10% threshold. A lower C.V. implies better reliability and precision in the model's reproducibility. The adequacy precision value was 12.3015, as shown in Table 5, which is greater than 4, further demonstrating the model's reliability [9]. Additionally, the statistical analysis indicated that both factors had a significant impact on the removal efficiency of COD and color.

Table 4 Fit statistical results for COD removal using the ozonation process

Std. Dev.	3.86	**R^2**	0.9535
Mean	48.91	**Adjusted R^2**	0.9303
C.V. %	8.40	**Predicted R^2**	0.7701
Adequacy precision			21.9545

Table 5 Fit statistical results for color removal using the ozonation process

Std. Dev.	1.60	**R^2**	0.9205
Mean	70.17	**Adjusted R^2**	0.8637
C.V. %	2.28	**Predicted R^2**	0.8560
Adequacy precision			12.3015

The experimental data can be used to construct a mathematical model (Actual Equation) as shown in Equations 9 and 10 for COD and color removal efficiencies, respectively.

$$\%R.E.COD = - 196.48857 + 0.099158A + 3.25477B – 0.000690AB - 0.010815B^2 \quad (9)$$

$$\%R.E.\ Color = 34.54805 – 0.003865A + 0.629209B + 0.0000024AB + 2.33716*10^{-6}A^2 \quad (10)$$

Where A is the ozone dosage rate (mg/hr) and B is the contact time (min).

Conditional optimization for the COD and color removal using ozonation

From the conditional optimization for treating wastewater from the ethanol production process using ozonation and based on the CCD model, a total of seven conditions were identified. However, the model recommended the optimal condition for both COD and color removal to be at an ozone dosage rate of 1,500 mg/hr and a contact time of 116.88 minutes. Under these conditions, the COD removal efficiency was 63.99%, and the color removal efficiency was 75.79%, with an overall desirability score of 0.995, as shown in Figure 3. Since this value is close to 1.00, it indicates that the optimal condition for treating ethanol production wastewater using the ozonation process, derived from the mathematical model, is highly reliable [20].

A set of experiments was conducted to validate the optimal treatment conditions obtained from the model. The experiment was performed in triplicate using the conditions recommended by the model, an ozone dosage rate of 1,500 mg/hr and a contact time of 117 minutes. The average COD removal efficiency was found to be 62.99 ± 0.68%. This experimental result was very close to the model's predicted value, with only a 1.602% deviation. The average color removal efficiency was 73.22 ± 0.62%, also closely matching the model's prediction, with a 3.51% deviation. These results confirm that the CCD model is both reliable and suitable for determining the optimal conditions for treating wastewater from the ethanol production process using ozonation, as the deviation between the experimental results and the mathematical model was less than 10% [10].

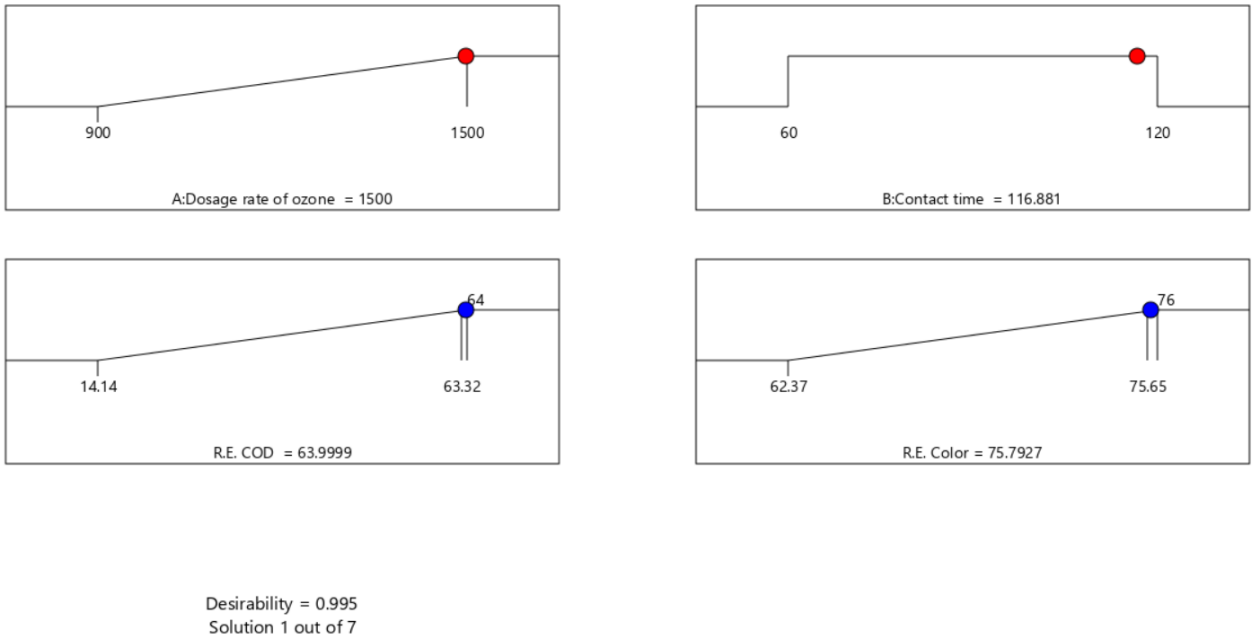


Figure 3 Desirability ramps for COD and color removal using ozonation at the optimal conditions

CONCLUSION

This research focuses on the treatment of wastewater from ethanol production using the ozonation process. Two key factors affecting the treatment efficiency were considered: the ozone dosage rate and contact time. It was found that an ozone dosage rate of 1,500 mg/hr and a contact time of 120 minutes resulted in the highest removal efficiencies of COD and color, which were 63.32 ± 1.28% and 75.65 ± 1.42%, respectively.

Statistical analysis revealed that both factors significantly influenced COD and color removal efficiencies. A quadratic model was found to be suitable for predicting COD removal efficiency, while a linear model was appropriate for predicting color removal efficiency. Based on conditional optimization, the model recommended the optimal conditions for COD and color removal at an ozone dosage rate of 1,500 mg/hr and a contact time of 116.88 minutes, yielding a COD removal efficiency of 63.99% and a color removal efficiency of 75.79%, with a desirability of 0.995, indicating a high level of suitability. The findings from this research can be applied to wastewater treatment in ethanol production plants or other processes with similar wastewater characteristics.

ACKNOWLEDGEMENT

Thanks to the Undergraduate Program in Environmental Engineering, Department of Chemical Engineering, Ubon Ratchathani University, for providing chemicals, experimental equipment, research facilities, and support for presenting this research.

REFERENCE

[1] Energy Research and Development, Institute Nakornping, Chiang Mai University. 2022. Study on Color and Organic Matter Reduction in Wastewater from Biogas Power Plants Using Wastewater from the Ethanol Industry; https://erdi.cmu.ac.th/?p=1827+eritute+Nako

[2] Selaruck, K. and Dhiravisi, A. 2014. Social Impact Assessment of Bioethanol Factory to Communities; Proceedings in Graduate Research Conference. https://gsbooks.gs.kku.ac.th/57/grc15/files/hmo15.pdf?utm_source=chatgpt.com

[3] Yoosook, W., Kasayapanand, N., and Yoochatchaval, W. 2015. Treatment of wastewater from bioethanol distillate by anaerobic fluidized bed reactor. Proceedings of 53rd Kasetsart University Annual Conference: Science, Genetic Engineering, Architecture and Engineering, Agro-Industry, Natural Resources and Environment. Kasetsart University, Bangkok, 617-624.

[4] Klumsuae, P. 2017. Removal of colour and odour of wastewater from spray paint room by ozone. Thammasat University Theses. Thammasat University, Bangkok. https://ethesisarchive.library.tu.ac.th/thesis/2017/TU_2017_5410036460_9025_8444.pdf

[5] Wichitsathian, B. 2018. Enhancement of water recycle with combined ozonation and ultrafiltration processes. Research Report. Suranaree University of Technology, Nakhon Ratchasima. http://sutir.sut.ac.th:8080/jspui/bitstream/123456789/8195/2/Fulltext.pdf

[6] Lin, S.H. and Yeh, K.L. 1993. Looking to treat wastewater try ozone. Chemical Engineering. 100(5): 112 – 116.

[7] Çetinkaya, N., Pazarlar, S., and Paylan, I.C. 2022. Ozone treatment inactivates common bacteria and fungi associated with selected crop seeds and ornamental bulbs. Saudi Journal of Biological Sciences. 29(12). https://doi.org/10.1016/j.sjbs.2022.103480

[8] Christiane Gottschalk, C., Libra, J.A., and Saupe, A. 2009. Ozonation of Water and Waste Water: A Practical Guide to Understanding Ozone and its Applications. Wiley. online Library. DOI:10.1002/9783527628926

[9] Sanongraj, S., Dechapanya, W., Wongkamchao, Y., Mattaraj, S., Ratanapongleka, K., Rattanaweerapan, T., Wongcharee, S., and Suwannahong, K. 2025. Optimization of the Combined Fenton and Ozonation Processes for Efficient COD Removal in Rubber Wastewater Treatment. http://dx.doi.org/10.2139/ssrn.5122970

[10] Yongpasakornkun1, R., Mattaraj. S., Ratanapongleka, K., Sanongraj, S., Rattanaweerapan, T., and Dechapanya, W. 2023. Application of Response Surface Methodology for Statistical Analysis of Treatment of Wastewater from a Para Rubber Plant Using Ozonation. Science and Engineering Connect journal. 46(4):387-401. DOI: 10.14456/kmuttrd.2023.24

[11] Roudi, A. M., Salem, S., Abedini, M., Maslahati, A., and Imran, M. 2021. Response surface methodology (RSM)-based prediction and optimization of the Fenton process in landfill leachate decolorization. processes, 9(12): Article 2284, doi: https://doi.org/10.3390/pr9122284

[12] El-Mekkawi, S.A., Abdelghaffar, R.A., Abdelghaffar, F. and Abo El-Enin, S.A. 2021. Application of response surface methodology for color removing from dyeing effluent using de-oiled activated algal biomass. Bulletin of the National Research Centre. 45(80). doi: https://doi.org/10.1186/s42269-021-00542-w

[13] Powar, A. S., Perwuelz, A., Behary, N., Hoang, L., and Aussenac, T. 2020. Application of ozone treatment for the decolorization of the reactive-dyed fabrics in a pilot-scale process—optimization through response surface methodology. Sustainability. 12(2) : 471. doi: https://doi.org/10.3390/su12020471

[14] Montgomery, D.C. 2017. Design and Analysis of Experiments, 9th ed., John Wiley & Sons, Inc., Hoboken New Jersey.

[15] Department of Marine Chemistry and Geochemistry. Ozone Measurements in the Marine Boundary Layer from Ocean Buoys. Woods Hole Oceanographic Institution, Ozone Measurements - Background (whoi.edu). 13 April, 2025.

[16] Pollution Control Department. 2016. Announcement of the Ministry of Natural Resources and Environment on the Establishment of Effluent Discharge Standards for Industrial Factories, Industrial Estates, and Industrial Zones. Bangkok: Pollution Control Department. https://www.pcd.go.th/wp-content/uploads/2020/05/pcdnew-2020-05-20_03-06-17_069400.pdf

[17] Kaewploy, S. 2016. Optimal parameter in tempering of alloy steels using response surface methodology. Thai Industrial Engineering Network Journal. 2(2): 49-55. https://ph02.tci-thaijo.org/index.php/ienj/article/view/179539/127464

[18] Chodok, P. 2017. Optimization of culture conditions for extracellular 5-aminolevulinic acid production by Rhodopseudomonas palustris LBL15 using response surface methodology. Burapha Science Journal. 22(2): 300-316. https://ojs.lib.buu.ac.th/index.php/science/article/view/5187

[19] Phanyusoh, D., Somnuk, K., and Prateepchaikul, G. 2019. Optimization of ethyl ester production from palm fatty acid distillate (PFAD) using double-step esterification process: a response surface methodology approach. Engineering Journal Chiang Mai University. 26(1): 107-120. https://ph01.tci-thaijo.org/index.php/EngJCMU/issue/view/16552

[20] Awapak, D., Mahae, N., and Pitchairat, D., 2013. Optimization of polysaccharide extraction from gracilaria fisheri using response surface methodology. KKU Science Journal. 41(2): 414-430. https://ph01.tci-thaijo.org/index.php/KKUSciJ/article/view/249137/168929

20R6-14

Carbon Dioxide Adsorption Efficiency of Pig Bone from Food Waste by the Pyrolysis Process

Khemanat Phatrabuddha[1*], Waewprach Tweepharnichkul[1], Sataporn Kanoksikarin[1], Montian Songsiam[2] and Kowit Suwannahong[3]

[1] Grade 11 Student, Chonradsadornumrung School, Chonburi;*
[2]Senior Professional Teacher, Chonradsadornumrung School, Chonburi
[3]Associated Professor, Bachelor of Environmental Health, Public Health, Burapha University, Chonburi20131
[*]Phone : 061-9516639, Fax : 038-390041, E-mail : kowit.su@go.buu.ac.th

ABSTRACT

This research aimed to study the physical and chemical properties of biochar from pig bone, as well as analyzed the carbon dioxide (CO_2) adsorption of biochar that has been boiled and unboiled prior to pyrolysis at 500°C using a CO_2 sensor in an Internet of Things (IoT) system.

The findings showed that the physical characteristics of boiled bone char before pyrolysis were light in color, smooth, and brittle, whereas the unboiled bone char was dark brown, rough, with some fibrous tissue, and more rigid. After pyrolysis, the biochar from boiled bone was black, lightweight, and brittle, while the biochar from unboiled bone was also black, lightweight, and slightly brittle. The BET surface area of the biochar from boiled bone was 77.0285 m^2/g, with a pore diameter of 14.4510 nm and a pore volume of 0.6770 cm^3/g, which was greater than that of the biochar from unboiled bone, which had a surface area of 33.3830 m^2/g, a pore diameter of 9.9720 nm, and a pore volume of 0.1027 cm^3/g. The C:N ratio of the biochar from boiled bone before pyrolysis was 0.75:13.87, which was similar to the unboiled biochar at 0.68:13.55. However, the carbon and nitrogen contents in the biochar from boiled bone were higher. The iodine number of the boiled and unboiled bone char before pyrolysis was 35.4% and 19.55%, respectively. The analysis of CO_2 adsorption revealed that the biochar from boiled bone adsorbed CO_2 better than the unboiled biochar, with a 15.25% higher CO_2 adsorption efficiency. Based on the findings, the study suggests that the duration of CO_2 release should be extended, and further research should be conducted on the oil by-products obtained from the pyrolysis of pig bone biochar.

Keywords : CO_2 adsorption, pig bone, food waste, pyrolysis

INTRODUCTION

Currently, food waste is a global problem due to its increasing volume every year, with an average of approximately 79 kilograms per person per year [1]. In Thailand, the average food waste is 86 kilograms per person per year, which is higher than the global average. The Pollution Control Department [2] reported the waste and pollution situation in Thailand for the year 2023, revealing that the country generated a staggering 26.95 million tons of waste, with "food waste" accounting for a significant portion. Food waste amounts to more than 10.24 million tons, or 38% of the total waste. In the food industry, pig bones or spare ribs are a significant form of food waste that contributes to greenhouse gas emissions, which is a major cause of climate change, leading to global warming. Carbon dioxide is one of the greenhouse gases that contribute to global warming. In terms of health effects, exposure to high concentrations of this gas can cause rapid breathing, fast pulse, rapid heartbeat, brain pressure, drowsiness, dizziness, confusion, unconsciousness, and may even lead to death [3].

Biochar is a carbon-rich material derived from biomass feedstocks, consisting of carbonyl groups, hydroxyl groups, and aromatic compounds. It is produced through a thermochemical decomposition process in the absence of oxygen, known as slow pyrolysis. Pyrolysis is a thermal decomposition process that occurs at temperatures ranging from 400 to 700 ^{O}C. This process differs from incineration, which burns waste to ash in a furnace. Because incineration involves direct exothermic combustion with air. In contrast, pyrolysis is an endothermic reaction that requires heat as an energy source to break down various components, causing them to vaporize from the organic material. The pyrolysis of biomass results in the production of three products: biochar, bio-oil, and gas. This process alters the surface characteristics of the biomass, creating pores and increasing surface area, which allows it to adsorb carbon dioxide and store it in its porous structure [4]. Most

biochar production uses waste materials from the agricultural sector, such as tree bark, wood scraps, animal manure, corn stalks, and food waste from the industrial sector, such as animal bones, for environmental or sustainable agricultural purposes [5]. Biochar from food waste has various benefits, including improving soil, reducing greenhouse gas emissions [6], and helping absorb nutrients in the soil, as well as color, odor, and toxic substances like fluoride from drinking water [7]. “Leng” is short for “Eia Leng”, a Teochew Chinese term that means pork spine. Thai people commonly shorten it to just “Leng”. Pig bones or “Leng” are bones derived from the sacrum, a section of the spine. The sacrum is the bone that connects the pelvic bone and the coccygeal (tail) bone. Pig bones, a type of food waste from households, are usually boiled, while those from the industrial sector, which are in larger quantities, are not boiled. Therefore, we are interested in comparing the efficiency of CO_2 absorption, a greenhouse gas, in biochar made from food waste, specifically pig bone, after preparing the samples by boiling and unboiling them before pyrolysis. The findings of this study will contribute to identifying effective methods for enhancing the efficiency of carbon absorption. In addition, this study outcomes would provide meaningful results for reducing industrial waste to zero and lower greenhouse gas emissions in line with the goal of sustainable development.

METHODOLOGY

This research is an experimental design study, and data were collected from October to December 2024. The experimental process began with taking pig bones from the industrial company to sun dry for 10 days. The dried pig bones were boiled at approximately 100 ºC, then baked at 60 ºC for 12 hours. Then, biochar was taken to grind, and stored in a desiccator for further study of its physical and chemical properties. The preparation of biochar, from both the boiled and unboiled samples, was conducted prior to slow pyrolysis at 500°C for 2 hours as shown in Figure 1.

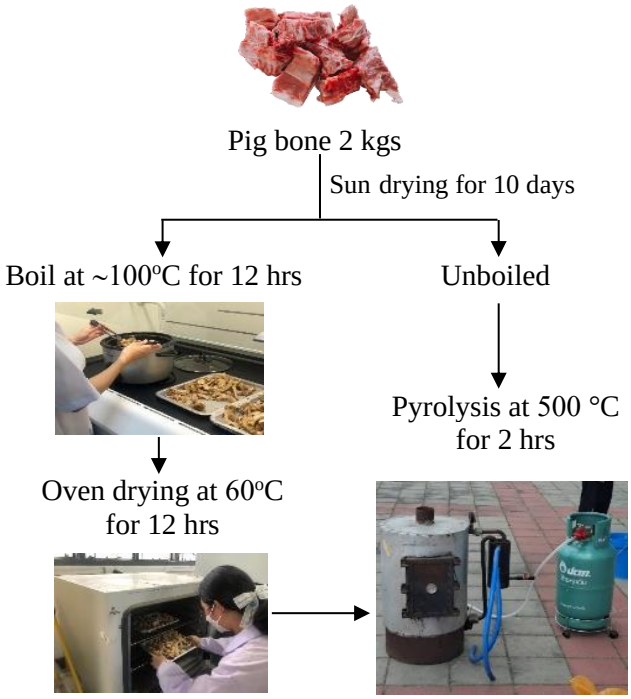


Figure 1 Biochar preparation process

The biochar samples are then studied for their structural characteristics using a surface area and porosity analyzer, based on the fundamental theory of Brunauer S., Emmett P.H. and Teller E. (BET), C/N ratio, Iodine number by following standard method of ASTM 4607-86. The carbon dioxide adsorption of biochar derived from pig bones were analyzed by using a CO_2 sensor with Internet of Things **(**IOT) system as shown in Figure 2. Biochar from the boiled and unboiled pig bones were placed into the container. Then, the timer was set to release carbon dioxide and record the concentration of CO_2 inlet and outlet every 1 minute. The experiment has done repeatly three times and recorded the results.

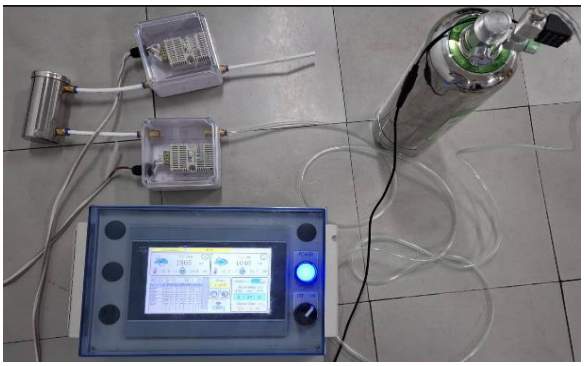


Figure 2 CO_2 sensor with Internet of Things **(**IOT) system

RESULTS AND DISCUSSIONS

The physical characteristics of the boiled pig bone showed a light color, smooth texture, and brittleness. In contrast, the unboiled pig bone was dark brown, uneven in texture, with some remaining tissue, and was harder (Figure 3). After pyrolysis, the boiled biochar turned black, was lightweight, and brittle, while the unboiled biochar also turned black, lightweight, and slightly brittle (Figure 4). The properties and basic composition of biochar differ from those of conventional charcoal. Biochar with pyrolysis contains a higher carbon content by weight than other elements and does not transform into carbon dioxide because it is not exposed to oxygen during the heating process. Additionally, the carbon in biochar is aromatic, consisting of six-carbon atom rings connected by covalent bonds, with no oxygen or hydrogen [8].

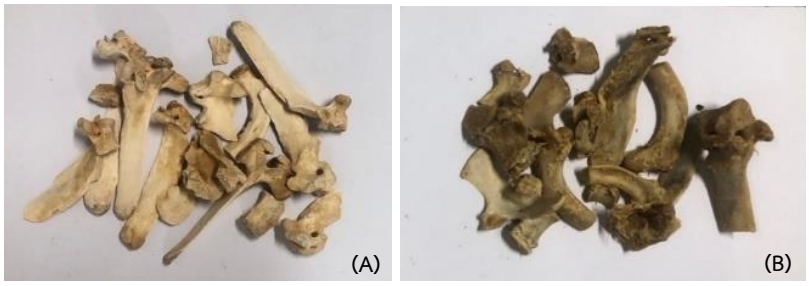


Figure 3 Pig bone (A) Boiled (B) Unboiled



Figure 4 Biochar after slow pyrolysis (A) Boiled (B) Unboiled

About chemical properties of biochar, we found that the biochar derived from the boiled pig bone had higher specific surface area, pore diameter, and pore volume compared to the biochar from the unboiled pig bone (Table 1). These indicated that boiling can enhance the carbon adsorption efficiency. Therefore, pig bone, which are a large quantity of food waste from the industrial sectors, should be boiled before pyrolysis because boiling helps remove fats and impurities that may be block the porous structure of the material, resulting in a cleaner and more porous surface area [9] . This leads to significantly improved carbon absorption capacity.

Table 1 Chemical characteristics of pig bone biochar

Types of biochar	Surface area (m^2/g)	Pore diameter (nm)	Pore volume (cm^3/g)
Boiled pig bones	77.0285	14.4510	0.6770
Unboiled pig bones	33.3830	9.9720	0.1027

The C:N ratio of biochar from boiled pig bone before pyrolysis was 0.75:13.87, which is similar to the ratio of biochar from unboiled pig bone, which was 0.68 : 13.55. However, carbon and nitrogen content in the boiled biochar was higher. The iodine number is an important value used to indicate the adsorption efficiency of biochar. For this study, we found that the iodine number of biochar from boiled and unboiled pig bones was 467 and 415.1 mg/g, respectively (Table 2).

Table 2 Iodine number of biochar from pig bone

Type of biochar	Iodine Number (mg/g)			
	I	II	III	Mean±S.D.
Boiled pig bones	455.5	473.0	468.5	465.7±9.2
Un-boiled pig bones	415.0	412.3	417.8	415.0±2.0

The CO_2 adsorption efficiency of the biochar from boiled pig bone was 15.25% higher than that of the unboiled pig bone. It was consistent with research by Leung & Wang [6], which found that slow pyrolysis process of food waste can help to reduce greenhouse gas emissions. Pyrolysis temperature also influences pH, surface area, and other properties of biochars made from various feedstocks. In general, biochar produced from slow pyrolysis was found to have a considerably higher carbon content than that by the fast pyrolysis [10,11]. With this optimized condition, this study was designed to do the pyrolysis process at $500^{O}C$. This study suggested that temperature and boiling time of pig bones should be increased to enhance the efficiency of carbon dioxide adsorption.

Suggestions for future research are 1) to study biochar from other food waste materials, such as fish bones 2) to analyze the environmental economics of using pig bone char for product development to reduce food waste in the industrial sector, which is produced in large quantities 3) to compare the removal efficiency of the synthesized biochar with that of the commercial adsorbent and 4) to study the utilization of oil by-product from pyrolysis process.

CONCLUSION

The biochar derived from the boiled pig bone before slow pyrolysis process demonstrated better CO_2 adsorption than biochar from unboiled bone. The CO_2 adsorption efficiency of the biochar from boiled pig bone was 15.25% higher than that of the unboiled bone char, which is consistent with the physical and chemical properties.

ACKNOWLEDGEMENT

Our research team is grateful acknowledge CPRAM Company for generously providing the pork bones to study. We would like to express my gratitude to the Department of Environmental Health, Faculty of Public Health, and the Department of Biochemistry, Faculty of Science, Burapha University, for their provision of equipments and facilities in this research study. Finally, we most gratefully Assoc. Prof. Kowit Suwannahong for their support throughout the period of this study.

REFERENCE

[1] United Nations Environment Programme; UNEP. Food waste index report. Think Eat Save: Tracking Progress to Halve Global Food Waste, 2024.

[2] Pollution Control Department. 2023. Thailand State of Pollution Report. Available from: https://www.pcd.go.th/wp-content/uploads/2024/06/pcdnew-2024-06-21_06-42-54_474054.pdf (cited January 5, 2025).

[3] Faculty of Science, Prince of Songkla University. 2021. Hazard of carbon dioxide. Available from: https://www.sci.psu.ac.th/news/2021/07/get-to-know-carbon-dioxide/ (cited January 5, 2025).

[4] U.S. Department of Agriculture; USDA. 2025. What is pyrolysis? Available from : https://www.ars.usda.gov/northeast-area/wyndmoor-pa/eastern-regional-research-center/docs/biomass-pyrolysis-research-1/what-is-pyrolysis/ (cited January 5, 2025).

[5] Waicharoen, D. and Chumpa, K. 2019. Biochar, Soil quality improvement assistant. Khai Hin Son Development Study Center, a royal initiative in Chachoengsao. Available from: https://www.opsmoac.go.th/chachoengsao-article_prov-files-4313917 91813 (cited January 5, 2025).

[6] Leung, D.Y.C. and Wang, J. 2016. An overview on biogas generation from anaerobic digestion of food waste. *International Journal of Green Energy* 13(2) https://doi.org/10.1080/15435075.2014.909355

[7] Alkurdi, S.S., Al-Juboori, R.A., Bundschuh, J. and Hamawand, I. 2019. Bone char as a green sorbent for removing health threatening fluoride from drinking water. *Environment International*. 127: 704-19. https://doi.org/10.1016/J.ENVINT.2019.03.017

[8] Agusti, A., Celli, B.R., Criner, G.J., Halpin, D.M.G., Anzueto, A., Barnes, P.J., et al. 2022. Global strategy for the diagnosis, management, and prevention of chronic obstructive lung disease report. GOLD executive summary. *American Journal of Respiratory and Critical Care Medicine*. 195(5): 557-582. https://doi.org/10.1164/rccm.202204-0864PP

[9] Piccirillo, C. 2023. Preparation, characterization and applications of bonechar, a food waste-derived sustainable material: A review. *Journal of Environmental Management*, 339, 117896. https://doi.org/10.1016/j.jenvman.2023.117896

[10] Tomczyk, A., Sokolowska, Z. and Boguta, P. 2020. Biochar physicochemical properties: pyrolysis temperature and feedstock kind effects. *Reviews in Environmental Science and Biotechnology*. 19: 191-215. https://doi.org/10.1007/s11157-020-09523-3

[11] Power, R.V. and Gangil, S. 2015. Effect of temperature on iodine value and total carbon contain in bio-char produced from soybean stalk in continuous feed reactor. *International Journal of Agricultural Engineering*. 8(1): 26-30. DOI: 10.15740/HAS/IJAE/8.1/26-30

Enhancing the Value of Air Filtration Media Fabricated from Natural Waste Materials

Jasmin Mayi[1], Wasna Ngulee[1], Wikanda Thongnueakhaeng[2], Peerapol Kaoien[3], Nantaporn Noosai[4], Vineeth Vijayan[5] and Supandee Maneelok[6]*

[1]Student, Occupational Health and Safety Program, Faculty of Health and Sports Science, Thaksin University, Phatthalung 93210, Thailand
[2]Lecturer, Environmental Science Program, Faculty of Science and Digital Innovation, Thaksin University, Phatthalung 93210, Thailand
[3]Researcher, Siam General Technology Co., Ltd., Trang 92140, Thailand
[4]Lecturer, Department of Civil and Environmental Engineering, Faculty of Engineering, Prince of Songkla University, Songkhla 90112, Thailand
5Lecturer, Department of Mechanical and Mechatronics Engineering, Faculty of Engineering, Prince of Songkla University, Songkhla 90112, Thailand
[6]Lecturer, Occupational Health and Safety Program, Faculty of Health and Sports Science, Thaksin University, Phatthalung 93210, Thailand

[*]Phone : 074609613, Fax : 074609613, E-mail : msupandee@tsu.ac.th.

ABSTRACT

Air filter sheets fabricated from natural agricultural waste materials as pineapple leaf fibers and bamboo fibers. Filter sheets were fabricated using fiber quantities of 100, 200, and 300 grams, in combination with binder concentrations ranging from 5% to 20% by weight. The physical properties of air filter sheets exhibited favorable surface characteristics, including smooth texture, uniform coloration, and structurally intact fibers with no evidence of tearing. Morphological analysis revealed that the fibers were longitudinally aligned, densely packed, and mechanically robust. Comparative physical assessments showed that pineapple leaf fiber demonstrated lower water absorption and moisture retention than bamboo fiber, contributing to its higher dust removal efficiency, reaching up to 70%, compared to 50% for bamboo-based filters. Despite these advantages, long-term application revealed challenges such as increased moisture accumulation and susceptibility to microbial growth. These findings indicate that pineapple leaf fiber is a promising biodegradable material for air filtration applications. However, further optimization is required to improve moisture resistance and incorporate antimicrobial functionality for sustained performance.

Keywords : air filter; natural waste materials; particulate matter; pineapple leave; bamboo leave

INTRODUCTION

Indoor air pollution has emerged as a pressing environmental and public health concern, especially as modern lifestyles result in individuals spending over 90% of their time within enclosed environments such as homes, schools, offices, hospitals, and other public buildings [1]. Exposure to indoor air pollutants including fine particulate matter ($PM_{2.5}$ and PM_{10}), carbon monoxide (CO), ozone (O_3), black carbon (BC), sulfur dioxide (SO_2), and nitrogen oxides (NO_x), it has been strongly associated with a range of health issues [2]. These include respiratory and cardiovascular conditions, as well as Sick Building Syndrome (SBS) and Building-Related Illnesses (BRI), which manifest through symptoms such as headaches, fatigue, nausea, and allergic reactions [2,3]. Indoor air contaminants originate from both external and internal sources. Pollutants can enter buildings via ventilation systems or arise from within due to factors such as poor air circulation, accumulation of dust mites, chemical emissions from furnishings and paint, excessive humidity, and microbial proliferation on damp surfaces [2,3]. As the prevalence and persistence of these pollutants increase, there is a growing need for effective air filtration technologies that can maintain indoor air quality and mitigate adverse health effects.

Air pollution control devices (air cleaners) play a critical role in the reduction and elimination of airborne contaminants. Various systems are employed depending on the scale and nature of the pollution, including setting chambers, clean air shelters, cyclones, bag filters, electrostatic precipitators, spray chambers, and packed scrubbers. However, within indoor environments, the most commonly utilized devices are air filtration systems [2]. Air filters are essential components designed to remove airborne pollutants and

contaminants, operating primarily through two mechanisms: (1) Mechanical filtration, which involves using a filter medium composed of fibers of varying sizes woven or arranged to create a porous structure. As contaminated air flows through the medium, particulates are trapped by the fibers and (2) Chemical filtration, which relies on mechanisms such as absorption and chemisorption to capture extremely small gaseous particles, typically smaller than 0.01 microns. The efficiency of chemical filtration depends on several factors, including air velocity (residence time), temperature, and humidity [2]. Regarding, High efficiency air filtration systems such as High-Efficiency Particulate Air (HEPA) and UltraLow Penetration Air (ULPA) filters, they are widely recognized for their ability to remove up to 99.97% of airborne particles. However, the reliance on synthetic polymers in their production presents challenges, including high manufacturing costs and environmental concerns regarding disposal. In light of increasing demand for affordable and environmentally sustainable alternatives, researchers have turned their attention to natural, biodegradable materials for air filter fabrication [4].

Agricultural residues and natural fibers have shown significant promise in this context. Materials such as pineapple leaves, bamboo leaves, sugarcane bagasse, rice straw, corn stalks, rice husk, coconut fiber, and palm leaves are not only renewable and biodegradable but also possess mechanical and absorption properties conducive to filtration [4-12]. Among these, pineapple leaf fiber is distinguished by its high tensile strength and moisture absorption capacity [2,5,9,10], while bamboo fiber is noted for its breathability, flexibility, and structural integrity [2,5,7].

This study focuses on the development of air filter media derived from waste pineapple leaves and bamboo leaves materials that would otherwise contribute to agricultural waste. Specifically, the objectives are to investigate the physical and structural properties of these natural fibers, identify the optimal conditions for production of air filter sheets, including the type and amount of binder used, and evaluate the filtration performance of the fabricated media produced from waste pineapple leaves and bamboo leaves.

METHODOLOGY

1.Air Filter Sheet Production Method

The process for producing air filter sheets from pineapple or bamboo leaf fiber involves the following steps:(1) Preparation of Raw Material: Obtain discarded pineapple (PN) or bamboo (BN) leaves from agricultural waste and cut them into small, uniformly sized pieces as required.(2) Alkaline Treatment: Boil the leaves in 2.5 liters of water mixed with sodium hydroxide at a ratio of 1:10 for 3 hour.(3) Oxidizing Treatment: Repeat the boiling process with hydrogen peroxide solution (H_2O_2), to further bleach and refine the fibers. (4) Washing: Filter out the liquid and rinse the fibers thoroughly with clean water to remove any residual chemicals. (5) Blending with Binder: mixing the fibers and a starch-based adhesive with varying proportions of 5%, 10%, 15%, and 20% relative to the dry weight of the fiber of 100, 200, and 300 grams respectively. (6) Sheet Formation: Scoop the fiber pulp onto a mesh screen and spread it evenly to form a uniform layer of fiber pulp. (7) Drying and Finishing: Allow the formed sheet to dry at 60^{o}C for 12 hours, then peel the filter sheet off the mesh screen.

2.Characteristics and performances

2.1 Physical Characterization: Water Absorption Capacity and Moisture Content Analysis were evaluated in accordance with ASTM D3285 standard and ASTM D6304 standard, respectively.

2.2. Morphological and Functional Analysis

Morphological Characterization of Fibers was performed using Scanning Electron Microscopy (SEM) and Filtration Efficiency for Total Dust Particles were conducted using the NIOSH Method 0500 see in Fig 1.

2.3. Application Testing: Operational Performance Test were conducted by apply the air filtration media into fan unit for 8 hour working time at 25^{o}C for 5 days to evaluate the usability and effectiveness of the developed air filter sheets

RESULTS AND DISCUSSIONS

The air filter sheet characteristic must demonstrate cohesive structure, resistance to tearing, and uniform thickness throughout. According to the specified criteria [13], the filter sheets should be free from perforations, tears, visible contaminants, or mold. Additionally, they must exhibit a clean and consistent surface without smudging, peeling, flaking, or irregular coloration. It can be seen in Figure 2, the air filter sheets fabricated from pineapple and bamboo leaf fibers met these quality standards. The surfaces were free of visible defects, including tears, contaminants, and discoloration. The sheets also demonstrated a smooth

texture and consistent coloration, with no signs of surface irregularities. The results of this study demonstrate that natural fibers derived

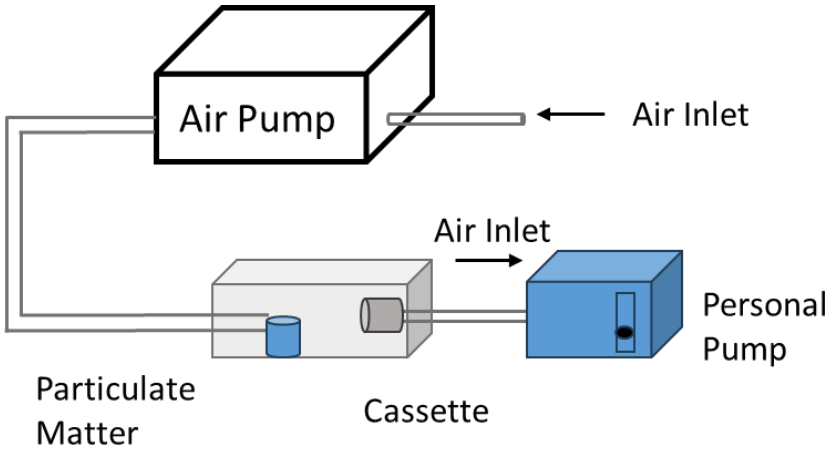
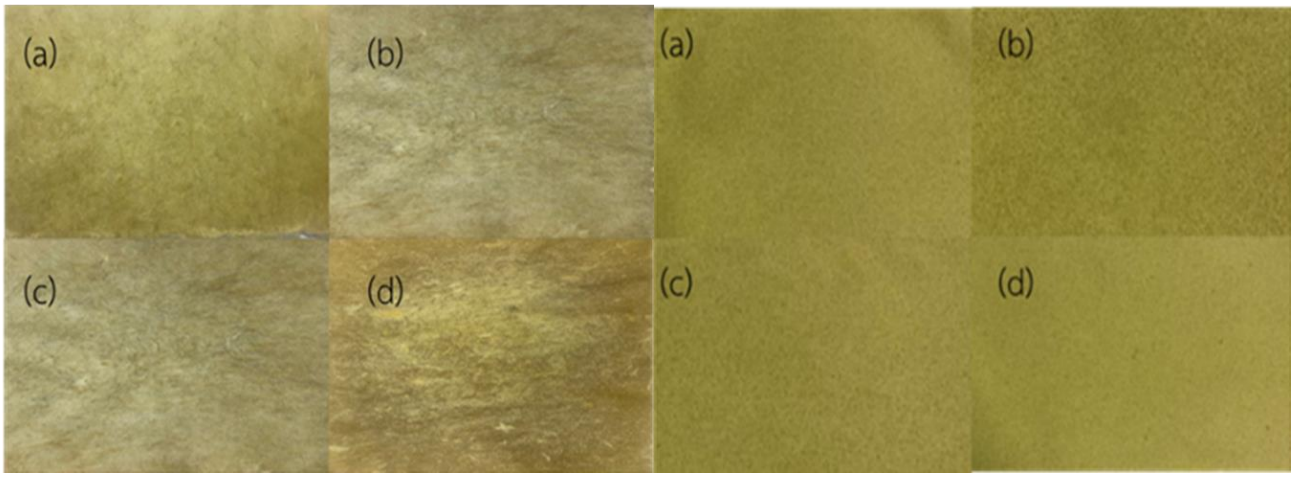


Figure 1 Schemetic of Filtration Experimental

from agricultural waste, specifically pineapple and bamboo leaves, can be effectively used to produce air filter sheets that meet essential quality standards. The physical evaluation of the filter sheets revealed satisfactory performance across all samples, with particular attention to criteria such as surface cohesion, resistance to tearing, uniform thickness, and overall aesthetic integrity. These characteristics are critical for maintaining mechanical filtration efficiency and ensuring durability during use. Notably, the preparation method had a significant influence on the visual and structural properties of the filter sheets. The incorporation of hydrogen peroxide (H_2O_2) in the PN+H_2O_2 method resulted in a visibly smoother surface and lighter coloration of the pineapple fiber sheets, compared to those prepared using only sodium hydroxide (PN). This finding supports previous literature [2,6,13] which attributes such effects to the oxidative bleaching action of H_2O_2 on plant-based fibers. The bleaching not only improves the aesthetic quality of the material but may also enhance fiber porosity and cleanliness, which are favorable attributes in air filtration applications.

Furthermore, the physical appearance of the filter sheets remained consistent or improved with increasing fiber content. Samples prepared with 200 and 300 grams of fiber maintained high scores in overall quality, indicating that increased fiber loading did not compromise structural integrity. This suggests that the manufacturing process is robust and scalable for producing thicker or denser filter media when required for higher filtration demands. Interestingly, although the PN+H_2O_2 at 100 grams sample was rated “good” in overall appearance, it received only a “fair” rating in pattern quality. This may indicate that lower fiber quantities result in less defined structural formation during the sheet-forming process, which could affect uniformity in pore distribution and potentially reduce filtration performance. As such, optimization of fiber concentration is not only crucial for mechanical integrity but also for ensuring consistent pattern and pore structure.



(A) Pineapple fiber leaves (B) Bamboo fiber leaves

Figure 2 The surface characteristic of air filters fabricated from 300 g of (A) Pineapple and (B) Bamboo leaves at a function of binder concentration of (a) 5%, (b) 10%, (c) 15% and (d) 20%.

In the production of air filter sheets using the PN method with a binder ratio of 5% relative to varying amounts of fiber, it was observed that the fibers exhibited a continuous, elongated, and rounded morphology without fragmentation, forming overlapping clusters with the binder distributed between the fibers. Similarly, in the production of air filter sheets using the PN+H_2O_2 method, the fibers maintained a continuous, elongated, and rounded morphology without breakage, but the fibers appeared to be more densely packed compared to the PN method. Furthermore, when comparing samples with equal amounts of fiber but different binder ratios, it was found that the fibers consistently formed overlapping clusters, maintaining a continuous and rounded structure, with the binder present between the fibers [2].

Scanning electron microscopy (SEM) technique is frequently employed to study surface morphology of fibers as see in Figure 3-5. Figure 3 presents the morphology of air filter sheets fabricated with 300 grams of fiber at magnification of 500x. Both fiber types exhibited continuous, elongated, and rounded structures without signs of fragmentation, forming overlapping clusters with the binder distributed throughout the fiber network [9,11]. Notably, the BN fibers appeared more densely packed compared to those produced using the PN method.

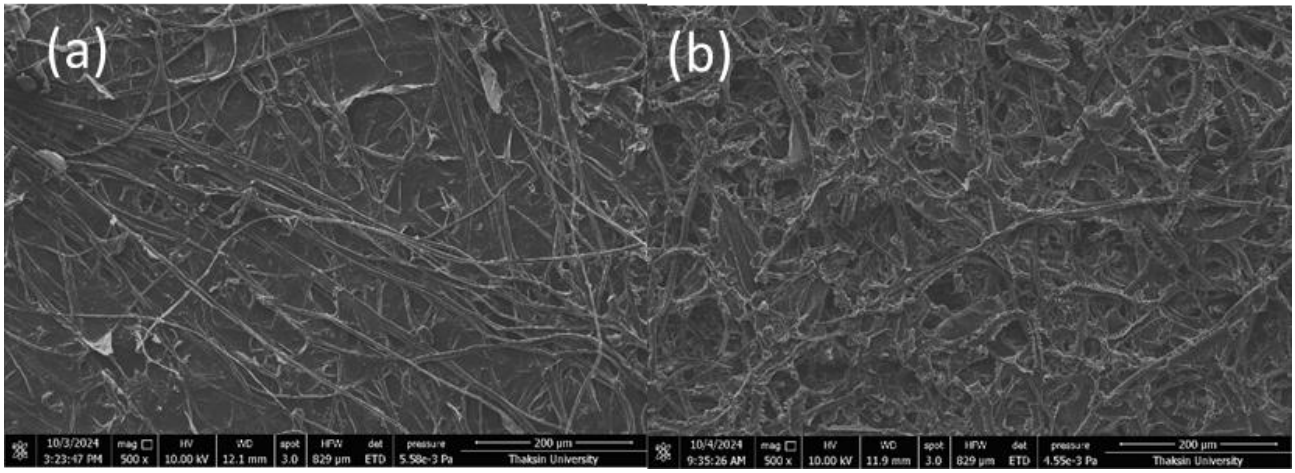


Figure 3 SEM image of the surface of air filter sheets fabricated from 300 g at magnification of 500x of (a) Pineapple fiber and (b) Bamboo fiber

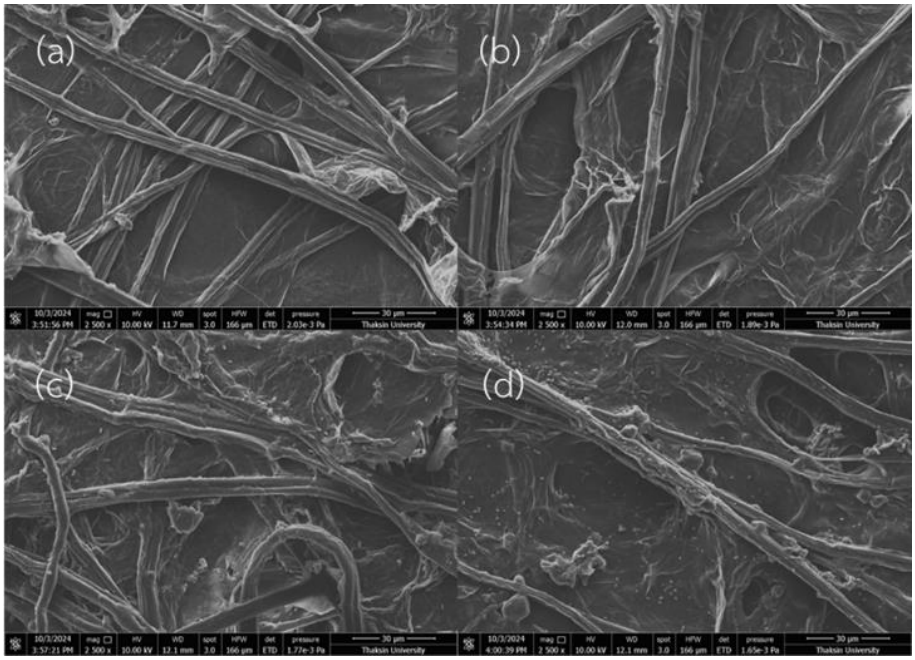


Figure 4 SEM image of the surface of Pineapple air filter sheets fabricated from 300 g at a function of binder concentration of (a) 5%, (b) 10%, (c) 15% and (d) 20%

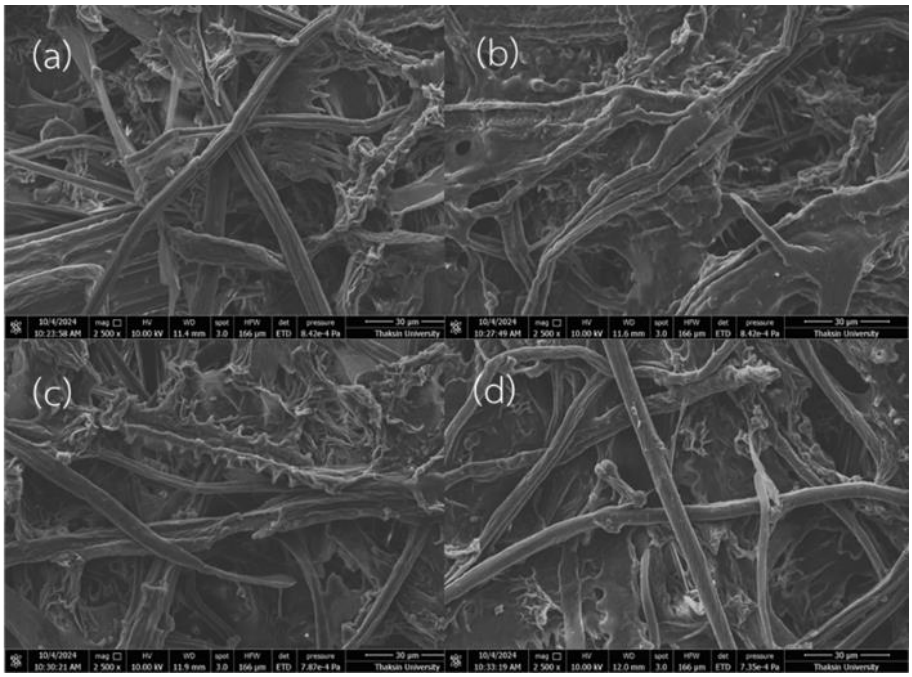


Figure 5 SEM image of the surface of bamboo air filter sheets fabricated from 300 g at a function of binder concentration of (a) 5%, (b) 10%, (c) 15% and (d) 20%

Pineapple leaf fibers exhibited a long and slender morphology as seen in Fig.4. Particularly, the fiber morphology remained consistent irrespective of the extraction method. At a magnification of 2,500× (Fig. 4), the surface texture was distinctly visible, revealing a rough and irregular structure composed of densely packed fibrils compare to those in Fig.5.

Figures 6 and 7 demonstrate the water absorption and moisture content of air filter sheets fabricated using the PN (pineapple leaf fiber) and BN (bamboo leaf fiber) methods with varying fiber quantities (100, 200, and 300 grams) and binder concentrations (5% to 20%). The results demonstrate a consistent decreasing trend in both water absorption and moisture content as binder concentration increased. Regarding air filter sheets produced using the PN method, initial water absorption levels at a 5% binder ratio were approximately 66.97%, 66.85%, and 62.40% for fiber weights of 100, 200, and 300 grams, respectively. As the binder ratio increased to 20%, water absorption correspondingly declined to 62.40%, 56.23%, and 44.75%. This reduction can be attributed to the increased binder coating the fiber surfaces, thereby decreasing the material's capacity to retain water. The denser fiber-binder matrix likely restricted the availability of hydrophilic sites on the fibers and minimized capillary action. This trend was similarly observed in sheets prepared with the BN method, although the overall water absorption levels were slightly higher than those of the PN samples across all binder ratios and fiber quantities.

The superior performance of PN filter sheets in terms of lower moisture retention can be explained by the intrinsic properties of pineapple leaf fibers. These fibers are less hygroscopic and possess a denser microstructure compared to bamboo fibers, which tend to exhibit higher porosity and greater moisture affinity [2, 5, 8, 10]. This characteristic is crucial in air filtration applications, where excessive moisture can not only impair filtration efficiency but also facilitate microbial growth.

The lowest water absorption and moisture content were observed in the PN300/20% sample, suggesting that this formulation is optimal for minimizing water retention. This is particularly beneficial for filter durability and performance, as high moisture content can reduce airflow, promote clogging, and degrade filter materials over time.

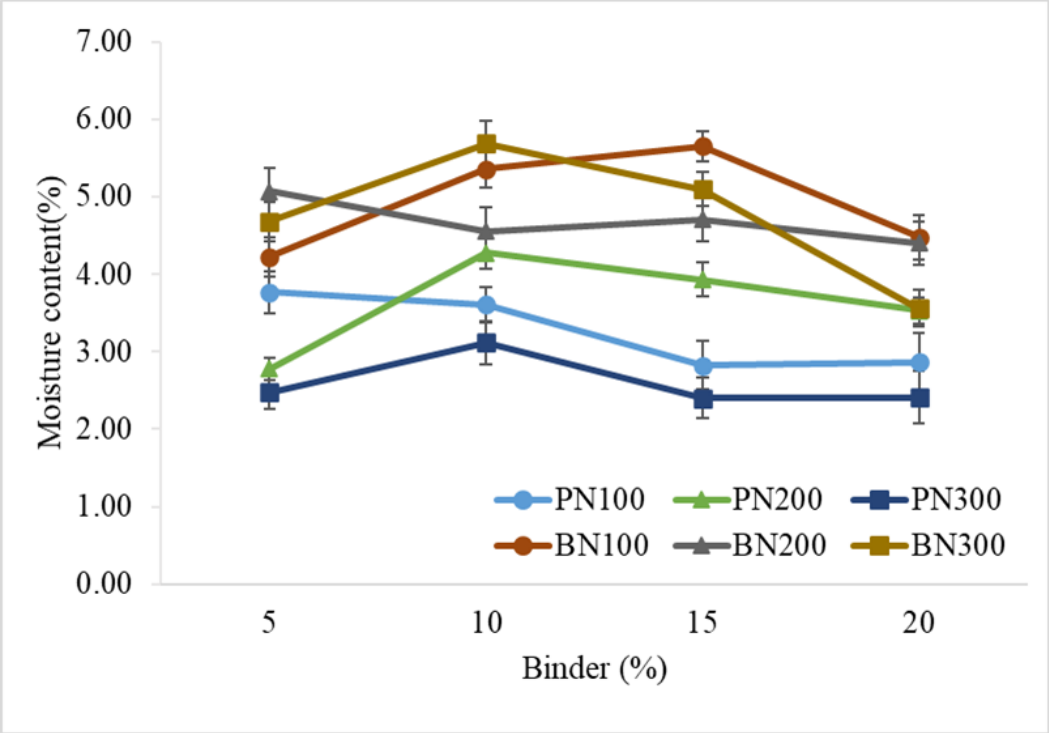


Figure 6 The water absorption of PN and BN air filter as a function binder concentration.

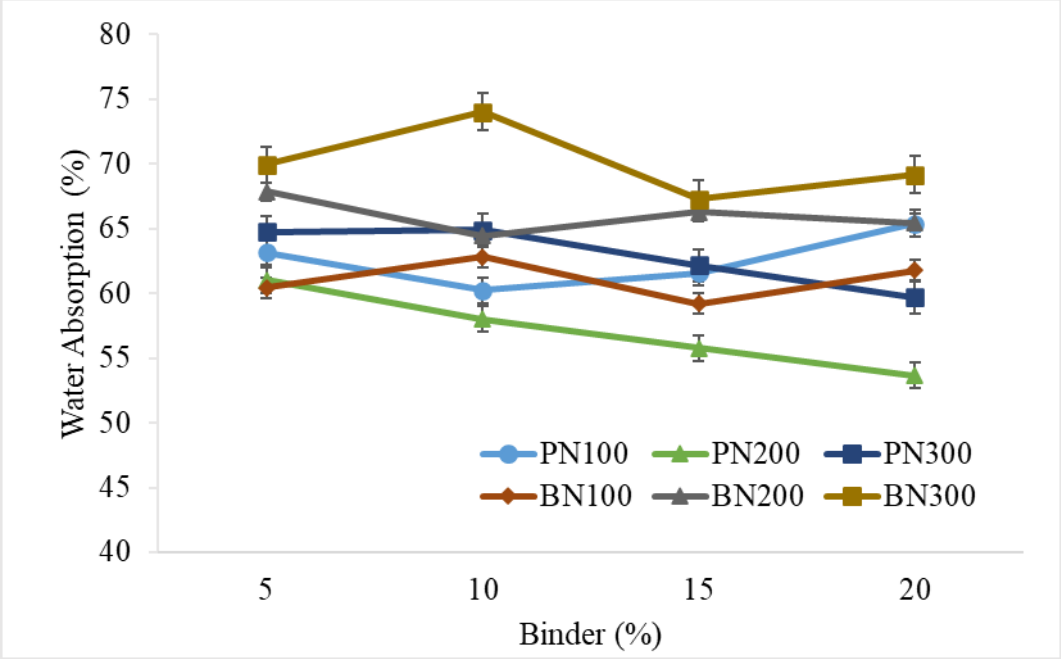


Figure 7 The moisture content of air filter sheets from PN and BN as a function binder concentration.

The particulate matter (PM) removal efficiency of air filters fabricated using the PN300 and BN300 formulations with a 20% binder concentration was evaluated under controlled laboratory conditions. The result showed in fig.8. It can be seen that the PN300 sample exhibited a removal efficiency in the range of ca. 60% - 70% as a function of binder, significantly higher than the 50% observed for the BN300 sample. This performance difference may be attributed to the microstructural properties of the filters. SEM analysis revealed that while both fiber types formed overlapping fiber networks, the BN300 filters were more densely packed with reduced porosity, which may hinder airflow and reduce effective dust entrapment.

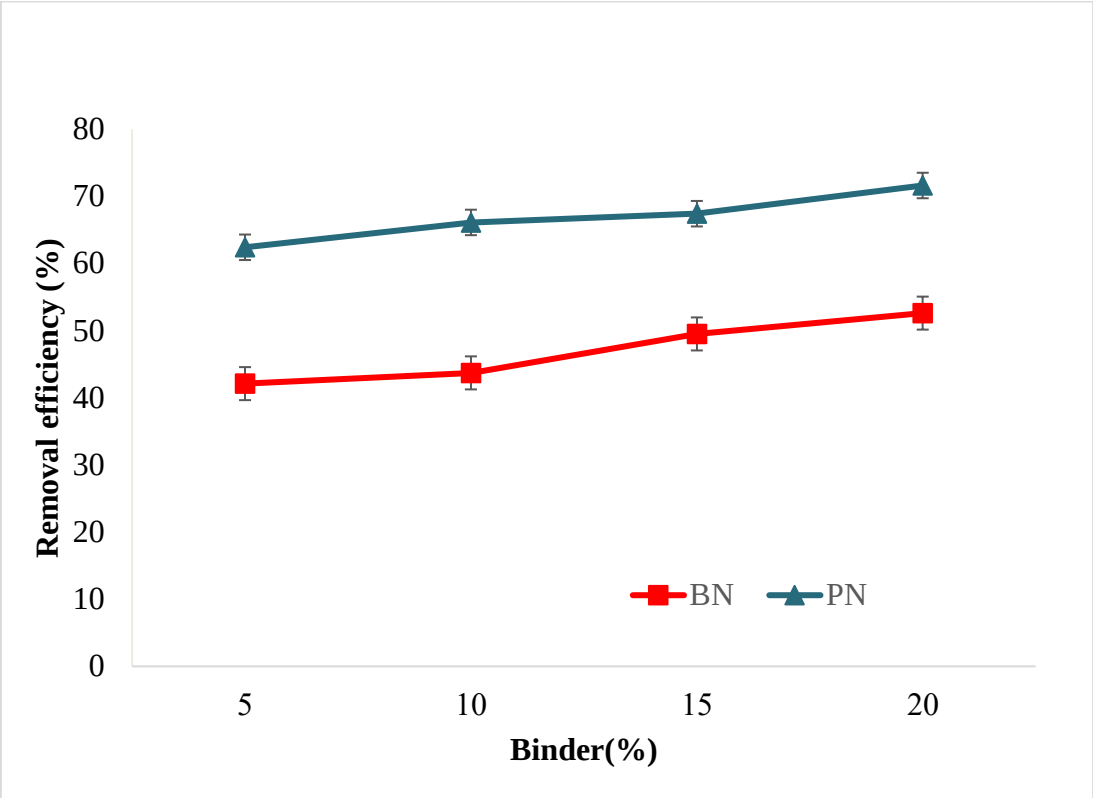


Figure 8 The particulate matter removal efficiency of air filters fabricated using Pineapple fiber and Bamboo fiber

With respect to practical performance, both PN300 and BN300 filters were subjected to real environmental conditions at a controlled temperature of 25°C over a five-day period. Post-exposure evaluations revealed an increase in moisture content relative to the initial state. Additionally, microbial growth was observed on the surface of both filters, particularly in the form of small black spots, indicative of fungal colonization. This outcome underscores the importance of addressing moisture accumulation and microbial resistance in biodegradable filter materials.

These findings highlight the potential of pineapple leaf fiber as a promising candidate for sustainable air filter production, particularly when paired with optimized binder concentrations. However, improvements in moisture resistance and the incorporation of antimicrobial agents are recommended for enhancing long-term performance under ambient environmental conditions.

CONCLUSION

Air filters produced from pineapple leaf fibers and bamboo fibers demonstrated favorable surface characteristics, including smoothness, uniform coloration, and structurally intact fibers without evidence of tearing. Morphological observations confirmed that the fibers were longitudinally aligned, densely packed, and exhibited high durability. Physical evaluations indicated that pineapple leaf fibers possessed lower water absorption and moisture retention compared to bamboo fibers, contributing to their superior dust removal efficiency (70%) relative to bamboo fiber filters (50%). However, during practical application over an extended period, issues such as increased moisture accumulation and microbial growth were observed. These findings suggest that while pineapple leaf fiber is a promising material for air filtration, further development is needed to enhance moisture resistance and antimicrobial properties for prolonged use.

ACKNOWLEDGEMENT

This study was supported by the Institute of Research and Innovation, Thaksin University: Pre-TSU Move for Industry.

REFERENCE

[1] Chirdsiri Ninpai, Kanpitcha Kiatkitroj, Suwannee Jharmchuree.2016. The Study of Indoor Air Quality Affect on The Sick Building Syndrome of Photocopier Operators. Princess of Naradhiwas University Journal, 9(3), 106–120.

[2] Suthanai Leelaaudom and Supaporn Noila. 2021. Development of an inner filter product of an air purifier made of bamboo fibers mixed with essential oils from Boesenbergia thorelii (Gagnep.) Loes. (Kaempfer) for effective PM 2.5 removal and microorganism inhibition, retrieved https://sci.rmutp.ac.th/web2558/.pdf

[3] M. Prasomwong, W. Ho, T. Boonchua, J. Kongcharoen, and N. Onmek, 2018. Indoor air quality in hotel buildings & sickbuilding syndrome of hotel staff, Surat Tani Province, Journal of Science & Technology, Ubon Ratchathani University, vol. 20, no. 3, pp. 64–73.

[4] Noel Lalhruaitluangi, Debashis Mandal. 2024. Utilization of pineapple leaf: an alternative for paper and textile industries. Journal of Postharvest Technology, 12 (3): 1-10.

[5] Kushwaha, A., Chaudhary, K. & Prakash, C. 2024. A study on the mechanical properties of pineapple, bamboo, and cotton woven fabrics. Biomass Conv. Bioref. 14, 16307–16318.

[6] Weera Chotithammaporn. 2023. Producing Craft Papers from Fibers of Pineapple leaves, Rice Straws and Banana Leaf Sheaths. Advanced Science Journal, Vol. 23 No. 1, R1-R12

[7] Suryani, T Rihayat, Nurhanifa, J P Siregar, J Jaafar, T Cionita and Fitria. 2020. Green composites of natural fiber bamboo/pineapple leaf/coconut husk as hybrid materials.IOP Conf. Ser.: Mater. Sci. Eng. **788** 012038

[8] Cesarino, I., Carnietto, M.B., Bronzato, G.R.F., Leao, A.L. (2020). Fabrication of Pineapple Leaf Fibers Reinforced Composites. In: Jawaid, M., Asim, M., Tahir, P., Nasir, M. (eds) Pineapple Leaf Fibers. Green Energy and Technology. Springer, Singapore pp. 265-277.

[9] Supanicha Srivorradatpaisan, Kriangsak Khiaomang, Sakorn Chonsakorn. 2022. The Study of Physical Properties and Fabric Properties from Filagen Fibers Mixed Pineapple Leafs Fibers using Natural Indigo Dyed. Swujournal,14(27), 156–164

[10] Charnont Moonwan, Ganwarich Pluphrach. 2015. Product Development from Palf Refinforced Composites: Literature Review. Kasem Bundit Engineering Journal,5(1), 65-78

[11] De Queiroz, R.S., da Silva, A.P.V., Broega, A.C.L. et al. 2020. New Brazilian pineapple leaf fibers for textile application: cottonization and dyeing performance. SN Appl. Sci. 2, 72.

[12] Syifa Hanifah, & Giarto. (2019). A Study of Making Nonwoven Fabric as an Air Filter Based on Pineapple Leaf Fiber by Thermal Bonding Method. Proceeding Indonesian Textile Conference (ITC), Indonesia. https://doi.org/10.5281/zenodo.3470775

[13] Poemyot Wongbua-Ngam, Kamonchanok YuenYao, Watcharawut Nuandee et.al. 2023. Effects of the Quantity of Sodium Hydroxide on Properties of Water Hyacinth Paper. KOCH CHA SARN JOURNAL OF SCIENCE Vol. 45 (1), pp. 30-35.

.

Long-Term Analysis of PM2.5 Concentrations and Seasonal Variation in Bangkok and Chiang Mai, Thailand: Impacts of COVID-19 Lockdowns and Fire Control Measures

Vineeth Vijayan[1] Supandee Maneelok[2] and Nantaporn Noosai[3*]

[1]Lecturer, Department of Mechanical and Mechatronics Engineering, Faculty of Engineering, Prince of Songkla University, Hat Yai, Songkhla, 90110, Thailand;
[2] Lecturer, Department of Occupational Health and Safety, Faculty of Health and Sports Science, Thaksin University, Phatthalung 93210, Thailand
*[3]*Lecturer, Department of Civil and Environmental Engineering, Faculty of Engineering, Prince of Songkla University, Hat Yai, Songkhla 90110, Thailand*
[3]

[*]Phone : (+66) 74-287115, Fax : (+66) 74-287012., E-mail : nantaporn.no@psu.ac.th

ABSTRACT

PM2.5 pollution remains a major environmental and health concern in Thailand, particularly in urban centers and biomass-burning regions. This study presents a 10-year analysis (2015–2024) of PM2.5 data from Bangkok (station 59T) and Chiang Mai (station 36T), using datasets from the Pollution Control Department (PCD)[1]. Results show distinct regional patterns: Bangkok exhibits dry-season peaks linked to traffic and industrial emissions [2,3], while Chiang Mai experiences sharp PM2.5 surges during January–April, coinciding with biomass burning [4,5]. A significant decline in PM2.5 was observed in Bangkok during the first COVID-19 lockdown (March–May 2020), indicating strong anthropogenic influence [6,7]. In Chiang Mai, the 2022 introduction of fire control regulations and the FireD system led to a temporary reduction in PM2.5 [8], though levels rebounded in subsequent years [9]. These findings highlight the effectiveness and limitations of policy interventions, underscoring the need for sustained, region-specific strategies for PM2.5 mitigation.

Keywords : PM2.5; COVID-19; Chiang Mai; Bangkok; biomass burning; lockdown effects

INTRODUCTION

PM2.5 is recognized as one of the most harmful air pollutants due to its ability to penetrate deep into the respiratory system, causing various health problems [2]. In Thailand, PM2.5 levels often exceed both national and international standards, especially during dry seasons [1].

This study focuses on Bangkok and Chiang Mai due to their distinct pollution characteristics. Bangkok, a highly urbanized metropolis, faces pollution primarily from traffic, industry, construction and other anthropogenic activities [3,4]. Chiang Mai, situated in northern Thailand, suffers from seasonal haze events caused by open biomass burning [5]. Although several air quality monitoring stations exist in both regions, stations ID 59T (Bangkok) and 36T (Chiang Mai) were selected for their long-term data availability and representativeness.

The study aims to examine PM2.5 trends over a 10-year period and evaluate the influence of major policy interventions: (1) COVID-19 lockdowns (Wave 1 to Wave 4) in Bangkok [6, 7]and (2) the FireD burning control system introduced in Chiang Mai in 2022 [8, 9].

METHODOLOGY

Daily PM2.5 data (2015–2024) were sourced from the Pollution Control Department (PCD) [1]. Two following PM2.5 monitoring stations were selected for this study [1]:

- Stations ID 59T
    - Latitude: 13.783185
    - Longitude: 100.540489
    - Station name: The Government Public Relations Department
    - Sub district: Phaya Thai
    - District: Khet Phaya Thai,

  - Province: Bangkok
- Station ID 36T
  - Latitude: 18.7909333
  - Longitude: 98.99
  - Station name: Yupparaj Wittayalai School
  - Sub district: Si Phum
  - District: Meuang
  - Province: Chiang Mai

Key analytical steps:

- Aggregation of daily data to compute monthly and annual averages.
- Comparison of 24-hour averages to Thailand's 24-hour standard (37.5 µg/m³) and annual standard (15 µg/m³) [1].
- Identification and comparison of COVID-19 lockdown phases:
  - Wave 1: Mar 22 – May 31, 2020 (strictest)
  - Wave 2: Dec 21, 2020 – Jan 31, 2021
  - Wave 3: Apr 1 – May 31, 2021
  - Wave 4: Jan 1 – Mar 31, 2022
- Assessment of fire control enforcement in Chiang Mai (Jan 1 – Apr 30, 2022 onwards) [2]

Data preprocessing involved cleaning, merging, and aggregating 24-hour averages. Seasonal and annual trends were computed using Python. The lockdown periods in Bangkok and fire control regulation periods in Chiang Mai were analyzed in relation to the PM2.5 data. These were compared to prior periods to estimate policy effects.

This study references prior analyses of seasonal and regional air quality in Thailand, including Sherin et al. [3], Inlaung et al. [5], Amnuaylojaroen et al. [10], and Thongboonchoo et al. [11], who conducted spatiotemporal PM2.5 modeling using WRF-Chem.

RESULTS AND DISCUSSIONS

Seasonal Patterns and Yearly Trends

Figures 1 presents the 24-hour average PM2.5 values for 59T station in Bangkok. Bangkok's PM2.5 levels are elevated between November and April, corresponding with the dry season and higher urban activity. From May to October (rainy season), values decrease.

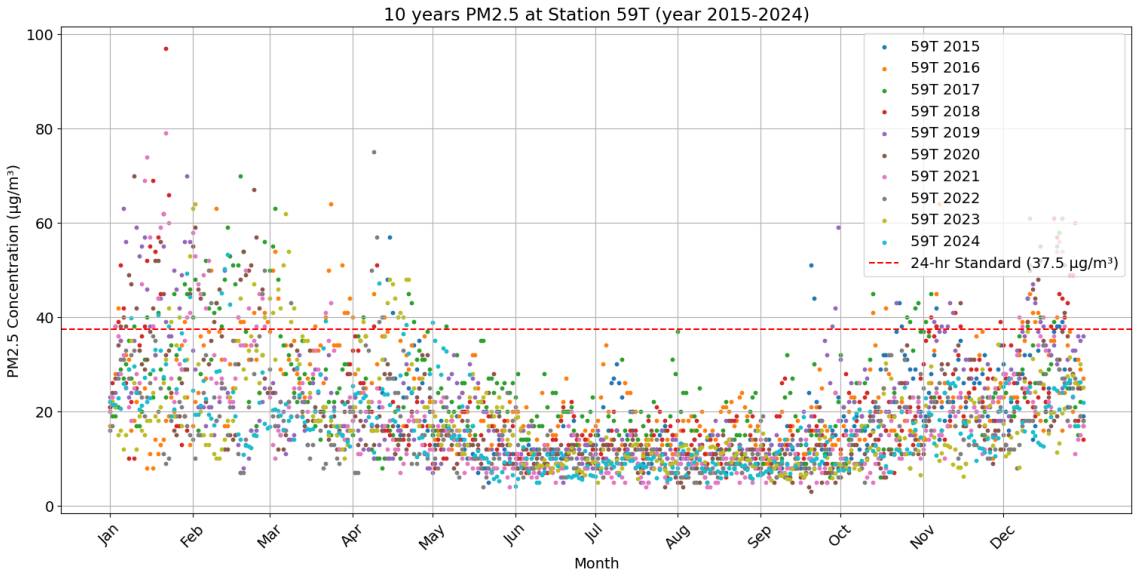


Figure 1 24-hour average PM2.5 concentration at station 59T (2015-2024)

Although Bangkok exhibits a clear seasonal trend of lower PM2.5 concentrations during the wet season (May–October) due to enhanced atmospheric cleansing from rainfall, the data during the dry season (November–April) presents a notably wider distribution of PM2.5 values without a consistent or predictable daily pattern. This intra-seasonal variability, especially evident in January through March, can be attributed to the interplay of multiple uncontrolled and episodic emission sources.

Several factors likely contribute to this phenomenon:

- Variable Emission Intensity: Daily fluctuations in traffic volume, industrial activity, and localized construction work lead to irregular emissions.
- Meteorological Influences: During the dry season, weak wind speeds, frequent temperature inversions, and stable atmospheric conditions may trap pollutants near the surface on some days, while on other days, better dispersion conditions may prevail.
- Regional Transport: Bangkok is also affected by transboundary or upwind pollution, especially during episodes of haze from neighboring regions or provinces.
- Lack of Point-Source Dominance: Unlike biomass burning events in Chiang Mai which occur in defined periods, Bangkok's emissions are more diffuse and continuous, creating a broader variability in the observed concentrations.

In summary, the lack of a clear pattern in the dry season suggests that while seasonal averages are helpful, they may obscure significant short-term air quality episodes. This underlines the need for both real-time monitoring and episodic control measures in addition to seasonal policy planning.

Figure 2 present the 24-hour average PM2.5 values for 36T station in Chiang Mai exhibits strong seasonal PM2.5 spikes from January to April, attributed to biomass burning. The data highlights a consistent pattern of haze during these months, underscoring the need for fire management.

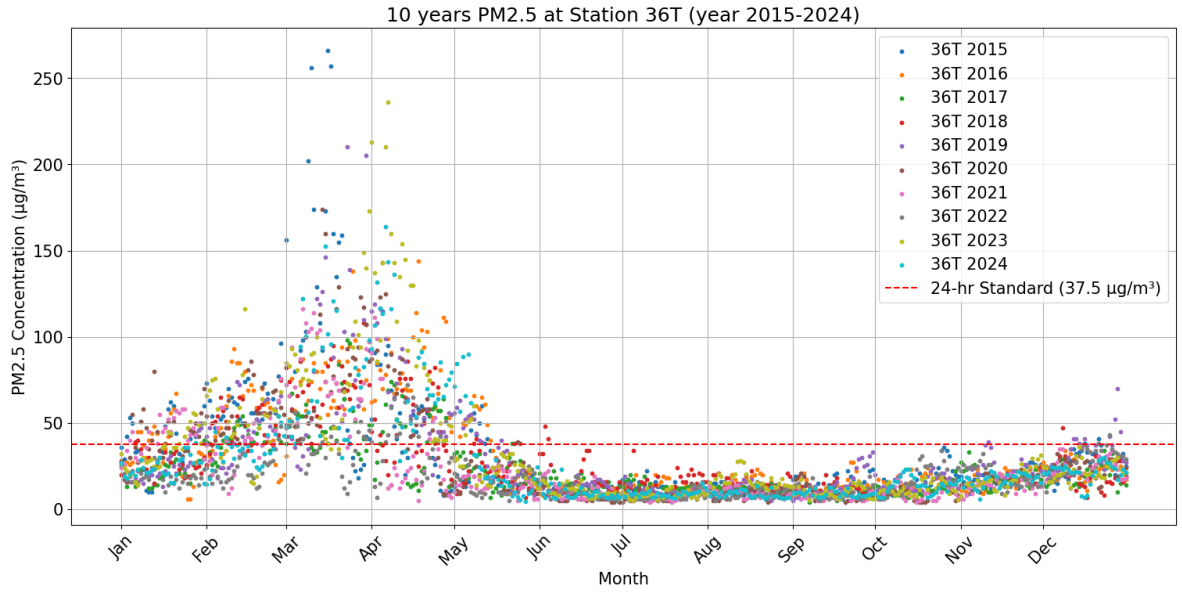


Figure 2 24-hour average PM2.5 concentration at Station 36T (2015–2024).

Based on the graph for Chiang Mai (Station 36T, 2015–2024), we can clearly observe a pronounced seasonal trend in PM2.5 concentrations:

- Peak concentrations are observed consistently between January and April, with multiple years showing spikes exceeding 100–250 µg/m³, far above the 24-hour standard (37.5 µg/m³).

- From May onward, there's a sharp drop, and PM2.5 remains relatively low and stable through October, before slightly rising in November–December.
- This consistent pattern strongly suggests that biomass burning is the dominant PM2.5 source during the dry season in Chiang Mai. Unlike Bangkok—where urban emissions stem from a complex mix of traffic, construction, and industrial activities—Chiang Mai's pollution source is highly seasonal and linked to rural land use and fire activities.
- The drastic contrast between high and low periods further confirms:
    - Biomass burning is the primary cause of elevated PM2.5 in northern Thailand.
    - Air quality improvement in the wet season isn't gradual but it's abrupt, correlating with the end of burning season and onset of rain.

Sherin et al. (2024) [3], Inlaung et al. (2024) [5], Bhattacharjee et al. (2023) [4], and Thongboonchoo et al. (2020) [11], which found that Chiang Mai's PM2.5 is heavily influenced by agricultural fires and transboundary haze.

COVID-19 Lockdown Effects in Bangkok

To assess the impact of pandemic-related restrictions on air quality, Figure 3 compares daily PM2.5 concentrations at station 59T during the strictest COVID-19 Wave 1 lockdown period (March 22–May 31, 2020) against the same period in 2017, a year selected to represent typical pre-COVID conditions with no influence from pandemic-related interventions.

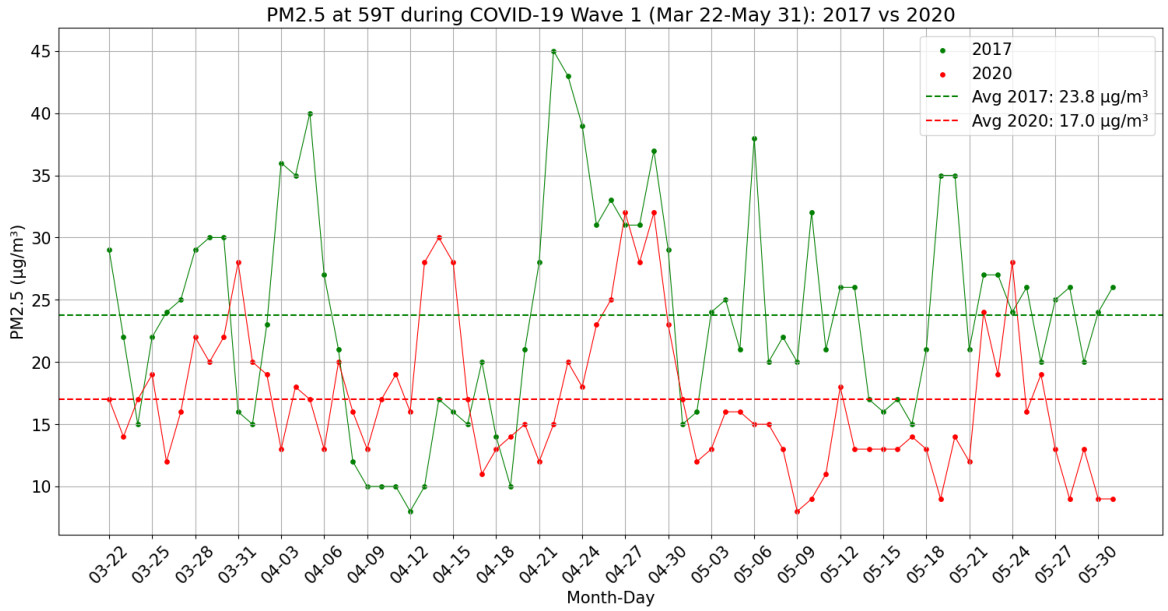


Figure 3 24-hour average PM2.5 concentration at station 59T during COVID19 Wave 1 (Mar 22 – May 31, 2020) compared with the same period of 2017 (no effect of COVID19).

The average PM2.5 concentration during this lockdown window in 2017 was 23.8 µg/m³, whereas in 2020, it dropped to 17.0 µg/m³, marking a 28.6% reduction. This decrease is significant and aligns with the timing of strict mobility restrictions and closures of schools, businesses, and construction sites. The drop in PM2.5 levels reflects a sharp decline in anthropogenic sources, particularly: vehicular emissions (from drastically reduced traffic), construction dust, Industrial activity, and other urban combustion sources. The comparison of PM2.5 levels in Bangkok during the COVID-19 Wave 1 lockdown (2020) and pre-COVID (2017) reflects similar findings in regional studies [6][7].

Although reductions in PM2.5 were most noticeable during this early lockdown, subsequent years (2021–2024) did not show continued declines but rather a stabilization at levels slightly above 2020. This suggests

that while COVID-19 restrictions highlighted the strong influence of urban human activity on PM2.5 in Bangkok [, longer-term reductions likely require structural interventions, such as: adoption of cleaner transportation technologies (e.g., EVs), stricter emission regulations, promotion of green public transit, urban zoning and pollution control policies.

This comparison confirms that PM2.5 levels in Bangkok are strongly driven by anthropogenic factors, and that targeted policy action can yield measurable improvements in air quality.

Fire Control Measures in Chiang Mai

To evaluate the effectiveness of fire control interventions in northern Thailand, Figure 4 illustrates the PM2.5 concentrations at station 36T in Chiang Mai during the fire control enforcement period (January 1 to April 30) in both 2019 and 2022. The year 2019 was selected as a representative baseline, when no fire control policy was actively implemented, while 2022 marks the official rollout of burning control regulations and the FireD system for open biomass burning registration and enforcement.

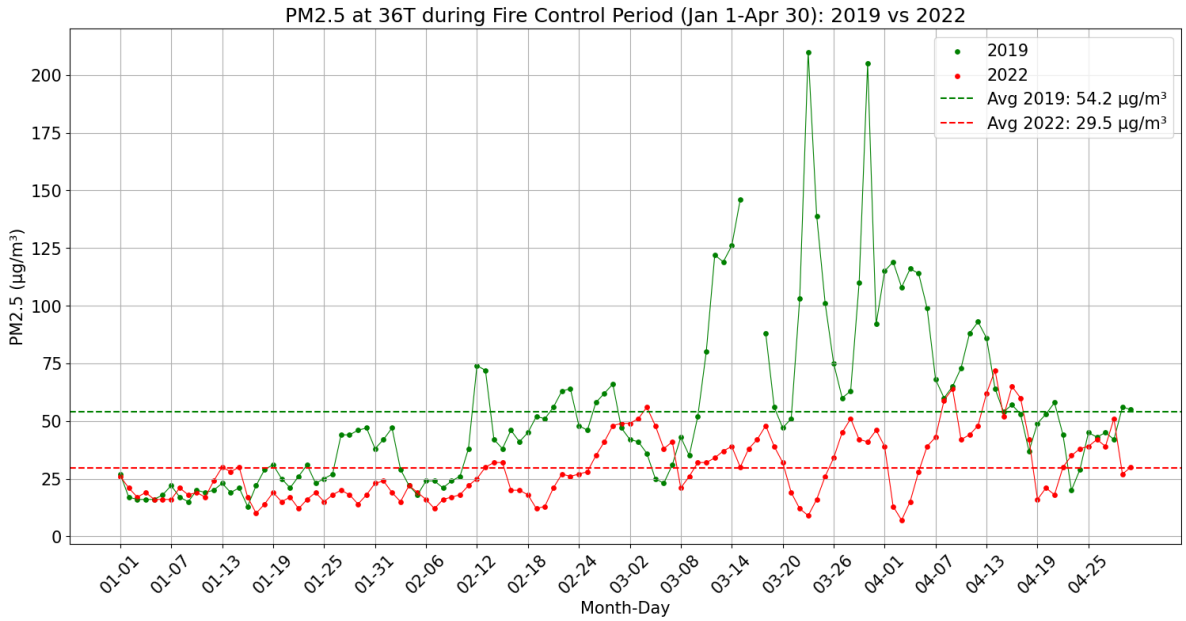


Figure 4 24-hour average PM2.5 concentration at station 36T during the fire-controlled enforcements were initially introduced (Jan 1 – April 30, 2022) compared with the same period of 2019 (no effect of the regulation).

During this 4-month period, the average PM2.5 in 2019 was 54.2 µg/m³, whereas it dropped significantly to 29.5 µg/m³ in 2022, a reduction of nearly 45%. This dramatic improvement clearly highlights the short-term effectiveness of the fire control policies in suppressing emissions from agricultural and forest biomass burning. The sharp decline in peak values and daily fluctuations also demonstrates a successful reduction in the intensity and frequency of fire-related pollution events.

However, while 2022 shows promising reductions, the annual average data presented in next Section (Yearly and Monthly Average Analysis) indicate that this improvement was not sustained in the following year (2023). PM2.5 levels in 2023 (32.8 µg/m³) rebounded above even the pre-policy year 2019 (30.3 µg/m³). This suggests that despite the initial enforcement, challenges such as enforcement fatigue, unregistered burning, or transboundary smoke transport may have limited the long-term success of the FireD system.

In conclusion, while the fire control policy showed clear positive outcomes in its initial phase, consistent enforcement and broader regional collaboration will be critical for achieving sustained air quality improvements in Chiang Mai and surrounding northern provinces.

Yearly and Monthly Average Analysis

Table 1 summarizes annual PM2.5 averages. Both sites frequently exceeded the Thai standard (15 µg/m³ post-2021). Chiang Mai surpassed Bangkok in most years, indicating biomass burning's severe impact.

Table 1 Annual average of PM2.5 concentrations at Station 59T, 36T and annual standard (µg/m³)

Year	Bangkok (59T)	Chiang Mai (36T)	Thai Standard
2015	18.4	32.6	25
2016	23.1	31.9	25
2017	24.9	23.1	25
2018	20.41	29.5	25
2019	20.9	30.3	25
2020	19.1	28.4	25
2021	18.3	24.0	25
2022	16.4	19.3	25/15
2023	18.4	32.8	15
2024	16.4	27.6	15

From Table 1, it is evident that PM2.5 concentrations in both Bangkok (59T) and Chiang Mai (36T) have frequently exceeded the national annual standard set by Thailand (red text), which was 25 µg/m³ prior to 2022 and lowered to 15 µg/m³ starting June 2022.

In Bangkok, all years from 2015 to 2021 recorded annual averages above the new 15 µg/m³ standard. Notably, the concentrations decreased steadily from 24.9 µg/m³ in 2017 to 16.4 µg/m³ by 2024, with a distinct decline after 2020—the first year of the COVID-19 pandemic. While the strict lockdown in Wave 1 (March–May 2020) clearly curtailed emissions from traffic and construction, the continued reduction afterward suggests a combination of other contributing factors. These may include: increased public awareness, the adoption of cleaner technologies (e.g., electric vehicles), stricter urban traffic regulations, and regulatory pressure following the 2022 standard revision. Despite occasional fluctuations (e.g., a slight increase in 2023), the post-2020 trend indicates a relative stabilization of PM2.5 levels below pre-COVID levels, reflecting both behavioral changes and regulatory improvements.

In Chiang Mai, the annual average was well above 25 µg/m³ in most years except 2017 (23.1 µg/m³), and even after the new 15 µg/m³ threshold in 2022, only that year met the standard (19.3 µg/m³). The sharp decline in 2022 can be linked directly to the implementation of fire control measures, including the FireD registration app and enforced bans during the burning season (Jan–Apr). However, PM2.5 levels spiked again in 2023 (32.8 µg/m³) and remained high in 2024 (27.6 µg/m³). This rebound may reflect challenges

such as: limited compliance or enforcement fatigue with fire regulations, increased illegal or cross-border burning, and meteorological variability that hindered dispersion during those years.

The pattern in Chiang Mai underscores the seasonal dominance of biomass burning, as seen in Figure 2. In contrast to Bangkok, where sources are more diffuse and influenced by human activity across seasons, Chiang Mai's PM2.5 peaks are highly concentrated in the dry season. Thus, effective and consistent fire management remains crucial for sustained improvement in air quality in northern Thailand.

CONCLUSION

This decade-long analysis of PM2.5 concentrations at Bangkok (59T) and Chiang Mai (36T) reveals critical insights into regional pollution dynamics and the efficacy of policy interventions.

In Bangkok, PM2.5 concentrations are predominantly driven by anthropogenic sources—vehicular traffic, industrial operations, and construction activities. The city exhibits a seasonal trend with higher PM2.5 levels during the dry season (November–April) and lower levels during the wet season (May–October) due to natural atmospheric cleansing by rainfall. However, within the dry season, no clear daily trend is evident, indicating that emission variability is influenced by multiple episodic sources and meteorological factors. The first wave of COVID-19 lockdown (March–May 2020) resulted in a 28.6% reduction in PM2.5 levels compared to the same period in 2017, confirming the substantial role of human activity in PM2.5 generation. Although concentrations rose slightly afterward, they remained below pre-pandemic levels, suggesting the ongoing influence of complementary policies such as vehicle emission standards and the expansion of electric vehicle (EV) infrastructure.

In Chiang Mai, the pollution profile is strikingly different. The PM2.5 trend is highly seasonal, with dramatic spikes during the burning season (January–April), clearly attributed to agricultural and forest biomass burning. This pattern is consistent across years, reinforcing the role of open burning as the dominant emission source. The fire control measures introduced in 2022, including burning bans and the FireD registration system, significantly reduced average PM2.5 levels by 45% during the enforcement period compared to 2019. However, this success was not sustained; PM2.5 rebounded in 2023 and 2024, surpassing pre-policy levels. This suggests enforcement challenges, non-compliance, and possibly transboundary smoke transport undermining local efforts.

From 2015 to 2021, both cities frequently exceeded the Thai annual standard of 25 µg/m³. After the standard was revised to 15 µg/m³ in June 2022, both cities continued to exceed the threshold in subsequent years, except for Chiang Mai in 2022. Bangkok showed a gradual and consistent reduction post-2020, while Chiang Mai's reduction was short-lived, emphasizing the need for continuous enforcement and broader collaboration across regions.

In summary, Bangkok's PM2.5 concentrations are influenced by diffuse, year-round anthropogenic emissions with seasonal modulation, whereas Chiang Mai faces a concentrated pollution crisis driven by biomass burning during the dry season. Both cases highlight the importance of sustained, region-specific interventions: emissions regulation and clean transport in urban centers like Bangkok, and fire control enforcement and rural land management in biomass-affected areas like Chiang Mai. Future policies must also consider enforcement sustainability, cross-border coordination, and integration of real-time monitoring to ensure long-term air quality improvements in Thailand.

REFERENCE (Please see format of the reference in the Manuscript Format and Style)

[1] Pollution Control Department (PCD). 2024. Thailand Air Quality Monitoring Report 2015–2024. www. https://www.pcd.go.th/

[2] World Health Organization (WHO). 2021. Global Air Quality Guidelines.

[3] Sherin H. B., et al. 2024. Understanding the seasonal dynamics of surface PM2.5 mass distribution and source contributions over Thailand. Atmospheric Environment, 331, 2024.120613 https://doi.org/10.1016/j.atmosenv.2024.120613

[4] Bhattacharjee, U., et al. 2023. Temporal trends and source apportionment of PM2.5 in Southeast Asia: A multi-city comparative analysis. Science of the Total Environment, 891, 164631. https://doi.org/10.1016/j.scitotenv.2023.164631

[5] Inlaung, K., et al. 2024. Assessment of Transboundary PM2.5 from Biomass Burning in Northern Thailand Using the WRF-Chem Model. Toxics. 12(7): 462.. https://doi.org/10.3390/toxics12070462

[6] Sahu, L. K., et al. 2020. Impacts of lockdown due to COVID-19 on air quality and PM2.5 chemical composition over urban sites in Thailand. Environmental Research, 191, 110190. https://doi.org/10.1016/j.envres.2020.110190

[7] Wang, P., et al. 2022. Air quality improvement and PM2.5 reduction during COVID-19 lockdown in Asia: Evidence from ground and satellite observations. *Environmental Pollution*, 302, 119043. https://doi.org/10.1016/j.envpol.2022.119043

[8] Chiang Mai University. 2021. FireD Application for Controlled Burning Registration.

[9] Pornsri, S., et al. 2023. Effectiveness of fire bans on reducing PM2.5 levels in Northern Thailand: A case study of Chiang Mai. *Atmospheric Pollution Research*, 14(5), 101621. https://doi.org/10.1016/j.apr.2023.101621

[10] Amnuaylojaroen, T., et al. 2021. Climatological analysis of PM2.5 across Thailand and its link to meteorological drivers. *Air Quality, Atmosphere & Health*, 14, 345–359. https://doi.org/10.1007/s11869-021-00992-w

[11] Thongboonchoo, N., et al. 2020. Spatiotemporal distribution and long-range transport of PM2.5 in Thailand: A modeling study using WRF-Chem. *Atmospheric Environment*, 229, 117464. https://doi.org/10.1016/j.atmosenv.2020.117464

21R4-03

Genotypic and Phenotypic Characterization of ESBL-Producing *E. coli* from Livestock Waster and Manure

Phub Zam [1], Thitima Srathongneam [2], Phongsawat Paisantham [2], Montakarn Sresung [2], Supitchaya Theplhar [2], Nisanart Charoenlap [2,3], Paiboon Vattanaviboon [1,2,3], Skorn Mongkolsuk [2,3], Kwanrawee Sirikanchana [2,3,*]

[1]Graduate Student;[2,3,]Senior Research Scientist II* (*Assoc. Prof. level*), *[1]Program in Applied Biological Sciences-Environmental Health, Chulabhorn Graduate Institute, Bangkok 10210, Thailand;[2,3,*] Research Laboratory of Biotechnology, Chulabhorn Research Institute, Bangkok, Thailand*
[1]Phone : 0630327578; E-mail: phub@cgi.ac.th; [2,3,]Phone: 08-0611-0555, Fax : 0-2553-8572, E-mail : kwanrawee@cri.or.th*

ABSTRACT

Antimicrobial resistance (AMR) is an raising global health crisis, with over use and misuse of antibiotics not only by humans but also seen in agricultural settings (1). This study aimed to characterize Extended-Spectrum Beta-Lactamase (ESBL)-producing *Escherichia coli* (*E. coli*) isolated from livestock wastewater and manure, using both genotypic and phenotypic approaches to assess prevalence and resistance profiles in various livestock farms. A total of 102 isolates were collected from fecal and wastewater samples across 35 animal farms, including pigs, cows, chickens, ducks, and goats in Thailand. Presumptive ESBL-producing *E. coli* were selected on MacConkey agar supplemented with cefotaxime (4 µg/mL) and confirmed using conventional PCR with *E. coli* specific primers.

Molecular screening identified 86 isolates (84%) as ESBL-producing *E. coli*. Among these, 73 isolates harbored $bla_{CTX\text{-}M}$ group 1 genes, 13 showed positive for $bla_{CTX\text{-}M}$ group 9, 1 isolate harbored $bla_{CTX\text{-}M}$ group 8 and 1 isolate showed positive for $bla_{OXA\text{-}1}$ respectively. Furthermore, five isolates from pig influent samples tested positive for colistin resistance genes (*mcr-1*, *mcr-2*, and *mcr-3*), while no $bla_{NDM\text{-}1}$, bla_{VIM}, bla_{IMP}, bla_{KPC}, $bla_{OXA\text{-}48}$ carbapenemase genes were detected. Phenotypic antimicrobial susceptibility testing (AST) by minimum inhibitory concentration (MIC) assessments revealed high resistance rates, particularly among isolates from pig farms, with levels ranging from 4 µg/mL to >8 µg/mL.

This study highlights the importance of integrating genotypic and phenotypic methods to track resistance patterns and supports strong One Health strategies to address AMR across human, animal, and environmental health. Frequent detection of $bla_{CTX\text{-}M}$ and *mcr* genes in pig farm samples underscores the need for targeted monitoring and control. Future research should explore additional resistance mechanisms and assess horizontal gene transfer potential. Strengthening One Health AMR surveillance is essential for limiting resistant bacteria spread in agriculture and for investigating resistance phenotypes lacking known genes, pointing to alternative mechanisms.

Keywords: Antimicrobial resistance; Extended-Spectrum Beta-Lactamase (ESBL)-producing *Escherichia coli* (*E. coli*); Livestock; Resistance gene

INTRODUCTION

Antimicrobial resistance (AMR) has emerged as a significant global health concern, posing severe challenges to the effective treatment of infectious diseases in humans and animals (2). The misuse and overuse of antibiotics in human medicine and livestock production have accelerated the development and dissemination of resistant bacterial strains. Among these, extended-spectrum β-lactamase (ESBL)-producing *Escherichia coli* have captured particular attention due to their ability to hydrolyze a wide range of β-lactam antibiotics, rendering treatments ineffective. The presence of such resistant bacteria in livestock waste is alarming, as it facilitates the spread of resistance genes through environmental pathways (3).

In Thailand, studies have reported a high prevalence of ESBL-producing *E. coli* in dairy farm wastewater. For instance, research conducted in Chiang Mai found that 88.7% of dairy farms were positive for ESBL-producing *E. coli*, with the $bla_{CTX\text{-}M}$ gene present in all isolates. Similarly, in Indonesia's Yogyakarta province, ESBL-producing *E. coli* were identified in 54% of dairy farms, with fecal samples being the most commonly positive. These findings underscore the widespread nature of antimicrobial-resistant bacteria in livestock environments within the region (4, 5).Furthermore, the detection of colistin resistance genes (*mcr* variants) in livestock is particularly concerning, given colistin's role as a last-resort antibiotic. A systematic review reported the presence of *mcr-1* and *mcr-3* genes in *E. coli* isolates from pigs and pork meat in Southeast Asia, indicating the potential for zoonotic transmission. (6).

While these studies highlight the prevalence of AMR in livestock environments, comprehensive studies that integrate both molecular characterization of resistance genes and phenotypic antimicrobial susceptibility testing involving various livestock farms rather than just few farms are still scarce in the region, limiting our understanding of resistance profiles within agricultural settings under the One Health framework. Addressing AMR in livestock waste is not only vital for animal and human health but also aligns with global sustainability efforts. Specifically, it contributes to Sustainable Development Goal (SDG) 3 (Good Health and Well-being) by combating infectious diseases, and SDG 6 (Clean Water and Sanitation) by preventing the contamination of water sources with resistant pathogens (7). Effective management of livestock waste can thus play a pivotal role in achieving these objectives.

This study aims to identify ESBL-producing *E. coli* in various livestock waste samples (influent wastewater, effluent waste water, feces). Detect the presence of key antibiotic resistance genes, including *bla*, *mcr*, and *CTX-M*, associated with resistance to beta-lactams, colistin, and cephalosporin. Assess the antimicrobial susceptibility testing by broth macro dilution. By integrating genotypic and phenotypic analyses from various livestock farms within a One Health framework, this research seeks to provide a comprehensive understanding of AMR dynamics in various livestock waste, thereby informing effective surveillance and intervention strategies.

Methodology

Collection of samples and preparation of isolates

Samples were collected from 35 different animal farms in Ratchaburi Province, Thailand, including 10 pig farms, 10 cow farms, and 5 farms each for chickens, ducks, and goats. Sample comprised of influent wastewater and effluent wastewater and from those farm where there was no availability of wastewater, fecal sample was collected. For liquid samples (both untreated and treated wastewater), 1000 mL was collected from each site. For solid fecal samples, around 1 kilogram was collected per farm. Samples were immediately stored on ice and transported to the laboratory for processing.

Upon reaching the laboratory, the samples were being processed further. The protocol specified in the Global Tricycle Surveillance Guidelines for ESBL-producing *E. coli* (WHO, 2021) was followed (8). wastewater samples were diluted using a 10-fold serial dilution with PBS buffer, while the fecal samples were homogenized (1 gram was combined with 9 mL of PBS buffer), thoroughly mixed, and then subjected to another 10-fold serial dilution with PBS. Next, 100 µL of the appropriate dilution was plated onto MacConkey agar (BD Difco, USA) to enumerate total *E. coli*, and onto MacConkey agar supplemented with

4 µg/mL cefotaxime (Sigma-Aldrich, USA) to isolate ESBL-producing *E. coli*. The plates were incubated at 35±2°C for 16-18 hours. Colonies that exhibited pink or red coloration were counted as total presumptive *E. coli* and ESBL-producing presumptive *E. coli*, respectively. A maximum of five presumptive ESBL-producing *E. coli* colonies were selected from the plates for further analysis. Each selected colony was restreaked on MacConkey agar supplemented with 4 µg/mL cefotaxime and then cultured in tryptic soy broth (TSB) (Merck, Germany) with 2 µg/mL cefotaxime to confirm resistance. One colony from each of the five presumptive *E. coli* colonies was preserved in a 15% glycerol stock and stored at -80°C for subsequent molecular characterization and antimicrobial resistance profiling.

Confirmation of ESBL- producing *E. coli and* determation of antibiotic resistance genes

All stored isolates were subcultured by streaking onto tryptic soy agar (BD Difco, Sparks, MD, USA) and incubated at 37°C for 16-18 hours. A single pure colony was then selected and subcultured in 5 mL tryptic soy broth (TSB) at 37°C for another 16-18 hours. DNA was extracted using the QIAamp Blood Mini DNA Extraction Kit (QIAGEN, Germany) with the addition of ATL buffer. The concentration of the extracted DNA was quantified using a NanoDrop 2000 spectrophotometer (Thermo Fisher Scientific, Waltham, MA, USA). Duplex PCR was conducted with primers designed for the amplification of *E. coli*, including the 16S rRNA gene as an internal control for bacterial detection (9, 10). *E. coli* ATCC 25922 and a no-template control were included as standards. Each sample was analyzed in duplicate, and if the results were inconsistent, a third run was performed to validate the findings.

Confirmed ESBL-producing *E. coli* isolates were subjected to further screening for antibiotic resistance genes (ARGs), including colistin resistance genes (mcr-1 to mcr-10), β-lactamase genes associated with third-generation cephalosporin resistance ($bla_{CTX\text{-}M\text{-}1}$, $bla_{CTX\text{-}M\text{-}2}$, $bla_{CTX\text{-}M\text{-}8}$, $bla_{CTX\text{-}M\text{-}9}$, $bla_{CTX\text{-}M\text{-}25}$), and carbapenemase-encoding genes such as metallo-β-lactamases ($bla_{NDM\text{-}1}$, bla_{VIM}, bla_{IMP}) and serine β-lactamases (bla_{KPC}, $bla_{OXA\text{-}1}$, $bla_{OXA\text{-}48}$). Separate Multiplex PCR assays were carried out for *Mcr*, *bla* genes targeting $bla_{\text{-}KPC}$, $bla\text{-}_{IMP}$, $bla\text{-}_{OXA\text{-}1}$, and $bla_{OXA\text{-}48}$. The duplex PCR for $bla_{CTX\text{-}M\text{-}1}$and $bla_{CTX\text{-}M\text{-}2}$ and $bla_{NDM\text{-}1}$ and bla_{VIM} was performed. Singleplex PCR assays were conducted for $bla_{CTX\text{-}M\text{-}8}$, $bla_{CTX\text{-}M\text{-}9}$, and $bla_{CTX\text{-}M\text{-}25}$. The PCR products were analyzed via electrophoresis on agarose gels (1.8% to 3%, depending on the expected amplicon size) and visualized using ethidium bromide staining. Each isolate was tested in duplicate, and if discrepancies were observed, a third PCR run was performed to confirm the results.

Determination of colistin Minimum Inhibitory Concentration by Broth Macro-dilution

The minimum inhibitory concentration (MIC) of colistin was determined according to the Clinical and Laboratory Standards Institute (CLSI) guidelines, 34th edition (CLSI, 2024), using the broth macro dilution method in polypropylene tubes. Confirmed ESBL-producing *E. coli* isolates, along with the reference strain *E. coli* ATCC 25922, were cultured on tryptic soy agar at 35°C for 16-18 hours. Bacterial suspensions were prepared in cation-adjusted Mueller-Hinton broth (CAMHB) (Becton, Dickinson, Le Pont-de-Claix, France) and adjusted to match a 0.5 McFarland standard. A 1,000 µg/mL stock solution of colistin sulfate (Sigma–Aldrich, USA) was prepared, from which a working solution (≥48 µg/mL) was made. Two-fold serial dilutions were performed to achieve final concentrations of 8, 4, 2, 1, and 0.5 µg/mL. Each isolate was tested in duplicate, and any inconsistent results were addressed with a repeat test. The reference strain *E. coli* ATCC 25922 (with an MIC range of 0.25–8 µg/mL) was used as a quality control. Inoculated tubes were incubated at 35°C for 16-18 hours with shaking, and the MIC was determined by assessing visible bacterial growth. Positive controls (bacterial suspension without colistin) and negative controls (CAMHB without bacterial inoculation) were included to ensure result validity.

RESULTS AND DISCUSSIONS

Results demonstrated 86 out of 102 presumptive ESBL- producing *E. coli* isolates was confirmed as ESBL-producing *E. coli*. The result shows a high prevalence of ESBL- *E. coli* across various types of animal farms in Ratchaburi, Thailand. Positive detection rates were significantly high, with some sources, such as duck effluent, duck feces, and goat feces, showing a 100% prevalence. This indicates, ESBL-producing *E. coli* is

not only prevalent in dairy farms or swine shown in most of the previous studies but also other domestic farms. Similarly, wastewater samples from pig farms (both influent and effluent) exhibited consistently high positivity rates of 84.2% and 87.5%, respectively. In contrast, cow wastewater had the lowest positivity rate (55.5%) among all tested sources, indicating a comparatively reduced prevalence. Chicken feces showed moderate positivity at 66.6%, still contributing significantly to the presence of ESBL- *E. coli* (Figure1).

Further testing of the 86 ESBL-producing *E. coli* isolates revealed the presence of mobile colistin resistance (*mcr*) genes and extended-spectrum β-lactamase (ESBL) genes. Among them, three isolates harbored the *mcr*-1 gene, two had *mcr*-2, and two carried *mcr*-3, suggesting a low but presence of transferable colistin resistance. Notably all these isolates were from the pig influent (Table1). ESBL genes were highly prevalent, with $bla_{CTX\text{-}M\text{-}1}$ detected in 73 isolates, followed by $bla_{CTX\text{-}M\text{-}9}$ in 13 isolates, $bla_{CTX\text{-}M\text{-}8}$ and $bla_{OXA\text{-}1}$ in one isolate each. The detection of multiple *mcr* variants, including co-occurrence of *mcr*-1 and *mcr*-2 in some pig isolates highlights the risk of multidrug resistance in livestock environments. Carbapenem genes such as $bla_{NDM\text{-}1}$, bla_{VIM}, bla_{IMP}, bla_{KPC}, $bla_{OXA\text{-}48}$ was not detected.

Colistin minimum inhibitory concentration (MIC) testing further revealed phenotypic resistance patterns. Isolates carrying *mcr* genes showed MICs ranging from 4 to >8 µg/mL, confirming their resistance to colistin. Notably, two isolates from pig influent, both harboring *mcr*-3, exhibited MIC values of ≥8 µg/mL, consistent with a resistant phenotype. Some pig influent isolates also displayed high MICs (>8 µg/mL) despite the absence of detectable *mcr* genes, suggesting potential alternative resistance mechanisms such as chromosomal mutations or efflux pump activity (11). Intermediate resistance was observed in isolates from cow and duck feces, with MICs ranging from 1–2 µg/mL, and most of these lacked detectable *mcr* genes.

These findings underscore the importance of integrated One Health surveillance, as resistance genes were detected across multiple farm animals including pigs, cows, and ducks. The co-occurrence of ESBL and *mcr* genes in several isolates, along with presence of phenotypic resistance without corresponding genes is of particular concern, as it may limit therapeutic options and facilitate the spread of resistance via other means of resistance mechanism. Regular monitoring of both phenotypic resistance and resistance genes is essential to guide antibiotic stewardship in veterinary and agricultural settings.

Conclusion

This study highlights a high prevalence of ESBL-producing *E. coli* across various livestock farms in Ratchaburi, Thailand, with particularly elevated rates in duck and pig farm samples. The widespread detection of ESBL genes, especially $bla_{CTX\text{-}M\text{-}1}$, and the presence of mobile colistin resistance genes (*mcr*-1, *mcr*-2, and *mcr*-3), although at lower frequencies, raise significant concerns about the dissemination of multidrug-resistant bacteria in animal farming environments. The phenotypic resistance patterns observed, including colistin resistance in isolates lacking known *mcr* genes, further suggest the emergence of alternative resistance mechanisms (11). These findings emphasize the need for integrated One Health surveillance and targeted antimicrobial stewardship in agricultural systems to curb the spread of critical resistance determinants and safeguard both animal and public health.

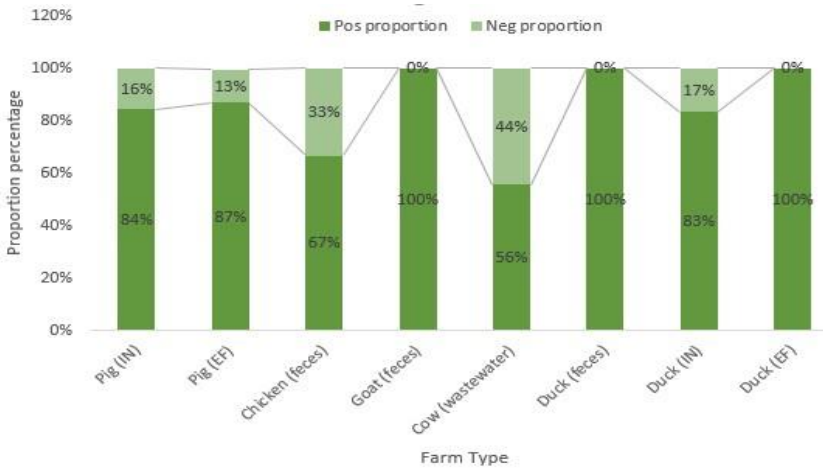


Figure1: Proportion of ESBL-*E. coli* in various livestock

Table1: ESBL-*E. coli* isolates positive for *Mcr*-gene

Sl. Number	Farm	Isolate Code	source of isolate	Mcr-gene
1	Farm 02	02_PIN_EC1	Pig Influent	*Mcr*-1, *Mcr*-2
2		02_PIN_EC4		*Mcr*-1, *Mcr*-2
3		02_PIN_EC6		*Mcr*-1
4		02_PIN_EC5		*Mcr*-3
5	Farm 29	29_PIN_EC1		*Mcr*-3

Acknowledgement

I would like to express my sincere gratitude to all those who have supported and contributed to the completion of this research. Special thanks to my supervisors, Emeritus Professor Dr. Skorn Mongkolsuk and Dr. Kwanrawee Sirikanchana, whose guidance, patience, and expertise were invaluable throughout this study. I also extend my appreciation to the faculty and staff of microbial source tracking laboratory of research laboratory of biotechnology at Chulabhorn Research Institute for their continuous support and resources. I would also like to thank Chulabhorn Graduate Institute for providing the financial support that made this research possible.

Finally, I am deeply grateful to my family, friends and colleagues back at home (Bhutan) for their unwavering support and understanding throughout this project. Without their encouragement and belief in me, this work would not have been possible.

References

1. Samtiya M, Matthews KR, Dhewa T, Puniya AK. Antimicrobial Resistance in the Food Chain: Trends, Mechanisms, Pathways, and Possible Regulation Strategies. Foods. 2022;11(19).
2. Aljohni MS, Harun-Ur-Rashid M, Selim S. Emerging threats: Antimicrobial resistance in extended-spectrum beta-lactamase and carbapenem-resistant Escherichia coli. Microbial Pathogenesis. 2025;200:107275.
3. Zhang YL, Huang FY, Gan LL, Yu X, Cai DJ, Fang J, et al. High prevalence of bla(CTX-M) and bla(SHV) among ESBL producing E. coli isolates from beef cattle in China's Sichuan-Chongqing Circle. Sci Rep. 2021;11(1):13725.
4. Saekhow P, Sriphannam C. Prevalence of extended-spectrum beta-lactamase-producing Escherichia coli strains in dairy farm wastewater in Chiang Mai: https://doi.org/10.12982/VIS.2021.030. Veterinary Integrative Sciences. 2021;19(3):349-62.
5. Yuli Maulana K, Pichpol D, Rohmi Farhani N, Ayu Widiasih D, Unger F, Punyapornwithaya V, et al. Antimicrobial resistance characteristics of Extended Spectrum Beta Lactamase (ESBL)- producing Escherichia coli from dairy farms in the Sleman district of Yogyakarta province, Indonesia: https://doi.org/10.12982/VIS.2021.041. Veterinary Integrative Sciences. 2021;19(3):525-35.
6. Sudatip D, Tiengrim S, Chasiri K, Kritiyakan A, Phanprasit W, Morand S, et al. One Health Surveillance of Antimicrobial Resistance Phenotypes in Selected Communities in Thailand. Antibiotics (Basel). 2022;11(5).
7. Nations U. Transforming our world: the 2030 Agenda for Sustainable Development. New York; 2015. Report No.: A/RES/70/1.
8. WHO. WHO integrated global surveillance on ESBL-producing E. coli using a “One Health” approach: implementation and opportunities. 16 March 2021.
9. Ferris MJ, Muyzer G, Ward DM. Denaturing gradient gel electrophoresis profiles of 16S rRNA-defined populations inhabiting a hot spring microbial mat community. Appl Environ Microbiol. 1996;62(2):340-6.
10. Sabat G, Rose P, Hickey WJ, Harkin JM. Selective and sensitive method for PCR amplification of Escherichia coli 16S rRNA genes in soil. Appl Environ Microbiol. 2000;66(2):844-9.
11. Reygaert WC. An overview of the antimicrobial resistance mechanisms of bacteria. AIMS Microbiol. 2018;4(3):482-501.

21R4-04

Article Type: Research & Analysis
Title: Optimization of batch electrocoagulation process with Al-Fe plate electrodes in TDS removal using Box-Behnken design for hospital wastewater

Suchira Thongson[1], Raweeporn Pomthong[1], Suthida Theepharaksapan[1,2*], Yanika Lerkmahalikit[3] Khanit Matra[4], and Sirilak Prasertkulsak[5]

[1]Department of Civil and Environmental Engineering, Srinakharinwirot University, 63 Moo 7 Ongkharak, Nakhon Nayok, 26120 Thailand ; [2] Central Instruments Center Building, Excellent Center Sustainable, Engineering faculty, Srinakharinwirot University, Nakhon Nayok, 26120, Thailand [3] Department of Electrical Engineering, Engineering Faculty, Srinakharinwirot University, Nakhon Nayok, 26120, Thailand [4] Department of Environmental Engineering, Faculty of Engineering and Architecture, Rajamanga University of Technology Suvarnabhumi, Thailand*

[*]Phone : 026495000 ext. 27065, E-mail : Suthidat@g.swu.ac.th

ABSTRACT

This study investigates the optimization of the electrocoagulation (EC) process using combined aluminum (Al) and iron (Fe) electrodes for the removal of total dissolved solids (TDS) from hospital wastewater. A Box-Behnken Design (BBD), under the framework of Response Surface Methodology (RSM), was employed to examine the effects of three operational parameters: initial pH, current density, and electrolysis time. Real hospital wastewater collected from Nakhon Nayok Province, Thailand, was characterized by high levels of TDS, BOD, and COD, exceeding Thai regulatory discharge limits. Experimental results demonstrated that current density was the most significant factor influencing TDS removal, followed by electrolysis time, while pH exhibited a non-linear effect. The optimized conditions—pH 7.0, current density 25 mA/cm², and electrolysis time 90 minutes—achieved a maximum TDS removal efficiency of 37.8%. Despite limitations in model predictability at boundary conditions, the regression model showed strong correlation (R^2 = 97.34%) with the experimental data within the central design region. These findings highlight the potential of Al–Fe based EC systems for improving hospital wastewater treatment, with implications for scaling and regulatory compliance.

Keywords : Hospital wastewater; Box-Behnken design (BBD); Electrocoagulation; Total Dissolved Solid (TDS)

INTRODUCTION

Hospital wastewater contains a diverse range of contaminants, including pharmaceuticals, pathogens, heavy metals, and organic pollutants. These pollutants originate from medical activities such as drug administration, laboratory processes, and sanitation. If inadequately treated, hospital wastewater poses serious environmental risks, contributing to antibiotic resistance, toxic metal accumulation, and microbial imbalances in aquatic ecosystems [1,2]. Conventional treatment methods, such as activated sludge and chemical coagulation, often fail to effectively remove persistent pollutants, particularly dissolved solids, heavy metals, and pharmaceutical residues [3]. Electrocoagulation (EC) has emerged as a promising alternative due to its electrochemical mechanisms, which facilitate the destabilization and removal of contaminants. The process generates coagulants in situ from sacrificial electrodes, allowing pollutants to aggregate and precipitate. However, the effectiveness of EC depends on critical operational parameters, including initial pH, current density, and electrolysis time, all of which influence pollutant removal efficiency, energy consumption, and electrode longevity [4]. To mitigate the environmental impact of hospital wastewater, many countries have established stringent regulations limiting the discharge of heavy metals, pharmaceutical residues, and total dissolved solids (TDS). Achieving compliance with these regulations necessitates advanced treatment technologies capable of addressing the complex nature of hospital effluents [5,6]. Optimizing EC parameters enhances treatment efficiency and ensures sustainable operation. Response Surface Methodology (RSM) offers a structured approach for optimizing treatment conditions while minimizing experimental trials. Among various RSM techniques, the Box-Behnken Design (BBD) is particularly useful for evaluating interactions among process variables and determining optimal

treatment conditions [7]. Despite its advantages, EC faces challenges such as electrode passivation, excessive sludge production, and operational costs when applied on a larger scale. Recent research has explored advanced electrode materials, hybrid EC configurations, and automated parameter control to enhance process efficiency and cost-effectiveness [8]. However, further investigation is needed to improve scalability and long-term sustainability, particularly in hospital wastewater treatment. Beyond hospital wastewater, EC has demonstrated effectiveness in treating various complex effluents, including industrial wastewater, pharmaceutical production discharges, and landfill leachates. Establishing optimized EC conditions for hospital wastewater treatment could pave the way for broader applications across other challenging wastewater streams [9]. Recent studies have highlighted the advantages of using a combined aluminum (Al) and iron (Fe) electrode system in a single electrochemical cell. This configuration harnesses the coagulant-generating capabilities of both metals, providing a synergistic effect that enhances pollutant destabilization and precipitation. Al electrodes predominantly produce Al^{3+} ions that form Al $(OH)_3$ flocs, known for their high adsorption capacity, while Fe electrodes release Fe^{2+} / Fe^{3+} ions that contribute to redox reactions and co-precipitation processes. Moreover, the combined use of Al and Fe can mitigate some limitations of using either metal alone, such as electrode passivation and pH sensitivity. This approach has shown promise not only in improving pollutant removal rates but also in reducing sludge volume and improving overall process stability. These benefits make the Al–Fe system a viable strategy for advanced wastewater treatment, particularly in dealing with the complex matrices of hospital effluents [10 ,11]. This study focuses on optimizing EC using aluminum (Al) and iron (Fe) electrodes to improve the removal of TDS from hospital wastewater. The primary objectives are: (i) to assess the influence of pH, current density, and electrolysis time on TDS removal efficiency, (ii) to utilize the BBD approach to identify optimal operating conditions for maximum treatment performance, and (iii) to evaluate the feasibility of implementing the optimized EC system in real-world wastewater treatment scenarios. By achieving these objectives, this study aims to contribute to the development of more effective and sustainable wastewater treatment strategies while ensuring regulatory compliance.

METHODOLOGY

1.Hospital wastewater

As a case study, 60 L of hospital wastewater was collected from a medical center in Nakhon Nayok Province, Thailand. The collected wastewater was stored at 4°C throughout the experimental period to preserve its characteristics. For each experimental run, a 0.8 L sample was taken directly from the stored wastewater at the time of testing. The properties of the collected hospital wastewater are summarized in **Table 1**.

2.Electrocoagulation Unit

A schematic representation of the electrocoagulation system is provided in **Figure 1** . The system consisted of a DC power supply unit capable of delivering a current range of 0–5 A, connected to a set of monopolar electrodes arranged in series. The electrocoagulation process was conducted in batch mode using a glass cylinder reactor with dimensions of 20 cm × 12 cm × 10 cm and a working volume of 1.0 L. A combination of aluminum (Al) and iron (Fe) electrodes was used to enhance treatment efficiency, with Al serving as the anode to release Al^{3+} ions for coagulation, while Fe acted as the cathode, aiding in the reduction of contaminants. The electrodes were arranged in a monopolar parallel configuration, ensuring efficient electrochemical reactions. Each experimental run utilized four electrodes, each measuring 8 cm × 14 cm × 0.3 cm, with an inter-electrode distance of 1.2 cm and a total surface area of 96 cm^2 per electrode. To ensure uniform mixing and prevent sedimentation, the reactor was placed on a magnetic stirrer operating at 300 rpm throughout the process. Each experimental run was conducted with 800 mL of wastewater to evaluate the electrocoagulation performance. pH measurement was achieved by using a digital pH meter (HNNA Instrument Inc.PH211, Romania) while adjusting pH value was accomplished using 0.1 M NaOH or 0.1 M H_2SO_4 solutions. Total Dissolved Solid (TDS) and conductivity were measured using (YSI 60, USA).

Table 1 Characteristics of the real hospital wastewater

Parameters	unit	Average ± SD	Standard*
pH	-	8.25 ± 0.55	5-9
EC	µS/cm	974.43 ± 171.76	-
Turbidity	NTU	150. 84±66 .83	-
SS	mg/l	80. 5±43 .4	<500
TDS	mg/l	725. 3±538 .1	<30
BOD	mg/l	140.83 ± 108.54	<35
COD	mg/l	569.33 ±4 43.04	<20
BOD/COD	mg/l	0.25 ± 0.24	-
TKN	mg/l	89.38 ± 60.60	<35
Oil and grease	mg/l	24.58 ± 30.73	<20
Sulfide	mg/l	2.35 ± 1.79	<1

Remark: * Notification of the Ministry of Natural Resources and Environment on Establishing Standards for Wastewater Discharge Control from Certain Types and Sizes of Buildings.

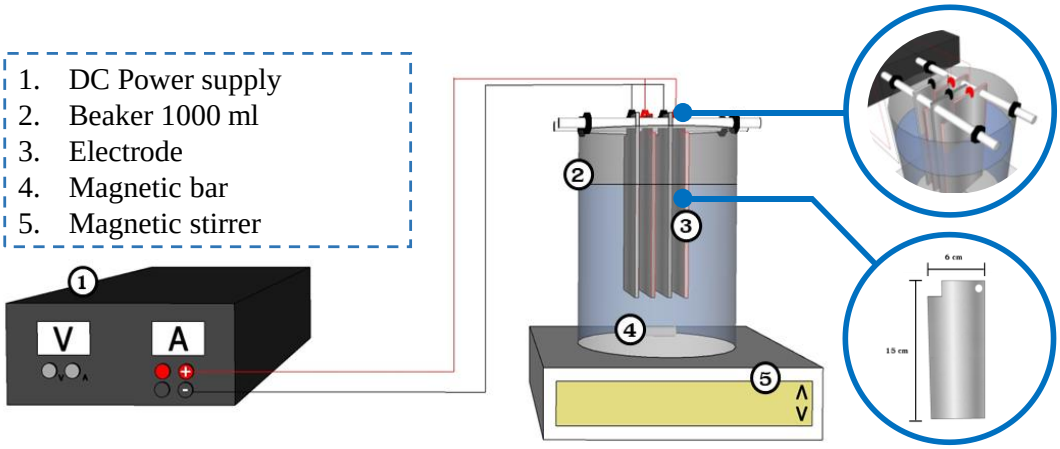


Figure 1: Experimental setup for the electrochemical process

3. Design of experiment for optimization

This study employed a Box Bhenken design (BBD), a well-known RSM technique, using historical data to optimize and get the effect of 3 influencing factors, i.e., initial pH, current density, and electrolysis time on the TDS removal. The choice of pH, current density, and electrolysis time was based on their direct influence on coagulant generation, pollutant destabilization, and treatment kinetics [12]. Other factors such as electrode material and spacing were considered in preliminary planning but kept constant to isolate the effects of key operating conditions. The study utilized Minitab-17 software to generate an optimized experimental design comprising 15 experimental runs, including three repetitions of the center point for statistical reliability. Each independent variable was coded at three levels between - 1 and + 1, where the variables initial pH (X_1), current density (X_2), and electrolysis time (X_3) were set in the range of pH 4–10, 5 –25mA/cm^2, 1.0 – 4.0 cm, and 30 – 90 min, respectively. The coded and actual values of variables are showed in **Table 2.** The effects of the selected independent variables and their interactions on responses according to BBD were described using the second order polynomial equation.

$$Y_i = \beta_0 + \sum_{i=1}^{k} \beta_i X_i + \sum_{i=1}^{k} \beta_{ii} X_i^2 + \sum_{i>j}^{k} \sum_{j}^{k} \beta_{ij} X_i X_j + C \quad \textbf{(1)}$$

where β_0, β_i, β_{ii}, and β_{ij} are constant, linear, quadratic, and cross-factor interaction coefficients, respectively; X_i and X_j represent the independent variables; Y_i is the predicted response; and k and C are the number of factors and the residual terms, respectively.

Table 2 Coded and actual values of the variables of the design of experiments for the electrocoagulation process

Independent variable	**actor**	**Coded level of variable**		
		-1	0	1
Initial pH	X_1	4	7	10
Current density (mA/m^2)	X_2	5	15	25
Electrolysis time (min)	X_3	30	60	90

4. Analysis

4.1 TDS removal (%)

The % TDS removal was calculated using **Eq. (2)**

$$TDS\ removal\ efficiency\ (\%) = \frac{(TDS_i) - (TDS_t)}{TDS_i} \quad \textbf{(2)}$$

4.2 Electrode and Power consumption

The power consumption for the removal of % TDS from hospital wastewater using the electrocoagulation process was calculated using **Eq. (3).**

$$C_{energy} = \frac{U \times I \times t_{\mathrm{EC}}}{\forall} \quad \textbf{(3)}$$

Where C_energy represents the amount of energy consumed (kWh/m^3), U represents the applied voltage, I denote the electrical current (A), t_{EC} refers to the reaction time (hours), $\forall$ is the volume of water used (m^3)

$$C_{electrod} = \frac{I \times t_{\mathrm{EC}} \times M_W}{Z \times F \times \forall} \quad \textbf{(4)}$$

Where C_electrode denotes the amount of electrode material used (kg/m^3), M_W represents the molecular weight of Al or Fe (26.98 or 55.84, respectively), Z is the number of electrons involved in the oxidation/reduction reaction (z = 3 for Al, z = 2 for Fe), and F is Faraday's constant (96,487 C/mole).

4.3 Statistical analysis

Analysis of Variance (ANOVA) was applied to evaluate statistical significance, with a maximum *p-value* threshold of 0.1. Variables exceeding this threshold were excluded to refine the predictive model and ensure optimal material properties.

RESULTS AND DISCUSSIONS

1. Characteristics of hospital wastewater

The physico-chemical characteristics of the wastewater are summarized in **Table 2**. The wastewater exhibited alkaline properties, with an average pH of 8.25 ± 0.55. Electrical conductivity was measured at 974.43 ± 171.76 µS/cm, indicating a significant presence of dissolved ions. The BOD and COD concentrations were 140.83 ± 108.54 mg/L and 569.33 ± 443.04 mg/L, respectively. Similarly, when compared to the Notification of the Ministry of Natural Resources and Environment on Establishing Standards for Wastewater Discharge, the wastewater does not meet the Thai regulatory standards, particularly for BOD, COD, and TDS concentrations. The excessive concentration of these pollutants poses environmental risks, requiring appropriate treatment before discharge. The BOD/COD ratio of 0.25 ± 0.24 suggests that conventional biological treatment methods would be ineffective for this wastewater.

2. Box Bhenken design

A three-factor, three-level Box-Behnken Design (BBD) was employed to optimize the operating parameters of the electrocoagulation process, focusing on TDS removal efficiency (%) and power consumption. The experimental design consisted of 15 runs, including three replications at the central point to estimate pure error. The experimental conditions, observed responses for TDS removal and power consumption, along with the predicted values, are summarized in **Table 3**

Table 3 Experimental design matrix and response based on the experimental runs and predicted values on the TDS removal (%) and power consumption proposed by the BBD

Run	X_1	X_2	X_3	TDS Removal %		Electrode Consumption (kg/m^3)	
				Actual	Predicted	Actual	Predicted
1	0	0	0	29.44	31.81	0.3359	0.3120
2	1	0	1	0.63	64.33	0.5275	0.4581
3	-1	0	1	16.70	54.65	0.3025	0.2011
4	0	1	1	41.02	48.45	0.7951	0.5697
5	0	-1	1	20.02	31.53	0.1686	0.2075
6	0	0	0	31.69	31.81	0.2997	0.3120
7	-1	1	0	10.14	66.00	0.1646	0.3105
8	1	1	0	11.49	64.68	0.1097	0.6803
9	-1	-1	0	0.18	51.96	0.1173	0.3403
10	1	-1	0	0.45	49.56	0.4037	0.3689
11	0	0	0	34.29	31.81	0.2992	0.3120
12	-1	0	-1	1.80	60.47	0.1682	0.4617
13	1	0	-1	8.80	47.07	0.5088	0.6031
14	0	1	-1	30.61	40.39	0.2444	0.5511
15	0	-1	-1	14.27	28.15	0.0609	0.6317

TDS removal ranged from 0.18% to 41.02%, with the highest value observed at neutral pH, high current density, and extended electrolysis time (Run 4). Electrode consumption varied from 0.0609 to 0.7951 kg/m³, with higher removal generally corresponding to increased electrode usage. Central point runs showed consistent results, confirming system stability under mid-range conditions. Predicted values from the quadratic model aligned well with experimental results near the design center but showed noticeable discrepancies at the design boundaries. For example, in Run 7, the actual TDS removal was 10.14%, while the predicted value was 66.00%. A similar overestimation occurred in Run 2 (Actual = 0.63%, Predicted = 64.33%). Model performance evaluation indicated limited predictive accuracy, with RMSE values of 38.24% for TDS removal and 0.256 kg/m³ for electrode consumption. Negative R^2 values (–7.28 and –0.83, respectively) suggest that the quadratic model did not adequately represent system behavior under certain operating conditions. These findings highlight the need for model refinement through additional data, incorporation of higher-order terms, or alternative modeling approaches to improve reliability.

3. Evaluation of experimental results with design of experiments

The predictive model developed from the Box-Behnken Design was further evaluated through response surface analysis and ANOVA. The quadratic response function for TDS removal is presented in **Equation (4)**, incorporating linear, interaction, and quadratic terms of the coded variables.

$$Y = 31.81 - 0.93\ X_1 + 7.29\ X_2 + 2.86\ X_3 - 22.87\ X_1{*}X_1 - 3.37\ X_2{*}X_2 - 1.95\ X_3{*}X_3 + 0.27\ X_1{*}X_2 - 5.77\ X_1{*}X_3 + 1.17\ X_2{*}X_3 \quad \textbf{(4)}$$

The model exhibited strong correlation with the experimental data, with R^2 = 97.34%, adjusted R^2 = 92.54%, and predicted R^2 = 63.49%. Despite the prediction errors discussed in Section 3.2, these coefficients suggest that the model can reasonably explain the observed variation within the experimental range, particularly near the central region. The ANOVA results (Table 4) confirmed the overall significance of the model (p = 0.002), supporting its adequacy for representing the system. Among the linear factors, **current density** had the most significant impact on TDS removal (p = 0.003), while **initial pH** was not statistically significant (p = 0.514). Electrolysis time had a moderate effect (p = 0.084), suggesting its contribution may depend on interaction with other factors. Quadratic terms were particularly influential, especially for pH, indicating a nonlinear relationship that may not be apparent from the linear analysis alone. The interaction between pH and electrolysis time (X_1X_3) also showed notable influence. However, the model was less predictive for electrode consumption, as indicated by the non-significant regression (p = 0.511) and lower F-values. These results complement the findings in Section 3.2 by clarifying the statistical significance of each factor and interaction. They also highlight the model's strengths and limitations, offering a basis for refining future process optimization strategies.

4. Optimization with RSM

Response Surface Methodology (RSM) is a statistical approach used to optimize complex processes influenced by multiple variables. It integrates experimental design, model fitting, and validation to determine optimal operating conditions. In this study, Box-Behnken Design (BBD) was employed to identify the best conditions for TDS removal efficiency using a regression model. The optimization process was conducted through Design of Experiments (DoE) software, which

CONCLUSION

This study developed a mathematical model for optimizing the electrocoagulation process using a Box-Behnken Design to treat hospital wastewater. The effects of pH, current density, and electrolysis time on TDS removal were systematically evaluated. The optimal conditions pH 7.0, current density 25 mA/m², and electrolysis time 90 minutes resulted in a maximum TDS removal efficiency of 37.8%. The close match between experimental and predicted results confirms the model's reliability. These findings not only demonstrate the potential of electrocoagulation for hospital wastewater treatment but also provide a basis for scaling up the process in real-world applications. The optimized conditions offer a practical framework for achieving regulatory compliance while maintaining operational efficiency.

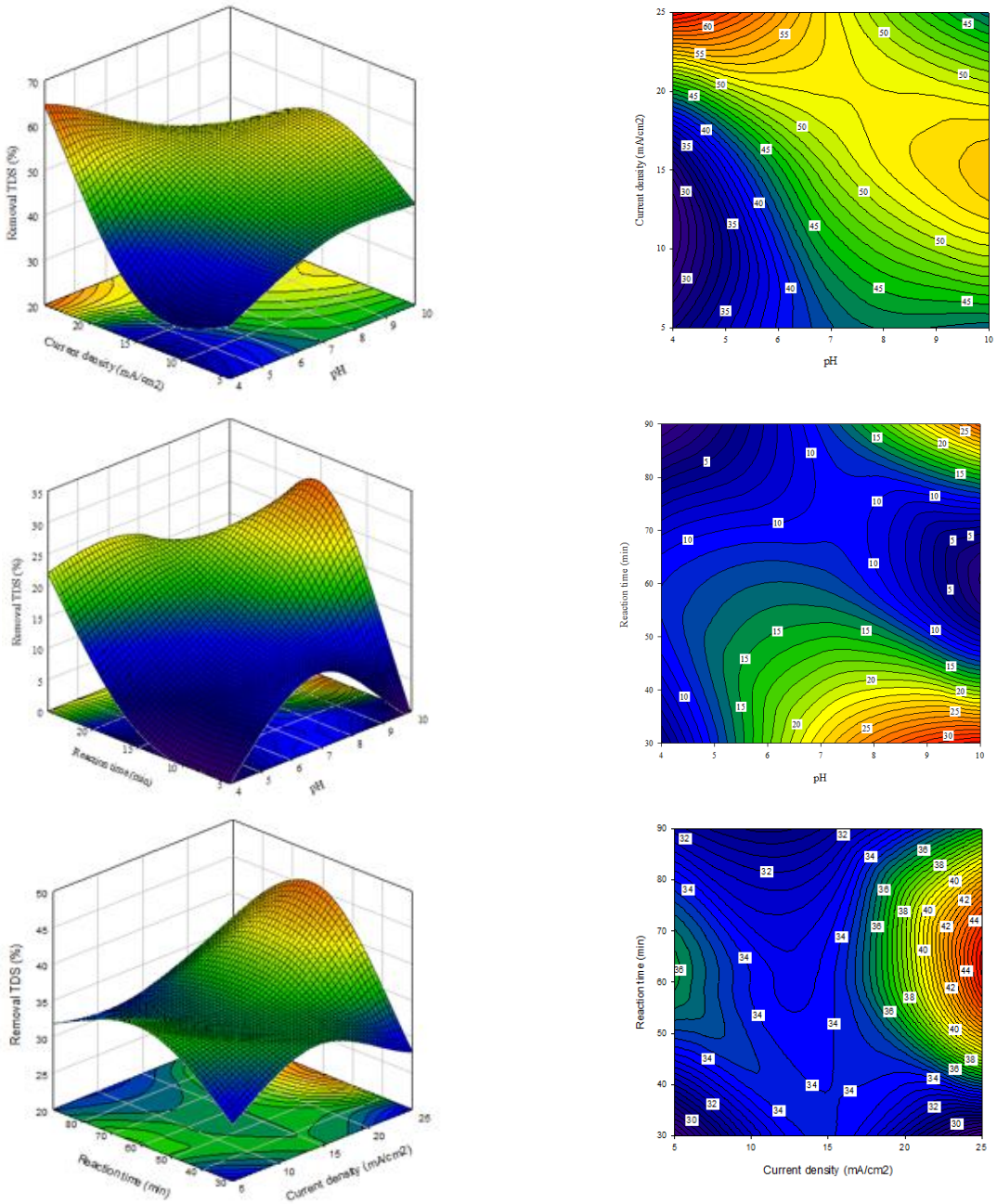


Figure 2 RSM plot and contour plots between parameters with responses on TDS removal.

ACKNOWLEDGEMENT

This work was supported by the Thailand Science Research and Innovation (TSRI) via Srinakharinwirot University (SWU) (Fundamental Fund: Grant no. 182342/2566). Appreciation is also extended to the Central Instruments Center and the Excellent Center for Sustainable Engineering at SWU for their invaluable assistance and provision of facilities.

REFERENCE

[1] Gorito, A.M., et al. (2022). Pharmaceutical removal from hospital wastewater: Advanced treatment technologies and future perspectives. *Science of the Total Environment*, 851, 158227.
[2] Couto, C.F., et al. (2021). Hospital wastewater treatment: A review on its characteristics, environmental risks, and possible solutions. *Environmental Research*, 198, 111242.
[3] Babu, B.R., et al. (2021). Electrocoagulation technology for hospital wastewater treatment: Mechanisms, performance, and optimization. *Environmental Science and Pollution Research*, 28(32), 43890-43910.
[4] Silva, C.A., et al. (2023). Application of response surface methodology in optimizing electrocoagulation processes for industrial and hospital wastewater. *Environmental Technology & Innovation*, 30, 103120.
[5] Sharma, R. & Verma, N. (2021). Response surface methodology for electrocoagulation process optimization in wastewater treatment. *Water Science & Technology*, 84(2), 330-345.
[6] World Health Organization (2020). Guidelines on sanitation and health. *WHO Press*.
[7] Ahmed, S., et al. (2022). Optimization of electrocoagulation for wastewater treatment: A review of design and operational parameters. *Journal of Environmental Chemical Engineering*, 10(4), 108202.
[8] Zhao, Y., et al. (2023). Advances in electrocoagulation for wastewater treatment: Challenges and future perspectives. *Chemical Engineering Journal*, 452, 139433.
[9] Zhang, X., et al. (2022). Electrocoagulation applications beyond wastewater treatment: Emerging trends and opportunities. *Environmental Science & Technology*, 56(14), 9921-9935.
[10] Kobya, M., Akyol, A., & Demirbas, E. (2015). Treatment of pharmaceutical wastewater by electrocoagulation using aluminum and iron electrodes. Environmental Progress & Sustainable Energy, 34(4), 1100–1111. https://doi.org/10.1002/ep.12056
[11] Zodi, S., Potier, O., Lapicque, F., & Leclerc, J. P. (2010). Treatment of the industrial wastewaters by electrocoagulation: Optimization of coupled Al–Fe electrode system using response surface methodology. Chemical Engineering and Processing: Process Intensification, 49(7), 718–726. https://doi.org/10.1016/j.cep.2010.01.002
[12] Vasudevan, S. (2013). Prospective application of electrocoagulation for wastewater treatment: A review. Desalination and Water Treatment, 51(19–21), 3384–3397. https://doi.org/10.1080/19443994.2012.749141

21R4-05

Analysis of Spatial Distribution Patterns of Non-Communicable Diseases (NCDs) and Risk Factors with GIS in Central Regions of Thailand

May Myat Myat Aung[1*], Kritsanat Surakit[2], Nawatch Surinkul[3] and Romanee Thongdara[3]

[1]Graduate student; [2]Lecturer; [3]Assistant Professor, Department of Civil and Environmental Engineering, Faculty of Engineering, Mahidol University, Thailand.*
[*]Phone : 0950030570, E-mail :maymyatmyataung27@gmail.com

ABSTRACT

Noncommunicable diseases (NCDs) are leading causes of mortality in Thailand, representing 74% of all deaths. Behavioral, social and environmental issues are the primary drivers contributing to the increasing incidence of NCDs across Thailand. This study aims to examine factors related to NCDs; and analyze spatial distribution patterns and cluster analysis of NCDs and related factors. In this study, Coronary Heart Diseases, Hypertension and Diabetes from Health Data Center (HDC) website published by the Ministry of Public Health (MOPH) in Thailand for 2023; and environmental and behavior factors will be analyzed to understand spatial distribution pattern. As methodology, NCDs diseases and risk factors will be conducted by spatial distribution analysis and checked the correlation of factors and diseases with SPSS; and 3 NCDs diseases in 3 zones will be analyzed by the spatial cluster analysis with local Moran's I. As a result, Mueang Districts, Bangkok Metropolitan Regions (BMR) - Nonthaburi, Ratchaburi, Samut Sakhon, Nakhon Pathom, Samut Prakan Provinces and industrialized provinces – Chonburi and Rayong Provinces were seriously affected from the diseases, environmental and social factors based on the result of spatial distribution pattern and clustered analysis. And the most severe air pollution was occurred in winter season therefore the government should focus on the tackle of air pollution affected on the community in this season, especially in the Mueang Samut Songkhram, Mueang Ratchaburi, Mueang Phetchaburi, Mueang Supanburi, Mueang Samut Sakhon Districts and Saraburi Province. Finally, this study can support the recommendations of prioritization provinces and districts in the cases of NCDs control and prevention. By combining GIS and spatial statistical analysis on health data, it would be helpful to expose the relationship of NCDs risk factors and beneficial to policy makers in decision making of prevention and surveillance NCDs.

Keywords: NCDs; risk factors; spatial statistical analysis; Local Moran's I; GIS

INTRODUCTION

Noncommunicable diseases (NCDs) are a kind of chronic disease that derives from genetic, physiological, environmental and behavioral factors. According to the statistical data of WHO, 41 million people died every year due to NCDs [1]. NCDs such as cardiovascular diseases, chronic obstructive pulmonary diseases, diabetes, and cancers are leading causes of mortality in Thailand, which is 400,000 deaths each year, referring 74% of all deaths nationally. The risk factors – tobacco use, harmful alcohol consumption, unhealthy diets, physical inactivity and environmental pollution are the primary drivers contributing to the increasing incidence of noncommunicable diseases (NCDs) across Thailand [2]. The Thai Health Report 2023 indicates that Samut Sakhon, located in the Central Region of Thailand, is among the provinces with the lowest percentage of adequate physical activity, with only 25.4%. Air pollution is the most significant factor, causing 6.7 million deaths worldwide, with around 5.7 million of these due to NCDs [3]. Besides air pollution, solid and hazardous industrial wastes continue to be a challenge across Thailand. The highest levels of hazardous industrial waste were found in provinces with significant industrial activity, such as Rayong, Chonburi, and Samut Prakan [3]. From an economic perspective, the government uses THB 1.6 trillion annually for NCDs and its amount is equivalent to 9.7% of its 2019 Gross Domestic Product (GDP). The treatment for NCDs cost THB 139 billion; and THB 1.5 trillion is charged for lost human resources capacity due to premature death or disability, which accounts for 91% of all NCDs-related costs. Therefore, NCDs adversely affect socioeconomic development and fiscal sustainability of government and public services [2]. Addressing NCDs issues as urgency, 2030 Agenda for Sustainable Development identifies NCDs as a significant obstacle to sustainable development. By 2030, one third of premature mortality from non-communicable diseases will be reduced through prevention and treatment and promote mental health and well-being [4]. This study aims to examine factors and causes related to NCDs in 24

provinces (201 districts) and to identify and analyze spatial patterns and cluster analysis of NCDs and related factors. Furthermore, real-time mapping could greatly assist public health officials in promptly responding to outbreaks. GIS can provide a conceptual framework for understanding the geographic variability of human disease and health. To effectively control NCDs transmission, it's crucial to prioritize regions with the high incidence of NCDs by applying GIS tools. Based on this analysis, policymakers and health authorities could strategically execute the control plan of NCDs and devote resources to strengthen NCDs prevention and control activities.

METHODOLOGY

The yearly incident data of NCDs - Coronary Heart Diseases, Hypertension and Diabetes which occurred in the Regional Health Zone 4, 5 and 6 were collected from the Ministry of Public Health for 5 years spanning 2019 to 2023 [5]. The social data including total population, age group and number of hospitals were also downloaded from the Ministry of Public Health for the year 2023. And income data was collected from the Community Development Department (CDD). For environmental factors, the updated landuse data for each district was downloaded from Land Development Department (LDD) between 2019, 2021 and 2023 [6], as well as the daily PM 2.5 data in 2023 were collected from the Pollution Control Department (PCD). The social data – total population, age, number of hospitals and income were manipulated to be useful and applicable in ArcGIS by data cleaning, sorting, filtering and joining. For PM 2.5 analysis, the locations of PM 2.5 monitoring stations and the daily PM 2.5 value across stations were obtained from Air4Thai for year of 2023 [7]. After calculating monthly PM 2.5 value by averaging daily data, Inverse Distance Weighting (IDW) calculation was applied to find the missing data of monthly PM 2.5. Similarly, the annual data of 2023 was received by averaging monthly data at each monitoring station. Once the process of data preparation was completed, the monthly and annual point value of PM2.5 were converted into polygon value with IDW interpolation and zonal statistics in ArcGIS, enabling an estimated pollution value for each district. Furthermore, the landuse was classified into 5 classes – Agriculture, Forest, Urban, Water and Miscellaneous to identify the influenced land area in the study area. After getting all data at the district level, the spatial distribution pattern of diseases and related factors was evaluated in order to understand the distribution pattern across districts. And then, the correlation analysis was conducted to find the relationship between them by using SPSS. If the data were statistically correlated with each other, the clustered analysis with Local Moran's I was carried out to investigate the specific districts of high and low prevalence rate of diseases and other factors as illustrated in Figure 1 by describing studying area in Figure 2.

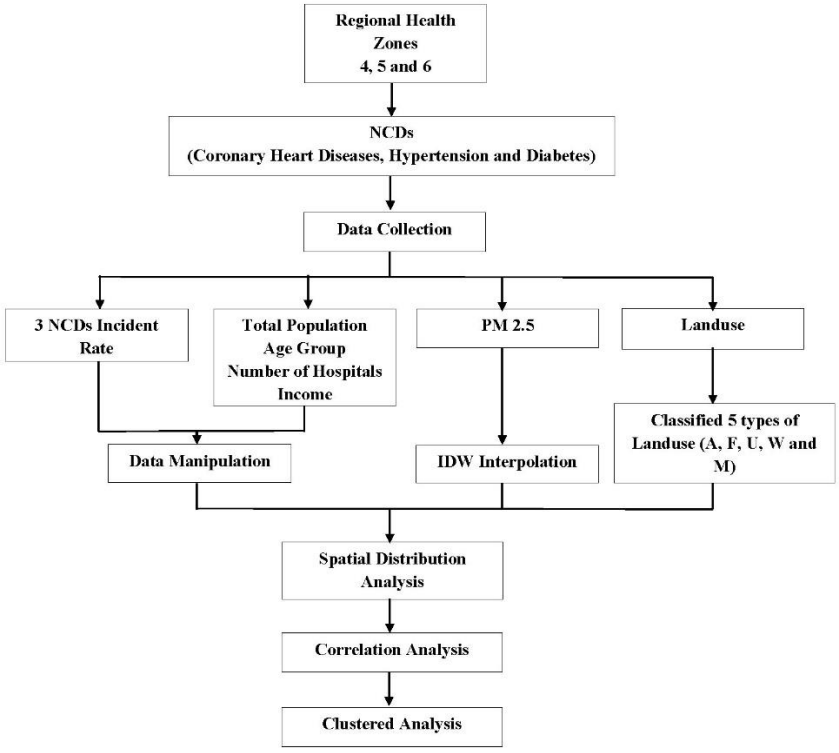


Figure 1 Conceptual Framework of the Study

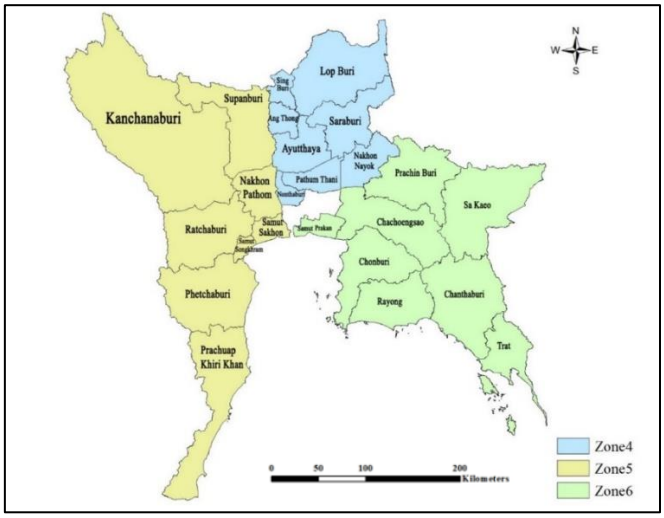


Figure 2 Locations of Regional Health Zone 4, 5 and 6

RESULTS AND DISCUSSIONS

The current situation of NCDs prevalence rates were significantly increasing in hypertension and diabetes from 2019 to 2023 while there was a little increase in coronary heart diseases as shown in Figure 3. The number of patients who suffered from hypertension gradually rose from approximately 1,800,000 patients in 2019 to 2,000,000 patients in 2023. The trend of diabetes was similar with that of hypertension, which started at nearly 800,000 patients in 2019 and increased to 1,000,000 in 2023. While 3 diseases revealed a steady growth in the prevalence of NCDs for 5 years, the most widespread disease was in hypertension cases and coronary heart diseases remained the lowest occurrence. Due to the data limitation of environmental and social factors, the data in 2023 for all diseases and factors were analyzed in this study.

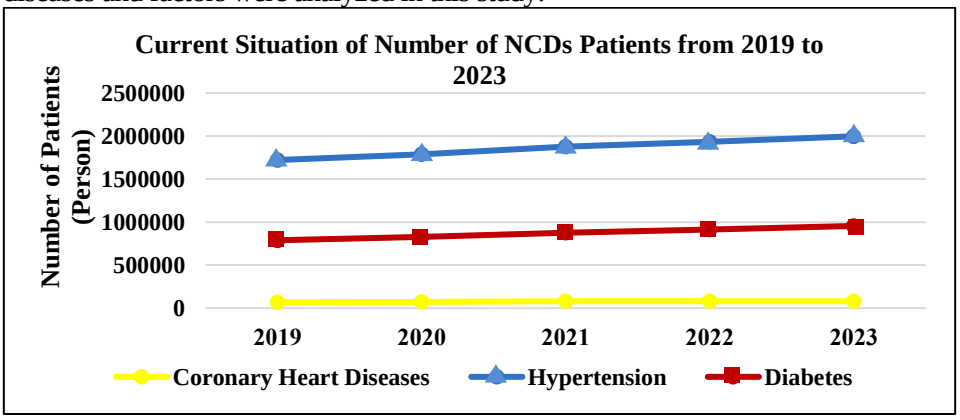


Figure 3 Current Situation of NCDs Prevalence from 2019 to 2023

Spatial Distribution Analysis

The spatial distribution patterns revealed that the lighter to darker color of the regions can be defined as the pattern of lowest to highest value of maps, except map (f) and (g) in Figure 4. The map (f) was illustrated as the graduated symbol of the pattern, showing the biggest cycle of a huge number of hospitals and smallest cycle directing the minimum number of hospitals. And the map (g) was described the classification of landuse; agriculture with yellow color, forest showing green color, miscellaneous referring brown color, urban highlighting with red color and water body with blue color. As result of the analysis, the distribution pattern of coronary heart diseases, hypertension and diabetes showed that a significant number of patients were highlighted with the darkest color, suggesting regions with greater prevalence of NCDs. The highest severe affected NCDs have been widespread in Mueang Nonthaburi District with 4,015 coronary heart diseases patients and Mueang Samut Prakan District with 42,690 patients and 23,049 patients who suffered hypertension and diabetes respectively. Among 3 diseases, the high prevalence rate of hypertension and diabetes were nearly identical in shown in map (b) and (c), especially in these provinces: Nonthaburi Province in Zone 4, Ratchaburi, Samut Sakhon and Nakhon Pathom Provinces in Zone 5 and Chonburi, Samut Prakan and Rayong Provinces in Zone 6. Combined with landuse applications, the red color of urban

areas mostly occurred in these provinces. It proved that the provinces in Thai Health 2023 report [3] as having the highest levels of hazardous industrial waste were definitely same with the provinces of highest prevalence NCDs rate in Zone 6. When the lowest prevalence rate of NCDs across the provinces and districts were analyzed, Ko Kut District in Trat Province is the lowest patients for all 3 diseases, showing the coastal regions suffering low incidence case of NCDs. And the findings from the urban density and total population maps were that the dark red regions of urban density absolutely aligned with the some of the dark green regions of total population, showing that areas with high total population occupied high urban-density area. The significant volume of total population was found in Mueang Nonthaburi District with 371,899 people having the highest urban area density. For hospital mapping, larger circles represented the districts with more hospitals including rural and sub-district areas. The highest number of hospitals with 37 hospitals in total can be found in Mueang Nakhon Pathom District, indicating most hospitals were found in places where NCDs were most prevalent. For the social factors, the highest income level was in Khao Khitchakut District, Chanthaburi Province with 501,573 baht annually, showing a low prevalence rate of NCDs in high-income region. From the environmental point of view, another indicator of PM2.5 pattern highlighted regions with high PM 2.5 concentrations, particularly in Phraphutthabat District, Saraburi Province with the highest level of 30.686 µg/m^3, where transportation and agricultural burning can be contributed to poor air quality. The lowest PM2.5 levels with 16.325 µg/m^3 was observed in Mueang Trat District which is near coastal areas, resulting fewer pollution sources. Finally, the spatial distribution patterns of NCDs and risk factors can be pointed out that the most widespread distribution pattern mostly happened in Mueang (City) of the districts and Nonthaburi, Ratchaburi, Samut Sakhon, Nakhon Pathom, Chonburi, Samut Prakan, Rayong and Saraburi provinces should be focused on handling of NCDs controlling process based on the results of spatial distribution pattern.

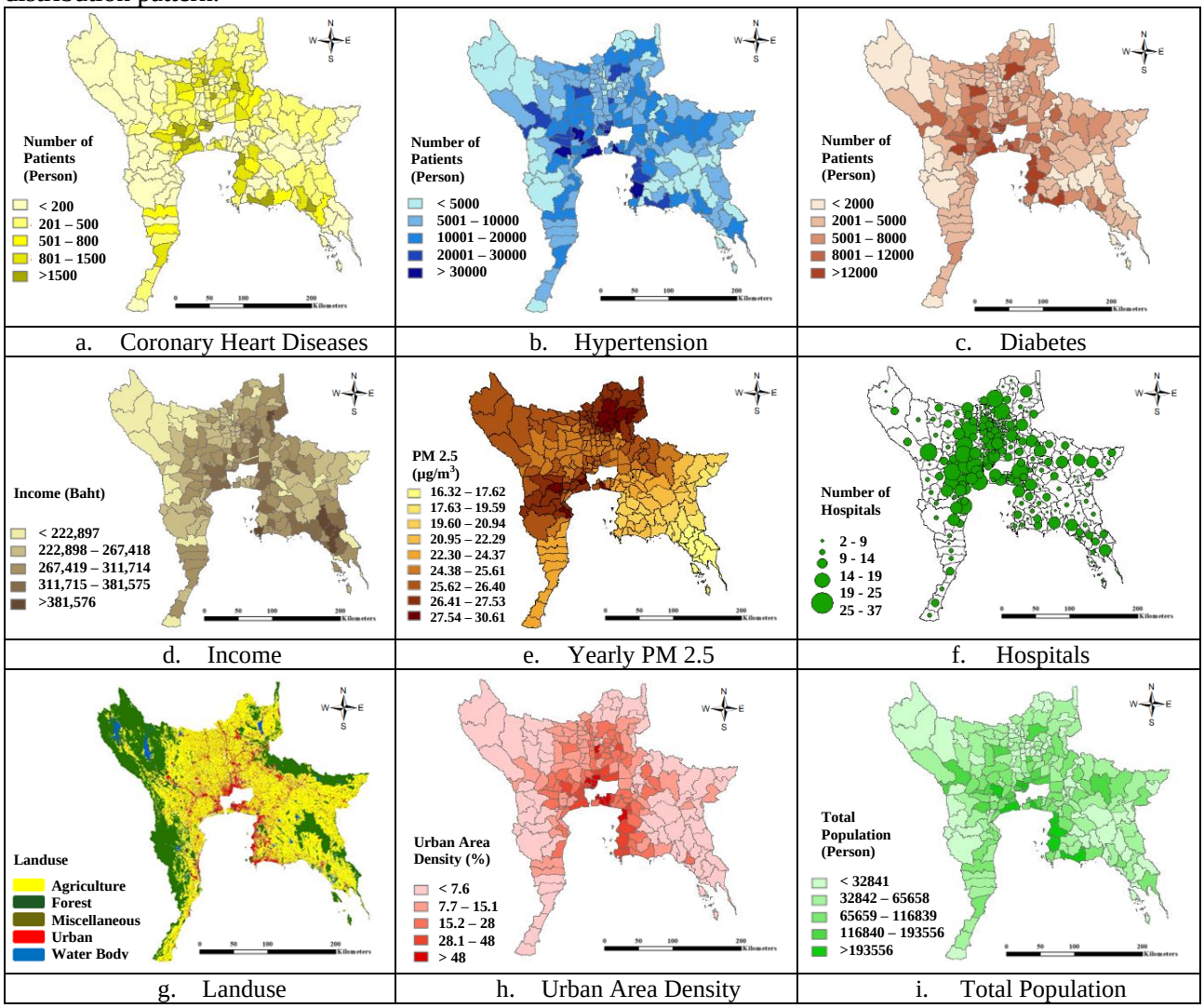


Figure 4 Maps of Spatial Distribution Patterns of NCDs and related Factors in 2023

Additionally, PM2.5 is one of the critical environmental factors influencing the patterns of NCDs. According to the air pollution concentration equivalent to Air Quality Index (AQI) defined by PCD, the range of PM 2.5 (0 to 15 µg/m^3) defined with blue color code which is showing excellent level of very good air quality, followed by 15.1 to 25 µg/m^3 with green color of defining satisfactory for good air quality, 25.1 to 37.5 µg/m^3 with yellow color with moderate level of air quality, 37.6 to 75 µg/m^3 with orange color of indicating unhealthy air quality and above 75.1 µg/m^3 with red color which is mentioned to avoid outdoor activities and wear masks due to very unhealthy air conditions [7]. The monthly distribution pattern of PM 2.5 value in 2023 showed the same defined value of AQI value in Figure 5. It revealed that the PM 2.5 value captured during January, February, March, April and December in 2023 exceeded the standard value of 37.5 µg/m^3, covering the orange color in most districts in the maps. In the remaining months, monthly PM 2.5 value captured the low value which was below the standard number of 37.5 µg/m^3. Therefore, further analysis was carried out in 5 months which were over the standard limit of AQI.

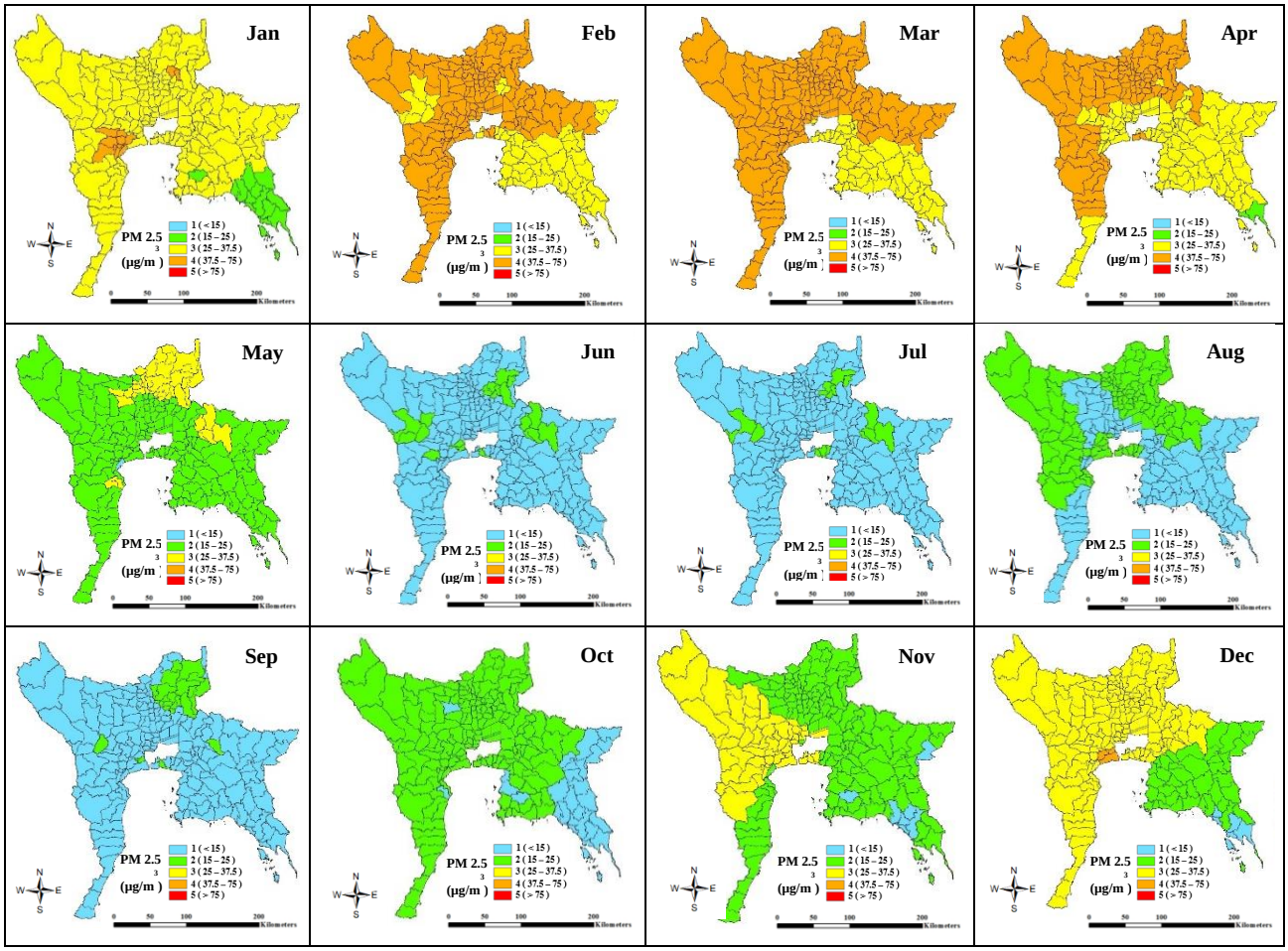
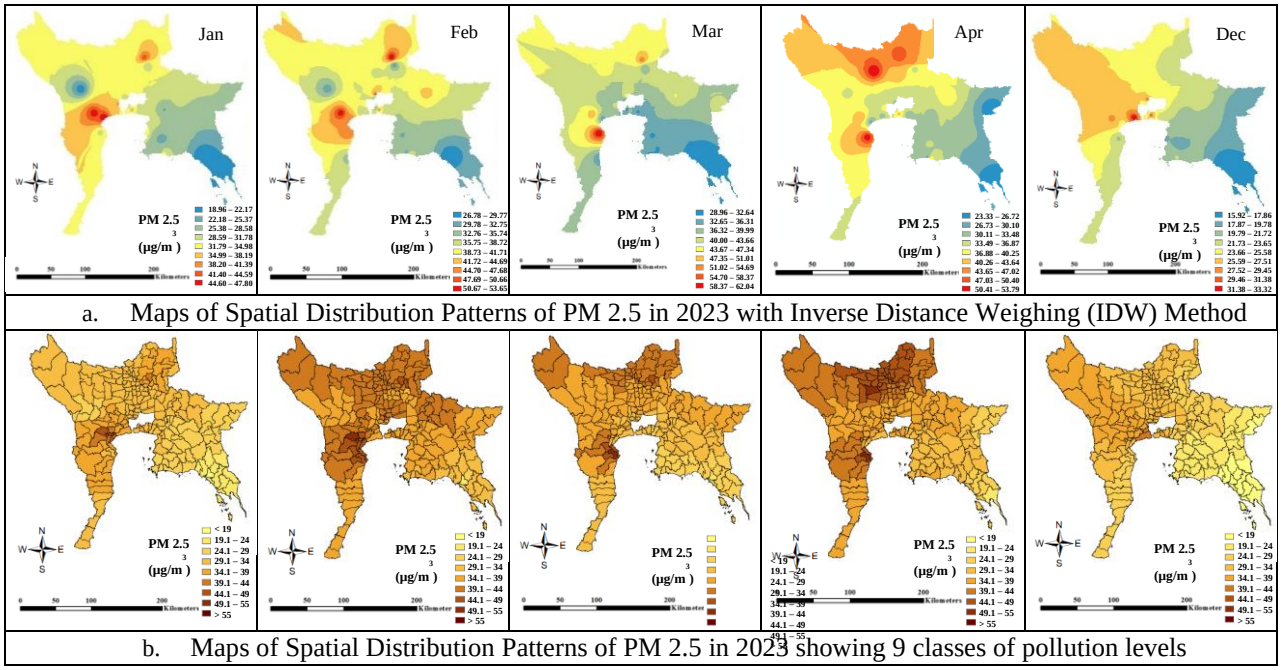


Figure 5 Maps of Spatial Distribution Patterns of Monthly PM 2.5 Value in 2023 according to AQI of PCD

The maps of spatial distribution patterns of PM 2.5 across (January, February, March, April and December) in 2023 by using IDW method were illustrated in map (a). High concentrations of PM 2.5 were shown in red while low concentrations were displayed in blue color. From IDW mapping, the worse air quality with red color occurred in some specific regions. The most significant regions polluted with bad air pollution were around Ratchaburi, Phetchaburi and Saraburi provinces in January, February and March with red and orange color. When the month was entered into April, severe pollution had happened near Supanburi, Phetchaburi and Kanchanaburi provinces. In December, the distribution of PM 2.5 was mostly directed to Samut Sakhon, Kanchanaburi and Ratchaburi provinces. When the months which received severe air contamination were identified, the air pollution levels which are above the standard limit of 37.5 µg/m^3 mostly happened in the months of February, March and April. In addition, the PM 2.5 values were classified into 9 classes (from 19 to 55 µg/m^3) to highlight the specific regions where suffered the worst air pollution across the months as shown in image (b). When the spatial distribution patterns of PM 2.5 in January were analyzed, it was observed that the hazardous air pollution levels over 37.5 µg/m^3 was recorded in Mueang

Samut Songkhram District at 45.27 µg/m^3. In February, Mueang Ratchaburi District was obtained the highest polluted level of 49.55 µg/m^3. Notably, Mueang Phetchaburi District recorded the highest values in March with 58.13 µg/m^3 and in April, the highest air quality of 51.51 µg/m^3 was reached in Mueang Supanburi District. In December, Mueang Samut Sakhon District experienced the region which affected the most air pollution with 41.29 µg/m^3. Therefore, the peak air pollution which causes unhealthy conditions for the community mostly occurred in winter season and Mueang Districts of Samut Songkhram, Ratchaburi, Phetchaburi, Supanburi and Samut Sakhon Provinces in Zone 5 were significantly polluted the worse air concentrations among districts as illustrated in Figure 6.



a. Maps of Spatial Distribution Patterns of PM 2.5 in 2023 with Inverse Distance Weighing (IDW) Method

b. Maps of Spatial Distribution Patterns of PM 2.5 in 2023 showing 9 classes of pollution levels

Figure 6 Maps of Spatial Distribution Patterns of PM 2.5 in 2023 showing the months which are over standard value (37.5 µg/m^3)

Correlation Analysis

Once the spatial distribution pattern of NCDs and risk factors was accomplished, the specific provinces to be focused on controlling NCDs were pointed out. Continuously, the correlation analysis was conducted to analyze the range of influence and relationship between factors. The sign of correlation coefficient showed the direction of the relationship between variables and the magnitude of correlation indicated the strength of relationship. If the range is between 0.1 and 0.3, it means weak correlation. The value is from 0.3 to 0.5 which indicates moderate correlation and if it is greater than 0.5, it directs strong correlation [8]. Another study analyzed that NCDs were statistically correlated with unmodifiable risk factors which were affecting the prevalence of NCDs by surveying local population [9]. Due to this fact, a correlation analysis was carried out to understand the influence of factors statistically. According to Table 1, the number of patients who suffered hypertension exhibited a strong and statistically significant correlation with all factors (All Age Group, Number of Hospitals and Urban Area), except PM 2.5 and income. Diabetes was high correction with factors except PM 2.5 and income also while coronary heart diseases were highly correlated with only the working age and elderly age group. While only PM 2.5 was not statistically correlated with the prevalence of NCDs, it is recommended to consider other influenced factors such as transportation, industries and wind direction which can impact on the pattern of air pollution. One of the social factors – income was low correlated with diseases, showing that income is not a strong indicator for NCDs. As a conclude, Hypertension and Diabetes have the highest correlations across multiple factors, indicating their strong association with both population growth and aging demographics, emphasizing the need for targeted healthcare policies in urban and aging populations.

Table 1 Correlation of NCDs and Factors

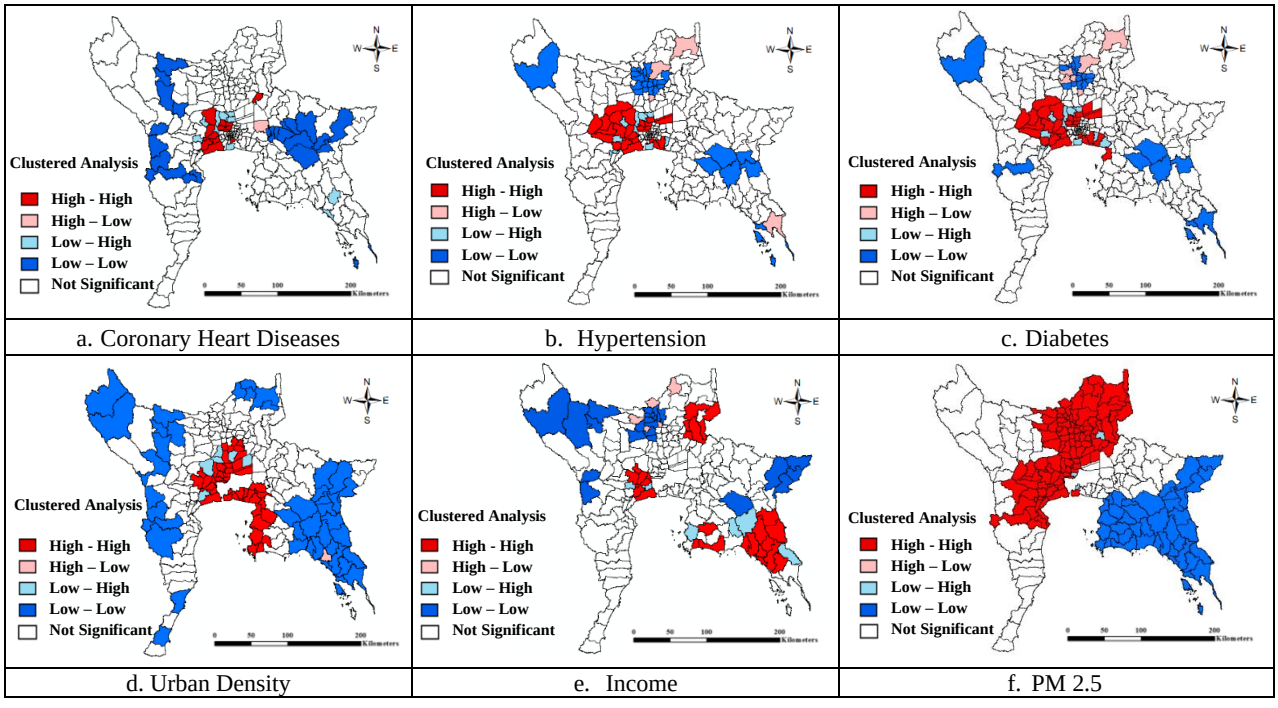
Factors	Coronary Heart Diseases	Hypertension	Diabetes
Less than 16 years	0.495**	0.88**	0.89**
16 – 60 years	0.646**	0.929**	0.936**
Greater than 60 years	0.704**	0.951**	0.951**
No. of Hospitals	0.367**	0.708**	0.676**
Urban Areas	0.392**	0.742**	0.743**
PM 2.5	-0.12	0.125	0.119
Income	0.223**	0.168*	0.174*

** Correlation is significant at the 0.01 level (2-tailed).

* Correlation is significant at the 0.05 level (2-tailed).

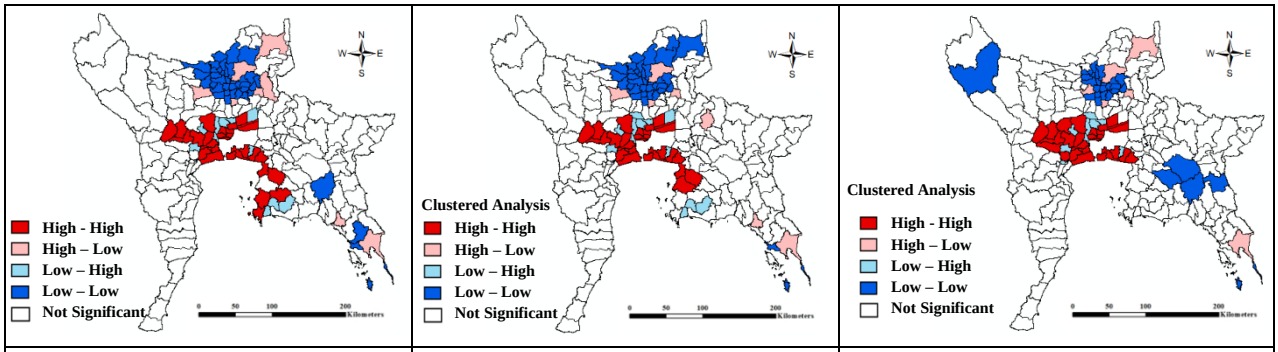
Clustered Analysis

The clustered analysis described the spatial clustering pattern that indicated the relationship of NCDs and risk factors in the study area. The cluster mapping illustrated that High-High was specifically defined as the areas surrounded by other high value. Similarly, the areas with low values surrounded by low value were described as Low-Low. High-Low means the high areas surrounded by other low values and Low-High means the low areas surrounded by high values. In this study, High-High and Low-Low clusters were considered to define the groups of regions which were affected by NCDs and risk factors. As illustrated in Figure 7, the high-high clusters of coronary heart diseases, hypertension and diabetes predominantly happened in the Bangkok Metropolitan Regions (BMR) - Nakhon Pathom, Samut Sakhon, Samut Prakan and Nonthaburi regions, demonstrating areas of a high prevalence of NCDs with similar spatial patterns while low-low cluster of diseases mostly occurred in And Thong, Ayutthaya, Chanthaburi, Chachoengsao and Kanchanaburi regions. Compared to all diseases, the high-high clustered regions of hypertension and diabetes were more widespread than those of coronary heart diseases. Analyzing the factors, the clustered risk factors described that urban areas were predominantly concentrated in the BMR, Chonburi and Rayong, which corresponded to densely populated areas. Clustered populations who are less than 60 years were also similar pattern of urban density, but the High-High cluster pattern of elderly people was not found in Chonburi and Rayong. Therefore, the NCDs pattern was mostly influenced by the older people group. While certain red colors of PM2.5 concentrations overlapped with urbanized and highly populated regions, one of the highly clustered groups of income – Chanthaburi province was found in the regions of low prevalence of NCDs, pollution and good air quality. When examining the link between diseases and risk factors, the high-high clustered pattern of NCDs (a, b and c) correlated with urban density (d) and aging communities (g, h and i) regions and it was found that the region which received highest income was not much suffered from NCDs.



a. Coronary Heart Diseases | b. Hypertension | c. Diabetes

d. Urban Density | e. Income | f. PM 2.5



g. Population who are less than 16 years | h. Population who are 16 – 60 years | i. Population who greater than 60 years

Figure 7 Maps of Cluster Analysis of NCDs and Risk Factors

CONCLUSION

The trend of prevalence rate of NCDs was gradually increasing so the prioritized provinces should be tackled and controlled to reduce the causes of NCDs. From this study, social factors and urban areas were mostly influenced by prevalence of NCDs and air pollution was hazardous in winter season of the year. By analyzing spatial distribution patterns and cluster analysis for both NCDs and factors, the severely affected regions - Mueang Districts and Nonthaburi, Ratchaburi, Samut Sakhon, Nakhon Pathom, Chonburi, Samut Prakan, Rayong and Saraburi Provinces should be prioritized to support the effective action plan environmentally, socially and economically. Even though correlation analysis cannot statistically provide proven results between factors, pattern of mapping can point out the spread of diseases and influencing factors across the specific and affected provinces. By applying GIS in the health field, it enables the visualized mapping and decision support systems to the policy makers for the controlling of NCDs together with the Ministry of Public Health.

ACKNOWLEDGEMENT

The researcher would like to express gratitude to Faculty of Engineering, Mahidol University to support the precious guidance and encouragement through the journey of the research. And the author thanks the Office of the Permanent Secretary, Ministry of Natural Resources and Environment for providing GIS data and information.

REFERENCE

[1] WHO. 2016. Noncommunicable Diseases. Available: https://www.who.int/news-room/fact-sheets/detail/noncommunicable-diseases. [Accessed 20 July 2024].

[2] Ministry of Public Health of Thailand, W.H.O., the United Nations Development Programme (UNDP), and the United Nations Inter-Agency Task Force (UNIATF). 2021. Prevention and Control of Noncommunicable Diseases in Thailand: The Case for Investment.

[3] Institute for Population and Social Research. 2023. Thai Health 2023: Thailand's Commitment in COP (Conference of Parties) & Responses to Climate Change Mahidol University. Nakhon Pathom.

[4] WHO. 2017. Noncommunicable Diseases. Available: https://www.who.int/health-topics/noncommunicable-diseases#tab=tab. [Accessed 20 July 2024].

[5] HDC. Health and Medical Data Center. Available: https://hdc.moph.go.th/center/public/standard-report/3e9b22afedc152096c7caf484c7d9629/6a1fdf282fd28180eed7d1cfe0155e11. [Accessed 10 September 2024].

[6] LDD. Soil and Landuse Information Service. Available: https://dinonline.ldd.go.th/Default.aspx. [Accessed 20 October 2024].

[7] Air4Thai. Air4Thai. Available: http://air4thai.pcd.go.th/webV3/#/History. [Accessed January 2025].

[8] Kent State University. 2021. Pearson Correlation. Available: https://libguides.library.kent.edu/SPSS/PearsonCorr. [Accessed 3 Jan 2025].

[9] Nawamawat, J., Prasittichok, W., Prompradit, T., et.al. 2020. Prevalence and characteristics of risk factors for non-communicable diseases in semi-urban communities: Nakhonsawan, Thailand. Journal of Health Research, Vol. 34. No. 4, 2020; 295-303.

21R4-06

Assessing Knowledge, Attitudes, and Practices Regarding $PM_{2.5}$ Among Students at Chulalongkorn University: Implications for Public Health Policy and Education.

Sophara Chhim[1*] Thammanitchpol Denpetkul[2] and Achariya Suriyawong[3]

[1]Master student; [1*]Department of Environmental and Sustainable Engineering, Faculty of Engineering, Chulalongkorn University, Bangkok 10330, Thailand.*

[2] Asst. Professor, [2]Department of Social and Environmental Medicine, Faculty of Tropical Medicine, Mahidol University, Bangkok 10400, Thailand

[3] Asst. Professor, [3]Department of Environmental and Sustainable Engineering, Faculty of Engineering, Chulalongkorn University, Bangkok 10330, Thailand.

E-mail: Sachariya@yahoo.com

ABSTRACT

$PM_{2.5}$ pollution remains a critical environmental and public health issue, particularly in rapidly urbanizing regions like Bangkok, Thailand. This study aimed to examine the Knowledge, Attitudes and Practice (KAP) regarding $PM_{2.5}$ among university students and to explore the factors associated with this KAP. A cross-sectional survey was conducted, involving demographic profiling and assessments of students' knowledge (13 items), attitudes (16 items), and practices (10 items) related to $PM_{2.5}$. The survey employed a combination of three-option questions for knowledge and a 5-point Likert scale for attitudes and practices. Data analysis included descriptive statistics, correlation and regression analysis using IBM SPSS software. Results from this study indicated a moderate level of knowledge and practice concerning $PM_{2.5}$ among the students, but high preventive attitudes. The average knowledge score was 10 (SD = 2) out of 13, translating to an accuracy rate of 77.3%, while attitudes and practices scored 87.02% and 75.77%, respectively. Correlation analyses revealed moderate to strong positive relationships between knowledge and practices, and between attitudes and practices, suggesting that enhanced knowledge and positive attitudes significantly impact preventive practices. Additionally, attitudes were positively associated with the Eastern region ($p = 0.027$) and Central region ($p = 0.033$). Preventive practices were positively associated with faculty of engineering ($p = 0.019$) and art ($p = 0.023$), and who is having rash problems ($p = 0.038$). These findings support the potential of educational interventions in improving $PM_{2.5}$ preventive behaviors among students, highlighting the importance of integrated educational and community engagement strategies to effectively address the challenges of air pollution.

Keywords: $PM_{2.5}$, Knowledge, Attitudes, Preventive Practice, Students

INTRODUCTION

Air pollution is a pressing environmental concern that demands attention at local, regional, and global levels. Bangkok, Thailand's capital, has undergone rapid development and accelerated urbanization, exacerbating environmental concerns. For years, the city has faced significant air pollution challenges [1]. The South Asian region faces significant air pollution challenges stemming from factors such as agricultural activities, rising vehicle emissions, rapid urbanization, and population growth. It is crucial to recognize that these problems transcend national borders, heightening their urgency [2, 3]. In 2017, the average PM2.5 concentrations in the Bangkok Metropolitan Region (BMR) surpassed Thailand's standard of 50 μg/m³ for 24-hour exposure on approximately 40 to 50 days between January and March [1]. According to recent assessments by the World Health Organization, air pollution has been recognized as the world's most significant environmental health threat, underscoring its severe impact on public wellbeing [4]. Exposure to polluted air can result in a variety of negative health impacts, such as respiratory problems, heart-related conditions, and even the development of cancer [2]. Research has shown that some individuals face greater exposure to air pollution due to the nature of their occupations [5-7]. A recent study indicates that implementing strategies at both the individual and community levels can help mitigate health issues caused by air pollution [8]. To effectively develop these strategies, it is crucial to comprehend the knowledge, attitudes, and practices related to air pollution at both the individual and community levels. A cross-sectional study revealed that although 75% of people in the community are concerned about air pollution, they are

uncertain about how to address it. [9].

The high levels of air pollution Thailand, driven by heavy traffic, industrial emissions, and open burning, may pose significant health risks to university students. Given their frequent transitions between indoor and outdoor environments, these students are particularly susceptible to the variable concentrations of $PM_{2.5}$ they encounter. Furthermore, there is limited research on students' knowledge, perception and preventive practices regarding $PM_{2.5}$ exposure in Thailand. This study aims to examine the Knowledge, Attitude and Practice (KAP) regarding $PM_{2.5}$ among university students and explore the factors associated with this KAP in order to develop more precise strategies leading to enhance effective protective practices and improved public health outcomes.

METHODOLOGY

The research was conducted through the survey at Chulalongkorn University, focusing on students, and data collection was conducted with a pilot testing include 60 samples. The questionnaire was designed to comprehensively measure the four dimensions of interest such as demographic information, knowledge about $PM_{2.5}$ pollution, attitudes towards $PM_{2.5}$ pollution, and practices adopted to mitigate exposure:

- Section 1: Demographic Characteristics - This section collects basic demographic data and health status to provide context about the respondents (e.g., age, gender, education level, income, etc.).
- Section 2: Knowledge about $PM_{2.5}$ - The Items were designed to assess students' understanding of $PM_{2.5}$, including its sources, health risks, and using a 3-point Likert scale (e.g., "Is $PM_{2.5}$ a fine particulate matter in the air?", with the options: "Yes", "No", "Not sure"). A response of "Yes" will receive a score of 1, while "No" and "Not sure" will each receive a score of 0. A higher score indicates a more comprehensive understanding of $PM_{2.5}$ pollution, its sources, effects, and the necessary preventive measures.
- Section 3: Preventive Attitude towards $PM_{2.5}$ - This section assesses the students' attitudes toward preventive measures against $PM_{2.5}$ pollution. It is structured around a series of questions designed to assess respondents' perceptions and attitudes using a 5-point Likert scale (e.g., "When $PM_{2.5}$ levels are high, do you feel concerned about its impact on your health?"). The scale ranges from 5 for "Strongly Agree" to 1 for "Strongly Disagree". A higher score indicates a better attitude about $PM_{2.5}$.
- Section 4: Preventive Practices for $PM_{2.5}$ - This section was focused on behaviors and actions taken by students to protect themselves from $PM_{2.5}$ exposure, using a 5-point Likert scale from 1 to 5 (coded as follows: "Never" is scored as "1," "Rarely" as "2," "Sometimes" as "3," "Often" as "4," and "Always" as "5"). A higher score indicates better preventive practices regarding $PM_{2.5}$.

The data underwent a thorough statistical analysis using various software tools, beginning with essential data cleaning and organization processes. Once prepared, the data was analyzed using IBM SPSS software to compute descriptive statistics, including percentages, means, and standard deviations for demographic characteristics and KAP scores. To explore the relationships among these KAP measures, Pearson's correlation was employed for data exhibiting linearity, while Spearman's Rank Correlation Coefficient was utilized for non-parametric data. Spearman's rank, a non-parametric measure of correlation, does not require the data to be normally distributed, making it ideal for datasets that do not meet the normality assumptions necessary for Pearson's correlation. Furthermore, both bivariate and multivariate regression analyses were conducted to investigate the factors influencing the KAP scores, with statistical significance set at $p < 0.05$. Bivariate analysis is pivotal for evaluating the direct relationship between two variables. In contrast, multivariate regression is essential for including multiple variables within the same model, allowing for a comprehensive understanding of the impacts of various independent variables on a dependent variable while controlling for other potential confounders.

RESULTS AND DISCUSSIONS

The pilot survey, conducted among 60 university students at Chulalongkorn University, revealed a predominance of female participants, with 61.67% females and 38.33% male respondents. The average distribution was 20 years old. In term of faculty of study, most student are in the Engineering, with 43.33% following by science accounted for 26.67% and 18.33%, while school of agriculture resources was 11.67%. Regarding education level, most respondents were in the first year of their bachelor's degree, accounting for

56.67%, followed by the fourth year with 25%, the second year with 11.67%, and the third year with 6.67%. Financially, 50% of the student receive a monthly allowance between 50,001 – 10,000 Thai baht, and 25% received 10,001 – 15,000 Thai baht, while 0 – 5,000 (18.33%) and higher than 15,000 (6.67%). The majority of the student are from central region of Thailand (55%), Northeastern region, Northern region, Southern region are the same percentage (11.67%) and Western region accounted for 3.33%. Additionally, the students are reported about their health status related with $PM_{2.5}$ with 51.67% having eye irritates, 28% rash, 60% allergic, 51.67% coughing problem, 73.33% have sneezing problem, chronic disease 5% and cardiovascular disease 0% (table 1).

Table 1 Descriptive demographic characteristic

Variables		**N**	**%**
Gender	Female	37	61.67
	Male	23	38.33
Faculty	Engineering	26	43.33
	Faculty of Arts	11	18.33
	School of agricultural resources	7	11.67
	Science	16	26.67
Education level	Bachelor Year 1	34	56.67
	Bachelor Year 2	7	11.67
	Bachelor Year 3	4	6.67
	Bachelor Year 4	15	25
Monthly income (THB)	0- 5,000	11	18.33
	5,001-10,000	30	50.00
	10,001-15,000	15	25.00
	15,001-35,000	4	6.67
Eye irritates	No	29	48.33
	Yes	31	51.67
Rash	No	43	71.67
	Yes	17	28.33
Allergic to dust	No	24	40.00
	Yes	36	60.00
Cardiovascular disease	No	60	100.00
	Yes	0	0.00
Coughing problem	No	29	48.33
	Yes	31	51.67
Sneezing problem	No	16	26.67
	Yes	44	73.33
Chronic disease	No	57	95.00
	Yes	3	5.00
Origin	Central region	33	55
	Eastern region	4	6.67
	Northeastern region	7	11.67
	Northern region	7	11.67
	Southern region	7	11.67
	Western region	2	3.33

The table 2 show the mean score of each item of knowledge about $PM_{2.5}$, which is K1 to K16, where a score closes to 1 indicates a correct understanding and a score close to 0 indicates a lack of knowledge. The knowledge mean score show a variation from low to good. The data for K10 indeed shows an interesting trend where the mean (0.32) is significantly lower than the standard deviation (0.47). This indicates that there is a high variability in responses and that most respondents likely answered “no” and “not sure”, while the question is "Is WHO's $PM_{2.5}$ safety limit 5 micrograms/m^3 on an annual average?". The results regarding attitudes and preventive practice, using a 5-point Likert scale, indicates that there is a high mean score

among 16 items in $PM_{2.5}$ in preventive attitudes suggesting that students tend to have a good perception. Furthermore, the mean score of items in the preventive practice range from moderate to high score, suggesting a variation preventive practice regarding to $PM_{2.5}$ prevention among students.

Table 2 Summary statistic of factor consider in survey

Factor	Item	Mean	SD	Factor	Item	Mean	SD	Factor	Item	Mean	SD
Knowledge	K1	0.98	0.13	Attitudes	A1	4.35	0.78	Preventive Practice	P1	3.13	1.08
	K2	0.83	0.38		A2	4	0.88		P2	3.77	1.16
	K3	0.98	0.13		A3	4.6	0.69		P3	3.20	1.48
	K4	0.83	0.38		A4	4.17	0.92		P4	4.02	1.19
	K5	0.73	0.45		A5	4.63	0.76		P5	3.98	1.07
	K6	0.88	0.32		A6	4.37	1.16		P6	4.07	0.86
	K7	0.72	0.45		A7	4.02	0.87		P7	3.75	1.11
	K8	0.70	0.46		A8	4.25	0.99		P8	3.95	1.00
	K9	0.83	0.38		A9	4.22	0.76		P9	3.80	1.10
	K10	0.32	0.47		A10	4.12	1.03		P10	4.22	0.83
	K11	0.70	0.46		A11	4.58	0.74				
	K12	0.63	0.49		A12	4.60	0.79				
	K13	0.92	0.28		A13	4.63	0.76				
					A14	4.62	0.88				
					A15	4.13	0.85				
					A16	4.33	0.88				

The average knowledge score was 10 (SD = 2) out of 13, reflecting an overall accuracy rate of 77.3%; The relatively high mean score of 4.35 out of 5 for $PM_{2.5}$ preventive attitudes (87.02%) is encouraging as it reflects a strong positive disposition towards engaging in behaviors that mitigate exposure to $PM_{2.5}$. The practice score, with an average of 3.8 out of 5 accounting for 75.77%, indicates moderate engagement in preventive practices. This score highlights a discrepancy between knowledge and attitudes versus actual practices (table 3).

Table 3 The score of knowledge, attitudes and preventive practice

Variables	Mean	Standard Deviation	Percentages (%)
$PM_{2.5}$ Knowledge	10	2	77.3
$PM_{2.5}$ Preventive Attitude	4.35	0.58	87.02
$PM_{2.5}$ Preventive Practice	3.8	0.7	75.77

$PM_{2.5}$ = particulate matter with a diameter of 2.5 μm or less.

The results of Spearman rank correlation indicate that $PM_{2.5}$ knowledge is moderate positively correlate with the preventive practice $r = 0.303$ ($p < 0.05$), and there is a moderate positive correlation between knowledge and practice $r = 320$ ($p < 0.05$). Furthermore, $PM_{2.5}$ preventive attitudes is positively correlated to preventive practice $r = 0.473$ ($p < 0.01$) (table 3). Our results show that, students $PM_{2.5}$ knowledge has a significant positive impact on their $PM_{2.5}$ attitudes toward preventive and $PM_{2.5}$ Preventive Practice, and students $PM_{2.5}$ attitude toward preventive has a strong positive correlation with their $PM_{2.5}$ preventive practice. Our findings indicate that enhancing students' knowledge of $PM_{2.5}$ and their attitudes towards preventive measures can lead to more effective $PM_{2.5}$ prevention practices among them [10]. This results also align with previous research, indicates that an individual's understanding of air pollution and their attitudes towards preventing it can influence their intentions to engage in behaviors aimed at controlling and mitigating air pollution [11]. These findings suggest that enhancing knowledge and attitudes towards

$PM_{2.5}$ can significantly improve preventive practices among students. This aligns with previous research indicating that better understanding and positive attitudes towards air pollution can profoundly influence proactive behaviors aimed at reducing exposure and mitigating its effects. Thus, educational interventions that effectively increase awareness and foster favorable attitudes could be key strategies in enhancing $PM_{2.5}$ preventive practices among university students

Table 4 Correlation analysis of knowledge, attitude and preventive practice

Variable	$PM_{2.5}$ Knowledge (K)	$PM_{2.5}$ Preventive Attitude (A)	$PM_{2.5}$ Preventive Practice (P)
$PM_{2.5}$ Knowledge (K)	1	.303*	.320*
$PM_{2.5}$ Preventive Attitude (A)	--	1	.473**
$PM_{2.5}$ Preventive Practice (P)	--	--	1

*. Correlation is significant at the 0.05 level (2-tailed).
**. Correlation is significant at the 0. 01 level (2-tailed).

From the bivariate and multivariate regression analysis, no demographic factors were found to influence student knowledge about $PM_{2.5}$, which is why knowledge about $PM_{2.5}$ was not included as the table. Table 5 presents the results of regression analysis predicting attitudes toward $PM_{2.5}$ prevention. The analysis demonstrates that several factors are positively associated with attitudes, including the Eastern region ($\beta = 2.27$, $p = 0.027$) and the Central region ($\beta = 2.19$, $p = 0.033$), compared to the Southern region of Thailand. This pilot study revealed that students from the Eastern and Central regions of Thailand have a more preventive attitude toward $PM_{2.5}$ compared to students from the Southern region. The Central and Eastern regions, especially around Bangkok and nearby areas, often face significant air pollution challenges. The increased exposure to $PM_{2.5}$ and other pollutants in these areas can heighten public awareness and concern, leading to more proactive attitudes toward pollution prevention. Meanwhile, other variables, including gender, academic faculty, income, and health conditions, showed negligible or non-significant influences on the results. Future studies will analyze these factors with a more sample size to further explore other factors that may influence attitudes toward prevention.

Table 5 Regression analysis predict attitudes regarding $PM_{2.5}$ prevention

Variable	Mean (SD)	Bivariate Regression					Multivariate Regression				
		B	SE	Beta	t	p-value	B	SE	Beta	t	p-value
Gender											
Male	68.62 (10.07)	Ref.					Ref.				
Female	71.22 (7.96)	-2.60	2.48	-0.14	-1.05	0.299	3.1	4.0	0.2	0.8	0.448
Faculty											
Science	69.06 (8.13)	Ref.					Ref.				
Engineer	71.04 (6.2)	1.98	3.01	0.11	0.66	0.515	-0.1	5.3	-0.09	-0.09	0.991
SAR	68 (10.7)	-1.06	4.30	-0.04	-0.25	0.806	-0.8	6.0	-0.02	-0.1	0.898
Arts	68.09 (15.47)	-0.97	3.72	-0.04	-0.26	0.795	-3.8	5.9	-0.2	-0.7	0.518
Education Level											
Year 1	69.82 (7.9)	Ref.					Ref.				
Year 2	68.57 (9.66)	-1.17	3.89	-0.04	-0.30	0.765	-1.7	6.4	-0.1	-0.3	0.789
Year 3	69.0 (14.48)	9.26	9.61	0.13	0.96	0.339	8.9	12.2	0.1	0.7	0.469
Year 4	69.1 (7.54)	-0.67	3.04	-0.03	-0.22	0.827	5.4	5.9	0.2	0.9	0.364

SAR = School of agricultural resources, SE = Standard Error, t = t-value, Beta = Standardized Coefficients (Beta), B = Unstandardized Coefficients.

Table 5 Regression analysis predict attitudes regarding $PM_{2.5}$ prevention (continued)

Variable	Mean (SD)	Bivariate Regression					Multivariate Regression				
		B	SE	Beta	t	p-value	B	SE	Beta	t	p-value
Region											
Southern	61.71(19.92)	Ref.					Ref.				
North-eastern	71.29 (4.86)	9.57	4.91	0.33	1.95	0.056	12.2	5.9	0.4	2.1	0.046
Northern	69.86 (7.12)	8.14	4.91	0.28	1.66	0.103	11.1	7.0	0.4	1.6	0.122
Eastern	74.75 (2.75)	13.04	5.75	0.35	2.27	**0.027**	17.1	8.1	0.5	2.1	0.041
Western	73 (4.24)	11.29	7.36	0.22	1.53	0.131	9.1	10.0	0.2	0.9	0.367
Central	70.06 (7.26)	8.35	3.82	0.45	2.19	**0.033**	10.9	5.5	0.6	2.0	0.057
Income											
0 – 5,001	71.82 (6.03)	Ref.					Ref.				
5,001 - 10,000	68.87 (8.19)	-2.95	3.32	-0.16	-0.89	0.378	-1.5	4.5	-0.1	-0.3	0.744
10,001 - 15,000	71.7 (17.97)	-2.29	3.57	-0.12	-0.64	0.524	-0.7	4.7	-0.03	-0.2	0.875
Rash											
No	Ref.						Ref.				
Yes	69.1 (12.71)	-0.78	2.70	-0.04	-0.29	0.774	0.7	4.6	0.03	0.1	0.886
Breathing problem											
No	Ref.						Ref.				
Yes	69.48 (7.2)	-0.26	2.43	-0.01	-0.11	0.915	1.1	3.1	0.1	0.3	0.734

SE = Standard Error, t = t-Value, Beta = Standardized Coefficients (Beta), B = Unstandardized Coefficients.

Table 6 displays the regression analysis of the practices related to $PM_{2.5}$. Bivariate regression analysis identified several factors positively associated with practice scores, including: (i) student who study at faculty engineering ($\beta = 0.37$, $p = 0.019$), art ($\beta = 0.34$, $p = 0.023$) in reference to science, (ii) having rash problems ($\beta = 0.27$, $p = 0.038$) in reference to not having rash problem.

This pilot study indicated that students in the engineering and arts faculties engage significantly more in $PM_{2.5}$ preventive practices than faculty of science. Consequently, science students may be at a higher risk of $PM_{2.5}$ exposure compared to those studying engineering and arts. Therefore, it may be beneficial for students in the science faculty to receive more education and training regarding $PM_{2.5}$ prevention, based on the insights from this pilot study.

The positive association between having rash problems and increased $PM_{2.5}$ preventive practices suggests a direct impact of $PM_{2.5}$ on personal health that drives behavior change (e.g., students experiencing health issues like rashes, which can be exacerbated by poor air quality, are likely more motivated to adopt practices that mitigate their exposure to pollutants). These results support earlier research that having specific health conditions is positively associated with practices related to air pollution [12]. The link between health problems caused by poor air quality and heightened preventive measures underscores the need to incorporate health education within wider environmental protection initiatives. This strategy could greatly improve student participation in preventive behaviors, particularly in areas at greater risk.

Future research will involve increasing the sample size to confirm these initial results and investigate further factors that shape student knowledge, preventive attitudes and behaviors. These expanded studies are crucial for gaining a deeper insight into the various factors that impact student responses to $PM_{2.5}$.

Table 6 Regression analysis predict preventive practice regarding $PM_{2.5}$

Variable	Mean (SD)	Bivariate Regression					Multivariate Regression				
		B	**SE**	**Beta**	**t**	**p-value**	**B**	**SE**	**Beta**	**t**	**p-value**
Gender											
Male	37.35 (8.37)	Ref.					Ref.				
Female	38.22 (5.72)	0.87	1.82	0.06	0.48	0.635	0.50	2.59	0.04	0.19	0.848
Faculty											
Science	34.54 (7.43)	Ref.					Ref.				
Engineer	39.5 (6.21)	5.00	2.07	0.37	2.42	**0.019**	5.17	3.40	0.38	1.52	0.136
SAR	35.57 (5.91)	1.07	2.95	0.05	0.36	0.718	-0.66	3.85	-0.03	-0.17	0.865
Arts	40.45 (6.03)	5.96	2.55	0.34	2.34	**0.023**	2.84	3.76	0.16	0.76	0.455
Education Level											
Year 1	38.15 (6.36)	Ref.					Ref.				
Year 2	31.86 (8.31)	-6.2	2.68	-0.30	-2.3	0.02	-3.29	4.10	-0.16	-0.80	0.422
Year 3	39.75 (5.37)	2.95	6.61	0.06	0.45	0.657	3.56	7.84	0.07	0.45	0.653
Year 4	40.38 (5.81)	2.33	2.09	0.14	1.12	0.269	2.11	3.77	0.13	0.56	0.579
Region											
Southern		Ref.					Ref.				
North-eastern	37.29 (5.52)	-0.67	2.75	-0.03	-0.24	0.807	0.75	3.7	0.04	0.203	0.840
Northern	35.8 (99.26)	-2.3	2.74	-0.11	-0.83	0.406	1.7	4.28	0.08	0.40	0.688
Eastern	40 (10.92)	2.26	3.53	0.08	0.64	0.524	2.44	4.66	0.09	0.53	0.602
Western	40 (2.82)	2.2	4.92	0.06	0.44	0.658	5.87	6.00	0.15	0.98	0.332
Central	38.09 (6.25)	0.46	1.78	0.03	0.26	0.79	1.58	3.38	0.24	0.98	0.330
Income											
	38 (7.61)	Ref.					Ref.				
5,001-10,000	35.6 (6.91)	-2.4	2.26	-0.18	-1.1	0.292	2.47	2.91	0.18	0.85	0.402
10,001-15,000	43.01 (4.08)	3.42	2.43	0.24	1.41	0.164	3.95	3.01	0.27	1.31	0.197
Rash											
No	36.74 (6.4)	Ref.						Ref.			
Yes	40.76 (5.73)	4.02	1.89	0.27	2.12	**0.038**	5.66	2.92	0.38	1.94	0.06
Breathing problem											
No	39.26 (7.81)	Ref.					Ref.				
Yes	36.41 (5.26)	-2.8	1.73	-0.2	-1.6	0.10	-2.2	1.97	-0.16	-1.1	0.271

SAR = School of agricultural resources, SE = Standard Error, t = t-value, Beta = Standardized Coefficients (Beta), B = Unstandardized Coefficients.

CONCLUSION

The research at Chulalongkorn University, assessing students' knowledge, attitudes, and practices regarding $PM_{2.5}$, showed that although knowledge and practice levels were moderate, there was a strong attitude toward preventive measures. The study also found significant positive correlations between knowledge, attitudes, and practices, underscoring the need to improve educational initiatives. Furthermore, this study provides foundational data that suggest significant regional disparities in attitudes about $PM_{2.5}$, education and health problem significant associated preventive practices regarding $PM_{2.5}$. The findings advocate for targeted interventions that address specific educational and regional gaps in pollution awareness and response. Such tailored strategies are crucial for equipping students with the knowledge and tools necessary to protect themselves against environmental hazards effectively. By enhancing these programs, students' practical involvement and effectiveness in managing $PM_{2.5}$ can be significantly increased.

Integrating these educational strategies into broader public health policies and community efforts is crucial for effectively tackling air pollution and enhancing public health safety.

REFERENCE

[1] S. Chirasophon and P. Pochanart, "The long-term characteristics of PM10 and PM2. 5 in Bangkok, Thailand," *Asian Journal of Atmospheric Environment*, vol. 14, no. 1, pp. 73-83, 2020.

[2] S. Abdul Jabbar *et al.*, "Air quality, pollution and sustainability trends in South Asia: a population-based study," *International journal of environmental research and public health*, vol. 19, no. 12, p. 7534, 2022.

[3] B. A. Begum, P. K. Hopke, and A. Markwitz, "Air pollution by fine particulate matter in Bangladesh," *Atmospheric Pollution Research*, vol. 4, no. 1, pp. 75-86, 2013.

[4] J. Samet and D. Krewski, "Health effects associated with exposure to ambient air pollution," *Journal of toxicology and environmental health, Part A*, vol. 70, no. 3-4, pp. 227-242, 2007.

[5] S. Lim, B. Barratt, L. Holliday, C. J. Griffiths, and I. S. Mudway, "Characterising professional drivers' exposure to traffic-related air pollution: Evidence for reduction strategies from in-vehicle personal exposure monitoring," *Environment International*, vol. 153, p. 106532, 2021.

[6] A. Patra and H. C. Phuleria, "Inequalities in occupational exposures among people using popular commute modes," *Environmental Pollution*, vol. 298, p. 118797, 2022/04/01/ 2022, doi: https://doi.org/10.1016/j.envpol.2022.118797.

[7] S. Zhao, Y. Fan, P. Zhao, A. Mansourian, and H. C. Ho, "How do taxi drivers expose to fine particulate matter (PM2. 5) in a Chinese megacity: a rapid assessment incorporating with satellite-derived information and urban mobility data," *International Journal of Health Geographics*, vol. 23, no. 1, p. 9, 2024.

[8] L. V. Giles *et al.*, "From good intentions to proven interventions: effectiveness of actions to reduce the health impacts of air pollution," *Environmental health perspectives*, vol. 119, no. 1, pp. 29-36, 2011.

[9] I. Degroot, W. Loring, A. Rihm Jr, S. W. Samuels, and W. Winkelstein Jr, "People and air pollution: A study of attitudes in Buffalo, NY," *Journal of the Air Pollution Control Association*, vol. 16, no. 5, pp. 245-247, 1966.

[10] X. Liu *et al.*, "Public's Health Risk Awareness on Urban Air Pollution in Chinese Megacities: The Cases of Shanghai, Wuhan and Nanchang," *International Journal of Environmental Research and Public Health*, vol. 13, no. 9, p. 845, 2016. [Online]. Available: https://www.mdpi.com/1660-4601/13/9/845.

[11] L. De Pretto, S. Acreman, M. J. Ashfold, S. K. Mohankumar, and A. Campos-Arceiz, "The link between knowledge, attitudes and practices in relation to atmospheric haze pollution in Peninsular Malaysia," *PloS one*, vol. 10, no. 12, p. e0143655, 2015.

[12] R. B. Hashem, A. B. Siddique, S. M. Rasel, and M. S. Hossain, "Assessment of knowledge, attitudes, and practices regarding air pollution among traffic polices in Dhaka city, Bangladesh: a cross-sectional study," *BMC Public Health*, vol. 24, no. 1, p. 3593, 2024.

21R4-07

Treatment of Fishery Wastewater Using a Floating Treatment Wetland Planted with Umbrella Sedge

Parichat Supasee[1] Supreeda Homklin[2] Satawat Tanarat[2] Anusorn Boonpoke[2] and Somanat Somprasert[2*]

[1]Graduate Student in Environmental Engineering, School of Energy and Environment, University of Phayao 56000; [2]Lecturer at School of Energy and Environment, University of Phayao 56000.
[*]Phone: 0850361741, E-mail : somanat.so@up.ac.th

ABSTRACT

This study evaluates the effectiveness of floating treatment wetlands (FTWs) using umbrella sedge (*Cyperus* spp.) for removing organic and nitrogen from fishery wastewater in Thailand. Aquaculture in Thailand produces significant wastewater with high organic matter and nitrogen, necessitating effective treatment solutions. FTWs are designed to float in fishponds, providing a flexible and space-saving method for wastewater treatment compared to traditional wetlands. The study used four laboratory-scale FTW reactors with varying hydraulic loading rates (5, 10, 15, and 20 cm/d) to assess their impact on pollutant removal. The FTW with the lowest hydraulic loading rate (5 cm/d) achieved the highest removal efficiencies of 45% 63% and 61% for COD TKN and NH_3-N, respectively, demonstrating the effectiveness of the system. The growth of the umbrella sedge was optimal in the 5 cm/d reactors, enhancing aerobic conditions and promoting effective decomposition of pollutants. The study concludes that FTWs are a sustainable and efficient solution for treating aquaculture wastewater, particularly at lower hydraulic loading rates, thus supporting better aquaculture practices.

Keywords: floating treatment wetland; synthetic fishery wastewater; nitrogen removal; organic removal; umbrella sedge.

INTRODUCTION

Aquaculture in Thailand is a significant source of wastewater from agricultural activities in the country. Leftover fish food and excrement results in high levels of organic matter and nitrogen in the water discharged from fishponds. Generally, tilapia farming involves transferring water from upstream ponds to downstream ponds without wastewater treatment. This leads to the accumulation of organic matter and nitrogen in the water of the downstream ponds, reducing oxygen levels and making the water unsuitable for fish growth. Additionally, it affects public water sources when wastewater is discharged from the farming area, causing pollution in the receiving water bodies. Aquaculture farmers need a simple and low-cost wastewater treatment system, and constructed wetlands suit this purpose. However, traditionally constructed wetlands require large areas, reducing the space available for aquaculture. Therefore, floating treatment wetlands (FTW) have been designed to float in fishponds, reducing the additional space needed for treatment. They are also flexible to changes in water levels in the ponds. Floating treatment wetlands (FTW) were created using floating rafts for growing wetland plants without soil, which is recognized as an effective mechanism of water treatment and is used in a wide range of applications. The raft will float on the surface of the water. The pollutant removal mechanism occurs in the root zone of plants under the water surface, which helps increase the amount of oxygen in the water to microorganisms living both around the roots and suspended in the water, causing a reaction to decompose organic matter and other pollutants. Newman [1] found that FTW systems provide design flexibility that can be built in small spaces. The system can be scaled to fit a pond or water source. It is a habitat for living creatures, enhancing their beauty and creating fascinating scenery. Water level fluctuations, as long as they are attached to the bottom or water source, thus the system is not damaged. Therefore, FTW systems are an interesting option used to treat wastewater from fish ponds. Floating treatment wetlands use a variety of plants to help improve water quality by absorbing excess nutrients and breaking down contaminants. Some commonly used plants in FTW such as cattail (*Typha* spp.) umbrella sedge (*Cyperus* spp.) and bulrushes (*Schoenoplectus* spp.). These plants absorb nutrients and contaminants and provide a habitat for beneficial microbes that further enhance the water purification process. The plants in floating constructed wetlands that provide good treatment efficiency include *Cyperus spp*. These plants are tolerant of pollutants in wastewater, grow quickly, and increase biomass, resulting in a high accumulation of organic matter and nitrogen. Additionally, their long roots help distribute oxygen in the water, enhancing the efficiency of pollutant treatment in wastewater. The FTWs

planted with umbrella sedges show higher organic and nitrogen removal efficiency than other plants, which were 85% and 77% for organic in the form of COD and TKN, respectively [2]. This study aims to find the optimal HLR to effectively treat organic matter and nitrogen. The results of the study will guide the application of tilapia farming to reduce the environmental impact of fish farming activities effectively and sustainably.

METHODOLOGY

Four laboratory-scale floating treatment wetland reactors were used in this study, as shown in Figure 1. Each reactor is 0.5 meters wide, 1.0 meters long, and has a water depth of 0.6 meters with 0.1 meters as a freeboard. The 40x80 cm floating raft was planted with an umbrella sedge (*Cyperus* spp.) 2-3 clumps per raft. The experiment was set in four different hydraulic loading rates (HLR) of 5, 10, 15, and 20 cm/d (C1, C2, C3 and C4, respectively).

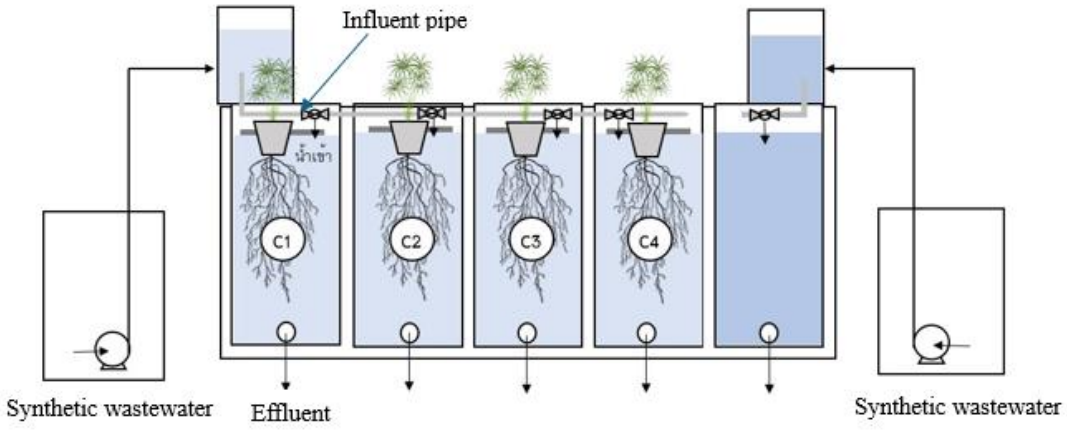


Figure 1 Schematics of the lab-scale reactor

The fishery wastewater was synthesized by mixing molasses and urea as an organic and nitrogen source to match the COD NH_3-N and TKN concentrations of 80-200 mg/L and 20-50 mg/L, respectively shown in Table 1. Synthetic wastewater with an average COD of 168 mg/L, NH_3-N, and TKN at 26 mg/L was pumped into the floating treatment wetland reactor continuously. The Influent and effluent samples were collected every week and analyzed for COD TKN. The steady state of the experiment was determined primarily by the ammonia nitrogen concentration in the effluent.

Table 1 Comparison of synthetic and fishery wastewater

Parameters	**Averaged concentration, mg/L**	
	Fishery wastewater	**Synthetic wastewater**
COD	80-200	168
TKN	20-50	26
NH_3-N		26
SS	2	1.5
pH	6-7.5	7.29

This experiment uses umbrella sedge as a plant in the FTW reactor because the previous study reports that the FTWs planted with umbrella sedge provide good efficiency in removing pollutants, specifically, nitrogen removal. This plant can be found in general and is also popular to grow as an ornamental plant. An umbrella sedge grows well in wastewater, can increase the height and number of plants quickly, and has a well-distributed root system. The square raft was made of PVC pipes with a 1-inch diameter a width of 40 cm and a length of 80 cm. In the middle of the raft were cut for planting pots. At the

beginning of the experiment, plants were cut to the same initial height of 30 centimeters and an average initial root length of 30 cm and planted 1 clump per pot as shown in Figure 2. At the beginning of the experiment, the wastewater was diluted to a concentration of about 25-30% so that the plants could grow easier. The 100% wastewater was fed when the average height of the plants increased from 20 cm to 30 cm, and new plant shoots had grown. Plant height and root length were measured at the beginning and the end of the experiment.



Figure 2 Umbrella sedge at the beginning of the experiment

RESULTS AND DISCUSSIONS

The reactors C1, C2, C3 and C4 were fed at HLR 5, 10, 15 and 20 cm/d (15, 30, 45 and 60 L/d, respectively). During the 3-month data collection period, it was found that the average COD TKN and NH_3-N concentration in the influent and effluent is shown in Table 2. The root length and plant height at the end of the experiment are also shown in Table 2.

Table 2 Average concentration of influent effluent plant height and plant root length

Parameter	**Influent**	**Average Concentration**			
		5 cm/d (C1)	**10 cm/d (C2)**	**15 cm/d (C3)**	**20 cm/d (C4)**
HRT, d		20	10	6.7	1.4
pH	6.6 (SD 0.16)	6.8 (SD 0.07)	7.2 (SD 0.23)	7.4 (SD 0.20)	7.3 (SD 0.18)
COD, mg/L	171 (SD 4.8)	94 (SD 20)	102 (SD 23)	108 (SD 24)	116 (SD 24)
TKN, mg/L	27 (SD 0.3)	10 (SD 1.1)	15 (SD 1.2)	16 (SD 0.7)	17 (SD 0.5)
NH_3-N, mg/L	26 (SD 0.3)	10 (SD 0.3)	13 (SD 0.4)	16 (SD 0.2)	18 (SD 0.7)
Root Length, cm		70.8	57.8	65.8	54.2
Plant Height, cm		50.3	60.3	50.8	58.9

The COD removal efficiency was nearly the same in every reactor, which was in the range of 32-45%. The COD in the effluent tendency increased as the experimental period lengthened, as shown in Figure 3. A large amount of algae was found to occur in the system because the vegetation on the raft was not dense enough. Therefore, light could penetrate the water, stimulating the growth of algae and fall off with the effluent.

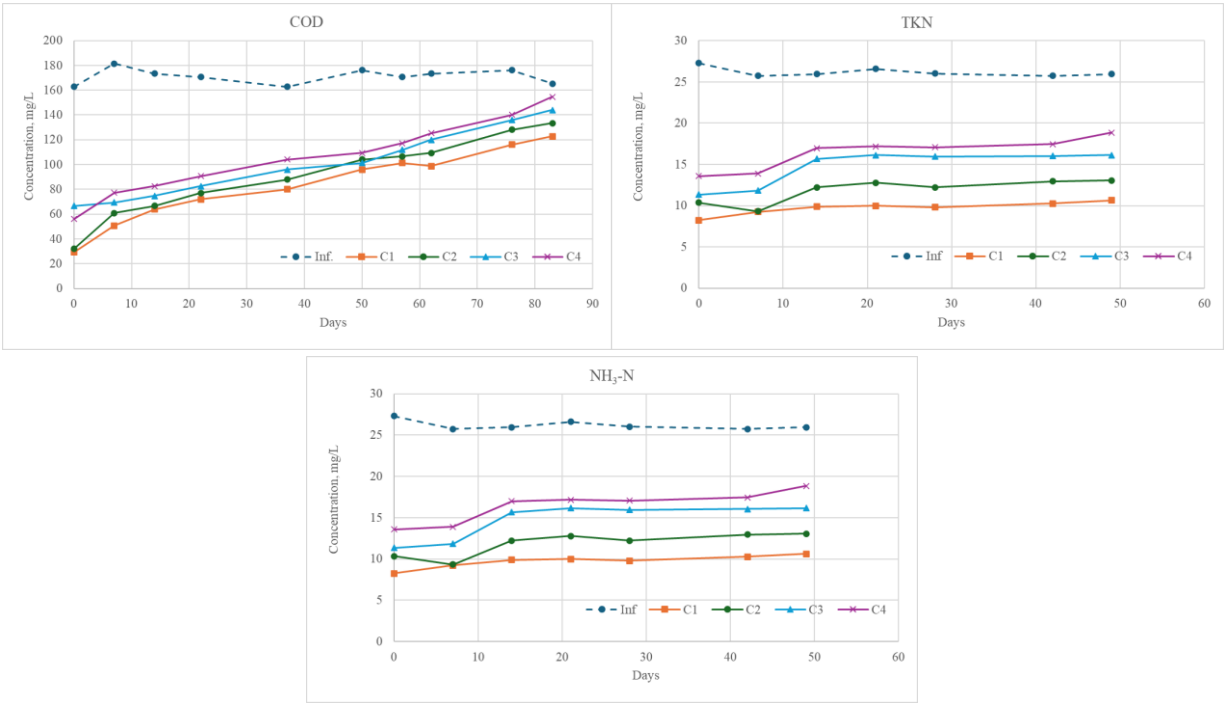


Figure 3 Changes in COD TNK and NH_3-N concentrations

The TKN and ammonia nitrogen in the influent were similar because the synthesis of wastewater used urea fertilizer as a representative of nitrogen in the wastewater, which gave nitrogen in the form of ammonia rather than organic nitrogen. The nitrogen in the effluent both TKN and NH3-N shows a steady state after 14 days of the experiment as shown in Fig 3. At the HLR 5 cm/d (C1) showed the highest nitrogen removal efficiency for both TKN and NH_3-N, 63% and 61%, respectively. It was found that as the hydraulic loading rate increased, the treatment efficiency decreased, as shown in Figure 4. The TKN removal efficiency was slightly less than the NH_3-N removal efficiency because the algae formed in the system were also mixed in the effluent. It was found that the C1 model provided similar TKN and NH_3-N removal efficiency because the plants in the system grew well above the water, thus blocking the light and reducing the growth of algae more compared to the C2, C3, and C4 models, which had less dense above-water plants (Fig 5).

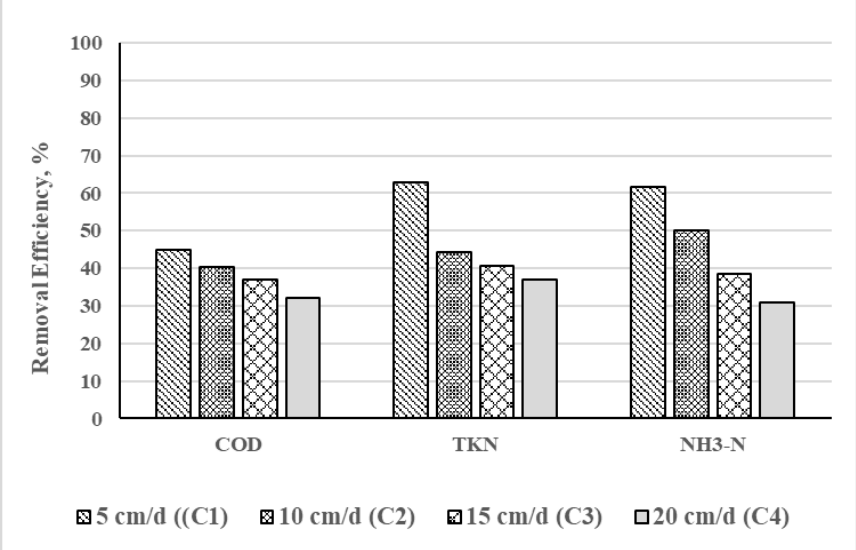


Figure 4 Removal efficiencies compared to HLRs



Figure 5 Plant shoot above the water surface in C1 C2 C3 and C4 at the end of the experiment

The reactors with 5 cm/d HLR showed the best removal efficiency for both organic and nitrogen. In this reactor, the umbrella sedge grew well both in the shoot and root length and plant density as shown in Fig 4. After 120 days of experiment, the umbrella sedge was increased by an average height of 50.3 centimeters and the average root length by 70.8 centimeters. The plant roots in C1 are dense and distributed along the wide sides of the reactor as shown in Fig 6.



Figure 6 Plant root at the end of the experiment at 5 cm/d (C1)

A well-distributed root system allows for aerobic conditions in which microorganisms can decompose organic matter well. Zhang et al. [3] studied the causes of oxygen environments and the response characteristics of plant oxygen release (POR) in subsurface-flow constructed wetlands and reported that the root zone DO increased significantly to 2.05–4.37 mg/L, and was positively correlated with the TN and TP removal rates. *Cyperus* spp. showed a good tendency to release oxygen in the root zone. Yao et al. [4] showed that oxygen released by *Vetiveria zizanioides* L. roots through the biochemical process contributed to 77% and 74% of total root oxygen release under nutrient solution conditions and artificial wastewater conditions, respectively, and that was 72% and 71% of total root oxygen release for *Cyperus alternifolius* L.

The plants in the C2, C3, and C4 reactors had a height and root length similar to C1 at the end of the experiment, but the density of the plant shoot and roots was much less. As a result, the efficiency of organic matter and nitrogen removal is lower than that of the C1 model because aerobic conditions occur only in areas with plant roots. In addition, as the hydraulic load rate rises, the flow becomes even more turbulent. This shortens the duration of the wastewater in the model and provides less treatment efficiency. Asaeda and Rashid [5] studied the effect of water turbulence motion and the growth of three types of aquatic plants. The study found that high turbulence velocity inhibits the normal metabolic activities of all three plants, while low to medium turbulence does not harm the floating-leaved plants.

The removal efficiency in this study was higher compared to the other studies. Barco and Borin [6] report that FTW in Northern Italy has significantly reduced COD and NH_4-N by 16.7% and 25.2%, respectively, whose effectiveness depends on the concentration in the inlet and the wastewater temperature. According to a study by Nichols et al. [7] which used FTW to treat stormwater runoff over 2 months, it was found that 53% of phosphorus and 17% of total nitrogen could be treated. In this study, long, dispersed plant roots throughout the width and length of the reactor provide aerobic conditions. Combined with a long hydraulic retention time (20 days) resulting in the complete degradation reaction for both organic and ammonia nitrogen.

CONCLUSION

This study concluded that FTW planted with an umbrella sedge was effective in removing organic and nitrogen from fishery wastewater, especially at lower hydraulic loading rates. The lowest HLR (5 cm/d) showed the highest removal efficiency for both organic and nitrogen 45% and nitrogen removal at 63% and 61% for TKN and NH_3-N, respectively. Well-distribution of plant roots has a positive effect on the efficiency of organic matter and nitrogen treatment. This method provides a sustainable and space-saving solution for aquaculture wastewater treatment.

ACKNOWLEDGEMENT

This research project was financially supported by the Thailand Science Research and Innovation Fund and the University of Phayao (Grant No. FF65- RIM007).

REFERENCE

[1] Majer Newman, J., Clausen, J. C., and Neafsey, J. A. (1999). Seasonal performance of a wetland constructed to process dairy milkhouse wastewater in Connecticut. Ecological Engineering, 14(1), 181-198.

[2] Wiphada Wongruankaew and Somanat Somprasert. (2016). Nitrogen Removal Efficiency of Floating Constructed Wetland System in Treating Catfish Farming Wastewater. Thai Environmental Engineering Journal, 30(3), 75-83.

[3] Jingying Zhang, Qiuhui Yan, Ge Bai, Dun Guo, Yanbin Chi, Bin Li, Lei Yang, Yongxiang Ren, (2023). Inducing root redundant development to release oxygen: An efficient natural oxygenation approach for subsurface flow constructed wetland, Environmental Research, Volume 239, Part 1, 117377.

[4] Fang Yao, Gen-xiang Shen, Xue-lian Li, Huai-zheng Li, Hong Hu, Wu-zhong Ni. (2011). A comparative study on the potential of oxygen release by roots of selected wetland plants, Physics and Chemistry of the Earth, Parts A/B/C, Volume 36, Issues 9–11, Pages 475-478.

[5] Takashi Asaeda, M.H. Rashid. (2017). Effects of turbulence motion on the growth and physiology of aquatic plants, Limnologica, Volume 62, Pages 181-187

[6] Alberto Barco, and Maurizio Borin. (2020). Treatment performances of floating wetlands: A decade of studies in North Italy, Ecological Engineering, Volume 158, 106016.

[7] Nichols, P., Lucke, T., Drapper, D., and Walker, C. (2016). Performance Evaluation of a Floating Treatment Wetland in an Urban Catchment. Water, 8, 244.

21R4-08

Heavy Metals from Fishing Gears: Potential Risks to Marine Environment

Khine Yin Nyien[1*], Yotwadee Hawangchu[2] and Dao Janjaroen[3]

[1]Masters Student; [3]Associate Professor, Department of Environmental and Sustainable Engineering, Faculty of Engineering, Chulalongkorn University, Bangkok, 10330, Thailand
[2]Researcher, Aquatic Resources and Research Institute, Chulalongkorn University, Bangkok, 10330, Thailand
[*]Phone : (66) 08 1549 2006, E-mail : khaiyinnyein98@gamil.com

ABSTRACT

Among ocean-based sources of marine debris, abandoned, lost or otherwise discarded fishing gear (ALDFG) made from synthetic polymers plays a significant role. Over time, these materials degrade into microplastics and potentially release toxic additives and heavy metals into the environment. This study investigates the polymer composition and heavy metals content in pristine fishing nets and evaluates ecological risk using the potential ecological risk index (PERI) approach developed by Hakanson. FTIR analysis identified polyethylene (PE), polyamide (PA) and polypropylene (PP) as main polymers. ICP-OES analysis detected trace levels of arsenic (As), barium (Ba), chromium (Cr) and lead (Pb) in some samples. Based on PERI, all samples posed a low ecological risk to marine pollution. However, the potential long-term effects of metal release from degrading nets highlight the need for continued assessments and the development of safer alternatives to support sustainable fishing practices.

Keywords : heavy metals; plastic; fishing gear; marine pollution; risk assessment

INTRODUCTION

Plastic pollution in the natural environment has been an emerging concern for several decades due to its widespread presence in terrestrial and aquatic ecosystems from various sources [1]. In the marine environment, plastics originates from various sources and can be found either floating on the surface or accumulating in sediments and water columns [2]. Such global widespread had become a serious concern due to its negative impacts on marine ecosystem and human health [3]. Among the major contributors to marine plastic pollution, fisheries and shipping industries are significant ocean-based sources [4]. Fishing operations use plastic fishing gears commonly made of nylon or polyolefins, are sometimes abandoned, lost or even discarded in the oceans during their use [5], forming ALDFGs (Abandoned, Lost or Discarded Fishing Gears) which continue to entangle marine species through a process known as ghost fishing [6]. Despite the high durability of polymers, they can undergo embrittlement, cracking and reduction in mechanical properties which eventually leads to fragmentation and formation of secondary microplastics[6, 7]. These microplastics not only persist in the environment but also pose negative impacts to marine environment, as they can potentially be ingested by marine organisms through food chain [8, 9]. Additionally, when plastics are degraded into microplastics, chemical additives and heavy metals from plastics can be released into the environment, increasing ecotoxicological risk to marine organisms[10].

Historically, additives used in plastics are based on toxic heavy metals [11] and some studies highlight that the presence of heavy metals present as metal based pigments and additives in fishing gears[12-14]. These toxic, persistent, bioaccumulate heavy metals are an emerging environmental concern, causing long-term effects on both human and marine ecosystems [15-17]. However, the specific polymer used in fishing gears, the extent of heavy metals contamination, and the process of degradation and release are still not clearly understood. Therefore, this study aims to identify the polymer composition and quantify heavy metals in fishing gear using laboratory-based methods, assess the potential environmental and ecotoxicological risks, and propose alternatives and policy recommendations to support sustainable fisheries and marine protection.

METHODOLOGY

Sample Preparation

Six samples of pristine fishing net namely, Small Green Net (SGN), Medium Green Net (MGN), Large Green Net (LGN), Small Blue Net (SBN), Large Blue Net (LBN) and Yellow Rope for Netting (YRN) were obtained as commercial products in unused condition with no prior environmental exposure or operational deployment. The samples were rinsed thoroughly with deionized (DI) water to get rid of any impurities and dried in the oven at medium heat until a constant weight was achieved.

Sample Characterization

Samples were characterized by identifying the polymer type and analyzing the amount of heavy metal present. The polymer type of each sample was determined by Attenuated Total Reflection-Fourier Transform Infrared (ATR-FTIR) spectroscopy. For heavy metal analysis, samples were first digested using microwave assisted acid digestion in accordance with the U.S Environmental Protection Agency's Method 3051A [18]. After digestion, concentrations of arsenic(As), mercury(Pb), cadmium(Cd), chromium(Cr), lead(Pb), barium (Ba) and selenium(Se) were determined using Inductively Coupled Plasma Optical Emission Spectroscopy (ICP-OES),based on the standards methods for the examination of water and waste water Method 3500B (3120) [19].

Risk Assessment

The ecological risk assessment of heavy metals from fishing nets was evaluated by using potential ecological risk index (PERI) by Hakanson [20]. Although PERI is generally applied to sediment and soils, it is used in this study for fishing net materials. This approach is justified as polymers in fishing nets can release heavy metals into the marine environment through degradation process, with the release increase over time [21] that may pose similar ecological risk to those caused by heavy metal contamination in sediments. PERI calculated according to the following equations:

$$C_f^i = \frac{C_S^i}{C_n^i} \tag{1}$$

$$C_d = \sum_{i=1}^{n} C_f^i \tag{2}$$

Where C^i_f is the contamination factor, Cis represents the concentration of i^{th} heavy metal in each sample, and C^i_n is the natural or background concentration of the corresponding heavy metals in mg/kg. C_d is the degree of contamination.

$$E_r^i = T_r^i \times C_f^i \tag{3}$$

$$PERI = \sum_{i=1}^{n} E_r^i \tag{4}$$

E^i_r is the potential ecological risk factor of each metal, while T^i_r refers to the toxic response factor associated with each metal. The classification criteria for risk indices are listed in Table 1.

Table 1. Classification of risk indices

Index	Criteria (Value Range)	Risk level
Risk factor (E^i_r)	$E^i_r < 40$	Low
	$40 \leq E^i_r < 80$	Moderate
	$80 \leq E^i_r < 160$	Considerable
	$160 \leq E^i_r < 320$	High
	$E^i_r \geq 320$	Very High
Potential ecological risk index (PERI)	PERI < 150	Low
	150 ≤ PERI < 300	Moderate
	300 ≤ PERI < 600	Considerable
	PERI ≥ 600	High

The toxic response factor values are based on Hakanson's approach and are listed in Table 2. In this study, PERI was calculated for five elements: As, Hg, Cd, Cr and Pb. It could not be calculated for Se and Br as there is no specified toxic response factor value in existing literature. Regarding background concentrations, the value were obtained from MESS-4:Marine Sediment Certified Reference Material for total and extractable metal content from National Research Council of Canada [22] and Turekian & Wedepohl (1961)[23] as site specific data were unavailable or incomplete. Although site specific data are ideal and would enhance data accuracy, literature-based values are also reliable for preliminary assessment of ecological risk associated with the release of heavy metals from fishing nets.

Table 2. Background concentration and Toxic response factor values [20, 22, 23]

Heavy metal	Background Concentration ($C^i_{n)}$	Toxic response factor ($T^i_{r)}$
Arsenic (As)	13[a]	10[c]
Mercury (Hg)	0.091[a]	40[c]
Cadmium (Cd)	0.42[b]	30[c]
Chromium (Cr)	90[a]	2[c]
Lead (Pb)	80[a]	5[c]

[a]MESS-4: Marine Sediment Certified Reference Material for total and extractable metal content from National Research Council of Canada
[b]Turekian & Wedepohl 1961
[c]Hakanson 1980

RESULTS AND DISCUSSIONS

Polymer Identification

Fishing net samples were analyzed using Fourier Transform Infrared Spectroscopy (FTIR) to determine their polymer composition. The observed absorption bands were compared with characteristics bands reported in literature [24-28].

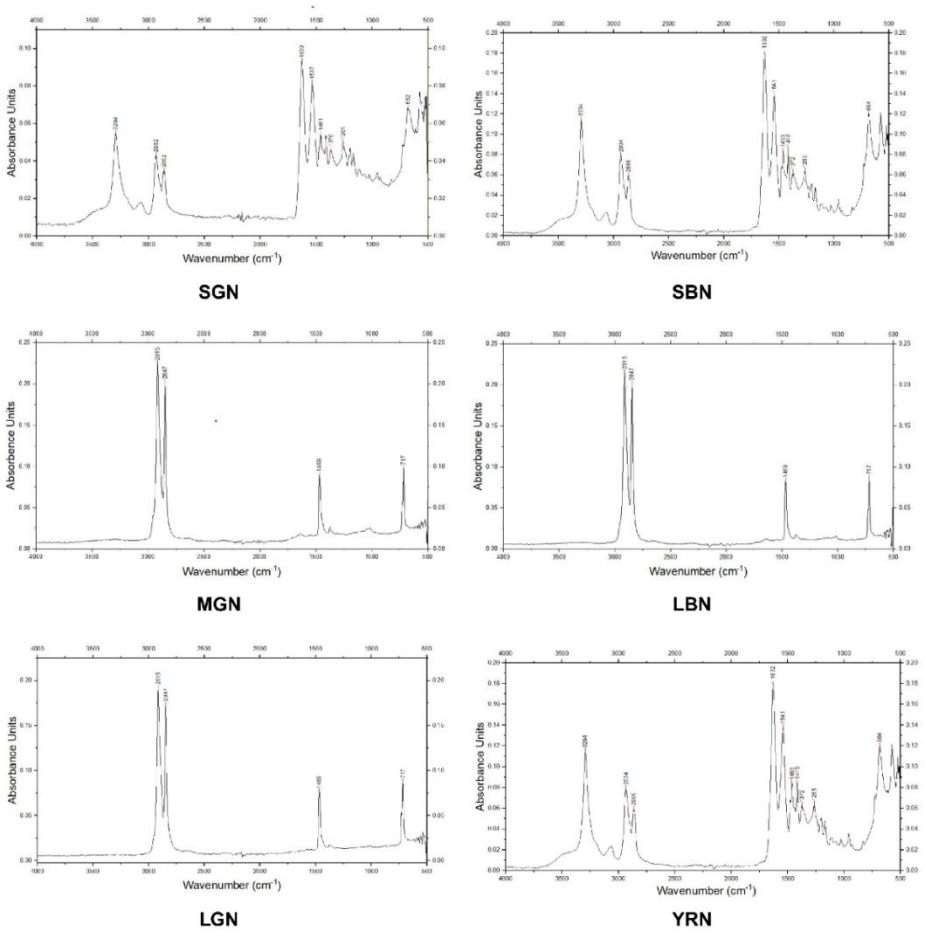


Figure 1. FTIR Spectra of Fishing Net Samples

The results revealed the distinct spectral features that confirm the polymer identification for each sample. Samples MGN, LGN and LBN exhibited characteristic peaks of polyethylene (PE) approximately at 2915 and 2847 cm^{-1} (C-H stretching), 1469 cm^{-1} (CH_2 bending) and 717 cm^{-1} (CH_2 rocking). FTIR spectra of SGN and SBN displayed distinct absorption bands at 3294 cm^{-1} (N-H stretching), 2930-2860 cm^{-1} (C-H stretching of aliphatic chains), and amide bands at 1630 cm^{-1} (C=O stretching) and 1540 cm^{-1} (N-H bending) that are consistent with the spectral profile of polyamide (Nylon). Sample YRN exhibited CH stretching vibrations between 2950 and 2849 cm^{-1}, bending at 1461 and 1379 cm^{-1} and a few peaks between 1168 and 810 cm^{-1} which are all consistent with spectral characteristics of polypropylene (PP). These results align with the findings by other literature. Fishing gears made of polymers has been using since the 1960s due to their cost-effectiveness, lightweight, long-lasting and availability where the choice of polymer is determined by their specific characteristics such as density, strength, diameter and weather resistance[29]. The table below represents a comparison of polymer types used in fishing gears across different locations based on literature records.

Table 3. Polymer types identified in Fishing Gears around the world

Study	Location	Polymer type observed	Remarks
In this study	Thailand	PE, PA, PP	
Corniuk et al., 2023 [29]	O'ahu, Hawai'i	HDPE, PP, Nylon	Majority of samples were HDPE
Kanehiro, 2004 [30]	Japan	Nylon, PE	
Turner 2017 [14]	England	PE, PE/PP blend, Nylon	Majority of samples were HDPE
Weissbach et al., 2022 [31]	Baltic Sea	PA, PP, polyethylene terephthalate (PET)	

Heavy Metal Analysis

The concentration of heavy metal in the six samples were measured using ICP-OES and the results were presented in Table 4. Overall, the mean concentration of metals in all samples was generally low. For concentrations below detection limit (<0.5 mg/kg), half detection limit approach was applied. Arsenic (As) was detected only in large nets (LGN and LBN) at concentrations of 4.235 mg/kg and 6.425 mg/kg respectively while the other samples remained below detection limit. The presence of As in the samples may be attribute to use of additives, production residues or contaminants from the materials during the manufacturing of the nets [11]. However, the specific source is unclear as there is limited information about arsenic in plastic materials. In comparison, Mora et al. (2023) reported that arsenic concentration on environmentally exposed microplastics that range between non-detectable limits to 6.53mg/kg [32] which indicates that the detected values in this study fall within the reported range.

Table 4. Detected concentration of heavy metals in the fishing net samples

Heavy Metal (mg/kg)	SGN	MGN	LGN	SBN	LBN	YRN	Mean	SD
As	<0.5	<0.5	4.235	<0.5	6.425	<0.5	**1.57**	**2.48**
Ba	<0.5	**10.36**	**17.8**	**1.547**	**8.809**	**1.079**	**7.56**	**6.91**
Cd	<0.5	<0.5	<0.5	<0.5	<0.5	<0.5	0.25	0
Cr	**0.539**	**1.205**	**2.414**	<0.5	**1.312**	**2.727**	**1.5**	**1.05**
Hg	<0.5	<0.5	<0.5	<0.5	<0.5	<0.5	0.25	0
Pb	<0.5	<0.5	**0.936**	<0.5	<0.5	**7.374**	**2.15**	**2.87**
Se	<0.5	<0.5	<0.5	<0.5	<0.5	<0.5	0.25	0

Mercury (Hg), cadmium (Cd) and selenium (Se) were all found below the detection limit in all samples which indicates that their concentration is either absent or present at concentrations too low to be quantified under analytical conditions. Nonetheless, previous studies have documented the presence of metals in plastic materials. Mercury concentrations ranging from 5 to 8216 nmol/kg have been reported in the beached plastics, particularly in black, red and brown samples [33]. Cadmium has been used as colorant in the plastic industry. Normally, 0.05 to 1.5% by weight of Cd pigment is added to the plastic and is often associated with yellow, orange and red pigments [34]. Massos and Turner (2017) reported the presence of Cd in beached microplastics [35]. Turner

(2017) also identified Cd and Se in fishing nets and plastic litter in England, likely originating from cadmium sulphoselenide-based pigments.[14].

Chromium (Cr) was found in all samples except SBN, with concentration ranging from 0.539 mg/kg to 2.727 mg/kg where the highest concentration was found in yellow PE rope (YRN). Lead (Pb) was detected only in green and yellow nets, LGN and YRN with concentrations of 0.936 mg/kg and 7.374 mg/kg respectively. Turner (2017) observed strong correlation between Cr and Pb concentration in orange and yellow samples suggesting the use of lead chromate ($PbCrO_4$) pigments[14]. The Pb and Cr concentration in YRN and LGN may indicate the possible use of lead chromate based yellow pigments in fishing nets. Barium (Ba) concentration ranged between 1.079 mg/kg and 17.8 mg/kg in five samples while SGN remained below the detection limit. Barium is largely found in plastic as barium sulfate $BaSO_4$, used as a filler in plastic production. Ba additives were detected in the beached plastics samples in southern England [36].

The concentrations of heavy metals in the analyzed fishing nets were compared with regulatory safety limits established by various international guidelines as in Table 5. The detected concentration in all samples were found to be well below the safety limits set by those guidelines. This indicates that the modern fishing nets comply with current safety standards regarding heavy metal content. Additionally, the concentration observed in this study is significantly lower than those reported in previous studies, suggesting improvements in material formulations and regulatory oversight in recent manufacturing practices. However, despite the low concentrations, the release of heavy metals from plastic material during degradation remains a concern due to their long-term environmental impacts. It is still necessary to monitor and develop safer alternatives of heavy metal use in fishing gear and plastic manufacturing.

Table 5. Regulatory limits of heavy metal concentrations in plastic materials set by various international standards and guidelines (mg/kg) [37-39]

Heavy Metals	TS	ISO	TIS
As	47	25	25
Ba	18750	1000	1000
Cd	17	75	75
Cr	460 (Cr III) 0.053 (Cr IV)	60	60
Hg	94	90	90
Pb	23	60	60
Se	460	500	500

*TS: Migration limits of heavy metals in 0.07 M HCl as specified by the EU Toy Safety Directive (2009/48/EC, Annex II), ISO: ISO 8124-3:2020 (Toy Safety – Part 3: Migration of Certain Elements), TIS: TIS 685 Part-1: 2562 (2019): Toys: Safety Requirements: Part 1 – Requirements. 2019.

Risk Assessment

PERI was calculated for all samples using Hakanson's approach, and the results are presented in Table 6. Although the concentrations in Cd and Hg were consistently lower than the detection limit, they were included in the calculation due to their persistence, toxicity, high toxic response factor and potential ecological significance even at trace concentrations. To minimize the risk of underestimating or overestimating the concentrations, the half detection limit method was applied by assigning a proxy concentration equal to half the analytical detection limit (<0.5mg/kg was adjusted to 0.25 mg/kg for all values below detection limit in this study).

Table 6. Potential Ecological Risk Index (PERI) and Individual Risk Factors (E^i_r) for Heavy Metals in Fishing Net Samples

	E^i_r					**PERI**	**Risk level**
	As	**Cd**	**Cr**	**Hg**	**Pb**		
SGN	0.19	17.86	0.012	109.89	0.016	127.97	Low
MGN	0.19	17.86	0.027	109.89	0.016	127.98	Low
LGN	3.26	17.86	0.054	109.89	0.059	131.12	Low
SBN	0.19	17.86	0.006	109.89	0.016	127.96	Low
LBN	4.94	17.86	0.029	109.89	0.016	132.73	Low
YRN	0.19	17.86	0.061	109.89	0.461	128.46	Low
Mean	1.5	17.86	0.032	109.89	0.097	129.37	
SD	2.09	0	0.022	0	0.18	2.05	

Among all metals evaluated, Hg and Cd exhibited the most toxic factor E^i_r values where Hg falls within considerable risk level when compared to classification of risk levels. However, this high score is primarily attributed to high toxic response factor values of Hg and its assumed presence using half detection limit approach across all samples. This highlights the significance of Hg's potential toxicity, even at trace levels. Generally plastics materials contains Hg-based additives as catalyst or pigments [11] and the use of those additives in fishing net production should be minimized. Cd also showed a significant amount of $E^i_{r\ value}$ across all samples, which is the second highest contributor to PERI. Similar to Hg, the high value in the metal is also a reason of the high toxic response factor value due to its substantial impact. However, when compared against the risk criteria for E^i_r, it still remains within the low-risk level. The E^i_r values of remaining metals —As, Cr and Pb — were all relatively low, falling within the low-risk category.

Overall, PERI values are low as they fall within the low-risk category, suggesting that their current potential ecological risk as classified by the PERI is considered low. This means the likelihood of adverse ecological impacts and marine pollution from these metals from those fish net samples is minimal. However, this low-risk classification needs to be interpreted carefully in the context of long-term environmental exposure. As noted earlier, fishing nets are commonly composed of plastics. Since plastics are difficult to degrade, their accumulation in aquatic environment increases over time and eventually broken down into marine environment[40]. Since metal additives in polymers are not chemically bonded to the polymers, they have the tendency to migrate out through diffusion and mass transfer, particularly in aqueous environments[11], thus increasing the likelihood of metal contaminants leaching into surrounding water sources. Additionally, microplastics from fishing gear can act as a vector of heavy metal in marine environment. Due to their surface characteristics, microplastics are easier to adsorb and accumulate chemical contaminants from the environment [41]. Furthermore, anthropogenic activities and changes in the marine conditions, such as pH, temperature, salinity, and organic matter content, could also contribute to cumulative pollution. While current ecological risk appears low, long-term cumulative risks from degradation of discarded fishing gears in the marine environment should not be overlooked. Additional studies are necessary to enhance understanding of heavy metal release from the discarded fishing gears in the marine environment and its impact on marine ecosystems.

CONCLUSION

This study assessed the ecological risk of heavy metals in discarded fishing gears using Hakanson's potential ecological risk index (PERI). Six samples were analyzed to determine their polymer composition and identified as PE, PP and PA, which are commonly used material for fishing gears globally. Heavy metal analysis detected metal concentrations of As, Ba, Br and Pb in some samples while the concentration of Hg Se and Cd were below detection limits. The PERI evaluation indicated that the overall risk from heavy metals in the analyzed fishing nets was low, suggesting the current heavy metal concentrations are unlikely to pose significant pollution to marine environment. However, microplastics from degradation of fishing gears and their tendency of persistent metal ions from plastic additives to leach into surrounding waters and their ability to adsorb metals from the environment remain concerns for long-term cumulative risks.

Although the findings from this study suggest the minimal risks, further research is essential to investigate heavy metal release from discarded fishing gear, particularly when they degrade and fragment into microplastics. Long-term ecological consequences in the marine ecosystem could be significant and continue study of cumulative impacts of heavy metals from discarded fishing gears and other natural and anthropogenic pollution sources. Given the persistence of plastic in the environment, the development of safer, heavy metal-free and sustainable alternatives for fishing gear is crucial to mitigate potential ecological impacts.

ACKNOWLEDGEMENT

The authors would like to express their sincere gratitude to the Department of Environmental and Sustainable Engineering, Faculty of Engineering, Chulalongkorn University for providing laboratory facilities and academic resources that enabled the successful completion of this study. We are also deeply grateful for the financial support provided by the ASEAN and Non-ASEAN Scholarship at Chulalongkorn University. This scholarship played a vital role in facilitating the research activities and academic development of the corresponding author throughout the study period. Special thanks are extended to the laboratory staff, administrative personnel, and fellow researchers who contributed their time, assistance, and thoughtful feedback during various stages of this research. Their support and cooperation greatly enhanced the overall quality of the work.

REFERENCE

[1] P. F. Tasseron *et al.*, "Defining plastic pollution hotspots," *Science of The Total Environment*, vol. 934, p. 173294, 2024/07/15/ 2024, doi: https://doi.org/10.1016/j.scitotenv.2024.173294.

[2] N. E. Kelly *et al.*, "Long term trends in floating plastic pollution within a marine protected area identifies threats for Endangered northern bottlenose whales," *Environmental Research*, vol. 227, p. 115686, 2023/06/15/ 2023, doi: https://doi.org/10.1016/j.envres.2023.115686.

[3] P. Yose, G. Thondhlana, and G. Fraser, "Conceptualizing the socio-cultural impacts of marine plastic pollution on human well-being – A perspective," *Marine Pollution Bulletin*, vol. 194, p. 115285, 2023/09/01/ 2023, doi: https://doi.org/10.1016/j.marpolbul.2023.115285.

[4] A. Pandey, A. Saha, B. Ganguly, R. Hansell, and T. Sanyal, "How Plastics Affect the Marine Environment: Its Sources, Threats, and Consequences, Potential Countermeasures for a Healthy Ocean Environment," 2023, pp. 520-540.

[5] A. L. Andrady, "Microplastics in the marine environment," *Marine Pollution Bulletin*, vol. 62, no. 8, pp. 1596-1605, 2011/08/01/ 2011, doi: https://doi.org/10.1016/j.marpolbul.2011.05.030.

[6] G. Macfadyen, T. Huntington, and R. Cappell, "Abandoned, Lost or Otherwise Discarded Fishing Gear," *UNEP Regional Seas Reports and Studies*, vol. 185, 01/01 2009.

[7] I. E. Napper and R. C. Thompson, "Plastic Debris in the Marine Environment: History and Future Challenges," *Global Challenges*, vol. 4, no. 6, 2020, doi: 10.1002/gch2.201900081.

[8] L. Bradney *et al.*, "Particulate plastics as a vector for toxic trace-element uptake by aquatic and terrestrial organisms and human health risk," *Environment International*, vol. 131, p. 104937, 2019/10/01/ 2019, doi: https://doi.org/10.1016/j.envint.2019.104937.

[9] N. A. Welden and P. R. Cowie, "Degradation of common polymer ropes in a sublittoral marine environment," *Marine Pollution Bulletin*, vol. 118, no. 1, pp. 248-253, 2017/05/15/ 2017, doi: https://doi.org/10.1016/j.marpolbul.2017.02.072.

[10] H. Luo, C. Liu, D. He, J. Sun, J. Li, and X. Pan, "Effects of aging on environmental behavior of plastic additives: Migration, leaching, and ecotoxicity," *Science of The Total Environment*, vol. 849, p. 157951, 2022/11/25/ 2022, doi: https://doi.org/10.1016/j.scitotenv.2022.157951.

[11] A. Turner and M. Filella, "Hazardous metal additives in plastics and their environmental impacts," *Environment International*, vol. 156, p. 106622, 2021/11/01/ 2021, doi: https://doi.org/10.1016/j.envint.2021.106622.

[12] G. Amariei, M. L. Henriksen, J. B. Friis, P. K. Pedersen, and M. Hinge, "In-line identification of Pb-based pigments in fishing nets and ropes based on hyperspectral imaging and machine learning," *Mar Pollut Bull*, vol. 191, p. 114910, Jun 2023, doi: 10.1016/j.marpolbul.2023.114910.

[13] N. Pasumpon and S. Vasudevan, "Baseline study of trace metal concentrations in abandoned, lost or otherwise discarded fishing gear along Thondi coast, Palk Bay, India," *Journal of Sea Research*, vol. 182, p. 102189, 2022/04/01/ 2022, doi: https://doi.org/10.1016/j.seares.2022.102189.

[14] A. Turner, "Trace elements in fragments of fishing net and other filamentous plastic litter from two beaches in SW England," *Environmental Pollution*, vol. 224, pp. 722-728, 2017/05/01/ 2017, doi: https://doi.org/10.1016/j.envpol.2016.11.034.

[15] C. C. M. Ip, X.-D. Li, G. Zhang, O. W. H. Wai, and Y.-S. Li, "Trace metal distribution in sediments of the Pearl River Estuary and the surrounding coastal area, South China," *Environmental Pollution*, vol. 147, no. 2, pp. 311-323, 2007/05/01/ 2007, doi: https://doi.org/10.1016/j.envpol.2006.06.028.

[16] K. S. Vieira *et al.*, "Occurrence of microplastics and heavy metals accumulation in native oysters Crassostrea Gasar in the Paranaguá estuarine system, Brazil," *Marine Pollution Bulletin*, vol. 166, p. 112225, 2021/05/01/ 2021, doi: https://doi.org/10.1016/j.marpolbul.2021.112225.

[17] G. Zhao, S. Ye, H. Yuan, X. Ding, and J. Wang, "Surface sediment properties and heavy metal pollution assessment in the Pearl River Estuary, China," *Environmental Science and Pollution Research*, vol. 24, no. 3, pp. 2966-2979, 2017/01/01 2017, doi: 10.1007/s11356-016-8003-4.

[18] U. S. E. P. Agency, *Method 3051A: Microwave Assisted Acid Digestion of Sediments, Sludges, Soils and Oils*. Washington, DC: U.S Environmental Protection Agency, 2007.

[19] A. W. W. A. A. American Public Health Association (APHA), Water Environment Federation (WEF), *Standard Methods for the Examination of Water and Wastewater, 23rd Edition*. APHA, 2017.

[20] L. Hakanson, "An ecological risk index for aquatic pollution control.a sedimentological approach," *Water Research*, vol. 14, no. 8, pp. 975-1001, 1980/01/01/ 1980, doi: https://doi.org/10.1016/0043-1354(80)90143-8.

[21] Y. Yu *et al.*, "Study on the photoaging process and metal ion release of plastic films with two kinds of structures in marine environment: Aliphatic and aromatic polymers," *Marine Pollution Bulletin*, vol. 203, p. 116474, 2024/06/01/ 2024, doi: https://doi.org/10.1016/j.marpolbul.2024.116474.
[22] S. Willie *et al.*, "MESS-4: Marine Sediment Certified Reference Material for total and extractable metal contentMESS-4 : Matériau de référence certifié pour la teneur en métaux totaux et extractibles des sédiments marins," ed: National Research Council of CanadaConseil national de recherches du Canada, 2014.
[23] K. K. Turekian and K. H. Wedepohl, "Distribution of the Elements in Some Major Units of the Earth's Crust," *GSA Bulletin*, vol. 72, no. 2, pp. 175-192, 1961, doi: 10.1130/0016-7606(1961)72[175:DOTEIS]2.0.CO;2.
[24] B. C. Smith, "Infrared Spectroscopy of Polymers, XI: Introduction to Organic Nitrogen Polymers," *Spectroscopy*, pp. 14-18, 2023, doi: 10.56530/spectroscopy.vd3180b5.
[25] B. C. Smith, "The Infrared Spectra of Polymers II: Polyethylene," *Spectroscopy*, pp. 24-29, 2021, doi: 10.56530/spectroscopy.xp7081p7.
[26] B. C. Smith, "The Infrared Spectra of Polymers III: Hydrocarbon Polymers," *Spectroscopy*, pp. 22-25, 2021, doi: 10.56530/spectroscopy.mh7872q7.
[27] InstaNano. FTIR Functional Group Database Table with Search
[28] S. Veerasingam *et al.*, "Contributions of Fourier transform infrared spectroscopy in microplastic pollution research: A review," *Critical Reviews in Environmental Science and Technology*, vol. 51, no. 22, pp. 2681-2743, 2020, doi: 10.1080/10643389.2020.1807450.
[29] R. N. Corniuk, K. R. Shaw, A. McWhirter, H. W. Lynch, S.-J. Royer, and J. M. Lynch, "Polymer identification of floating derelict fishing gear from O'ahu, Hawai'i," *Marine Pollution Bulletin*, vol. 196, p. 115570, 2023/11/01/ 2023, doi: https://doi.org/10.1016/j.marpolbul.2023.115570.
[30] H. Kanehiro, "Disposal and recycling of fisheries plastic wastes:Fishing net and expanded polystyrene," *Developments in Food Science*, vol. 42, 12/31 2004, doi: 10.1016/S0167-4501(04)80027-X.
[31] G. Weissbach, G. Gerke, A. Stolte, and F. Schneider, "Material studies for the recycling of abandoned, lost or otherwise discarded fishing gear (ALDFG)," *Waste Manag Res*, vol. 40, no. 7, pp. 1039-1046, Jul 2022, doi: 10.1177/0734242X211052850.
[32] A. Mora, J. Dueñas-Moreno, and J. Mahlknecht, "Microplastics as a vector of arsenic contamination," *Current Opinion in Environmental Science & Health*, vol. 33, p. 100461, 2023/06/01/ 2023, doi: https://doi.org/10.1016/j.coesh.2023.100461.
[33] J. Santos-Echeandía, J. R. Rivera-Hernández, J. P. Rodrigues, and V. Moltó, "Interaction of mercury with beached plastics with special attention to zonation, degradation status and polymer type," *Marine Chemistry*, vol. 222, p. 103788, 2020/05/20/ 2020, doi: https://doi.org/10.1016/j.marchem.2020.103788.
[34] A. Turner, "Cadmium pigments in consumer products and their health risks," *Science of The Total Environment*, vol. 657, pp. 1409-1418, 2019/03/20/ 2019, doi: https://doi.org/10.1016/j.scitotenv.2018.12.096.
[35] A. Massos and A. Turner, "Cadmium, lead and bromine in beached microplastics," *Environmental Pollution*, vol. 227, pp. 139-145, 2017/08/01/ 2017, doi: https://doi.org/10.1016/j.envpol.2017.04.034.
[36] A. Turner and M. Filella, "The influence of additives on the fate of plastics in the marine environment, exemplified with barium sulphate," *Marine Pollution Bulletin*, vol. 158, p. 111352, 2020/09/01/ 2020, doi: https://doi.org/10.1016/j.marpolbul.2020.111352.
[37] *Directive 2009/48/EC of the European Parliament and of the Council of 18 June 2009 on the safety of toys (Consolidated version 05.12.2022)*, 2022.
[38] *ISO 8124-3:2020: Safety of toys – Part 3: Migration of certain elements*, 2020.
[39] *TIS 685 Part-1: 2562 (2019): Toys: Safety Requirements: Part 1 – Requirements*, 2019.
[40] R. Muthuraja, B. Ou, M. Thangavelu, T. N. Narhayanan, N. Chittamart, and D. Janjaroen, "Effects of particle size and aging on heavy metal adsorption by polypropylene and polystyrene microplastics under varying environmental conditions," *Chemosphere*, vol. 369, p. 143843, 2024/12/01/ 2024, doi: https://doi.org/10.1016/j.chemosphere.2024.143843.
[41] S. Liu *et al.*, "Microplastics as a vehicle of heavy metals in aquatic environments: A review of adsorption factors, mechanisms, and biological effects," *Journal of Environmental Management*, vol. 302, p. 113995, 2022/01/15/ 2022, doi: https://doi.org/10.1016/j.jenvman.2021.113995.

21R4-09

Upcycling Aluminum Dross into Magnetic Gamma Alumina Adsorbent

Thae Su Su Hninn[1,2], Vorapot Kanokkantapong[3,*]

[1]International Program in Hazardous Substance and Environmental Management,
Graduate School, Chulalongkorn University, Bangkok 10330, Thailand
[2]Center of Excellence on Hazardous Substance Management (HSM),
Chulalongkorn University, Bangkok 10330, Thailand
[3]Department of Environmental Science, Faculty of Science,
Chulalongkorn University, Bangkok 10330, Thailand
Email: Vorapot.ka@chula.ac.th

Abstract

Among the industrial wastes, aluminum dross is a kind of waste that can be valorized including preparation of aluminum oxides gamma alumina due to its adsorbent property. Meanwhile, there is increasing interest in the preparation of magnetic adsorbents as a potential remediation method for pollutant removal. In this study, the magnetic gamma alumina was prepared from aluminum dross waste. Firstly, gamma alumina was prepared from aluminum dross via acid leaching process followed by precipitation with ammonia. Precipitated aluminum hydroxide was converted into gamma alumina by calcination at 600^0C and 900^0C respectively. Gamma alumina was then magnetized by co-precipitation using iron precursors. The characteristics of magnetic gamma alumina were investigated by X-ray florescence (XRF), X-ray diffraction (XRD), and vibrating sample magnetometer (VSM). Additionally, the potential release of elements from the product was assessed. The results from the analysis revealed significant peaks formation in gamma alumina preparation according to XRD, XRF analysis indicated a prominent increase in alumina content following calcination, from 58.9% in aluminum dross to 79.2% in GA 600 and 91.3% in GA 900. Moreover, the magnetic saturation values of the prepared magnetic adsorbents, 11 emu/g for MGA 600 and 40 emu/g for MGA 900, were higher than those reported in some previous studies and no detectable release of hazardous substances was observed from the prepared adsorbent Overall, its facile preparation, eco-friendly nature presents a solution for preparing magnetic adsorbent from aluminum dross waste and provides some insights into the potential application of industrial waste as a value-added product.

Keywords: Waste utilization, Superparamagnetism, Industrial waste

Introduction

Aluminum dross (AD) is a by-product generated during the refining of aluminum and its alloy or as residual waste from the smelting process [1]. If AD were disposed improperly, serious environmental problems including surface water and groundwater pollution or generation of gaseous pollutants when it contacts with water, water vapor or moisture can happen. Moreover, it also contributed to greenhouse effect and ozone layer depletion significantly [2]. Therefore, improper disposal of this waste not only harms the environment but also leads to the loss of valuable components in AD that could be recycled [3]. Some studies investigated the recycling of AD into other products, for instance, a base material for high-quality aluminum-silicon alloys production, generation of hydrogen and other gases or adsorbent preparation depending on the applied method [2, 4, 5]. Pyrometallurgical and hydrometallurgical processes are applied commonly to for the recovery of material from AD, an alumina-rich inorganic residue. The former process consumes high energy, requires high temperature and is costly whereas the latter is energy efficient, lower temperature, and less expensive [6].

The gamma alumina recycled from AD has high surface area, thermal and chemical stability, and effective adsorption properties. The application of gamma alumina can be found not only as an adsorbent for pollutants

removal but also as a catalyst support for syngas preparation [7, 8]. For instance, gamma alumina can remove up to 57 mg/g of methylene blue, crystal violet, basic fuchsin, 245 mg/g of congo red dye according to Fernandes, Silva [9] and Ji, Ling [10]s' studies. Interestingly, utilization of gamma alumina as a magnetic adsorbent by modification has not been established very well in literature.

Gamma-alumina is commonly prepared with acid leaching process by using sulfuric acid [1, 7, 11, 12] although some studies applied hydrochloric acid [6] or nitric acid [13]. The calcination temperature ranges usually between $600^0$and 900^0C [6, 7, 12]. Meanwhile, the development of magnetic adsorbents has also gained increased attention due to their specific properties such as non-toxicity, environmental-friendliness, ease of separation [14]. The studies about magnetic adsorbents development are mostly composites with magnetic nanoparticles [15], synthetic silicate MCM-41 [16], nanocarbons, activated carbons, biochar, graphene derivatives, metal-organic frameworks, carbon nanotubes [17], and magnetic biochar [18, 19] etc. The methods used in those studies are complicated and costly although the magnetic values are not that significant in some preparations. However, the focus on modification of gamma alumina which already has adsorbent property, into magnetic adsorbent has rarely been established. In this study, an attempt is performed to modify the gamma alumina prepared from AD was into magnetic adsorbent. Every stage including gamma-alumina preparation and magnetization is facile in this work and acid leaching process, calcination at $600^0$and 900^0C, co-precipitation with iron precursors were applied.

Methodology

Preparation of Gamma Alumina

There are various types of alumina and not all alumina exhibits adsorbent properties. It can be categorized as low temperature alumina (ρ, χ, η, $\gamma - Al_2O_3$) and high-temperature alumina (α, δ, κ, $\theta - Al_2O_3$) depending on their calcination temperature [1]. Since gamma alumina formation starts from calcination temperature at 600 ^{o}C and ends at 900 ^{o}C [11], the lowest and highest temperature were applied in this study. This study adopted the experimental setups from How's and Roslan's works along with some adjustments [1, 7].

AD was first ground using a Jaw crusher and then a ball mill for further grinding at 1,000 rpm. The resulting grey AD powder was then sieved using a No. 100 sieve shaker. Deionized water was used to wash AD powder, stirred at 200 rpm for 30 mins at room temperature. The solution was dried in the oven at 90^o C and ground.

A 2M sulfuric acid solution was used for acid leaching process, reacting with AD (4:1) at 70^0C for 30 minutes. he resulting grey solution was then filtered to obtain a clear solution. Ammonia (25%) was added dropwise until pH 9 to obtain the white precipitate, aluminum hydroxide. The collected precipitate was then washed with distilled water several times in order to reduce the unwanted soluble materials. The precipitate was dried in the oven at 100^0C and then calcination process at 600^0 C and 900^0C are followed. In this study, the white powders of gamma alumina (GA 600) and gamma alumina (GA900) were obtained for further process.

Preparation of Magnetic Gamma Alumina

Magnetization process was the co-precipitation with iron precursors. Deoxygenated water was firstly prepared using N_2 gas which can prevent critical oxidation. The molar ratio (1:1.95) of iron (III) chloride hexahydrate ($FeCl_3.6H_2O$), iron(II) chloride tetrahydrate ($FeCl_2.4H_2O$) were mixed with gamma alumina in the deoxygenated water along with the presence of sodium hydroxide (NaOH) and stirred vigorously at 70^0C for 30 minutes until pH becomes 10-11. The chemical ratios are described in Table 1. The produced dark-colored nanomaterials were washed with a deionized water and ethanol mixture (1:1) several times until the pH of the washed solution became neutral. After then, the magnetic gamma alumina (MGA 600 and MGA 900) were obtained by drying

the washed product in oven at 105^0C overnight and grinding. Vibrating sample magnetometer (VSM) was used for analysis of magnetic gamma alumina.

Table 1. Chemicals required for magnetization of 2 g-gamma alumina

No	Material Name	Quantity	Unit
1	Deoxygenated water	136	ml
2	Ferrous chloride tetrahydrate	4	g
3	Ferric chloride hexahydrate	~ 10.72	g
4	Sodium hydroxide	~ 7-8	g

Characterization methods

X-ray diffraction (XRD) analysis was performed to identify the formation of gamma alumina by using Bruker D8 Discover (Germany). X-ray florescence (XRF) analysis was also conducted to evaluate the alumina content by using Bruker S8 Tiger (Germany). The magnetic saturation values of magnetic gamma alumina were obtained by using Vibrating sample magnetometer (VSM, 8600 series, Lakeshore Cryotronics, USA). The release of harmful substances was analyzed by using Inductively Coupled Plasma Optical Emission Spectroscopy (ICP-OES, iCAP Pro, Germany).

Results and Discussion

The possible reactions during the acid leaching process and calcination to produce gamma alumina are as follows:

$$2\,Al_2O_3\,(s) + 6\,H_2SO_4\,(aq) \longrightarrow Al_2(SO_4)_3\,(aq) + 3SO_2\,(g) + 6H_2O\,(l) \qquad (1.1)$$

The leached liquor, aluminum sulfate after treated with sulfuric acid reacted with the ammonia solution to produce aluminum hydroxide as a white precipitate. The chemical reaction is represented as:

$$Al_2(SO_4)_3\,(aq) + 6\;NH_4OH\,(aq) \longrightarrow 2\,Al(OH)_3\,(s) + 3\,(NH_4)_2SO_4\,(aq) \qquad (1.2)$$

Finally, the chemical reaction during the calcination step (600^0C and 900^0C) is as follows:

$$2\,Al(OH)_3\,(s) \longrightarrow Al_2O_3\,(s) + 3H_2O\,(l) \qquad (1.3)$$

The formation of gamma alumina from aluminum dross can be shown in Figure 1. (a, b).

The gamma alumina was then magnetized with iron precursors along with sodium hydroxide, resulting in dark-brown precipitate called magnetic gamma alumina (Fig 1.c).

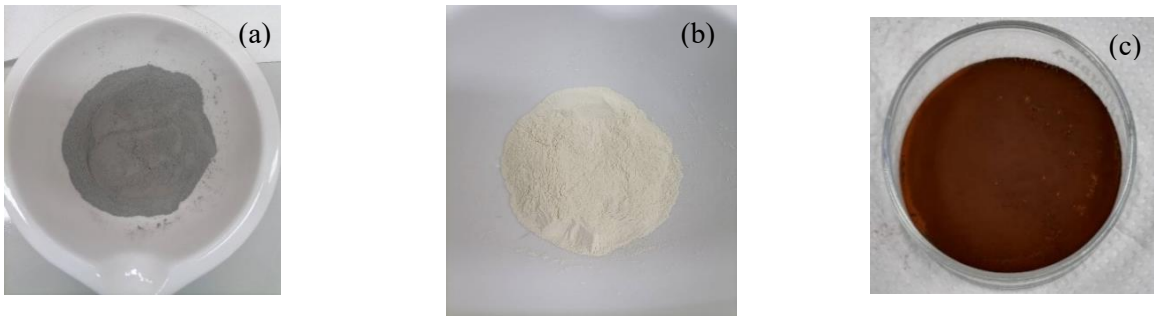


Figure.1. (a) Aluminum dross; (b) Gamma alumina; (c) Magnetic gamma alumina

Characterization of gamma alumina

X-ray Florescence (XRF) & X-ray diffraction (XRD analysis

According to XRF result, the composition of alumina in aluminum dross, GA 600 and GA 900 can be seen in Table 2. The alumina content became higher after transformation of gamma alumina. Presence of gamma alumina was further investigated by XRD analysis. Alumina content became significant after calcinating the aluminum hydroxide powder, from 58.9 (mass %) in aluminum dross to 79.2 (mass %) in GA 600 and 91.3 (mass %) in GA 900, respectively. In Roslan's study, it reported that the composition of gamma alumina after acid leaching was 97 (wt %) derived from AD containing 64.7% of Al_2O_3 [7]. The higher content of Al_2O_3 from AD likely explains this difference in results.

Table 2. Alumina Presence in the materials

Chemical composition	Aluminum dross (Mass %)	GA 600 (Mass %)	GA 900 (Mass %)
Al_2O_3	58.9	79.2	91.3

The XRD results in (Fig 2. a & b) showed the formation of gamma alumina with different peaks at $2\theta = 10 – 80^{o}$. The results indicated the potential of gamma alumina transformation developing at 600^{0}C calcination temperature especially at the 2θ values of 25.5^{0} , 67.42^{0} [20], and 45.54^{0} [21]. For gamma alumina calcined at 900^{0}C, the significant peaks which are similar to many studies can be seen such as 19.6^{0}, 39.56^{0}, 46.84^{0} [1], 32^{0}, 47.48^{0}, 52.56^{0} [22], 35.16 [23], 61.14^{0} [1, 7, 24] and 67.34 [1, 7, 9, 20, 21, 23], confirming that gamma alumina was formed at pH 9. The peak differences in GA 600 and GA 900 indicated that gamma alumina transformation began at 600 and complete its formation at 900 which shows the similar result with Salahudeen's study [11].

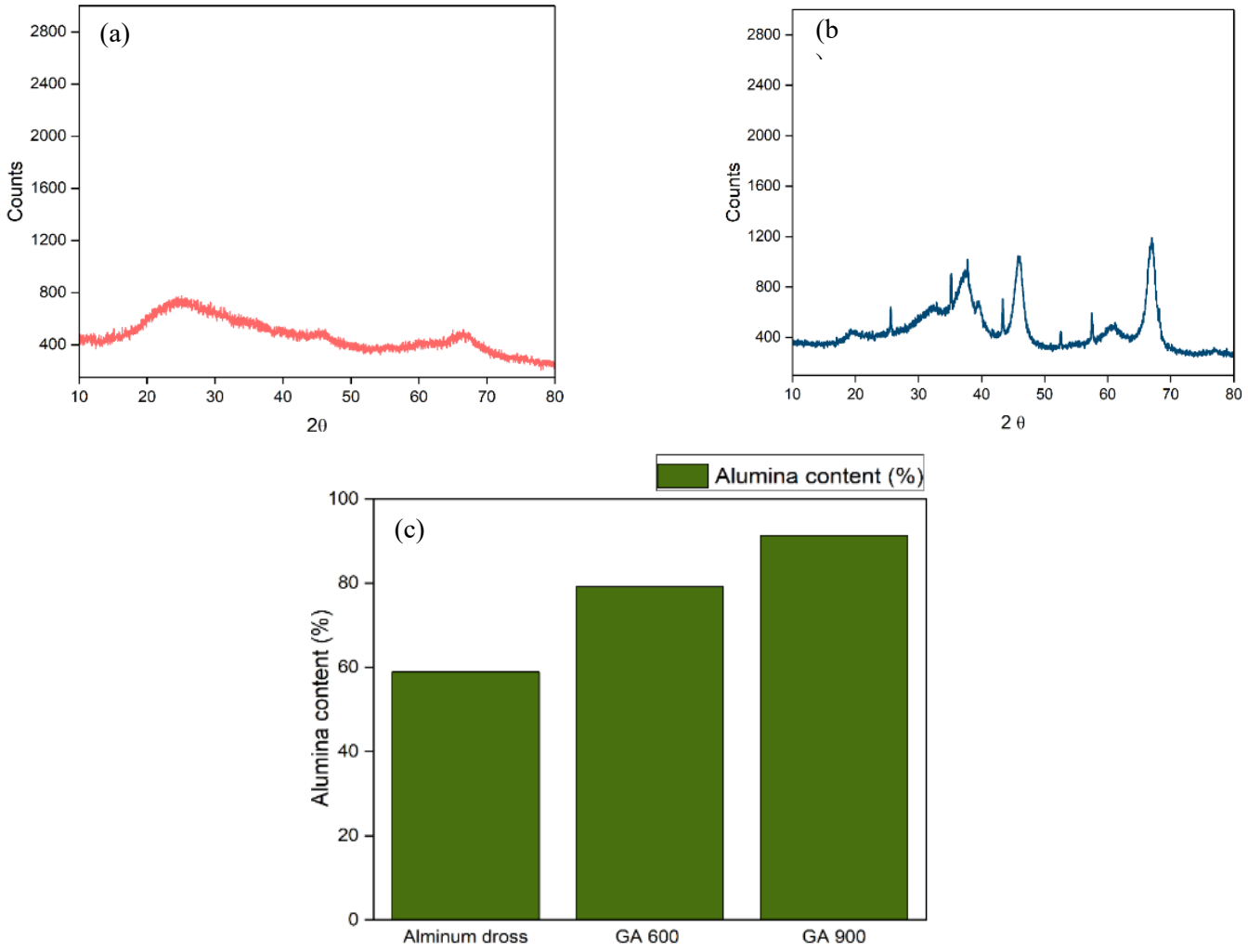


Figure 2. XRD results of gamma alumina calcined at (a) 600^0C; (b) 900^0C (c) Alumina content comparison between AD, GA 600 and GA 900

Magnetic Properties

To investigate the magnetic properties of MGA 600 and MGA 900, vibrating sample magnetometer was applied and the result can be seen in Fig 3. As shown from hysteresis of each sample, the magnetic saturation values of MGA 600 and MGA 900 were around 11 emu/g and 40 emu/g respectively. These results confirm the successful preparation of magnetic gamma alumina. The magnetic saturation values obtained in this study are higher than other studies, such as 8.3 emu/g in Kim's study and 19 emu/g in Arabkhani and Asfarams' study [25, 26]. The magnetic value differences suggested that the different preparation process of magnetic adsorbents has influence on those magnetic saturation values; for instance, the previous literature utilized a $FeSO_4$ solution.

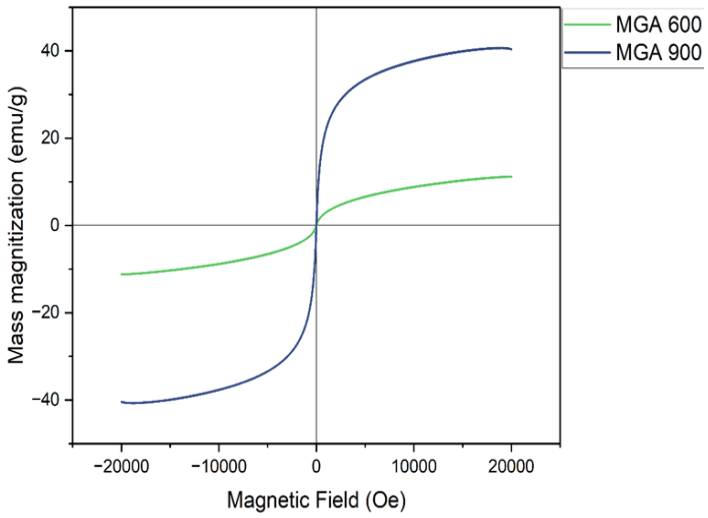


Figure 3. VSM hysteresis for MGA 600 and MGA 900

Table 3. Comparison of magnetic values with other studies

Material Name	Coercivity Value (emu/g)	Reference
MGA 600	11	This study
MGA 900	40	This study
Magnetic MCM 41	8.3	Kim et al., 2001
Biowaste-derived magnetic adsorbent	19	Arabkhani & Asfaram, 2025

Release of harmful substances

ICP-OES analysis, as presented in Table 4, was conducted to determine the elemental release from the magnetic adsorbent and to assess the safety of the prepared magnetic gamma alumina, given that industrial waste was used as the raw material. The results indicated that no release of harmful element except aluminum which was the major component of the product. Therefore, it can be concluded that the prepared adsorbent, derived from industrial waste, poses no significant environmental risk and can be considered an environmentally friendly material."

Table 4. Detection of elements in magnetic gamma alumina

No	Element	Mean Concentration (mg/l)	Remark
1	Al	0.3551	Detected
2	As, Cd, Co, Cr, Cu, Fe, Ni, Pb, Mn, Zn	< LOD*	Non-detected

LOD* limit of detection

Conclusion

The prepartion of gamma alumina from AD waste and magnetic gamma alumina modification was evaluated by different analyses. The significant peaks of 2 θ angles between 10 and 80^{o} showed the presence of gamma alumina in both different calcination temperatures. The magnetic saturation values also indicated that the production of magnetic gamma alumina was achieved. Therefore, the valorization of industrial waste into an environmental-friendly functional material can be an alternative choice for the magnetic adsorbent preparation. Since magnetic adsorbents have been used for pollutants removal, future research should be focused on the application of magnetic gamma alumina in pollutants removal or degradation along with the preparation to obtain more magnetic saturation intensity.

Acknowlegement

This research is supported by IP-HSM research grant, Graduate School, Chulalongkorn Univeristy. The first author
would like to show gratitute to the Faculty of Science, Department of Environmental Science and IP-HSM laboratory, Chulalongkorn Univeristy for providing the facilitation and resources to perform this study.

References

[1] How, L.F., A. Islam, M.S. Jaafar, and Y.H. Taufiq-Yap, Extraction and Characterization of γ-Alumina from Waste Aluminium Dross. Waste and Biomass Valorization, 2017. 8(2): p. 321-327.
[2] Verma, S.K., V.K. Dwivedi, and S.P. Dwivedi, Utilization of aluminium dross for the development of valuable product – A review. Materials Today: Proceedings, 2021. 43: p. 547-550.
[3] Xueqin, L., et al., Feasibility assessment of recycling waste aluminum dross as a basic catalyst for biomass pyrolysis to produce hydrogen-rich gas. International Journal of Hydrogen Energy, 2023. 48(93): p. 36361-36376.
[4] Asencios, Y.J.O. and M.R. Sun-Kou, Synthesis of high-surface-area γ-Al2O3 from aluminum scrap and its use for the adsorption of metals: Pb(II), Cd(II) and Zn(II). Applied Surface Science, 2012. 258(24): p. 10002-10011.
[5] Davoodi, E., et al., Nano-porous anodic alumina: fundamentals and applications in tissue engineering. Journal of Materials Science: Materials in Medicine, 2020. 31(7): p. 60.
[6] Mahinroosta, M. and A. Allahverdi, Enhanced alumina recovery from secondary aluminum dross for high purity nanostructured γ-alumina powder production: Kinetic study. Journal of Environmental Management, 2018. 212: p. 278-291.
[7] Roslan, N.A., et al., Extracted γ-Al2O3 from aluminum dross as a catalyst support for glycerol dry reforming reaction. Materials Today: Proceedings, 2021. 42: p. 63-68.
[8] Mahinroosta, M. and A. Allahverdi, Pilot-scale valorization of hazardous aluminum dross into γ-Al2O3 nanoadsorbent for efficient removal of fluoride. Environmental Technology & Innovation, 2021. 23: p. 101549.

[9] Fernandes, E.P., et al., Efficient adsorption of dyes by γ-alumina synthesized from aluminum wastes: Kinetics, isotherms, thermodynamics and toxicity assessment. Journal of Environmental Chemical Engineering, 2021. 9(5): p. 106198.
[10] Ji, H.-h., et al., Preparation of rod-like γ-alumina/volcanic rock porous material and the adsorption property of Congo red. Journal of Fuel Chemistry and Technology, 2021. 49(7): p. 1049-1056.
[11] Salahudeen, N., et al., Synthesis of gamma alumina from Kankara kaolin using a novel technique. Applied Clay Science, 2015. 105-106: p. 170-177.
[12] Zhang, S., Zhu, W. , Li, Q. , Zhang, W. and Yi, X. , Recycling of Secondary Aluminum Dross to Fabricate Porous γ-Al2O3 Assisted by Corn Straw as Biotemplate. Journal of Materials Science and Chemical Engineering, 2019. 7.
[13] Parida, K.M., A.C. Pradhan, J. Das, and N. Sahu, Synthesis and characterization of nano-sized porous gamma-alumina by control precipitation method. Materials Chemistry and Physics, 2009. 113(1): p. 244-248.
[14] Niu, C., et al., A rapid one-step process for the isolation of antibacterial peptides by silica-decorated Fe3O4nanoparticles. LWT, 2022. 155: p. 112858.
[15] Babaei, A.B., A. Dara, and H.S. Taheri, Efficacious removal of mercury metal in food industry sewerage utilizing reduced graphene oxide adsorbent composited with magnetic nanoparticles. South African Journal of Chemical Engineering, 2025. 52: p. 97-103.
[16] Chen, X., et al., Synthesis of Highly Selective Magnetic Mesoporous Adsorbent. The Journal of Physical Chemistry C, 2009. 113(22): p. 9804-9813.
[17] Di, S., et al., Recent advances and applications of magnetic nanomaterials in environmental sample analysis. TrAC Trends in Analytical Chemistry, 2020. 126: p. 115864.
[18] Rasheed, T., Magnetic nanomaterials: Greener and sustainable alternatives for the adsorption of hazardous environmental contaminants. Journal of Cleaner Production, 2022. 362: p. 132338.
[19] Shahzad, K., et al., Recent advances and factors affecting the adsorption of nano/microplastics by magnetic biochar. Chemosphere, 2025. 370: p. 143936.
[20] Ali, S., Y. Abbas, Z. Zuhra, and I.S. Butler, Synthesis of γ-alumina (Al2O3) nanoparticles and their potential for use as an adsorbent in the removal of methylene blue dye from industrial wastewater. Nanoscale Advances, 2019. 1(1): p. 213-218.
[21] Van Truong, T. and D.-J. Kim, Synthesis of high quality boehmite and γ-alumina for phosphorus removal from water works sludge by extraction and hydrothermal treatment. Environmental Research, 2022. 212: p. 113448.
[22] El-Sawaf, A.K., et al., Green synthesis and characterization of magnetic gamma alumina nanoparticlesfor copper ions adsorption from synthetic wastewater. Results in Engineering, 2024. 22: p. 101971.
[23] Sun, C., et al., Magnetic mesoporous γ-Al2O3/ZnFe2O4 micro-bowls realizing enhanced adsorption, separation and recycle performance towards waste water. Microporous and Mesoporous Materials, 2018. 270: p. 120-126.
[24] Ebadollahzadeh, H. and M. Zabihi, Competitive adsorption of methylene blue and Pb (II) ions on the nano-magnetic activated carbon and alumina. Materials Chemistry and Physics, 2020. 248: p. 122893.
[25] Kim, D.K., et al., Synthesis and characterization of surfactant-coated superparamagnetic monodispersed iron oxide nanoparticles. Journal of Magnetism and Magnetic Materials, 2001. 225(1): p. 30-36.
[26] Arabkhani, P. and A. Asfaram, A novel biowaste-derived magnetic adsorbent for efficient removal of cadmium, cobalt and strontium ions from industrial wastewater. Inorganic Chemistry Communications, 2025. 174: p. 113956.

Plastic Waste Monitoring Via Plastic Product Brand Audit from Marine Debris in Bang Tao Bay, Phuket, Thailand

Sineenart Puangmanee[1*] and Phaothep Cherdsukjai[2]

[1*]*Lecturer, Environmental Science, Phuket Rajabhat University, Phuket, Thailand, 83000*
[2]*Research, Phuket Marine Biological Center Phuket, Thailand, 83000*
[*]*Phone : 0819909707, Fax : 076218806, E-mail : sineenart.p@pkru.ac.th*

ABSTRACT

This research focused on plastic waste in Bang Tao Bay, Phuket, Thailand. The study aimed to analyze the sources of plastic waste by plastic brand audit (product brand) at three beaches in Bang Tao Bay during the Northeast Monsoon season (April) and the Southwest Monsoon season (July) of 2022. The sources and quantities of marine debris were recorded and segregated using the UNEP/IOC Guideline on Survey and Monitoring of Marine Litter (2009) method. The results showed that the product brands could be classified into five major groups of materials that consisted of 1) well-known domestic Thai brands manufactured in the major metropolitan areas outside of Phuket Province, 2) foreign brands manufactured in Thailand, 3) local brands manufactured in Phuket and nearby areas, 4) foreign brands where the origin of the manufacturer could not be identified, and 5) brands where the origin of the manufacturer could not be identified. The greatest number of product brands was Thai brands (74 brands). The most frequently found brands were M-150 and Crystal brands followed by foreign brands (27 brands), local brands (22 brands), foreign brands that could not be identified (17 brands), and product brands of unidentified producers (49 brands). The most frequently found global foreign product brands were Coca-Cola and Nestlé.

Keywords : plastic waste monitoring; plastic product brand audit; marine debris; Bang Tao Bay; Phuket

INTRODUCTION

Plastic waste is a major global issue because it diffuses around the world by many pathways, which may be called transboundary pollution. People around the world are paying attention to plastic waste because the amount of this form of pollution is trending up every year. Recent research revealed that more than 13 million tonnes of plastic waste found its way into the ocean each year [1]. From a ranking of foreign websites, the highest amounts of marine debris in 2021 from plastic waste products came from India (126.50 million kilograms), China (70.70 million kilograms), and Thailand (22.80 million kilograms), which put Thailand within the top 10 [2]. In Thailand, the sources of marine debris were from land and coastal activities (communities, land dumps, port areas, and beach tourism), which accounted for 80%, while activities on the sea (maritime transport, fishing, marine tourism) accounted for 20% [3]. Waste materials can be carried or swept out to sea by wind, currents, waves or rain and may be carried from the sea to the shore. Waste materials may also be intentionally dumped into the sea by humans [1]. A report prepared in Thailand found plastic waste mismanagement amounted to 1.03 million tonnes per year of which 0.41 million tonnes per year were swept into the sea. The types of plastic materials consisted of foam containers (12%), food packaging (10%), plastic shopping bags (8%), plastic bottles (7%), and plastic straws (5%), most of which were from human behavior [4]. These waste materials have an impact on the ecosystem of the seas and oceans, especially on the coral reefs, sea grass, mangroves, and rare marine animals (dolphins, whales, turtles, and dugongs). Furthermore, waste materials affect the economic system, tourism, health, and food contamination due to microplastics [5].

Even though all sectors attempt to mitigate the problems of plastic waste through public relations, campaigns, new policies, laws, plans, and measures, the real sources and causes of the problems have not been addressed. Furthermore, no measures have been implemented to control the recall of end-of-life products and packaging by manufacturers and consumers. Some organizations and producers have started the recall of end-of-life products; however, the public relations budgets are limited and many areas do not have drop-off points for end-of-life products. Moreover, these projects are weak due to voluntary participation. However, the governments of developed countries have established policies called Extended Producer Responsibility (EPR) to control producers by establishing systems to reclaim packaging waste after consumption (Take-Back System) [6] to improve the efficiency of solid waste management.

The purpose of this research was to study plastic waste found at Bang Tao Bay, Phuket, Thailand and explore the sources of plastic waste. This research study carried out a plastic brand audit (product brand) of the sources and quantities of plastic waste at three beaches in 2022 at Bang Tao Bay, Thailand during the northeast monsoon season (April) and the southwest monsoon season (July).

METHODOLOGY

Field sampling: The study site was Bang Tao Bay located in Thalang District, Phuket Province. The data collection in this study design and determination of the experimental area size were determined with modifications from the UNEP/IOC Guideline on Survey and Monitoring of Marine Litter (2009) [7]. The samples were collected from a length of 2,700 meters along the beach at Bang Tao Bay, which was separated into three stations at three beaches: 1) Le Phang Beach; 2) Laguna Beach; and 3) Bang Tao Beach. Each beach was separated into nine points that covered the entire length. The points were spaced every 100 meters for a total distance of 900 meters for each beach (Figure 1).



Figure 1 Coastline of Interest at Bang Tao Bay

The width of the area was from the plant line along the beach to the low tide line (Figure 2). All waste materials one inch and larger were collected from the high tide line each day. The tidal reference was from the Annual Tide Tables Thai Waters Mae Nam Chaophraya - Gulf of Thailand - Andaman Sea A.D. 2022, Hydrographic Department Royal Thai Navy [8].

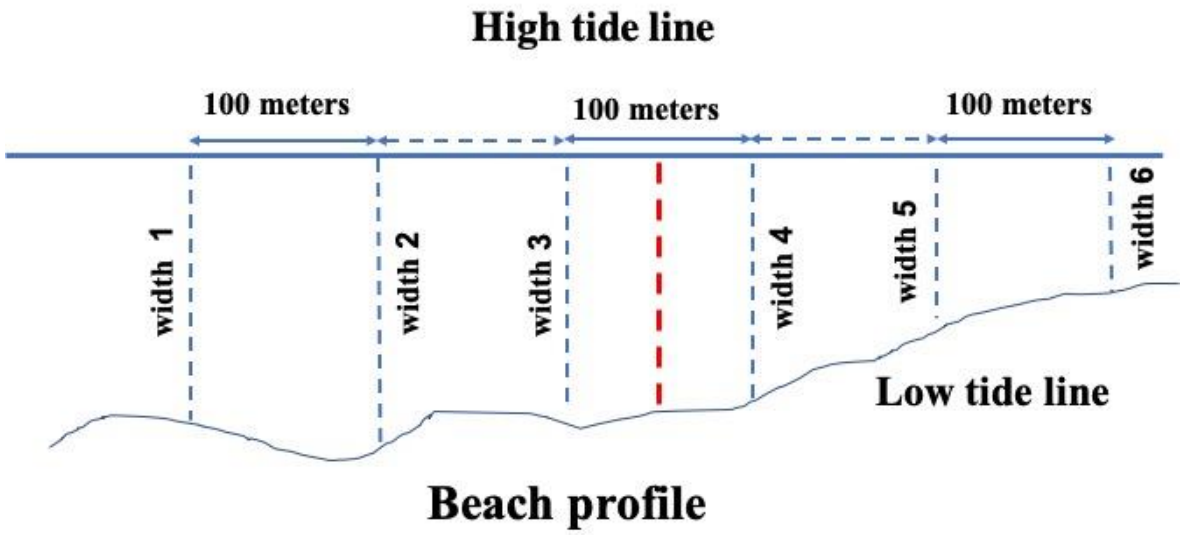


Figure 2 Beach Profile

Data acquisition and processing: The plastic waste and solid waste materials were collected and classified according to sources and quantities by performing a plastic brand audit (product brand) by recording the name of the product. All waste was sorted and recorded with a photo and a piece count of waste that followed the standard method according to the UNEP/IOC Guideline on Survey and Monitoring of Marine Litter (2009) [7].

RESULTS AND DISCUSSIONS

Sources and quantities of plastic waste by product brand audit: During the northeast monsoon season, the product brands were assorted into five groups. Group 1 included 41 Thai brands from 37 Thai companies, which are available in other countries, for a total of 71 pieces. The M-150 brand (Figure 3A) was found to have the greatest amount (10 pieces) followed by Sponsor, Lactasoy, Carabao Dang, Crystal, Red Bull, Vitamilk, Singha, Tiparos, and Shark with 5, 5, 4, 4, 3, 3, 2, 2, and 2 pieces, respectively. Group 2 included product brands from foreign producers in Thailand that included 12 brands from 10 companies for a total of 25 pieces. Coca-Cola (Figure 4C) had the highest number of pieces for a total of 11 pieces followed by Geonbae and Mirinda with 3 and 2 pieces, respectively. Group 3 included 13 local Thai brands from four provinces for a total of 15 pieces. The brands were PP (3 pieces) followed by Top Water (2 pieces) and Kowit Drinking Water (1 piece). Group 4 included nine pieces of seven foreign product brands from three countries. The specific manufacturing locations of these products could not be identified. The brands were L&M (3 pieces) followed by One2Drink, Summer, Twister, and Petronas Gas with 1 piece each. These five brands are from Malaysia. The next two brands were one piece of Real from Singapore and one piece of Soju from South Korea. Group 5 included 16 pieces from 15 brands that could not be identified.

During the southwest monsoon season, the product brands were assorted into five groups. Group 1 included Thai products produced in Thailand. There were 33 brands from 29 companies for a total of 54 pieces. Four pieces of the Crystal brand (Figure 3B) were found followed by M-150, DeeDo, Singha, LEO, Carabao Dang, MAMA, Ichitan Greentea, and Srisuda Bakery with 4, 4, 4, 3, 3, 3, 2, and 2 pieces, respectively. Group 2 included foreign producers in Thailand. A total of 15 brands from 8 companies for a total of 44 pieces were found. The brands were Nestlé (17 pieces) (Figure 4D) followed by Coca-Cola, Ajinomoto, Sprite, Lays, and Nescafé with 12, 2, 2, 1, and 1 pieces, respectively. Group 3 included local Thai brands, which were nine brands from three provinces for a total of 12 pieces. The brands were Kowit Drinking Water (3 pieces) followed by Sand Drinking Water and Sea Horse Drinking Water with 2 pieces and 1 piece, respectively. Group 4 included 13 pieces of 10 foreign brands from five countries. The specific locations for the manufacturing of these products could not be identified. The brands were AQUA (4 pieces) and GOLDA (1 piece). These two brands are from Indonesia and are also available in India, Malaysia, Sri Lanka, and Singapore. Group 5 included 34 brands for a total of 35 pieces that could not be identified.



A **B**

Figure 3 Product Brands of Thailand
(A) M-150 and (B) Crystal



C **D**

Figure 4 Foreign Product Brands
(C) Coca-Cola and (D) Nestlé

The plastic waste that was classified by product brand during the northeast and southwest monsoon seasons identified 189 brands from five types of product brands: 1) Thai products produced in Thailand included 74 brands from 66 companies; 2) foreign products produced in Thailand included 27 brands from 18 companies; 3) local Thai brands included 22 brands from 7 provinces; 4) foreign product brands of unidentified producers included 17 brands from 8 countries; and 5) product brands of unidentified producers included 49 brands. Notably, the most common foreign brands produced in Thailand that were found during both monsoon seasons were Coca-Cola and Nestlé. These two brands were also found to be among the most common top three brands in many countries and over many years. Coca-Cola and Nestlé brands were found in a report by the Department of Marine and Coastal Resources [9], which mentioned that Coca-Cola and Nestlé brands were found at a beach in Thailand in 2020 and 2021 during the northeast and southwest monsoon seasons. Moreover, Coca-Cola and Nestlé were found most frequently in the Canadian cities of Vancouver, Toronto, Montreal, Halifax, and at Sable Island in a study by Baxter et al (2022) that evaluated single-use plastic mitigation policies [10]. Also, these two brands were found in a brand audit of anthropogenic litter by Stanton et al (2022) [11]. That study found plastic waste products related to Coca-Cola, Anheuser-Busch InBev, and PepsiCo. In addition, Coca-Cola was found to be the leading plastic bottle polluter in Kenya in the sodas category in a report published by CLEAN UP KENYA (2021) that focused on the 2021 PET Rubbish Report, which was the first national brand audit report [12]. Moreover, survey reports by Green Queen (2021) [13] and Trash Hero World (2020) [14] found that the top polluting

companies to produce plastic waste were Coca-Cola, PepsiCo, and Nestlé/Unilever. Coca-Cola, PepsiCo, and Nestlé were also found in a report by Break Free From Plastic (2018) [15].

The results of a plastic brand audit conducted in Thailand (2021) by Greenpeace Thailand (2021) showed that under the COVID-19 situation the same brands were found in many areas that included Samut Prakan Province, Chiang Rai Province, Prachuap Khiri Khan Province, Rayong Province, and Bangkok [16]. In addition, Greenpeace conducted a brand audit of plastic waste using the Home Brand Audit method in homes and dormitories at Burapha University (Chanthaburi Campus) that identified Nestlé, Coca-Cola, PepsiCo, Mondelēz, and Unilever. In 2020, a plastic brand audit conducted in Thailand by Greenpeace Thailand [17] found Nestlé and Coca-Cola waste products in many areas such as Wonnapha Beach (Chon Buri Province) and Chiang Mai Province. In 2019, Coca-Cola and Nestlé waste products were found in Chiang Mai Province and Songkhla Province, and in 2018 the same products were found at Wonnapha Beach (Chon Buri Province).

It can be noted that the major product brands, especially Coca-Cola and Nestlé, and others that distribute to many areas around the world do not control waste packaging after use by either the companies or the consumers. Some organizations, especially non-government organizations, appeal to the companies that own the product brands to solve the problems concerning plastic waste by stressing the use of EPR. In addition, legal pressure has been used in many countries of the European Union (Germany, Sweden, Netherland) [18], Japan, South Korea, Taiwan, Singapore, Vietnam, Indonesia, Philippines, and Thailand [19]. In Thailand the policies, strategies, and plans for plastic waste management that cover ERP policy include the Thailand Environment Quality Management Plan 2017-2022, Thailand's Road Map on Plastic Waste Management 2018-2030, National Waste Management Action Plan: Volume 2 (2022-2027), and the Plastic Waste Management Action Plan: Phase 1. Although each country attempts to solve the problems of plastic waste, management of the problem is difficult due to the need to integrate and improve the policies and legal aspects that require joint cooperation and participation from all stakeholders. In addition, Thailand just started to solve the problems of plastic waste products by using laws and measures to control plastic waste, especially EPR policies, but it is not efficient as most of producers/manufactures lack the knowledge and understanding of EPR policies and lack awareness in environmentally friendly production.

CONCLUSION

The product brands of plastic waste from marine debris at the three beaches in Bang Tao Bay in both seasons were classified into five groups: 1) Thai products produced in Thailand; 2) foreign products produced in Thailand; 3) local Thai brands; 4) foreign product brands of unidentified producers, and 5) product brands of unidentified producers. In both monsoon seasons, the two most common Thai brands found were M-150 and Crystal, and the two most found foreign brands produced in Thailand were Coca-Cola and Nestlé. Although Thailand has many policies, strategies, and plans for plastic waste management, the problems of plastic waste have not been solved. Therefore, all sectors need to cooperate in solving this problem.

ACKNOWLEDGEMENT

The authors would like to thank Phuket Rajabhat University for financial support (PKRU Fund), Phuket Marine Biology Center for information and data support, Cherngtalay Subdistrict Municipality, and Laguna Phuket for their area site support.

REFERENCES

[1] https://www.sdgmove.com/2023/07/26/plastic-pollution-sea-thailand/
[2] https://www.onep.go.th/
[3] https://km.dmcr.go.th/c_260/d_19695
[4] https://www.bangkokbiznews.com/lifestyle/942359
[5] https://www.dmcr.go.th/detailAll/35501/nws/191
[6] https://ej.eric.chula.ac.th/article/view/277
[7] https://www.unep.org/resources/report/unepioc-guidelines-survey-and-monitoring-marine-litter
[8] The tide reference from Annual Tide Tables Thai Waters Mae Nam Chaophraya - Gulf of Thailand - Andaman Sea A.D. 2022, Hydrographic Department Royal Thai Navy (2020)xx
[9] Report of Department of Marine and Coastal Resources (2022)
[10] L. Baxter, Z. Lucas, TR. Walker, Marine Pollution Bulletin, 176, (2022)

[11] https://www.sciencedirect.com/science/article/pii/
[12] https://brandaudit.breakfreefromplastic.org/wp-content/updoads/2022/11/2021-PET-Rubbish-Report-Final-Web.pdf
[13] https://www.greenqueen.com.hk/break-free-from-plastic-2021-brand-audit/
[14] https://trashhero.org/brand-audit-report-2020/
[15] https://brandaudit.breakfreefromplastic.org/wp-content/uploads/2022/11/BRANDED-Report-2018_compressed.pdf
[16] https://act.seasia.greenpeace.org/th/brand-audit-report-2022?_ga=2.22582131.917446341.1723548876-2113776397.1723548876
[17] https://www.greenpeace.org/thailand/publication/18363/plastic-brand-audit-result-thailand-2020/
[18] https://ej.eric.chula.ac.th/article/view/318
[19] https://packaginglibrary.agro.ku.ac.th/knowledge/0-293-

21R5-02

Effects of Pyrolysis Temperature and Chemical Activation on Characteristics and Yields of Biochar Produced from Coconut Husk Biomass

Leangse Meng[1], Thaksina Poyai[2], Ratchanan Chamnanmor[3], Saret Bun[4], and Pisut Painmanakul[5,6,7*]

[1]Master student; [3]Doctoral student; [5]Professor, Department of Environmental and Sustainable Engineering, Faculty of Engineering, Chulalongkorn University, Bangkok 10330, Thailand
[2]Lecturer, Department of Environmental Engineering, Faculty of Engineering, Kasetsart University, Bangkok 10900, Thailand
[4]Professor, Water and Environmental Engineering, Faculty of Hydrology and Water Resources Engineering, Institute of Technology of Cambodia, Phnom Penh, Cambodia
[6]Director, Carbon Institute for Sustainability, Chulalongkorn University, Bangkok 10330, Thailand
[7]Professor, Center of Excellence in Treatment Technology and Management of Petroleum Contaminants and Environmental Pollution, Chulalongkorn University, Bangkok 10330, Thailand
[*]Phone : (66)08 9413 1392, E-mail : leangsemeng715@gmail.com

ABSTRACT

Carbon dioxide (CO_2) is known as the main greenhouse gas emission. The increase of CO_2 concentration has significantly caused global warming and affected climate change by trapping heat in the atmosphere. There is an urge to develop innovative technologies to balance the surface carbon dioxide. Biochar is a long-term form of carbon structure, scalability and cost-effectiveness for manufacturing. To tackle this, we will investigate the conversion of biochar made from coconut husk (CH), a common agricultural waste that is abundant source in tropical countries. The study attempts to turn CH biomass into a useful CO_2 adsorbent. This work focuses on pyrolysis at various temperatures (500 ℃ and 600℃), followed by alkali activation using potassium carbonate to well improve pore structure and enhancing biochar surface area. Advanced characterization approaches, including BET surface analysis, FTIR, and scanning electron microscopy, have been used to study the structural changes in biochar. The results anticipate that the alkali-activated biochar will have a significantly larger adsorption capacity than the non-activated biochar due to its increased surface area and porosity. This research will demonstrate the practicality of biochar as a cost-effective and environmentally friendly adsorbent material, as well as its role in encouraging environmental sustainability by transforming agricultural waste into valuable resources. The coconut husk biochar has the potential to play a key part in global carbon management and climate change mitigation efforts.

Keywords : Agricultural waste; Pyrolysis; Coconut husk biochar; K_2CO_3 activation

INTRODUCTION

Biochar is a carbon-rich material produced from biomass through pyrolysis in the absence of oxygen. Biochar has become one of the most popular carbonaceous physical adsorbents due to its large surface area, porous structure, and slightly polar surface. Furthermore, it has a cheaper manufacturing cost compared to various solid adsorbents since it has its stability under humid conditions and at low to moderate operating temperatures[1]. Additionally, biochar is most broadly used to remove contaminants from water and wastewater, soil amendment , and air purification. Additionally, it was found to be effective in reducing solid and food waste, supporting waste mitigation, and contributing to sustainable solutions for climate change, energy production, and pollution [2]. The research of vitamin C modified cow manure biochar significantly enhanced the removal efficiency of tetracycline from water, with a maximum adsorption capacity of 50.90 mg/g, compared to 31.72 mg/g for unmodified cow dung biochar [3]. The study of biochar produced from agricultural waste has been improved with hydrogen peroxide and magnetization modifications to adsorb hexavalent uranium from aqueous solutions. The adjustments raised the biochar's specific surface area from 17.606 m^2/g to 195.62 m^2/g and pore volume from 0.037 cm^3/g to 0.132 cm^3/g, improving its adsorption magnetized HBC (MBC) of 77.58 mg/g and hydrogen peroxide modified biochar (HBC) of 69.50 mg/g[4]. The biochar conversion from argan paste cake produced by a two-step chemical

activation technique using KOH as activation agent at three different activation temperatures at 700°C, 800°C, and 850°C was applied. The activated carbon sample which generated at 700°C had the maximum CO_2 adsorption capacity, reaching 4.89 mmol/g at 0°C and 2.98 mmol/g at 25°C. The developed activated carbons were highly porous, with specific surface areas that varied between 1211 to 2046 m^2/g. Micropores, which are crucial for CO_2 adsorption, were most abundant in the sample processed at 700°C. The carbon content of the activated carbon went up with activation temperature, with 700°C providing the maximum results[5]. Biochar is an effective form of carbon storage, capable of locking carbon away for potentially hundreds to thousands of years. Globally, the implementation of biochar could sequester between 0.3 to 2 gigatons of CO_2 equivalent per year by 2050[6]. It is regarded as an innovative technology which can help mitigate and balance excessive CO_2 in the atmosphere.

Due to population growth, urbanization and industrialization worldwide would release so much negative impact to the environment like solid waste, liquid waste, soil contamination and air pollution. All these problems can cause a threat of global warming and lead to affect climate change and ecosystem. Human activities are expressed to have raised the Earth's global average temperature by around 1 ℃ (1.8 ℉) from the pre-industrial period, with an increase of more than 0.2 ℃ (0.36 ℉) every decade nowadays. The present pattern of warming seems to be the product of human activities since the 1950s, and it is occurring at an unprecedented rate spanning over centuries [7]. The Paris Agreement on Climate Change was ratified in 2015 by 194 nations, establishes a global framework to limit the average temperature rise to well below 2 degrees Celsius above pre-industrial levels, while endeavoring to restrict the temperature increase even further to 1.5 degrees Celsius to control the emission of GHGs [8]. Carbon dioxide (CO_2) contributes to almost 80% of all greenhouse gasses emission which are primary caused by both natural processes and human activities. The increase of CO_2 concentration significantly led to global warming and affected climate change by trapping heat in the atmosphere. In 2023, the global average surface CO_2 concentration reached 419.3 ppm while recent global trend was about 425 ppm[9, 10]. Waste management is also one of the main problems which are leading to substantial impacts on climate change besides fossil fuel combustion, agriculture, deforestation, and industrial processes. To address these challenges, biochar is an urge innovative technology corresponding to both solid waste and climate change mitigation. Since Coconut husk is a common waste product in tropical nations. In 2022, the global generation of coconut husk was at 62.4 million tons by Statista 2024 [11]. Therefore, production of coconut husk biochar should provide two environmental benefits by utilizing solid waste and reducing greenhouse gas emission.

Therefore, the objective of study was to investigate the potential of coconut husk as a suitable feedstock for biochar production by the slow pyrolysis process, and to assess the effects of pyrolysis temperatures on biochar yield and subsequent physicochemical properties. The pyrolysis temperatures of 500 and 600 °C with a constant residence time of 60 min and a heating rate of 5 °C/min were selected as process parameters for the slow pyrolysis process follow by activation. The resulting biochars were characterized in terms of the mass yield, proximate and ultimate analysis, specific surface area, morphological and functional group analysis (FTIR).

METHODOLOGY

Sample Preparation

Biomass feedstock used in this study is coconut husk waste which was purchased from the local farm in Thailand. The coconut husk (CH) was cut into small pieces and oven dried at 105 ℃ for 24h then grinding and sieving before pyrolysis process. Potassium carbonate (K_2CO_3) is an activating agent used as the activating agent for producing activated biochar and 1 mol/L HCL was applied to wash the impregnated samples to get off ash and organic matter before activation. All reagents used were of analytical grade.

Biochar Production

The prepared coconut husk was pyrolyzed in pyrolysis reactor under slow pyrolysis conditions with a heating rate of 5 ℃/min, N_2 flow rate of 100 mL/min for 1h. The pyrolysis experiments were conducted at temperatures of 500 °C and 600 °C. The flow chart of pyrolysis process is exhibited in **Figure 1**. The coconut husk biochar would be kept in vacuum seal bags (MAP or Nitrogen Packaging) in an airtight container store in a dry environment, stable temperature and avoid direct sunlight. The samples of biochars were labeled as R500 and R600 (R represented raw biochar before impregnation). The coconut husk biochar was impregnated with potassium carbonate solution (1:1 ratio by mass, in previous study they used 2 g of CHBC mixed with 50 mL of DI water with contained concentration of K_2CO_3[12]). Subsequently, the mixture was first dried in the oven at 80 ℃ to evaporate moisture, and then further dried overnight at 110 °C.

After drying, the biochars were mixed with 1 mol/L of HCl to remove the ash and impurity in the pore biochar and then washed with deionized water until the conductivity of the wash liquor was less than 10 mS/cm or reached neutral condition. At last, the biochars were dried at 105 ℃ for 1 hour.

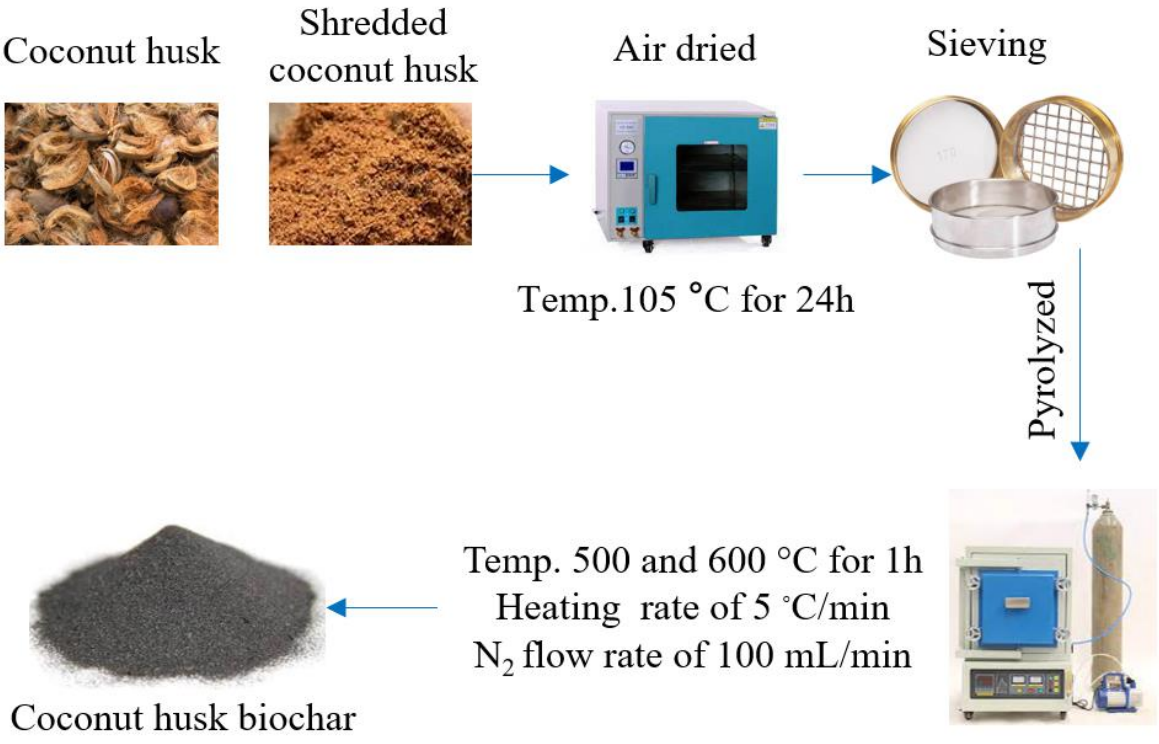


Figure 1 Flow Chart of Pyrolysis Process

The biochars were then activated at 700 °C under a N_2 flow. The control biochar was prepared directly from coconut husk, without impregnation and addition of potassium carbonate. The activated biochars were labeled as BC500-700, BC600-700. The samples were stored in sealed containers for further analysis.

Biochar Characterization

Particle Size Distribution of coconut husk feedstock was performed by sieve analysis. Proximate analyses were implemented by thermogravimetric analyzer. The proximate analysis was taken out to determine the volatile matter, ash content, fixed carbon, and moisture content in weight percentage of the biomass and pyrolyzed biochars. Fixed carbon content was determined by difference. The percent fixed carbon (%FC) and percent ash free fixed carbon (% FC ash-free) were determined using Eq. (1) and (2), described by [13]

$$\% FC = \left(\frac{M_{FC+ash-} M_{Ash}}{M_{OD-BC}}\right) \times 100 \quad (1)$$

$$\% FC_{ash-free} = \left(\frac{M_{FC+ash} - M_{ash}}{M_{OD-BC} - M_{ash}}\right) \times 100 \quad (2)$$

Where M_{OD-BC} is the mass in grams of the sample after oven drying at 105 ◦C, M_{ash} is the sample mass in grams after combustion M_{FC+Ash} is the mass in grams of fixed carbon and ash in the sample

Ultimate analyses were performed by dry combustion with a CHNS Analyzer. Oxygen was calculated as formula shown in Eq.(3) followed by Gaur & Poonia, 2024 [14].

$$O\% = 100\ (\%) - C\ (\%) - H\ (\%) - N\ (\%) - Ash\ (\%) \quad (3)$$

The weight of feedstock (W_1) and the produced biochar (W_2) from the feedstock were measured to calculate the conversion efficiency using Eq.(4) followed by Gonzaga et al., 2017 [15]

$$\text{Conversion Efficiency} = \frac{W_2}{W_1} \times 100\% \quad (4)$$

Surface areas and pore volumes of the biochars were determined by BET and BJH method. The morphologies, the structure and size distribution of activated biochar materials were observed by Field Emission Scanning Electron Microscope and Energy Dispersive X-Ray Spectrometer (FESEM-EDS). Chemical functional groups were determined by Fourier transform infrared spectroscopy (FTIR).

RESULTS AND DISCUSSIONS

Particle Size Distribution of Biomass Feedstock

The graphs shown in **Figure 2** represent the particle size distribution of the coconut husk feedstock, essential for assessing its suitability in biochar production. Graph A displays a bar chart of the percentage of particles within specific screen size classes in millimeters, illustrating a main size class between 0.250 and 0.255 mm, where over 50% of the particles are concentrated. This indicates a highly specific granular composition, which is critical for uniform pyrolysis in biochar production. Graph B, the gradation curve, further details the cumulative percentage of particles finer than each size class. It shows that approximately 58% of the particles are finer than 0.63 mm and more than 86% are under 1 mm, emphasizing fine particle distribution. Mostly all particles (98.90%) are finer than 2.3 mm, ideal for ensuring a high surface area, beneficial for applications such as CO_2 adsorption, soil amendment and filtration, where increased surface area and reactivity are crucial. The combination of these graphs provides a comprehensive overview of the particle size distribution, highlighting the feedstock's potential for producing high-quality biochar with desirable physical and chemical properties for environmental applications.

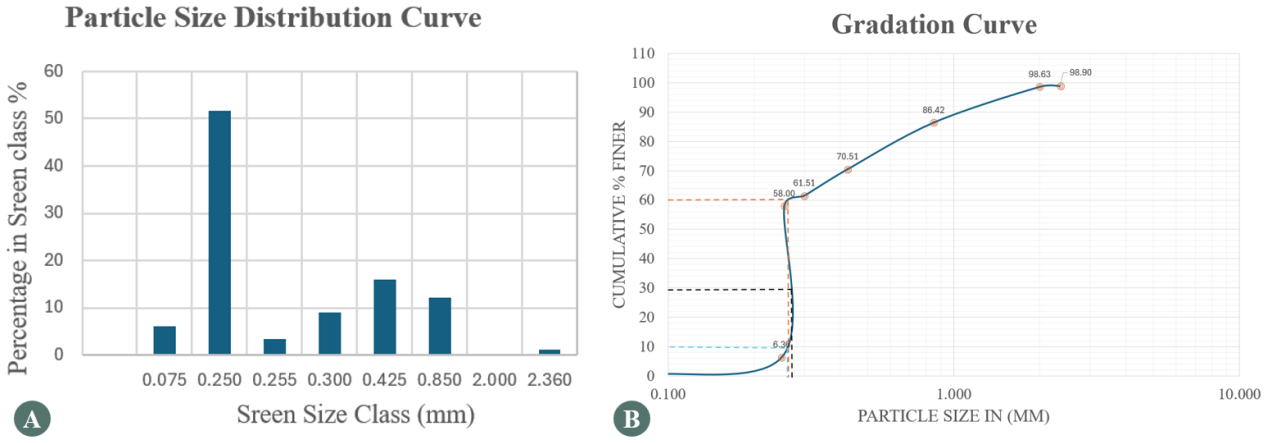


Figure 2 Sieve analysis: A. Particle Size Distribution and B. Gradation Curve

Biochar Yield

The biochar yield was calculated based on the dry weight of the coconut husk feedstock before and after pyrolysis. Preliminary results suggest that the yield of coconut biochar varies depending on the pyrolysis temperature and time. For instance, at a temperature of 500°C maintained for 1 hour, the yield was approximately 59 % of the initial coconut husk feedstock mass. This yield decreased to about 48% as the temperature increased to 600°C, demonstrating a typical trend where higher temperatures lead to more extensive decomposition of organic material. The moisture contained in the feedstock is one of the factors that affect biochar production yield. When the initial coconut husk is well dried it will generate lower weight loss after pyrolysis. In this study drying condition of raw materials before pyrolysis is at 105 ℃ for 24h. I get only 34% average weight compared to the raw materials before drying.

Proximate Analysis

The proximate analysis was intended to characterize the biochar in percentage such as moisture content (%MC) , volatile matter(%VM), fixed carbon(%FC), and ash content(%Ash). The ash content is a measure of the non-volatile matter and non-combustible component of the biochar. Regarding the coconut husk as a feedstock provided low ash content less than 17.32 % which is essential for high pore volume and

surface area shown in **Table 1**. While higher ash content could provide nutrient for soil[16] but not suitable for other applications such as energy recovery or CO_2 adsorption, due to ash may clog pore of biochar lead to decrease adsorption capacity.

Ultimate Analysis

Consequence of Elemental analysis illustrated that biochar largely has five elements hydrogen (H), oxygen (O), nitrogen (N), sulfur (S) and carbon (C). A higher carbon content signifies increased stability and long-term carbon sequestration capability. The aromaticity of biochar is also impacted by its hydrogen and oxygen levels. The low H/C and O/C ratios indicate a higher degree of carbonization, consequential in more stable biochar and less degradation over time[17]. According to the current study illustrated in **Table 1**, coconut husk biomass could produce high fixed carbon approximately 83.76% which is crucial for biochar production great carbon structure and high surface area.

Table 1 Elemental Composition of Coconut Residues and Coconut Husk in this Recent Work

Part of coconut residue	MC (%)	VM (%)	FC (%)	Ash (%)	C (%)	N (%)	H (%)	S (%)	Yield (%)	Reference:
Husk	-	5.33	77.35	17.32	67.31	0.87	2.67	0.17	34	[18]
Flesh	2.36	12.71	79.09	8.19	83.25	2.98	1.45	1.33	40.65	[19]
Husk	1.69	5.99	83.76	8.56	>60.0	-	-	-	33.7	[20]
Coconut frond	7.08	78.03	17.01	4.96	34.01	0.46	7.71	0.94	-	[19]
Coconut frond	0.37	89.96	5.37	4.67	42.81	-	7.23	0.77	~38.76	[21]
Coconut Husk	0.18	84.13	15.54	0.33	47.36	7.02	1.43	0.03	~40.45	[21]
Coconut Husk(500℃)	-	-	-	-	-	-	-	-	59	This study
Coconut Husk(600℃)	-	-	-	-	-	-	-	-	48	This study

FTIR Analysis

The infrared spectrum of coconut husk biochar which were analyzed by FTIR, are shown in Fig 3(a) and Fig 1(b). Characterization of biochar samples using FTIR to detect functional groups of carbon, impurities, and water that can change the sequestration ability. The FTIR spectra of raw coconut husk (CH) and coconut husk biochar (CHC) produced at varying pyrolysis temperatures (400°C, 600°C, 800°C, and 1000°C) are presented in **Figure 3(a)** [18].

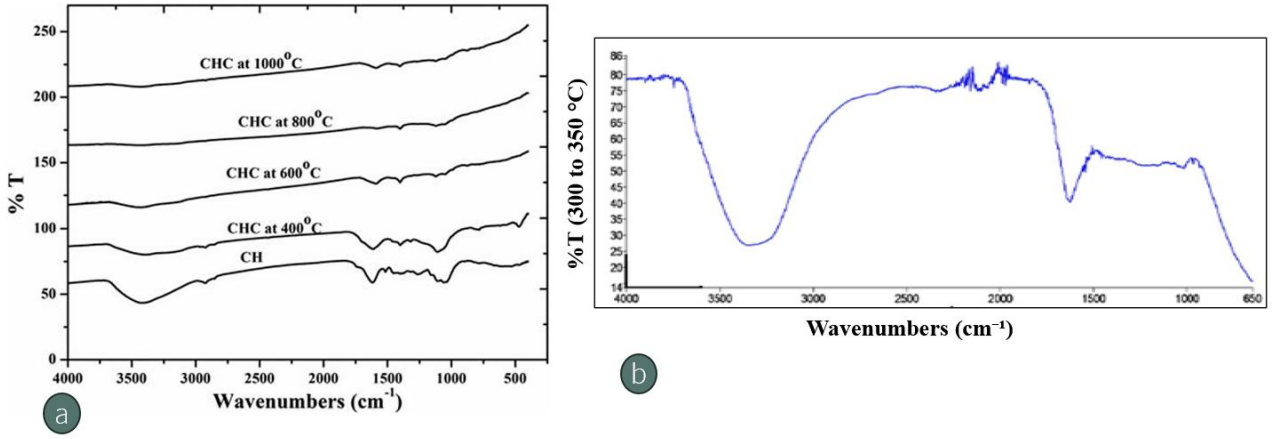


Figure 3 FTIR analysis: a. coconut husk biochar (400°C, 600°C, 800°C, and 1000°C) and b. coconut husk biochar (300 to 350 °C)

The raw CH sample exhibits prominent absorption bands around 3400 cm^{-1}, 2900 cm^{-1}, 1700 cm^{-1}, and 1000–1200 cm^{-1}, corresponding to O–H stretching (hydroxyl groups), C–H stretching (aliphatic groups), C=O stretching (carbonyl groups), and C–O stretching (cellulose and hemicellulose), respectively. As pyrolysis temperature increases, these peaks gradually diminish in intensity, indicating the thermal

degradation and volatilization of oxygen-containing functional groups. At temperatures above 600°C, the spectra show a significant reduction in polar functional groups, and at 1000°C, most peaks nearly disappear, suggesting the formation of highly aromatic, carbon-rich structures. This transformation confirms the increasing carbonization and chemical stability of the biochar with temperature, highlighting its potential suitability for long-term carbon sequestration and other environmental applications. In contrast, the single-spectrum biochar in **Figure 3(b)**[22], representing a specific pyrolysis condition temperature range of 300–350°C, still shows prominent bands at 3400 cm^{-1} (O–H), around 1700 cm^{-1} (C=O), and 1000–1200 cm^{-1} (C–O), indicating the partial retention of surface oxygenated groups. This suggests that the biochar retains a moderate level of reactivity and adsorption capacity, making it suitable for applications such as wastewater treatment or soil amendment.

BET Surface Areas and Pore Volumes

The BET surface analysis will observe biochar produced from Coconut Husk biomass. BET surface area, pore volume and pore diameter of biochar are significant to identify the adsorption capacity of biochar. The study of coconut husk fiber, surface area increased from 193.7 to 278.58 m^2/g rapidly as the pyrolysis temperature increased from 450 to 500 °C. That could be attributed to the complete devolatilization within that temperature range and structural modification of higher crystalline lignin contents of the feedstock and 600 °C, the surface area of the coconut fiber biochar was 286.68 m^2/g [23]. Another previous studies indicated that the activated K_2CO_3 of coconut husk demonstrated a well-developed porous structure, with a BET surface area of 1356.25 m^2/g, total pore volume of 0.780 cm^3/g and adsorption capacity of 418.15 mg/g for methylene blue[24].

CONCLUSION

This study confirms that pyrolysis temperature is a critical factor in determining the yield and quality of biochar produced from coconut husk biomass. The preliminary results show that as the temperature increased, the biochar yield decreased from 59% to 48%. Alkali activating agent could enhance the BET surface area and pore volume of biochar, which is advantageous for adsorption application regarding to the study of K. Y. Foo and B. H. Hameed[24]. By improving the biochar's physical characteristics through controlled pyrolysis and chemical activation, this research highlights a viable pathway for the use of agricultural waste in mitigating climate change impacts. This study sure provides essential data and information for further researchers to explore wisely realistic applications of coconut husk biochar in real-world scenarios.

ACKNOWLEDGEMENT

The authors thankfully Department of Environmental and Sustainable Engineering, Faculty of Engineering, Chulalongkorn University for this research.

REFERENCE (Please see format of the reference in the Manuscript Format and Style)

[1] A. N. Shafawi, A. R. Mohamed, P. Lahijani, and M. Mohammadi, "Recent advances in developing engineered biochar for CO2 capture: An insight into the biochar modification approaches," Journal of Environmental Chemical Engineering, vol. 9, no. 6, 2021.

[2] A. Kumar et al., "Multifaceted applications of biochar in environmental management: a bibliometric profile," Biochar, vol. 5, no. 1, 2023.

[3] H. Ma et al., "Enhanced removal of tetracycline by vitamin C-modified cow manure biochar in water," Sci Rep, vol. 14, no. 1, p. 22362, Sep 27 2024.

[4] Z. Xu, H. Li, Y. Zhang, and B. Zu, "Enhanced Adsorption of Uranium (VI) from Aqueous Solutions by Hydrogen Peroxide-Modified Magnetic Biochar: Performance Evaluation and Mechanistic Study," Water, Air, & Soil Pollution, vol. 235, no. 11, 2024.

[5] E. H. Yahia et al., "Valorization of argan paste cake waste: Enhanced CO2 adsorption on chemically activated carbon," Journal of Analytical and Applied Pyrolysis, vol. 181, 2024.

[6] L. L. Maury and O. M. Hande, "Biochar for Climate Change Mitigation: Turning Carbon into a Climate Solution," The Science World, vol. Vol.4(9),, 2024.

[7] NOAA. "No sign of greenhouse gases increases slowing in 2023Global Climate change." Oceanic and Atmospheric Research or NOAA Research. https://research.noaa.gov/2024/04/05/no-sign-of-greenhouse-gases-increases-slowing-in-2023/ (accessed.

[8] Jos G.J. Olivier, Greet Janssens-Maenhout, Marilena Muntean, and J. A. H. W. Peters., "Trends in global CO2 emissions: 2016 Report," 2016. [Online]. Available: https://www.pbl.nl/en/publications/trends-in-global-co2-emissions-2016-report

[9] NOAA. "Climate Change: Atmospheric Carbon Dioxide." NOAA Climate.gov based on data from Lüthi, et al., 2008. https://www.climate.gov/news-features/understanding-climate/climate-change-atmospheric-carbon-dioxide (accessed 15 oct 2024.

[10] R. L. Verma and G. Borongan, "Emissions of Greenhouse Gases from Municipal Solid Waste Management System in Ho Chi Minh City of Viet Nam," Urban Science, vol. 6, no. 4, 2022.

[11] A. P. D'Almeida and T. L. de Albuquerque, "Coconut husk valorization: innovations in bioproducts and environmental sustainability," Biomass Conversion and Biorefinery, 2024.

[12] J. M. Illingworth, B. Rand, and P. T. Williams, "Understanding the mechanism of two-step, pyrolysis-alkali chemical activation of fibrous biomass for the production of activated carbon fibre matting," Fuel Processing Technology, vol. 235, p. 107348, 2022/10/01/ 2022.

[13] F. Ronsse, S. van Hecke, D. Dickinson, and W. Prins, "Production and characterization of slow pyrolysis biochar: influence of feedstock type and pyrolysis conditions," GCB Bioenergy, vol. 5, no. 2, pp. 104-115, 2012.

[14] L. Gaur and P. Poonia, "Synthesis, Characterization, and Process Optimization of Invasive Weed Tephrosia purpurea Biochar," Environment and Ecology, vol. 42, no. 3B, pp. 1332-1341, 2024.

[15] M. I. S. Gonzaga, C. L. Mackowiak, N. B. Comerford, E. F. d. V. Moline, J. P. Shirley, and D. V. Guimaraes, "Pyrolysis methods impact biosolids-derived biochar composition, maize growth and nutrition," Soil and Tillage Research, vol. 165, pp. 59-65, 2017.

[16] S. Ma, S. Ma, W. Yin, S. Wang, H. Sheng, and X. Wang, "Effects of Biochar on the Availability of Trace Elements in Different Types of Soil," Toxics, vol. 13, no. 3, Feb 27 2025, doi: 10.3390/toxics13030169.

[17] H. Sanei et al., "Assessing biochar's permanence: An inertinite benchmark," International Journal of Coal Geology, vol. 281, 2024.

[18] S. Suman and S. Gautam, "Pyrolysis of coconut husk biomass: Analysis of its biochar properties," Energy Sources, Part A: Recovery, Utilization, and Environmental Effects, vol. 39, no. 8, pp. 761-767, 2017, doi: 10.1080/15567036.2016.1263252.

[19] N. S. M. Aziz , Adilah Shariff, Nurhayati Abdullah, and N. M. Noor, "Characteristics of coconut frond as a potential feedstock for biochar via slow pyrolysis," Fundamental and Applied Sciences, 2018.

[20] T. Thongsamer, S. Vinitnantharat, A. Pinisakul, and D. Werner, "Chitosan impregnation of coconut husk biochar pellets improves their nutrient removal from eutrophic surface water," Sustainable Environment Research, vol. 32, no. 1, 2022.

[21] Adilah Shariff, Nur Syairah Mohamad Aziz , Norsyahidah Md Saleh, and N. S. I. Ruzali., "The Effect of Feedstock Type and Slow Pyrolysis Temperature on Biochar Yield from Coconut Wastes," Chemical, Molecular, Nuclear, Materials and Metallurgical Engineering, 2016.

[22] S. M. Zemriyetti, Refnizuida, Rosmaria Girsang and Benny Hidayat., "Characterization Biochar Properties from Waste of Cassava, Sugarcane, and Coconut," Journal of Environmental and Agricultural Studies, 2022.

[23] S. A. Dhar, T. U. Sakib, and L. N. Hilary, "Effects of pyrolysis temperature on production and physicochemical characterization of biochar derived from coconut fiber biomass through slow pyrolysis process," Biomass Conversion and Biorefinery, vol. 12, no. 7, pp. 2631-2647, 2020.

[24] K. Y. Foo and B. H. Hameed, "Coconut husk derived activated carbon via microwave induced activation: Effects of activation agents, preparation parameters and adsorption performance," Chemical Engineering Journal, vol. 184, pp. 57-65, 2011.

The Optimal Conditions for Enhancing High Heating Value of Rubberwood Briquettes from Sawdust Residues via Torrefaction Process

Sutthipat Khamwichit[1] Surathai Khamwichit[1] Weerapol Lapkoed[2] Nattaya Jaibun[3] Nattawat Panthong[3] and Wipawee Dechapanya[3*]

[1]High school student; [2]Teacher, Health Science and Technology (HT) Program, Srinakharinwirot University Prasarnmit Demonstration Senior High School, Bangkok 10110, Thailand
[3]Undergrad student; [3]Associate Professor, Department of Chemical Engineering, School of Engineering and Technology, Nakhon Si Thammarat 80160, Thailand*
[*]Phone : +66945958895, Fax : +6675672399, E-mail : khamwipawee@gmail.com

ABSTRACT

This study investigates the valorization of rubberwood sawdust residues through torrefaction to produce enhanced quality solid biofuels. Briquettes were subjected to varying torrefaction conditions, with temperatures ranging from 200°C to 350°C and residence times of 30, 60, and 120 minutes. The effects of these parameters on the fuel properties were systematically analyzed through proximate composition, density measurements, and calorific value determination. Results showed that torrefaction significantly improved the fuel characteristics of the briquettes. As torrefaction severity increased, moisture content decreased from 2.44% to 0.11%, while fixed carbon content increased substantially from 13.29% to 55.32%. The higher heating value (HHV) was enhanced from 4480 kcal/kg in untreated samples to 6631 kcal/kg at the most severe conditions (350°C, 120 min), representing a 48% improvement. Although torrefaction reduced the mass yield to as low as 34.84%, the energy yield remained consistently above 100%, reaching 148.05% under the most severe conditions. Temperature exhibited a stronger influence than residence time on the briquette properties, though synergistic effects between both parameters were observed at higher temperatures. The density of briquettes decreased with torrefaction severity, from 748 kg/m³ to 523 kg/m³, indicating structural changes in the biomass. This study demonstrates that torrefaction is an effective approach for upgrading rubberwood sawdust residues into high-quality biofuels, with optimal conditions dependent on specific application requirements. Moderate torrefaction conditions (250-300°C for 60 minutes) provide a balanced compromise between energy enhancement and mass retention, offering a practical solution for the valorization of these low-cost abundant agricultural residues.

Keywords: rubberwood briquette; torrefaction; biomass valorization; waste management; bioenergy.

INTRODUCTION

The growing energy crisis, driven by dwindling fossil fuel reserves, increasing global demand, and environmental challenges, has heightened the urgency for sustainable and dependable energy solutions. In Southern Thailand, the rubberwood processing industry is one of the main industrial sectors that contributes to the economic growth of the region. Traditional rubberwood processing generates a considerable amount of sawdust, typically around 10% of the total wood volume [1]. In 2020, an estimated throughput of sawdust and wood chips amounting to around 485,000 tons being generated from the rubberwood processing industry [2], These residues present both challenges and opportunities for the rubberwood industry; effective utilization can promote sustainable practices and enhance economic viability. This study utilizes leftover sawdust to produce biomass briquettes suitable to be used as an alternative renewable solid fuel.

The fuel properties of these wood briquettes can be enhanced by torrefaction, a thermal treatment process, to improve the energy density and combustion efficiency of biomass [3]. The torrefaction process is typically carried out at 200–300°C for 30–120 min, respectively. The process parameters, including temperature and residence time, play crucial roles in determining the quality of the torrefied product [4]. Various agroforestry wastes, including rubberwood, have been investigated in torrefaction studies to improve their fuel properties that can be potentially used in bioenergy applications [5]. It has been reported that the calorific value of the biomass increased by 25% (20 to 25 MJ kg^{-1}) from the raw biomass after being treated under suitable torrefaction conditions [6]. In addition, the energy density and combustion characteristics of torrefied biomass can be enhanced for easier transportation and storage [7]. By integrating this method, the rubberwood industry can significantly reduce its carbon footprint while creating new job opportunities

in pellet production and distribution [8]. This not only makes the pellets more efficient for heating and electricity generation but also expands their market potential as a sustainable alternative to fossil fuels [9].

While torrefaction significantly improves the fuel properties of rubberwood sawdust briquettes, challenges remain in optimizing the process for large-scale applications. The balance between energy yield and production cost is crucial for commercial viability. Additionally, the environmental benefits of reduced emissions and improved eco-efficiency make torrefied briquettes a promising alternative to fossil fuels.

METHODOLOGY

Rubberwood Briquette Preparation

Rubberwood sawdust residues (approximately 1.50 THB/kg) were well mixed with molasse (18 THB/kg), the physical binder, at a ratio of 9 to 1 by weight (total weight of 640 g) in a mixing container before being filled into a slab mold (25×25×1 cm). The filled mold was placed in a hydraulic hot press machine, and compressed under a pressure of 1,500 MPa, 210^{o}C for 10 min. The obtained briquette was dried in a hot air oven at 105^{o}C for 24 hr.

Torrefaction

The obtained rubberwood briquette slab was cut into samples (about 2.5×1.5×1 cm), filled in a closed ceramic reactor, and placed inside a muffle furnace. Torrefaction was carried on at various temperatures (200, 250, 300, and 350 °C) at different residence times (30, 60, and 120 min). The torrefied rubberwood briquette (TWB) samples were kept in a desiccator before being subjected to characterization.

Characterization

The mass density of the TWB was measured and calculated by equation (1), as follows:

$$\text{Mass density} = m/V \quad (1)$$

Where m is the weight (kg), and V is the volume (m^3) of the TWB samples.

Proximate analysis was performed to determine the moisture (MC), volatile matter (VM), and ash (AC) contents, following the standard test methods ASTM E871, ASTM E832, and ASTM E870, respectively. Fixed carbon was calculated from equation (2):

$$FC\ (wt.\%) = 100 - [MC+VM + AC] \quad (2)$$

The mass yield (Y_m) of the TWB was calculated from equation (3):

$$Y_m\ (\%) = m_{TWB}/m_0 \times 100 \quad (3)$$

Where m_{TWB} is the mass of the torrefied TWB sample, and m_0 is the mass of the sample before being torrefied.

The higher heating value (HHV) of the samples (kcal/kg) was measured using a Bomb Calorimeter, following the ASTM E711 procedure. The energy yield (Y_e) was calculated as the ratio of the HHV of treated TWB to that of the untreated WB, as presented in equation (4).

$$Y_e\ (\%) = HHV_{TWB}/HHV_0 \times 100 \quad (4)$$

Where HHV_{TWB} and HHV_0 are the higher heating values of the WB sample before and after torrefaction, respectively.

RESULTS AND DISCUSSIONS

The physical appearance of the TWB samples after torrefaction at various temperatures and times is shown in Figure 1. Following torrefaction, the briquettes exhibited a progressive color transformation that directly correlated with increasing torrefaction severity. The untreated briquettes (WB) displayed a characteristic light brown color typical of natural rubberwood sawdust. At mild torrefaction conditions (200°C, 30 minutes), the briquettes began showing a slight darkening to medium brown. As treatment intensity increased to moderate conditions (250°C), the color deepened to dark brown, while severe torrefaction (300–350°C) produced distinctly black briquettes. This color evolution serves as a visual indicator of the chemical transformations occurring within the biomass structure [10]. The darkening could be attributed to several simultaneous processes, including thermal degradation of lignocellulose compounds (e.g., hemicellulose, cellulose, and lignin) [11] , devolatilization of volatile matter [12], and thermochemical reactions of the presented reactive components [13].



Figure 1 The appearance of TWB samples prepared at various torrefaction temperatures and times.

Table 1 summarizes the characterization results of the TWB samples. During torrefaction, TWB initially underwent drying, followed by thermal degradation and potential thermochemical reactions, leading to composition shifts in MC, VM, AC, and FC contents. In addition, the effects of torrefaction temperature and time on the physical properties, including density, HHV, mass and energy yields, are presented.

Table 1 Characterization Results

Temp (°C)	Time (min)	MC (wt%)	VM (wt%)	AC (wt%)	FC (wt%)	Density (kg/cm^3)	HHV (kcal/kg)	Mass yield Y_m (%)	Energy Yield Y_e (%)
Untreated	-	2.44	82.69	1.58	13.29	748	4480	-	-
200	30	0.94	83.57	1.64	13.85	748	4498	99.83	100.40
	60	0.69	82.74	1.65	14.92	736	4544	93.34	101.42
	120	0.43	81.12	1.89	16.56	725	4585	92.22	102.34
250	30	0.71	80.75	2.1	16.44	692	4524	94.54	100.99
	60	0.52	79.82	2.03	17.63	664	4648	89.39	103.75
	120	0.35	71.94	2.5	25.21	617	4998	76.16	111.56
300	30	0.51	71.48	3.25	24.76	662	4648	87.38	103.75
	60	0.32	67.09	4.1	28.49	611	5532	64.72	123.48
	120	0.22	45.37	6.5	47.91	566	6340	45.2	141.52
350	30	0.43	58.62	5.36	35.59	571	5633	51.01	125.74
	60	0.28	46.98	6.5	46.24	550	6551	39.95	146.22
	120	0.11	36.48	8.09	55.32	523	6631	34.84	148.05

Effects of Torrefaction Conditions on Proximate Analysis

The proximate analysis data in Table 1 demonstrates significant changes in the rubberwood briquettes' composition as a function of torrefaction temperature and residence time. The effects of torrefaction temperature and residence time on the proximate compositions are illustrated in Figure 2.

Moisture Content (MC)

The moisture content decreased markedly with increasing torrefaction severity. The untreated briquettes had an initial MC of 2.44 wt%, which reduced to as low as 0.11 wt% at the most severe condition (350°C, 120 min), as shown in Figure 2a. This reduction is attributed to the dehydration reactions and evaporation of bound water during torrefaction. Even mild torrefaction (200°C, 30 min) resulted in a 61.5% decrease in moisture content compared to the untreated sample.

Volatile Matter (VM)

The volatile matter content exhibited a clear declining trend with increasing torrefaction intensity (see Figure 2b). The untreated sample contained 82.69 wt% VM, which remained relatively stable at mild torrefaction conditions (200°C). However, as temperature increased to 300°C and 350°C, VM content decreased substantially, reaching a minimum of 36.48 wt% at 350°C for 120 min. This represents a 55.9% reduction from the untreated sample and indicates the significant thermal decomposition of hemicellulose and partial degradation of cellulose at higher temperatures.

Ash Content (AC)

From Figure 2c, the ash content increased progressively with torrefaction severity, from 1.58 wt% in the untreated sample to 8.09 wt% at the most severe condition (350°C, 120 min). This increase is not due to ash generation but rather represents the concentration effect as organic components are thermally degraded and released as volatiles, while the inorganic minerals remain in the solid product.

Fixed Carbon (FC)

Fixed carbon content demonstrated the most dramatic increase among all proximate parameters. From an initial value of 13.29 wt% in the untreated briquettes, FC increased to 55.32 wt% at 350°C for 120 min, representing a 316% increase, as shown in Figure 2d. This substantial rise in FC is directly correlated with the decrease in volatile matter and results from the carbonization reactions that occur during torrefaction, particularly at higher temperatures.

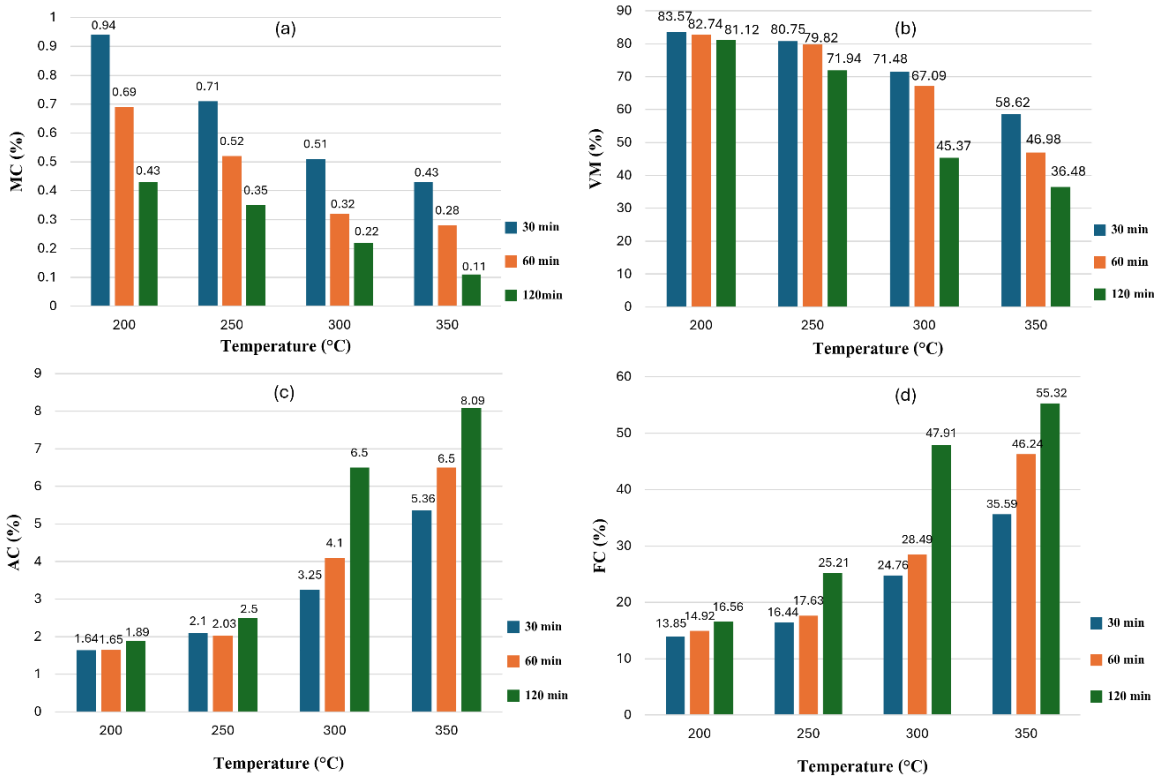


Figure 2 Proximate Analysis Results: (a) Moisture Content, MC, (b) Volatile Matter, VM, (c) Ash Content, AC (%), and (d) Fixed Carbon Content.

Effects on Physical and Energy Properties

Density

The density of the briquettes decreased consistently with increasing torrefaction severity. From Figure 3, the untreated sample had a density of 748 kg/m³, which remained unchanged after mild torrefaction at 200°C for 30 minutes. However, as the treatment became more severe, density decreased progressively, reaching 523 kg/m³ at 350°C for 120 min. This 30% reduction in density is attributed to the loss of mass during devolatilization and the formation of a more porous structure as volatiles escape.

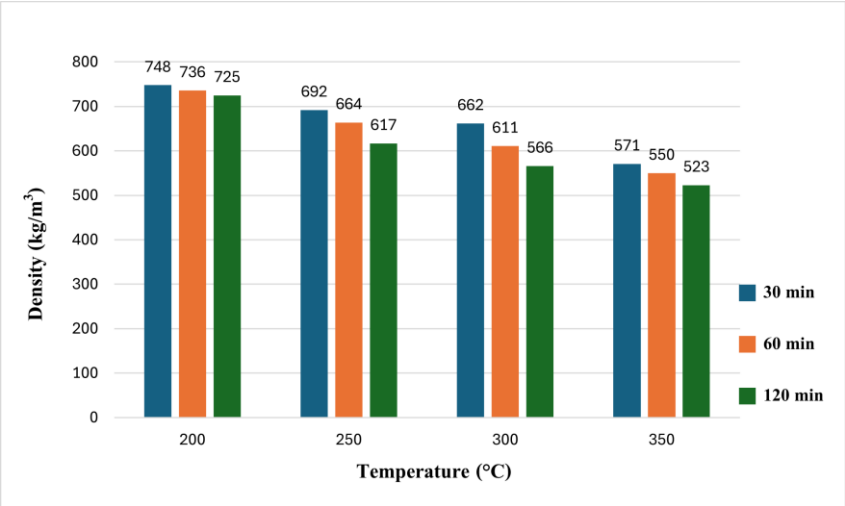


Figure 3 Effect of Torrefaction Temperature and Time on the Density of TWB Samples

Higher Heating Value (HHV)

The higher heating value showed a consistent increase with torrefaction severity. From Figure 4, the untreated sample had an HHV of 4480 kcal/kg, which increased to 6631 kcal/kg at 350°C for 120 min, representing a 48% enhancement. This significant improvement in calorific value is directly related to the increase in fixed carbon content and the relative decrease in oxygen-to-carbon ratio due to the preferential removal of oxygen-rich compounds during torrefaction.

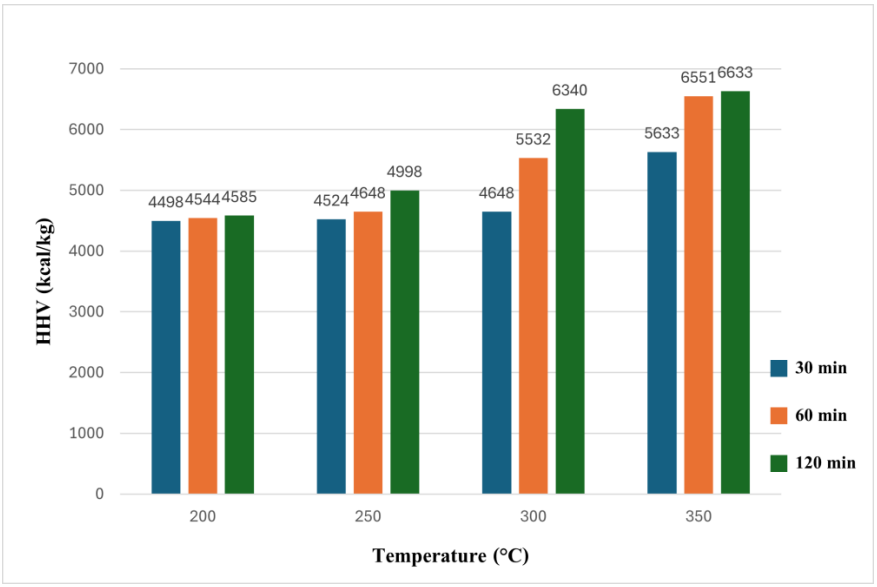


Figure 4 Effect of Torrefaction Temperature and Time on HHV of TWB Samples

Mass Yield (Y_m) vs Energy Yield (Y_e)

Mass yield decreased progressively with torrefaction severity, from 99.83% at mild conditions (200°C, 30 min) to only 34.84% at severe conditions (350°C, 120 min), see Figure 5a. This trend reflects the increasing mass loss through the devolatilization of hemicellulose and cellulose components as torrefaction intensity increases. The mass loss was particularly pronounced at temperatures above 250°C, with residence time further amplifying this effect.

Despite the significant mass loss, energy yield remained above 100% for all torrefaction conditions, indicating that the increase in calorific value compensated for the mass reduction. The energy yield increased from 100.40% at mild conditions to 148.05% at the most severe conditions (350°C, 120 min), as shown in Figure 5b. This demonstrates the effectiveness of torrefaction in concentrating the energy content in the remaining solid mass.

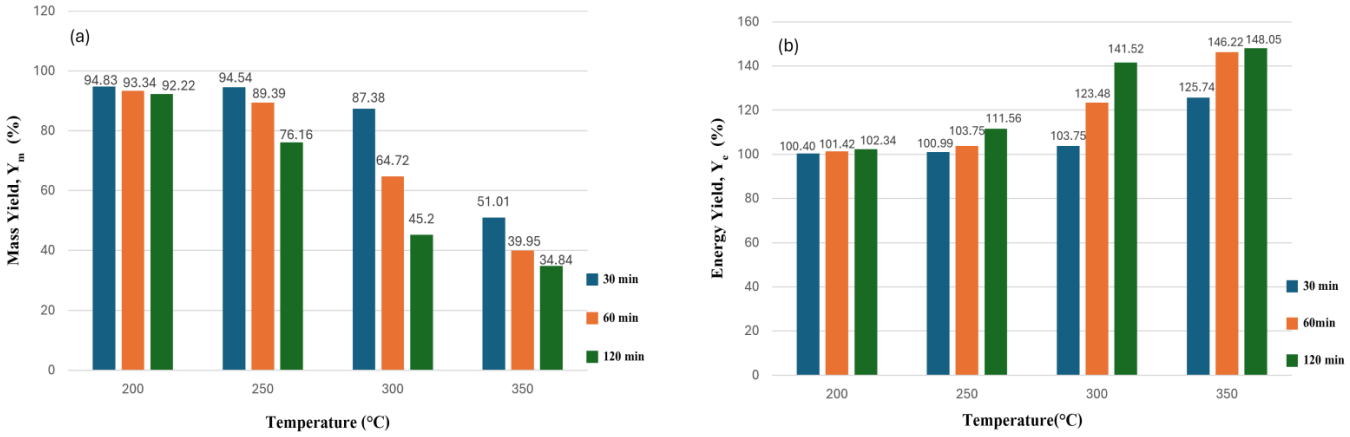


Figure 5 Effect of Torrefaction Temperature and Time on (a) Mass Yield, and (b) Energy Yield of TWB Samples

The relationship between mass yield (Y_m) and energy yield (Y_e) was observed to be inversely correlated across all torrefaction conditions. As the mass yield decreases with increasing torrefaction severity, the energy yield consistently increases. This inverse relationship can be explained by examining the fundamental changes occurring during the torrefaction process. The energy yield incorporates both the changes in calorific value and the mass retention. While mass yield decreases with torrefaction severity, the significant increase in HHV counterbalances this loss, resulting in net energy gains.

Temperature vs. Residence Time Effects

Temperature exhibited a stronger influence on briquette properties than residence time. For instance, increasing the temperature from 200°C to 350°C at a fixed residence time of 30 minutes caused the HHV to increase from 4498 to 5633 kcal/kg (25.2% increase) while extending the residence time from 30 to 120 minutes at 200°C only increased the HHV from 4498 to 4585 kcal/kg (1.9% increase). However, residence time showed a more pronounced effect at higher temperatures. At 350°C, extending the residence time from 30 to 120 minutes resulted in an HHV increase from 5633 to 6631 kcal/kg (17.7% increase), indicating synergistic effects between temperature and time at more severe conditions.

Optimal Torrefaction Conditions

At mild conditions (200°C, all residence times), the energy yield increases only marginally while maintaining high mass yields (>92%). In contrast, at severe conditions (350°C, 120 min), the energy yield reaches its maximum (148.05%) but at the expense of substantial mass loss (mass yield reduced to 34.84%). The most significant energy densification occurs between 250–300°C, particularly at longer residence times. For instance, at 300°C for 120 minutes, the energy yield reaches 141.52% with a mass yield of 45.20%, representing an excellent balance between energy enhancement and mass retention. The relationship can be summarized as follows:

1. Mild torrefaction (200°C): Minimal mass loss, minimal energy gain
2. Moderate torrefaction (250°C): Modest mass loss, significant energy gain
3. Severe torrefaction (300–350°C): Substantial mass loss, maximum energy gain

This trade-off between mass yield and energy yield is crucial for determining the optimal torrefaction conditions based on specific application requirements. The results suggest that moderate conditions (250°C, 120 min) or (300°C, 30–60 min) may provide the optimal balance for most applications, achieving significant energy densification while maintaining acceptable mass yields. However, the optimal torrefaction conditions could depend on the desired balance between energy density enhancement and mass yield. For applications prioritizing maximum energy content, severe torrefaction (350°C, 120 min) provided the highest HHV (6631 kcal/kg) and energy yield (148.05%), but at the cost of significant mass loss (34.84% yield) and reduced density. For applications where maintaining higher mass yield and density is important while still achieving reasonable energy enhancement, moderate torrefaction conditions (250°C, 120 min) offer a good compromise. At these conditions, the briquettes retained 76.16% of their mass while achieving an HHV of 4998 kcal/kg (11.6% increase from untreated) and an energy yield of 111.56%. The results from this study are comparative and in good agreement with other related studies reported elsewhere [3, 4, 6].

CONCLUSION

This study investigated the effects of torrefaction temperature (200–350°C) and residence time (30–120 minutes) on the properties of rubberwood briquettes produced from left-over sawdust residues. The results demonstrated that torrefaction is an effective thermochemical process for upgrading these biomass residues into value-added solid biofuels with enhanced properties.

The proximate analysis revealed significant compositional changes in the torrefied briquettes, characterized by decreased moisture content (from 2.44% to as low as 0.11%) and volatile matter (from 82.69% to 36.48%), alongside substantial increases in fixed carbon content (from 13.29% to 55.32%) and ash content (from 1.58% to 8.09%) at the most severe conditions. These changes directly contributed to the enhancement of the fuel's higher heating value, which increased from 4480 kcal/kg for untreated briquettes to 6631 kcal/kg at 350°C for 120 minutes, representing a 48% improvement.

Torrefaction severity exhibited an inverse relationship between mass yield and energy yield. Higher temperatures and longer residence times resulted in greater mass loss but correspondingly higher energy densification. Temperature had a more pronounced effect than residence time on briquette properties, though residence time showed increased influence at higher temperatures, indicating synergistic effects between the two parameters.

The optimal torrefaction conditions depend on the specific application requirements. For applications prioritizing maximum energy content, severe torrefaction (300–350°C, 60–120 min) is preferable, while moderate conditions (250°C, 60–120 min) offer a balanced compromise between energy enhancement and mass retention. These findings provide valuable insights for the practical implementation of torrefaction technology in converting rubberwood sawdust residues into high-quality biofuels as renewable low-cost solid fuels in southern Thailand.

ACKNOWLEDGEMENT

The authors would like to thank the Department of Chemical Engineering at Walailak University for their laboratory support. We also extend our thanks to the Health Science and Technology (HT) program at Srinakharinwirot University Prasarnmit Demonstration Senior High School for their collaborative contributions to our research efforts.

REFERENCE

[1] Saosee P, Sajjakulnukit B, Gheewala SH. Environmental externalities of wood pellets from fast-growing and para-rubber trees for sustainable energy production: A case in Thailand. Energy Conversion and Management: 2022;14:100183. https://doi.org/10.1016/j.ecmx.2022.100183.

[2] Mirski R, Dukarska D, Derkowski A, et al. By-products of sawmill industry as raw materials for manufacture of chip-sawdust boards. Journal of Building Engineering 2020;32:101460. https://doi.org/10.1016/j.jobe.2020.101460.

[3] Riaz S, Al-Abdeli YM, Oluwoye I, et al. Torrefaction of Densified Woody Biomass: The Effect of Pellet Size on Thermochemical and Thermophysical Characteristics. Bioenergy Res 2022;15:544–58. https://doi.org/10.1007/s12155-021-10319-8.

[4] Kasawapat J, Khamwichit A, Dechapanya W. Waste-to-Energy Conversion of Rubberwood Residues for Enhanced Biomass Fuels: Process Optimization and Eco-Efficiency Evaluation. Energies. 2024;17:5444. https://doi.org/10.3390/en17215444.

[5] Nunes LJR, Matias JCO, Catalão JPS. A review on torrefied biomass pellets as a sustainable alternative to coal in power generation. Renewable and Sustainable Energy Reviews 2014;40:153–60. https://doi.org/10.1016/j.rser.2014.07.181.

[6] Thengane SK, Kung KS, Gomez-Barea A, et al. Advances in biomass torrefaction: Parameters, models, reactors, applications, deployment, and market. Prog Energy Combust Sci 2022;93:101040. https://doi.org/10.1016/j.pecs.2022.101040.

[7] Adeleke AA, Odusote JK, Ikubanni PP, et al. Essential basics on biomass torrefaction, densification and utilization. Int J Energy Res 2021;45:1375–95. https://doi.org/10.1002/er.5884.

[8] Saosee P, Sajjakulnukit B, Gheewala S. Life Cycle Assessment of Wood Pellet Production in Thailand. Sustainability 2020;12:6996. https://doi.org/10.3390/su12176996.

[9] Bui-Duy L, Le LT, Vu-Thi-Minh N, et al. Economic and environmental analysis of biomass pellet supply chain using simulation-based approach. Asia Pacific Management Review 2023;28:470–86. https://doi.org/10.1016/j.apmrv.2023.02.002.

[10] Chen W-H, Wang C-W, Kumar G, et al. Effect of torrefaction pretreatment on the pyrolysis of rubber wood sawdust analyzed by Py-GC/MS. Bioresour Technol 2018;259:469–73. https://doi.org/10.1016/j.biortech.2018.03.033.
[11] Adeleke AA, Odusote JK, Ikubanni PP, et al. Essential basics on biomass torrefaction, densification and utilization. Int J Energy Res 2021;45:1375–95. https://doi.org/10.1002/er.5884.
[12] Bridgeman TG, Jones JM, Shield I, et al. Torrefaction of reed canary grass, wheat straw and willow to enhance solid fuel qualities and combustion properties. Fuel 2008;87:844–56. https://doi.org/10.1016/j.fuel.2007.05.041.
[13] Khamwichit A, Kasawapat J, Seekao N, et al. Enhanced Torrefied Oil-Palm Biomass as an Alternative Bio-Circular Solid Fuel: Innovative Modeling of Optimal Conditions and Ecoefficiency Analysis. Energies (Basel) 2024;17:2192. https://doi.org/10.3390/en17092192.

21R5-04

Study of Effecting Factors for Formalin Removal Efficiency in Lab Gross using the Biochar Air Pollution Treatment Unit

Surathai Khamwichit[1], Sutthipat Khamwichit[1], Arisa Arwaehama[2], Nareekan Dokket[1], and Wipawee Dechapanya[2*]

[1]*Health Science and Technology (HT) Program, Srinakharinwirot University Prasarnmit Demonstration Senior High School, Bangkok 10110, Thailand*

[2*]*Department of Chemical Engineering, School of Engineering and Technology, Nakhon Si Thammarat 80160, Thailand* [*]*Phone 0945958895, Fax : 075672399, E-mail : khamwipawee@gmail.com*

ABSTRACT

This study explores the effectiveness of palm kernel shell (PKS) biochar as an adsorbent material for air pollution treatment, focusing on the removal of formaldehyde in an Anatomy Gloss laboratory at Walailak University. PKS biochar, a porous and carbon-rich substance produced through a pyrolysis process at around 350-500 □C for 4 hours, offers high adsorption potential due to its large surface area and microporous structure. The Design Expert (DE) program was exploited to design the experiments and optimize the optimal operating conditions for an air treatment prototype unit to remove formaldehyde in an anatomy gloss lab. FTIR analysis confirmed the successful adsorption of formaldehyde, iodine, and Methylene Blue onto the biochar surface, identifying key spectral peaks associated with N–H, C–N, C=C, C–H, and C=O bonds. SEM imaging revealed significant morphological changes in the PKS structure after pyrolysis, with increased surface damage and pore development. Iodine adsorption tests showed values ranging from 450 to 1550 mg/g, supporting the conclusion that PKS biochar possesses high adsorption capacity. The prototype unit, incorporating biochar within its filtration system, was tested for formaldehyde adsorption efficiency. The highest removal efficiency achieved was 90.76%, using an airflow rate of 0.24 m^3/s, 750 grams of biochar, and a treatment time of 120 minutes. While longer treatment durations improved efficiency, the gains plateaued after 100 minutes. Conversely, higher airflow rates negatively impacted performance, indicating an inverse relationship between airflow velocity and adsorption capacity. These findings suggest that PKS biochar is an effective, low-cost, and sustainable material for air purification, particularly in indoor environments with formaldehyde exposure. The study also supports the use of agricultural waste in environmental applications, aligning with circular economy principles and zero-waste strategies.

Keywords : PKS biochar, circular economy, waste minimization, formaldehyde removal

INTRODUCTION

Formaldehyde is currently a widely used chemical in medicine, industry, and agriculture, especially in hospitals and anatomy laboratories for disinfection and tissue preservation [1]. However, long-term accumulation of formaldehyde vapors can cause health hazards, such as skin, eye, and respiratory irritation at concentrations of 0.01–30 ppm, and can be fatal at concentrations greater than 100 ppm [2]. Formaldehyde is also a known human carcinogen [3]. OSHA sets a standard for occupational contamination of 0.75 ppm over 8 hours and 2 ppm over a short period of 15 minutes [4].

In Thailand, biomass feedstock is primarily sourced from by-products of the wood and agricultural industries, including palm kernel shell (PKS), a residue generated during palm oil refining. Palm oil is a globally significant commodity and plays a crucial role in the economy of Southeast Asia. While Malaysia and Indonesia are the world's leading producers, Thailand ranks third globally in palm oil production. In this industry, fresh fruit bunches (FFB) are delivered to crude palm oil (CPO) mills, where the oil extraction process generates several types of biomass waste, including palm fiber (PF), empty fruit bunches (EFB), and PKS. On average, FFB consists of approximately 21% CPO, 22–23% EFB, 13.5–15% PF, and 5.5–7% PKS. Following oil extraction, a substantial volume of solid biomass waste is produced, primarily composed of EFB, PF, and PKS. It is estimated that for every ton of CPO extracted, around 1.8 tons of solid biomass waste are generated by a typical oil palm process. The substantial volume of biomass generated from oil palm extraction presents a promising opportunity for biochar production.

Biochar offers several advantages as an adsorbent for the removal of air pollutants. Its highly porous structure and large surface area enhance its capacity to capture and retain a wide range of airborne contaminants, including volatile organic compounds (VOCs), particulate matter, and gaseous pollutants such as ammonia (NH_3), sulfur dioxide (SO_2), and nitrogen oxides (NO_x). The surface chemistry of biochar, which

includes various functional groups, facilitates the adsorption of both polar and non-polar compounds. Additionally, biochar can be engineered or chemically modified to improve its selectivity and adsorption efficiency for specific pollutants. Its production from renewable biomass sources also makes it a cost-effective and sustainable alternative to conventional adsorbents like activated carbon. Moreover, biochar contributes to carbon sequestration, thereby providing co-benefits in climate change mitigation alongside pollution control.

This research aimed to study the effectiveness of air pollution treatment using biochar as a pollutant adsorbent. The study found that biochar is a porous and carbon-rich material obtained from the pyrolysis process of palm kernel shell (PKS), where biochar's properties depend on the biomass type, temperature, and pyrolysis duration [5]. The study applied optimization function in the Design Expert (DE) program to obtain the optimal air treatment unit operation conditions to remove formaldehyde in lab gross at Walailak University. The developed air pollution treatment unit used biochar in the filter to absorb formaldehyde from the air in the lab gross, reducing health risks and improving air quality in the work area.

METHODOLOGY

Preparation of PSK biochar

PSK obtained from local palm oil industries was baked at 110 °C for 3 hours in the hot air oven to remove moisture before being pyrolyzed in a low-oxygen kiln (as shown in Figure 1) at 350–500 °C for 4 hours. After letting the biochar cool down to room temperature, it was ground and sieved to a size of 250 microns. Then, the grounded biochar was stored in the desiccator for further use in the air treatment unit.



Figure 1 Pyrolysis Kiln for Biochar Production

Properties analysis of PKS biochar

The FTIR spectra of the biochar samples were examined in an ATR-FTIR spectrometer (model Tensor 27; Bruker, Germany) under the wavelength range of 530-4,000 cm^{-1}. A scanning electron microscope (SEM; Model Merlin Compact, Carl Zeiss Co., Ltd., Bangkok, Thailand) was employed to examine the morphological structure of the biomass, providing insights into the structural modifications induced by the torrefaction process at varying temperatures. The SEM images were analyzed using Micro Sun 2000/s image analysis software to assess the nano structural characteristics of the biochar. Image analysis was conducted at a magnification of 10,000× with an accelerating voltage of 5 kV.

Air pollution treatment unit

The research team developed a prototype air purification system based on a principle-driven design framework for indoor air pollution treatment. The system was designed with three compartments as displayed in Figure 2 to effectively reduce airborne pollutants, including volatile organic compounds (VOCs). This was achieved through a biochar adsorption unit with high VOC absorption efficiency. Additionally, the system incorporates HEPA filtration to capture fine particulate matter such as dust and paint mist, particularly in areas near emission sources.

To further enhance air quality, the system includes a UV-C sterilization unit capable of eliminating airborne pathogens. The prototype is designed for durability, mobility, and ease of maintenance, allowing for simple replacement of components such as the biochar filter, HEPA filter, and UV-C lamp. Moreover, the system is adaptable, with adjustable airflow and modular filter and adsorption units, making it suitable for varying industrial environments and pollution levels.

The prototype of air pollution treatment unit is shown in Figure 3 (dimensions of 30 × 50 × 150 cm, layers of filters: a pre-filter, a biochar filter, and a HEPA filter). A total of 15 kg of biochar was obtained for testing in a prototype air treatment unit. The airflow rate could be adjusted in 5 levels (0.07–3.4 m/sec). The mechanism of an air treatment unit uses a combination of filters to effectively clean indoor air, starting with a prefilter. The prefilter captures large airborne particles such as dust. Next, the air passes through a biochar filter, which is designed to remove gaseous pollutants, odors, and VOCs. Its large surface area enables it to adsorb harmful gases and chemicals from the air. Finally, the air flows through a High-Efficiency Particulate Air (HEPA) filter, which captures very fine particles such as pollen, capable of removing at least 99.97% of particles as small as 0.3 microns

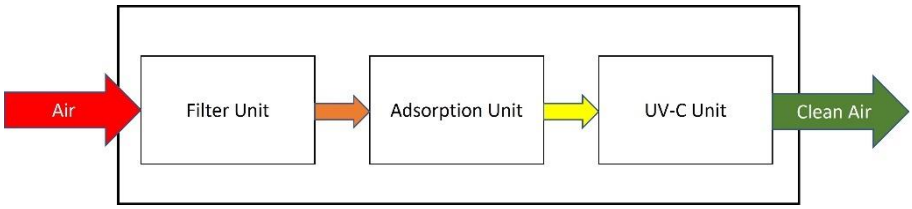


Figure 2 The Schematic Design of Air Pollution Treatment Unit

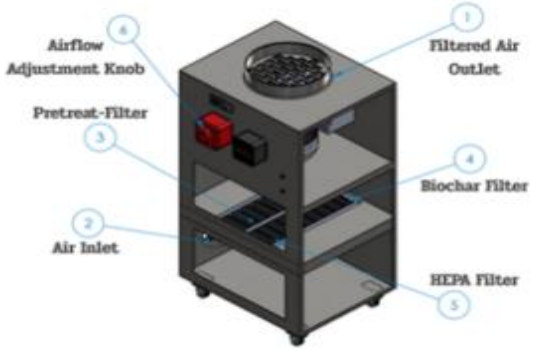


Figure 3 Air Pollution Treatment Unit

Adsorption of Iodine and Methylene Blue using PKS biochar

Adsorption of Iodine and Methylene Blue test using PKS biochar was performed according to the ASTM D4607 standard. The procedure involves drying the biochar sample, grinding it to a uniform particle size (usually below 150 µm), and mixing a known mass with a standard iodine solution. This study mixed 0.5, 1.0, and 1.5 g of PKS biochar with a standard iodine solution. After a set agitation period, the mixture is filtered to separate the solid, and the remaining iodine concentration in the filtrate is determined through back titration with sodium thiosulfate, using starch as an indicator. The amount of iodine adsorbed is calculated based on the difference between the initial and final iodine concentrations. The result, expressed in milligrams of iodine adsorbed per gram of biochar (mg/g), indicates the material's adsorption capacity. A higher iodine number reflects greater surface area and microporosity, making this test a valuable tool for evaluating biochar quality in adsorption applications. Iodine number was calculated using Equation 1

$$\text{Iodine number (mg/g)} = (C_0 - C_e) \times V \times 126.9/M \qquad \text{Equation 1}$$

Where C_0 = initial iodine concentration (mol/L)
C_e = equilibrium iodine concentration after adsorption
V = volume of iodine solution (L)
M = mass of biochar sample (g)
126.9 = molar mass of iodine (g/mol)

Formaldehyde removal utilizing air pollution treatment unit

To study the optimal conditions of the operation to remove formaldehyde in the lab gross at Walailak University using the phototype air pollution treatment unit, the experiment was designed using Design Expert (DE). The following parameters which were biochar amount of 500–1000 g, duration of 60–120 min, and airflow rate of 0.07–0.413 m/s were input into the DE program. The air pollution treatment unit

was put in a closed lab gross room of 4 × 3 × 3 m for 17 experiment sets. Formaldehyde concentration was measured using a Formaldehyde Monitor GM8801 brand Benetech. Optimization function in the DE analyzed the results to evaluate the optimal conditions for formaldehyde removal efficiency. Formaldehyde removal efficiency was evaluated according to Equation 2. In which, C_0 and C_e is formaldehyde initial and equilibrium concentration, respectively.

$$RE\ (\%) = \frac{(Ce-Co)}{Co} \times 100 \qquad \text{Equation 2}$$

RESULTS AND DISCUSSIONS

Biochar Synthesis and Characterization

Figure 4 illustrates the PKS, PKS biochar, and grounded PKS biochar after the pyrolysis process. As illustrated in Figure 4, the raw PKS initially exhibited light brown coloration. However, after the pyrolysis process PKS biochar progressively darkened, transitioning from light brown to a deep brown hue.



Figure 4 PKS, PKS Biochar, and Grounded PKS Biochar

SEM analysis provides insight into the surface morphology of the biomass, highlighting changes in texture and structure resulting from the pyrolysis process. As shown in Figure 5, SEM images of the raw PKS and PKS biochar reveal notable alterations post-pyrolysis. The originally intact, interconnected cell walls within the tubular porous structure exhibit visible surface damage. Additionally, an increase in both pore volume was evident, attributed to the thermochemical degradation of lignocellulosic components during pyrolysis.

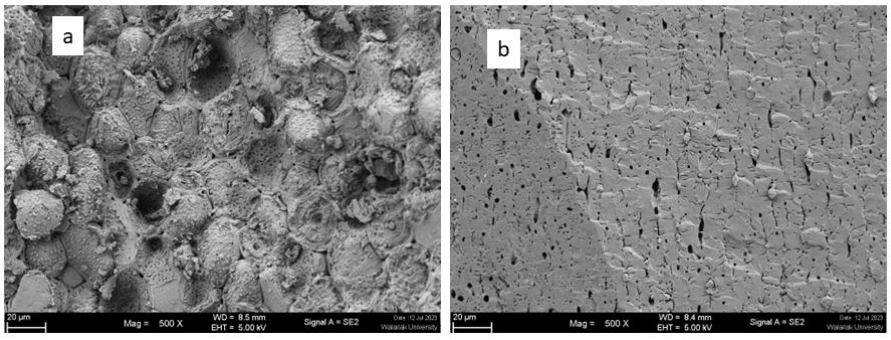


Figure 5 SEM Image of a) Raw PKS and b) PKS Biochar

The FTIR spectra showed the peaks of Methylene Blue adsorbed on biochar, with the main peaks corresponding to the structure, namely N–H bond stretching [3,200–3,500 cm^{-1}] [6], C–N bond stretching [1,200–1,350 cm^{-1}], and benzene ring vibration (C=C) [1,600 cm^{-1}], which confirmed the adsorption of Methylene Blue [7]. In addition, the peaks of Formaldehyde were also observed in the spectra, namely C–H stretching [2,800–3,000 cm^{-1}] [8]. C=O stretching [1,720–1,740 cm^{-1}] [9], and C–H bending [1,350–1,500 cm^{-1}] [9]. These may reflect the interaction between formaldehyde and the biochar surface.

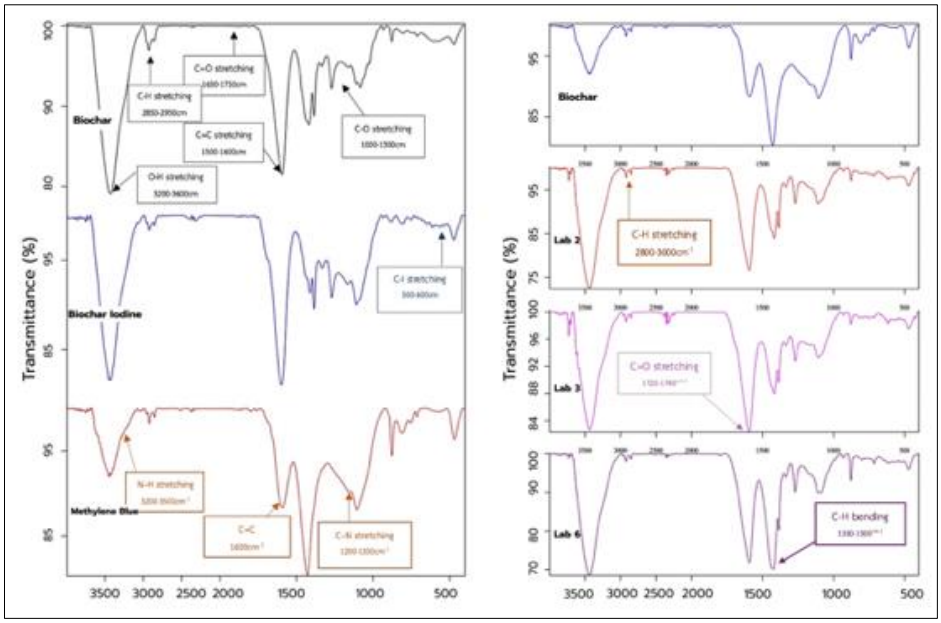


Figure 6 FTIR of biochar and biochar after adsorption of iodine, methylene blue, and formaldehyde

Adsorption Using PKS Biochar

Adsorption of iodine using different amount of PKS biochar (0.5, 1.0, and 1.5 g) is illustrated in Figure 7 and Table 1. As seen in the Figure, an inverse correlation between biochar mass and X/M (mg/g) was observed. As the biochar mass increases from 0.5 g to 1.5 g, the X/M value decreases significantly, suggesting that higher biochar mass leads to lower iodine adsorption per unit mass. The iodine adsorption results, expressed as the (X/M) value, ranged from 450 to 1550 mg/g when different amounts of biochar were used in the experiment. This indicates the high adsorption capacity of the biochar, suggesting a large surface area and significant microporosity. These properties can be used to assess the quality of the biochar for formaldehyde adsorption applications

Table 1 X/M of biochar for different amount of biochar samples

Parameter	Biochar 0.5 g		Biochar 1.0 g		Biochar 1.5 g	
	Average	SD	Average	SD	Average	SD
N1 (N)	0.1	-	0.1	-	0.1	-
N2 (N)	0.1	-	0.1	-	0.1	-
A (mg)	1269.3	-	1269.3	-	1269.3	-
B (mg/ml)	12.69	-	12.69	-	12.69	-
S (ml)	17.63	0.32	19.27	0.5	19.73	
X/M (mg/g)	1537.41	19.49	728.85	13.41	476.50	6.64

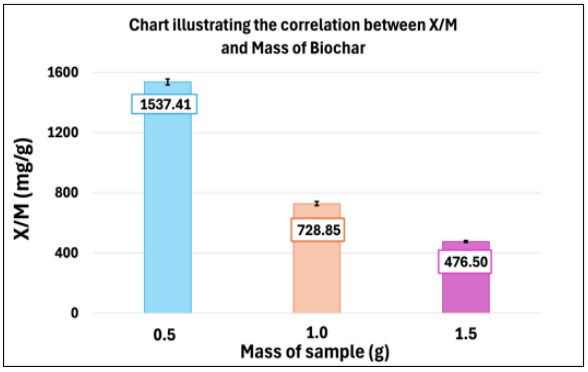


Figure 7 Effect of biochar mass on X/M

Formaldehyde Removal using Air pollution Treatment Unit

Table 2 presents the formaldehyde removal efficiency from 17 experimental trials conducted in the lab gross. The highest removal efficiency (90.76%) was observed in Experiment 5, which utilized an airflow rate of 0.24 m^3/s, 750 grams of biochar, and a treatment duration of 120 minutes. The data indicate that removal efficiency increased with longer treatment durations; however, improvements became marginal beyond 100 minutes. Conversely, higher airflow rates were associated with reduced removal efficiency, suggesting an inverse relationship between airflow velocity and adsorption performance. Among the tested conditions, 750 grams of biochar proved to be the most effective quantity for use in the filter medium.

Table 2 Formaldehyde Removal Efficiency for 17 Experimental Conditions

Run	Factor A (biochar, g)	Factor B (Air flowrate, m^3/s)	Factor C (time, min)	C_e (ppm)	RE. (%)
1	750	0.24	60	0.0146	59.40
2	500	0.41	60	0.065	53.84
3	750	0.24	90	0.081	71.70
4	500	0.07	120	0.024	87.50
5	750	0.24	120	0.032	90.76
6	750	0.24	90	0.081	72.96
7	500	0.41	120	0.024	83.01
8	1000	0.41	120	0.008	84.99
9	750	0.07	90	0.032	73.33
10	1000	0.24	90	0.024	69.99
11	1000	0.07	60	0.032	64.71
12	750	0.24	90	0.081	71.70
13	500	0.07	60	0.032	67.56
14	500	0.24	90	0.041	73.21
15	750	0.41	90	0.105	70.45
16	1000	0.07	120	0.016	85.36
17	1000	0.41	60	0.057	57.14

Figure 8 displays formaldehyde RE of 17 experiments from 0 to 120 minutes. RE increased rapidly at the beginning of the experiment and potentially approached stable around 90 minutes for all labs. The formaldehyde removal efficiency achieved in this study (over 90.97%) using PKS biochar demonstrates exceptional performance compared to other biochar-based adsorbents reported in the literature. For instance, Zouari et al. [10] reported a maximum removal efficiency of 64% using biochar derived from Arundo donax and olive seeds at 800°C. Similarly, Ahn et al. (2021) also demonstrated high adsorption capacity (1811 mg/g) using metal-doped biochar synthesized from acid mine drainage sludge and spent coffee grounds.

In comparison, the PKS-derived biochar used in this study showed not only comparable or superior removal efficiency but also the potential advantages of being derived from an abundant agricultural byproduct. Its effectiveness highlights its suitability for practical indoor air purification applications, particularly in environments such as anatomical laboratories where formaldehyde is prevalent.

By using the optimization function in the DE program, the optimal conditions for the operation of the phototype air treatment unit to remove formaldehyde in the lab gross was obtained as illustrated by Figure9. Figure 9 shows the optimal conditions of operating the air pollution treatment unit to remove formaldehyde in the lab gross. From Figure 9, the optimal conditions of formaldehyde treatment suggested by RSM were biochar amount of 995.97 g, air flowrate of 0.12 m^3/s, treatment time of 114.14 min yielded RE of 82.61%, and concentration of 0.0078 ppm.

The observed trend of increasing removal efficiency with longer treatment durations is consistent with established adsorption behavior, where extended contact time allows for greater interaction between the adsorbent surface and target gas molecules. However, the diminishing improvements beyond 100 minutes suggest that equilibrium may have been reached, where additional exposure time yields only marginal gains in removal efficiency. In contrast, increasing the airflow rate negatively impacted performance, likely due to the reduced contact time between the formaldehyde molecules and the biochar surface. Higher flow rates may also promote channeling effects, reducing the overall utilization of the adsorbent's surface area. This

inverse relationship emphasizes the importance of balancing airflow and residence time to achieve effective pollutant capture. The results also highlight that 750 grams of biochar was the optimal amount for the filter configuration used. This suggests that beyond this quantity, additional biochar may not significantly enhance performance, potentially due to limitations in gas distribution or saturation of the active surface.

Overall, the findings confirm that careful optimization of biochar quantity, airflow rate, and treatment time is essential for achieving high formaldehyde removal efficiency. These insights are valuable for guiding the design of biochar-based air treatment systems, particularly in environments with high concentrations of indoor air pollutants such as formaldehyde.

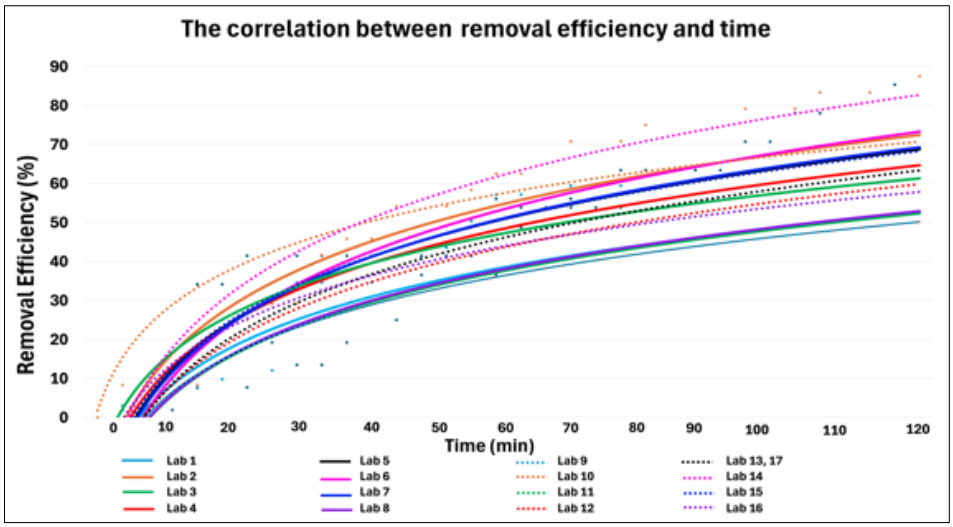


Figure 8 Formaldehyde Removal Efficiency

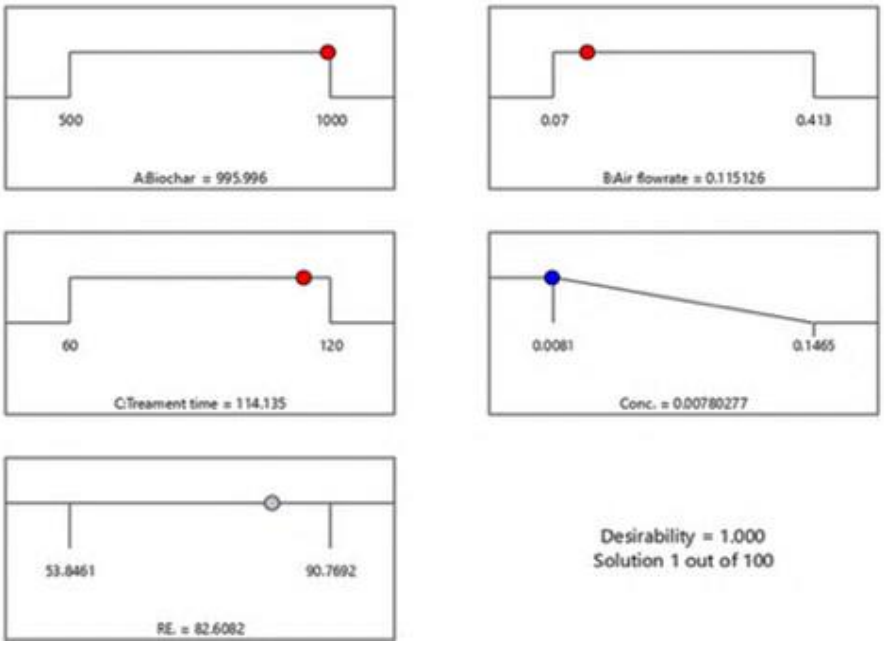


Figure 9 Optimal Conditions for Formaldehyde Removal using Air Pollition Treament Unit

CONCLUSION

The maximum removal effectiveness of a prototype air treatment unit utilizing biochar adsorbents in the anatomy lab was determined to be greater than 90% for the starting formaldehyde content in the range of 0.34–0.36 ppm. PKS biochar produced in this study using the prototype treatment unit is hence effective at treating air pollution. By utilizing the CCD in the DE's optimization function, the ideal operating conditions for the air treatment unit were achieved. The use of industrial or agricultural waste was shown in the study's results to be consistent with the circular economy and zero waste strategy.

ACKNOWLEDGEMENT

School of Engineering and Technology, Walailak University
Health Science and Technology (HT) Program, Srinakharinwirot University Prasarnmit Demonstration Senior High School

REFERENCE (Please see format of the reference in the Manuscript Format and Style)

[1] A. Resae, M.H. Yousefi, S. Naeimi, A. Mahdavi, Effects of Occupational Formaldehyde Exposure on Passive Avoidance Conditioning and Anxiety Levels in Wistar rats, Iran J Vet Med 17 2023. 65–74. https://doi.org/10.32598/IJVM.17.1.1005241.

[2] K.-H. Kim, S.A. Jahan, J.-T. Lee, Exposure to Formaldehyde and Its Potential Human Health Hazards, Journal of Environmental Science and Health, Part C 29 2011. 277–299. https://doi.org/10.1080/10590501.2011.629972

[3] G.D. Nielsen, P. Wolkoff, Cancer effects of formaldehyde: a proposal for an indoor air guideline value, Arch Toxicol 84 2010. 423–446. https://doi.org/10.1007/s00204-010-0549-1.

[4] M. Hassan, A. Bermak, Threshold detection of carcinogenic odor of formaldehyde with wireless electronic nose, in: IEEE SENSORS 2014. Proceedings, IEEE, 2014: pp. 1368–1371. https://doi.org/10.1109/ICSENS.2014.6985266

[5] T. Xie, K.R. Reddy, C. Wang, E. Yargicoglu, K. Spokas, Characteristics and Applications of Biochar for Environmental Remediation: A Review, Crit Rev Environ Sci Technol 45 2015. 939-969.

[6] H. Fidder, M. Yang, E.T.J. Nibbering, T. Elsaesser, K. Röttger, F. Temps, N–H Stretching Vibrations of Guanosine–Cytidine Base Pairs in Solution: Ultrafast Dynamics, Couplings, and Line Shapes, J Phys Chem A 117 2013. 845–854. https://doi.org/10.1021/jp309237u.

[7] O. V. Ovchinnikov, A. V. Evtukhova, T.S. Kondratenko, M.S. Smirnov, V.Yu. Khokhlov, O. V. Erina, Manifestation of intermolecular interactions in FTIR spectra of methylene blue molecules, Vib Spectrosc 86 2016. 181–189. https://doi.org/10.1016/j.vibspec.2016.06.016.

[8] Y. Dwivedi, S.B. Rai, Spectroscopic study of overtone and combination bands in aliphatic aldehydes, Vib Spectrosc 49 2009. 278–283. https://doi.org/10.1016/j.vibspec.2008.10.009.

[9] M.A. Algatti, R.P. Mota, R.Y. Honda, M.E. Kayama, K.G. Kostov, R.S. Fernandes, T.C.A.M. Azevedo, N.C. Cruz, Study of optical properties and molecular structure of plasma polymerized diethylene glycol dimethyl ether, The European Physical Journal D 54 2009. 325–328. https://doi.org/10.1140/epjd/e2009-00043-7.

[10] Zouari, M., Marrot, L., & DeVallance, D. B. (2023). Evaluation of properties and formaldehyde removal efficiency of biocarbon prepared at variable pyrolytic temperatures. Frontiers in Environmental Science, 11, 1252926. https://doi.org/10.3389/fenvs.2023.1252926

[11] Ahn, Y., et al. (2021). Efficient removal of formaldehyde using metal-biochar derived from acid mine drainage sludge and spent coffee waste. Journal of Environmental Management, 298, 113468. https://doi.org/10.1016/j.jenvman.2021.113468

Determination of Mechanical, Physical and Microstructural Properties of Hemp Fibers added with Polyacetic Acid Bio Composites

Pongsathorn Kongkeaw [1*] Thanin Rudchapo[1] and Apisit Khetcharioen[1]

[1] Lecturer; Program of Physics, Faculty of Science and Technology, Rajabhat Maha Sarakham University, Maha Sarakham, Thailand*

[*]Phone : 0896023249, , E-mail : Pongsathorn.ko@rmu.ac.th

ABSTRACT

This research investigated the mechanical, physical, and microstructural properties of hemp fiber reinforced polylactic acid (PLA) bio composites across multiple fiber-to-matrix ratios. Using a Completely Randomized Design (CRD), the study examined four different hemp weight ratios (5:95, 10:90, 15:85, and 20:80 %wt) to determine optimal composition for enhanced performance. Bio composites were fabricated via compression molding at 210°C under 140 bar pressure. Mechanical testing revealed significant variations in tensile strength ($p < 0.05$) and flexural modulus ($p < 0.05$) across compositions, with 10:90 %wt hemp demonstrating superior tensile properties (4.54 ± 0.55 MPa strength, 0.972 ± 0.014 MPa modulus). Physical property analysis showed increasing density trends with higher fiber content, from 0.528 ± 0.058 g/cm³ at 5:95 %wt to 0.600 ± 0.071 g/cm³ at 20:80 %wt, while water absorption exhibited non-linear behavior peaking at 15:85 %wt (0.718 ± 0.987%). Microstructural examination via SEM confirmed good fiber-matrix adhesion at 10% fiber content but revealed significant interfacial defects and agglomeration at 20% loading. Thermogravimetric analysis demonstrated enhanced thermal stability with moderate fiber incorporation, with decomposition temperatures reaching 349.37°C at 15% hemp content. The findings establish that 10% hemp fiber represents the optimal balance between reinforcement benefits and interfacial limitations in PLA-based bio composites, providing valuable insights for developing sustainable alternatives to petroleum-based composites with tailored mechanical and physical properties.

Keywords: Hemp fiber; Polylactic acid; Bio composites; Mechanical properties; Thermal stability; Microstructure

INTRODUCTION

While "cannabis" has been gaining significant attention as a new economic crop, hemp (*Cannabis sativa* L.) shares similar botanical characteristics but lacks the psychoactive properties of cannabis. Both hemp and cannabis originated from the same plant species, native to the temperate regions of southern Siberia, Persia (modern-day Iran), northern Kashmir in India, and northern China [1]. The use of hemp stem fibers for industrial applications has been documented throughout history, with evidence dating back several millennia [2]. In Thailand, the Ministry of Public Health currently promotes and supports hemp cultivation across various regions, subject to proper licensing requirements and regulatory frameworks [3]. Hemp has gained recognition for its exceptional mechanical properties, particularly its fiber characteristics. Research has shown that hemp fibers demonstrate remarkable tensile strength ranging from 350-800 MPa and Young's modulus of 30-60 GPa. These properties, combined with their low density (1.4-1.5 g/cm³), make hemp fibers particularly attractive for composite applications [4]. The integration of hemp fibers with PLA (Polylactic Acid) matrices has shown promising results in creating sustainable biocomposites. Studies have demonstrated that hemp-PLA composites can achieve tensile strengths of up to 55 MPa with 30% fiber loading, representing a significant improvement over neat PLA. Furthermore, these biocomposites exhibit enhanced biodegradability compared to conventional petroleum-based composites, with complete degradation possible within 6-24 months under appropriate conditions.

Recent investigations into the microstructural properties of hemp fibers have revealed complex hierarchical structures that contribute to their superior mechanical properties. Electron microscopy studies have shown that hemp fibers possess a unique multi-layered cell wall structure, with microfibrils oriented at specific angles that enhance their mechanical performance. This structural arrangement, combined with their high cellulose content (approximately 70-74%), makes hemp fibers particularly suitable for reinforcement in biocomposite applications.Therefore, investigating various properties and developing prototype products

from hemp fibers in agricultural areas could benefit agencies and farmers interested in future hemp cultivation.

This research aims to explore appropriate applications of hemp specific to local areas, diversify agricultural uses, and advance commercial production and development of hemp-based products and packaging, while addressing the growing demand for sustainable materials in various industrial sectors.

METHODOLOGY

The experiment employed a Completely Randomized Design (CRD) with fixed effect model, consisting of 5 treatments with 3 replications each, investigating different weight ratios of hemp fibers and Polylactic Acid (PLA): 5:95, 10:90, 15:85, and 20:80 %wt. The experimental procedure began with hemp fiber modification using sodium hydroxide (NaOH), followed by grinding and sieving through mesh No. 16, then hot air drying. Concurrently, PLA pellets were dried in a vacuum oven at 80°C for 24 hours. The dried hemp fibers and PLA were then mixed according to the specified weight ratios and placed in prepared molds. Composites were fabricated using compression molding at 210°C under 140 bar pressure for 7 minutes, after which the specimens were cut and shaped using a jigsaw according to ASTM standards for mechanical and thermal property testing. Finally, all mechanical and thermal properties data were statistically analyzed using One-way ANOVA at 95% confidence level. This methodology follows established procedures documented in relevant literature, including ASTM International standards for mechanical testing of polymer matrix composite materials.

RESULTS AND DISCUSSIONS

1.Mechanical Properties

The mechanical performance of hemp fiber/PLA bio composites was evaluated across four different fiber-to-matrix ratios (5:95, 10:90, 15:85, and 20:80 %wt). As shown in Table 1 and illustrated in Figure 1(a-e)

Table 1 Mechanical and Physical Properties of Hemp Fibers added with Polyacetic Acid Bio Composites

Fiber Content (Polylactic acid: Hemp fiber)	Density (g/cm^3)	Water absorption (%)	Tensile Strength (Mpa)	Tensile Modulus (Mpa)	Flexural Strength (Mpa)	Flexural Modulus (Mpa)	Impact Strength (kJ/mm^2)
95:5	0.528±.058	0.339±.756	4.36±.152	0.755±.442	0.62±.024	0.932±.025	14.246±3.113
90:10	0.562±.054	0.339±.756	4.54±.055	0.972±.014	0.67±.009	0.966±.017	14.690±1.201
85:15	0.540±.079	0.718±.987	4.3±.235	0.586±.509	0.57±.138	0.966±.005	14.6997±2.159
80:20	0.600±.071	0.644±.881	2.14±.089	0.594±.488	0.59±.061	0.989±.009	14.692±3.269
P-value	.365	.841	.000*	.431	.247	.001*	.990

where *is significantly difference at p<0.05

The tensile strength results (Table 1 and Figure 1a) reveal a significant variation ($p < .05$) among different hemp fiber concentrations. The data shows that 10:90 %wt hemp composition achieved the highest tensile strength (4.54 ± 0.55 MPa), followed by 5:95 %wt (4.36 ± 1.52 MPa) and 15:85 (4.3 ± 2.35 MPa), with a sharp decline at 20:80 (2.14 ± 0.89 MPa). This performance pattern follows the critical fiber content theory proposed by [5] which suggests that exceeding the optimal fiber volume fraction leads to fiber agglomeration and poor interfacial adhesion. The statistical significance ($p < 0.05$) confirms that this pattern is not due to random variation. Similarly, tensile modulus data (Figure 1b) shows peak performance at 10% hemp content (0.972 ± 0.014 MPa), though the differences were not statistically significant ($p > 0.05$).

According to [6], this behavior reflects the competing mechanisms of fiber reinforcement and interfacial defect introduction.

The flexural modulus (Figure 1d) demonstrates a statistically significant difference across compositions ($p < 0.05$), increasing progressively with fiber content from 0.932 ± 0.025 MPa at 5:95 %wt to 0.989 ± 0.009 MPa at 20:80 %wt. This trend aligns with [7] findings that natural fibers can enhance composite stiffness even when other mechanical properties decline, due to the inherently higher modulus of cellulosic fibers compared to PLA. Flexural strength values (Figure 1c) peaked at 10:90 %wt composition (0.67 ± 0.009 MPa) and were lowest at 15:85 %wt (0.57 ± 0.138 MPa), though these variations were not statistically significant ($p > 0.05$). The non-significance suggests that fiber content within this range does not substantially alter the flexural strength.

Impact strength values (Figure 1e) remained remarkably consistent across all compositions ($p > 0.05$), ranging from 14.246 ± 3.13 kJ/m² (5:95) to 14.699 ± 2.159 kJ/m² (15:85). This consistency indicates that within the studied range, hemp fiber content has negligible effect on impact performance. Yuanjian et al. [8] explained that in plant fiber composites, impact properties are influenced more by fiber-matrix adhesion quality than by fiber quantity, which explains why statistical analysis shows no significant differences.

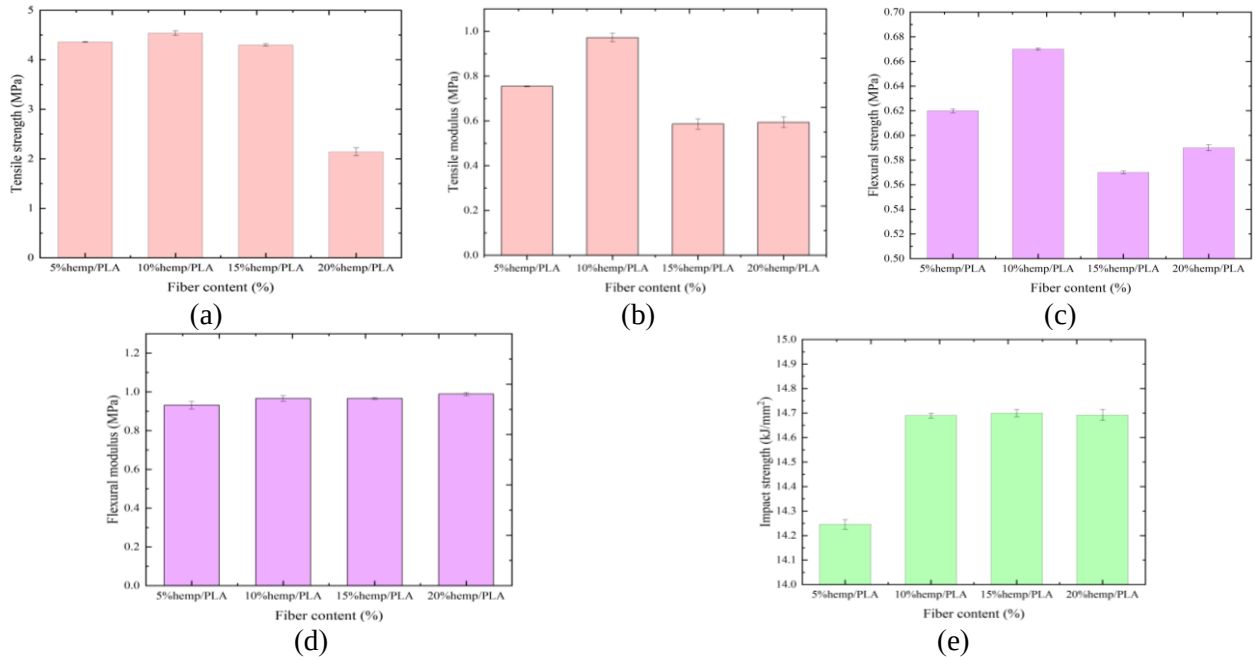
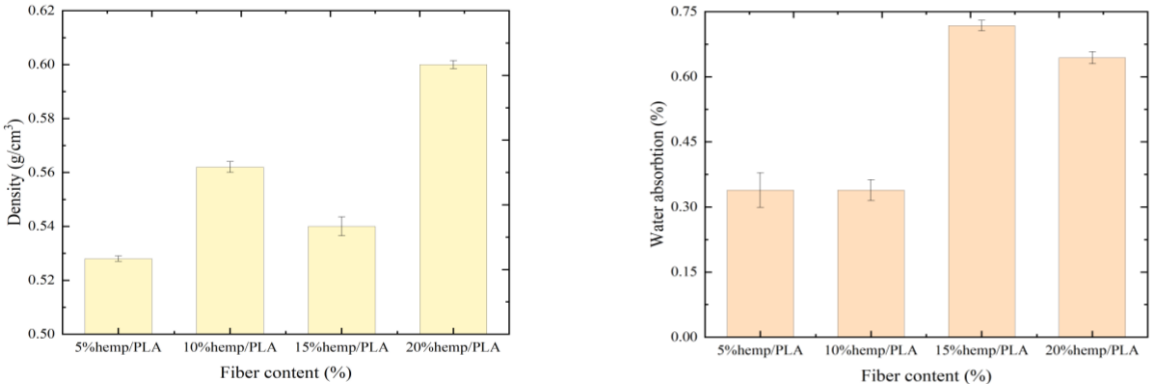


Figure 1 Mechanical Properties of Bio Composites (a) Tensile strength (b) Tensile modulus (c) Flexural strength (d) Flexural modulus and (e) Impact strength

2.Physical Properties

The physical properties of hemp fiber/PLA bio composites demonstrated interesting variations across different fiber loadings as shown in Table 1. Density measurements revealed a modest increasing trend from 0.528 ± 0.058 g/cm³ at 5:95 %wt hemp to 0.600 ± 0.071 g/cm³ at 20:80 %wt composition, though statistical analysis indicated non-significance ($p > 0.05$). This subtle density increase corresponds with the visual density patterns observable in Figure 2(a), where microstructural arrangement becomes more compact with increasing fiber content, consistent with findings by [9]. Water absorption behavior followed a non-linear pattern as shown in figure 2(b), with lowest values at 5:95 %wt and 10:90 %wt (both 0.339 ± 0.756%), peaking at 15:85 %wt (0.718 ± 0.987%), then slightly decreasing at 20:80 %wt (0.644 ± 0.881%), though these differences were not statistically significant ($p > 0.05$). The initially increasing water absorption trend aligns with hemp's hydrophilic nature as documented by [10], while the slight decrease at highest fiber content may reflect reduced matrix-fiber interface area due to fiber agglomeration visible in Figure 3's

microstructural images, a phenomenon previously observed by [11], where densely packed fiber regions create fewer pathways for water penetration despite higher overall fiber content.

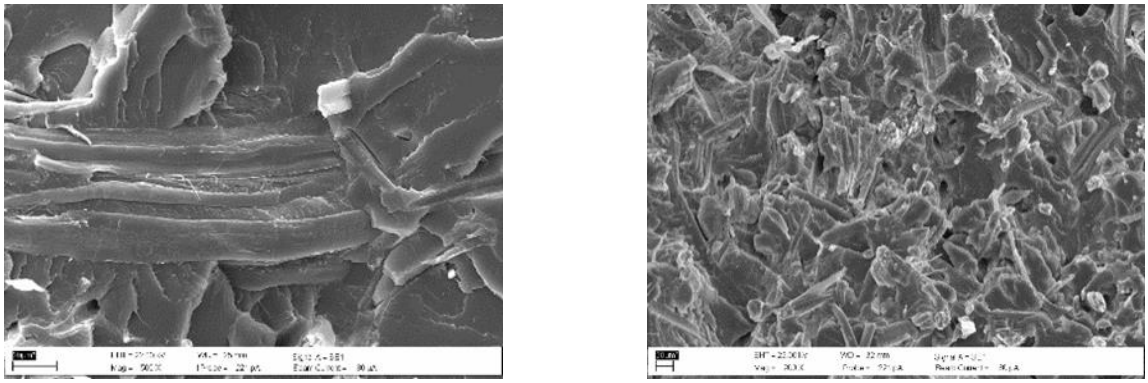


(a) (b)

Figure 2 Physical properties of Bio Composites (a) Density and (b) Water absorption

3.Microstructure of Bio Composites

Figure 3 reveals distinct microstructural characteristics of hemp/PLA bio composites at different fiber loadings following tensile testing. The 10:90 %wt (Figure 3a) displays a relatively smooth, layered fracture surface with visible fiber alignment and good interfacial adhesion between hemp fibers and the PLA matrix, as evidenced by the limited fiber pullout and continuous matrix areas. This microstructural arrangement supports the superior tensile properties observed at this composition (4.54 ± 0.55 MPa), aligning with [12] findings that optimal fiber-matrix adhesion occurs at moderate fiber loadings. In contrast, the 80:20 %wt (Figure 3b) exhibits a significantly rougher surface characterized by numerous short, randomly oriented fibers with poor matrix wetting and visible void formations at fiber-matrix interfaces. These microstructural defects explain the substantial decline in tensile strength (2.14 ± 0.89 MPa) at higher fiber content, consistent with [13] observations that excessive fiber loading creates interfacial weaknesses and [14] documentation of critical fiber volume fractions beyond which agglomeration dominates over reinforcement effects in natural fiber bio composites.



(a) (b)

Figure 3 Microstructure of composite specimens after tensile strength test (a) 90:10 %wt (b) 80:20 %wt

4. Thermal Properties

The thermal degradation behavior of hemp/PLA bio composites displays significant variations across different fiber loadings as illustrated in Figure 4(a-d). The thermogravimetric (TG) and derivative thermogravimetric (DTG) curves reveal a distinct single-stage decomposition pattern for all compositions, with decomposition temperatures progressively increasing from 337.15°C at 95:5 %wt (Figure 4a) to 346.59°C at 90:10 %wt (Figure 4b), 349.37°C at 85:15 %wt (Figure 4c), and reaching 343.16°C at 80:20

%wt (Figure 4d). This trend indicates enhanced thermal stability with moderate fiber incorporation, consistent with [15] findings that natural fibers can create tortuous pathways for volatile degradation products. The weight loss percentage (Delta Y) also shows a systematic increase from 86.734% (95:5 %wt) to 92.751% (80:20 %wt), reflecting the greater proportion of thermally stable cellulosic components as fiber content increases, as documented by [16]. Notably, the peak decomposition rate (peak height) shows the inverse trend, decreasing from 3.0845 mg/min at 95:5 %wt to 2.7225 mg/min at 80:20 %wt, suggesting slower decomposition kinetics with higher fiber loading, a phenomenon [17] attributed to the formation of a char layer from hemp components that provides a temporary barrier against thermal degradation of the underlying polymer matrix.

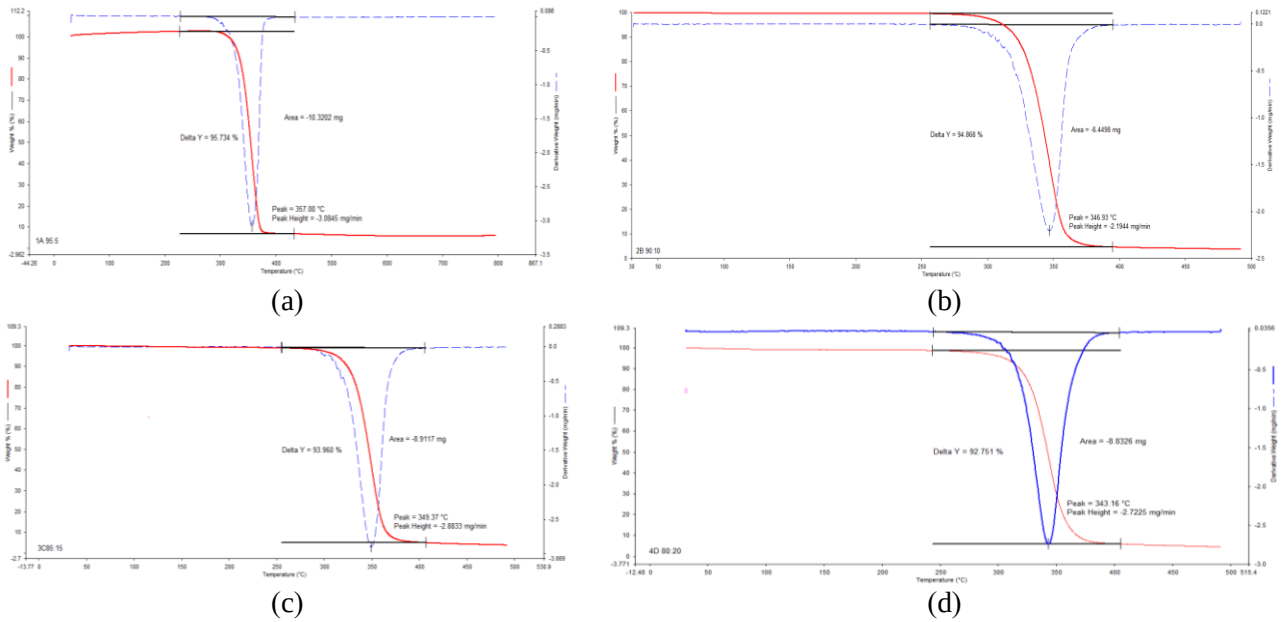


Figure 4 Decomposition temperature of hemp fiber reinforced biocomposites at different ratios (a) 95:5 %wt (b) 90:10%wt (c) 85:15 %wt and (d) 80:20 %wt

CONCLUSION

This study comprehensively investigated the mechanical, physical, and microstructural properties of hemp fiber/PLA bio composites across various fiber-to-matrix ratios (5:95, 10:90, 15:85, and 20:80 %wt). The results revealed that 10:90 % wt hemp composition achieved optimal mechanical performance with the highest tensile strength (4.54 ± 0.55 MPa) and tensile modulus (0.972 ± 0.014 MPa), while flexural modulus increased progressively with fiber content ($p < 0.05$). Physical property analysis showed a slight increase in density with fiber loading, though not statistically significant ($p > 0.05$), and non-linear water absorption behavior that peaked at 15:85 %wt. Microstructural examination confirmed good interfacial adhesion at 10% fiber loading with smooth, layered structures, contrasting with the agglomerated, poorly wetted fibers at 20% content. Thermal stability improved with moderate fiber incorporation, with decomposition temperatures peaking at 349.37°C for 85:15 %wt. These findings demonstrate that hemp fiber content must be carefully optimized to balance interfacial adhesion effects against reinforcement benefits, with 10% hemp fiber representing the ideal compromise for overall performance in sustainable bio composites targeted for lightweight, moderate-strength applications where environmental considerations are paramount.

ACKNOWLEDGEMENT

The authors would like to acknowledge the financial support provided by the Science, Research and Innovation Fund, Fundamental Fund (FF.) for the fiscal year 2024.

REFERENCE

[1] R.C. Clarke & M.D. Merlin. 2013 – Cannabis: Evolution and Ethnobotany. Plant Ecology and Evolution, 147(1), 149–149.

[2] Müssig, J., Amaducci, S., Bourmaud, A., Beaugrand, J., & Shah, D. U. 2020. Transdisciplinary top-down review of hemp fibre composites: From an advanced product design to crop variety selection. Composites Part C: Open Access, 2, 100010.

[3] Pickering, K. L., Efendy, M. G. A., & Le, T. M. 2016. A review of recent developments in natural fibre composites and their mechanical performance. Composites Part A: Applied Science and Manufacturing, 83, 98–112.

[4] Manaia, J. P., Manaia, A. T., & Rodriges, L. 2019. Industrial Hemp Fibers: An Overview. Fibers, 7(12), 106.

[5] Yoo, D.-Y., Lee, J.-H., & Yoon, Y.-S. 2013. Effect of fiber content on mechanical and fracture properties of ultra high-performance fiber reinforced cementitious composites. Composite Structures, 106, 742–753.

[6] Fu, Y., & Yao, X. 2022. A review on manufacturing defects and their detection of fiber reinforced resin matrix composites. Composites Part C: Open Access, 8, 100276.

[7] Gholampour, A., & Ozbakkaloglu, T. 2020. A review of natural fiber composites: properties, modification and processing techniques, characterization, applications. Journal of Materials Science, 55(3), 829–892.

[8] Yuanjian, T., & Isaac, D. H. 2007. Impact and fatigue behaviour of hemp fibre composites. Composites Science and Technology, 67(15–16), 3300–3307.

[9] Faruk, O., Bledzki, A. K., Fink, H.-P., & Sain, M. 2012. Bio composites reinforced with natural fibers: 2000–2010. Progress in Polymer Science, 37(11), 1552–1596.

[10] Hussain, A., Calabria-Holley, J., Lawrence, M., & Jiang, Y. 2019. Resilient hemp shiv aggregates with engineered hygroscopic properties for the building industry. Construction and Building Materials, 212, 247–253.

[11] Hoto, R., Furundarena, G., Torres, J. P., Muñoz, E., Andrés, J., & García, J. A. 2014. Flexural behavior and water absorption of asymmetrical sandwich composites from natural fibers and cork agglomerate core. Materials Letters, 127, 48–52.

[12] Zuccarello, B., & Zingales, M. 2017. Toward high performance renewable agave reinforced bio composites: Optimization of fiber performance and fiber-matrix adhesion analysis. Composites Part B: Engineering, 122, 109–120.

[13] Sethi, S., & Ray, B. C. 2015. Environmental effects on fibre reinforced polymeric composites: Evolving reasons and remarks on interfacial strength and stability. Advances in Colloid and Interface Science, 217, 43–67.

[14] Zuccarello, B., & Zingales, M. 2017. Toward high performance renewable agave reinforced bio composites: Optimization of fiber performance and fiber-matrix adhesion analysis. Composites Part B: Engineering, 122, 109–120.

[15] Fan, M., & Naughton, A. 2016. Mechanisms of thermal decomposition of natural fibre composites. Composites Part B: Engineering, 88, 1–10.

[16] Chen, X., Yu, J., Zhang, Z., & Lu, C. 2011. Study on structure and thermal stability properties of cellulose fibers from rice straw. Carbohydrate Polymers, 85(1), 245–250.

[17] Branca, C., & Di Blasi, C. 2021. Thermal degradation behavior and kinetics of industrial hemp stalks and shives. Thermochimica Acta, 697, 178878.

20P-16

Fume Exposure During Arc Welding Practices among Vocational Students: A Case Study

Phongsakorn Kumpeera[1], Pornthip Yenjai[2] and Pongsit Boonruksa[3*]

[1]Students, School of Occupational Health, Safety, and Environmental, Institute of Public Health, Suranaree University of Technology, Nakhon Ratchasima 30000, Thailand

[2,3]Assistant Professor, School of Occupational Health and Safety, Institute of Public Health, Suranaree University of Technology, Nakhon Ratchasima 30000, Thailand*

[*]Phone : 0 4422 3938, Fax : 0 4422 3952, E-mail: pongsitb@sut.ac.th

ABSTRACT

Shielding Metal Arc Welding (SMAW) is widely used in various industries, and general metal repair works. SMAW produces welding fumes identified as carcinogenic to humans. Prolonged exposure to welding fumes can lead to a range of health effects including respiratory diseases, metal fume fever, and lung cancer. This study aimed to investigate welding and metal fume exposure, and particle morphology during SMAW practices among 9 students enrolled in a basic welding course at a vocational college. Welding fumes were collected from each student's breathing zone using an MCE filter and a personal pump with a flow rate of 2 L/min. The filter was analyzed using the gravimetric method to determine welding fume concentration. Subsequently, it was analyzed using ICP-MS to determine the metal fume concentrations of 8 elements: Fe, Zn, Mn, Cu, Cr, Ni, Cd, and Ag. Moreover, the fumes were collected on a nucleopore membrane filter with a flow rate of 2 L/min for morphology analysis using a field emission scanning electron microscopy. The results showed that during the SMAW practices, students were exposed to welding fume concentrations of 2.10 - 10.40 mg/m³, with an average of 4.50 ± 2.36 mg/m³. The concentrations of welding fume exposure increased with higher electric current. The highest welding fume exposure concentration at a mean of 7.15 ± 3.31 mg/m^3 when welding using an electric current at 85 A, followed by the current at 80 A, and 70 A. For metal fume concentrations, the highest percentage of metal in welding fumes was Fe, followed by Zn and Mn, respectively, across all electric currents. For morphology analysis, fumes were typically arranged as chain-like agglomerates of ultrafine and nanoparticles. Therefore, control measures including local exhaust ventilation systems, and the selection of appropriate electric currents should be implemented to minimize the exposures during SMAW practices.

Keywords: fume exposure, morphology, shielding metal arc welding practice, vocational students

INTRODUCTION

Arc welding or Shielded Metal Arc Welding (SMAW) is a metal joining process that utilizes an electric current to generate heat, which melts the electrode and fuses the metal components, forming a weld bead [1]. It is widely utilized across various industries such as automotive assembly, construction, and general metal equipment repair works.

During SMAW, welders are at risk of exposure to various hazards including welding fumes [2]. Exposure to this major hazard causes adverse health effects such as respiratory diseases [3], metal fume fever, inflammation [4], pneumonia, and asthma [5]. Moreover, The International Agency for Research on Cancer (IARC) classified welding fumes as carcinogenic to humans (Group 1) [9]. Moreover, morphological characteristics are closely linked to health impacts, as particle size plays a critical role in the capture and accumulation of particulate matter within the respiratory system [10].

Several studies reported that SMAW welders were exposed to welding fumes above the ACGIH (5 mg/m^3) for an 8-hour time-weighted average (TWA) [11, 12, 13]. For example, a study illustrated that SMAW welders in Iran were exposed to total welding fume at a mean TWA of 7.9 mg/m^3 [14]. Moreover, a health risk assessment study revealed that welders were exposed to metal fumes, including Fe, Cr, and Ni at concentrations of 17.89, 0.44, and 0.14 mg/m³, respectively [15]. Welding fume concentrations emitted from SMAW are affected by various factors including electric current, arc voltage, travel speed, electrode type, welding position, and environmental conditions [16].

However, research on exposure to welding fumes from SMAW in Thailand remains limited, particularly in the context of short-term exposure including during the SMAW practices in a basic welding course among vocational students focusing on industrial works. Therefore, this study aimed to investigate welding fume, metal fume, and particle morphology that these students were exposed to during SMAW practices.

METHODOLOGY

Study and Population

This research was a cross-sectional descriptive study conducted among 9 students enrolling in a basic welding course at a vocational college in Nakhon Ratchasima. All participants were male, with an average age of 17.67 ± 0.5 years. Following the procedure, each student performed a SMAW welding of low carbon steel (SS400) with E6013 welding electrodes to create two bead-on-plate welds in a flat position using electric currents at a range of 70 - 85 amperes (A).

Welding Fume Sampling

Personal welding fume samplings were collected using a cassette with a mixed cellulose ester filter (37 mm with 0.8 μm pore size) attached to the breathing zone of each subject and a personal pump (Gilian, GilAir Plus) was operated at a flow rate of 2 L/min. The duration of sampling time depended on an individual welding practice with a range of 5 - 10 minutes.

For fume morphology sampling, welding fumes were collected on nucleopore membrane filters (25 mm with 0.2 μm pore size) with a flow rate of 2 L/min. The cassette was placed above the floor at 1.5 meters (the breathing zone level). The sampling time was set at a minute, allowing welding particles on the filter at a moderate density.

Welding Fume and Metal Fume Analysis

The welding fume concentrations during arc welding practice were analyzed using the gravimetric analysis method. The mass concentration is calculated using Equation 1.

$$C = \frac{(W_2\text{-}W_1) - (B_2\text{-}B_1) \times 10^3}{V} (mg/m^3) \qquad (1)$$

Where C represents the welding fumes concentration (mg/m³). W_1 and W_2 are the weights of the filter (mg) before and after sample collection, respectively. B_1 and B_2 are the weights of the filter (mg) of blank before and after sampling, respectively. V is the volume of sampling air (L).

The metal fume concentrations were analyzed using ICP-MS (Agilent/7900) to measure elements including Ag, Cd, Cr, Cu, Fe, Mn, Ni, and Zn that are required by NIOSH method for welding and brazing fumes. Each element concentration is calculated using Equation (2) [17]

$$C = \frac{(C_sV_s - C_bV_b)}{V} (mg/m^3) \qquad (2)$$

Where C represents the concentration of metal fume in the sample solution (μg/L, equivalent to mg/m³). C_s and C_b are the concentration of the metal fume of the sample and blank (μg/L), respectively. V_s and V_b are the final volume (ml) of the sample and blank, respectively. V is the volume of sampling air (L).

Morphological Analysis

The nucleopore membrane filter was coated with gold to a thickness of 3.2 nm in the vacuum of $5x\ 10^{-2}$ mbar, using a current of 30 mA for 20 minutes on a rotating stage. The filter was subsequently analyzed using a Field Emission Scanning Electron Microscope (FESEM, Carl Zeiss/AURIGA) for particle morphology.

RESULTS AND DISCUSSIONS

Exposure to Welding Fume

During the SMAW practices, students were exposed to welding fume concentrations ranging from 2.10 - 10.40 mg/m³, with a mean of 4.50 ± 2.36 mg/m³. When considering the data based on the electric current, it showed that welding fume exposure concentrations are higher with increasing the electric current. Using the current at 85 A led to the highest welding fume exposure concentration at a mean of 7.15 ± 3.31 mg/m^3, followed by the current at 80 A (3.74 ± 0.06 mg/m^3), and 70 A (2.62 ± 0.56 mg/m^3) (Figure 1).

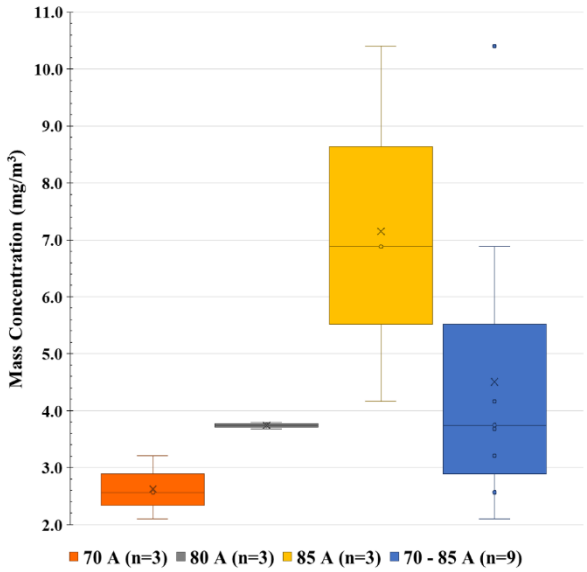


Figure 1 Box-whisker plot of welding fume exposure concentration during SMAW practices under different electric currents.

The results were consistent with a study by Abdull et.al [18]. It reported that using a high electric current (130A) for a welding process generated a mean welding fume concentration of 0.122 mg/m³ that higher than 1.91 times of using a low electric current (60 A).

Metal Fume Exposure Concentration

Table 1 illustrates the metal fume exposure concentrations among students performing SMAW practice using various electric currents. The results showed that the highest percentage of metal in welding fumes was Fe, followed by Zn and Mn, respectively, for all electric currents. These findings aligned with a study by Pourhassan et al. [19], which showed the top 3 highest metal fume exposure concentrations of Fe (1.05 mg/m³), Zn (0.11 mg/m³) and Mn (0.03 mg/m³) from the sampling according with 4-hour sampling time.

The intensity of electric current may influence metal fume exposure. The highest exposure was observed at 85 A, followed by 70 A and 80 A. An experiment revealed that increased electric current during SMAW operations with a core wire and base material using IS 2062 low carbon steel resulted in elevated generation of Fe and Mn fumes [20] However, this study showed that the average metal fume exposure during welding with an electric current of 70 A was higher than that with a current of 80 A. According to our observations, welding with low currents may compromise welding quality, leading to students requiring additional time to complete their tasks. This may result in increased exposure to metal fumes compared to using a current of 80 A. A study reported that longer welding time has significantly affected the risk of metal fume exposure [19]. Further studies should be conducted.

Welding Fume Morphology

The images of welding fume morphology at a FESEM magnification of 2,500x and 30,000x are illustrated in Figure 2. Welding fume consisted of various shapes and sizes such as spherical particles with a size of 4.78 µm and aggregations of ultrafine particles (Figure 2A). A study reported that large particles of welding fumes were mainly composed of Fe, C, and O [21]. When increasing the magnification to 30,000x, it revealed aggregations of ultrafine particles at the nanoscale. They formed into clusters that resemble agglomerate chain-like structures (Figure 2B).

The findings were aligned with previous studies. They have reported that particles generated from welding processes are non-uniform and spherical shapes with sizes less than 10 µm. These larger particles result from metal spatter during metal arc welding [12, 19]. Moreover, they also found the morphology of metal fumes contains ultrafine particles (0.01 - 1 µm) with chain-like agglomerates consisting of nanoparticles with a range of 5 - 20 nm [22, 23, 24].

Table 1 Metal fume exposure concentration based on using various electric currents.

Metal Fume	Concentration (µg/m^3)							
	70 (A)		80 (A)		85 (A)		70 – 85 (A)	
	$\bar{x}$ (SD)	%	$\bar{x}$ (SD)	%	$\bar{x}$ (SD)	%	$\bar{x}$ (SD)	%
Fe	125.25 (74.55)	76.41	44.45 (10.91)	66.88	201.95 (34.12)	80.57	123.88 (79.77)	77.26
Zn	15.76 (12.63)	9.61	9.58 (5.39)	14.41	19.38 (20.51)	7.73	14.91 (13.07)	9.30
Mn	15.21 (6.67)	9.28	4.63 (3.22)	7.06	18.68 (16.37)	7.45	12.86 (10.98)	8.02
Cu	5.57 (1.38)	3.40	5.71 (1.19)	8.59	7.60 (3.95)	3.03	6.29 (2.39)	3.92
Cr	1.17 (0.20)	0.71	1.02 (0.09)	1.53	1.95 (1.48)	0.78	1.38 (0.87)	0.86
Ni	0.94 (0.35)	0.57	0.90 (0.06)	1.35	1.09 (0.51)	0.43	0.98 (0.32)	0.61
Cd	0.01 (0.01)	0.01	0.11 (0.11)	0.17	<0.01	<0.01	0.04 (0.08)	0.02
Ag	<0.01	<0.01	<0.01	<0.01	<0.01	<0.01	<0.01	<0.01
Total	163.91 (95.79)	100	66.44 (20.97)	100	250.66 (76.95)	100	160.34 (107.46)	100

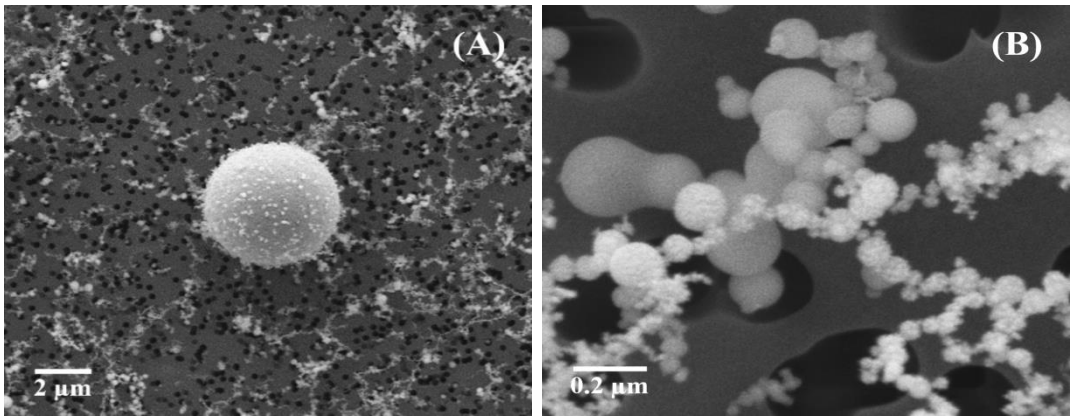


Figure 2 FESEM image of the welding fume collected near a breathing zone of subjects during SMAW practice; (A) a magnification of 2,500x, (B) a magnification of 30,000x

According to the findings, measures to mitigate exposure to welding and metal fumes during SMAW practices should be considered. Local exhaust ventilation systems must be implemented at each workstation. Additionally, students should be instructed to recognize the hazards of welding and metal fumes, as well as to acknowledge the factors that contribute to fume exposures, such as the selection of appropriate electric currents during SWAW operation.

CONCLUSION

During SMAW practices, vocational students were at risk of exposure to welding fumes. The higher the electric current use, the more welding fumes exposure concentration students were exposed. Fe, Zn, and Mn were the metal fumes of the top 3 highest exposure concentrations. Moreover, toxic trace elements such as Cr, Ni, Cd, and Ag were observed in welding fumes. The welding fume morphology was agglomerate chain-like structures consisting of nanoparticles. Therefore, control measures including a local exhaust ventilation systems, and the selection of appropriate electric currents should be implemented to reduce exposure to welding and metal fumes among the students performing SMAW practices.

ACKNOWLEDGEMENT

The authors appreciate the vocational college for their excellent cooperation and Science and Technology Instrumentation Center, Suranaree University of Technology for their consultation on the sample analysis in this study.

REFERENCE

[1] Montri, S., & Prayoon, S. 2019. Study of Microstructure and Creep Resistance of Electrical Welding Process in Spheroidal Graphite Cast-iron. EAU Heritage Journal Science and Technology

[2] Murugan, S. S., & Sathiya, P. 2024. Analysis of welding hazards from an occupational safety perspective. Vietnam journal of science, technology, and engineering, 66(3), 63-74.

[3] Riccelli, M. G., Goldoni, M., Poli, D., Mozzoni, P., Cavallo, D., & Corradi, M. 2020. Welding fumes, a risk factor for lung diseases. International journal of environmental research and public health, 17(7), 2552.

[4] Suárez, G., Niculita-Hirzel, H., Correia, D., Pralong, J. A., & Vernez, D. 2022. A proposed synergetic mechanism for metal fume fever involving ZnO and Fe3O4 nanoparticles. Scientific Reports, 12(1), 15643.

[5] Cha, E. W., Jeon, D., Kang, D., Kim, Y. K., & Kim, S. Y. 2022. Chemical Pneumonitis Caused by the Inhalation of Zinc Oxide Fumes in an Arc Welder. International Journal of Environmental Research and Public Health, 19(13), 7954.

[6] Sriram, K., Lin, G. X., Jefferson, A. M., Roberts, J. R., Chapman, R. S., Chen, B. T., ... & Antonini, J. M. 2010. Dopaminergic neurotoxicity following pulmonary exposure to manganese-containing welding fumes. Archives of toxicology, 84, 521-540.

[7] Kuempel, E. D., Roberts, J. R., Roth, G., Zumwalde, R. D., Nathan, D., Hubbs, A. F., ... & Holdsworth, G. 2021. Health effects of occupational exposure to silver nanomaterials.

[8] Charkiewicz, A. E., Omeljaniuk, W. J., Nowak, K., Garley, M., & Nikliński, J. 2023. Cadmium toxicity and health effects—a brief summary. Molecules, 28(18), 6620.

[9] IARC Working Group on the Evaluation of Carcinogenic Risks to Humans. 2018. Welding, molybdenum trioxide, and indium tin oxide. International Agency for Research on Cancer.

[10] Wyciślik-Sośnierz, J., Matusiak, J., Adamiec, J., Urbańczyk, M., Lemanowicz, M., Kusiorowski, R., & Gerle, A. 2024. Morphology of Welding Fume Derived from Stainless Steel Arc Welding. In Proceedings (Vol. 108, No. 1, p. 8). MDPI.

[11] Matczak, W., & Przybylska-Stanisławska, M. 2004. Oznaczanie dymów i ich składników powstajacych podczas spawania drutami proszkowymi [Determination of fumes and their elements from flux cored arc welding]. Medycyna pracy, 55(6), 481–489.

[12] Boelter, F. W., Simmons, C. E., Berman, L., & Scheff, P. 2009. Two-zone model application to breathing zone and area welding fume concentration data. Journal of occupational and environmental hygiene, 6(5), 298-306.

[13] Balkhyour, M. A., & Goknil, M. K. 2010. Total fume and metal concentrations during welding in selected factories in Jeddah, Saudi Arabia. International Journal of Environmental Research and Public Health, 7(7), 2978-2987.
[14] Pourtaghi, G., Kakooei, H., Salem, M., Pourtaghi, F., & Lahmi, M. 2009. Pulmonary effects of occupational exposure to welding fumes. Australian Journal of Basic and Applied Sciences, 3(4), 3291-3296.
[15] Soltanpour, Z., Rasoulzadeh, Y., Ansarin, K., Seyedrezazadeh, E., & Mohammadian, Y. 2023. Carcinogenic and non-carcinogenic risk of exposure to metal fume in different types of welding processes. Environmental Science and Pollution Research, 30(35), 83728-83734.
[16] Czuchryj, J., & Sikora, S. 2007. Problems with assessing, quality of welded joints, made on the basis of visual examinations Recommended by EN ISO 5817: 2003 standard. Welding International, 21(12), 871-878.
[17] NIOSH. 2003. ELEMENTS by ICP 7300 (Nitric/Perchloric Acid Ashing). In NIOSH Manual of Analytical Methods (NMAM) Fourth Edition.
[18] Abdull, N., Muhammad, N. S. I., Mokhtar, K. M., & Shahri, Z. 2024. Occurrence, characterization, and transport mechanism of welding fumes particles emitted during the welding process. In Journal of Physics: Conference Series (Vol. 2688, No. 1, p. 012010). IOP Publishing.
[19] Pourhassan, B., Beigzadeh, Z., Nasirzadeh, N., & Karimi, A. 2024. Application of multiple occupational health risk assessment models for metal fumes in welding process. Biological Trace Element Research, 202(3), 811-823.
[20] Sivapirakasam, S. P., Mohan, S., Santhosh Kumar, M. C., & Surianarayanan, M. 2017. Modeling of fume formation from shielded metal arc welding process. Metallurgical and Materials Transactions B, 48, 1268-1278.
[21] Oprya, M., Kiro, S., Worobiec, A., Horemans, B., Darchuk, L., Novakovic, V., ... & Van Grieken, R. 2012. Size distribution and chemical properties of welding fumes of inhalable particles. Journal of Aerosol Science, 45, 50-57.
[22] Su, W. C., Chen, Y., Bezerra, M., & Wang, J. 2019. Respiratory deposition of ultrafine welding fume particles. Journal of Occupational and Environmental Hygiene, 16(10), 694-706.
[23] Antonini, J. M., Keane, M., Chen, B. T., Stone, S., Roberts, J. R., Schwegler-Berry, D., Andrews, R. N., Frazer, D. G., & Sriram, K. 2011. Alterations in welding process voltage affect the generation of ultrafine particles, fume composition, and pulmonary toxicity. Nanotoxicology, 5(4),700–710. https://doi.org/10.3109/17435390.2010.550695
[24] Stebounova, L. V., Gonzalez-Pech, N. I., Peters, T. M., & Grassian, V. H. 2018. Physicochemical properties of air discharge-generated manganese oxide nanoparticles: comparison to welding fumes. Environmental Science: Nano, 5(3), 696-707.

The Awareness of Residents Regarding Influence on Water Quality in the Local Environment

Momone Kanno[1], Sarunnoud Phuphisith[2], Yurina Otaki[3] and Masahiro Otaki[4*]

[1] Undergraduate student, Department of Human Environmental Science, Faculty of Human Life and Environmental Science/Undergraduate School, Ochanomizu University, Tokyo, Japan 112-8610
[2]Assistant Professor, Department of Environmental Engineering, Faculty of Engineering/Graduate School, Chiang Mai University, Chiang Mai, Thailand 50200
[3] Professor, Department of Social Sciences, Faculty of Social Sciences/Graduate School, Hitotsubashi University, Tokyo, Japan 186-8601
[4]Professor, Department of Human Environmental Science, Faculty of Human Life and Environmental / Graduate School of Humanities and Science, Ochanomizu University, Tokyo, Japan 112-8610*
[*]Phone : +81-3-5978-5748, Fax : +81-3-5978-2049, E-mail : otaki.masahiro@ocha.ac.jp

ABSTRACT

In much of Southeast Asia, domestic graywater, which is wastewater generated by households except for that from toilets, is typically discharged without treatment from the household, contributing the deterioration of the local water environments. Therefore, this study explores the level of awareness among local residents regarding this issue. A questionnaire survey was conducted with 150 residents from 25 communities along the Mae Kha Canal flowing through Chiang Mai City. The results showed that residents rated the lower impact from their own houses on the Mae Kha Canal and the Ping River significantly than other sources, such as restaurants or hotels. Furthermore, when the term "Mae Kha Canal" was replaced with "Canal Near Your House," residents were more likely to acknowledge their houses' impact. This suggests that residents recognize their graywater discharge as affecting small canals near their houses but not to larger water environment, such as the Mae Kha Canal and the Ping River, even though they are directly connected. These findings indicate a limited sense of responsibility for the broader water environment and further research should be considered to explore how they perceive the relationship between the nearby canals and larger water bodies and strategies to enhance the residents' awareness.

Keywords: graywater discharge; water quality; residents' awareness

INTRODUCTION

In much of Southeast Asia, the local water environment is strongly influenced by domestic graywater, which is wastewater generated by households except for that from toilets and is typically discharged without treatment.

In the case of Chiang Mai City, some household drainage connects to the sewage system, which covers 67.5% of the city, and is treated at a wastewater treatment plant [1]. In other areas, drainage is discharged into the city's canals. While some canal water undergoes treatment at a wastewater plant, the rest remains untreated and is released to the section of Ping River that flows through Chiang Mai province.

Manene et al. (2024) examined the water qualities at 7 sites of the Mae Kha Canal, which flows through Chiang Mai [2]. The study measured eight water quality parameters inclusive of water temperature, pH, electrical conductivity, saturated oxygen based on dissolved oxygen, BOD, ammonium nitrogen, nitrate nitrogen, and orthophosphate, and calculated Merck's chemical index (MCI) using these eight parameters. **Table 1** shows the classification of the water quality using the value of MCI and **Table 2** shows the resulting MCI values and the classifications of 7 sites across the three seasons. The results indicate that the water quality of the Mae Kha Canal was assessed as "polluted" in all seasons except for the most upstream site. Additionally, poor water quality was recorded in both the dry and wet seasons, with a maximum Biochemical Oxygen Demand (BOD) exceeding 2500 mg/L and a minimum Dissolved Oxygen (DO) level of approximately 1 mg/L observed at the site MK 4 in February 2023.

Table 1 Classification of Merck's chemical index

Class	Range of chemical index	Classification
I	83-100	Very clean
I-II	73-83	Clean
II	56-73	Fairly clean
II-Ⅲ	44-56	Moderate
Ⅲ	27-44	Polluted
Ⅲ-Ⅳ	17-27	Heavily polluted
Ⅳ	0-17	Very heavily polluted

Table 2 Merck's chemical index results with their corresponding water quality classes.

Sites	Cool dry	Hot dry	Rainy	Average
MK1 (most upstream)	84(I)	54(II-Ⅲ)	47(II-Ⅲ)	62(II)
MK2	33(Ⅲ)	23(Ⅲ-Ⅳ)	31(Ⅲ)	29(Ⅲ)
MK3	14(Ⅳ)	18(Ⅲ-Ⅳ)	12(Ⅳ)	14(Ⅳ)
MK4 (in Chiang Mai City)	8(Ⅳ)	7(Ⅳ)	7(Ⅳ)	7(Ⅳ)
MK5 (in Chiang Mai City)	12(Ⅳ)	9(Ⅳ)	12(Ⅳ)	11(Ⅳ)
MK6	14(Ⅳ)	11(Ⅳ)	8(Ⅳ)	11(Ⅳ)
MK7 (most downstream)	15(Ⅳ)	12(Ⅳ)	13(Ⅳ)	13(Ⅳ)
Average	16(Ⅳ)	13(Ⅳ)	14(Ⅳ)	14(Ⅳ)

Concerning the water quality of the Ping River, the Environmental and Pollution Control Office (2020) measured five parameters at five sampling sites and calculated the water quality index, the results of which are presented in **Table 3** [3]. The water quality of the Ping River was classified as good or moderate at all sampling sites. However, after passing through Chiang Mai City, the concentrations of total coliform bacteria and ammonium nitrogen increased, and in terms of nitrogen concentration, the value exceeded the regulatory standard for the moderate class. This suggests that the water quality of the Ping River is affected by discharges from Chiang Mai City. Therefore, the water quality of both the Ping River and the Mae Kha Canal is likely affected by urban human activities, with the Mae Kha Canal being heavily polluted.

Table 3 Results of surface water quality at each location in the Ping River in March 2020

Sites	DO (mg/L)	BOD (mg/L)	TCB (MPN/100mL)	FCB (MPN/100mL)	NH_3 (mg/L)	WQI	Water quality class
Pl14 (most upstream)	4.75	1.37	2.3×10^2	4.5×10^1	0.26	72	2 (Good)
Pl13 (in Chiang Mai City)	6.63	1.55	9.2×10^3	1.3×10^3	0.45	70	3 (Fair)
Pl12 (in Chiang Mai City)	6.00	1.49	9.2×10^3	4.0×10^1	0.47	65	3 (Fair)
Pl11.1	5.30	1.29	1.6×10^4	3.2×10^2	0.77	61	3 (Fair)
Pl11	6.68	1.31	4.9×10^2	2.2×10^2	0.98	64	3 (Fair)
Pl10 (most downstream)	7.88	1.43	9.2×10^3	2.1×10^2	0.96	61	3 (Fair)
Class 3 standard	>4.0	< 2.0	$< 2.0\times10^4$	$< 4.0\times10^3$	0.50		

In the context of studies on public awareness of water environments in Southeast Asia, Otaki et al. (2025) investigated how residents in Ho Chi Minh City, Vietnam, perceive the current situation of domestic wastewater, the extent to which they consider it a problem, and what approach to domestic wastewater treatment they consider appropriate [4]. The study found that residents were more aware of the problem with the canal than with the major river, and the level of awareness was linked to their education, regardless of the distance to the canal or river and the frequency of seeing them.

To better understand public awareness of water pollution issues, this study conducted a questionnaire survey among residents of communities near the Mae Kha Canal referring to previous studies. It explored how residents perceive domestic wastewater treatment and the state of the local water related to graywater discharge.

METHODOLOGY

This study focused on Chiang Mai City, a major economic, cultural, and educational hub in northern Thailand. Chiang Mai Municipality covers an area of 40.2 km² [5] and had a population of 117,086 in 2022 [6]. In 2009, the main water supply service unit in Chiang Mai provided 31,962,634 m³ of water per year for 71,448 residents [7]. To the east of the city, the Ping River flows from north to south, while the Mae Kha Canal runs through the more central part of the city, west of the Ping River. According to water resource data from the Nawarat Bridge monitoring station on the Ping River, the average annual water volume measured over the period from 1921 to 2000 is 1,825 million m³ [7]. Along the Mae Kha Canal and the Ping River, many residential communities, markets, and hotels are located.

The survey area consisted of 25 communities located along the Mae Kha Canal, and the responses were collected from 5 to 10 households per community using snowball sampling, a sampling method in which existing participants introduce new ones. Permission to conduct the survey was obtained by contacting each community leader. A total of 150 households were interviewed which was sufficient for the required sample size of 128 for analyzing an unpaired two-tailed t-test, as calculated using G*Power (ver. 3.1.9.6) [8]. Due to the flooding of the Ping River, the survey period was divided into two phases: September 20 to 26, 2024, and November 3 to 10, 2024. There was one difference in the wording used between the first and second survey: the specific name “Mae Kha Canal” was used in the survey questions about the canal, and it was replaced with the more general term “Canal Near Your House” in the second survey. The locations of the surveyed communities, the Mae Kha Canal, and the Ping River are shown in **Figure 1**. Red numbers indicate the communities surveyed in the first phase, while blue numbers represent those surveyed in the latter phase.

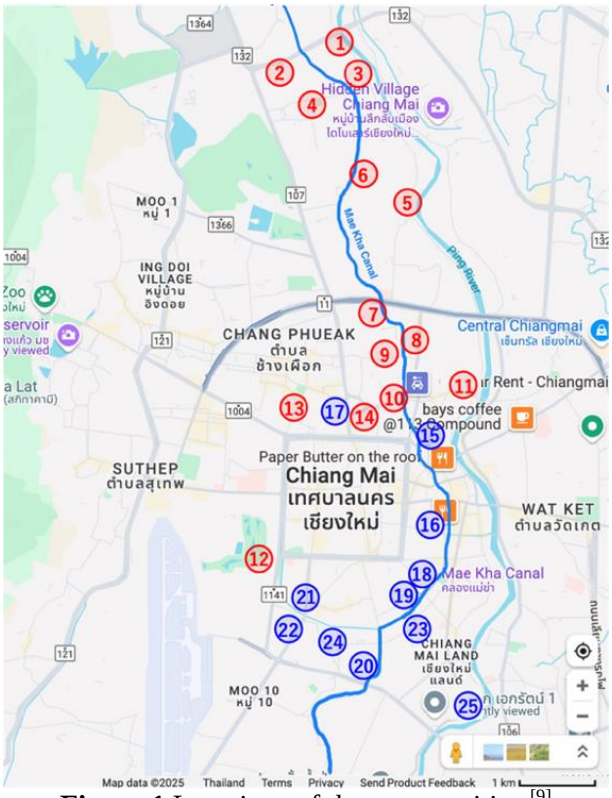


Figure 1 Locations of the communities [9]

The questionnaire survey was conducted by Qualtrics, a questionnaire development platform. To measure the level of residents' awareness, the survey used a Visual Analog Scale (VAS), in which respondents were asked to rate their awareness on 100 levels.

The questionnaire consisted of four components: aspects of the local water environment that respondents liked or found problematic, awareness of the local water environment, awareness and behavior related to graywater discharge, and demographics. This study focuses on two survey questions: "How much do you think that the following sources influence water quality in the Ping River and Mae Kha Canal?" The seven sources were asked to the respondents including your house, surrounding houses, restaurants, tourists, factories, commercial buildings/offices, and hotels. The sources of restaurants and hotels were included

because many restaurants and hotels are located along the Ping River and the Mae Kha Canal. Based on the information available on Google Maps [9], 39 restaurants and 34 hotels are situated along the Ping River, while 95 restaurants and 47 hotels are located along the Mae Kha Canal within the survey area. The respondents were requested to rate their answers using a scale from 0 to 100, where 0 indicated no influence at all, and 100 represented a very strong influence.

RESULTS AND DISCUSSIONS

Before assessing residents' awareness regarding the impact on water quality in the local environment, this study considered how residents perceive and interact with local waterfront spaces. **Table 4** displays the waterfront spaces that respondents mentioned positively in the open-ended responses, while **Table 5** presents those they identified as problematic.

The findings suggest that both the Ping River and the Mae Kha Canal, were frequently mentioned in both categories. This indicates that residents feel an attachment to these waterfront spaces, but at the same time, they also consider them to have problems. As for problematic these waterfront spaces while also recognizing their issues. Regarding problematic spaces, small branches of the Mae Kha Canal were also mentioned. In total, half of the respondents identified the Mae Kha Canal and its branches as problematic. It is likely to reflect concerns about the poor water quality of the Mae Kha Canal.

Table 4 Favorite waterfront spaces (selected from those with the highest number of answers)

Favorite waterfront space	Number of answers
Ping River (including answers that refer to specific locations)	**47**
Mae Kha Canal (including answers that refer to specific locations)	**29**
Huai Tueng Thao Reservoir	9
Moat around the old city	6
Nothing in particular	49

Table 5 Problematic waterfront spaces (selected from those with the highest number of answers)

Problematic waterfront space	Number of answers
Mae Kha Canal (including answers that refer to specific locations)	**60**
Ping River (including answers that refer to specific locations)	**17**
Rong Krachae (A tributary of the Mae Kha Canal)	7
Lam Khu Wai (A tributary of the Mae Kha Canal)	6
Moat around the old city	6
Lam Mueang Klang (A tributary of the Mae Kha Canal)	2
Nothing in particular	48

The results regarding the impact of the seven sources on the local water environment (Ping River and Mae Kha Canal) are presented. **Figure 2** illustrates the perceived impact of these seven sources on the Ping River. Residents rated the impact of restaurants significantly higher, while they rated the impact of their own homes significantly lower (Friedman test, $p < 0.01$). Regarding hotels, residents did not perceive the impact to be as great as that of restaurants, despite their similar presence along the Ping River.

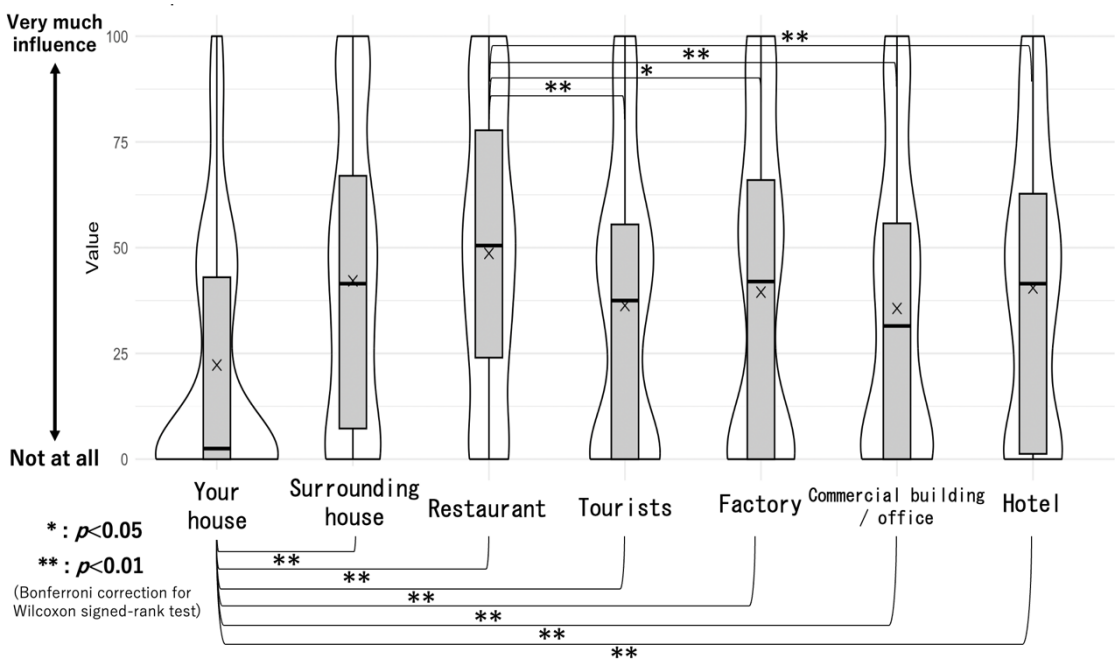


Figure 2 Influences of 7 sources on the Ping River

The same question was asked about the Mae Kha Canal, which is heavily polluted, and the results are shown in **Figure 3**. Residents rated the impact of their own houses significantly lower than that of other houses, restaurants, tourists, and hotels (Friedman test, $p < 0.01$). These results indicate a tendency to perceive the impact of their own houses on both the Ping River and the Mae Kha Canal as significantly lower than that of other sources.

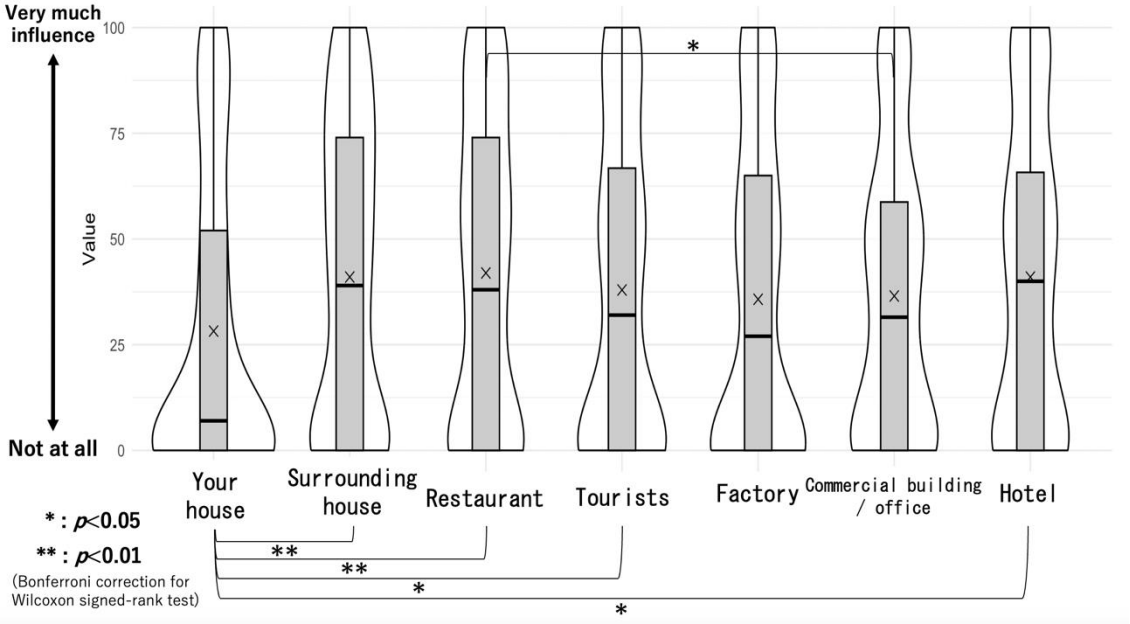


Figure 3 Influences of 7 sources on the Mae Kha Canal

Concerning this question about the Canal, when the individual name “Mae Kha Canal” was replaced with the general term “Canal Near Your House” in the latter part of the survey, a significant difference was observed in the response to “Your house” (Mann-Whitney U-test, $p < 0.001$). **Figure 4** compares the responses between the two groups: one was asked about the “Mae Kha Canal”, and the other was asked about the “Canal Near Your House.” The comparison suggests that some residents perceive their houses as having an impact on “canals near their homes” but not on “the Mae Kha Canal.” The use of the term "Mae Kha Canal" may have given the impression that it was merely a proper name or an unfamiliar canal, even though it is a familiar canal.

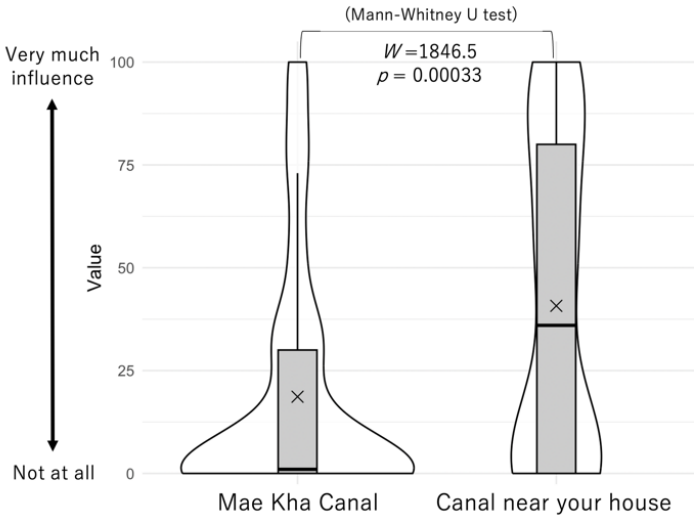


Figure 4 Comparison of item "Your house"
(How much do you think your house influences water quality in the Canal?)

CONCLUSION

The objective of this study is to assess residents' awareness and opinions regarding the impact of their household discharge on water quality in the local environment. The findings indicate that residents of communities near the Mae Kha Canal tend to perceive their graywater discharges as affecting only the nearby canals, with significantly lower awareness of its impact on the Mae Kha Canal and the Ping River, which were the subjects with a so-called objective name, compared to other sources. While residents feel a sense of attachment to the city's main canal and river and acknowledge their problems, they recognize that not their graywater discharge but other elements such as tourism or restaurants impact the main canal and river, despite the connection between nearby canals and the larger canal and river.

To clarify the extent of the residents' awareness of their own impact, further research should explore about how they perceive the relationship between the canals near their houses, the Mae Kha Canal and the Ping River. Additionally, strategies such as visualizing the entire flow of graywater discharge to the Ping River using videos or other technology, as well as engaging residents in community initiatives like canal cleanups or water quality monitoring, should be considered in future studies.

ACKNOWLEDGEMENT

I would like to thank Associate Professor Aunnop Wongrueng for his extensive support in designing and conducting the survey. I am grateful to the officers of Chiang Mai Municipality for assisting with site selection and community coordination, as well as to the students of the Department of Environmental Engineering, Faculty of Engineering, Chiang Mai University for translating the questionnaire into Thai and helping to conduct the field surveys. I also sincerely thank the community leaders and 150 residents of Chiang Mai who participated in the survey. Additionally, I would like to acknowledge the contributions of Chika Tokunaga and Hiro Nagai, whose previous research provided valuable references for developing the survey and analysis methods. Finally, I am grateful to all members of the Environmental Engineering Laboratory at Ochanomizu University for their insightful feedback and support throughout my research.

REFERENCE

[1] Environmental and Pollution Control Office 1. 2020. Community Wastewater Management Report and monitoring of wastewater treatment system situation fiscal year 2020. 26-37. https://x.gd/YlTQj

[2] Manene, O., Deadman, N., Techakijvej, C., Kullasoot, S., Sapewisut, P., Sareein, N., Phalaraksh, C. 2024. Ecological health assessment of Mae Kha Canal, Chiang Mai Province, Thailand in 2023. Journal of Ecology and Environment, 48, 11. doi=10.5141/jee.23.061

[3] Environmental and Pollution Control Office 1. 2020. Situation report, results of monitoring and surveillance of water quality, surface water sources Ping River (upper part), Kuang River, Li River, Kok River 2020. 2-3. https://x.gd/fqF4I

[4] Otaki, Y., Otaki, M., Do, Q.T.T, Shibao, E., Nagai, H., Tokunaga, C. 2025. Current status and views on the discharge of domestic wastewater to the environment in developing Asia. Water Practice and Technology, 20, 2; 375–384. https://doi.org/10.2166/wpt.2025.012

[5] Digital Economy Promotion Agency. 2025. ABOUT "CHIANG MAI MUNICIPALITY". https://www.citydata.in.th/chiangmai-municipality/en/homepage/

[6] Chiangmai Provincial Statistical Office, National Statistical Office. 2023. Chiangmai Provincial Statistical Report.7-12. https://chiangmai.nso.go.th/images/2023/repport/Statistics%202566_1.pdf

[7] Hydro-Informatics Institute. 2012. Data Collection and Data Analysis Implementation Project for the Development of a Data Warehouse System for 25 River Basins and Flood and Drought Modeling Ping River Basin. 13-18, 59-60. https://tiwrm.hii.or.th/web/attachments/25basins/06-ping.pdf

[8] Faul, F., Erdfelder, E., Lang, A.G., Buchner, A. 2007. G*Power 3: A flexible statistical power analysis program for the social, behavioral, and biomedical sciences. Behavior Research Methods, 39; 175-191. doi.org/10.3758/BF03193146

[9] Google. n.d. [Google Maps location of Chiang Mai City]. retrieved from https://x.gd/dejtW, viewed 18/02/2025